بیست و نهمین
کنفرانس شیمی آلی ایران

۱۰ تا ۱۲ آبان ۱۴۰۲ | دانشگاه قم

بسم الله الرحمن الرحيم

Dear Participant

Welcome to 29th Iranian Organic Chemistry Conference, that will be held during November 1-3, 2023 (Aban 10-12, 1402) at the Department of Chemistry, Faculty of Science, University of Qom with the collaboration of the Iranian Chemical Society to expand upon the knowledge and technology in Organic Chemistry, dependent fields and applications in industries, nanotechnology, environment, etc.

The scientific program covers a wide variety of topics in Organic Chemistry, including synthesis, methodology, physical organic chemistry, stereochemistry, spectroscopy, polymer, nano-chemistry and all subjects related to the Organic Chemistry.

The scientific and organizing committee would like to express their deep gratitude to all authors for their contribution in this conference. We hope that you will have a wonderful experience in Qom city and University of Qom will stay in your memories forever.

With the best regards, we would like to heartly appreciate the Chancellor, Finance Vice Chancellor and Research Vice Chancellor of the University of Qom, and Iranian Chemical Society, Scientific Committee, Department of Chemistry and Organizing Committee for their valuable contribution.

With the best regards

Mostafa Kiamehr

Associate Professor in Organic Chemistry

The Scientific Secretary of 29th Iranian Organic Chemistry Conference

شرکت کنندگان محترم

مفتخریم که بیست و نهمین کنفرانس شیمی آلی ایران با همکاری انجمن شیمی ایران در تاریخ ۱۰-۱۲ آبان ماه ۱۴۰۲ در **دانشگاه قم** برگزار شد و میزبان اساتید، دانشجویان، پژوهشگران، صنعتگران و علاقمندان این رویداد علمی بودیم. در این کنفرانس سه روزه، آخرین دستاوردهای علمی و پژوهشی در حوزه های مختلف شیمی آلی شامل: سنتز ترکیبات آلی، کاتالیزگرها، صنایع شیمیایی، محیط زیست و ... مطابق محورهای کنفرانس برگزار شد.

مقالات ارسالی همکاران ارجمند، دانشجویان عزیز، محققان و صنعتگران از طرف کمیته علمی بررسی و در دو قالب سخنرانی و پوستر ارائه شد. در مجموع در بیست و نهمین کنفرانس شیمی آلی ایران ۵۹۴ مقاله علمی و ۲۸ سخنرانی علمی ارایه شد.

در بخش دیگر این همایش، جهت بهره مندی بیشتر شرکت کنندگان با جدیدترین یافته های علمی و پژوهشی در حوزه موضوعات مرتبط با شیمی آلی و صنعت شیمی نشست های تخصصی با همکاری متخصصین در حوزه های مرتبط برگزار شد. در ضمن در طول برگزاری کنفرانس، کارگاه های آموزشی کاربردی با حضور اساتید برجسته برگزار گردید. برگزاری نمایشگاه های تخصصی در حاشیه همایش از دیگر برنامه های این رویداد علمی است.

در آخر از تمام اساتید، همکاران، مسئولین دانشگاه قم و دانشجویان عزیزی که در برگزاری هرچه بهتر بیست و نهمین کنفرانس شیمی آلی ایران- دانشگاه قم ما را یاری نمودند، بخصوص جناب دکتر احمدحسین شریفی ریاست محترم دانشگاه قم و دکتر محمود زارعی دبیر اجرایی کنفرانس کمال تشکر و قدردانی را دارم.

ارادتمند شما

دکتر مصطفی کیامهر

دبیر علمی بیست و نهمین کنفرانس شیمی آلی ایران

Scientific Committee

Dr.Mostafa Kiamehr	University of Qom
Dr.Mahmood Zarei	University of Qom
Dr.Amin Ahmadpoor	
Dr.Hadi Adibi	Kermanshah University of Medical Sciences
Dr.Abbas ali Esmaeili	Ferdowsi University of Mashhad
Dr.Bagher Eftekhari	University of Maragheh
Dr.Amin Ansari	Bu-Ali Sina University
Dr.Saeid Balalaei	K. N. Toosi University
Dr.Hamid Beizaei	University of Zabol
Dr.Behzad Jafari	Universität Rostock
Dr.Sadegh Rostamnia	Iran University of Science and Technology
Dr.Atie Rezvanian	Al-Zahra University
Dr.Reza RanjbarKarimi	Vali-e-Asr University of Rafsanjan
Dr.Hasan Zandi	University of Qom
Dr.Nasrin Zohre	University of Qom
Dr.Afshin Sarvari	Noshirvani university of technology
Dr.Hamid Saeidian	Payam Noor Alborz University
Dr.Mahdi Shakourian Fard Jahromi	Birjand University of Technology
Dr.Morteza Shiri	Al-Zahra University
Dr.Javad Safaei Ghomi	University of Kashan
Dr.Azim Ziaei Halime Jani	Sharif University of Technology
Dr.Salman Taheri	Chemistry & Chemical Engineering Research Center of Iran
Dr.Afsaneh Arefi Oskooei	Beheshti University of Medical Sciences
Dr.Alireza Abbasi	University of Qom
Dr.Mir Mohammad Alavi Nikje	Imam Khomeini International University
Dr.Mohammad Ali Ghasem Zadeh	Qom Islamic Azad University
Dr.Ramin Ghorbani Vaghei	Bu-Ali Sina University
Dr.Mahdi Kalhor	Payam Noor Qom University
Dr.Ali Maleki	Iran University of Science and Technology
Dr.Gholamreza Mahdavi Nia	University of Maragheh
Dr.Zohre Mirjafari	Islamic Azad University Science and Research Branch
Dr.Reza Najjar	University of Tabriz
Dr.Mahmood Nasrollah Zade	University of Qom
Dr.Nader Norouzi Pesyan	University of Oroumieh
Dr.Ehasan Noroozi Zadeh	

Student Committee

Fatemeh Abiri

Mohadeseh Afshar

Elahe Afshari

Fatemeh AliAbadi

Zeinab AmanGanje

MohammadReza AmjadTabrizi

Fahimeh Arezoomandi

Zeinab Asadi

Neda Bahadori

Mina Bakhtiari

Masoomeh Bekmohammadi

Nima Divani

Haniye FeyzAbadi

Masoomeh Ghadiri

Zahra Ghamkhar

FatemehSadat Honarvar

Fatemeh Mardani

Elahesadat Miri

Shahgol Mohammadi

Maryam Mohammadloo

Saeideh Mohammadnia

Mohadeseh MolaAghaBaba

Mahnaz Montazeri

Zohre Moradalian

Atie Mousavi

SeyedehHale Razi

Fatemeh SabzeKhah

Mohadeseh Sajadi

MohammadReza Sattari

Ahmad Sharafi

Sahar Shavikloo

Maryam Sobhani

Fatemeh ZareZadeh

سخـــــنرانان کلـــیدی

بیست و نهمین کنفرانس شیمی آلی ایران

سخـــــنرانان کلـــیدی

بیست و نهمین کنفرانس شیمی آلی ایران

حامیان مالی کنفرانس

شرکت مصباح انرژی

وزارت علوم، تحقیقات و فناوری

شرکت راد کیمیا گران

انجمن شیمی ایران

مرکز توسعه فناوری شیمیایی CIG

دانشگاه قم

Synthesis and characterization of porous covalent triazine polymers

Somayeh Nasrian, Massoumeh Bagheri*

Department of Chemistry, Faculty of Science, Azarbaijan Shahid Madani University, Tabriz, Iran, s_nasryan@yahoo.com, massoumehbagheri@yahoo.com.

Keywords: Porous organic polymers, Covalent triazine polymers, Melamine

Porous organic polymers are a new class of nanoporous materials that have been discovered in recent decades. Due to their very porous nature and covalent bond structures, they have a wide surface area and high stability. These properties make them useful in a number of advanced practical applications [1]. Covalent triazine polymers (CTPs) are a new class of porous organic polymers that contain aromatic triazine units with π-bonding properties. CTP frameworks are useful for application in gas adsorption/separation and catalysis, photocatalyst, Lithium-ion batteries, luminance and pollutant removal. CTPs have high thermal stability, and also show high stability in the presence of strong acids and bases [2], which makes them superior to other porous materials and has a strong potential for use in industrial applications.

In this study, we report the synthesis and characterization of melamine-based CTPs using 1,3,5-Triazine-2,4,6-triamine and dicarboxylic acids under different reaction conditions such as various molar ratios of initial materials, different reaction temperature and solvent by catalyst free polycondensation via solvothermal method. The structure of the synthesized melamine-based CTPs was characterized by scanning electron microscopy (SEM), Fourier transform infrared spectroscopy (FT-IR), thermaogravimetric analysis (TGA) and X-ray diffraction (XRD). The porosity analyses were also done via BET measurements. Furthermore, the effect of different synthesis conditions on the porosity, thermal stability, solubility and crystallinity of the prepared CTP was examined.

References

[1] Das, S.; Heasman, P.; Ben, T.; & Qiu, S. Porous organic materials: strategic design and structure–function correlation. *Chem. Rev*. 2017, *117*(3), 1515-1563.

[2] Zhang, Y.; & Jin, S. Recent advancements in the synthesis of covalent triazine frameworks for energy and environmental applications. *Polymers* 2018, *11*(1), 31.

An efficient and green route for one-pot synthesis of 5-substituted indole chromeno[2,3-b]pyridines

Fatemeh Molaei Yielzoleh, Maryam Saffari and Kobra Nikoofar*

Department of Organic Chemistry, Faculty of Chemistry, Alzahra University, Tehran, Iran
f.molaei@alzahra.ac.ir; fateme.molaei69@gmail.com, K.nikoofar@alzahra.ac.ir.

Keywords: Multi-component reaction, Indole, Indole chromeno[2,3-b]pyridines, Heterogeneous nanocatalyst

A heterogenous nanostructure containing tartaric acid, silica, and magnesium bismuthate (SiO_2/*L*-tar/$MgBi_2O_4$) prepared for the first time and used as catalyst in the one-pot, pseudo four-component condensation of salicylaldehydes, indoles, and malononitrile to achieve 5-substituted indol chromeno[2,3-b]pyridines in the excellent yields at 50 °C under solvent-free condition (**Scheme 1**). The valuable features of this method are: broad substrate scope, simple procedure, green solvent-free conditions, recovery and reusability, and short reaction times. Chromenopyridines are fused heterocycles that display broad range of biological activities such as cancer chemopreventive, antibacterial, antimyopic, antiproliferative, antiasthmatic, and antihistaminic [1-3].

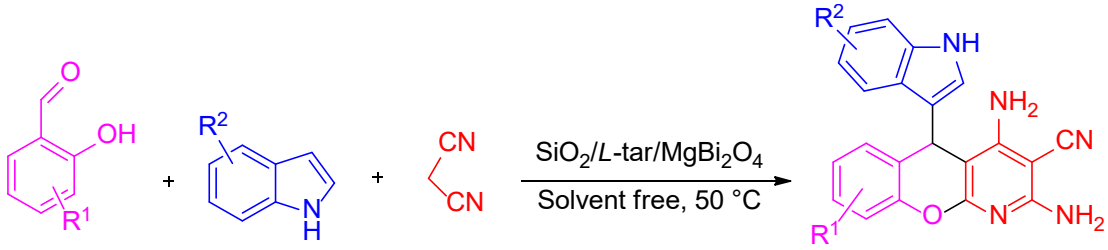

Scheme 1: Synthesis of 5-substituted indole chromeno[2,3-b]pyridines by SiO_2/*L*-tar/$MgBi_2O_4$.

References

[3] Srivastava, S. K.; Tripathi, R. P.; Ramachandran, R. nad$^+$-dependent DNA ligase (rv3014c) from mycobacterium tuberculosis: crystal structure of the adenylation domain and identification of novel inhibitors, *J. Biol. Chem* 2005, *280*, 30273–30281.

[4] Brotz-Oesterhelt, H.; Knezevic, L.; Bartel, S.; Lampe, T.; Warnecke-Eberz, U.; Ziegelbauer, K.; Habich, D.; Labischinski, H. Specific and potent inhibition of NAD$^+$- dependent DNA ligase by pyridochromanones, *J. Biol. Chem*. 2003, *278*, 39435–39442.

[5] Zhang, M.; Chen, M. N.; Zhang, Z. H. Visible Light-Initiated Catalyst-Free One-Pot, Multicomponent Construction of 5-Substituted Indole Chromeno [2, 3-b] pyridines. *Adv. Synth. Catal*. 2019, *361*, 5182-5190.

A Convenient Synthesis of Functionalized Indenopyrazolones from Indan-1,2,3-trione, Benzaldehydes, and Phenylhydrazine

Issa Yavari [a*], Samereh Seyfi[a] and Stavroula Skoulika[b]

a) Department of Chemistry, Tarbiat Modares University, Tehran, Iran, yavarisa@modares.ac.ir

b) Laboratory of Physical Chemistry, Department of Chemistry, The University of Ioannina, GR-451 10 Ioannina

Keywords: Indenopyrazolones, Benzaldehydes, Phenylhydrazine, Indan- 1,2,3-trione.

As part of our current studies on the development of new routes in heterocyclic synthesis [1 – 3], we report the results of our studies involving the reaction of phenylhydrazones, derived from phenylhydrazine (1) and bezaldehydes, with indan-1,2,3-trione (=1H-indene-1,2-3-trione; 3) in MeCN, which constitutes a synthesis of cis-3-aryl-3a,8b-dihydro-3a,8b-dihydroxy-1-phenylindeno[1,2-c]pyrazol- 4(1H)-ones 4 in good yields (**Scheme 1**).

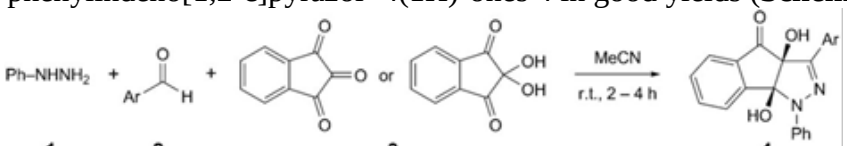

	Ar	Product	Yield [%]
2a	Ph	4a	84
2b	4-MeO–C_6H_4	4b	80
2c	4-Me–C_6H_4	4c	74
2d	4-Cl–C_6H_4	4d	88
2e	4-Br–C_6H_4	4e	90
2f	4-NO_2–C_6H_4	4f	80
2g	3-NO_2–C_6H_4	4g	78
2h	2-OH–C_6H_4	4h	78
2i	2-OH,3-$NO_2C_6H_3$	4i	76

Scheme1: Synthesis of Functionalized Indenopyrazolones

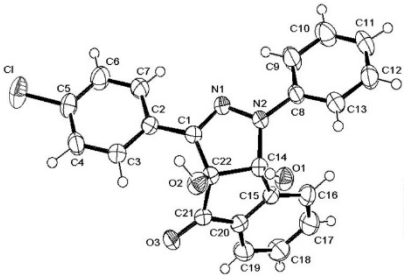

Fig.1. X-Ray crystal structure of **4d**. ORTEP-III Plot [4]; arbitrary atom numbering.

References

[6] Yavari, I.; Khalili, G.; Mirzaei, A.; *Helv. Chim. Acta* 2010, 93, 277.
[7] Yavari, I.; Khalili, G.; *Synlett* 2010, 1862.
[8] Yavari, I.; Moradi, L.; *Helv. Chim. Acta* 2006, 89, 1942.
[9] Burnett, A. M. N.; Johnson, C. K.; *Oak Ridge National Laboratory Report ORNL*-6895, 1996.

The new sulfonic-acid-based Ce-Mn-Layered Doble Hydroxide as a capable nano-catalyst for the green-synthesis of spiro[indoline-pyran]ones and spiro[acenaphthylene-pyran]ones

Samira Javadi* **and Davood Habibi**

Organic Chemistry Laboratory, Faculty of Chemistry, University of Bu-Alisina, Hamedan, Iran, samira.javadi9223@gmail.com.

Keywords: Solvent-free, Green synthesis, Spiro[acenaphthylene-pyran]ones, Sulfonic-acid-based Ce-Mn-LDH, Nano catalyst.

The new sulfonic-acid-based Ce-Mn-Layered Doble Hydroxide (Ce-Mn-LDH@ CPTMS @NAP@SO_3H) was prepared by modiication of the Ce-Mn-layered double Hydroxide (Ce-Mn-LDH) with 3-chloropropyltrimethoxysilane and N-amino Phthalimide and functionalized with chlorosulfonic acid. Then, It was characterized with the FT-IR, XRD, EDX, SEM, SEM-mapping, UV/vis, TEM, And TGA-DTA Techniques and used as a new and efficient heterogeneous acid catalyst for the green solvent-free synthesis of spiro[induline-pyran]ones and spiro[acenaphthylene-pyran] ones from the one-pot multicomponent condensation reaction of isatin or acenaphthoquinone, malononitrile, and 1,3-diketone in very short reaction times and excellent yields. Also, the catalyst is stable under reaction conditions and can be reused without the significant loss of catalytic activity (**Scheme**).

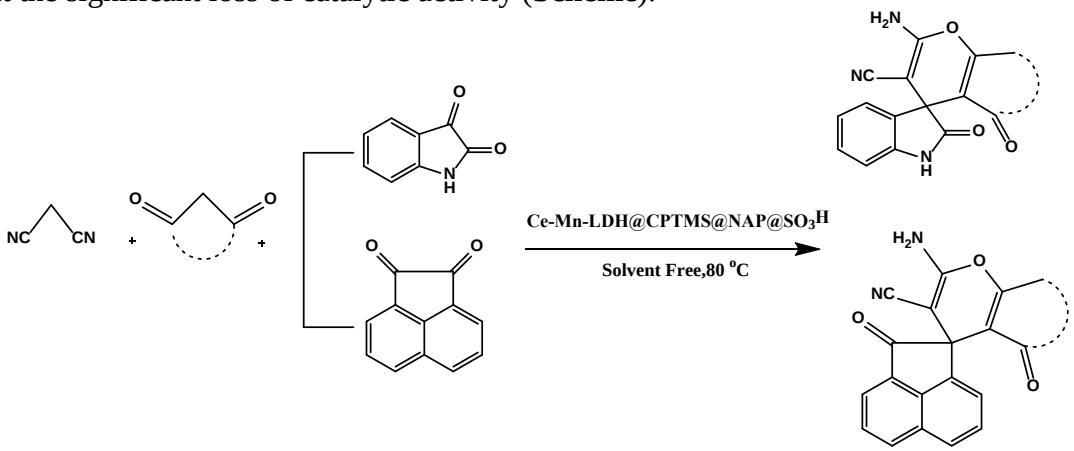

Scheme: Synthesis of spiro[indoline-pyran]ones and spiro[acenaphthylene-pyran]ones.

References

[10] Bach, L.; Islam, M.R.; Cao, X.T.; Lim, K.T.; Park, J.M. A novel photoluminescent nanohybrid of poly(ε-caprolactone) grafted Mg/Al layered double hydroxides and Tb^{3+} ions: synthesis and characterization. *J. Alloy. Compd* 2014, *22*, 582.

[11] Dou, R.; Huang, J. Ma, D.; Fan,C.; Zhao,W.; Komarneni,S.; Peng, M. Bisulfite assisted photocatalytic degradation of methylene blue by Ni-Fe-Mn oxide from MnO_4 inter-calated LDH. *Appl. Clay Sci* 2018, *161*, 235.

Synthesis of new magnetic nanocatalyst on Halloysite substrate and investigation of their performance in the synthesis of spirooxindole Derivatives

Zahra Younesi[a*], Mahmood Tajbakhsh Jadidi[a] and Mansoureh Daraie[b]

a) Organic Chemistry Laboratory, Faculty of Chemistry, University of Mazandaran, Babolsar, Iran, zahra_younesi@yahoo.com,
b) Department of Chemistry, Science and Research Branch, Islamic Azad University, Tehran, Iran

Keywords: Halloysite nanotubes, Catalyst, Magnetic nanoparticle, Spirooxindole, Multicomponent reactions (MCRs)

In recent years, halloysite nanotubes (HNTs) have garnered significant attention due to their unique properties and wide applications in various fields. One of the key advantages of HNTs is their ability to be modified and functionalized, allowing for the incorporation of different nanoparticles to enhance their properties and create novel nanocomposites.
In this study, a new bio-based nanocomposite was designed based on the modification of magnetic halloysite with arginine. The combination of HNTs and Fe_3O_4 nanoparticles created a unique platform for the catalyst, which enabled easy separation and recycling of the catalyst and also improved the catalytic performance. Various analyzes were performed to confirm the formation of the catalyst [1]. After that, it was tested as a Lewis acid catalyst for the multicomponent one-pot synthesis of spirooxindole. Among the spiro compounds, spirooxindoles have gained significant attention due to their unique structural array and highly pronounced pharmacological activity. Effective parameters such as catalyst amount, temperature and reaction time were optimized. The catalyst was also reusable and could be reused up to five times. Therefore, the synthesis of spirooxindoles has become a topic of interest for researchers [2].

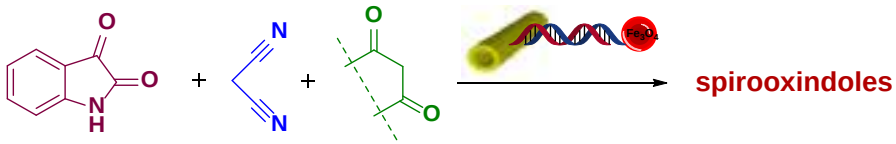

Scheme: Synthesis of different spirooxindoles in the presence of Hal-arg-Dy.

References:

[12] Sadjadi, S.; Samadi, S.; Samadi, M. $Cu(CH_3CN)_4PF_6$ immobilized on halloysite as efficient heterogeneous catalyst for oxidation of allylic C–H bonds in olefins under mild reaction condition. *Res. Chem. Intermed*. 2019; 45: 2441- 55.
[13] Wang, L. M.; Jiao, N.; Qiu, J.; Yu, JJ.; Liu, JQ.; Guo, FL.; Liu, Y. Sodium stearate-catalyzed multicomponent reactions for efficient synthesis of spirooxindoles in aqueous micellar media. *Tetrahedron* 2010; 66(1): 339- 43.

29TH IRANIAN ORGANIC CHEMISTRY CONFERENCE
1_3 NOV, 2023
UNIVERSITY OF QOM, IRAN

Synthesis new derivatives of 1-methyl-3-phenylpyrazolo[4',3':5,6]pyrano[3,4-c]quinolin-5(3H)-one and 1H-pyrimido[5',4':5,6]pyrano[3,4-c]quinoline-1,3,6(2H,4H)-trione compounds

Sobhan Ghazimoradi*, Sorour Ramezanpour

Medicinal Chemistry Laboratory, Faculty of Chemistry, University of K. N. Toosi, Tehran, Iran, sobhan.ghmr@yahoo.com

Keywords: Quinolines, Multicomponent, activity.

In this research, we have been able to synthesize different derivatives of two groups of 1-methyl-3-phenylpyrazolo [4',3':5,6] pyrano[3,4-c] quinolin-5(3H)-one (a) and 1H-pyrimido [5',4':5,6] pyrano [3,4-c] quinoline-1,3,6(2H,4H)-trione (b) (**Scheme1**) compounds using multicomponent reactions with a similar method. 1-Methyl-3-phenylpyrazolo[4',3':5,6]pyrano[3,4-c]quinolin-5(3H)-one(a) compounds based on their structural skeleton can show properties such as: antibacterial, antioxidant [1], anti-cancer activity, Also, and 1H-pyrimido[5',4':5,6]pyrano[3,4-c]quinoline-1,3,6(2H,4H)-trione(b) Important scaffolding in organic and medicinal chemistry, with activities such as 5-HT3 receptor antagonist, topoisomerase II inhibitors, etc. [2].

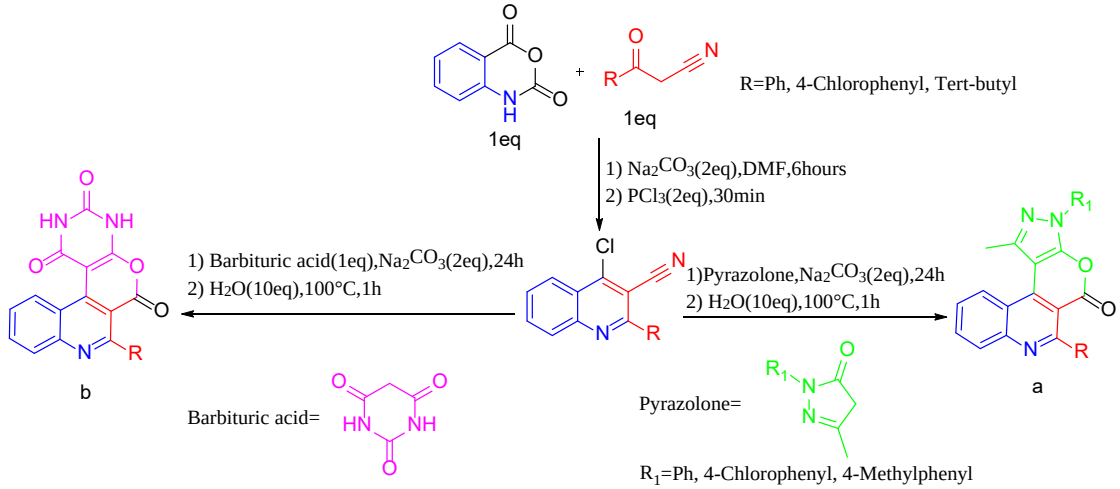

Scheme1: Overview of how to synthesize products.

References:

[1] Arasakumar, T.; Mathusalini, S.; Gopalan, S.; Shyamsivappan, S.; Ata, A.; Mohan, P. S. Biologically Active Perspective Synthesis of Heteroannulated 8-Nitroquinolines with Green Chemistry Approach. *Bioorganic Med. Chem. Lett.* **2017**, *27* (7), 1538–1546.

[2] Raji Reddy, C.; Bodasu, S.; Mallesh, K.; Prapurna, Y. L. Synthesis of Fused Pyrimido[1,6- a]Indolones via Rhodium(III)-Catalyzed Cascade Annulations. *Synth.* **2021**, *53* (6), 1127–1136.

New epidermal strain sensors based on magnetic κ-carrageenan-containing hydrogels

Sakineh Alipour, Ali Pourjavadi *

Polymer Research Laboratory, Department of Chemistry, Sharif University of Technology, Tehran, Iran, purjavad@sharif.edu, skalipoor@gmail.com

Keywords: Strain sensor, Magnetic hydrogel, Carrageenan.

Hydrogel-based-strain sensors are applied to monitor human motions helping to diagnose movement diseases. The smartness of hydrogels adds new features to the corresponding sensors that improve their performance [1]. We previously prepared electrical conductive hydrogels using Fe_3O_4 nanoparticles and κ-carrageenan, representing temperature-sensitive shape memory [2]. The electrical conductivity was created only with carrageenan and acrylic acid (no additional salt was added). The hydrogels (as tensile strain sensors) showed strong and reproducible signals during 500 stretching and shortening cycles. Herein, the performance of the hydrogels in human motion monitoring was investigated (**Scheme**). Results showed strong signals in the knee, wrist, and finger movements. This consequence was extraordinary, considering the lack of additional salt in the hydrogel composition.

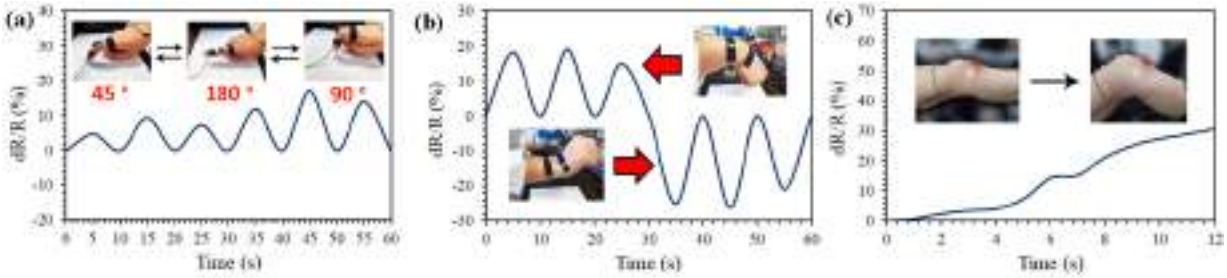

Scheme: Monitoring of (a) the finger, (b) wrist, and (c) knee motions by the magnetic hydrogel.

References

[1] Yang, Q.; Gao, C.; Zhang, X.; Zhao, X.; Fu, Y.; Tsou, C.; Zeng, C.; Yuan, L.; Pu, Z.; Xia, Y., Dual-responsive shape memory hydrogels with self-healing and dual-responsive swelling behaviors. *J. Appl. Polym. Sci.* **2021,** *138* (13), 50308.

[2] Alipour, S.; Pourjavadi, A.; Hosseini, S. H., Magnetite embedded κ-carrageenan-based double network nanocomposite hydrogel with two-way shape memory properties for flexible electronics and magnetic actuators. *Carbohydr. Polym.* **2023,** *310*, 120610.

Synthesis of pyrido[2,3-d:5,6-d′]dipyrimidine derivatives in the presence of ZnO NPs as highly efficient catalyst

Atieh Ahmadi, Leila Moradi*

Department of Organic Chemistry, Faculty of Chemistry, University of Kashan, P.O. Box 8731753153, Kashan, I. R., Iran, 8731753153, ahmadiatieh99@gmail.com, *L_Moradi@kashanu.ac.ir*

Keywords: Pyrido[2,3-d:5,6-d′]dipyrimidines, ZnO Nanoparticles, Multicomponent reactions, Barbituric acid.

One-pot multicomponent reactions are a highly versatile strategy for the synthesis of valuable nitrogen containing heterocyclic compounds [1]. Pyridopyrimidines are an important class of N-containing fused heterocyclic systems, that have many biological and pharmacological properties such as anti-allergic, antiviral activities, anti-tumor, anticonvulsants activity and anti-inflammatory. Since the past until now, various approaches have been reported for the synthesis of these compounds [2,3]. In this study, we decided to present the synthesis of pyrido[2,3-d:5,6-d´]dipyrimidine derivatives via the one-pot three component condensation reaction of 6-aminouracil, barbituric acid and aromatic aldehydes in the presence of an efficient nanocatalyst (ZnO NPs) in ethanol under thermal conditions **(Scheme 1).** Reusable catalyst, green reaction conditions and high to excellent yield of products are the advantageous of presented method.

Scheme 1: One pot synthesis of pyrido[2,3-d:5,6-d′]dipyrimidine derivatives in the presence of ZnO.

References

[1] Nandi, S., Jamatia, R., Sarkar, R., Sarkar, F. K., Alam, S., & Pal, A. K. (2022). *ChemistrySelect*, *7*(33), e202201901.
[2] Saeidiroshan, H., & Moradi, L. (2019). *J. Organomet. Chem. 893*, 1-10.
[3] Mamaghani, M., Moslemi, L., & Badrian, A. (2018). *React Modern Org Chem Res*, *3*(1), 8.

Advanced Photocatalytic System for Reduction of Nitro aromatic compounds in Magnetized water

Amir Farkhondeh[a*], Foad Kazemi[a] and Mostafa Gholizadeh[b]

a) Department of Chemistry, Institute for Advanced Studies in Basic Sciences (IASBS), Zanjan, Iran, Amir.farkhondeh@iasbs.ac.ir, Kazemi_f@iasbs.ac.ir
b) Department of Chemistry, Faculty of Science, Ferdowsi University of Mashhad, Mashhad, Iran

Keywords: Biphase systems, β-Cyclodextrin, Magnetized water, Photocatalytic reduction, Nitro aromatic,

One of the key objectives of chemists is to achieve high-speed chemical reactions. A method that can be adopted to obtain such a goal is to conduct reactions in magnetic solvents. When water is subjected to a magnetic field, it exhibits remarkable changes, including alterations in refractive index, electric dipole moment, electrical conductivity, specific heat, permeability, enthalpy of vaporization, surface tension, viscosity, and density.

In photocatalytic reduction processes using semiconductor nanoparticles, the utilization of beta-cyclodextrin (β-CD) on the surface of titanium dioxide (TiO_2) enables the inclusion of organic molecules within the β-CD pore, resulting in improved performance of the modified catalyst TiO_2-β-CD in photocatalytic reactions. One of the major challenges in photocatalytic reduction processes using semiconductor nanoparticles is the limited amount of raw material. Therefore, finding a pathway to address this issue is highly significant. It can be expected that the use of a biphasic system alongside beta-cyclodextrin as a phase transfer catalyst (PTC) would lead to reduced reaction time, lower solvent requirements, fewer side reactions, and consequently, increased reaction efficiency. In this project, a novel approach is reported for the reduction of nitro aromatic compounds by increasing the amount of raw material and utilizing biphasic systems with magnetized water in the presence of β-CD-modified TiO_2 as a phase transfer catalyst (PTC) under UV LED light.

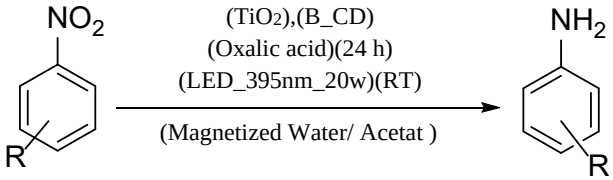

Scheme: The Photocatalytic Reduction of Nitro aromatic compounds using TiO_2-β-CD in Biphase system.

References

[14] Bakherad. M, Farkhondeh. A, Keivanloo. A, Amin. A. Catalyst-free, a Green, and Efficient Protocol for the Synthesis of 1, 8-dioxooctahydroxanthenes in Magnetized Water. *J. M. Chem. Soc*. (**2019**) 63(4):199-207.
[15] Zand. Z, Kazemi. F, Partovi. A. Photocatalytic synthesis of anilides from nitrobenzenes under visible light irradiation: 2 in 1 reaction. *J. Photoch. Photobio. B.* (**2015**) 1.152:58-62.

New Magnetic Nanoparticles Supported Bimetallic CoCu as an Efficient Catalyst in Water

Mahboobe Eskandari, Mohammad Gholinejad* and Mohammad Ali Saidiansar

Department of Chemistry, Institute for Advanced Studies in Basic Sciences (IASBS), Gava Zang, Zanjan 49195-1159, Iran. meskandari517@gmail.com, mohammad_gholinejad@yahoo.com

Keywords: Magnetic catalyst, Bimetallic CoCu, Reduction, Nitrophenols, Organic dyes.

In this work, synthesis of a new magnetic catalyst, Fe_3O_4@IL-APD-CoCu, and its application in the reduction of nitrophenol compounds, decolorization of dyes, and degradation of tetracycline is studied. The structure of the catalyst was identified and analyzed by various techniques such as TEM, XRD, XPS, FT-IR, and UV-vis. In the following, catalytic performance in the reduction of nitrophenol compounds including 4-nitrophenol (4-NP), 3-nitrophenol (3-NP), and 2-nitrophenol (2-NP), decolorization of organic dyes such as methyl orange (MO), methyl red (MR), and rhodamine B (Rh B) and degradation of tetracycline were investigated (**Scheme**). The recyclability of the desired catalyst was also investigated and showed 14 runs of recyclability without a significant reduction in catalytic activity.

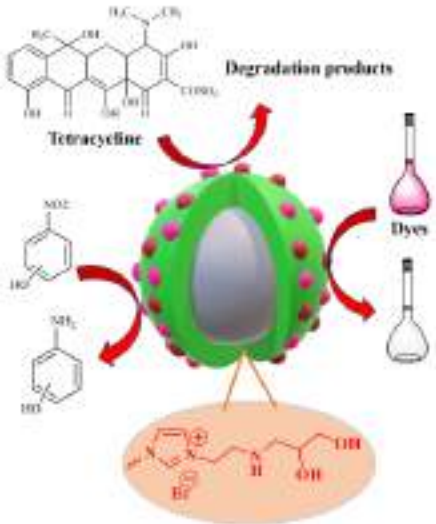

Scheme: New Magnetic Nanoparticles Supported Bimetallic CoCu as an Efficient Catalyst in Water.

References:

[16] Gholinejad, M., Naghshbandi, Z., Sansano, J.M.: Co/Cu bimetallic ZIF as new heterogeneous catalyst for reduction of nitroarenes and dyes. *Appl. Organomet. Chem*. 34, 5522 (**2020**).
[17] Gholinejad, M., Mirmohammadi, S., Sansano, J.M.: Novel Water Dispersible and Magnetically Recoverable Palladium Nano Catalyst for Room-Temperature Suzuki-Miyaura Coupling Reaction. *Chem. Select*. 6, 13906-13917 (**2021**).

A new synthetic method for β,γ-unsaturated α-aminophosphonates and investigation of their aza-Claisen rearrangement

Babak Kaboudin*, Mojtaba Ghashghaee

Organic Chemistry Laboratory, Department of Chemistry, Institute for Advanced Studies in Basic Sciences (IASBS), Gava Zang, Zanjan 45137-66731, Iran, kaboudin@iasbs.ac.ir and mojtabaghashghaee@iasbs.ac.ir

Keywords: Aminophosphonates, Claisen, Rearrangement

In the past decade, organophosphorus compounds and their derivatives have received considerable attention due to their biological, pharmacological, agricultural and medicinal chemistry proprieties as well as their utility as synthetic intermediates [1]. We tried to design a simple and efficient method for the synthesis of β,γ-unsaturated α-aminophosphonates (Scheme 1). The Claisen rearrangements of vinyl and aryl allyl ether are exploited as an expeditious approach to carbon-carbon bond formation in organic syntheses. In contrast, the amino-Claisen rearrangement, the nitrogen analogue of Claisen rearrangement has attracted little attention due to several limitations including slow rates, the need of higher temperature and low yields due to simultaneous allylic cleavage or cyclization leading to C-N bond formation [2]. The aza-Claisen rearrangement of the β,γ-unsaturated α-aminophosphonates will be also studied in various reaction condition. The resulting product is considered a valuable reagent for starting a reaction due to the presence of active sites in the structure (**Scheme**).

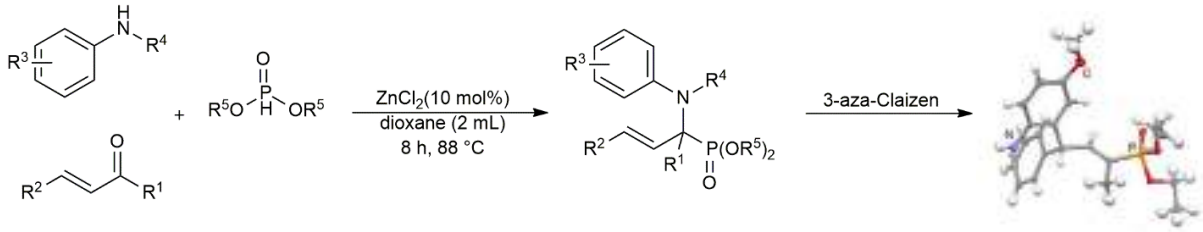

Scheme: General procedure for the synthesis of α-aminophosphonates and its rearrangement.

References

[18] Amira, A., Aouf, Z., K'tir, H., Chemam, Y., Ghodbane, R., Zerrouki, R., & Aouf, N. E. Recent Advances in the Synthesis of α-Aminophosphonates: A Review. *ChemistrySelect*, **2021**, *6*, 6137-6149.

[19] Jain, S. Zinc Chloride Catalyzed Amino Claisen Rearrangement of 1-N-Allylindolines: An Expedient Protocol for the Synthesis of Functionalized 7-Allylindolines. *Heterocycl. Commun.*, **2019**, *25*, 22-26.

29TH IRANIAN ORGANIC CHEMISTRY CONFERENCE
1_3 NOV, 2023
UNIVERSITY OF QOM, IRAN

Phosphoramidate synthesis via copper-catalysed oxidative coupling of amines and H-phosphonates

Fatemeh Darvish*, Zahra Abdi

Department of Chemistry, Faculty of Science, K.N. Toosi University of Technology, Tehran, Iran, darvish@kntu.ac.ir, zahraabdi20@yahoo.com

Keywords: Phosphoramidate, Atherton-Todd reaction, H-phosphonate, Dialkyl phosphite.

P-N bond creation is one of the great important research area owing to their myriad applications in organic synthesis. Between the various organophosphorous, including P(O)-N structural moiety, phosphoramidates are more efficient compounds in biologically active molecules, medicinal chemistry and industrial important products. For example, Sofosbuvir is an antiviral medicine that is used to treat chronic hepatitis C [1].

Traditional method of P(O)-N bond formation mainly relies on coupling of amines as a nucleophile with H-phosphinates. The Atherton-Todd reaction which generates phosphoryl chloride intermediate by halogenation of P(O)-H compounds with toxic halogenating agent such as CCl_4, followed by the attack of nucleophile to phosphoryl chloride, give desire product. It is noticeable that traditional methods are inclined to suffer from low yields, react with restricted amines and the major drawbacks of the method include the use of toxic halogen sources. In this research, it has been tried to provide a more efficient method [2].

In the present study, we used CuI as the catalyst and Di-tert-butyl peroxide (DTBP) as the oxidant to obtain the phosphoramidate synthesis via copper-catalyzed oxidative coupling of amines and H-phosphonates. The purpose of this work is to synthesis of phosphoramidates with various amines in short time and highly yield products (**Scheme1**).

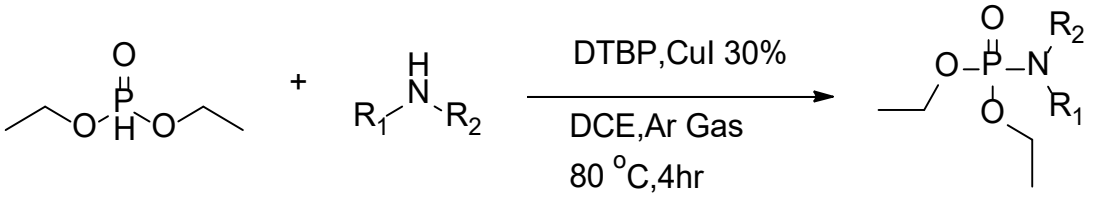

Scheme1: Synthesis of Phosphoramidates.

References

[1] Zhu, Y.-Y.; Niu, Y.; Niu, Y.-N.; Yang, S.-D., Recent advances in the synthesis and applications of phosphoramides. *Organic & Biomolecular Chemistry* **2021**, 19(47), 10296-10313.

[2] Itumoh, E. J.; Data, S.; Leitao, E. M., Opening up the toolbox: synthesis and mechanisms of phosphoramidates. *Molecules* **2020**, 25(16), 3684.

29TH IRANIAN ORGANIC CHEMISTRY CONFERENCE
1_3 NOV, 2023
UNIVERSITY OF QOM, IRAN

Tandem synthesis of imidazoles and benzimidazoles from diamines and aromatic aldehydes using potassium cyanide

Fatemeh Ahmadi and Ghasem Aghapour*

School of Chemistry, Damghan University, Damghan 36715-364, ahmadifatemeh447@gmail.com, gh_aghapour@du.ac.ir

Keywords: Aldehyde; Imidazole; Benzimidazole; Green oxidant; Potassium cyanide.

Imidazoles and benzimidazoles are very valuable and useful heterocycles in pharmaceutical chemistry. These derivatives have a lot of biological and pharmacological properties such as analgesic, antioxidant, anti-viral, antiulcer, antibacterial, antihypertensive, anticancer, anticonvulsant, herbicidal, anti-inflammatory, and antifungal and their structures are found in diverse drugs such as clotrimazole, telmisartan and omeprazole [1-2]. One way synthesizing these compounds is the reaction of aldehydes with ethylenediamines and o-phenylenediamines respectively [3]. However some procedures in this way have some restrictions such as use of acidic conditions, use of an unavailable catalyst or a special oxidant, high reaction temperature and so on. Thus, finding novel methods synthesizing these valuable compounds has become an at ractive field for synthetic chemists. Here, we describe an efficient method for the synthesis of imidazoles and benzimidazoles via reaction of different aromatic aldehydes with ethylenediamine and o-phenylenediamine respectively using O_2 from air in the presence of potassium cyanide in an oxidatively and tandem manner (**Scheme 1**). The present method is in agreement with green chemistry due to its tandem nature and use of oxygen from air as green oxidant. Mild reaction conditions, easy work up, excellent yields and also excellent chemoselectivity are considered as other advantages of this method.

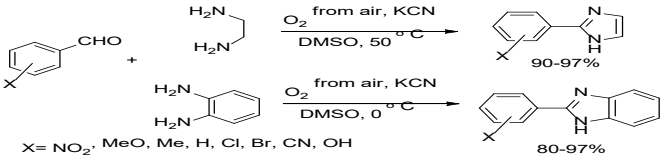

Scheme 1: Tandem synthesis of imidazoles and benzimidazoles from aldehydes using potassium cyanide.

References

[1] Satija, G.; Sharma, B.; Madan, A.; Iqubal, A.; Shaquiquzzaman, M.; et al. Benzimidazole based derivatives as anticancer agents: Structure activity relationship analysis for various targets. *J. Heterocycl. Chem*. 2022, *59*, 22-66.

[2] Faheem, M.; Rathaur, A.; Pandey, A.; Singh, V. K.; Tiwary, A. K. A Review on the Modern Synthetic Approach of Benzimidazole Candidate. *Chemistryselect* 2020, *5*, 3981-3994.

[3] Pardeshi, V. A. S.; Chundawat, N. S.; Pathan, S. I.; Sukhwal, P.; Chundawat, T. P. S.; Singh, G. P. A review on synthetic approaches of benzimidazoles. *Synth. Commun*. 2021, *51*, 485-513.

Drug delivery and controlled release of gemcitabine in polymer nano-capsules for pancreatic cancer therapy

Amirali Rafati*

School of Medicine, Tehran University of Medical Sciences, Tehran, Iran, amiralirafati2@gmail.com

Keywords: Gemcitabine, Drug delivery systems, Controlled drug release, Pancreatic cancer, Polymer nanoparticles.

Gemcitabine is a nucleoside analogue widely used for the treatment of pancreatic cancer, but its clinical efficacy is limited by its short half-life, rapid metabolism, and drug resistance. In this study, we developed a novel drug delivery system based on polymer nanocapsules for the controlled release of gemcitabine. The polymer nanocapsules were prepared by self-assembly of poly(N-vinylcaprolactam) (PVCL) containing solid lipid polymer hybrid nanoparticles (SLPHNs) that were loaded with gemcitabine and decorated with folic acid for targeted delivery. The physicochemical properties, drug loading and release, cellular uptake, cytotoxicity, and antitumor activity of the nanocapsules were evaluated in vitro and in vivo. The nanocapsules exhibited enhanced cellular uptake and cytotoxicity against pancreatic cancer cells compared to free gemcitabine, especially in the presence of folic acid.

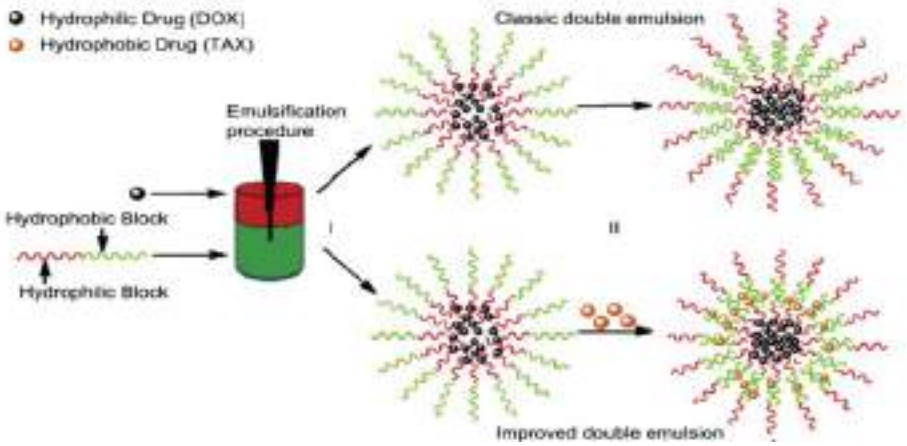

Scheme1. Core–shell polymeric nanoparticles for hydrophilic and hydrophobic drug loading.

References:

[20] Das, M; Li, J; Bao, M.; Huang, L. Nano-delivery of Gemcitabine Derivative as a Therapeutic Strategy in a Desmoplastic KRAS Mutant Pancreatic Cancer. *AAPS J.* 2020, *22*, 88−97

[21] Surapaneni S. G.; Ambade; A. V. Poly(N-vinylcaprolactam) containing solid lipid polymer hybrid nanoparticles for controlled delivery of a hydrophilic drug gemcitabine hydrochloride. *RSC Adv*. 2022, *12*, 17621–17628.

Synthesis and multifaceted functionalization silica nano hollow sphere for controlled drug delivery of zidovudine

Amirali Rafati*

School of Medicine, Tehran University of Medical Sciences, Tehran, Iran, amiralirafati2@gmail.com

Keywords: Organic mesoporous silica, Drug delivery systems, Core-shell structure, Hollow structure, Zidovudine.

Zidovudine is an antiretroviral drug that can cause adverse effects when administered systemically. In this study, we synthesized and functionalized hollow silica nanoparticles (HSNPs) as drug carriers for controlled and targeted delivery of zidovudine to HIV-infected cells. HSNPs were prepared by using a microwave-based sol-gel method with fructose as a sacrificial template. The resulting HSNPs had uniform size, shape, and porosity, and high water retention capability. The in vitro release of zidovudine from HSNPs showed a sustained and pH-dependent profile, indicating the potential of HSNPs for controlled drug delivery. The cellular uptake and cytotoxicity of HSNPs were evaluated using human peripheral blood mononuclear cells (PBMCs) and CEM-SS cells, a T-lymphoblastoid cell line infected with HIV-1.

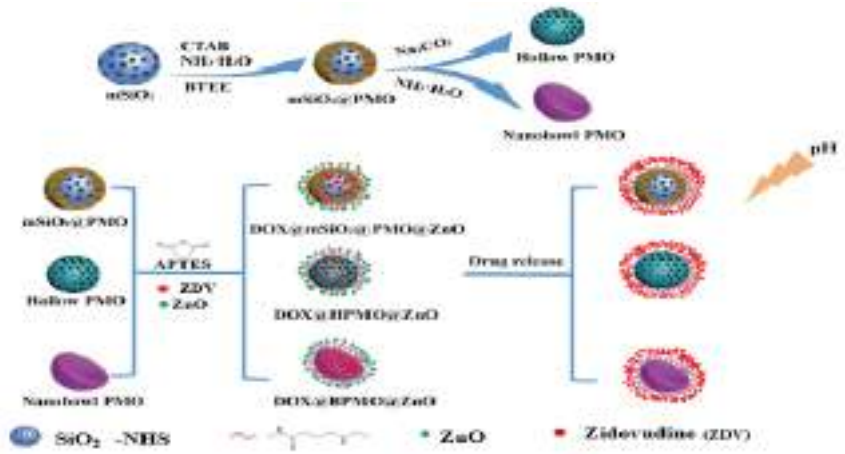

Scheme1. Schematic diagram of the synthesis and controlled drug release of ZDV@PMOs@ZnO.

References:

[22] Hafiz, A.; Shyam S. G.; Eluri, P.; Prabakaran, A.; Mukta, A.; Amit A. Biomedical applications of mesoporous silica nanoparticles as a drug delivery carrier. *J. Drug Deliv. Sci. Technol.* 2022, *76*, 103729.

[23] Shi; G.; Li, Z.; Zhang, Z.; Yin, Q.; Li, N.; Wang, S.; Qi, G.; Hao, L. Functionalized europium-doped hollow mesoporous silica nanospheres as a cell imaging and drug delivery agents. *Biochem. Biophys. Res. Commun.* 2023, *674*, 1-9.

An improve synthesis of 6-O-Monotosyl-6-deoxy-ß-cyclodextrin

Babak Kaboudin[a*], Ali Sabzalipour

Department of Chemistry, Institute for Advanced Studies in Basic Sciences (IASBS), Gava Zang, Zanjan, Iran, kaboudin@iasbs.ac.ir, sabzalipour@iasbs.ac.ir

Keywords: cyclodextrin, 6-O-Monotosyl-6-deoxy-ß-cyclodextrin, synthesis.

Supramolecular hosts called cyclodextrins are widely used across various applications. One way to attach a clearly defined host unit to complex systems is through the basic process of replacing a single glucose unit in the native cyclodextrins with a covalent bond at position C-6. The process of preparing these derivatives is quite simple, which is why there are over 1400 publications describing their preparation methods, with many of the reported synthetic techniques being very similar. Deciding on the best-published method for the intended purpose can be quite challenging [1]. The aim of our project is to demonstrate the most efficient and comprehensively elucidated methods for producing 6-O-Monotosyl-6-deoxy-ß-cyclodextrin (**Scheme 1**).

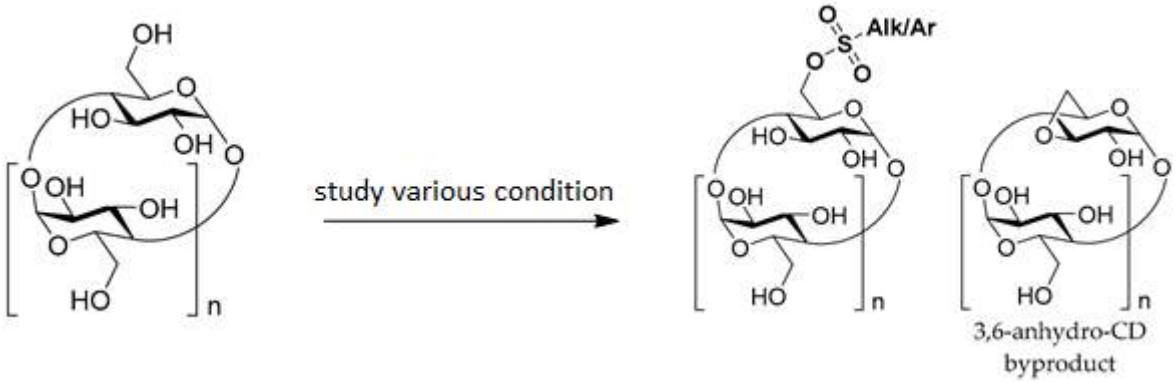

Scheme 1: Schematic representation of 6-O-Monotosyl-6-deoxy-ß-cyclodextrin.[2]

References

[24] Tang, W., & Ng, S. C. (2007). Synthesis of cationic single-isomer cyclodextrins for the chiral separation of amino acids and anionic pharmaceuticals. Nature Protocols, 2(12), 3195-3200.

[25] Kasal, P., & Jindřich, J. (2021). Mono-6-Substituted Cyclodextrins—Synthesis and Applications. Molecules, 26(16), 5065.

Catalytic activity of B, S co-doped g-C_3N_4 supported copper-based MOF in nitroarenes reduction reaction

Marzie Sadat Mirhosseyni* **and Ghodsi Mohammadi Ziarani**

Department of Organic Chemistry, Alzahra University, Tehran, Iran, M.Mirhosseyni@alzahra.ac.ir

Keywords: Heterogenous catalyst, Metal-Organic Framework, Heteroatom-doped g-C_3N_4, Nitroarenes Reduction.

Nowadays, the heteroatom-doped mesoporous solid substrates were attracted the researcher interest due to their notable properties such as thermal and chemical stability, high specific surface area, facile synthetic procedure and also abundance precursor [1-3]. So, in this study, the innovative and applicable Boron and Sulphur-doped g-C_3N_4 supported Cu-MOF (Cu@g-BSCN) was prepared through in situ growth of Cu-MOF on the surface of B, S-Doped g-C_3N_4. The synergistic effect of B and S as the heteroatoms was caused the abundance activated sites due to the structural defect on the surface of the solid substrate. The catalytic effect of this sample was improved by in situ formation of copper-based MOF. The synthesized Cu@g-BSCN) was applied as the efficient heterogenous catalyst in nitroarenes reduction reaction (**Scheme 1**). High performance and desired recoverability are some of the advantageous of this catalytic system.

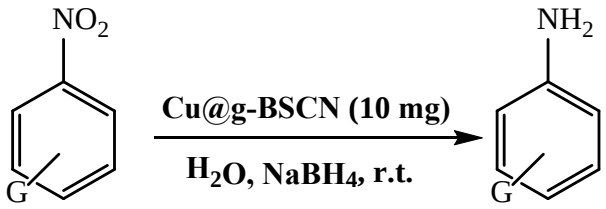

Scheme 1: Catalytic activity of Cu@g-BSCN toward alcohols oxidation

References

[1] Hao, M.; Qiu, M.; Yang, H.; Hu, B.; and Wang, X. Recent advances on preparation and environmental applications of MOF-derived carbons in catalysis *Sci. Total Environ* 2021, *760*, 143333.

[2] Mohtasham, H.; Gholipour, B.; Rostamnia, S.; Ghiasi-Moaser, A.; Farajzadeh, M. N. Nouruzi, Jang, H.W.; Varma, R.S.; Shokouhimehr, M. Hydrothermally exfoliated P-doped g-C_3N_4 decorated with gold nanorods for highly efficient reduction of 4- nitrophenol, *Colloids Surf. A Physicochem. Eng. Asp*. 2021, *614*, 126187.

[3] Rani Verma, P.; Payra, S.; Khan, F.; Penta, S.; Banerjee, S. $CuBr_2$@g-C_3N_4-Catalyzed highly selective aerobic oxidation of alcohol and toluene derivatives, *Chemistry*, 2020, *5*, 1950–1955.

29TH IRANIAN ORGANIC CHEMISTRY CONFERENCE
1_3 NOV, 2023
UNIVERSITY OF QOM, IRAN

Antibacterial evaluation, in silico characters and molecular docking studies of newly synthesized Schiff base hexamethylenediamine and dimethylaminobenzaldehyde

Parisa Babaei*, Vahideh Hadigheh Rezvan

Department of chemistry, Ardabil branch, Islamic Azad University, Ardabil, Iran, parisababaei0914@gmail.com

Keywords: Schiff base, Molecular docking, Ligand-receptor interaction, MTT test, Antibacterial.

Schiff base ligands have attracted a lot of attention in recent years due to their pharmacological and biological applications such as antimalarial, antiproliferative, analgesic, anti-inflammatory, antibacterial, antiviral, antipyretic, antifungal, antitumor and antioxidant [1,2]. In this research, the Schiff base ligand (L) was synthesized through the reaction between hexamethylenediamine and N,N-dimethylaminobenzaldehyde in the presence of methanol solvent and a few drops of concentrated acetic acid under reflux conditions. The structure of the reaction product has been identified using FT-IR, ^{1}H NMR, ^{13}C NMR and CHN spectral data. Then, in order to perform molecular docking by Auto Dock Vina software, the crystallographic structures of protein receptors 1STE, 1HSG, 1Z11 and 1AJ6 were extracted from the protein data base (RCSB PDB). Among them, the best conformation with the strongest binding is related to the interaction between the ligand and the active site of the 1HSG (-8.37 kcal/mol) receptor. Also, according to the results obtained from the disk diffusion, MIC and MBC tests, it can be concluded that the synthesized ligand shows antibacterial properties against bacteria. IC_{50} values of MCF-7 cell lines obtained show that at the concentration of 6.27 mg/ml, 50% of cancer cells were killed (**Scheme 1**).

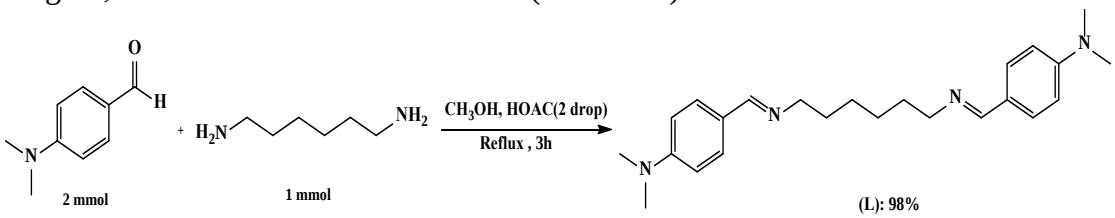

Scheme1: The synthesis route of ligand (L_1) was designed.

References

[26] Rama, I.;Selvameena, R. Manganese (II), cobalt (II), nickel (II), copper (II) and zinc (II) complexes of sulfathiazole functionalised Schiff base: Synthesis, characterization, redox behavior, antioxidant and antimicrobial activities. *J. Indian Chem. Soc*. 2020,*97*, 2144-2154.

[27] Kumar, S.; Devi, J.; Dubey, A.; Kumar, D.; Jindal, D. K.; Asija, S.; Sharma, A. Co (II), Ni (II), Cu (II) and Zn (II) complexes of Schiff base ligands: Synthesis, characterization, DFT, in vitro antimicrobial activity and molecular docking studies. *Res. Chem. Intermed.* 2023, *49*, 939-965.

Vanadium-Oxo Tetrapyridinoporphyrazine: an Efficient and Heterogenious Catalyst for the Unsymmetrical Synthesis of Hantzsch Reaction

Mahtab Moeinimehr[a], Maliheh Safaiee[b]* and Avat Arman Taherpour[a]*

c) Department of Organic Chemistry, Faculty of Chemistry, Razi University, Kermanshah, 67149-67346, Iran. avatarman.taherpour@gmail.com. mahtab.moeinimehr@yahoo.com
d) Department of Organic Chemistry, Faculty of Chemistry, Bu-Ali Sina University, Hamedan, 6517838683, Iran. M.safaiee@basu.ac.ir

Keywords: Hantzsch reaction, Heterogeneous catalyst, Tetrapyridinoporphyrazine.

Multi-component reactions (MCRs), such as Biginelli, Ugi, and Hantzsch, are widely used for the synthesis of a large variety of heterocyclic compounds. N- Heterocycle compounds such as 1,4- dihydropyridine structures are an important class of organic compounds with unique medicinal and biological properties. Also, scaffolds based on 1,4-dihydropyran moieties have been studied in various pharmaceutical fields such as anti-inflammatory, antitumor, painkillerand bronchodilator [1]. *Tetrapyridinoporphyrazines* are *phthalocyanine derivatives* in which the *outer benzene ring has* been replaced by *pyridines*. In continuation of our efforts to synthesize of novel catalysts and multi-component reactions we wish to report the synthesis of vanadium-oxo tetrapyridinoporphyrazine [VO(TPPA)] as an efficient catalyst for the synthesis of polyhydroquinolines through the condensation reaction of aryl aldehydes, ethyl acetoacetate, dimedone, and ammoniumacetate in EtOH under reflux condition (**Scheme 1**).

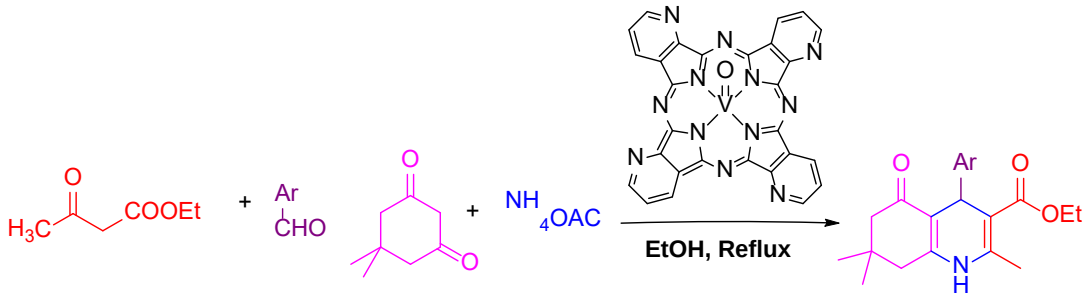

Scheme 1: Synthesis of different polyhydroquinolines by the [VO(TPPA)]

References

[28] Zhang, Q;Xiao-Ming Ma; W, Huai-Xin ; Zhao, X and Luo, J. Covalently anchored tertiary amine functionalizedionic liquid on silica coated nano-Fe_3O_4 as a novel,efficient and magnetically recoverable catalyst forthe unsymmetrical Hantzsch reaction andKnoevenagel condensation. *RSC Adv* 2017, *7*, 53861.

A Highly Efficient and Practical Synthesis of Chromene Derivatives Using Vanadium-Oxo Tetrapyridinoporphyrazine [VO(TPPA)]

Mahtab Moeinimehr[a], Maliheh Safaiee[b]* and Avat Arman Taherpour[a]*

e) Department of Organic Chemistry, Faculty of Chemistry, Razi University, Kermanshah, 67149-67346, Iran. avatarman.taherpour@gmail.com. mahtab.moeinimehr@yahoo.com
f) Department of Organic Chemistry, Faculty of Chemistry, Bu-Ali Sina University, Hamedan, 6517838683, Iran. M.safaiee@basu.ac.ir

Keywords: Chromene, Multi-component Reaction, Tetrapyridoporphyrazine.

Chromenes constitute chemically important class of heterocyclic compounds having diverse biological and chemical importance. Development of environmentally benign, efficient and economical methods for the synthesis of chromenes remains a significant challenge in synthetic chemistry. Therefore, synthesis of chromenes has attracted enormous attention from medicinal and organic chemists [1]. Tetrapyridoporphyrazines containing four pyridinoid rings in place of four benzenoid. Tetrapyridoporphyrazine derivatives are important commercial pigments and dyes for a number of years, and their chemical and heat stabilities are well known [2]. In continuation of our interest in the application of heterogeneous catalyst in organic transformation, we report the simple and efficient procedure for one pot synthesis of tetrahydro-4*H*-chromene derivatives using [VO(TPPA] as catalyst in EtOH under reflux condition (**Scheme 1**).

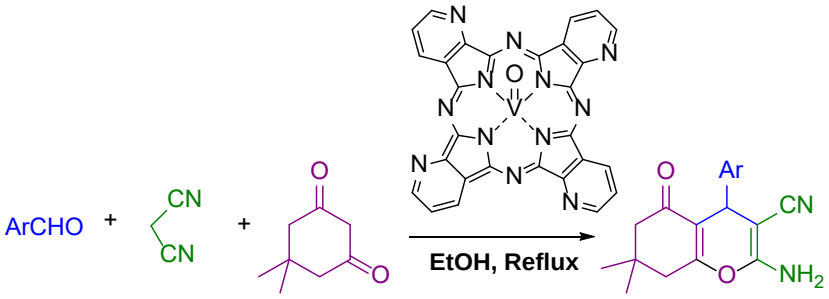

Scheme 1: Synthesis of tetrahydro-4*H*-chromene derivatives catalyzed by [VO(TPPA)]

References

[29] Mashhadinezhad, M; Mamaghani, M; Rassa, M and Shirini, F. A Facile Green Synthesis of Chromene Derivatives as Antioxidant and Antibacterial Agents Through a Modified Natural Soil. *ChemistrySelect* 2019, *4*, 4920 –4932.
[30] Sakamotoa, K; Katoa, T; Ohno-Okumurab, E; Watanabea, M and C,Michael J. Synthesis of novel cationic amphiphilic phthalocyanine derivatives for next generation photosensitizer using photodynamic therapy of cancer. *Dyes and Pigments* 2005, *64*, 63–71.

Design, synthesis, molecular docking study and biological evaluation of new Schiff base ligand as COVID-19 protease inhibitors

Parisa Babaei*

Department of Chemistry, Ardabil Branch, Islamic Azad University, Ardabil, Iran, parisababaei0914@gmail.com

Keywords: COVID-19, Molecular Docking Simulation, Schiff base, HIV.

Advent of COVID-19 attracted the attentions of researchers to develop drugs for its treatment. Besides efforts on developing new drugs, screening available drugs to see their efficacy on COVID-19 could be an urgent action of initiating its pharmacotherapy. In this study, efficacy of HIV protease inhibitors on COVID-19 protease has been examined [1-2]. In this research, new Schiff base ligand (L) was synthesized, and the structure of the reaction product has been identified using spectral data (**Scheme 1**). Molecular docking based screening by AutoDock software has been done to examine the efficacy of ligand-receptor interactions. Obtained results of binding energy, inhibitory constant and interactions quality have approved the idea of efficacy of HIV protease inhibitors on COVID-19 protease. Quantitative results indicated different levels of efficacy of investigated ligand for inhibitory activity of COVID-19 and qualitative results indicated localization of ligand in the proposed active site of protease.

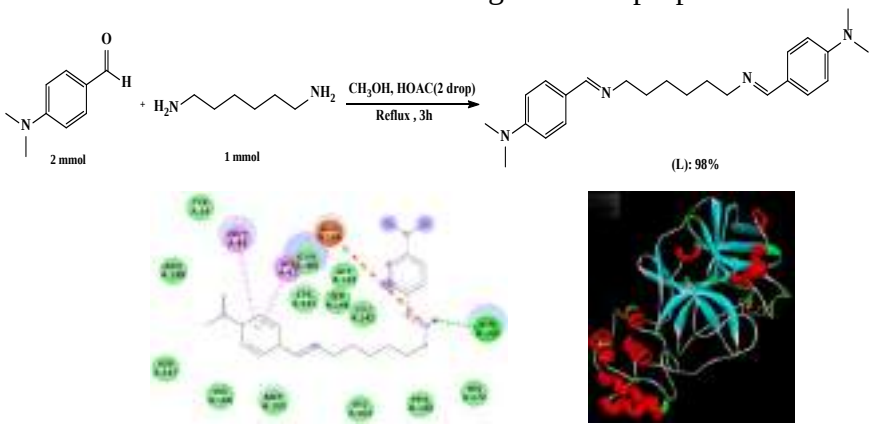

Scheme1: The synthesis route of ligand (L_1), and ligand-receptor interaction

References

[31] Farnoosh, G.; Alishiri, G.; Hosseini Zijoud, S. R.; Dorostkar, R.; Jalali Farahani, A. Understanding the Severe Acute Respiratory Syndrome Coronavirus 2 (SARS-CoV-2) and Coronavirus Disease (COVID-19) Based on Available Evidence - A Narrative Review. *J Mil Med*. 2020, *22*,1-11.

[32] (a) Ahmed, S. F.; Quadeer, A. A.; McKay, M. R. Preliminary identification of potential vaccine targets for the COVID-19 coronavirus (SARS-CoV-2) based on SARS-CoV immunological studies. *Viruses* 2020,*12*, 254; (b) Liu, X.; Zhang, B.; Jin, Z.; Yang, H.; Rao, Z. The crystal structure of COVID-19 main protease in complex with an inhibitor N3. 2020.

A new one-pot method for the synthesis of acenaphtopyrroles

Fatemeh Gourkani, Poya Portaher* and Mohammad Reaz Mohammadizadeh*

Chemistry Department, Faculty of Nano- and Bio-Science and Technology, Persian Gulf University, Bushehr 75169, Iran, fatemeh.goorakani@gmail.com, poyaportaher@gmail.com, mrmohamadizadeh@pgu.ac.ir.

Keywords: One-pot reactions, Acenaphtopyrrole, Pyrrolopyrimidine, Pyrroloimidazole.

Among heterocycles, compounds containing pyrrole derivatives are of the important organic compounds in nature [1]. They exhibit different pharmacological applications including antibacterial, anti-infammatory, antitumor, antifungal and antiviral activities [2]. As a result, much attention has been paid to the synthesis of pyrrole skeleton, and significant progress has been made.

In continuation of our previous works on the synthesis of various heterocycles [3], here we report a new method for the synthesis of acenaphtopyrroles via one-pot four component reaction of 1,1-bis(methylthio)-2-nitroethene, various amines, acenaphtoquinone and barbituric acid in ethanol under reflux condition. The corresponding acenaphtopyrroles were easily prepared using *para*-toluensulfonic acid as catalyst (**Scheme1**).

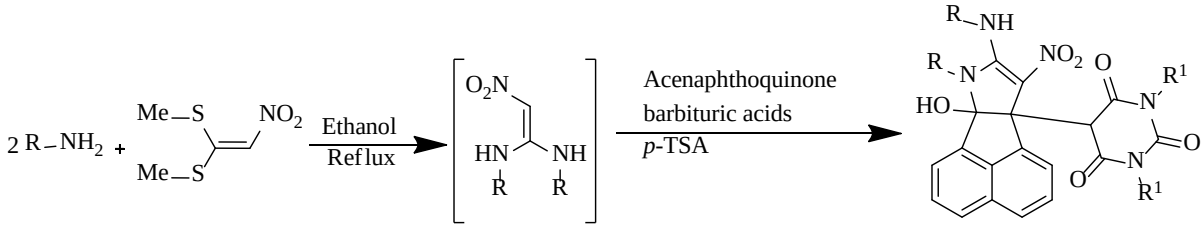

Scheme1: One-pot synthesis of acenaphtopyrrole derivatives.

References

[33] Rostami, H.; Lotfi, S. Chen, X.; Jin, J.; Wang, Y.; & Lu, P. Review on synthesis of pyrrole derivatives promoted by nanoparticles. *Appl Organomet Chem.* 2021, *35*, e6209.

[34] Kurian, J.; Shurooque, K. S.; Ramkumar, V.; Chakkumkumarath, L.; Kannoth, M. *Org. Lett.* 2021, *23*, 3354-3358.

[35] Alipoor, R.; Mohammadizadeh, M. R.; Saberi, D. New one-pot pathway for the synthesis of 2*H*–pyrrolo[2,3-*d*]pyrimidine-2,4-(3*H*)-diones and 1*H*-benzo[*f*]indole-4,9-dione derivatives substituted 3-hydroxy-1,4-naphthoquinonyl. *Polycyclic Arom. Comp*. 2023, *43*, 1602-1618.

29TH IRANIAN ORGANIC CHEMISTRY CONFERENCE
1_3 NOV, 2023
UNIVERSITY OF QOM, IRAN

Synthesis of N-aryl pyrrole derivatives in the presence of titanium (IV) tetrachloride immobilized on nanocellulose

Mohsen Rostamian, Abdolhamid Bamoniri*

Department of Organic Chemistry, Faculty of Chemistry, University of Kashan, Kashan, I. R. Iran, mohsenrostamiean@yahoo.com, bamoniri@kashanu.ac.ir.

Keywords: N-aryl pyrroles, Nanocatalyst, Aromatic amines, 2,5-hexanedione.

Undoubtedly, heterocyclic chemistry forms the largest and the most diverse family of organic chemistry. In particular, nitrogen-containing heterocyclic compounds have always played a key role in the pharmaceutical and agrochemical industries[1]. Pyrroles are the most ubiquitous heterocycles as they are found in the structural fragments of various natural products and pharmaceutical compounds. Owing to their varied pharmacological properties like antibacterial, antiviral, antioxidant, antifungal and anticancer significant efforts are directed towards development of newer protocols for the synthesis of functionalized pyrroles[2]. The most commonly method for the preparation of pyrroles is the Paal–Knor of 1,4-dicarbonyl compound with a vast variety of primary aromatic amines, which requires a special reagent or force reaction conditions[3]. Many procedures for the synthesis of N-aryl pyrroles have been reported in the presence of various catalysts. Herein, we wish report the synthesis of N-aryl pyrroles using various primary aromatic amines and 2,5-hexanedione in the presence of nanocellulose/$TiCl_4$ as a green catalyst under different conditions (**Scheme1**). The advantages of this work are simple work-up, mild condition, short reaction time and high yields.

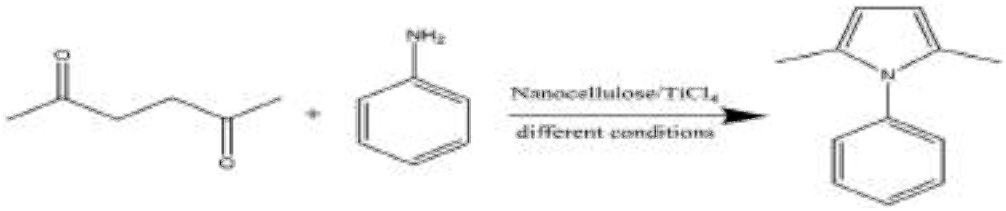

Scheme1

References

[1] Bamoniri, A., B.F. Mirjalili, and R. Tarazian, Nano-$TiCl_4/SiO_2$: An efficient heterogeneous solid acid catalyst for the one pot cascade five-component synthesis of densely functionalized tetrahydropyridines. *J. Chem. Sic*, 2015. 127, 885-895.

[2] Magoo, D., Aggarwal, K., Gupta, S., and Meena, K., Enamines and their variants as intermediates for synthesis of aza-heterocycles with applications in MCRs. *Tetrahedron*, 2022. 103, 132545.

[3] Azizi, N., F. Heidarzadeh, and F. Farzaneh, Facile fabrication of porous magnetic covalent organic frameworks as robust platform for multicomponent reaction. *Appl. Organomet .Chem*, 2021. 35(11), e6373.

Tetrazole synthesis and its application as chemosensors

Faezeh Farzandi, Ghodsi Mohammadi Ziarani*, Marzie Sadat Mirhosseyni, Zeinab Rastegaran

Department of Organic Chemistry, Faculty of Chemistry, Alzahra University, Tehran, Iran. f.farzandi@alzahra.ac.ir, & F.Farzandi@gmail.com, gmohammadi@alzahra.ac.ir

Keywords: Sensor activity, Tetrazole, Fluorescent chemosensors.

In recent years, the development of fluorescent chemosensors in both biological and environmental application have attracted increasing attention due to their high sensitivity, simplicity, and real-time monitoring with rapid response time [1]. In this study, the tetrazole derivative, 1,2-Bis(5-Tetrazole) ethane, was synthesized (Scheme 1) [2]. Due to π-electron donating property of the tetrazole rings and also their ability to form the metal complex [3], in this work, the sensor activity of the mentioned sample was studied. For this purpose, a series of different cations, including Cu^{2+}, Co^{2+}, Zn^{2+}, Cr^{3+}, Mg^{2+}, Hg^{2+}, Fe^{3+}, Cd^{2+}, Pb^{2+}, Al^{3+}, K^{+}, Na^{+}, Ca^{2+}, Ag^{+}, Mn^{2+}, Ni^{2+} were applied.

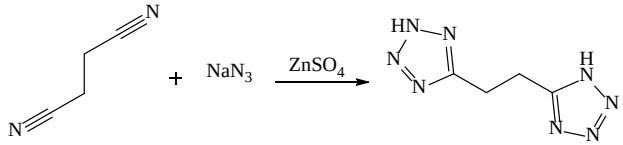

Scheme 1: Synthesis of 1,2-Bis(5-Tetrazole) ethane [2].

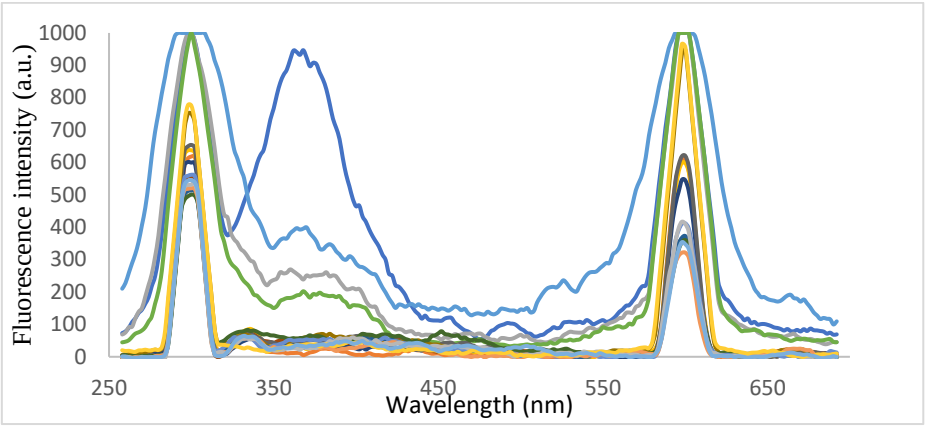

References

[36] Ding, WH.; Cao, W.; Zheng, XJ.; Ding, WJ.; Qiao, JP.; Jin LP. A tetrazole-based fluorescence "turn-on" sensor for Al (III) and Zn (II) ions and its application in bioimaging. *Dalton Transactions*. 2014, 43(17), 6429-35.

[37] Chafin, A.; Irvin, DJ.; Mason, MH.; Mason, SL. Synthesis of multifunctional hydroxyethyl tetrazoles. *Tetrahedron Lett*. 2008, 49(23), 3823-6.

[38] Popova, EA.; Trifonov, RE.; Ostrovskii, VA. Advances in the synthesis of tetrazoles coordinated to metal ions. *ARKIVOC*, 2012 (i), 45-65.

29TH IRANIAN ORGANIC CHEMISTRY CONFERENCE
1_3 NOV, 2023
UNIVERSITY OF QOM, IRAN

Synthesis of N-aryl pyrrole derivatives using borane trifluoride supported on nano kaolin in various conditions

Ramtin Moradi Chafjiri, Abdolhamid Bamoniri*, Parisa Moharrami Korblagh

Department of Organic Chemistry, Faculty of Chemistry, University of Kashan, Kashan, IR Iran, ramtinmoradi77@gmail.com, bamoniri@kashanu.ac.ir

Keywords: N-aryl pyrroles, 2,5-hexanedione, borane trifluoride, nano kaolin.

In this research, the preparation of pyrrole derivatives using 2,5-hexane dione and primary aromatic amines in the presence of borane trifluoride stabilized on nano kaolin was investigated under different conditions. Boron trifluoride immobilized on nano kaolin is readily available, heterogeneous, and recyclable. After preparation of the catalyst, it was detected using spectroscopy, imaging, and pattern-finding methods such as FT-IR, XRD, TGA, SEM, and TEM. In this research, N-aryl pyrrole derivatives were prepared using 2,5-hexane dione as raw material and primary aromatic amines under different conditions [1-4] (**Scheme1**). Products were identified using spectroscopic ways such as FT-IR and ^{1}H NMR. Among the advantages of this method is the use of affordable and available raw materials, high efficiency, short reaction time, and one-pot-reaction; ease of separation and purification of the products.

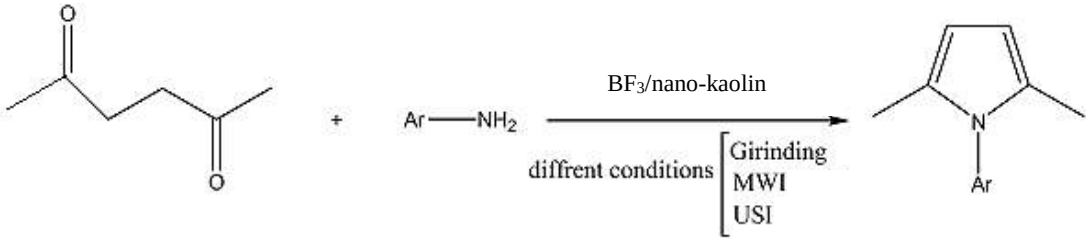

Scheme 1. Synthesis of N-aryl pyrrole derivatives

References

[1] Kerru N, Gummidi L, Maddila S, Jonnalagadda SB. A review of recent advances in the green synthesis of azole-and pyran-based fused heterocycles using MCRs and sustainable catalysts. *Curr. Org. Chem.* **2021**, 25, 4- 39.

[2] Kotha S, Singh D. Synthesis of pyrrole derivatives via ring closing metathesis, Clauson-Kaas reaction and Paal-Knorr condensation as key steps. *J. Mol. Struct.* **2023**, 5, 1275- 1346.

[3] Aronica LA, Albano G. Supported metal catalysts for the synthesis of N-heterocycles. *Catalysts*. **2022**, 12, 68- 78

[4] Fuentes-Morales L, Miranda LD. Recent Trends in Metal-catalyzed MCRs Toward Heterocycles. Multicomponent Reactions towards Heterocycles: *Concepts Appl.* **2022**, 7, 51- 82.

Synthesis of chromenes by Talc as a natural mineral catalyst

Motahare Hajihasani Bafghi[a], Abdolhamid Bamoniri[a*], Bi Bi Fatemeh Mirjalili[b]

a) Department of Organic Chemistry, Faculty of Chemistry, University of Kashan, Kashan, I.R. Iran, m.hajihasani74@gmail.com, bamoniri@kashanu.ac.ir.
b) Department of Chemistry, College of Science, Yazd University, Yazd, I.R.Iran.

Keywords: Mineral, Talc, Benzo[*f*]chromene, Dihydropyrano[3,2-*c*]chromene, Tetrahydrobenzo[*b*]pyran.

Talc is a natural mineral catalyst known by the chemical composition of $MgSi_4O_{10}(OH)_2$, which in its pure state consists of 31.88% magnesium oxide, 63.37% silicon oxide and 4.75% water. The abundance of this material, the ease of extraction and its properties have made talc an important mineral in industries [1]. In this research, Talc, which was extracted directly from the mine, after decontamination, was used for the synthesis of benzo[*f*]chromene [2] (**Scheme1**), dihydropyrano[3,2-*c*]chromene [3], tetrahydrobenzo[*b*]pyran [4] derivatives. Product were identified by spectroscopic methods. Such as FT-IR, ^{1}H NMR, and etc.

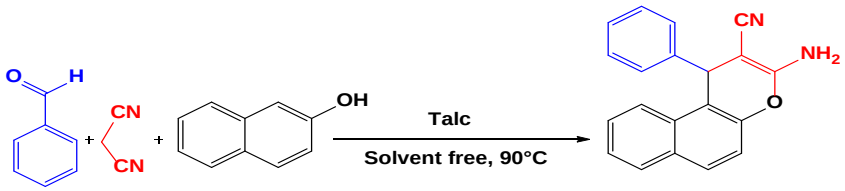

Scheme1.

References

[1] Zafari, S.; Ghorbani-Vaghei, R.; Alavinia, S., Poly (sulfonamide-thiourea) grafted γ-Fe2O3@ talc as a green catalyst for the synthesis of substituted tetrahydropyridines. *Mater. Chem. Phys*. **2021,** *270*, 124840-124852.

[2] Sadek, K. U.; Mekhimer, R. A. H.; Abd-Elmonem, M.; Abdel-Hameed, A.; Elnagdi, M. H., Recent developments in the enantioselective synthesis of polyfunctionalized pyran and chromene derivatives. *Tetrahedron: Asymm.* **2017,** *28* (11), 1462-1485.

[3] Mashhadinezhad, M.; Mamaghani, M.; Rassa, M.; Shirini, F., A facile green synthesis of chromene derivatives as antioxidant and antibacterial agents through a modified natural soil. *ChemistrySelect*. **2019**, *4* (17), 4920-4932.

[4] Tanna, J. A.; Chaudhary, R. G.; Gandhare, N. V.; Rai, A. R.; Yerpude, S.; Juneja, H. D., Copper nanoparticles catalysed an efficient one-pot multicomponents synthesis of chromenes derivatives and its antibacterial activity. *J. Exper. Nanosci.* **2016,** *11* (11), 884-900.

Preparation of pyrimidines in the presence of titanium (IV) chloride supported on silica nanoparticles under different conditions

Zahra Imani, Abdolhamid Bamoniri*, Parisa Moharrami Korblagh

Department of Organic Chemistry, Faculty of Chemistry, University of Kashan, Kashan, IR Iran,
zahraimani188@gmail.com, bamoniri@kashanu.ac.ir

Keywords: Titanium tetrachloride, Lewis's acid, Silica nanoparticles, Pyrimidines, 1,8- Naphthalene diamine.

Perimidines are a type of heterocyclic compounds consisting of quinazoline and another benzene ring. The limitations in this type of reactions, including time limit, environmental parameters, and reuse of the desired catalyst, have led to more studies on pyrimidine derivatives. Preparation of some pharmaceutical derivates of pyrimidine in the presence of non-oxidizing catalyst is the safest way for the environment [1-3]. In this research, the reaction between 1,8-naphthalene diamine and various aromatic aldehydes has been investigated using titanium tetrachloride catalyst stabilized on silica nanoparticles under microwave, ultrasonic, thermal and grinding conditions **(Scheme1)**. Titanium tetrachloride immobilized on silica nanoparticles is known as one of the heterogeneous catalysts. The structure of the catalyst was investigated using a SEM, TEM, XRD and etc. The structures of dihydropyridine derivatives were investigated by ^{1}H NMR and FT-IR.

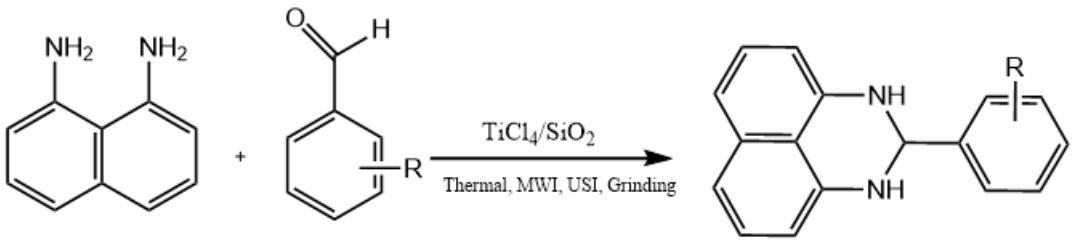

Scheme 2

References:
[1] Kalhor M, Zarnegar Z. Fe_3O_4/SO_3H@Zeolite-Y as a novel multi-functional and magnetic nanocatalyst for clean and soft synthesis of imidazole and perimidine derivatives. *RSC Adv*. **2019**. 9. 19333-19346.

[2] Khopkar S, Shankarling G. Squaric acid: an impressive organocatalyst for the synthesis of biologically relevant 2, 3-dihydro-1H-perimidines in water. *J. Chem. Sci*. **2020**. 132. 1-10.

[3] Sahiba N, Sethiya A, Soni J, Agarwal S. Metal free sulfonic acid functionalized carbon catalyst for green and mechanochemical synthesis of perimidines. *ChemistrySelect*. **2020**. 13. 13076-13080.

A vitamin C-based natural deep eutectic solvent for the synthesis of chromene and pyran derivatives

Zohreh Valipour*, Rahman Hosseinzadeh, Yaghoub Sarrafi, Behrooz Maleki

Department of Organic Chemistry, Faculty of Chemistry, University of Mazandaran, Babolsar, Iran, zohrehvalipoor@gmail.com

Keywords: Green chemistry, Natural deep eutectic solvents, Ascorbic acid, Tetrahydrobenzo[b]pyran, Dihyropyrano[c]chromene.

Dihyropyrano[c]chromene and tetrahydrobenzo[b]pyran derivatives are found in many naturally occurring compounds. These compounds have been used as cognitive enhancers to treat neurodegenerative diseases such as Alzheimer's disease, Parkinson's disease, and Down's syndrome [1]. Using different catalysts, chemists have improved the synthesis of tetrahydrobenzo[b]pyran and dihydropyrano[c]chromene derivatives through the three-component reaction of an aldehyde, malononitrile and a β-dicarbonyl compound [2]. Despite the remarkable efficiency of these catalytic systems, they have several disadvantages, such as the need for a cumbersome method of catalyst separation, release of hazardous substances into the environment, and long reaction times.

In the past decade, Deep Eutectic Solvents (DESs) have been investigated as reaction media and catalysts for organic syntheses. In our current work, we report the use of choline chloride (ChCl) / ascorbic acid (AA, or vitamin C) as a Natural Deep Eutectic Solvents (NADES) for the multicomponent-synthesis of pyrans and chromenes (**Scheme**).

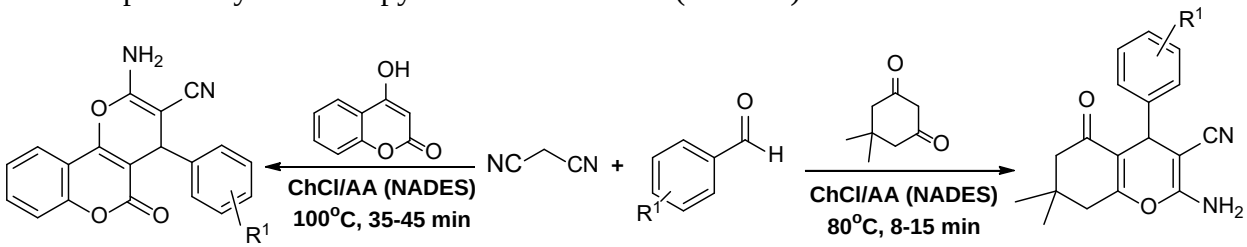

Scheme: Synthesis of chromene and 4H-pyran derivatives using ChCl/AA

References

[39] Singh, P.; Yadav, P.; Mishra, A.; Awasthi, S. K. Green and mechanochemical one-pot multicomponent synthesis of bioactive 2-amino-4 H-benzo [b] pyrans via highly efficient amine-functionalized SiO2@ Fe3O4 nanoparticles. *ACS omega* 2020, 5(8), 4223-4232

[40] Nawaz, A.; Aslam, S.; Ahmad, M.; Zahoor, A. F.; Naqvi, S. A. R. Synthetic strategies of pyran derivatives by multicomponent reaction (MCR) approach. *J. Iran. Chem. Soc* 2022, 19(9), 3721-3768.

29TH IRANIAN ORGANIC CHEMISTRY CONFERENCE
1_3 NOV, 2023
UNIVERSITY OF QOM, IRAN

Design of MOF(Fe)-TUR as a new porous H-bond catalyst based on MIL-88B(Fe)-NH_2 for the synthesis of new nicotinonitriles and chromeno[4,3-*b*]pyridines

Mahrokh Farrokh, Hassan Sepehrmansourie, Mohammad Ali Zolfigol*, Maryam Hajjami* and Elham Tavakoli

Department of Organic Chemistry, Faculty of Chemistry, Bu-Ali Sina University, Hamedan 6517838683, Iran, mah.farrokh1878@gmail.com, zolfi@basu.ac.ir & mzolfigol@yahoo.com, m.hajjami@yahoo.com.

Keywords: Anomeric effect, H-Bond catalyst, Metal-organic frameworks (MOFs).

Fe-based MOFs are a class of porous materials composed of metal ions coordinated to organic ligands. Fe-based MOFs have unique advantages compared to other types of MOFs. The incorporation of iron as the metal center provides several desirable properties. Fe-based MOFs often have good thermal and chemical stability, which is very important for their practical applications [1]. H-bonded porous catalysts are catalysts that use hydrogen bonding interactions in their porous structure to carry out chemical reactions. In the field of catalysis, a porous material with hydrogen bonding capability can provide a unique environment to promote specific reactions [2]. In this regard, the goal is to create a MOF(Fe)-TUR catalyst, which turns it into a hydrogen bonding catalyst. The designed catalyst is used in the synthesis of nicotinonitriles which have biological components, and in their structure, there are indole, triazole, and nicotinonitrile, whose importance in pharmaceutical compounds has been proven [3] (**Scheme 1**).

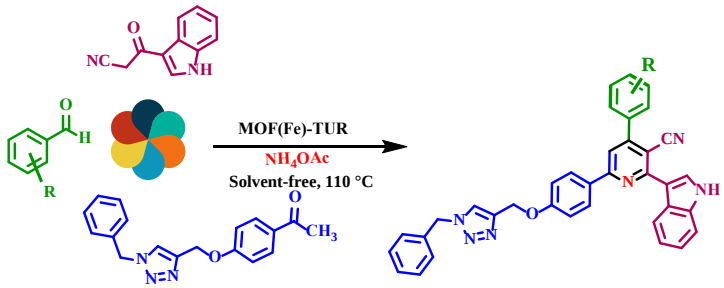

Scheme 1: Synthesis of new nicotinonitriles using MOF(Fe)-TUR.

References

[41] Guo, T.; Wang, K.; Zhang, G.; Wu, X. A novel α-Fe_2O_3@ g-C_3N_4 catalyst: synthesis derived from Fe-based MOF and its superior photo-Fenton performance. *Applied Surface Science* 2019, *469*, 331-339.

[42] Doyle, A. G.; Jacobsen, E. N. Small-molecule H-bond donors in asymmetric catalysis. *Chemical Reviews* 2007, *107(12)*, 5713-5743.

[43] Soliman, E. A.; Panda, S. S.; Aziz, M. N.; Shalaby, E. M.; Mishriky, N.; Asaad, F. M.; Girgis, A. S. Synthesis, molecular modeling studies and bronchodilation properties of nicotinonitrile containing-compounds. *European Journal of Medicinal Chemistry* 2017, *138*, 920-931.

29TH IRANIAN ORGANIC CHEMISTRY CONFERENCE
1_3 NOV, 2023
UNIVERSITY OF QOM, IRAN

Architecture copper complex based on Bimetallic-MOFs in the synthesis of phenylnicotinonitriles via CVABO mechanism

Mahrokh Farrokh, Milad Mohammadi Rasooll, Hassan Sepehrmansourie, Mohammad Ali Zolfigol* and Maryam Hajjami*

Department of Organic Chemistry, Faculty of Chemistry, Bu-Ali Sina University, Hamedan 6517838683, Iran, mah.farrokh1878@gmail.com, zolfi@basu.ac.ir & mzolfigol@yahoo.com, m.hajjami@yahoo.com.

Keywords: Bimetallic-Organic Frameworks, Heterogeneous catalyst, Phenylnicotinonitriles.

Today, metal-organic frameworks (MOFs) have attracted a lot of attention due to their high surface areas, high content of metal centres and impressive topological richness. MOFs based on two metals (bimetallic-MOFs) are a new class of MOFs that have found wide applications such as gas storage, drug delivery, energy storage, and catalyst [1]. The different properties of these porous materials make them a good catalytic candidate for cross coupling, oxidation/reduction, and multicomponent reactions. Many chemical reactions are carried out by Lewis's acid-based catalysts. Copper complex is widely used as a catalyst in many organic reactions [2]. Nicotinonitriles has diverse important biological activities such as anti-oxidant anti-inflammatory and anti-cancer [3]. In the above work, a Lewis acid was synthesized based on bimetallic-MOFs with high surface area and high pore volume. The above catalyst was used in the synthesis of phenylnicotinonitriles derivatives. The high reaction speed, high reaction efficiency, short reaction time, reducing the production of side products and the ability to recycle the catalyst are among the features of the above work **(Scheme 1)**.

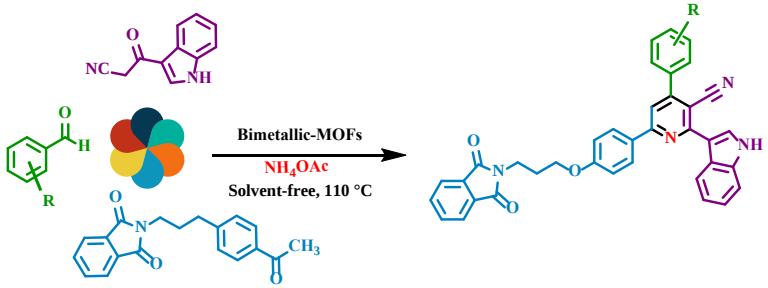

Scheme 1: Preparation of new phenylnicotinonitriles using copper complex based on Bimetallic-MOFs.

References

[44] Chen, L.; Wang, H. F.; Li, C.; Xu, Q. Bimetallic metal-organic frameworks and their derivatives. *Chemical Science* 2020, *11*, 5369-5403.

[45] Tavakoli, E.; Sepehrmansourie, H.; Zarei, M.; Zolfigol, M. A.; Khazaei, A.; As' Habi, M. A. Application of Zr-MOFs based copper complex in synthesis of pyrazolo[3,4-*b*]pyridine-5-carbonitriles via anomeric-based oxidation. *Scientific Reports* 2023, *13*, 9388.

[46] Hassan, H.; Hisham, M.; Osman, M.; Hayallah, A. Nicotinonitrile as an essential scaffold in medicinal chemistry: an updated review (2015–present). *Journal of advanced Biomedical and Pharmaceutical Sciences* 2023, *6*, 1-11.

29TH IRANIAN ORGANIC CHEMISTRY CONFERENCE
1_3 NOV, 2023
UNIVERSITY OF QOM, IRAN

Application of Oxone/hydrogen peroxide (Oxone/H_2O_2) in the synthesis of nitrogen-containing heterocycles from alcohols

Zahra Mohammadi, S. Ghasem Aghapour*

School of Chemistry, Damghan University, Damghan 36715-364 Iran, zahramohammadi142@yahoo.com, gh_aghapour@du.ac.ir

Keywords: Benzimidazole, Quinoxaline, Oxone, Hydrogen peroxide, Potassium cyanide.

Benzimidazoles and quinoxalines are considered as very important heterocyclic groups especially in pharmaceutical chemistry due to their very desirable properties such as anticancer, anti-inflammatory, antihypertensive, antiviral, antifungal, antibacterial, antioxidant and so on [1]. Very drugs and biological active compounds contain these structural scaffolds in their structures such as mebendazole as antiparasite, lansoprazole as antiulcer, and levomycin as antibiotic [2]. Here in the present work, an oxidative and one-pot method is described for the efficient conversion of alcohols and *o*-phenylenediamine to these valuable nitrogen containing heterocycles using Oxone/H_2O_2 as an oxidant system in the presence of potassium cyanide (**Scheme 1**). Different benzylic alcohols containing electron donating or withdrawing groups on aromatic ring can be converted to their corresponding benzimidazoles and also quinoxalines in good to excellent yields by this method. It was found that selective conversion of alcohols to desired benzimidazoles or quinoxalines is possible with controlling of reaction conditions such as solvent, the molar ratio of *o*-phenylenediamine to alcohol, and also reaction temperature. In addition, some other functional groups easily tolerate this chemoselective procedure so that they remain intact. The present work is important in terms of green chemistry due to its one-pot nature so that there is no need to separate aldehyde as intermediate product.

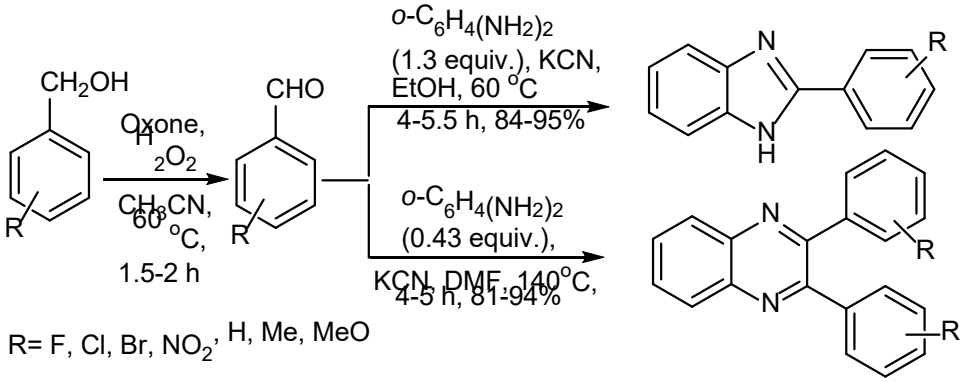

Scheme 1: Synthesis of benzimidazoles and quinoxalines from alcohols using Oxone/H_2O_2 and KCN.

References:

[1] Kumar, R.; Singh, G. Substituted benzimidazoles as antibacterial and antifungal agents: A review. *Pharmacophore* 2022, *13*, 41-55.

[2] Khatoon, H.; Abdulmalek, E. Novel synthetic routes to prepare biologically active quinoxalines and their derivatives: A synthetic review for the last two decades. *Molecules* 2021, *26*, 1055.

The study of hydrophobicity-plugging synergistic effect on the catalytic performance of sulfonic acid based bifunctional periodic mesoporous organosilica (PMOs) in Esterification reactions

Babak Karimi *, **Hesamodin Moradi**

Organic Chemistry Laboratory, Faculty of Organic Chemistry, Department of Chemistry, Institute for Advanced Studies in Basic Sciences (IASBS), Zanjan, 45137-66731, Iran, h.moradi@iasbs.ac.ir.

Keywords: BFPMO materials, Ionic liquids (ILs), Supported sulfonic acid catalyst, Esterification reaction

In this report, we decide to study the catalysis of sulfonic acids on supports with and without plugs on bifunctional periodic mesoporous organosilicas in esterification reactions. Since water is the product in the esterification reaction and sulfonic acid is poisoned in addition to water, control of the hydrophobicity of the mesochannels is very important. Considering the role of IL in the stability of the catalysts and the amphiphilic character near the hydrophobic ethane and/or phenyl groups and the hydrophilic plugs, we expect these materials to have good performance in the esterification reaction. Moreover, the counterion of IL can be replaced by HSO_4^- to achieve a synergistic effect with the sulfonic acid catalyst (**Table 1**).

Table 1: a typical esterification reaction using supported sulfonic acid catalyst supported on plugged (P) and unplugged (U) bifunctional periodic mesoporous organosilica with ionic liquid and ethylene (E15) or phenyl (B15) groups.

Entry	catalyst	Yield[a]
1	SO_3H@P-E15	98
2	SO_3H@U-E15	41
3	SO_3H@P-B15	70
4	SO_3H@U-B15	50

a: GC yield

References

[47] Karimi, R.; Khorasani, M.; Vali, H.; Luque, R. Control of plugging in bifunctional periodic mesoporous organosilica with imidazolium framework (BFPMO) via stepwise addition of silica precursors, *J. Mater. Chem. A.* **2015**, *3*, 6575.

[48] Karimi, B.; Vafaeezadeh, M. SBA-15-functionalized sulfonic acid confined acidic ionic liquid: a powerful and water-tolerant catalyst for solvent-free esterifications, *Chem. Commun*. **2012**, *48*, 3327.

Comparison of DSC curves Copolymerization of vinyl acetate- butyl acrylate with different percentage of PVA

Farahnaz Hamdi Holasoo*

Sugar Beet Seed Institute (SBSI)- Agricultural Research Education and Extension Organization (AREEO), Karaj, Iran, f.hamdi@areeo.ac.ir

Keywords: Copolymerization, DSC, Polyvinyl alcohol, Tg.

In this study, the DSC (Differential Scanning Calorimetry) curves of copolymerization of vinyl acetate- butyl acrylate in the presence of different percentage of PVA investigated [1]. A vinyl acetate- butyl acrylate Copolymer was prepared by aqueous emulsion polymerization which contained 70 to 30 % of monomers in the presence of anionic surfactants and Potassium Persulfate (KPS) initiator, PVA 10% and PVA 15% at 70 ° C and at 3 hours [2]. Results show that the Tg value in different percentage are difference (**Scheme**) and copolymerization has taken place between vinyl acetate and butyl acrylate. Therefore, it is possible, the influence of protective colloid in this type of emulsion copolymerization [1,3].

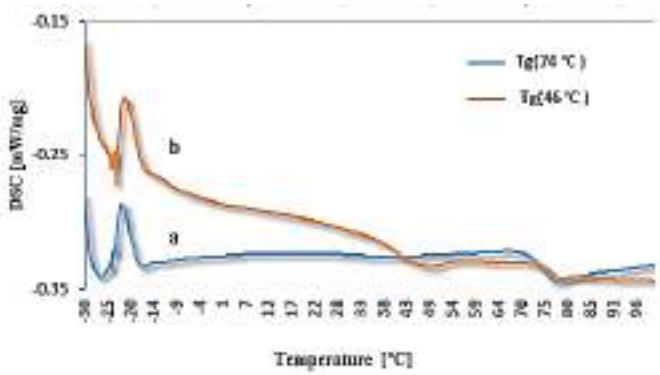

Scheme: DSC curves of optimized copolymer (VAc/BuA) with different percentage of (a) PVA 10%, (b) PVA 15%.

References

[1] Seul, S. D., Lim, J. M. Emulsion Polymerization of Vinyl acetate-Butyl acrylate Copolymer. Polymer (Korea), 2004, 28(2), 135-142.

[2] Hamdi Holasooa, F., Nemati, F., Amoozadeha, A., Sajjadi, S. M., Taleghani, D. Synthesis and delayed germination of vinyl acetate-butyl acrylate copolymer for coating of sugar beet seeds using combined experimental design and image analysis. *J. Appl. Chem*. 2019, 13 (49), 21- 28.

[3] Nagakawa, Y., Kato, M., Suye, S. I., Fujita, S. Fabrication of tough, anisotropic, chemicalcrosslinker- free poly (vinyl alcohol) nanofibrous cryogels via electrospinning. *RSC Adv*. 2020, 10, 38045–38054.

29TH IRANIAN ORGANIC CHEMISTRY CONFERENCE
1_3 NOV, 2023
UNIVERSITY OF QOM, IRAN

Tandem conversion of alcohols and protected alcohols to oximes using Oxone and hydroxylamine hydrochloride

Elham Zahiri Rad, S. Ghasem Aghapour*

School of Chemistry, Damghan University, Damghan 36715-364 Iran, elham.zahiri.rad@gmail.com;, gh_aghapour@du.ac.ir

Keywords: Alcohol, Silyl ether, Oxime, Oxone, Hydroxylamine hydrochloride.

Oximes are an important group in organic chemistry. This importance stems from a range of their very desirable industrial, pharmaceutical and biological properties such as antiviral, antidepressant, antitumor, antimicrobial, insecticide, enzyme inhibitory, and antioxidant [1]. These compounds are also important from the synthetic point of view. It is possible to covert the oxime functional group to many different other kinds of functional groups such as nitrone, nitrile, amide, nitrile oxide, amine, and pyridine structures [2, 3]. Here in this work, the tandem conversion of alcohols and silyl ethers as protected alcohols to oximes is described using Oxone which is an inorganic triple salts with the formula $2KHSO_5.KHSO_4.K_2SO_4$ and hydroxylamine hydrochloride (**Scheme 1**). Different types of alcohols and silyl ethers containing electron donating or withdrawing groups on aromatic ring are efficiently and oxidatively converted to their corresponding oximes *via* this procedure in good to excellent yields. This method is in accordance with green chemistry principles due to its one pot and tandem nature. On the other hand, an unknown alcohol or silyl ether can be identified by this method *via* determination of melting point of product oxime. Excellent chemoselectivity and easy work up can be considered as other advantages of the present method.

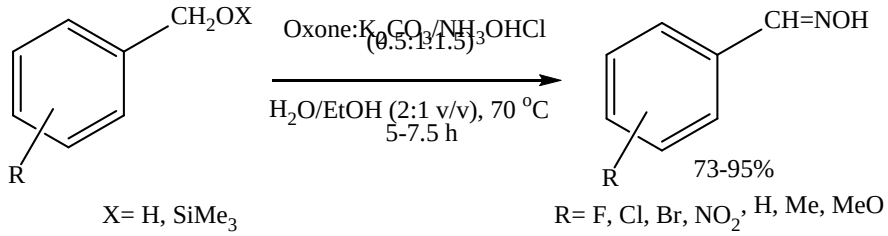

Scheme 1: Tandem conversion of alcohols and silyl ethers to oximes.

References

[1] Kurbah, S. D. Dioxido-vanadium (V) complex catalyzed oxidation of alcohols and tandem synthesis of oximes: a simple catalytic protocol for C–N bond formation. *J. Coord. Chem*. 2021, *74*, 905-918.

[2] Horvat, M.; Weilch, V.; Radisch, R.; Hecko, S.; Schiefer, A.; et al. Chemoenzymatic one-pot reaction from carboxylic acid to nitrile via oxime. *Catal. Sci. Technol*. 2022, *12*, 62-66.

[3] Li, Y.; Yang, K.; Cao, L. Copper-catalyzed [3+3] annulation of ketones with oxime acetates for the synthesis of pyridines. *RSC Adv*. 2022, *12*, 27546-27549.

Synthesis and evaluation of thermal stability of melamine dinitrate explosive

Sajjad Damiri *, Karim Esmaeil pour, Bahare Fadaei Tehrani

Department of Applied Chemistry, Malek-Ashtar University of Technology, Shahin-Shahr, Esfahan, Iran, s_damir@mut-es.ac.ir

Keywords: Melamine dinitrate, synthesis, thermal stability, explosives.

Considering the role of common high-energy materials such as ammonium nitrate in civil blasting applications, it is valuable to produce materials with higher explosive strength and higher thermal stability than ammonium nitrate. Melamine, 2,4,6-triamino-1,3,5-triazine, is a white, odorless, crystalline substance with a melting point of 345 ^{o}C, which is produced in our country on a large scale. Melamine dinitrate (MDN) is a thermally stable salt of melamine and nitric acid that maintains its thermal stability at a temperature of about 330 ^{o}C for at least 48 hours [1-2]. In this research, the heat resistant MDN explosive was prepared using the reaction of melamine in nitric acid at a temperature of 95-100 °C with an efficiency near to 87.0% . Also, the main factors affecting on the quality of process were optimized, and some necessary quantitative and qualitative analyses, including Fourier transform infrared spectroscopy (FT-IR), hydrogen nuclear magnetic resonance spectroscopy (^{1}H-NMR), and elemental analysis were performed to identify and confirm the quality of the product. Also, the degree of stability of the MDN in accelerated aging conditions, and its thermal decomposition was evaluated by thermogravimetric (TGA) method. The results showed that the nitrogen element content of MDN is near to 44.24%, and the substance begins to decompose in the temperature range of 248.77 ^{o}C to of 329.12 ^{o}C (see Scheme).

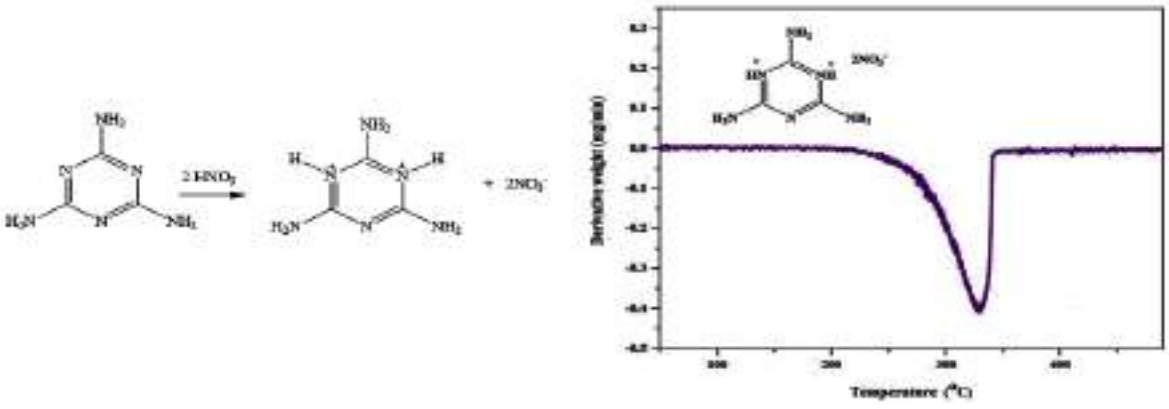

Scheme: Chemical reaction and thermo-gravimetric decomposition of MDN

References

[1] K. Bretterbauer and C. Schwarzinger, Melamine derivatives-a review on synthesis and application, Current Organic Synthesis, 9 (2012) 342-356.

[2] P. Kneisl, Application of high temperature explosive to downhole use, Patent No. WO2010042258A2, 2012.

Synthesis, thermokinetics, and detonation performance of 4- amino-1,2,4-triazolium nitrate (4-ATN) energetic ionic liquid

Sajjad Damiri*, Leila Makvandi and Mohammad Hossein Keshavarz

Department of Applied Chemistry, Malek-Ashtar University of Technology, Shahin-Shahr, Esfahan, Iran, s_damir@mut-es.ac.ir

Keywords: 4-ATN, energetic ionic liquid, thermokinetics, detonation performance.

The synthesis of energetic ion liquids (EILs) with favourable physical properties as well as detonation and combustion performance is attractive for military applications. They may provide low sensitivity without adverse effects of the overall performance. Since energetic ionic liquids have a low melting point, they can be used as melt-cast explosive charges, the same as 2,4,6-trinitrotoluene (TNT), in different molds. Among a different kind of EILs, 4-amino-1,2,4-triazolium nitrate (4-ATN) is an energetic and non-sensitive ionic liquid, being a good candidate for the replacement of TNT [1-2]. In this work, synthesis of 4-ATN with concentrated nitric acid was performed and various spectroscopic methods such as Fourier transform infrared spectroscopy (FT-IR), hydrogen nuclear magnetic resonance spectroscopy (^{1}H-NMR), and elemental analysis were used to identify and confirm the quality of the product. Also, thermal stability with differential thermo-gravimetric method and detonation performance of 4-ATN were assessed and compared with TNT (see Scheme). Here, four model-free techniques including Ozawa, Kissinger, OFW, and KAS methods were used to calculate thermokinetic properties of 4-ATN. The results showed that calculated activation energies are in the range of 78.7-87.7 kJ.mol^{-1}, and the activation energies, detonation pressure, velocity and thermal stability of 4-ATN are more than that of TNT.

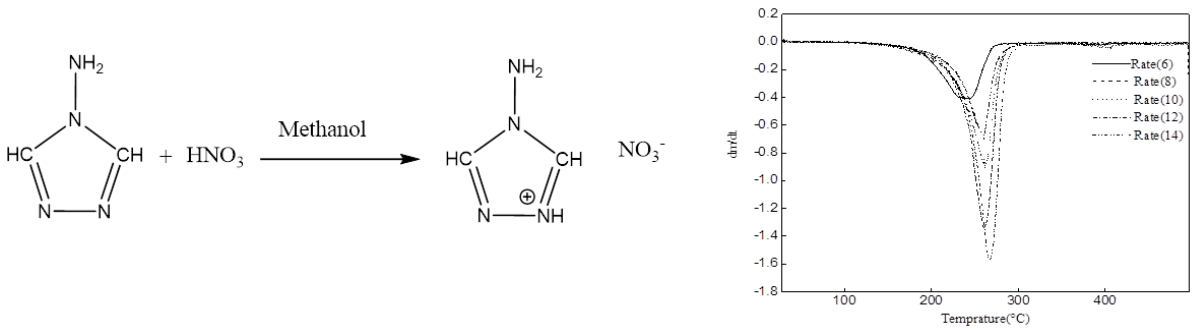

Scheme: Synthesis reaction and thermal analysis of 4-ATN ionic liquid

References

[1] Drake G., Hawkins T., Brand A., Hall L., Mckay M., Vij A., and Ismail I., Energetic, low-melting salts of simple heterocycles, Propellants, Explosives, Pyrotechnics, 2003, 28(4), 174-180.

[2] Leonard P.W., Chavez D.E., Bowden P.R., and Francois E.G., Nitrate Salt Based Melt Cast Materials, Propellants, Explosives, Pyrotechnics, 2018, 43(1), 11-14.

preparation of pyrimidinones in the presence of borane trifluoride stabilized on nano-kaolin under abrasive and solvent-free conditions

Maryam Hariri, Abdolhamid Bamoniri*, Parisa Moharrami Korblagh

Department of Organic Chemistry, Faculty of Chemistry, University of Kashan, Kashan, I.R. Iran,
ma.hariri.online@gmail.com, bamoniri@kashanu.ac.ir

Keywords: Green chemistry, Pyrimidinone, Biomass, Nano kaolin, Borane trifluoride

Green chemistry is a new way to produce medicinal compounds that uses biomass to produce industrial quantities. Heterocyclic compounds are abundant in nature. These compounds have many biological properties and medicines have one or more heterocyclic structures. These compounds have two nitrogen atoms in the positions of 1,3-hexagonal rings [1]. The antifungal, antioxidant, antimicrobial and anticancer properties of pyrimidinone medicals have long been considered by many pharmaceutical researchers [2]. The main problem with steels and their alloys are corrosions in acidic environments. Pyrimidinones prevent the corrosion of alloys by acid many of the proposed methods for the synthesis of these compounds have been associated with the use of toxic solvents, expensive reagents, long time and the formation of by-products. Therefore, the synthesis of these compounds is accompanied by the use of milder conditions and environmentally friendly catalysts in a short reaction time and mild conditions that are economically available. In this research, the preparation of pyrimidinone in the presence of borane trifluoride stabilized on nano-kaolin as catalyst under abrasive and solvent-free conditions has been investigated (**Scheme1**). Performing reactions in a green environment is one of the most important features of researchers.

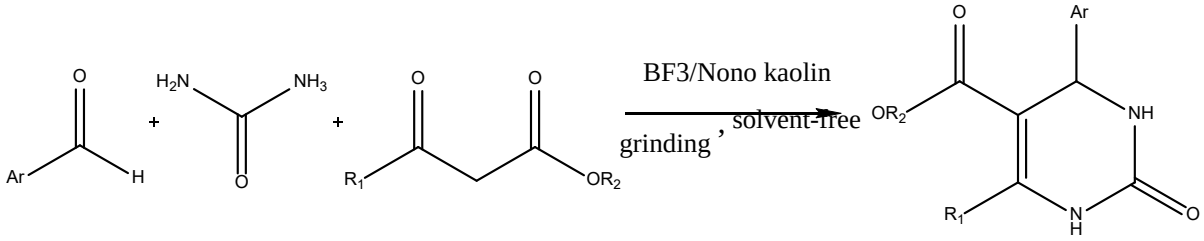

Scheme1

References:
[1] Farahmand. T, Hashemian. S, Sheibani. A, Efficient one-pot synthesis of pyrano[2,3-d] pyrimidinone and pyrido [2,3-d] pyrimidine derivatives by using of Mn-ZIF-8@ZnT Nano catalyst, *J. Mol. Struct*. **2020**, ١٢٠٦ ,127667.
[2] Helwa. A. A, Gedawy. E. M, About-Seri. S. M, Taher. A. T. E1 ,Ansary. K, Synthesis and bioactivity evaluation of new pyrimidinone-5-carbonitriles as potential anticancer and antimicrobial agents*, Res. Chem. Intermed.* **2018**, 44, 2685-2702.

Green benzylation of phenols in water using trimethyl-beta-cyclodextrin as phase-transfer catalyst

Fatemeh Sardarabadi, Esmail Rezaei Seresht*, Behnam Mahdavi

Department of Chemistry, School of Sciences, Hakim Sabzevari University, Sabzevar, Iran, fatemesardar75@gmail.com, *e.rezaei@hsu.ac.ir*

Keywords: Phase-transfer catalysis, Trimethyl-beta-cyclodextrin, Benzylation, Phenols.

Phase-transfer catalysis (PTC) has long been recognized as a versatile method for organic synthesis in industrial and academic laboratories [1]. A catalyst enables a phase-transfer reaction in a heterogeneous system between general organic compounds soluble in organic solvents and water-soluble compounds such as mineral salts. A phase-transfer catalyst is soluble in both solvents and transports the anions of mineral salts to organic solvents and returns them to the water phase [2].

Cyclodextrins are a family of natural macrocycles. The cavity size of beta-cyclodextrin is more suitable than other cyclodextrins to include a wide range of is organic molecules [3]. Benzylation of phenol is one of the important organic reactions. The importance of this reaction is due to the application of benzyl phenol products in various fields such as the production of antioxidants, rubbers and plastics and other intermediate materials [4]. In this work, we want to report the use of trimethyl beta-cyclodextrin (TM-β-CD), as a phase- transfer catalyst for green benzylation of phenols in water.

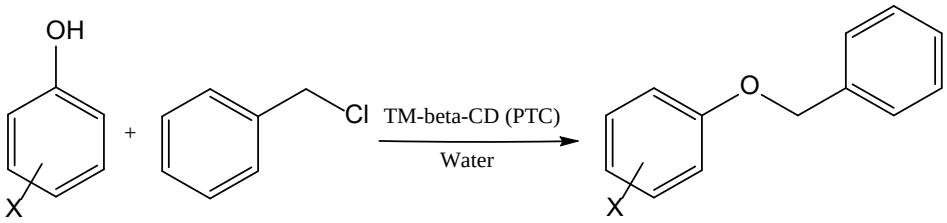

Scheme 1. Green Benzylation of phenols in water by PTC using TM-β-CD.

References

[1] Hashimoto, T. and K. Maruoka, Recent development and application of chiral phase-transfer catalysts. *Chemical Reviews*, 2007. **107**(12): p. 5656-5682.

[2] OHTA, N. and Y. IWAKI. Department of Chemistry, Graduate School of Science, Kyoto University, *Kyoto 606-8502, Japan*. in *Proceedings of 2000 International Conference on Excitonic Processes in Condensed Matter: Osaka, Japan, August 22-25, 2000*. 2001. World Scientific.

[3] Roy, M.N., et al., Exploration of inclusion complexes of neurotransmitters with β-cyclodextrin by physicochemical techniques. Chemical Physics Letters, 2016. 655: p. 43-50.

[4] Wang, H., et al., Tetrabutyl ammonium bromide-mediated benzylation of phenols in water under mild condition. Tetrahedron, 2014. 70(16): p. 2669-2673.

Preparation of polytetramethyleneglycol(PTMEG) using phosphotungstic acid(HPW) and investigation of the effect of temperature

Alireza Banan*, Mohammad Javanmardi

Department of Chemistry, Faculty of Imam Hossein Comprehensive University, Tehran, Iran, bananjahromi@yahoo.com, mohammadjavanmardi1998@gmail.com

Keywords: Polytetramethyleneglycol, PTMEG, HPW, Ceiling temperature.

PTMEG is an important intermediate in manufacturing thermoplastic polyurethane elastomers, polyetheresters and polyetherimides. These products are used for the production of highly abrasion-resistant and flexible hoses, films and cable sheathings [1]. THF polymerization is accounted as a reversible polymerization reaction. There is actually a monomer-polymer equilibrium which at certain temperatures the polymerization reaction is favored and at other temperatures the depolymerization reaction is favored [2]. Ceiling temperature (T_c) is defined as the temperature at which the rate of polymerization and depolymerization of the polymer are equal. T_c can be determined by investigating the conversion percentage different temperatures [3]. Type of catalyst can affect the ceiling temperature of reversible polymerization reaction. We studied this concept in the case of using HPW as catalyst. First, we investigated the synthesis of PTMEG by a cationic ring opening polymerization (Scheme1) and characterized it using ^{1}H NMR, ^{13}C NMR and FT-IR spectroscopy then, the polymerization reaction was performed at different temperatures in order to determine the T_c of the reaction. By comparing the yield of the reactions at different temperatures the highest yield was obtained at 50 °C which was considered as T_c. At temperatures higher than 50 °C the polymerization yield started to decrease because the monomer-polymer equilibrium will be changed and depolymerization reaction occurs [3].

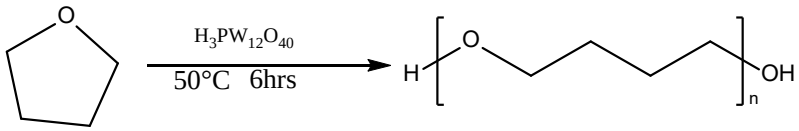

Scheme 1: Synthesis of PTMEG.

References

1. Deng, H., et al., Real-time monitoring of ring-opening polymerization of tetrahydrofuran via in situ Fourier Transform Infrared Spectroscopy. *J. Appl. Polym. Sci.*, 2014. **131**(15).
2. Penczek, S., J. Pretula, and S. Slomkowski, Ring-opening polymerization. *Chem. Teach. Int.*, 2021. **3**(2): p. 33-57.
3. Ivin, K.J. and J. Leonard, The equilibrium polymerization of monomers which are solvents for their polymers: Case of tetrahydrofuran. *Polymer*, 1965. **6**(11): p. 621-624.

Synthesis of polytetrahydrofuran-co-epichlorohydrin (poly(THF-co-ECH) by cationic ring opening polymerization

Alireza Banan*, Mohammad Javanmardi and SeyedMojtaba Keshavarz

Department of Chemistry, Faculty of Imam Hossein Comprehensive University, Tehran, Iran, bananjahromi@yahoo.com, mohammadjavanmardi1998@gmail.com

Keywords: Poly(THF-co-ECH), Ring opening polymerization, Phosphotungstic acid

Polytetrahydrofuran (PTHF) is utilized as the precursor for the synthesis of polyurethane elastic fibers, polyurethane elastomers, and ester–ether copolymers [1]. The cationic ring opening polymerization of THF is the main route for preparation of PTHF. However, the self-polymerization of THF is a challenging process since the ring tension of THF is low. So not only it is necessary to utilize a promoter such as epichlorohydrin but also it needs a strong acidic catalyst for polymerization [2]. In several studies heteropoly acids such as phosphotungstic acid (HPW) has been used as an efficient catalyst for THF polymerization promoted by heterocycles such as ECH [3, 4]. HPW is a strong acid with three acidic protons in its structure [4]. In our study we synthesized poly(THF-co-ECH) by a cationic ring opening polymerization. In this reaction, ECH was used as a promoter and HPW was used as a catalyst. Because the oxirane ring is more reactive than THF ring, it becomes first protonated and the ring opening reaction starts (scheme 1). In order to the polymerization process was terminated by adding water to the reaction mixture. The resulted product was characterized by gel permeation chromatography (GPC), ^{1}H NMR, ^{13}C NMR and FT-IR spectroscopy.

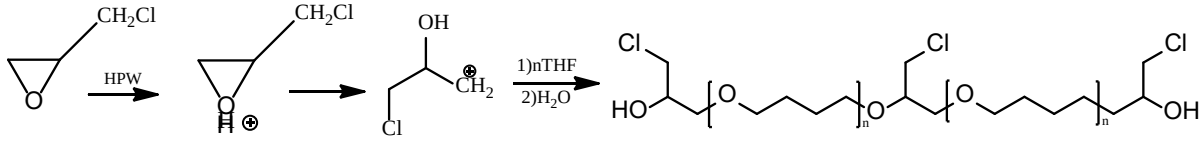

Scheme1: Synthetic process of poly(THF-co-ECH).

References

[1] Penczek, S., J. Pretula, and S. Slomkowski, Ring-opening polymerization. *Chem. Teach. Int.* 2021. **3**(2): p. 33-57.

[2] Hamam, N., et al., Synthesis and Characterization of poly (Epichlorohydrin-co-Tetrahydrofuran) Using Green Catalyst Montmorillonite Algerian (Maghnite-H+). *Alger. J. Eng. Technol.* 2019. **5**(3).

[3] Zhu, Y., et al., Sustainable synthesis of bio-based PTMEG and methane beyond the Reppe method. *Green Chem.* 2022. **24**(15): p. 5770-5778.

[4] Deng, H., et al., Real-time monitoring of ring-opening polymerization of tetrahydrofuran via in situ Fourier Transform Infrared Spectroscopy. *J. Appl. Polym. Sci.*, 2014. **131**(15).

29TH IRANIAN ORGANIC CHEMISTRY CONFERENCE
1_3 NOV, 2023
UNIVERSITY OF QOM, IRAN

DFT study on the mechanism of aza-Diels Alder reaction of cyclic and acyclic enamides with 1,2-diaza-1,3-dienes

Mahsa Bakhshian* **and Mina Haghdadi**

Department of chemistry, Babol Branch, Islamic of Azad university of Babol, Iran, mahsabakhshian3@gmail.com

Keywords: Tetrahydropyridazine, DFT study, Aza-Diels Alder reaction, Regioselectivity.

Tetrahydropyridazine rings, as six-membered N-containing heterocyclic blocks, are widespread in many pharmaceutically active molecules and biologically natural compounds [1]. In this regard, the [4+2] cycloaddition reaction of 1,2-diaza-1,3-dienes and various alkenes would be a straightforward approach for the construction of 1,4,5,6-tetrahydropyridazine skeletons. In 2021 Shen *et al.* reported some aza-Diels−Alder reactions of enamides with 1,2-diaza-1,3-dienes, which successfully formed a wide range of fused polycyclic tetrahydropyridazines [2]. Herein, we investigated the mechanistic details of these reactions through computational analysis by the DFT method. It was found that, enamides applied as electron-rich participants and irrespective of locality, electronic property, and number of the substituents could be suitable for the inverse electron-demand [4+2] cycloaddition reaction. Moreover, regardless of electron-withdrawing or electron-donating group on the aryl ring (Ar) of acyclic enamides, did not have significant influence on the reactivity. All of cycloaddition reactions are completely regioselective and take place via a polar and asynchronous process. Analysis of the reactivity indices shows that 1,2-diaza-1,3-dienes present a strong electrophilic character and enamides have a strong nucleophilic character.

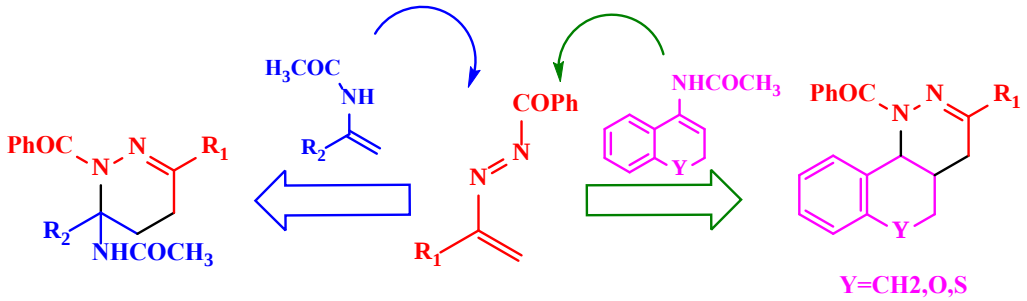

Scheme: Aza-Diels-Alder reactions between 1,2-diaza-1,3-butadiene with cyclic and acyclic enamides.

References

[49] D. W.; Albert, D. H.; Dyer, R. D.; Bouska, J. B.; Young, P.; Rotert, G.; Machinist, J. M.; Carter, G. W. 1-Phenyl-[2H]- tetrahydropyridazin-3-one, A-53612, a selective orally active 5-lipoxygenase inhibitor. *Bioorg. Med. Chem. Lett.* 1992, 2, 1353-1370.

[50] Shen,L-W.; Li,T-T.; You,Y.; Zhao,J-Q.; Wang ,Z-H.; and Yuan ,W-C.; Inverse Electron-Demand Aza-Diels−Alder Reaction of Cyclic Enamides with 1,2-Diaza-1,3-dienes in Situ Generated from α-Halogeno Hydrazones: Access to Fused Polycyclic Tetrahydropyridazine Derivatives, *J. Org. Chem.* 2021, 86, 17, 11472–11481.

The One-Pot Synthesis of Amidoalkyl Naphthols Derivatives by Using Sulfonic Acid Functionalized Graphene Oxide as an Efficient Catalyst

Nafisehsadat Sheikhan*, Ghazaleh khajeh Saeidi

Department of Chemistry, Najafabad Branch, Islamic Azad University, Najafabad, Iran, ns_sheikhan@yahoo.com

Keywords: One-pot, Graphene oxide, Amidoalkyl naphtols, Solvent-free, solid acid.

One-pot multicomponent reactions are known as important and environmentally benign processes in synthetic chemistry because they decrease the number of steps and reduce energy consumption and waste production. 1-amidoalkyl 2-naphthols can be converted to useful and important biological building blocks and to 1-amino methyl 2-naphthols by an amide hydrolysis reaction, since compounds exhibit depressor and bradycardia effects in humans [1]. Regarding the importance of amidoalkyl 2-naphthols and the great need for environmentally benign chemical productions, the development of suitable green synthetic methods for these compounds has attracted considerable interest. Recently, Solid acids have many advantages such as easy handling, decreasing reactor and plant corrosion problem and environmentally safe disposal over conventional mineral acids. Graphene oxide (GO) includes high density of hydrophilic organic functional groups including hydroxyl, carboxyl and epoxy functional groups. However, GO and such kind of modified GO is a capable candidate as heterogeneous acid catalyst for organic transformation as well as industrial applications [2]. So herein we report a mild and efficient method for the one-pot preparation of amidoalkyl naphthols from condensation of aldehydes with amides or urea and 2-naphthol in the presence of sulfonic acid functionalized graphene oxide (GO-SO_3H) as an effective solid acid under thermal solvent-free conditions (**Scheme**).

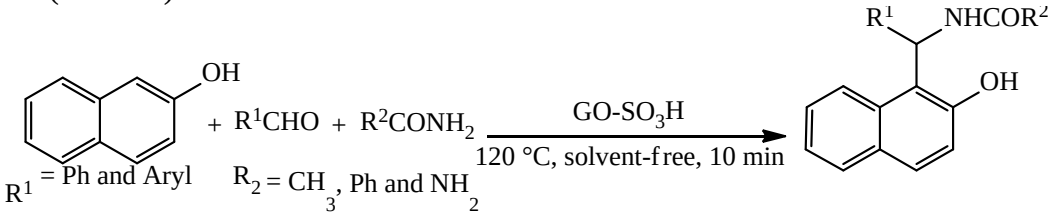

Scheme: The one-pot synthesis of amidoalkyl naphthols derivatives by using GO-SO_3H

References

[51] Hakimi, F.; Mirjalili, F.; Fallah-mehrjardi, M. One-pot synthesis of 1-amidoalkyl-2-naphthols catalyzed by nano-graphene oxide under solvent-free conditions. *Asian J. Green Chem.* 2019, 4, 183–191.

[52] Hanoon, H.; Kowsari, E.; Abdouss, M.; Zandi, H.; Ghasemi, M. Efficient preparation of acidic ionic liquid- functionalized reduced graphene oxide and its catalytic performance in synthesis of benzimidazole derivatives. *Res. Chem. Intermed.* 2017, 43, 1751–1766.

The preparation of tetrahydrobenzo[*b*]pyrans in the presene of a novel manetic heteropoly acid nanocatalyst

Seyedeh Fatemeh Hojati*, Zahra Borghebani

Department of Chemistry, Hakim Sabzevari University, Sabzevar 96179-76487 Iran, sf.hojati@hsu.ac.ir, Zahra.b.1221.m@gmail.com

Keywords: Tetrahydrobenzo[b]pyran, Magnetic heteropoly acid, Nanocatalyst.

Heteropoly acids (HPAs) are an important class of inorganic materials [1,2] that are made up of a particular combination of oxygen and hydrogen with specific metals such as tungsten, molobdenium or vanadium and non-metals [3]. They are extensively used in diverse fields of science and have been applied as highly efficient catalysts in different chemical transformations [4]. In this work, a new keggin-type heteropoly acid ($H_3PMo_{11}WO_{40}$. xH_2O) was synthesized and modified by a core-sell Fe_3O_4@Silica-aminopropyl nanocomposite. After characterization by IR, SEM and EDX analyses, this new magnetic nanocomposite was applied in the preparation of benzo[*b*]pyran derivatives from aldehydes, malononitrile/ethyl cyanoacetate and active methylene-containing compounds (Scheme 1). High yields of products, mild reaction conditions, short reaction times, easy separation of the catalyst and reusability of the catalyst are valuable advantages of the current work.

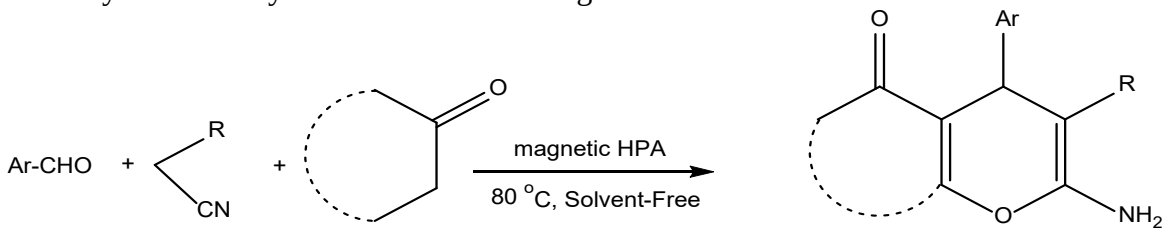

Scheme 1. The preparation of tetrahydrobenzo[*b*]pyrans in the presence of magnetic HPA.

References:

[53] Pope, Michael Thor, and Achim Müller."Introduction to polyoxometalate chemistry: from topology via self-assembly to applications."Polyoxometalate Chemistry from Topology *via* Self-Assembly to Applications. Dordrecht, Springer Netherlands,2001. 1-6.

[54] Pope, Michael Thor,Yves Jeannin, and Michel Fournier. Heteropoly and isopoly oxometalates.*Vol*.8. Berlin: Springer-Verlag, 1983.

[55] Dufaud, V.; Lefebvre, F. Inorganic hybrid materials with encapsulated polyoxometalates." *Materials* 2010, 3, 682-703.

[56] Amiri,Amirhassan,et al."Preparation and characterization of magnetic Wells–Dawson heteropoly acid nanoparticles for magnetic solid-phase extraction of aromatic amines in water samples. *J. Chromatogr. A* 1483,2017,64-70.

Magnetically responsive graphene oxide and multi-wall carbon nanotubes as demulsifier for oil removal from crude oil-in-water emulsion

Behnaz Havakhah Hallaj[a], Behrooz Maleki[b]*, Hamid Reza Ezatpour[a], Fariba Jafari-Soghieh[a]

a) Department of Chemistry, School of Sciences, Hakim Sabzevari University, Sabzevar, Iran, b.havakhah.ms@gmail.com
b) Department of Organic Chemistry, Faculty of Chemistry, Mazandaran University, Babolsar, Iran

Keywords: Emulsion, Demulsifier, Asphaltene, Carbon nanotubes, Grafen oxide, Magnetic.

Large oil spills and crude oil-in-water (O/W) emulsion discharges from industrial activities have serious impacts on the environment with potentially major economic impacts [1, 2]. A magnetically responsive mixture frommulti-walled carbon nanotubes and grafen oxide (M-MWCNT-GO) appropriate for acidic to alkaline conditions of crude O/W emulsion was designed and prepared via regulating the content of surface functional groups (such as -NH_2, -OH and -COOH). The M-MWCNT-GO was confirmed as an efficient demulsifier and the corresponding demulsification efficiency achieved the highest when its dosage was increased to 300 mg/L. Significantly, the M-MWCNT-GO has superior demulsification performance under wide pH levels (**Scheme**).

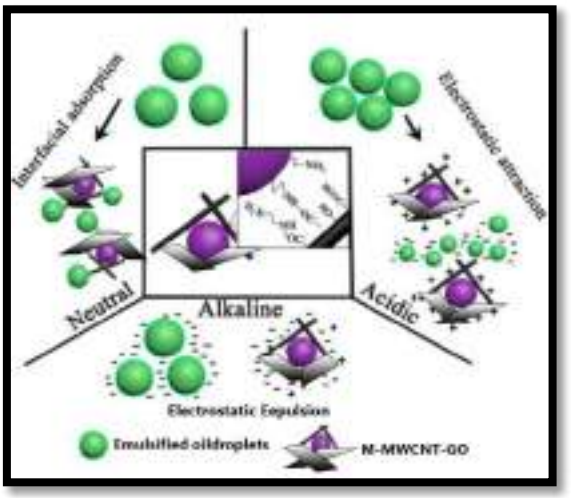

Scheme: Demulsification of M-MWCNTS-GO.

References

[1] Li, S.; Li, N.; Yang, S.; Liu. F.; Zhou, J. The synthesis of a novel magnetic demulsifier and its application for the demulsification of oil-charged industrial wastewaters, *J Mater Chem A* 2014, *2*, 94-99.
[2] Mirshahghassemi. S.; Lead, J. R. Oil recovery from water under environmentally relevant conditions using magnetic nanoparticles. *Environ Sci Technol* 2015; *49*,11729-36.

29TH IRANIAN ORGANIC CHEMISTRY CONFERENCE
1_3 NOV, 2023
UNIVERSITY OF QOM, IRAN

Evaluation of the mechanism, regio-, and chemoselectivity of cycloaddition reactions of 1,2-diaza-butadienes with thioesters

Fateme Hajati*, Mina Haghdadi and Hassan Ghasemnejad Bosra

Department of chemistry, Babol Branch, Islamic of Azad university of babol, Iran, Shamim.hajati@yahoo.com, mhaghdadi2@gmail.cm, hghasem2000@yahoo.it

Keywords: Thiadiazine, Chemoselectivity, DFT study, Thioesters.

1,3,4-thiadiazine skeletons show a prominent and important role in many biologically active compounds. [1] They can react with, C=C, C=N, N=N and C=S dienophiles, to realize aza-Diels−Alder reactions, leading to the generation of nitrogen heterocyclic skeletons, such as tetrahydropyridazines or thiadiazines. In this regard, the highly regioselective and inverse electron-demand of aza-Diels alder reaction of the 1,2-diaza-1,3-dienes with α,β-unsaturated thioesters reported by *Shen et.al*.[2] Herein, we studied all competitive cycloaddition reactions of 1,2-diaza-1,3-dienes with α,β-unsaturated thioesters, which some of them were not observed in the experimental results. The mechanistic details were explored using the DFT method at the M06- 2X/6-311g(d,p) level of theory. DFT calculations indicated that thioester preferred to participate as a heterodienophile through the C=S group toward diene to afford the 1,3,4thiadiazine products. Then, the electron-donating and electron-withdrawing groups at the para position of the benzene ring of 1,2-diaza-1,3-dienes and α,β-unsaturated thioester were investigated, and the results indicated that the reactions were compatible according to the type of substitution. Analysis of the global reactivity indices allows classifying 1,2-diaza-1,3-dienes and thioester as strong electrophile and nucleophile, respectively, which is in clear agreement with the GEDT directions at the TSs.

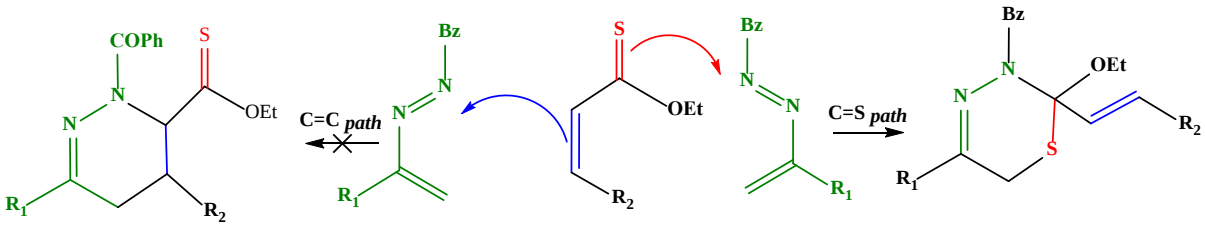

Scheme: The possible reaction pathway of aza-Diels-Alder reactions of 1,2-diaza-1,3-butadiene with thioesters.

References

[57] Gouda, M. A.; Abu-Hashem, A. A.; Hussein, H. A. R.; Aly, A. S. Recent Progress on Fused Thiadiazines: A Literature Review. *Polycycl. Aromat. Compd.* 2020, 1.

[58] Shen, L-W.; Zhang, Y-P.; You, Y.; Zhao, J-Q.; Wang, Z-H.; and Yuan, W-Ch Inverse Electron-Demand Aza-Diels−Alder Reaction of α,β-Unsaturated Thioesters with In Situ-Generated 1,2-Diaza-1,3-dienes for the Synthesis of 1,3,4-Thiadiazines s: *J. Org. Chem*. 2022, 87, 4232−4240

Olaparib polycaprolactone-coated nanocapsules as an efficient and controlled drug delivery system for cancer therapy: in vitro release and cytotoxicity studies

Maryam Shojaeifard[a], Noorhan J. M. Al-Juaifari[a], Zohreh Mirjafary[a,*], Hamid Saeidian[b]

a) Department of Chemistry, Science and Research Branch, Islamic Azad University, Tehran, Iran, m.shojaeifard@gmail.com, zmirjafary@srbiau.ac.ir
b) Department of Science, Payame Noor University (PNU), P.O. Box: 19395-3697, Tehran, Iran

Keywords: Olaparib, Nanocapsules, Polycaprolactone, Drug delivery system

Breast cancer is the most common cancer among women. Olaparib (OLP) is one of the drugs approved for the treatment of this type of cancer. Due to its low solubility in an aqueous medium and its high dosage, it is necessary to design an effective drug delivery system (DDS) for it. In the present study, an efficient and new DDS for OLP was prepared using polycaprolactone (PCL) nanocapsules [1, 2] and its physicochemical properties were investigated over a period of 40 days. The amount of drug loaded in nanocapsules was obtained 89%. The average particle size of nanocapsules was 221 nm with a polydispersity index = 0.196 and zeta potential = -25.8 mV, which indicate the complete stability of OLP@PCL nanocapsules. In vitro release profile studies confirmed that there is a controlled release of OLP from PCL nanocapsules (**Fig. 1**).

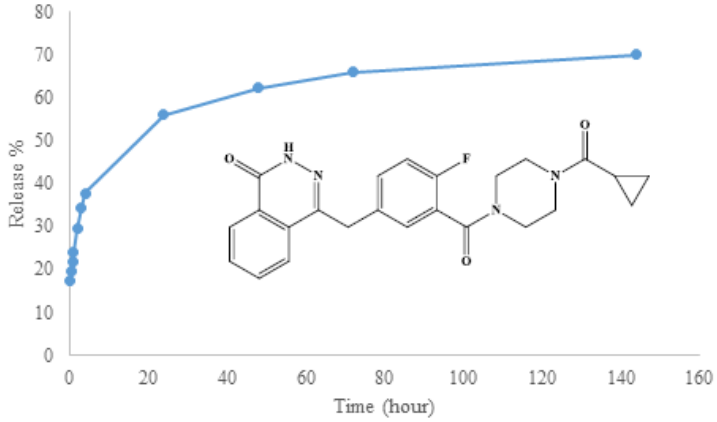

Fig. 1. Chemical structure of Olaparib and *in vitro* release profile for OLP@PCL nanocapsules

References

[1] Diyanat, M.; Saeidian, H. The metribuzin herbicide in polycaprolactone nanocapsules shows less plant chromosome aberration than non-encapsulated metribuzin. *Environmental Chem. Lett.* 2019, *17*, 1881-1888.

[2] Mahmoudi, M.; Saeidian, H.; Mirjafary, Z.; Mokhtari, J.; Preparation and characterization of memantine loaded polycaprolactone nanocapsules for Alzheimer's disease. *J. Porous Mater*. 2021, *28*, 205-212.

29TH IRANIAN ORGANIC CHEMISTRY CONFERENCE
1_3 NOV, 2023
UNIVERSITY OF QOM, IRAN

The Synthesis and Characterization of Sulfamic Acid Functionalized Graphene Oxide and its Catalytic Application in One-Pot Synthesis of Imidazol Derivatives

Nafisehsadat Sheikhan*, Kimia Yavari

Department of Chemistry, Najafabad Branch, Islamic Azad University, Najafabad, Iran, ns_sheikhan@yahoo.com

Keywords: One-pot, Graphene oxide, Imidazol, Solvent-free, sulfamic acid.

The oxidized graphene sheets, namely, graphene oxide (GO) contains high density of hydrophilic organic functional groups such as hydroxyl, carboxyl, and epoxy groups. Recently, GO have attracted significant attention for its extensive range of applications. Functionalization of graphene oxide can basically alteration graphene oxide's properties. There are many methods in which graphene oxide can be functionalized depending on the favorite application [1,2]. Regarding, sulfamic acid functionalized graphene oxide was prepared and characterized by FESEM, TEM and FT-IR.

Recently, one-pot multicomponent reactions have played an increasingly important role in organic and medicinal chemistry for decreasing a number of reaction steps, lower costs, high atom-economy, energy saving, the prevention of time consuming, waste consumption and expensive purification processes. Therefore, Multicomponent reactions are very important for the construction of many heterocyclic compounds such as imidazole derivatives. The synthesis of these compounds due to large number of biological and pharmacological properties has received a great deal of attention. The aims of this research were to synthesize and characterize the sulfamic acid functionalized graphene oxide. Its catalytic properties were also investigated in the synthesis of imidazole derivatives. (**Scheme**).

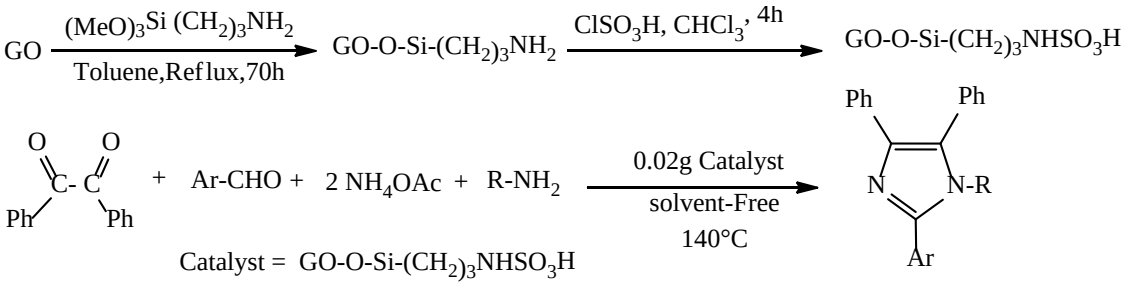

Scheme: The synthesis of sulfamic acid functionalized graphene oxide and its application

References

[59] Wang, C.; Ge, H.; Zhao, Y.; Liu, Sh.; Zou, Y.; Zhang, W. Study on the adsorption of Cu(II) by folic acid functionalized magnetic graphene oxide. *J. Magn. Magn. Mater.* 2017, 423 421–43.

[60] Kazemi Movahed, S.; Esmatpoursalmani, R., Bazgir, A. N-Heterocyclic carbene palladium complex supported on ionic liquid-modified graphene oxide as an efficient and recyclable catalyst for Suzuki reaction. *RSC Advances* 2014, 4, 14586-14591.

29TH IRANIAN ORGANIC CHEMISTRY CONFERENCE
1_3 NOV, 2023
UNIVERSITY OF QOM, IRAN

Starch-Copper (II) complex supported on Hercynite nanoparticles as an efficient nanomagnetic catalyst for synthesis of highly-substituted imidazoles

Ahmad Nikseresht[a*], Masoud Mohammadi[b]

a) Department of Chemistry, Payame Noor University (PNU), 19395-4697 Tehran, Iran, a_nik55@yahoo.com.
b) Department of Chemistry, Faculty of Science, Ilam University, P.O. Box 69315516, Ilam, Iran, tbr.masoud@gmail.com

Keywords: Tetrasubstituted imidazoles, Starch, Hercynite, Green catalyst, multicomponent reactions.

Tetrasubstituted imidazoles are a class of heterocyclic compounds that contain an imidazole ring with four different substituents attached to its carbon atoms. Tetrasubstituted imidazoles are of significant interest in medicinal chemistry and drug discovery due to their potential pharmacological activities [1]. The synthesis of tetrasubstituted imidazoles can be achieved through various methods, such as multicomponent reactions, condensation reactions, and cyclization reactions involving appropriate starting materials [2]. In this study, we used the Starch-Cu complex supported on the surface of Hercynite as a catalyst in the synthesis of tetrasubstituted imidazoles. The Starch-Cu-Hercynite complex was prepared using a green chemistry approach, incorporating a renewable and biodegradable Starch ligand coordinated with Cu ions on the magnetic spinel oxide, Hercynite. Characterization of the catalyst was performed using various spectroscopic and microscopic techniques, including FT-IR, XRD, TGA, EDAX, Mapping, SEM, TEM, VSM and XPS, to assess its structural and morphological properties. The catalyst exhibited high efficiency and selectivity in promoting the formation of tetrasubstituted imidazoles, accompanied by reduced reaction times and minimized waste generation.

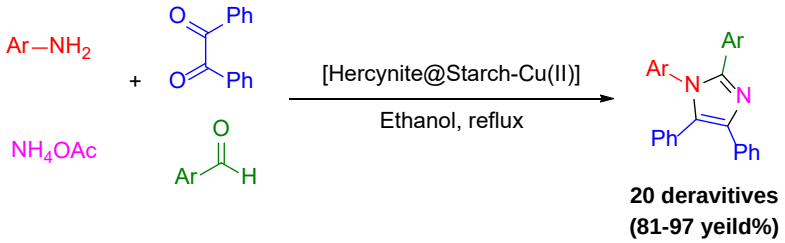

Scheme: Synthesis of tetrasubstituted imidazoles catalyzed by [Hercynite@Starch–Cu$^{(II)}$].

References

[1] Nagara, B. G. Green Synthesis of Bioactive Molecules : A Review. *Int. J. Pharm. Res. Technol.* 2020, *12* (1), 1.
[2] Mekki, S.; Laichi, Y.; Benourrad, F.; Lagha, N.; Chebout, R.; Bachari, K.; Saidi-Besbes, S. Copper Triazole Complex Supported on Fe3O4@SiO2 Nanoparticles as Eco-Friendly Nanocatalysts in Solvent-Free Biginelli Reaction. *Appl. Organomet. Chem.* 2023.

Selective Esterification of α-Haloacetic acids to Desired α-Halo esters over the catalysis of Amberlyst®-15

Ahmad Nikseresht[a*], Leila Matin[a], and Masoud Mohammadi[b]

a) Department of Chemistry, Payame Noor University (PNU), 19395-4697 Tehran, Iran, a_nik55@yahoo.com.
b) Department of Chemistry, Faculty of Science, Ilam University, P.O. Box 69315516, Ilam, Iran, tbr.masoud@gmail.com.

Keywords: α-Halo esters, Haloacetic acid, Amberlyst® 15, Heterogeneous catalyst, Esterification.

α-Halo esters are a class of organic compounds that contain a halogen atom attached to the carbon adjacent to the carbonyl group in an ester. These compounds are versatile synthetic intermediates widely used in organic synthesis for the preparation of various complex molecules [1]. However, the synthesis of α-halo esters presents several challenges, including achieving selectivity for the desired regioisomer, managing the reactivity of the α-halogenated carbonyl compounds with nucleophiles, and addressing compatibility issues with sensitive functional groups [2]. In this study, we used Amberlyst®-15 as an efficient, cost-effective, and recyclable strong acid catalyst for the selective esterification of a wide variety of haloacetic acids, without any Williamson ether by-product formation, by employing an excess amount of different alcohols. The α-halo ester derivatives were obtained through a one-pot condensation of linear alcohols and haloacetic acids under green conditions, resulting in short reaction times and excellent yields (**Scheme** 1). Furthermore, we assessed the stability of the Amberlyst®-15 catalyst during these reactions by conducting FT-IR, XRD, EDAX, SEM, TEM and BET analyses. The results demonstrated that the Amberlyst®-15 catalyst remained completely stable throughout the reactions and could be reused for up to eight cycles of reaction.

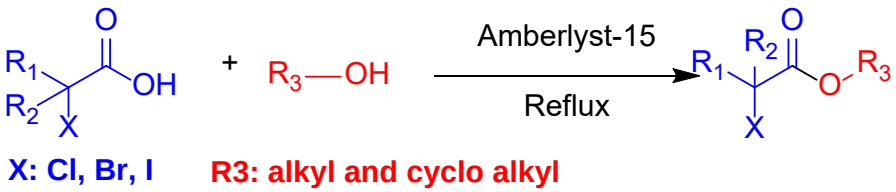

Scheme: Esterification of α-Haloacetic acids over the catalysis of Amberlyst®-15.

References

[1] Nguyen, V. C.; Bui, N. Q.; Mascunan, P.; Vu, T. T. H.; Fongarland, P.; Essayem, N. Esterification of Aqueous Lactic Acid Solutions with Ethanol Using Carbon Solid Acid Catalysts: Amberlyst 15, Sulfonated Pyrolyzed Wood and Graphene Oxide. *Appl. Catal. A Gen.* 2018, *552*, 184–191.
[2] Patwardhan, A. A.; Sharma, M. M. Esterification of Carboxylic Acids with Olefins Using Cation Exchange Resins as Catalysts. *React. Polym.* 1990, *13* (1–2), 161–176.

one-pot cyclopropanation reaction of benzoyl acetone with BrCN and various aldehydes in presence of Et_3N

Mahsa Golmohamadi and Nader Noroozi Pesyan*

Department of Organic Chemistry, Faculty of Chemistry, Urmia University, 57159 Urmia, Iran, m.golmohamadi0211@gmail.com.

Keywords: Benzoyl acetone, Cyanogen Bromide, Aldehyde, Cyclopropane.

The synthesis and application of multi-substituted cyclopropanes has been a subject of great interest due to their roles as the basic structural elements in a wide range of biologically active compounds and important intermediates in organic synthesis diverse applications in synthetic, agricultural, and medicinal chemistry as well as in material science [1]. Cyclopropane ring systems are ubiquitous in nature and are contained in a large number of natural products, insecticides, and pharmaceutical drug candidates. Cyclopropane analogues have been found to exhibit diverse biological applications such as antibacterial, antifungal, antiviral, anti-HIV, anticancer, antitumor, antibacterial, antiestrogenic, agonist, COX-II inhibitor properties [2].

Owing to the importance of full-substituted cyclopropanes, a new route for the synthesis of 1,1'-(1,2-dibenzoyl-3-(aryl(alkyl)) cyclopropane-1,2-diyl) bis(ethan-1-one) (**3**) is described. This method a new one-pot reaction of aldehydes (**1**) with benzoyl acetone (**2**) and BrCN to give (**3**) in the presence of Et_3N and/or sodium ethoxide (EtONa) in excellent yields in a very short time (Scheme 1). All structures were characterized using IR, ^1H NMR, and ^{13}C NMR spectroscopy techniques.

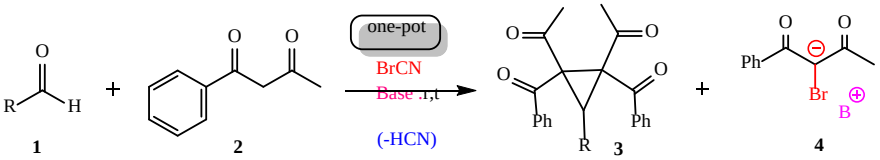

R = H (**a**), *p*-OMe-Ph (**b**), *m*-OH-Ph (**c**), *m*-NO_2-Ph (**d**), *p*-NO_2-Ph (**e**), *p*- Br-Ph (**f**), *p*-Cl-Ph (**g**), *p*-CN-Ph (**h**), *o*-NO_2-Ph (**i**), 2,4-di-Cl-Ph (**j**), *p*-Me-Ph (**k**), Ph (**l**)

Scheme1: Synthesis of cyclopropane derivatives in the presence of BrCN under alkali conditions.

References

[1] Aalinejad M, Noroozi Pesyan N. One-pot, fast cyclopropanation reaction of indandione with various aldehydes in the presence of cyanogen bromide and trimethylamine. J. Chin. Chem. Soc. 2019 Nov;66(11):1523-30.

[2] Kumar A. Brief review on cyclopropane analogs: synthesis and their pharmacological applications. *Int. J. Pharm. Pharm. Sci.* 2013;5(1):467-72.

The novel DES-assisted fast and green synthesis of benzo[6,7]-chromeno[2,3-*d*]pyrimidines

Arezo Monem, Davood Habibi *, Hadis Goudarzi, Maryam Mahmoudiani Gilan

Department of Organic Chemistry, Faculty of Chemistry, Bu-Ali Sina University, Hamedan, Iran, arezomonem@yahoo.com, davood.habibi@gmail.com

Keywords: Deep Eutectic Solvent, Benzo[6,7]chromeno[2,3-*d*]pyrimidine-tetraones, Catalysis

Abbott's research in 2003 led to what we call deep eutectic solvents (DES) [1]. DES is a mixture of two or three (often inexpensive and safe) with a high melting point are mixed and forms a eutectic compound with a lower melting point than each component [2].

DESs are considered green solvents due to properties such as being non-volatile, stable, non-flammable, and non-toxic. Barbituric acids are an important class of medically important pyrimidine derivatives. which is used as an anticonvulsant, sedative, antioxidant, antifungal, and blood pressure. It has recently been estimated that more than 70% of all drugs and agrochemicals have at least one heterocyclic ring in their structure [3]. Pyrano[2,3-d]pyrimidines consist of a pyran ring fused to a pyrimidine. As such, their main framework consists of both nitrogen and oxygen in their carbocyclic structure and has significant pharmacological properties, including cardiac, antitumor, bronchodilator, anti-bronchitis, and antihypertensive activities [4]. In this project, a cheap, simple, and non-toxic method for the synthesis of pyrano[2,3-d]pyrimidines derivatives was considered using a DES catalyst. The structure and properties of the DES catalyst were investigated by FT-IR, TGA/DTA, condensation, eutectic point, and ^{1}HNMR. Among the advantages presented by this study, we can mention the reaction in solvent-free conditions (reduction of pollution), short reaction time, high productivity, easy recycling and separation of the catalyst, as well as high selectivity.

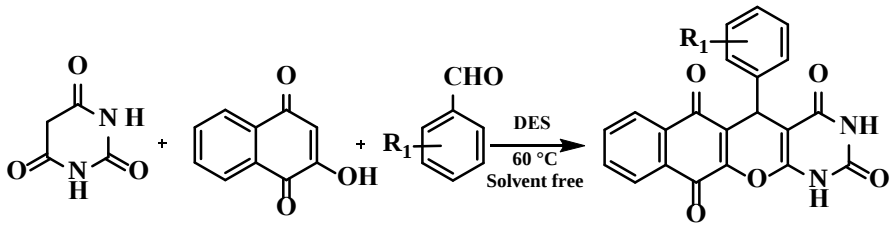

References

[61] Abbott, A.P.; Capper, G.; Davies, D. L.; Rasheed, R. K.; Tambyrajah, V.; Novel solvent properties of choline chloride/urea mixtures, *Chem. Commun.* 2003, *1*, 70-71.

[62] Hayyan, M.; Hashim, M. A.; Hayyan, A.; Al-Saadi, M. A.; AlNashef, I. M.; Mirghani, M. E. Are deep eutectic solvents benign or toxic?, Chemosphere 2013, *90*, 2193-2195.

[63] Rathee, P.; Tonk, R. K.; Dalal, A.; Ruhil, M. K. Synthesis and application of thiobarbituric acid derivatives as antifungal agents, *Cell. Mol. Biol.* 2016, *62*, 141-145.

[64] Furuya, S.; Ohtaki, S. T.; Pyrido[2,3-*d*]pyrimidines and their uses as anatagonists, *Chem. Abst.* 1994, *121*, 205395w.

29TH IRANIAN ORGANIC CHEMISTRY CONFERENCE
1_3 NOV, 2023
UNIVERSITY OF QOM, IRAN

Identifying Novel Small Organic Allosteric Modulators for Fumarate Hydratase

Hamid Reza Kalhor*, Elahe Navaee Lavasani

Biochemistry and Chemical Biology Research Laboratory, Faculty of Chemistry, Sharif University of Technology, Tehran, Iran, kalhor@sharif.edu, elahenavaeelavasani@gmail.com

Keywords: Fumarate hydratase, Double Strand Breaks, Allosteric modulators.

Fumarate hydratase, also known as “Fumarase” is an enzyme of the tricarboxylic acid (TCA) cycle in mitochondria which converts fumarate to L-malate. In recent years, fumarase has emerged as an important player in response to DNA double strand breaks (DSBs) in the nucleus[1].The maintenance of genome integrity constitutes major challenges for all living organisms, and fumarase deficiency has been linked to several pathologies including cancers in humans. The aim of the present study, is to identify allosteric modulators leading to changes in the enzyme function, without competing with its main substrate, working specifically and in a low concentration. Using PCR-cloning, the fumarase gene (from *Saccharomyces cerevisiae*) was amplified and cloned into a bacterial expression vector. The expression and purification of the recombinant enzyme was confirmed using gel electrophoresis. The kinetic parameters including K_m and k_{cat} were measured for the enzyme. To search for allosteric modulators, a library of small organic molecules is screened virtually, by molecular docking. The best candidate molecules are then identified experimentally, using the recombinant fumarase.

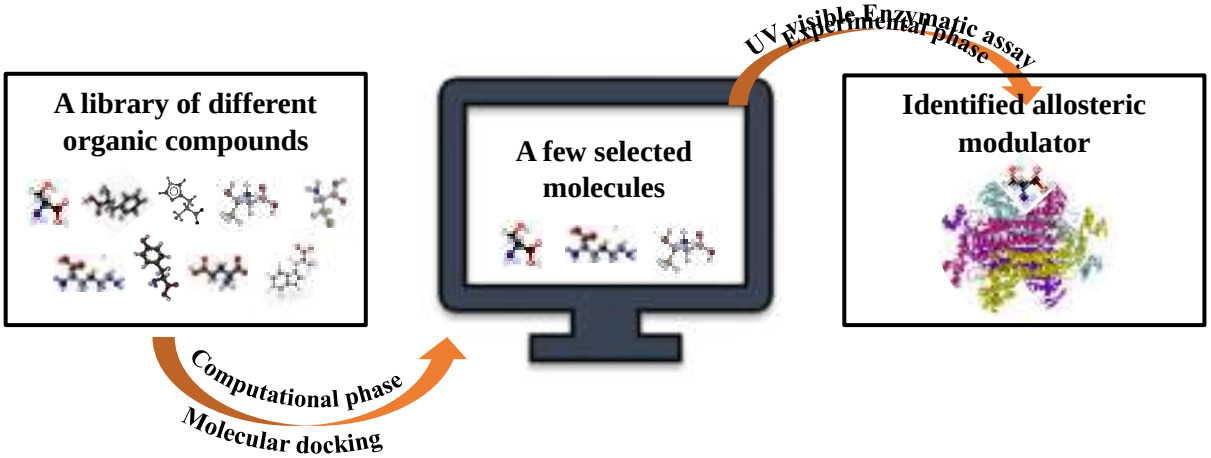

Scheme: General project steps is shown here, consisting computational and experimental phases

References

[1] Leshets, M.; Silas, Y. B. H.; Lehming, N.; Pines, O. Fumarase: From the TCA Cycle to DNA Damage Response and Tumor Suppression. *Front. Mol. Biosci.* **2018**, *5*, 68. https://doi.org/10.3389/fmolb.2018.00068.

29TH IRANIAN ORGANIC CHEMISTRY CONFERENCE
1_3 NOV, 2023
UNIVERSITY OF QOM, IRAN

Trimethyl-β-cyclodextrin as a phase-transfer catalyst for green cleavage of styrene oxide in aqueous medium

Saeed Taghizadeh Khorasanian, Esmail Rezaei Seresht*, Behnam Mahdavi

Department of Chemistry, School of Sciences, Hakim Sabzevari University, Sabzevar, Iran, e.rezaei@hsu.ac.ir

Keywords: Phase-transfer catalysis, Trimethyl-Beta-cyclodextrin, Styrene oxide, Green cleavage.

Phase-transfer catalysis is a general method applicable to many types of reactions in which organic and inorganic anions as well as carbenes and other active species react with organic compounds. Contrary to the general tendency to carry out chemical reactions in homogeneous environments, according to the concept of phase-transfer catalyst reactions, the reaction is carried out in a heterogeneous two-phase system where the first phase is a source of reaction anions or a game to produce organic anions. while organic reactants and catalysts (source of lipophilic cations) are in the second phase, the organic phase [1].

Cyclodextrins (CDs) can form selective host-guest complexes in aqueous media through supramolecular interactions, and therefore, they are suitable host molecules for designing phase-transfer catalysts operating in aqueous media [2].In this work, we intend to report the green ring-cleavage reaction of styrene oxide, a water-insoluble epoxide, in water by different nucleophiles in the presence of trimethyl-β-cyclodextrin (TM-β-CD) as the nanoreactor. In addition, reaction parameters involved in the ring-cleavage reaction, such as temperature, time, amount of nanoreactor, and regiochemistry of the ring-cleavage, have been investigated (**Scheme 1**).

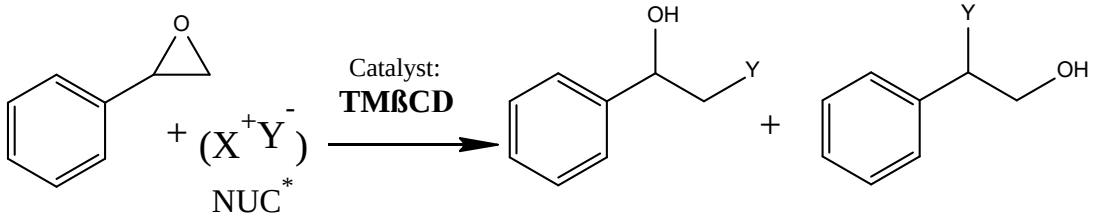

Scheme 1. Green cleavage of styrene oxide in the aqueous medium.

References

[65] Dehmlow, Eckehard V., Sigrid S. Dehmlow, and Hans F. Ebel. Phase transfer catalysis. Vol. 11. Weinheim: Verlag Chemie, 1980.

[66] Szejtli, J., et al., *Synthesis and 13C-NMR Spectroscopy of Methylated beta-Cyclodextrins.* Starch-Stärke, 1980. 32(5): p. 165-169.

29TH IRANIAN ORGANIC CHEMISTRY CONFERENCE
1_3 NOV, 2023
UNIVERSITY OF QOM, IRAN

The gentisic acid-based deep eutectic solvent mediated green synthesis of *N*-substituted decahydroacridine-1,8-diones

Hadis Goudarzi, Davood Habibi*, Arezo Monem, Maryam Mahmoudiani Gilan

Department of Organic Chemistry, Faculty of Chemistry, Bu-Ali Sina University, Hamedan, Iran, hadisgoudarzi9271@gmail.com, davood.habibi@gmail.com

Keywords: Deep Eutectic Solvent, Acridines, Catalysis.

Recently, a new generation of green solvents, namely deep eutectic solvents (DESs), have emerged as a suitable alternative to hazardous organic solvents in various applications, they were introduced as a low-cost alternative to ionic liquids (ILs) [1]. DESes are be made of mixture a hydrogen-bond acceptors (HBA) and hydrogen-bond donors (HBD). Generally, a DES is a type of solvent composed of a mixing two or more components under simple operation of that forms an eutectic with a much lower melting point than either of the individual components [2]. Substituted acridines and acridine-1,8-dione have been successfully used as antimalarials for many years, and several of them have shown excellent results such as anticancer activity, antimicrobial activity and cytotoxicity [3]. Due to their structural similarity with 1,4-dihydropyridines, these substances are used as intermediates for the synthesis of some drugs, such as drugs for the treatment of cardiovascular diseases and high blood pressure [4]. In this study, a novel, efficient, and recoverable DES was designed and made from a mixture of triphenylphosphonium derivative as HBA and Gentisic acid as HBD with ration 1:1 and it characterized using fourier transform infrared spectroscopy (FT-IR), thermal analysis/differential thermal analysis (TGA/DTA), densitometry, and 1HNMR. This DES used as catalyst for the synthesis of piperidine derivatives.

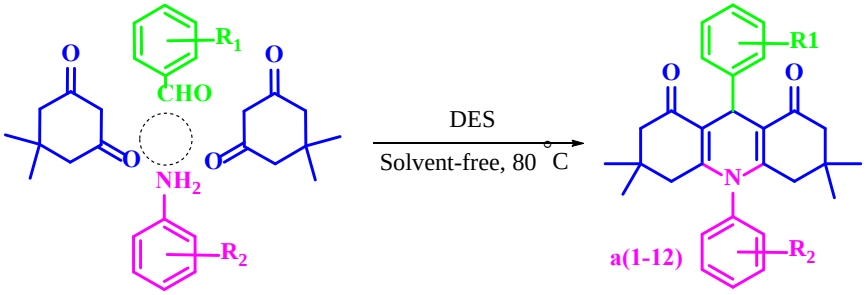

References

[1] Azizi, N.; Ahooie, T. S.; Hashemi, M. M. Multicomponent domino reactions in deep eutectic solvent: An efficient strategy to synthesize multisubstituted cyclohexa-1, 3-dienamines. *J. Mol. Liq*. 2017, 246, 221-224.

[2] Maugeri, Z.; De María, P. D. Novel choline-chloride-based deep-eutectic-solvents with renewable hydrogen bond donors: levulinic acid and sugar-based polyols, *RSC Adv*. 2012, 2, 421–425.

[3] Patel, M.M.; Mali, M.D.; Patel, S.K. Bernthsen synthesis, antimicrobial activities, and cytotoxicity of acridine derivatives. *Bioorg. Med. Chem. Lett*. 2010, *20*, 6324-6326.

One-pot, cyclopropanation reaction of diethyl malonate with various aldehydes in presence of BrCN and trimethylamine

Faezeh Salmanpour and Nader Noroozi Pesyan*

Department of Organic Chemistry, Faculty of Chemistry, Urmia University, 57159, Urmia, Iran

Keywords: Cyanogen bromide, Cyclopropane, Diethyl malonate, One-pot reaction

A new, fast, and easy one-pot cyclopropanation reaction of aromatic and aliphatic aldehydes with diethyl malonate and cyanogen bromide (BrCN) was developed for synthesizing tetraethyl 3-(aryl(alkyl))cyclopropane-1,1,2,2-tetracarboxylate in excellent yields in a short time (about 15s) under basic media. All structures were characterized using IR, ^{1}H NMR, and ^{13}C NMR spectroscopy techniques. This article describes a new one-pot reaction of aldehydes (**1**) with diethyl malonate (**2**) and BrCN to give 3- (aryl(alkyl))cyclopropane-1,1,2,2-tetracarboxylate in the presence of trimethylamine (Et_3N) and/or sodium ethoxide (EtONa) in excellent yields in a very short time (15 s) (**Scheme 1**).

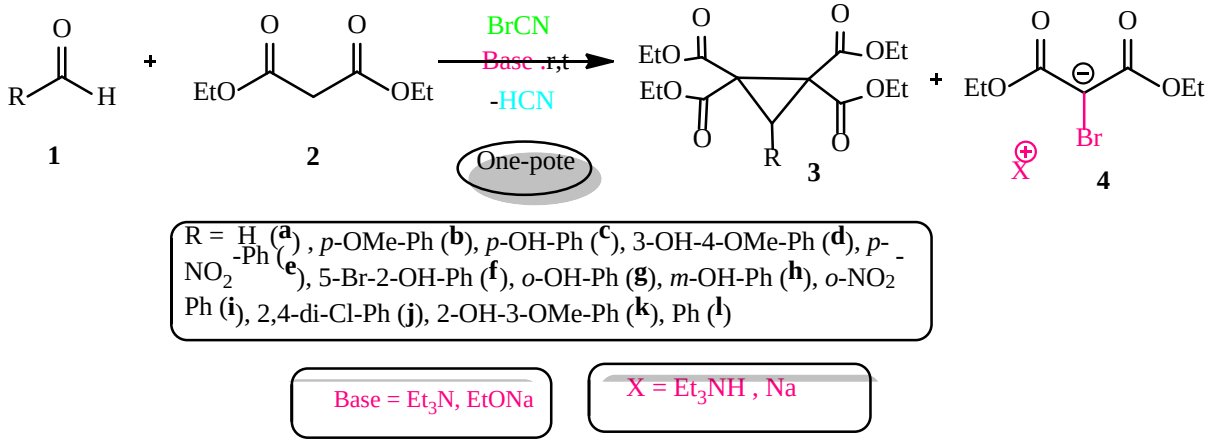

Scheme 1: Synthesis of **3** in the reaction of aldehyde (**1**) with diethyl malonate (**2**) in the presence of BrCN under alkali conditions

References:

[1] Aalinejad M., Noroozi Pesyan N. One-pot, fast cyclopropanation reaction of indandione with various aldehydes in the presence of cyanogen bromide and trimethylamine, *J. Chin. Chem. Soc*. 2019 Nov;66(11):1523-30.

[2] Noroozi Pesyan N., Kimia M.A., Jalilzadeh M., Şahin E. A New, Fast and Easy Strategy for One-pot Synthesis of Full Substituted Cyclopropanes: Direct Transformation of Aldehydes to 3-Aryl-1, 1, 2, 2-tetracyanocyclopropanes, *J. Chin. Chem. Soc*. 2013 Jan;60(1):35-44.

Carbon Quantum Dots as Nano catalysts for Transamidation Reactions

Hamid Reza Kalhor*, Fatemeh Rahgozar

Biochemistry and Chemical Biology Research laboratory, Faculty of Chemistry, Sharif University of Technology, Tehran, Iran, kalhor@sharif.edu, Faezeh.sk7102211@gmail.com

Keywords: Carbon dot, CQD, Transamidation, "Nano catalyst.

Carbon quantum dots (CQDs), as a new type of carbon-based nanomaterial, have attracted a broad research interest in recent years. Diverse physiochemical properties and other attributes including good biocompatibility, unique optical properties, low cost, eco-friendliness, and abundant functional groups have made CQDs amendable for research. Turning CQDs into catalysts to perform organic reactions, has been under spotlight in recent yerars [1]. Our goal in this project is using doped CQD with various biomolecules including amino acids, to perform transamidation reactions. In the present study, amino acid-doped carbon quantum dots were synthesized, using a bottom-up hydrothermal method. The catalysts were characterized by various analytical tools including FTIR, XRD, NMR, and gel electrophoresis. The synthesized CQD were then used in various transamidation reactions. Finally, the products are confirmed by ^{13}C NMR and ^{1}H NMR spectroscopy (**Scheme**).

Scheme: Transamidation reaction by CQD nano catalysis.

References

[1] Hasani, M.; Kalhor, H. R. Enzyme-Inspired Lysine-Modified Carbon Quantum Dots Performing Carbonylation Using Urea and a Cascade Reaction for Synthesizing 2-Benzoxazolinone. *ACS Catal.* **2021**, *11* (17), 10778–10788. https://doi.org/10.1021/acscatal.1c01276.

Synthesis and investigation of structural and optical characterizations of coordination polymers arylenediimides with metal cations

Seyyed Abolfazl Seyyedi*, Mohammad Reza Zamanloo and Gholamhasan Imanzadeh

Department of Applied Chemistry, University of Mohaghegh Ardabili, P.O. Box 56199-11367, Ardabil, Iran, sa.seyyedi95@gmail.com, mrzamanloo@uma.ac.ir

Keywords: Arylenediimides, Photochemical activity, High redox activity, Coordination polymer

Arylenediimides, such as naphthalene diimides (NDIs) and pyromellitic diimides (PMDIs), have received much attention due to their unique chemical and physical properties as a class of organic dyes with high photochemical activity and high redox activity [1]. Also, arylenediimids considerable interest attributing to their photoinduced electron transfer to form stable radical anions upon irradiation in the presence of electron donors [2]. The overall aim of this research is the synthesis and investigation of structural features and optical properties of coordination polymers based on azo-containing arylenediimid ligands with metal cations. The structure of the ligands were confirmed by IR, NMR, Mass spectra. These coordination polymers characterized by single-crystal X-ray diffraction, elemental analyses, IR spectroscopy, powder X-ray diffraction, and theromgravimetric analysis. Because of the presence of electron-deficient NDI and PMDI moieties, they exhibit reversible photochromic properties [3].

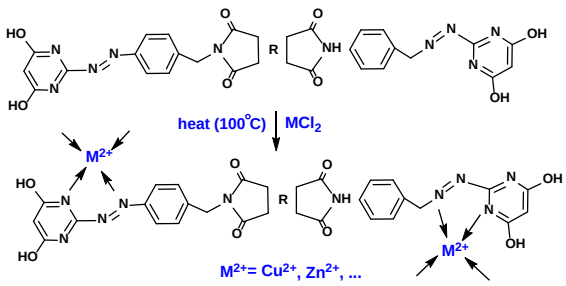

Scheme: Schematic diagram for the syntheses of coordination polymers.

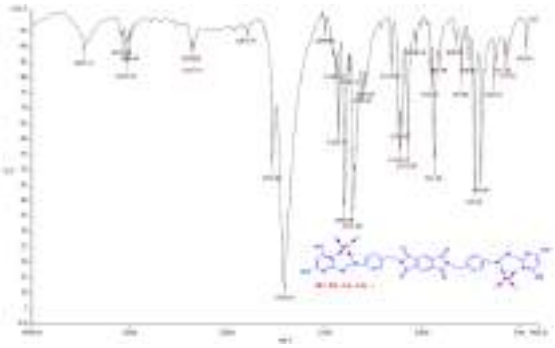

Fig. FT-IR spectrum of pure coordination polymers

References

[1] Jian-Jun, L.; Teng, L.; Chang-Cang, H. Synthesis and characterization of a photochromic magnesium(II) coordination polymer based on a naphthalene diimide ligand. *Acta Cryst* 2017, C73, 437–441.

[2] Jian-Jun, L.; Yao W.; Yu-Jian, H.; Mei-Jin, L.; Chang-Cang, H.; Wen-Xin, D. A photochromic naphthalene diimide coordination network sensitized by polyoxometalates. *Dalton Trans* 2014, 43, 17908–17911.

[3] Jian-Jun, L.; Shu-Biao, X.; Dan, L.; Juying, H.; Hongbo, S.; Fei-Xiang, C. Multifunctional naphthalene diimide-based coordination polymers: Photochromism and solventchromism. *Dyes and Pigments* 2020, 177, 1-7.

A new magnetic covalent organic framework: catalytic application for the preparation of sulfonamide-linked pyridines

Meysam Yarie*, Amir Masoud Hosseini and Morteza Torabi

Organic Chemistry Laboratory, Faculty of Chemistry, University of Bu-Ali Sina, Hamedan, Iran, myarie.5266@gmail.com, hosseiniamirmasoud@yahoo.com

Keywords: Covalent organic frameworks, Pyridine, Sulfonamide

Covalent organic frameworks (COFs) emerging as a new class of porous and crystalline polymers linked by strong covalent bonds, have received considerable attention for their great potential applications in gas storage and separation, catalysis, smart sensors, optoelectronics, energy storage, among others. The high porosity, functional versatility, easy modification and outstanding stability of COFs make them ideal materials for catalysis applications [1]. Pyridine, as the heart of heterocycle chemistry, has been used in various areas such as catalysis, coordination chemistry, supramolecular structures, materials and surfaces engineering, and polymer science [2]. At the same time, heterocyclic compounds with sulfonamide groups ($-S\,(=O)_2-NH-$) are considered important chemical compounds in terms of chemical and biological activities. These compounds have a crucial functionality because of theirs wide variety of biological and pharmacological activities such as anticancer, carbonic anhydrase inhibitory, antibacterial, antitumor, anti-inflammatory and antiprotozoal activities [3]. Therefore, our goal was focused on the preparation of heterocyclic compounds, consisting pyridine fragment and the sulfonamide group by using a new magnetic COF as catalyst (**Scheme 1**).

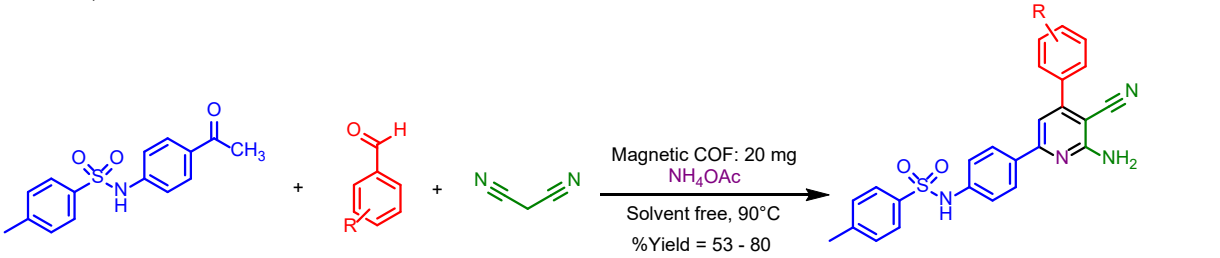

Scheme 1: Catalytic application of a new magnetic COF for the preparation of sulfonamide-linked pyridines

References

[1] Hu, H.; Yan, Q.; Ge, R.; Gao, Y. Covalent organic framework as heterogeneous catalysts. *Chinese journal of catalysis* 2018, *39*, 1167-1179.

[2] Torabi, M.; Yarie, M.; Zolfigol, M. A.; Rouhani, S.; Azizi, S.; Olomola, T. O.; Maaza, M.; Msagati, T. A. M. Synthesis of new pyridines with sulfonamide moiety via a cooperative vinylogous anomeric-based oxidation mechanism in the presence of a novel quinoline-based dendrimer-like ionic liquid. *RSC Advances* 2021, *11*, 31- 43.

[3] Allabergenova, S. M.; Yakubov, U. M.; Tojiboev, A. G.; Turgunov, K. K.; Ashurov, J. M.; Elmuradov, B. Z. Synthesis, crystal structure and hirshfeld surface analysis of 3-butyl-4-oxo-3,4-dihydroquinazoline-6-sulfonamide. *Chemical data collections* 2022, *41*, 100926.

Quantum Dot@Hydrogen-Bonded Organic Framework for Highly Efficient Fluorescent Sensing of metronidazole

Alieh Moeinipour, Abbas Afkhami*

Analytical Chemistry Laboratory, Faculty of Chemistry, University of Bu-Ali Sina University, Hamedan, Iran, aliehmoeinipour@gmail.com, abbas.afkhami@gmail.com

Keywords: Quantum dots, Hydrogen bonded organic framework, Metronidazole

The structure of n,n′-diethyl-p-phenylenediamine quantum dots prepared via solvent-free methods was studied. Then, core-shell structure of this QD was synthesized by hydrogen bonded organic framework. NMR characterization method demonstrate HOF structure. In addition, XRD and FE-SEM characterization methods confirm which it is a hollow cubic tube crystal structure that it has covered the quantum dot structure. The quantum dot structure showed green color under ultraviolet light. It is excited at 335 nm and emitted in the range of 480-650 nm and maximum wavelength 514. The fluorescence intensity of the QD@HOF could be quenched by the addition of a small amount of metronidazole aqueous solution to %98.

References

[1] Bin Wang, Ru He, Lin-Hua Xie, Zu-Jin Lin, Xin Zhang, Jing Wang, Hongliang Huang, Zhangjing Zhang, Kirk S. Schanze, Jian Zhang, Shengchang Xiang, and Banglin Chen, A Microporous Hydrogen-Bonded Organic Framework for Highly Efficient Turn-Up Fluorescent Sensing of Aniline, *J. Am. Chem. Soc.* 2020, 142, 28, 12478–12485.

[2] Ling Xu, Kunji Chen, Jianming Zhu, Hongming Chen, Hongbin Huang, Jun Xu, Xinfan Huang, Core-shell structure and quantum effect of CdSe/HgSe/CdSe quantum dot quantum well, *Superlattices and Microstructures.* 2001, *27*, 67-72.

A facile one-pot, solvent-free synthesis of novel pyrazolone-1,3-thiazolidine hybrids

Zahra Dehghani*, Farough Nasiri and Jaber Salehzadeh

Department of Applied Chemistry, University of Mohaghegh Ardabili, P.O. Box 56199-11367, Ardabil, Iran, zaaahraaadehghani@gmail.com.

Keywords: Pyrazolone-1,3-thiazolidine, Hybrid molecules, Green synthesis, One pot reaction.

Pyrazolone scaffolds are important heterocycles that constitute an interesting core for the construction of various biologically active molecules. Pyrazolones have attracted the attention of researchers due to possessing a variety of applications in the field of corrosion, dyeing, optical as well as in biology, including antimicrobial, anti-inflammatory, antioxidant, antitumor, and anti-cancer. Also, in medicinal chemistry, metal complexes of pyrazolones have received much attention in recent years [1-3]. These features have led to the design and development of new pyrazolone or sulfur-containing heterocycles with similar properties. In this study, an efficient one-pot, solvent-free synthesis of pyrazolone-1,3-thiazolidine hybrids from the reaction between pyrazolones and *α*-chloroacetaldehyde in the presence of phenyl isothiocyanate is reported. This reaction was carried out in the presence of triethylamine at room temperature (**Scheme 1**).

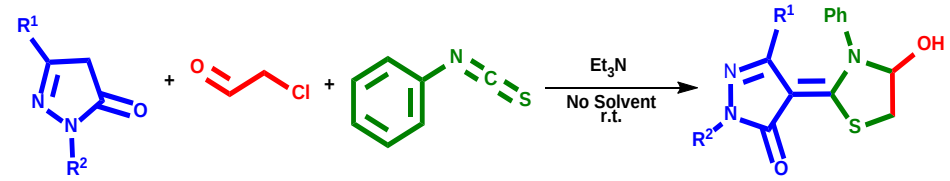

R^1= Me, Ph, Pr, CH_2CO_2Me,CO_2Me, CO_2Et;
R^2=H, Ph

Scheme1: One-pot reaction for the synthesis of pyrazolone-1,3-thiazolidine hybrids.

References

[1] Adhikari, S.; Singh, M.; Sharma, P.; Arora, S. Pyrazolones as a potential anti-cancer scaffold: Recent trends and future perspectives. *J. Appl. Pharm. Sci*. 2021,*11*, 026-037.

[2] You, H.; Su, X.; Su, G. Novel thiazole-pyrazolone hybrids as potent ACE inhibitors and their cardioprotective effect on isoproterenol-induced myocardial infarction. *Arch. Pharm*, 2020, *353*, e200- 0140.

[3] Salehzadeh, J.; Nasiri, F.A versatile solvent‐free synthesis of novel pyrazolone‐1,3‐dithiolan and pyrazolone‐1,3‐dithiole hybrids, *Res. Chem. Intermed.* 2023, *49*, 1-17.

A study of E/Z isomerism of some aryl-hydrazones synthesized by linking aryldiazonium chlorides to 6-butyl-4-hydroxyquinoline-2(1*H*)-one

Fatemeh Ashouri Mirsadeghi, Enayatollah Moradi Rufchahi*

Department of Chemistry, Faculty of Science, Islamic Azad University, Lahijan Branch, Lahijan, Iran, fatemeh.ashouri.mirsadeghi@gmail.com, moradierufchahi1350@gmail.com

Keywords: 4-Hydroxyquinolin-2(1H)-one, Azo-hydrazone tautomerism, DFT, Solvatochromism

A series of 3-(2-arylhydrazono)-quinolin-2,4-diones were synthesized by the reaction of aryldiazonium chlorides with 6-butyl-4-hydroxyquinolin-2(1*H*)-one dissolved in water containing equimolar amount of sodium hydroxide. According to ^{1}H NMR and Ultraviolet-visible results, there are two kinds of intramolecular hydrogen bonds in these synthesized aryl-hydrazones which enable the compounds to be rotated about the hydrazone C=N bond and lead to a reversible isomerization between their E and Z configurations. The isomers populations and the rotation phenomenon can be controlled by changing the polarity of the solvents. The results reveal that a decrease in solvent polarity (upon changing the solvent from deuterated DMSO to $CDCl_3$) shifts the isomeric balance to Z-geometrical form and substantially increase the E/Z ratios. The results obtained from density functional theory (DFT) calculations at B3LYP/6-31G(d) level of theory, demonstrated that the hydrazone tautomeric forms are more stable with the lowest total energy and showed a good agreement with the experimental findings in both gas and solution states.

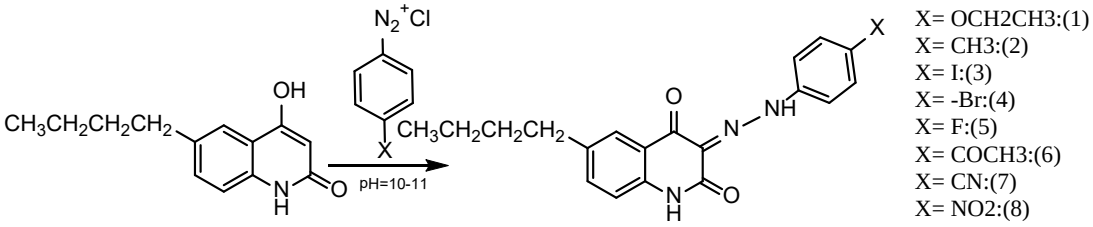

Scheme: Synthetic rout to 3-(2-arylhydrazono)-quinolin-2,4-diones

References

[1] MoradiRufchahi, E.O.; Ghanadzadeh Gilani, A. Synthesis, characterization and spectroscopic properties of some new azo disperse dyes derived from 4-hydroxybenzo[h]quinolin-2-(1H)-one as a new synthesized enol type coupling component. *Dyes Pigm.*2012, 96, 632–638.

[2] MoradiRufchahi, E.O.; Pouramir, H.; Yazdanbakhsh, M.R.; Bagheri, M.; Rassa, M. Novel azo dyes derived from 8-methyl-4-hydroxyl-2-quinolone: Synthesis, UV–vis studies and biological activity. *Chin. Chem. Lett.* 2013, 24, 425–428.

[3] MoradiRufchahi, E.O.; Yousefi, H.; Mohammadinia, M.6-Butyl-4-hydroxyquinolin-2-(1*H*)-one as an enol type coupling component for the synthesis of some new azo disperse dyes. *J. Mol. Liq.* 2014, 199, 393 400.

Preparation of RGO Aerogel/TEPA/ZnO-CuO catalyst and its use in Knoevenagel condensation

Fatemeh Golmiri*, Pouya Taheri, Mahmood Tajbakhsh and Hamid Emadi

Department of Organic Chemistry, Faculty of Chemistry, University of Mazandaran, Babolsar, Iran, fatemehgolmiri76@gmail.com

Keywords: Aerogels, Reduced graphene oxide aerogels, 4h-Benzopyran.

Aerogels, a unique class of materials known for their high porosity and low density, have found application as catalysts in various organic reactions. One particular area where aerogels have shown promise is in asymmetric direct aldol reactions in aqueous solutions [1]. Aerogels also exhibit outstanding capabilities for the sorption of spills and gases [2], being useful in selective captures for catalysis and analytical purposes and remediation. Herein, First, reduced graphene oxide aerogel was synthesized hydrothermally, and then tetraethylene pentamine, zinc and copper nanoparticles (precipitated by co-precipitation) were added to the RGO Aerogel/TEPA/ZnO-CuO nanocomposite. Produced nanocomposites showed significant catalytic activity in the synthesis of tetrahydrobenzopyran compounds using benzaldehyde, dimedone, and malononitrile derivatives in ethanol solvent at reflux condition. 4H-benzo[b]pyrans represent one of the most important classes of heterocyclic compounds that have substantial pharmaceutical and biological activities. These compounds are used as anticancer agents [3], for example, the 4H-benzo[b]pyran derivative, topotecan, which is an inhibitor of topoisomerase I.

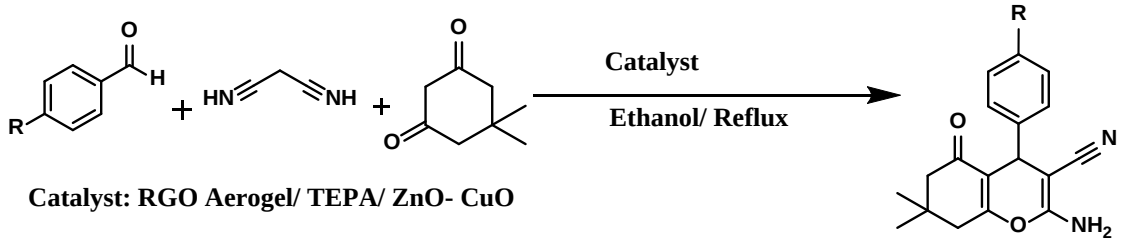

Catalyst: RGO Aerogel/ TEPA/ ZnO- CuO

Scheme: Synthesis of 4H-Benzopyran derivatives using RGO Aerogel/ TEPA/ZnO-CuO

References

[1] Ricci A, Bernardi L, Gioia C, Vierucci S, Robitzer M, Quignard F. Chitosan aerogel: A recyclable, heterogeneous organocatalyst for the asymmetric direct aldol reaction in water. *Chem. Comm*. 2010; 46(34): 6288-90.

[2] Keshavarz L, Ghaani MR, MacElroy JD, English NJ. A comprehensive review on the application of aerogels in CO2-adsorption: Materials and characterisation. *Chem. Eng. J*. 2021 May 15;412:128604.

[3] Roy R, Rakshit S, Bhowmik T, Khan S, Ghatak A, Bhar S. Substituted 3-E-styryl-2 H-chromenes and 3-E-styryl-2 H-thiochromenes: synthesis, photophysical studies, anticancer activity, and exploration to tricyclic benzopyran skeleton. *J. Org. Chem.* 2014; 79(14): 6603–14.

Synthesis of new spiropyrans including biological section using modification of Ti-based MOFs with acetic acid

Zahra Torkashvand, Hassan Sepehrmansourie and Mohammad Ali Zolfigol*

Department of Organic Chemistry, Faculty of Chemistry, Bu-Ali Sina University, Hamedan 6517838683, Iran, shakilatorkashvand@gmail.com, zolfi@basu.ac.ir & mzolfigol@yahoo.com.

Keywords: Metal-organic frameworks (MOFs), Ti-based MOF, Porous catalyst, Spiropyran.

Metal-organic frameworks (MOFs) are architectural structures consisting of the coupling of a metal group and an organic group. These structures are composed of metal elements that are ionic inside or outside their core and organic ligands that coordinate with metals [1]. MOFs are used in various fields such as storage and transport of gases, separation of materials, removal of pollutants from the environment, synthetic catalysis and pharmaceuticals [2]. Spiropyrans are a class of organic compounds that contain two or more rings fused together at a single atom. One of the remarkable features of spiropyrans is their three-dimensional shape, which can provide structural rigidity and influence their chemical properties [3]. In this report, based on the characteristics of MOFs, especially the Ti-based MOFs, the aim is design and synthesize porous catalyst. The catalytic activity of (MOF-Ti)/TCT/Im/$[CH_2CO_2H]$Br in the preparation of spiropyrans was investigated as an important group of organic compounds with biological properties (**Scheme 1**).

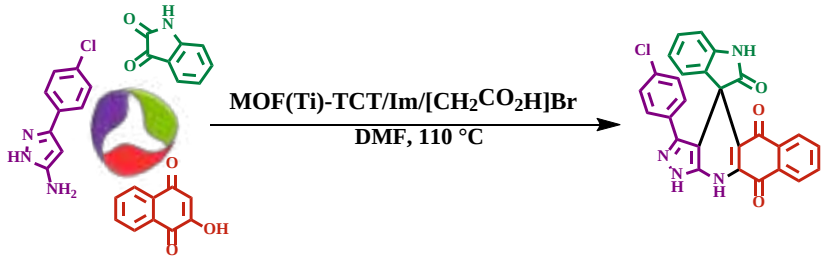

Scheme 1: Preparation of new spiropyrans using Ti-based MOFs functionalized with acetic acid.

References

[1] James, S. L. Metal-organic frameworks. *Chemical Society Reviews* 2003, *32*, 276-288.
[2] Zhou, H. C.; Long, J. R. Yaghi, O. M. Introduction to metal–organic frameworks. *Chemical Reviews* 2012, *112*, 673-674.
[3] Saragi, T. P.; Spehr, T.; Siebert, A.; Fuhrmann-Lieker, T.; Salbeck, J. Spiro compounds for organic optoelectronics. *Chemical Reviews* 2007, *107*, 1011-1065.

$MgCu_2Al_2O_6$: A Simple and Efficient Metal Oxide Nanocatalyst for the Synthesis of 1,4-Dihydropyridine

Marzieh Mahmoodi Keshtiban[a*], Abbas Nikoo[b] and Bakhshali Massoumi[a]

a) Department of Chemistry, Payame Noor University, Tabriz, Iran, b_massoumi@pnu.ac.ir, mahmoodimarzieh99@gmail.com
b) Department of Organic Chemistry, Faculty of Chemistry, Urmia University, Urmia, Iran, a.nikoo@urmia.ac.ir

Keywords: Sol-Gel auto-combustion, One-pot synthesis, 1,4-Dihydropyridine, Metal oxide nanocatalyst

In modern synthetic organic chemistry, one-pot multi-component reactions (MCR) are a powerful synthetic tool that produces complex heterocyclic molecules [1]. Several methods with various catalysts and in the different reaction conditions for the synthesis of 1,4-dihydropyridine have been reported in scientific research articles such as $La_{1-x}Sr_xMn_{1-y}Zn_yO_3$ [2]. $MgCu_2Al_2O_6$ heterogeneous nanocatalyst was synthesized for the first time by sol–gel auto-combustion method with a simple, cheap and non-toxic preparation method. This solid nanocatalyst does not lose its effect in the long term and is stable and does not deteriorate under the influence of heat, air and moisture. Next, by one-pot reaction, 1,4-DHP derivatives were prepared in green solvent water at 80 °C with high efficiency and short duration with excellent yield (80-95) %. It is worth noting that the catalytic property was maintained in five consecutive reactions, and the $MgCu_2Al_2O_6$ nanocatalyst can be separated after the end of the reaction and reused for next reaction. (**Scheme**). The solid catalyst was confirmed by XRD, BET, FTIR, FESEM and EDX, and the substituted 1,4-dihydropyridines were characterized by melting point, ^1H and ^{13}C NMR.

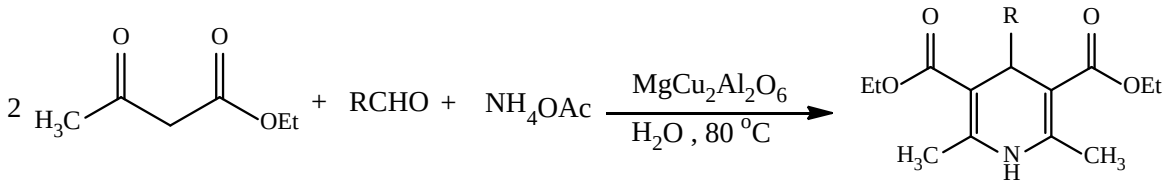

Scheme: Synthesis of 1,4-DHP derivatives by $MgCu_2Al_2O_6$ as metal oxide nanocatalyst.

References

[1] Kurniawan, Y. S.; Priyangga, K. T. A.; Krisbiantoro, P. A.; Imawan, A. C. Green Chemistry Influences in Organic Synthesis: A Review. *J. Multidiscip. Appl. Nat. Sci.* 2021, *1(1)*, 1-12.
[2] Khaled, A.; Stiti, M. Z.; Habila, T.; Ferkhi, M.; Pirotte, B.; Pireaux, J. J.; Khelili, S. Synthesis and characterization of $La_{1-x}Sr_xMn_{1-y}ZnyO_3$ perovskites as an efficient and recoverable catalyst for the Hantzsch reaction. *J. Chem. Sci.* 2022, *134(3)*, 1-14.

Ultrasmall Platinum Nanoparticles Supported Inside the PMO-IL for Aerobic Oxidation of Unactivated Alcohols in Water

Masoumeh Hatami[a], Zahra Naderi[a] and Babak Karimi[a,b*]

a) Department of Chemistry, Institute for Advanced Studies in Basic Sciences (IASBS), Prof. Sobouti Boulevard, Zanjan 45137-66731, Iran, masomhatami@iasbs.ac.ir, karimi@iasbs.ac.ir
b) Research Center for Basic Sciences & Modern Technologies (RBST), Institute for Advanced Studies in Basic Sciences (IASBS), Prof. Sobouti Boulevard, Zanjan 45137-66731, Iran.

Keywords: Periodic Mesoporous Organosilica, Ionic liquids, Oxidation of Alcohols, Nanoparticles, Platinum

A novel Pt nanoparticle supported on periodic mesoporous organosilica with imidazolium framework (PtNPs@PMO-IL) was prepared. Ultrasmall Pt nanoparticles (<1.5 nm) allowed the formation of a catalyst system with significant activity and recyclability. The catalyst exhibited high activity in the oxidation of unactivated primary alcohols and sterically encumbered secondary aliphatic alcohols. which remain challenging substrates for many catalytic aerobic protocols **(Scheme)** [1,2].

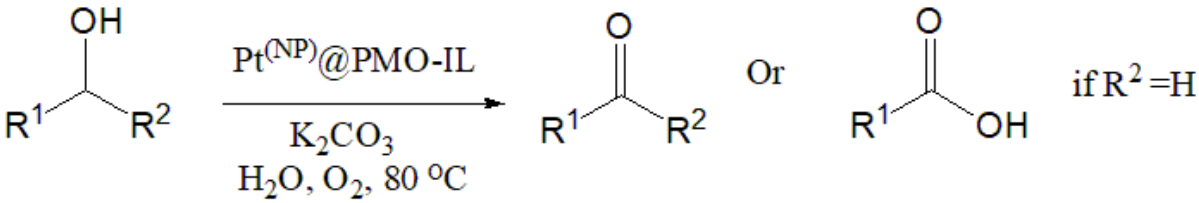

Scheme: Aerobic Oxidation of Alcohols with PtNPs@PMO-IL

References

1. Karimi, B.; Zamani, A.; Abedi, S.; Clark, J. H., Aerobic oxidation of alcohols using various types of immobilized palladium catalyst: the synergistic role of functionalized ligands, morphology of support, and solvent in generating and stabilizing nanoparticles. *Green Chem.* **2009,** *11* (1), 109-119.
2. Karimi, B.; Naderi, Z.; Khorasani, M.; Mirzaei, H. M.; Vali, H., Ultrasmall platinum nanoparticles supported inside the nanospaces of periodic mesoporous organosilica with an imidazolium network: an efficient catalyst for the aerobic oxidation of unactivated alcohols in water. *ChemCatChem* **2016,** *8* (5), 906-910.

Application of N, S-doped ordered mesoporous carbon as a solid acid-base bifunctional catalyst in Biginelli reaction

Nahid Moghaddam[a], Babak Karimi[a,b]*

a) Department of Chemistry, Institute for Advanced Studies in Basic Sciences (IASBS), Prof. Sobouti Boulevard, Zanjan 45137-66731, Iran, Nahidmoghaddam@iasbs.ac.ir, karimi@iasbs.ac.ir
b) Research Center for Basic Sciences & Modern Technologies (RBST), Institute for Advanced Studies in Basic Sciences (IASBS), Prof. Sobouti Boulevard, Zanjan 45137-66731, Iran.

Keywords: Ordered mesoporous carbon, Nanocasting, Ionic liquids, Acid-base bifunctional catalyst, Biginelli reaction

A novel bifunctional acid-base ordered mesoporous carbon, denoted "Ionic liquid derived Bimodal cubic Ordered Mesoporous Carbon" (IBOMC), was prepared using a nanocasting protocol with KIT-6 as a hard template and a mixture of an imidazolium-based ionic liquid as the main organic precursor. The coexistence of acidic and basic sites on this carbocatalyst made it suitable for one-pot cascade reactions that require both acid and base, such as the Biginelli reaction. The dual acid-base activity of our catalyst was verified in the Biginelli reaction, which requires basic functional groups for deprotonation of ethyl acetoacetate and also acidic sites for activation of aldehydes and aldol condensation to synthesize the Biginelli product [1] (**Scheme**).

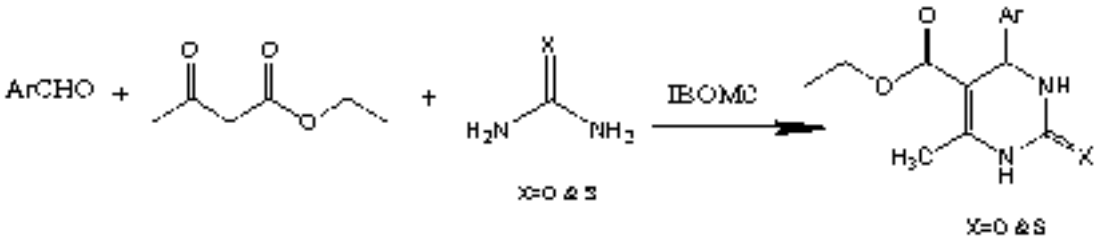

Scheme: Biginelli reaction.

References

[1] Veisi, H. H.; Akbari, M.; Karimi, B.; Vali, H.; Luque, R. "One-pot acid–base catalysed tandem reactions using a bimodal N, S-doped cubic mesoporous carbon." *Green Chem.*, **2023**, *25*, 4076-4089.

Photocatalytic conversion of carbon dioxide to methanol in the presence of metal-organic framework nanocomposite (UiO-66/ZIF-67)

Mahtab Abareshi, Mahdi Niknam Shahrak*

Department of Chemical Engineering, Quchan University of Technology, Quchan, Iran, abareshimahtab@gmail.com, m.niknam.sh@qiet.ac.ir

Keywords: UiO-66, Photocatalyst, Methanol, ZIF-67

The continuous increase in the combustion of hydrocarbon fuels along with the high levels of carbon dioxide emission has led to the global energy crisis and environmental changes. Photocatalyst-based methods are an effective way to deal with this energy and environmental crisis. Solar energy, which is a clean and renewable energy, is a very desirable path for photocatalytic conversion of CO_2 into value-added products to deal with energy and environmental problems. Synthesis of various products such as: CH_4, CO, EtOH, CH_3OH and so on through the photocatalytic reduction of CO_2 has been expanded. Among these products, methanol is one of the most important and widely used chemicals that are widely used in industry and in daily life [1,2]. In this paper, novel metal-organic framework nanocomposite (UiO-66/ZIF-67) will be investigated for CO_2 reduction to methanol under ultraviolet/visible (UV/Vis) light irradiation at room temperature. UiO-66 & ZIF-67 have been used due to their suitable specific surface area, high thermal and chemical stability. The trueness of the nanocomposite synthesis was determined using XRD, FT-IR, FESEM, TEM, N_2 adsorption-desorption, EDS, PL spectroscopy and DRS analyses. The area obtained from the analysis BET is 647.83 ($m^2.g^{-1}$), which shows the efficiency of the catalyst. Finally, using the desired nanocomposite, photocatalytic tests were performed under ultraviolet irradiation and in different environments, and the results are as follows **(table).**

Table: Methanol efficiency of photocatalytic test($\mu mol.g^{-1}.h^{-1}$)

Photocatalyst	DI water	NaOH	Na_2SO_3
UiO-66/ZIF-67	848.93	873.90	610.79

References

[1] Gajanan Y. Shinde, Abhishek S. Mote and Manoj B. Gawande. Recent Advances of Photocatalytic Hydrogenation of CO_2 to Methanol. *Catalysts* 2022, 12, 94.

[2] Muhammad T, Rana Muhammad N. Javed, Amani Al-Othman, Fares Al. The novel contribution of non-noble metal catalysts for intensified carbon dioxide hydrogenation: Recent challenges and opportunities. *J. Enconman*. 2023.116755

The one-pot synthesis of 2-(3-(2-imino-3-methyl-5-oxoimidazolidin-4-yl)-2-oxoindolin-3-yl)malononitrile using SiO_2-Pr-SO_3H under solvent-free conditions

Nikoo Shamkhali and Ghodsi Mohammadi Ziarani*

Department of Organic Chemistry, Faculty of Chemistry, Alzahra University, Tehran, Iran, nikoosh1378@gmail.com, gmahammadi@alzahra.ac.ir

Keywords: Multicomponent reactions, Heterogenous catalyst, SiO_2-Pr-SO_3H, Green chemistry

Nowadays, due to growing demands for green, and efficient chemical processes, the chemical reactions under solvent-free conditions have become very important. In addition, the use of heterogeneous nanocatalysts makes this process easier and more economical due to their easy separation from the reaction mixture, reusability, and eco-friendly conditions.

In this study, SiO_2-Pr-SO_3H was used as a highly efficient heterogeneous solid acid catalyst [1] in a one-pot multicomponent reaction between isatin, malononitrile, and creatinine [2] for the synthesis of 2-(3-(2-imino-3-methyl-5-oxoimidazolidin-4-yl)-2-oxoindolin-3-yl)malononitrile under the solvent-free and mild condition in a short reaction time and high yield (98%) (**Scheme 1**).

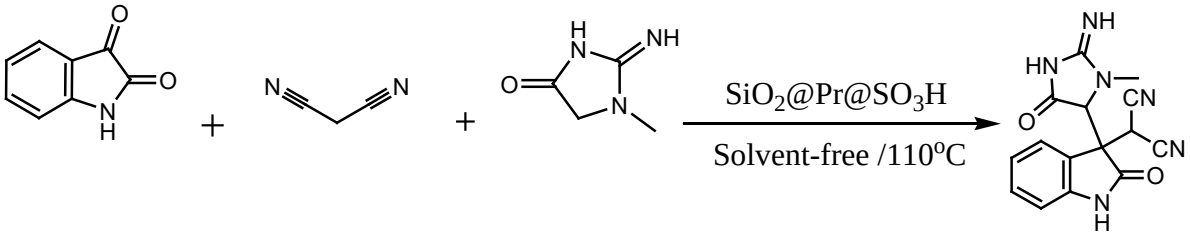

Scheme 1: Multicomponent reaction of isatin, malononitrile, and creatinine with SiO_2-Pr-SO_3H

References

[1] Mohammadi Ziarani, G. ; Badiei, A. R.; Azizi, M. The one-pot synthesis of 14-aryl-14H-dibenzo [a, j] xanthene derivatives using sulfonic acid functionalized silica (SiO2-Pr-SO3H) under solvent-free conditions. *Sci. Iran.* 2011, *18*(3), 453-457.

[2] Parthasarathy, K.; Ponpandian, T.; Praveen, C. Gold-catalyzed addition reaction between creatinine and isatin: A sustainable and green chemistry approach for the diastereoselective synthesis of 3-substituted-3-hydroxyisatins. *Chinese J. Catal.* 2017,*38*(5), 775-783.

One-pot synthesis of novel polycyclic quinoline derivatives *via* Knoevenagel condensation-Michael addition and cyclization reaction

Mostafa Kiamehr [*], **Samane Haddadi**

Department of Chemistry, Faculty of Science, University of Qom, Ghadir Blvd, P.O. Box 37146-6611, Qom, Iran, mkiamehr@yahoo.com, m.kiamehr@qom.ac.ir, smanehaddadi7574@gmail.com

Keywords: Knoevenagel condensation, Michael addition, Cyclization reaction, Quinoline derivatives

Quinoline skeleton is an important part in natural compounds with a wide spectrum of biological and medicinal activities. Due to the fact that quinoline and its derivatives show excellent biological properties, it has received a lot of attention in recent years. The chemistry of quinoline is particular interest due to their potential applications in medicinal chemistry as antimicrobial, analgesic, antitumor and therapeutic agents [1-2]. In this research, we succeeded in synthesizing of new heterocyclic compounds that are derivatives of benzoyl-3-tetrazolo[1,5-a]quinoline through one-pot Knoevenagel condensation, Michael addition and cyclization reactions (**Scheme**).

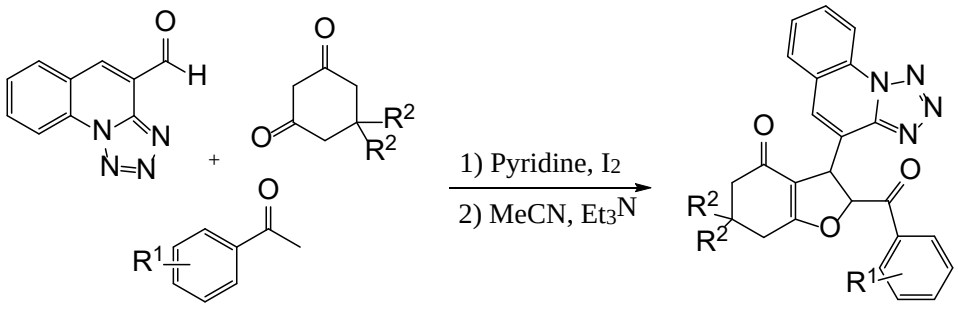

Scheme: One-pot synthesis of novel polycyclic quinoline derivatives.

References

[1] Dib, M.; Ouchetto, H.; Ouchetto, K.; Hafid, A.; & Khouili, M. Recent developments of quinoline derivatives and their potential biological activities. *Curr. Org. Synth.* 2021, *18*(3), 248-269.

[2] Beteck, R. M.; Jordaan, A.; Seldon, R.; Laming, D.; Hoppe, H. C.; Warner, D. F.; & Khanye, S. D. Easy-to-access quinolone derivatives exhibiting antibacterial and anti-parasitic activities. *Molecules* 2021, *26*(4), 1141.

Preparation of Ni-Fe layered double hydroxide/ graphitic carbon nitride nanocomposite for enhanced sonocatalytic degradation of chloramphenicole

Omid Khanbeiki, Shahram Ghasemimir* and Hamid Emadi

Faculty of Chemistry, University of Mazandaran, Postal code 47416-95447, Babolsar, Iran, omidkhanbeikiii@gmail.com, sghasemimir@yahoo.com, sghasemi@umz.ac.ir.

Keywords: Sonocatalytic degradation, Layered double hydroxide, Graphitic carbon nitride, Chloramphenicole

Pharmaceuticals and personal care products (PPCPs) are becoming a growing concern in aquatic environments due to their impact on human health and the environment. Chloramphenicol (CAP) [1] is a commonly used antibiotic that is difficult to remove from water sources and can lead to drug-resistant bacteria. Advanced Oxidation Processes (AOPs) [2] and sonochemistry are effective methods for removing pollutants from water, and Layered Double Hydroxide (LDH) has excellent adsorption properties for heavy metal ions. Layered metal-free graphitic carbon nitride g-C_3N_4 [3] has potential as a sonocatalyst for degrading pollutants, but its efficiency can be improved by loading heteroatoms or creating heterojunctions with other semiconductors. The NiFe LDH/g-C_3N_4 double layered hydroxide nanocomposite shows promise for efficient sonocatalytic degradation of pharmaceutical pollutants.

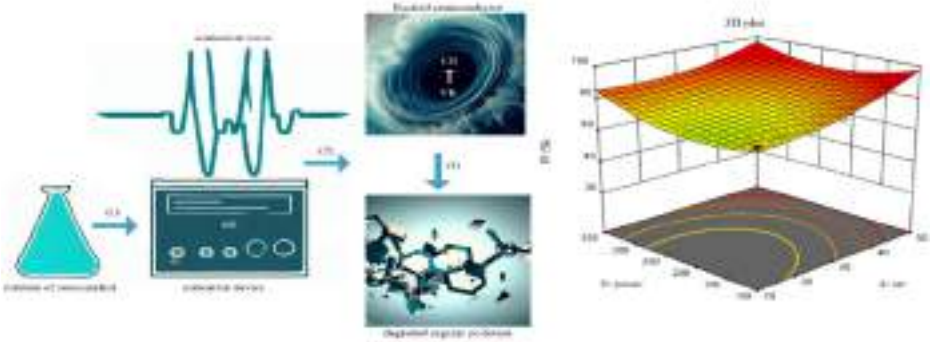

References:

[1] Xu, Q., Song, Z., Ji, S., Xu, G., Shi, W., & Shen, L. The photocatalytic degradation of chloramphenicol with electrospun $Bi_2O_2CO_3$-poly (ethylene oxide) nanofibers: the synthesis of crosslinked polymer, degradation kinetics, mechanism and cytotoxicity. *RSC advances*, 2019, 9(51), 29917-29926.

[2] Miklos, D. B., Remy, C., Jekel, M., Linden, K. G., Drewes, J. E., & Hübner, U. Evaluation of advanced oxidation processes for water and wastewater treatment–A critical review. *Water Research*, 2018, *139*, 118-131.

[3] Guo, Y., Sun, X., Chen, Q., Liu, Y., Lou, X., Zhang, L., ... & Guan, J. Photocatalytic Applications of g-C_3N_4 Based on Bibliometric Analysis. *Catalysts*, 2022, *12*(9), 1017.

Preparation of Ni-Fe layered double hydroxide/ graphitic carbon nitride nanocomposite for enhanced sonocatalytic degradation of tetracycline hydrochloride

Omid Khanbeiki, Shahram Ghasemimir* and Hamid Emadi

Faculty of Chemistry, University of Mazandaran, Postal code 47416-95447, Babolsar, Iran, omidkhanbeikiii@gmail.com, sghasemimir@yahoo.com, sghasemi@umz.ac.ir

Keywords: Sonocatalytic degradation, Layered double hydroxide, Graphitic carbon nitride, Tetracycline hydrochloride

Pharmaceutical residues enter the environment and pose risks. Antibiotics are widely used in human and animal production. Tetracycline (TCH) is commonly used but its residues are difficult to remove. Advanced oxidation processes (AOPs) that generate hydroxyl radicals can remove organic pollutants in wastewater. Sonochemistry based on acoustic cavitation can also oxidize contaminants. Layered double hydroxides (LDH) like NiFe LDH have excellent adsorption properties and can remove heavy metals. Graphitic carbon nitride (g-C_3N_4) is a metal-free sonocatalyst but has low activity. Doping g-C_3N_4 with heteroatoms and combining it with LDH can improve its sonocatalytic activity. The nanolayer structure of NiFe LDH/g-C_3N_4 can generate more electron-hole pairs, improving degradation of TCH residues.

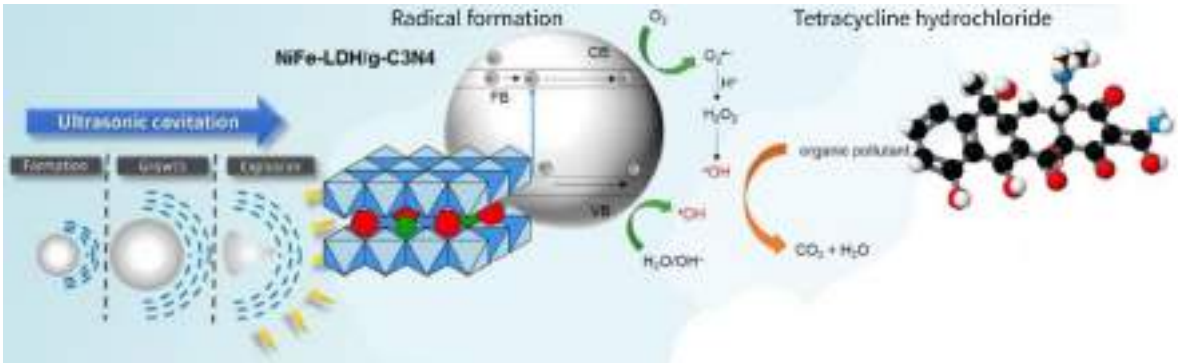

References

[1] L.L. Ji, Y.Q. Wan, S.R. Zheng, D.Q. Zhu, Adsorption of tetracycline and sulfamethoxazole on crop residue derived ashes: implication for the relative importance of black carbon to soil sorption, *Environ. Sci. Technol.* 45 (2011) 5580–5586.

[2] Miklos, D. B., Remy, C., Jekel, M., Linden, K. G., Drewes, J. E., & Hübner, U. (2018). Evaluation of advanced oxidation processes for water and wastewater treatment–A critical review. *Water Research*, *139*, 118-131

[3] Guo, Y., Sun, X., Chen, Q., Liu, Y., Lou, X., Zhang, L., ... & Guan, J. (2022). Photocatalytic Applications of g-C3N4 Based on Bibliometric Analysis. *Catalysts*, *12*(9), 1017.

Synthesis of 1- and 2-substituted tetrazole derivatives with dimethyl sulfoxide and acetic anhydride

Zeinab Motamedi and Nader Noroozi Pesyan*

Department of Organic Chemistry, Faculty of Chemistry, Urmia University, 57159 Urmia, Iran, zainabmotamdi@gmail.com

Keywords: Modified Swern oxidation, Tetrazole derivatives, Dimethyl Sulfoxide, Acetic anhydride.

Tetrazoles belong to the class of twice unsaturated fivemembered ring aromatic heterocycles, consisting of one carbon and four nitrogen atoms. They do not exist in nature. Interestingly, they have the highest number of nitrogen atoms among the stable heterocycles because pentazoles are highly explosive compounds even at low temperature. [1]. Tetrazole derivatives possess various biological activities due to the fact that a tetrazole functional group serves successfully as a metabolically stable replacement for carboxylic acid. In most cases, the methods of preparation and biological activity have been the point of interest. Tetrazoles have been widely used in various reactions such as: protection reactions, methylation, organometallic, thermolysis and photolysis, insertion reaction via nitrenes, and more [2]. In this research, the reaction of 5-aryl(aryloxy) tetrazole with dimethyl sulfoxide and acetic anhydride formed two kinds of products; 1- and 2-thiomethoxymethyl-5-aryl(aryloxy) tetrazoles via modified Swern reaction (**Scheme 1**).

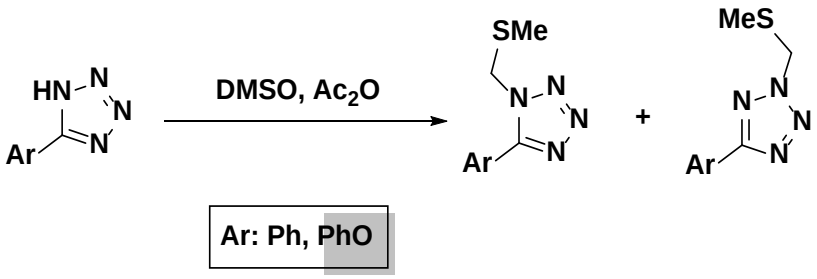

Scheme 1: Reaction of 5-aryl(aryloxy) tetrazole with dimethyl sulfoxide.

References

[1] Dabbagh H. A and Bagheri A. Thiomethoxymethylation of 5-aryloxytetrazoles via modified Swern Reagents. *J. Chem. Res.* 2005, 202–204.

[2] Neochoritis, C. G., Zhao, T., & Dömling, A. Tetrazoles via Multicomponent Reactions. *Chem. Rev*. 2019, 119, 3, 1970–2042.

Knoevenagel–Michael cyclocondensation in the Presence of Biochar Functionalized with Amine as Efficient Nano catalyst

Reza Hazbavi, Maryam Hajjami*

Organic Chemistry Laboratory, Faculty of Chemistry, Bu-Ali Sina University, Hamedan, Iran, hazbavireza37@gmail.com, m.hajjami@basu.ac.ir & mhajjami@yahoo.com.

Keywords: Multicomponent reactions, Knoevenagel–Michael, Cyclocondensation, Biochar, Walnut shells

Multicomponent reactions (MCRs) are referred to one-pot, convergent chemical reactions utilizing more than two starting materials, where final product retains significant portions of all starting materials. This advanced approach has emerged as an efficient, economical, and eco-friendly substitute for conventional sequential multi-step synthesis of various biologically active pharmacophores [1]. In this study, first biochar was produced from air-dried walnut shells [2]. Then, the surface of this nano-substrate was functionalized with amine. then Knoevenagel–Michael cyclocondensation of aryl aldehydes, malononitrile, and resorcinol were performed in the presence of biochar functionalized amine at room temperature in excellent yields and very short reaction times.

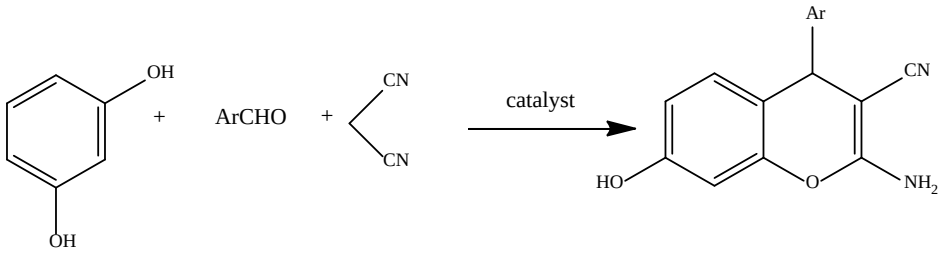

Scheme. Three-component reaction of resorcinol, aldehydes and malononitrile in the Presence of Biochar Functionalized with Amine as catalyst in reflux (water: ethanol) condition.

Reference

[1] Rashidi, S., Gholamian, F., Hajjami, M. Immobilization of Ni(II)-4-phenylthiosemicarbazide into functionalized MCM-41 as nano catalyst in synthesis of tetrahydrobenzo[b]pyran and 1,4-dihydropyrano[2,3-c]pyrazole. *J. Nanopart. Res.* 2023, 25, 102–120.

[2] Moradi, P., Hajjami, M. Magnetization of biochar nanoparticles as novel support for fabrication of organo nickel as selective, reusable and magnetic nanocatalyst in organic reactions. *New J. Chem.* 2021, 25, 2981-2994.

Curcumine-copper functionalized magnetic graphene oxide as an efficient nanocatalyst for one-pot synthesis of polyhydroquinoline derivatives

Alireza Gharehkhani, Maryam Hajjami*

Department of Organic Chemistry, Faculty of Chemistry, Bu-Ali Sina University, Hamedan, Iran, alireza.gharehkhani110@gmail.com & m.hajjami@basu.ac.ir

Keywords: Curcumine, Magnetic graphene oxide, Multicomponent reaction, Nanocatalys

Recently, the design of efficient and recoverable catalysts has become an important in organic reactions [1]. When the size of the support is decreased to the nanometer scale, the surface area is increased [2]. Among carbon nanomaterials, graphene oxide (GO) has been considered for use as support materials due to its tensile strength, large surface area, thermal stability, ease of recyclability. In the meantime, the use of naturally- derived ligands such as Curcumin extracted from natural resources has been taken into consideration. Curcumin, as a natural ligand, can be coordinated to metal ions. In this light, herein, an efficient protocol has been developed for design of Cu-curcumin functionalized magnetic graphene oxide nanoparticles ($GO@Fe_3O_4@SiO_2@Cur–Cu$) as nano catalyst for mild and green synthesis of polyhydroquinoline derivatives. The one-pot multicomponent reaction of aldehydes, ethylacetoacetate, ammonium acetate, and dimedone in the presence of $GO@Fe_3O_4@SiO_2@Cur–Cu$ was investigated at 100 °C in solvent-free condition. $GO@Fe_3O_4@SiO_2@Cur–Cu$ showed remarkable advantages in comparison with previous methods. Advantages of the method presented here include easy purification, reusability of the catalyst, green and mild procedure, and synthesis of new derivatives in high yields within short reaction time.

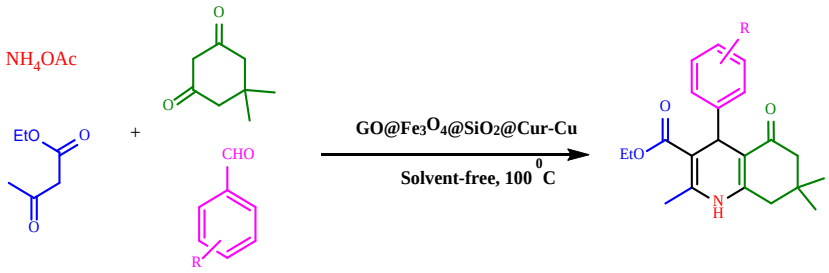

Scheme. General procedure for $GO@Fe_3O_4@SiO_2@Cur/Cu$-catalyzed synthesis of polyhydroquinoline derivatives

References

[1] Rashidi, S. Gholamian, F. Hajjami, M. Immobilization of Ni(II)-4-phenylthiosemicarbazide into functionalized MCM-41 as nano catalyst in synthesis of tetrahydrobenzo[b]pyran and 1,4-dihydropyrano[2,3-c]pyrazole. *J Nanopart. Res*, 2023, 25, 102.

[2] Ghafouri-Nejad, R. Hajjami, M. Nejat, R. Preparation and Characterization of Ni-Modified Graphene Oxide Complex as an Efficient Catalyst for the Synthesis of Sulfides via Reaction of Arylhalides with S 8 or Thiourea: Preparation of Ni-modified GO complex for the synthesis of sulfides *Appl. Organomet. Chem*., 2018, 32, 4248.

Covalent Triazine Framework as Catalyst Support for CO_2 Utilization

Mozhdeh Pourmansouri [a], **Mojtaba Khorasani** [a,b*]

a) Department of Chemistry, Institute for Advanced Studies in Basic Sciences (IASBS), No. 444, Prof. Yousef Sobouti Boulevard, Zanjan 45137-66731, Iran, mozhdepm@iasbs.ac.ir, m_khorasani@iasbs.ac.ir.
b) Research Center for Basic Sciences & Modern Technologies (RBST), Institute for Advanced Studies in Basic Sciences, IASBS, Zanjan 45137-66731, Iran.

Keywords: Carbon Dioxide, CO_2 Conversion, Cyclic Carbonates, Covalent Triazine Frameworks

Today, the excessive use of fossil fuels has caused to release of significant amounts of carbon dioxide (CO_2) gas that has posed major risks to the environment and ecosystem. To solve this problem, researchers have presented different solutions including smart recovery and conversion of this gas to value-added products considering the green chemistry points of view. Among them, the direct coupling of CO_2 with epoxides to firm cyclic carbonates have been received more attention since the carbonates have extensively been used as pharmaceutical intermediates and apolar solvents [1]. However, due to the high thermodynamic stability of CO_2, its utilization is typically required an active catalyst. The covalent triazine frameworks (CTF) categorized as nitrogen-rich materials have been recently employed as effective catalysts for the mentioned CO_2 conversion due to their unique properties [2]. Herein, we would like to report that cycloaddition of CO_2 to terminal epoxide could be selectively performed in the presence of a metal supported on nitrogen-rich CTF catalyst and tetrabutylammonium bromide (TBAB) as co-catalyst under 10 bar CO_2 at 70 ºC as mild reaction conditions.

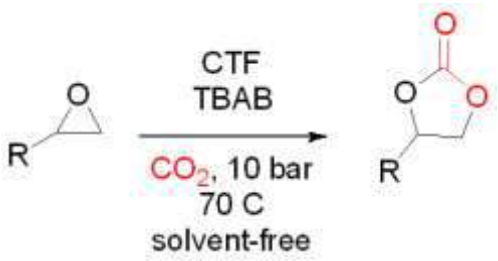

Scheme: Coupling reaction of carbon dioxide with epoxide in the presence of CTF catalyst

References

[1] Khorasani, M.; Karimi, B.; Vali, H. Coupling of CO_2 with epoxides catalyzed by bifunctional periodic mesoporous organosilica with ionic liquid framework. *React. Chem. Eng*. **2022**, *7*, 2618-2628.
[2] Ji, G.; Zhao, Y.; Liu, Z. Design of porous organic polymer catalysts for transformation of carbon dioxide. *Green Chem. Eng*. **2022**, *3*, 96-11.

CO_2 Conversion by Ionic Liquid Decorated Covalent Triazine Framework

Niloofar Abbasi [a], **Mojtaba Khorasani** [a,b]*

a) Department of Chemistry, Institute for Advanced Studies in Basic Sciences (IASBS), No. 444, Prof. Yousef Sobouti Boulevard, Zanjan 45137-66731, Iran, niloofarabbassi@iasbs.ac.ir, m_khorasani@iasbs.ac.ir
b) Research Center for Basic Sciences & Modern Technologies (RBST), Institute for Advanced Studies in Basic Sciences, IASBS, Zanjan 45137-66731, Iran.

Keywords: CO_2 Conversation, Ionic Liquid, Cyclic Carbonate, Covalent Triazine Framework.

In recent years, the combustion of fossil fuels and deforestation through uncontrolled emissions of carbon dioxide (CO_2) have led to climate change. To address this issue, carbon capture and utilization (CCU) defined as capturing CO_2 and converting it to useful chemicals, has attracted much attention. In this regard, the production of valuable cyclic carbonates through the direct coupling of CO_2 with epoxides is one of the most efficient processes for the mitigation of CO_2 emissions. For this important transformation, ionic liquids as a family of organocatalysts, are paid more attention due to their stability and non-toxicity [1]. On the other hand, covalent triazine frameworks (CTFs) as a class of porous polymers have been widely studied as heterogeneous catalysts for chemical CO_2 conversion [2]. Herein, we wish to disclose that a covalent triazine framework functionalized by ionic liquid (IL-CTF) linkers could exhibit superior activity toward direct coupling of CO_2 with terminal epoxides through the coexistence of triazine basic site and halide ions (**Scheme 1**).

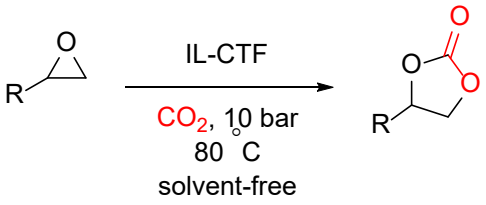

Scheme 1. Direct coupling of CO_2 with epoxide catalyzed by IL-CTF

[1] M, Khorasani; B, Karimi; Vali, H. Coupling of CO_2 with epoxides catalyzed by bifunctional periodic mesoporous organosilica with ionic liquid framework. *React. Chem. Eng.* 2022, *7*, 2618-2628.

[2] Buyukcakir, O.; Je, S. H.; Talapaneni, S. N.; Kim, D.; Coskun, *A.* Charged Covalent Triazine Frameworks for CO_2 Capture and Conversion. *ACS Appl. Mater. Interfaces* 2017, *9*, 7209-7216.

A^3 coupling reaction in the presence of Fumed-Pr-Pi@Ag

Masoome Atef, Ghodsi Mohammadi Ziarani*

Department of Organic Chemistry, Alzahra University, Tehran, Iran, masoomeatef777@gmail.com, gmohammadi@alzahra.ac.ir

Keywords: Nano catalyst, Fumed silica, A^3 coupling reactions, Propargyl amines.

According to the economical aspect of the chemical reaction, the heterogeneous catalytic system was attracted the researcher's attentions due to their simple separation process and also their recoverability [1]. Among the various solid supports, the Fumed silica is one of the most applicable candidate due to its amorphous structure, low density, high specific surface area, and also the nano size of the particles (5-50 nm) [2]. So, in this research, the Fumed silica was functionalized by (3-chloropropyl)-triethoxysilane, piperazine [3]. Subsequently, the silver was immobilized on the surface of Fumed silica to obtain Fumed-Pr-Pi@Ag as the efficient heterogeneous catalyst, which was used in the A^3 coupling reaction to produce propargyl amines which are active in biological compounds (e.g., antitumor and antioxidant) [4] (**Scheme 1**).

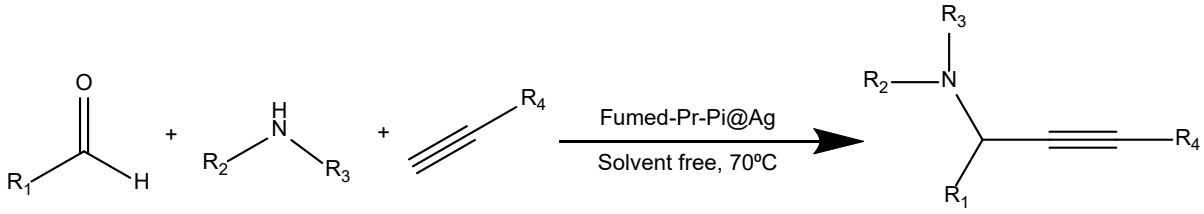

Scheme 1: catalytic activity of Fumed-Pr-Pi@Ag in A^3 coupling reaction

References

[1] Samandi, A.; Nemati, F.; Mirhosseyni, MS.; Sabaqian, S. Magnetic selenium and dual-doped mesoporous carbon for immobilization of Pd nanoparticles: The utilitarian heterogeneous catalyst in Heck-cross coupling reaction. *Appl. Organomet. Chem.* 2022, *37*, e6988.

[2] Barthel H.; Heinemann M.; Stintz M.; Wessely B. Particle sizes of fumed silica. *Chem. Eng. Technol.* 1998, *21*, 21745-52.

[3] Afshar, S. S.; Ziarani, G. M.; Mohajer, F.; Badiei, A.; Iravani, S.; & Varma, R. S. Synthesis of Fumed-Pr-Pi-TCT as a Fluorescent Chemosensor for the Detection of Cyanide Ions in Aqueous Media. *Water* 2022, *14*, 4137.

[4] Lo, V. K. Y.; Liu, Y.; Wong, M. K.; & Che, C. M. Gold (III) salen complex-catalyzed synthesis of propargylamines via a three-component coupling reaction. *Org. Lett.* 2006, *8*, 1529-1532.

Preparation charge-transfer complex and investigation of its physicochemical properties through mechanical quantum method

Nasrin Azizi Balabeigloo*, Vahideh Hadigheh Rezvan

Department of Chemistry, Ardabil Branch, Islamic Azad University, Ardabil, Iran, azizi.na65@gmail.com

Keywords: Charge transfer complexes, Electrons acceptor-π-donor, DFT, Melamine

The chemistry of charge transfer (CT) complexes has become important in materials and biological science in recent years. CT complexes show a vital characteristic in the area of electric and optical properties [1-3]. The new chemistry of the hydrogen-bonded charge and proton transfer complex (HB CT) between electron-donor Melamine and electron-acceptor para-Nitro benzoic acid has been studied using electronic absorption spectroscopy in aqua media (**Scheme 1**). The HBCT complexstructure was confirmed by different characterization techniques, such as FT-IR, NMR, TGA-DTA, and SEM-EDX analysis. Computational analysis was carried out by DFT studies using the B3LYP function with a basis set of 6-311G(d,p)-6 in the gas phase. The computational studies further supported the experimental results by confirming the charge and proton transfer complex.

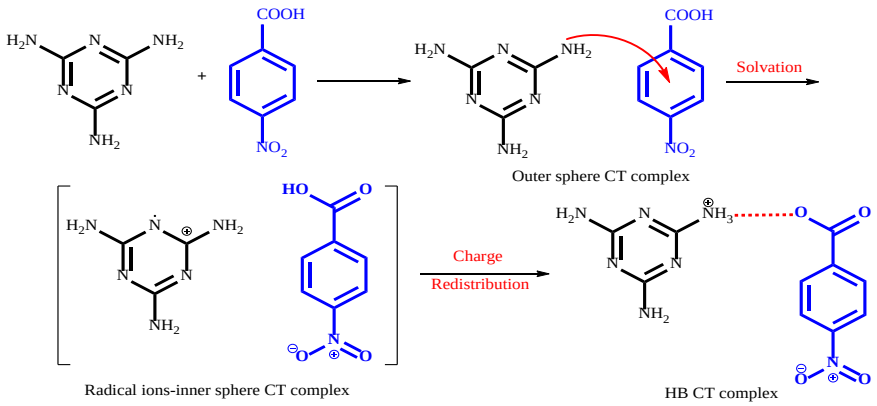

Scheme1: Probable mechanism of the HB CT complex.

References

[1] Goetz, K. P.;Vermeulen, D.; Payne, M. E.;Kloc, C.; McNeil, L. E.;Jurchescu, O. D. Charge-transfer complexes: new perspectives on an old class of compounds. *J. Mater. Chem. C* 2014, *2 (17)*, 3065-3076.

[2] Khan, I. M.;Alam, K.;Alam, M. J. Exploring charge transfer dynamics and photocatalytic behavior of designed donor-acceptor complex: characterization, spectrophotometric and theoretical studies (DFT/TD-DFT). *J. Mol. Liq.* 2020,*310*, 113213.

[3] Mohammad, M.; Al RasidGazi, H.;Pandav, K.; Pandya, P.; Islam, M. M. Evidence for dual site binding of nile blue a toward DNA: Spectroscopic, thermodynamic, and molecular modeling studies. *ACS omega* 2021, *6(4)*, 2613-2625.

Novel Hollow Mesoporous Organosilica Nanoparticle Decorated with Imidazolium Units (Im-HMON) as Recoverable Catalyst for CO_2 Conversion

Ghazale Anvarian-Asl[a] and Mojtaba Khorasani[a,b]*

a) Department of Chemistry, Institute for Advanced Studies in Basic Sciences (IASBS), No. 444, Prof. Yousef Sobouti Boulevard, Zanjan 45137-66731, Iran, ghazale.anvarian@iasbs.ac.ir, m_khorasani@iasbs.ac.ir
b) Research Center for Basic Sciences & Modern Technologies (RBST), Institute for Advanced Studies in Basic Sciences, IASBS, Zanjan 45137-66731, Iran,

Keywords: Hollow mesoporous Organosilica silica sphere, Ionic liquids, CO_2 Fixation

One of the methods of converting and consuming CO_2 greenhouse gas, which has increased in the earth's atmosphere in the current century, into valuable chemicals is to combine it with epoxides and form five-membered ring carbonates [1]. Hollow mesoporous materials (HMMs) have attracted much attention in the last decade. HMMs have the advantages of low density, large void space, and large specific surface area. One of the main tips for designing catalysts for the conversion of CO_2 gas is the use of hollow catalysts which have a significant tendency toward CO_2 capture and storage [2]. Considering the importance of hollow structures for gas phase reactions and the catalytic role of imidazolium units in the conversion of carbon dioxide, a new catalyst based on bis imidazolium groups incorporated into pore walls of hollow mesoporous organosilica nanoparticles (Im-HMON) has been introduced. The coupling reaction of the CO_2 with various types of terminal epoxides could be selectively achieved under mild reaction conditions in the presence of Im-HMON (**Scheme 1**). The catalyst was successfully reused for six reaction runs without any remarkable decrease in its activity and selectivity.

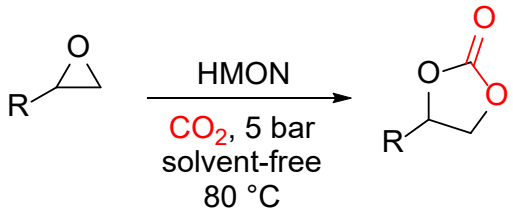

Scheme: Reaction of CO_2 with epoxides in the presence of a prepared catalyst.

References

[1] Bhanja, P.; Modak, A.; Bhaumik, A. Supported Porous Nanomaterials as Efficient Heterogeneous Catalysts for CO_2 Fixation Reactions. *Chem. Eur. J.*, **2018**, *24*, 7278-7297.
[2] Razaghi, M.; Khorasani, M. Boosting the quaternary ammonium halides catalyzed CO_2 coupling with epoxides on the hollow mesoporous silica sphere. *J. CO_2 Util.* **2022**, *61*, 102028.

Supported Ni(II) on Mesoporous Organosilica Nanoparticles for CO_2 Conversions

Tohid Nouri[a] and Mojtaba Khorasani[a,b*]

a) Department of Chemistry, Institute for Advanced Studies in Basic Sciences (IASBS), No. 444, Prof. Yousef Sobouti Boulevard, Zanjan 45137-66731, Iran, tohidnouri@iasbs.ac.ir, m_khorasani@iasbs.ac.ir
b) Research Center for Basic Sciences & Modern Technologies (RBST), Institute for Advanced Studies in Basic Sciences, IASBS, Zanjan 45137-66731, Iran.

Keywords: CO_2 utilization, Pincer catalyst, Mesoporous Organosilica Nanoparticle

In recent years, the concentration of carbon dioxide (CO_2) in the air has reached its highest level due to human activities. Therefor, the improvement sustainable strategies to capture CO_2 and then its conversion into valuable compounds has received greater attention [1]. For example, cyclic carbonates widely used in the industry can be produced *via* the coupling of CO_2 with epoxides. In recent years, mesoporous organosilica materials have attracted much attention as a kind of porous organic-inorganic hybrids due to their specific features [2]. Herein, nickel(II) supported on the mesoporous organosilica nanoparticle with the dipicolinic thioester frameworks (Ni@SNS-MON) has been described as an efficient recoverable catalyst for title reaction. It was found that CO_2 could couple with various types of epoxides to the corresponding cyclic carbonates in the presence of 0.1 mol% Ni@SNS-MON and 0.3 mol% tetrabutylammonium bromide (TBAB) as co-catalyst at 100 °C (**Scheme 1**).

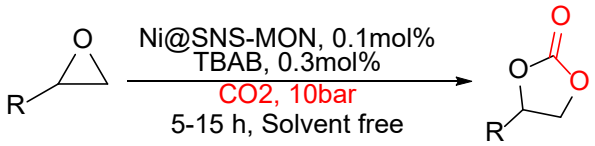

Scheme: Direct coupling of CO_2 with epoxides by using Ni@SNS-MON.

References

[1] Pescarmona, P. P. Cyclic carbonates synthesized from CO_2: Applications, challenges and recent research trends. *Curr. Opin. Green. Sustain. Chem.* **2021**, *29*, 100457.
[2] M. Razaghi.; M. Khorasani. Boosting the quaternary ammonium halides catalyzed CO_2 coupling with epoxides on the hollow mesoporous silica sphere. *J. CO_2 Util.* 2022, *61*, 102028

Synthesis of Ethyl 1-naphthylacetate Using $MgFe_2CuO_5$ as a Nanocatalyst under Solvent-free Condition

Marzieh Mahmoodi Keshtiban[a*], Bakhshali Massoumi[a] and Abbas Nikoo[b]

a) Department of Chemistry, Payame Noor University, Tabriz, Iran, mahmoodimarzieh99@gmail.com, b_massoumi@pnu.ac.ir,
b) Department of Organic Chemistry, Faculty of Chemistry, Urmia University, Urmia, Iran, a.nikoo@urmia.ac.ir

Keywords: Naphthalene, Ethyl chloroacetate, Mixed metal oxide

1-naphthylacetic acid, also known as naphthylacetic acid and α-naphthylacetic acid, is a broad-spectrum plant growth regulator, it has been successfully developed by Union Car-hide in the United States [1]. Its physiological function and mechanism are similar to that of indole acetic acid, which can promote cell division and expansion, induce the formation of adventitious roots, increase fruit setting and prevent fruit drop, change the ratio of female and male flowers, etc. Through the leaves, branches of the tender epidermis, seeds into the plant, with the flow of nutrients to the whole plant [2].

With naphthalene as raw material, under the action of $MgFe_2CuO_5$ and potassium bromide, the reaction was carried out with ethyl chloroacetate and ethyl 1-naphthylacetate was directly prepared (**Scheme**). In the absence of KBr, no ethyl 1-naphthylacetate was formed. After the completion of the reaction, the unreacted naphthalene was removed, the ethyl 1-naphthylacetate was filtered out, washed with cold water, and recrystallized to obtain pure ethyl 1-naphthylacetate.

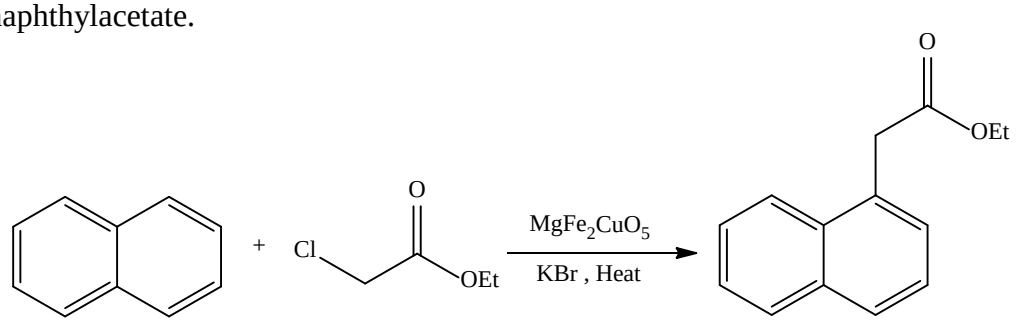

Scheme: Synthesis of ethyl 1-naphthaleneacetate by $MgFe_2CuO_5$.

References

[1] Basuchaudhuri, P. 1-Naphthaleneacetic acid in rice cultivation. *Curr. Sci.* 2016, *110(1)*, 52-56.
[2] Al- Duraid, M. H.; Al-Taey, K. A.; Al-Kikhani, A. H. J. Effect of Phenylalanine and Naphthalene Acetic Acid on Growth, Yield and Antioxidant Activity of Fenugreek Trigonella foenum-graecum. *IOP Conf. Ser.: Earth Environ. Sci.* 2019, *388*, 012073.

Synthesis and Characterization of hydrogel based on beta –cyclodextrin-polyacrylic acid supported on nano silica

Farzad Zolfaghari*, Ali Reza Kiasat

Department of Chemistry, Faculty of Science, Shahid Chamran University of Ahvaz, Ahvaz, Iran, farzad.chemistry99@gmail.com

Keywords: Hydrogel, Nano silica, Polyacrylic acid, Beta-cyclodextrin

In recent years, the drug delivery systems have expanded greatly with the development of the synthesis of various hydrogels. In this study, beta –cyclodextrin- polyacrylic acid supported on nano silica has been synthesized and characterized. For this goal, the surface of nano silica was first modified by mercapto propyl trimethoxy silane in toluene. Free radical polymerization of the thiolated silica with acrylic acid by AIBN initiator produced polyacrylic acid supported nanosilica. The reaction of composite by thionyl chloride and then beta –cyclodextrin produced the SiO_2-PAA-β-CD hydrogel (**Scheme 1**).

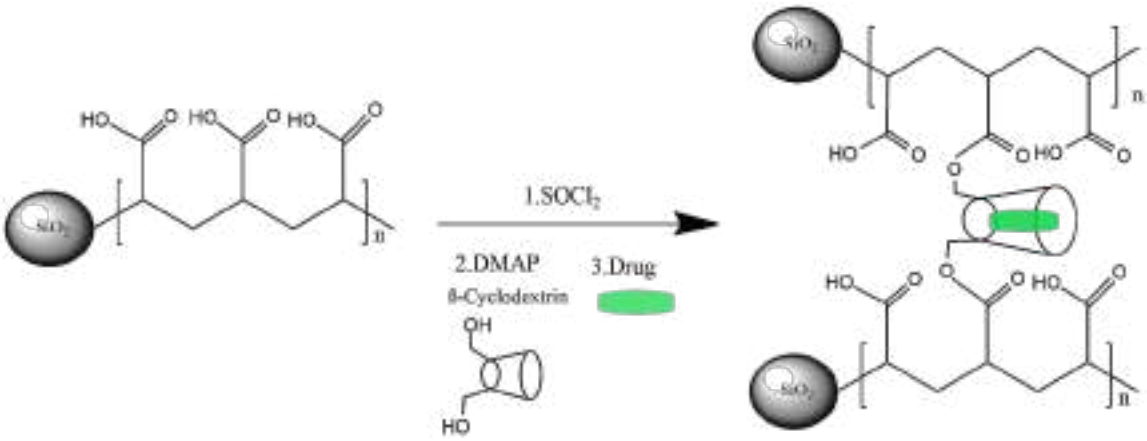

Scheme 1: Synthesis of drug-loaded SiO2-PAA-β-CD hydrogel.

References

[1] Kutyła MJ, Lambert LK, Davies NM, McGeary RP, Shaw PN, Ross BP. Cyclodextrin-crosslinked poly (acrylic acid): synthesis, physicochemical characterization and controlled release of diflunisal and fluconazole from hydrogels. *Inter. J Pharm*, 2013, *444(1-2)*,175-84.

[2] Guo X, Wang J, Li L, Pham DT, Clements P, Lincoln SF, May BL, Chen Q, Zheng L, Prud'Homme RK. Tailoring polymeric hydrogels through cyclodextrin host–guest complexation. *Macr. Rapid Commun*, 2010, *31(3)*,300-4.

A SERS platform for determination of Dydrogesterone using CQD-gold nanoparticle conjugate

Aref Tanavardi-Nasab and Mohamad Mahani*

Department of Chemistry, Faculty of Chemistry and Chemical Engineering, Graduate University of Advanced Technology, Kerman, Iran, aref93tanavardi@gmail.com, mohmahani@gmail.com.

Keywords: Dydrogesterone, Carbon quantum dots, Surface-enhanced Raman scattering, SERS platform, Gold nanoparticle.

Dydrogesterone is a selective agonist of the progesterone receptor, with greater oral bioavailability and is commonly used for regulating certain life-sustaining processes in living organisms [1]. Recently, sensors based on carbon quantum dots are used for biological measurements [2]. In this work a surface enhanced Raman scattering (SERS) platform was developed for determination of Dydrogestrone. Carbon quantum dots were synthesized by hydrothermal method and characterized using HRTEM, DLS, UV-Vis spectrophotometry and spectrofluorimetry. Gold nanoparticles were synthesized by reduction of chloroauric acid and also characterized. Different types of carbon quantum dots were synthesized and covalently conjugated to gold nanoparticles. The interaction mechanism of Dydrogestrone with different type of carbon nano dots and different gold nanostructures were studied. A novel conjugate of carbon quantum dots and gold nanoparticles was developed as a SERS platform for the determination of Dydrogesterone. The fluorescence of carbon quantum dots quenched in CQD-GNP conjugate and 2-fold increase in the Raman intensities was observed. The lower limit of quantitation of 10 µg mL^{-1} (RSD:22.9%) with a linear dynamic range of 10–50 µg mL^{-1} were obtained for the determination of Dydrogestrone.

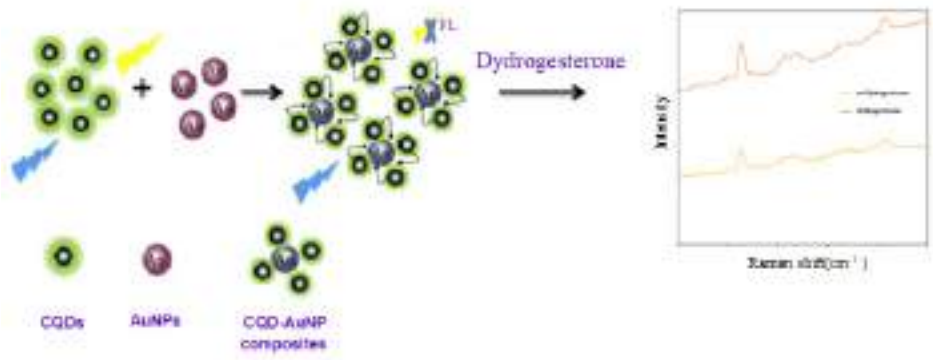

Scheme: The CQD− GNP SERS sensor for the determination of Dydrogesterone.

References:

[1] Mary, Y. S; Mary, Y. S. Utilization of doped/undoped graphene quantum dots for ultrasensitive detection of duphaston, a SERS platform. *Spectrochim. Acta - A: Mol. Biomol. Spectrosc.* 2021, *244*, 118865.

[2] Neri, G; Fazio, E; Mineo, P. G; Scala, A; Piperno, A. SERS sensing properties of new graphene/gold nanocomposite. *Nanomaterials* 2019, *9*, 1236.

Synthesis, characterization and investigation of degradation of organic dye from wastewater using γ-Fe_2O_3@graphene oxide as an efficient composite

Seyedeh Maryam Mousavi, Mohammad Ali Ghasemzadeh*, Boshra Mirhosseini-Eshkevari

Department of Chemistry, Qom Branch, Islamic Azad University, Qom, I. R. Iran,
maryammousavi9371@gmail.com, m.a.qasemzade@gmail.com

Keywords: γFe_2O_3, Graphene oxide, Dye degradation.

About 90 million tons of dye polluted wastewater are discharged into environment without proper treatment every year, which account for roughly 20% of the industrial wastewater [1]. Among organic dyes, synthetic dyes (such as malachite green (MG), Rhodamine B (RhB), and methyl orange (MO)) are considered to be as important pollutant sources [2].
In This study, γ-Fe_2O_3@GO were successfully prepared via a facile hydrothermal method. The prepared structure was characterized using XRD, SEM, FT-IR and UV–Vis, and DLS analysis. The photocatalytic activity of the mentioned hybrids was evaluated by identifying and removing dyes in water. It has been determined that methyl orange was removed from 20% to 80% after the addition of the above compound. This work paves a new way to use carbon-based nanomaterial in efficient design for organic pollution degradation in wastewater [3].The photocatalytic activities of the synthesized composite were investigated through the degradation of dye in water under visible light irradiation. The degradation of photocatalytic dyes followed the first-order kinetic equation well, and increasing the catalyst dosage and the optimal initial concentration of dyes were responsible for increasing the photocatalytic degradation. In addition, the reusability of the composite was also studied [4].

References

[1] B. Hayati, N.M. Mahmoodi, M. Arami, F. Mazaheri, Dye removal from colored textile wastewater by poly(propylene imine) dendrimer: operational parameters and isotherm studies, *Clean - Soil, Air, Water* 39 (2011) 673–679.
[2] K.T. Kubra, M.S. Salman, M.N. Hasan, Enhanced toxic dye removal from wastewater using biodegradable polymeric natural adsorbent, *J. Mol. Liq.* 328 (2021).
[3] C. Zhang, L. Ai, J. Jiang, Graphene hybridized photoactive iron terephthalate with enhanced photocatalytic activity for the degradation of rhodamine B under visible light, *Ind. Eng. Chem. Res.* 54 (2015) 153–163.
[4] L. Hu, G. Deng, W. Lu, S. Pang, X. Hu, Deposition of CdS nanoparticles on MIL-53(Fe) metal-organic framework with enhanced photocatalytic degradation of RhB under visible light irradiation, *Appl. Surf. Sci.* 410 (2017) 401–413.

Synthesis of 3,4-Dihydropyrimidinones using boron tri fluoride supported on silica nano particles as an efficient catalyst in different conditions

Mahdieh Hosseinpoor Fini, Abdolhamid Bamoniri*

Department of Organic Chemistry, Faculty of Chemistry, University of Kashan, Kashan, I. R. Iran, mahdieh.h.f@gmail.com, bamoniri@kashanu.ac.ir

Keywords: Dihydropyrimidinones, Green chemistry, Multicomponent reaction, Nano silica

Pyrimidinones are heterocyclic rings that are similar to pyridines. They show many medicinal properties. In this research, using suitable conditions, pyrimidinones were synthesized with the highest efficiency. The use of borane trifluoride stabilized on nano silica was used for the synthesis of dihydropyrimidinones. This catalyst is cheap, available and easily prepared. Investigation and analysis of the manufactured catalyst was done using methods such as FT-IR, TEM, FESEM, XRD, EDS, TGA and BET. Derivatives of 3,4-dihydropyrimidinones were synthesized from borane trifluoride stabilized on nano silica as catalyst in one-pot conditions, using various aldehydes, beta-diketo and urea or thiourea (Scheme 1). Finally, the manufactured derivatives were analysed by FT-IR and ^{1}H NMR spectroscopy. Among the advantages of this research, we can mention the greenness of the catalyst and the synthesis of derivatives with high efficiency using different methods.

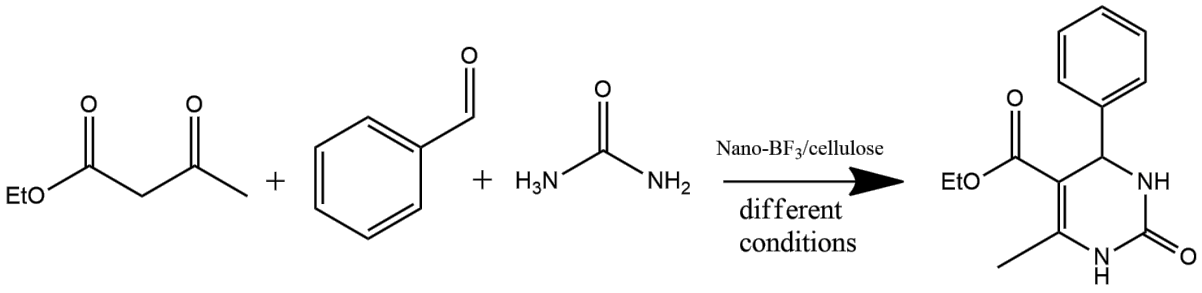

Scheme 1. Synthesis of 3,4-Dihydropyrimidinones

References

[1] Gong, K., Wang, H., Wang, S., Ren, X., β-Cyclodextrin-propyl sulfonic acid: a new and eco-friendly catalyst for one-pot multi-component synthesis of 3, 4-dihydropyrimidones via Biginelli reaction. *Tetrahedron*, **2015**, *71*(29), 4830-4834.

[2] Maurya, M. R., Chauhan, A., Arora, S., Gupta, P., Triazole based oxidovanadium (V) complex supported on chloromethylated polymer and its catalytic activity for the synthesis of dihydropyrimidinones (DHPMs). *Catal. Today*, **2022**, *397*,3-15.

Green synthesis of pyrazolopyranopyrimidine derivatives using glutamic acid under thermal conditions

Hanieh Amini Moghaddam[a*], Leila Moradi

Department of Organic Chemistry, Faculty of Chemistry, University of Kashan, Kashan, I.R. Iran, h.moghaddam130@gmail.com.

Keywords: Multi component reactions, Fused heterocycles, Green chemistry, Glutamic acid, Pyrazolopyranopyrimidine.

Multicomponent reactions are reactions in which more than two starting materials are used to form the product [1]. Pyrazolopyranopyrimidines are heterocycles contain pyrimidine, pyran and pyrazole groups, which have many biological and medicinal properties [2], including analgesic, anti-inflammatory, anticancer and anti-depressant [3]. In this research, glutamic acid wase used as catalyst in the four-component reaction of hydrazine hydrate, ethyl acetate, aromatic aldehydes and barbituric acid derivatives to the optimal preparation of pyrazolopyranopyrimidines under thermal conditions. The green reaction conditions (using water as a solvent and green catalysts), short reaction time and high yeild of products are some of the advantages of the present research.

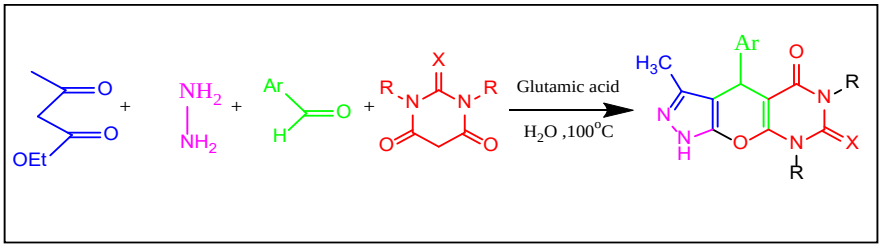

Scheme: Synthesis of pyrazolopyranopyrimidine under thermal condition in the presence of glutamic acid.

References:

[1] Bo. Jiang, T. Rajale “Multicomponent Reactions for the Synthesis of Heterocycles”, *Chem. Asian J.* 2010, 5, 2318 – 2335.

[2] S. Sadjadi, M.M. Heravi, “Heteropolyacid supported on amine-functionalized halloysite nano clay as an efficient catalyst for the synthesis of pyrazolopyranopyrimidines via four-component domino reaction”, *Res. Chem. Intermed.* 2017, 43, 2201–2214.

[3] S. Dastkhoon, Z. Tavakoli, “Nanocatalytic one-pot, four-component synthesis of some new triheterocyclic compounds consisting of pyrazole, pyran, and pyrimidinone rings”, *New J. Chem.* 2015, 39, 7268–7271.

29TH IRANIAN ORGANIC CHEMISTRY CONFERENCE
1_3 NOV, 2023
UNIVERSITY OF QOM, IRAN

The application of selanyl tetrazoles/HY zeolite hybrids as an organic-inorganic hybrid catalyst in the synthesis of pyrroles

Soheila Khaghaninejad* and Mojgan Zendehdel

Organic Chemistry Laboratory, Faculty of Chemistry, University of Arak, Arak, Iran, soheila.khaghani@yahoo.com, s-khaghani@araku.ac.ir, mojganzendehdel@yahoo.com, m-zendehdel@araku.ac.ir

Keywords: Pyrrole, Tetrazole, Selenium, Zeolite Hybrid

Pyrroles have board applications as pharmaceutical agents, conducting polymers, molecular optics, electronics and gas sensors for organic compounds [1]. This ring system is a key component of alkaloids, synthetic materials, bioactive molecules such as vitamin B12, Heme and cytochromes, and biologically active compounds such as indolizine, unsaturated γ-lactams and bicyclic lactams. However, there are several methods for the synthesis of pyrroles. The Paal-Knorr reaction is one of the most significant important and simple methods to synthesis a pyrrole derivatives. In the Paal-Knorr reaction, 1,4-dicarbonyl derivatives are converted to pyrroles *via* acid mediated cyclization with primary amines which remains most common and attractive [2]. In continuation of our previous work on the applications of heterogeneous acid catalysts [TMSP-S-Tet.]HY-Z in the synthesis of organic compounds [3]. herein, we report the preparation and characterization of a novel organic-inorganic hybrid catalyst, namely three ethoxy silan propyl selenium tetrazole [TMSP-Se-Tet.] HY-Z functionalized on HY zeolite and examined in the synthesis of pyrroles derivatives *via* the Paal-Knorr reaction (**Scheme**).

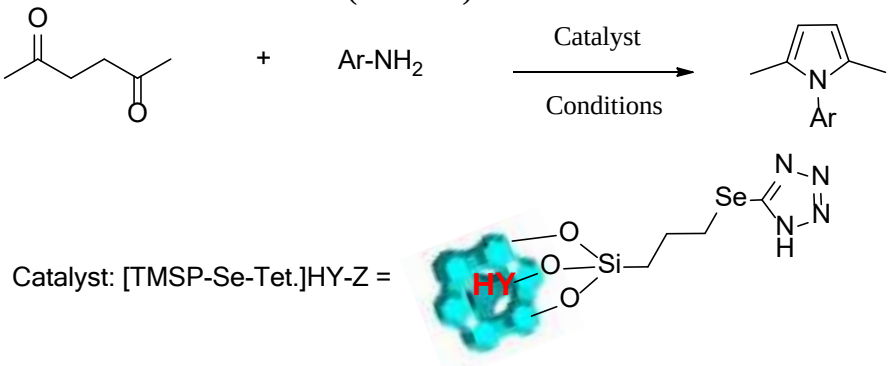

Scheme: The preparation of pyrrole in the presence of [TMSP-Se-Tet.]HY-Z catalyst *via* Paal-Knorr reaction

References

[1] Higgins, S.; Conjugated polymers incorporating pendant functional groups-synthesis and characterization. *Chem. Soc. Rev.* 1997, 26, 247-257.

[2] Khaghaninejad S.; Heravi M.M. Chapter three - Paal-Knorr reaction in the synthesis of heterocyclic compounds. *Adv. Heterocycl. Chem.* 2014, 111, 95-146.

[3] Zendehdel, M.; Khaghaninejad S.; Kheiri, A. Preparation, Characterization of Sulfonyl Tetrazoles/ HY Zeolite Hybrids as a Catalyst in the Synthesis of Pyrrole *via* Paal-Knorr Reaction. *Silicon* 2022, 14, 9959-9971.

Carbon-nanofiber/taurine as a novel and metal-free catalyst for the synthesis of coumarins and 1,2,4,5-tetra-substituted imidazoles

Dina Mallah[a], Bi Bi Fatemeh Mirjalili[*a] and Abdolhamid Bamoniri[b]

a) Department of Chemistry, College of Science, Yazd University, Yazd, Iran, mallah.diana@gmail.com, fmirjalili@yazd.ac.ir.
b) Department of Organic Chemistry, Faculty of Chemistry, University of Kashan, Kashan, Iran.

Keywords: Nano-scale, Carbon nanofiber, Taurine, 7-hydroxycoumarin, Tetra-substituted imidazole.

In recent years, carbon nanofibers have attracted a lot of attention due to their unique properties, including the inertness of the surface, and the presence of stabilizing surface groups. Due to the inertness of the surface, carbon nanofibers prevent unnecessary reactions with the reagent. Hence, it can be a suitable support for the replacement of conventional catalysts [1]. Taurine as an amino sulfonic acid is essential for proper heart function, healthy sleep, and promoting calmness. Several reports have suggested that taurine, in addition to its medicinal properties, also plays a role in the preparation of catalysts and the synthesis of heterocyclic compounds [2]. Biologically active compounds mainly have a polycyclic heteroatom structure. Among known heterocyclic compounds, coumarin and imidazoles are of great importance because of the medicinal and biological properties of these heterocyclic compounds [3, 4] (**Scheme**).

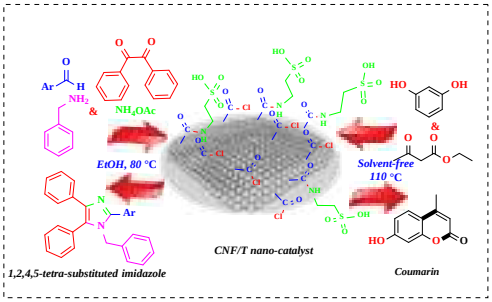

Scheme: Application of Carbon nanofiber/Taurine nano-catalyst.

References

[1] Zhou, X.; Wang, Y.; Gong, C.; Liu, B.; Wei, G. Production, structural design, functional control, and broad applications of carbon nanofiber-based nanomaterials: A comprehensive review, *Chem. Eng. J.* 2020, *402*, 126189.
[2] Ripps, H.; Shen, W. Taurine: a very essential amino acid. *Mol. Vis.* 2012, *18*, 2673.
[3] Tolba, M.; El-Dean, A.; Geies, A.; Radwan, S.; Zaki, R.; Sayed, M.; Mohamed, S.; Abdel-Raheem, S. An overview on synthesis and reactions of coumarin based compounds, *Curr. Chem. Lett.* 2022, *11*, 29-42.
[4] Hossain, M.; Nanda, A. K. A review on heterocyclic: synthesis and their application in medicinal chemistry of imidazole moiety, *Science* 2018, *6*, 83-94.

Preparation and complexation of 2, 2'-[l ,2-ethanediylbis-(nitrilomethylidene)] bis-furane as catalyst in the synthesis of 1-(benzothiazolylamino)aryl methyl-2-naphtol

Javad Safaei Qomi*, Parisa Gholami Hasan Abadi, Elahe Mashhadi

Department of Organic Chemistry, Faculty of Chemistry, University of Kashan, Kashan, 51167, I. R. Iran, gh.pariisa@gmail.com, safaei@kashanu.ac.ir,

Keywords: Complex, Homogeneous, Schiff base, Zinc (II), (benzothiazolylamino) aryl methyl-2-naphtols

A heterocyclic structure frequently encountered within medicinal chemistry is the derivative of 1-(benzothiazolylamino)arylmethyl-2-naphthol, an amalgamated heterocyclic compound with diverse applications in the pharmaceutical sector [1]. These compounds play a pivotal role as fundamental structural components in the creation of valuable pharmaceuticals, including anticonvulsants, antitumor agents, and anticancer drugs [2]. Schiff base can interact with most metal ions and produce various complexes. Within this investigation, we successfully synthesized a zinc(II) Schiff-base complex [3]. This synthesized Schiff base was used as an efficient homogeneous catalytic system for the one-pot multicomponent synthesis of 1-(benzothiazolylamino)arylmethyl-2-naphthol (**Scheme 1**). The method offers several advantages, including less time, high efficiency, green chemistry conditions, simplicity of work, and use of non-toxic solvents.

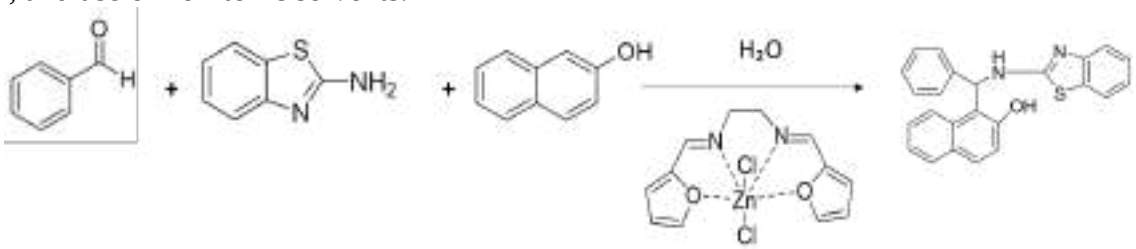

Scheme 1: Using various aldehydes, 2-naphthol and 2-aminobenzothiazole with Schiff base complex as a catalyst in H_2O, 80 ^{0}C.

References

[1] S. Sobhani, S. Asadi, M. Salimi, F. Zarifi, Cu-isatin schiff base complex supported on magnetic nanoparticles as an efficient and recyclable catalyst for the synthesis of bis(indolyl)methanes and bis(pyrazolyl)methanes in aqueous media, *J. Organomet. Chem.* 2016, 822, 154–164.

[2] A. Moradi, R. Heydari, M.T. Maghsoodlou, Agar: A novel, efficient, and biodegradable catalyst for the one-pot three-component and green synthesis of 2,3-dihydroquinazolin-4(1H)-one, 4H-pyrimidobenzothiazole and 2-aminobenzothiazolomethylnaphthol derivatives, *Res. Chem. Intermed.* 2015, 41, 7377–7391.

[3] K.C. Gupta, A. Kumar Sutar, C.C. Lin, Polymer-supported Schiff base complexes in oxidation reactions, *Coord. Chem. Rev.* 2009, 253, 1926–1946.

Architecture of click chemistry on bimetal-organic frameworks (Bimetalic-MOFs) for the preparation of new spiro-oxindoles

Mohammad Ali Zolfigol,* Elham Tavakoli, Hassan Sepehrmansourie, and Ardeshir Khazaei

Department of Organic Chemistry, Faculty of Chemistry, Bu-Ali Sina University, Hamedan 6517838683, Iran, zolfi@basu.ac.ir & mzolfigol@yahoo.com, elham.tavakoli1990@yahoo.com.

Keywords: Bimetallic-Organic Frameworks, Click chemistry, Spiro-oxindoles.

Metal-organic frameworks (MOFs) are a new class of new generation nanoreactors that are composed of various metals and organic compounds as ligands. Recently, various metals such as Zr, Co, Fe, Ti have been used in bimetallic MOFs architectures. These nanostructures have shown unique properties and the limitations of monometallic MOFs can be compensated with such hybrid systems [1]. Click chemistry is one of the most effective methods of producing organic compounds and various catalysts, which has attracted the attention of many scientists and industries in the last decade. By using click chemistry, it is possible to modify the structure of many MOFs and turn them into targeted and effective catalysts for catalytic and photocatalytic purposes [2-3]. Our aim is to design a MOF based on two metals Co and Fe to create a bimetal-organic frameworks. The catalytic application of this structure has been evaluated in the reaction of preparing spiro compounds under green and mild conditions, and the results prove the suitability of such a catalytic system (**Scheme 1**).

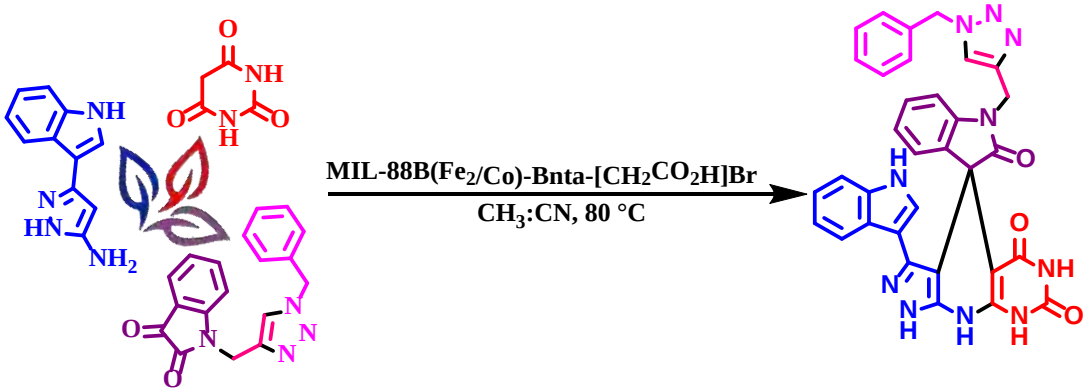

Scheme 1: Synthesis of new spiro-oxindole derivatives using bimetal-organic frameworks as a novel porous catalyst.

References

[1] Sanati, S.; Abazari, R.; Albero, J.; Morsali, A.; García, H.; Liang, Z.; Zou, R. Metal–organic framework derived bimetallic materials for electrochemical energy storage. *Angew. Chem., Int. Ed.* 2021, *60*, 11048-11067.

[2] Franc, G.; Kakkar, A. K. Click" methodologies: efficient, simple and greener routes to design dendrimers. *Chem. Soc. Rev*. 2010, *39*, 1536-1544.

[3] Ball-Jones, N. R.; Badillo, J. J.; Franz, A. K. *Org. Biomol. Chem.* 2012, *10*, 5165-5181

Catalytic application of TMU-52-UR as an efficient H-bond catalyst in the preparation of biological active macromolecules

Mohammad Ali Zolfigol,*[a] Mahmoud Zarei,[b] Elham Tavakoli,[a] Hassan Sepehrmansourie,[a] and Ardeshir Khazaei[a]

a) Department of Organic Chemistry, Faculty of Chemistry, Bu-Ali Sina University, Hamedan 6517838683, Iran, zolfi@basu.ac.ir & mzolfigol@yahoo.com.
b) Department of Chemistry, Faculty of Science, University of Qom, Qom, 37185-359, Iran, mahmoud8103@yahoo.com.

Keywords: Anomeric effect, H-bond catalyst, TMU-52-UR, Macromolecules.

The utilization of a hydrogen bond-donating approach represents a clever and appropriate technique for developing novel heterogeneous catalysts based on metal-organic frameworks (MOFs). Pillar-layered Metal-organic frameworks (MOFs) represent a unique class of MOFs distinguished by their structure, which comprises alternating layers of metal-containing pillars and organic ligands. The presence of two linking ligands that can facilitate basic functions makes pillar-layered MOFs promising for heterogeneous catalytic applications [1]. H-bond donating-MOFs catalysis has been acknowledged as a useful method for producing essential intermediate products utilized in the pharmaceutical and agricultural sectors. These catalysts are capable of selectively binding and activating reactive substrates through either hydrogen bonding or noncovalent interactions [2,3]. We aim to design a MOF based on Zn metal, which uses carboxylic acid and pyridine ligands in its structure, and turns it into a pillar-layered metal-organic frameworks (MOFs). The catalytic application of TMU-52-UR as a novel H-bond Zn-MOF-based in the preparation reaction of macromolecule compounds has been evaluated in green and mild conditions, and the results prove the suitability of such a catalytic system (**Scheme 1**).

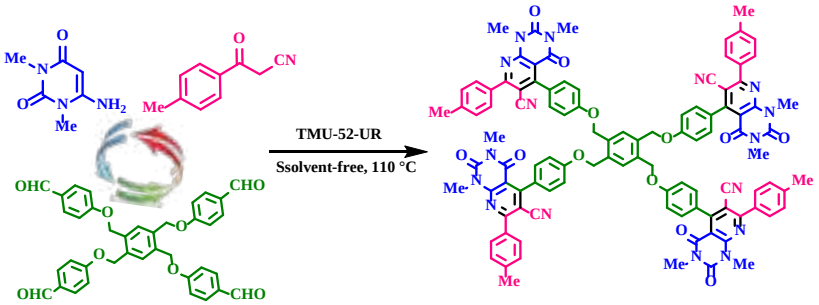

Scheme 1: Synthesis of target macromolecules using TMU-52-UR.

References

[1] Hashemi, L.; Morsali, A. Pillared Metal-Organic Frameworks: Properties and Applications. *John Wile & Sons* 2019.
[2] Chen, L.; Zhang, B.; Chen, L.; Liu, H.; Hu, Y.; Qiao, S. Hydrogen-bonded organic frameworks: design, applications, and prospects. *Adv. Mater* 2022, *3*, 3680-3708.
[3] Lutz, J. F. Solution self-assembly of tailor-made macromolecular building blocks prepared by controlled radical polymerization techniques. *Polym. Int* 2006, *55*, 979-993.

Plasma induced graft polymerization of acrylic acid on chitosan

Zeinab Chehrazi[a], Ali Reza Kiasat[a,b*] , Seifollah Jamalpour [c] and Mohammad Sabaeian[d,e]

a) Department of Chemistry, Faculty of Science, Shahid Chamran University of Ahvaz, Ahvaz, Iran, zeinabchehrazi76@gmail.com.
b) Petroleum Geology and Geochemistry Research Centre (PGGRC), Shahid Chamran University of Ahvaz, Ahvaz, Iran.
c) Department of Chemical Engineering, Faculty of Engineering, Shahid Chamran University of Ahvaz, Ahvaz, Iran.
d) Department of Physics, Faculty of Science, Shahid Chamran University of Ahvaz, Ahvaz, Iran.
e) Center for Research on Laser and Plasma, Shahid Chamran University of Ahvaz, Ahvaz, Iran.

Keywords: Chitosan, Acrylic acid, Polymerization, Plasma

Graft polymerization is a suitable method for modifying natural polymers. In this study, acrylic acid (AA) was grafted onto chitosan (Cs) through plasma in order to achieve the desirable properties of chitosan. Atmospheric Pressure Plasma (APP) treatment is a green technology that can induce the radical formation and crosslinking of polymers in liquid phases [1]. The structure of chitosan grafted acrylic acid (CsAA) copolymer have been characterised by FTIR spectroscopy. After grafting, the new band at 1698 cm^{-1} appears in CsAA spectrum. It corresponds to stretching vibrations of carboxyl groups which is attributed to grafting of AA onto the Cs. The presence of the asymmetrical and symmetrical AA COO− groups at 1516-1541 cm^{-1} confirm the interaction of Cs with AA. The synthesis steps are shown in **Scheme**.

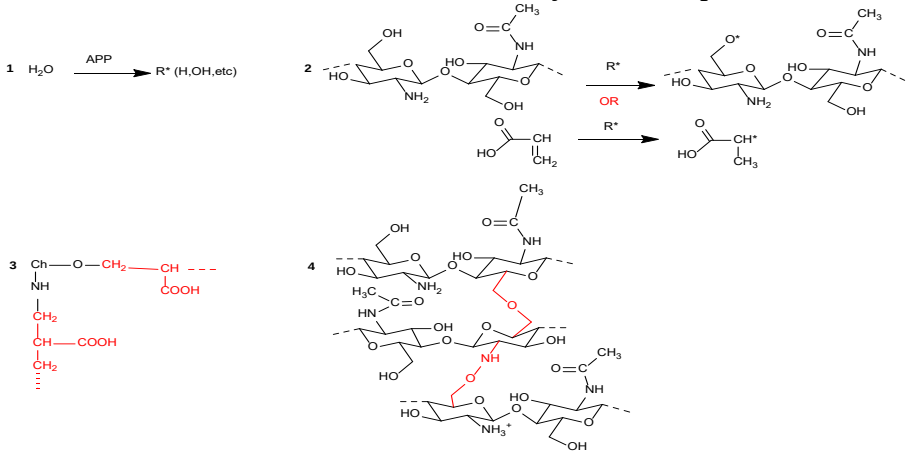

Scheme: Possible chemical reactions involved in the plasma treatment of CsAA solutions during synthesis.

References:

[1] Taaca, K. L. M.; De Leon, M. J. D.; Thumanu, K.; Nakajima, H.; Chanlek, N.; Prieto, E. I.; Vasquez Jr, M. R. Probing the structural features of a plasma-treated chitosan-acrylic acid hydrogel. *Colloids Surf. A: Physicochem. Eng. Asp.* **2022**, *637*, 128233.

Synthesis of new Chalcone containing Triarylmethane units

Fahimeh Asadi, Reza Ranjbar-Karimi* and Kazem Mohammadiannejad

Department of Chemistry, Faculty of Science, University of Vali-e-Asr Rafsanjan, Kerman, Iran, fahimehasadi2569@gmail.com, r.ranjbarkarimi@vru.ac.ir and kmmohammadi@gmail.com

Keywords: Chalcone, Triarylmethane, SiO_2-H_2SO_4

Chalcones are an aromatic ketone in which two aromatic rings are linked through a three carbon α, β unsaturated carbonyl system, and they are a novel category of compounds with substantial properties such as antimicrobial, antifungal, antiviral, anticancer and etc... [1,2] The present work involves a new chalcone which is containing triarylmethane (TARM) units that are synthesized in 3 steps. At first, the coupling reaction of 4-formylphenylboronic acid with 4-bromoacetophenone has occurred. Secondly, the solventless Fridel-crafts alkylation reaction of arenes such as veratrole with the aldehyde, catalyzed by SiO_2-H_2SO_4 was done. In the last step nucleophilic reaction was carried out between 4-methylbenzaldehyde and TARM and obtained chalcone. The structure of all compounds elucidated by ^{1}H-NMR and ^{13}C-NMR Spectroscopy.

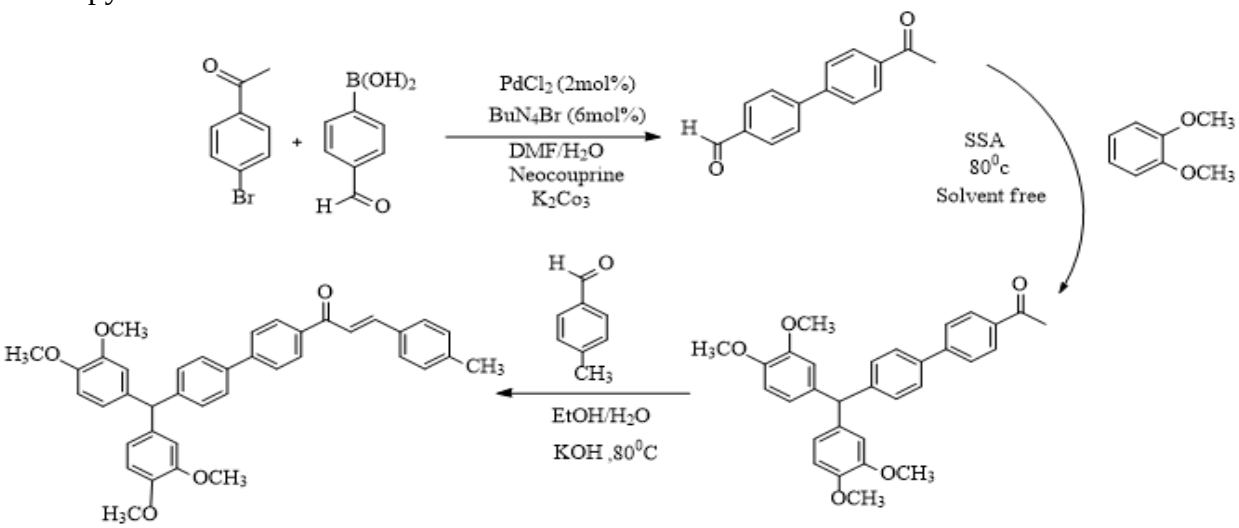

Scheme: 3 steps of chalcone synthesis

References

[1] Rammohan, A., Reddy, J. S., Sravya, G., Rao, C. N., & Zyryanov, G. V. "Chalcone synthesis, properties and medicinal applications: a review. *Environ. Chem. Lett.* 2020, 18, 433-458.

[2] Gaonkar, S. L., & Vignesh, U. N. Synthesis and pharmacological properties of chalcones: a review. *Res. Chem. Intermed.* 2017, *43*, 6043-6077.

Valorization of CO_2 catalyzed by nitrogen-rich covalent triazine framework

Mohadeseh Rashvand[a] **and Mojtaba Khorasani**[a,b*]

a) Department of Chemistry, Institute for Advanced Studies in Basic Sciences (IASBS), No. 444, Prof. Yousef Sobouti Boulevard, Zanjan 45137-66731, Iran, rashvand.m@iasbs.ac.ir, m_khorasani@iasbs.ac.ir.
b) Research Center for Basic Sciences & Modern Technologies (RBST), Institute for Advanced Studies in Basic Sciences, IASBS, Zanjan 45137-66731, Iran.

Keywords: Covalent triazine frameworks, CO_2 fixation, Cyclic carbonate, Nitrogen-rich

The catalytic coupling of carbon dioxide (CO_2) with epoxides to produce the cyclic carbonates which is extensively used as an important synthetic intermediate or apolar solvent, is considered one of the most important organic transformations [1]. However, this transformation practically needs a catalyst due to the inherent stability of CO_2. Although hydrogen-bond-donor (HBD) catalysts in either homogeneous or supported forms have been extensively explored for various types of organic transformations, have been rarely investigated for direct coupling of carbon dioxide with epoxides. Covalent triazine frameworks have been attracting tremendous interest as promising heterogeneous catalysis for this kind of CO_2 conversion [2]. We would like to report a nitrogen-rich CTF with diamino pyridine linkers with the combination of tetrabutylammonium iodide (TBAI) as a co-catalyst was found to reveal excellent activity and selectivity for the direct coupling of carbon dioxide with various types of terminal epoxides. It is believed that the described CTF architecture appears to capture CO_2 while the hydrogen bonding site facilitates the ring opening of epoxide as the first step of the reaction.

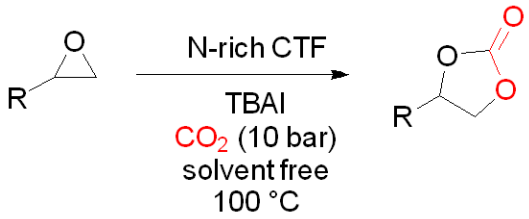

Scheme: Catalytic coupling of various types of epoxides with CO_2 by N-rich CTF.

References

[1] Razaghi, M.; Khorasani, Boosting the quaternary ammonium halides catalyzed CO_2 coupling with epoxides on the hollow mesoporous silica sphere, *J. CO_2 Util*. **2022**, *61*, 102028.
[2] Luo, R.; Yang, Y.; Chen, K.; Liu, X.; Chen, M.; Xu, W.; Liu, B.; Ji, H.; Fang, Y. Tailored covalent organic frameworks for simultaneously capturing and converting CO_2 into cyclic carbonates. *J. Mater. Chem. A*. **2021**, **9**, 20941-20956.

Diphenylglyoxime gapped Ni^{2+} immobilized on multi-walled carbon nanotube: A new nanocatalyst for one-pot cyclopropanation reaction

Shadi Namdar and Nader Noroozi Pesyan*

Department of Organic Chemistry, Faculty of Chemistry, Urmia University, 57159 Urmia, Iran, namdar70arshad@gmail.com

Keywords: CNT, Diphenylglyoxime, Cyclopropane

Magnetic carbon nanotubes (CNTs) in the form multi-walled (MWCNT) hybrid materials have attracted considerable attention from scientific communities owing to their promising applications in a variety of technical fields, such as medical and biosensor [۱]. The use of Ni species as catalyst can be of great importance since Ni is a great alternative to precious metals for reactions from viewpoint of cost-efficiency [2]. A new heterogeneous nanocatalyst containing Ni and diphenylglyoxime as ligand, complex grafted to MWCNT was synthesized. This recoverable nanocomposite was applied as a highly effective, green, thermally stable catalyst for the one-pot cyclopropanation reaction (**Scheme 1**). The heterogeneous nanocomposite was well identified using SEM, TEM, XRD, FTIR, EDX analysis techniques. The eco-friendly nanocatalyst demonstrated excellent recyclability.

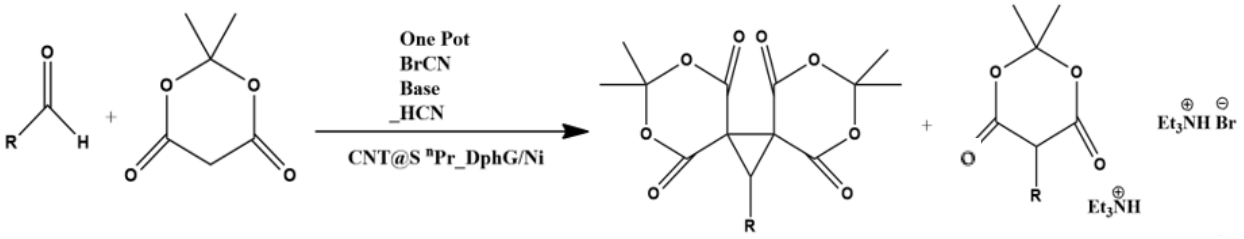

Scheme1: Cyclopropanation reaction in the presence of CNT@S^{n}Pr-DPhG/Ni nanocatalyst.

References:

[1] Hosseinzadeha S, Hosseinzadeh H, Pashaei SH, Khodaparasta Z., Synthesis of magnetic functionalized MWCNT nanocomposite through surface RAFT co-polymerization of acrylic acid and N-isopropyl acrylamide for removal of cationic dyes from aqueous solutions. *Ecotoxicol. Environ. Saf.* 2018, 161, 34-44.

[2] Aalinejad M, Noroozi Pesyan N, Doustkhahb E., Diaza crown-type macromocycle (kryptofix 22) functionalised carbon nanotube for efficient Ni^{2+} loading; A unique catalyst for cross-coupling reactions. *Mol. Catal.* 2020, 494, 111117.

THE SYNTHESIS OF FAP-2286 ACETATE AS A PEPTIDE RADIOPHARMACEUTICAL FOR THE DIAGNOSIS AND TARGETED THERAPHY OF 30 TYPES OF CANCER TUMORS

Seyyed Mohammad Shahcheragh*, Maryam Khoshdoun and Arsalan Pashapour

Aprin Sama Pharmed Company, Tehran, Iran, M.shahcheragh.oc@gmail.com

Keywords: Targeted Therapy, Peptide, Radiopharmaceuticals, Cancer

Fibroblast activation protein (FAP) is a membrane-bound protease that has limited expression in normal adult tissues but is highly expressed in the tumor microenvironment of many solid cancers. Currently, FAP family radiopharmaceuticals are considered the most unique and effective radiopharmaceuticals in the world in terms of their scope of action, and this active substance is used as a radiopharmaceutical in the diagnosis and treatment of 30 different types of cancer tumors [1]. In this article, the Fap-2286 acetate, which is a cyclic peptide with a complex structure, has been synthesized using a creative method. The synthesis of this structure has been done by performing the reaction on the solid phase, as shown as in **Scheme1**. After obtaining crude reaction, the final product was purified through preparative HPLC and identified by mass analysis. Also, its purity percentage was determined by analytical HPLC on C18 column. The preclinical and clinical studies of this peptide are currently being conducted at the Atomic Energy Organization of Iran.

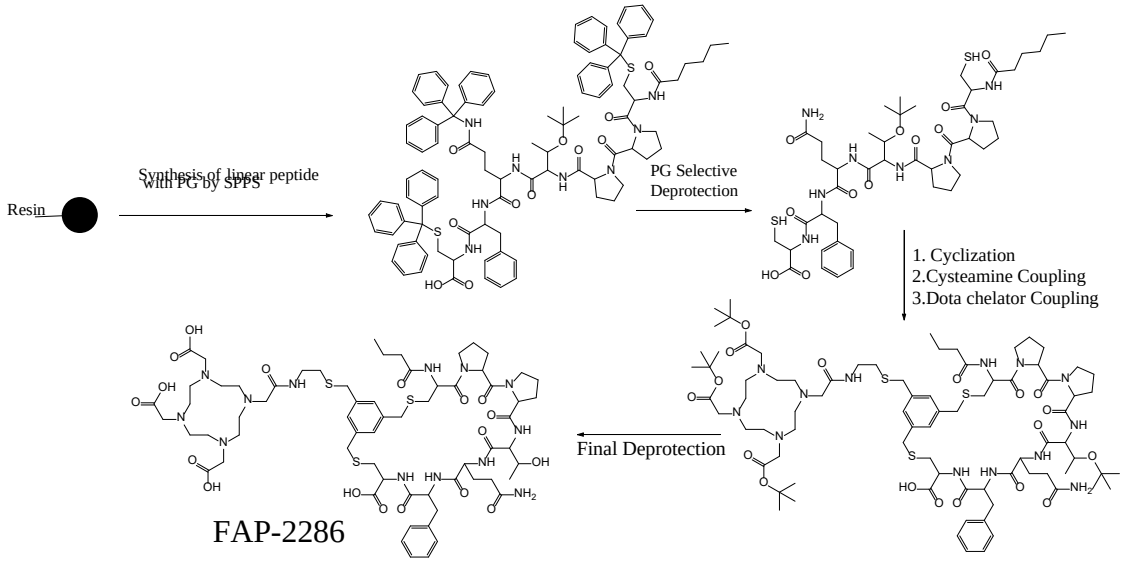

Scheme1: The Main Steps of FAP-2286 Synthesis

References:
[1]. Zboralski, Dirk, et al. Preclinical evaluation of FAP-2286 for fibroblast activation protein targeted radionuclide imaging and therapy. *Eur. J. Nucl. Med. Mol. Imaging* 49.11 (2022): 3651-3667.

Synthesis of 5-amino-1H-pyrazole-4-carbonitrile Derivatives in the presence of Biochar/Zinc Oxide Nanocatalyst

Maryam Noori, Maryam Hajjami*

Department of Organic Chemistry, Faculty of Chemistry, Bu-Ali Sina University, Hamedan 6517838683, Iran, mohsenfardarani@gmail.com, m.hajaami@basu.ac.ir & m.hajjami@yahoo.com

Keywords: Biochar, Zinc Oxide Catalyst, Multi-component reaction (MCRs), Nanoparticles.

Biochar is a highly porous, carbon - based material produced from a range of different biomass, usually either vegetal or animal waste, under low - oxygen conditions that I have significant aromatization and anti - decomposition capabilities. Biochar is reported to have a high specific surface area and contain a wide variety of negative surface functional groups (e.g., hydroxyl, carboxyl, amino), and therefore it has gained the interest of the scientific community in multifunctional fields such as support for catalysis synthesis [1]. Novel catalyst based on zinc oxide on biochar is prepared through a simple route and is proposed for the synthesis of 5-amino-1H-pyrazole-4-carbonitrile derivatives. Highly effective biochar/ZnO catalysed via one-pot multi-component reaction, by Using the phenyl hydrazine, malononitrile and aldehyde under optimal conditions. The salient features of this nanocomposite as catalyst are: easy preparation, cost effective, high stability and reusability of the catalyst [2] **(Schem1).**

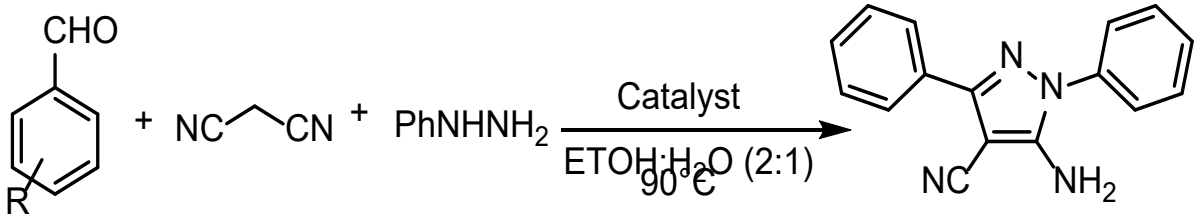

Scheme: Synthesis of 5-amino-1H-pyrazole-4-carbonitrile using Zinc Oxide catalyst

References

[1] Rodriguez-Navaez, O. M; Peralta-Hernandez, J. M; Goonetilleke, A; Bandala, E. R. Biochar-supported nanomaterials for environmental applications, *Ind Eng Chem Fund*. 2019, 78, 21-33.

[2] Moradi, P; Hajjami, M. Magnetization of biochar nanoparticles as a novel support for fabrication of oregano nickel as a selective, reusable and magnetic Nano catalyst in organic reactions, *New J. Chem*. 2021, 25, 2981-2994.

Immobilization of Lysozyme in ZIF-8 for Enhancing Reusability and Activity of Enzyme

Hamid Reza Kalhor*, Zeinab Piraman

Biochemistry and Chemical Biology Research Laboratory, Faculty of Chemistry, Sharif University of Technology, Tehran, Iran, kalhor@sharif.edu, zeinabpiraman@gmail.com

Keywords: Zeolitic imidazolate framework, Biocatalyst, Immobilization.

A subclass of Metal-organic framework known as Zeolitic Imidazolate Frameworks (ZIFs), which are made of Zn ions as metal nodes and 2-methylimidazole as an organic ligand, typically consists of huge cavities connected by small windows. Due to gentle synthesis conditions, enormous specific surface area, and great water stability, ZIF-8 has been used widely as a template for enzymes immobilization [1]. The aim of the present study has been to immobilize an enzyme using a metal-organic framework in order to enhance the enzymatic reaction. Lysozyme, as a very common and well-characterized enzyme, was used to immobilize in ZIF-8. As shown in Scheme I, immobilization was done by de-novo encapsulation method [2]. The Fourier Transform Infrared spectra indicated that the lysozyme was well immobilized in ZIF-8. Scanning Electron Microscopy and X-ray diffraction analysis were also performed, indicating that the sodalite topology for immobilized lysozyme was similar to simulated ZIF-8 and the presence of the enzyme in the structure did not change the ZIF structure. To examine the activity and reusability of the encapsulated enzyme, immobilized lysozyme was used in some C-C coupling reactions. The results indicated that the yield of the reaction and its reusability were significantly enhanced as compared to nonencapsulated enzymes.

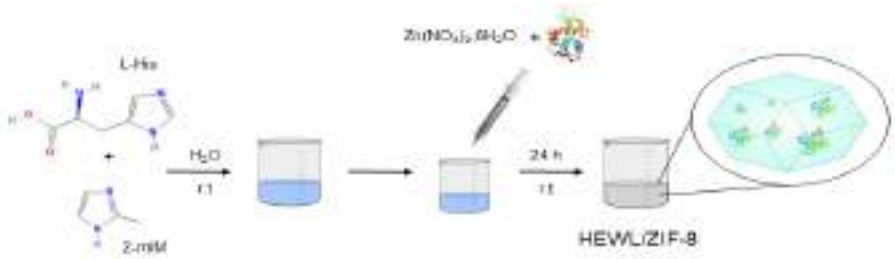

Scheme I: Encapsulation of lysozyme in ZIF-8, to enhance activity and recyclability.

References

[1] Zhao, J.; Li, H.; Han, Y.; Li, R.; Ding, X.; Feng, X.; Wang, B. Chirality from Substitution: Enantiomer Separation via a Modified Metal–Organic Framework. *J. Mater. Chem. A* **2015**, *3* (23), 12145–12148.

[2] Shen, X.; Du, Y.; Du, Z.; Tang, X.; Li, P.; Cheng, J.; Yan, R.; Cui, J. Construction of Enzyme@Glutathione Hybrid Metal-Organic Frameworks: Glutathione-Boosted Microenvironment Fine-Tuning of Biomimetic Immobilization for Improving Catalytic Performance. *Mater. Today Chem.* **2023**, 27, 101326.

Green in-situ preparation of chitosan/gallic acid metal-organic framework nanocomposite hydrogel beads as an antibacterial agent

Hanieh Hamedi, Siamak Javanbakht and Reza Mohammadi*

Polymer Research Laboratory, Faculty of Chemistry, University of Tabriz, Tabriz, Iran, Haniehhamedihagi@gmail.com, r.mohammadi@tabrizu.ac.ir

Keywords: Antibacterial, Chitosan, Nanocomposite, Metal-organic frameworks, Hydrogel

In the history of modern medicine, there has been a serious risk of antibacterial drugs as losing their effectiveness against bacteria [1]. In this regard, nanocomposite hydrogel beads based on natural polymers such as chitosan (CS) have been recently proposed as antibacterial platform [2]. In this work, antibacterial gallic acid-based metal-organic framework (GA-MOF) were developed to increase the biological efficiency of CS hydrogel beads (**Scheme**). Various analysis techniques were utilized for the validation of successful construction of the nanocomposites. In-vitro GA release in the simulated physiological environmental (PBS, pH 7.4) were considered, revealing a controlled and sustained release profile during 72 h. Antibacterial studies showed inhibition zone of 18 ± 0.5 mm for the *Staphylococcus aureus* bacteria, respectively. Considering obtained results, the prepared nanocomposite hydrogel beads have good potential to be employed as antibacterial bio-platform.

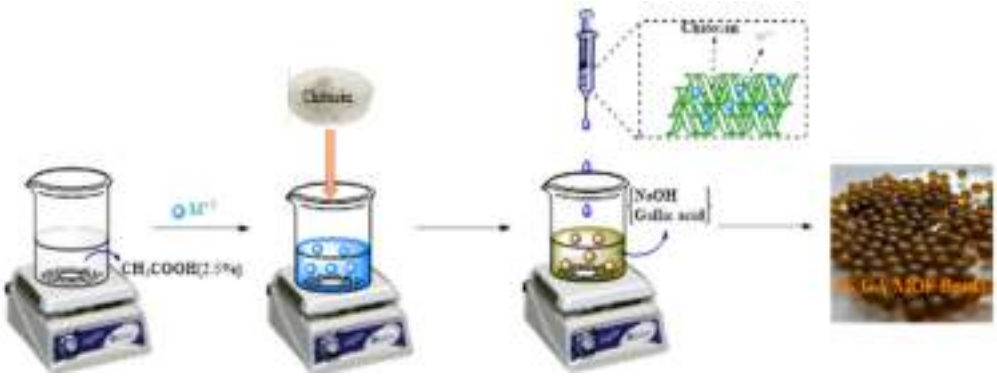

Scheme: Schematic procedure for preparation of CS/GA-MOF nanocomposite hydrogel bead.

References

[1] Alkekhia, D.; LaRose, C.; Shukla, A. β-Lactamase-Responsive hydrogel drug delivery platform for bacteria-triggered cargo release. *ACS Appl. Mater. Interfaces* 2022, *14* (24), 27538-27550.
[2] El Bourakadi, K.; Merghoub, N.; Fardioui, M.; Mekhzoum, M. E. M.; Kadmiri, I. M.; Essassi, E. M.; Bouhfid, R. Chitosan/polyvinyl alcohol/thiabendazoluim-montmorillonite bio-nanocomposite films: Mechanical, morphological and antimicrobial properties. *Compos. B: Eng.* 2019, *172*, 103-110.

A new highly active Zn-based metal-organic frameworks (Zn-MOFs) functionalized with CuO nanoparticles for the azide-alkyne cycloaddition

Sima Kalhor[a], Hassan Sepehrmansourie[a], Mahmoud Zarei[*b] and Mohammad Ali Zolfigol[*a]

a) Department of Organic Chemistry, Faculty of Chemistry, Bu-Ali Sina University, PO Box 6517838683, Hamedan, Iran, simakalhor@ymail.com, zolfi@basu.ac.ir & mzolfigol@yahoo.com
b) Department of Chemistry, Faculty of Science, University of Qom, Qom, 3716146611, Iran, mahmoud8103@yahoo.com

Keywords: Click chemistry, Heterogeneous catalyst, Metal-organic frameworks

In the quest for the best catalytic materials, metal-organic frameworks (MOFs) have garnered significant attention. MOFs are a class of porous materials composed of metal ions or clusters interconnected by organic ligands [1-2]. The importance of multi-component reactions with diversity in raw materials as well as click reactions as an important group of material coupling methods has been well defined and the need to improve synthesis conditions and perform such reactions in terms of their environmental and economic efficiency is very important. The main goal of this report is to discuss the expansion of click chemistry. In the present study, a new metal-organic framework was designed and synthesized. In the design of the catalyst, it was tried to place CuO nanoparticles on the Zn-MOF so that the properties of both CuO and Zn-MOF can be used. This catalyst was used to synthesize 1,4-other substituted-1,2,3-triazoles derivatives. The method represents a truly green process with good sustainability and economics (**Scheme 1**).

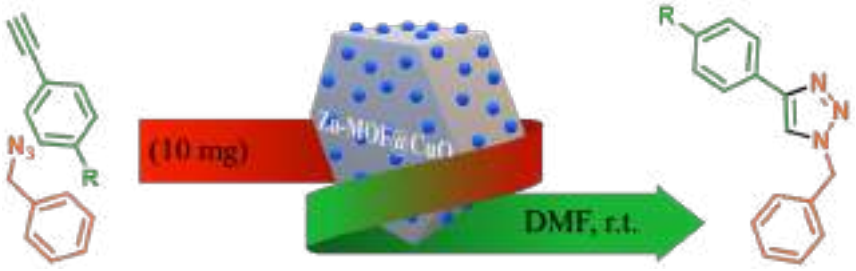

Scheme 1: Copper-catalyzed azide-alkyne cycloaddition (CuAAC) via Zn-MOF@CuO as a catalyst.

References

[1] Kitagawa, S. Metal-organic frameworks (MOFs). *Chem. Soc. Rev.* **2014**, *43* (16), 5415-5418.
[2] Wang, Q.; Astruc, D. State of the art and prospects in metal-organic framework (MOF)-based and MOF-derived nanocatalysis. *Chem. Rev.* **2019**, *120* (2), 1438-1511.
[3] Chen, L.; Jiang, C.; Xu, Q.; Jin, J.; Wang, X.; Li, X.; Hu, Y.; Lu, X.; Duan, S.; Gao, Z. Biphasic Release of Betamethasone from an Injectable Ha Hydrogel Implant for Alleviating Ldh Induced Sciatica. *Acta Biomater*. http://dx.doi.org/10.2139/ssrn.4484332

Efficient and simple rout for the synthesis of (tetrahydro-2H-thiazolo[3,2,b][1,2,4,5]tetrazin-7-yl)-2-(triphenylphosphoranylidene)acetate derivatives

Maryam Oudi *, **Mohammad Anary-Abbasinejad**

Department of Chemistry, Faculty of Science, University of Vali-e-Asr Rafsanjan, Kerman, Iran, maryamoudi298@gmail.com, m.anary@vru.ac.ir

Keywords: Three-component reaction, 1,2,4,5-Tetrazinane-3-thion derivatives, Dialkylacetylenedicarboxylate, Triphenylphosphine

Heterocyclic compounds are widely present in the structure of natural and synthetic compounds. Thiazoles are five-membered heterocycles containing nitrogen and sulphur atoms. The medicinal significance of the thiazoles such as antibiotics, antimicrobials, antineoplastic, anti-inflammatory and anti-thyroids [1]. Three-component reactions of 1,2,4,5-tetrazinane-3-thione derivatives, triphenylphosphine and dialkylacetylenedicarboxylate were carried out at room temperature in DMF solvent, and(tetrahydro-2H-thiazolo[3,2,b][1,2,4,5]tetrazin-7-yl)-2-(triphenylphosphoranylidene)acetate derivatives were synthesized efficiently and simply. (**Scheme 1**).

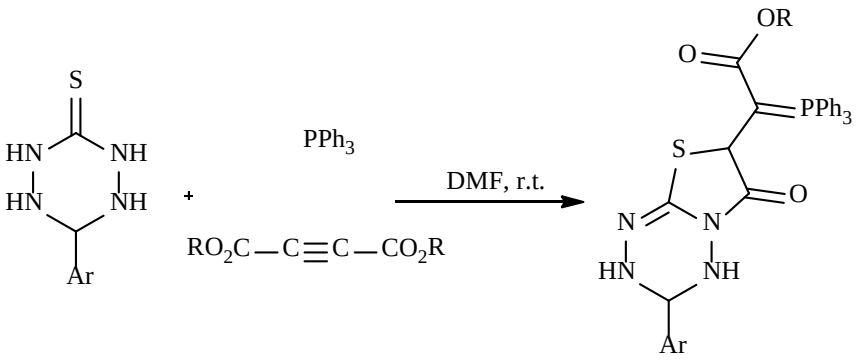

Scheme 1: Synthesis of (tetrahydro-2H-thiazolo[3,2,b][1,2,4,5]tetrazin-7-yl)-2-(triphenylphosphoranylidene)acetate derivatives

References

[1] Abdu-Rahem, L. R.; Ahmad, A. K.; Abachi, F. T. Synthesis and medicinal attributes of thiazole derivatives: A review. *Sys. Rev. Pharm* 2021, *12*, 290-295.

synthesis of 1,2-Dihydro-1-arylnaphtho[1,2-e][1,3]oxazine-3-ones compounds with the help of surfactant in water and the effect of ultrasound

Mohsen Moradian* and Saeedeh Asadian

Department of Organic Chemistry, Faculty of Chemistry, University of Kashan, Kashan, Iran, m.moradian@kashanu.ac.ir, s.p.asadian@gmail.com.

Keywords: Naphthoxazine, Surfactant, Green chemistry, Anionic micelles

An efficient and greener protocol for the synthesis of 1,2-dihydro-1-aryl-naphtho[1,2-e][1,3]oxazine-3-ones [1] using commercial surfactants, including anionic micelles, cationic micelles and nonionic micelles in water without using any organic cosolvents is described [2]. These studies will donate to reducing the use of injurious organic solvents and to progress efficient catalytic organizations which cannot be realized in conventional organic solvents (**Scheme**).

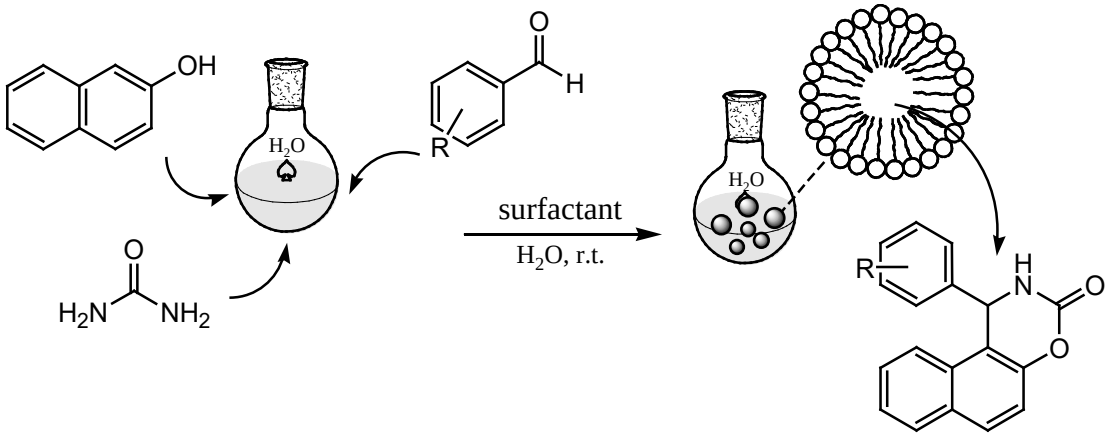

Scheme: Micelle-promoted synthesis of Naphthoxazinone derivatives

References

[1] Goodarzi, N.; Rashidizadeh, A.; Ghafuri, H. Ompg-C3N4/SO3H organocatalyst-mediated green synthesis of 1,2-dihydro-1-arylnaphtho[1,2-e][1,3] oxazin-3-ones under solvent-free and mild conditions: a fast and facile one-pot three-component approach. *Monatsh. Chem.* 2020, *151*, 791−798.

[2] Shinde, P. V.; Kategaonkar, A. H.; Shingate, B. B.; Shingare, M. S. Surfactant catalyzed convenient and greener synthesis of tetrahydrobenzo[a]xanthene-11-ones at ambient temperature. *Beilstein J. Org. Chem.* 2011, *7*, 53−58.

Catalytic Synthesis of Acridinedione Derivatives by Using a Dinuclear Iron(III) Complex

Elaheh Shahmoradi,[a] Rahman Bikas,*[b] Fatemeh Ajormal,[a] and Nader Noshiranzadeh[a]

a) Department of Chemistry, Faculty of Science, University of Zanjan, 45371-38791 Zanjan, Iran, elaheh.shahmoradi@yahoo.com

b) Department of Chemistry, Faculty of Science, Imam Khomeini International University, 34148-96818 Qazvin, Iran.

Keywords: Catalyst, Synthesis, Acridinedione, Iron complex

The special characteristics of acridinedione compounds, including the presence of N-heteroatom, the presence of acridine ring, their electronic behaviour, and the possibility of synthesis of extensive derivatives, as well as their bichromophoric structure and ability to interact with various proteins, render them a captivating framework in the realms of synthesis, heterocyclic, and medicinal chemistry [1]. The last years have seen an impressive improvement of the use of iron complexes as fascinating and valuable catalysts in organic synthetic transformations [2]. In this work, we report the synthesis, characterization, crystal structure of and catalytic activity of a new dinucelar iron(III) complex, $[Fe_2(L)_2Cl_2]$ (**1**). Compound **1** was synthesized by a reaction of $FeCl_2{\cdot}6H_2O$, H_2L (where ligand H_2L is 2,2'-((*1E,1'E*)-(ethane-1,2-diylbis(azanylylidene))bis(methanylylidene))bis(4-bromophenol)) in ethanol. The crystals of compound **1** were obtained by slow solvent evaporating method during one week. This compound was characterized by elemental analysis and FT-IR, UV-Vis spectroscopy and single crystal X-ray analysis. The results of these analyses show the formation of the phenolato bridged dinuclear iron complex. Compound **1** was used as catalyst for the green synthesis of acridinedione derivatives (**Scheme 1**) under mild condition. The results indicated that that this complex is an efficient catalyst for this reaction and enables the synthesis of acridinedione derivatives with high yields.

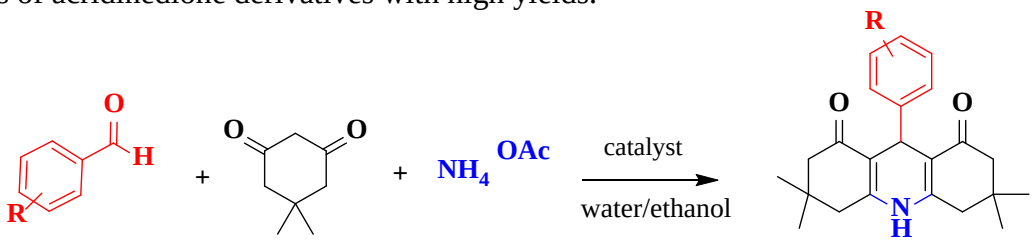

Scheme: Synthesis of acridinedione derivatives by using iron(III) complex as a catalyst.

References

[1] Sahiba, N.; Sethiya, A.; Soni, J.; Agarwal, S. Acridine-1,8-diones: Synthesis and Biological Applications. *ChemistrySelect* 2021, *6* (9), 2210-2251.

[2] Rana, S.; Biswas, J. P.; Paul, S.; Paik, A.; Maiti, D. Organic synthesis with the most abundant transition metal–iron:from rust to multitasking catalysts. *Chem. Soc. Rev.* 2021, *50*,243-472.

Synthesis of 3,4-Dihydropyrimidine Compounds via the Biginelli Reaction Catalyzed by Cu-1,3-Oxazolidine Complex

Fatemeh Ajormal,[a]* Rahman Bikas,[b] Nader Noshiranzadeh[a], Elaheh Shahmoradi[a]

a) Department of Chemistry, Faculty of Science, University of Zanjan, 45371-38791 Zanjan, Iran.
b) Department of Chemistry, Faculty of Science, Imam Khomeini International University, 34148-96818 Qazvin, Iran

Keywords: Catalyst, Synthesis, Biginelli, Multicomponent Reactions

Multicomponent reactions have become indispensable tools in modern synthetic chemistry and medicine. These reactions are highly significant in organic chemistry due to their remarkable pharmaceutical properties. Biginelli is the well-known reaction in organic chemistry for the synthesis of valuable biological compounds with neuroprotective, antiparasitic, antiviral, antitumor, anti-inflammatory, and anticancer activities [1]. The Biginelli reaction is typically performed using aromatic aldehydes, urea/thiourea, and ethyl acetoacetate or its derivatives [2]. In the absence of a catalyst, it is difficult to form products with a good yield and catalysts play an essential role in this reaction. Copper catalysts can efficiently catalyze this reaction and they have attracted considerable attention in recent years [3]. In this work, a mononuclear Cu(II) complex, ($[Cu(L)Cl_2]\cdot CH_3OH$ where L is (2-pyridin-2-yl-1,3-oxazolidine-4,4-diyl)dimethanol), was synthesized by the reaction of $CuCl_2.H_2O$ with N- and O-donor ligand in methanol. The complex was characterized by FT-IR, UV-Vis, and elemental analysis. The crystal structure of the synthesized Cu(II) complex has been determined by single-crystal X-ray diffraction analysis which indicates that the Cu(II) ion adopts distorted square pyramidal geometry. The catalytic activity of Cu(II) complex was investigated in the synthesis of 3,4-dihydropyrimidine compounds via classical Biginelli reaction. The results demonstrate this complex exhibits high catalytic activity (low reaction times and high yields) in the synthesis of 3,4-dihydropyrimidine compounds.

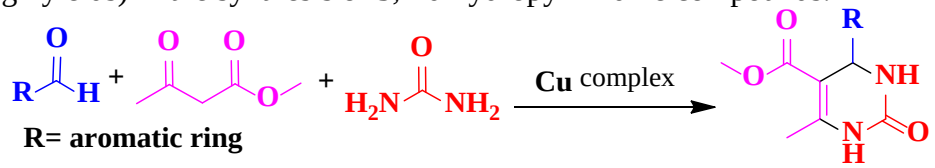

Scheme: Synthesis of 3,4-dihydropyrimidine by three component one-pot Biginelli reaction.

References

[1] Nagarajaiah, H.; Mukhopadhyay, A.; Moorthy, J. N. Biginelli reaction: an overview. *Tetrahedron Lett.* 2016, *57* (47), 5135-5149.
[2] Patil, R. V.; Chavan, J. U.; Dalal, D. S.; Shinde, V. S.; Beldar, A. G. Biginelli Reaction: Polymer Supported Catalytic Approaches. *ACS Comb. Sci.* 2019, *21* (3), 105-148.
[3] Willig, J. C. M.; Granetto, G.; Reginato, D.; Dutra, F. R.; Poruczinski, É. F.; de Oliveira, I. M.; Stefani, H. A.; de Campos, S. D.; de Campos, É. A.; Manarin, F. A comparative study between Cu (INA) 2-MOF and [Cu $(INA)_2$ $(H_2O)_4$] complex for a click reaction and the Biginelli reaction under solvent-free conditions. *RSC Adv.* 2020, *10* (6), 3407-3415.

The preparation of inclusion complex of menthol in β-cyclodextrin

Azita Khodabandeh, Behnam Mahdavi*, Esmail Rezaei-Seresht

Department of Chemistry Faculty of Science, Hakim Sabzevari University, Sabzevar, Iran, azitanote@gmail.com, b.mahdavi@hsu.ac.ir

Keywords: Menthol essential oil (EO), ß-cyclodextrin (ß-CD), encapsulated complex (EO/ß-CD)

Cyclodextrins (CD) are cyclical oligosaccharides that are derived from starch. The spatial orientation of the glucopyranose units in β-CD molecules forms a truncated cone with a hydrophobic interior space and a hydrophilic exterior surface [1]. The essential oils and terpenoids compounds like menthol are known as hydrophobic compounds. In recent years, the encapsulation techniques improve the water solubility of these compounds. β-CD derivatives such as methylated β-CD are a class of hosts for this propose [2]. In the present study, we have investigated the preparation of menthol encapsulation in β -CD. The FT-IR technique was run to endorse the preparation of menthol/β-CD.

Method: the co-precipitation method was used to prepare the inclusion complex of menthol/β-CD. A hydroalcoholic solution of β-CD was prepared by dissolving of β-CD (1 g) in 10 mL water:ethanol (1:1). Then, 2 ml of menthol was added to β-CD solution. The mixture was electromagnetically stirred at 55°C for 30 minutes, and then followed by continuous stirring for 4 hours at room temperature. The samples were then kept at 4°C for 12 hours. Finally, the formed precipitate was separated through vacuum filtration and was dried in an oven at 50°C for 24 hours. Figure 1 shows the FT-IR spectra of β-CD, menthol, and menthol/β-CD complex. The similarity of the spectrum of menthol/β-CD to those of β-CD and menthol confirm the preparation of the inclusion complex of menthol/β-CD successfully.

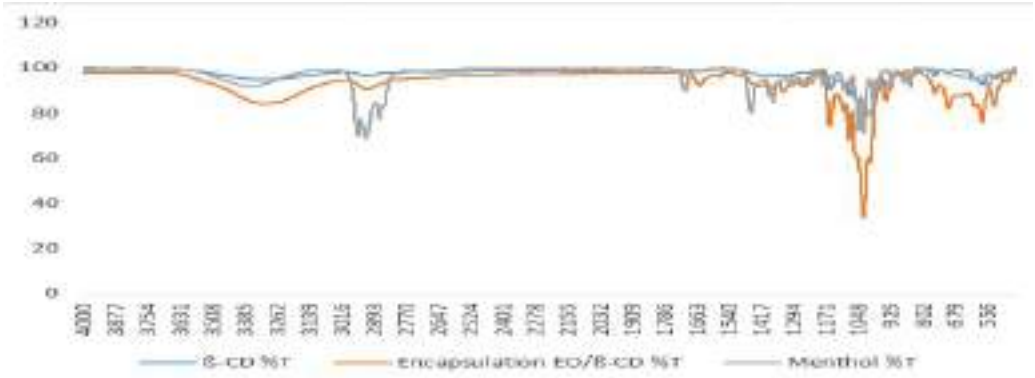

References

[1] Hill, Laura E., Carmen Gomes, and T. Matthew Taylor. "Characterization of beta-cyclodextrin inclusion complexes containing essential oils (trans-cinnamaldehyde, eugenol, cinnamon bark, and clove bud extracts) for antimicrobial delivery applications." *LWT - Food Sci. Technol.* 51.1 (2013): 86-93.

[2] A. PEGGY, P. CEVALLOS, MP. BUERA, BE. ELIZALDE. Encapsulation of cinnamon and thyme Essential oils components (cinnamaldehyde and thymol) in ù-cyclodextrin: Effect of interactions with Water on complex stability. *J. Food Eng.*,99, 70-75 (2010).

A Novel and Efficient Procedure for the Synthesis of Spiro[acridine-9,3'-indoline]-1,2'-dione

Neda Khedri, Mohammad Reza Mohammadizadeh,* Forough Zahedpour, Zahra Rastipour

Department of Chemistry, Faculty of Nano- and Bio-Science and Technology, Persian Gulf University, Bushehr 75169, Iran, mrmohamadizadeh@pgu.ac.ir, z.rastipoor@gmail.com

Keywords: Isatin, N-aryl enaminones, Spiro[acridine-9,3'-indoline]-1,2'-diones

New drug discovery and development continues to be an area of intensive investigation. Acridine scaffold has highly efficient anti-inflammatory, anticancer, antimicrobial, antitubercular, antiparasitic, antimalarial, antiviral and fungicidal activities [1]. Furthermore, the spirocyclic oxindoles exhibit diverse biological activities including anticancer potentials [2]. In continues of our studies on the synthesis of spiro-heterocyclic compounds [3], we recently investigated the reaction of N-substituted isatin and N-aryl-enaminones, which led to introduction of a new and efficient method for the synthesis of spiro [acridine-9-3'-indoline]-1, 2'-dione derivatives. The reactions were carried out in acetic acid under reflux conditions and the desired products obtained in excellent yields (**Scheme 1**).

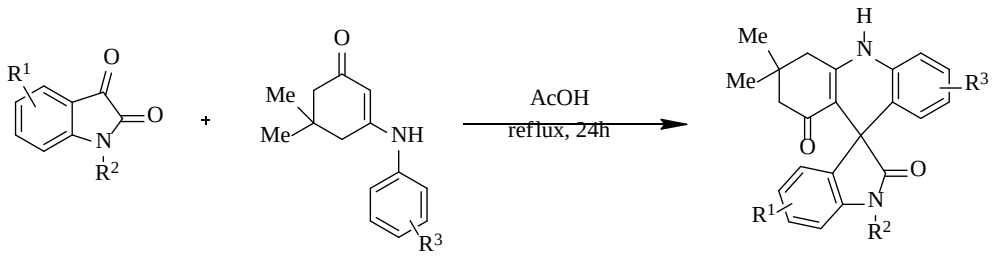

Scheme 1: Novel synthesis of spiro [acridine-9,3'-indoline]-1,2-diones

References:

[1] Gensicka-Kowalewska, M.; Cholewinski, G.; Dzierzbicka, K. Recent developments in the synthesis and biological activity of acridine/acridone analogues. *RSC Adv.* 2017, *7*, 15776-15804.

[2] Yu, B.; Yu, D. Q.; Liu, H. M. Spirooxindoles: Promising scaffolds for anticancer agents. *Eur. J. Med. Chem.* 2015, *97*, 673-98.

[3] Mousavi, S. H.; Mohammadizadeh, M. R.; Roshan, Z.; Jamaleddini, A.; Arimitsu, S. One-pot synthesis of spiro-isobenzofuran compounds *via* the sequential condensation/oxidation reaction of ninhydrin with 4-amino-1,2-naphthoquinones/2-amino-1,4-naphthoquinones under mild conditions. *ACS Omega*, 2020, *5*, 18273-18288.

One-pot synthesis of quinoline derivatives by modified nanomagnetic graphitic carbon nitride as a green nanocatalyst

Fatemeh Rezaei, Heshmatollah Alinezhad* and Behrooz Maleki

Department of Organic Chemistry, Faculty of Chemistry, University of Mazandaran, Babolsar, Iran, fatemehrezaei416@yahoo.com, alinejad@umz.ac.ir

Keywords: Graphitic carbon nitride, Mild reaction conditions, Green nanocatalyst, Quinoline

One of the effective strategies to take advantage of these compounds and simultaneously benefit from the privilege of the heterogeneous catalytic system, including stability, reusability, and easy recovery, is the functionalization of solid supports with organic molecules and active biomolecules [1]. Carbon-based nanomaterials are known as interesting solid support compounds, specifically two-dimensional nanosheet constituents, and their unique structure has led to charming physicochemical properties [2]. Among them, graphitic carbon nitride (g-C_3N_4) is recognized as a layered polymer whose attractive properties such as high stability, eco-friendly property, large surface area, rich in N, and nontoxicity have converted it into a valuable and useful class of carbon nanomaterials. Therefore, an environmentally organic compound was attached to the surface of magnetic graphene nitride by employing a linker agent. The synthesized composite efficiently catalyzed the multicomponent reaction including the synthesis of quinoline derivatives (**Scheme**). A large library of functional targeted products was synthesized in mild reaction conditions. More importantly, this catalyst was stable and magnetically recycled and reused for at least five runs without losing catalytic activity.

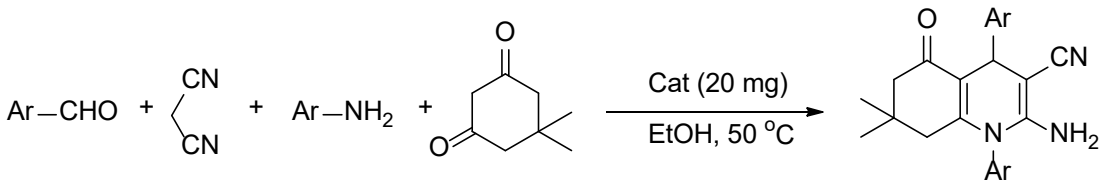

Scheme: The synthesis of quinoline derivatives using MNPs @g-C_3N_4-Pr-Cp.

References

[1] Lam, E.; H.T.Luong, J. Carbon materials as catalyst supports and catalysts in the transformation of biomass to fuels and chemicals. *ACS Catal.* 2014, *4*, 3393−3410.

[2] Dubertret, B., Heine, T. & Terrones, M. The rise of two-dimensional materials. *Acc. Chem. Res* 2015, *48*, 1-2.

Green and efficient synthesis of pyranopyrazole derivatives using SBA-15 supported ionic liquid (SBA-IL)

Sara Mohseni Tavana and Ghodsi Mohammadi Ziarani*

Department of Organic Chemistry, Faculty of Chemistry, Alzahra University, Tehran, Iran, saramohsenitavana@gmail.com, gmohammadi@alzahra.ac.ir

Keywords: Pyranopyrazole, Multicomponent reaction, SBA-IL, Heterogeneous catalyst

Dihydropyrano[2,3-c]pyrazole derivatives are a significant class of heterocyclic compounds known for their pharmaceutical activities [1]. The synthesis of these compounds involves a multicomponent reaction of ethyl acetoacetate, hydrazine hydrate, malononitrile, and aldehyde/ketone [2]. Ionic liquids are considered environmentally friendly alternatives because they can exhibit low environmental toxicities. As a result, researchers have been attracted to using ILs in various applications, including catalysis [3]. In This research, the reaction is conducted using SBA-IL as an efficient and heterogeneous catalyst in short reaction time with acceptable yield, which offers advantages such as easy separation and reusability (**Scheme 1**). The use of ionic liquids (ILs) in this research is particularly interesting due to their "green" nature.

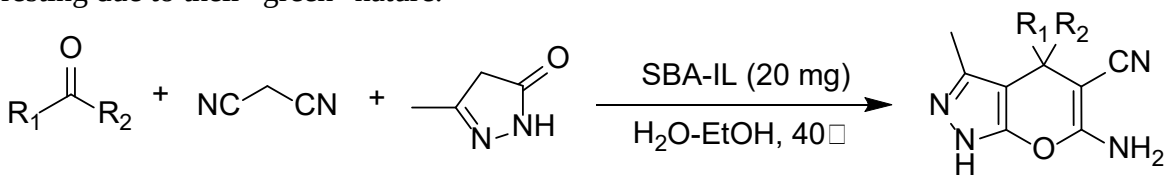

Scheme 1: Synthesis of Dihydropyrano[2,3-c]pyrazole by SBA-IL

References

[1] Dalal, K. S.; Tayade, Y. A.; Wagh, Y. B.; Trivedi, D. R.; Dalal, D. S.; Chaudhari, B. L. Bovine serum albumin catalyzed one-pot, three-component synthesis of dihydropyrano[2,3-c]pyrazole derivatives in aqueous ethanol. *RSC Adv.* 2016, *6*, 14868–14879.

[2] Guo, R. Y.; An, Z. M.; Mo, L. P.; Yang, S. T.; Liu, H. X.; Wang, S. X.; Zhang, Z. H. Meglumine promoted one-pot, four-component synthesis of pyranopyrazole derivatives. *Tetrahedron* 2013, *69*, 9931–9938.

[3] Mohammadi Ziarani, G.; Seyedakbari, L.; Asadi, S.; Badiei, A.; Yadavi, M. Ionic liquid supported nanoporous silica (SBA-IL) as an efficient and heterogeneous catalyst in the domino synthesis of polyhydroquinoline derivatives. *Res. Chem. Intermed.* 2016, *42*, 499–509.

Architecture of MIL-88B(Fe_2/Co)-UR as the new porous bimetallic H-bond catalyst for the preparation pyrazolo[3,4-*b*]quinolines via CVABO

Milad Mohammadi Rasooll, Hassan Sepehrmansourie and Mohammad Ali Zolfigol*

Department of Organic Chemistry, Faculty of Chemistry, Bu-Ali Sina University, Hamedan 6517838683, Iran, milad74628m@gmail.com, zolfi@basu.ac.ir & mzolfigol@yahoo.com

Keywords: Anomeric effect, Bimetal-organic frameworks, H-bond catalyst, Pyrazolo[3,4-*b*]quinolines

Nowadays, metal-organic frameworks (MOFs), are known as new generation nanoreactors. These compounds are formed as porous coordinated polymers by connecting metals and organic ligands. Drug delivery, energy and gas storage, chemical and biological sensor, water purification, catalyst and photocatalyst are applications of MOFs. Recently, the use of metal-organic frameworks (MOFs) containing two metals has found wide application which are known as bimetallic-MOFs. Studies have shown that in this category of catalysts, the two metals present in the MOF structure cause a synergistic effect [1]. In recent years, the use of heterogeneous catalysts modified with organic compounds such as urea and thiourea as hydrogen-bonding catalysts has become widespread. Catalysts based on hydrogen bonding have high selectivity and this ability has improved their catalytic properties because in this case they can play both an acidic and a basic role [2]. Pyrazolo[3,4-*b*]quinolines have been found to exhibit a wide range of biological activities, including antitumor, antiviral, and anti-inflammatory properties [3]. Considering the mentioned characteristics, we became interested in the synthesis of this group of compounds with the help of a new generation of hydrogen bond catalysts based on metal-organic frameworks (MOFs). Among the features of the above work is easy synthesis, high efficiency of products, reduction of side products and the ability to recycle the catalyst.

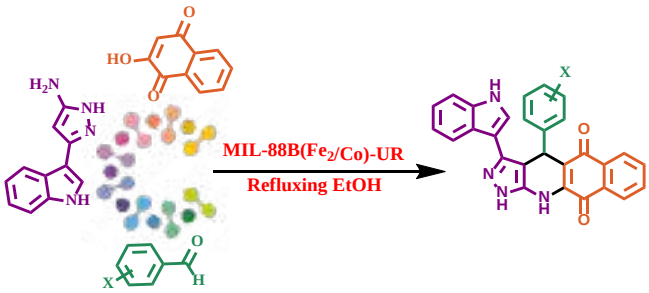

Scheme 1: Preparation of new pyrazolo[3,4-*b*]quinolines using MIL-88B(Fe_2/Co)-UR.

References

[1] Chen, L.; Wang, H. F.; Li, C.; Xu, Q. Bimetallic metal-organic frameworks and their derivatives. *Chem. Sci.* 2020, *11*, 5369-5403.

[2] Mayfield, A. B.; Metternich, J. B.; Trotta, A. H.; Jacobsen, E. N. Stereospecific furanosylations catalyzed by bis-thiourea hydrogen-bond donors. *J. Am. Chem. Soc.* 2020, *142*, 4061-4069.

[3] Safaei, S.; Mohammadpoor-Baltork, I.; Khosropour, A. R.; Moghadam, M.; Tangestaninejad, S.; Mirkhani, V.; Khavasi, H. R. One-pot three-component synthesis of pyrano[3,2-*b*]pyrazolo[4, 3-*e*]pyridin-8(1*H*)-ones. *ACS Comb. Sci.* 2013, *15*, 141-146.

Synthesis and application of novel TMU-17-UR as hydrogen bonding catalyst for the preparation of pyrazolo[3,4-*b*]quinolin-5-one derivatives

Milad Mohammadi Rasooll, Hassan Sepehrmansourie and Mohammad Ali Zolfigol*

Department of Organic Chemistry, Faculty of Chemistry, Bu-Ali Sina University, Hamedan 6517838683, Iran, milad74628m@gmail.com, zolfi@basu.ac.ir & mzolfigol@yahoo.com

Keywords: H-bond catalyst, Metal-organic frameworks (MOFs), Pyrazolo[3,4-*b*]quinolin-5-one, TMU-17-UR.

Metal-organic frameworks (MOFs) are an attractive class of hybrid crystalline materials that consist of organic linkers and metal nodes. Metal-organic frameworks have found wide applications in various fields due to their high surface area, adjustable holes, suitable morphology and designability. The defined reaction environments, tunable nature and purposeful preparation of MOFs has made this class of catalysts suitable candidates for catalytic purposes [1]. In recent years, the use of catalysts based on hydrogen bond activation has made significant progress. This category of catalysts has been used in various reactions such as Diels-Alder reactions, Mannich reactions, Claisen rearrangements, multi-component reactions, etc. Therefore, hydrogen bond catalysts are suitable candidates for catalyzing chemical reactions [2]. Quinoline compounds are a group of organic compounds that are classified in the heterocycle group. Compounds containing quinoline are used as antimalarial, antifungals, antibacterial and local anesthetics [3]. In this report, we used TMU-17-UR, which is a novel hydrogen bond catalyst, to synthesize pyrazolo[3,4-*b*]quinolin-5-one derivatives. High reaction speed, proper efficiency, recycling and reuse of the catalyst are among the features of this research work.

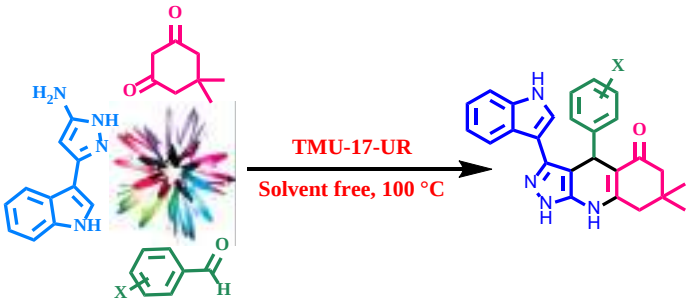

Scheme 1: Preparation of new pyrazolo[3,4-*b*]quinolin-5-one using TMU-17-UR.

References

[1] Safarifard, V.; Beheshti, S.; Morsali, A. An interpenetrating amine-functionalized metal-organic framework as an efficient and reusable catalyst for the selective synthesis of tetrahydro-chromenes. *CrystEngComm* 2015, *17*, 1680-1685.

[2] Mayfield, A. B.; Metternich, J. B.; Trotta, A. H.; Jacobsen, E. N. Stereospecific furanosylations catalyzed by bis-thiourea hydrogen-bond donors. *J. Am. Chem. Soc.* 2020, *142*, 4061-4069.

[3] Musiol, R.; Serda, M.; Hensel-Bielowka, S.; Polanski, J. Quinoline-based antifungals. *Current Med. Chem.* 2010, *17*, 1960-1973.

Preparation of modified nanomagnetic alginate as a green catalyst for the multicomponent synthesis of 1,4-dihydropyridine

Moghadaseh Keshvari Kenari, Sakineh Asghari* and Behrooz Maleki

Department of Organic Chemistry, Faculty of Chemistry, University of Mazandaran, Babolsar, Iran, moghadasekeshvari416@yahoo.com, s.asghari@umz.ac.ir

Keywords: Magnetic biocatalyst, Alginate, 1,4-dihydropyridine, Green reaction conditions

Magnetic nanoparticles have attracted great attention due to their extensive applications in various scientific topics, including catalysis [1]. Their facile magnetic separation process in compare son with centrifugation, extraction, and filtration has been considered their best advantage. Their wonderful properties like high surface area, low toxicity, oxidation resistance, biocompatibility, and magnetic properties converted these materials into worthwhile supports in the design of development reusable catalysts [2]. Synthesis of biocompatible magnetic nanoparticles employing natural polymers is distinguished as an imperative subject in green chemistry. So, a novel acid nanobiocatalyst (MNPs@Alg-Pr-His) was synthesized using available materials (nanomagnetic alginate core) via a facile strategy. After characterization, its efficiency was investigated in the synthesis of 1,4-dihydropyridine derivatives (**Scheme**). This nanobiocatalyst showed remarkable catalytic activity in reaction under mild reaction conditions. This catalyst showed good recyclability with no significant loss of catalytic activity after five runs.

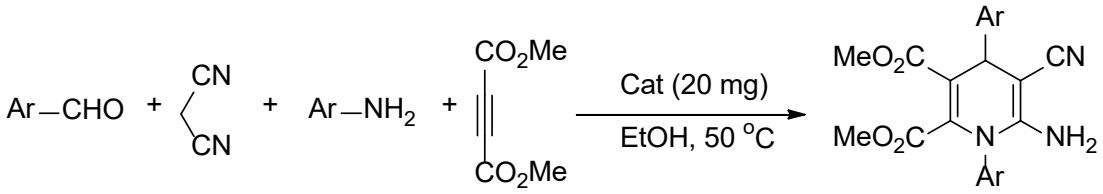

Scheme: The synthesis of 1,4-dihydropyridine using MNPs@Alg-Pr-His.

References

[1] Kheilkordi, Z.; Ziarani, G. M.; Badiei, A.; Sillanpää, M. Recent advances in the application of magnetic bio-polymers as catalysts in multicomponent reactions. *RSC adv* 2022, *12*, 12672-12701.

[2] Hudson, R.; Feng, Y.; Varma R. S.; Moores, A. Bare magnetic nanoparticles: sustainable synthesis and applications in catalytic organic transformations. *Green Chem.* 2014, *16*, 493-505.

Design and synthesis of novel Zr-based MOF and its application in the synthesis of dihydropyrano[3,2]chromenes compounds

Amin Benrashid*, Davood Habibi, Masoumeh Beiranvand

Department of Organic Chemistry, Faculty of Chemistry, Bu-Ali Sina University, Hamedan, Iran, aminbenrashid1@gmail.com,

Keywords: Zr-based metal-organic framework, One-pot synthesis, Dihydropyrano[3,2]chromenes.

Metal−organic frameworks (MOFs) are an emerging type of porous coordination network with promising catalytic capabilities that fabricate by self-assembly from a diversity of organic ligands and inorganic metal clusters [1]. Chromenes are a group of heterocyclic biological compounds found in many natural products and pharmaceutically useful intermediates [2,3]. Among them, dihydropyrano[3,2-*c*]chromenes have shown a potential application to treat diseases such as Alzheimer, Parkinson, schizophrenia, myoclonus, Huntington, and Down's syndrome [4]. In this study, a novel, reusable, and efficient novel Zr-based MOF was synthesized based on Zr cations, BDC-NH_2 and pyridine ligands. Then, the catalytic performance of the synthesized framework was assessed in the one-pot synthesis of dihydropyrano[3,2]chromenes under mild conditions. The catalyst exhibited a better efficiency than some of the already reported protocols in terms of higher yields and stability, lower reaction times, and simple separation.

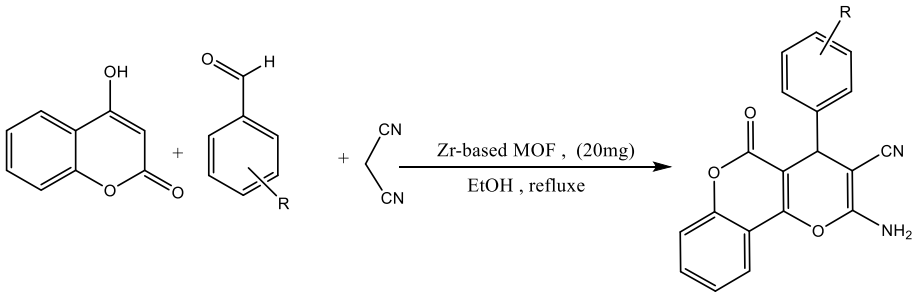

References

[1] Li, Y.; Wei, Z.; Zhang, Y.; Guo, Z.; Chen, D.; Jia, P.; Chen, P.; Xing, H. Dual-emitting EY@ Zr-MOF composite as self-calibrating luminescent sensor for selective detection of inorganic ions and nitroaromatics. *ACS Sustainable Chem. Eng.* 2019, *7*, 6196-6203.

[2] He, X.; Li, R.; Choy, P. Y.; Liu, T.; Wang, J.; Yuen, O. Y.; Leung, M. P.; Shang, Y.; Kwong, F. Y. DMAP-catalyzed annulation approach for modular assembly of furan-fused chromenes. *Org. Lett.* 2020, *22*, 9444-9449.

[3] Mogharabi-Manzari, M.; Ghahremani, M. H.; Sedaghat, T.; Shayan, F.; Faramarzi, M. A. A Laccase heterogeneous magnetic fibrous silica-based biocatalyst for green and one-pot cascade synthesis of chromene derivatives. *Eur. J. Org. Chem.* 2019, *8*, 1741-1747.

[4] Abdella, A. M.; Mohamed, M. F.; Mohamed, A. F.; Elwahy, A. H.; Abdelhamid, I. A. Novel bis(dihydropyrano[3,2-*c*]chromenes): Synthesis, antiproliferative effect and molecular docking simulation. *J. Heterocycl. Chem.* 2018, *55*, 498-507.

Gold and Palladium Supported on Ionic Liquid Modified Fe-based Metal–Organic Framework (MOF) as Highly Efficient Catalysts for Reductions and Sonogashira-Hagihara Reactions

Shirin Karimi,[a] Mohammad Gholinejad,[a,b]* Rahimeh Khezri,[c] José M. Sansano,[d,e] Carmen Nájera,[e] and Miguel Yus[e]

[a] Department of Chemistry, Institute for Advanced Studies in Basic Sciences (IASBS), P. O. Box 45195-1159, Gavazang, Zanjan 45137-66731, Iran, sh.karimi@iasbs.ac.ir.
[b] Research Center for Basic Sciences & Modern Technologies (RBST). Institute for Advanced Studies in Basic Sciences (IASBS), Zanjan 45137-66731, Iran.
[c] Department of Chemistry, Faculty of Sciences, Persian Gulf University, Bushehr, 75169, Iran.
[d] Departamento de Química Orgánica and Instituto de Síntesis Orgánica, Universidad de Alicante, Apdo. 99, 03690-Alicante, Spain.
[e] Centro de Innovación en Química Avanzada (ORFEO-CINQA), Universidad de Alicante, Apdo. 99, 03690-Alicante, Spain.

Keywords: Post-modified MOFs, Ionic liquid, Nitrophenols reduction, Dyes reduction, Sonogashira-Hagihara coupling

Two supported nanoparticles gold and palladium anchored on an ionic liquid-modified Fe-based metal-organic framework (MOF) were successfully synthesized and characterized by FT-IR, XRD, TEM, XPS, SEM, EDX, and elemental mapping. This ionic liquid post-modified MOFs were used for anchoring Au or Pd at ppm levels, and the resulting materials were employed as catalysts in the reduction of nitrophenol isomers, dyes, and Sonogashira-Hagihara reactions. Using Au@Fe-MOF-IL catalyst, reduction of nitrophenol isomers, as well as the removal of dyes, *e.g*., methylene blue (MB), methyl orange (MO), and methyl red (MR) were performed efficiently in water. On the other hand, Pd@Fe-MOF-Im was used as an effective catalyst in the Sonogashira-Hagihara coupling reaction of aryl iodides and bromides using very low amounts of Pd. These catalysts were recycled and reused for several runs without deteriorating remarkably in catalytic performance.

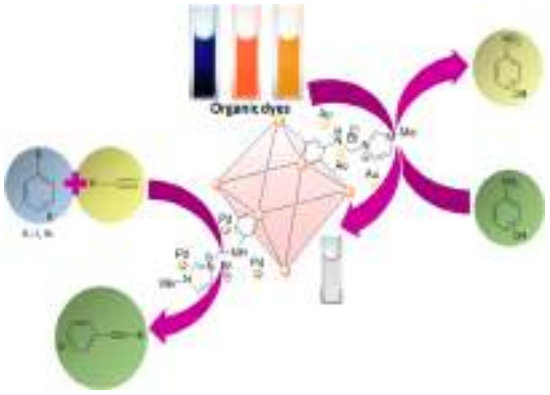

[1] Khosravi, F.; Gholinejad, M.; Sansano, J. M.; Luque, R. Bimetallic Fe–Cu Metal Organic Frameworks for Room Temperature Catalysis. *Appl. Organomet. Chem.* **2022**, *36*, e6749.
[2] Bagley, M. C.; Dale, J. W.; Merritt, E. A.; Xiong, X. Thiopeptide Antibiotics, *Chem. Rev.* **2005**, *105*, 685-714.

An efficient and green route for one-pot synthesis of 5-substituted indol chromeno[2,3-b]pyridines

Fatemeh Molaei Yielzoleh, Maryam saffari darbarzi and Kobra Nikoofar*

Department of Organic Chemistry, Faculty of Chemistry, Alzahra University, Tehran, Iran, f.molaei@alzahra.ac.ir; fateme.molaei69@gmail.com, K.nikoofar@alzahra.ac.ir.

Keywords: Multi-component reaction, Indole, Indole chromeno[2,3-b]pyridines, Heterogeneous nanocatalyst

A heterogenous nanostructure containing tartaric acid, silica, and magnesium bismuthate (SiO_2/*L*-tar/$MgBi_2O_4$) prepared for the first time and used as catalyst in the one-pot, pseudo four-component condensation of salicylaldehydes, indoles, and malononitrile to achieve 5-substituted indol chromeno[2,3-b]pyridines in the excellent yields at 50 °C under solvent-free condition (**Scheme 1**). The valuable features of this method are: broad substrate scope, simple procedure, green solvent-free conditions, recovery and reusability, and short reaction times. Chromenopyridines are fused heterocycles that display broad range of biological activities such as cancer chemopreventive, antibacterial, antimyopic, antiproliferative, antiasthmatic, and antihistaminic [1-3].

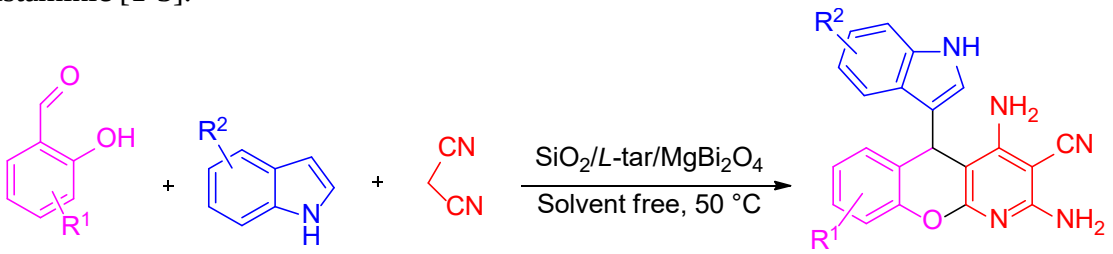

Scheme 1: Synthesis of 5-substituted indol chromeno[2,3-b]pyridines by SiO_2/*L*-tar/$MgBi_2O_4$.

References

[1] Srivastava, S. K.; Tripathi, R. P.; Ramachandran, R. nad$^+$-dependent DNA ligase (rv3014c) from mycobacterium tuberculosis: crystal structure of the adenylation domain and identification of novel inhibitors, *J. Biol. Chem* 2005, 280, 30273–30281.

[2] Brotz-Oesterhelt, H.; Knezevic, L.; Bartel, S.; Lampe, T.; Warnecke-Eberz, U.; Ziegelbauer, K.; Habich, D.; Labischinski, H. Specific and potent inhibition of NAD$^+$- dependent DNA ligase by pyridochromanones, *J. Biol. Chem*. 2003, 278, 39435–39442.

[3] Zhang, M.; Chen, M. N.; Zhang, Z. H. Visible Light-Initiated Catalyst-Free One-Pot, Multicomponent Construction of 5-Substituted Indole Chromeno [2, 3-b] pyridines. *Adv. Synth. Catal.* 2019, *361*, 5182-5190.

Investigating Promiscuous Activity in Recombinant NADH-dependent Flavin Reductase

Hamid R. Kalhor*, Amene Navaser

Biochemistry and Chemical Biology Research Laboratory, Chemistry Department, Sharif University of Technology, Tehran, Iran, kalhor@sharif.edu, Amenenavaser@gmail.com.

Keywords: Enzyme promiscuity, Biocatalyst, Flavin reductase, Knoevenagel condensation-Michael addition reaction, Tetraketone synthesis.

Enzymes which are well known for their high regio, chemo, and stereo-selectivity, have been increasingly used as biocatalysts in synthesizing various organic compounds. Many enzymes have shown promiscuous activity by serving a non-native substrate or demonstrating non-native catalytic activity [1]. Recently, enzyme promiscuity; has earned much attention in organic synthesis. Introducing novel approaches to evolve a promiscuous activity in enzymes would improve the traditional organic synthesis routes. In the present study, promiscuous activities were developed in the *E.coli* NADH-dependent flavin reductase by removing the enzyme's cofactor. However, in the absence of the cofactor; the flavin reductase was able to catalyze the Knoevenagel condensation and Michael addition reactions. Additionally, the enzyme's promiscuous performance was enhanced by optimizing the reaction condition including various solvents and temperature for the Knoevenagel-Michael addition cascade to produce tetraketones (**Scheme 1**). The scope of reaction indicated that a wide range of compounds including aliphatic, aromatic, and heterocyclic aldehydes can be used by the enzyme to generate the desired products. In the presence of the NADH, both Knoevenagel condensation and Michael addition reactions were blocked and no desired product was achieved. Molecular docking and molecular dynamics were exploited to identify key residues that play roles in the tetraketone synthesis. Removing the cofactor can stand as a novel method to induce promiscuity in enzymes. Furthermore, the NADH and its regenerating system are considered expensive, therefore, deletion of the cofactor could be a cost-effective approach for organic synthesis.

Scheme 1: Promiscuous activity of flavin reductase.

References

[1] Copley, S. D., Shining a light on enzyme promiscuity. *Curr. Opin. Struct. Biol.* 2017, *47*, 167-175.

Synthesis of New 4-Aryl-benzo[g]chromene Bearing N-Benzyl Triazole Moiety

Mohammad Majid Mojtahedi *, Elham Ashuri Moghaddam, Hoda Mollabagher

Chemistry & Chemical Engineering Research Center of Iran, Tehran, Iran, mojtahedi@ccerci.ac.ir, elhamashory@gmail.com

Keywords: One-pot reaction, Triazole, Chromene, Lawsone

Among the nitrogen-containing heterocyclic compounds, triazoles stand out due to their remarkable pharmacological applications. Triazoles and their derivatives exhibit significant biological properties, including antimicrobial, antitubercular, anticancer, and antioxidant activities, among others [1,2].

Consequently, these compounds find a wide range of therapeutic uses with continuously expanding potential across various scientific fields [3].

In this study, a novel series of chromene derivatives linked to the N-benzyl triazole group were synthesized by employing Lawsone (2-hydroxy-1,4-naphthoquinone), along with azide (**Scheme 1**). The final compounds were isolated, purified, and characterized using techniques such as IR, ^{1}HNMR, ^{13}CNMR, Mass, and UV.

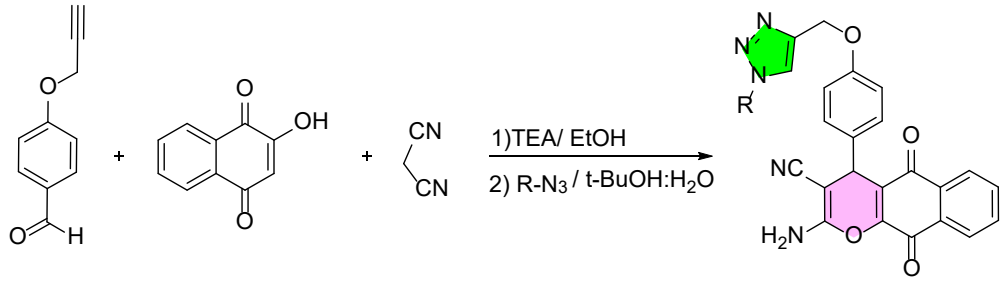

Scheme 1: one-pot synthesis of new 4-aryl-benzo[g]chromene Bearing N-Benzyl Triazole Moiety

References

[1] Zhou, X., Xu, X., Liu, K., Gao, H., Wang, W., and Li, W. Organocatalytic 1,3-Dipolar Cyclo-addition Reaction of β-Keto Amides with Azides - Direct Access to 1,4,5-Trisubstituted 1,2,3-Triazole-4-C-arb-oxamides. *Eur. J. Org. Chem*. 2016, *10*, 1886- 1890.

[2] Zaher, N. H., Mostafa, M. I., and Altaher, A. Y. Design, synthesis and molecular docking of novel triazole derivatives as potential CoV helicase inhibitors. *Acta Pharm*. 2020, 70, *2*, 145–159.

[3] Surendra Reddy, G., Suresh Kumar, A., and Ramachary, D. B. Organocatalytic enone-azide [3 + 2]-cycloaddition: synthesis of functionally rich C/N-double vinyl 1,2,3-triazoles, *Org. Biomol. Chem.* 2020, 18, 4470–4478.

Biosynthesis of pH-responsive magnetic nanocomposite hydrogels based on biopolymers/M-Ag bio nanoparticles: Antibacterial carrier for potential targeted anticancer drug delivery

Roghayeh Fathi, Reza Mohammadi*

Polymer Research Laboratory, Department of Organic and Biochemistry, Faculty of Chemistry, University of Tabriz, Tabriz, Iran, roghayeh.fathi@gmail.com, r.mohammadi@tabrizu.ac.ir

Keywords: Chitosan; Drug delivery; Antibacterial

Today, the antimicrobial activity of various nanoparticles such as Fe_3O_4, CuO, ZnO, Au, Ag, etc. is well known. Among the various metals, silver (Ag), particularly silver nanoparticles (Ag NP_S), exhibits significant antiviral, antimicrobial, and biocompatible properties, showing great potential for biomedical applications. Until now, the green synthesis of Ag NP_S has been reported using a wide range of plant extracts, bio-based sources, and microorganisms [1-2]. This study reports the development of new pH-responsive drug delivery systems that are important for the treatment of cancer. First, the Mentha plant extract was obtained and then used for the biosynthesis of magnetic Ag bio nanoparticles (M-Ag bio-NPs). They were added in the formulation of hybrid hydrogel of *k*-carrageenan (*k*-Cr) and chitosan (CS) toward the synthesis of magnetic nanocomposite hydrogels [3]. Their chemical structure and morphology were characterized by different analyses. Doxorubicin (DOX) was used as a model anticancer drug to study the targeted drug release behavior of the synthesized nanocomposite hydrogels (loading capacity (about 98%). *In vitro* drug release studies showed that the release profile was noticeably controlled in a pH-dependent manner (higher drug release at pH 5). The antibacterial assessment confirmed the high antibacterial activity for the synthesized hydrogel against *S. aureus* (MIC values 39.06 µg/mL) and *E. coli* (MIC values > 19.53). *In-vitro* cytotoxicity results (MTT assay) demonstrated good biocompatibility (higher than 88%) for the blank nanocomposite hydrogels, while DOX-loaded nanocomposite hydrogels showed high toxicity (about 22% in the concentration of 20 µg/mL) against HeLa cells. The results showed that the present nanocomposite hydrogels can be suggested for potential application as an antibacterial and anticancer carrier.

References

[1] S. Simon, N.R.S. Sibuyi, A.O. Fadaka, S. Meyer, J. Josephs, M.O. Onani, M. Meyer, A.M. Madiehe, Biomedical Applications of Plant Extract-Synthesized Silver Nanoparticles, *Biomedicines* 10(11) (2022) 2792.

[2] M.S. Samuel, M. Ravikumar, A. John J, E. Selvarajan, H. Patel, P.S. Chander, J. Soundarya, S. Vuppala, R. Balaji, N. Chandrasekar, A Review on Green Synthesis of Nanoparticles and Their Diverse Biomedical and Environmental Applications, *Catalysts* 12(5) (2022) 459.

[3] P. Lavrador, M.R. Esteves, V.M. Gaspar, J.F. Mano, Stimuli-responsive nanocomposite hydrogels for biomedical applications, *Advanced Functional Materials* 31(8) (2021) 2005941.

Green synthesis of pH-responsive nanocomposite hydrogels based on biopolymers/LDH bio nanoparticles: for potential targeted anticancer drug delivery

Roghayeh Fathi, Reza Mohammadi*

Polymer Research Laboratory, Department of Organic and Biochemistry, Faculty of Chemistry, University of Tabriz, Tabriz, Iran, roghayeh.fathi@gmail.com, r.mohammadi@tabrizu.ac.ir

Keywords: Biosynthesis, LDH, Drug delivery

There are many medicinal plants in Iranian traditional medicine with significant therapeutic properties. Among the various biological sources, plant extracts are safe, easily available, biocompatible, and provide good control over morphology and resistance [1]. Layered double hydroxides (LDHs) are an emergent class of inorganic lamellar nanomaterials having a 2D structure and belong to the class of hydrotalcite or anionic clays [2]. LDH is a good carrier for drug and gene delivery. It can carry the drug and delay its release. The drugs intercalated within LDH will be releasing slowly and thereby the frequency of administration of drugs can be decreased LDH is a good carrier for drug and gene delivery. It can carry the drug and delay its release. The drugs intercalated within LDH will be releasing slowly and thereby the frequency of administration of drugs can be decreased [3]. This study reports the development of new pH-responsive drug delivery systems that are important for the treatment of cancer. First, the Mentha plant extract was obtained and then used for the biosynthesis of LDH (Al/Zn) bio nanoparticles. They were added in the formulation of hybrid hydrogel of chitosan and pectin toward the synthesis of nanocomposite hydrogels. Their chemical structure and morphology were characterized by FT-IR, XRD, SEM and EDS analyses. Doxorubicin was used as a model anticancer drug to study the targeted drug release behavior of the synthesized nanocomposite hydrogels (pre-loading capacity (about 96%)). *In vitro* drug release studies showed that the release profile was noticeably controlled in a pH-dependent manner (higher drug release at pH 7/4). *In-vitro* cytotoxicity results (MTT assay) demonstrated good biocompatibility (higher than 86%) for the blank nanocomposite hydrogels, while DOX-loaded nanocomposite hydrogels showed high toxicity (about 25% in the concentration of 20 µg/mL) against HeLa cells. The results showed that the present nanocomposite hydrogels can be suggested for potential application as an anticancer carrier for oral delivery systems.

References

[1] Shahriari, M.; et al. "Biosynthesis of gold nanoparticles using Allium noeanum Reut. ex Regel leaves aqueous extract; characterization and analysis of their cytotoxicity, antioxidant, and antibacterial properties." *Appl. Organomet. Chem*. 33.11 (2019): e5189.

[2] Shirin, VK Ameena, et al. "Advanced drug delivery applications of layered double hydroxide." *J. Control. Release*. 330 (2021): 398-426.

[3] Pooresmaeil, M.; Nia, S. B.; Namazi, H. "Green encapsulation of LDH (Zn/Al)-5-Fu with carboxymethyl cellulose biopolymer; new nanovehicle for oral colorectal cancer treatment." *Int. J. Biol. Macromol.* 139 (2019): 994-1001.

A novel Zr-based MOF as an excellent catalyst for synthesis of 6*H*-chromeno[4,3-*b*]quinolin-6-ones

Masoumeh Beiranvand, Davood Habibi*, Maryam Mahmoudiani Gilani

Department of Organic Chemistry, Faculty of Chemistry, Bu-Ali Sina University, Hamedan, Iran, masumeh.beiranvand@gmail.com

Keywords: Metal-organic framework, *Exo*-bidentate, Zirconium, Three-component.

Metal-organic frameworks (MOFs), are a class of functional meso-/micro-porous crystalline materials constituted by the auto-assemblage of metal ions or metal oxide clusters and organic ligands through covalent connection [1]. In all reported MOFs, the Zr-MOFs stand out due to the strong Zr-O coordination bond, practicable synthetic conditions, and facility of reproducibility. The strong Zr-O coordination bond, along with the robust polynuclear molecular building blocks, cause Zr-MOFs an exceptional family of structures that are promising because of their tenability, stability, and design ability [2]. Chromeno-quinolines show remarkable properties in biological, medicinal, and fluorescence areas [3].

A new Zr-MOF was synthesized based on zirconium cations, an amine-functionalized ligand, and a linear *exo*-bidentate bis-pyridine ligand. Then, catalytic application of the synthesized Zr-based MOF was successfully explored in the synthesis of 6*H*-chromeno[4,3-*b*]quinolin-6-ones via a one-pot three-component condensation reaction under solvent-free conditions at 110 °C (Scheme 1).

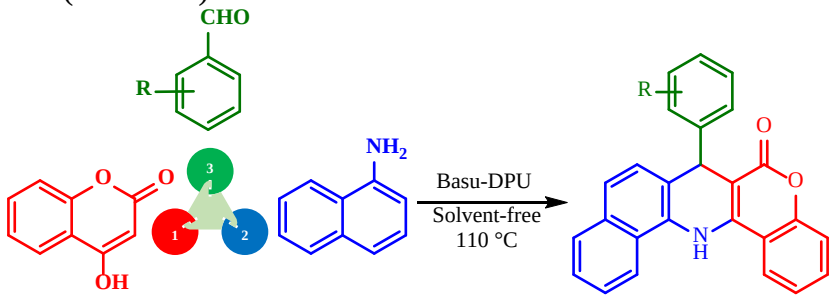

Scheme 1: Synthesis of 6*H*-chromeno[4,3-*b*]quinolin-6-ones catalysed by Basu-DPU.

References

[1] Yuan, S.; Qin, J. S.; Zou, L.; Chen, Y. P.; Wang, X.; Zhang, Q.; Zhou, H. C. Thermodynamically guided synthesis of mixed-linker Zr-MOFs with enhanced tenability. *J. Am. Chem. Soc.* 2016, *138*, 6636-6642.

[2] Chen, Z., Li, P., Wang, X., Otake, K. I., Zhang, X., Robison, L.; Farha, O. K. Ligand-directed reticular synthesis of catalytically active missing zirconium-based metal-organic frameworks. *J. Am. Chem. Soc.* 2019, 141, 12229-12235.

[3] Shen, G.; Wang, Z.; Huang, X.; Hong, M.; Fan, S.; Lv, X. Palladium/copper co-catalyzed C-H activation and C-C bond regioselective cleavage reaction for the synthesis of fused chromeno quinolines. *Org. Lett.* 2020, *22*, 8860-8865.

Design and synthesis of reusable Biochar phosphoric acid nanocatalyst for 1,8-Dioxo-octahydroxanthene and Tetrahydrobenzo[b]pyran Derivatives synthesis

Fatemeh Nezafatpour, Zahra Siahpour, Maryam Hajjami*

Organic Chemistry Laboratory, Faculty of Chemistry, Bu-Ali Sina University, Hamedan, Iran, fatemeh.np78@gmail.com, m.hajjami@basu.ac.ir & mhajjami@yahoo.com

Keywords: Biochar, Nanocatalysts, Multicomponent reaction, 1,8-Dioxo-octahydroxanthene, Tetrahydrobenzo[b]pyran

Multicomponent reaction (MCR) condensations involve three or more simple substrates is considered that approach close to the "ideal synthesis" due to atomic economy, and high bond forming efficiency. [1]. Recently, nanoparticles were emerged in various fields including science, industry, pharmacy, medicine, and green chemistry [2]. Biochar is one of the novel nanoparticles, which is a stable carbon solid and used in various fields in past few years for science and engineering. Biochar is made *via* pyrolysis of biological source such as woody materials, agricultural wastes, green waste, animal manures and other waste products [3], therefore it is inexpensive and environmentally friendly. In this work Phosphoric acid-activated walnut shell biochar as efficiently catalysis prepared and uses for one-pot multi-component synthesis 1,8-Dioxo-octahydroxanthene and Tetrahydrobenzo[b]pyran Derivatives in excellent yields and in very short reaction times.

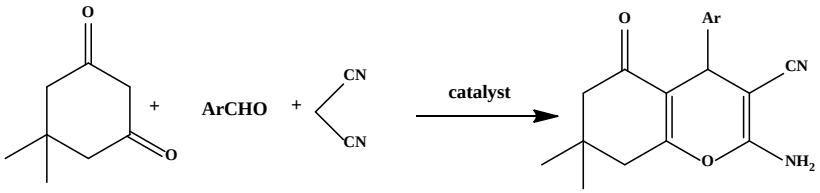

Scheme Three-component reaction of dimedone aldehydes and malononitrile in the presence of Biochar phosphoric acid as catalyst in reflux (water: ethanol) condition.

References

[1] Hajjami, M., Ghorbani-Choghamarani, A., Gholamian, F., Multicomponent synthesis of bioactive 1-amidoalkyl-2-naphtols under solvent-free Conditions, *Bulg. Chem. Commun.* 2015**,** 47, 119.

[2] Govan, J., Gun'ko, Y. K., Recent Advances in the Application of Magnetic Nanoparticles as a Support for Homogeneous Catalysts, *Nanomater.* 2014, 4, 222.

[3] Moradi, P., Hajjami, M., Valizadeh-Kakhki, F. Biochar as heterogeneous support for immobilization of Pd as efficient and reusable biocatalyst in C–C coupling reactions, *Appl. Organomet. Chem.* 2019**,** 33, e5205.

Highly selective reduction of nitro compounds catalyzed by Cu-MOF-derived $CoFe_2O_4$ under mild conditions

Masoume Malmir and Majid M. Heravi*

Department of Organic Chemistry, Faculty of Chemistry, Alzahra University, Tehran, Iran, m.malmir@alzahra.ac.ir, mmheravi@alzahra.ac.ir.

Keywords: MOF, Nitroarene, Reduction, Heterogeneous Catalyst, Copper

Today, studies on the catalytic reduction of nitroarenes and dyes are of great importance, because nitroarenes and dyes are considered as important pollutants in wastewater, which can pose risks to humans [1]. Therefore, providing an efficient method to achieve these compounds and protect the environment is very important. Following of our research [2], herein, the magnetic MOF-based catalyst containing Cu species as an active site offers unique and cost-effective route for the catalytic reduction of nitroarenes. In details, magnetic $CoFe_2O_4$ as a core is prepared, functionalized with aspartic acid and then magnetic-MOF catalyst is formed by using TAZ-IMI and $Cu(OAc)_2$. Notably, TAZ-IMI was synthesized from cyanuric chloride and imidazole as a precursor for the synthesis of MOF. The catalytic capability of $CoFe_2O_4$@Cu-TAZ-IMI catalyst was examined in the reduction of nitroarenes under aqueous and mild conditions. The result shows that this heterogeneous catalyst represents the excellent catalytic activity, high stability towards reduction reaction and facile recyclability up to seven consecutive cycles without significant loss of activity (**Scheme**).

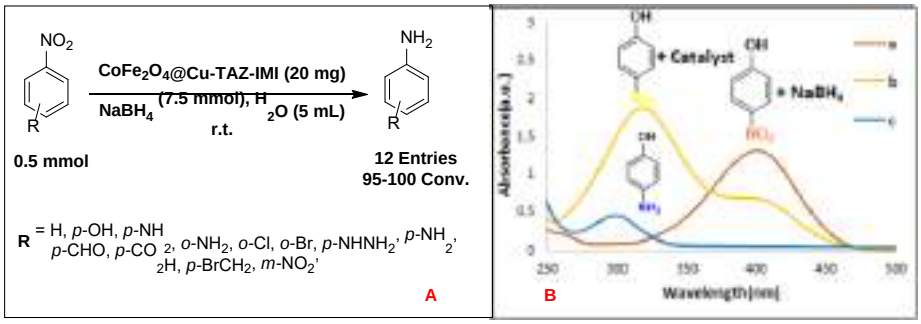

Scheme: (A) Reduction of nitro compounds by $CoFe_2O_4$@Cu-TAZ-IMI. (B) UV-Vis spectra of degradation of 4-nitrophenol with $NaBH_4$ in 0 min (a) without $NaBH_4$ after 10 min (b) with $NaBH_4$ and catalyst in r.t. and 10 min (c).

References

[1] Nasrollahzadeh, M.; Issaabadi, Z.; Safari, R., Synthesis, characterization and application of Fe_3O_4@SiO_2 nanoparticles supported palladium(II) complex as a magnetically catalyst for the reduction of 2,4-dinitrophenylhydrazine, 4-nitrophenol and chromium(VI): A combined theoretical (DFT) and experimental study. *Sep. Purif. Technol.* 2019, *209*, 136-144.

[2] Jahani, G.; Malmir, M.; Heravi, M. M., Catalytic Oxidation of Alcohols over a Nitrogen- and Sulfur-Doped Graphitic Carbon Dot-Modified Magnetic Nanocomposite. *Ind. Eng. Chem. Res.* 2022, *61* (5), 2010-2018.

Fabrication, comparison and evaluation of membrane modified with xanthate and sulphated C_3N_4 to improving performance

Soulmaz Seyyed Shahabi* **and Sepahbod Karimi**

Petrochemical Research and Technology Company, National Petrochemical Company, P.O. Box 14358-84711, Tehran, Iran, soulmaz.shahabi@yahoo.com

Keywords: UF membrane, Waste water, Heavy methal ion, Xanthate

Ultrafiltration members fabricated from xanthate mix were processed by phase inversion method using 12% PS in DMF. A 1000 ppm zinc nitrate solution was used in this study to adsorb heavy metal ions, and the membranes were characterized by pure water flux, contact angle, and rejection of metal ions to determine the effect of the additive on membrane properties. A dead-end setup was used to test the membrane and to detect the presence of zinc ions quantitatively. Ultrafiltration membranes exhibit a greatly increased permeability and ion adsorption properties, according to the results. A second stage consisted of the addition of solfunated C3N4 to increase hydrophilicity. Both components cooperated and result showed the water flux and rejection of heavy methal has grown 16% compared to initial state.

References

[1] Zhang,X.; Zhang, D.; Kong, L.; Shao, Z.; Lv, Y.; Duan, H. Prepration and characterization of xanthated cotton fiber modified cellulose triacetate ultrafiltration membrane. *Desalin. Water Treat.* 2016, 57, 10188- 10199.

[2] Seyyed Shahabi, S.; Azizi, N.; Vatanpour, V. Synthesis and characterization of novel g-C3N4 modified thin film nanocomposite reverse osmosis membranes to enhance desalination performance and fouling resistance. *Sep. Purif. Technol. 2019, 215*, 430-440.

Electrochemical Oxidation of 5-aminosalicylic acid in the Presence of 2-methyl indole

Ameneh Amani*

Nahavand Higher Education Complex, Bu-Ali Sina University, Hamedan, Iran,
amani.iran@gmail.com

Keywords: Mesalazine, Electrochemical Oxidation, Cyclic Voltammetry, 2-methyl indole

Organic electrosynthesis is a strong tool to produce a variety of functional compounds *via* electrochemically generated species as a key intermediate. [1]. Our previous studies show that the electrochemically generated *p*-quinone imine is a reactive intermediate and as a Michael acceptor, participates in different types of reactions [2,3]. In this work electrochemical oxidation of 5-aminosalicylic acid (mesalazine drug) has been studied in the presence of 2-methyl indole (**3**) as a nucleophile (**Scheme 1**). Some electrochemical techniques such as: cyclic voltammetry using diagnostic criteria derived by Nicholson and Shain for various electrode mechanisms and controlled-potential coulometry were used. Our results indicate the participation of electrochemically generated *p*-quinones in Michael-type addition reaction with 2-methyl indole (**3**) to form new indole derivatives. Diagnostic criteria of cyclic voltammetry, the consumption of 4e$^-$ electrons per molecule of mesalazine, and the spectroscopic data of the isolated products, indicated that the reaction mechanism of electrooxidation of **1** in the presence of **3** is the *ECE* mechanism. The natural stability of *p*-quinone imine in comparison with *o*-quinones is responsible for remaining the final product in quinone imine form.

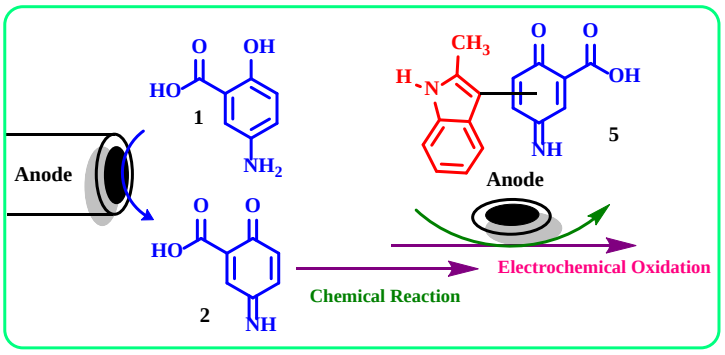

Scheme 1

References

[1] Marken, F.; Atobe, M.; Modern Electrosynthetic Methods in Organic Chemistry., *Taylor & Francis Group*. 2018, 1st Edition.

[2] Amani, A.; Torabi, S.; Electrochemical oxidation of 4-amino phenol in the presence of 2-mercaptobenzimidazoles and synthesis of new organosulfur compounds, *J. Appl. Chem*., 2021, 16, 79-94.

[3] Amani, A.; Nematollahi, D. Electrochemical Synthesis Based on the Oxidation of 1-(4-(4-Hydroxyphenyl)piperazin-1-yl)ethanone in the Presence of Nucleophiles *J. Org. Chem*., 2012, 77, 11302-11306.

Electrochemical Study of Mefenamic Acid in the Presence of Coumarin Derivatives to Synthesis of New Organic Compounds

Sadegh Khazalpour*, Mobina Hajihosini, Maryam Mehrdadian and Ameneh Amani

Department of Analytical Chemistry, Faculty of Chemistry and Petroleum Sciences, Bu-Ali Sina University, Hamedan, Iran, s.Khazalpour@basu.ac.ir, Iran, Mobina.hajihosini77@gmail.com

Keywords: Electrochemical, Mefenamic Acid, Coumarin

Mefenamic acid, which includes non-steroidal anti-inflammatory drugs. It is used in the treatment of pain, arthritis and dysmenorrhea [1]. Coumarins are polyphenolic compounds This group is anti-inflammatory, anti-oxidant, anti-microbial, anti-allergic, anti-fungal, anti-HIV and anti-cancer is also used [2]. Considering the unique properties of mefenamic acid and the specific properties of coumarins, we decided to synthesize a compound that includes both functional groups.

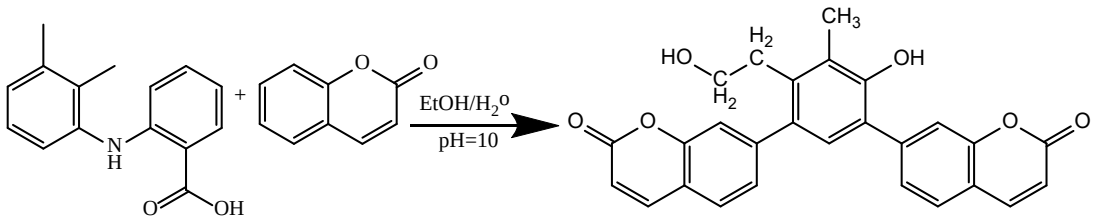

Scheme: Proposed mechanism of the product of electrochemical synthesis of mefenamic acid and coumarin

References

[1] Amooshahi, P.; Khazalpour, S.; and Amani, A. Electrochemical Evidence in Mechanism of Toxicity of Mefenamic Acid Overdose in the Presence of Glutathione and N-Acetyl-L-Cysteine. *J. Electrochem. Soc*. 2020,*167*, 045503,

[2] Madari, H.; Panda, D.; Wilson, L.; and Jacobs, R. Dicoumarol a unique microtubule stabilizing natural product that is synergistic with Taxol. *J. Cancer Res*. 2003, *63*, 1214-1220,

Mannich-mediated amination of sulfated Kraft lignin: A Brønsted acid catalyst for the synthesis of 5-hydroxymethylfurfural from fructose

Zahra Nezafat,[a] Mahmoud Nasrollahzadeh,[b*] and Shahrzad Javanshir[a]

a) Pharmaceutical and Heterocyclic Chemistry Research Laboratory, Department of Chemistry, Iran University of Science and Technology, Tehran 16846-13114, Iran, znezafat95@yahoo.com.
b) Department of Chemistry, Faculty of Science, University of Qom, Qom 37185-359, Iran, mahmoudnasr81@gmail.com.

Keywords: Mannich reaction, Kraft lignin, Brønsted acid, 5-Hydroxymethylfurfural, 5-Amino-1*H*-tetrazole

One of the most important materials which attracted much consideration is 5-hydroxymethylfurfural (5-HMF). The 5-HMF is a multifunctional material which has many applications in different industries [1,2]. In this study, we synthesized 5-HMF using aminated lignin functionalized SO_3H as an efficient Brønsted acid catalyst. The catalyst was prepared via Mannich reaction of 5-amino-1*H*-tetrazole with Kraft lignin following functionalized by chlorosulfonic acid (Mani-Tet-SO_3H) and characterized by Fourier transform infrared (FT-IR), X-ray diffraction (XRD), thermogravimetry-differential scanning calorimetry (TG-DSC), and Field emission scanning electron microscopy (FESEM). The catalyst was applied for the synthesis of 5-HMF from fructose via an acid hydrolysis reaction (**Scheme 1**). Finally, the catalyst can be recycled and reused for 4 times without significant loss of in its performance.

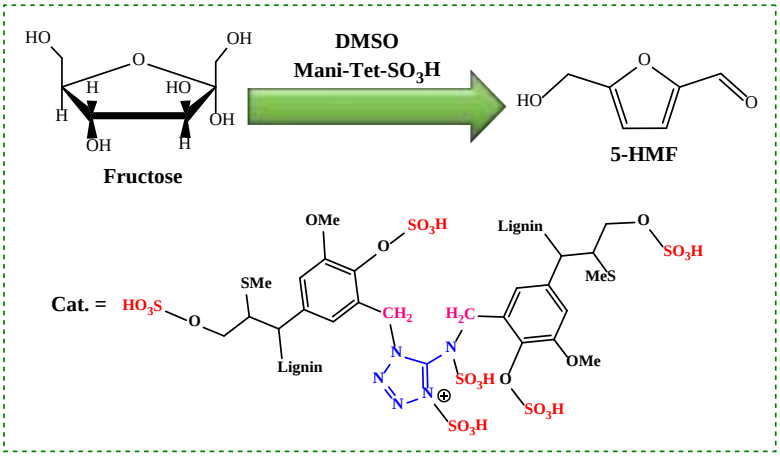

Scheme 1: Synthesis of 5-HMF using Mani-Tet-SO_3H.

References

[1] Nasrollahzadeh, M.; Nezafat, Z.; Momenbeik, F.; Orooji, Y. Polystyrene immobilized Brønsted acid ionic liquid as an efficient and recyclable catalyst for the synthesis of 5-hydroxymethylfurfural from fructose. *J. Mol. Liq.* **2022**, *345*, 117811.
[2] Nasrollahzadeh, M.; Soheili Bidgoli, N. S.; Shafiei, N.; Momenbeik, F. Biomass valorization: Sulfated lignin-catalyzed production of 5-hydroxymethylfurfural from fructose, *Int. J. Biol. Macromol.* **2021**, *182*, 59-64.

Efficient synthesis of full substituted dihydrofuran-2(5*H*)-ones using GO@dopamine-Cu as a green nanocatalyst

Neda Niknam and Nader Noroozi Pesyan*

Department of Organic Chemistry, Faculty of Chemistry, Urmia University, 57159, Urmia, Iran, msc.nedaniknam@yahoo.com

Keywords: Dihydrofuran-2(5*H*)-one, Graphene oxide, Green, Dopamine

Recently, preparing new composite structures using graphene oxide (GO) has attracted great attention in the world. In this regard, in order to design catalysts, GO supports can be highly applicable. Some of advantages for GO, i.e. having active pores and sites, thermal stability, high selectivity and high mechanical strength [1,2]. Furan and dihydrofun skeletons display several biological and pharmaceutical behaviors such as anticancer [3] and etc. Herein, we have used the GO@dopamine-Cu as a recoverable nanocatalyst for the one-pot synthesis of methyl 5-oxo-2-aryl-4-(arylamino)-2,5-dihydrofuran-3-carboxylate derivatives (**4**) in high yield.

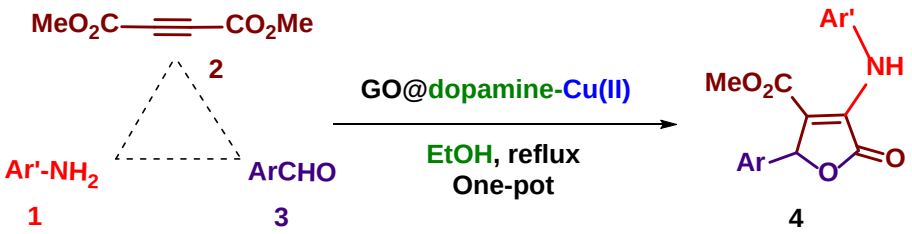

Scheme 1: Synthesis of dihydrofuran-2(5*H*)-one derivatives in the presence of GO@dopamine-Cu nanocatalyst

References:

[1] Presolski S., Pumera M., Graphene oxide: carbocatalyst or reagent? *Angew. Chem. Int. Ed.* 2018, 57: 16713–16715.

[2] Zhang M., Liu Y.H., Shang Z.R., Hu H.C., Zhang Z.H., Supported molybdenum on graphene oxide/Fe3O4: an efficient, magnetically separable catalyst for one-pot construction of spiro-oxindole dihydropyridines in deep eutectic solvent under microwave irradiation, *Catal. Commun*. 2017, 88: 39–44.

[3] Takahashi S., Kubota A., Nakata T., Total synthesis of muconin, *Tetrahedron Lett.* 2002, 43: 8661-8664.

Iono-C@Si-Py/$CuFe_2O_4$: An effective catalyst for promoting Ullmann coupling reaction

Negin Rasoulian[a], Masoume Malmir[a*] and Majid M. Heravi[a*]

Department of Organic Chemistry, Faculty of Chemistry, Alzahra University, Tehran, Iran, rasouliannegin@gmail.com, m.malmir@alzahra.ac.ir, mmheravi@alzahra.ac.ir

Keywords: Heterogeneous catalyst, Magnetic nanoparticles, Mesoporous carbon, Ullmann reaction.

Heterogeneous catalysis plays a part in the production of more than 80% of all chemical products. It is therefore essential that all chemists and chemical engineers have an understanding of the fundamental principles as well as the applications of heterogeneous catalysts. Ullmann-type *N*-arylations have long been employed for the synthesis of various molecules and intermediates, suitable for a large number of biological, medicinal, and pharmaceutical applications [1], and, therefore, they belong to the most important transition metal-catalyzed cross-coupling reactions. Continuing our research [2], herein, Iono-C@Si-Py/$CuFe_2O_4$ was synthesized and applied for promoting Ullmann reaction in aqueous media. First, a mesoporous carbon was synthesized via Ionothermal method. Then, the obtained mesoporous carbon functionalized and magnetized with $CuFe_2O_4$. The catalytic capability of Iono-C@Si-Py/$CuFe_2O_4$ catalyst was examined in Ullmann reduction of aryl halides and aromatic and aliphatic amines under aqueous and mild conditions. The result shows that this heterogeneous catalyst represents the excellent catalytic activity and high stability towards Ullmann reaction. Moreover, the catalyst could be successfully removed from the reaction mixture by using a magnetic field and also recycled for 9 consecutive reaction times with slight loss of the catalytic activity (**Scheme 1**).

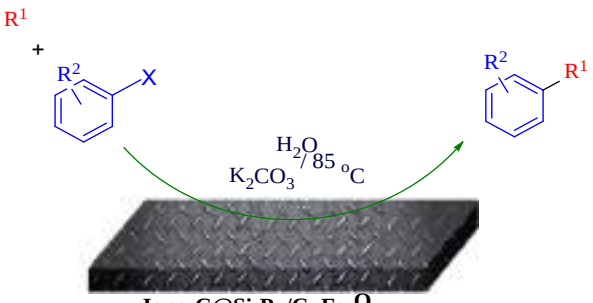

X= I, Br, Cl
R^1= Imidazole, Morpholine, Piperidine
R^2= H, OMe, NH_2, NO_2

Scheme 1: Ullmann coupling reaction of aryl halides and amines in the presence of Iono-C@Si-Py/$CuFe_2O_4$ and K_2CO_3.

References

[1] Dai, L.X., C-S coupling with nitro group as leaving group via inorganic salt catalysis. *Prog. Chem.* **2018**, *30*, 1257.
[2] Malmir, M.; Heravi, M. M.; Yekke-Ghasemi, Z.; Mirzaei, M., Incorporating heterogeneous lacunary Keggin anions as efficient catalysts for solvent-free cyanosilylation of aldehydes and ketones. *Sci. Rep.* **2022,** *12*, 11573.

Synthesis of 2,6-Di Aryl Benzophenones From Grignard Reagents

Ali Ebrahimi Turkamani[a*], Akbar Saednya[b]

a) Department of Chemistry, Faculty of Nano and Bio Science and Technology, Persian Gulf University, Bushehr, Iran, Aliebrahimiturkmani@yahoo.com.
b) Department of Organic Chemistry, Faculty of Chemistry, University of Tabriz, Tabriz, Iran.

Keywords: 2,6-Di Aryl Benzophenones, 2,6-dichloro iodobenzene, Aryl Grignard

In this research work we reported a method for the synthesis of 2,6-diaryl benzophenones from the reaction of excess aryl Grignards and 2,6-dichloro iodobenzene formed m-terphenyl-2′-magnesium bromide (1) [1,2] were treated with benzoyl chloride then hydrolysis. Via the reactions three carbon-carbon bonds are constructed and 2,6-di aryl benzophenones are obtained in good yields (**Scheme 1**).

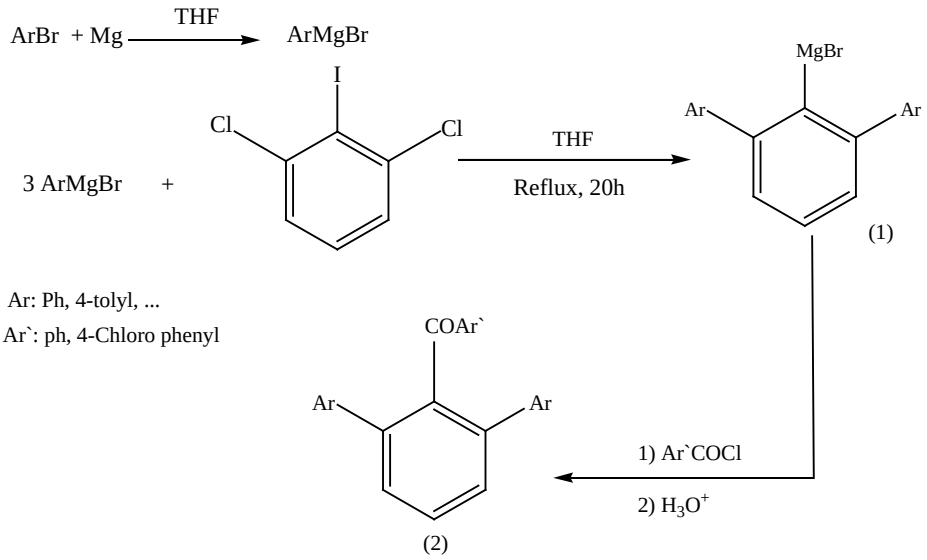

Scheme 1: Synthesis of 2,6-diaryl benzophenones.

References

[1] B. Rashidzadeh, F. Jafarpour, A. Saednya, One-pot synthesis of m-terphenyl-2'-carbaldehydes, *ARKIVOC* vii (2008) 167-172.
[2] R. S. Wright, T. K. Vinod, Synthesis of m-terphenyl derivatives for potential use as tectons in crystal engineering, *Tetrahedron Lett*. 44 (2003) 7129-7132.

Engineered Ta-doped ZnO based on hydroxyapatite composites as a robust catalyst in the preparation of perhydrotriazolotriazoles

Narjes Sadat Mireei , Javad Safaei-Ghomi* and Pooria Babaei

Department of Organic Chemistry, Faculty of Chemistry, University of Kashan, Kashan, P.O. Box 87317-51167, I. R. Iran, narjes.s.mirei@gmail.com

Keywords: Hydroxyapatite, Ta-doped ZnO, Engineered composites, Perhydrotriazolotriazoles.

Engineered Ta-doped ZnO based on Hydroxyapatite nanocomposites have been fabricated via the green approach [1]. Herein, nano-sized Ta-doped ZnO/HAp composites with diverse morphologies are fabricated in different conditions (*e.g.* Green routes, various pH adjusters, temperatures, *etc*.). The designed composite was characterized using scanning electron microscopy (SEM), energy dispersive X-ray spectroscopy (EDS) and X-ray diffraction (XRD) techniques. The Ta-doped ZnO/HAp composites has been applied as an efficient catalyst for the preparation of perhydrotriazolotriazoles [2] in acetonitrile solvent at room temperature at the shortest reaction time. Furthermore, green route, easy separation of nanocatalyst, reusability without noticeable loss of catalytic efficiency are other advantages.

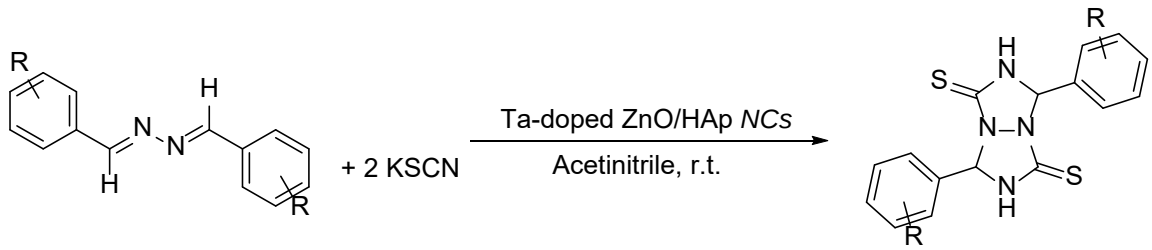

Scheme 1: Syntheses of perhydrotriazolotriazoles in the presence of Ta-doped ZnO/HAp nanocomposites

References

[1] Babaei, P.; Safai-Ghomi J.; Rashki S. Engineered dual-purpose Ta-doped ZnO/Hydroxyapatite nanocomposites: Antibacterial activity and robust catalyst in MW-Induced synthesis of chromopyrimidines. *Ceram. Int.* **2022**, *48*, 8359- 8373.

[2] Safari J. and Javadian L. An efficient synthesis of perhydro[1,2,4]triazolo[1,2-a][1,2,4] triazole-1,5-dithiones catalyzed by TiO_2-functionalized nano-Fe_3O_4 encapsulated-silica particles as a reusable magnetic nanocatalyst. *RSC. Adv.* **2015**, *5*, 104973-104980.

Investigating the Effect of Nitrogen–Doped Carbon Quantum Dots in Phenazine Sensitized Solar Cells

Shabnam Jahanbani Korabbaslo[a], Rahim Ghadari[b*]

a) Organic Chemistry Laboratory, Faculty of Chemistry, University of Tabriz, Iran, shabnam.jahanbani@gmail.com
b) Department of Organic and Biochemistry, Faculty of Chemistry, University of Tabriz, 5166616471 Tabriz, Iran, r-ghadari@tabrizu.ac.ir

Keywords: DSSC, Phenazine, Carbon quantum dots, Nitrogen–doped carbon quantum dots

Dye-sensitized Solar cells are the most promising devices among third-generation solar cells because of low cost, easy production, environmental friendliness, and relatively high conversion efficiency [1]. Among the third-generation photovoltaics, quantum dot solar cells (QDSCs) are emerging as a promising candidate due to the unique and versatile characteristics of quantum dots (QDs) including tunable band gap and high absorption coefficient [2]. The design of organic dyes with the architecture of the donor-π bridge-acceptor (D-π-A) to be used in DSSC is a common procedure which is due to the creation of a flexible and highly effective structures [3]. Nitrogen-containing carbon dots were applied to improve the performance of phenazine-sensitized solar cells. The structure of dyes and quantum dots synthesized was confirmed by FT-IR, TEM, XRD, EDS-Map, AFM, DLS, and PL analyses. Current-voltage properties of solar cells sensitized with phenazine and (phenazine/N-CQD) in simulated sunlight with radiation intensity of 100 $mWcm^{-2}$ at 1.5 AM were evaluated.

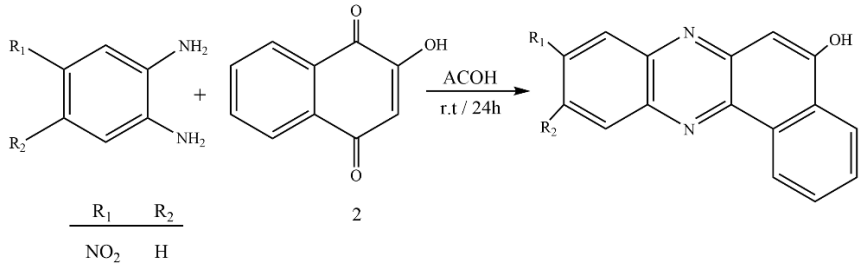

Scheme.1. Synthesis of Dye.

References

[1] Bagavathi, N., & Dhanemozhi, A. C. Fabrication of Dye Sensitized Solar Cells by the Plasmonic Effect of Silver Nanoparticles and Basella Alba Dye. *Mater. Today: Proc.* 2019, *8*, 271-278.
[2] Wang, H., Sun, P., Cong, S., Wu, J., Gao, L., Wang, Y., ... & Zou, G. Nitrogen-doped carbon dots for "green" quantum dot solar cells, *Nanoscale Res. Lett.*, 2016, *11*, 1-6.
[3] Sharmoukh, W., Cong, J., Gao, J., Liu, P., Daniel, Q., & Kloo, L. Molecular engineering of D–D− π–A-based organic sensitizers for enhanced dye-sensitized solar cell performance. *ACS Omega*, 2018, *3*(4), 3819-3829.

A DFT/TD-DFT Investigation on the Efficiency of Dyes Based on Phenazine as a Dye-Sensitized Solar Cell Light-Absorbing Material

Shabnam Jahanbani Korabbaslo[a], Rahim Ghadari[b*]

a) Organic Chemistry Laboratory, Faculty of Chemistry, University of Tabriz, Iran, shabnam.jahanbani@gmail.com
b) Department of Organic and Biochemistry, Faculty of Chemistry, University of Tabriz, 5166616471 Tabriz, Iran, r-ghadari@tabrizu.ac.ir

Keywords: Dye-sensitized solar cells, DFT, Solar cell, Opto-electronic property

The electronic structures and photophysical properties of phenazine derivatives have been studied. In this work, all computations were done with the Gaussian 09 package was used as a graphical interface [1]. The ground state geometry of all the synthesized structures is optimized by density functional theory (DFT) along with the correlation functions of B3LYP (Becke-Lee-Yang-Parr) and 6-31G (d) as the basis set at gas phase [1, 2]. In the following, since the absorption phenomenon is to time-dependent, to obtain the absorption properties in dimethylformamide solvent of time-dependent-DFT (TD-DFT) study was used [1, 2]. Therefore, some of the important parameters such as (HOMO/LUMO) shape and energy level, gap bad energy (E_{gap}), absorption spectrum, oscillator strengths (OS), vertical excitation energy (E_{ex}), main transition (MO), molecular electrostatic potential (MEP) maps, and photovoltaic parameters like open-circuit voltage (V_{oc}) employing DFT and TD-DFT methods in the theory level of theory B3LYP/6-31G(d) were studied and investigated [1, 2].

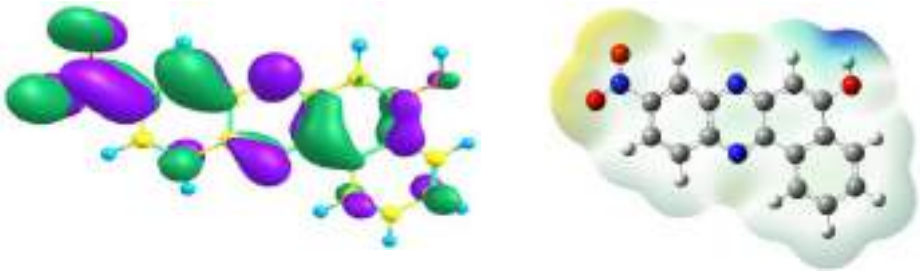

Scheme: Calculated frontier molecular orbital and MEP map of synthesized phenazine derivative obtained at B3LYP/6-31G(d) level of theory.

References:

[1] M. Qiu, W. Pei, Q. Lu, Z. Li, Y. Li, and J. Liang, DFT characteristics of charge transport in DBTP-based hole transport materials, *Appl. Sci.*, 2019, 9, 2244.

[2] G. H. Lee and Y. S. Kim, Theoretical Study of Effect of Introducing π-Conjugation on Efficiency of Dye-Sensitized Solar Cell, *J. Nanosci. Nanotechnol.*, 2018, 18, 6640–6644.

A competent MOF Catalyst of Gold-Nanoparticles-Decorated Graphitic Carbon Nitride (g-C_3N_4) @ Functionalized UiO-66-COOH as a novel and efficient MOF-Catalyst for Reduction of Nitro Aromatic Compounds

Leila Mohammadi*, Mohammadreza Vaezi

Department of Nano Technology and Advanced Materials, Materials and Energy Research Center, Iran, l.mohammadi80@yahoo.com.

Keywords: UiO-66, UiO-66-COOH, Graphitic Carbon Nitride (g-C_3N_4), Au-NPs, Reduction Reaction

This research is motivated to identify newly synthesized MOF nano-catalyst *via* metal-organic frameworks UiO-66-Type with free carboxylic acid as an efficient MOF functionalized graphitic carbon nitride (g-C_3N_4) *via* stabilization of Gold Nanoparticles. In order to prepare a highly efficient catalyst UiO-66-COOH @ g-C_3N_4 @ Au-NPs as a heterogeneous catalyst for applying in reduction of nitro aromatic compounds which have been investigated. In this process, the design, synthesis and construction of a type of metal-organic framework UiO-66 under the title UiO-66-COOH was investigated [1]. UiO-66 (Zr)-type metal organic framework with free carboxylic acid was synthesized in one step from zirconium chloride ($ZrCl_4$) and 1,2,4-BTC (1,2,4-benzene tricarboxylic acid) [1]. Graphitic carbon nitride (g-C_3N_4), as a polymeric semiconductor, is promising for some applications because of its suitable electronic structures, together with the low cost, facile preparation, and metal-free feature [2]. Since it exhibits a stacked structure, g-C_3N_4 is often considered as sp^2-hybridized nitrogen-substituted graphene. So, UiO-66-COOH can be functionalized to Au metal nanoparticles using g-C_3N_4 nitrogen-substituted (Scheme).

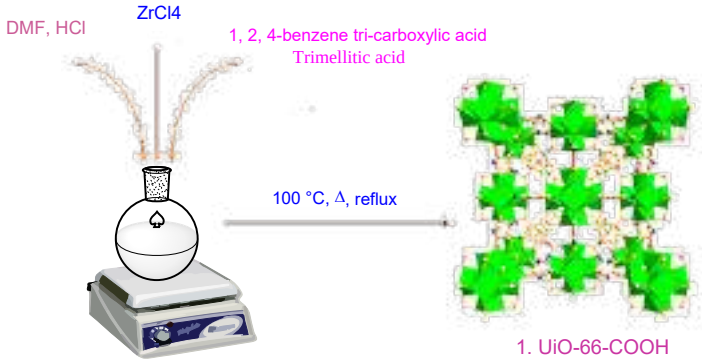

Scheme: Synthesis of UiO-66-COOH

References

[1] Zhang, L.; Li, L.; Hu, E.; Yang, L.; Shao, K.; Yao, L.; Jiang, K.; Cui, Y.; Yang, Y.; Li, B., Boosting Ethylene/Ethane Separation within Copper (I)-Chelated Metal–Organic Frameworks through Tailor-Made Aperture and Specific π-Complexation. *Adv. Sci* 2020, *7* (2), 1901918.

[2] El-marghany, A.; Sillanpää, M.; Manzoor, S.; Abid, A. G.; Nisa, M. U., Solvothermally fabricated cobalt selenide supported on graphitic carbon nitride for enhanced oxygen evolution reaction. *Appl. Phys. A* 2023, *129* (8), 605.

A Narrative and Proficient MOF Catalyst of Gold-Nanoparticles-Decorated Epichlorohydrine @Poly dopamine Functionalized UiO-66-NH_2 as a Novel and Efficient MOF-Catalyst for Preparation of Spirochromenes

Leila Mohammadi*, Mohammadreza Vaezi

Department of Nano Technology and Advanced Materials, Materials and Energy Research Center, Iran

Keywords: UiO-66-NH_2, Gold-Nanoparticles, Poly dopamine, Spirochromenes

The general principles in this research is the synthesis of new catalysts based on metal-organic frameworks (MOF) by coating with Epichlorohydrine and poly dopamine, then stabilizing with Metal (Au) nanoparticles have been included. In this process, the design, synthesis and construction of a type of metal-organic framework UiO-66 under the title UiO-66-NH_2 was investigated. In the following, the amino-target compound *via* nitrogen-containing was conjugated with epichlorohydrine, and epoxy-ring was opened by amino group attached UiO-66-NH_2. Then, poly dopamine was coated with UiO-66-NH_2@epichlorohydrin, and finally synthesized by stabilizing gold nanoparticles. In the following, he synthesis of the desired nano-catalyst was carried out, and the authority of the synthesized catalyst was confirmed with analyzes such as FT-IR, XRD, EDS-Mapping, FE-SEM, VSM, TEM, BET. In the following, application of the heterogeneous catalyst was used in organic reactions such as the A^3-coupling reaction, which is one of the most important reactions in the synthesis of organic compounds same as spirochromenes [1]. The high efficiency in the reaction process indicates the effect of the activity and very high efficiency of the synthesized catalyst. In addition, the effect of recycling the catalyst was also investigated (**Scheme**).

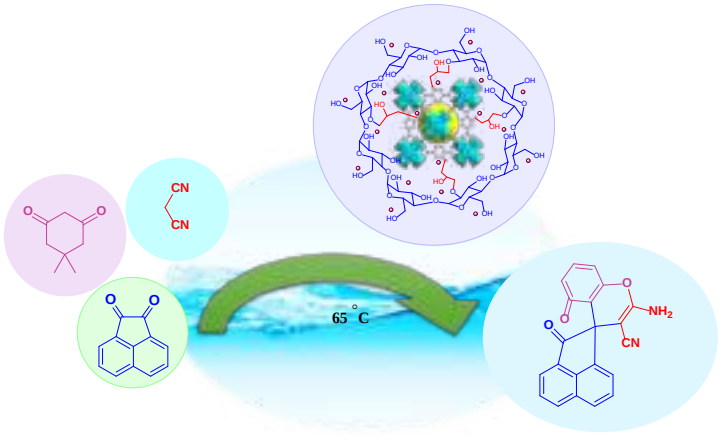

Scheme: The efficient newly synthesized nano-catalyst for preparation spirochromene

References

[1] Balalaie, S.; Nayebzadeh, B.; Amiri, K.; Khosravi, H. Synthesis of Spiro[chromene-imidazo[1,2-*a*]pyridin]-3′-imines via 6-*exo*-dig Cyclization Reaction. *J. Org. Chem.* 2021, 86 (19), 13693–13701.

Synthesis of Benzopyrano[2,3-d]pyrimidines in the Presence of Sodium Carbonate Silica Catalyst

Ziba Daroughezadeh, Hamzeh Kiyani*

School of Chemistry, Damghan University, Damghan, Iran, ziba.daroughe@gmail.com

Keywords: Benzopyrano[2,3-*d*]pyrimidines, Green synthesis, Sodium carbonate silica

These benzopyrano[2,3-*d*]pyrimidines are attractive class of heterocyclic compounds with biological activities, including in vivo antitumor, antibacterial, antioxidant, antiangiogenic, analgesic, in vitro anti-aggregating, and antigenotoxic [1]. Due to the widespread applications of benzopyrano[2,3-*d*]pyrimidines, the development of new methods aimed at the synthesis of these valuable heterocycles is an striking topic of current research in many laboratories [2]. In this contribution, sodium carbonate silica (SCC) was synthesized and its catalytic activity was studied for the synthesis of derivatives of benzopyrano[2,3-*d*]pyrimidines (**Scheme 1**). The approach began with the development of the optimal conditions using salicylaldehyde, malonitrile, and piperidine as the model in various conditions. A screening of various amounts of catalyst showed the optimal amount of 0.05 g of catalyst led to 80 % of product in 70 min in ethanolic conditions. The condensation of malonitrile with different salicylaldehydes and various secondary amines under these optimized conditions led to a variety of benzopyrano[2,3-*d*]pyrimidines. Salicylaldehydes bearing either electron-withdrawing or electron-donating groups reacted successfully with malonitrile and secondary amines under green conditions in the presence of 0.05 g of catalyst refluxing ethanol to give the corresponding benzopyrano[2,3-*d*]pyrimidines in good to excellent yields. In addition, SSC catalyst was shown to be recyclable without significant loss of efficiency after fourth use.

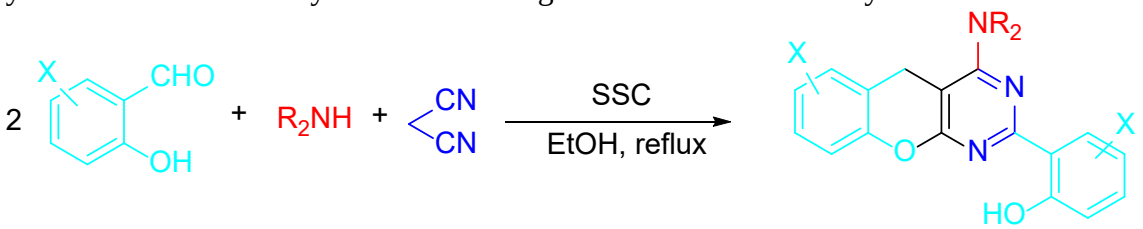

Scheme 1: Green synthesis of benzopyrano[2,3-*d*]pyrimidines.

References

[1] Ghorbani-Vaghei, R.; Shirzadi-Ahodashti, M.; Eslami, F.; Malaekehpoor, S.M.; Salimi, Z.; Toghraei-Semiromi, Z.; Noori, S. Efficient One-Pot Synthesis of Quinazoline and Benzopyrano[2,3-d]pyrimidine Derivatives Catalyzed by *N*-Bromosulfonamides. *J. Heterocycl. Chem.* **2017**, *54*, 215–225.

[2] Mostafavi, M.M.; Movahedi, F.; Synthesis, Characterization, and Heterogeneous Catalytic Activity of Sulfamic Acid Functionalized Magnetic IRMOF-3. *Eur. J. Inorg. Chem.*, **2019**, 2019, 787.

Fabrication, Characterization, and Investigation of Application of Engineered Ta-doped ZnO/Hydroxyapatite Nanostructures in the Fabrication of Quinoline-3-carbonitriles as an Efficient Catalyst

Pooria Babaei*

Department of Organic Chemistry, Faculty of Chemistry, University of Kashan, Kashan, P.O. Box 87317-51167, I. R. Iran, drpbabaee@gmail.com.

Keywords: Engineered nanostructures, Ta-doped ZnO composite, Hydroxyapatite, Quinoline-3-carbonitriles.

Engineered nano-sized Ta-doped ZnO based/hydroxyapatite composites have been prepared by hydrothermal protocol [1]. Herein, Ta-doped ZnO/HAp composites with difference shapes are prepared in various conditions (various pH adjusters, green routes, temperatures, *etc*.). The designed nanostructure was characterized applying X-ray diffraction (XRD), energy dispersive X-ray spectroscopy (EDS), and scanning electron microscopy (SEM) analysis. The Ta-doped ZnO/HAp composite has been used as an efficient catalyst for the fabrication of quinoline-3-carbonitriles [2] in ethanol solvent at reflux conditions at the shortest reaction time. Moreover, green solvent, easy separation of nanocatalyst, reusability without noticeable loss of catalytic efficiency are other advantages.

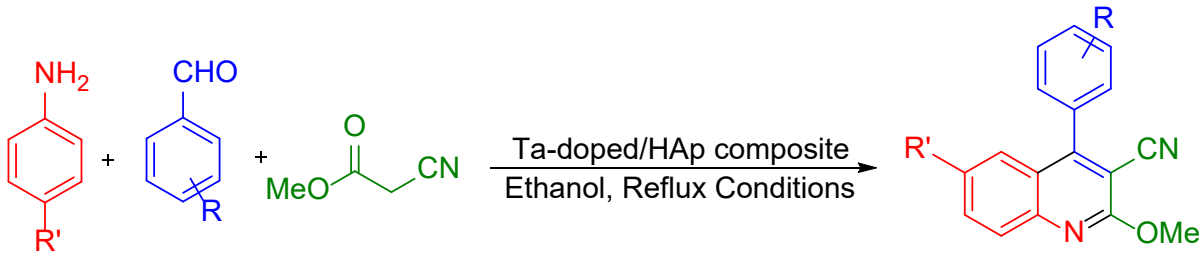

Scheme 1: Fabrication of quinoline-3-carbonitriles using Ta-doped ZnO/HAp nanocomposite

References

[1] Babaei, P.; Safai-Ghomi J. Engineered dual-purpose Ta-doped ZnO/Hydroxyapatite nanocomposites: Antibacterial activity and robust catalyst in MW-Induced synthesis of chromopyrimidines. *Ceram. Int.* **2022**, *48*, 8359- 8373.

[2] R. Musharrfieh, J. Zhang, P. Tuohy, N. Kitamura, S. S. Bellampalli, Y. Hu, R. Khanna and J. Wang, Discovery of quinoline analogues as potent antivirals against enterovirus D68 (EV-D68) *J. Med. Chem*., **2019**, *62*, 4074–4090.

Increased photocatalysis processes *via* merging π-conjugated covalent organic framework and nickel photoredox complex for synthesis of benzimidazole drugs

Mohammad Bashiri, Mona Hosseini-Sarvari*

Nanophotocatalysis Lab., Department of Chemistry, Shiraz University, Shiraz 7194684795, I.R. Iran, mohammad_bashiri_mb@yahoo.com

Keywords: Nickel catalysis; Photoredox; Covalent Organic Framework (COF); Benzimidazole; Visible light.

Covalent organic frameworks (COFs) have attracted large interest owing to their constant porosity, high stability, and tunable functionalities. COFs with widespread π-conjugation and light-sensitizing structures have been investigated for various photoredox processes [1]. Nickel catalysts are an appropriate replacement for noble metal complexes such as Pd, Pt, *etc.*, especially by changing their valance in during the reaction [2]. Benzimidazoles, as a special class of heterocyclic compounds, have been widely recognized as an important structure in biologically active molecules and pharmaceutical products [3]. Herein, we demonstrate the first study of COF-based electron transfer nickel catalysis. To investigate the performance of this catalyst under visible irradiation, the tandem reaction of toluene oxidation and benzimidazole cyclization has been examined. The COF/ Ni complex showed high efficiency in these reactions and could be recovered and reused without significant loss of catalytic activity (**Scheme 1**).

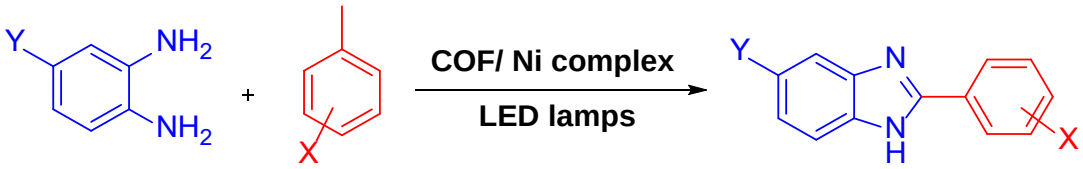

Scheme1: Synthesis of benzimidazoles with COF/ Ni complex under visible light irradiation

References:

[1]. Li, L.-H.; Feng, X.-L.; Cui, X.-H.; Ma, Y.-X.; Ding, S.-Y.; Wang, W. Salen-based covalent organic framework. *J. Am. Chem. Soc.* **2017**, *139* (17), 6042-6045.

[2] Sahari, A.; Puumi, J.; Mannisto, J. K.; Repo, T. Dual Nickel Photocatalysis for O-Aryl Carbamate Synthesis from Carbon Dioxide. *J. Org. Chem.* **2023**, *88* (6), 3822-3829.

[3]. Ebenezer, O.; Oyetunde-Joshua, F.; Omotoso, O. D.; Shapi, M. Benzimidazole and its derivatives: Recent Advances (2020-2022). *Results Chem.* **2023**, 100925.

Graphene quantum dots/copper tannic acid nanocomposite as an efficient antibacterial bioplatform

Jahangir Azizi, Siamak Javanbakht and Reza Mohammadi*

Polymer Research Laboratory, Faculty of Chemistry, University of Tabriz, Tabriz, Iran, jahangir.azizi1101@gmail.com, r.mohammadi@tabrizu.ac.ir

Keywords: **A**ntibacterial, Graphen quantum dot, Nanocomposite, Metal-organic frameworks, Green chemistry

The infection caused by harmful bacteria is a notable danger for global public health, leading to many deaths every year. It is essential to develop antibiotic alternatives or antibiotic delivery systems for deactivating bacteria with drug resistance. This work presents the synthesis of a copper tannic acid metal-organic framework (CuTA) and graphene quantum dot (GQD) nanocomposite, GQD/CuTA, using a simple, environmentally-friendly, and cost-effective method. The nanocomposite exhibits exceptional colloidal and antibacterial properties. First, GQDs were synthesized from citric acid through a novel and straightforward approach. Then, CuTA was grown in the presence of GQDs via an in-situ synthesis method to form the GQD/CuTA nanocomposite. Characterization using various techniques confirmed the successful synthesis of the nanomaterials. The GQD/CuTA nanocomposite demonstrated significant antibacterial activity against both E. coli and S. aureus. Furthermore, cytocompatibility studies showed good compatibility of the nanocomposite with human dermal fibroblast cells (HFF-2). Overall, the synthesized GQD/CuTA nanocomposite holds promise as a safe photoluminescent nanoplatform with strong antimicrobial properties.

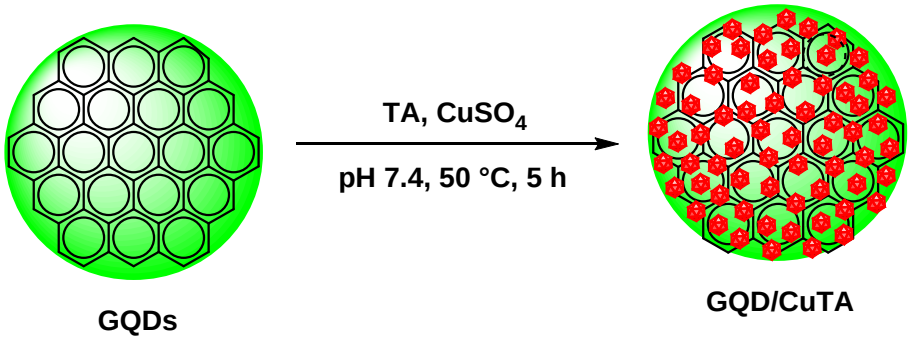

Scheme: Illustration of the synthesis of GQD/CuTA nanocomposite.

References

[1] T. Wei, Q. Yu, H. Chen, Responsive and synergistic antibacterial coatings: fighting against bacteria in a smart and effective way, *Adv. Healthc. Mater*. 8(3) (2019) 1801381.
[2] R.K. Alavijeh, S. Beheshti, K. Akhbari, A. Morsali, Investigation of reasons for metal–organic framework's antibacterial activities, *Polyhedron* 156 (2018) 257-278.

Magnetic starch as support for the growth of hyaluronic acid terminated covalent organic framework: A pH-controlled drug carrier

Malihe Pooresmaeil[a*], **Hassan Namazi**[a,b]

a) Polymer Research Laboratory, Department of Organic and Biochemistry, Faculty of Chemistry, University of Tabriz, Tabriz, Iran, m.pooresmaeil@tabrizu.ac.ir
b) Research Center for Pharmaceutical Nanotechnology, Biomedicine Institute, Tabriz University of Medical Science, Tabriz, Iran, namazi@tabrizu.ac.ir

Keywords: Cobalt ferrite; Starch; Covalent organic framework; Hyaluronic acid; Daunorubicin.

Cancer is one of the greatest fearsome diseases with the leading cause of death that results because of the uncontrolled growth of cells [1]. In recent years the development of nanomaterials has taken new chances and challenges in numerous aspects so there is no doubt that these materials accomplish well in tumor therapy [2-3]. Therefore, herein, a new multifunctional nanosystem was designed and fabricated benefiting from the cobalt ferrite nanoparticles ($CoFe_2O_4$), starch (St), covalent organic framework (COF), and hyaluronic acid (HA) features. The outcomes of the explored physicochemical properties confirmed the success of the DNR@$CoFe_2O_4$@St@COF(DtTb)-HA synthesis. BET analysis obtained the surface area and mean pore diameter respectively 55.458 m^2 g^{-1} and 6.3855 nm. Daunorubicin as a model anticancer drug was loaded into the final system. The release pattern revealed the enhanced drug release in simulated tumor cell conditions. More importantly, the outcome of the MTT, DAPI, and cell cycle tests as the important aspect of toxicological assessments exhibited that the $CoFe_2O_4$@St@COF(DtTb)-HA is biocompatible, while the drug-loaded system leads to further inhibition of cell proliferation.

Scheme: Schematic of $CoFe_2O_4$@St@COF(DtTb)-HA synthesis way.

References

[1] Parvaneh, S.; Pourmadadi, M.; Abdouss, M.; Pourmousavi, S.A.; Yazdian, F.; Rahdar, A.; Díez-Pascual, A.M.; Carboxymethyl cellulose/starch/reduced graphene oxide composite as a pH-sensitive nanocarrier for curcumin drug delivery, *Int. J. Biol. Macromol. 241* (2023) 124566.
[2] Meng, Q.; Zhou, L.; Zhong, S.; Wang, J.; Wang, J.; Gao, Y.; Cui, X; Stimulus-responsive starch-based nanocapsules for targeted delivery and antibacterial applications, *Int. J. Biol. Macromol. 241* (2023) 124664.
[3] Pooresmaeil, M.; Namazi, H.; Surface modification of graphene oxide with stimuli-responsive polymer brush containing β-cyclodextrin as a pendant group: Preparation, characterization, and evaluation as controlled drug delivery agent, *Colloids Surf. B . Biointerfaces 172* (2018) 17-25.

Carboxymethyl starch-gelatin coated COF/5-Fu as pH-sensitive drug delivery vehicle

Malihe Pooresmaeil[a*], Hassan Namazi[a,b]

a) Polymer Research Laboratory, Department of Organic and Biochemistry, Faculty of Chemistry, University of Tabriz, Tabriz, Iran, m.pooresmaeil@tabrizu.ac.ir.
b) Research Center for Pharmaceutical Nanotechnology, Biomedicine Institute, Tabriz University of Medical Science, Tabriz, Iran, namazi@tabrizu.ac.ir.

Keywords: Covalent organic framework; Carboxymethyl starch; Gelatin; pH-responsive system.

Colon cancer is one of the important cases of a risk to human health which has commonly been a major concern worldwide [1]. Therefore, today, the enormous amount of effort spent to treat it. Newly, oral drug carriers based on porous materials and polysaccharides have been recognized to be efficient in therapeutic drug delivery to the colon [2-3]. Therefore, in the current study, we constructed covalent organic framework with a spherical structure as a platform for 5-fluorouracil (5-Fu) loading at about ~93.33% (COF/5-Fu). However, their imine bond is relatively unstable in harsh acidic conditions. Hence, there is an urgent and strong need to cap COF/5-Fu into carboxymethyl starch-gelatin (CMS-Gel) coat (COF/5-Fu@CMS-Gel). Drug release tests showed that the loaded 5-Fu was released highly at pH 7.4, but only 14.11 % of 5-Fu releases occurred at pH 1.2. All together the results can guarantee that the COF/5-Fu@CMS-Gel is promising for controlled colon drug delivery.

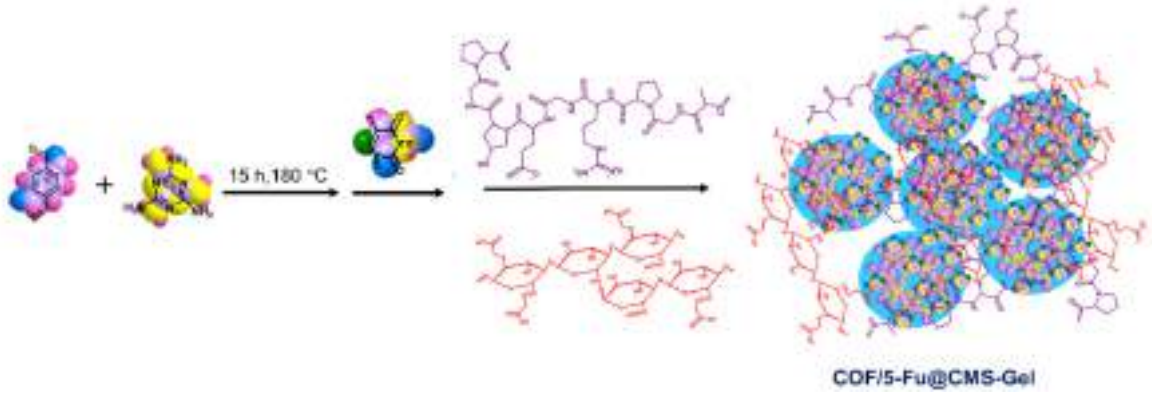

Scheme: Schematic of $CoFe_2O_4$@St@COF(DtTb)-HA synthesis way.

References

[1] Kaur, V.; Goyal, AK.; Ghosh, G.; Si, SC.; Rath, G.; Development and characterization of pellets for targeted delivery of 5-fluorouracil and phytic acid for treatment of colon cancer in Wistar rat. *Heliyon. 6(1)* (2020) e03125.
[2] An, K.; Kang, H.; Zhang, L.; Guan, L.; Tian, D.; Preparation and properties of thermosensitive molecularly imprinted polymer based on konjac glucomannan and its controlled recognition and delivery of 5-fluorouracil. *J. Drug Deliv. Sci. Technol. 60* (2020) 101977.
[3] M, Pooresmaeil.; H, Namazi.; Development of the new pH-driven carrier from alginate/carboxymethyl starch bio-coated co-drugs@ COF-OH for controlled and concomitant colon cancer treatment. *Int. J. Biol. Macromol. 239* (2023): 124322.

pyrido[2,3-d:5,6-d′]dipyrimidinesare synthesized using a new and effective nanocatalyst, KCC-1 solvents-free.

Seyyed Hojjat Sadeghi, Sadegh Rostamnia*

Organic and Nano Group (ONG), Department of Chemistry, Iran University of Science and Technology (IUST), Tehran 16846-13114, Iran, tkd.isf@gmail.com.

Keywords: KCC-1, Multicomponent reactions, Heterogeneous catalys, Filamentous silica nanoparticles”

Due to their extensive range of biological and therapeutic properties and inclusion in the natural goods' structures, heterocyclic compounds are a significant class of organic molecules. Pyrido[2,3-d:5,6-d′]dipyrimidines . are a specific family of heterocyclic substances that have a pyrimidine ring in their structure. Derivatives of Pyridodipyrimidine have numerous biochemical effects, including antitumor [1,2]. In this study, we reported pyrido[2,3-d:5,6-d′]dipyrimidine compound synthesis solvent-free using KCC-1 NPs.(**Scheme**).

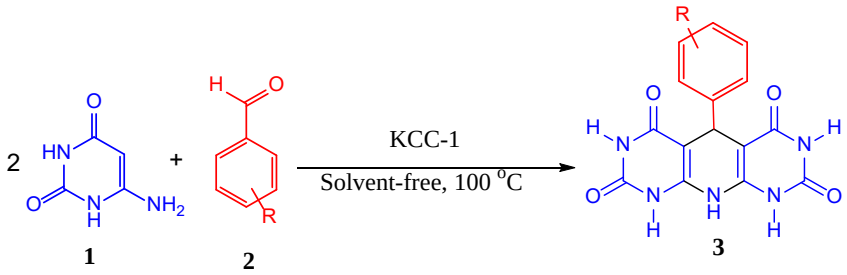

1 **2** **3**

Scheme: Synthesis of pyrido[2,3-d:5,6-d′]dipyrimidines by KCC-1NPs.

References

[1] Yavari I, Moradi L. A synthesis of isoxazoles through the reaction of activated acetylenes and alkyl 2-nitroethanoates in the presence of triphenylphosphine. *Tetrahedron Lett.*2006,*47*,1627.

[2] Ghorbani-Vaghei R, Sarmast N. Hexamethylenetetramine grafted layered double hydroxides as a novel and green heterogeneous ionic liquid catalyst for the synthesis of pyrido [2, 3-d] pyrimidine derivatives. *Res.Chem.Intermed.* 2018,*44*,4483–501.

pyrido[2,3-d:5,6-d/]dipyrimidinesare synthesized using $NiFe_2O_4$ a magnetically recoverable nanocatalyst solvent-free.

Seyyed Hojjat Sadeghi, Sadegh Rostamnia*

Organic and Nano Group (ONG), Department of Chemistry, Iran University of Science and Technology (IUST), Tehran 16846-13114, Iran, tkd.isf@gmail.com.

Keywords: Multicomponent reactions, Heterogeneous catalyst, $NiFe_2O_4$ magnetically nanoparticles

Due to their extensive range of biological and therapeutic properties and inclusion in the natural goods' structures, heterocyclic compounds are a significant class of organic molecules. Pyrido[2,3-d:5,6-d′]dipyrimidines . are a specific family of heterocyclic substances that have a pyrimidine ring in their structure. Derivatives of Pyridodipyrimidine have numerous biochemical effects, including antitumor [1,2]. In this study, we reported pyrido[2,3-d:5,6-d′]dipyrimidine compound synthesis solvent-free using $NiFe_2O_4$ NPs.(Scheme).

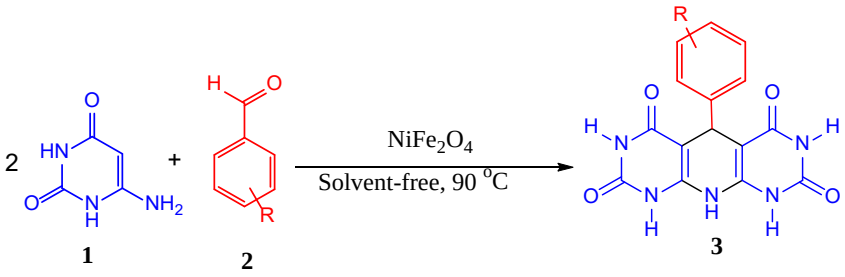

Scheme: Synthesis of pyrido[2,3-d:5,6-d0]dipyrimidines by KCC-1NPs.

References

[1] I. Yavari, L. Moradi, A synthesis of isoxazoles through the reaction of activated acetylenes and alkyl 2-nitroethanoates in the presence of triphenylphosphine, *Tetrahedron Lett*. 2006 , *47*, 1627–1629.

[2] R. Ghorbani-Vaghei, N. Sarmast, Hexamethylenetetramine grafted layered double hydroxides as a novel and green heterogeneous ionic liquid catalyst for the synthesis of pyrido [2,3-d] pyrimidine derivatives, *Res. Chem. Intermed.* 2018, *44*, 4483–4501.

Urea-based porous organic polymer as a hydrogen bond catalyst in Knoevenagel condensation reaction

Narges Zarei, Mohammad Ali Zolfigol*, Morteza Torabi, Meysam Yarie

Department of Organic Chemistry, Faculty of Chemistry, Bu-Ali Sina University, Hamedan 6517838683, Iran, nargesza70@gmail.com, zolfi@basu.ac.ir, myarie.5266@gmail.com.

Keywords: Polymer, Hydrogen bond Catalyst, Knoevenagel condensation

Recently, porous organic polymers (POPs) have attracted increasing attention and have emerged as a new research area in polymer chemistry [1]. These materials have so much applications in gas adsorption/separation, energy storage, H_2 production from water, photocatalysis, chemical sensing, solar cells, water purification, optical devices, catalytic transformations and biomedicine [2]. The product of Knoevenagel condensation reaction is made from the reaction between aldehydes or ketones and active methylene compounds [3]. In this study, the synthesis of some organic compounds based on Knoevenagel reaction in the presence of new urea-based POP as a hydrogen bond catalyst is reported (**Scheme 1**).

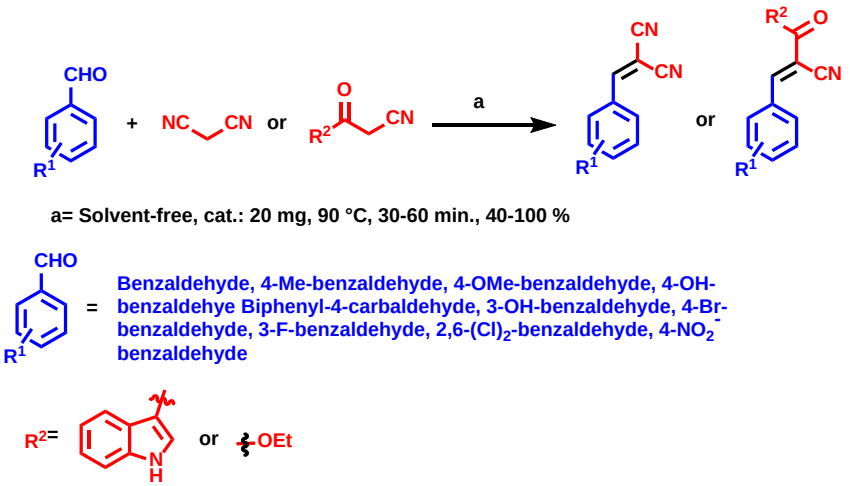

Scheme 1: General procedure for the catalytic synthesis of Knoevenagel adducts.

References

[1] Das, S.; Heasman, P.; Ben, T.; Qiu, S. Porous organic materials: strategic design and structure–function correlation. *Chem. Rev.* 2017, *117*, 1515-1563.

[2] Mohamed, M. G.; EL-Mahdy, A. F.; Kotp, M. G.; Kuo, S. W. Advances in porous organic polymers: Syntheses, structures, and diverse applications. *Mater. Adv.* 2022, *3*, 707-733.

[3] Pandey, R.; Singh, D.; Thakur, N.; Raj, K. K. Catalytic C–H bond activation and Knoevenagel condensation using pyridine-2, 3-dicarboxylate-based metal–organic frameworks. *ACS Omega* 2021, *6*, 13240-13259.

Synthesis, characterization, solvatochromic, computational and antibacterial studies of a series of new 4-imino-3-(2-heteroarylhydrazono)chroman-2-one dyes

Sara Fotovati[a], Gholamhasan Imanzadeh[a]*, Asieh Yahyazadeh[b], Enayatollah Moradi Rufchahi[c*]

a) Departement of Chemistry, Faculty of Science, University of Mohaghegh Ardabili, Ardabil, Iran, sarafotovati@yahoo.com
b) Department of Chemistry, Faculty of Science, University of Guilan, Rasht, Iran
c) Department of Chemistry, Faculty of Science, Lahijan Branch, Islamic Azad University, Lahijan, Iran

Keywords: 4-Aminocoumarin, Azo dyes, Solvatochromism, DFT

4-Aminocoumarin was synthesized and reacted with some diazonium salts derived from substituted 2-aminothiazoles to produce corresponding new azo dye [1]. (**Scheme1**). The results testified that the obtained products exclusively adopt hydrazone tautomeric form in both solid and solution states and there was seen no spectral evidence of azo structure. The visible absorption spectral changes of the dyes were also studied and discussed according to possible electronic transitions in the compounds [2,3]. Furthermore, the geometries of the proposed azo and hydrazone tautomeric forms of the dyes were optimized at B3LYP/6–311++G (d, p) level of theory. DFT calculations have performed to evaluate the stability of azo and hydrazone tautomeric forms of the prepared dyes. Antibacterial activities of the dyes evaluated using well diffusion method against *Staphylococcus aureus* and *E.coli* bacterial.

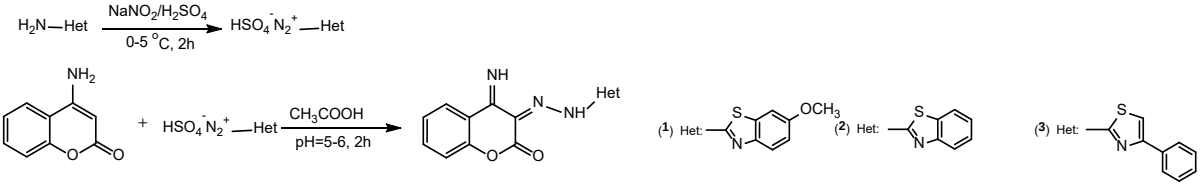

Scheme1: Azo coupling of 4-aminocoumarin

References

[1] Debnath, D.; Roy, S.; Li, B.; Lin, Ch.; Misra, T. K. Synthesis, structure and study of azo-hydrazone tautomeric equilibrium of 1,3-dimethyl-5-(arylazo)-6-amino-uracil derivatives. *Spectrochim. Acta A Mol. Biomol.* 2015,140,185-197.
[2] Yousefi, H.; Yahyazadeh, A.; Yazdanbakhsh, M. R.; Rassa, M.; Moradi-e-Rufchahi, E. O. Synthesis, spectral features and biological activity of some novel hetarylazo dyes derived from 6-amino-1, 3-dimethyluracil. *J. Mol.* Struct. 2012, 1015, 27-32.
[3] Debnath, D.; Roy, S.; Li, B.-H.; Lin, Ch.-H.; Misra, T. K. Synthesis, structure and study of azo-hydrazone tautomeric equilibrium of 1,3-dimethyl-5-(arylazo)-6-amino-uracil derivatives. *Spectrochim. Acta A Mol. Biomol.* 2015, 140, 185–197.

Magnetic Cu-Ni Bimetallic System as an Efficient Nanocatalyst for Hantzsch Reaction

Fatemeh Nasseri[a, b], **Mohammad Ali Nasseri**[b*] **and Mohammad Zaman Kassaee**[a]

a) Department of Chemistry, Tarbiat Modares University, Tehran, Iran, fatemehnaseri123@yahoo.com
b) Department of Chemistry, Birjand University, Birjand, Iran, manaseri@birjand.ac.ir

Keywords: Bimetallic catalyst, Hantzsch reaction, 1,4-Dihydropyridines, Magnetic NPs

In the field of drugs and pharmaceuticals, Hantzsch 1,4-dihydropyridines (1,4-DHPs) and their derivatives represent a significant class of bioactive molecules [1]. In recent decades, bimetallic catalysts have been getting more attention in academic and industrial applications. The electronic effect, along with structural changes, helps them to act as a better catalyst than their monometallic counterparts [2]. By supporting the catalysts on the surface of Fe_3O_4 NPs, they can be easily separated from the reaction medium using a magnet [3]. In our study, we synthesized a magnetically recyclable copper/nickel bimetallic nanocatalyst (Fe_3O_4@SiO_2@L/Cu-Ni) with high performance for the Hantzsch reaction (**Scheme**).

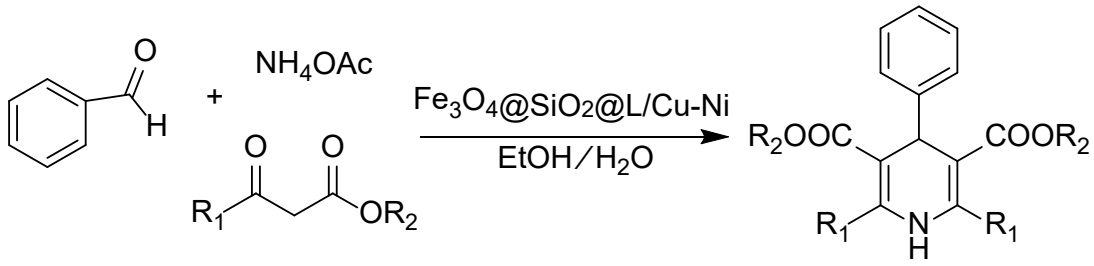

Scheme: Synthesis of 1,4-dihydropyridine derivatives by Fe_3O_4@SiO_2/Cu-Ni catalyst.

References

[1] Allahresani, A.; Mohammadpour Sangani, M.; Nasseri, M. A. CoFe2O4@ SiO2-NH2-CoII NPs catalyzed Hantzsch reaction as an efficient, reusable catalyst for the facile, green, one-pot synthesis of novel functionalized 1, 4-dihydropyridine derivatives. *Appl. Organomet. Chem* 2020, *34* (9), e5759.
[2] Singh, R. Use of bimetallic nanoparticles in the synthesis of heterocyclic molecules. *Curr. Org. Chem* 2021, *25* (3), 351-360.
[3] Sobhani, S.; Nasseri, F.; Zarifi, F. Unique role of 2-hydroxyethylammonium acetate as an ionic liquid in the synthesis of Fe 3 O 4 magnetic nanoparticles and preparation of pyridine derivatives in the presence of a new magnetically recyclable heterogeneous catalyst. *J. Iran. Chem. Soc* 2018, *15*, 2721-2732.

Electrocatalytic application of a Schiff base copper(II) complex-based catalyst

Mohaddeseh Sajjadi[a], Ali Ghaffarinejad[b,*], Mahmoud Nasrollahzadeh[c,*] and Hossein Ghafuri[a]

a) Catalysts and Organic Synthesis Research Laboratory, Department of Chemistry, Iran University of Science and Technology, Tehran, 16846-13114, Iran, mhd.sajjadi@gmail.com.
b) Research Laboratory of Real Samples Analysis, Faculty of Chemistry, Iran University of Science and Technology (IUST), Tehran 1684613114, Iran, ghaffarinejad@iust.ac.ir.
c) Faculty of Chemistry, University of Qom, Qom, Iran, mahmoudnasr81@gmail.com.

Keywords: Magnetic lignin, Electrocatalyst, Hydrogen evolution, Tetrazole complex

Meeting society's demands needs alternative bio-friendly and sustainable energy resources. Hydrogen is the key component in terms of energy economy, and electrochemical water splitting is one of the most important techniques to replace the commonly used fossil fuels [1-2]. Here, for the first time, magnetic lignosulfonate-supported Schiff base copper(II) complex (**Scheme 1**) was prepared and used as an efficient electrocatalyst in carbon paste electrode (MLig-SchTet-Cu(II)-CPE) for hydrogen evolution reaction (HER). The fabricated electrocatalyst comprising magnetic biopolymer, Schiff base Cu(II) complex was added to CPE to improve the HER activity of bare CPE. The HER efficiency/stability of the prepared electrode was measured by LSV, CV, EIS, and CP methods in acidic and alkaline media. The best result for HER was achieved in 0.5 M H_2SO_4 and 2.5% of the electrocatalyst percent. The optimal electrode (2.5% MLig-SchTet-Cu(II)-CPE) has an excellent electrocatalytic activity for HER in acidic media equal to -0.54 mV overpotential at a current density of 10 $mA \cdot cm^{-2}$.

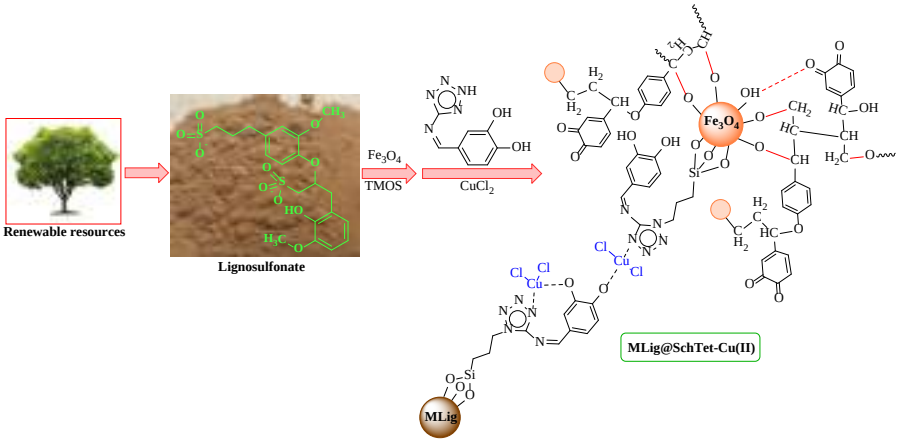

Scheme 1: Schematic representation of MLig-SchTet-Cu(II) preparation.

References

[1] Mohazzab, B. F.; Jaleh, B.; Nasrollahzadeh, M.; Khazalpour, S.; Sajjadi, M.; Varma, R. S. Upgraded valorization of biowaste: laser-assisted synthesis of Pd/calcium lignosulfonate nanocomposite for hydrogen storage and environmental remediation. *ACS Omega* **2020**, *5*, 5888-5899.
[2] Arabi, M.; Ghaffarinejad, A.; Darband, G. B. Electrodeposition of nanoporous nickel selenide on graphite rod as a bifunctional electrocatalyst for hydrogen and oxygen evolution reactions. *J. Electroanal. Chem.* **2022**, *907*, 116066.

A Hydrophilic Heterogeneous Copper Nanocatalyst for Suzuki Coupling Reaction in Water

Fatemeh Nasseri[a, b], Mohammad Ali Nasseri[b*] and Mohammad Zaman Kassaee[a]

a) Department of Chemistry, Tarbiat Modares University, Tehran, Iran, fatemehnaseri123@yahoo.com
b) Department of Chemistry, Birjand University, Birjand, Iran, manaseri@birjand.ac.ir

Keywords: Suzuki reaction, Hydrophilic catalyst, Magnetic nanoparticles, Copper, Water

Suzuki-Miyaura cross-coupling reaction of aryl halides with arylboronic acids catalyzed by copper compounds provides a versatile synthetic tool for the formation of biaryls as essential motifs found in bioactive compounds and pharmaceuticals [1]. As a cheap, safe, non-toxic, and green medium, water has attracted considerable interest for organic reactions. Some effective ligands with metals can catalyze the reactions efficiently in water, which is attributed to the Breslow hydrophobic effect, hydrogen bonding effect, and polarity effect [2]. magnetic nanoparticles as the support for catalysts have attracted increasing attention because of their facile separation from the reaction mixture using an external magnet [3]. Here, we have immobilized copper (II) onto magnetic nanoparticles stabilized by a hydrophilic ligand and applied it as a nanocatalyst in the Suzuki cross-coupling reaction (**Scheme**).

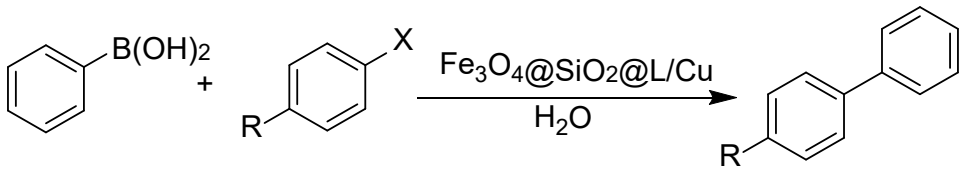

Scheme: Suzuki reaction by Fe_3O_4@SiO_2@L/Cu nanocatalyst.

References

[1] Priya, V. B.; Venkatesan, K.; Jagadish, T.; Koppala, S.; Karthikeyan, P. Immobilized copper (II)-containing imidazolium functionalized ionic liquid: A highly active, effective and ecological heterogeneous catalyst for the Suzuki-Miyaura reaction. *J. Organomet. Chem* 2023, *999*, 122821.
[2] Zhou, G.; Chen, W.; Zhang, S.; Liu, X.; Yang, Z.; Ge, X.; Fan, H.-J. A newly designed carbohydrate-derived alkylamine promotes Ullmann type C–N coupling catalyzed by copper in water. *Synlett* 2019, *30* (02), 193-198.
[3] Sobhani, S.; Nasseri, F.; Zarifi, F. Unique role of 2-hydroxyethylammonium acetate as an ionic liquid in the synthesis of Fe 3 O 4 magnetic nanoparticles and preparation of pyridine derivatives in the presence of a new magnetically recyclable heterogeneous catalyst. *J. Iran. Chem. Soc* 2018, *15*, 2721-2732.

Production of 5-hydroxymethylfurfural using a novel chitosan-based catalyst

Mohaddeseh Sajjadi[a], Mahmoud Nasrollahzadeh[b,*] and Hossein Ghafuri[a]

a) Catalysts and Organic Synthesis Research Laboratory, Department of Chemistry, Iran University of Science and Technology, Tehran, 16846-13114, Iran, mhd.sajjadi@gmail.com.
b) Faculty of Chemistry, University of Qom, Qom, Iran, mahmoudnasr81@gmail.com.

Keywords: 5-Hydroxymethylfurfural, Chitosan, Acidic catalyst, Ionic liquid, Fructose

5-Hydroxymethylfurfural (5-HMF) is one of the most significant building components based on biomass, which is a significant precursor in view of the presence of aldehyde and hydroxymethyl functional groups, and thus is very valuable in generating polymers, pharmaceuticals, fine chemicals, and related organics in the industry [1,2]. Recently, the preparation of heterogeneous catalysts using biopolymers has been considered due to their unique advantages [3]. Ionic liquids have attracted particular attention as novel and efficient catalysts owing to their critical properties e.g., environmental friendliness, high thermal stability, selective solubility, activity, *etc*. [2]. Herein, this study has demonstrated a novel method to prepare magnetic chitosan-supported ionic liquid copper(II) complex and its application to produce 5-HMF from fructose (**Scheme 1**).

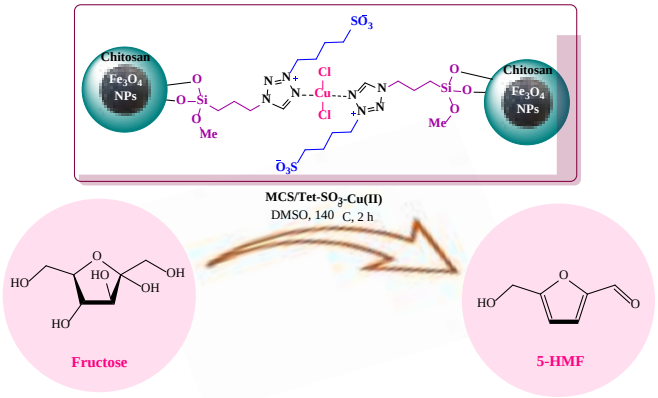

Scheme 1: Synthesis of 5-HMF catalyzed by MCS/Tet-SO_3-Cu(II).

References

[1] Nasrollahzadeh, M.; Bidgoli, N. S. S.; Shafiei, N.; Momenbeik, F. Biomass valorization: Sulfated lignin-catalyzed production of 5-hydroxymethylfurfural from fructose. *Int. J. Biol. Macromol.* **2021**, *182*, 59-64.

[2] Nasrollahzadeh, M.; Nezafat, Z.; Momenbeik, F.; Orooji, Y. Polystyrene immobilized Brønsted acid ionic liquid as an efficient and recyclable catalyst for the synthesis of 5-hydroxymethylfurfural from fructose. *J. Mol. Liq.* **2022**, *345*, 117811.

[3] Sajjadi, M.; Nasrollahzadeh, M.; Ghafuri, H.; Baran, T.; Orooji, Y.; Baran, N. Y.; Shokouhimehr, M. Modified chitosan-zeolite supported Pd nanoparticles: A reusable catalyst for the synthesis of 5-substituted-1*H*-tetrazoles from aryl halides. *Int. J. Biol. Macromol.* **2022**, *209*, 1573-1585.

Efficient Catalytic Degradation of 4-nitrophenol in the presence of Cu-Zn-MOF

Hossein Yarahmadi*

Department of Chemical Engineering, Sirjan University of Technology, Sirjan, Iran, hyarahmadi61@gmail.com.

Keywords: Degradation, 4-Nitrophenol, MOF

Efficient water treatment methods are necessary to remove hazardous dyes from industrial wastewater, which poses a threat to human health and the environment in developing countries [1]. Various techniques have been utilized for the treatment and remediation of contaminated wastewater, with catalytic degradation being a promising and widely used method for environmental pollution treatment. Researchers have focused on developing and optimizing novel low-cost catalysts with high catalytic efficiency and recyclability, including activated carbon, coal, clay, fly ash, zeolites, and metal-organic frameworks (MOFs) [2, 3]. This study focuses on exploring the potential of bimetallic MOFs for enhancing catalytic activity in water treatment. Specifically, it investigates the preparation of modified Cu-Zn-MOF nanocomposites using Waste PET Bottles (WPTS), aiming to degrade organic pollutant dyes (OPDs) in aqueous media under mild conditions. A bimetallic Cu-Zn-MOF is successfully synthesized and utilized as a heterogeneous catalyst. The cost-effective and environmentally friendly approach involves using terephthalic acid on MOF structure derived from the degradation of WPTS, with the incorporation of Cu to enhance catalytic efficiency for the chemical degradation of OPDs.

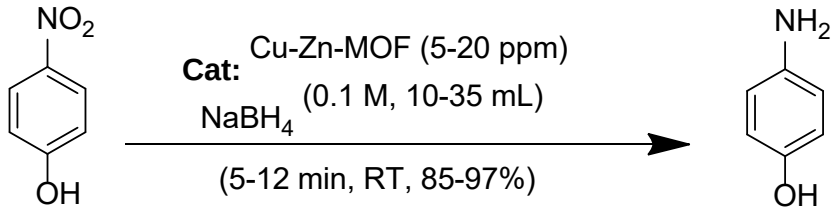

Scheme: Degradation of OPDs in the presence of Cu-Zn-MOF.

References

[1] Uddin, F. Environmental hazard in textile dyeing wastewater from local textile industry. *Cellulose* 2021, *28*, 10715-10739.

[2] Durán, A., Monteagudo, J. M. & San Martín, I. Operation costs of the solar photo-catalytic degradation of pharmaceuticals in water: A mini-review. *Chemosphere* 2018, *211*, 482-488.

[3] Poonia, K. et al. Recent advances in Metal Organic Framework (MOF)-based hierarchical composites for water treatment by adsorptional photocatalysis: A review. *Environ. Res.* 2023, *222*, 115349.

Immobilized Bronsted acidic ionic liquid on magnetic cellulose as a novel catalyst for the synthesis of triazolo[4,3-*a*]pyrimidine derivatives

Azar Jahanbakhshi and Mahnaz Farahi*

Department of Chemistry, Yasouj University, 75918-74831, Yasouj, jahanbakhshi.azar@yahoo.com, Iran, farahimb@yu.ac.ir.

Keywords: Cellulose, Fe_3O_4, Ionic liquid, Triazolo[4,3-*a*]pyrimidine

Cellulose, as one of the most critical natural organic polymers, can be used as nanocomposite, support materials, and emulsions because of various advantages such as biocompatible, thermal stability, and ability to modify its surface chemistry and hydrophilicity. The hydroxyl groups on the surface of cellulose are reactive and facilitate chemical modification with organic and inorganic groups, thereby enhance the properties of cellulose-based materials. Ionic liquids (ILs) as eco-friendly have substantial benefits to the organic and acid-catalysis reactions. However, the immobilization of ionic liquids on different solid supports such as cellulose facilitate easy catalyst recovery, high selectivity, recyclability and less contamination of products with a catalyst [1,2]. Herein, we report the immobilization of the Bronsted acidic ionic liquid 1-(propyl-3-sulfonate) vinyl imidazolium hydrogen sulfate [IL] onto magnetically-modified cellulose. The catalytic activity of this nanocomposite was investigated in the synthesis of triazolo[4,3-*a*]pyrimidine derivatives (**Scheme**).

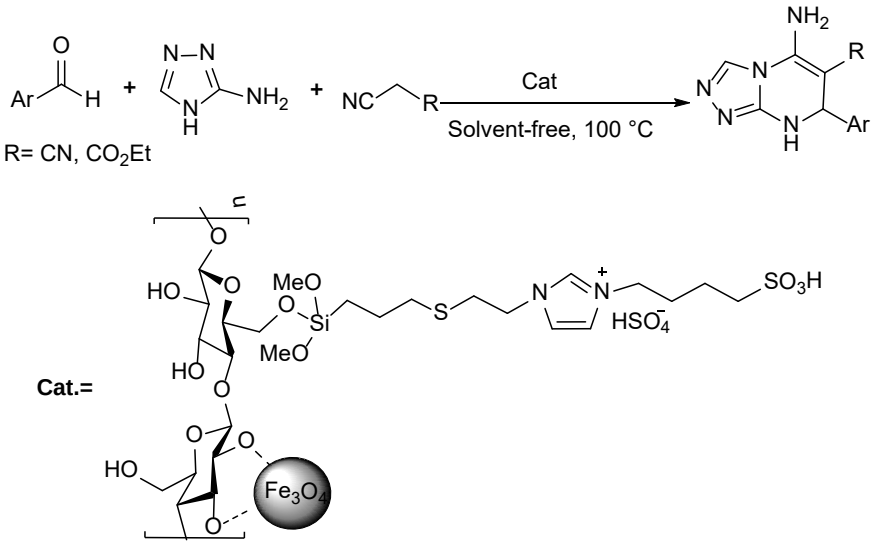

Scheme: Synthesis of triazolo [4,3-*a*]pyrimidine derivatives in the presence of Fe_3O_4/MPC-[IL].

References

[1] Abdelhameed, R. M.; El-Shahat, M.; Emam, H. E. Employable metal (Ag & Pd)@MIL-125-NH_2@cellulose acetate film for visible-light driven photocatalysis for reduction of nitro-aromatics. *Carbohydr. Polym.* 2020, *247*, 116695-116721.

[2] Kerru, N.; Gummidi, L.; Maddila, S. N.; Bhaskaruni, S. B.; Jonnalagadda, S. V. Bi_2O_3/FAp, a sustainable catalyst for synthesis of dihydro- [1,2,4]triazolo[1,5-*a*]pyrimidine derivatives through green strategy. *Appl. Organomet. Chem.* 2020, *34*, 5590-5599.

Preparation and investigation of new derivatives of Heterocyclic bis-thiazole compounds

Akram Hosseinian*

Department of Engineering Science, College of Engineering, University of Tehran, P.O. Box 11365-4563, Tehran, Iran, Hoseinian@ut.ac.ir

Keywords: Preparation, Investigation, Heterocyclic, Thiazole

The thiazole ring system represents the active handle in many biologically-active heterocyclic compounds. Thiazole derivatives have attracted the attention of the scientific community in general and pharmaceutical chemists in particular. This interest is largely fuelled by the thiazole diverse pharmacological and biological activities. Many bis-thiazoles are also as reactive as their thiazole counterparts and their biological activity as antibacterial, antifungal, and anticancer were reported [1, 2]. In this regard, we describe the preparation synthesis of new derivatives of heterocyclic bis-thiazole using a simple method. The characterization of these compounds was done by IR, ^{1}H, ^{13}C NMR spectroscopy and elemental analyses. This heterocyclic compound was structurally characterized by single-crystal X-ray diffraction. The crystal packing is mainly stabilized by intermolecular hydrogen bonding interactions. The heterocyclic compound was further characterized by UV-visible spectrophotometric measurements and fluorescence spectra.

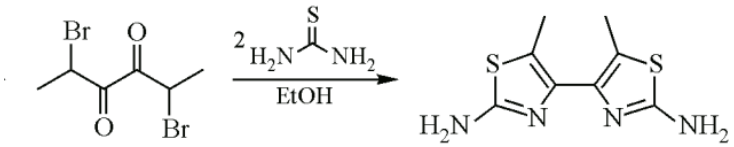

Scheme: Schematic of synthesis of compound

References:

[1] Mahmoud, H.K., Abbas, A.A., Gomha, S.M., Synthesis, Antimicrobial Evaluation and Molecular Docking of New FuncSynthesis and in-silico studies of new bis-thiazole derivatives 13 tionalized Bis(1,3,4-Thiadiazole) and Bis (Thiazole) Derivatives. *Polycycl. Aromat. Compd.*, 2020.41, 2029-2041.

[2] Gomha, S.M., Badrey, M.G., Edrees, M.M., Heterocyclisation of 2,5-diacetyl-3,4-disubstituted-thieno[2,3-b] Thiophene BisThiosemicarbazones Leading to Bis-Thiazoles and Bis-1,3,4-thiadiazoles as Anti-breast Cancer Agents. *J. Chem. Res.* 2016, 40 (2), 120– 125.

A DFT Study of a novel series of bithiazole derivatives

Akram Hosseinian*

Department of Engineering Science, College of Engineering, University of Tehran, P.O. Box 11365-4563, Tehran, Iran, Hoseinian@ut.ac.ir

Keywords: DFT, HOMO, LUMO, Bithiazole

DFT is a computational quantum mechanical modelling method used in physics, chemistry and materials science to investigate the electronic structure. In the case of DFT, these are functionals of the spatially dependent electron density. DFT is among the most popular and versatile methods available in condensed-matter physics, computational physics, and computational chemistry.

The electronic structure and PDOS of the material were simulated via density functional theory, using the Castep software. In Fig. It can be seen that the energy gap between HOMO and LUMO was calculated as 2.40 eV. Due to different Nitrogen atoms in the system which can have different participation in formation of energy levels, we labeled N1 atoms as N* and N2 atoms as N (amine).

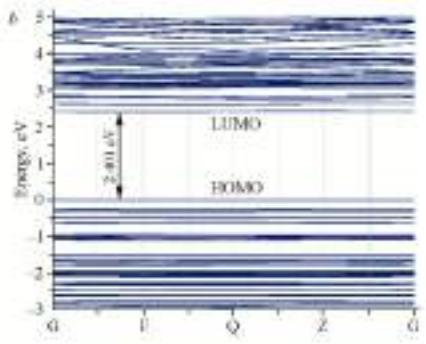

References:

[1] Abo Dena, A.S., Muhammad, Z.A., Hassan, W.M.I., Spectroscopic, DFT studies and electronic properties of novel functionalized bis-1,3,4-thiadiazoles. *Chem. Pap.* 2019, **73**, 2803–2812.

[2] Chamack, M. Hosseinian, A. Khazaee, Z. Synthesis, crystal structure, and DFT insight of a new trigonal bipyramidal zinc (II) complex, *J. Struct. Chem.* 2021, 62, 1043-1055.

29TH IRANIAN ORGANIC CHEMISTRY CONFERENCE
1_3 NOV, 2023
UNIVERSITY OF QOM, IRAN

Mont@SiO_2-NAA-H_2PO_4IL: An efficient catalyst for the synthesis of pyrazolopyranopyrimidines

Fatemeh Ghorbani, Masoume Malmir* and Majid M. Heravi*

Department of Organic Chemistry, Faculty of Chemistry, Alzahra University, Tehran, Iran, fghorbani9313@gmail.com, m.malmir@alzahra.ac.ir and mmheravi@alzahra.ac.ir.

Keywords: Ionic liquids, Multicomponent reactions, Montmorillonite, Heterogeneous Catalyst, Pyranopyrazolopyrimidine.

In order to take advantage of the advantages of heterogeneous catalysts [1,2] in improving the process of organic chemistry reactions, this project tries to report a cost-effective and environmentally friendly method to synthesis of heterogeneous catalyst and investigation of its activity in multi-component reactions. In this research, montmorillonite was functionalized by TEOS, CPTES, nitriloacetic acid and H_3PO_4 and a nanocatalyst containing acidic ionic liquid, Mont@SiO_2-NAA-H_2PO_4IL, was synthesized. Further, the catalyst structure was identified by TEM, ICP-OES, XRD, FTIR, BET, TGA and SEM/EDX techniques. The catalytic activity of Mont@SiO_2-NAA-H_2PO_4IL was investigated in the multicomponent reaction of pyranopyrazolopyrimidine with the synthesis of 36 derivatives, and all compounds obtained with high yields in short times. In addition, this catalyst was easily separated from the reaction mixture by simple filtration and was reused up to 10 times without significant decrease in catalytic activity (**Scheme**).

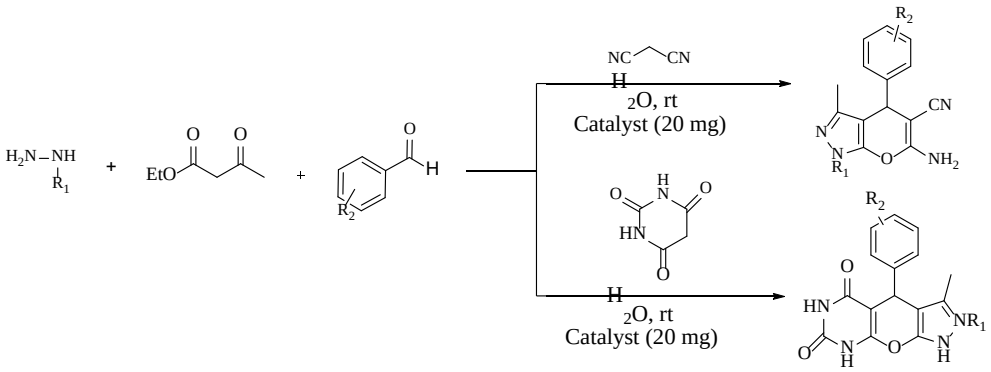

Scheme: Synthesis of pyrazolopyranopyrimidines.

References

[1] Nasrollahzadeh, M.; Issaabadi, Z.; Safari, R., Synthesis, characterization and application of Fe_3O_4@SiO_2 nanoparticles supported palladium(II) complex as a magnetically catalyst for the reduction of 2,4-dinitrophenylhydrazine, 4-nitrophenol and chromium(VI): A combined theoretical (DFT) and experimental study. *Sep. Purif. Technol.* 2019, *209*, 136-144.

[2] Jahani, G.; Malmir, M.; Heravi, M. M., Catalytic Oxidation of Alcohols over a Nitrogen- and Sulfur-Doped Graphitic Carbon Dot-Modified Magnetic Nanocomposite. *Ind. Eng. Chem. Res.* 2022, *61* (5), 2010-2018.

Economically viable and efficient heterogeneous catalysts based niobium for coupling reaction

Hamed Gholami, MohammadNasir Shambayati, Maryam Hajjami*

Organic Chemistry Laboratory, Faculty of Chemistry, Bu-Ali Sina University, Hamedan, Iran, hamedgholamichemistry@gmail.com, m.hajjami@basu.ac.ir & mhajjami@yahoo.com

Keywords: Niobium, Coupling reaction, Organic synthesis, Heterogeneous catalysts

In organic chemistry, a coupling reaction is a type of reaction in which two reactant molecules are bonded together. Such reactions often require the aid of a metal catalyst. Niobium is the third most exported metal in terms of value, losing only to iron ores and gold [1]. The world niobium consumption has grown a hundredfold since the 1960s, and the emergence of new technologies may contribute to increasing the niobium market in future. Niobium catalysts generally possess a good Lewis acidity and have received increased attention in recent years. Materials containing niobium have increased the activity and selectivity in several catalytic reactions, therefore it has awakened the interest among researchers [2,3]. This study reports a simple, reusable, and recoverable niobium-based heterogeneous catalysts for coupling reaction. Additionally, a feasible reaction pathway was suggested for coupling reaction using niobium-based heterogeneous catalysts.

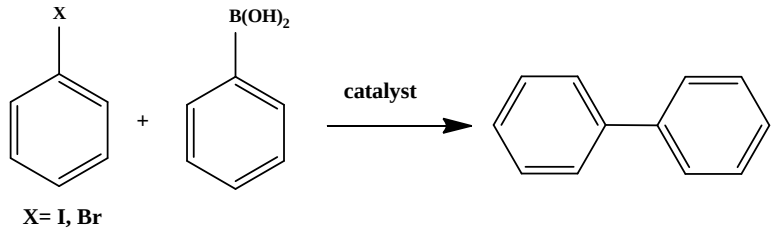

Scheme. Carbon–carbon bond formation in the presence niobium-based heterogeneous catalysts.

Reference

[1] Silveira, J.W.; Resende, M. Competition in the international niobium market: *A residual demand approach. Resour. Policy* 2020, 65, 101564.

[2] Shao, Y.; Xia, Q.; Dong, L.; Liu, X.; Han, X.; Parker, S. F.; Cheng, Y.; Daemen, L. L.; Ramirez-Cuesta, A. J.; Yang, S.; et al. Selective Production of Arenes via Direct Lignin Upgrading over a Niobium-Based Catalyst. *Nat. Commun.* 2017, 8, 16104.

[3] Lin, L.; Sheveleva, A. M.; da Silva, I.; Parlett, C. M. A.; Tang, Z.; Liu, Y.; Fan, M.; Han, X.; Carter, J. H.; Tuna, F.; et al. Quantitative production of butenes from biomass-derived γvalerolactone catalysed by hetero-atomic MFI zeolite. *Nat. Mater* 2020, 19, 86–93.

6,8-Dimethyl-4-hydroxyquinolin-2(1*H*)-one as a versatile coupling component for the synthesis of some new heterocyclic azo dyes

Sara Fotovati[a], Enayatollah Moradi Rufchahi[b*], Asieh Yahyazadeh[c], Gholamhasan Imanzadeh[a]

a) Department of Chemistry, Faculty of Science, University of Mohaghegh Ardabili, Ardabil, Iran.
b) Department of Chemistry, Faculty of Science, Lahijan Branch, Islamic Azad University, Lahijan, Iran
c) Department of Chemistry, Faculty of Science, University of Guilan, Rasht, Iran

Keywords: 4-Hydroxyquinolin-2(1*H*)-one, Azo dyes, Benzothiazole, Enol-type coupling component

4-Hydroxyquinoline-2(1*H*)-ones have been investigated as heterocyclic backbones to produce some of the early examples of azo disperse dyes [1]. For example, 4-hydroxyquinolin-2(1*H*)-one (2,4-dihydroxyquinoline) and *N*-butyl-4-hydroxyquinolin-2(1*H*)-one were respectively employed for the synthesis of C.I. Pigment Yellow 7 and C.I. Mordant Yellow 30 [2, 3].
Inspired by the aforementioned results, herein a series of 2-aminobenzothiazoles have been diazotized and coupled with 6, 8-dimethyl-4-hydroxyquinoline-2(1*H*)-one in basic solution at 0-5°C (**Scheme1**).The structures assigned by IR, ^{1}H NMR and Mass analyses. The visible absorption spectra along with ^{1}H NMR findings of all the 4-hydroxyquinolin-2-one based azo dyes revealed that there is a mixture of tautomeric forms in the solution state in solvents with different polarities. The effects of acid and base on the visible absorption spectra of the dyes in ethanol were also studied and showed that the spectral changes are clearly dependent upon the protonation-deprotonation of the dye molecules.

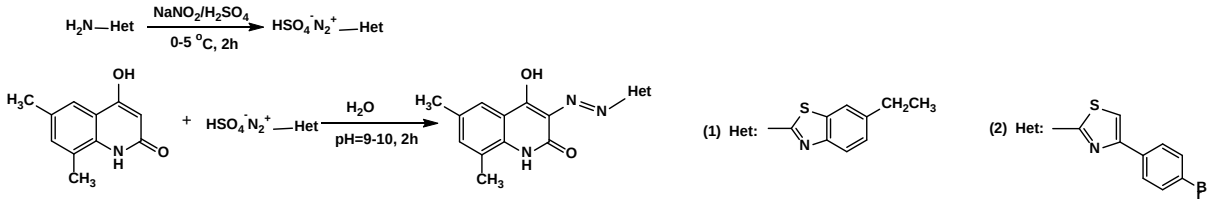

Scheme1. Synthesis of some new heterocyclic azo dyes.

References

[1] Abrahart, E. N. Dyes and Their Intermediates, 2nd edition, London NW1 3BH UK, Hodder Arnold, **1977**, p. 250.
[2] Tanabe, T.; Ishikawa, N. Preparation of 5,6,7,8-tetrafluoro-2,4-quinolinediol and some azo colors derived therefrom, *Nippon. Kagaku Kaishi* **1972**, 7, 1255-1258.
[3] Clark, T. Handbook of Textile and Industrial Dyeing, Sawston, first ed., Woodhead Publishing Limited, Cambridge CB22 3HJ, UK, **2011**, p. 495.

Fabrication of Ni@zeolite-Y supported 4-methylpyridinium ionic liquid and its application as a multi-functional nanocatalyst in the green synthesis of 4-aryl-1,3-oxazolones

Mehdi Kalhor*, Fatemeh Janghorban

Department of Chemistry, Payame Noor University, 19395-4697, Tehran, Iran,
mekalhor@yahoo.com

Keywords: Multi-functional nanocatalyst, Ionic liquid, Ni/zeolite-Y, 4-Methylpyridinium chloride, 1,3-oxazolone.

From the fundamental principles and goals of green chemistry is to design environmentally friendly reactions to minimize the harm caused by the utilization of chemicals. One of the basic ways to achieve this is the use of catalysts in chemical reactions. For this reason, the design and synthesis of heterogeneous nanocatalysts, especially multi-functional ones, are these days a hot topic of researches [1]. In view of this fact, further development of research on the synthesis of zeolite-based nanocatalysts and its application in the easy preparation of *N*-heterocycles [2] herein, we decided to report design and manufacturing of Ni/[(MPy)$^+$Cl$^-$]@ZY nanoprous through loading 4-methylpyridinium chloride ionic liquid on Ni-zeolite-Y. Its structure was identified and confirmed by various analyzes including: FT-IR, FE-SEM, EDX, XRD, TGA and N_2 adsorption–desorption (BET). It also used as a recoverable and multi-functional nanocatalyst for the simple and rapid synthesis of 4-arylidene-2-phenyl-5(4*H*) oxazolones through the one-pot reaction of hippuric acid, arylaldehydes, acetic anhydride under mild and solvent-free conditions with excellent yields. (**Scheme**).

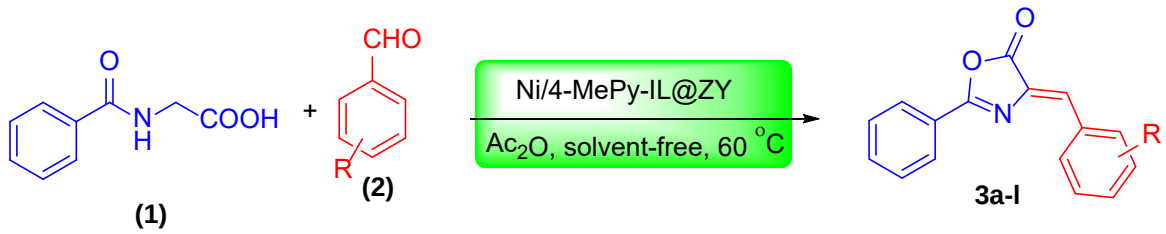

Scheme: The synthetic pathway of 4-arylidene oxazolones using Ni/[(MPy)$^+$Cl$^-$]@ZY

References

[1] Jagadeesan, D.; a review: multifunctional nanocatalysts for tandem reactions: A leap toward sustainability. *Appl. Catal. A-Gen.* 2016, *511*, 59-77.

[2] Kalhor, M.; Zarnegar, Z.; Fe_3O_4/SO_3H@zeolite-Y as a novel multi-functional and magnetic nanocatalyst for clean and soft synthesis of imidazole and perimidine derivatives. *RSC Adv.* 2019, *9*, 19333-19346.

[3] Kalhor, M.; Banibairami, S.; Mirshokraie, S. A.; Ni@zeolite-Y nanoporous; a valuable and efficient nanocatalyst for the synthesis of *N*-benzimidazole-1,3-thiazolidinones. *Green Chem. Lett. Rev.* 2018, *11*, 334-344.

Evaluation of pyrolysis methods and their effects on the environment: a review

Seyedeh Bahareh Azimi[a*], Payam Joharchi[b]

a) Assessment and Environment Risks Department, Research Centre and Environment and Sustainable Development (RCESD), Tehran, Iran, azimib@rcesd.ac.ir
b) Researcher of the Department of Environmental Protection, Tehran, Iran, Payamjoharchi@gmail.com

Keywords: Pyrolysis, Environment, Waste management

Pyrolysis is one of the thermochemical methods for converting agricultural waste (biomass) into biochar, bio-oil and biogas. This method has been considered as a potential solution for waste management and environmental impact reduction. In this article, some key points regarding the reduction of environmental impacts using pyrolysis are explained.
Waste reduction: Pyrolysis can be used to convert all kinds of organic waste, including biomass, into valuable products such as biochar. That helps to reduce the volume of waste and environmental challenges.

Greenhouse gas emissions: Pyrolysis can help reduce greenhouse gas emissions compared to traditional methods such as burning of biomass. This process can produce biochar, that be used as a soil amendment for carbon sequestration and mitigating climate change.

Air pollution: while pyrolysis can provide environmental benefits, it is essential to address potential pollutants emitted during the process. proper design and operation, including the use of appropriate technologies, can minimize the emission of harmful gases and suspended particles.

Pyrolysis with waste conversion to valuable resources enhances the circle economy and can help sustainable resource management by recycling energy and useful products from waste.

These points are only a few examples of cases mentioned in this paper. the effects of pyrolysis can vary depending on factors such as starting materials, process condition, and the implementation of emission control measures. Proper regulation, monitoring and continuous improvement in pyrolysis technologies is necessary to ensure maximum environmental benefits and at the same time minimize any possible forms

References

[1] Hamidzadeh, Z., Ghorbannezhad, P., Ketabchi, M. R., & Yeganeh, B. Biomass-derived biochar and its application in agriculture. *Fuel* 2023, *341*, 127701
[2] Durak, HComprehensive Assessment of Thermochemical Processes for Sustainable Waste Management and Resource Recovery. *Processes* 2023, *11*(7), 2092.
[3] Hu, X., & Gholizadeh, MBiomass pyrolysis: A review of the process development and challenges from initial researches up to the commercialisation stage. *Energy Chemistry*. 2019, *39*, 109-143.

29TH IRANIAN ORGANIC CHEMISTRY CONFERENCE
1_3 NOV, 2023
UNIVERSITY OF QOM, IRAN

Synthesis of 1-(benzothiazole-2-yl)-3-phenylthiourea under the ionic liquid condition: Theoretical and experimental approach on NMR spectra

Elahe Sadat Mousavi-Kherad[a*], Leila Hajiaghababaei[a], Jamshid Najafpour[a], Ashraf Sadat Shahvelayati [a], Shiva Dehghan Abkenar[b]

a) Department of Chemistry, Yadegar-e-Imam Khomeini (RAH) Shahre Rey Branch, Islamic Azad University, Tehran, Iran, elahe.mousavi69@gmail.com.*
b) Department of Chemistry, Islamic Azad University, Savadkooh Branch, Savadkooh, Iran.

Keywords: "Green synthesis", "1-(~~benzothiazole~~Benzothiazole-2-yl)-3-phenylthiourea", "Ionic liquid", "Density Functional Theory"

The compound 1-(benzothiazole-2-yl)-3-phenylthiourea has been successfully synthesized under Ethyl Pyridinium iodide [EPy] as a green media[1]. The substance was analyzed using Thin Layer Chromatography (TLC), Nuclear Magnetic Resonance (NMR) spectroscopy, and Density Functional Theory (DFT) calculations. The synthesis of 1-(benzothiazole-2-yl)-3-phenylthiourea involves a stepwise reaction between 2-amino benzo thiazole and phenyl isothiocyanate in Ethyl Pyridinium iodide [EPy] as a green solvent (Scheme 1). The best yielding was obtained at 40°C for 12 hours.

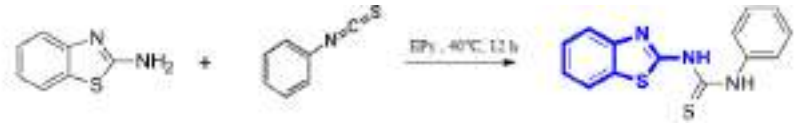

Scheme 1: Reaction of 2-amino benzothiazole with phenyl isothiocyanate

The synthesized compound's energetics, geometry, and electronic structure are explored through DFT calculations at the B3LYP/6-31G(d,p) level of theory. Chemical shielding calculations were performed using the GIAO method at B3LYP/6-31G(d,p) level of theory. Theoretical NMR spectra were obtained and compared with experimental NMR. The results showed that the experimental NMR spectrum is in good agreement with the theoretical data.

References

[~~(~~1~~)~~] Banerjee, S.; Payra, S.; Saha, A. A review on synthesis of benzothiazole derivatives. Curr. Organocatalysis **2017**, *4* (3), 164-181.

A molecular dynamics (MD) study on the ether functionalized COF42 as temperature-sensitive drug delivery system for taxol anti-cancer drug

Sara Mobashsher Aghdam[a], Rahim Ghadari[b*]

a) Organic Chemistry Laboratory, Faculty of Chemistry, University of Tabriz, Iran, sara.lost98.bts77@gmail.com
b) Department of Organic and Biochemistry, Faculty of Chemistry, University of Tabriz, 5166616471 Tabriz, Iran, r-ghadari@tabrizu.ac.ir

Keywords: covalent organic frameworks, drug delivery, molecular dynamics, anti-cancer

The covalent organic frameworks (COFs) are very useful materials in nanotechnology, research and other industries due to their inherent porosity and high-level porosity, biocompatibility, high sustainability, multidimensional structure, post-synthesis and other benefits. In such a way, the applications of COFs continue from gas storage and separation to smart drug delivery and are increasing day by day [1]. In this work, a molecular dynamics (MD) study of a temperature-sensitive smart drug delivery system based on the two-dimensional COF42 functionalized with ether groups, as a carrier of the anticancer drug taxol, was performed. MD simulations were performed at 298.15, 310.15, 315.15, and 323.15 K, and it was shown that the binding energy changes with the change of temperature. Also, among the intermolecular interactions, van der Waals (vdw) interactions contributed the most, and electrostatic interactions and hydrogen bonding had a small share in binding energy, which makes this framework suitable for smart drug delivery [2].

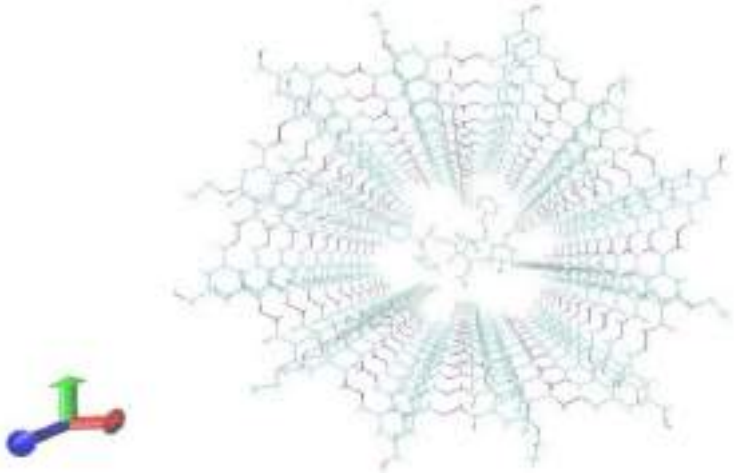

Scheme 1: 10 layers of ether functionalized COF42 with drug.

References:

[1] Wu MX, Yang YW. Applications of covalent organic frameworks (COFs): From gas storage and separation to drug delivery. *Synlett* 2017 Jun 1;28(6):1135-43.
[2] Ghadari R, Ghanbari S, Mohammadzadeh Y. A computational study on the interactions between a layered imine-based COF structure and selected anticancer drugs. *Synlett* 2021 Feb;27:1-0.

Synthesis and characterization of palladium nanoparticles decorated in Crown ether/MCM-41 mesoporous as heterogeneous and recyclability catalyst

Somayeh Shariatzadeh-Kyasari, **Nader Noroozi-Pesyan***

Department of Organic, Inorganic Chemistry- Urmia University,Urmia, Iran, somyshari2@gmail.com

Keywords: PdNPs, Cross coupling reaction, MCM-41

In this thesis, palladium intermediate metal complex was synthesized based on silicate nanocavity mcm_41, which was used as efficient and reusable nanocatalysts in carbon-carbon, carbon-nitrogen and carbon-oxygen coupling reactions. Short reaction time, better yield of products, separation of the path of catalysts due to their heterogeneous characteristics and the use of green solvent are some of the advantages of this method. Then, the nature and construction of the catalyst using Fourier transform (FT-IR), energy diffraction measurement (EDX), inductively coupled plasma emission spectrometer (ICP-OES), transmission electron microscopy image (TEM), microscope image - Scanning Electron (SEM), X-Ray Diffraction (XRD) and Porosimetry measurement of absorption and desorption (BET) were investigated.

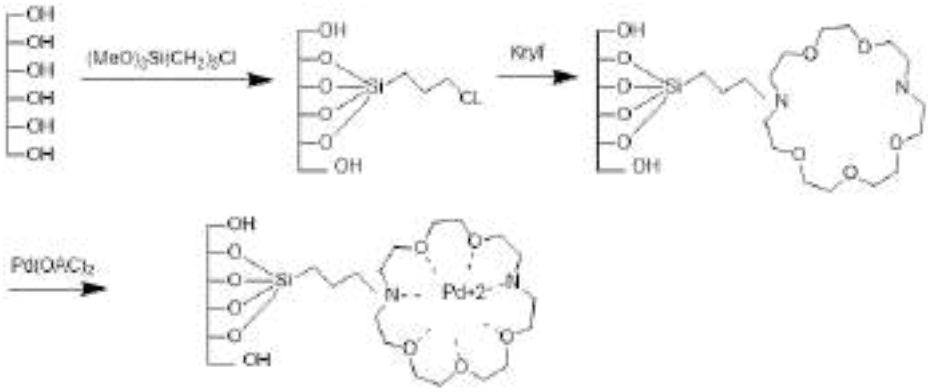

Scheme: Attaching palladium metal to MCM-41-Sp-Kryf-pd

References:

[1] Song, J., Shen, Q., Xu, F., & Lu, X. Cationic Pd (II)-catalyzed enantioselective cyclization of aroylmethyl 2-alkynoates initiated by carbopalladation of alkynes with arylboronic acids. *Org. Lett.*, (2007). *9*(15), 2947-2950.

[2] Batmani, H., Noroozi Pesyan, N., & Havasi, F, Synthesis and characterization of MCM-41-Biurea-Pd as a heterogeneous nanocatalyst and using its catalytic efficacy in C–C, C–N and C–O coupling reactions. *Appl. Organomet. Chem.* (2018), *32(8)*, e4419.

Green Synthesis of 1-(4,6-dimethylpyrimidin-2-yl)-3-phenylthiourea and Comparison of its experimental and theoretical NMR spectra

Masoumeh Jafari*, Leila Hajiaghababaei, Jamshid Najafpour, Ashraf Sadat Shahvelayati

Department of Chemistry, Yadegar-e-Imam Khomeini (RAH) Shahre Rey Branch, Islamic Azad University, Tehran, Iran, masomeh.jafari2020@gmail.com

Keywords: Green Synthesis, 1-(4,6-dimethylpyrimidin-2-yl)-3-phenylthiourea, Density Functional Theory, Ionic Liquid

In this study, to preparation of 1-(4,6-dimethylpyrimidin-2-yl)-3-phenylthiourea, phenyl isothiocyanate was added to 2-amino-4,6-dimethyl pyrimidine in the presence of ionic liquid of ethyl pyridinium iodide [EPy]I as a green solvent. The reaction was carried out at temperature 40-50℃ for 12 hours with good yield [1]. Thin layer chromatography was used to product confirmation. The structure was verified via Nuclear Magnetic Resonance (NMR).

Fig. 1: 1-(4,6-dimethylpyrimidin-2-yl)-3-phenylthiourea

Theoretical studies were done on synthesized compound. The geometry of the conformers has been optimized (Fig. 1). Calculations were done by Density Functional Theory with B3LYP method and 6-31G (d, p) basis set in the vacuum and in the chloroform. ^{1}H chemical isotropic shielding of compounds was calculated by Gauge Including Atomic Orbitals method at B3LYP/6-31G (d, p) levels of theory. Calculated theoretical ^{1}H chemical shift values in terms of ppm for N-H_6, N-H_{10}, C-H_{19}, C-H_{21}, C-H_{30} were 7.7, 13.3, 9.3, 7.1, 7.5 respectively, and also the experimental values in terms of ppm for N-H_6, N-H_{10}, C-H_{19}, C-H_{21}, C-H_{30} were 7.7, 13.2, 9.2, 7.2, 7.7 respectively. The obtained results showed that the experimental NMR results are is good agreement with the theoretical ^{1}H chemical shifts.

References

[1] Tolba, M.; Dean, A.; Ahmed, M.; Hassanien, R.; Saved, M.; Zaki, R.; Mohamed, S. Synthesis, reactions, and applications of pyrimidine derivatives. *Curr. Chem. Lett.* **2022**, *11(1)*, 121-138.

Intermolecular addition of alkenes to aldehydes in visible-light photoredox-catalyzed radical condensation

Ali Akbari*, Muhammad Saleh Faryabi

Organic Chemistry Laboratory, Faculty of Chemistry, University of Jiroft, Jiroft, P.O. Box 8767161167, Iran, a.akbari@ujiroft.ac.ir, ms.faryabi@ujiroft.ac.ir

Keywords: Benzyl alcohols, Visible-light, Photoredox-catalyzed

Alkenes are the core structure of building blocks in natural products and have found wide applications in chemical synthesis and material science [1-2]. Hence, the development of efficient methods for the functionalization of alkenes has become an important and well-studied research topic in organic synthesis. In particular, radical-mediated functionalization of alkenes has emerged as a protocol to increase molecule complexity with atom-economic efficiency, and excellent functional group tolerance [3].

we report here a new method for the addition of alkenes to aldehydes in visible-light photoredox-catalyzed in intermolecular carbon radical addition to afford benzyl alcohol derivatives (**Scheme**).

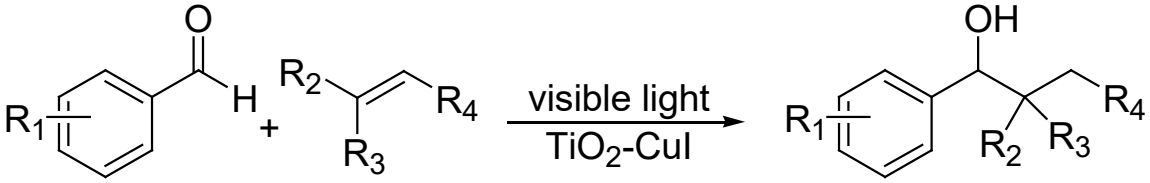

Scheme: Proposed synthetic routes of benzyl alcohol derivatives.

References

[1]. Calmanti, R.; Selva, M.; Perosa, A., Tandem catalysis: one-pot synthesis of cyclic organic carbonates from olefins and carbon dioxide. *Green Chem.* **2021,** *23* (5), 1921-1941.

[2]. Zhao, T.; Long, G.; Liang, H.; Xiong, W.; Hu, X., One-pot synthesis of cyclic carbonates from olefins and CO2 catalyzed by silica-supported imidazolium hydrogen carbonate ionic liquids. *Microporous Mesoporous Mater.* **2023,** *356*, 112576.

[3]. Liu, Y.-L.; Ouyang, Y.-J.; Zheng, H.; Liu, H.; Wei, W.-T., Recent advances in acyl radical enabled reactions between aldehydes and alkenes. *Chem. Comm.* **2021,** *57* (50), 6111-6120.

A new method for the synthesis of 2*H*-Indazoles

Ali Akbari*, Muhammad Saleh Faryabi

Organic Chemistry Laboratory, Faculty of Chemistry, University of Jiroft, Jiroft, P.O. Box 8767161167, Iran, a.akbari@ujiroft.ac.ir, ms.faryabi@ujiroft.ac.ir

Keywords: Indazoles, Visible-light, photoredox-catalyzed

Indazoles, the introductory class of nitrogen-containing heterocycles, are the core structure of building blocks in natural products. 2*H*-Indazoles of this class have shown a broad area of biological activity, such as anticancer agents [1-2], and anti-inflammatory activities [3].

we report here a new method for the preparation of 2-phenyl-2*H*-indazole derivatives by condensation of substituted o-bromobenzaldehyde with aniline derivatives and photocatalytic in the presented sodium azide in visible-light photoredox-catalyzed nitrogen radical cyclization (**Scheme**).

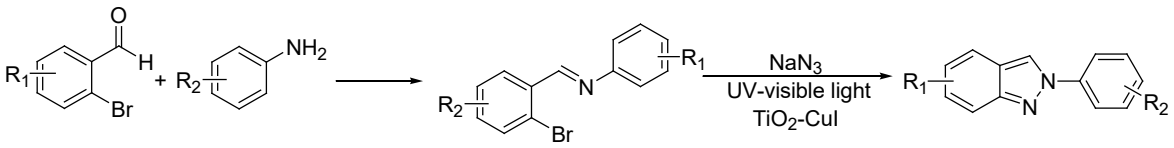

Scheme: Proposed synthetic routes of 2-phenyl-2*H*-indazole derivatives.

References

[1]. Liu, J.; Qian, C.; Zhu, Y.; Cai, J.; He, Y.; Li, J.; Wang, T.; Zhu, H.; Li, Z.; Li, W., Design, synthesis and evaluate of novel dual FGFR1 and HDAC inhibitors bearing an indazole scaffold. *Bioorg. Med. Chem.* **2018,** *26* (3), 747-757.

[2]. Puri, S.; Sawant, S.; Juvale, K., A comprehensive review on the indazole based derivatives as targeted anticancer agents. *J. Mol. Struct.* **2023,** *1284,* 135327.

[3]. Pérez-Villanueva, J.; Yépez-Mulia, L.; González-Sánchez, I.; Palacios-Espinosa, J. F.; Soria-Arteche, O.; Sainz-Espunes, T. d. R.; Cerbón, M. A.; Rodríguez-Villar, K.; Rodríguez-Vicente, A. K.; Cortés-Gines, M., Synthesis and biological evaluation of 2 H-indazole derivatives: Towards antimicrobial and anti-inflammatory dual agents. *Molecules* **2017,** *22* (11), 1864.

Synthesis of treacetin by glycerol acetylation using acidic catalyst and ethyl acetate as an entrainer

Zohreh Mortezaei [a,b*], **Azam Sadeghi** [b]

a) Department of Chemistry, Faculty of Science, Arak University, Arak 38156-8-8349, Iran, zeo.sercher@yahoo.com

b) Department of Research and Development, Hallal Pouyan Co., Arak, Iran

Keywords: Hydroxyl group, Ethyl acetate, Esterification, Triacetin

Glycerol is a triol and up to its three hydroxyl groups can be functionalized [1]. Triacetin is a triglyceride obtained by acetylation of the three hydroxyl groups of glycerol. Esterification of glycerol with acetic acid in the presence of ethyl acetate as an entrainer was performed over p-toluene sulfonic acid (PTSA) as acidic catalyst in a batch reactor (**Scheme**). Ethyl acetate continuously removed the reaction water; thus, the chemical equilibrium was effectively shifted; the selectivity for the most desired product triacetin was dramatically increased [2]. The influence of reaction conditions such as reaction time, acetic acid: glycerol molar ratio and catalyst amount were investigated. The results showed that the more than 99% selectivity to triacetin at complete glycerol conversion was obtained.

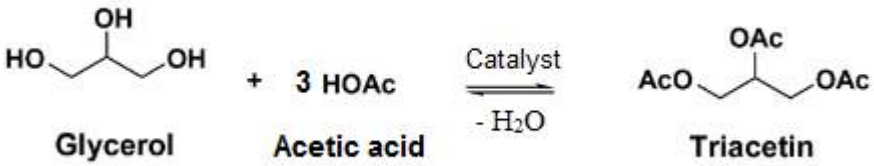

Scheme: Reaction scheme of glycerol acetylation.

References

[1] Valter L.C. Gonc¸alves, Bianca P. Pinto, Joao C. Silva, Claudio J.A. Mota. Acetylation of glycerol catalyzed by different solid acids. *Catal. Today* 2008, *133–135*, 673–677.

[2] S. Kale, S.B. Umbarkar, M.K. Dongare, R. Eckelt, U. Armbruster, A. Martin. Selective formation of triacetin by glycerol acetylation using acidic ion-exchange resins as catalyst and toluene as an entrainer. *Appl. Catal. A: Gen.* 2015, *490*, 10–16.

Surface Functionalization of SBA-15 with 2-Chloroquinoline-3-carbaldehyde and Arylamines for Enhanced Sensor Performance

Ala Arvish and Ghodsi Mohammadi Ziarani*

Department of Organic Chemistry, Faculty of Chemistry, Alzahra University, Tehran, Iran, ala.arvish3505@gmail.com, gmohammadi@alzahra.ac.ir

Keywords: Chemosensors, SBA-15, 2-Chloroquinoline-3-carbaldehyde, amine

Nanosilica supports, like SBA-15, are very important in nanochemistry due to their availability, easy surface modification, and favorable properties such as porosity, high thermal and mechanical stability, low toxicity, and biocompatibility. They have valuable applications as chemosensors, catalysis, and in drug delivery. In recent years, there has been a growing interest in chemical sensors capable of detecting environmentally important ions. SBA-15, a two-dimensional hexagonal mesoporous silica, offers a valuable substrate for modification with various organic chelating groups such as aldehydes and amines. SBA-Pr-Cl can be reacted with 2-Chloroquinoline-3-carbaldehyde to provide SBA-Pr-CQC, followed by the reaction with aryl amine compound to synthesis SBA-Pr-CQC-Arylamine, which can be used as efficient chemosensor.

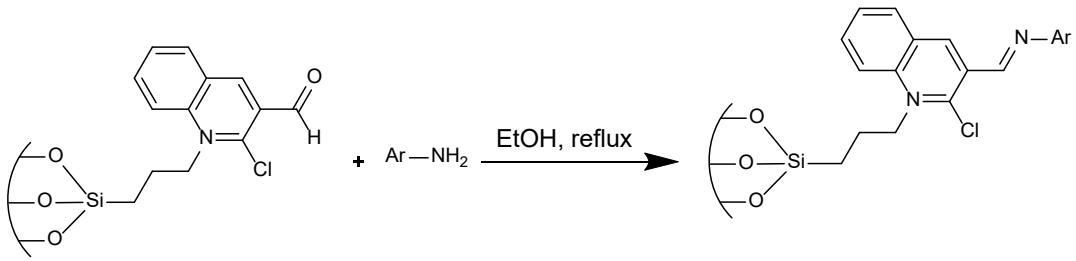

Scheme 1: The synthesis of SBA-Pr-CQC-Arylamine

References

[1] Lashgari, N.; Badiei, A.; Mohammadi Ziarani, G., Modification of mesoporous silica SBA-15 with different organic molecules to gain chemical sensors: a review. *J. Nanochem. Res.* 2016, 1 (1), 127-141.

[2] Wang, X.; Lin, K. S. K.; Chan, J. C. C.; Cheng, S., Preparation of ordered large pore SBA-15 silica functionalized with aminopropyl groups through one-pot synthesis. *Chem. Comm.* 2004, (23), 2762-2763.

Synthesis, characterization and adsorption study of dyes on melamine-formaldehyde microspheres

Mina Mohammadi, Fahimeh Farshi Azhar and Massoumeh Bagheri*

Department of Chemistry, Faculty of Science, Azarbaijan Shahid Madani University, Tabriz, Iran, mohamadimina877@gmail.com, massoumehbagheri@yahoo.com.

Keywords: Melamine-formaldehyde resin, Microspheres, Dyes, Adsorption

Water pollution caused by colours from diverse industries such as textiles, leather, paper, medications, beauty products, printing, and dye production has become a global issue that has harmed both human and aquatic life [1]. Porous polymer, especially resin microsphere, has gained heightened attention as the adsorption material for their characteristics of high dispersibility in solvents and large surface area of network [2, 3]. Melamine-formaldehyde (MF) resin microspheres were synthesized from melamine and formaldehyde solution via dispersion polymerization method. The chemical structure, thermal properties and the surface morphology of adsorbent were investigated by Fourier transform infrared (FT-IR), X-ray diffraction (XRD), scanning electron microscopy (SEM) and energy dispersive X-ray spectroscopy (EDS). Furthermore, the effects of initial pH value and ionic strength in dye solution, contact time and initial concentration of dyes on the adsorption capacities of dyes on the adsorbent have been also investigated. In addition, the adsorption isotherm and kinetics were also studied to evaluate the behavior of the adsorbent. The prepared adsorbent exhibited excellent elution effect and recovery efficiency in five cycles.

References

[1] Selvakumar, T.; Rajaram, M.; Natarajan, A.; Harikrishnan, L.; Alwar, K.; and Rajaram, A. Highly Efficient Sulfur and Nitrogen Codoped Graphene Quantum Dots as a Metal-Free Green Photocatalyst for Photocatalysis and Fluorescent Ink Applications. *ACS Omega* 2022, 7, 12825-12834.

[2] Chen, J.; Jiang, M.; Han, J.; Liu, K.; Liu, M.; and, Wu, Q. Syntheses of magnetic GO @ melamine formaldehyde resin for dyes adsorption. *Mater. Res. Express* 2019, 6, 086103.

[3] Liang Ma, C.; Ran Wang, Z.; Hui Hu, Z.; Wang, Y.; Zhao, Y.; and, Jing Shi. Preparation of submicron monodisperse melamine resin microspheres and nitrogen-doped carbon microspheres derived from them. *New Carbon Mater.*, 2020, 35(3): 269-285.

Facile fabrication of Fe_2O_3@SiO_2/CuO-MoO_3 nanocomposite for degradation of methylene blue

Somaye Badri, Nader Noroozi Pesyan*, and Hassan Alamgholiloo

Department of Organic Chemistry, Faculty of Chemistry, Urmia University 57159, Urmia, Iran, somayebadri7676@gmail.com.

Keywords: Degradation, Fe_2O_3@SiO_2/CuO-MoO_3, Metal oxide-based material, Methylene blue,

Designing metal oxide-based materials as a highly efficient catalyst is essential in environmental remediation. Herein, a new type of Fe_2O_3@SiO_2/CuO-MoO_3 nanocomposite was synthesized and employed as an efficient and reusable nanostructure for methylene blue degradation. The nature and structure of the catalyst were investigated using Fourier Transform Infrared Spectroscopy (FT-IR), Transmission Electron Microscopy (TEM), Scanning Electron Microscopy (SEM), X-ray Diffraction (XRD), Vibrating Sample Magnetometry (VSM), and Diffuse Reflectance Spectroscopy (DRS). The short reaction time, easy separation of the catalyst due to its magnetic property using a magnet, and contribution to environmental preservation and health are the advantages of this approach. The current study provides new insight to develop metal oxide-based materials for improvement in water treatment and remediation.

References:

[1] Hassanloie, N., Noroozi Pesyan, N., Sheykhaghaei, G., Aalinejad, M., Ojaghi Aghbash, K., & Alamgholiloo, H. Preparation of Fe3O4@ SiO2@ Cu-MoO3 core–shell nanostructures: synergistics effects of copper and molybdenum for catalytic enhancement. *J. Porous Mater.* 2023, 30(3), 859-869.

[2] Liu, J., Liu, J., Zhao, Z., Tan, J., Wei, Y., & Song, W. Fe/Beta@ SBA-15 core-shell catalyst: Interface stable effect and propene poisoning resistance for no abatement. *AIChE J.* 2018, 64(11), 3967-3978.

Design of the MMT-BAC@ Fe_3O_4@CuNi as highly efficient nanocatalyst for the synthesis of pyrimidines

Hossein Eshghi *, **Fatemeh Pirani**

Department of Chemistry, Faculty of Science, Ferdowsi University of Mashhad, Mashhad 91775-1436, Iran, heshghi@um.ac.ir, f.pirani7040@gmail.com

Keywords: Heterogeneous nanocatalyst, Nanoclay, Solvent-free conditions, Pyrimidine derivatives

In this project, we have successfully designed a new Cu-Ni alloys nanoparticles immobilized in magnetic organo-modified clay (MMT-BAC@ Fe_3O_4@CuNi) nanocatalyst for the first time through a simple method. Clay minerals have prominent, different, and interesting features. Due to their high selectivity, compatibility with the environment, low cost and low toxicity, and high surface area, they are considered very effective catalysts for a wide range of organic reactions [1]. The structure of the synthesized catalyst was confirmed by EDX, XRD, TEM, IR, SEM, and ICP techniques. The Heterogeneous nanocatalyst was used in the synthesis of pyrimidines, as highly active pharmaceutical compounds in mild condition [2]. The salient features of this protocol include short reaction time, good to excellent product yield, biocompatible conditions, reusable catalyst, low catalyst loading, wide substrate scope, solvent-free conditions and easy workup conditions (**Scheme**).

Scheme: Nanoclay as an eco-friendly and reusable catalyst for green synthesis of pyrimidines

References

[1] Eftekhari far, B.; Nasr-Esfahani, M. Synthesis, characterization and application of Fe_3O_4@ SiO_2@ CPTMO@ DEA-SO_3H nanoparticles supported on bentonite nanoclay as a magnetic catalyst for the synthesis of 1, 4-dihydropyrano [2, 3-c] pyrazoles. *Appl. Organomet. Chem.* 2020**,** *34*, e5406.

[2] Nasab, N. H.; Raza, H.; Hassan, M.; Kloczkowski, A.; Kim, S. J. A facile green synthesis of 3, 4-dihydropyrimidin-2 (1*H*)-ones using cysteine as a bio-organic catalyst: Potent urease inhibitors, in vitro evaluation, kinetic mechanism, and molecular docking studies. *J. Mol. Struct.* 2023**,** *1286*, 135638.

Visible-Light-Mediated Synthesis of Substituted pyrroles Using Eosin Y as a Photoredox Catalyst

Akbar Heydari [a*], Masoumeh Jadidi Nejad [b]

a) Organic Chemistry Laboratory, Faculty of Chemistry, Tarbiat Modares University, Tehran, Iran, heydar_a@modares.ac.ir.
b) Department of Chemistry, Tarbiat Modares University, Tehran, Iran, mjadidi72m@gmail.com

Keywords: Photocatalyst, Eosin Y, Pyrrole

Several strategies are available for the synthesis of pyrrole derivatives. However, these synthetic methods have problems such as the need for metal catalysts and expensive substrates, in addition, mostly the reactions are carried out under harsh conditions and in long periods of time with low efficiency. According to the mentioned challenges, most of the scientists are looking for easy, efficient and environmentally safe methods that enhance the probability of performing organic reactions under effective conditions. This study offers a method for utilizing Eosin Y, a non-metallic organic dye, in the photochemical synthesis of pyrrole derivatives at room temperature under visible light. This is a straightforward, highly effective, and one-pot process for synthesis of substituted pyrroles.

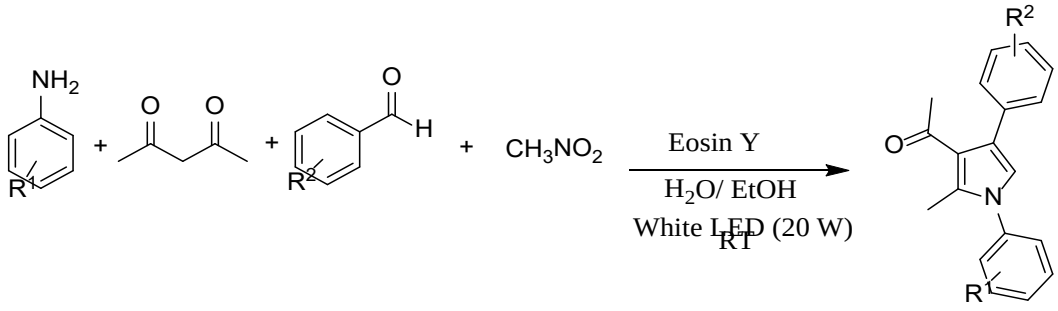

Scheme: Multicomponent reaction of pyrrole synthesis under light conditions.

References:

[1] B. Das, G. C. Reddy, P. Balasubramanyam, and B. Veeranjaneyulu, An efficient new method for the synthesis of polysubstituted pyrroles, *Synthesis*, 2010, 1625-1628.

[2] H. K. Singh, A. Kamal, S. Kumari, D. Kumar, S. K. Maury, V. Srivastava, and S. Singh, Eosin Y-catalyzed synthesis of 3-aminoimidazo [1, 2-a] pyridines via the HAT process under visible light through formation of the C–N bond, *ACS Omega,* 2020, 5, 29854-29863.

[3] A. K. Sahoo, A. Rakshit, A. Dahiya, A. Pan, and B. K. Patel, Visible-Light-Mediated Synthesis of Thio-Functionalized Pyrroles, *Org. Lett*, 2022, 24, 1918-1923.

Synthesis of new 1,4-disubstituted 1,2,3- triazole based perfluoropyridine derivatives

Fereshteh Khorasani, Reza Ranjbar-Karimi*

Department of Chemistry, Faculty of Science, University of Vali-e-Asr Rafsanjan, Kerman, Iran, fr.khorassani@gmail.com, r.ranjbarkarimi@vru.ac.ir

Keywords: 1,2,3-Triazole, Pentafluoropyridine, Click chemistry

1,2,3-Triazoles, as important heterocycles, play a significant role in the field of pharmaceuticals and agrochemicals. These compounds possess a diverse range of biological activities, including antibacterial, herbicidal, fungicidal, antiallergic, and anti-HIV properties [1,2]. New fluorinated containing 1,2,3-triazole units were prepared in three steps. First, the nucleophilic attack of *N*-methylpipirazine under mildly basic conditions took place solely at the C–4 position of PFP and the corresponding 1-methyl-4-(2,3,5,6-tetrafluoro-pyridine-4-yl)-piperazine were obtained in nearly quantitative yields. Upon treatment of 1-methyl-4-(2,3,5,6-tetrafluoro-pyridine-4-yl)-piperazine with sodium azide afforded new product. Finally, the 1,2,3-triazole based fluorinated were synthesis by click chemistry (**Scheme 1**). All the compounds were characterized using ^{1}H, ^{13}C and ^{19}F-NMR spectroscopies.

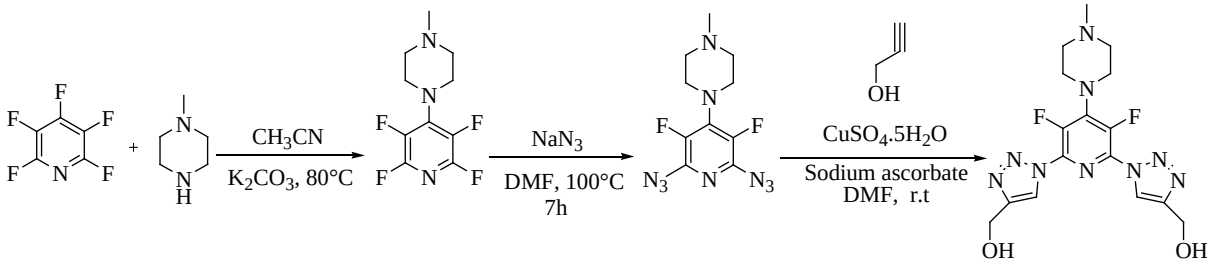

Scheme 1: Synthesis of new fluorinated 1,2,3-triazole.

References

[1] Zambri, M.T.; Hou, T.R.; Taylor, M.S. Synergistic Organoboron/Palladium Catalysis for Regioselective N-Allylations of Azoles with Allylic Alcohols. *Org. Lett.* 2022. *24*, 7617-7621.

[2] Lebeau, A.; Abrioux, C.; Bénimèlis, D.; Benfodda, Z., Meffre, P. Synthesis of 1, 4-disubstituted 1, 2, 3-triazole derivatives using click chemistry and their Src kinase activities. *Med. Chem.* 2017, *13*, 40-48.

Synthesis of benzimidazoles in the presence of nano cellulose supported Titanium tetrachloride in different conditions

Shima Shabani, Abdolhamid Bamoniri *, Javad Safaei-Ghomi

Department of Organic Chemistry, Faculty of Chemistry, University of Kashan, Kashan, I. R. Iran, shimshabani97@gmail.com, bamoniri@kashanu.ac.ir

Keywords: Benzimidazoles, Orthophenylenediamine, Nano cellulose, Titanium tetra chloride

Nowadays, a lot of research is done in the field of cyclic compounds. Benzimidazoles are widely used cyclic compounds that have properties such as anti-cancer, anti-allergic, anti-malarial, anti-hypertensive, anti-AIDS and etc. [1]. Because of the widespread use of benzaimidazoles, chemists turned their attention to efficient methods for their synthesis. Also, the design of nanoscale materials is of great importance due to its application in various fields [2]. In this research, a solid acid catalyst with a natural substrate was prepared from the reaction of titanium tetrachloride with cellulose nanoparticles. The structure of nano catalyst was investigated using imaging, spectroscopy and pattern recognition methods such as: BET, EDX(EDS), FESEM, TEM, TGA, XRD and FT-IR. In this research, aromatic diamines and aldehydes were used in the presence of titanium tetrachloride stabilized on nano cellulose as catalyst for the synthesis of benzimidazole derivatives under different conditions (**Scheme1**). The structure of products was investigated with the help of FT-IR and ^{1}H NMR spectroscopy.

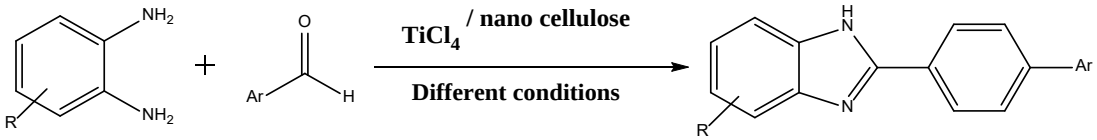

R = H / 4-Methyl / 4-Nitro

Scheme1. Synthesis of benzimidazoles

References

[1] Bodaghifard, M. A. Shafi, S. Ionic liquid-immobilized hybrid nanomaterial: an efficient catalyst in the synthesis of benzimidazoles and benzothiazoles via anomeric-based oxidation. *J. Iranian Chem. Soc*., **2021**, *18*, 677-687.

[2] Kumaraswamy, G., Sadanandam, G., Ledwaba, K., Maroju, R., An efficient photocatalytic synthesis of benzimidazole over cobalt-loaded TiO_2 catalysts under solar light irradiation. *J . Photochem. Photobiol. A: Chem.*, **2022**, *429*, 113888-113890.

Design and synthesis of covalent organic framework based on quinoline-4-carboxylic acid as a new catalyst in the preparation of α-aminobenzyl-4-hydroxycoumarin

Zahra Alishahi, Meysam Yarie, Morteza Torabi, Mohammad Ali Zolfigol*

Department of Organic Chemistry, Faculty of Chemistry, Bu-Ali Sina University, Hamedan 6517838683, Iran, zahraalishahi1999@gmail.com, myarie.5266@gmail.com, zolfi@basu.ac.ir

Keywords: Catalyst, COFs, α-Aminobenzyl 4-hydroxycoumarin, Multi-component reaction

Covalent organic frameworks (COFs) as a new class of porous organic materials, are assembled from organic monomers interconnected by covalent bonds. In the last decades, due to various applications of COFs such as energy storage, gas adsorption, drug delivery as well as catalytic processed, these materials great more attention. Distinguishingly, compositional characteristics of these materials such as ordered pore size, metal-free backbone, good thermal/chemical stability, low density, vast surface area and easy modification makes them as a highly promising paradigm [1-2]. In recent years, much attention has been directed towards the synthesis of 3-benzyl-substituted 4-hydroxycoumarins, particularly α-aminobenzyl-4-hydroxycoumarin derivatives owing to their tremendous application in various research fields such as biological science and medicinal chemistry [3]. In this research, the catalytic application of QC-COF@Nb_2O_5 was investigated in the synthesis of *α*-aminobenzyl-4-hydroxycoumarins (**Scheme 1**).

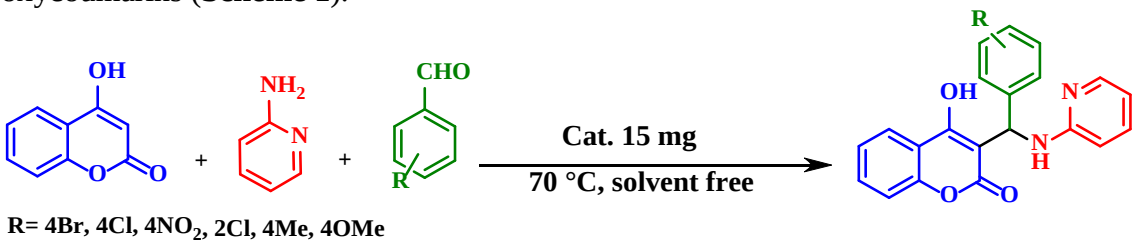

R= 4Br, 4Cl, 4NO_2, 2Cl, 4Me, 4OMe

Scheme1: Synthesis of *α*-aminobenzyl 4-hydroxycoumarin using QC-COF@Nb_2O_5

References

[1] Dong, Z.; Pan, H.; Gao, P.; Xiao, Y.; Fan, L.; Chen, J.; Wang, W. Palladium Immobilized on a Polyimide Covalent Organic Framework: An Efficient and Recyclable Heterogeneous Catalyst for the Suzuki–Miyaura Coupling Reaction and Nitroarene Reduction in Water. *Catal. Lett.* 2022, *152*, 299-306.

[2] Ding, S. Y.; Gao, J.; Wang, Q.; Zhang, Y.; Song, W. G.; Su, C. Y.; Wang, W. Construction of covalent organic framework for catalysis: Pd/COF-LZU1 in Suzuki–Miyaura coupling reaction. *J. Am. Chem. Soc.* 2011, *133*, 19816-19822.

[3] Olyaei, A.; Dortaj, E.; Khoeiniha, R.; Rajabi, F. One-pot Synthesis of Novel 3-(Aryl (heteroarylamino) methyl)-2*H*-chromen-2-one Derivatives. *J. Heterocycl. Chem.*2018, 55, 2971-2976.

Engineering iodine decorated porous organic polymer: A brilliant catalyst for the preparation of 2,4,6-trisubstituted pyridines

Morteza Torabi[a], Mohammad Ali Zolfigol*[a], Narges Zarei[a], Meysam Yarie*[a], Saeid Azizian[b]

a) Department of Organic Chemistry, Faculty of Chemistry, Bu-Ali Sina University, Hamedan, Iran, torabimorteza74@yahoo.com.
b) Department of Physical Chemistry, Faculty of Chemistry, Bu-Ali Sina University, Hamedan, Iran.

Keywords: Heterogeneous catalyst, Porous organic polymer, I_2 capture, 2,4,6-Trisubstituted pyridine.

In the last years, POPs have been converted to the cornerstone of heterogeneous catalysis. First and foremost, due to maintaining their highly ordered structure, POPs have intrinsic catalytic activity and iodine capture potential. Second, their permanent porosity leads to better mass transport and enhances their catalytic performance. catalytic utilities of POPs are including of photocatalytic reactions, coupling reactions, electrocatalytic processes such as water splitting, degradation processes, oxidation/reduction reactions, asymmetric catalysis and multicomponent reactions [1, 2]. Compounds containing pyridine moieties as one of the most inspiring and beneficial families of *N*-heterocycles gained the burgeoning attention of the society of researchers. The plethora of utility of pyridines in natural products, functional materials, pharmaceuticals, coordination chemistry and organic catalysis is undeniable [3]. Herein, we designed and synthesized new iodine decorated porous organic polymer by azo linkers and this was applied as a heterogeneous catalyst for the synthesis of divers 2,4,6-trisubstituted pyridine (**Scheme 1**).

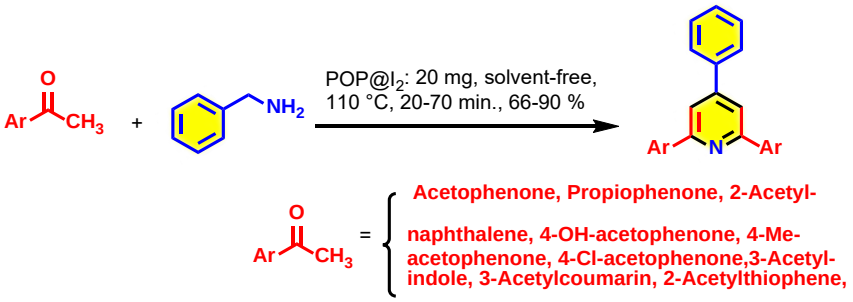

Scheme 1: The catalytic application of POP@I_2 for the preparation of 2,4,6-trisubstituted pyridines.

References

[1] Tian, Y.; Zhu, G.; Porous aromatic frameworks (PAFs). *Chem. Rev.* 2020, *120*, 8934-8986.
[2] Kaur, P.; Hupp, J. T.; Nguyen, S. T.; Porous organic polymers in catalysis: opportunities and challenges. *Acs Catal.* 2011, *1*, 819-835.
[3] Torabi, M.; Yarie, M.; Baghery, S.; Zolfigol, M. A.; Recent advances in catalytic synthesis of pyridine derivatives. Recent developments in the synthesis and applications of pyridines. *Elsevier Inc.* 2023, 503-580.

Synthesis and characterization of new high-energy polymers based on epihalohydrin and investigation of its compatibility with different energy-generating plasticizers

Mohammad Dashteh [a], Yadollah Bayat [*a], and Mohammad Ali Zolfigol [*b]

a) Faculty of Chemistry and Chemical Engineering, Malek Ashtar University of Technology, P.O. Box 16765-3454 Tehran, Iran, mohammaddashteh1994@gmail.com.
b) Department of Organic Chemistry, Faculty of Chemistry, Bu-Ali Sina University, PO Box 6517838683, Hamedan, Iran, zolfi@basu.ac.ir & mzolfigol@yahoo.com

Keywords: High-energy polymers, Binder, Propellants

A binder is a polymeric system that keeps a propellant's components together, and determines the mechanical properties of the propellant and the formulation of the energetic material [1]. Neutral binders have a loading capacity for solids as well as low energy content in the propellant system. An appropriate polymeric binder can improve the mechanical and thermal properties of a propellant, control the propellant's safety when it is exposed to crucial situations, such as variations in temperature, and pressure [2]. The main goal of this report is to discuss the expansion of the polymerization of neutral binders with a flexible polymeric backbone that can improve its mechanical and thermal properties. In the present study, a new high-energy polymer based on epihalohydrin was designed and synthesized. In the design of the catalyst and properties such as glass transition temperature, mechanical properties such as (strength, elongation, modulus, etc.) were examined in the propellant. The method represents a truly green process with good sustainability and economics (**Scheme 1**).

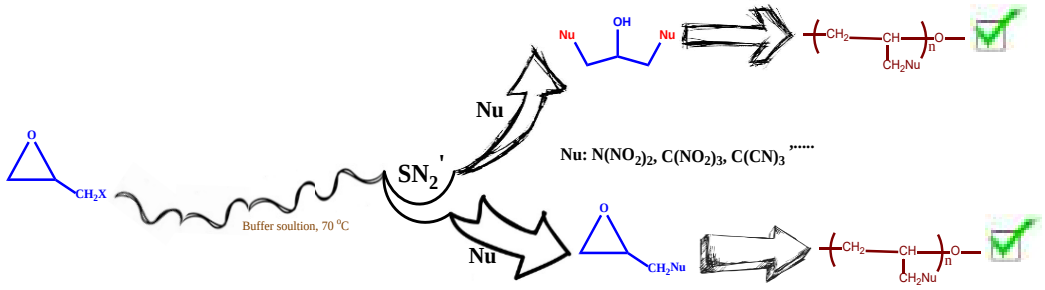

Scheme 1: Copper-catalyzed azide-alkyne cycloaddition (CuAAC) via Zn-MOF@CuO as a catalyst.

References

[1] Vala, M. M., Bayat, Y., and Bayat, M. Synthesis and Thermal Decomposition Kinetics of Epoxy Poly Glycidyl Nitrate as an Energetic Binder. *Def. Sci. J.* **2020**, *70* (4), 110-125.
[2] Ghoroghchian, F., Bayat, Y., and Abrishami, F. Study on the Thermal Stability and Decomposition Kinetics of Polypropylene Glycol–Glycidyl Azide Polymer–Polypropylene Glycol (PPG-GAP-PPG) as a Novel Triblock Copolymer Binder. *Cent. Eur. J. Energ. Mater.* **2020**, *17* (2), 1235-1251.

Reusable magnetized carbon nanotube heterogeneous catalysts for multicomponent reactions

Rahman Karimi-Nami*, Yadegar Rahimi*

Department of Chemistry, Faculty of Science, University of Maragheh, Maragheh, Iran, r.kariminami@gmail.com, yadegarrahimi19966@gmail.com

Keywords: Carbon Nanotubes, Nanocatalyst, Magnatic, Multicomponent reactions.

In this research, initially, modified surface multiwall carbon nanotubes clinoptilolite with Fe_2O_3 were synthesized. Then, genuinely eco-friendly, low-cost magnetic nanocomposite and fast approach for synthesizing diverse chromeno[4,3-b]chromene-6,8-dione derivatives in the presence of synthetic functionalized Fe_2O_3@CNT/COOH as novel heterogeneous and reusable Nanocatalyst was developed [1,2]. This green procedure encompasses multiple advantages, including excellent product yields, simple workup, short reaction times, high catalytic activity, and reusability of the Nanocatalyst. The structure of this synthetic Nanocatalyst is fully characterized with different techniques, including FT-IR, XRD, SEM, EDS, BET, and TGA analyses [3] (**Scheme 1**).

Scheme 1: Synthesis of chromeno[4,3-b]chromene-6,8-dione derivatives in the presence of Fe_2O_3@CNT/COOH catalyst

References

[1] Prasek, J.; Jana D.; Jana C.; Jaromir H.; Ondrej J.; Vojtech A.; Rene K. Methods for carbon nanotubes synthesis. *J. Mater. Chem.* 2011, *21*, 15872-15884.

[2] Bilqees, S.; Saeedi, M.; Mahdavi, M.; Nadri, H.; Homayouni, F.; Amini, M. Synthesis, docking study and neuroprotective effects of some novel pyrano[3,2-c]chromene derivatives bearing morpholine/phenylpiperazine moiety. *Bioorg. Med. Chem.*, 2017, *25*, 3980-3988.

[3] Soni, S. K.; Benedict T.; Vishesh R. K. A Comprehensive Review on CNTs and CNT-Reinforced Composites: Syntheses, Characteristics and Applications. *Mater. Today Commun.* 2020, *25*, 101546.

Treatment methods for skin diseases and acne: A review

Nadia Jafaei*

Faculty of Chemical Engineering, Islamic Azad University, Science and Research Branch, Tehran, Iran, nadiajafaei@gmail.com

Keywords: Skin diseases, Acne, Treatment

Acne is a skin condition that causes blemishes and breakouts, especially on the face, shoulders, back, neck, chest, and arms. It happens when sebum and dead skin clog hair follicles and cause inflammation. Acne is one of the 10 most common diseases in the world and the most common inflammatory skin disease, despite its cosmetic appearance, its effects can be much deeper than the surface of the skin and impose a heavy emotional and psychological burden on patients, which may be much worse than the physical impact. be A change in skin appearance may lead to a change in body image, which in turn leads to anger, fear, shame, anxiety, depression, embarrassment, and bullying and stigma in the peer group. Lack of self-confidence, social isolation, feelings of insecurity and inferiority, limited job opportunities, functional and interpersonal problems at work, and suicidal tendencies have also been reported and attributed to the effects of acne. The severity of acne can range from mild to moderate to severe. An increasing number of young women also suffer from acne, which significantly reduces their quality of life.

The cause of acne is known to be multifactorial. This condition has many reasons, both external and internal, that contribute to its occurrence, including the main causes of hyperkeratosis of hair follicles and excessive production of sebum. Genetic factors also play an important role. It has been shown that about 50% of adult acne patients confirm the presence of the disease in their first-degree relatives.

Acne appears with non-inflammatory and inflammatory pimples on the skin. Most skin lesions appear in areas with the largest number of sebaceous glands. The so-called micro black seeds are created in the fat units of the hair. Then they turn into blackheads (open or closed) which subsequently turn into papules and finally into pustules. This condition may be mild and transient and only have a few blackheads that are easily removed by pressure. They may be mild and not worrisome, or they may be severe, persistent and very disfiguring, in more serious cases often leaving a permanent scar.

References

[1] Strauss J.S., Krowchuk D.P., Leyden J.J., et al. Guidelines of care for acne vulgaris management. *J. Am. Acad. Dermatol.* 2007, 56, 651-663.

[2] Eichenfield LF, Krakowski AC, Piggott C, et al. Evidence-based recommendations for the diagnosis and treatment of pediatric acne. *Pediatrics*, 2013, 131, S163-S186.

[3] Hayashi N, Akamatsu H, Kawashima M. Acne Study Group.Establishment of grading criteria for acne severity. *J. Derma-tol.* 2008, 35, 255-260.

Synthesis of carboxyl-terminated polyester resin for thermoset powder coating

Mina Erfani Ghazian, Gholamhossein Zohuri*, Navid Ramezanian, Yasser Delavar

Department of Chemistry, Faculty of Science, University of Ferdowsi, Mashhad Iran, Mina.Ghazian@gmail.com, zohuri@um.ac.ir

Keywords: Powder coating, Thermoset resins, TGIC-polyester system, Carboxyl-terminated polyester

A saturated carboxyl-terminated polyester resin was synthesized via two-stage process. To prepare the resin, an excess amount of glycol relation to acid was used in the esterification reaction, and a pre-polymer with predominantly hydroxyl groups at the terminal position was attained [1]. Following that, acidifying agent was added to the prepared resin to produce a carboxyl-terminated polyester **(Scheme)**. Based on formulation and acid value of the resin, triglycidyl isocyanurate was chosen as the best curing agent in the formula of the powder coating. Infrared radiation technique was used to characterize the resin structure [2]. The thermal behavior of a triglycidyl isocyanurate/polyester system was evaluated by means of Differential Scanning Calorimetry. The result indicated that the prepared resin in the present work exhibits acceptable performance to be used in the powder coating industry.

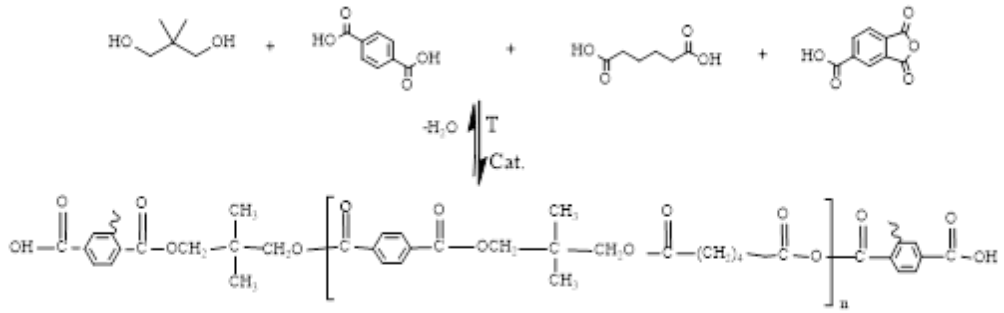

Scheme: Formation of carboxyl-terminated polyester.

References

[1] Xiufang, Y. E.; Jingxuan, L. I. N.; Dongchu, C. H. E. N.; Chang, M; and Hongyang, W. E. I. Design and Synthesis of Crystalline Carboxyl-terminated Polyester Resin. *J. Mater. Sci*. 2021, 27(2), 217-223.

[2] Yong, L.; Liu, L.; Gu, Y.; Xie, J.; Zhang, J. Improve surface levelling of powder coating with semi-crystalline polyester resin. *Prog. Org. Coat*. 2016, 99, 191-193.

Ion-exchanged zeolite Y as a heterogeneous catalyst for synthesis of some derivatives of 9-aryl-hexahydro acridine-1,8-dione

Mohsen Moradian [a,b*], Faeze Namayandeh-Niasar [a]

a) Department of Organic Chemistry, Faculty of Chemistry, University of Kashan, Kashan, Iran, m.moradian@kashanu.ac.ir, faezenamayandeh22@gmail.com
b) Institute of Nanoscience and Nanotechnology, University of Kashan, Kashan, Iran

Keywords: Acridin, Zeolite, Heterogeneous catalyst

The preparation of acridines and their derivatives is a three-component reaction. This reaction is part of an important group of organic reactions. Acridines have anticancer properties [1] as well as being enzyme and tumor cell inhibitors [2]. Zeolites are compounds with a porous structure and large internal cavities that composed of aluminium and silicate. Their origin is both natural and artificial. Extraction of aluminum from sodium zeolite framework Y was done for the first time by Kerr [3].

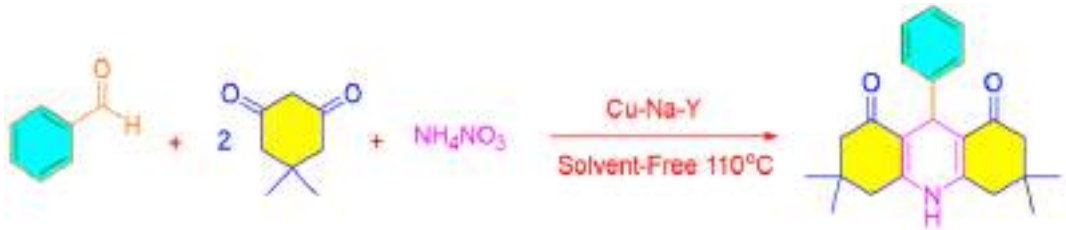

Scheme: Use of copper zeolite in the synthesis of acridines

References

[1] Ramesh, K. B.; Pasha, M.A. Study on one-pot four-component synthesis of 9-aryl-hexahydro-acridine-1, 8-diones using SiO2–I as a new heterogeneous catalyst and their anticancer activity. *Bioorganic Med. Chem. Lett.* 2014, *24(16)*, 3907-3913.
[2] Srividya, N.; Ramamurthy, P.; Shanmugasundaram, P.; Ramakrishnan, V.T. Synthesis, characterization, and electrochemistry of some acridine-1, 8-dione dyes. *J. Org. Chem.* 1996, *61(15)*, 5083-5089.
[3] Kerr, G.T. Chemistry of crystalline aluminosilicates. V. Preparation of aluminum-deficient faujasites. *J. Phys. Chem.* 1968, *72(7)*, 2594-2596.

Application of Novel Magnetic Metal-Organic Frameworks (CuBDC-NH_2) as a Catalyst for C-C Cross-Coupling Reactions

Rahman Karimi-Nami*, Amir Seyyedi Saghezchi

Department of Chemistry Faculty of Science, University of Maragheh, Maragheh, Iran, r.kariminami@gmail.com, seyedi.amir74@gmail.com

Keywords: CuBDC-NH_2 MOF, Nanocatalyst, Magnetic, C-C coupling reactions

C-C coupling reactions represent a fundamental synthetic methodology widely employed in academic and industrial settings. Herein, we present a report on developing and synthesizing a heterogeneous catalyst that is environmentally compatible and has recycling capabilities. Furthermore, the utilization of this catalyst for C-C coupling reactions was explored [1-3]. In this regard, a novel magnetic metal-organic framework (MMOF) consisting of supported 1,10-phenanthroline-2,9-dicarbaldehyde (Fe_3O_4@Cu(BDC)-NH_2-PHD) has been fabricated by post-synthetic modifications of Fe_3O_4@Cu(BDC)-NH_2. Subsequently, the prepared nanocomposites were modified using palladium chloride ions (Fe_3O_4@Cu(BDC)-NH_2-PdPHD) to impart catalytic sites. As a result, the fabricated magnetic porous catalyst exhibited great catalytic activity in the Heck cross-coupling reactions. The structure of this synthetic Nanocatalyst is fully characterized with different techniques, including FT-IR, XRD, SEM, EDS, VSM, and TGA analyses. (**Scheme 1**).

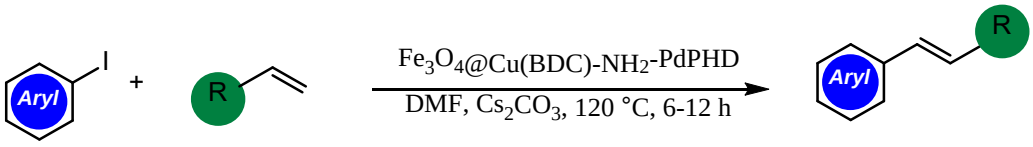

Scheme 1: Synthesis of diphenylethene derivatives in the presence of Fe_3O_4@Cu(BDC)-NH_2-PdPHD catalyst

References

[1] Leng, Y., et al., Generally applicable and efficient oxidative Heck reaction of arylboronic acids with olefins catalyzed by cyclopalladated ferrocenylimine under base-and ligand-free conditions. *Tetrahedron*, 2010. 66(6): p. 1244-1248.

[2] Wang, L., H. Li, and P. Li, Task-specific ionic liquid as a base, ligand, and reaction medium for the palladium-catalyzed Heck reaction. *Tetrahedron*, 2009. 65(1): p. 364-368.

[3] Sobhani, S. et al., Palladium-Schiff base complex immobilized covalently on magnetic nanoparticles as an efficient and recyclable catalyst for Heck and Suzuki cross-coupling reactions. *Catal. Lett.*, 2016. 146(1): p. 255-268.

Magnetically separable nanocatalyst for selective oxidation of sulfides to sulfoxides

Masomeh Balali [a*], **Hassan Keypour** [b]

a) Hamedan University of Technology, Hamedan, Iran, masomeh.balali@yahoo.com.
b) Chemistry Department, Bu-Ali Sina University, Hamedan, Iran.

Keywords: Oxidation of sulfides, Magnetic nanoparticles, Complex of molybdenum

A molybdenum complex, $[MoO_2Cl_2(DMSO)_2]$was immobilized on Schiff base magnetic $Fe_3O_4@SiO_2$ nanoparticles by covalent linkage. First, superparamagnetic Fe_3O_4 nanoparticles were prepared by the coprecipitation method. Secondly, the surface of Fe_3O_4 was encapsulated with silica in order to increase the functionality and stability of nanoparticles. Then, the Fe_3O_4 nanoparticles were surface-modified with 3-aminopropyltriethoxysilane (APTS) which introduced $-NH_2$ on to the surface of support. For preparation of $Fe_3O_4@SiO_2$/Schiff base, $Fe_3O_4@SiO_2$-NH_2 nanoparticles were reacted with dialdehyde and then reacted with the $MoO_2Cl_2(DMSO)_2$ complex to synthesize Mo(VI) nanocatalyst. The resulting nanocatalyst are used as an efficient and recyclable catalyst for the selective oxidation of sulfides to corresponding sulfoxides using urea hydrogen peroxide as the oxidant. Furthermore, the obtained catalysts showed not only high catalytic activity in oxidation reactions but also high degree of chemical stability in various organic solvents.

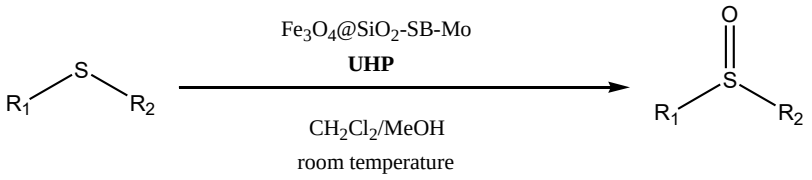

Scheme: Oxidation of sulfides to sulfoxides by nanocatalyst in the presence of UHP oxidant

References

[1] Bagherzadeh, M., Haghdoost, M. M, Shahbazirad, A., Nanoparticle supported, magnetically separable vanadium complex as catalyst for selective oxidation of sulfides *J. Coord. Chem.*, 2012, *65*, 591–601.
[2] Bagherzadeh, M., Haghdoost, M. M, Matlobi-Moghaddam, F., Koushki-Foroushani, B., Sarazdi, S., Payab, E., Mn(III) complex supported on Fe_3O_4 nanoparticles: magnetically separable nanocatalyst for selective oxidation of thiols to disulfides. *J. Coord. Chem.*, 2013, *66*, 3025–3036.

Novel in silico designed inhibitor for BTK enzyme and B-cell lymphoma treatment by natural fragments

Aliasghar Behzadi* **and Alireza Fattahi**

Organic Chemistry Department, Faculty of Chemistry, Sharif university of Technology, Tehran, Iran, aliasghar.behzadi@ch.sharif.edu

Keywords: Computational organic chemistry, Anti-cancer, Bioorganic chemistry, Drug design

Bruton's tyrosine kinase has been one the most challenging enzymes to inhibit and singerly recognized target to prevent B cell lymphoma [1]. In this work we have successfully designed a novel potential inhibitor by using computational methods based on molecular dynamic, Quantum mechanics and molecular mechanics, which bears two significant predominance over previous inhibitors: 1) natural based fragments namely amino acids and Cytosine, inspiring less side effects and more acceptance pharmacokinetically and lower production cost as well, 2) more promising inhibition activity by the outcomes obtained from comparison such as reasonably more negative free energy of binding and physical parameters of protein, including radius of gyration, RMSD and RMSF. Altogether a potential innovative non-covalent inhibitor that is safer, with less complex organic skeleton is presented.

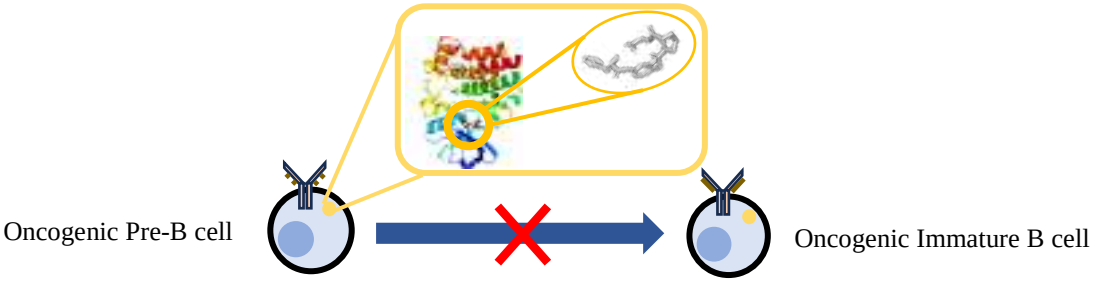

Scheme: Simplified demonstration of the effect of BTK inhibition on transformation of Pre-B cell to immature B cell in order to prevent oncogenic cells from growing.

Reference:

[1] Herman, S.E.M., et al., Bruton tyrosine kinase represents a promising therapeutic target for treatment of chronic lymphocytic leukemia and is effectively targeted by PCI-32765. *Blood*, The Journal of the American Society of Hematology, 2011. **117**(23): p. 6287-6296.

Four-component Synthesis of Pyrimido[4,5-*b*]quinoline Derivatives Using Acidic and Recyclable Magnetic Nanocatalyst Fe_3O_4@THAM-CH_2CH_2-SCH_2CO_2H

Mahla Sheikhveisi[a*], Nourallah Hazeri[a], Mojtaba Lashkari[b], Homayoun Faroughi Niya[a], and Maryam Fatahpour[a]

a) Department of Chemistry, Faculty of Science, University of Sistan and Baluchestan, Zahedan, Iran
b) Faculty of Science, Velayat University, Iranshahr, Iran.

Keywords: Pyrimido[4,5-b]quinoline, Magnetic Nanocatalyst, Fe_3O_4@THAM-CH_2CH_2-SCH_2CO_2H

In continuation of our team's research work in multi-component syntheses [1-2], here we report a four-component reaction using dimedone, aniline, barbituric acid and aldehyde for the synthesis of compounds pyrimido[4,5-b]quinoline. Magnetic nanocatalyst Fe_3O_4@THAM-CH_2CH_2-SCH_2CO_2H has high catalytic activity and can be used several times. Another advantage of this catalyst is easy and convenient separation from the reaction mixture with the help of an external magnet. In this synthesis, the reaction was carried out in solvent-free conditions (**Scheme**).

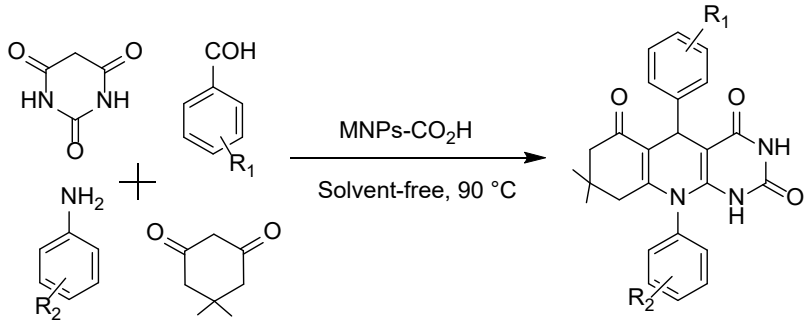

Scheme: Synthesis of pyrimido[4,5-b]quinoline derivatives with MNPs-CO_2H.

References

[1] Rezaie Kahkhaie, M.; Hazeri, N.; Maghsoodlou, M. T.; Yazdani-Elah-Abadi, A. Synthesis and characterization of a novel and reusable Fe_3O_4@ THAM-CH_2CH_2-SCH_2CO_2H magnetic nanocatalyst for highly efficient preparation of xanthenes and 3-aminoisoxazoles in green conditions. *Res. Chem. Intermed.* 2021, *47*, 5007-5025.

[2] Hazeri, N.; Lashkari, M.; Fatahpour, M.; Sheikhveisi, M. DABCO-Catalyzed the Synthesis of Densely Functionalized Cyclohexanones in a Benign Manner. *Bull. Korean. Chem. Soc.* 2020, *41*, 786−792.

Preparation of bio-based polyester resin for hybrid powder coating based on 1,3-propandiol

Mina Erfani Ghazian, Gholamhossein Zohuri*, Navid Ramezanian

Department of Chemistry, Faculty of Science, University of Ferdowsi, Mashhad Iran, Mina.Ghazian@gmail.com, zohuri@um.ac.ir

Keywords: Hybrids, 1,3-propandiol, Powder paint, Carboxyl functional polyester resin, Bio-based resin

A saturated polyester resin was prepared based on 1,3-propanediol. Utilizing bio-based monomers in synthesis of a resin can provide its quality in the structure of the resin. One of the most appropriate alternatives for this target is 1,3-propanediol. Since it has reasonable price and can produce in sufficient amounts via microbial fermentation of glucose from starch [1]. Hybrid powder coating is composed of carboxyl-terminated polyester and epoxy resin of bisphenol-A type as a crosslinker [2]. polyester resin was prepared via melt two-stage polycondensation process **(Scheme)**. To attain a resin with higher functionality than the normal polyester resin in polyester-TGIC systems, a higher molar percentage of polyacid was used [3]. Also, 20 % of neopentyl glycol was replaced with 1,3-propandiol in the preparation of formula. The structure and performance of the polyester resin was characterized using infrared radiation technique, and differential scanning calorimeter. The result indicated that the prepared polyester resin has lower glass transition temperature. Coating from this renewable polyester showed enhanced mechanical resistance like hardness and impact resistance which proves that this resin can be applied in coating industry.

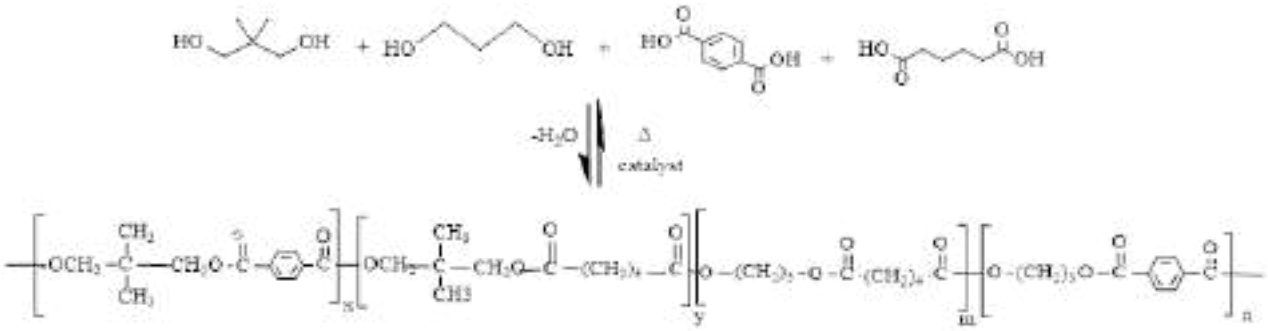

Scheme: Bio-based polyester based on 1,3-propandiol.

References

[1] Kluge, M.; Pérocheau Arnaud, S.; Robert, T. 1,3-Propanediol and its application in bio-based polyesters for resin applications. *Chem. Afr*. 2019, 2, 215-221.

[2] Noordover, B.; van Staalduinen, G.; Duchateau, R.; Koning, C. E.; van Benthem, R.; Mak, M.; Heise, A.; Frissen, A. E.; van Haveren, J. Co -and terpolyesters based on isosorbide and succinic acid for coating applications: synthesis and characterization. *J. Biol. Macromol.* 2006, 7(12), 3406–3416.

A new green synthesis of acridine-1,8-dione derivatives by carboxylated multi-walled carbon nanotubes

Reihaneh Siahkar, Azam Moazeni Bistgani and Leila Moradi*

Department of Organic Chemistry, Faculty of Chemistry, University of Kashan, 87317-51167, Kashan, Iran, siahkarreihaneh@gmail.com, moazeniazam1999@gmail.com, l_moradi@kashanu.ac.ir.

Keywords: Carboxylated multi-walled carbon nanotubes (MWCNTs/CO_2H), Hantzsch reaction, 1,4-Dihydropyridine (DHP), Acridine-1,8-dione derivatives

Acridine-1,8-diones as the most emerging fused 1,4-DHP molecules, have broad applications in the field of bio-organic, pharmaceutical, material, industrial, and synthetic organic chemistry. The presence of N-heteroatom, acridine ring skeleton and wide possibilities of diversified substitution, make it a ubiquitous heterocycle in many areas of life [1,2].

The use of solid acid catalysts simplified the reaction conditions in terms of product, selectivity, reaction time, recycling of the catalyst and isolation of the products. To this regard, the green pseudo-four-component synthesis of the acridine-1,8-dione in the presence of carboxylated multiwalled carbon nanotubes (MWCNTs) is presented. Carbon nanomaterials are one of the goals of green chemical pathways. Particular physical properties such as high oxidation stability, good chemical inertness, high surface area, and unusual electron conductivity, have made carbon nanomaterials as good supports for organic synthesis catalysts. [3]. In this study, the MWCNTs were carboxylated by a new method and used as solid acidic catalyst for the green synthesis of acridine-1,8-dione derivatives through the reaction of dimedone, ammonium acetate and various aldehydes in water (Scheme 1). Short reaction times, clean reaction profiles, and high-yield of products are the advantages of this method.

Scheme 1. synthesis of acridine-1,8-dione derivatives by MWCNTs/CO_2H

References

[1] Sahiba, N.; Sethiya, A.; Soni, J.; Agarwal, S. Acridine-1,8-diones: synthesis and biological applications. *ChemistrySelect* 2021, 6, 2210 –2251.

[2] Kumar Dutta, A.; G, Pinky.; Borah, R.; Synthesis of dibenzoxanthene and acridine derivatives catalyzed by 1,3-disulfonic acid imidazolium carboxylate ionic liquids, *RSC Adv.*, 2014, *4*, 41287-4191.

[3] Saeidiroshan, H.; Morad, L.; Multiwalled carbon nanotubes/guanidine/Ni (II): A new and effective organometallic catalyst for the green synthesis of pyrazolopyranopyrimidines. *Appl. Organomet. Chem.*, 2021, *35*, e6142.

5-Amino tetrazoles based Mn-complex as a reusable nanocatalyst for the synthesis of tetrahydrobenzopyrans

Hosein Khodakarami, Davood Habibi*, Maryam Mahmoudiani Gilani

Department of Organic Chemistry, Faculty of Chemistry, Bu-Ali Sina University, Hamedan, Iran, hossien.khodakarami@gmail.com

Keywords Magnetic nanocatalyst, $Mn(OAc)_2$, Multicomponent reactions, Tetrahydrobenzopyran.

Catalyst is one of the most important principles of green chemistry which is widely used these days in chemical processes. On the other hand, chemists are always looking to design and fabricate catalysts that can be easily separated from the reaction mixture in addition to their high activity, in other words, the two most important features of a suitable catalyst are catalyst separation and catalyst activity [1-3]. All of these problems can be overcome by using magnetic nanocatalysts or changing the surface of magnetic nanoparticles and stabilizing catalyst species on magnetic substrates.

Mn catalyst was used as a reusable catalyst for the green synthesis of tetrahydrobenzopyrans from the three-component condensation reaction of aryl aldehydes, dimedone, and malononitrile in refluxing ethanol. (Scheme 1).

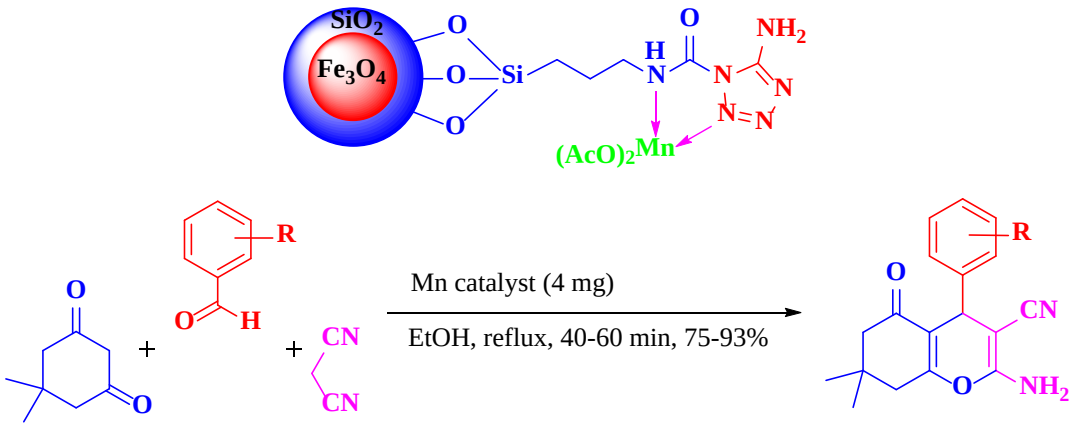

Scheme 1: Synthesis of tetrahydrobenzopyrans.

References

[1] Zabeti, M.; Daud, W. M. A. W.; Aroua, M. K. Activity of solid catalysts for biodiesel production: A review. *Fuel Process. Technol.* 2009, *90*, 770-777.

[2] Cheng, T.; Zhang, D.; Li, H.; Liu, G. Magnetically recoverable nanoparticles as efficient catalysts for organic transformations in aqueous medium. *Green Chem*. 2014, *16*, 3401-3427.

[3] Gloag, L.; Mehdipour, M.; Chen, D.; Tilley, R. D.; Gooding, J. J. Advances in the application of magnetic nanoparticles for sensing. *Adv. Mater.* 2019, *31*, 1904385.

Synthesis of amidoalkyl derivatives with the use of Thiourea bridged periodic mesoporous organosilica as a catalyst under solvent-free

Zahra Karbalaie, Seyyed Hojjat Sadeghi, Tannaz Mahmoudi and Sadegh Rostamnia*

Organic Chemistry Laboratory, Faculty of Chemistry, Iran University of Science & Technology, Tehran, Iran, zahrakarbalaie123@gmail.com

Keywords: Periodic mesoporous organosilica, Amidoalkyl, Catalyst

Periodic mesoporous organosilicas are a group of nanoporous materials that were first reported in 1999 by three groups from Canada, the United States, and Japan [1] .

We have synthesized a thiourea bridged PMO using 1,3-bis(3-(triethoxysilyl)propyl) thiourea (bis-thiourea) [2]. We have used thiourea-bridged PMO to demonstrate its ability to act as a catalyst in amidoalkyl derivatives synthesis.

Amidoalkyls derivatives belong to a group of organic compounds that are synthesized through multicomponent reactions. These compounds exist in the structure of natural products and have biological activities such as antibacterial and antiviral properties [3] . In this article, we intend to use periodic mesoporous organosilica containing sulfur as a catalyst for the synthesis of amidoalkyl derivatives (**Scheme**).

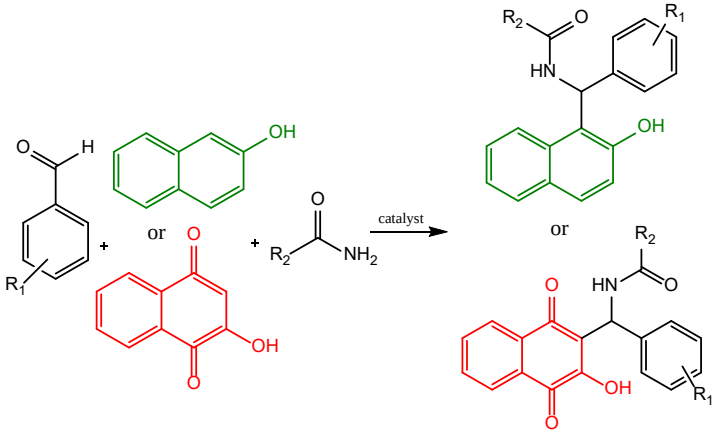

Scheme: Synthesis of amidoalkyl derivatives in the presence of TU-PMO.

References

[1] Asefa T, MacLachlan MJ, Coombs N, Ozin GA. Periodic mesoporous organosilicas with organic groups inside the channel walls. Nature. 1999;402(6764):867–71.

[2] Doustkhah E, Rostamnia S, Imura M, Ide Y, Mohammadi S, Hyland CJT, et al. Thiourea bridged periodic mesoporous organosilica with ultra-small Pd nanoparticles for coupling reactions. RSC Adv. 2017;7(89):56306–10.

[3] Dömling A. Recent developments in isocyanide based multicomponent reactions in applied chemistry. Chem Rev. 2006;106(1):17–89.

Use Thiourea bridged periodic mesoporous organosilica as a catalyst for synthesis of 1,4-dihydropyridine derivatives

Zahra Karbalaie, Seyyed Hojjat Sadeghi, Tannaz Mahmoudi and Sadegh Rostamnia*

Organic Chemistry Laboratory, Faculty of Chemistry, Iran University of Science & Technology, Tehran, Iran, zahrakarbalaie123@gmail.com

Keywords: Periodic mesoporous organosilica, 1,4-Dihydropyridine, Catalyst

Nanoporous materials contain nanometer pores, which are only a fraction of nanomaterials. periodic mesoporous organosilica are an exciting group of nanoporous materials that were first reported independently in 1999 by three groups from Canada, the United States, and Japan [1]. We synthesized a thiourea-bridged PMO using 1,3-bis(3-(triethoxysilyl)propyl)thiourea (bis-thiourea) [2]. We have used thiourea-bridged PMO to demonstrate its ability to act as a catalyst in the synthesis of 1,4-dihydropyridine. 1,4-DHPs are recognized as an important class of organic heterocyclic compounds because of their biological, medicinal, and pharmacological activities [3]. In this article, we intend to use sulfur-containing mesoporous organic silica as a catalyst to increase efficiency and reduce the reaction time for the synthesis of 1,4-DHP. (**Scheme**).

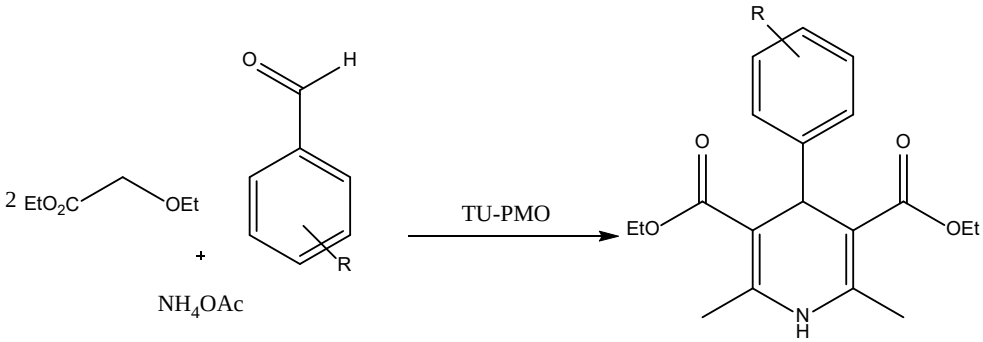

Scheme: Synthesis of 1,4-dihydropyridine derivatives in the presence of TU-PMO.

References

[1] Asefa T, MacLachlan MJ, Coombs N, Ozin GA. Periodic mesoporous organosilicas with organic groups inside the channel walls. *Nature*. 1999;402(6764):867–71.

[2] Doustkhah E, Rostamnia S, Imura M, Ide Y, Mohammadi S, Hyland CJT, et al. Thiourea bridged periodic mesoporous organosilica with ultra-small Pd nanoparticles for coupling reactions. *RSC Adv.* 2017;7(89):56306–10.

[3] Khaligh NG. 1, 1′-butylenebis (3-methyl-3 H-imidazol-1-ium) Hydrogen Sulfate Catalyzed One-Pot Multi-Component Synthesis of Unsymmetrical Polyhydroquinoline Derivatives. *Polycycl. Aromat. Compd.* 2016;36(4):284–94.

Remarkably catalytic performance in preparation of tetrahydropyridines by using ionic magnetic covalent organic framework

Erfan Abdoli, Mohammad Ali Zolfigol*, Morteza Torabi, Meysam Yarie

Department of Organic Chemistry, Faculty of Chemistry, Bu-Ali Sina University, Hamedan, Iran, erfanabdoli7697@gmail.com, zolfi@basu.ac.ir; mzolfigol@yahoo.com.

Keywords: COFs, Magnetic nanoparticles, Tetrahydropyridines

By the emergence of covalent organic frameworks (COFs) as covalently linked two- and three-dimensional organic structures, these materials have gained more interest. These versatile, reticular, sustainable and environmentally friendly materials are highly promising and have unique properties such as high thermal and chemical stability, regulatable physicochemical properties, metal-free and flexible scaffolds. Recently, COFs were applied as robust catalyst in many of organic transformations such as oxidation/reduction, coupling reactions, photocatalytic processes and multi-component reactions [1, 2]. According to literature, tetrahydropyridine containing heterocycles have a brilliant background in the many researches such as natural products, biological compounds, pharmaceutical molecules and many of miscellaneous areas [3]. Herein, we used a new ionic magnetic COF as catalyst for the synthesis of tetrahydropyridine derivatives (**Scheme**).

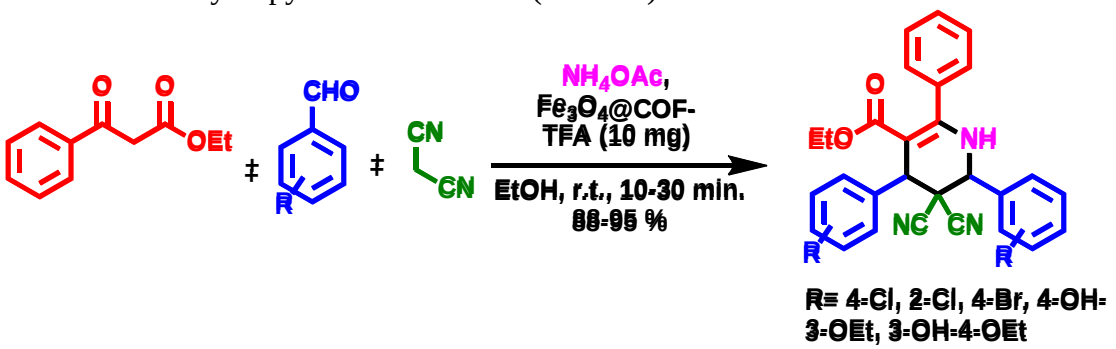

Scheme: Synthesis of tetrahydropyridines in the presence of Fe_3O_4@COF-TFA as catalyst.

References

[1] Ozdemir, J.; Mosleh, I.; Abolhassani, M.; Greenlee, L. F.; Beitle Jr, R. R.; Beyzavi, M. H. Covalent organic frameworks for the capture, fixation, or reduction of CO2. *Front. Energy Res.* 2019, *7*, 77-82.

[2] Shubayev, V. I.; Pisanic II, T. R.; Jin, S. Magnetic nanoparticles for theragnostics. *Adv. Drug Deliv. Rev.* 2009, *61*(6), 467-477.

[3] Yang, Q.; Luo, M.; Liu, K.; Cao, H.; Yan, H. (2020). Covalent organic frameworks for photocatalytic applications. *Appl. Catal. B: Environ.* 2020, *276*, 119-174.

Highly regioselective three-component synthesis of novel 4H-pyrano[2,3-b]quinoline derivatives

Masumeh Heydari*, Ali A. Mohammadi and Mohammad R. Mosleh

Chemistry and Chemical Engineering Research Center of Iran (ccerci), Tehran, Iran, heydari.chemmas@gmail.com, aliamohammadi@ccerci.ac.ir

Keywords: Regioselective, Multicomponent, Metal-free, Pyranoquinoline, Heterocyclization

A highly regioselective multicomponent synthesis via Knoevenagel condensation/heterocyclization sequence has been executed. An efficient and fast-track protocol has been used for preparing *O*-heterocyclic compounds under metal-free conditions. The three-component reaction of 2-chloroquinoline-3-carbaldehyde and two diverse cyclic active methylenes (dimedone and barbituric acid) for the synthesis of 4*H*-pyrano[2,3-b]quinoline has been accomplished under mild condition. The strategy included herein shows significant advantages including a facile process with easy purification, excellent yields, wide applicability, available substrates and cost-effective and eco-friendly solvent and catalyst. (**Scheme 1**).

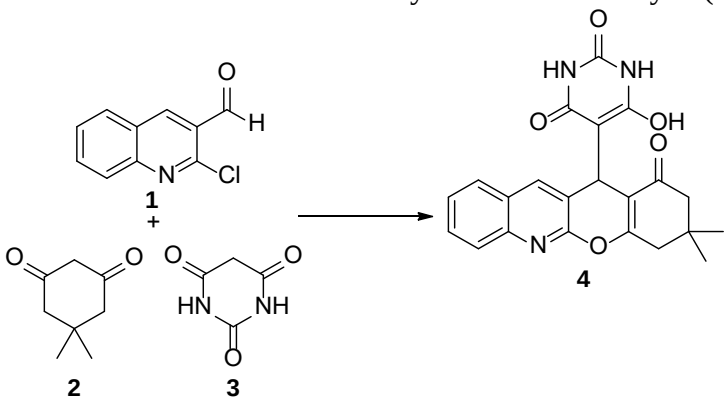

Scheme 1: Regioselective synthesis of pyranoquinoline

References

[1] Ruijter, E.; Scheffelaar, R.; Orru, R. V. Multicomponent reaction design in the quest for molecular complexity and diversity. *Angew. Chem. Int. Ed.* 2011. *50*, 6234-6246.
[2] Prajapati, S. M.; Patel, K. D.; Vekariya, R. H.; Panchal, S. N.; Patel. H. D. Recent advances in the synthesis of quinolines: a review. *RSC Adv.* 2014. *4*, 24463-24476.
[3] Hamama, W. S.; Ibrahim, M. E.; Gooda, A. A.; Zoorob, H. H. Recent advances in the chemistry of 2-chloroquinoline-3-carbaldehyde and related analogs. *RSC Adv.* 2018. *8*, 8484-8515.
[4] Shiri, M.; Heydari, M.; Zadsirjan, V. Efficient synthesis of novel functionalized pyrazolo-pyranoquinoline and tetrahydrodibenzo-[1, 8] naphthyridinone derivatives. *Tetrahedron* 2017. *73*, 2116-2122.

Four-component domino protocol toward the synthesis of novel functionalized 4H-pyrano[2,3-b]quinoline derivatives

Masumeh Heydari*, Ali A. Mohammadi and Mohammad R. Mosleh

Chemistry and Chemical Engineering Research Center of Iran (ccerci), Tehran, Iran, heydari.chemmas@gmail.com, aliamohammadi@ccerci.ac.ir

Keywords: 4H-Pyrano[2,3-b]quinolone, 2-Chloroquinoline-3-carbaldehydes, Cyclic active methylene, Organocatalyst, Regioselective

An efficient and facile domino protocol for the synthesis of novel functionalized 4H-pyrano[2,3-b]quinolones at 82–92% yield was reported. The four-component reaction of 2-chloroquinoline-3-carbaldehydes, 1,3-cyclodione compounds (as cyclic active methylene), ethyl acetoacetate (as β-keto ester), and hydrazine hydrate in the presence of organocatalyst was done. The significant advantages of this multi component reaction are C-O bond formation under metal-free conditions, simple procedure, mild and green condition, high yield, easy purification and, excellent regioselectivity (**Scheme 1**).

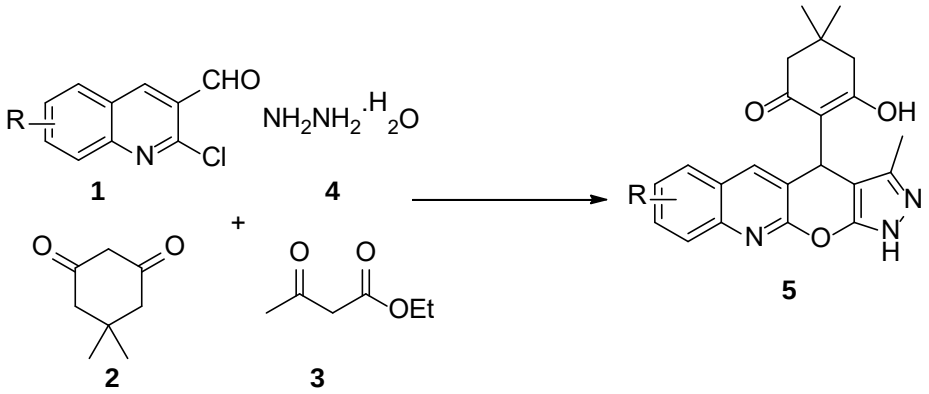

Scheme 1: Regioselective synthesis of pyranoquinoline

References

[1] Ganem, B. Strategies for innovation in multicomponent reaction design. *Acc. Chem. Res.* 2009, 42, 463-472.
[2] Nikoofar, K.; Yielzoleh, F. M. A concise study on dimedone: A versatile molecule in multi-component reactions, an outlook to the green reaction media. *J. Saudi Chem. Soc.* 2018. *22*, 715-741.
[3] Massoud, M. A. M.; Bayoumi, W. A.; Farahat, A. A.; El-Sayed, M.; Mansour, A. B. 2-Chloroquinoline-3-carbaldehydes: synthesis and reactions. *Arkivoc* 2018, *i*, 244-287.
[4] Fu, L.; Feng, X.; Wang, J. J.; Xun, Z.; Hu, J. D.; Zhang, J. J.; Zhao, Y. W.; Huang, Z. B.; Shi, D. Q. Efficient Synthesis and Evaluation of Antitumor Activities of Novel Functionalized 1,8-Naphthyridine Derivatives. *ACS Com Sci.* 2014, *17*, 24-31.

Design, synthesis and biological activities evaluation of novel resveratrol derivatives

Abdolrasoul H. Ebrahimabadi*, Ali Yousefi

Essential Oils Research Institute, University of Kashan, Kashan, Iran, aebrahimabadi@kashanu.ac.ir, aliyousefiir7@gmail.com

Keywords: Synthesis, Cytotoxicity, Anticancer, Resveratrol, Antioxidant

Resveratrol is a natural phytoalexin found in grapes, pine, legumes, pomegranate, beans, soybeans and peanuts [1]. It is known as a representative of polyphenolic trans-stilbenes. Stilbenes, especially resveratrol, have shown a lot of significant biological activities such as antifungal, antimicrobial, anticancer, antiestrogen, antiplatelet aggregation, antioxidant, heart protector, antimalarial, light protector, anti-inflammatory and antipyretic [2,3]. The use of resveratrol as a potentially beneficial agent is promising. But, due to some unfavourable pharmacokinetic/pharmacodynamic characteristics such as weak bioavailability, its use is limited. This study was conducted to design, synthesize and evaluate the biological activities of new derivatives of resveratrol using the bio-isosteric concept to overcome these limitations and improve the biological effects. Three derivatives of resveratrol with spatial variation of hydroxyl groups on phenyl rings were synthesized by a new synthesis method. The chemical structures of produced products were confirmed via ^{1}H NMR, ^{13}C NMR, FT-IR analysis and analytical HPLC. Then important biological properties such as anti-oxidant properties with a valid DPPH test, anti-cancer properties with the brine shrimp lethality test, the cytotoxicity test with the MTT method and antimicrobial properties against various pathogenic bacteria was performed.

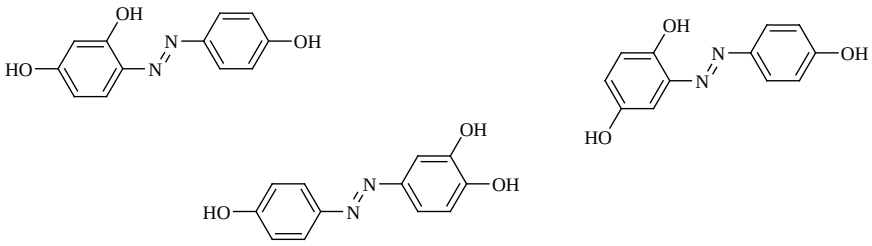

Scheme: Azoresveratrol and its two novel derivatives

References

[1] Uzura, S.; et al. A facile and rapid access to resveratrol derivatives and their radioprotective activity. *J. Bioorg. Med. Chem. Lett*. 2016; 26, 3886.
[2] Shaifi-Rad, J.; Quispe, C.; Durazzo, A.; et al. Resveratrol' biotechnological applications: Enlightening its antimicrobial and antioxidant properties. *J. Herb. Med.* 2022, 32, 100550.
[3] Ahmadi, R.; Ebrahimzadeh, M. A. Resveratrol – A comprehensive review of recent advances in anticancer drug design and development. *Eur. J. Med. chem.* 2020; 200, 112356.

Exploring the Potential of Fe_3O_4@SiO_2-Pr-NH-IC as a Nano-Magnetic Optical Sensor: Design, Preparation, and Characterization

Fatemeh Zamiran, **Ghodsi Mohammadi Ziarani***

Department of organic Chemistry, Faculty of Chemistry, Alzahra University, Tehran, Iran, fatemehzamiran278@gmail.com, gmohammadi@alzahra.ac.ir

Keywords: Fe_3O_4@SiO_2-Pr-NH-IC, Chemo sensor, Indole-3-carbaldehyde

The selective coordination potential of fluorescent organic sensors with diverse metal ions has captured the attention of researchers in the pursuit of advanced fluorescent material [1]. Researchers have employed the technique of depositing organic fluorescent ligands onto the surface of magnetic nanocomposites (Fe_3O_4@SiO_2) to generate novel heterogeneous compounds. This approach enables convenient separation of the nano-magnetic optical sensor After each utilization [2,3]. So, in this research, the magnetic nanoparticles (Fe_3O_4@SiO_2) were functionalized by (3-aminopropyl)-triethoxysilane (APTES) to provide Fe_3O_4@SiO_2-Pr-NH2, which was modified by indole-3-carbaldehyde to obtain Fe_3O_4@SiO_2-Pr-NH-IC (scheme 1). It can be used as a high-performance probe for the detection of trace amounts of some ions in water.

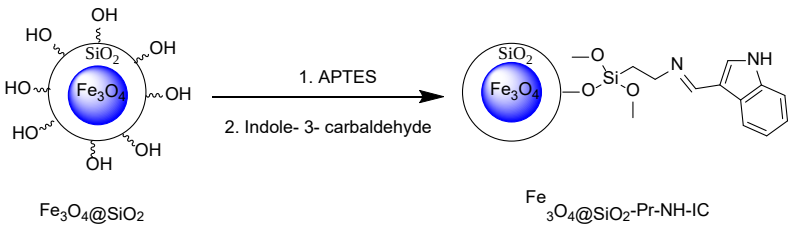

Scheme 1: Synthetic procedure of Fe_3O_4@SiO_2-Pr-NH-IC

References

[1]. Zhu, B.; Zhao, J.; Yu, H.; Yan, L.; Wei, Q.; Du, B. Development of novel naphthalimide-functionalized magnetic fluorescent nanoparticle for simultaneous determination and removal of Hg^{2+}. *Opt. Mater* 2013, 35, 2220-2225.

[2]. Xu, Y.; Zhou, Y.; Ma, W.; Wang, S.; Li, S. Highly sensitive and selective OFF-ON fluorescent sensor based on functionalized Fe_3O_4@ SiO_2 nanoparticles for detection of Zn^{2+} in acetonitrile media. *Appl. Surf. Sci.* 2013, *276*, 705-710.

[3]. Mir, N.; Karimi, P.; Castano, C. E.; Norouzi, N.; Rojas, J. V.; Mohammadi, R. Functionalizing Fe_3O_4@SiO_2 with a novel mercaptobenzothiazole derivative: Application to trace fluorometric and colorimetric detection of Fe^{3+} in water. *Appl. Surf. Sci.* 2019**,** 487**,** 876-888.

Cheep and available method preparation release for yankee dryer use in tissue making

Zahra Chenani*

Harir Khozestan Company, Hafttappeh, Ahvaz, Iran, z.chenani3053@gmail.com.

Keywords: Release, Sylandr yankee, Tissue making

Tissue products such as facial tissue and paper towels have been playing a crucial role in promoting hygiene and maintaining good health, since they are commonly available and widely used nowadays. The production of low-density tissue paper typically involves a key creping process that contains pressing and adhering the wet web onto a high-speed Yankee cylinder, followed by releasing the creped sheet with a stationary creping blade to form periodic micro-folds within the tissue structure. This paper discusses and reviews the mechanisms of tissue creping technology, as well as the factors that impact the creping process and tissue properties. These factors primarily include the dryness of the tissue web, creping rate, properties of the pulp raw material, Yankee coating, crepe doctor blade, and tissue drying machines. It is indicated that the creping process, as a multifaceted and integrated treatment for tissue production, can be significantly enhanced through the concerted efforts of the aforementioned factors to achieve greater creping efficiency [1]. At the interface between the Yankee dryer surface and the tissue web resides a thin film comprising an agglomeration of materials we call a Yankee coating. The Yankee coating is composed of chemical additives applied to facilitate development of specific film properties(e.g. adhesion and release) and “natural” components from the wet end, process water along with cellulosic material from the sheet. For a coating to provide “Best Practice” results it must be able to protect the Yankee surface and be optimized to deliver the proper level of uniform adhesion for commercial creping operations [2]. Release is one of the components of Yankee cylinder coating. In this invention, we were able to prepare an effective and good release with cheap and available materials. We tested the made release in the production line of Khuzestan Silk Company. Good results were obtained. The sample made from foreign samples such as ncr company materials was better. In the present invention,the oil-based formulation and the components therein can be food-grade and/or non-toxicand/or can be entirely or primarily from renewable resources.

References

[1] Qin, Tong, et al. Creping technology and its factors for tissue paper production: a review. *Eur. J. Wood Wood Prod.* 2023, 1-17.

[2] Archer, Sam; FURMAN, Gary. Yankee Coating Systems-The Functional Interface. UBM Asia Trade Fairs Ptd., Ltd., March18–21, Tissue world, Barcelona, Spain, 2013.

Highly stable magnetically Cu-nanocatalyst as an efficient catalyst for C(sp^2)−C(sp) and C(sp^2)–C(sp^2) cross coupling reactions

Masomeh Balali [a*], Hassan Keypour [b], Mojtaba Bagherzadeh[c]

a) Hamedan University of Technology, Hamedan, Iran, masomeh.balali@yahoo.com.
b) Chemistry Department, Bu-Ali Sina University, Hamedan, Iran
c) Chemistry Department, Sharif University of Technology, Tehran, Iran

Keywords: Magnetic nanoparticles, Cross-coupling reactions, Nanocatalysts.

Cu-catalyzed has been explored as an efficient and recyclable catalyst to effect on Sonogashira and Suzuki cross-coupling reactions. After the modification of 2-(((piperazin-1-ylmethyl)imino)methyl)phenol on the surface of amorphous silica coated iron oxide (Fe_3O_4@SiO_2@Cl) magnetic core–shell nanocomposite, Copper(II) chloride was employed to synthesize the Fe_3O_4@SiO_2@SH@-Cu catalyst, affording a copper loading of 1.52 mmol g^{-1}. High yield, low reaction times, non-toxicity and recyclability of the catalyst are the main merits of this protocol. The catalyst has been characterized by FT-IR, XRD, SEM, TEM, XPS, EDX, VSM and ICP-AES. The Fe_3O_4@SiO_2@SH@Cu nanocatalyst shows good activity towards Sonogashira and Suzuki cross-coupling reactions in an environmentally friendly solvent (water–DMF) under mild conditions. The catalyst shows not only high catalytic activity, but also offers many practical advantages such recyclability and air stability.

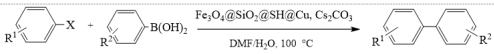

Entry	Ar^{1}X	Boronic acid	Time (h)	Yield (%)[b]	Entry	Ar^{1}X	Boronic acid	Time (h)	Yield (%)[b]
1		PhB(OH)$_2$	2	90	6		2-NaphthylB(OH)$_2$	4	86
2		PhB(OH)$_2$	3	85	7		PhB(OH)$_2$	3	85
3	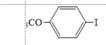	PhB(OH)$_2$	1.30	80	8		PhB(OH)$_2$	3 h	80
4	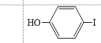	PhB(OH)$_2$	2	85	9		PhB(OH)$_2$	4 h	83
5		4-NO$_2$C$_6$H$_4$B(OH)$_2$	1	89	10		PhB(OH)$_2$	2.30	84

[a] Reaction condition: Fe_3O_4@SiO_2@SH@Cu (0.01 g), aryl halide (1 mmol), aryl boronic acid (1.5 mmol) and Cs_2CO_3 (2 mmol). [b] Isolated yield.

Table: Suzuki reaction of arylboronic acids with aryl halides[a]

References

[1] Riadi, Y., M. Kadhim M., Jawad Shoja S., Hussein Ali, M., Fakri Mustafa, Y., Sajjadi, A. Copper (II) complex supported on the surface of magnetic nanoparticles modified with S-benzylisothiourea (Fe_3O_4@SiO_2-SMTU-Cu): A new and efficient nanomagnetic catalyst for the synthesis of quinazolines and amides. *Synth. Commun.* 2022, *52*, 875−887.

[2] Bagherzadeh, M., Haghdoost, M. M, Shahbazirad, A., Nanoparticle supported, magnetically separable vanadium complex as catalyst for selective oxidation of sulfides *J. Coord. Chem.*, 2012, *65*, 591–601.

Supramolecular architecture of $((C_6H_5CH_2)_2N)(C_6H_4)(NH)_2P(O)$

Fahimeh Sabbaghi[a]* and Mehrdad Pourayoubi[b]

a) Department of Chemistry, Zanjan Branch, Islamic Azad University, Zanjan, Iran, fahimeh_sabbaghi@yahoo.com
b) Department of Chemistry, Faculty of Science, Ferdowsi University of Mashhad, Mashhad, Iran, pourayoubi@um.ac.ir

Keywords: Phosphoric triamide, Diazaphosphole, X-ray crystallography

Phosphoric triamides are well-known for their biological activities and some other applications as extractant, solvent and ligand [1]. The crystal structure of a new diazaphosphole-holding phosphoric triamide with the formula $((C_6H_5CH_2)_2N)(C_6H_4)(NH)_2P(O)$ is studied (**Figure**). The P—N bond made by the $(C_6H_5CH_2)_2N$ moiety is slightly shorter than the P—N bonds of diazaphosphole ring. The benzyl moieties adopt the *+ac–sc+ac+sp* and *+ac–sc+ac+ap* conformations (*ac* = anticlinal, *sc* = synclinal, *sp* = synperiplanar, *ap* = antiperiplanar), based on the 2×C—C—C—N/C—C—N—P/C—N—P═O torsion angles. In the crystal structure, the molecules are aggregated through N—H…O═P hydrogen bonds in a tape arrangement along the *a* axis. This assembly includes centrosymmetric eight-membered ring hydrogen bond motifs, in which the P═O group takes part as a double-hydrogen bond acceptor. The C—H…π interactions extend the supramolecular assembly to a two-dimensional array parallel to the *ab* plane.

Figure: The molecular structure, showing the atom-numbering scheme for the title compound, with displacement ellipsoids drawn at the 50% probability level.

References

[1] Corbridge, D. E. C. In Phosphorus: An Outline of Its Chemistry, Biochemistry and Technology, 5th ed. Amsterdam: Elsevier, 1995.

Preparation of new nicotinonitrile derivatives catalyzed by magnetic nanoparticles as the new magnetic H-bond catalyst *via* CVABO mechanism

Mahdiyeh Navazeni,[a] Hossein Ahmadi,[a] Hassan Sepehrmansourie,[a] Mohammad Ali Zolfigol,*[a] Ardeshir Khazaei,[a] Mohammad Ali Bodaghi Fard[b] and Mojtaba Hosseinifard[c]

a) Department of Organic Chemistry, Faculty of Chemistry, Bu-Ali Sina University, Hamedan 6517838683, Iran, mahdieh.navazani@gmail.com, zolfi@basu.ac.ir & mzolfigol@yahoo.com, Khazaei_1326@yahoo.com

b) Department of Chemistry, Faculty of Science, Arak University, Arak, Iran

c) Department of Energy, Materials and Energy Research Centre, P.O. Box 31787-316, Karaj, 401602, Iran.

Keywords: Anomeric effect, Nicotinonitriles, Nano-magnetic catalyst

Herein, we have designed a magnetic catalyst by modifying magnetic nanoparticles. In this method, by using these compounds, an organic structure with urea part has been created on magnetic nanoparticles, which can function as a hydrogen bond catalyst. Hydrogen bond catalysts play both the role of acid catalyst and the role of basic catalyst [1]. The catalytic application of catalyst as the new magnetic H-bond catalyst in the synthesis of new nicotinonitrile compounds was evaluated by multicomponent reaction in solvent-free and green conditions, which showed good performance. These compounds have antibacterial, antifungal, anti-depressant, anti-aging, anti-inflammatory and anti-Alzheimer properties [2] (**Scheme**).

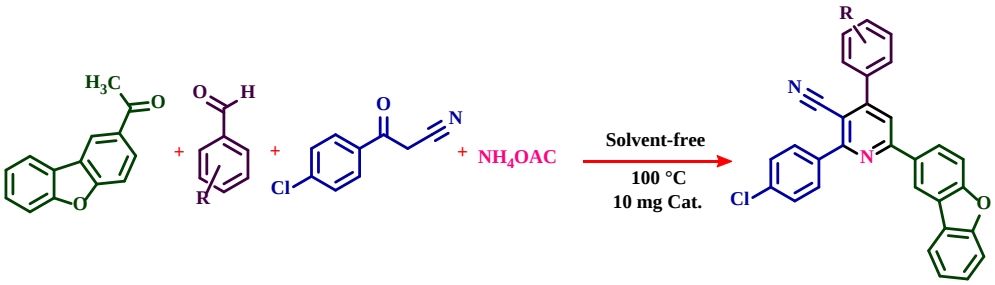

Scheme: Synthesis of nicotinonitrile derivatives catalysed by magnetic nanoparticles as the new magnetic H-bond catalyst.

References

[1] Torkashvand, Z.; Sepehrmansourie, H.; Zolfigol, M. A.; As' Habi, M. A. Application of Ti-MOF-UR as a new porous catalyst for the preparation of pyrazolo [3, 4-*b*] quinoline and pyrazolo [4, 3-*e*] pyridines. *Mol. Catal.* 2023, *541*, 113107.

[2] Shamroukh, A. H.; Kotb, E. R.; Anwar, M. M.; Sharaf, M. A Review on the Chemistry of Nicotinonitriles and Their applications. *Egypt. J. Chem.* 2021, *64*, 4509-4529.

Crystal structure of a new diazaphosphorinane-based amidophosphoester: $(C_6H_5O)(C_{10}H_6)(NH)_2P(O)$

Fahimeh Sabbaghi[a]* and Mehrdad Pourayoubi[b]

a) Department of Chemistry, Zanjan Branch, Islamic Azad University, Zanjan, Iran, fahimeh_sabbaghi@yahoo.com
b) Department of Chemistry, Faculty of Science, Ferdowsi University of Mashhad, Mashhad, Iran, pourayoubi@um.ac.ir

Keywords: Amidophosphoester, Diazaphosphorinane, X-ray crystallography

Amidophosphoester moieties are structural motifs often found in a variety of bioactive products as well as in different classes of drugs [1]. In this work, the crystal structure of a new diazaphosphorinane-holding amidophosphoester with the formula $(C_6H_5O)(C_{10}H_6)(NH)_2P(O)$ is studied (**Figure**). The asymmetric unit is composed of three independent molecules, which are similar in viewpoint of bond lengths/angles. The main differences of these molecules are related to some torsion angles, especially the ones defining the orientation of C_6H_5O moiety with regard to the P═O group. The C—O—P═O torsion angles of 167.1 (5)°, –66.1 (5)° and –78.8 (6)° show the +*ap*, –*sc* and –*sc* conformations (*ap* = antiperiplanar and *sc* = synclinal). Thus, the distances of phenyl groups (of C_6H_5O segments) from the naphthalene rings are different in three symmetry-independent molecules. In the crystal structure, the molecules are aggregated through N—H…O═P hydrogen bonds in a tape arrangement. This assembly includes eight-membered ring hydrogen bond motifs, constructed from connection between both symmetry-related and symmetry-independent molecules. The P═O groups take part as a double-hydrogen bond acceptor.

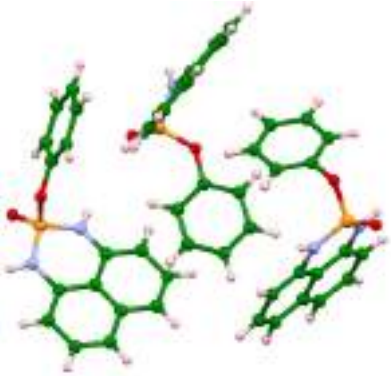

Figure: The molecular structure of asymmetric unit of the title compound, atom color codes: P orange, O red, N blue, and H pink.

References

[1] Warren, T. K.; Jordan, R.; Lo, M. K.; Ray, A. S.; Mackman, R. L.; Soloveva, V.; *et al*. Therapeutic efficacy of the small molecule GS-5734 against Ebola virus in rhesus monkeys. *Nature*, 2016, *531*, 381–385.

The new synthesis of pyrrole-fused dibenzo[*b,f*][1,4]oxazepine/thiazepines by the pseudo-Joullié-Ugi reaction *via* an unexpected route with high chemoselectivity

Mohammad Taghi Nazeri, Masoomeh Ahmadi, Maryam Ghasemi, Ahmad Shaabani* and Behrouz Notas

Department of Organic Chemistry, Shahid Beheshti University, Daneshjou Boulevard Street, Tehran, 1983969411, Iran, Nazeri1985@gmail.com

Keywords: Joullié-Ugi reaction, Cyclic imine, Dibenzoxazepine, Pyrrole, Isocyanide.

In this paper, we designed a new and unexpected route for the synthesis of pyrrole-fused dibenzoxazepines/thiazepines based on the modified Ugi reaction of cyclic imines with isocyanides and acetylenedicarboxylates under catalyst-free conditions. Mechanism investigation indicates that this process is carried out through the production of zwitterion species (Huisgen's 1,4-dipole), which is a key intermediate in the chemo selectivity of products. This Huisgen's 1,4-dipole is trapped in situ with isocyanides, and various pyrrole-fused dibenzoxazepines/thiazepines are synthesized in a simple one-pot operation with high yields and chemoselectivity [1]. This strategy opens a new route in Ugi reactions (pseudo-Joullié-Ugi reaction) for synthesizing pyrrole-fused heterocycles as unique pharmaceutical scaffolds. This efficient, simple and catalyst-free method can be successfully performed in gram-scale reactions. In addition, the new approach is repeatable for other cyclic imines. Interestingly, the pyrrole-fused dibenzoxazepines/thiazepine derivative has remarkable emission, which could be a potential candidate for optoelectronic conjugated materials [2].

Scheme: Use Times New Roman 11 to explain your scheme.

References

[1] Nazeri, M. T.; Shaabani, A.; Notash, B. Chemoselective synthesis of fully substituted pyrroles via a one-pot four-component isocyanide-based reaction. *Org. Biomol. Chem.* **2021**, *19* (16), 3722-3734.

[2] Nazeri, M. T.; Farhid, H.; Mohammadian, R.; Shaabani, A. Cyclic imines in Ugi and Ugi-type reactions. *ACS Comb. Sci.* **2020**, *22* (8), 361-400.

[3] Nazeri, M. T.; Ahmadi, M.; Ghasemi, M.; Shaabani, A.; Notash, B. The new synthesis of pyrrole-fused dibenzo [b, f][1, 4] oxazepine/thiazepines by the pseudo-Joullié–Ugi reaction via an unexpected route with high chemoselectivity. *Org. Biomol. Chem.* **2023**, *21* (19), 4095-4108.

In situ synthesis of MOF(Ag) in carboxymethyl starch nanoplatform: Synthesis and characterization

Rahim Safarpour[a], Malihe Pooresmaeil[a], Hassan Namazi[a,b*]

a) Polymer Research Laboratory, Department of Organic and Biochemistry, Faculty of Chemistry, University of Tabriz, Tabriz, Iran, r.safarpour99@ms.tabrizu.ac.ir.
b) Research Center for Pharmaceutical Nanotechnology, Biomedicine Institute, Tabriz University of Medical Science, Tabriz, Iran, namazi@tabrizu.ac.ir.

Keywords: Starch, Carboxymethyl starch, Metal-organic framework.

In recent years, metal-organic frameworks (MOFs) received more attention from researchers in most areas [1]. Adjustable specific surface areas, porosity, and chemical structure are some advantages of MOF-based materials. Unfortunately, the fabrication of MOFs in a neat state leads to some aggregation. Therefore the synthesis of these materials in the presence of other materials especially biopolymers is welcome [2]. Considering these, in this research work, at first, the starch polymer (St) was modified with chloroacetic acid to introduce the carboxylic acid functional groups in the structure (CMSt). In the next step, CMSt nanoparticles (CMSt NPs) were prepared via precipitation in ethanol. Eventually, the fabricated CMSt NPs acted as a green platform for Ag based MOFs synthesis (CMSt NPs/MOF(Ag)). The analysis of the physical and chemical properties displayed the successful formation of Ag MOF in the presence of CMSt NPs. For example, the appearance of the peaks at the 2θ value of 44.32º, 38.24º and 32.28º which are related to (002)، (111)، (011) is in good accordance with the crystalline structure of MOF(Ag) approves its successful formation in the CMSt NPs platform. Scanning electron microscope (SEM) analysis presented a rod-like morphology for the prepared MOF(Ag). Overall the outcome of this research showed the possibility of the CMSt NPs use as a green platform for in situ synthesis of MOFs.

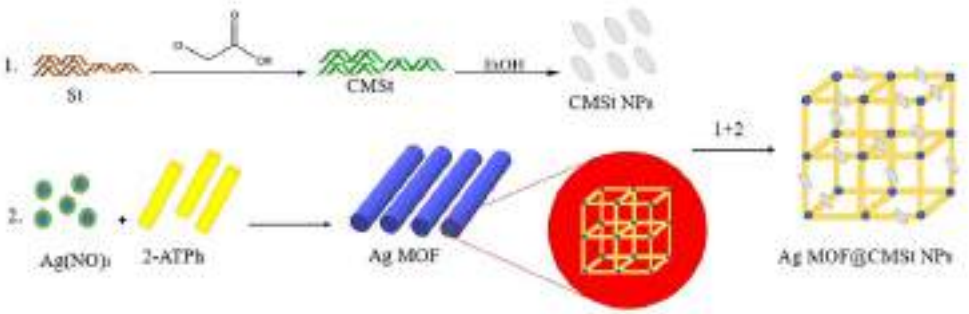

Scheme. Schematic of CMNSt/MOF(Ag) synthesis way.

References

[1] Qian, Y.; Zhang, F.; Pang, H., A review of MOFs and their composites-based photocatalysts: synthesis and applications. *Adv. Funct. Mater.* 2021, *31* (37), 2104231.
[2] Pooresmaeil, M.; Namazi, H., Developments on carboxymethyl starch-based smart systems as promising drug carriers: A review. *Carbohydr. Polym.* 2021, *258*, 117654.

Design, synthesis, and characterization of new nanohybrid of starch/bio-based carbon dots as a promising photoluminescent platform for biomedicinal applications

Rahim Safarpour[a], Malihe Pooresmaeil[a], Hassan Namazi[a,b*]

a) Polymer Research Laboratory, Department of Organic and Biochemistry, Faculty of Chemistry, University of Tabriz, Tabriz, Iran, r.safarpour99@ms.tabrizu.ac.ir.
b) Research Center for Pharmaceutical Nanotechnology, Biomedicine Institute, Tabriz University of Medical Science, Tabriz, Iran, namazi@tabrizu.ac.ir.

Keywords: Starch; Carbon quantum dots; Cancer.

Cancer is one of the leading causes of death worldwide [1]. Up to now, several methods have been used for cancer treatment. In between, chemotherapy is one of the most important methods in the clinics. Despite the advantages of this way, it suffers from several issues, therefore, today there are enormous efforts to achieve smart drug delivery systems based on nanomaterials [2]. Considering these, in this research, the new photoluminescent nanohybrid was prepared based on starch nanoparticles (St NPs) and pre-synthesized carbon dots (CDs). The performed Fourier-transform infrared spectroscopy (FT-IR), scanning electron microscope (SEM), atomic force microscopy (AFM), and X-ray diffraction (XRD) analysis approved the success of St/CDs nanohybrid synthesis. DLS obtained the mean diameter of the St/CDs at about 42 nm. Additionally, the photoluminescence (PL) test approved the photoluminescence nature via the detection of the blue emission under the UV lamp along with a peak at 421 nm of its PL spectrum. Altogether, the findings show that the prepared system can be proposed as an anticancer drug delivery agent owing to its structure, as well as a bioimaging system due to its photoluminescent nature.

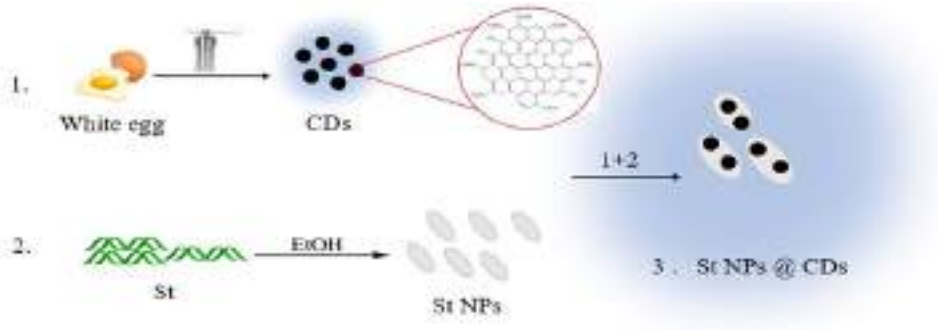

Scheme. Schematic of St NPs/CDs synthesis way

References

[1] Bose, N.; Danagody, B.; Rajappan, K.; Ramanujam, G. M.; Anilkumar, A. K. Development and characterization of AgHNTs@ SPU film loaded with letrozole as drug delivery system and its anticancer activity. *J. Drug Deliv. Sci. Technol.* 2023, *85*, 104557.
[2] Pooresmaeil, M.; Namazi, H. Metal-organic framework/carboxymethyl starch/graphene quantum dots ternary hybrid as a pH sensitive anticancer drug carrier for co-delivery of curcumin and doxorubicin. *J. Taiwan Inst. Chem. Eng.* 2022, *141*, 104573.

NaY Zeolite Modified with diethanol Amine (DEA-NaY) as a Green and Reusable Catalyst for the One pot Three-Component Synthesis of Tetrahydrobenzo[b]pyran in Water

Mohammadreza Fakhimi Abarghouei*

Central Laboratory, Pardis Petrochemical Company, Assalouyeh, Iran, Fakh5656@gmail.com

Keywords: Tetrahydrobenzo[b]pyran, NaY Zeolite, Diethanol Amine

Modified zeolite (DEA-NAY) has been applied as an effective heterogeneous catalyst for one-pot synthesis of tetrahydrobenzo[b]pyran via reaction of various isatins with malonitrile and dimedone in water at 100 ^{o}C [1, 2]. The prepared catalysts were recovered and reused several times with minor reductions in activity. The high efficiency, short time and use of green solvent in mild conditions are the benefits of these methods (**Scheme**).

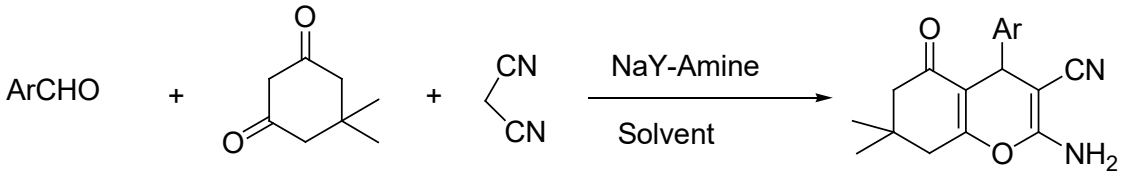

Scheme: Synthesis of Tetrahydrobenzo[b]pyran derivatives.

References

[1] Hu, H., Qiu, F., Ying, A., Yang, J., & Meng, H. An environmentally benign protocol for aqueous synthesis of tetrahydrobenzo [b] pyrans catalyzed by cost-effective ionic liquid. *Int. J. Mol. Sci.* 2014, *15*(4), 6897-6909.

[2] Gurumurthi, S., Sundari, V., & Valliappan, R. An efficient and convenient approach to synthesis of tetrahydrobenzo [b] pyran derivatives using tetrabutylammonium bromide as catalyst. *J. Chem.* 2009, *6*(S1), S466-S472.

Mesoporous MCM-41@S^{n}Pr-Kryf.23-Mn a versatile and reusable nanocatalyst for the oxidation of primary and secondary alcohols in the presence of hydrogen peroxide as oxidant

Shirin Mahjabin and Nader Noroozi Pesyan *

Department of Organic Chemistry, Faculty of Chemistry, Urmia University, 57159 Urmia, Iran, shirinmahjabin97@gmail.com.

Keywords: Ring opening oxidation, Kryptofix 23, MCM-41, Alcohols

Mesoporous materials are porous materials with periodically ordered pore in the range of 2 ~ 50 nm. They have large accessible surface areas and tunable pore sizes, which are of particular benefit for mass transport and dispersion of electrons/reactants [1]. Mesoporous silica materials like MCM-41 has attracted much attention because of their different usages, and have versatile applications in materials science and several unique properties including good thermal stability, large surface area, unique channel structure, large pore volume, good biocompatibility and also easy surface functionalization [2]. Herein, we decided to introduce new nanocatalyst MCM-41@S^{n}Pr-Kryf.23-Mn to catalyse the oxidation of primary and secondary alcohols to corresponding oxidized carbonylated compounds in the presence of hydrogen peroxide in acetonitrile and acetic acid in high yields under mild condition (**Scheme 1**).

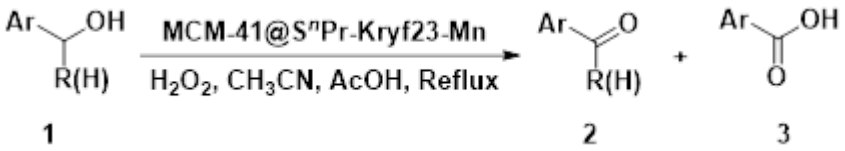

Scheme 1: Oxidation of primary and secondary alcohols (1) to corresponding carbonylated compounds (2 and/or 3) with catalytic amount of MCM-41@S^{n}Pr-Kryf.23-Mn nanocatalyst.

References

[1] Zhang, L., Jin, L., Liu, B., & He, J. Templated growth of crystalline mesoporous materials: from soft/hard templates to colloidal templates. *Front. Chem. 2019*, 7, 22.

[2] Manzano, M., Aina, V., Arean, C. O., Balas, F., Cauda, V., Colilla, M., ... & Vallet-Regi, M. Studies on MCM-41 mesoporous silica for drug delivery: effect of particle morphology and amine functionalization. *Chem. Eng. J. 2008*, 137(1), 30-37.

Elimination of MG and CR from water with Cerium-based MOF

Mohammad Sepehr Salimi, Hossein Molavi*

Analytical Chemistry Laboratory, Faculty of Chemistry, University of iasbs, Zanjan, Iran, sepehrsalimi@iasbs.ac.ir, h.molavi@iasbs.ac.ir

Keywords: Malachite Green (MG), Congo Red (CR), Water treatment, Green synthesis

Today the water purification is one of the most challenging problems for the human of 21'st century. Water is necessary in all aspects of life, being the defining characteristic of our planet. Most of the chemical and bio chemical reactions are done in presence of water, the life of the living species are dependent on water, water is used to cool down the industrial devices and etc [1]. This is obvious that water treatment is very important and unfortunately due to novel anthropogenic pollutants this problem increasingly has become a dangerous issue for whole world. Metal-organic frameworks (MOFs) have recently achieved much attention to eliminating toxic pollutants because of their attractive attributes, including large specific surface area, ultra-high porosity, abundant active adsorption sites, tuneable surface chemistry, well-controlled pore size distribution, and strong host–guest interactions. Among the many developed MOFs, the Ce-based MOFs, particularly the UiO-66 family, are considered extremely attractive for wastewater treatment applications. The fascinating properties of UiO-66 such as high thermal stability, superior chemical resistance towards several solvents, including benzene, acetone, different alcohols, dimethylformamide, acidic and basic solution, excellent chemical stability against various conditions such as air, water, and chloroform, and exceptional resistance to high external pressure, mainly due to strong Ce-O bond and high coordination number between the Ce clusters and organic ligands have led to numerous potential applications in wastewater treatment [2]. MOFs are known as a new class of highly porous materials for gas storage and adsorption, photocatalysis, bio medical imaging, ion exchange, water purification, drug delivering and adsorbent and sensing [3]. In this job the Malachite Green (MG) and Congo Red (CR) dyes are pollutant models. Furthermore the Cerium based UiO-66 MOF (Ce-UiO-66) is used as pollutant adsorbent. Many factors Influences the adsorption capacity of the adsorbent. Green synthesis of this MOF is the purpose of this job. Based on the obtained results, this MOF can successfully adsorb both dyes from water with different amounts.

References:

[1] Rojas, S.; Horcajada, P. Metal–organic frameworks for the removal of emerging organic contaminants in water. *Chem. Rev.* **2020**, *120* (16), 8378-8415.

[2] Ahmadijokani, F.; Molavi, H.; Rezakazemi, M.; Tajahmadi, S.; Bahi, A.; Ko, F.; Aminabhavi, T. M.; Li, J.-R.; Arjmand, M. UiO-66 metal–organic frameworks in water treatment: A critical review. *Prog. Mater. Sci.* **2022**, *125*, 100904.

[3] Ahmadijokani, F.; Ahmadipouya, S.; Molavi, H.; Arjmand, M. Amino-silane-grafted NH 2-MIL-53 (Al)/polyethersulfone mixed matrix membranes for CO 2/CH 4 separation. *Dalton Trans.* **2019**, *48* (36), 13555-13566.

Design of novel Strong Superbases Based of diquinonimino: Computational DFT Analysis in the Gas Phase.

Tayyebeh Koneshlou [a,*], Morteza Rouhani [a,*], Hamid Saeidian [b,*], Javad Mokhtari Aliabad [a]

a) Department of Chemistry, Science and Research Branch, Islamic Azad University, Tehran, Iran, tkoneshlou@gmail.com
b) Department of Science, Payame Noor University (PNU), P.O. Box: 19395-4697, Tehran, Iran

Keywords: Guanidine, Superbase, Hyperbase, Computational, DFT

In this investigation, we are trying to design appropriate super/hyperbasic structures on the basis of guanidine and the application of electron-donating of substituted R groups, aromaticity stabilization of seven-membered and two six-membered fused rings via the calculation of Proton Affinity (PA) and Gas-phase Basicity (GB), using Density Functional Theory (DFT). The results showed that the effective push-pull effect has been existed from R donating groups to guanidine moiety. In order to monitoring aromaticity alterations in the rings before and after protonation, Nucleus-independent Chemical Shift (NICS), Harmonic Oscillator Model of Aromaticity (HOMA), and Harmonic Oscillator Model of Electron Delocalization (HOMED) indexes were used. Results ascertained that all of the designed structures have the PA value further than superbasicity threshold and also even four structures offered PA values higher than hyperbasicity threshold (**11**, **13**, **18**, and **19**) (**Scheme**).

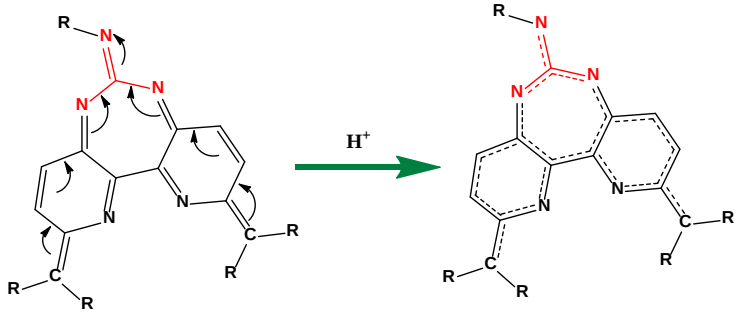

Scheme: Effect of guanidine Aromaticity Synergistic for increasing Super/hyperbasicity.

References

[1] Ishikawa, T.; Margetić, D.; In Perspectives//Superbases for Organic Synthesis Guanidines, Amidines, Phosphazenes and Related Organocatalysts; Ishikawa, John Wiley & Sons Ltd: Chichester, West Sussex, 2009.
[2] Maksic, Z.B.; Kovacevic, B, Spatial and electronic structure of highly basic organic molecules: cyclopropeneimines and some related systems, *J. Phys. Chem. A* 103(1999) 6678–6684.
[3] Raczyńska, E.D.; Maria.; P.-C. Decouzon J.-F. Gal, M. Superbases in the gas phase.Part II. Further extension of the basicity scale using acyclic and cyclic guanidines,*J. Phys. Org. Chem.* 7 (1994) 725–733.

Efficient nanocatalyst for one-pot synthesis of 2,3-disubstituted benzo[b]furans

Samaneh Koosha, Sedigheh Alavinia and Ramin Ghorbani-Vaghei *

Department of Organic Chemistry, Faculty of Chemistry, Bu-Ali Sina University, 6517838683, Hamadan, Iran, kooshasamaneh@gmail.com, rgvaghei@yahoo.com & ghorbani@basu.ac.ir

Keywords: IRMOF-3, MOF-polymer composite, Nano porousmaterials, Benzo[b]furan, Copper iodide

This study was conducted to synthesize and characterize a new Polymer/MOF stabilizer *via* the reaction between a sulfonamide-triazine-based porous organic polymer (poly(sulfonamide-triazine)-PSTA) and an amino-functionalized zinc metal-organic framework (IRMOF-3). Next, the prepared nanocomposites (IRMOF-3/PSTA/Cu) were modified using copper iodide nanoparticles (CuI NPs). Finally, the application of the prepared nanocomposites was investigated through the one-pot synthesis of 2,3-disubstituted benzo[b]furans. To this end, alkyne, salicylaldehydes, and amines were subjected to a three-component domino reaction. All products were obtained in high turnover frequency (TOF) up to 142.42, suggesting this catalyst's high selectivity and activity in the mentioned domino reactions. Notably, the synthesized nanocatalyst is reusable up to seven times with no considerable catalytic efficiency loss. Overall, the high yields of products, nanocatalyst's facile recovery, short reaction time, and wide substrate scopes make this procedure eco-friendly, practical, and economically justified (**Scheme**).

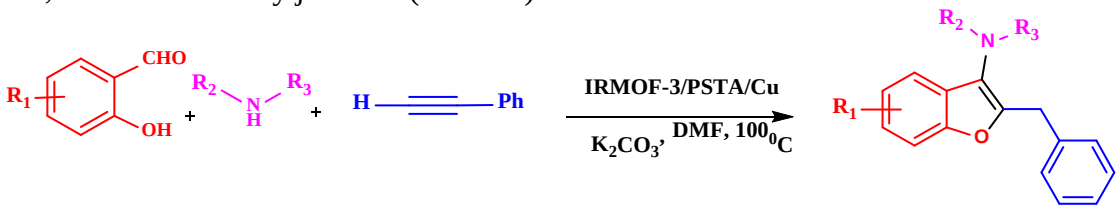

Scheme: Synthesis of 2,3-disubstituted benzo[b]furans using IRMOF-3/PSTA/Cu.

References

[1] G.A. Coppola, S. Pillitteri, E. V Van der Eycken, S.-L. You, U.K. Sharma, Multicomponent reactions and photo/electrochemistry join forces: atom economy meets energy efficiency, *Chem. Soc. Rev*. 51 (2022) 2313–2382.

[2] L. Levi, T.J.J. Müller, Multicomponent syntheses of functional chromophores, *Chem. Soc. Rev.* 45 (2016) 2825–2846.

[3] M. Kazemi, M. Mohammadi, Magnetically Recoverable Catalysts: Catalysis in Synthesis of Polyhydroquinolines, *Appl. Organomet. Chem*. 34 (2020) e5400.

[4] M. Mohammadi, A. Ghorbani-Choghamarani, Hercynite silica sulfuric acid: a novel inorganic sulfurous solid acid catalyst for one-pot cascade organic transformations, *RSC Adv.* 12 (2022) 26023–26041.

Synthesis of new benzo imidazole pyrrolidine carbothioate *via* thiol ester linkage

Zahra Ashoori, Mohammad Bayat* and Shima Nasri

Department of Chemistry, Faculty of Science, Imam Khomeini International University, Qazvin, Iran, z.ashoori1997@gmail.com, bayat_mo@yahoo.com; m.bayat@sci.ikiu.ac.ir

Keywords: Benzimidazole-2-thiol, L-proline, Benzo imidazole pyrrolidine carbothioate.

Recently, some procedures were reported for the synthesis of substituted benzoheterocycles such as benzimidazole-2-thiol which are vital blocks of some medical agents or biologically active compounds. Various derivatives of 2-mercapto benzimidazole have exhibited a wide range of biological activities such as antimicrobial, antihistamine, neutropic, and analgesic activities. Also, it serves as a plant growth regulator and is used as a corrosion inhibitor, as well as a well-known analytical reagent for mercury and some metal ions in sewage water and industrial wastewater samples [1]. Generally, compounds containing benzimidazole-2-thiol core synthesized from alkylation of 2- mercapto benzimidazole under basic conditions using different alkyl halides and aryl halides gave the thioether derivatives [2]. On the other hand, thioesters can be prepared by condensation of carboxylic acids with an alkali metal salt of a thiol in the presence of dehydrating agents. In order to increase the therapeutic properties of mercapto benzimidazole core with a green approach, here we synthetically attached the L-proline as a proteinogenic amino acid with a broad range of biological activity to 2-benzimidazolethiol in EtOH without using any catalyst to form benzo imidazole pyrrolidine carbothioate with a chiral center in excellent yields as shown in **Scheme**. This reaction can be extended to other amino acids and the structural diversity of the product as well as its biological applications can be increased.

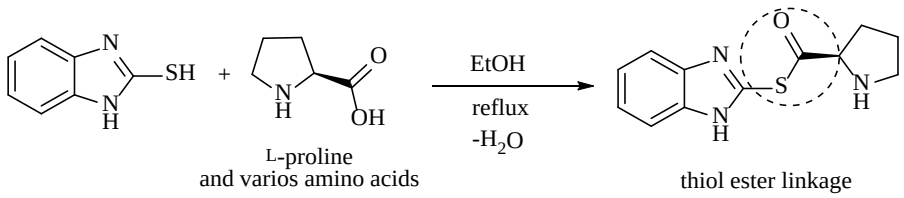

Scheme: Synthetic scheme for the generation of benzo imidazole pyrrolidine carbothioate.

References

[1] Latif, A.; Bibi, S.; Ali, S.; Ammara, A.; Ahmad, M.; Khan, A.; Ali, M. New multitarget directed benzimidazole-2-thiol-based heterocycles as prospective anti-radical and anti-Alzheimer's agents. *Drug Dev. Res.* 2021, *82*, 207-216.

[2] Ahamed, M. R.; Narren, S. F.; Sadiq, A. S. Synthesis of 2-mercaptobenzimidazole and some of its derivatives. *Al-Nahrain J. Sci.* 2013, *16*, 77-83.

Synthetic approach toward thiazolone-fused benzo imidazole scaffold using 2-benzimidazolethiol

Zahra Ashoori, Mohammad Bayat* and Shima Nasri

Department of Chemistry, Faculty of Science, Imam Khomeini International University, Qazvin, Iran, z.ashoori1997@gmail.com, bayat_mo@yahoo.com; m.bayat@sci.ikiu.ac.ir

Keywords: 2-Benzimidazolethiol, Chloroacetic acid, Thiazolone-fused benzo imidazole.

2-Mercaptobenzimidazole is the organosulfur compound derived from benzimidazole with a thiol group in the 2-position. 2-Mercaptobenzimidazole contains a thioamide group (-N-C=S), therefore it is considered one of the thioamide compounds for its ability to react under special conditions to give derivatives having a substituent at either nitrogen or sulfur atoms [1]. The benzimidazole-2-thiol containing compounds are attractive synthetic targets due to their medicinal activity such as antibacterial agents, antibacterial, antifungal agents, potent anticonvulsant, anti-inflammatory/analgesic agents, antimicrobial, anti-inflammatory, and analgesic agents. Some drugs such as Fabomotizole used as potent anxiolytic drugs, and 2-MBI oxadiazoles as antidiabetic agents [2]. With this background of biological activities of mercapto benzimidazole and the necessary need for the formation of molecular architectures with wide potential biological activities, here we designed and introduced a new protocol involving the reaction of the 2-benzimidazolethiol, chloroacetic acid under mild reaction conditions leads to benzo imidazo thiazolone in good yields (Scheme). The direction of heterocyclization and the structure of the final product were identified spectroscopically. In the following, this synthesized intermediate will be used in condensation with various benzaldehydes.

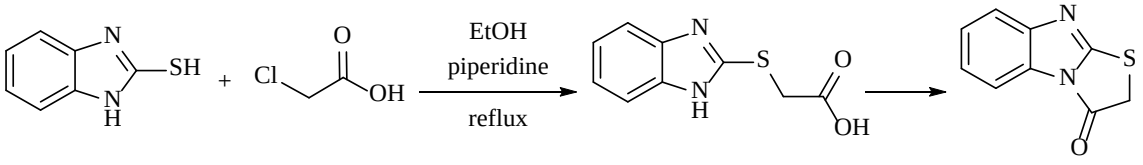

Scheme: Synthetic scheme for the formation of benzo imidazo thiazolone.

References

[1] Al-Rashood, K. A.; Abdel-Aziz, H. A. Thiazolo [3,2-*a*]-benzimidazoles: synthetic strategies, chemical transformations and biological activities. *Molecules* 2010, *15*, 3775-3815.

[2] Coulbali, S.; Zoakouma, R. S. P.; Akpa, S. J.; Say, V. M.; Bamba, F.; Sissouma, D.; Adjou, A. Synthesis of novel thiazolobenzimidazoles. *Int. J. Biol. Chem. Sci.* 2017, *11*, 1320-1335.

Utilizing Biguanide-dihydropyrimidine dual scaffolds in the Design of New Organic Superbases in gas phase

Tayyebeh Koneshlou [a,*], **Morteza Rouhani** [a,*], **Hamid Saeidian** [b,*], **Javad Mokhtari Aliabad** [a]

a) Department of Chemistry, Science and Research Branch, Islamic Azad University, Tehran, Iran, tkoneshlou@gmail.com.
b) Department of Science, Payame Noor University (PNU), P.O. Box: 19395-4697, Tehran, Iran

Keywords: Biguanide, Dihydropyrimidine, Basicity, Aromaticity, DFT

Gas phase basicities (GBs) and proton affinities (PAs) of a new class of uncharged organo-superbases based on biguanide-dihydropyrimidine dual scaffolds with several electron donating groups, were computationally assessed by DFT- B3LYP/6-311+G(d,p) calculations. Two remarkable strategies for superbase designing based on intramolecular hydrogen bonds (IHBs) and aromatization of the unsaturated rings were implemented to obtain structures with high basicity properties. The employed protocol leads to the design of novel super/hyperbases with significant basicity range of 1089.45–1262.69 kJ mol□ 1. To examine aromaticity changes in the unsaturated rings upon protonation, Harmonic Oscillator Model of Aromaticity (HOMA), Harmonic oscillator model of electron delocalization (HOMED) parameters and the nucleus-independent chemical shift (NICS) were utilized.Electrostatic potential maps for all designed structures were further applied for electron density distribution evaluation. Furthermore, Natural Bond Orbital (NBO) method was used to study the nature of the formed IHBs in the structures 1–11. (**Scheme**).

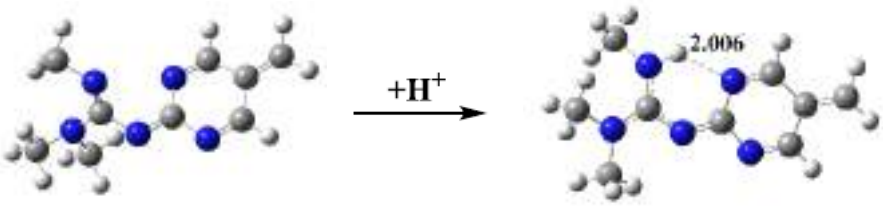

Scheme: Biguanide-dihydropyrimidine synergistic effect for improving basicity strengths via intramolecular hydrogen bonding, heterocyclic aromaticity and electrondonating of substituents.

References

[1] Vazdar, K.; Margetic, D.; Kovacevic, B.; Sundermeyer, J.; Leito, I.; Jahn, U. Design of novel uncharged organic superbases: merging basicity and functionality, *Acc.Chem. Res.* 26 (2021) 3108–3123.1627–1634.
[2] Kulsha, A.V.; Ragoyja, E.G.; Ivashkevich, O.A. Strong bases design: Predicted limits of basicity, *J. Phys. Chem. A* 126 (2022) 3642–3652.
[3] Fortun, S.; Schmitzer, A.R. The chemistry of biguanides: from synthetic routes to applications in organic chemistry, *Can. J. Chem.* 98 (2020) 251–260.
[4] Bachrach, S.M. Chiral superbases with extended hydrogen bond networks, *J. Org.Chem.* 84 (2019) 3467–3476.

Synthesis of 1,2,3-triazolyl-pyridine derivatives through a multicomponent reactions and using a new nano-magnetic catalyst based on urea

Monireh Navazeni,[a] Morteza Torabi,[a] Mohammad Ali Zolfigol,*[a] Ardeshir Khazaei,[a] and Kaveh Khosravi [b]

a) Department of Organic Chemistry, Faculty of Chemistry, Bu-Ali Sina University, Hamedan 6517838683, Iran, monireh.navazani@gmail.com, zolfi@basu.ac.ir & mzolfigol@yahoo.com.
b) Department of Chemistry, Faculty of Science, Arak University, Arak, Zip Code 38156-8-8349, Iran.

Keywords: Urea, 1,2,3-Triazole pyridine, Nano-magnetic catalyst

Herein, we have designed a recyclable, reusable and environmentally friendly urea-containing catalyst which is modified on magnetic nanoparticles surface and can use in the manufacture of valuable chemical compounds. Then, by using this catalyst, a new class of derivatives 1,2,3-triazolyl-pyridine was synthesized in solvent-free conditions. The results showed that this catalyst has a good efficiency in the synthesis of the mentioned compounds due to the dispersion of nanoparticles, and the strong interactions of linker on the nanoparticle surface, as well as the interaction of hydrogen donor species with the compounds present in reactions.

Because of having pyridine ring, substitution containing 1,2,3-triazole and as well as -NH_2 and -CN functional groups in position 2 and 3 [1], the synthesized compounds have properties such as antimicrobial, antitumor, anticancer, antifungal, antibacterial, antiinflammatory, alpha reductase inhibitors, LSD1 inhibitors and alpha glycosidase inhibitors. Therefore, they are widely used as a precursor for the preparation of molecules that have various medicinal and biological applications [2].

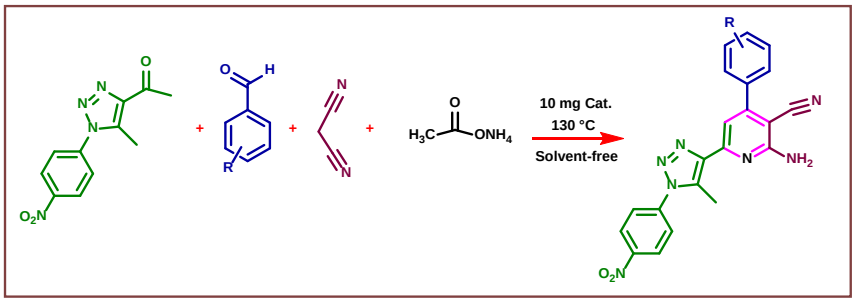

Scheme: Synthesis of 1,2,3-triazole pyridines through a new nano-magnetic catalyst.

References

[1] Troschütz, R., Dennstedt, T. Substituierte 2-Aminonicotinonitrile. *Archiv der Pharmazie*, 1994, 327(2), 85-89.
[2] Rashdan, H. R., Shehadi, I. A., Abdelmonsef, A. H. Synthesis, anticancer evaluation, computer-aided docking studies, and ADMET prediction of 1, 2, 3-triazolyl-pyridine hybrids as human aurora B kinase inhibitors. *ACS Omega*, 2021, 6(2), 1445-1455.

Anderson type hexamolybdate [$CrMo_6O_{18}$] catalyst: Highly efficient for the synthesis of benzothiazoles

Mohadese Zarei and Ali Zarnegaryan*

Department of Chemistry, College of Sciences, Yasouj University, Yasouj, 75918-74831, Iran, mohadesezaree.1998@gmail.com, zarnegaryana@ yu.ac.ir.

Keywords: Polyoxometalate, Benzothiazoles, Anderson

Polyoxometalate (POM) are anionic metal oxide group with different nuclearizes, sizes, and shapes. Their special features can be mentioned such as high thermal stability, excellent redox abilities, high negative charges, and the to form dynamic structures that can have a size from nano to micro-scale. They represent a new class of molecular systems that have applications in nanotechnology, pharmaceuticals, magnetism, materials science, biology, and catalysis. Polyoxometalate (POM) is a group of anionic clusters of transition metal oxides in their highest oxidation state, which are made through bonding by oxygen atoms, to represent metal-oxo units, where the metal ion is a multifaceted building block [1,2]. Benzothiazoles are some of the most effective heterocyclic organic compounds, which are used as valuable intermediates in organic synthesis. Benzothiazoles derivatives were synthesized from the condensation of aldehydes and 1,2-phenylenediamine with aromatic aldehydes under oxidative or strongly acidic conditions [3]. Herein, we report the design of a $[N(C_4H_9)_4]_2[[Cr\ Mo_6O_{18}(OH)_3]$ The catalytic efficiencies in the catalytic properties and stabilities of the synthesized catalyst in the preparation of various benzothiazoles were also investigated **(Scheme**)

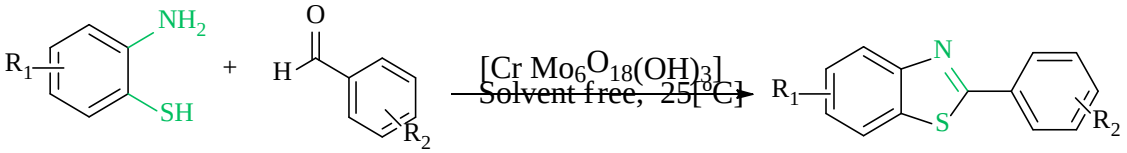

Scheme: Synthesis of benzothiazoles catalyzed by [$CrMo_6O_{18}$]

References

[1] Wu, P.; Wang, Y.; Huang, B.; Xiao, Z. Anderson-type polyoxometalates: from structures to functions. *Nanoscale.* 2021, *13*, 7119-7133.
[2] Ogiwara, N.; Iwano, T.; Ito, T.; Uchida, S. Proton conduction in ionic crystals based on polyoxometalates. *Coord. Chem. Rev.* 2022, *462*, 214524.
[3] Weinstock, I. A.; Schreiber, R. E.; Neumann, R. Dioxygen in polyoxometalate mediated reactions. *Chem. Rev.* 2017, *118*, 2680-2717.

Developing the novel fluorescent chemosensor based on the carbazole derivatives

Nasrin Dehghani, Ghodsi Mohammadi Ziarani *

Department of Organic Chemistry, Faculty of Chemistry, Alzahra University, Tehran, Iran, nasrin_deh65@yahoo.com,gmohammadi@alzahra.ac.ir.

Keywords: Chemosensor, Organic synthesis, Fluorescent activity, Carbazole

Identification of the metal ions is very important in various sciences including the biological and industrial sciences. Thus, it is necessary to investigate trustworthy and simple techniques to identify and remove the heavy metal ions from the aqueous solutions to preserve the water resources [1]. Recently, fluorescence probes have attracted a lot of attention due to their sensitivity, high selectivity, cost-effective, fast response, large dynamic concentration range, noninversion, and simplicity in identification of the metal ions [2]. In the present study, the efficient synthesis of carbazole derivatives through Vilsmeier–Haack reaction was reported (Scheme 1). The fluorescence properties of 9H-Carbazole-9-carbazole derivative were investigated in the presence of various cations and anions. The results showed that the designed selective fluorescent can be used as the new chemical sensor probe with high sensitivity and selectivity to identify and isolating the ions. The competitive test of the synthesized compound in the presence of various ions proved the high selectivity and also the specific fluorescence for the desired ions.

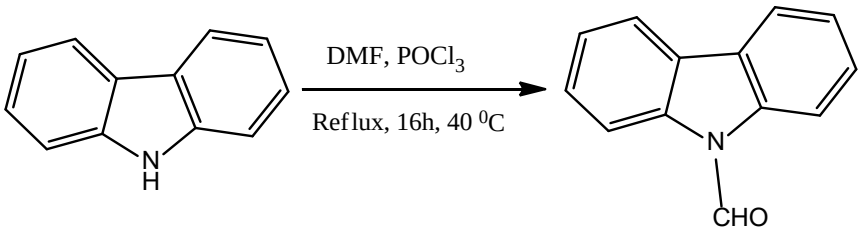

Scheme: The synthesis of 9H-Carbazole-9-carbaldehyde.

References

[1] Kadam, A. N., Moniruzzaman, M., & Lee, S. W. Dual functional S-doped g-C3N4 pinhole porous nanosheets for selective fluorescence sensing of Ag+ and visible-light photocatalysis of dyes. *Molecules* 2019, 24(3), 450.

[2] Lin, D. S.; Lai, J. P.; Sun, H.; Yang, Z.; and Zuo, Y. A turn-on fluorescein spirolactam derivative as a high selective fluorescence probe for detection of silver ion (I) in water, *Anal. Methods* 2014, 6, 1517.

Synthesis of new Schiff bases based on 5-(imidazol-1-yl)salicylaldehyde and their metal complexes

Zarrin Ghasemi*, Mahsa Hadian and Somayeh Rashtabadi

Department of Organic Chemistry and Biochemistry, Faculty of Chemistry, University of Tabriz, Tabriz, Iran, z.ghasemi@tabrizu.ac.ir, mahsahadian45@gmail.com

Keywords: Metal complexes of Schiff bases, Tetraarylimidazole, Duff reaction

The metal complexes of Schiff bases have attracted a lot of attention in the scientific community due to their unique properties and comprehensive applications in various fields of industry and biology [1]. On the other hand, organic materials with high π-conjugation and resonance often show interesting and valuable optical and electrochemical properties [2]. In this research work, we first prepared phenolic derivatives containing tetraarylimidazole moiety by using multi-component reaction and then synthesize the corresponding salicylaldehyde derivatives by Duff reaction (**Scheme1**). In the next step, these products were converted into the corresponding Schiff bases during the condensation reaction with primary aromatic or aliphatic amines that accompanied with the removal of water during the condensation process. In order to synthesis metal complexes, we then treated these Schiff base derivatives with transition metal salts [3]. The structure of all products was established by analytical and spectroscopy methods.

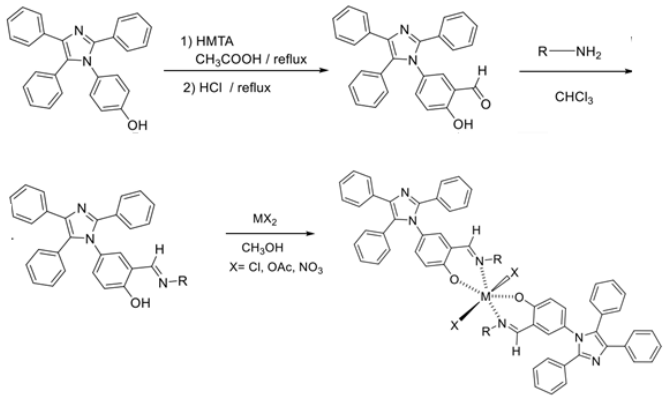

Scheme1: Synthesis of novel Schiff base complexes

References

[1] Arulmurugan, S.; Kavitha, H. P.; Venkatraman, B., Biological activities of Schiff base and its complexes: a review. *Rasayan. J. Chem*. 2010, 3 (3), 385-410.

[2] Hashem, H. E.; Mohamed, E. A.; Farag, A. A.; Negm, N. A.; Azmy, E. A., New heterocyclic Schiff base-metal complex: Synthesis, characterization, density functional theory study, and antimicrobial evaluation. *Appl. Organomet. Chem.* 2021, 35 (9), e6322.

[3] Alkış, M. E.; Buldurun, K.; Turan, N.; Alan, Y.; Yılmaz, Ü. K.; Mantarcı, A., Synthesis, characterization, antiproliferative of pyrimidine based ligand and its Ni (II) and Pd (II) complexes and effectiveness of electroporation. *J. Biomol. Struct. Dyn.* 2022, 40 (9), 4073-4083.

Highly efficient oxidation of aldehydes to carboxylic acids using an Anderson type polyoxometalate

Mohadese Zarei and Ali Zarnegaryan*

Department of Chemistry, College of Sciences, Yasouj University, Yasouj, 75918-74831, Iran, zarnegaryana@ yu.ac.ir.

Keywords: Carboxylic acids, Polyoxometalate, oxidation of aldehydes

The oxidation of aldehydes to produce carboxylic acids is an important transformation in the chemical industry. Aldehydes are widely used as intermediates for the production of perfumes, agrochemicals, cosmetics, and pharmaceuticals. As part of the growing tendency towards green chemistry, current research in this area has focused on the development of environmentally benign catalytic processes involving the use hydrogen peroxide or molecular oxygen as an oxidant. Work towards the use of H_2O_2 assisted methods, in particular, has attracted considerable interest because this oxidant is providing a high active oxygen content, generates water as its sole byproduct, and readily available [1].

Polyoxometalates (POMs) have attracted much attention in the fields of acid and oxidation catalysis, because their acidic and redox properties can be designed and tuned at molecular or atomic level. However, the Anderson-type POMs are not well known as catalysts. Anderson-type heteropolyanions ($[YM_6O_{24}H^x]^{n-}$) possess a heteroatom (Y) in a central octahedral cavity of the crown by edge-sharing six octahedral MO_6 (M = Mo or W) These polyanions become a family for a number of 2+, 3+, 4+, 6+ and 7+ ions as the heteroatom. They are classified into types of A (x = 0) and B (x = 6) by the number of attached protons [2,3]. Herein, we report the design of a $[N(C_4H_9)_4]_2[[Cr\ Mo_6O_{18}(OH)_3]$ the catalytic efficiencies in the catalytic properties and stabilities of the synthesized catalyst in the preparation of various carboxylic acids were also investigated **(**Scheme 1).

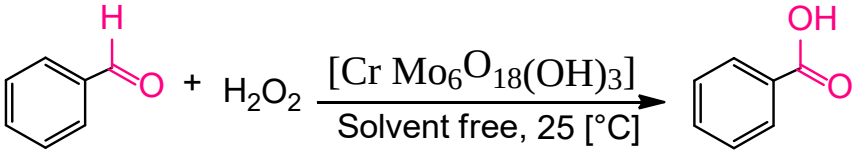

Scheme 1: Synthesis of of carboxylic acids catalyzed by $[CrMo_6O_{18}]$

References

[1] Li, J.; Huang, C. Y.; Li, C. J. Deoxygenative functionalizations of aldehydes, ketones and carboxylic acids. *Angew. Chem. Int. Ed. Engl.* 2022, *134*, e202112770.

[2] Nomiya, K.; Takahashi, T.; Shirai, T.; Miwa, M. Anderson-type heteropolyanions of molybdenum (VI) and tungsten (VI). *Polyhedron* 1987, *6*, 213-218.

[3] Lü, H.; Zhang, Y.; Jiang, Z.; Li, C. Aerobic oxidative desulfurization of benzothiophene, dibenzothiophene and 4, 6-dimethyldibenzothiophene using an Anderson-type catalyst [(C 18 H 37) 2 N (CH 3) 2] 5 [IMo 6 O 24]. *Green Chem.* 2010, *12*, 1954-1958.

Synthesis of new conjugated derivatives of dihydro-indenopyrrole and study of their reduction reactions

Zarrin Ghasemi*, Maedeh Zolfalizadeh and Forough Nasuhipur

Department of Organic Chemistry and Biochemistry, Faculty of Chemistry, University of Tabriz, Tabriz, Iran, z.ghasemi@tabrizu.ac.ir, maedezolfalizade@gmail.com

Keywords: Three-component reactions, Dihydroxy-indenopyrrole, Fluorescence emission

Conjugated polycyclic aromatic substances have always attracted the attention of many scientists, mainly due to their applications as light-emitting diodes (OLED), their electrochemical activities and their applications in solar cells. The electron-rich planar rings can also bind to numerous biomolecules through π-π interactions. Indenopyrroles are among the most important heterocyclic compounds which are mainly found in natural and synthetic organic compounds and have biological activities as protein kinase inhibitors. In this work, we report the three-component reactions between 1-aminopyren (or 1-aminonaphthalene), a 1,3-dicarbonyl and ninhydrin to synthesize new derivatives of dihydroxy-indenopyrrole (**Scheme 1**). The obtained products were then treated with $POCl_3$ in DMF which led to dehydroxylation (removal of vicinal OH groups), as well as chlorination (at 2-methyl position) to give the corresponding 2-chloromethyl-indenopyrrole derivatives. Thermal hydrolysis of the benzylic chlorides resulted in the final 2-hydroxymethyl substituted products. All the synthesized molecules were characterized by spectroscopy methods and studied in view of emission properties.

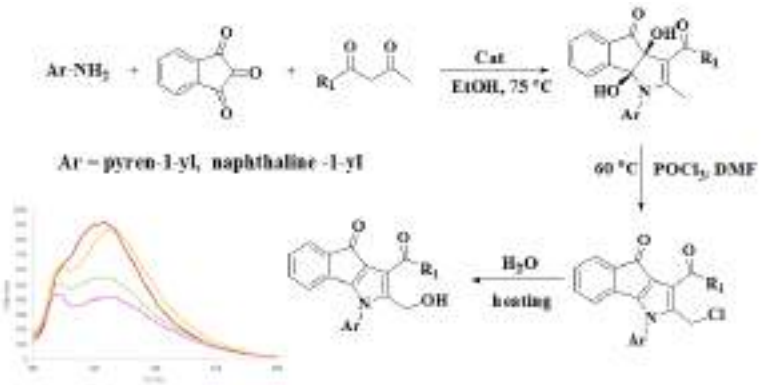

Scheme 1: Synthesis of new conjugated derivatives of dihydro-indenopyrrole

References

[1] Islam, M. M.; Hu, Z.; Wang, Q.; Redshaw, C.; Feng, X., Pyrene-based aggregation-induced emission luminogens and their applications. *Mater. Chem. Front.* **2019,** *3* (5), 762-781.

[2] Kumar, M.; Padmini, V.; Bhuvanesh, N., Stereo-selective green protocol for the synthesis of highly substituted 1-phenyl-tetrahydro indeno [1, 2-b] pyrroles. *Res. Chem. Intermed.* **2017,** *43*, 4517-4530.

[3] Pathak, S.; Kundu, A.; Pramanik, A., Facile synthesis of substituted pyrrole-fused isocoumarins from ninhydrin. *Tetrahedron lett.* **2011,** *52* (40), 5180-5183.

One-pot two-step synthesis of novel 4-substitiuted tetrazolo[1,5-a]quinoline derivatives *via* a sequential Ugi-4CR– nucleophilic substitution and intramolecular cyclization reaction

Mostafa Kiamehr *, **Zahra Fahimi**

Department of Chemistry, Faculty of Science, University of Qom, Ghadir Blvd, P.O. Box 37146-6611, Qom, Iran, mkiamehr@yahoo.com, m.kiamehr@qom.ac.ir, z.fahimi1997@gmail.com

Keywords: Quinoline derivatives, Ugi reaction, Nucleophilic addition, Intramolecular cyclization, 2-Chloro-3-formylquinoline

Multi-component reactions (MCRs) are powerful synthetic tools, in which more than two starting materials react with each other to form multi-functionalized compounds in a one-pot procedure. Nowadays, MCRs are an exceptional strategy to synthesize many pharmaceutical and drug-like structure compounds due to their atom economy, high efficiency, low cost and simple experimental procedure. One of the most important subsets of this group of reactions is the Ugi reaction, that become increasingly efficient in the synthesis of many natural products and macro-cyclic molecules [1]. Due to the increasing application of heterocyclic compounds, especially quinoline derivatives and compounds containing tetrazole ring [2], in this research, new derivatives of these compounds have been synthesized *via* one- pot two-step reactions with high efficiency (**Scheme 1**).

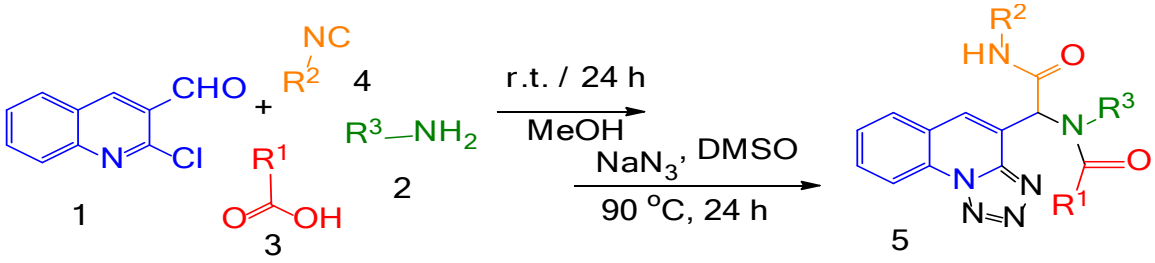

Scheme 1. One-pot two-step synthesis of novel quinoline derivatives.

References

[1] Balalaie, S.; Vaezghaemi, A.; Zarezadeh, N.; Rominger, F.; Bijanzadeh, H. R. Catalyst-Free Synthesis of Fused Triazolo-Diazepino[5,6-b]Quinoline Derivatives via a Sequential Ugi-4CR–Nucleophilic Substitution–Intramolecular Click Reaction. *Synlett* 2018; *29*(08): 1095-1101.

[2] Mirzaei, S.; Hadizadeh, F.; Eisvand, F.; Mosaffa, F.; Ghodsi, R. Synthesis, structure-activity relationship and molecular docking studies of novel quinoline-chalcone hybrids as potential anticancer agents and tubulin inhibitors, *J. Mol. Struct.*, 2020, *1202*, 127310.

Comprehensive DFT calculations on Salvigenin, Eupatorin and Cirsilol

Zahra Inanloo, Hamid Saeidian*, Abbas Maleki, Niloufar Bahramipanah

Department of Science, Payame Noor University (PNU), P.O. Box: 19395-3697, Tehran, Iran, inanlo.za@gmail.com, Saeidian1980@pnu.ac.ir

Keywords: Density functional theory, antioxidant, flavonoid, bond dissociation enthalpy

Salvigenin (Sal), Eupatorin (Eup) and Cirsilol (Cir) are methoxylated flavonoids extracted from various natural sources and have high biological properties. Structural, electronic and spectral data of these three compounds were obtained using B3LYP/6-31G+(d,p) calculation method. Further, their antioxidant activity was investigated with two mechanisms of hydrogen atom transfer (HAT) and single electron transfer then proton transfer (SET-PT) in the gas phase. The results show that these flavones have acceptable antioxidant properties. The presence of two methoxy electron-donating groups on ring A in all three flavones makes its antioxidant properties higher than phenol through the SET-PT mechanism. The results show that these flavones have acceptable antioxidant properties. The presence of two methoxy electron-donating groups on ring A in all three flavones makes its antioxidant properties higher than phenol through the SET-PT mechanism. Among these flavones, the antioxidant activity of Cir is higher than the others. Examining the reactivity of the studied compounds with oxygen radicals shows that the possible reaction to remove the hydrogen radical from these flavones will occur by OH˙ and OOH˙ and the compound Cir is more active than Sal and Eup [1, 2].

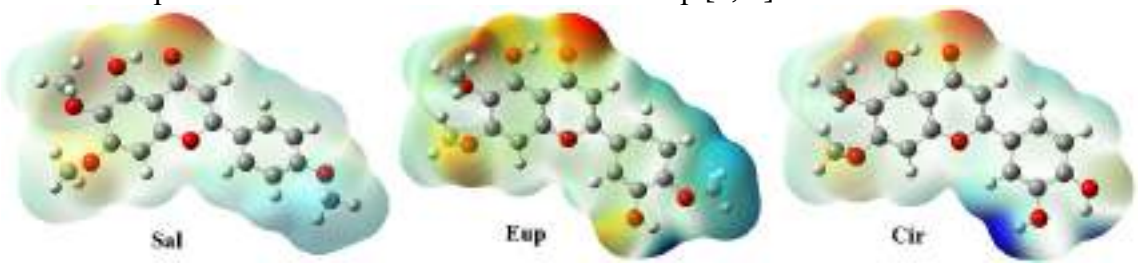

Fig. 1. The molecular electrostatic potential of methoxylated flavones, Sal, Eup and Cir.

References

[1] Khademloo, E.; Kadhodaeian, H. A.; Jameie, S. B.; Farhadi, M. Saeidian, H. A detailed density functional theory investigation on physicochemical properties of ciclopirox derivatives: A potential candidate for prevention of age-related macular degeneration. *J. Mol. Struct*. **2022**, *1268*, 133678.

[2] Jalezadeh, A.; Mirjafary, Z.; Rouhani, M.; Saeidian, H. Investigation of structural, electronic, and antioxidant properties of calycopetrin and xanthomicrol as two polymethoxylated flavones using DFT calculations. *Struct. Chem*. **2022**, *33*, 1241.

Synthesis of 1,4-dihydropyridine by magnetic nanoparticles ($NiFe_2o_4$) as a catalyst

Tannaz Mahmoudi, Seyyed Hojjat Sadeghi, Zahra Karbalaie and Sadegh Rostamnia*

Organic and Nano Group (ONG), Department of Chemistry, Iran University of Science and Technology (IUST), Tehran, Iran, tanaz.mahmoudi@gmail.com

Keywords: Magnetic nanoparticles, 1,4-dihydropyridine, Nickel ferrite"

One of the key components of chemical reactions is catalysis, which provides selectivity, a high yield of the products, and faster reaction rates. The use of magnetic nanoparticles (MNPs) of transition metal oxides as solid supports has recently received a lot of research attention. They are simple to make and good candidates to immobilize a variety of homogeneous catalysts due to the extreme surface area of nanoparticles, stability, magnetic characteristics, and inherent electronic impact of transition metal elements. The use of cubic spinel nickel ferrite ($NiFe_2O_4$) has been researched in this area. For simple separation from the reaction mixture, this magnetic material's excellent heat stability (up to 900 ˚C) and superparamagnetic properties are advantageous [1].

DHPs, or 1,4-dihydropyridine derivatives, are present in a wide variety of pharmacological substances. Due to their many therapeutic and medical properties, these chemicals have attracted a lot of interest. These are medicines that can be used to protect the liver and dilate blood vessels. The DHPs also function as anti-aging, anti-tumor, anti-asthma, and anti-diabetic medications. As a result, many different techniques have been described for the synthesis of 1,4-dihydropyridine derivatives up to this point [2] (**Scheme**).

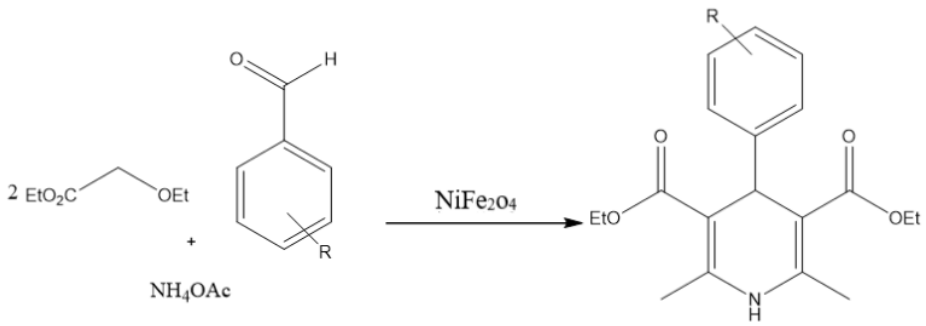

Scheme: Synthesis of 1,4-dihydropyridine by magnetic nanoparticles (NiFe2o4).

References

[1] Zeynizadeh, B.; Rahmani, S.; Eghbali, E. Anchored Sulfonic Acid on Silica-Layered NiFe2O4: A Magnetically Reusable Nanocatalyst for Hantzsch Synthesis of 1, 4-Dihydropyridines. *Polyhedron* 2019, *168*, 57–66.

[2] Kamalzare, P.; Mirza, B.; Soleimani-Amiri, S. Chitosan Magnetic Nanocomposite: A Magnetically Reusable Nanocatalyst for Green Synthesis of Hantzsch 1, 4-Dihydropyridines under Solvent-Free Conditions. *J. Nanostructure Chem.* 2021, *11*, 229–243.

Synthesis of Amido alkyl derivatives in the presence of magnetic nickel ferrite nanoparticles as a catalyst under solvent-free

Tannaz Mahmoudi, Seyyed Hojjat Sadeghi, Zahra Karbalaie and Sadegh Rostamnia*

Organic and Nano Group (ONG), Department of Chemistry, Iran University of Science and Technology (IUST), Tehran, Iran, tanaz.mahmoudi@gmail.com

Keywords: Magnetic nanoparticles, Amido alkyl derivatives, Nanocatalysts"

The Amido alkyl derivatives have a range of biological activities, including antiviral, antibacterial, antifungal, and antiparasitic effects. Besides possessing intriguing features, amido alkyl derivatives are useful raw materials for creating other bioactive compounds. These substances can be employed as ligands for chelation with organometallic reagents during synthesis and asymmetric catalysis [1]. The development of novel techniques for amido alkyl production is of great synthetic significance given these advantageous features [1,2].

As a new class of nanocatalysts for organic reactions, magnetic nanoparticles ($NiFe_2O_4$) exist. The ability to separate these nanocatalysts with just an external magnet and no filtration is crucial to these catalysts [2]. Most importantly, the MNPs-supported catalysts exhibit excellent levels of chemical stability and do not swell in organic solvents in addition to good catalytic activity. With the aid of an external magnetic field, MNPs-supported nanocatalysts can be restored, and even after numerous repetitions of reactions, their catalytic activity endures [2,3] (**Scheme**).

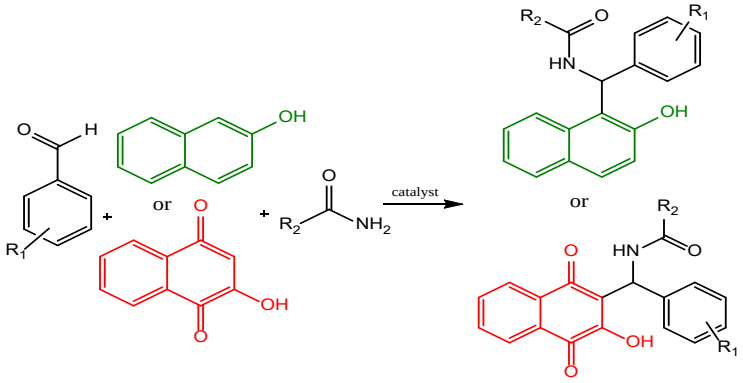

Scheme: Synthesis of amidoalkyl derivatives in the presence of $NiFe_2O_4$.

References

[1] Petkov, H.; Simeonov, S. P. Amidoalkyl Naphthols as Important Bioactive Substances and Building Blocks: A Review on the Current Catalytic Mannich-Type Synthetic Approaches. *Appl. Sci.* 2023, *13* (11), 6616.

[2] Safari, J.; Zarnegar, Z. Synthesis of Amidoalkyl Naphthols by Nano-Fe3O4 Modified Carbon Nanotubes via a Multicomponent Strategy in the Presence of Microwaves. *J. Ind. Eng. Chem.* 2014, *20* (4), 2292–2297.

[3] Maleki, B.; Sheikh, E.; Seresht, E. R.; Eshghi, H.; Ashrafi, S. S.; Khojastehnezhad, A.; Veisi, H. One-Pot Synthesis of 1-Amidoalkyl-2-Naphthols Catalyzed by Polyphosphoric Acid Supported on Silica-Coated NiFe2O4 Nanoaparticles. *Org. Prep. Proced. Int.* 2016, *48* (1), 37–44.

In-situ synthesizing antibacterial Ag-MOF within the bio-polymer hydrogel film: A potential platform for wound dressing

Amin Hashemi Aghdam, Siamak Javanbakht and Reza Mohammadi*

Polymer Research Laboratory, Faculty of Chemistry, University of Tabriz, Tabriz, Iran, amin.hastam141@gmail.com, r.mohammadi@tabrizu.ac.ir

Keywords: Antibacterial, Wound dressing, Hydrogel film

In the history of modern medicine, there has been a serious risk of antibacterial drugs as losing their effectiveness against bacteria [1]. In this regard, nanocomposite hydrogel films based on natural polymers such as cellulose have been recently proposed as antibacterial platform[2]. In this work, antibacterial Ag-based metal-organic framework (Ag@NH_2-BDC) were developed to increase the biological efficiency of cellulose hydrogel films. Also NH2-BDC ligands were synthesized in the lab, various analysis methods were utilized for the validation of successful formation of the nanocomposites such as EDX, Mapping, SEM, AFM and etc. Antibacterial studies showed inhibition zone of 17 ± 0.5 mm for the *Staphylococcus aureus* bacteria, respectively. Considering obtained results, the prepared nanocomposite hydrogel films have good potential to be employed as antibacterial bio-platform.

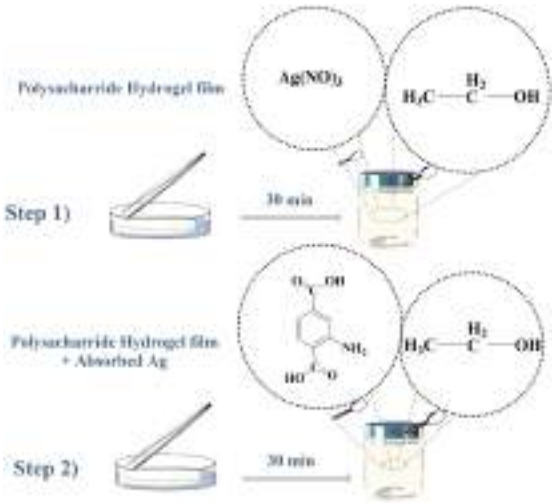

Scheme: Preparation of Ag@NH_2-BDC nanocomposite hydrogel film.

References

[1] Levy, S. B.; Marshall, B. Antibacterial resistance worldwide: causes, challenges and responses. *Nat. Med.* 2004, *10* (Suppl 12), S122-S129.

[2] Zheng, L.; Li, S.; Luo, J.; Wang, X. Latest advances on bacterial cellulose-based antibacterial materials as wound dressings. *Front. Bioeng. Biotechnol.* 2020, *8*, 593768.

Zif-8/Polysaccharide nanocomposite hydrogel films as a potential platform for wound dressing

Amin Hashemi Aghdam, Hanieh Hamedi Haghi, Siamak Javanbakht and Reza Mohammadi*

Polymer Research Laboratory, Faculty of Chemistry, University of Tabriz, Tabriz, Iran, amin.hastam141@gmail.com, r.mohammadi@tabrizu.ac.ir

Keywords: Antibacterial, Wound dressing, Hydrogel film

In the history of modern medicine, there has been a serious risk of antibacterial drugs as losing their effectiveness against bacteria [1]. In this regard, nanocomposite hydrogel films based on natural polymers have been recently proposed as antibacterial platform [2]. In this work, antibacterial metal-organic frameworks were developed to increase the biological efficiency of the hydrogel films. Various analysis techniques were utilized for the validation of successful construction of the nanocomposites. Antibacterial studies showed inhibition zone of 14 ± 0.5 mm for the *Staphylococcus aureus* bacteria, respectively. Considering obtained results, the prepared nanocomposite hydrogel films have good potential to be employed as antibacterial bio-platform.

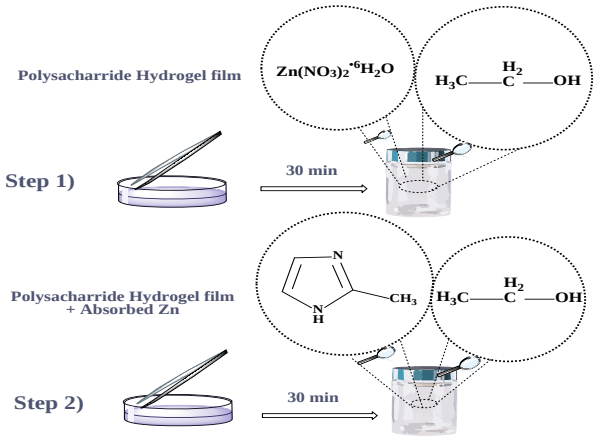

Scheme: Preparation of Zif-8/Polysaccharide nanocomposite hydrogel film.

References

[1] Ang, J. Y.; Ezike, E.; Asmar, B. I. Antibacterial resistance. IJP 2004, 71, 229-239.
[2] Zhang, X.; Qin, M.; Xu, M.; Miao, F.; Merzougui, C.; Zhang, X.; Wei, Y.; Chen, W.; Huang, D. The fabrication of antibacterial hydrogels for wound healing. *Eur. Polym. J.* 2021, *146*, 110268.

A Challenge on The Zeeman's Effect in Chemistry

Mostafa Gholizadeh*

Department of Chemistry, Faculty of Science, Ferdowsi University of Mashhad, Mashhad, I.R. of Iran, m_gholizadeh@um.ac.ir

Keywords: Magnetic effect, Magnetized solvent, Criticizing of Zeeman Effect, Magnetizing device

The present article reviewed the areas which Solvents Magnetizing Apparatus (SMA) have been applied, including chemistry, concrete, brick, agriculture, livestock and poultry, extraction of oil and its derivatives, automobile industries, and medicine. More information in all the above areas brought from the experiments of the author and taken from more than twenty years experiment on the magnetized solvents. The control of the condition has been investigated by the US-patent device (*US20180117562A1*), which invented in different sizes of micro, mid macro and macro by author. In addition, Zeeman effect was criticized for the first time in the way that solvents are able to keep and transfer the properties obtained from the magnetic source not just under magnetic source, but after passing from the magnetic source and these properties even remained after exposing high temperature and days. The last claim has resulted in the experiments carried out in all the mentioned areas. The main conclusions abstracted from the paper, are that magnetized solvents can include polar and non-polar solvents and it is not limited to just water. Furthermore, as a critique on the Zeeman Effect, the properties obtained from the magnetic source can retain and transfer after days and even exposing high temperature.

Scheme: Solvent Magnetizing Apparatus (SMA).

References:

[1] Eshaghi, Z. & Gholizadeh, M. The effect of magnetic field on the stability of (18-crown-6) complexes with potassium ion. *Talanta* **64**, 558–561 (2004).

[2] Afshin, H., Gholizadeh, M. & Khorshidi, N. Improving Mechanical Properties of High Strength Concrete by Magnetic Water Technology. *Trans. A Civ. Eng.* **17**, 74–79 (2010).

FDU-12@AGA-Pd: A novel, green, recyclable, and highly versatile catalyst for C-C bond formation and synthesis of 1H-tetrazoles derivatives

Hamid Aghavandi, Arash Ghorbani-Choghamarani*

Department of Organic Chemistry, Faculty of Chemistry, Bu-Ali Sina University, Hamedan, 6517838683, Iran, hamidaghavandichemist@gmail.com

Keywords: 1H-Tetrazole; FDU-12, Green, Nano, Catalyst.

In this work, a novel and efficient nanocatalyst through the immobilization of AGA-Pd onto the inside of mesoporous silica FDU-12 channels was successfully synthesized by a simple procedure. The catalytic activity of the described catalyst was investigated for the synthesis of the Suzuki reaction and 1H-tetrazole derivatives. In this research, the catalyst was prepared by the immobilization of Palladium on ordered mesoporous silica (FDU-12) coated with 2-Amino-5-guanidinovaleric acid (AGA). N2 adsorption-desorption isotherms indicated excellent BET surface area for FDU-12 and FDU-12@AGA-Pd is 627.27 and 106.69 (m2 /g) respectively. The physical and chemical properties of raw and modified samples (FDU-12, FDU-12@AGA-Pd) were characterized by TGA, EDX, BET, XRD, ICP, Map, and Fourier-transform infrared spectroscopy (FT-IR) analyses. This designed nanocatalyst offers several advantages including the use of inexpensive materials and commercially available, high yield, short reaction times, and simple procedure. The synthesized mesoporous nanocatalyst was recovered and reused in five continuous cycles without considerable change in its catalytic activity[1].

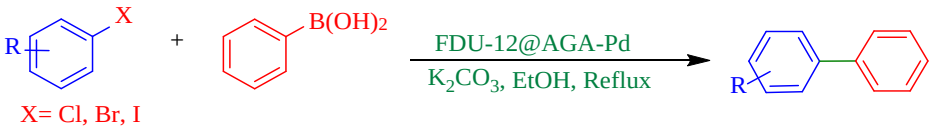

Scheme 1. Synthesis of Suzuki C-C cross-coupling catalyzed by FDU-12@AGA-Pd**.**

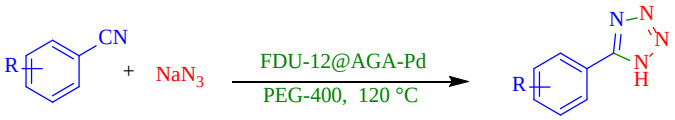

Scheme 2. Synthesis of 1H-tetrazole catalyzed by FDU-12@AGA-Pd**.**

References

[1] Khanmohammadi-Sarabi, F.; Ghorbani-Choghamarani, A.; Aghavandi, H.; Zolfigol, M. A. ZnFe2O4@SiO2-Ascorbic Acid: Green, Magnetic, and Versatile Catalyst for the Synthesis of Chromeno[2,3-d] Pyrimidine-8-Amine and Quinazoline Derivatives. *Appl. Organomet. Chem. n/a* (n/a). https://doi.org/https://doi.org/10.1002/aoc.6768.

FDU-12@n-Pr@PTD-Ni: green, novel and efficient catalysts for the synthesis of chromeno and amide derivatives

Hamid Aghavandi, Arash Ghorbani-Choghamarani*

Department of Organic Chemistry, Faculty of Chemistry, Bu-Ali Sina University, Hamedan, 6517838683, Iran, hamidaghavandichemist@gmail.com

Keywords: Chromeno; FDU-12, Green, Novel, Catalyst

The development of a highly efficient and green catalyst for the one-pot synthesis of chromeno and amides derivatives is an extremely important and ground challenging area in organic chemistry. In this study, the catalyst was prepared by the immobilization of Ni on ordered mesoporous silica (FDU-12) coated with 6-phenyl-1,3,5-triazine-2,4-diamine (PTD). The proposed catalysts were characterized by FT-IR, XRD, BET, TGA, EDX, and ICP studies and were successfully applied in the synthesis of chromeno and amide derivatives. This designed protocol offers several advantages including the use of commercially available and inexpensive materials, simple procedure, short reaction times, high yield, and easily separable and reusable catalyst [1].

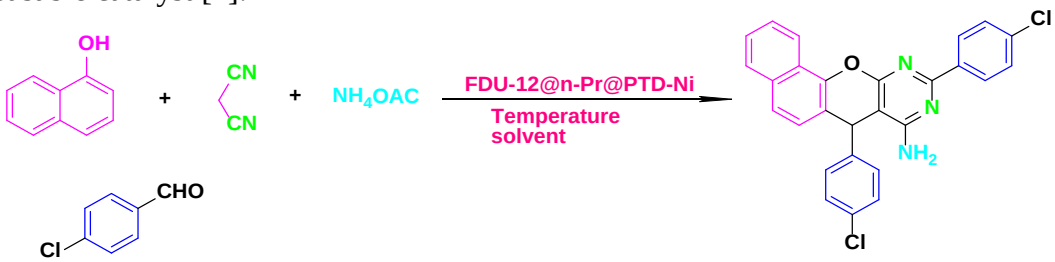

Scheme 1. Synthesis of chromeno catalyzed by FDU-12@n-Pr@PTD-Ni.

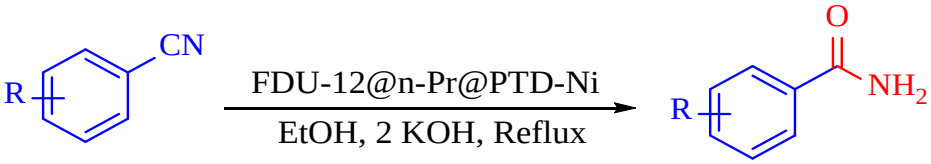

Scheme 2 Synthesis of amide catalyzed by FDU-12@n-Pr@PTD-Ni.

References

[1] Khanmohammadi-Sarabi, F.; Ghorbani-Choghamarani, A.; Aghavandi, H.; Zolfigol, M. A. ZnFe2O4@SiO2-Ascorbic Acid: Green, Magnetic, and Versatile Catalyst for the Synthesis of Chromeno[2,3-d] Pyrimidine-8-Amine and Quinazoline Derivatives. *Appl. Organomet. Chem. n/a* (n/a). https://doi.org/https://doi.org/10.1002/aoc.6768.

Palladium nanoparticles stabilized on the amino acids-functionalized Fe_3O_4 as the magnetically recoverable nanocatalysts for Suzuki reactions

Mahtab Naeim, Mohsen Sayadi, Ali Naghipour*

Department of Chemistry, Faculty of Science, Ilam University, Ilam, Iran, naeim.mahtab@gmail.com

Keywords: Magnetic nanocatalyst, C -C coupling reaction, Recyclable catalysts, Glutathione

Palladium is one of the most crucial metals in catalysis and it has been commonly applied as one of the most powerful tools for the formation of the carbon–carbon bond in organic synthesis [1]. Therefore, Palladium- catalyzed C-C cross coupling reactions, especially the Suzuki and Heck reactions (coupling of aryl halides with arylboronic acids and alkenes, respectively) have played a crucial role in the chemical industries and researches [2]. In recent years, among the various magnetic nanoparticles, Fe_3O_4 MNPs have been extensively emerged as efficient inorganic supports for stabilizing of homogeneous catalysts because of their unique properties such as easy preparation and functionalization, having a high surface area, good stability, as well as low toxicity and cost, and easy availability [3]. Taking advantage of multiple-functional groups in molecule, glutathione was usually used as reducing agent to synthesize metal nanoparticle with ultra-small diameter [4]. In this study, two amino acids, aspartic acid and glutathione, were used. Based on the aforementioned remarks, herein, we have illustrated the synthesis of efficient and reusable heterogeneous catalysts based on Pd nanoparticles supported on magnetic Fe_3O_4 nanoparticles which are functionalized by glutathione and aspartic acid. These new nanocomposites have been investigated as the magnetically separable and recyclable catalysts for Suzuki reactions.

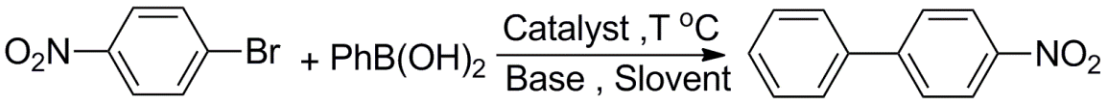

Scheme: Schematic of suzuki reaction of aryl iodides/bromides and chlorides catalyzed by Fe_3O_4@aspartic acid-Pd and Fe_3O_4@glutathione-Pd.

References

[1] B. Zhou, H. Wang, Z. Cao, J. Zhu, R. Liang, X. Hong, Y. Jia. Dearomative 1,4-difunctionalization of naphthalenes via palladium-catalyzed tandem Heck/Suzuki coupling reaction. *Nature.com*. 2020, 11, 4380.

[2] L. Xue, Z. Lin. Theoretical aspects of palladium-catalysed carbon–carbon cross-coupling reactions. *Chem. Soc. Rev*. 2010, 39, 1692–1705.

[3] G. Herve, G. Sartori, G. Enderlin, G. Mackenzie, C. Len. Palladium-catalyzed Suzuki reaction in aqueous solvents applied to unprotected nucleosides and nucleotides. *RSC Adv*, 2014, 4, 18558–18594.

[4] Y. Wang, J. Luo, Z. Liu. Synthesis, characterization and cytotoxicity of Pt(II), Pd(II), Cu(II) and Zn(II) complexes with 4'-substituted terpyridine. *Appl. Organometal. Chem*, 2013, 27, 601–605.

[60]Fullerene-Based Pd(0) complexes of phosphorus ylide as efficient heterogeneous nano-catalyst for Suzuki reaction

Mohsen Sayadi [a*] **and Mahtab Naeim** [b]

a) Department of Chemistry, Faculty of Chemistry, Bu-Ali Sina University, Hamedan, Iran, Sayadim80@yahoo.com
b) Department of Chemistry, Faculty of Science, Ilam University, Ilam, 69315-516, Iran

Keywords: Pd-[60]fullerene complexes, Phosphorus ylides, Suzuki reaction, Synthesis

In the recent years, functionalization of fullerenes C_{60} and investigation of their new properties, in particular biological, catalytic and reactivity studies of these compounds have attracted the attention of academic researchers [1]. During the last three decades, different palladium-fullerene complexes have been developed extensively as efficient nano-catalysts for a variety of reactions due to their unique nanostructures and higher surface area than traditional Pd-based catalysts [2–3]. This work reports the synthesis and catalytic properties of new mono- and bidentate Pd(0)-[60] fullerene complexes, prepared by reaction of α-keto stabilized phosphorus ylides $[Ph_2P(CH_2)_nPPh_2C(H)C(O)C_6H_4\text{-}m\text{-}OMe]$ (n=1, (**Y**^{1}); n=2, (**Y**^{2})) C60 and $Pd(dba)_2$ (dibenzylideneacetone(dba)). The synthesized complexes exhibit different structures, including P,C-chelated $[(\eta^2\text{-}C_{60})Pd(\kappa^2\text{-}Y^1)]$ (**1**) and P-coordinated $[(\eta^2\text{-}C_{60})Pd(Y^2)_2]$ (**2**) complexes. These complexes have been fully characterized by spectroscopic methods and other conventional techniques such as IR, UV-Vis, SEM and TEM analyses. Also, a comparison between the catalytic activity of Pd complexes **1** and **2** was evaluated in the Suzuki reaction of various aryl halides with phenylboronic acid. (**Scheme**)

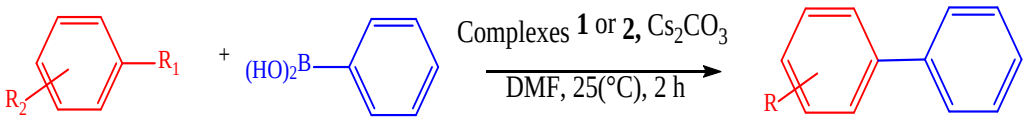

Scheme: Suzuki reaction of various aryl halides catalyzed by **1** and **2** complexes.

References

[1] Jennepalli, S.; Pyne, S. G.; Keller, P. A. [60]Fullerenyl amino acids and peptides: a review of their synthesis and applications. *RSC Adv.*, 2014, 4, 46383−46398.
[2] Yanov, M. I.; Leszczynski, J.; Sulman, E.; Matveeva, V.; Semagina, N. Modeling of the molecular structure and catalytic activity of the new fullerene-based catalyst $(\eta^2\text{-}C_{60})Pd(PPh_3)_2$: An application in the reaction of selective hydrogenation of acetylenic alcohols. *Int. J. Quantum. Chem.*, 2004, 100, 810–817.
[3] Sabounchei, S. J.; Hashemi, A.; Hosseinzadeh, M.; Salehzadeh, S.; Maleki, F. [60]Fullerene-Based Pd(0) Complexes of Phosphorus Ylides as Efcient Nanocatalyst for Homo- and Heterogeneous Mizoroki–Heck Coupling Reactions. *Catal. Lett.*, 2017,147, 2319-2331.

Ultrasonicated Green Synthesis of Isoxazolones using Sodium Cyclamate

Ziba Daroughezadeh[a] and Hamzeh Kiyani[a,b*]

a) School of Chemistry, Damghan University, Damghan, Iran, hkiyani@du.ac.ir, hkiyani@sku.ac.ir.
b) Department of Chemistry, Faculty of Science, Shahrekord University, Shahrekord, Iran.

Keywords: Sonication, Isoxazolone, Green synthesis

Nitrogen and oxygen-containing heterocycles, including isoxazoles, serve as key structural units that are found in pharmaceuticals, natural products, some marketed drugs, agrochemicals, functional materials, and organic dyes [1]. Isoxazolone heterocycles are among the most attractive isoxazoles that have a wide range of biological properties, including anticancer, anti-inflammatory, antimycobacterial, antibacterial, antiviral, antitubercular, anti-Alzheimer's, antioxidant, insecticide, and anti-nociceptive. These heterocycles will provide fruitful leads for future open innovation drug discovery [2-3]. In this research investigation, the three-component cyclocondensation route was applied to synthesizing isoxazolones (**Scheme 1**). Isoxazolone compounds were synthesized by a cyclization of various aldehydes with hydroxylamine and *β*-oxo esters using ultrasound waves. Optimization studies revealed that 5 mol% of sodium cyclamate in water at room temperature is sufficient to perform the experiment. In these experiments, water was used as a green solvent and ultrasonication was applied as the non-conventional source of green energy. The structures of the synthesized heterocycles were identified via spectroscopic methods (FT-IR and NMR spectroscopies) and elemental analysis.

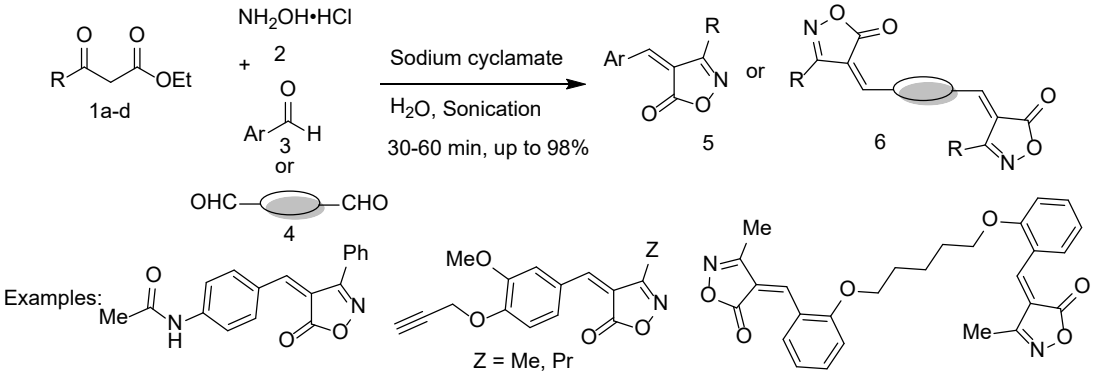

Scheme 1: Ultrasonicated synthesis of isoxazolones.

References

[1] Barmade, M. A.; Murumkar, P. R.; Sharma, M. K.; Yadav, M. R. Medicinal Chemistry Perspective of Fused Isoxazole Derivatives. *Curr. Top. Med. Chem*. **2016**, *16*, 2863-2883.
[2] Reihani, N.; Kiyani, H. Three-component Synthesis of 4-Arylidene-3-alkylisoxazol-5(4*H*)-ones in the Presence of Potassium 2,5-dioxoimidazolidin-1-ide. *Curr. Org. Chem.* **2021**, *25*, 950-962.
[3] Faramarzi, Z.; Kiyani, H. Steglich's Base Catalyzed Three-Component Synthesis of Isoxazol-5-ones. *Polycycl. Aromat. Compd*. **2023**, *43*, 3099-3121.

29TH IRANIAN ORGANIC CHEMISTRY CONFERENCE
1_3 NOV, 2023
UNIVERSITY OF QOM, IRAN

Pd@Mont/ImI-IL-SO_3H: An efficient catalyst for the synthesis of Hantzsch pyridine

Fatemeh Ghorbani, Masoume Malmir* and Majid M. Heravi*

Department of Organic Chemistry, Faculty of Chemistry, Alzahra University, Tehran, Iran, fghorbani9313@gmail.com, m.malmir@alzahra.ac.ir, mmheravi@alzahra.ac.ir.

Keywords: Ionic liquids, Multicomponent reactions, Montmorillonite, Heterogeneous Catalyst, Hantzsch pyridine.

In order to take advantage of the advantages of heterogeneous catalysts [1,2] in improving the process of organic chemistry reactions, this project tries to report a cost-effective and environmentally friendly method to synthesis of heterogeneous catalyst and investigation of its activity in multi-component reactions..a magnetic catalyst based on montmorillonite and ionic liquid containing Pd nanoparticles was designed. Pd@Mont/ImI-IL-SO_3H catalyst was used in one-pot Hantzsch pyridine synthesis and its activity was investigated on a wide range of aldehyde derivatives. Moreover, this catalyst was easily separated from the reaction mixture by simple filtration and reused up to 7 times without a significant decrease in catalytic activity. It should be noted that the activity of Pd@Mont/ImI-IL-SO_3H was compared with other recent catalytic reports, and one of the advantages of this protocol is the introduction of an environmentally friendly method in the presence of a recyclable catalyst (**Scheme**).

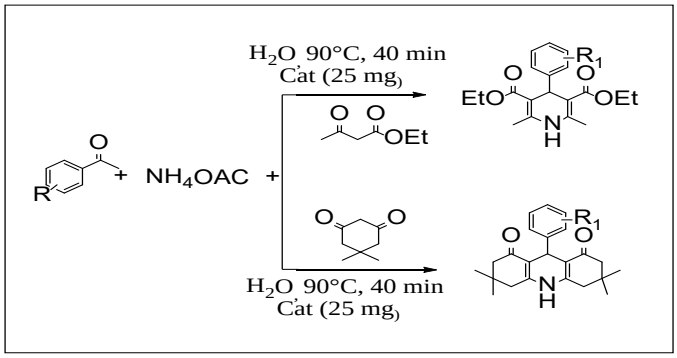

Scheme: Synthesis of Hantzsch pyridine.

References

[1] Karrabi, M.; Malmir, M.; Heravi, M.M.; Hosseinnejad, T., A theoretical and experimental study on ecofriendly-one-pot synthesis of pyrazolopyranopyrimidines catalysed by CuO functionalized montmorillonite. *Inorg. Chem. Commun.* 2023. *149*, 110367.

[2] Rostamnia, S.; Alamgholiloo, H.; Jafari, M., Ethylene diamine post-synthesis modification on open metal site Cr-MOF to access efficient bifunctional catalyst for the Hantzsch condensation reaction. *Appl. Organoment. Chem*. 2018. *32* (8), 4370.

New Rh(III) complex of 5-methyl-5-(2-pyridyl)2,4-imidazolidenedione; Synthesis, X-ray structure and high catalytic activity toward hydrogenation of ketones

Mohsen Sayadi*

Department of Chemistry, Faculty of Chemistry, Bu-Ali Sina University, Hamedan, Iran, Sayadim80@yahoo.com.

Keywords: Rh(III) complex, X-ray structure, Hydrogenation, Synthesis

In recent years, the importance of metal complexes of hydantoins has been studied due to applications such as catalytic and biological activity of this class of compounds and new structural features presented by the metal complexes of such ligands. In late nineteenth century, chemistry of a variety of Rh(III) complexes with several N-heterocycles and their derivatives have been widely investigated and it was attracted more attention in recent years [1, 2]. As seen from literature[3], Rh(III) complexes with N-heterocycles ligands can applied as efficient catalysts in the organic reactions (transfer hydrogenation reaction of ketones) [4]. In this work we describe the reaction of anion $[RhCl_6]^{3-}$ with hydantoin ligand (**HL**= 5-methyl-5-(2-pyridyl)-2,4-imidazolidenedione). Based on the spectroscopies (^1H and ^{13}C NMR), elemental and MS analyses, the complex has the general formula $K[RhCl_2(L)_2]$. Next, dissolution of this complex in DMSO leads to elimination of one KL ligand and coordination of two DMSO molecules as ligand and transformation of this complex to $[RhCl_2L(DMSO)_2]$ (**1**) complex. The X-ray analysis results showed that this complex was crystallized as solvated complex cis-$[RhCl_2L(DMSO)_2]$. The catalytic activity of this complex was then evaluated for the hydrogenation of various ketones. (**Scheme**)

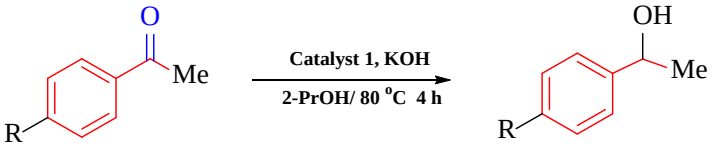

Scheme: Transfer hydrogenation of ketones catalyzed by Rh(III) catalyst.

References

[1] Bayon, J. C.; Net, G.; Real, J.; Rasussen, P. J. Synthesis and reactivity of rhodium(I) and iridium(I) complexes of the dianions of 2,3-pyrazinedicarboxylic and 2,5 pyrazinedicarboxylic acid. *J. Organomet. Chem.* 1990, 385, 409−415.

[2] Kumar, A.; Kumar, A.; Gupta, R. K.; Paitandi, R. P.; Singh, K. B.; Trigun, S. K.; Hundal, M. S.; Pandey, D. S. Cationic Ru(II), Rh(III) and Ir(III) complexes containing cyclic π-perimeter and 2-aminophenyl benzimidazole ligands: Synthesis, molecular structure, DNA and protein binding, cytotoxicity and anticancer activity. *J. Organomet. Chem*. 2016, 801, 68−79.

[3] Gu, P.; Xu, Q.; Shi, M. Synthesis and structural studies on the chiral phosphine-NHC rhodium and palladium complexes for their performances in the metal-catalyzed reactions. *Tetrahedron*. 2014, 70, 7886−7892.

[4] Singh, P.; Das, D.; Singh, M.; Singh, A. K. Rhodium(III) complexes of N-{2 (arylseleno/telluro)ethyl} morpholine: Synthesis, structure and applications as efficient catalyst for transfer hydrogenation reaction of ketones. *Inorg. Chem. Comm*. 2010, 13, 988−991.

Intercalation of supramolecule into LDH for solid-phase extraction of NSAIDs in water and urine sample

Saied Shafiei Navid[a*], Rahman Hosseizadeh[a] and Milad Ghani[b]

a) Department of Organic Chemistry, Faculty of Chemistry, University of Mazandaran, 47416-95447 Babolsar, Iran, s.shafiei@stu.umz.ac.ir

b) Department of Analytical Chemistry, Faculty of Chemistry, University of Mazandaran, 47416-95447 Babolsar, Iran

Keywords: Layered double hydroxide, Supramolecular chemistry, Real samples, Calix[4]arene

The present research aims to prepare a new sorbent based on an acidic calixarene (A_2CA) intercalated into a Mg/Al layered double hydroxide (LDH) to achieve the new sorbent (A_2CA@LDH) (**Scheme**) which was confirmed by utilizing techniques [1]. The prepared sorbent's ability to extract specific nonsteroidal anti-inflammatory drugs (NSAIDs), from water and real urine samples was examined using the pack column strategy. Plackett-Burman and Box-Behnken designs, two components of the response surface methodology (RSM), were utilized to fine-tune and optimize the parameters controlling the extraction and desorption process by using an HPLC-UV. The results demonstrated that this new sorbent and current method may be helpful for accurately, easily, and affordably identifying NSAIDs in actual samples [2].

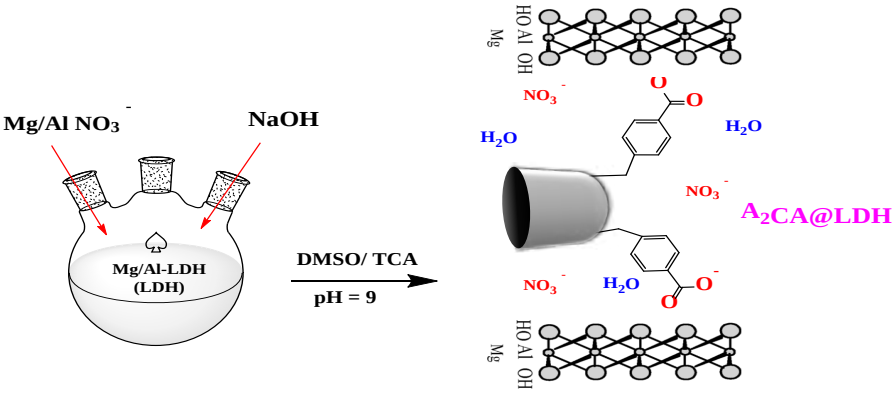

Scheme: Preparation of A_2CA@LDH as the new sorbent.

References

[1] Hajibeygi, M. Shafiei-Navid, S. Shabanian, M. Vahabi, H. Novel poly (amide-azomethine) nanocomposites reinforced with polyacrylic acid-co-2-acrylamido-2-methylpropanesulfonic acid modified LDH: Synthesis and properties. *Appl. Clay Sci.* 2018, *157*, 165-76.

[2] Cui, F. Zhao, L. Optimization of xylanase production from Penicillium sp. WX-Z1 by a two-step statistical strategy: Plackett-Burman and Box-Behnken experimental design. *Int. J. Mol. Sci.* 2012,*13*, 10630-46.

The Mechanism investigation of Acetaminophen's Interaction with L-Cysteine and L-Methionine by Electrochemical Techniques

Sh. Moeini-Far, H. Shayani-Jam * and M. R. Yaftian

Phase Equilibria Research laboratory, Department of Chemistry, Faculty of Science, The University of Zanjan, Postal Code 45371–38791, Zanjan, Iran, shayan@znu.ac.ir

Keywords: Acetaminophen, Electrosynthesis, Drug Interaction, Electrochemistry

Electrochemistry can be a useful tool in understanding the mechanism of compound reactions in chemistry. Electrosynthesis also allows for the use of the moderate reaction conditions, reducing the need for harsh reagents or high temperatures. This can be beneficial for sensitive compounds or reactions that are difficult to achieve using traditional techniques [1, 2]. The aim of this research is performing a thorough analysis in order to determine the reaction mechanism between amino acids (L-cysteine and L-methionine) and acetaminophen by using cyclic voltammetry and coulometry techniques. The final product was synthesized using coulometry in aqueous solution through a catalyst-free environmentally friendly method at room temperature under green conditions. The product was then separated and purified. It was characterized by NMR, FT-IR and MS techniques. The obtained results reveals N-acetyl-P-benzoquinone (NAPQI) induced by acetaminophen oxidation, can undergo reactions with L-cysteine and L-methionine. As resulting, these amino acids potentially possessing the ability to reduce or eliminate the toxicity of NAPQI (Scheme1). As a result, these amino acids can be considered as potential antidotes for acetaminophen overdoses.

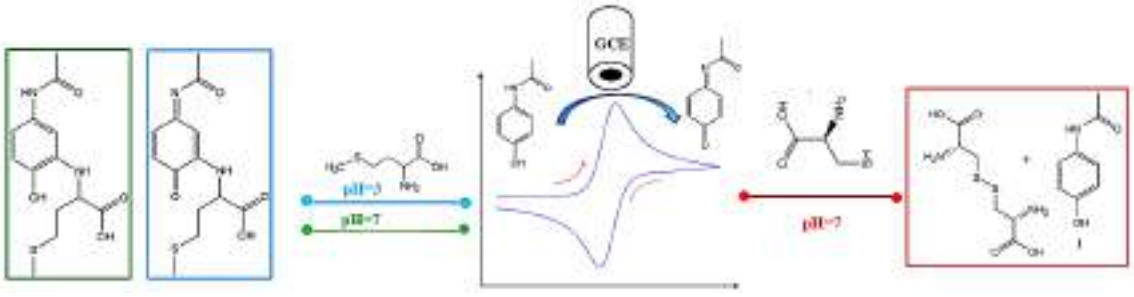

Scheme1: Proposed mechanism for reaction between amino acids and acetaminophen

References

[1] Francke, R., R.D. Little, and S. Inagi, Organic electrosynthesis. 2019, *Wiley Online Library*. p. 4065-4066.
[2] Frontana-Uribe, B.A., et al., Organic electrosynthesis: a promising green methodology in organic chemistry. *Green Chem.*, 2010. 12(12): p. 2099-2119.

Electrochemical Study of the Acetaminophen and Pomegranate Extract Interaction

R. Babereh, H. Shayani-Jam *, M. R. Yaftian, B. Farajmand, M.H. Moeini, Sh. Moeini-Far

Phase Equilibria Research laboratory, Department of Chemistry, Faculty of Science, The University of Zanjan, Postal Code 45371–38791, Zanjan, Iran. shayan@znu.ac.ir, mohammad.h.moeini@gmail.com

Keywords: Reaction mechanism, Electrochemistry, Drug interaction, Toxicity mitigation, Oxidation reactions.

This research used electrochemical techniques to investigate the reaction mechanisms of acetaminophen oxidation and its interactions with pomegranate extract. Cyclic voltammetry (CV) and coulometry provided direct, quantitative analysis of the redox behavior of acetaminophen and its corresponding products [1]. Electrosynthesis can also be a powerful tool in revealing the mechanisms of compounds in chemistry. By using electricity to start and continue chemical reactions, researchers can gain insights into the step-by-step processes involved in the formation of compounds. These techniques allow precise control over reaction conditions and can provide valuable information about reaction intermediates and reaction pathways [2]. Changes in cathodic and anodic peak currents of CV in the presence of pomegranate extract showed that the extract interacts with N-acetyl-p-benzoquinone imine (NAPQI), leading to its subsequent chemical pathways and mechanisms. Our electrochemical analysis provides valuable mechanistic information on the multistep process of acetaminophen and pomegranate extract reactions that are difficult to obtain through traditional methods. This information can be used to identify antidotal like pomegranate extracts that can mitigate acetaminophen toxicity. Overall, our study demonstrates the advantages of electrochemical techniques to identify the reaction mechanisms for screening plant extracts as therapeutic alternatives for acetaminophen poisoning.

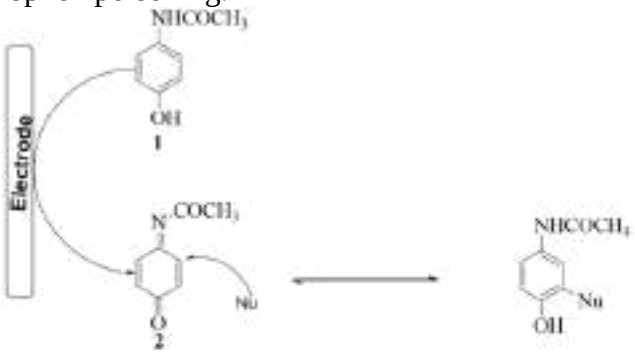

Scheme 1: Proposed mechanism for reaction between pomegranate extract and acetaminophen

References

[1] Elgrishi, N., et al., A practical beginner's guide to cyclic voltammetry. *J. Chem. Educ.*, 2018. **95**(2): p. 197-206.

[2] Kaur, M., Development of electrosynthetic methods for the functionalisation of tertiary amides. 2016, *Manchester Metropolitan University*.

Utilization of $AgNO_3$ over a novel amide-based covalent organic framework (COF) as a heterogeneous reusable catalyst for the synthesis of ß-amino carbonyl compounds

Salman Taheri*, Maryam Nazifi

Organic Chemistry Laboratory, Faculty of Chemistry, Chemistry and Chemical Engineering Research Center of Iran, Tehran, Iran, Taheri@ccerci.ac.ir, Maryam.nazifi1991@gmail.com

Keywords: Covalent organic frameworks, Ag-COF, Mannich Reaction

Covalent organic frameworks (COFs) are a class of highly porous organic polymers. Functional modification of the COFs has become an efficient strategy to enlarge their application in diverse fields. The novel porous covalent organic framework was successfully functionalized with $AgNO_3$. The high surface area Ag-COF could exhibit superior catalytic activity. The characterization of the novel catalyst was determined by FT-IR, SEM, EDS, PXRD, and TGA analysis. Ag-COF was used as an efficient heterogeneous catalyst. Therefore, it can be recovered by centrifugation and used for 4 cycles without reducing the catalytic activity. Simple operation, easy preparation of the catalyst, availability of raw materials, high stability, environmentally friendly catalyst and solvent, excellent efficiency, and simple work-up are the salient features of this methodology.

A simple, easy, and efficient synthesis of β-aminocarbonyl derivatives has been carried out through the multicomponent Mannich reaction of aldehydes, amines, and various acetophenones in ethanol solvent using Ag-COF as a catalyst. β-aminocarbonyl compounds were produced with an efficiency ranging between 75% and 98% within a period of 4 hours.

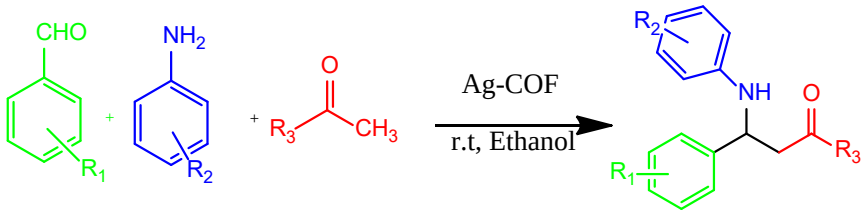

Scheme: Ag-COF catalyzed synthesis of ß-amino carbonyl products.

References

[1] Simplício AL, Clancy JM, Gilmer JF. β-Aminoketones as prodrugs with pH-controlled activation. *Int. J. Pharm.* 2007;336(2):208-14.

[2] Zhi Y, Wang Z, Zhang HL, Zhang Q. Recent progress in metal-free covalent organic frameworks as heterogeneous catalysts. *Small*. 2020;16(24):2001070.

[3] Källström S, Leino R. Synthesis of pharmaceutically active compounds containing a disubstituted piperidine framework. *Bioorg. Med. Chem.* 2008;16(2):601-35.

Functionalized (g-C_3N_4)/biochar support by Polyethyleneimine (PEI) as efficient nano catalyst for synthesis of 2-amino-4H-chromenes Derivatives

MohammadNasir Shambayati, Hamed Gholami, Maryam Hajjami*

Organic Chemistry Laboratory, Faculty of Chemistry, Faculty of Chemistry, Bu-Ali Sina University, Hamedan, Iran, nasirshambayati@gmail.com, m.hajjami@basu.ac.ir & mhajjami@yahoo.com

Keywords: Polyethyleneimine, Graphitic carbon nitride, Biochar, Recyclable catalysts

Design and synthesis of green and recyclable catalysts in order to improve the efficiency of organic chemistry reactions is a significant challenge [1]. 2-amino-4H-chromenes are known to have diverse biological and pharmacological activities [2]. In this study, first, graphitic carbon nitride (g-C_3N_4) /biochar nanosheets with high surface area and chemical stability were synthesized. Afterwards, the surface of this nano-substrate was modified with polyethyleneimine to obtain g-C_3N_4 biochar/PEI. The synthesis of 2-amino-4H-chromenes derivatives was performed in reflux (water: ethanol) condition, with high yield. The advantages of this reaction include easy catalyst separation and reusability thanks to its heterogeneous nature, with good to excellent efficiency, and finally short reaction time.

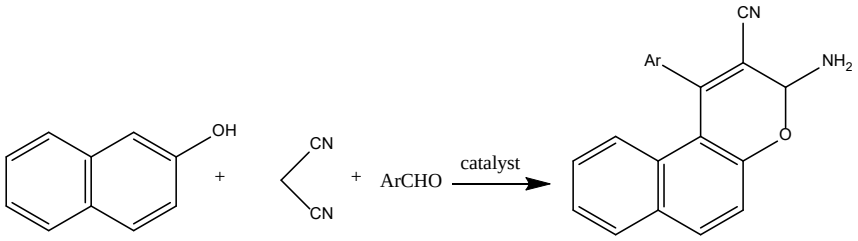

Scheme Three-component reaction of malononitrile, aldehydes and beta-naphthol in the presence of (g-C3N4)/biochar support by Polyethyleneimine (PEI) as catalyst in reflux (water: ethanol) condition

Reference

[1] Moradi, P., Hajjami, M. Stabilization of ruthenium on biochar-nickel magnetic nanoparticles as a heterogeneous, practical, selective, and reusable nanocatalyst for Suzuki C-C coupling reaction in water. *RSC Advances* 2022 12, 13523-13534.

[2] Sheibani, H.; Saidi, K.; Abbasnejad, M.; Derakhshani, A.; Mohammadzadeh, I. A convenient one-pot synthesis and anxietic activity of 3-cyano-2(1H)-iminopyridines and halogen derivatives of benzo[h]chromenes, *Arab. J. Chem.* 2016 9, S901-S906.

Fabrication of 2-amino-4-phenyl-4a,5,6,7-tetrahydronaphthalene-1,3,3(4*H*)-tricarbonitriles in the presence of the nano-scale $NiFe_2O_4$ composites

Javad Safaei-Ghomi*, Aliasghar Mahmoudi Kharazm and Pooria Babaei

Department of Organic Chemistry, Faculty of Chemistry, University of Kashan, Kashan, P.O. Box 87317-51167, I. R. Iran, mahmoodiali135913@gmail.com.

Keywords: Multicomponent reactions, Tetrahydronaphthalene,3,3(4H)-carbonitrile, Nano-scale $NiFe_2O_4$, Nanocomposites,

Multi-component reactions or MCRs are one of the most excellent strategies to extend the molecular skeleton diversity via facile methods. They can furnish facile, prompt, and efficient tactics in novel products and medical chemistry. Hence, it is taken into considerable to fabricate these products by applying robust catalysts and optimal methods. The bicyclic *ortho*-aminocarbonitriles are crucial intermediate structures in the synthesis of organic compounds. Under varied conditions, cyclic malononitrile, ketones, and various benzaldehydes are converted into bicyclic *ortho*-aminocarbonitrile derivatives through *K*noevenagel condensation and Michael addition [1]. In this study, nano-scale $NiFe_2O_4$ composites was applied as a magnetically and robust catalyst to prepared the bicyclic *ortho*-aminocarbonitriles. Not expensive, air-stable, magnetically separable, and affordable another advantages of nano-scale $NiFe_2O_4$ composite. References regarding the catalytic characteristics of $NiFe_2O_4$ MNPs are extremely scarce [2]. These spinel-type bimetal oxides have shown considerable promise for use in catalysis (**Scheme 1**).

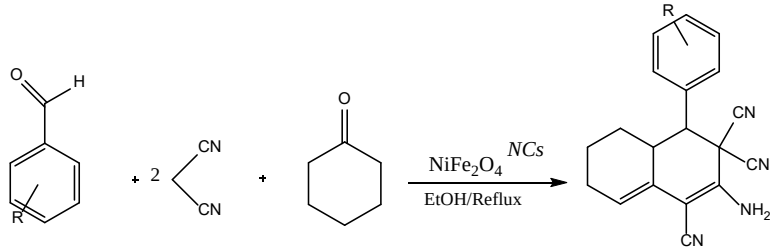

Scheme 1: Preparation of *ortho*-aminocarbonitrile derivatives

References

[1] B. Maleki, R. Rooky, E. Rezaei-Seresht, and R. Tayebee. One-Pot synthesis of bicyclic *Ortho*-aminocarbonitrile and multisubstituted cyclohexa-1, 3-dienamine derivatives. *Org. Prep. Proced. Int.*, **2017**, *49*, 557-67.

[2] P. Sivakumar, R. Ramesh, A. Ramanand, S. Ponnusamy, C. Muthamizhchelvan. Preparation and properties of nickel ferrite ($NiFe_2O_4$) nanoparticles via sol–gel auto-combustion method. *Mater. Res. Bull*. **2011**, *46*, 2204-2207.

Core-shell Cu based metal organic framework coated with fluorouracil imprinted methacrylamid polymer: A PH-responsive anticancer nanocarrier

Hossein Hosseinzadeh, Siamak Javanbakht and Reza Mohammadi *

Polymer Research Laboratory, Faculty of Chemistry, University of Tabriz, Tabriz, Iran, hosseincr6@gmail.com, r.mohammadi@tabrizu.ac.ir

Keywords: Nanocarrier, Molecular imprinted polymer, Fluorouracil, Metal-organic frameworks, Drug delivery

Recent research has increasingly received more attention to molecularly imprinted polymers (MIPs) and their application in the biomedical nanoplatforms [1]. In this study, an innovative fluorouracil (5-FU) imprinted polymer via the precipitation free radical polymerization strategy was developed as shell on the Cu-based metal organic framework (MOF) as core for drug delivery system. The prepared materials were characterized by different analysis such as Fourier transform infrared (FT-IR), scanning electron microscopy (SEM) and X-Ray Diffraction (XRD). Binding kinetics of 5-FU established specific recognition binding sites in the core shell nanoscale molecularly imprinted polymer structure [1]. In vitro drug release behaviors exhibited a pH-controlled release in a indicated that a 5-FU-loaded nanocarrier against cancer cells has notable cytotoxicity. According to the obtained results, the prepared pH-responsive core shell has the potential to be employed as an anticancer drug delivery platform [2].

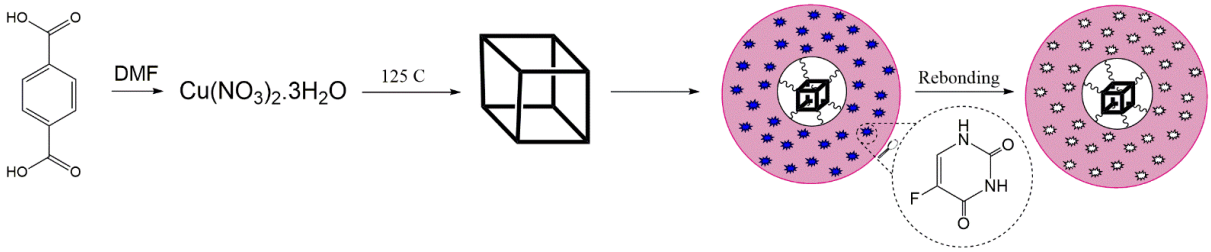

Scheme: Schematic procedure for preparation of MOF@MIP nanocomposite

References

[1] Javanbakht, S.; Saboury, A.; Shaabani, A.; Mohammadi, R.; Ghorbani, M., Doxorubicin imprinted photoluminescent polymer as a pH-responsive nanocarrier. *ACS Appl. Bio Mater.* **2020,** *3* (7), 4168-4178.

[2] Han, S.; Song, Y.; Liu, S.; Zhao, L.; Sun, R., Dual responsive molecularly imprinted polymers based on UiO-66-DOX for selective targeting tumor cells and controlled drug release. *Eur. Polym. J.* **2022,** *171*, 111219.

Ring-opening Polymerization of Tetrahydrofuran

Alireza Banan*, Reza Zamani Chehrania

Faculty of Science, Imam Hossein University, Tehran, Iran. Corresponding Author E-mail: bananjahromi@yahoo.com

Keywords: Ring-opening Polymerization, Tetrahydrofuran, Heteropolyacid ($H_3PW_{12}O_{40}$), Acetic anhydride, Poly(tetramethylene ether glycol)

The ring-opening polymerization is a useful method to prepare polymers and copolymers with controlled microstructure, chain length and functionality that are otherwise difficult to obtain by conventional polymerization methods [1]. This method is usually used for the production of high performance polymeric materials and engineering plastics. Poly(tetramethylene ether glycol) (PTMG), also called poly(tetrahydrofuran), is a colorless waxy polymer that is widely used as a soft segment for the production of thermoplastic elastomers and as an intermediate for the synthesis of elastic fibers, polyurethanes, and polyesters [2] Due to its unique physical and chemical properties and its use in advanced applications, it is very demanding to design efficient methods for the synthesis of PTMG.

In this study a catalytic prodecure has been developed for the synthesis of PTMG by ring opening polymerization of THF.Herein,a heteropolyacid ($H_3PW_{12}O_{40}$) and acetic anhydride as a co-catalyst are used to control the molecular weight of the resulting polymer. The heteropolyacid has high acid strength and forms stable polyanions and in combination with acetic anhydride can activate THF ring. The activated THF rings are opened and polymerized to form the acetate-terminated polymer. Polymerization was terminated and the acetate end-groups are hydrolyzed with the addition of NaOH aqueous solution. The overall synthetic procedure is shown in Scheme 1. The resulting product was characterized by gel permeation chromatography (GPC) and ^{1}H NMR, ^{13}C NMR and FT-IR spectroscopy.

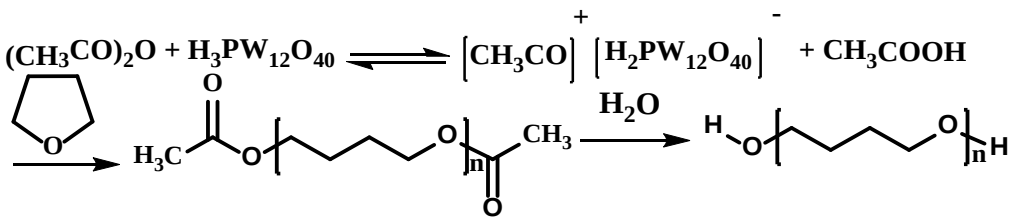

Scheme: Synthesis of PTMG by ring opening polymerization of THF.

References

[1] Jia, Z. Q., Zhao, M., Gao, C. G., & Zhao, Y. X. (2011). Effect of surface acidity and pore size of Al-substituted plugs-containing SBA-15 and MCM-41 silicas on the polymerization of THF. *Chin. Chem. Lett.*, *22*(1), 105-108.

[2] Yang, H. J., Yoon, S. W., Park, H. S., Lee, K. H., & Hur, N. H. (2019). Highly efficient ring-opening polymerization of tetrahydrofuran by anhydrous ferric chloride. *J. Appl. Polym. Sci*, *136*(39), 47999.

Cu(II) supported on Chitosan/LDH/Fe_3O_4 magnetic nanocomposite as heterogeneous nanocatalyst for synthesizing *bis*(indolyl)methanes under ultrasonic conditions

Asra Rashtiani & Ramin Ghorbani-Vaghei *

Department of Organic Chemistry, Faculty of Chemistry, Bu-Ali Sina University, Hamadan, Iran, asra.rashtiani@gmail.com, rgvaghei@yahoo.com & ghorbani@basu.ac.ir

Keywords: Layered double hydroxides (LDHs) , Chitosan, *Bis*(indolyl)methanes (BIMs)

Chitosan is a natural, nontoxic biopolymer with amine and hydroxyl functional groups which make it easy for chitosan molecules to form intermolecular and intramolecular hydrogen bonds. In that context, the present study reports Cu(II) supported on Chitosan@LDH@Fe_3O_4 magnetic nanocomposite (Fe_3O_4@MgCuAl-LDH@CS/Cu(II)) as an effective and a novel heterogeneous catalyst to perform electrophilic substitution reaction between indoles and aromatic aldehydes to yield bis(indolyl)methane derivatives (BIMs) in shorter reaction time under ultrasonic conditions **(Scheme)**. Copper ions were mainly adsorbed onto the core-shell magnetic nanocomposite (Fe_3O_4@LDH) modified with chitosan by the chelating capacity of chitosan and LDH. Overall, the results show that Sonication significantly enhanced the catalytic performances compared to conventional heating. Also, the prepared catalyst could be easily separated from the solution using an external magnetic field and reused up to nine times without considerable leaching or loss in its catalytic activity.

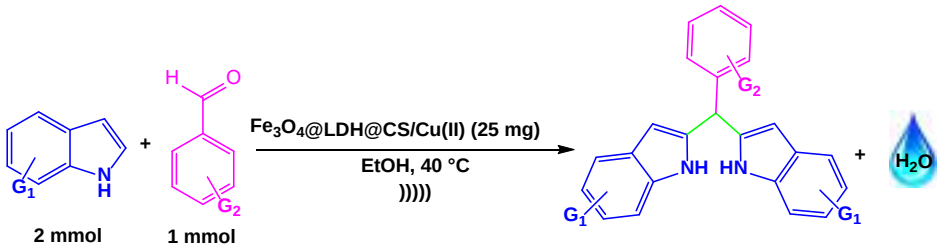

Scheme: Synthesis of bis(indolyl)methane derivatives using (Fe_3O_4@MgCuAl-LDH@CS/Cu(II)).

Reference

[1] Ghorbani-Vaghei, R.; Veisi, H.; Keypour, H.; Dehghani-Firouzabadi, A. A. A practical and efficient synthesis of bis(indolyl)methanes in water, and synthesis of di-, tri-, and tetra(bis-indolyl)methanes under thermal conditions catalyzed by oxalic acid dihydrate. *Mol. Divers* 2010, *14*, 87-96.

[2] Shiri, M.; Zolfigol, M. A.; Gerhardus Kruger, H.; Tanbakouchian, Z. Bis-and trisindolylmethanes (BIMs and TIMs). *Chem. Rev.* 2010, *4*, 2250-2293.

[3] Veisi, H.; Joshani, Z.; Karmakar, B.; Tamoradi, T.; Heravi, M. M.; Gholami, J. Ultrasound assisted synthesis of Pd NPs decorated chitosan-starch functionalized Fe3O4 nanocomposite catalyst towards Suzuki-Miyaura coupling and reduction of 4-nitrophenol. *Int. J. Biol. Macromol* 2021, 172, 104-113.

Facile synthesis of COF@$ZnFe_2O_4$ composite as a heterogeneous and reusable catalyst for the preparation of benzodiazepine derivatives

Fatemeh Ghomi [a], **Mohammad Ali Ghasemzadeh** [a,*], **Ali Javadi** [b]

a) Department of Chemistry, Qom Branch, Islamic Azad University, Qom, Iran, fateme.qomi9520@gmail.com, m.a.qasemzade@gmail.com; ma.ghasemzadeh@iau.ac.ir
b) Department of Medical Sciences, Faculty of Medicine, Qom Medical Sciences, Islamic Azad University, Qom, Iran

Keywords: COF@$ZnFe_2O_4$, Multi-component reaction, Covalent organic frameworks, Benzodiazepine, Heterocycle

Recently, the development of new catalysts to promote organic reactions has become an integral part of research plans [1,2]. In this research, the catalytic behavior of COF@$ZnFe_2O_4$ composite was explored in the preparation of by a one-three-component reaction of benzaldehydew, dimdone, and phenylenediamine. COF@$ZnFe_2O_4$ is introduced as a new catalyst with high efficiency for the synthesis of benzodiazepines. The structure of the synthesized materials was elucidated using various spectral techniques such as: X-ray crystallography (XRD), scanning electron microscopy (SEM), energy dispersive X-ray spectroscopy (EDX/Mapping), Fourier transform infrared (FTIR), Brunauer-Emmett-Teller (BET), The present method brought several advantages, including: short reaction times, high yield of products, high catalytic activity and high thermal stability **(Scheme**).

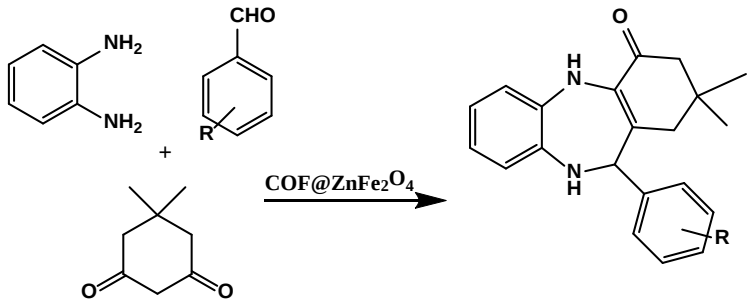

Scheme: Synthesis of Benzodiazepine derivatives using COF@$ZnFe_2O_4$.

References

[1] F. Pan, Z. Liu, B. Deng, Y. Dong, X. Zhu, C. Huang, W. Lu, Lotus leaf-derived gradient hierarchical porous C/MoS_2 morphology genetic composites with wideband and tunable electromagnetic absorption performance, *Nano-Micro Lett*. 2021, *13*, 43.
[2] X. Zhang, Z. Liu, B. Deng, L. Cai, Y. Dong, X. Zhu, W. Lu, Microwave absorption on a bare biomass derived holey silica-hybridized carbon absorbent, *Chem. Eng. J*. 2021, *419*, 129547.

Electronic structure calculations on Angelicin by Density functional theory method

Tooba Abdizadeh*

Clinical Biochemistry Research Center, Basic Health Sciences Institute, Shahrekord University of Medical Sciences, Shahrekord, Iran, t.abdizadeh@gmail.com

Keywords: Angelicin, DFT, Electronic structure

Angelicin (**Scheme**) as a natural coumarin compound known for its effective therapeutic effects in phototherapy and has a wide range of applications for the treatment of various conditions, such as psoriasis, eczema, cancer, diabetes, and osteoporosis. [1,2]. Density functional theory (DFT) is a computational quantum mechanical (QM) method that is used to investigate the electronic structure and also to be employed in pharmaceutical studies [3]. In this study, the DFT calculation for the angelicin compound was performed at the B3LYP level and using the 6-31++G(d,p) basis set in the gas phase by Gaussion 09 software. Also, some molecular parameters including chemical potential, chemical hardness and softness and electrophilicity index were investigated. In the angelicin, Homo (E=-6.57 ev) and LUMO (-2.13 ev) orbitals were localized over the benzofuran and coumarin rings, respectively. The values of 0.23 and 4.25 ev for the chemical softness (s) and the electrophilicity (ω) for angelicin showed that this compound with the less hardness (η) value has the high chemical reactivity. According to these results, the compound of angelicin can be investigated for various diseases.

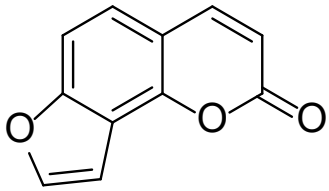

Scheme: Angelicin structure

References

[1] Mahendra, C. K.; Tan, L.T.; Lee, W. L.; Yap, W. H.; Pusparajah, P.; Low, L. E.; Tang, S. Y.; Chan, K. G.; Lee, L. H.; Goh, B. H. Angelicin-A Furocoumarin compound with vast biological potential. *Front. Pharmacol.* 2020, 11, 366.

[2] Ge, L.; Cui, Y.; Liu, B.; Yin, X.; Pang, J.; Han, J. ERα and Wnt/β-catenin signaling pathways are involved in angelicin-dependent promotion of osteogenesis. *Mol. Med. Rep.* 2019, 19, 3469-3476.

[3] Mazurek, A. H.; Szeleszczuk, Ł.; Pisklak, D. M. Periodic DFT calculations-review of applications in the pharmaceutical sciences. *Pharmaceutics* 2020, 12, 415.

Investigating the chemical properties of dihydrofolate reductase as a therapeutic target and investigation of pyrimethamine drug based on DFT

Hanieh Amini Tazehkand [a], Nasrin Mollania [a]*, Hossein Asghar Rahnama[b], Fariba Mollania[c], Malihe Azadparvar[b]

a) Department of Biology, Faculty of Basic Sciences, Hakim Sabzevari University, Sabzevar, Iran, hanieamini06@gmail.com, n.mollania@hsu.ac.ir.
b) Department of physic, Faculty of Basic Sciences, Hakim Sabzevari University, Sabzevar, Iran.
c) Department of Chemistry, University of Torbat, Torbat Heydaie, Iran.

Keywords: DHFR, Folate antagonists, Pyrimethamine, Medicinal chemicals, Inhibitors.

Folate antagonists, such as trimethoprim and pyrimethamine (**Figure 1**) [1], are medicinal chemicals that target dihydrofolate reductase (DHFR) [2], a crucial enzyme in DNA production. These specific medicines exploit variations in host and parasite enzyme active sites, with pyrimethamine being a popular anticancer medication.

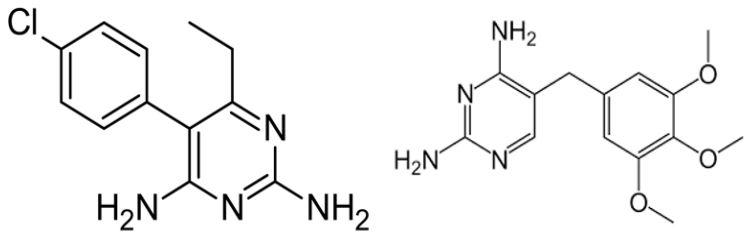

Figure 1: Structures of DHFR inhibitors. A) DHFR inhibitors used in medicine: methotrexate, trimethoprim, pyrimethamine.

References

[1] Schweitzer, B. I.; Dicker, A. P.; Bertino, J. R. Dihydrofolate Reductase as a Therapeutic Target. *FASEB J.* **1990**, *4* (8), 2441–2452.

[2] Knighton, D. R.; Kan, C.-C.; Howland, E. F.; Janson, C. A.; Zuzana Hostomska; Welsh, K. A.; Matthews, D. A. Structure of and Kinetic Channelling in Bifunctional Dihydrofolate Reductase–Thymidylate Synthase. *Nat. Struct. Mol. Biol.* **1994**, *1* (3), 186–194.

Synthesis of novel polymer nanocomposite based on ferrite cobalt/ silver bromide for removal of dye

Abdollah Fallah Shojaei *, Farzaneh Naghdi Dizgah

Department of Chemistry, Faculty of Science, University of Guilan, Rasht, Iran, a.f.shojaie@guilan.ac.ir, farzanehn563@gmail.com

Keywords: $CoFe_2O_4$, AgBr, Hydrothermal process, Precipitation method, Polyacrylic acid

Among the treatment technologies discussed about the removal of dyes, the adsorption technique has been taken into consideration in which incorporation of nanotechnology by applying nanomaterials as adsorbents has been given prime importance [1]. In this regard, the use of metal nanocomposites such as ferrite cobalt promoted the role of nanomaterials due to their unique physical and chemical properties compared with conventional materials [2]. In this work, first synthesized $CoFe_2O_4$ nanoparticles with properties their high coactivity, magneto crystalline anisotropy, moderate saturation magnetization, chemical stability, wear resistance, and electrical insulation by hydrothermal process and then $CoFe_2O_4$/AgBr nanocomposite by easy and efficient precipitation method. Citric acid, $Co(NO_3)_2.6H_2O$, $Fe(NO_3)_3.9H_2O$, NaBr, and $AgNO_3$ were used as primary chemicals. Then polymer nanocomposite by adding polyacrylic acid (PAA) was made into $CoFe_2O_4$/AgBr nanocomposite. The effects of various factors on the removal efficiency of methylene blue dye were studied such as pH, concentration, catalyst dosage, and time. The prepared materials were characterized by X-ray diffraction (XRD) analysis and Fourier transform infrared (FTIR) spectroscopy.

Scheme: Magnetic ferrite cobalt/ silver bromide/ PPA.

References

[1] Sidhaarth KA, Jeyanthi J, Baskar S, Kumar MV. Adsorption of congo red dye using cobalt ferrite nanoparticles. *Int. J. Res. Civ. Eng. Technol.* 2018, 9, 1335-47.

[2] Kazemi M, Zolgharnein J. Cobalt (II) phthalocyanine dye removal from aqueous solution using cobalt ferrite nanoparticles as an efficient adsorbent. *Water Supply.* 2020, 20, 2547-63.

DFT study on the structural and chemical properties of the Kirenol

Tooba Abdizadeh*

Clinical Biochemistry Research Center, Basic Health Sciences Institute, Shahrekord University of Medical Sciences, Shahrekord, Iran, t.abdizadeh@gmail.com

Keywords: Kirenol, DFT, Chemical properties

Kirenol (**Scheme**) is a major diterpenoid components derived from Herba Siegesbeckiae, which has anti-inflammatory, antiarthritic, antibacterial, cardioprotective and immunoregulatory effects [1,2]. Density functional theory (DFT) computational technique provides an effective tool to complement experimental findings and understand the reactivity of various molecular structures [3]. In this research, DFT, with the B3LYP functional, 6-31++G(d, p) basis set for the kirenol atoms was used to optimize the kirenol compound. Also, some molecular parameters including chemical potential, chemical hardness and softness and electrophilicity index were investigated. The results of the theoretical DFT calculations showed that HOMO (E=-6.55 ev) and LUMO (-0.55 ev) orbitals of the kirenol were localized over the cyclohexen and ethane-1,2-diol groups. The values of 3.00 and 2.10 ev for the chemical hardness (η) and the electrophilicity (ω) for kirenol showed that this compound with an energy gap of 6.0 ev has the high stability and the hardness and can be investigated for different diseases.

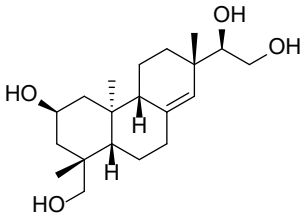

Scheme: Kirenol structure

References

[1] Nasir, N. N.; Sekar, M.; Fuloria, S.; Gan, S. H.; Rani, N. N.; Ravi, S.; Begum, M. Y.; Chidambaram, K.; Sathasivam, K. V.; Jeyabalan, S.; Dhiravidamani, A. Kirenol: a potential natural lead molecule for a new drug design, development, and therapy for inflammation. *Molecules* 2022, 27, 734.

[2] Ibrahim, S. R.; Altyar, A. E.; Sindi, I. A.; El-Agamy, D. S.; Abdallah, H. M.; Mohamed, S. G.; Mohamed, G. A. Kirenol: A promising bioactive metabolite from siegesbeckia species: A detailed review. *J Ethnopharmacol* 2021, 281, 114552.

[3] Adekoya, O. C.; Adekoya, G. J.; Sadiku, E. R.; Hamam, Y.; Ray, S. S. Application of DFT calculations in designing polymer-based drug delivery systems: An overview. *Pharmaceutics* 2022, 14, 1972.

Modification of cryptomelane (K-OMS-2) and its application in reduction of nitriles to amides

Alireza Khorshidi*, Fatemeh Namjoyan

Department of Chemistry, Faculty of Science, University of Guilan, Rasht, Iran, khorshidi@guilan.ac.ir, fatemehnamjoyan@gmail.com

Keywords: k-OMS-2, Nitrile, Amide

The conversion of nitriles to amides is one of the most important reactions in organic syntheses and chemical industries, because amides are versatile synthetic intermediates in the production of pharmaceutical products, polymers and Detergents. A common methodology for the title reaction is using a catalyst in the presence of organic solvents. However, the main problems of classical methods include: a) the need for harsh reaction conditions that can be harmful for sensitive functional groups b) complexity in recycling and reuse of catalyst, c) use of organic solvents [1]. development of Cryptomelan (k-OMS-2) is a crystalline solid with a hollow structure.This catalyst is unique due to high activity, small particle size, and high surface area [2]. Here in, we report the application of transition metal modifird cryptomelane (M-OMS-2, where M = Ni, Ag) as an efficient catalyst for selective reduction of nitriles to amides in aqueous solution

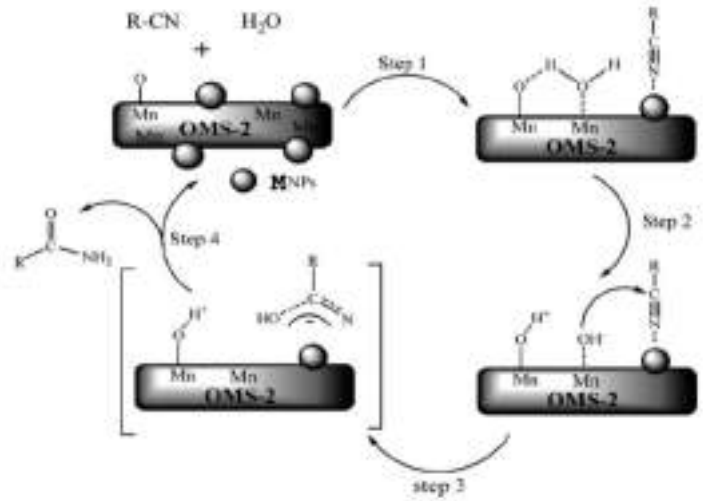

Scheme: A possible mechanistic pathway for M-OMS-2 catalysed reducation *of nitriles (M = Ni, Ag).*

References:

[1] Salam, N., et al. "Ag-grafted covalent imine network material for one-pot three-component coupling and hydration of nitriles to amides in aqueous medium." RSC adv. 4.88 (2014): 47593-47604.

[2] Hajnajafi, Ma., et al. Catalytic degradation of malachite green in aqueous solution by porous manganese oxide octahedral molecular sieve (OMS-2) nanorods. Res. Chem. Intermed. 44 (2018): 3313-3323

Application of Periodic Mesoporous Organosilica with Imidazolium Frameworks for CO_2 Conversions

Sadegh Joudian[a] and Mojtaba Khorasani[a, b*]

a) Department of Chemistry, Institute for Advanced Studies in Basic Sciences (IASBS), No. 444, Prof. Yousef Sobouti Boulevard, Zanjan 45137-66731, Iran, sadeghjoudian@iasbs.ac.ir, m_khorasani@iasbs.ac.ir.
b) Research Center for Basic Sciences & Modern Technologies (RBST), Institute for Advanced Studies in Basic Sciences, IASBS, Zanjan 45137-66731, Iran.

Keywords: CO_2 fixation, Cyclic Carbonate, Periodic Mesoporous Organosilica

A major contributor to climate change is carbon dioxide which also plays an important role in global warming. Therefore, any organic reactions that consume CO2 under sustainable conditions can be desirable from green chemistry. Coupling carbon dioxide with epoxides and producing cyclic carbonates is one of the 100% atom economic reactions [1]. Recently, mesoporous organosilica materials have received considerable attention due to their high porosity, large surface area, and ability to adjust pore size [2]. Herein, a new periodic mesoporous organosilica with the imidazolium frameworks (I@PMO) is described as a novel catalyst for this important transformation. Under optimized reaction conditions, various terminal epoxides have been converted to the corresponding cyclic carbonates in the presence of 0.5 mol% I@PMO at 80 °C within short reaction times (Scheme 1). Reaction selectivity and reactivity of the catalyst was not decreased even after five consecutive runs.

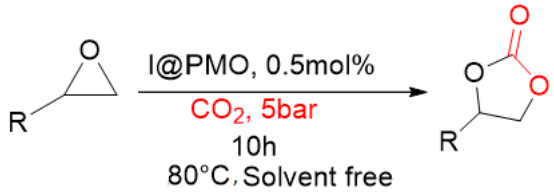

Scheme 1: Direct coupling of CO_2 with epoxides.

References

[1] Hoseini, K. S.; Razaghi, M.; Nouri, T.; Khorasani, M. Direct coupling of CO_2 with epoxides catalyzed by lanthanum (III) supported on magnetic mesoporous organosilica nanoparticles. *Sci. Rep*. **2023**, *13*, 5521.
[2] Khorasani, M.; Karimi, B.; Vali, H. Coupling of CO_2 with epoxides catalyzed by bifunctional periodic mesoporous organosilica with ionic liquid framework. *React. Chem. Eng*. **2022**, *7*, 2618-2628.

[Cu(l-proline)$_2$] complex modified magnetic UiO-66-NH$_2$(Zr) metal organic framework as a novel and reusable nanocatalyst for the one-pot synthesis of Knoevenagel condensation

Sobhan Rezayati and Ali Morsali*

Department of Chemistry, Faculty of Sciences, Tarbiat Modares University, P.O. Box 14117-13116, Tehran, Islamic Republic of Iran, sobhan.rezayati@yahoo.com

Keywords: Knoevenagel condensation; Magnetic nanoparticles; Heterogeneous catalysis

The essential need for today's methodologists is to design innovative approaches in organic synthesis to increase the environmental conservation by following the green chemistry principles [1-2]. Due to the importance of nanoparticles and MOFs, we synthesized and characterized of [Cu(l-proline)$_2$] complex modified magnetic UiO-66-NH$_2$(Zr) metal organic framework for the Knoevenagel condensation through malononitrile and various aldehydes in H_2O as green solvent at room temperature (Scheme 1). As prepared nanocatalysts were characterized and confirmed by FT-IR, TGA, XRD, VSM, FE-SEM, TEM, DLS, XPS, EDX, and BET analyses.

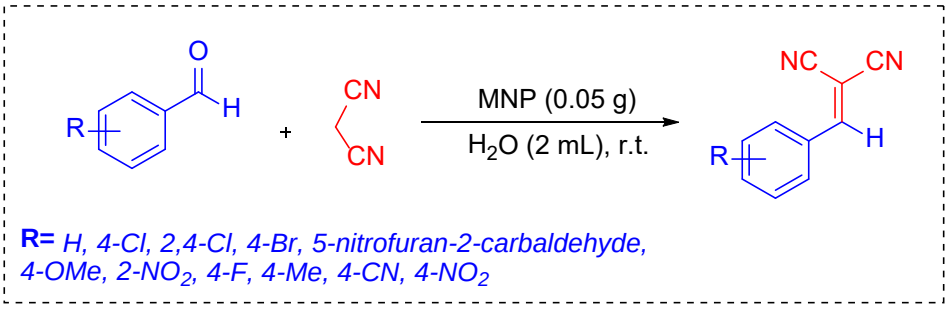

Scheme 1: Synthesis of Knoevenagel condensation catalyzed by MNP

References

[1] Panja, S. L.; Dwivedi, N.; Saha, S. First report of the application of simple molecular complexes as organo-catalysts for Knoevenagel condensation. *RSC Adv.*, 2015, 5, 65526-65531.

[2] Trindade, A. F.; Gois, P. M.; Afonso, C. A. Recyclable stereoselective catalysts. *Chem. Rev.*, 2009, *109*, 418-514.

In Situ forming Zeolite Imidazole Framework in the presence of ZnAl-LDH for Antibacterial drug delivery system

Arash Vahdatkhah, Siamak Javanbakht and Reza Mohammadi *

Polymer Research Laboratory, Faculty of Chemistry, University of Tabriz, Tabriz, Iran, arash.vahdatkhah@gmail.com, r.mohammadi@tabrizu.ac.ir

Keywords: Antibacterial, Layered double hydroxide, Nanocomposite, Metal-organic frameworks

The combination of layered double hydroxides (LDHs) and metal-organic frameworks (MOFs) has shown great potential for drug delivery applications [1]. LDHs are a class of layered materials with a positively charged brucite-like structure, while MOFs are porous materials with a three-dimensional network of metal ions or clusters connected by organic linkers [2].In this method, the Zn Al-LDH compound was first synthesized by the co-precipitation method, and in the presence of this substance, the ZIF-8 compound was synthesized in situ. The resulting nanocomposite has properties such as antibacterial, high portability, and high porosity.

Scheme: Schematic procedure for preparation of ZIF-8/ZnAL-LDH nanocarrier

References

[1] Pooresmaeil, M., & Namazi, H. D-mannose functionalized MgAl-LDH/Fe-MOF nanocomposite as a new intelligent nanoplatform for MTX and DOX co-drug delivery. *Int. J. Pharm.* 2022, *625*, 122112.

[2] Karimi, S., Rasuli, H., & Mohammadi, R. Facile preparation of pH-sensitive biocompatible alginate beads havening layered double hydroxide supported metal-organic framework for controlled release from doxorubicin to breast cancer cells. *Int. J. Biol. Macromol.*, 2023, *234*, 123538.

Extraction of "*Acroptilon repens*" essential oil compounds for green synthesis of iron oxide nanoparticles

Amir Azizi* **and Mahboobeh Nazari**

Applied Chemistry Laboratory, Faculty of Chemistry, University of Arak, Arak, Iran, a-azizi@araku.ac.ir

Keywords: Essential oil, Acroptilon Repens, GC-MS, Iron oxide, Characterization

In this study, the essential oil of *Acroptilon Repens* plant aerial parts, which was collected from Mahalat city, was extracted using water distillation method. In order to quantitatively and qualitatively identify the chemical compounds in the extracted essential oil, a gas chromatography device connected to a mass spectrometer (GC-MS) was used [1,2]. In the following, the capability of extracted essential oil in the preparation of iron oxide nanoparticles was evaluated [3]. The specifications and characteristics of the produced product were investigated by UV-Vis, FTIR, XRD, SEM, DLS and VSM methods. In this study, the efficiency of essential oil extraction was determined to be 1.1%. 21 chemical compounds in essential oil were identified from 22 components detected, separated and recorded by gas chromatograph (GC). Caryophyllene oxide (10.99%), beta-caryophyllene (14.14%), camphor (16.32%), O8-cineole (17.18%) and alpha-pinene (8.75%) were the main components of essential oil, which The total is 67.38% of the total essential oil. Based on the XRD results, as a result of the reaction of the extracted essential oil with a solution of Fe (III) salt, a mixture of iron oxides with the chemical structures of Fe_3O_4 and Fe_2O_3 has been prepared. The results of SEM, DLS and VSM analyzes respectively showed that the produced structure has an average particle size of 31.5 nm, a surface charge of +22.73 mV and a magnetic property of 1.5 electromagnetic units per gram. These results confirm the ability of bitter essential oil as an environmentally friendly reaction in the green preparation of iron oxide nanoparticles.

References

[1] Razavi, S, M, Narouei, M, Majrohi, A, A, Mohammaddust Chamanabad, H, R, Chemical constituents and phytotoxic activity of the essential oil of acroptilon repens (L.) Dc from Iran, *J. Essent. Oil-Bear. Plants* 2012, 15(6), 943-948.

[2] Adams, R, P, Identufication of essential oil components by gas choromatography/mass spectroscopy, *Allured Publishing Corporation, IIIinoise*, 1995.

[3] Shah, M, Green synthesis of metallic nanoparticles via biological entities, *Materials*, 2015, 8(11), 7278-7308.

Introduction of a new DABCO-based ionic liquid as an efficient catalyst for the synthesis of benzimidazoquinazolinone derivatives

Fatemeh Mirzaei Eslamlou, Maryam Mousapour and Farhad Shirini*

Department of Chemistry, Faculty of Science, University of Guilan, Rasht, Iran, fatimamirzaie76@gmail.com, shirini@guilan.ac.ir

Keywords: DABCO, multi-component reactions, ionic liquid catalyst, benzimidazoquinazolinones

Benzimidazoquinazolinones are heterocyclic compounds that have been shown various pharmacological activities such as anti-cancer, anti-inflammatory, anti-oxidant, antimicrobial and neuroprotective activity. The diverse pharmacological activities exhibited by benzimidazoquinazolinone make it a promising lead compound for the development of novel therapeutic agents. These attempts resulted in the introduction of a variety of reagents for the promotion of the synthesis of these compounds [1]. Although, each of these methods have their own advantages, some of them often suffer from one or more disadvantages such as use of stoichiometric amounts of reagents, expensive metal precursors, tedious work-up, long reaction times, unsatisfactory product yields, excess of organic solvent, high temperatures, harsh reaction conditions, and difficulty in preparation of the catalyst, which limit the use of these methods. Therefore, it is important to find more convenient methods for the synthesis of benzimidazoquinazolinone derivatives [2]. In this research, we have reported the preparation of a new DABCO-based ionic liquid catalyst which can be used for the promotion of the synthesis of benzimidazoquinazolinone derivatives. It is expected that using the mentioned dicationic ionic liquid with its remarkable features be useful for the elimination of some of the disadvantages of the previously reported methods (**Scheme**).

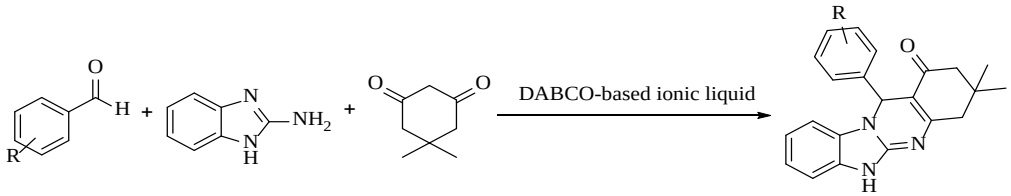

Scheme: synthesis of benzimidazoquinazolinones in the presence of DABCO-based catalyst.

References

[1] Shirini, F., Seddighi, M., Goli-Jolodar, O. (2016). Facile and efficient synthesis of pyrimido [1, 2-*a*] benzimidazole and tetrahydrobenzimidazo [2, 1-*b*] quinazolin-1(2*H*)-one derivatives using Brönsted acidic ionic liquid supported on rice husk ash (RHA-[pmim] HSO $_4$). *J. Iran. Chem. Soc.*, *13*, 2013-2018.

[2] Jadhavar, P. S., Patel, K. I., Dhameliya, T. M., Saha, N., Vaja, M. D., Krishna, V. S, Chakraborti, A. K. (2020). Benzimidazoquinazolines as new potent anti-TB chemotypes: Design, synthesis, and biological evaluation. *Bioorg.Chem.*, *99*, 103774.

Green synthesis of magnetic Tin oxide nanocomposite and its application for degradation of Rhodamin B

Amir Azizi* **and Saba Hatamipour**

Applied Chemistry Laboratory, Faculty of Chemistry, University of Arak, Arak, Iran, a-azizi@araku.ac.ir

Keywords: Green synthesis, Magnetic Tin Oxide, Photocatalytic degradation, Rhodamine B.

In this study, photocatalytic degradation of rhodamine B dye has been investigated as an efficient method to remove this contaminant from aqueous solutions [2,1]. In this regard, using green synthesis as one of the cleanest methods to produce metal oxides, a magnetic composite of tin oxide was prepared for use as a photocatalyst [3]. The specifications of synthesized composite were then determined by common methods [4]. The results of characterizing the prepared composite as a photocatalyst showed that the synthesized structure has an average particle size of 22.5 nm, surface charge + 38 mV and a magnetic property of 20 emu/g. In addition, in order to achieve the maximum photodegradation efficiency (PDE), the effect of important factors such as pH, amount of photocatalyst, initial dye concentration, plus the presence of oxidizing H_2O_2 and Fe^{2+} ion was investigated and optimized. Effective on the process, pH = 5.5, dye concentration of 52.5 mg/L, and value of 0.75 g/L of the magnetic nanocomposite were determined as the best operating conditions, degradation efficiency was 83.4%. The results of the study of the effect of Fentoni agents showed that the addition of concentrations of 200 mg/L of hydrogen peroxide and 3.5 mg/L of ferrous ions resulted in 100% dye degradation only 45 min after the start of the process.

References

[1] Hoffmann, M, R, Martin, S, Choi, W, Bahnemann, D, W, Environmental applications of semiconductor photocatalysis", *Chem. Rev.*, 1995. 95. 69–96.

[2] Herrmann, J, M, Heterogeneous photocatalysis: fundamentals and applications to the removal of various types of aqueous pollutants, *Catal. Today*, 1999. 53. 113–129.

[3] Shah, M, Green synthesis of metallic nanoparticles via biological entities, *Materials*, 2015, 8(11). 7278-7308.

[4] Pirzadeh, M, Caporaso Nicola, R, A, Shariati, M, A, Yessimbekov, Z, Usmankhan M, Pomegranate as a source of bioactive constituents: a review on their characterization, properties and applications, *Crit. Rev. Food Sci. Nutr.*, 2021, 61(6), 982-999.

The synthesis and characterization a green Bronsted-Lewis Acidic Ionic Liquid catalyst in the preparation of Carbamatoalkyl naphthols

Soheila Khaghaninejad*

Organic Chemistry Laboratory, Faculty of Chemistry, University of Arak, Arak, Iran, soheila.khaghani@yahoo.com, s-khaghani@araku.ac.ir

Keywords: Bronsted-Lewis acidic Ionic Liquid catalyst, Aminoacid of histidine, Green, Carbamatoalkyl naphthols

Ionic liquids (ILs), have been widely applied in many reactions as catalyst, solvent or dual catalyst-solvents due to their strong dissolving capacity, negligible vapor pressure, reusability, and high thermal and chemical stability [1,2]. The appearance of functionalized ILs ranges the application fields of ILs. Acidic ILs are a kind of functionalized ILs, have attracted more interest due to their advantages of both solid and liquid acid.

In this work, a green acidic IL catalyst was prepared of aminoacid of histidine with both Brønsted and Lewis acidic sites in the cation and examinated in organic synthesis such as the preparation of carbamatoalkyl naphthols (Scheme 1).

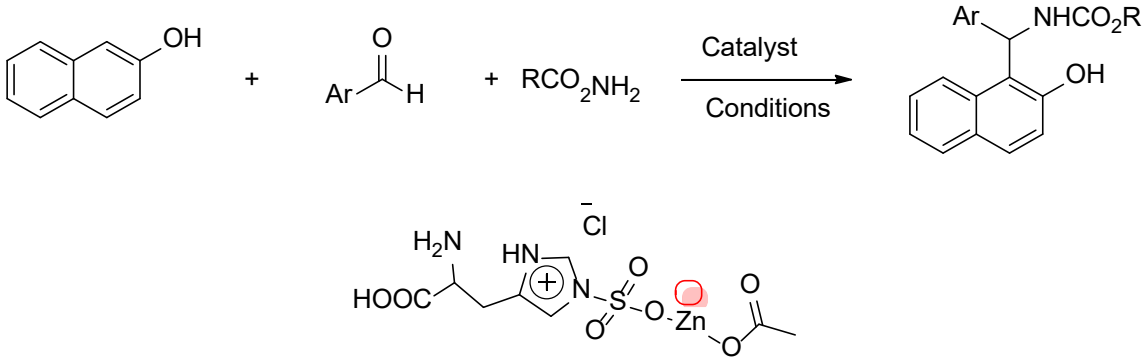

Scheme 1: Bronsted-Lewis acidic Ionic Liquid catalyst

References

[1] Ranu, B. C.; Banerjee, S. Ionic liquid as catalyst and reaction medium: The dramatic influence of a task-specific ionic liquid, [bmlm]OH, in Michael addition of active methylene compounds to conjugated ketones, carboxylic esters, and nitriles. *Org. Lett.* 2005, 7, 3049-3052.

[2] Du, D. M.; Chen, X. New advances of organic synthetic reactions and catalytic asymmetric reaction in ionic liquid media. Chin. *J. Org. Chem.* 2003, 23, 331-343.

Synthesis of inorganic hybrid bromide perovskites with green emission and encapsulation in organometallic frameworks as a stable substrate

Mahtab Naeim[a], Reza Sahraei [a]*, Ali Naghipour[a], Ehsan Soheyli[b]

a) Department of Chemistry, Faculty of Science, Ilam University, Ilam, Iran, naeim.mahtab@gmail.com

b) Department of Physics, Faculty of Science, Ilam University, Ilam, Iran, r.sahraei@ilam.ac.ir

Keywords: Inorganic hybrid bromide perovskites (HBPs), Metal-organic frameworks (MOFs), Green emission, Photoluminescence.

Inorganic hybrid bromide perovskites (HBPs) are a subset of hybrid halide perovskites with the general formula APbBr (where A is a monovalent organic cation) due to band-gap tunable photoactive materials with high absorption coefficients and small exciton binding energies have received a lot of attention [1]. However, their practical applications face many challenges due to their strong combination effects and poor resistance to heat, moisture, polar solvents, and light [2]. In recent years, the use of MOF-based composites has made significant progress. The reason for this is having regular cavities that can accommodate a range of nano-sized guest molecules. It also minimizes the accumulation of particles and increases the stability of guest molecules [3, 4]. In this work, a new HBPs with green was synthesized by ligand-assisted reprecipitation technique (LARP), then it was embeded in the MOF-5 mesostructure in order to improve the stability. HBPs /MOF-5 composites powder resulting has green emission, higher thermal and environmental stability than HBPs.

References

[1] D. Zhang, Y. Xu, Q. Liu, Z. Xia, Encapsulation of $CH_3NH_3PbBr_3$ Perovskite Quantum Dots in MOF-5 Microcrystals as a Stable Platform for Temperature and Aqueous Heavy Metal Ion Detection. *Inorg. Chem. ACS Nano* 2021, *15* (7), 10775-10981.

[2] S. Laha, D. Rambabu, S. Bhattacharyya, Modulating Hierarchical Micro/Mesoporosity by a Mixed Solvent Approach in Al-MOF: Stabilization of $MAPbBr_3$ Quantum Dots. K. Maji, *Inorg. Chem.*, 2020, 17, 14671-14678.

[3] S. Ahmed, S. Lahkar, P. Saikia, D. Mohanta, J. Das, S. Dolui, Stable and highly luminescent $CsPbX_3$ (X= Br, Br/Cl) perovskite quantum dot embedded into Zinc (II) imidazole-4,5-dicarboxylate metal organic framework as a luminescent probe for metal ion detection. *Mater. Chem. Phys*, 2023, 295, 127093.

[4] J. Liu, Y. Zhao, X. Li, J. Wu, Y. Han, X. Zhang, Y. Xu, Dual-Emissive $CsPbBr_3$@Eu-BTC Composite for Self-Calibrating Temperature Sensing Application. *Cryst. GrowthDes*, 2020, 20, 454-459.

Removal of Tetracycline From aqueous solution by Cu-modified γ–MnO_2

Alireza Khorshidi*, Masoumeh Kramati

Department of chemistry, faculty of science, University of Guilan, Rasht, Iran, khorshidi@guilan.ac.ir, masoumekramati637@gmail.com

Keywords: Modification, Removal, γ–MnO_2, Tetracycline

In the last decade, pharmaceutical compounds have become an emerging group of organic pollutants. These products are used in human and veterinary medicine. Presence of these compounds,in water sources can be considered as a serious threat to public health and the environment. It should be noted that antibiotics have low biodegradability and high toxicity compared to other pollutants. In addition, even at very low concentrations, antibiotics have a negative effect on living organisms (for example, algae and bacteria), so it is very important and necessary to remove these compounds from aquatic environments. Tetracycline is one of the most widely used antibiotics produced worldwide. Several treatment methods, including coagulation-precipitation/biosorption,ozonation, biodegradation,and advanced oxidation processes have been used to remove TC from contaminated water sources. Hydrogen peroxide can lead to the production of HO• radicals. Therefore, it can play the role of an oxidizing agent in this process [1,2]. Manganese oxide (MnO_2) due to its availability, tunable crystal structure, and high mobility of network oxygen is widely used.as a heterogeneous catalysts for aerobic oxidations. A variety of MnO_2 materials are formed by octahedral MnO_6 units sharing corners or edges, which form different tunnel and layered structures (such as α-, β-, γ- and δ-MnO_2 etc.) Among the four crystallographic structures, γ-MnO_2 has shown the best electrochemical properties [3]. In this research, γ-MnO_2 was modified with copper and then the product was characterized by X-Ray diffraction (XRD),FTIR,EDX analyses.Eventually, it was used as an efficient catalyst for removal of TC from aqueous Solution [4].

References:

[1].Michalova, E., & Schlegelova, J. (2004). Tetracyclines in veterinary medicine and bacterial resistance to them. *Vet. Med.*, 49(3), 79.

[2].Jaafarzadeh, N., Kakavandi, B., Takdastan, A., Kalantary, R. R., Azizi, M., & Jorfi, S. (2015). Powder activated carbon/Fe 3 O 4 hybrid composite as a highly efficient heterogeneous catalyst for Fenton oxidation of tetracycline: degradation mechanism and kinetic. *RSC adv.*, 5(103), 84718-84728.

[3]. Xie, A., Tao, F., Jiang, C., Sun, W., Li, Y., Hu, L., ... & Yao, C. (2017). A coralliform-structured γ MnO2/polyaniline nanocomposite for high-performance supercapacitors. *J. Electroanal. Chem.*, 789, 29-37.

[4]. Wang, P., Duan, J., Wang, J., Mei, F., & Liu, P. (2020). Elucidating structure-performance correlations in gas-phase selective ethanol oxidation and CO oxidation over metal-doped γ-MnO_2. *Chinese J. Catal.*, 41(8), 1298-1310.

Nano-Drug Carriers: Synthesis, Drug loading, Characterization and Biological Evaluation

Ali Hossein Rezayan*, Hale Alvandi

Division of Nanobiotechnology, Department of Life Science Engineering, Faculty of New Sciences and Technologies, University of Tehran, P.O. Box 14395-1561, Tehran, Iran, ahrezayan@ut.ac.ir

Keywords: Drug Delivery, Drug Carriers, Bioconjugation, Nanotechnology

With the emergence of nanotechnology, integrating science fields became more critical. Drug delivery through nanostructures improves treatment by increasing therapeutic efficacy, reducing toxicity, and increasing patient acceptance. The use of bioconjugation methods, which refers to the covalent linkage of a biological and a chemical molecule facilitates the permeability, retention time, and targeted delivery of nanoparticles [1-4]. In continuation of our research in the field of synthesis of drug-carrying nanostructures, here we intend to introduce nanocarriers made in our research laboratory for targeted drug delivery to cancerous tissues or repair of damaged tissues (**Scheme**).

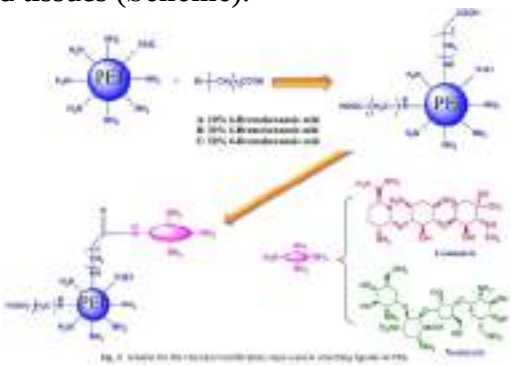

Scheme: illustration of chemical modification steps used in attaching ligands to PEIs.

References

1) Oroojalian, F., Rezayan, A.H., Mehrnejad, F., Nia, A.H., Shier, W.T., Abnous, K. and Ramezani, M. Efficient megalin targeted delivery to renal proximal tubular cells mediated by modified-polymyxin B-polyethylenimine based nano-gene-carriers. *Mater. Sci. Eng. C*, 2017, *79*, 770-782.
2) Hamedinasab, H., Rezayan, A.H., Mellat, M., Mashreghi, M. and Jaafari, M.R. Development of chitosan-coated liposome for pulmonary delivery of N-acetylcysteine. *Int. J. Biol. Macromol.*, 2020, *156*, 1455-1463.
3) Mirmajidi, T., Chogan, F., Rezayan, A.H., Sharifi, A.M., In vitro and in vivo evaluation of a nanofiber wound dressing loaded with melatonin, *Int. J. Pharm.*, 2021, *596*, 120213.
4) Chogan, F., Mirmajidi, T., Rezayan, A.H., Sharifi, A.M., Ghahary, A., Nourmohammadi, J., Kamali, A., Rahaie, M., Design, fabrication, and optimization of a dual function three-layer scaffold f or controlled release of metformin hydrochloride to alleviate fibrosis and accelerate wound healing, *Acta Biomater.*, 2020, *113*, 144–163.

Salicylaldehydes in multicomponent reactions: Synthesis of new heterocycles

Afshin Sarvary *

Department of Chemistry, Faculty of Science, Babol Noshirvani University of Technology, Shariati Ave., Babol, Iran, Post Code: 47148-71167, a.sarvary@nit.ac.ir

Keywords: Salicylaldehyde, Multicomponent reactions, Heterocycle

Salicylaldehydes, which have one aldehyde and one phenolic functional group, show a different behaviour and lead to compounds with different structures in comparison to other aromatic aldehydes in certain multicomponent reactions (MCRs) [1-2]. In this study, salicylaldehydes with different substitutions as the aldehyde component in the Strecker and Groebke-Blackburn-Bienayme (GBB) 3-component reactions (3CR) were investigated in the absence of the any catalyst. The results showed that the Strecker reaction with salicylaldehydes resulting the benzofuro[2,3-b]pyrazin-2(1H)-ones and in the GBB-3CR salicylaldehyde substitution plays an effective role in the reaction process. Salicylaldehydes with Br and Cl substitution groups led to a pseudo four-components reaction, producing 4H-1,3-benzodioxine-4,4-dicarboxamides. Conversely, salicylaldehydes with NO_2 substitution participated in the GBB-3CR and produced 2-(3-aminoimidazo[1,2-a]pyridin-2-yl)phenols (**Scheme**).

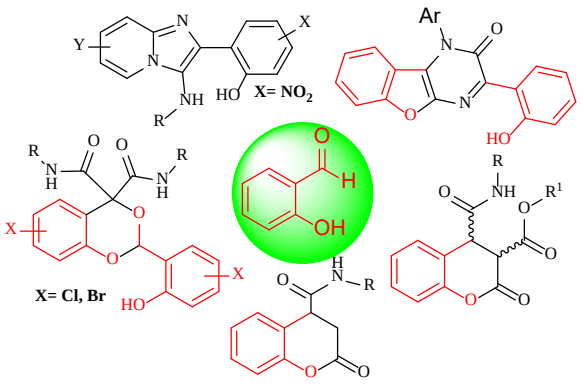

Scheme: Salicylaldehydes in multicomponent reactions

References

[1] Heravi, M. M.; Zadsirjan, V.; Mollaiye, M.; Heydari, M.; Koshvandi, A. T. K. Salicylaldehydes as privileged synthons in multicomponent reactions. *Russ. Chem. Rev.* 2018, 87, 553–585.

[2] Mousazadeh, M.; Sarvary, A.; Notash, B. Experimental investigation of salicylaldehydes in Groebke-Blackburn-Bienayme -3-component reaction, *Tetrahedron* 2023, *138*, 133415.

Synthesis and Characterization of MPy@GQD as Hybrid of Porous Organic Polymers with Graphen Quantum Dots

Haniyeh Farrokhi, Massoumeh Bagheri*

Department of Chemistry, Faculty of Science, Azarbaijan Shahid Madani University, Tabriz, Iran, farrokhi_hanie@yahoo.com, massoumehbagheri@yahoo.com

Keywords: Porous organic polymers, Melamine, Graphene Quantum Dots, 6-Pyridine dicarboxylic acid

Porous organic frameworks/polymers (POFs/POPs) are an intriguing class of porous materials distinguished by their distinctive characteristics, including a straightforward synthesis process, enduring and adjustable porosity, a high specific surface area, robust thermal stability, and low density [1]. On the other hand, Graphene Quantum Dots (GQDs) have garnered significant attention due to their exceptional optical properties and their potential applications in sensing, diagnostics, imaging, and optoelectronic devices. Recently, a novel type of polyamine-functionalized CQD, achieved through capping with branched poly-(ethylenimine) (BPEI), has emerged as fluorescent probes for the selective and sensitive detection of copper ions [2]. In this study, we developed a hybrid material called MPy@GQD, which combines the features of Porous Organic Polymers (POPs) and Graphene Quantum Dots (GQDs). This was achieved through a one-pot polyamidation reaction involving melamine (M), 2,6-pyridine dicarboxylic acid (Py), and GQD. The reaction was carried out using different molar ratios of Py/M and GQD in solvothermal condition (**Scheme**). The successful synthesis of MPy@GQD was confirmed through various analyses, including XRD, FTIR, SEM, BET, and TGA. As a result, MPy@GQD was obtained as a mesoporous adsorbent, boasting an impressive surface area of 474 m^2/g, also systematically investigated how the molar ratio of GQDs in the synthesis of MPy@GQD affected its thermal stability, crystallinity, porosity, and morphology. Notably, all the synthesized MPy@GQDs exhibited an amorphous structure. Therefore, this material shows significant potential for use in applications related to the adsorption of metal ions.

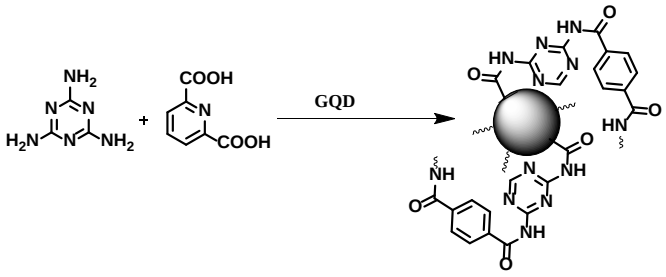

Scheme: Synthesis of MPy@GQD from the reaction of M, Py and GQD.

References

[1] L. Tan, B. Tan, Hypercrosslinked porous polymer materials: design, synthesis, and applications, *Chem. Soc. Rev.* 2017, 46, 3322–3356.

[2] Liu, Wang, Y.M. and Han, Fluorescent chemosensors for copper (II) ion: Structure, mechanism and application. *J. Photochem. Photobiol.* 2017, *32*, 78-103.

Catalytic behaviour of modified bone char nano compound in synthesis of organic compounds

Zahra Siahpour, Maryam Hajjami*

Department of Organic Chemistry, Faculty of Chemistry, Bu-Ali Sina University, Postal code 6517838683, Hamedan, Iran, m.hajjami@basu.ac.ir or mhajjami@yahoo.com

Keywords: Bone char, Nano catalyst, food waste, pyrimidine-5-carbonitrile

Bone char is a solid phosphorus rich food waste derived sustainable mesoporous material which is produced by the under controlled thermal conditions of animal bones [1]. Recently the mesoporous bone char has gained considerable attention owing to with excellent features such as large surface areas, very low cost, ease of preparation and biocompatibility [2]. In this work, bone char nanoparticles were prepared from pyrolysis of bone char and functionalization with 3-aminopropyl-triethoxsysilane then sulfonation supported with chlorosulfonic acid as reusable and environmental biocatalyst. The modified bone char as Bronsted acid catalyst was characterized by FT-IR, XRD, SEM, EDS and BET techniques. The modified bone char showed excellent catalytic activity for the synthesis of pyrimidine-5-carbonitrile derivatives (**Scheme**).

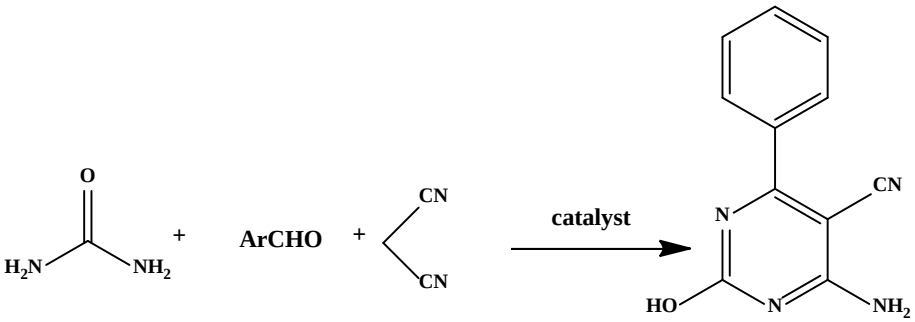

Scheme: Synthesis of pyrimidine-5-carbonitrile derivatives in the presence of sulfonated bone char as catalyst under solvent-free condition at 80 ℃

References

[1] Wang, M.; Liu, Y.; Yao Y.; Han, L.; Liu, X. Comparative evaluation of bone chars derived from bovine parts: Physicochemical properties and copper sorption behaviour. *Sci. Total Environ.* 2020, *700*, 134470-134485.

[2] Piccirillo, C. Preparation, characterisation and applications of bone char, a food waste-derived sustainable material: A review. *J. Environ. Manage.*, 2023, *339*, 117896-117920.

An efficient method for the degradation of picric acid using GO/$NiMn_2O_4$

Ayda Farajollahi*, Kolsum Mohammadsharifi , Ahmad Poursattar Marjani

Department of Organic Chemistry, Faculty of Chemistry, Urmia University, Urmia, Iran, aydafarajollahi@yahoo.com

Keywords: Degradation, GO/$NiMn_2O_4$ nanocomposite, Picric acid

The world has faced many environmental problems with the increase in population and the fast development of industry and technology [1]. The utilization of metal oxides based on carbon materials has gained increased attention for the degradation of organic pollutants [2, 3]. Herein, a new methodology was described for the fabrication of GO/$NiMn_2O_4$ nanocomposite for the removal of picric acid. The exfoliated GO sheets helped to control the crystallinity of $NiMn_2O_4$ spontaneously by inducing oxygen vacancies (OVs). Moreover, the active sites of nickel, manganese and the high electronic conductivity of GO in nanocomposite exhibited a vital role in degradation of picric acid. The prepared nanocomposite indicated the highest degradation rate of picric acid (97%) within 40 min The results indicated that the picric acid degradation in the presence of GO/$NiMn_2O_4$ was better than alone-$NiMn_2O_4$, confirming the synergistic effect of GO layers with metal oxides.

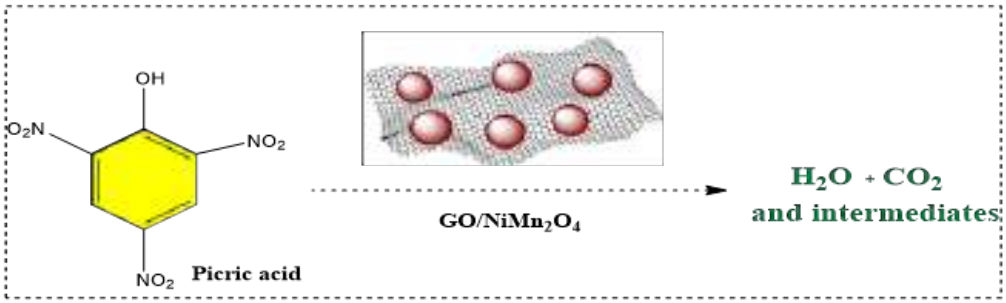

Scheme: Degradation of picric acid in the presence of GO/$NiMn_2O_4$

References

[1]. Alamgholiloo, H., et al., Synergistic advanced oxidation process for the fast degradation of ciprofloxacin antibiotics using a GO/CuMOF-magnetic ternary nanocomposite. *J. Environ. Chem. Eng.* 2021. **9**(4): p. 105486.

[2]. Zhao, L., et al., An efficient heterogeneous catalyst of $FeCo_2O_4$/g-C_3N_4 composite for catalytic peroxymonosulfate oxidation of organic pollutants under visible light. *Colloids Surf. A Physicochem. Eng. Asp.*, 2021. **610**: p. 125725.

[3]. Qiu, S., et al., An efficient and low-cost magnetic heterogenous Fenton-like catalyst for degrading antibiotics in wastewater: Mechanism, pathway and stability. *J. Environ. Manage.* 2022. **302**: p. 114119.

Development of $FeMn_2O_4$/CNT heterostructure for the synthesis of pyranoquinolines

Ayda Farajollahi*, Kolsum Mohammadsharifi , Ahmad Poursattar Marjani

Department of Organic Chemistry, Faculty of Chemistry, Urmia University, Urmia, Iran, aydafarajollahi@yahoo.com

Keywords: $FeMn_2O_4$/CNT, Multi-component reaction, Pyranoquinolines

With the increase in population and the emergence of various diseases, the need for drugs has increased, especially drugs that have heterocyclic compounds in their structure. Multicomponent reactions are one of the most important and effective reactions in the field of synthesis of heterocyclic compounds in chemistry, which makes the reaction easy and fast without the need to separate the intermediates [1, 2]. The pyranoquinoline derivatives are synthetically important due to their biological properties [3]. In this research, these derivatives were produced through an environmentally friendly method. This method includes the use of $FeMn_2O_4$/CNT as a nanocatalyst, which is easy to produce, has excellent performance, cost-effectiveness, and recyclability among its features, and also the use of water as a green solvent. Pyranoquinolines through the one-pot, the multi-component reaction between different derivatives of arylgloxal, ethyl cyanoacetate, and 4-hydroxyquinoline-2(1*H*)-one were synthesized using nanocatalyst, Na_2CO_3, and H_2O.

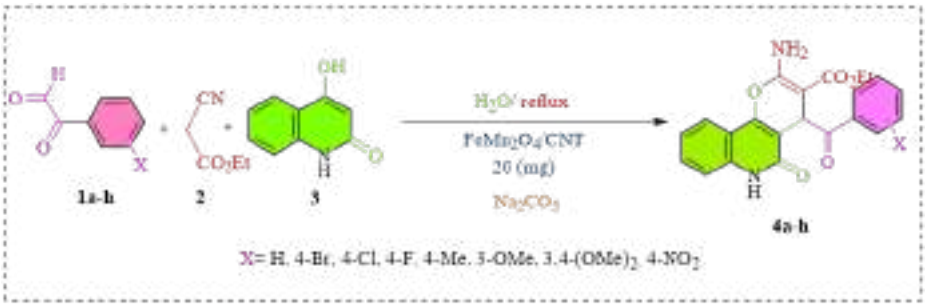

Scheme: One-pot preparation of pyranoquinolines.

References

[1]. Li, M., et al., Microwave-assisted combinatorial synthesis of hexa-substituted 1,4-dihydropyridines scaffolds using one-pot two-step multicomponent reaction followed by a S-alkylation. *J. Comb. Chem.*, 2008. **10**(3): p. 436-441.

[2]. Shaabani, A., Rahmati, A. and E. Farhangi, Water promoted one-pot synthesis of 2′-aminobenzothiazolomethyl naphthols and 5-(2′-aminobenzothiazolomethyl)-6-hydroxyquinolines. *Tetrahedron Lett.*, 2007. **48**(41): p. 7291-7294.

[3]. El-Agrody, A.M., Abd-Rabboh, H.S. and Al-Ghamdi, A.M. Synthesis, antitumor activity, and structure–activity relationship of some 4H-pyrano[3,2-H]quinoline and 7H-pyrimido[4′,5′:6,5]pyrano[3,2-h]quinoline derivatives. Med. Chem. Res., 2013. **22**: p. 1339-1355.

Application of magnetic molecularly imprinted polymer as a green catalyst in multicomponent reaction

Elaheh Hashemi *, **Nahid Pahlavani**

Department of Chemistry, Faculty of Sciences, Shahid Rajaee Teacher Training University, P.O. Box: 16785-163, Tehran, Iran, e.hashemi@sru.ac.ir, venus.npa@gmail.com

Keywords: Molecularly imprinted polymer, Magnetic nanoparticles, Multicomponent reaction, Dimedone.

Molecularly imprinted polymer (MMIP) catalysts are catalysts that are synthesized in the presence of a specific template molecule, which is usually the substrate or product of the desired reaction. The template molecule plays a crucial role in creating binding sites within the catalyst that are tailored to its structure. These binding sites are essential for selectively binding to the substrate and facilitating the desired reaction [1, 2].

In the synthesis of a targeted magnetically imprinted polymer (MMIP), octahydroquinazolinone was employed as the template, while 4-vinylpyridine served as the monomer, and vinylized magnetite nanoparticles acted as the carriers. The efficacy of MMIP catalyst was utilized in an octahydroquinazolinone synthesis through a multicomponent Biginelli reaction. The results showed that template and its analogue products were successfully synthesized in water as an absolutely green solvent in appropriate time under reflux condition (**Scheme 1**). In addition, reusability of catalyst was effectively examined for 5 successive cycle runs.

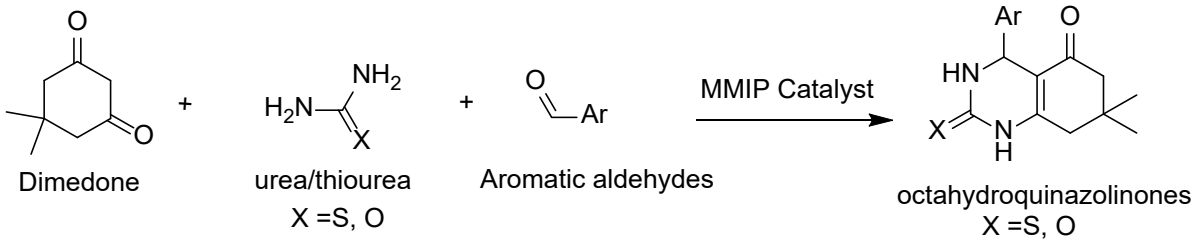

Scheme 1: Octahydroquinazolinones synthesis in the presence of MMIP catalyst

References

[1] Meseguer-Lloret, S.; Torres-Cartas, S.; Gómez-Benito, C.; Herrero-Martínez, J. M. Magnetic molecularly imprinted polymer for the simultaneous selective extraction of phenoxy acid herbicides from environmental water samples. *Talanta* 2022, *239*, 123082.

[2] Shaabani, A.; Afshari, R.; Hoshmand, S. E.; Keramati Nejad, M. Molecularly Imprinted Polymer as an Eco-Compatible Nanoreactor in Multicomponent Reactions: A Remarkable Synergy for Expedient Access to Highly Substituted Imidazoles. *ACS sustainable chem. eng.* 2017, *5*, 19396-4716.

Synthesis of 2-Substituted-7-trifluoromethyl-thiadiazolopyrimidones as alkaline phosphatase inhibitors

Behzad Jafari, Peter Langer *

Institut für Chemie, Universität Rostock, Albert-Einstein-Str. 3a, 18059 Rostock, Germany, behzadjafari961@yahoo.com, peter.langer@uni-rostock.de

Keywords: Suzuki-Miyaura reaction, Thiadiazolopyrimidones, Cross coupling reaction, Alkaline Phosphatase (AP).

Alkaline Phosphatases (APs) play a key role in maintaining a ratio of phosphate to inorganic pyrophosphate (P_i/PP_i) and thus regulate extracellular matrix calcification during bone formation and growth [1]. Among different isozymes of AP, aberrant increase in the level of tissue non-specific alkaline phosphatase (TNAP) is strongly associated with vascular calcification and end-stage renal diseases [2]. In this context, we synthesized a novel series of fluorinated pyrimidone derivatives, *i.e.*, 2-bromo-7-trifluoromethyl-5-oxo-5*H*-1,3,4-thiadiazolepyrimidones. The bromine functionality was further used for derivatisation palladium catalysed cross-coupling reactions (Scheme). The synthesized derivatives were found potent but non-selective inhibitors of both isozymes of AP. Arylated thiadiazolopyrimidones exhibited strong inhibitory activities [3].

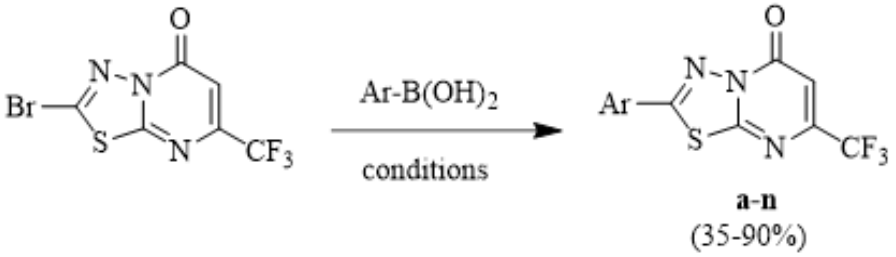

Scheme: Ar-$B(OH)_2$ (1.1 equiv.), $Pd(OAc)_2$ (10 mol%), XanthPhos (20 mol%), K_2CO_3 (2.0 equiv.), 1,4-dioxane, 100 °C, 16 h. Yields refer to isolated products.

References

[1] Sharma, U.; Pal, D.; Prasad, R. Alkaline phosphatase: an overview. *Indian J. Clin. Biochem* 2014, *29*, 269-278.

[2] Zimmermann, H. Extracellular metabolism of ATP and other nucleotides. *Arch. Pharmacol* 2000, *362*, 299-309.

[3] Jafari, B.; Langer, P. 2-Substituted-7-trifluoromethyl-thiadiazolopyrimidones as alkaline phosphatase inhibitors. Synthesis, structure activity relationship and molecular docking study. *Eur. J. Med. Chem* 2018, *144*, 116-127.

Removal of industrial contaminants from water: A review

Nadia Jafaei *

Faculty of Chemical Engineering, Islamic Azad University, Science and Research Branch, Tehran, Iran, nadiajafaei@gmail.com

Keywords: Heavy metals, Membrane filtration, Water

Fresh water is a valuable natural resource and can be easily contaminated. In the 21st century, water has become a scarce natural resource globally due to population growth, urbanization, and widespread agricultural practices. These factors cause industrial water pollution, groundwater depletion and greenhouse gas emissions, which in turn cause global warming. Human water demand in arid environments continues to increase, and groundwater supplies are limited, causing severe annual droughts. Industries such as mining and agriculture account for more than 70% of surface freshwater loss through pollution during mineral processing and over-irrigation of crops, respectively. Various sources such as heavy metals, dyes, pathogenic and organic compounds lead to a decrease in water quality. Pollution of surface and underground water sources by industrial wastes aggravates water shortages and as a result severe health risks that threaten aquatic and terrestrial life. does, intensifies. Increasing industrialization and urbanization have put pressure on water resources. This eventually leads to the contamination of clean water. In low-lying areas, the dumping of industrial waste increases the chances of water pollution due to the high rate of infiltration into the soil. Pollutants can reach water sources both through underground water and through surface water and by the release of solid, liquid or gas particles from different industries. Pollutants can be reduced through physical, chemical and biological methods, thereby reducing the health and environmental effects caused by it. Several alternative treatment processes, such as membrane filtration, have been proposed as final treatment methods. The purpose of this article is to summarize the types of pollutant compounds, filtration processes and membranes that have been studied the most in this field, with special emphasis on how changing the membranes, whether the manufacturing process or the composition of nanomaterials, affects their performance. Based on past research, these techniques significantly remove one or more pollutants, but are not sufficient to effectively remove most toxic pollutants from wastewater. Technologies combined with nanomaterials may be a skilful approach to remove various pollutants from wastewater.

References

[1] Lee CS, Robinson J, Chong MF. A review on application of flocculants in wastewater treatment. *Process Saf. Environ. Prot.* 2014;92(6):489-508.
[2] Howard, G.; Calow, R.; Macdonald, A.; Bartram, J. Climate Change and Water and Sanitation: Likely Impacts and Emerging Trends for Action. Annu. Rev. Environ. Resour. 2016, 41, 253–276.
[3] Afroz, R., Rahman, A., and Rahman, A. Health Impact of River Water Pollution in Malaysia. *Int. J. Adv. Appl. Sci.* 2017, 4 (5), 78–85.

Removal of methylene blue dye using nanocomposite based on branched polyethyleneimine

Maryam Khademian[a*], Yaghub Sarrafi[a], Mahmood Tajbakh[a], Shahla Azimi[a]

a) Department of Organic Chemistry, Faculty of Chemistry, University of Mazandaran, Babolsar, 47416-95447, Iran, m.khademian.gh@gmail.com.
b) Department of Medical Sciences, Faculty of Nursing, University of Iran, 14197-33171, Iran.

Keywords: Methylene blue, Polyethylenimine, Adsorption

Methylene blue (MB), a cationic dye, is used as a dyeing agent for cotton, wool, and silk. Various techniques such as flocculation, absorption, oxidation, electrolysis, biodegradation and ion exchange are used to remove color from wastewater [1]. Among the different techniques, absorption has attracted much attention due to its several advantages, including lower cost, ease of operation, flexibility and simplicity of design, and insensitivity to toxins [2-3]. In the present study, PEI/SA/cMWCNTs nanocomposite was synthesized to remove harmful cationic methylene blue from wastewater. Then, the influence of several factors including adsorbent dose, contact time, pH, rotation speed, MB dye concentration, as well as isotherms, kinetics and thermodynamics of adsorption were investigated. The advantages of the synthesized nanocomposite include high absorbency in a short time, easy separation from wastewater, retrievability and cost-effectiveness.

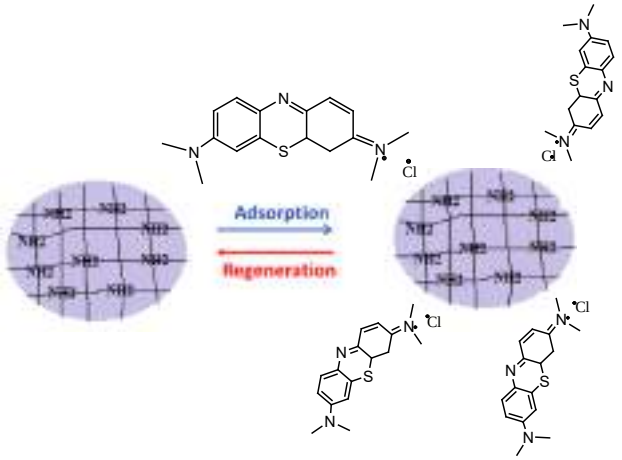

Scheme: Adsorption of methylene blue.

References

[1] Soni, M.; Sharma, AK.; Srivastava, JK.; Yadav, JS. Adsorptive removal of Methylene blue dye from an aqueous solution using water hyacinth root powder as a low cost adsorbent. Int. J. Chem. Sci. Appl. 2012, 3(3), 338–45.
[2] Bhatnagar A.; Sillanpaa M. Utilization of agro-industrial and municipal waste materials as potential adsorbents for water treatment – A review. *Chem. Eng. J.* 2010, 157(2-3), 277–96.
[3] Crini G. Non-conventional low-cost adsorbents for dye removal: a review. *Bioresour Technol.* 2005, 97, 1061–85.

Modification of magnetic nanoparticles surface by Copper(II) complex as a heterogeneous nanocatalyst for the Synthesis of 2,3-Dihydroquinazolin-4(1H)-ones

Tara Miladi, Masoomeh Norouzi*

Department of Chemistry, Faculty of Science, Ilam University, P.O. Box 69315516, Ilam, Iran, taramiladi707@gmail.com, m.norozi@ilam.ac.ir

Keywords: Nanocatalyst, Copper complex, 2,3-Dihydroquinazolin-4(1H)-one

Nanoscale materials have attracted worldwide attention for their unique physical and chemical properties, which is different than their bulk counterparts. Due to this property, they have emerged as a powerful technique in catalysis, chemistry, biology, and physics [1-2]. Nanoparticles (NPs) have attracted the attention of scientists because of their wide range of advantages such as modified structure, surface area to volume ratio and high activity. An efficient and heterogeneous novel magnetic silica-coated phenylenediamine copper complex [$ZrFe_2O_4$@SiO_2@Phenylenediamine-Cu(II)] was employed in the synthesis of 2,3-dihydroquinazolin-4(1H)-one. The aforementioned nanocatalyst were characterized by FTIR, XRD, TGA, FESEM, and EDS. These results disclosed that the chemical grafting was successfully performed. The high activity in mild condition and the simple recoverable from the reaction are the suitable characteristics of this catalyst. Finally, the catalyst sustained activity for five cycles of reaction (**Scheme**).

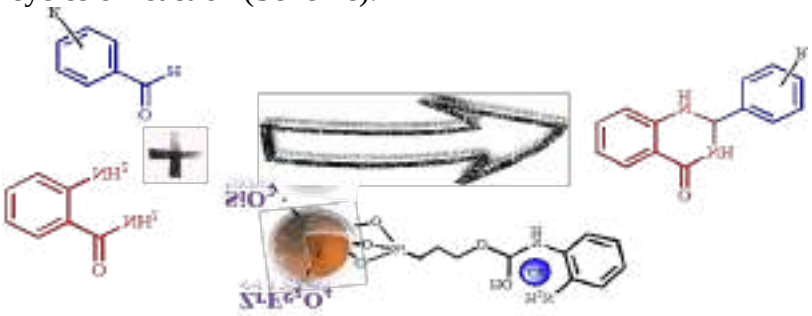

Scheme: Synthesis of 2,3-dihydroquinazolin-4(1H)-one catalyzed by $ZrFe_2O_4$@SiO_2@Phenylenediamine-Cu(II)

References

[1] Li, H.; Chen, X.; Shen, D.; Wu, F.; Pleixats, R.; Pan, J. Functionalized silica nanoparticles: classification, synthetic approaches and recent advances in adsorption applications. *Nanoscale* 2021, *38*, 15998-16016.

[2] Norouzi, M.; Beiranvand, S. Fe_3O_4@SiO_2@BHA-Cu(II) as a new, effective, and magnetically recoverable catalyst for the synthesis of polyhydroquinoline and tetrazole derivatives. *J. Chem. Sci.* 2023, *135*,1-13.

Synthesis and characterization of Zinc ferrite nanocomposite based on polymer for dye pollutant removal

Abdollah Fallah Shojaei*, Maryam Pourjamal

Department of Chemistry, Faculty of Science, University of Guilan, Rasht, Iran, a.f.shojaie@guilan.ac.ir, maryampourjamal76@gmail.com

Keywords: Zinc ferrite, Silver iodide, Photocatalytic, Degradation

Zinc ferrite as one of the transition-metal spinal ferrites has attracted widespread attention because of its low cost, visible light absorbance (Eg≈1.9 eV), extraordinary photochemical stability and magnetic recyclability [1]. Owing to the proper band gap (~2.77 eV) and giant photosensitivity, AgI has for a long time been expected to be a promising material for photocatalysis applications. It is often used to modify other semiconductors to simultaneously improve the poor charge carrier transfer rate and the optical absorption capacity [2]. In this work, $ZnFe_2O_4$/AgI nanocomposites were favorably prepared through a feasible one-step hydrothermal approach. The efficiency of the $ZnFe_2O_4$/AgI nanocomposite as a nanophotocatalyst is screened in the photo degradation processes of Rhodamine B (RhB), under visible-light irradiation. The effect of catalyst loading, H_2O_2 concentration and contact time on the photocatalytic activity of $ZnFe_2O_4$/AgI nanoparticles will be investigated. Finally, to enhance the photocatalytic activity, polyether sulfone was introduced into the $ZnFe_2O_4$/AgI nanocomposite, resulting in the formation of a polymer nanocomposite. This synthesis was investigated by FT-IR, EDX and XRD spectra.

References

[1] Liang, P. L., Yuan, L. Y., Deng, H., Wang, X. C., Wang, L., Li, Z. J., ... & Shi, W. Q. Photocatalytic reduction of uranium (VI) by magnetic $ZnFe_2O_4$ under visible light. *Appl. Catal. B: Environ.* 2020, *267*, 118688-118712.

[2] Zhang, X. G., Guan, D. L., Niu, C. G., Cao, Z., Liang, C., Tang, N., ... & Zeng, G. M. (2019). Constructing magnetic and high-efficiency AgI/$CuFe_2O_4$ photocatalysts for inactivation of Escherichia coli and Staphylococcus aureus under visible light: Inactivation performance and mechanism analysis. *Sci. Total Environ.*, *668*, 730-742.

Investigating of the targeted release of curcumin attached to COOH-functionalized carbon nanotubes through molecular mechanics

Roya Moeinzadeh [a*], Hooriye Yahyaei [b] and Fariba Jafari [a]

a) Department of Chemistry, Dezful Branch, Islamic Azad University, Dezful, Iran, Ro_moein@yahoo.com

b) Chemistry Department, Zanjan Branch, Islamic Azad University, Zanjan, Iran.

Keywords: Curcumin, Carbon nanotubes, Solvent effect, Molecular mechanics, Force field.

Curcumin, or diferuloylmethane, is a bright yellow chemical with anticancer, antioxidant and anti-inflammatory properties. It is the major bioactive polyphenol acquired in the rhizome of *Curcuma longa* (turmeric) and in others *Curcuma* spp. The structure of curcumin consists of: two aromatic O-methoxy phenolic groups joined by a seven- carbon linker including an α,β-unsaturated β-diketone moiety. The bioactive ability of curcumin is due to the presence of two aromatic phenolic groups and diketone moiety in its structure [1-2]. In this study, the interaction of curcumin with COOH-functionalized carbon nanotubes was examined using AMBER, OPLS, CHARMM and MM^+ force fields through the molecular mechanic (MM) method. The calculations were performed through the Monte Carlo simulation methods at different temperatures. The effects of gas phase and various solvent media with different dielectric constants were investigated on the interaction of curcumin with COOH-functionalized carbon nanotubes using the above-mentioned force fields [3]. Moreover, the absorption energy of curcumin on COOH-functionalized carbon nanotubes increased compared to curcumin. On the other hand, if curcumin can penetrate the cancer cells, it has the ability to cause apoptosis, or programmed cell death. The results show that COOH-functionalized carbon nanotubes are more efficient than carbon nanotubes. They are better able to complex with curcumin and penetrate the cancer cells more easily.

References

[1] Hamilton, A. E.; Gilbert, R. J.; Curcumin release from biomaterials for enhanced tissue regeneration following injury or disease. *Bioengineering* 2023, *10*, 262.

[2] Priyadarsini, K. I.; The chemistry of curcumin: from extraction to therapeutic agent. *Molecules*. 2014, *19*, 20091-20112.

[3] Yahyaei, H.; Sharifi, S.; Shahab, S.; Sheikhi, M.; Ahmadianarog, M., Theoretical study of adsorption of solriamfetol drug on surface of the B12N12 fullerene: a DFT/TD-DFT approach. *Lett. Org. Chem.* 2021, *18*, 115-127.

Monte Carlo calculation of the interaction between zonisamide and boron nitride nanotubes

Roya Moeinzadeh[a*], Fariba Jafari [a] and Hooriye Yahyaei [b]

a) Department of Chemistry, Dezful Branch, Islamic Azad University, Dezful, Iran, Ro_moein@yahoo.com

b) Chemistry Department, Zanjan Branch, Islamic Azad University, Zanjan, Iran.

Keywords: Zonisamide, Boron nitride nanotubes, Solvent effect, Molecular mechanics, Monte Carlo.

Zonisamide, brand name zonegran, is used to treat parkinson's disease and is a novel antiepileptic drug (AED). It is considered a benzisoxazole derivative and is a sulfonamide anticonvulsant that is structurally different from other AEDs [1]. This study evaluated the interaction between zonisamide and boron nitride nanotubes (BNNTs). The calculations were performed using the two methods of quantum mechanics and molecular mechanics. The effect of different solvents on the interaction between zonisamide and BNNTs was investigated through Onsager self-consistent reaction field (SCRF) model. Also Using the DFT method, the effect of temperature on the stability of interactions of the compounds in various solvents was investigated. Moreover, the interaction of zonisamide with BNNTs was investigated through OPLS force field by using the molecular mechanic (MM) method. Calculations were performed using Monte Carlo simulation methods at different temperatures. The effects of gas phase and diverse solvent environments with different dielectric constants were investigated on the interaction of zonisamide by using the aforementioned force fields [2]. Calculations show that S=O functional groups play an important role in drug release through boron nitride nanotubes, and the effect of solvents, especially methanol, is reflected in this interaction.

References

[1] Matsunaga, S.; Kishi, T.; Iwata, N. Combination therapy with zonisamide and antiparkinson drugs for parkinson's disease: A meta-analysis. *J. Alzheimer's Dis.* 2017, *56* ,1229–1239.

[2] Piryaei, F.; Shajari, N.; Yahyaei, H. Efficient ZrO (NO_3) 2.2 H_2O catalyzed synthesis of 1H-indazolo [1,2-b] phthalazine-1,6,11 (13H)-triones and electronic properties analyses, vibrational frequencies, NMR chemical shift analysis, MEP: A DFT study. *Heteroat. Chem.* 2020, NA-NA.

Fabrication and characterization of nanocomposite membranes based on Poly lactic acid

Abdollah Fallah Shojaei[a*], Katayoun Hasanpour[a]

Department of Chemistry, Faculty of Science, University of Guilan, Rasht, Iran, a.f.shojaie@guilan.ac.ir, katyhp646@gmail.com.

Keywords: Poly lactic acid, γ-Fe_2O_3, Nanocomposite, Wet chemical method.

Herein, a novel electrospun composite membrane with a dual-scaled porous structure and nano-raised structure on each fiber was fabricated through electrospinning using biodegradable poly lactic acid (PLA) and magnetic γ-Fe_2O_3 nanoparticles [1]. In this work, magnetic nanoparticle was synthesized by a wet chemical method [2]. The magnetic nanocomposite used in this study was synthesized through the addition of metal compounds such as Ag, Cu, Ti, and Zn to the γ-Fe_2O_3 nanoparticles. Finally, the nanocomposite membranes were fabricated using the electrospinning method, and application of the prepared nanocomposites was investigated. The fabricated nanocomposite membrane shows high hydrophobic properties and excellent ability to completely remove oil from water. Furthermore, the characterization of nanocomposite was investigated using Fourier-transform infrared spectrum (FT-IR), energy-dispersive X-ray spectroscopy (EDX), and x-ray diffraction (XRD). The morphological aspect of the nanocomposite membrane was identified by scanning electron microscopy (SEM). This study revealed that the addition of metal elements to the nanocomposite illustrated better performance at oily pollutant adsorption.

References

[1] Zhang, Di, et al. "Electrospun fibrous membranes with dual-scaled porous structure: super hydrophobicity, super lipophilicity, excellent water adhesion, and anti-icing for highly efficient oil adsorption/separation." *ACS Appl. Mater. Interfaces* 11.5 (2019): 5073-5083.

[2] Darezereshki, Esmaeel. "Synthesis of maghemite (γ-Fe_2O_3) nanoparticles by wet chemical method at room temperature." *Mater. Lett.* 64.13 (2010): 1471-1472.

Synthesis and Characterization of catalyst based on cinchonine - polyacrylic acid supported on nano silica

Farzad Zolfaghari, Yasmin Noori, Ali Reza Kiasat*

Department of Chemistry, Faculty of Science, Shahid Chamran University of Ahvaz, Ahvaz, Iran, farzad.chemistry99@gmail.com, akiasat@scu.ac.ir

Keywords: Catalyst, Nano silica, Polyacrylic acid, Cinchonine

In the past decades, the use of catalysts has been used to increase the speed of reactions and minimize hazardous waste materials. One of the most widely used catalysts is silica-based catalysts. In this work, the surface of nano silica was first modified by mercapto propyl trimethoxy silane in toluene. Free radical polymerization of the thiolated silica with acrylic acid and cinchonine by AIBN initiator produced acrylic acid-cinchonine random copolymer supported nanosilica. (Scheme 1). Then, the synthesized catalyst was used in the multi-component Hantzsch reaction. (Scheme 2).

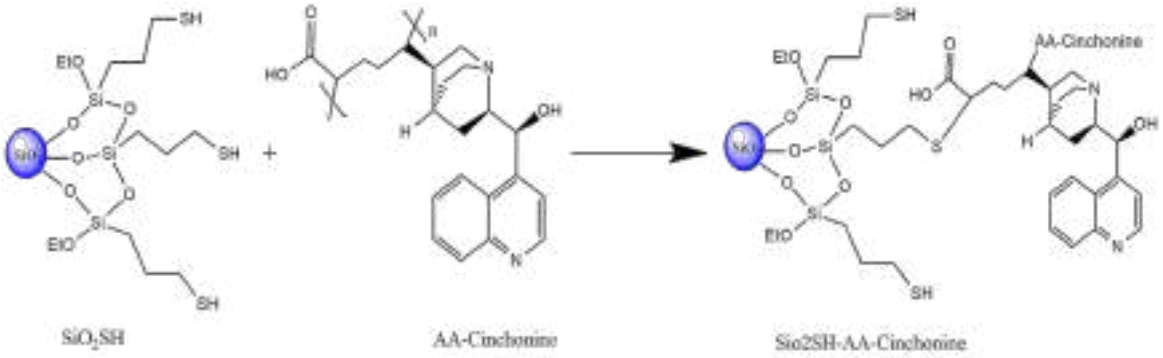

Scheme 1: Synthesis of catalyst random copolymer AA-cinchonine supported on nanosilica.

Scheme 2: The synthesized catalyst was used in the multi-component Hantzsch reaction.

References

[1] Kiasat, A. R., & Nazari, S. Magnetic nanoparticles grafted with β-cyclodextrin–polyurethane polymer as a novel nanomagnetic polymer brush catalyst for nucleophilic substitution reactions of benzyl halides in water. *J. Mol. Catal. A Chem.*, 2012, *365*, 80-86.

[2] Kardooni, R., Kiasat, A. R., & Motamedi, H. Designing of a novel dual-function silica-iron oxide hybrid based nanocomposite, Fe3O4@ SiO2PEG/NH2, and its application as an eco-catalyst for the solvent-free synthesis of polyhydroacridines and polyhydroquinolines. *J. Taiwan Inst. Chem. Eng.*, 2017, *81*, 373-382.

Synthesis of new azabenzene systems with triazole and sulfonamide moieties by a novel magnetic H-bonding catalyst

AmirMahdi Tavassoli, Morteza Torabi, Meysam Yarie*, Mohammad Ali Zolfigol*

Department of Organic Chemistry, Faculty of Chemistry, Bu-Ali Sina University, Hamedan 6517838683, Iran, tavassoli@live.com, mzolfigol@yahoo.com, myarie.5266@gmail.com.

Keywords: Magnetic nanoparticles, Multicomponent reactions, Azabenzene systems.

Magnetic nanoparticles (MNPs), through extraordinary capability for instance non-toxicity, retrievability and accessibility have become a vital part of heterogeneous catalysis. Catalysts which have benefited with this kind of supports, supply appropriate conditions to affixing organic linkers [1,2]. A huge range of heterocyclic compounds have been prepared by multicomponent reactions (MCRs) which offering multidimensional pharmaceutical applications [3]. In this study, in the continuation of our research in this field we attempted to synthesize some novel and complex hybrid pyridines incorporated triazole, indole or sulfonamide moieties by using a magnetic H-bonding catalyst which is based on Fe_3O_4@SiO_2.

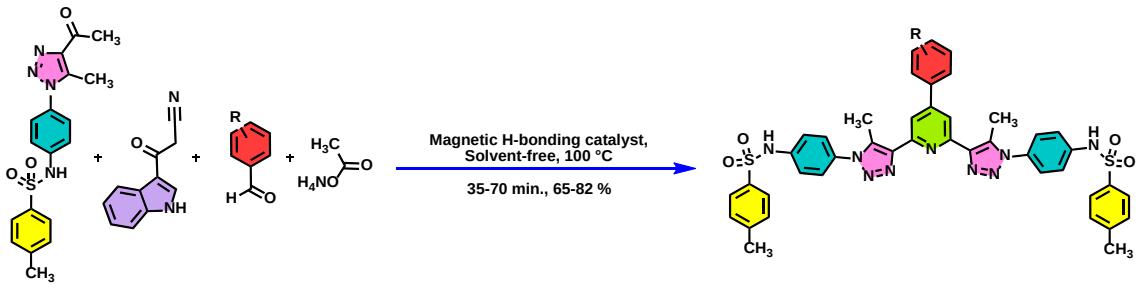

Scheme 1: Synthesize of complex azabenzene systems by the usage of a magnetic H-bonding catalyst.

References:

[1] Hudson, R., Feng, Y., Varma, R.S., Moores, A., Bare magnetic nanoparticles: sustainable synthesis and applications in catalytic organic transformations. *Green Chem*. 2014,16, 4493.

[2] Wu, L., Mendoza-Garcia, A., Li, Q., Sun, S., Organic phase syntheses of magnetic nanoparticles and their applications. *Chem. Rev*. 2016, 116, 10473.

[3] Younus, H.A., Al-Rashida, M., Hameed, A., Uroos, M., Salar, U., Rana, S., Khan, K.M., Multicomponent reactions (MCR) in medicinal chemistry: a patent review. *Expert Opin. Ther. Pat.* 2021, 31, 267.

Synthesis of 2-hydroxy-1,4-naphthoquinone derivatives in the presence of nanocomposite based on polyvinyl alcohol

Samira Bayazidi, Seied Ali Pourmousavi*, Shefa Miraninezhad and Ehsan Nazarzadeh Zare

School of Chemistry, Damghan University, Damghan, 36716-45667, Iran, samirabayazidi67@gmail.com.

Keywords: Nanocomposite, Polymer-based catalysts, 2-Hydroxy-1,4-naphthoquinone

The most important advantage in using functionalized polymer as a reagent or catalyst is high efficiency, simplification of work and easy separation of the catalyst. In order to improve the catalytic efficiency of polymers, active functional groups are included in polymer chains in different ways [1]. Nano-scale metal-based catalysts increase surface area and form homogeneous emulsions. Magnetic nanoparticles are widely used as catalyst supports because of their high surface area, stability, high loading capacity, and easy recycling. Magnetic separation simplifies catalyst recovery and tolerates most chemical environments except highly acidic or corrosive environments. In this research, the nanocomposite of polymer-based catalysts was prepared and the advantages of nanocomposite as a catalyst were investigated. The catalyst was prepared in three steps, including (1) cross-linking of polyvinyl alcohol, (2) sulfonation using chlorosulfonic acid, and (3) preparing nanocomposite using ferrite nanoparticles. The nanocomposite was used as a catalyst to synthesize 2-hydroxy-1,4-naphthoquinone derivatives. (Scheme 1).

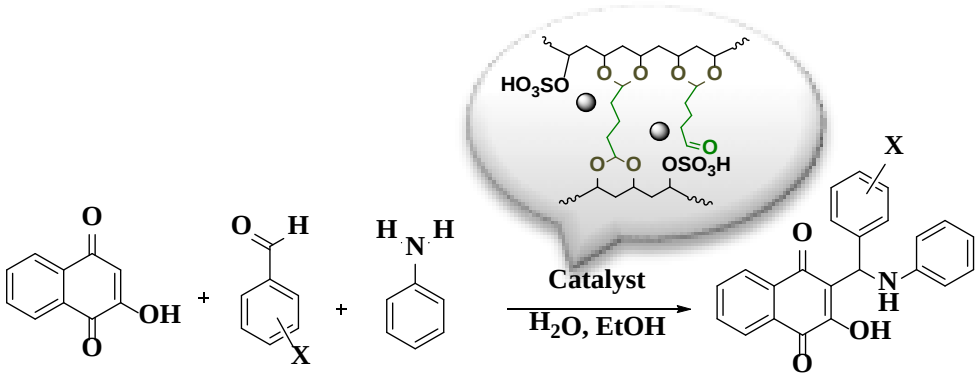

Scheme 1: Synthesis of 2-hydroxy-1,4-naphthoquinone derivatives.

References

[1] Nezhad, S. M., Pourmousavi, S. A., & Zare, E. N. Superparamagnetic Poly (aniline-co-m-phenylenediamine)@Fe_3O_4 Nanocomposite as an Efficient Heterogeneous Catalyst for the Synthesis of 1*H*-pyrazolo [1, 2-*a*] pyridazine-5, 8-diones & 1*H*-pyrazolo [1, 2-*b*] phthalazine-5, 10-diones Derivatives. *Curr. Org. Chem.* 2022, 19, 246-266.

[2] Behrens, S., & Appel, I. Magnetic nanocomposites. *Curr. Opin. Biotechnol.* 2016, 39, 89-96.

[3] Zhu, Y., Stubbs, L. P., Ho, F., Liu, R., Ship, C. P., Maguire, J. A., & Hosmane, N. S. Magnetic nanocomposites: a new perspective in catalysis. *ChemCatChem*, 2010, *2*, 365-374.

Synthesis and characterization of a novel Nanomagnetic/GO- GTSC-Cu nano-composite and its efficient catalytic activity in the synthesis of 5-substituted-1-*H* Tetrazoles

Hadis Safarbeigi*, Masoomeh Norouzi

Department of Chemistry, Faculty of Science, Ilam University, P.O. Box 69315516, Ilam, Iran. E-mail: m.norozi@ilam.ac.ir

Keywords: Tetrazole, Copper complex, Magnetic Graphene Oxide, Heterogeneous Catalysis

In recent years, heterogeneous catalysts have been used in organic reactions and modern synthesis [1]. However, separation of used catalysts is an important issue in the use of heterogeneous catalysts. One of the ways to overcome this problem is to magnetize the catalyst and separate it by a magnet from the liquid reaction system [2, 3]. Herein we report the synthesis of a magnetically separable graphene oxide [Nanomagnetic /GO-GTSC-Cu] as an environmentally friendly heterogeneous catalyst. The as-prepared nanocatalyst was well characterized by various techniques such as FT-IR, XRD, BET, FE-SEM, EDX, TGA, VSM, ICP-OES, and elemental analysis and evaluated for the synthesized 5-substituted-1*H*-tetrazole derivatives in PEG as a green solvent. The separation of the nanocatalyst was easily performed by an external magnet and applied again for eight fresh runs with no considerable loss of catalytic activity (**Scheme**).

.

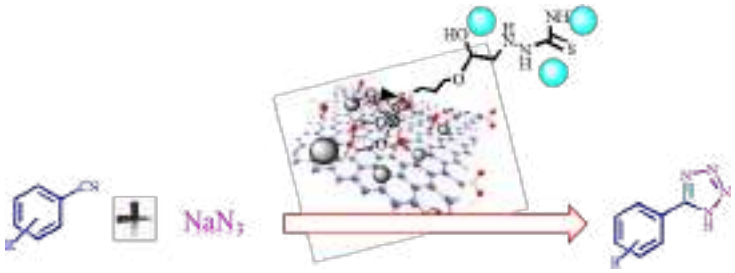

Scheme: Synthesis of 5-substituted 1-H tetrazoles by Nanomagnetic/GO- GTSC-Cu.

References

[1] Wang, Q.; Astruc, D. State of the art and prospects in metal–organic framework (MOF)-based and MOF-derived nanocatalysis. *Chem. Rev.* 2019, *120*, 1438-1511.
[2] Rai, P.; Gupta, D. Magnetic nanoparticles as green catalysts in organic synthesis-a review. *Synth. Commun.* 2021, *51*, 3059-3083.
[3] Neochoritis, C. G.; Zhao, T.; Dömling, A. Tetrazoles via multicomponent reactions. *Chem. Rev.* 2019, *119*,1970-2042.

Cr-EDTA-MOF: A green and versatile catalyst for the production of biodiesel fuel from oleic acid

Arash Ghorbani-Choghamarani*, Ahmad Jafari, Hamid Aghavandi

Department of Organic Chemistry, Faculty of Chemistry, Bu-Ali Sina University, Hamedan, 6517838683, Iran, a.ghorbani@basu.ac.ir or arashghch58@yahoo.com

Keywords: EDTA, MOF, Cr-EDTA, Biodiesel, Esterification, Oleic acid.

Herein, we reported an efficient, novel metal-organic framework designed and fabricated via hydrothermal reaction of Chromium (III) nitrate nonahydrate salt with EDTA as an organic ligand. The structure of prepared MOF was investigated by PXRD, BET, SEM, EDS, FT-IR, and X-ray mapping techniques. N_2 adsorption-desorption isotherms indicated excellent BET surface area for Cr-EDTA-MOF which is 234.55 (m^2/g). The prepared Cr-EDTA-MOF exhibits efficient and potential performance for the esterification of oleic acid under gentle reaction conditions. Furthermore, this nanostructure material afforded several benefits including excellent product yields, stability, easy methodology, easy workup, and greener situations. Furthermore, this heterogeneous nanocatalyst (Cr-EDTA-MOF) could be easily recovered from the reaction mixture by centrifugation and reused for four consecutive runs with a minimum loss of catalytic activity [1].

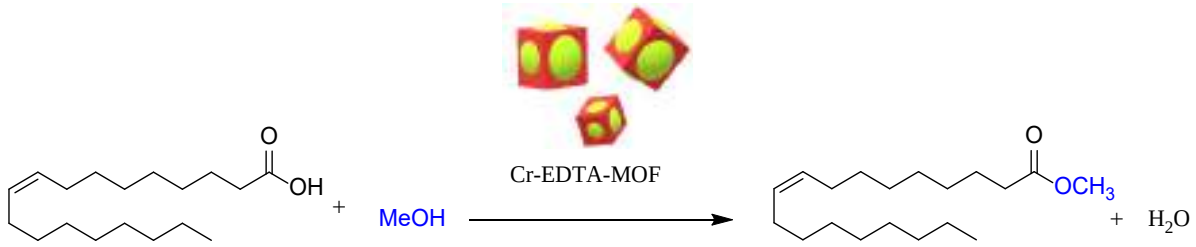

Scheme 2. Esterification of oleic acid

References

[1] Khanmohammadi-Sarabi, F.; Ghorbani-Choghamarani, A.; Aghavandi, H.; Zolfigol, M. A. ZnFe2O4@SiO2-Ascorbic Acid: Green, Magnetic, and Versatile Catalyst for the Synthesis of Chromeno[2,3-d] Pyrimidine-8-Amine and Quinazoline Derivatives. *Appl. Organomet. Chem. n/a* (n/a).

Use of an amine-functionalized metal-organic framework for high selectivity fluorometric determination of chromium

Ali Morsali *, **Mahsa Abbasiazad**

Department of Chemistry, Faculty of Sciences, Tarbiat Modares University, Tehran, Iran, morsali_a@yahoo.com, mahsaabbasiazad@gmail.com

Keywords: Metal-organic Framework, Nano structure, Sensing Chromium ions

An amine functionalized metal-organic framework (MOF), ([Zn(L*)(OBA)]. DMF) (L*=5,6-dipyridin-4-yl-1,2,3,4 tetrahydropyrazine, OBA= 4,4′-oxybisbenzoic acid) (TMU-60), used for chromium ion sensing in aqueous solution. To achieve the optimal structure for the purpose and to evaluate the effect of size on the sensing performance, in addition to solvothermal method the TMU-60 nano-sample was prepared by ultrasonic-assisted synthetic methods [1]. Then, the performance of bulk and optimized nano TMU-60 were studied as sensors of heavy metal (HM) ions such as Pb^{2+}, Hg^{2+}, Cu^{2+}, Cd^{2+}, Cr^{2+}, Ni^{2+}, and Cr^{3+}. Based on the results, it was found that TMU-60 has a remarkable potential for selective detection of Cr^{3+} ions in attendance of other HM cations in an aqueous solution [2]. The detection limit for Cr^{3+} in water was 0.89 nM ($Ksv = 2 \times 10^6$) for nano TMU-60 which was the best result among other reported MOFs. Finally, we found that amine is an effective function for Cr^{3+} sensing and the size of the structure has a significant impact on its sensing performance.

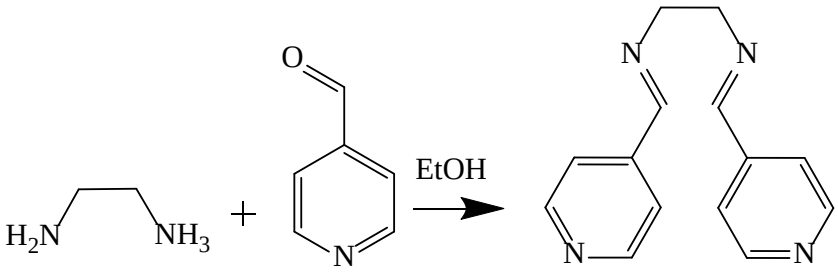

Scheme: Scheme of synthesis of ligand L

References

[1] Chen, Z. F.; Zhao, Y.; Zhu, Y.; Yang, X.; Qiao, J.; Tian, Q.; Zhang, Q., Health risks of heavy metals in sewage-irrigated soils and edible seeds in Langfang of Hebei province, China. *J. Sci. Food Agric.* 2010, *90* (2), 314-320.

[2] Bilal, M.; Rasheed, T.; Mehmood, S.; Tang, H.; Ferreira, L. F. R.; Bharagava, R. N.; Iqbal, H. M., Mitigation of environmentally-related hazardous pollutants from water matrices using nanostructured materials–A review. *Chemosphere* 2020, *253*, 126770.

Multifunctional Roles of Dihydrotetrazine Decorated Zr-MOFs in Photoluminescence and Colorimerism for Discrimination of Arsenate and Phosphate Ions in Water

Sayed Ali Akbar Razavi, Elham Habibzadeh and Ali Morsali*

Department of Chemistry, Faculty of Sciences, Tarbiat Modares University, Tehran, Islamic Republic of Iran. P.O. Box 14117-13116, elihabibzadeh73@yahoo.com.

Keywords: Metal-organic frameworks, Dihydrotetrazine, Arsenate, Phosphate, photoluminescence detection.

High chemical and structural stability of zirconium (Zr)-based metal-organic frameworks (MOFs) in aquatic media introduce them as an ideal candidate for waste water treatment and rational decoration with functional groups can significantly extend their application in this area. In this work, two well-known Zr-MOFs, UiO-66 and MIL-140-A, were functionalized with dihydrotetrazine function to increase their capability in water treatment. Investigations reveal that these two dihydrotetrazine (DHTZ) functionalized MOFs, named UiO-66(Zr)-DHTZ and MIL-140(Zr)-DHTZ, can be applied as a two-components array for highly selective and sensitive discrimination of arsenate (AsO_4^{3-}) and phosphate (PO_4^{3-}) ions in water in presence of other anions. Photoluminescence (PL) tests using UiO-66(Zr)-DHTZ show that this MOF can detect arsenate and phosphate ions via a ratiometric response. The ratiometric PL response of UiO-66(Zr)-DHTZ toward arsenate and phosphate anions raised from possible hydrogen bonding between these ions and dihydrotetrazine functions of this MOFs. In the next step, colorimetric tests using MIL-140(Zr)-DHTZ were conducted to discriminate the arsenate from phosphate. This MOFs undergoes a yellow-to-pink color change in the presence of arsenate ions, while no color change is observed in the presence of phosphate. This color change is observed through conversion of dihydrotetrazine sites inside the pores of MIL-140(Zr)-DHTZ into tetrazine. Altogether, the PL response of UiO-66(Zr)-DHTZ is originated from the hydrogen bond donating/accepting character of DHTZ function, while the colorimetric response of MIL-140(Zr)-DHTZ is based on chemical conversion of DHTZ function. This work clearly shows that the decoration of Zr-based MOFs with multi-character functional groups can develop their application in waste water treatment as multi-purpose platforms.

References

[1] Kreno, L. E.; Leong, K.; Farha, O. K.; Allendorf, M.; Van Duyne, R. P.; Hupp, J. T. Metal–Organic Framework Materials as Chemical Sensors. *Chem. Rev.* **2011**, *112* (2), 1105–112
[2] Yi, F.; Chen, D.; Wu, M.; Han, L.; Jiang, H. Chemical Sensors Based on Metal–Organic Frameworks. *Chempluschem* **2016**, *81* (8), 675–690.
[3] Kitagawa, S. Metal–Organic Frameworks (MOFs). *Chem. Soc. Rev.* **2014**, *43* (16), 5415–5418.
[4] Furukawa, H.; Cordova, K. E.; O'Keeffe, M.; Yaghi, O. M. The Chemistry and Applications of Metal-Organic Frameworks. *Science* **2013**, *341* (6149), 1230444.

4-MePy IL@zeolite-MnY: Fabrication and application as a multi-functional nanocatalyst in the green and three-component synthesis of 4-Aryl-4*H*-Chromenes

Mehdi Kalhor*, Fatemeh Janghorban

Department of Chemistry, Payame Noor University, 19395-4697, Tehran, Iran, fatemehjan.2020@yahoo.com

Keywords: Multi-functional nanocatalyst, Ionic liquid, Zeolite-MnY, 4-Methylpyridinium chloride, 4*H*-Chromene

Today, the use of heterogeneous solid catalysts in the synthesis and industrial production of chemicals has become very important and has received much attention due to its good acidity, insoluble in organic solvents, thermal stability, easy separation, recycling, and cheapness. They are also a green replacement to homogeneous catalysts. Among these structures, we can mention aluminosilicates or zeolites, which have been significantly developed in recent decades, especially as catalysts in various organic reactions. According to this, the design and synthesis of heterogeneous nanocatalysts, especially multifunctional nanocatalysts, is a hot topic of researchers these days [1,2]. On the other hand, 2-amino-chromes are widely used as pigments, cosmetics and potential agrochemicals and represent an important group of chemical compounds that are the main components of many natural products [3]. Looking at the mentioned points and continuing research in this field, we decided to design, fabricate, identify and perform the nanostructure of the zeolite-MnY functionalized with 4-methylpyridinium chloride ionic liquid (Mn/4-MePy-IL@ZY), as an effective nanocatalyst for the three-component synthesis of 2-amino-4*H*-chromenes from the starting materials of aldehydes, malenonitrile and resorcinol under a three-component condensation reaction in water (**Scheme**). One of the obvious advantages of this nanocatalyst is the presence of Lewis acid sites (Mn^{2+}) and basic ionic liquid (4-MePy-Cl) fixed on zeolite nanoporous (multifunctional), which can be very useful in multicomponent reactions.

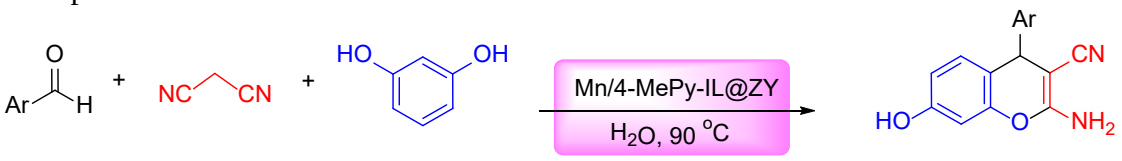

Scheme: The synthetic pathway of Chromenes using Mn/4-MePy IL@ZY

References

[1] Jagadeesan, D.; a review: multifunctional nanocatalysts for tandem reactions: A leap toward sustainability. *Appl. Catal. A-Gen.* 2016, *511*, 59-77.

[2] Kalhor, M.; Orouji, Z.; Khalaj, M.; 4-Methylpyridinium chloride ionic liquid grafted on Mn@zeolite-Y: Design, fabrication and performance as a novel, multi-functional nano-catalyst in the four-component synthesis of pyrazolophthalazine-diones. *Micropor. Mesopor. Mater.* 2022, *329*, 111498.

[3] Ellis, G. P.; The Chemistry of Heterocyclic Compounds in Chromenes, Chromanes, and Chromones, ed. by A. Weissberger, EC *Taylor*, 1977.

The triazine-based COF showcases its radiant catalytic prowess in synthesis both thiazole and dihydroquinazolin components with exquisite finesse

AmirMahdi Tavassoli, Morteza Torabi, Mohammad Ali Zolfigol*, Meysam Yarie*

Department of Organic Chemistry, Faculty of Chemistry, Bu-Ali Sina University, Hamedan 6517838683, Iran, tavassoli@live.com, mzolfigol@yahoo.com, myarie.5266@gmail.com

Keywords: COFs, Covalent organic frameworks, Thiazole, Dihydroquinazolin

Covalent organic frameworks (COFs) are a class of porous materials that have recently emerged as a promising platform for a wide range of applications in various fields such as catalysis, gas storage, and separation, sensing, and electronics [1]. Thiazole is an important building block in many biological and synthetic compounds due to its unique properties [2]. The most notable properties of dihydroquinazolin are its ability to act as a bioisostere of various natural products and drugs. This property arises due to the structural similarity of dihydroquinazolin to many natural products and drugs, allowing it to act as a mimetic of these compounds. This makes dihydroquinazolin an important tool in the development of new drugs with improved pharmacological properties [3].

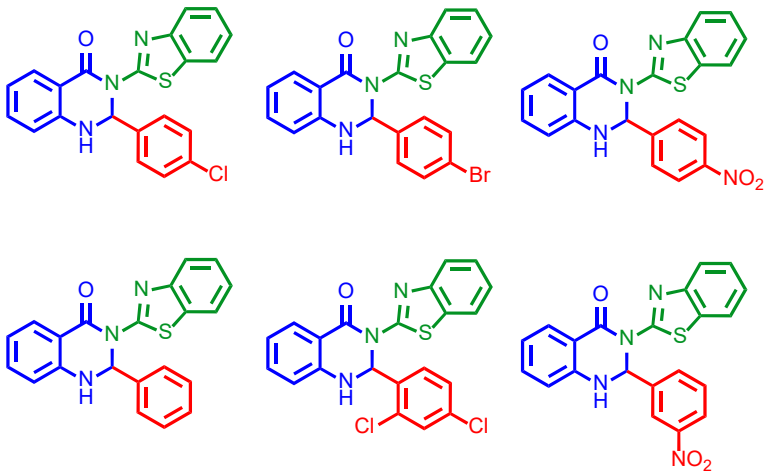

Scheme 1: Catalytic application of triazine-based COF in synthesize of thiazole and dihydroquinazolin components.

References:

[1] Wu, M. X., & Yang, Y. W. Applications of covalent organic frameworks (COFs): From gas storage and separation to drug delivery. *Chin. Chem. Lett.*, 2017, 28, 1135-1143.

[2] Ayati, A., Emami, S., Asadipour, A., Shafiee, A., & Foroumadi, A. Recent applications of 1, 3-thiazole core structure in the identification of new lead compounds and drug discovery. *Eur. J. Med. Chem.*, 2015, 97, 699-718.

[3] Kim, J. H.; Jeong, H. R.; Yoon, H. B.; Kim, S. Y.; Kim, H. J.; Lee, K. T.; Gadotti, V. M.; Huang, V.; Zhang, F. X.; Zamponi, W. G.; Lee, J. Y. Synthesis and biological evaluation of fluoro-substituted 3, 4-dihydroquinazoline derivatives for cytotoxic and analgesic effects. *Bioorg. Med. Chem.*2017, 25, 4656-4664.

Synthesis of chitosan-zinc-oxide-silver nanoplate composite as a new coating for solid phase microextraction fiber

Reza Alizadeh*, Mina Kadkhodazadeh and Elham Rostami

Department of Chemistry, Faculty of Science, University of Qom, Qom, Iran, r_alizadeh2005@yahoo.com, m.kadkhodazadeh9@gmail.com

Keywords: Nanocomposite, Chitosan/ZnO/Ag, Microfluidic chip, Solid phase microextraction

Nanomaterials have been developed due to their small dimensions and high surface to volume ratio, high chemical and thermal stability. The use of nanocomposites has been widely spread in the coating of solid phase microextraction fibers. The nanostructure metal oxides have been developed as high surface to volume ratio coatings which improves the extraction efficiency [1]. Among the metallic and metal oxide nanomaterials, silver (Ag) and zinc oxide (ZnO) nanoparticles (NPs) are widely used, which increases the absorbent surface and improves the chemical and physical properties and selectivity are also increased [2]. Zinc oxide /Silver (ZnO/Ag) nanocomposite were synthesized by a hydrothermal and co-precipitation method using $Zn(CH_3COO)_2$ and $AgNO_3$.

Polymer hydrogels, as natural polymers, are three dimensional cross-linked networks that have high porosity. Chitosan is a natural cationized polymer that is produced from the deacetylation of chitin. The special properties of this natural polysaccharide are its non-toxicity and high biocompatibility and their safety pointed out [1]. In recent years, chitosan-based hybrid materials have been developed due to the excellent properties of individual components and their outstanding synergistic effects.

In this project, first the synthesis of zinc oxide/ silver nanoplates is formed and its collected and washed, then its nanocomposite is formed with chitosan. The successful formation of nanoplates (ZnO/ Ag) was confirmed by scanning electron microscopy (SEM) and X-ray diffraction (XRD) instrument. Zinc oxide/silver nanoplates and chitosan as a solid phase microextraction fiber coating are used for the extraction and determination of organophosphorus pesticides (diazinon, chlorpyrifos) in environmental samples as a novel and efficient method on a microfluidic chip that were identified by high performance liquid chromatography (HPLC). It provides efficient and acceptable results.

References

[1] Alizadeh, R. (2016). Chlorophenol's ultra-trace analysis in environmental samples by chitosan–zinc oxide nanorod composite as a novel coating for solid phase micro-extraction combined with high performance liquid chromatography. *Talanta*, *146*, 831-838.

[2] Jobe, M. C., Mthiyane, D. M., Mwanza, M., & Onwudiwe, D. C. (2022). Biosynthesis of zinc oxide and silver/zinc oxide nanoparticles from Urginea epigea for antibacterial and antioxidant applications. Heliyon, 8(12), e12243.

Molybdenum disulphide nanoparticles synthesis and their potential assessment as catalyst for Gewald reaction

Fatemeh Zahra Bagherinezhad[a], Nasrin Mollania [a]*, Mohammad Zirak[b], Hamid Mollania[c], Maryam Moudi[d]

a) Department of Biology, Faculty of Basic Sciences, Hakim Sabzevari University, Sabzevar, Iran, fatemehzhra248@gmail.com, n.mollania@hsu.ac.ir.
b) Department of Physic, Faculty of Basic Sciences, Hakim Sabzevari University, Sabzevar, Iran.
c) Ferdowsi University of Mashhad, Department of Electrical Engineering, Mashhad, Iran.
d) Department of Biology, Faculty of Science, University of Birjand, Birjand, Iran.

Keywords: Molybdenum Disulfide (MoS_2), Sodium Molybdate, L-Cysteine, Hydrothermal Method

Two-dimensional molybdenum disulfide (MoS_2) nanoparticle are regarded as a valuable inorganic material with high physicochemical and mechanical stability [1]. These intriguing nanomaterials have unique electrical and optical properties, making them appealing candidates for applications ranging from nanoelectronics to biomedicine and biotechnology [2]. In this direction, we utilize the hydrothermal approach for synthesizing MoS_2 nanoparticles. 0.3 g of sodium molybdate and 0.8 g of L-cysteine were dissolved in deionized water (40 ml) and stirred for one hour in a typical synthesis. Then 30 drops of hydrochloric acid were added and the obtained clear solution was incubated in the oven for 48 hours at 180 °C. Finally, the obtained black powder was washed 3 times, dried, and utilized for characterization by X-Ray diffraction analysis (XRD) and Dynamic light scattering (DLS). The MoS_2 nanoparticles exhibited excellent catalytic activity in the Gewald reaction (Scheme 1).

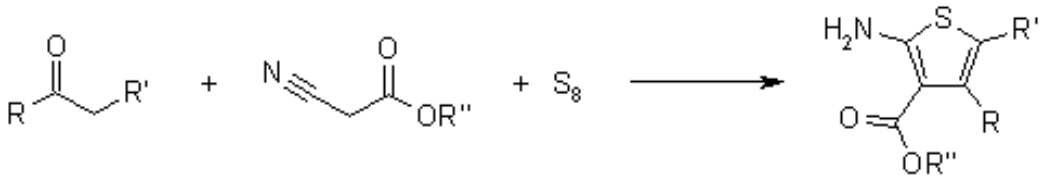

Scheme 1: Gewald reaction

References

[1] Vidya, C. Manjunatha, C. Pranjal, A. Faraaz, I. Prashantha, K. A multifunctional nanostructured molybdenum disulphide (MoS2): an overview on synthesis, structural features, and potential applications. *Mater. Res. Innov*. 2022, 27(3), 177-193.
[2] Ecer, Ü. Şahan, T. Zengin, A. synthesis and characterization of an efficient catalyst based on MoS2 decorated magnetic pumice: An experimental design study for methyl orange degradation. *J. Environ. Chem. Eng*. 2021, 9 (3), 105265.

Catalytic application of Pillar-layered Zr-MOF as a new catalyst in the preparation of new pyrido[2,3-*d*]pyrimidine derivatives

Hossein Ahmadi,[a] Mahmoud Zarei,[b] Mohammad Ali Zolfigol,*[a] Maryam Hajjami and Mojtaba Hosseinifard [c]

a) Department of Organic Chemistry, Faculty of Chemistry, Bu-Ali Sina University, Hamedan, Iran, hossein9754@gmail.com, zolfi@basu.ac.ir & mzolfigol@yahoo.com.
b) Department of Chemistry, Faculty of Science, University of Qom, Qom, Iran, mahmoud8103@yahoo.com.
c) Department of Energy, Materials and Energy Research Centre, P.O. Box 31787-316, Karaj, Iran.

Keywords: Pillar-layered Zr-MOF, Pyrido[2,3-*d*]pyrimidine, Zr-MOF

Metal-Organic Frameworks (MOFs) have gained significant attention in the field of solid-state chemistry over the past two decades. These promising materials have various applications, including gas adsorption, separation, catalysis, sensing, and drug delivery. Among the research areas in crystalline materials, Pillar-layered Metal-Organic Frameworks (MOFs) stand out. Exploring their diverse structures, properties, and potential as multi donor porous frameworks is of great interest due to the numerous reports on pillar-layered MOFs. By modifying the pillar moieties along with metal nodes and oxygen donor linkers, it is possible to improve control over structure assembly and obtain structures with specific properties. The incorporation of the pyridine ring system into the structure of bioactive compounds is quite popular among N-heteroaromatics. This ring system is also found in natural products like nicotinic acid, nicotinamide, and vitamin B6, which play crucial roles in metabolism. (**Scheme**).

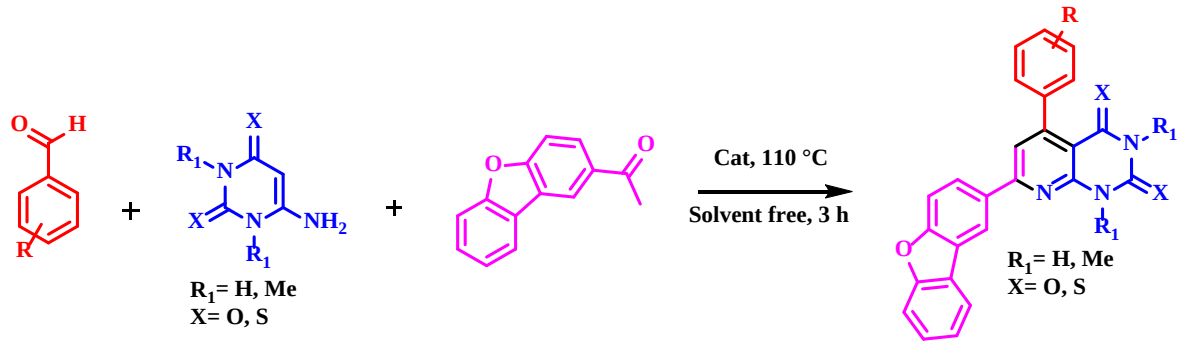

Scheme: Synthesis of nicotinonitrile derivatives catalysed by magnetic nanoparticles as the new magnetic H-bond catalyst.

References

[1] ZareKarizi, F., Joharian, M., & Morsali, A. (2018). Pillar-layered MOFs: functionality, interpenetration, flexibility and applications. *J. Mater. Chem. A.* 6(40), 19288-19329.

[2] Shamroukh, A. H.; Kotb, E. R.; Anwar, M. M.; Sharaf, M. A Review on the Chemistry of Nicotinonitriles and Their applications. *Egypt. J. Chem.* 2021, *64*, 4509-4529.

Synthesis of Chitosan/ PVA/ ZnO/ GA nanocomposite as sorbent for drug extraction from urine sample

Reza Alizadeh*, Elham Rostami, Mina Kadkhodazadeh

Department of chemistry, Faculty of science, University of Qom, Qom, Iran, e.rostami1996@gmail.com.

Keywords: Chitosan/ PVA/ ZnO/ GA nanocomposite, Solid phase microextraction, Organic- inorganic nanocomposite

The use of natural polymers has received considerable attention due to their safety [1]. Chitosan is a cationized polymer from the deacetylation of chitin. This natural polysaccharide has favourable characteristics such as non-toxicity and high biocompatibility, which can be used in clinical fields [2]. Polyvinyl alcohol is a water-soluble polymer that has polar hydroxyl groups. This polymer has the ability to form a film and good emulsification and shows good adhesion [3]. Unfortunately, this polymer has a low absorption capacity and a small surface area. However, it has large and interconnected pores that allow the diffusion of solutes of any size and mass transfer of nano and even micro particles. Therefore, trapping the absorbent particles inside the polymer increased its specific surface area and high extraction efficiency is obtained [3]. Networking of chitosan in the presence of polyvinyl alcohol led to the construction of polymers with suitable physical, mechanical and chemical properties [4]. This composite has attracted a lot of attention recently due to its biodegradability along with good physical properties. The use of nanostructures in this composite has led to an increase in the absorbent surface and improved its physical properties.

In this project, an attempt is made to modify the surface of zinc oxide nanorods by gallic acid in the chitosan/polyvinyl alcohol composite, in addition to improving the physical properties of the nanocomposite, its chemical properties and selectivity are also increased. The said composite will be used in the manufacture of solid phase microextraction fibers (SPME). The SPME fiber was used to extract diazepam and oxazepam from urine sample and the drugs were determined by high performance liquid chromatography (HPLC) technique. The results show the suitable analytical data such as LODs, LOQs, LDRs, repeatability and reproducibility.

References

[1] Açikgöz, M., Kaş, H. S., Hascelik, Z., Milli, U., & Hincal, A. A. Chitosan microspheres of diclofenac sodium, II: In vitro and in vivo evaluation. *Die Pharmazie*, 1995, 50(4), 275-277.

[2] Hirano, S., Seino, H., Akiyama, Y., & Nonaka, I. Progress in biomedical polymers. In Proceedings of an American Chemical Society Symposium 1990, 283-290.

[3] Wang, Y., Zhang, Y., Cui, J., Li, S., Yuan, M., Wang, T., ... & Hou, X. Fabrication and characterization of metal organic frameworks/polyvinyl alcohol cryogel and their application in extraction of non-steroidal antiinflammatory drugs in water samples. *Anal. Chim. Acta*, 2018, 1022, 45-52

[4] Liu, J., Li, H., Jiang, X., Zhang, C., & Ping, Q. Novel pH-sensitive chitosan-derived micelles loaded with paclitaxel. *Carbohydr. Polym.*, 2010, 82(2), 432-439.

An efficient synthesis of new spiroindenopyridotriazine-4*H*-pyran derivatives

Monireh Rezaei and Mohammad Bayat*

Department of Chemistry, Faculty of Science, Imam Khomeini International University, Qazvin, Iran, monireh.rezaei1370@gmail.com

Keywords: 1,6-Diaminopyridinone, Ninhydrin, Malononitrile, C-H acids, Spiro-4*H*-pyran

Spiroheterocycles have recently attracted a lot of attention as an important category of heterocyclic compounds which have biological and pharmacological properties [1-2]. Due to the biological activities of spiropyran compounds, we were interested in developing a convenient approach for the synthesis of spiroindenopyridotriazine-4*H*-pyran derivatives which has not yet been reported. We have developed a convenient one-pot protocol for the synthesis of novel spiro[indeno[1,2-*e*]pyrido[1,2-*b*][1,2,4]triazine-7,5'-pyran]-1,3,6'-tricarbonitrile **5a-l** *via* the reaction of 1,6-diaminopyridinone derivatives **1a-g**, ninhydrin **2**, malononitrile **3** and C-H acids **4** under reflux condition in ethanol. The important features of this protocol are the availability of starting materials, mild reaction conditions, excellent yields and easy isolation of products with no chromatographic technique. The structures of the products were confirmed by ^{1}H NMR, ^{13}C NMR, IR and Mass analyses.

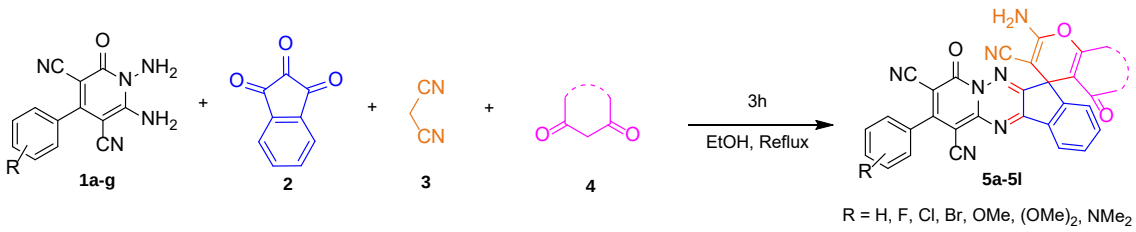

Scheme: Synthesis of spiroindenopyridotriazine-4*H*-pyran **5a-l**.

References

[1] Bayat, M.; Hosseini, H. An efficient synthesis of novel spiroindenopyridazine-4*H*-pyran derivatives. *New J. Chem.*, 2017, *41*, 14954-14959.

[2] Saigal, Irfan, M.; Khan, P.; Abid, M.; Khan, M.M. Design, synthesis, and biological evaluation of novel fused spiro-4*H*-pyran derivatives as bacterial biofilm disruptor. *ACS Omega.*, 2019, *4*, 16794-16807.

Nickel-impregnated magnetic UiO-66 for Mizoroki–Heck and Suzuki–Miyaura cross-coupling reactions

Reza Taghavi, Sadegh Rostamnia *

Organic and Nano Group (ONG), Faculty of Chemistry, Iran University of Science and Technology, Tehran, Iran, Reza.taghavee@gmail.com, Srostamnia@gmail.com.

Keywords: Ni species, Metal-organic frameworks, Cross-coupling reaction, Magnetic NPs.

Suzuki-Miyaura reactions include the cross-coupling of organoboronic acids with aryl halides to generate biaryls [1]. Heck cross-coupling reactions, also known as Mizoroki-Heck reactions, involve the coupling of an unsaturated halide with an alkene. Metal species are extremely appealing catalysts because they have large surface-to-volume ratios and active surface atoms [3]. A core-shell magnetic Fe_3O_4@UiO-66 was synthesized and selected as a good Ni support (Scheme 1). Magnetic NPs were used as a green catalyst in high-yielding cross-coupling processes. The structure and morphology of the produced composite were studied using SEM and XRD techniques. The EDS method was also used to characterize the levels of Ni loading. Catalyst recyclability revealed 5 successful reactions.

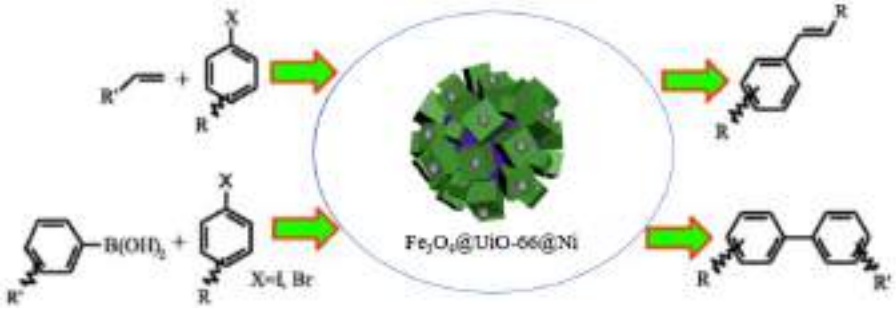

Scheme 1: Schematic illustration of the C-C coupling reaction using nickel imbedded Fe_3O_4@UiO-66

References

[1] Sadegh Rostamnia; Turaj Rahmani. Ordered mesoporous SBA-15/PrSO3Pd and SBA-15/PrSO3PdNP as active, reusable and selective phosphine-free catalysts in C-X activation Heck coupling process, *Appl. Organomet. Chem.*, 2015, 471-474.

[2] Arefeh Ahadi; Sadegh Rostamnia; Paria Panahi; Lee D Wilson, Qingshan Kong; Zengjian An; Mohammadreza Shokouhimehr. Palladium Comprising Dicationic Bipyridinium Supported Periodic Mesoporous Organosilica (PMO): Pd@Bipy–PMO as an Efficient Hybrid Catalyst for Suzuki–Miyaura Cross-Coupling Reaction in Water, *Catal*. 2019, 9, 140.

[3] Leng Leng Chng; Nandanan Erathodiyil; and Jackie Y. Ying. Nanostructured Catalysts for Organic Transformations, *Acc. Chem. Res*. 2013, 46, 8, 1825–1837.

Biosynthesis of iron oxide nanoparticles by the extracellular metabolite compounds produced by *Bacillus cereus HMH1*

Sara Ramezani [a], Nasrin Mollania [a*], Halimeh Hassanzadeh[b], Fariba Mollania [c]

a) Department of Biology, Faculty of Basic Sciences, Hakim Sabzevari University, Sabzevar, Iran, sara.ramezani1376@gmail.com , n.mollania@hsu.ac.ir
b) Stem Cells and Regenerative Medicine Department, Academic Center for Education, Culture, and Research (ACECR)-Khorasan Razavi, Mashhad, Iran.
c) Visiting Professor, PhD in chemistry, Department of plant production, University of Torbate Heydarieh, Iran.

Keywords: biosynthesis, iron oxide nanoparticles, *Bacillus cereus*

Nanostructured materials, including iron oxide nanoparticles (IONPs), have received growing attention due to their unique properties (1). Various studies have been conducted to synthesize metal nanoparticles using biological materials such as fungi, plant extracts, and extremophile bacteria (2). The aim of this study was to optimize iron oxide nanoparticle biosynthesis by Bacillus cereus HMH1 supernatant. The biosynthesized IONP was characterized by UV-vis spectrophotometry, X-ray Diffraction (XRD), and Fourier Transform Infrared Spectroscopy (FTIR). The synthesis of iron-oxide nanoparticles was validated by UV-Visible spectroscopy which showed higher peak at 370 nm as valid standard reference (Fig. 1). Changing the medium reaction color to dark brown indicated the biosynthesis of iron oxide nanoparticles. The FT-IR analysis aimed to identify interactions between nanoparticles and bacterial metabolites involved in biosynthesis.

Fig. 1: UV-visible spectra of nanoparticle biosynthesized

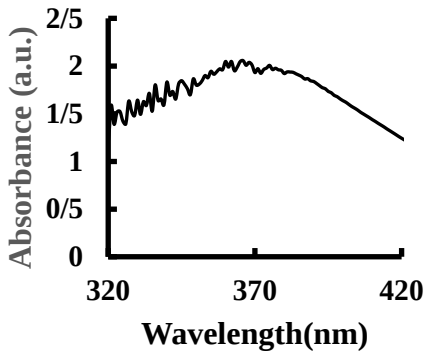

References:

[1] Elnouby, M.S., Taha, T.H., Abu-Saied, M.A. Alamri, S.A., Mostafa Y.S.M., Hashem M., Green and chemically synthesized magnetic iron oxide nanoparticles-based chitosan composites: preparation, characterization, and future perspectives. *J Mater Sci: Mater Electron* 2021, 32, 10587–10599.

[2] Jeevanandam, J., Chan, Y.S. and Danquah, M.K., Biosynthesis of Metal and Metal Oxide Nanoparticles. ChemBioEng Reviews, 2016, 3, 55-67.

Investigation of the effect of silver nanoparticles on the angiogenesis process in chick chorioallantoic membrane model (CAM)

Seyedeh Samaneh Feizabadi, Ehsan Koushki and Madjid Momeni Moghaddam*

Faculty of Sciences, Hakim Sabzevari University, Sabzevar, Iran, Samaneh.f7272@gmail.com, m.momeni@hsu.ac.ir

Keywords: Silver nanoparticles, Angiogenesis, Chick chorioallantoic membrane

Nanotechnology is a new technology in which nanoparticles have been widely used in various fields, particularly in medicine and biology [1]. Angiogenesis plays a vital role in many diseases, especially in cancer. Silver nanoparticles have antibacterial and antimicrobial properties [2]. The effect of silver nanoparticles on angiogenesis on chick chorioallantoic membrane has been investigated. Silver nanoparticles were synthesized using the Turkevich method (Fig. 1) [3]. In this research, 54 fertilized eggs of ROSS breed were divided into 9 groups, including 1 sham group and 8 experimental groups. On the 8th day of incubation, the fertilized eggs were injected with concentrations of 162.5, 325, 650, 1300 µg/mL of silver nanoparticles. Imaging was conducted on the 12th day to examine the number and length of branches, and they were compared with the control group. The results showed that the concentration of 162.5 µg/mL of silver nanoparticles has no significant effect on the angiogenesis process, but the concentrations of 650 and 1300 µg/mL have a significant decrease in the number and length of blood vessels. Silver nanoparticles can affect angiogenesis in various diseases such as cancer.

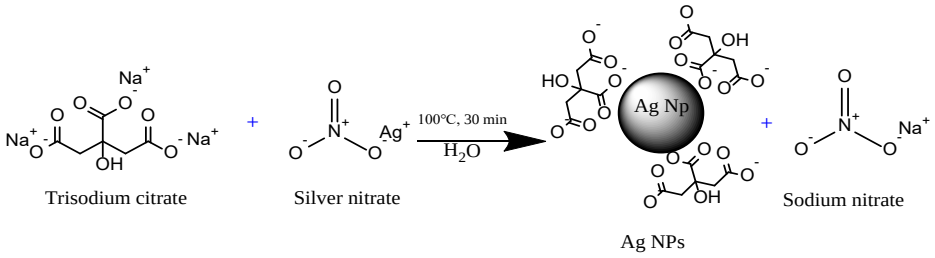

Fig.1: Ag Np synthesized by Turkevich method

References

[1] McNeil, S.E., Nanotechnology for the biologist. *J. Leukoc. Biol.*, 2005. 78(3): p. 585-594.
[2] Krutyakov, Y.A., et al., Synthesis and properties of silver nanoparticles: advances and prospects. *Russ. Chem. Rev.*, 2008. 77(3): p. 233.
[3] Souza Neto, F., et al., Modification of Turkevich method of synthesis of silver nanoparticles.

Synthesis and dye adsorption study on nanohybrids of porous covalent triazine polymers

Leila Jafari, Massoumeh Bagheri* and Rahim Mohammad Rezaei

Department of Chemistry, Faculty of Science, Azarbaijan Shahid Madani University, Tabriz, Iran, Leila.jafariiiii@gmail.com, MassoumehBagheri@yahoo.com, r.mohammadrezaei@ymail.com

Keywords: Porous polymers, Triazine covalent polymers, Adsorption, Dyes

Recently, covalent triazine polymers (CTPs) have received increasing research interest due to their potential in a wide variety of applications such as energy storage, gas storage/separation, chemical catalysis, chemical- and bio-sensing, and pollutants adsorption/decontamination, etc. CTPs are a promising type of porous materials with microporous or mesoporous structures formed by covalent bonding of organic structural units, which have clear advantages such as a large specific surface area, low skeleton density, good thermal and chemical stability, simple and diverse synthetic methods, and adjustable and designable pore properties. Nowadays, the development of nanoporous materials for water remediation has been of paramount interest [1]. Azo dyes are the largest and most versatile class of dyes that are toxic and threatening people's health seriously [2]. For decades, various types of nanomaterials such as carbon nanotubes, fullerenes, graphene oxide, and polymeric nanoparticles often combined with organic polymers to obtain functionalized hybrid materials [1]. Modification of CTPs using nanomaterials can significantly increase the performance of adsorption behavior of the modified CTPs because of their fascinating properties including, large surface area, more functional groups and chemical inertness.

In this study, we report the synthesis and characterization of nanohybrids of CTPs using melamine, difunctional aliphatic linkers and graphene-based nanomaterial for the removal of anionic Congo red molecules from water solution. The structures and properties of the prepared materials were systematically characterized by Fourier transform infrared spectroscopy (FT-IR), field emission scanning electron microscopy (FE-SEM), thermogravimetric analysis (TGA) and N_2 adsorption–desorption and BET techniques. This study demonstrates that the prepared nanohybrids of CTP is a promising adsorbent for the removal of anionic dyes from aqueous solutions.

References

[1] Dinari, M.; Mokhtari, N.; & Hatami, M. Covalent triazine based polymer with high nitrogen levels for removal of copper(II) ions from aqueous solutions. *J. Polym. Res.*, 2021, *28*, 1-11.

[2] Ou, H.; You, Q.; Li, J.; & Wang, D. A rich-amine porous organic polymer: an efficient and recyclable adsorbent for removal of azo dye and chlorophenol. *RSC Adv.*, 2016 *6*(100), 98487-98497.

A novel magnetic nanocomposite (Fe_3O_4@Saponin/Cr) as a potential recyclable catalyst for the synthesis of *β*- Acetamidoketones derivatives

Hossein Anaraki-Ardakani*

Department of Chemistry, Mahshahr Branch, Islamic Azad University, Mahshahr, Iran, hosseinanaraki@yahoo.com

Keywords: Nano-Fe_3O_4, Saponin, Chromium Chloride

Organic synthesis has been attractive to be used in multi-component reactions because they are capable of producing final materials through one reaction. These reactions do not need for intermediate isolation, therefore, operation time and required energy decreases [1-2].
In this report, a natural magnetic catalyst (nanoFe_3O_4@Saponin/Cr) was synthesized using $CrCl_3.6H_2O$ compounds on a nanoFe_3O_4@Saponin surface as a novel recyclable magnetic catalyst. nanoFe_3O_4@Saponin/Cr has been synthesized by coprecipitation of salts of Fe^{3+} and Fe^{2+} via eco-friendly solvent in saponin. Structural, morphological, and magnetic features of the synthesized novel catalyst were characterized by various methods like energy-dispersive X-ray spectroscopy (EDS), Brunauer-Emmett-Teller (BET), thermo-gravimetric analysis (TGA), high-resolution transmission electron microscopy (HR-TEM), vibrating sample magnetometer (VSM), Fourier transform infrared (FT-IR) spectroscopy, inductively coupled plasma (ICP), X-ray diffraction (XRD) and scanning electron microscopy (SEM).
It is totally accepted that heterogeneous catalysts show appropriate efficiency in synthesizing three-component reactions among 4-hydroxycoumarin, aromatic aldehydes, and amides under eco-friendly solvent, at RT. The procedure presented in this paper is an eco-friendly one that provides so many benefits such as higher yield, easier work-up, simply recovered by magnetic decantation, short reaction time, reusability for multiple and consecutive reactions without remarkable activity reduction. (**Scheme**1).

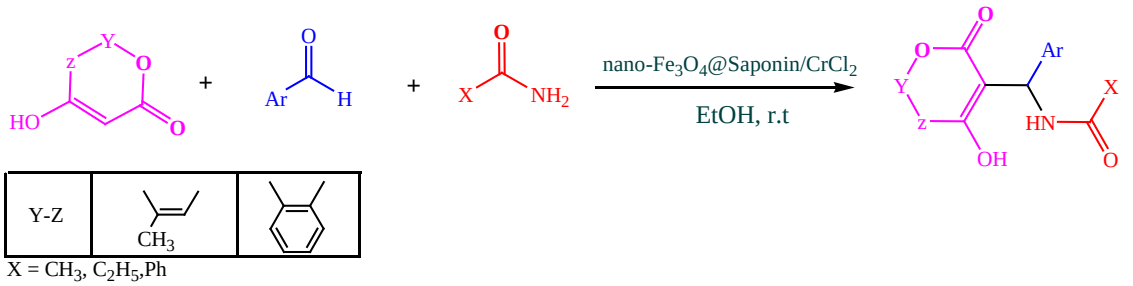

Scheme1: The one-pot synthesis of *β*- Acetamidoketones derivatives

References

[1] Shaterian, H. R.: Hosseinian, A.: Ghashang, M. A three-component novel synthesis of 1-carbamato-alkyl-2-naphthol derivatives. *Tetrahedron Lett.* 2008, *49*, 5804-5806.
[2] Khojastehnezhad, A.; Moeinpour, F.; Javid, A. NiFe $_2$ O $_4$ @SiO $_2$ –PPA Nanoparticle: A Green Nanocatalyst for the Synthesis of *β*-Acetamido Ketones. *Polycycl. Arom. Comp.* 2019, *39*, 404-412.

Theoretical investigation on enhancing reactivity of Carbonyl group via halogen bonding

Fereshteh Yaghoobi*

Nahavand Higher Education Complex, Bu-Ali Sina University, Hamedan, Iran, f.yaghoobi@basu.ac.ir

Keywords: Halogen bonding, Catalyst, DFT, Dihalogen

In this work, the halogen bonding between carbonyl (CO) group of H_2CO with F_2, I_2 and IF molecules has been investigated theoretically. The aim of this study is to examine the influence of dihalogens as a catalyst on the activation of the H_2CO carbonyl group as a neutral organic substrate through halogen bonding. Halogen bonding is a noncovalent interaction between halogen atom and a Lewis base [1], which plays a significant role in various areas of chemistry [2]. Therefore, using Diels-Alder [3] reaction as benchmark, the effect of halogen bonding on activation energy of this reaction has been studied (**Scheme**). The values of interaction energies between CO group of H_2CO with F_2, I_2 and IF molecules were calculated. Also, the activation strain model (ASM) [4] were used to analyze the effect of halogen bonding on activation energy of Deils-Alder reaction in Ts state. Calculations showed that dihalogens decrease the activation energies of D-A reaction via halogen bonding interactions. Also, calculations showed that the largest effect on activation energies of the reaction belongs to the IF molecule.

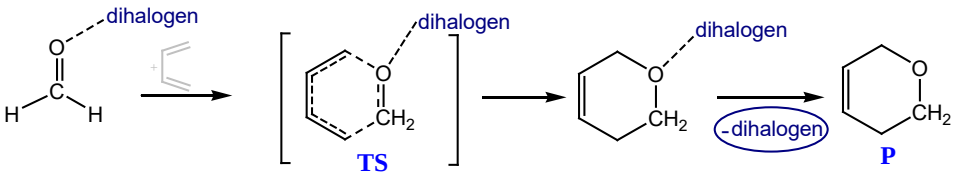

Scheme: Diels–Alder benchmark reaction in the presence of dihalogen molecule.

References

[1] Politzer, P.; Lane, P.; et al. An overview of halogen bonding. *J. Mol. Model* 2007, *13*, 305.
[2] Cavallo, G.; Metrangolo, P.; Milani, R.; Pilati, T.; Priimagi, A.; Resnati, G.; Terraneo, G. The halogen bond. *Chem. Rev.* 2016. *116*(4), 2478-2601.
[3] Diels, O.; Alder, K. Synthesis in der Hydroaromatischen Reihe, *Eur. J. Org. Chem*. 1928, *460*, 98-122.
[4] Ess, D. H.; Houk, K. N. Distortion/interaction energy control of 1, 3-dipolar cycloaddition reactivity, *J. Am. Chem. Soc*. 2007, *129*,10646-10647.

Application of tropine-based dicationic molten salt in acceleration of synthesis of 1,2,4-triazolo[4,3-*a*]pyrimidines

Janan Metghalchi Langroudi, Masoumeh Mazloumi, Farhad Shirini* and Hassan Tajik

Department of Chemistry, College of Science, University of Guilan, Rasht, 41335-19141, Iran, jananmetghalchi5@gmail.com.

Keywords: Dicationic molten salt, Pyrimidines, Tropine, $[(Tropine)_2C_3H_5OH].2Cl$

In recent years, dicationic ionic liquids (DILs) have attracted increasing interest, finding unique applications as electrolytes, catalysts and etc [1]. DIL's characteristic caused structural variability, high tunability, low volatility, high thermal stability and lower ecotoxicity to compare with parental monocationic ionic liquids. Tropine or 3-tropanol is an important member of azabicyclo compounds which contain a tropane ring. Pyrimidine and its derivatives are important heterocyclic compounds and the diversity of their chemical and biological importance have made them more vital in pharmaceutical chemistry [2]. On the other hand, 3-amino[1,2,4]triazole derivatives which are composed of two rings, one pentamerous and the other senary, connected by a nitrogen bridge, have the ability to induce the growth of the cancer cells in the thyroid gland of rats [3]. In this work, a green and efficient procedure is reported for the synthesis of 1,2,4-triazolo[4,3-*a*]pyrimidine derivatives using a suitable dicationic molten salt based on tropine $[(Tropine)_2C_3H_5OH].2Cl$ (**Scheme**). The simple catalyst preparation, straightforward separation and recovery of the catalyst from the reaction mixture, short reaction times and high yields of the products are the significant points of interest of this study.

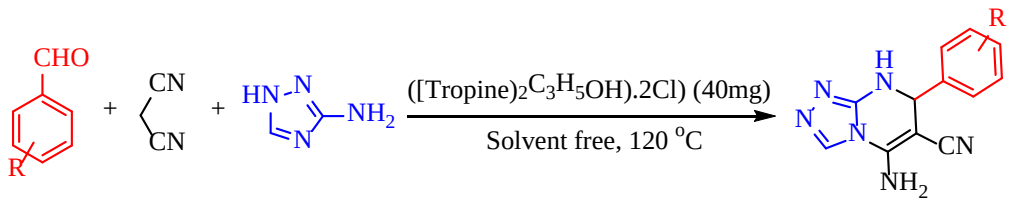

Scheme: synthesis of pyrimidine derivatives in presence of $[(Tropine)_2C_3H_5OH].2Cl$.

References

[1] Chinnappan, A.; Kim, H. Environmentally benign catalyst: Synthesis, characterization, and properties of pyridinium dicationic molten salts (ionic liquids) and use of application in esterification. *Chem. Eng. J.* **2012**, *187*, 283-288.

[2] Rai, U. S.; Isloor, A. M.; Vijesh, A.; Prabhu, N.; Isloor, S.; Thiageeswaran, M.; Fun, H.-K. Novel chromeno [2, 3-b]-pyrimidine derivatives as potential anti-microbial agents. *Eur. J. Med. Chem.* **2010**, *45* (6), 2695-2699.

[3] Demirbas, A.; Sahin, D.; Demirbas, N.; Karaoglu, S. A. Synthesis of some new 1, 3, 4-thiadiazol-2-ylmethyl-1, 2, 4-triazole derivatives and investigation of their antimicrobial activities. *Eur. J. Med. Chem.* **2009**, *44* (7), 2896-2903.

Application of tropine-based dicationic molten salt in acceleration of synthesis of pyrido[2,3-*d*]pyrimidine

Janan Metghalchi Langroudi, Masoumeh Mazloumi, Farhad Shirini* and Hassan Tajik

Department of Chemistry, College of Science, University of Guilan, Rasht, 41335-19141, Iran, jananmetghalchi5@gmail.com.

Keywords: Dicationic molten salt, Pyrimidines, Tropine, [(Tropine)$_2$C$_3$H$_5$OH].2Cl

In recent years, dicationic ionic liquids (DILs) have attracted increasing interest, finding unique applications as electrolytes, catalysts and etc [1]. DIL's characteristic caused structural variability, high tunability, low volatility, high thermal stability and lower ecotoxicity to compare with parental monocationic ionic liquids. Tropine or 3-tropanol is an important member of azabicyclo compounds which contain a tropane ring. Pyrimidine and its derivatives are important heterocyclic compounds and the diversity of their chemical and biological importance have made them more vital in pharmaceutical chemistry [2]. Pyrido[2,3-*d*] pyrimidines have a diverse range of activities such as antibacterial antimicrobial, tyrosine kinase, anti-inflammatory, analgesic, calcium channel antagonist, antileishmanial and anti-fungal [3]. In this work, a green and efficient procedure is reported for the synthesis of pyrido[2,3-*d*]pyrimidine derivatives using a suitable dicationic molten salt based on tropine [(Tropine)$_2$C$_3$H$_5$OH].2Cl (**Scheme**). The simple catalyst preparation, straightforward separation and recovery of the catalyst from the reaction mixture, short reaction times and high yields of the products are the significant points of interest of this study.

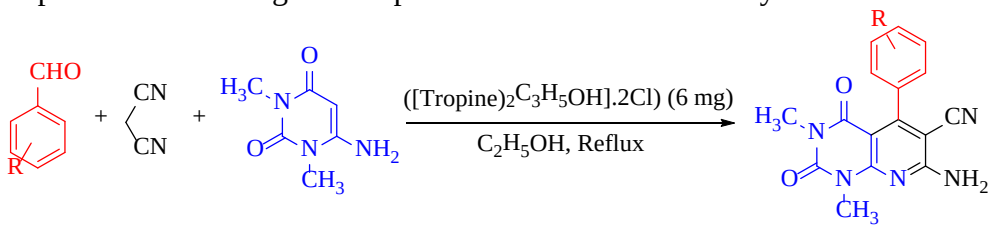

Scheme: synthesis of pyrimidine derivatives in presence of [(Tropine)$_2$C$_3$H$_5$OH].2Cl.

References

[1] Chinnappan, A.; Kim, H. Environmentally benign catalyst: Synthesis, characterization, and properties of pyridinium dicationic molten salts (ionic liquids) and use of application in esterification. *Chem. Eng. J.* **2012**, *187*, 283-288.

[2] Rai, U. S.; Isloor, A. M.; Vijesh, A.; Prabhu, N.; Isloor, S.; Thiageeswaran, M.; Fun, H.-K. Novel chromeno [2, 3-b]-pyrimidine derivatives as potential anti-microbial agents. *Eur. J. Med. Chem.* **2010**, *45* (6), 2695-2699.

[3] Quiroga, J.; Cisneros, C.; Insuasty, B.; Abonía, R,; Cruz, S.; Nogueras, M.; de la Torre, JM.; Sortino, M.; Zacchino, S. Microwave-assisted three-component synthesis and in vitro antifungal evaluation of 6-cyano-5, 8-dihydropyrido [2, 3-*d*] pyrimidin-4 (3*H*)-ones. *J. Heterocycl. Chem.* **2006**, *43* (2), 299-306.

Synthesis of Zn-MOF based on Arylenediimide tetra carboxylate ligand as a catalyst in the oxidation reactions

Ali Morsali*, Mohammad Rad

Department of Chemistry, Faculty of Sciences, Tarbiat Modares University, Tehran, Iran, morsali_a@yahoo.com, radmo@yahoo.com

Keywords: Tetra carboxylated ligand, Arylenediimid, Zn-MOF, catalyst

The compound 5,5'-(1,3,5,7-tetraoxopyrrolo[3,4-f]isoindole-2,6-diyl)diisophthalic acid, that one of the arylene diimide ligands, due to its particular oxygen sites, has the ability to create supramolecular interactions the usage of the guest-host approach. The presence of these groups can improve the properties of Metal-Organic frameworks based on this ligand, in catalytic procedures applications. Iodide have been placed in cavities of Zn-MOF, by post-synthetic modification to give Zn-MOF-I. under reaction situations of ambient temperature,Zn-MOF and Zn-MOF-I catalyzed the oxidation of alcohols, such as benzyl alcohol, with H_2O_2 as the oxidant. Halogen is generally used in oxidation reactions as oxygen-carrying species, referred to as active catalytic sites. Zn-MOF-I is introduced as the satisfactory catalyst in promoting the oxidation of alcohols. We aim to enhance the catalytic properties of alcohol oxidation within the case of this post-synthetic modification, as Zn-MOF includes large hydrogen-bonding networks that are to be had to bind with iodide.(Scheme1)

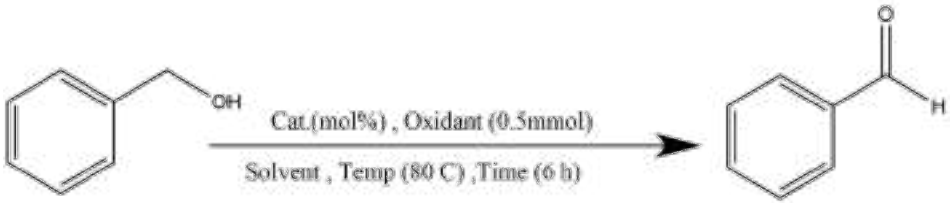

Scheme 1: General form of reaction and reaction conditions

References:

[1] An, G.; Zhang, X.; Zhang, C.; Gao, H.; Liu, S.; Qin, G.; Qi, H.; Kasemchainan, J.; Zhang, J.; Wang, G. J. C. J. o. C., Metal-organic-framework-based materials as green catalysts for alcohol oxidation. *Chinese J. Catal.*, 2023, 50, 126-174.

[2] Prasad, T. K.; Hong, D. H.; Suh, M. P. J. C. A. E. J., High Gas Sorption and Metal-Ion Exchange of Microporous Metal–Organic Frameworks with Incorporated Imide Groups. *Chem. Eur. J.*, 2010, 16 (47), 14043-14050.

[3] Das, S.; Chakraborty, P.; Shit, A.; Mondal, S.; Nandi, A. K. J. J. o. M. C. A., Robust hybrid hydrogels with good rectification properties and their application as active materials for dye-sensitized solar cells: insights from AC impedance spectroscopy. *J. Mater. Chem. A*, 2016, 4 (11), 4194-4210.

[4] Kataoka, Y.; Yano, N.; Mikuriya, M.; Handa, M. J. C. C. R., Coordination polymers and metal–organic frameworks based on paddlewheel-type dirhodium (II) tetracarboxylates. *Coord. Chem. Rev.*, 2022, 472, 214796.

Architecture of metal-organic frameworks for catalytic and photocatalytic applications; a review

Hassan Sepehrmansourie[a], **Mahmoud Zarei,***[b] **Mohammad Ali Zolfigol***[a]

[a] Department of Organic Chemistry, Faculty of Chemistry, Bu-Ali Sina University, Hamedan, Iran, sepehr9129@yahoo.com.

[b] Department of Chemistry, Faculty of Science, University of Qom, Qom, 37185-359, Iran.

Keywords: Catalytic applications, Metal-organic frameworks (MOFs), Porous catalyst

Metal-organic frameworks (MOFs) are a class of porous materials that have diverse properties such as thermal stability, uniform regular structure, very low density, and ease of synthesis. These remarkable properties have led to continuous research for the development of many new porous materials. At the elemental level, metal-organic frameworks represent the subtlety of chemical structures and the combination of inorganic and organic components. Metal-organic frameworks (MOFs) are a group of nanoreactors composed of metal and organic compounds as ligands. Metal-organic frameworks can be developed by connecting metal ions or metal oxides and organic bases or linkers together. Considering the progress of chemistry in recent years and the importance of the environment, catalysts are expected to be used for the synthesis of compounds that have high biological activity and selectivity. One of the most important applications of metal-organic frameworks (MOFs) is the catalytic application of this type of porous material. Metal-organic frameworks (MOFs) are used in chemical processes such as asymmetric reactions, synthesis of heterocyclic compounds, coupling reactions, etc. [1-2] (**Scheme 1)**.

Scheme 1: Catalytic application of metal-organic frameworks.

References

[1] Zhou, H. C.; Long, J. R.; Yaghi, O. M. Introduction to metal–organic frameworks. *Chem. Rev.*, 2102, 112, 673-674.

[2] Wang, Z.; Cohen, S. M. Postsynthetic modification of metal–organic frameworks. *Chem. Soc. Rev.*, 2009, 38, 1315-1329.

Rapid synthesis of some bis(indolyl)methanes by employing nano-cellulose-OSO_3H prepared from the peanut shell as a catalyst

Bahareh Sadeghi*

Department of Chemistry, Central Tehran Branch, Islamic Azad University, Tehran, Iran, bsadeghia@gmail.com

Keywords: Nano-cellulose-OSO_3H, Peanut shell, Aldehydes, Indole

Peanut shell is an agricultural waste and would be an excellent bio-resource for preparing solid acids because of its high supply, low cost, and easy sustainability. Much like other agricultural lignocellulolytic biomass, peanut shells are composed mainly of lignin, cellulose and hemicellulose. Consequently, peanut shells consist of a wide variety of hydroxyl groups that can be used as active sites for the preparation of solid acid catalysts. Several papers [1,2] have reported the preparation of solid acid catalysts by the sulfonation of the partially carbonized peanut shell and shown their high activity and excellent recyclability for biodiesel production and esterification reactions. In this study, the peanut shell has been applied as adsorbent for the preparation of nano-cellulose-OSO_3H whose average size is small and is well distributed. Nano-cellulose-OSO_3H is found to be an efficient catalyst for the electrophilic substitution reaction of indole with aldehydes to afford the corresponding bis(indolyl)methanes in good yields (**Scheme**).

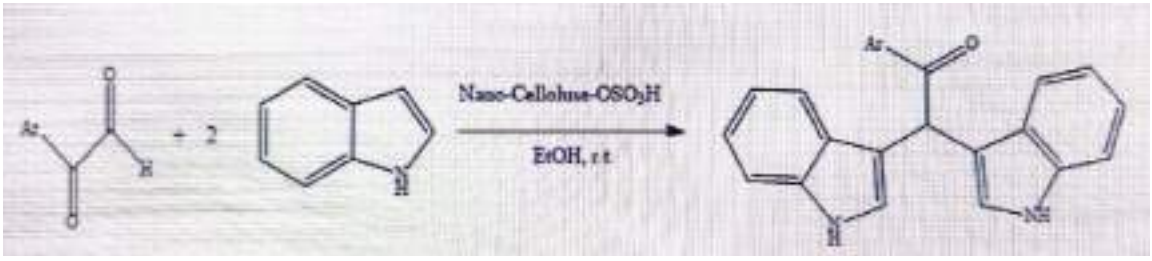

Scheme: Synthesis of bis(indolyl)methanes

References:

[1] Sadeghi, B.; Lasemi, Z.; Pisheh Abadi, M. Nano-peanut shell-OSO_3H: Green and natural-based renewable nanocatalyst for one-pot synthesis of dihydropyrano[3,2-*b*]chromenedione derivatives. *Iran. J. Catal.* 2019, *9*, 155-162.

[2] Zeng, D.; Liu, S.; Gong, W.; Wang, G.; Qiu, J.; Chen, H. Synthesis, characterization and acid catalysis of solid acid from peanut shell. *Appl. Catal. A.* 2014, *469*, 284-289.

Nano-coc-OSO_3H as an efficient catalyst for the one-pot synthesis of 3,4-dihydropyrimidine-2-(1*H*)-ones

Bahareh Sadeghi*

Department of Chemistry, Central Tehran Branch, Islamic Azad University, Tehran, Iran, bsadeghia@gmail.com

Keywords: Nano-cellulose, Chlorosulfonic acid, Coconut shell, Aldehydes, Pyrimidine

Nano-coc-OSO_3H has been prepared and shown to efficiently catalyst the one-pot, three-component reaction of an aromatic aldehyde, urea and a 1,3-diketone at reflux, to afford the corresponding 3,4-dihydropyrimidine-2-(1*H*)-ones (DHPMs) in high yield (Scheme). 3,4-dihydropyrimidine-2-(1*H*)-ones have received considerable attention due to the interesting pharmacological properties associated with this heterocyclic skeleton [1, 2]. Coconut shell is an agricultural waste and would be an excellent bio-resource for preparing solid acids because of its high supply, low cost, and easy sustainability. Much like other agricultural lignocellulolytic biomass, coconut shells are composed mainly of lignin, cellulose and hemicellulose. Consequently, coconut shells consist of a wide variety of hydroxyl groups that can be used as active sites for the preparation of solid acid catalysts. In this study, the coconut shell has been applied as adsorbent for the preparation of nano-coc-OSO_3H whose average size is small and is well distributed.

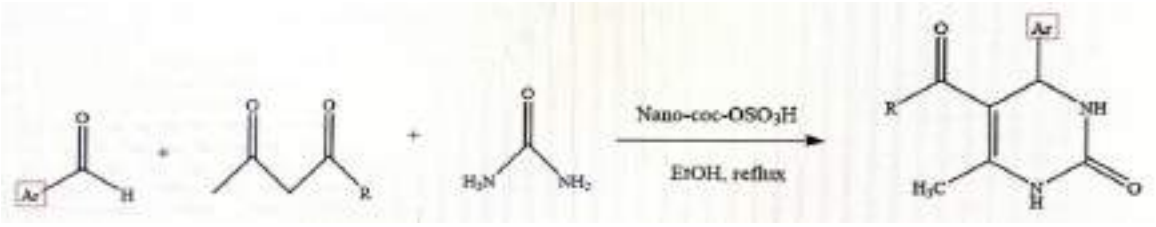

Scheme: Synthesis of 3,4-Dihydropyrimidine-2-(1*H*)-ones

References:

[1] Kappe, C. O. Biologically active dihydropyrimidones of the Biginelli-type a literature survey. *Eur. J. Med. Chem.* 2000, *35*, 1043-1052.

[2] Zorkun, I. S.; Sarac, S.; Celebi, S.; Erol, K. Synthesis of 4-aryl-3,4-dihydropyrimidin-2(1H)-thione derivatives as potential calcium channel blockers. *Biol. Med. Chem.* 2006, *14*, 8582-8589.

$ZrFe_2O_4@SiO_2@SO_3H$: A novel and reusable nanocatalyst for the synthesis of 2,3-dihydroquinazolin-4(1*H*)-ones

Maryam Borzooei *, **Masoomeh Norouzi**

Department of Chemistry, Faculty of Science, Ilam University, P.O. Box 69315516, Ilam, Iran, maryamborzooei78@gmail.com, m.norozi@ilam.ac.ir

Keywords: Nanocatalyst, 2,3-Dihydroquinazolin-4(1H)-one, Recoverable nanocatalyst

The preparation and the use of nanoparticles (NPs) in organic synthesis has become a subject of intense investigation [1]. In particular, magnetic nanoparticles (MNPs) offer advantages in clean and sustainable chemistry as they are non-toxic, readily accessible, and retrievable. In addition, the activity and selectivity of magnetic nano-catalysts can be manipulated by surface modification [2-3]. The present study describes the synthesis of a new magnetic solid sulfuric acid [$ZrFe_2O_4@SiO_2@SO_3H$] was synthesized and employed in the synthesis of 2,3-dihydroquinazolin-4(1H)-one. The aforementioned nanocatalyst were characterized by XRD, FTIR, FESEM, TGA and EDS. This results disclosed that the chemical grafting was successfully performed. The high activity in mild condition and the simple recoverable from the reaction are the suitable characteristics of this catalyst. Finally, the catalyst sustained activity for five cycles of reaction (**Scheme**).

Scheme: Synthesis of 2,3-dihydroquinazolin-4(1H)-one in the attendance of $ZrFe_2O_4@SiO_2@SO_3H$.

References

[1] Li, Y.; Zhang, L. A.; Qin, Y.; Chu, F.; Kong, Y.; Tao, Y.; Li, Y.; Bu, Y.; Ding, D.; Liu, M. Crystallinity dependence of ruthenium nanocatalyst toward hydrogen evolution reaction. *ACS Catal.* 2018, *22*, 5714-5720.

[2] Esmati, M.; Zeynizadeh, B. Introducing rGO@ Fe_3O_4@Ni as an efficient magnetic nanocatalyst for the synthesis of tetrahydrobenzopyranes via multicomponent coupling reactions of dimedone, malononitrile, and aromatic aldehydes. *Appl. Organomet. Chem.* 2022, *36*, 6496-6513.

[3] Ma, Z.; Mohapatra, J.; Wei, K.; Liu, J. P.; Sun, S. Magnetic nanoparticles: Synthesis, anisotropy, and applications. *Chem. Rev.* 2021, *123*, 3904-3943.

Synthesis of covalent organic framework/metal organic framework hybrid for headspace sampling of volatile and semi-volatile compounds in soil

Sara Maleki, Payman Hashemi* and Mohsen Adeli

Analytical Chemistry Laboratory, Faculty of Chemistry, Lorestan University, Khorramabad, Iran, Malekisd@yahoo.com, Hashemi.p@lu.ac.ir.

Keywords: Covalent organic framework, Metal-organic framework, Headspace solid-phase microextraction

Headspace solid-phase microextraction (HS-SPME) is a simple, rapid, solvent free and cost effective sample preparation method [1]. The key factor affecting the selectivity, extraction efficiency and sensitivity of analytes in SPME technique is choosing a suitable coating on the SPME fiber. Various porous materials with different physical, chemical, thermal, and mechanical properties have been reported as fiber coating for the analysis of different samples in recent years [2]. In this regard, porous crystalline materials, a combination of organic and inorganic materials, such as zeolites, metal-organic frameworks (MOFs), covalent organic frameworks (COFs), and porous organic cages with specific topologies and intrinsic porosities have been recently utilized for sampling and separation of organic and inorganic analytes in different matrices. In this work, a new hybrid of MOFs and COFs were synthesized and characterized by FE-SEM, XRD, BET, TGA and FTIR techniques. The HS-SPME method is evaluated for simultaneous sampling of volatile and semi-volatile compounds from polluted soil samples using the COF/MOF fiber. Optimization of the extraction parameters including extraction temperature, extraction time, moisture content of the sample, desorption time and desorption temperature was carried out using a GC-FID instrument and a simple method.

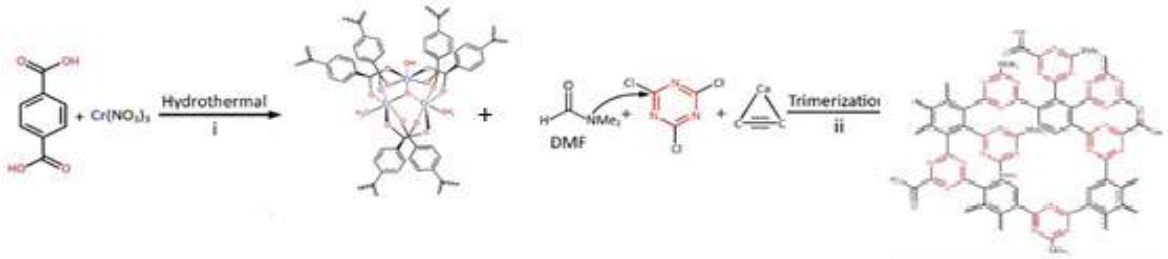

Scheme: Synthesis and structure of the COF/MOF hybrid.

References:

[1] Gong, S.-X.; Wang, X.; Chen, Y.; Cheng, C.-G.; Wang, M.-L.; Zhao, R.-S., Carboxylated solid carbon spheres as a novel solid-phase microextraction coating for sensitive determination of phenols in environmental water samples. *J. Chromatogr. A* **2015,** *1401*, 17-23.

[2] Delińska, K.; Rakowska, P. W.; Kloskowski, A., Porous material-based sorbent coatings in solid-phase microextraction technique: recent trends and future perspectives. *Trends Analyt. Chem.* **2021,** *143*, 116386.

29TH IRANIAN ORGANIC CHEMISTRY CONFERENCE
1_3 NOV, 2023
UNIVERSITY OF QOM, IRAN

Synthesis of adamantane-containing tetrahydrobenzo[*b*]pyrans and polyhydroquinolines

Hafez Janizadeh, Adeleh Moshtaghi Zonouz*, Mohammad Nori Ali Beg Candy

Departement of Chemistry, Faculty of Science, Azarbijan Shahid Madani University, Tabriz, Iran, hafezjanizadeh7878@gmail.com, adelehmz@yahoo.com.

Keywords: Adamantane motif, Diamondoid, Tetrahydrobenzo[*b*]pyrans, Polyhydroquinolines

Diamondoids are cage-saturated hydrocarbon molecules and superimposable on the diamond lattice, which can be described as hydrogen-terminated nanodiamonds [1]. Adamantane with the $C_{10}H_{15}$ formula is the smallest diamondoid. In addition to the existence of eight adamantane-based drugs in the world pharmaceutical market, the unique properties of adamantane, including the size, lipophilicity, rigidity, and biocompatibility make it special for modification of known drugs through an add-on strategy [2]. Hence, we decided to synthesize novel tetrahydrobenzo[*b*]pyrans and polyhydroquinolines derivatives incorporating an adamantane moiety. For this purpose, firstly N-1-adamantyl-2-(arylidene) acetoacetamides I were synthesized from the Knoevenagel reaction of N-1-adamantyl acetoacetamide 1 and aromatic aldehydes [3]. Then sequential Michael addition/cyclizatin reaction of arylidene derivatives I with dimedone or enaminone 2 afforded 4H-chromene derivatives II and polyhydroquinolines derivatives III, respectively (**Scheme**).

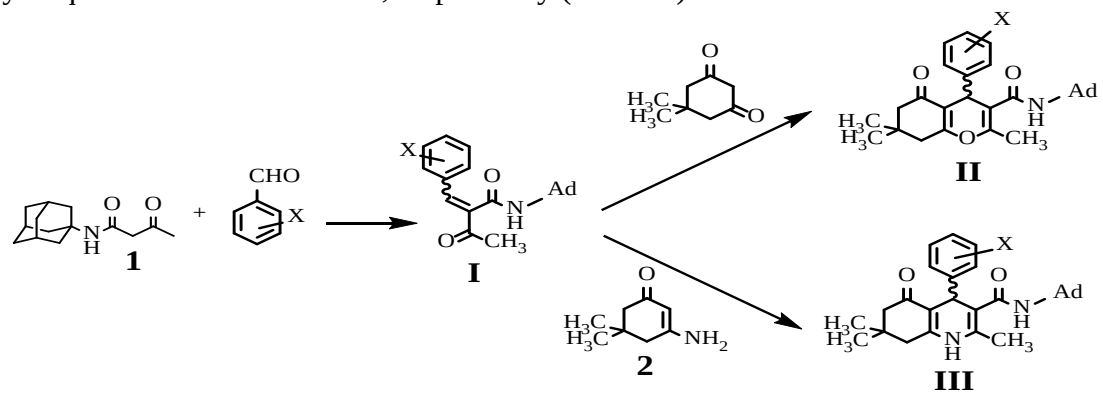

Scheme: Synthesis of 4H-chromene derivatives II and Polyhydroquinolines derivatives III

References

[1]. Gunawan, M.A.; Hierso, J-C; Poinsot, D.; Fokin, A.A.; Fokina, N.A.; et al. Diamondoids: functionalization and subsequent applications of perfectly defined molecular cage hydrocarbons. *New J. Chem.* 2014, *38*, 28-41.

[2]. Wanka, L.; Iqbal, K.; Schreiner, P.R. The lipophilic bullet hits the targets: medicinal chemistry of adamantane derivatives. *Chem. Rev.* 2013, *113*, 3516-604.

[3]. Abkar Aras, M.; Moshtaghi Zonouz, A. Synthesis of novel adamantane-containing dihydropyrimidines utilizing Biginelli condensation reaction. *J. Sulfur Chem.* 2023, *44*, 361-76.

Electrochemical Oxidation of *O*-Tolidine in the Presence of 4-Hydroxycoumarin to Synthesis of New Organic Compounds

Sadegh Khazalpour[a]*, Mehdi Pourahmad[a], Maryam Mehrdadian[a], Ameneh Amani[b]

a) Department of Analytical Chemistry, Faculty of Chemistry and Petroleum Sciences, Bu-Ali Sina University, Hamedan, Iran, S.Khazalpour@basu.ac.ir.
b) Nahavand Higher Education Complex, Bu-Ali Sina University, Hamedan 65178-38683, Iran.

Keywords: *Ortho*-Tolidine, 4-Hydroxycoumarin, Electrochemistry, Oxidation.

Aromatic amines are a worthy category of compounds in biological, materials, and pharmaceutical sciences [1]. *o*-tolidine (OTD) (3,3'-dimethylbenzidine) as an aromatic amine, is widely used in the formation of aniline dye and different azo dyes. It has been utilized to detect haemachrome, hemoglobin, hydrogen peroxide and red blood cells and, acts as a substrate for some peroxide enzymes. [2]. On the other hand, Coumarins are an important class of naturally occurring compounds which have been identified in plants and fungals. Many of them also, have been synthesized and studied for their pharmacological activities [3]. These properties prompted us to investigate the electrochemical oxidation of OTD in the presence of 4-hydroxycoumarin as nucleophile [4]. This method represents a facile and one-pot electrochemical process for the synthesis of new 4-hydroxycoumarin derivatives in good yields and purities.

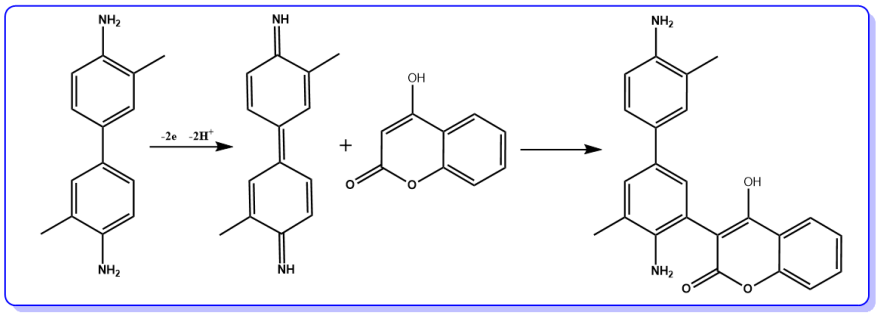

References:

1. Pietrzak, M.; Jędrzejewska, B. Aromatic Amines in Organic Synthesis. Part II. p-Aminocinnamaldehydes. Molecules. *Electrochim. Acta* 2021,52, 3883.
2. Ismail, K. M. Electrochemical preparation and kinetic study of poly (o-tolidine) in aqueous medium. *Electrochim. Acta.* 2007,52, 3883-3888.
3. Chang, C. J.; Floss, H. G.; Steck, W. Carbon-13 magnetic resonance spectroscopy of coumarins. Carbon-13-proton long-range couplings. *J. Org. Chem.* 1977 ,42, 1337-1340.
4. Amani, A.; Nematollahi, D. Electrochemical synthesis of new coumarin derivatives of potential biological significance. *J. Electroanal. Chem.*, 2012 ,681, 11-15.

Assessment and Design of reactor with capability of pyrolysis of urban green space

Seyedeh Bahareh Azimi*

Assessment and Environment Risks Department, Research Centre and Environment and Sustainable Development (RCESD), Tehran, Iran, azimib@rcesd.ac.ir

Keywords: Pyrolysis, Environment, Waste management

Every year in Iran and the world, very high amounts of biological waste are produced under the name of biomass. These wastes are disposed of inappropriately due to lack of proper management in the country. Improper disposal of biomass will cause serious damage to the environment and the ozone layer and ultimately increase the global temperature. According to some official and unofficial sources, these biological wastes constitute more than half of the world's wastes. Now, if there is no way to properly dispose of these wastes, it can harm the environment and society in several ways [1].

One of the best ways to dispose of waste is to recycle it. The pyrolysis process has received much less attention due to the high cost of its use. It also requires a permanent heat source, which limits its use. Production of a simple and suitable reactor for the pyrolysis process can improve the economic discussion of the pyrolysis process to some extent. In this article, design, assessment and construction of the biochar production device using the pyrolysis of agricultural waste was done. In addition of biochar (organic carbon), we also obtained activated carbon as a byproduct (**Scheme**). The designed pyrolysis system consists of a steel reactor and other inexpensive sub-components, which are connected to each other and performs the pyrolysis operation with the lowest amount of energy consumption. The results will show the contribution of each of the outputs depend on the control parameters and residence time. In this system, due to the one-way flow of gas exiting the reactor by the vacuum pump, it becomes impossible for oxygen to enter the reactor, and there is no need for continuous injection of nitrogen gas during the pyrolysis process.

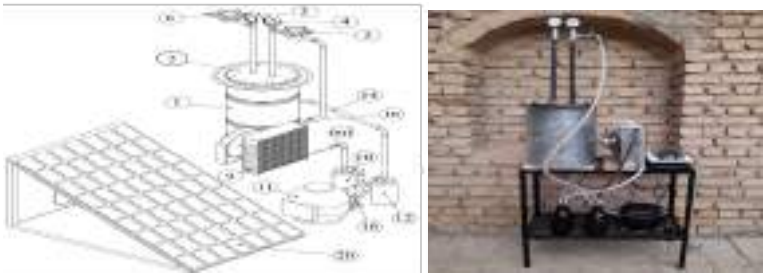

Scheme: system

References:

[1] Velmurugan, V. Review of research and development on pyrolysis process. *Materialstoday:* (2022), *49*, 3679-3686

Synthesis of anticancer Coumarin derivatives by new catalyst Cd/Zif-67

Somaye Kaboli*, Alireza Motavalizadehkakhky

Department of Chemistry, Neyshabur Branch, Islamic Azad University, Neyshabur, Iran, kaboli.somaye@yahoo.com, amotavalizadeh@yahoo.com

Keywords: Nanocatalyst, Cd/Zif-67, Coumarin, Anticancer Compounds

Coumarins are ring systems of benzene and pyrone, which are of particular importance in biological research due to their potential therapeutic properties [1]. It has immense anticancer potential with minimal side effects depending on the core substitution [2]. Coumarins have a remarkable ability to regulate a diverse range of cellular pathways that can be explored for selective anticancer activity.

In this project, considering the potential importance of coumarins, were synthesized using the reaction of phenol with ethyl acetoacetate. In the coumarin synthesized from this reaction, it was found that at a temperature of 90 degrees Celsius, acetonitrile solvent, Cd/Zif-67 catalyst (Cadmium/Zeolitic imidazolate framework-67) with a value of 0.05 and a time of 60 minutes, the best efficiency was 83% (Scheme).

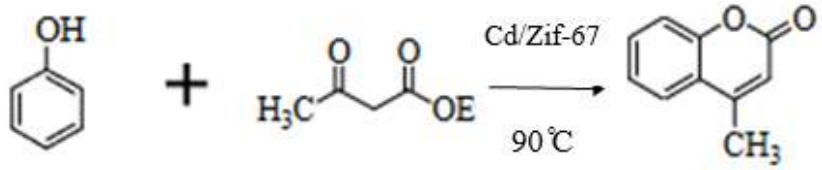

Scheme: General reaction of coumarin synthesis from phenol and ethyl acetoacetate

References

[1] Murray, R.D.H., Mendez, J. and Brown, S.A. (1982) The Natural Coumarins: Occurrence, Chemisty and Bio-chemistry (John Wiley & Sons Ltd, New York), p 21.

[2] Venugopala KN, Rashmi V, Odhav B. Review on Natural Coumarin Lead Compounds for Their Pharmacological Activity. *Biomed. Res. Int.*, 2013;2013:1-14.

Ag nanoparticles on cyanoguanidine decorated magnetic g-C_3N_4 as an efficient catalyst for hydrogenation of nitroaromatic compounds

Mansoureh Daraie[a], Mahmood Tajbakhsh[b], Ali Ayati[c], Sara Rashidi[a]

a) Department of Chemistry, Science and Research Branch, Islamic Azad University, Tehran, Iran, Daraie_m@yahoo.com
b) Department of Organic Chemistry, Faculty of Chemistry, University of Mazandaran, Babolsar, Iran.
c) Department of Chemical Engineering, Quchan University Technology, Quchan, Iran.

Keywords: Nanocatalyst, Magnetic g-C_3N_4, Nitroaromatic compound

Heterogeneous nanocatalysts have gained great attention from synthetic organic chemists during the past two decades for their precision engineering, design, and sustainable development. Compared to their homogeneous counterparts, they offer mild reaction conditions, easy separation, avoidance of decontamination, and recyclability without pre-activation [1,2]. In these years, the development of catalysts with high activity and selectivity that overcome these difficulties is a rapidly developing area in chemistry.
Based on these considerations, this study aimed to develop a robust, efficient, and readily separable catalyst for the reduction of nitroaromatic compounds. To improve its catalytic function, a novel g-C_3N_4-Cyanoguanidine nanoparticle-doped Ag nanoparticle compound was developed (Ag@Fe_3O_4-g-C_3N_4-CG). As a result of the promising results, Ag nanoparticles were synthesized using Portulaca oleracea herb as a reducing and stabilizing agent. In order to evaluate its catalytic performance, the hybrid nanostructure was applied to nitroaromatic compound reduction with $NaBH_4$. In addition, the recyclability of the nanocatalyst was discussed.

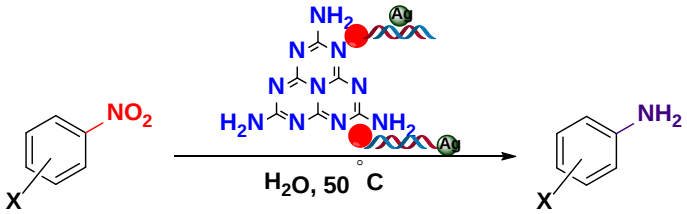

Scheme: The reaction of nitrobenzene reduction.

References

[1] Iqbal, O. et al. A review on the synthesis, properties, and characterizations of graphitic carbon nitride (g-C_3N_4) for energy conversion and storage applications. *Mater. Today Phys.* 2022, 34, 101080.
[2] Daraie, M., Heravi, M. M., Mohammadi, P. & Daraie, Silver incorporated into g-C_3N_4/Alginate as an efficient and heterogeneous catalyst for promoting click and A^3 and KA2 coupling reaction A. *Sci. Rep*. 2021, 11, 14086.

Magnetic core-shell nanoparticles based on alginate dialdehyde: A superior pH-responsive doxorubicin delivery system

Ali Mohammadzadeh, Siamak Javanbakht and Reza Mohammadi*

Polymer Research Laboratory, Faculty of Chemistry, University of Tabriz, Tabriz, IRAN, alimohammadzade778@gmail.com, r.mohammadi@tabrizu.ac.ir

Keywords: Alginate dialdehyde, Magnetic, Doxorubicin.

This research describes the development of a novel pH-responsive drug delivery system (DDS) for cervical cancer [1]. This project explores the use of Fe_3O_4 nanoparticles for drug collection and transfer, modifying their surfaces with natural polymers, and explaining their structure for cancer cell delivery [2]. According to the following schematic, Fe_3O_4@SiO_2@APTMS (3-Aminopropyl)trimethoxy silane@ alginate dialdehyde/DOX (FSA@ADA/DOX) and FSA/DOX nanocarriers were synthesized. The maximal drug-loading capacities of FSA and FSA@ADA nanocarriers were found to be 79.83 and 90.12%, respectively. Cytotoxicity results showed good biocompatibility for blank FSA/ADA. The obtained results showed that FSA@ADA/DOX nanocarriers can be proposed as an anticancer drug delivery system (**Scheme**).

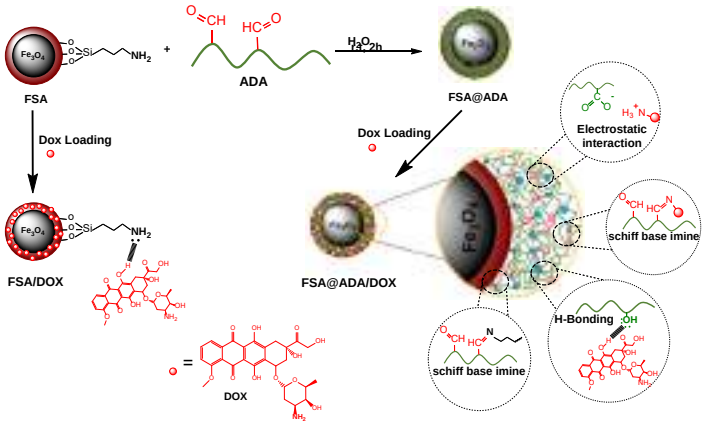

Scheme: Preparation of FSA/DOX and FSA@ADA/DOX nanocarriers.

References

[1] Sharma, S., Kumar, R., Rana, N.K. and Koch, B., The consequence of imine bond origination: Fabrication of rapid self-healing chitosan hydrogel as a drug delivery candidate for water-soluble drug. *Eur. Polym. J.*, 2022, *180*, p.111605.

[2] Jahanban-Esfahlan, R., Derakhshankhah, H., Haghshenas, B., Massoumi, B., Abbasian, M. and Jaymand, M., A bio-inspired magnetic natural hydrogel containing gelatin and alginate as a drug delivery system for cancer chemotherapy. *Int. J. Biol. Macromol.*, 2020, *156*, pp.438-445.

Synthesis and Complexation of *N*,*N*'-Bis-(pyridin-2-ylmethylene)-ethane-1,2-diamine as Homogeneous Catalyst in the Synthesis of Dihydroquinazolin-4(1*H*)-ones

Elahe Mashhadi, Javad Safaei-Ghomi*

Department of Organic Chemistry, Faculty of Chemistry, University of Kashan, Kashan, 51167, I. R. Iran, elahe.mashhadi74@gmail.com

Keywords: Cu(II) Schiff base, Homogeneous catalysis; Multi-component reaction, Dihydroquinazolin-4(1*H*)-ones

Dihydroquinazolin-4(*1H*)-one derivatives as one of the most frequently encountered fused heterocycles in medicinal chemistry various applications in the pharmaceutical industry. The compounds of this family have exhibited antitumor, anti-inflammatory, anticonvulsant and antibacterial activities [1, 2]. Because of their facile syntheses, electronic properties, easily tunable steric and good solubility in solvents, Schiff base ligands have been extensively studied in coordination chemistry. Schiff base with nitrogen donors can interact with most metal ions and produce various complexes [3, 4]. In this research, a successful design have been accomplished for the synthesis of a Cu(II) Schiff-base complex. This complex serves as an effective homogeneous catalyst in a one-step reaction involving different aldehydes, isatoic anhydride, and primary aromatic amine to produce derivatives of 2,3-dihydroquinazolin-4(1H)-one. The reaction occurs in an aqueous solution at a temperature of 80℃, as depicted in Scheme 1.

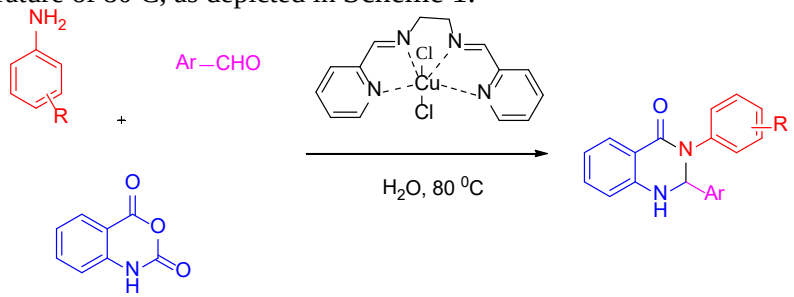

Scheme 1: using various aldehydes, isatoic anhydride, and primary aromatic amine with Schiff base complex as a catalyst in H_2O, 80 ^0C

References

[1] Safaei-Ghomi J, Teymuri R, Bakhtiari A. Co-aminobenzamid@ Al-SBA-15, a favorable catalyst in synthesis of 2, 3-dihydroquinazolin-4 (1H)-ones. *BMC Chemistry*. 2019, *13*, 1-12.

[2] Safaei-Ghomi J, Teymuri R. A favourable ultrasound-assisted method for the combinatorial synthesis of 2, 3-dihydroquinazolin-4 (1H)-ones via $CoAl_2O_4$ spinel nanocrystal as an efficient catalyst. *Iran. J. Catal.* 2021, *11*, 113-23.

[3] More, M. S., Joshi, P. G., Mishra, Y. K., & Khanna, P. K. Metal complexes driven from Schiff bases and semicarbazones for biomedical and allied applications: a review. *Mater. Today Chem.* 2019, *14*, 100195.

Synthesis of spiropyrans using catalyst synthesized by post-modification method based on vanadium-MOFs

Mina Bakhtiari,[a] Mahmoud Zarei,*[a] Hassan Sepehrmansourie [b]

a) Department of Chemistry, Faculty of Science, University of Qom, Qom, 37185-359, Iran, minabakhtiari2027@gmail.com, mahmoud8103@yahoo.com.

b) Department of Organic Chemistry, Faculty of Chemistry, Bu-Ali Sina University, Hamedan, Iran.

Keywords: Vanadium-MOFs, Post-modification, Spiropyrans.

Metal-organic frameworks (MOFs) are a new class of new generation nanoreactors that are composed of various metals and organic compounds as ligands. Recently, various metals such as Zr, Co, Fe, V, Ti have been used in MOFs architectures. This unique structure of MOFs has been used in various fields such as catalysis, photocatalyst, magnetic resonance imaging (MRI), gas separation and storage, biotechnology, drug delivery and other fields [1]. Metal-organic frameworks based on this metal have very interesting properties such as good stability MOFs have recently attracted attention in catalysis-related fields. Due to the coordination flexibility and multiple oxidation states of vanadium ions or clusters, vanadium-MOFs (V-MOFs) have unique structural features and beneficial catalytic properties [2]. Spiropyrans are a class of organic compounds that contain two or more rings fused together at a single atom. The presence of the spiro framework often gives these compounds unique biological activities and physical properties [3]. In this regard, the goal is to create a vanadium-based MOFs catalyst to be used as a suitable catalyst for the synthesis of spiropyran compounds. The importance of spiropyran compounds in medicinal compounds has been proven (**Scheme 1**).

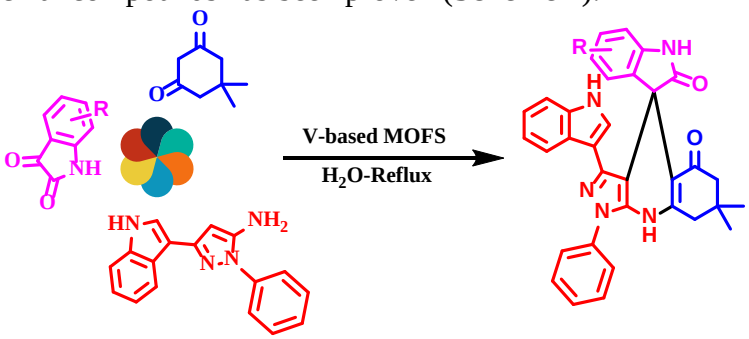

Scheme 1: Synthesis of spiropyrans using Vanadium-based MOFS.

References

[1] James, S. L. Metal-organic frameworks. *Chem. Soc. Rev.*, 2003, 32, 276-288.

[2] Phan, A.; Czaja, A. U.; Gándara, F.; Knobler, C. B.; Yaghi, O. M. Metal-organic frameworks of vanadium as catalysts for conversion of methane to acetic acid. *Inorg. Chem.*, 2011, 50, 7388-7390.

[3] Fagan, A.; Bartkowski, M.; Giordani, S. Spiropyran-based drug delivery systems. *Front. Chem.*, 2021, 9, 720087.

Synthesis of polytriazine frameworks by chemical and mechanochemical polymerization

Sara Bagheri, Abedin Zabardasti, Siamak Beyranvand and Mohsen Adeli*

Inorganic Chemistry Laboratory, Faculty of Chemistry, University of Lorestan, Khorramabad, Iran, baghrei_2018@yahoo.com, mohadeli@yahoo.com

Keywords: Polytriazine, Polymerization, Mechanochemical

Covalent triazine formwork (CTFs) are a subclass of two-dimensional polymers with unique optical, mechanical and chemical properties. The presence of strong covalent bonds, high chemical and thermal stability, high surface area results in interesting physicochemical properties that can be used in a wide range of applications including gas separation, energy storage, photocatalyst and heterogeneous decomposition.[1-2] Here, we report the synthesis of metal-assisted triazine polymer structures via a chemical and mechanochemical approach. Triazine monomers are polymerized in the presence of metal ions to be directed in different morphologies and optical activities.

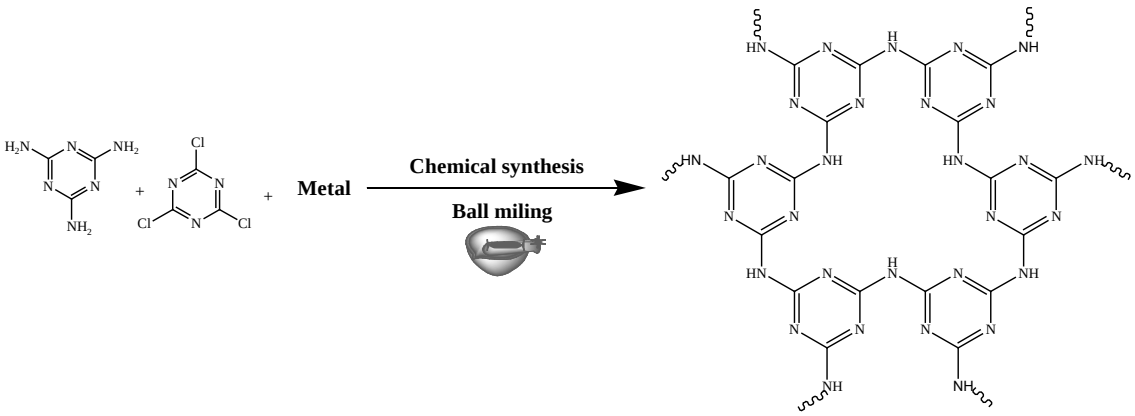

Scheme: Schematic illustration of the synthesis of CTFs by chemical synthesis and mechanochemistry.

References

[1] Liu, M.; Guo, L.; Jin, S.; Tan, B., Covalent triazine frameworks: synthesis and applications. *J. Mater. Chem. A* **2019,** *7* (10), 5153-5172.

[2] Krishnaraj, C.; Jena, H. S.; Leus, K.; Van Der Voort, P., Covalent triazine frameworks–a sustainable perspective. *Green Chem.* **2020,** *22* (4), 1038-1071.

Transition-Metal-Free Domino Cyclization Reaction of *o*-diisocyanoarenes for the Synthesis of Imidazo[1,2-*a*]pyridinobenzimidazole Backbones

Mohammad Rezaei-Gohar, Kamran Amiri, Kimia Aghaie, Behrouz Nayebzadeh and Saeed Balalaie*

Peptide Chemistry Research Institute, K. N. Toosi University of Technology, P. O. Box 15875-4416, Tehran, Iran, Balalaie@kntu.ac.ir

Keywords: Domino Cyclization Reaction, *o*-diisocyanoarenes, Imidazo[1,2-*a*]pyridin, Benzimidazole, Transition-Metal-Free.

An efficient procedure to access a variety of connected imidazo[1,2-*a*]pyridine and benzimidazole skeletons through the C-N bond was described as a new type of Buchwald-Hartwig reaction. Furthermore, the bis(Imidazo[1,2-*a*]pyridin-3-yl)aryl-1,2-diamine scaffolds were obtained by changing the equivalent ratio of aldehyde and 2-aminopyridine. Some advantages of the protocol are the formation of four new bonds (C=C, C-N), transition-metal-free domino reaction, scale-up reaction, high atomic economy, broad substrate scope, high yields, and mild reaction conditions. The proposed reaction mechanism was confirmed based on the DFT calculations (**Scheme**).

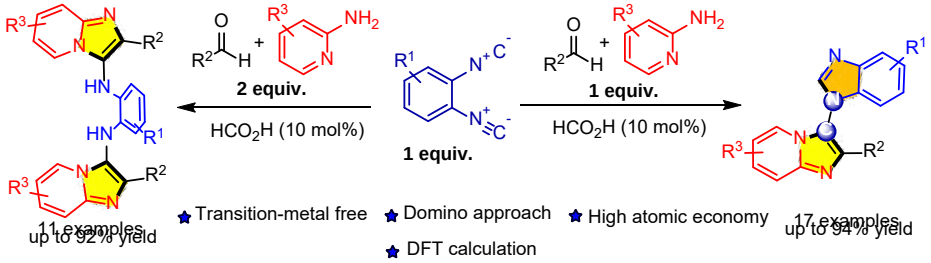

Scheme: Using of *o*-diisocyanoarenes for the synthesis of heterocyclic skeletones.

References

[1] Rezaei-Gohar, M.; Amiri, K.; Aghaie, K.; Nayebzadeh, B.; Ariafard, A.; Shiri, F.; Balalaie, S. Domino Cyclization Reaction of o-Diisocyanoarenes for the Synthesis of Imidazo [1,2-*a*] pyridinobenzimidazole Backbones. *Org. Lett*. **2023**, *25*, 5682-5686.

[2] Nayebzadeh, B.; Amiri, K.; Khosravi, H.; Mirzaei, S.; Rominger, F.; Dar'in, D.; Krasavin, M.; Bijanzadeh, H. R.; Balalaie, S. Synthesis of Spiro [chromene-imidazo [1, 2-*a*] pyridin]-3′-imines via 6-exo-dig Cyclization Reaction. *J. Org. Chem.* **2021**, *86*, 13693−13701.

[3] Leifert, D.; Studer, A. Iodinated (Perfluoro) alkyl Quinoxalines by Atom Transfer Radical Addition Using ortho-Diisocyanoarenes as Radical Acceptors. *Angew. Chem., Int. Ed.* **2016**, *55*, 11660−11663

[4] Boltjes, A.; Dömling, A. The Groebke-Blackburn-Bienaymé reaction. Eur. *J. Org. Chem*. **2019**, 2019 (42), 7007−7049.

Design of Vanadium-based MOFs as a new porous catalyst for the synthesis of spiropyrans

Fatemeh Zarezadeh,[a] Mahmoud Zarei,*[a] Hassan Sepehrmansourie [b]

a) Department of Chemistry, Faculty of Science, University of Qom, Qom, 37185-359, Iran, m.zarezadeh89@gmail.com, mahmoud8103@yahoo.com.

b) Department of Organic Chemistry, Faculty of Chemistry, Bu-Ali Sina University, Hamedan, Iran.

Keywords: Metal-organic frameworks (MOFs), Porous catalyst, Spiropyrans.

Metal-organic frameworks (MOFs) are organic-inorganic hybrid crystalline porous materials that consist of a regular array of positively charged metal ions surrounded by organic 'linker' molecules. The metal ions form nodes that bind the arms of the linkers together to form a repeating, cage-like structure. Due to this hollow structure, MOFs have an extraordinarily large internal surface area [1]. Vanadium-based MOFs are a class of porous materials composed of metal ions coordinated to organic ligands. Vanadium-based MOFs have unique advantages compared to other types of MOFs. The incorporation of iron as the metal center provides several desirable properties. Vanadium-based MOFs often have good thermal and chemical stability, which is very important for their practical applications [2]. Spiropyrans have also attracted much attention because of their application within the perovskite solar cells and pharmacological properties such as inhibitors of human NK-1 receptor, antitumoral, antimicrobial, and antibiotic agents [3]. In this regard, the goal is to create a vanadium-based MOFs catalyst to be used as a suitable catalyst for the synthesis of spiropyran compounds. The importance of spiropyran compounds in medicinal compounds has been proven (**Scheme 1**).

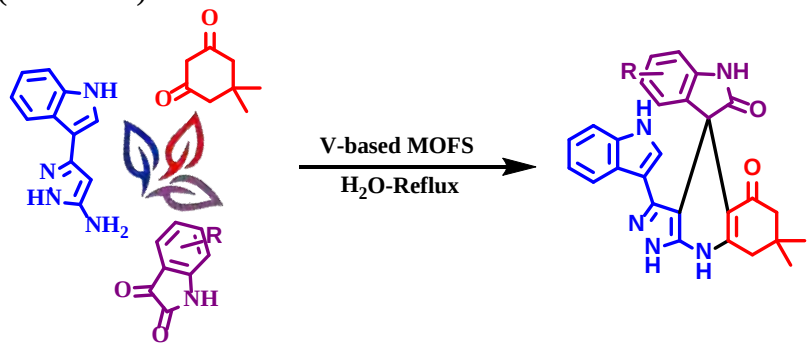

Scheme 1: Synthesis of spiropyrans using Vanadium-based MOFS.

References

[1] Zhou, H. C.; Long, J. R.; Yaghi, O. M. Introduction to metal–organic frameworks. *Chem. Rev.*, 2102, 112, 673-674.

[2] Gupta, Recent reports on vanadium-based coordination polymers and MOFs. *Rev. Inorg. Chem.*, 2023, 43, 465-493.

[3] Klajn, R. Spiropyran-based dynamic materials. *Chem. Soc. Rev.*, 2014, 43, 148-184.

Evaluation of tripartite motif Containing16 (TRIM16) protein expression gene in tumor and normal tissue of patients with gastric cancer

Jalil Afshar[a], Jamshid Mehrzad[a]*, Hassan Mehrad-Majd[b], Jafar Saeidi[c]

a) Department of Biochemistry, Neyshabur Branch, Islamic Azad University, Neyshabur, Iran, jalil.afshargoli@gmail.com, mehrzadjam@yahoo.com
b) Department of Gastroenterology and Hepatology, Mashhad University of Medical Sciences, Mashhad, Iran.
c) Department of Physiology, Neyshabur Branch, Islamic Azad University, Neyshabur, Iran.

Keywords: Gene encoding TRIM16 protein, Gastric cancer, Realtime

Gastric cancer (GC), it remains the third most common cancer and the fifth leading cause of death among all cancers. Identification of genetically predisposing genes to the development and incidence of gastric cancer in the first place, and the functional molecular mechanism of genes in the pathogenesis of the disease in the second place are among the essential requirements in defining effective treatment strategies and controlling and preventing the disease [1-2]. For this purpose, 40 pairs of samples were collected from patients with definitive diagnosis of GC and confirmed by pathological tests. Using TRIzol (TRIzol ($C_2H_3N_3$) is a widely used chemical solution used in the extraction of DNA, RNA, and proteins from cells) extraction kit, total RNA extraction and its quality were evaluated through absorption readings at 260 nm through the nanodrop device. Then, based on the existing protocols, cDNA was synthesized and quantitative PCR was performed to evaluate the expression of TRIM16 mRNA compared to the expression of a reference gene (beta-actin) by real-time PCR. The increase and decrease in expression of this gene was measured with this reference gene β-actin. It was observed that the expression of TRIM16 gene in cancer tissue was significantly reduced compared to adjacent healthy tissue (**Scheme**).

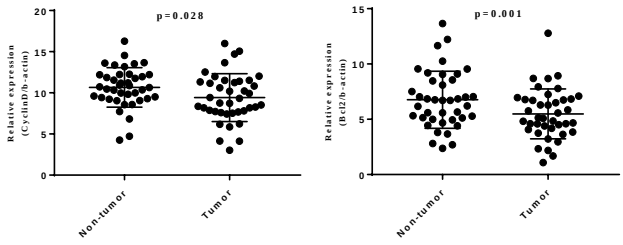

Scheme: Gene expression analysis in GC tissues and their non-cancerous control group

References

[1] Freddie Bray, Jacques Ferlay, Isabelle Soerjomataram, Rebecca L Siegel, Lindsey A Torre, Ahmedin Jemal (2018). Global cancer statistics 2018: GLOBOCAN estimates of incidence and mortality worldwide for 36 cancers in 185 countries. *CA Cancer J Clin*, 68, 394-424.

[2] Fischer, M. (2017). "Census and evaluation of p53 target genes." Oncogene 36(28): 3943-3956.

Investigation Relationship of Tripartite Motif Containing 44 (TRIM44) Expression in Patients with Gastric Cancer

Jalil Afshar[a], Jamshid Mehrzad[a]*, Hassan Mehrad-Majd [b], Jafar Saeidi [c]

a) Department of Biochemistry, Faculty of BasicScience, Neyshabur Branch, Islamic Azad University, Neyshabur, Iran, jalil.afshargoli@gmail.com, mehrzadjam@yahoo.com
b) Department of Gastroenterology and Hepatology, Faculty of Medical Sciences, Mashhad University of Medical Sciences, Mashhad, Iran.
c) Department of Physiology, Faculty of BasicScience, Neyshabur Branch, Islamic Azad University, Neyshabur, Iran.

Keywords: TRIM44- Gastric cancer (GC)- β-catenin

Considering the importance of signaling pathways such as NF-κB and the PI3K/Akt axes in the pathogenesis of GC we designed a study to explore the relationship between the expression of TRIM44 and the outcome of the GC patients and to propose a probable molecular mechanism through which this gene might participate in the progression of GC.

The paired-samples t-test was used to compare the mRNA expression levels of TRIM44(tripartite motif44), and β-catenin between cancerous and noncancerous tissues. According to the TRIM44 median expression level, patients were divided into two groups of high (tumor tissue expressed TRIM44 mRNA above the median value) and low (tumor tissue expressed TRIM44 mRNA below the median level) expression(**Scheme**).

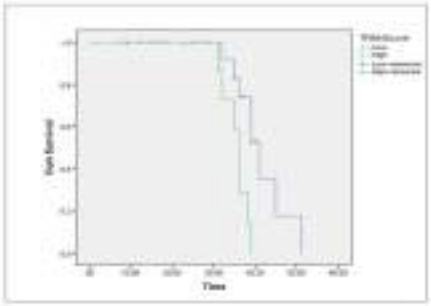

Scheme: The Correlation between TRIM44 Expression and the Overall Surviva

References

1) Elizabeth C Smyth, Magnus Nilsson, Heike I Grabsch, Nicole CT van Grieken, Florian Lordick (2020). Seminar Gastric cancer, Pages 635-648.
2) Il Ju Choi, Chan Gyoo Kim, Jong Yeul Lee, Young-Il Kim, Myeong-Cherl Kook, Boram Park, Jungnam Joo (2020). Family history of gastric cancer and Helicobacter pylori treatment. NEJM, 382, 427-36.
3) Rawla P, Barsouk A (2019). Epidemiology of gastric cancer: global trends, risk factors and prevention. Prz, 14, 26-38.

Magnetic Fe_3O_4@TiO_2 Core-Shell Supported Schiff-base/Pd(0) Complex: An Efficient Heterogenous Catalyst for Reduction of Nitroarenes

Leyla Mohammadkhani, Majid M. Heravi* and Parisa Mofatehnia

Department of Chemistry, Faculty of Chemistry, Alzahra University, Tehran, Iran, mohammadkhani.leyla@gmail.com, mmheravi@alzahra.ac.ir

Keywords: Palladium nanoparticles, Heterogeneous catalysis, Nitroarenes, Titanium dioxide, Core-shell

This study presents a novel approach for the rapid and selective reduction of nitroarenes to anilines, utilizing a newly developed complex consisting of palladium (Fe_3O_4@TiO_2@Schiff base@Pd(0)), in conjunction with sodium borohydride as the reducing agent, and water as a green solvent, all performed at room temperature. The heterogeneous catalyst was prepared through chemical attachment of Schiff-base groups on Fe_3O_4/TiO_2 nanoparticles followed by treatment with $Pd(OAc)_2$. The characterization of Fe_3O_4@TiO_2@Schiff base@Pd(0) was achieved using various analytical techniques such as FT-IR, SEM, XRD, EDS, BET, and HR-TEM analyses. The results demonstrate that this catalyst system is highly effective in reducing aromatic nitro-compounds, resulting in anilines with exceptional conversion rates, selectivity, and stability. Furthermore, the Fe_3O_4@TiO_2@Schiff base@Pd(0) catalyst can be reused for more than five cycles, while maintaining consistent efficiency (**Scheme**).

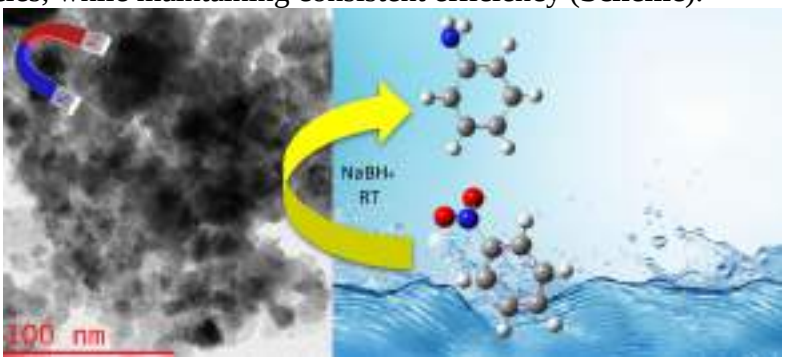

Scheme: Reduction of nitroarenes using Fe_3O_4@TiO_2@Schiff base@Pd(0)

References

[1] Liu, H.; Joo, J. B.; Dahl, M.; Fu, L.; Zeng, Z.; Yin, Y. Crystallinity control of TiO_2 hollow shells through resin-protected calcination for enhanced photocatalytic activity. *Energy Environ. Sci.* 2015, *8*, 286−296.

[2] Azadi, G.; Kazemi, F.; Firouzeh, E. Visible-light-driven photocatalytic Suzuki–Miyaura coupling reaction using novel retrievable magnetic photocatalyst. *ChemistrySelect* 2021, 6, 630−639.

[3] Mohammadkhani, L.; Heravi, M. M.; Panahi, F. Efficient and heterogeneous transfer hydrogenation of nitroarenes using immobilized palladium nanoparticles on silica–starch substrate (PNP-SSS). *Monatsh. Chem.* 2022, *153*, 623−633.

Investigation of copper (II) base heterogeneous photocatalyst in the synthesis of tetrahydroquinoline derivatives

Reza Teymouri Mofrad*, Darya Shabani Domoula and Aida Heidari

Department of Organic Chemistry and Biochemistry, Faculty of Chemistry, University of Tabriz, Tabriz, Iran, darya.shaabani@gmail.com, teymouri@tabrizu.ac.ir

Keywords: Photocatalyst, Tetrahydroquinoline, Electron transfer reaction, Photocatalytic cyclization reaction

The tetrahydroquinoline ring system is a prevalent structural compound in many biologically active natural products [1]. Moreover, tetrahydroquinolines with chiral structures have been investigated as coordination ligands in asymmetric synthesis [2,3]. Due to the importance of these compounds in drug discovery and medicinal chemistry, new methods for the synthesis of tetrahydroquinoline derivatives are very active research. This work aims to design photocatalysts based on copper for the synthesis of tetrahydroquinoline derivatives with a single electron transfer mechanism under visible light. The reaction of phenyl maleimide with *N, N*-dimethylaniline under air and visible light at room temperature was chosen as an electron transfer model reaction for investigation (Scheme 1).

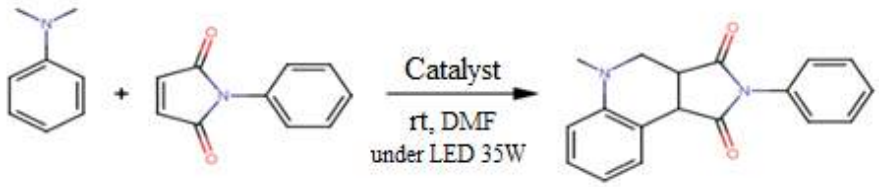

Scheme 1: The reaction of phenyl maleimide with *N, N*-dimethylaniline under air and visible light by using a catalyst

References

[1] Katritzky, A.R., Rachwal, S. and Rachwal, B., Recent progress in the synthesis of 1, 2, 3, 4,-tetrahydroquinolines. Tetrahedron, 1996, 52(48), pp.15031-15070.

[2] Pullmann, T., Engendahl, B., Zhang, Z., Hölscher, M., Zanotti-Gerosa, A., Dyke, A., Franciò, G. and Leitner, W., Quinaphos and Dihydro-Quinaphos Phosphine–Phosphoramidite Ligands for Asymmetric Hydrogenation. *Chem. Eur. J.* 2010, *16*(25), pp.7517-7526.

[3] Liu, W.B., He, H., Dai, L.X. and You, S.L., Synthesis of 2-methylindoline-and 2-methyl-1, 2, 3, 4-tetrahydroquinoline-derived phosphoramidites and their applications in iridium-catalyzed allylic alkylation of indoles. *Synthesis, 2009* (12), pp.2076-2082.

Supramolecular complexation for the bioavailability enhancement of poorly soluble drugs in water

Yasaman Yaghini, Nina Alizadeh*

Department of Chemistry, Faculty of Science, University of Guilan, Rasht, Iran, yasamanyaghini76@gmail.com, n-alizadeh@guilan.ac.ir

Keywords: Famotidine, Sulfobuthyl ether β-cyclodextrin, Inclusion complexes

Famotidine (FAM) is a strong H_2-blocker antagonist that is used to treat gastric and duodenal ulcers, recurrent ulcer disease, gastric reflux disease, etc. [1]. It has weak lipophilicity, low solubility in water, bitter taste and susceptibility to destruction in the stomach that may be the reason for the low and variable oral bioavailability of FAM [2]. In this study, to increase the bioavailability of the drug, highly soluble sulfobutyl ether beta-cyclodextrin (SBE-βCD), as supramolecular hollow cones was used [3]. For this an inclusion complex between FAM and SBE-βCD was prepared by mixing the two components in water and heating for one hour and stirring at room temperature, then solvent was separated using freeze drying method (**Scheme**). The stoichiometry of the complex was determined by the Job's method using a UV approach. This study showed the 1:1 ratio between the FAM and SBE-βCD. Stability constant of this inclusion complex by Benesi–Hildebrand method was determined as $K_{1:1}=1.526\times10^{3}M^{-1}$. Complex was studied by FTIR, SEM and NMR experiments. This inclusion complex may be valueable to the pharmaceutical industry especially in the preparation of tablets of FAM. These supramolecular systems will be developed in the field of pharmaceutical and medical application.

Scheme: Complex formation reaction of FAM and SBE-βCD.

References

[1] Islam, M.S.; Narurkar, M.M., The effect of 2-hydroxypropyl -cyclodextrin on the solubility, stability and dissolution rate of famotidine. *Drug Dev. Ind. Pharm.* 1991, 17, 1229–1239.

[2] Mady, F.; Abou-Taleb, A. E.; Khaled, A. K.; Yamasaki, K.; Iohara, D.; Ishiguro, T.; Hirayama, F.; Uekama, K.; Otagiri, M., Evaluation of carboxymethyl-β-cyclodextein with acid function: Improvement of chemical stability, oral bioavailability and bitter taste of FAM. *Int. J. Pharma.* 2010, 397, 1-8.

[3] Alizadeh, N.; Malakzadeh, S. Antioxidant, antibacterial and anti-cancer activities of ß- and y- CDs/ curcumin loaded in chitosan nanoparticles. *Inter. J. Bio. Macromol.* 2020, 147, pp 778-791.

Synthesis of 2,3-dihydro-4(1H) quinazolinones using a magnetic pectin-supported deep eutectic solvent

Mohsen Bakhtiarian [a], **Mohammad Mehdi Khodaei** [a,b*]

a) Department of Organic Chemistry, Razi University, 67149-67346 Kermanshah, Iran, mohsenorgc@gmail.com, mmkhoda@razi.ac.ir

b) Nanoscience and Nanotechnology Research Center (NNRC), Razi University, Kermanshah 67149-67346, Iran.

Keywords: Deep-eutectic solvent, Pectin, Sustainable catalysis, Magnetic nanocatalyst, Multicomponent reaction

Deep eutectic solvents (DESs) are an emerging type of ionic liquids (ILs) with benign and tuneable nature that are prepared by mixing and heating of a hydrogen bond acceptor (HBA) (mostly a quaternary ammonium salt) and a hydrogen-bond donor (HBD) [1]. Despite these advantages, recovery issues restrict their use, and immobilization serves as a viable solution. However, choosing a support material is a challenging step in view of sustainability and eco-friendliness. Therefore, in this work we introduced for the first time a recoverable deep eutectic solvent immobilized on pectin (Pec) as a naturally-occurring support using metformin (Met) as a hydrogen bond donor, and choline chloride (ChCl) as hydrogen bond acceptor. Then, these nanoparticles (Pec-Met-ChCl) were magnetized by immobilizing magnetic Fe_3O_4 nanoparticles to produce MNPs-Pec-Met-ChCl. Various aromatic and heteroaromatic 2,3-dihydro-4(1H)-quinazolinone derivatives were synthesized by MNPs-Pec-Met-ChCl under solvent-free conditions. The stable and heterogeneous nature, existence of hydrogen bond donating groups and subsequently an effective interaction with substrates specify the catalyst activity of MNPs-Pec-Met-ChCl nanocomposites. The presence of Fe_3O_4 magnetic nanoparticles not only provides a clean and simple recovery, but also improves the catalytic activity. (**Scheme 1**).

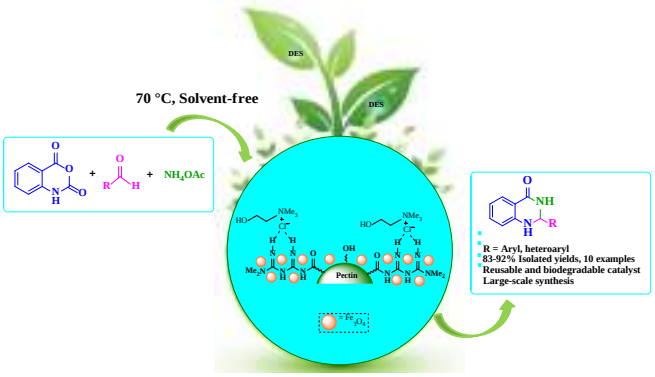

Scheme 1: Pectin-immobilized DES for the synthesis of 2,3-dihydro-4(1H) quinazolinones.

References

[1] Smith, E. L.; Abbott, A. P.; Ryder, K. S. Deep eutectic solvents (DESs) and their applications. *Chem. Rev.* 2014, *114*, 11060-11082.

Ag_3 Cluster as An Anticarcinogenic Agent: A DFT Quest

Batoul Alipour and Mohamad Zaman Kassaee*

Department of Chemistry, Tarbiat Modares University, P.O. Box 14115-175, Tehran, Iran, alipourbatoul@gmail.com, kassaeem@modares.ac.ir

Keywords: Cluster, DFT, Silver, Anticancer, BDE

The Ag_3 cluster acts as carcinogenic or anticarcinogenic by promoting or trapping free radicals. Continuing with group work, we compute the dual roles of the Ag_3 cluster in trapping $RO^{\bullet}$, or forming free radicals from RO–H, at the B_3LYP/ LANL2DZ level in water as solvent. The DFT results show that the bond dissociation energy (BDE) of RO–H and the spin density at the oxygen of $RO^{\bullet}$ decrease in the presence Ag_3 cluster. It can be found that the cleavage of the RO–H bond occurred and then the $RO^{\bullet}$ radicals scavenge. Since O–Ag, anchoring bond is responsible for the interaction of Ag_3 and ROH (or $RO^{\bullet}$), The results indicate that the O–Ag bond is stronger and has more covalent nature in $RO^{\bullet}$– Ag_3 than in ROH– Ag_3. Therefore, the silver cluster acts as a potential anticancer through scavenging free radicals (**Scheme**).

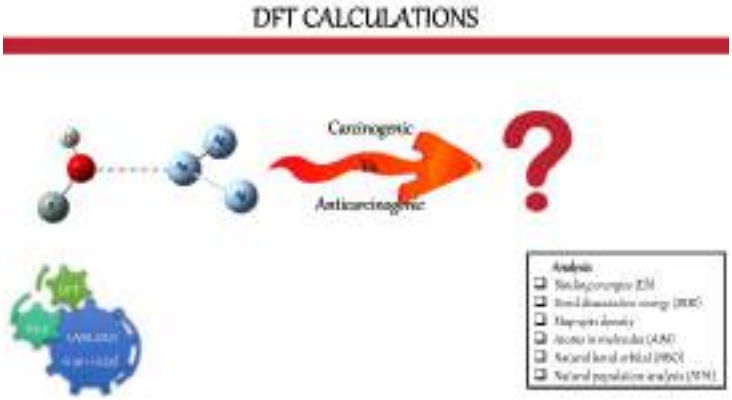

Scheme: A DFT study of the Ag_3 cluster as carcinogenic and anticarcinogenic agent

References

[1] Ahmadi, A.; Kassaee, M. Z.; Fattahi, A. Does gold cluster promote or scavenge radicals? A controversy at DFT. *J. Phys. Org. Chem.* 2018, *31*, e3776.
[2] Ahmadi, A.; Kassaee, M. Z.; Ayoubi-Chianeh, M.; Fattahi, A. Gold at crossroads of radical generation and scavenging at density functional theory level: Nitrogen and oxygen free radicals versus their precursors in the face of nanogold. *J. Phys. Org. Chem.* 2021, *34*, e4126.
[3] Miehlich, B.; Savin, A.; Stoll, H.; Preuss, H. Results obtained with the correlation energy density functionals of Becke and Lee, Yang and Parr. *Chem. Phys. Lett.* 1989, *157*, 200-206.

Contact Lenses Based on Two-Dimensional MoS_2 for Glaucoma Treatment

Behnaz Bastami[a], Mohsen Adeli[a]* and Marzieh Rashidipour[b]

a) Organic chemistry Laboratory, Faculty of Chemistry, Lorestan University, Khorramabad, Iran bastamibehnaz@gmail.com, mohadeli@yahoo.com
b) Environmental Health Research Center, Lorestan University of Medical Sciences, Khorramabad, Iran.

Keywords: Glaucoma, Chronic diseases, Molybdenum disulfide, Brimonidine, Two-dimensional nanomaterials.

Contact lens-based ocular drug delivery systems are useful alternatives to treatment of glaucoma (a chronic eye disease). But they are confronted with challenging issues including drug/formulation changes and abrupt release of drugs [1-3]. In this work, contact lenses based on two-dimensional molybdenum disulfide/gelatin are constructed and loaded with brimonidine and the ability of drug loaded lenses for the treatment of glaucoma has been investigated (**Scheme**). In vitro experiments and animal studies showed a slow release of brimonidine, over 8-12 hours, a reduction in the intra ocular pressure (IOP) of rabbit eyes till 240 min. The anti-inflammatory study as well as toxicity test and histological experiments indicated high biocompatibility of the constructed lenses. Taking advantage of the excellent mechanical and physicochemical properties of molybdenum disulfide/gelatin lenses as well as their biocompatibility and slow release of the loaded drug, they can be used as sustained drug delivery system for treatment of chronic ocular diseases.

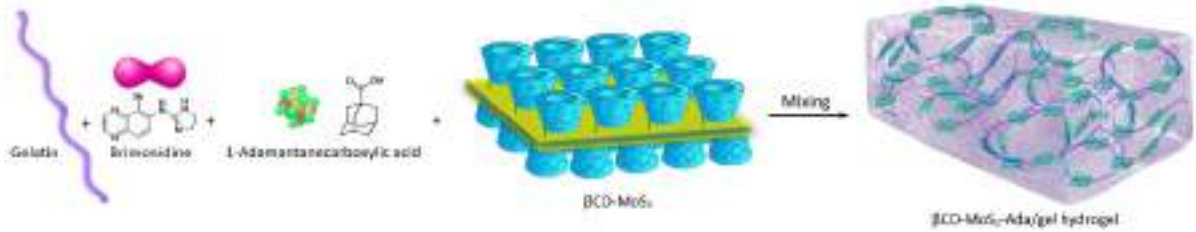

Scheme: schematic representation of preparation of hydrogel for treatment of glaucoma.

References

[1] Zhang, N., et al., Prevalence of primary open angle glaucoma in the last 20 years: a meta-analysis and systematic review. *Sci. Rep.*, 2021, 11(1), 1-12.
[2] Prager, A.J., J.M. Kang, and A.P. Tanna, Advances in perimetry for glaucoma. *Curr. Opin. Ophthalmol.*, 2021. 32(2), 92-97.
[3] Zohreband, Z., M. Adeli, and A. Zebardasti, Self-healable and flexible supramolecular gelatin/MoS2 hydrogels with molecular recognition properties. *Int. J. Biol. Macromol.*, 2021. **182**: p. 2048-2055.

Study on Simulation the Separation of SO_2 from CO_2, H_2 and N_2 using ZIF-1

Vahid Sokhanvaran, Atefe Dovlatabadi and Behzad Haghighi*

Department of Chemistry, Faculty of Basic Sciences, University of Neyshabur, Neyshabur, Iran, dolatabadi7168@gmail.com, bhaghighi@neyshabur.ac.ir

Keywords: Separation, Zeolite imidazolite framework, GCMC simulation, Sulfur dioxide

Zeolite imidazolate frameworks (ZIFs) have gained more attention in recent years [1]. ZIFs are a new and special class of metal–organic frameworks (MOFs), that potentially have the advantages of both inorganic zeolites (for instance, high stability) and of MOFs (for instance, high porosity, high surface area and organic functionality), which are applied to high performance in separation processes [2]. ZIFs comprised of imidazolate linkers and tetrahedral metal ions (e.g., Zn, Co), with structures similar to conventional aluminosilicate zeolites. Their intrinsic porous characteristics, abundant functionalities as well as exceptional thermal and chemical stabilities [3] have led to a wide range of potential applications for various ZIF porous materials. Their attractive and potential applications in gas sorption, gas separation, and catalysis, sensing, electronic devices, and drug delivery in the past years are discussed and reviewed [4]. This study investigates the separation based on adsorption of the binary gas mixture of SO_2 with CO_2, H_2 and N_2. Therefore, Grand canonical Monte Carlo (GCMC) simulation is used to study the adsorption of pure gases using ZIF-1 at 10-10000 kPa and 298 K. In all simulations, 1.5×10^7 of iterations were considered. The first half of iterations are used to set up the equilibrium of the system and the last half of iterations is used to calculate the ensemble average values of the thermodynamic parameters. The adsorption and separation behavior of SO_2-CO_2, SO_2-H_2 and SO_2-N_2 binary mixtures in ZIF-1 were investigated using GCMC, with mixture compositions of 50:50 mol%. The results showed that the selectivity of SO_2 is found to be maximum at a pressure less than 10 kPa and also, the calculated selectivity decreases with increasing pressure upper than 10 kPa. Furthermore, the maximum selectivity of SO_2 over CO_2, N_2 and H_2 are observed 6.8, 41.3 and 187.1, respectively.

References

[1] Sankar, S. S.; Karthick, K.; Sangeetha, K.; Karmakar, A.; Kundu, S.; Transition-metal-based zeolite imidazolate framework nanofibers via an electrospinning approach: a review, *ACS Omega*, 2019, 5, 57-67.

[2] Hayashi, H.; Côté, A. P.; Furukawa, H.; O'Keeffe, M.; Yaghi, O. M.; Zeolite A imidazolate frameworks, *Nat. Mater*, 2007, 6, 501-6

[3] Hertäg, L.; Bux, H.; Caro, J.; Chmelik, C.; Remsungnen,T.; Knauth, M.; Fritzsche, S.; Diffusion of CH_4 and $H_۲$ in ZIF-8, *J. Membr. Sci*, 2011, 377, 36-41.

[4] Chen, B.; Yang, Z.; Zhu, Y.; Xia, Y.; Zeolitic imidazolate framework materials: recent progress in synthesis and applications, *J. Mater. Chem. A*, 2014, 2, 16811-16831.

Synthesis of tetrahydroquinoline derivatives

Reza Teymouri Mofrad*, Darya Shabani Domoula

Department of Organic Chemistry and Biochemistry, Faculty of Chemistry, University of Tabriz, Tabriz, Iran, teymouri@tabrizu.ac.ir, darya.shaabani@gmail.com

Keywords: Photocatalyst, electron transfer reaction, Derivatives of tetrahydroquinoline, visible light

Tetrahydroquinoline is an organic compound in the form of a colorless oil, which is the product of incomplete hydrogenation of quinoline. Tetrahydroquinoline derivatives are usually prepared by the hydrogenation reaction of quinoline in the presence of heterogeneous catalysts [1]. The International Union of Pure and Applied Chemistry (IUPAC) defines a photocatalyst as changing the rate or starting point of a chemical reaction under light (ultraviolet, visible, infrared), in the presence of a substance capable of absorbing light, which is called photocatalyst, or in simpler terms, reactions that are carried out in the presence of semiconductors and light [2]. This work aims to design photocatalysts based on copper for the synthesis of tetrahydroquinoline derivatives with a single electron transfer mechanism under visible light (Scheme 1). All the synthesized derivatives were characterized by spectroscopy methods.

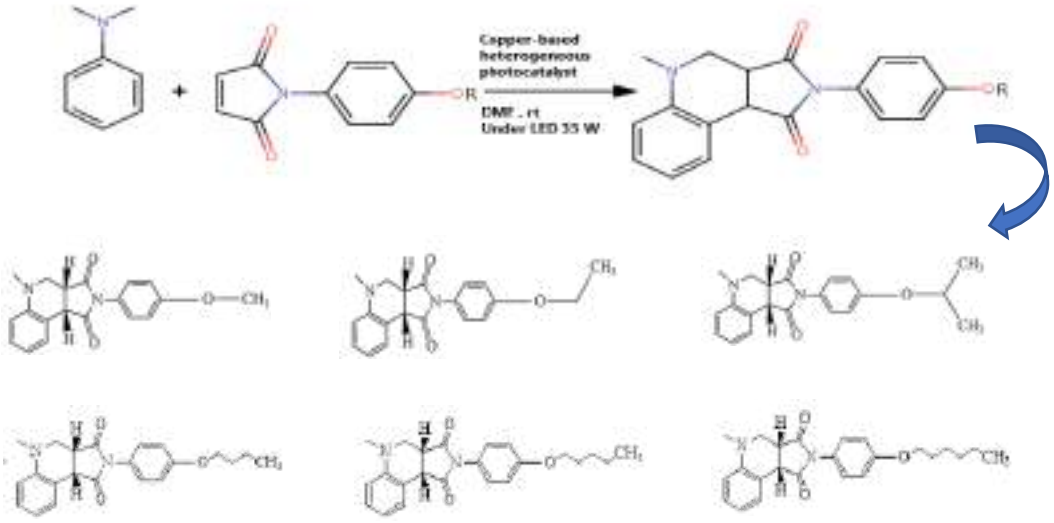

Scheme 1: The reaction of maleimide derivatives with N, N-dimethylaniline for the synthesis of tetrahydroquinoline derivatives

References

[1] Chen, F., Ding, Z.Y., He, Y.M. and Fan, Q.H., Synthesis of Optically Active 1, 2, 3, 4-Tetrahydroquinolines via Asymmetric Hydrogenation Using Iridium-Diamine Catalyst. Organic Syntheses, 2003, 92, 213-226.

[2] Ameta, R. and Ameta, S.C., Photocatalysis: principles and applications. Crc Press. 2016.

Nanostructured polymeric compounds for extraction and preconcentration of insecticides

Sharifeh Hormozi Jangi, Asma Khoobi*

Department of Chemistry, Faculty of Sciences, University of Sistan and Baluchestan, Zahedan 98135-674, Iran, hormozii77@gmail.com, a.khoobi@science.usb.ac.ir.

Keywords: Nanostructures, Polymeric compounds, Extraction, Preconcentration, Insecticides

In this research, the purpose is to design suitable methods for preconcentration and extraction of insecticides using nanostructured polymer compounds is reported. The nanostructures of o-hydroxyazobenzene are porous organic polymers (Hazo-POP) that have been synthesized using a reaction called diazo coupling reaction and has been characterized by different techniques (Scheme 1). Thus, this nanostructured polymer compounds are used for the extraction and preconcentration of neonicotinoid insecticides and steroid hormones in various environmental samples, including river water [1].

Also, another polymer compounds that are suitable for preconcentration of insecticides are zeolite imidazolate framework-67 and porous magnetic porphyrin organic polymer (ZIF-67@MPPOP) [2]. The compounds were synthesized by different methods and showed various applications in separation fields. [3].

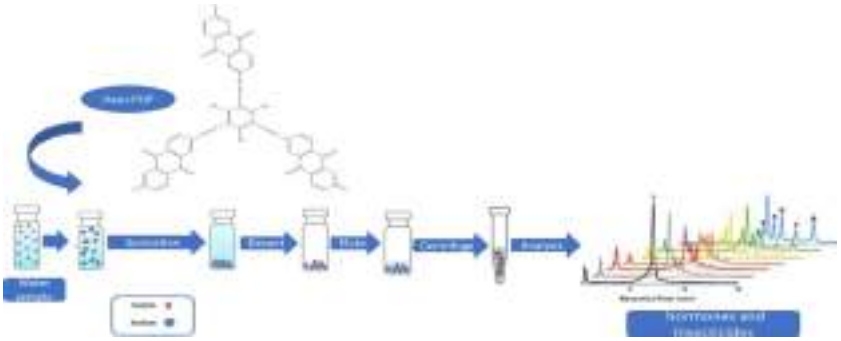

Scheme1. Synthesis steps of o-hydroxyazobenzene.

References

[1] Shirley, Kh. S.; Anele, M.; Azile, N.; Philiswa, N. N. Microchem J, 2022, 181, 107791
[2] Shirley, Kh. S.; Anele. M.; Philiswa, N. N. J Chromatogr A, 2022, 1661, 462685.
[3] Ling-Xiao, Ch.; Shi-Jun, Y.; Tong-Qing, Ch.; Jia-LiWang, Guo-Ying, Ch.;Xi Zhou and Feng-Qing, Y.; Ultra-High Adsorption Capacity of Core–Shell-Derived Magnetic Zeolite Imidazolate Framework-67 as Adsorbent for Selective Extraction of Theophylline, Molecules 2023, 28, 5573

Pyridinium-based dual acidic ionic liquid supported on pectin for the efficient synthesis of pyrazoles

Mohsen Bakhtiarian [a], **Mohammad Mehdi Khodaei** [a,b*]

a) Department of Organic Chemistry, Razi University, 67149-67346 Kermanshah, Iran, mohsenorgc@gmail.com, mmkhoda@razi.ac.ir

b) Nanoscience and Nanotechnology Research Center (NNRC), Razi University, Kermanshah 67149-67346

Keywords: Ionic liquids, Pectin, Sustainable catalysis, Biopolymes, Multicomponent reaction

Today, green chemistry or sustainable chemistry suggests the alternative ways in order to improve the overall efficiency and minimize the pollution generation [1]. In this work, we developed a pectin-supported acidic ionic liquid with rich sulfonic acid groups as an efficient and heterogeneousnanocatalyst for the synthesis of pyrazole derivatives. Pectin (Pec) as a biopolymer was initially modified by 2,6-diamino pyridine (DAP) to obtain the Pec-DAP nanoparticles. Then, the reaction of Pec-DAP with 1,4-butane sultone (BS) was carried out, followed by treatment with a H_2SO_4 solution to afford the Pec-DAP-BS catalyst. This catalyst presented a remarkable activity as a metal-free catalytic system for the three-component synthesis of pyrazoles from aldehydes, phenyl hydrazines, and malononitrile in aqueous ethanol as a green solvent. Moreover, the catalyst was reusable at least five cycles without significant loss of activity (**Scheme 1**).

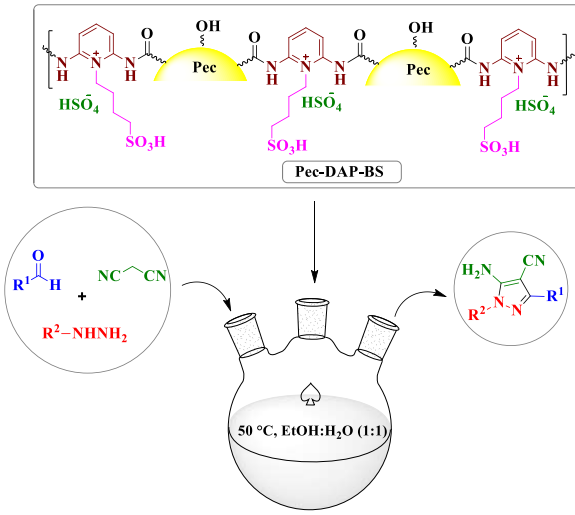

Scheme 1: Pec-DAP-BS-catalyzed synthesis of pyrazoles.

References:

[1] Hernandez, R. R.; Armstrong, A.; Burney, J.; Ryan, G.; Moore-O'Leary, K.; Diédhiou, I.; Grodsky, S. M.; Saul-Gershenz, L.; Davis, R.; Macknick, J. Techno–ecological synergies of solar energy for global sustainability. *Nat. Sustain.* 2019, *2*, 560-568.

Aza-Diels-Alder reaction of Danishefsky's Diene with Imines

Atenasadat Hosseini[a], Alireza Motavalizadehkakhky[a,*], Rahele Zhiani[a], Ehsan Zahedi[b] and Seyed Mohammad Mahdi Nouri[c]

a) Department of Chemistry, Neyshabur Branch, Islamic Azad University, Neyshabur, Iran, atena.hosseini73@gmail.com, amotavalizadeh@yahoo.com
b) Department of Chemistry, Shahrood Branch, Islamic Azad University, Shahrood, Iran.
c) Chemical Engineering Department, Hakim Sabzevari University, Sabzevar, Iran.

Keywords: Hetero-Diels–Alder, Aza-Diels-Alder, Danishefsky's Diene

Diels-Alder reactions drew a lot of attention because of their extensive applications needed of life today [1]. The hetero-Diels–Alder reaction of imines or related compounds (the aza Diels–Alder reaction) is also a useful method for constructing nitrogen-containing cyclic compounds. Due to the fundamental importance of nitrogen containing natural compounds, much attention has been given to the development of Aza-Diels–Alder reactions [2]. Danishefsky's dienes are effective and useful compounds for the synthesis of six-membered rings such as dihydropyrones, dihydropyridones and dihydropyrans [3]. The goal of this study is the synthesis of 2-substituted dihydro-4 pyridone derivatives using imines as the dienophile and Dainshefsky diene (1-methoxy-3-[(trimethylsilyl)oxy]-butadiene). This reaction can be also carried out in a three-component one-pot reaction manner. (**Scheme 1**). Various Lewis acids have been utilized to promote this reaction [4].

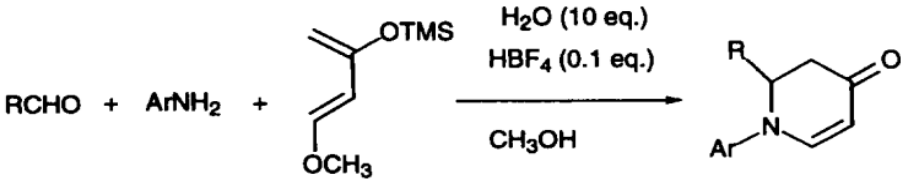

Scheme 1: Three-Component Synthesis of Dihydro-4-pyridone Derivatives by One-Pot Aza Diels-Alder Reaction.

References

[1] Kal-Koshvandi, A. T.; Heravi, M. M. Application of Danishefsky's dienes in asymmetric Oxo-Diels-Alder reactions. *Tetrahedron: Asymmetry* 2017, *28*, 1506–1556.
[2] Ishihara, K.; Sakakura, A. 5.10 Hetero-Diels–Alder Reactions. *Compr. Org. Synth. (2nd Ed.)* 2014, *5*, 409–465.
[3] Kal-Koshvandi, A. T.; Heravi, M. M. Applications of Dainshefsky's Dienes in the Asymmetric synthesis of Aza-Diels-Alder Reaction. *Chem. Rec.* 2019, *19*, 550–600.
[4] Yuan, Y.; Li, X.; Ding, K. Acid-Free Aza Diels−Alder Reaction of Danishefsky's Diene with Imines. *Org. Lett.* 2002, *4(19)*, 3309–3311.

Synthesis of Fused *N*-Bridged [3.3.1]nonadiquinoline Multicyclic Skeleton *via* Metal-Free Formal [4+2] Cycloaddition/Mannich/Dearomatization Domino Reaction

Kamran Amiri, Behrouz Nayebzadeh, Mohammad Kamangar, Mohammad Babazadeh and Saeed Balalaie*

Peptide Chemistry Research Institute, K. N. Toosi University of Technology, P. O. Box 15875-4416, Tehran, Iran, kamran.amiri67@gmail.com, Balalaie@kntu.ac.ir

Keywords: *N*-Bridged [3.3.1]nonadiquinoline, Formal [4+2] Cycloaddition, Mannich, Domino Reaction

We present a novel green synthetic protocol for the construction of a broad range of substituted fused azabicyclo[3.3.1]nonadiquinoline scaffolds, through formic acid catalyzed formal [4+2] annulation/ Mannich/ dearomatization domino reaction. This unified strategy supplies a broad substrate scope with high functional group tolerance in good to high yields under environmentally benign, transition-metal-free, low-cost, and operationally simple conditions. The current method outshines existing methods in terms of green and sustainable conditions. The reaction mechanism was confirmed based on the DFT calculations (**Scheme 1**).

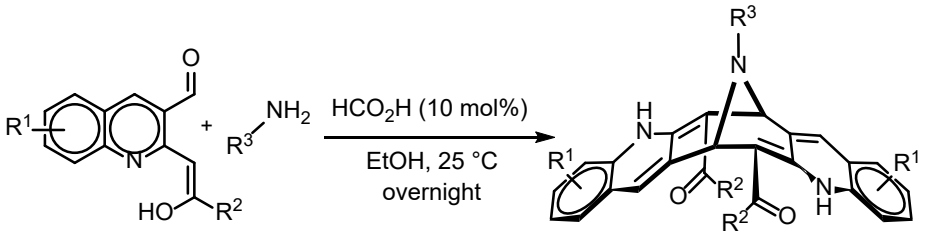

Scheme 1: Synthesis of fused azabicyclo[3.3.1]nonadiquinoline skeletons through novel domino reaction.

References

[1] Tan, J. P.; Li, K.; Shen, B.; Zhuang, C.; Liu, Z.; Xiao, K.; Yu, P.; Yi, B.; Ren, X.; Wang, T. Asymmetric synthesis of *N*-bridged [3.3.1] ring systems by phosphonium salt/Lewis acid relay ca-talysis, *Nat. Commun.*, **2022**, *13*, 357.

[2] Tan, Q.; Yang, Z.; Jiang, D.; Cheng, Y.; Yang, J.; Xi, S.; Zhang, M. Copper-Catalyzed Aerobic Oxidative Cyclization Cascade to Construct Bridged Skeletons: Total Synthesis of (-)-Suaveoline, *Angew. Chem., Int. Ed*. **2019**, *58*, 6420.

[3] Zhang, L.; Zhang, Y.; Li, W.; Qi, X. Total Synthesis of (−)-Alstofolinine A through a Furan Oxidation/Rearrangement and Indole Nucleophilic Cyclization Cascade, *Angew. Chem., Int. Ed*. **2019**, *58*, 4988.

Application of cyclopentadiene in Diels and Hetero-Diels-Alder reaction

Atenasadat Hosseini[a], Alireza Motavalizadehkakhky[a,*], Rahele Zhiani[a], Ehsan Zahedi[b] and Seyed Mohammad Mahdi Nouri[c]

a) Department of Chemistry, Neyshabur Branch, Islamic Azad University, Neyshabur, Iran, atena.hosseini73@gmail.com, amotavalizadeh@yahoo.com.
b) Department of Chemistry, Shahrood Branch, Islamic Azad University, Shahrood, Iran.
c) Chemical Engineering Department, Hakim Sabzevari University, Sabzevar, Iran.

Keywords: Diels-Alder-reaction, Hetero-Diels-Alder-reaction, Cyclopentadiene

Cyclopentadiene is one of the dienes frequently used in Diels–Alder reactions [1]. The Diels Alder (DA) reaction is a cycloaddition between a diene and a dienophile and has been known for a long time [2]. When one of the substrates has at least one hetero atom in its structure, the Diels-Alder reaction is called the Hetero-Diels-Alder (HDA) reaction [3]. Herein, we report the DA and HDA reaction was carried out by heating a mixture of cyclopentadiene and dienophiles (**scheme 1**). Cyclopentadiene, formed by heating of dicyclopentadiene and then reacted with the dienophile in a thermodynamically controlled reaction. In this study, we discuss the history of the cyclopentadiene cycloaddition as well as applications of cyclopentadiene in DA and HDA reactions.

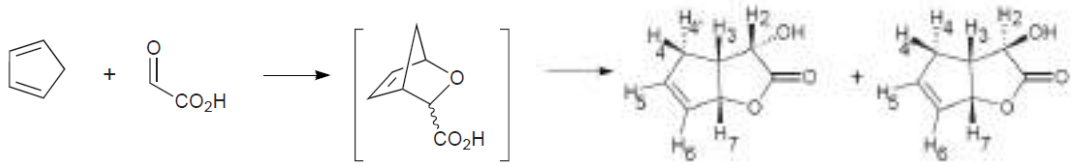

Scheme 1: Reaction between cyclopentadiene and glyoxylic acid

References

[1] Huertas, D.; Florscher, M.; Dragojlovic, V. Solvent-free Diels–Alder reactions of in situ generated cyclopentadiene. *Green Chem*. 2009, *11(1)*, 91–95.
[2] Benoit, B.; Améduri, B.; Boutevin, B. Trends in the Diels–Alder reaction in polymer chemistry. *Chem. Soc. Rev*. 2021, *50*, 11055-11097.
[3] Kal-Koshvandi, A. T.; Heravi, M. M. Application of Danishefsky's dienes in asymmetric Oxo-Diels-Alder reactions. *Tetrahedron: Asymmetry* 2017, *28*, 1506–1556.

Investigation of the effect of palladium nanoparticles on the angiogenesis process in chick chorioallantoic membrane model(CAM)

Fatemeh Zeidabadi, Behnam Mahdavi and Ehsan Koushki*

Faculty of Sciences, Hakim Sabzevari University, Sabzevar, Iran. Ftm.z1374@gmail.com, Ehsan.koushki@hsu.ac.ir.

Keywords: Palladium nanoparticles, Angiogenesis, Chick chorioallantoic membrane

CAM is a valuable model for tumor biology and angiogenesis due to the presence of many vessels (1). Palladium nanoparticles have high antioxidant and anti-angiogenesis activities (2). In this article, the effect of palladium nanoparticles on angiogenesis in chick chorioallantoic membrane has been investigated. Palladium nanoparticles were synthesized by Turkevich method (Fig.1)(3). In this research, 24 fertilized eggs of ROSS breed were divided into 4 groups, including 1 control group and 3 treatment groups. On the 8th day of incubation, the eggs were injected with a concentration of 83, 42.5, 20.75 µg/mL of palladium nanoparticles solution and on the 12th day of hatching, to investigate the effect of palladium nanoparticles on angiogenesis, the eggs were opened and the length and number of branches of the treatment group and the control group were examined and discussed. Based on the studies, the concentration of 21.75 µg/mL of palladium nanoparticles did not have much effect on the reduction of angiogenesis but concentrations of 83 and 42.5 µg/mL can be claimed to have a direct effect on the reduction of angiogenesis and the number and length of chicken vessels.According to the studies, it can be concluded that palladium nanoparticles can affect the angiogenesis of various diseases, including cancer and tumor.

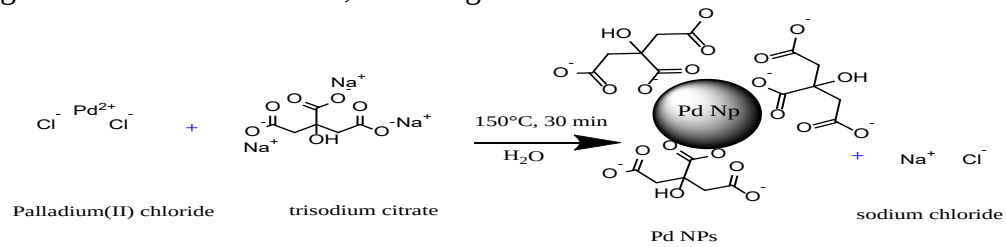

Fig.1: Pd Np synthesized by Turkevich method

References

1. Macrae CF, Edgington PR, McCabe P, Pidcock E, Shields GP, Taylor R, et al. Mercury: visualization and analysis of crystal structures. Journal of applied crystallography. 2006;39(3):453-7.
2. Merckx G, Tay H, Lo Monaco M, Van Zandvoort M, De Spiegelaere W, Lambrichts I, et al. Chorioallantoic membrane assay as model for angiogenesis in tissue engineering: Focus on stem cells. Tissue Engineering Part B: Reviews. 2020;26(6):519-39.
3. Turkevich J, Stevenson PC, Hillier J. A study of the nucleation and growth processes in the synthesis of colloidal gold. Discussions of the Faraday Society. 1951;11:55-75.

Proton tautomerism in (Z)-5-(Furan-2-ylmethylidene)-4-phenylaminothiazol-2(5H)-one: a Computational study

Fatemeh Salimi[a], Mahboobeh Alimoradi [b] and Nasrin Fallah [b]*

a) Department of Biology, Central Tehran Branch, Islamic Azad University, Tehran, Iran, ftemls14@gmail.com
b) Department of Chemistry, Science and Research Branch, Islamic Azad University, Tehran, Iran, nasrin.fallah@srbiau.ac.ir

Keywords: Tautomerism, Density Functional Theory (DFT), 4-Amino(imino)thiazolidinone.

Tautomerism has a vital role in modern medicinal chemistry. An understanding of tautomerism is required to understand the mechanistic pathways of many biochemical processes, especially those involved in dynamic interplay with proteins, enzymes, and DNA. Spectroscopic techniques, X-ray diffraction, and quantum chemical methods help to explore tautomerism. Quantum chemical evaluation of all possible tautomers of one compound and their energy differences, along with the estimation of their electronic characteristics, is a useful approach to understanding structural preferences.

In this study, due to the different structural possibilities forms for *(Z)-5-(Furan-2-ylmethylidene)-4-phenylaminothiazol-2(5H)-one* (**1**), their conformational and geometrical aspects were investigated computationally by the DFT/ B3LYP/6-311+G(d,p) method in the solvent (DMSO) phase. The results suggested that the amine-one is the more stable tautomeric form and a soft molecule with a larger dipole moment. (**Figure 1**). Therefore, compound **1** interacts with the DNA bases and shows better biological activity. This result was supported by a molecular docking study.

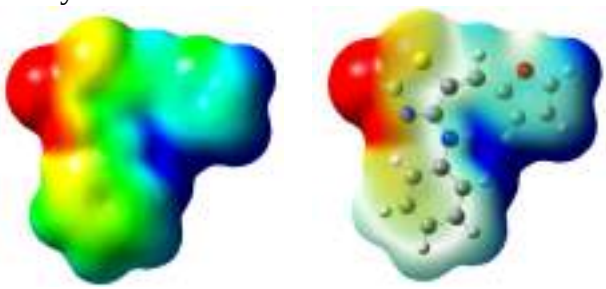

Fig. 1. Molecular electrostatic potential map of compound **1** in amine-one form.

References

[1] Gholivand, K., Faraghi, M., Fallah, N., Babaei, A., Pirastehfar, F., Dusek, M., ... & Salimi, F. Therapeutic potential of phospho-thiadiazole derivatives as anti-glioblastoma agents: synthesis, biological assessment and computational study. *Bioorg. Chem.*, 2022, *129*, 10612.
[2] Kaminskyy, D., Subtel'na, I., Zimenkovsky, B., Karpenko, O., Gzella, A., & Lesyk, R. Synthesis and evaluation of anticancer activity of 5-ylidene-4-aminothiazol-2 (5H)-one derivatives. *Med. Chem.*, 2015, *11*(6), 517-530.

A Computational study of (Z)-5-(4-Dimethylaminophenylmethylidene)-4-(4-hydroxy-5-isopropyl-2-methylphenylamino) thiazol-2(5H)-one

Fatemeh Salimi[a], Mahboobeh Alimoradi [b] and Nasrin Fallah [b]*

a) Department of Biology, Central Tehran Branch, Islamic Azad University, Tehran, Iran, ftemls14@gmail.com
b) Department of Chemistry, Science and Research Branch, Islamic Azad University, Tehran, Iran, nasrin.fallah@srbiau.ac.ir

Keywords: Density Functional Theory (DFT), NBO, IR, NMR.

The computational methods have become a very useful tool for chemists. Density functional theory (DFT) is a major part of computational methods which is utilized by organic and bioorganic chemists [1]. In 2015, Kaminskyy et al determined the crystal structure of *(Z)-5-(4-Dimethylaminophenylmethylidene)-4-(4-hydroxy-5-isopropyl-2-methylphenylamino) thiazol-2(5H)-one* (**1**) [2]. This group of compounds showed good anti-cancer properties [2]. Based on our limited knowledge, there is no published paper about DFT studies of compound **1** in the literature yet.

In this study, the geometry optimization is carried out for compound **1** by using the B3LYP/6-311+G (d,p) method in the gas and solvent phases. (Figure 1) The complete structural analysis such as electronic characterization, Molecular Electronic Potential (MEP), Natural Bond Orbital (NBO) as well as IR assignments are performed and discussed with details for mentioned molecule. According to results R^2 (squared correlation coefficients) and RMSE (root-mean-square error), good correlations were obtained between the predicted ^{1}H- and ^{13}C NMR spectra and the corresponding experimental ones.

Fig. 1. The optimized chemical structure of compound **1** ($C_{22}H_{25}N_3O_2S_1$).

References

[1] Fallah, N., Gholivand, K., Yousefi, M., & Azar, P. A. Synthesis, spectroscopic characterization, anti-urease activities of a novel bisphosphoramidate, a combined experimental and computational study. *J. Mol. Struct.*, 2018, *1173*, 801-813.
[2] Kaminskyy, D., Subtel'na, I., Zimenkovsky, B., Karpenko, O., Gzella, A., & Lesyk, R. Synthesis and evaluation of anticancer activity of 5-ylidene-4-aminothiazol-2 (5H)-one derivatives. *Med. Chem.*, 2015, *11*(6), 517-530.

Investigation of catalytic activity of phosphorous acid functionalized metal-organic framework in the production of 5-hydroxymethylfurfural

Akbar Rostami-Vartooni[a*], Mahmoud Zarei[a], Mohammad Mahdi Mohammad-Hasani[a], Hassan Sepehrmansourie[b]

a) Department of Chemistry, Faculty of Science, University of Qom, Qom, Iran, a.rostami@qom.ac.ir
b) Department of Organic Chemistry, Faculty of Chemistry, Bu-Ali Sina University, Hamedan, Iran

Keywords: Metal-organic frameworks, Catalyst, Phosphorous acid, HMF

Metal-organic frameworks (MOFs) with structural diversity, ordered pores and high surface area have shown potential in numerous fields, such as separation, gas storage, proton conductivity, biomedicine, sensing and catalysis [1]. These compounds based on the type of their ligands and functional groups on their surface exhibit different properties.

5-hydroxymethylfurfural (HMF) can undergo polymerization, halogenation, esterification, hydrolysis, hydrogenation, oxydehydrogenation, and other chemical reactions to produce many useful compounds such as plastic resins, medicines, diesel fuel additives, etc. The dehydration of C6 sugars, typically fructose, catalyzed by Brønsted or Lewis acid catalyst is the most effective method to synthesize 5-HMF [2].

In this work, a novel and heterogeneous MIL-125(Ti)-NH_2 containing phosphorous acid functional groups was employed to prepare 5-HMF via fructose dehydration in DMSO solvent (Scheme 1). With the purpose of finding the most appropriate conditions to achieve the highest yield of 5-HMF, several parameters such as time and temperature of the reaction and the amount of catalyst were optimized.

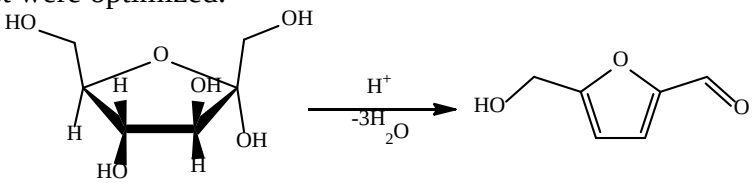

Scheme 1: Preparation of 5-HMF from fructose.

References

[1] Jalili, F.; Zarei, M., Zolfigol, M.A.; Khazaei, A. Application of novel metal–organic framework [Zr-UiO-66-PDC-SO_3H]$FeCl_4$ in the synthesis of dihydrobenzo[g]pyrimido[4,5-b]quinoline derivatives. *RSC Adv.*, 2022, 12, 9058-9068.

[2] Nasrollahzadeh, M; Soheili Bidgoli, N.S; Shafiei, N.; Momenbeik, F. Biomass valorization: Sulfated lignin-catalyzed production of 5-hydroxymethylfurfural from fructose. I*nt. J. Biol. Macromol*, 2021, 182, 59–64.

Preparation of Ag/ZnO/SiO_2 nanocomposite and investigation of its efficiency in the removal of organic dyes

Akbar Rostami-Vartooni[a*], Nedasadat Nikookalam Azim[a], Mohammad Mahdavi[b]

a) Department of Chemistry, Faculty of Science, University of Qom, Qom, Iran, a.rostami@qom.ac.ir
b) Department of Chemistry, Malek-ashtar University of Technology, Shahin-shahr, Iran.

Keywords: Catalyst, Photocatalyst, Pollutant, Azo dye, Reduction

The usage of metal nanoparticles (MNPs) has been significantly studied in recent years due to their high specific surface area and good catalytic activity [1]. Among several physical, chemical and biological approaches for the preparation of MNPs, biosynthetic route using plant extracts has some advantages including the elimination of toxic and expensive chemical compounds and providing gentle reaction conditions [2].

In this study, Ag nanoparticles (NPs) synthesized by biological (using the leaf extract of *Malva Sylvestris* plant) and irradiation (UV light) methods were suppoted on ZnO/SiO_2. Different techniques such as FTIR, XRD, EDS and FESEM were used for the characterization of prepared nanocomposites. According to the FESEM images (Scheme 1), the average particles size of well-dispersed spherical Ag NPs supported on the surface of ZnO/SiO_2 were below 50 nm. The Ag/ZnO/SiO_2 nanocomposites as a catalyst or photocatalyst were investigated in the reduction, oxidation and adsorption reactions of methyl orange (MO) and nile blue (NB).

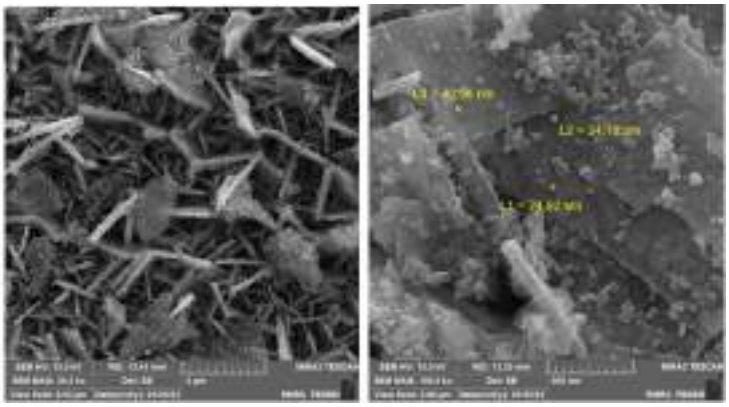

Scheme 1: FESEM images of the Ag/ZnO/SiO_2 nanocomposite.

References

[1] Saikia, P.; Miah, A.T.; Das, P.P. Highly efficient catalytic reductive degradation of various organic dyes by Au/CeO_2-TiO_2 nano-hybrid. *J. Chem. Sci*., 2017, 129, 81-93.
[2] Rostami-Vartooni, A.; Moradi-Saadatmand, A.; Bagherzadeh, M.; Mahdavi, M. Green synthesis of Ag/Fe_3O_4/ZrO_2 nanocomposite using aqueous *Centaurea cyanus* flower extract and its catalytic application for reduction of organic pollutants. *Iran. J. Catal.*, 2019, 9(1), 27-35.

Selective unsymmetrical Hantzsch coupling reaction using a green amine functionalized IRMOF-3

Mohammad Reza Mohammad Azimi, Sadegh Rostamnia*

Organic and Nano Group (ONG), Faculty of Chemistry, Iran University of Science and Technology, Tehran, Iran, Srostamnia@gmail.com

Keywords: Metal-organic frameworks, IRMOF-3, Hantzsch coupling reaction, Green catalysis

Hantzsch reaction is a multi-component organic reaction between an aldehyde, 2 equivalents of a β-keto ester, and a nitrogen donor [1]. The development of a simple, efficient, recoverable, and cost-efficient catalyst for organic transformations such as the Hantzsch reaction gained considerable attention in recent years [2]. Here, we employed a green and additive-free iso reticular metal–metal-organic framework (IRMOF-3) for selective and efficient progress of unsymmetrical Hantzsch coupling reaction. The proposed catalyst shows excellent reusability up to four cycles and as an advantage, the progress of the reaction was observed through a waste-free procedure.

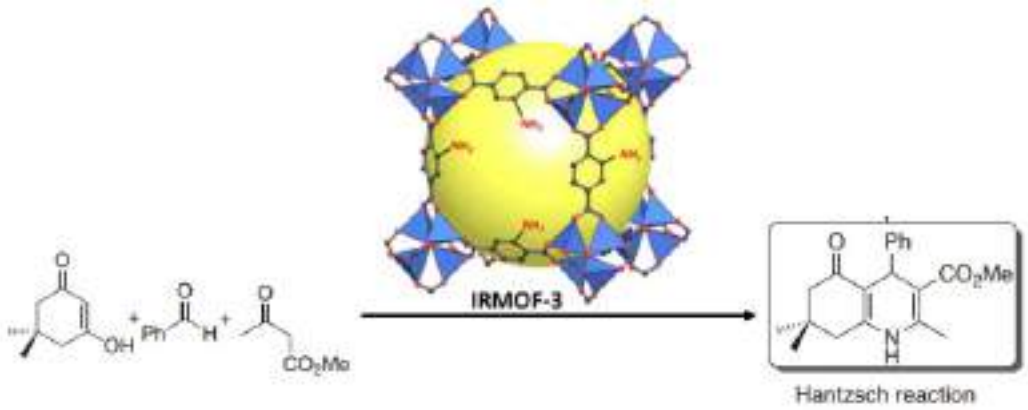

Scheme 1: Schematic illustration of IRMOF-3 as catalyst for Hantzsch reaction

References

[1] Yonghong Liu, Shuangjie Lin, Dandan Zhang, Bingkun Song, Yunhe Jin, Erjun Hao, and Lei Shi. Photochemical Nozaki–Hiyama–Kishi Coupling Enabled by Excited Hantzsch Ester. *Org. Lett.* 2022, 24, 18, 3331–3336

[2] Zhi-Yong Song, Chun-Lin Zhang, and Song Ye.Visible light promoted coupling of alkynyl bromides and Hantzsch esters for the synthesis of internal alkynes. Org. Biomol. Chem., 2019, 17, 181-185.

Solvent-free multicomponent condensation of Ugi-type reactions using amine-functionalized MIL-53(Al)

Mohammad Reza Mohammad Azimi, Sadegh Rostamnia*

Organic and Nano Group (ONG), Faculty of Chemistry, Iran University of Science and Technology, Tehran, Iran, Srostamnia@gmail.com

Keywords: Metal-organic frameworks, MIL-53(Al), Open metal sites, Ugi reaction.

The Ugi reaction is a multi-component reaction in organic chemistry involving a ketone or aldehyde, an amine, an isocyanide, and a carboxylic acid to form a bis-amide [1]. The hazardous environmental impact of volatile organic solvents increased the necessity of finding solvent-free pathways for the progress of organic reactions [2]. In this work, an open metal sites (OMS) rich MIL-53(Al) was employed as an efficient and recyclable catalyst for the Ugi reaction of an amine and aldehyde over isocyanide. Due to the high activity of the proposed catalyst, the Ugi reaction proceeded with a high yield in solvent-free conditions. The proposed catalyst shows high efficiency even after five cycles (**Scheme 1**).

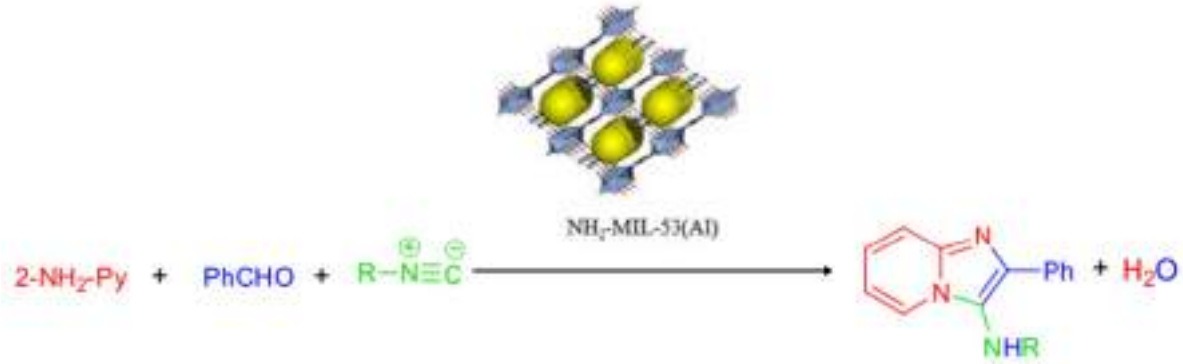

Scheme 1: Schematic illustration of MIL-53(Al) as catalyst for Ugi reaction

References

[1] Subhas Chandra Pan, Benjamin List. Catalytic Three-Component Ugi Reaction. *Angew. Chem. Int. Ed.*, 2008, 47, 19, 3622-3625

[2] Manar Ahmed Fouad, Hamida Abdel-Hamid and Mohammed Salah Ayoup. Two decades of recent advances of Ugi reactions: synthetic and pharmaceutical applications. *RSC Adv.*, 2020, 10, 42644-42681.

Facile electrosynthesis of Cu-, Ni-, Cu, Ni-MOF and their nanocomposites as a high-performance supercapacitor electrode material

Mostafa Kiamehr*, Elahesadat Miri and Ali Ehsani*

Department of Chemistry, Faculty of Science, University of Qom, Ghadir Blvd, P.O. Box 37146-6611, Qom, Iran, mkiamehr@yahoo.com, m.kiamehr@qom.ac.ir, mirielahe114@gmail.com, ehsani46847@yahoo.com

Keywords: Electrosynthesis, Metal-organic framework, Supercapacitor, Nanocomposite

In some applications of metal-organic frameworks (MOFs), to achieve high performance, it would be desirable to create hetero-systems combining two different MOFs [1]. In this paper, we fabricated three different MOFs samples including Cu-BTC, Ni-BTC, and new bimetallic MOF Cu,Ni-BTC by electrochemical method at room temperature. Furthermore, this work introduces new nanocomposite for electrochemical supercapacitors with advantages including ease synthesis and high active surface area [2]. Cu-BTC/POAP, Ni-BTC/POAP and Cu,Ni-BTC/POAP nanocomposites electrosynthesized by cyclic voltammetry. At the end their performances as supercapacitor electrode materials were evaluated and compared by Different electrochemical methods including galvanostatic charge discharge experiments, cyclic voltammetry and electrochemical impedance spectroscopy (**Scheme 1**).

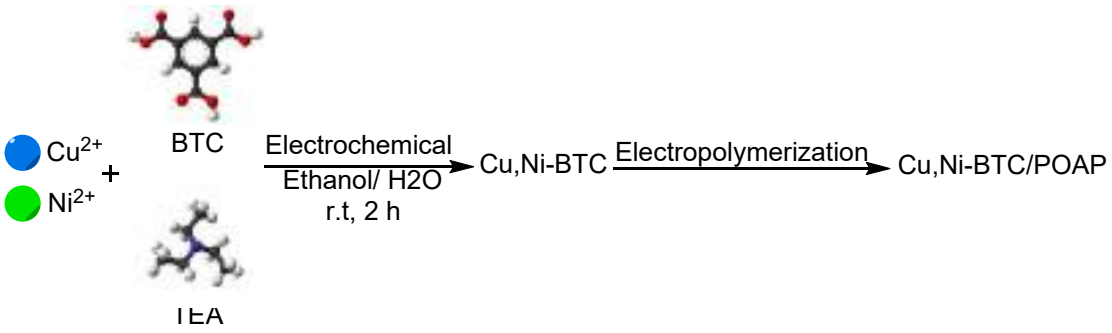

Scheme 1: Preparation of Cu,Ni-BTC/POAP nanocomposite.

References

[1] Jabarian, S., & Ghaffarinejad, A. Simultaneous electrosynthesis of Cu–BTC and Zn–BTC metal–organic frameworks on brass. *New J. Chem.* 2020, *44* (45), 19820-19826.

[2] Naseri, M., Fotouhi, L., Ehsani, A., & Dehghanpour, S. Facile electrosynthesis of nano flower like metal-organic framework and its nanocomposite with conjugated polymer as a novel and hybrid electrode material for highly capacitive pseudocapacitors. 2016, *J. Colloid Interface Sci.*, *484*, 314-319.

Modified polyaniline by graphene oxide and dithizone for adsorption of Cadmium (II)

Yasaman Yaghini[a*], A.S. Emami Meibodi[b]

a) Department of Chemistry, Faculty of Science, University of Yazd, Yazd, Iran, yasamanYaghini76@gmail.com
b) Department of Chemistry, Faculty of Science, Karaj Branch, Islamic Azad University, Iran, Azamsadat.emami@kiau.ac.ir

Keywords: Graphene oxide, Polyaniline, Cadmium (II), Emulsion polymerization, Dithizone

Graphene oxide (GO) was synthesized by using modified Hummers method [1]. Two composites were prepared through ultrasound assisted emulsion polymerization pathway from aniline (An) in a suspension of graphene oxide and ammonium peroxy disulfate (APS) with and without dithizone (Dz) [2, 3]. Then the composites were applied for pre-concentration of trace levels of Cd^{+2}. Optimization of adsorption condition was performed by design of experiment (DOE) method. Adsorption capacity in optimized condition for PolyAn/GO and PolyAn/GO/Dz composites to Cd^{+2} adsorption were obtained 18.2 mg/g and 34.3 mg/g respectively by atomic absorption spectroscopy experiments.

Scheme: Ultrasound assisted polymerization of Aniline in presence of GO, Dz, APS

References

[1] Zaaba, N. I.; Foo K. L.; Hashim, U.; Tan, S. J.; Wei-Wen Liu; Voon, C. H. Synthesis of Graphene Oxide using Modified Hummers Method: Solvent Influence. *Procedia Engineering* 2017, 469-477
[2] Palaniappan S. Preparation of polyaniline-sulfate salt by emulsion and aqueous polymerization pathway without using protonic acid. *Polym. Adv. Technol.* 2002, 13:54–9.
[3] Moayeri, A.; Ajji, A. Fabrication of polyaniline/poly (ethylene oxide)/non-covalently functionalized graphene nanofibers via electrospinning. *Synthetic Metals* 2015, 200:7-15

29TH IRANIAN ORGANIC CHEMISTRY CONFERENCE
1_3 NOV, 2023
UNIVERSITY OF QOM, IRAN

Optimal Loading and Release of Amitriptyline by a Modified Zeolite Carrier

Fatemeh Seyedi-Ardabil[a*], Alireza Nezamzadeh-Ejhieh[b]

Department of Chemistry, Shahreza Branch, Islamic Azad University, Isfahan, Iran, fatemeseyedi3@gmail.com, arnezamzadeh@iaush.ac.ir

Keywords: Release, Loading, RSM, Clinoptilolite, Chitosan, Histidine

The primary amine groups render special properties that make Chitosan very useful in pharmaceutical applications [1]. Texture and structure of clinoptilolite recommend its use as a biocompatible matrix for the development of modified release drug delivery systems [2]. Modifying the composite with histidine increases the loading rate and also improve the gradual release process. In this work, loading and releasing of amitriptyline as a function of operation parameters like pH, time, amount of carrier and drug concentration were optimized by response surface methodology (RSM) in order to obtain maximum loading and gradual release of the drug. In order to determine the structure and identify the characteristics of the prepared composite and carrier, SEM, FT-IR, XRD and TGA analysis techniques were used. Also, in order to measure the drug loading percentage and its release from the UV-VIS device used in all experiments.

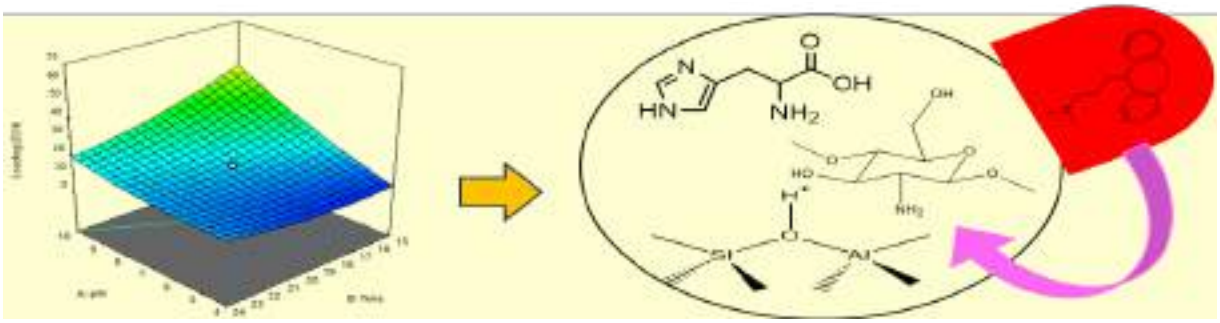

Scheme: Amitriptyline loading process using design of experiment

[1] P.C. Berscht, B. Nies, A. Liebendörfer, J. Kreuter, Incorporation of basic fibroblast growth factor into methylpyrrolidinone chitosan fleeces and determination of the in vitro release characteristics, *Biomaterials*, 15 (1994) 593-600.
[2] L. Ochiuz, C. Ghiciuc, M. Ignat, M. Popa, C.A. Peptu, A. Vasile, Development of a modified-release drug delivery system with bexarotene loaded in clinoptilolite, *Mater. Plast*, 54 (2017) 581-585.

Palladium doped-magnetic biochar as a heterogeneous catalyst for the reduction of nitroarenes

Mahsasadat Alizadeh[a*], Masoume Malmir[b*] and Majid M. Heravi[a*]

a) Department of Organic Chemistry, Faculty of Chemistry, Alzahra University, Tehran, Iran, m.malmir@alzahra.ac.ir, mmheravi@alzahra.ac.ir.
b) Department of Physical Chemistry and Nano, Faculty of Chemistry, Alzahra University, Tehran, Iran. alizadeh.mahsa1995@gmail.com

Keywords: Nanocatalyst, Biochar, Palladium Nanoparticle, Reduction.

Watermelon peel is considered as one of the available wastes in nature, which can be a suitable source of carbon for the production of biochars [1]. In this research, watermelon peel was used as a suitable source for preparing biochar. Then, the obtained biochar was used to prepare a heterogeneous catalyst using magnetic nanoparticles (Fe_3O_4) and palladium (Pd) by hydrothermal process. The structure of the prepared nanocatalyst, Fe_3O_4@Pd@biochar, was identified by several techniques and its activity in the reduction of nitroarene compounds [2] was investigated. Among the advantages of the above catalyst, we can mention the recovery of several nitroaromatic compounds with excellent efficiency and successful recovery and reuse (**Scheme**).

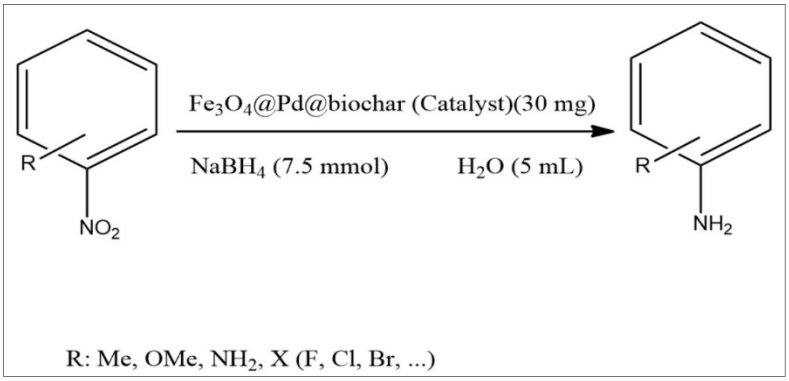

Scheme: Reduction of Nitro Compounds.

References

[1] Abad, S. S. A. M. K.; Javidan, P.; Baghdadi, M.; Mehrdadi, N. Green synthesis of Pd@ biochar using the extract and biochar of corn-husk wastes for electrochemical Cr (VI) reduction in plating wastewater. *J. Environ. Chem. Eng* 2023, *11* (3), 109911.
[2] Omole, M. A.; K'Owino, I. O.; Sadik, O. A., Palladium nanoparticles for catalytic reduction of Cr (VI) using formic acid. *Appl. Catal. B : Environ.* 2007, *76* (1-2), 158-167.

Synthesis, Characterization and X-ray Structure of (E)-4-((2-(2,4-dinitrophenyl)hydrazineylidene)methyl)pyridine: Insights into Weak Interactions in Molecular Design

Babak Mirtamizdoust *

Department of Chemistry, Faculty of Science, University of Qom, Qom, Islamic Republic of Iran, babak.mirtamizdoust@qom.ac.ir

Keywords: Organic compound, Weak interaction, X-ray crystallography

Weak interactions play a crucial role in shaping molecular structures in chemistry. These interactions, including hydrogen bonding, van der Waals forces, and hydrophobic interactions, are relatively weak compared to covalent bonds but are essential for holding molecules together and determining their overall shape. Understanding the significance of weak interactions in designing new drugs, catalysts, and materials with desired properties is critical [1,2]. In this work, we describe the synthesis, characterization, and X-ray structure of (E)-4-((2-(2,4-dinitrophenyl)hydrazinylidene)methyl)pyridine (**Figure 1**). The new compound has an orthorhombic crystal structure with $Pna2_1$ space group. The discrete structure of compound **1** interacts with neighboring objects through several weak interactions, resulting in the formation of three-dimensional structures.

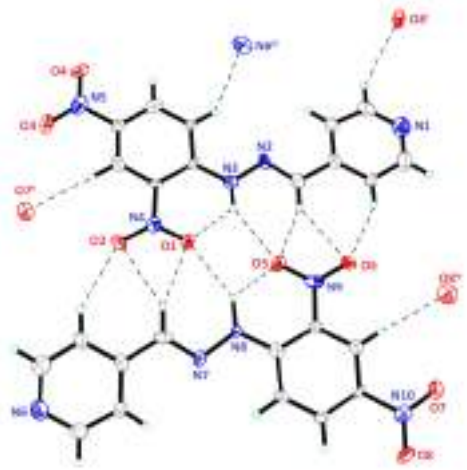

Figure 1- Crystal structure of compound **1**

References

[1] Harrowfield, J., Matt, D. Labile interactions defined in crystalline metal complexes. *J. Incl. Phenom. Macrocycl. Chem.*, 2004, *50*, 133-150.

[2] Ventouri, I. K., Loeber, S., Somsen, G. W., Schoenmakers, P. J., Astefanei, A. (2022). Field-flow fractionation for molecular-interaction studies of labile and complex systems: A critical review. *Anal. Chim. Acta*, 2022, *1193*, 339396.

Green synthesis of silver nanoparticles with *Artemisia* plant

Reyhaneh Sadat Davarpanah Shahri [a], Nasrin Mollania [a*], Hamid Mollania[b], Alireza Sadeghi-avalshahr[c]

a) Department of Biology, Faculty of Basic Sciences, Hakim Sabzevari University, Sabzevar, Iran, r_sadat72@yahoo.com, n.mollania@hsu.ac.ir.
b) Ferdowsi University of Mashhad, Department of Electrical Engineering, Mashhad, Iran.
c) Materials Research Department, Iranian Academic Center for Education, Culture and Research (ACECR), Khorasan Razavi Branch, Mashhad, Iran.

Keywords: Green synthesis, Silver nanoparticles, *Artemisia* plant

Considering the numerous applications of nanoparticles in various industries, their synthesis through traditional chemical processes is often toxic, expensive, and harmful to the environment. Hence, there is a growing interest in developing economical, environmentally friendly, and reproducible nanoparticle preparation methods. The production of biological nanoparticles such as silver nanoparticles (AgNPs) was increasing due to their effectiveness in bio-medicine sciences for example, in topical ointments to prevent infection in burns and open wounds. these eco-friendly nanoparticles also have anti-fungal, anti-inflammatory, anti-viral, anti-angiogenic, and anti-platelet activity.

An easy, eco-friendly, and low cost biological method is described for the synthesis of AgNPs by an *Artemisia* plant. For this purpose, the aqueous extract of the mountain artemisia plant was extracted by brewing method and was combined with silver nitrate salt. The AgNPs formation was observed by the reaction medium color change from colorless to dark brown. The prepared crystalline nanoparticles were then characterized by DLS, XRD, and UV-Vis spectroscopy. As results showed the obtained AgNPs, with the diameter of 77.45 nm and PDI of 0.193, were predominantly monodispersed and were stable for more than a few months without significant aggregation

References

[1] Moulaie, S. Mirzaie, A. Aliasgari, E. Antibacterial and anticancer activities of silver nanoparticles fabricated by the Artemisia scoparia extract against lung cancer cell line (A549). Feyz. 2018, 22(4), 487-496.
[2] Kaviani, N. Osfoori, M. Biological Preparation of Silver Nanoparticles Using Artemisia sieberi. Modar-es. *J. Biotechnol*. 2018, 9(1), 23-27.

29TH IRANIAN ORGANIC CHEMISTRY CONFERENCE
1_3 NOV, 2023
UNIVERSITY OF QOM, IRAN

Intra-molecular Transport Coefficients in Molecular Nanoelectronic Devices

Reza Safari[a*] and Hamid Hadi[b*]

a) Department of Chemistry, Physical Chemistry group, University of Qom, Qom, Iran, r.safari@qom.ac.ir
b) Department of Physical Chemistry, Faculty of Chemistry, University of Lorestan, Khorramabad, Iran, hadi.physicalchemistry@gmail.com

Keywords: Molecular devices, Nanoelectronics, QTAIM, Transport Coefficients

In this work, we compute some intra-molecular transport coefficients (such as intra-molecular Peltier and Joule coefficients), for a candidate organic-molecular device, Fig 1**.,** using B3LYP/6-311G*-LANLD2Z method and quantum theory of atoms-in-molecules (QTAIM) theory [1-2]. In this regards, external field effect on some of the electronic properties (such as atomic electron density and curent-voltage, I-V curve) of this molecular device are studied, using QTAIM and Landauer theory (LT). The analysis of the obtained results showed that some of these molecular transfer coefficients are linearly (such as Joule's coefficient) and some are nonlinearly (such as Peltier's coefficient) dependent on the intensity and direction of the applied electric field. It is expected that the results of this research can be used in the performance management of molecular electronic systems and providing the possibility of reducing disturbances caused by electrical-thermal effects.

Fig1: The molecular system studied in this work.

References

[1] Matta, C. F.; Boyd, R. J., *Quantum Biochemistry*, Wiley, Weinheim, 2010.
[2] Ratner, M. A brief history of molecular electronics, *Nature Nanotech.*, 2013, 8, 378–38

Computational evaluation of some electronic properties of a field-effect organic molecular switch

Hamid Hadi[a*] and Reza Safari[b*]

a) Department of Physical Chemistry, Faculty of Chemistry, University of Lorestan, Khorramabad, Iran, hadi.physicalchemistry@gmail.com
b) Department of Chemistry, Physical Chemistry group, University of Qom, Qom, Iran, r.safari@qom.ac.ir

Keywords: Molecular nanoelectronic, Molecular switch, QTAIM, DFT, Landauer theory

Organic electronics is one of the new approaches to material science that investigates the electronic properties of organic molecules or polymers in nanoelectronic circuities. In this regard, the design and synthesis of molecular devices (such as smart organic molecular switches), for use in nanoelectronic circuits, is a fundamental requirement [1-2]. A molecular switch plays the role of opening/closing the circuit in nanoelectronic systems. For example, as a result of applying external stimuli (such as applying a field or light), the molecular switch can be turned ON/OFF [3]. Therefore, in this work, the switching mechanism of an organic redox molecular switch (**Fig. 1**), are studied, using density functional theory (DFT), quantum theory of atoms in molecules (QTAIM), and Landauer theory (LT). The analysis of the obtained results showed that with the increase in the intensity of the applied electric field, this molecular switch changes its configuration and becomes ON.

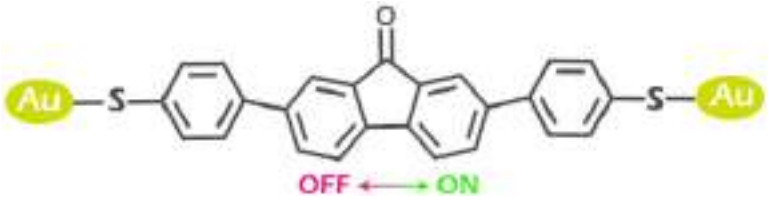

Fig 1: The organic molecular switch studied in this work.

References

[1] Paven, T. M.; Fengzhou, F., Advances in molecular electronics: A brief review. *Engin*. 2018, 4, 760-771.
[2] Lan, Y. K.; Cheng, H. Y.; Yang, H. C., Theoretical investigations of electronic structure and charge transport properties in polythiophene-based organic field-effect transistors, *Polym. Internat*. 2007, 59, 16-21.
[3] Feringa, B. L. *Molecular Switches*; Wiley, Weinheim, 2007.

Three new phosphinicamide structures: $(C_6H_5)_2(X)P(O)$ [X = 3,4-$(CH_3)_2$-C_6H_3NH, 2-Cl-$C_6H_4CH_2NH$ and $NH(CH_2)_3NHP(O)(C_6H_5)_2$]

Haniyeh Salari Jaieni , Farahnaz Hamzehee Harzanji and Mehrdad Pourayoubi*

Department of Chemistry, Faculty of Science, Ferdowsi University of Mashhad, Mashhad, Iran, haniiyesalari1@gmail.com, pourayoubi@um.ac.ir

Keywords: Phosphinicamide, X-ray crystallography, CSD

There are reports on the application of phosphinicamide in flame retardants, ligands and catalysts [1–2]. Here, the synthesis, spectroscopic characterization (IR, Mass, NMR (^{31}P, ^{1}H,^{13}C)) and X-ray crystal structures of three new phosphinicamide are investigated. The compounds are $(C_6H_5)_2$(3,4-$(CH_3)_2C_6H_3NH$)P(O) (**I**), $(C_6H_5)_2$(2-Cl-C_6H_4NH)P(O) (**II**), and $(C_6H_5)_2P(O)NH(CH_2)_3NHP(O)(C_6H_5)_2$ (**III**). In all structures, the phosphorus atom is within a distorted $C_2NP(O)$ tetrahedral environment and the compounds are assembled in a chain arrangement through NH…O═P hydrogen bonds, which typically is shown for structure (**I**), Figure. The P═O/P—N bond lengths and the N…O distances of NH…O hydrogen bonds of the title compounds were compared with analogous structures deposited in the Cambridge Structural Database (CSD) [3].

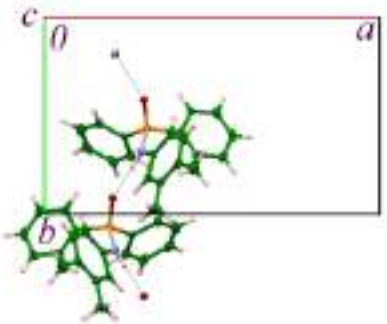

Figure: A view of the hydrogen bond pattern of the structure (**I**)

References

[1] Palacios, F.; Alonso, C.; de Los Santos, J. M. Synthesis of β-Aminophosphonates and-Phosphinates. *Chem. Rev* 2005,105, 899−931.

[2] Ferentinos, E.; Xu, M; Grigoropoulos, A; Bratsos, I; Raptopoulou, C.P; Psycharis, V; Jiang, S.D; Kyritsis, P. Field-induced slow relaxation of magnetization in the S= 3/2 octahedral complexes trans-[Co{$(OPPh_2)$ $(EPPh_2)$ $N\}_2$ $(dmf)_2$], E= S, Se: effects of Co–Se vs. Co–S coordination. *Inorg. Chem. Front* 2019,6, 1405-1414.

[3] Eslami, F.; Pourayoubi, M.; Sabbaghi, F.; Skořepová, E.; Dušek, M.; Baniyaghoob, S. Diastereotopic groups in two new single-enantiomer structures (R2) P (O)[NH-(+) CH $(C_2H_5)(C_6H_5)$](R= OC_6H_5 and C_6H_5). *Acta Cryst* 2023, E79, 769–776.

Synthesis and spectroscopic characterization of a new amidophosphoester, $(CH_3CH_2O)_2P(O)NH(C_6H_{10})NHP(O)(OCH_2CH_3)_2$

Narjess Peyman, Mehrdad Pourayoubi*

Department of Chemistry, Faculty of Science, Ferdowsi University of Mashhad, Mashhad, Iran, nargesspeyman@yahoo.com, pourayoubi@um.ac.ir

Keywords: Amidophosphoester, NMR spectroscopy, Phosphoramide

The phosphoramide compounds have been the focus of researchers for a long time, due to manifold applications, especially in medicine, agriculture, and preparation of flame retardants[1]. According to the different applications of these compounds, synthesis methods have been developed, including the reaction of amines with phosphoryl halides[2].

A new amidophosphoester, $(CH_3CH_2O)_2P(O)NH(C_6H_{10})NHP(O)(OCH_2CH_3)_2$, was prepared from the reaction of $(CH_3CH_2O)_2P(O)Cl$ reagent and trans1,4-diaminocyclohexane (2:1 mole ratio, in the presence of $N(C_2H_5)_3$) in dry chloroform (Scheme). The product was characterized by IR, ^{1}H-NMR, ^{13}C-NMR, and ^{31}P-NMR spectroscopies.

In the IR spectrum, the bands centered at 3201 and 1211 cm^{-1} are attributed to the NH and P=O stretching frequencies. The phosphorus signal appears at 8.84 ppm, which is in the range of analogous compound[3]. The phosphorus-hydrogen and phosphorus-carbon coupling constants of the title compound are reported.

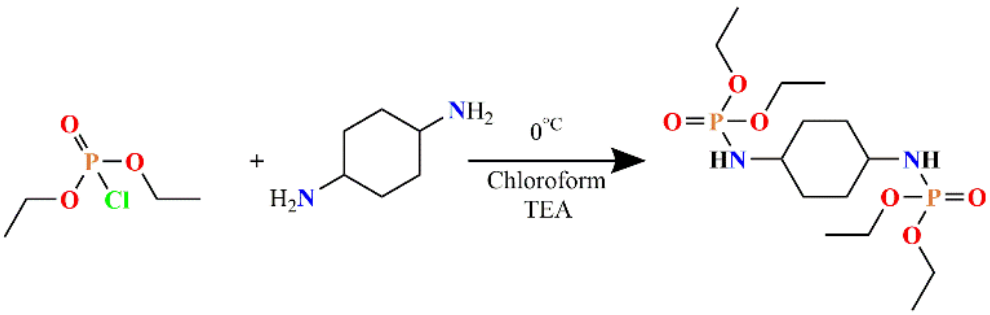

Scheme: Synthesis route of tetraethyl cyclohexane-1,4-diylbis(phosphoramidate).

References

[1] Moghaddam, S. N.; Shabari, A. R.; Sabbaghi, F.; Pourayoubi, M. Synthesis, spectroscopic characterization, crystal structure and Hirshfeld surface analysis of $(4\text{-}Cl\text{-}C_6H_4O)(OC_4H_8N)_2PO$ amidophosphoester. *Rev. Roum. Chim.* 2019, *64* (3), 209–215.

[2] Bouchareb, F.; Berredjem, M. Recent progress in the synthesis of phosphoramidate and phosphonamide derivatives: A review. *Phosphorus, Sulfur, and Silicon and the Related Elements* 2022, *197* (7), 711–731.

[3] Handoko.; Benslimane, Z.; Arora, P. S. Diselenide-mediated catalytic functionalization of hydrophosphoryl compounds. *Org. Lett.* 2020, *22* (15), 5811–5816.

Synthesis of Polysubstituted Pyrimidines through Palladium-Catalyzed Isocyanide Insertion to 2*H*-Azirines

Leyla Saeifard,[a] Kamran Amiri, [a] Frank Rominger, [b] Thomas J. J. Müller*, [c] and Saeed Balalaie* [a]

a) Peptide Chemistry Research Institute, K. N. Toosi University of Technology, P. O. Box 15875-4416, Tehran, Iran, leylasaiifard@yahoo.com, Balalaie@kntu.ac.ir.
b) Organisch-Chemisches Institut der Universität Heidelberg, Im Neuenheimer Feld 271, D-69120 Heidelberg, Germany.
c) Institut für Organische Chemie und Makromolekulare Chemie, Heinrich-Heine-Universität Düsseldorf, Universitätsstrasse 1, D-40225 Düsseldorf, Germany.

Keywords: Domino Cyclization Reaction, Isocyanide Insertion, 2*H*-Azirine, Polysubstituted Pyrimidines, Palladium-Catalyzed

The domino process of the palladium-catalyzed coupling reaction of isocyanides with 2*H*-azirine provides various tetrasubstituted pyrimidines via one C-C and two C-N bond formations with satisfactory yields. The title compounds are obtained with good functional group tolerance, high atom economy, and broad substrate scopes (**Scheme**).

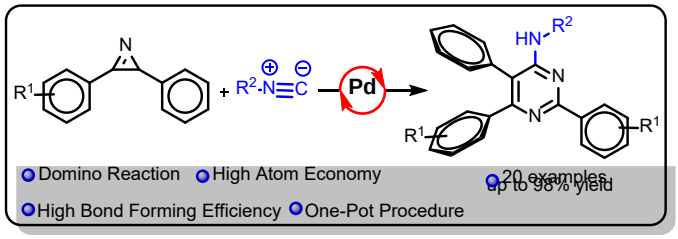

Scheme: Synthesis of tetra-Substituted Pyrimidines Derivatives.

References

[1] Roose, T. R.; Verdoorn, D. S.; Mampuys, P.; Ruijter, E.; Maes, B. U. W.; Orru, R. V. A. Transition Metal-Catalysed Carbene and Nitrene Transfer to Carbon Monoxide and Isocyanides. *Chem. Soc. Rev.* **2022**, *51*, 5842-5877.
[2] D'Souza, D. M.; Müller, T. J. J., Multi-component syntheses of heterocycles by transition-metal catalysis. *Chem. Soc. Rev.* **2007**, *36*, 1095-1108.
[3] Nikbakht, A.; Mohammadi, F.; Mousavi, M. S.; Amiri, K.; Balalaie, S.; Rominger, F.; Bijanzadeh, H. R. A Domino Approach for the Synthesis of 4-Carboxamide Oxazolines from Azirines. *Synthesis*. **2021**, *53*, 4654–4661.
[4] Vlaar, T.; Ruijter, E.; Maes, B. U. W.; Orru, R. V. A. Palladium-catalyzed Migratory Insertion of Isocyanides: An Emerging Platform in Cross-coupling Chemistry. *Angew. Chem. Int. Ed.* **2013**, *52*, 7084–7097.

Synthesis of Cyclic Azomethine Ylides and Their Applications in Designing of Novel 1,3-Dipolar Cycloaddition Reactions

Fatemeh Abdiyan Mobarakeh, **Saeed Balalaie** *

Peptide Chemistry Research Institute, K. N. Toosi University of Technology, Tehran, Iran, fatemeh.abdiyan@yahoo.com, balalaie@kntu.ac.ir;

Keywords: Azomethine ylide, 1,3-dipolar cycloaddition reaction, D-A cyclopropanes, tetrahydro-aza-phenanthrenes

Azomethine ylides are flat structures consisting of a nitrogen atom and two sp^2 carbon atoms at the ends.[1] Furthermore, they are frequently useful as starting materials for synthesizing specific substituted pyrroles, furans, cyclopropanes, and polyheterocycles. Azomethine ylides are known and useful 1,3-dipoles that could be used in designing of 1,3-dipolar cycloaddition reaction [2]. Herein, we wish to report the in-situ synthesis of azomethine ylides using 2-alkynyl benzaldehydes and their reaction with D-A cyclopropanes to access functionalized tetrahydro-aza-phenanthrenes catalyzed by silver triflate. (**Scheme**).

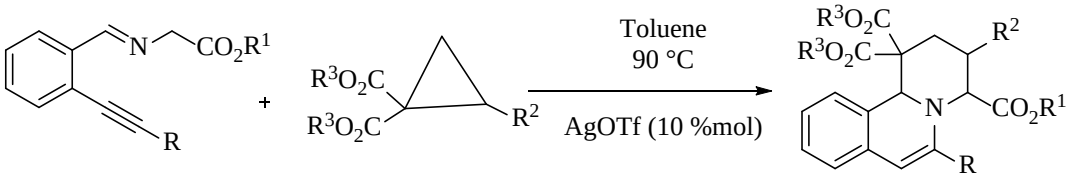

Scheme: The synthesis of nitrogen-containing heterocyclic compounds.

References

[1] Padwa, A.; Pearson, W. H. *Synthetic Applications of 1, 3-Dipolar Cycloaddition Chemistry toward Heterocycles and Natural Products*; John Wiley & Sons, 2003; Vol. 59.

[2] Nikbakht, A.; Balalaie, S.; Breit, B.; Synthesis of 2-(isoquinolin-1-yl) prop-2-en-1-ones via silver(I)- catalyzed one-pot tandem reaction of ortho-alkynylbenzaldoximes with propargylic alcohols, *Org. Lett.* **2019**, , 7645–7648.

Fabrication and application of Mn/SO_3H@zeolite-Y as bi-functional nano catalyst in three-component synthesis of *N*-benzo-imidazo- or -thiazole-1,3-thiazolidinones

Mehdi Kalhor* and Zahra Seyedzade

Department of Chemistry, Payame Noor University, Tehran, Iran, mekalhor@yahoo.com.

Keywords: Bi-functional nano-catalyst, SO_3H@zeolite-MnY, three-component synthesis, 1,3-thiazolidinone.

In recent years, the synthesis of multi-functional nanocatalysts in chemical processes and the preparation of hetrocyclic rings has been greatly welcomed. The presence of two catalytic agents in the structure of a nanosystem improves reaction efficiency, increases selectivity, variety of applications, and speed of a process. According to the advantages of these catalysts, the use of these nano catalysts in various synthesis has recently been reported [1,2]. Among the heterocyclic compounds, five-membered aromatic rings have occupied a wide area of heterocyclic chemistry due to the importance of the nuclei of these rings and the suitable positions for various reactions. Important members of this family are thiazoles and benzaimidazoles. Extensive studies have been conducted on these compounds and many compounds containing this heterocycle are known, which have biological and industrial importance. These heterocycles are used as anti-tumor, anti-bacterial, anti-HIV, anti-cancer, anti-viral, anti-allergic, anti-hypertensive, *etc* [3] .Considering the importance of improving the synthesis methods of these unusual rings and continuing the development of multi-functional nanocatalysts on basic zeolite, in this study, we synthesized *N*-benzo-imidazo- or -thiazole-1,3-thiazolidinone derivatives through a single reaction container and mild conditions, we synthesized Mn/SO_3H@zeolite-Y acidic bi-functional nanocatalyst stabilized on zeolite substrate. Among the benefits of this zeolitic catalyst, the following can be mentioned. This procedure offers several advantages, including operational simplicity without high temperature, fast reaction times, excellent yields and good reusability of the catalyst

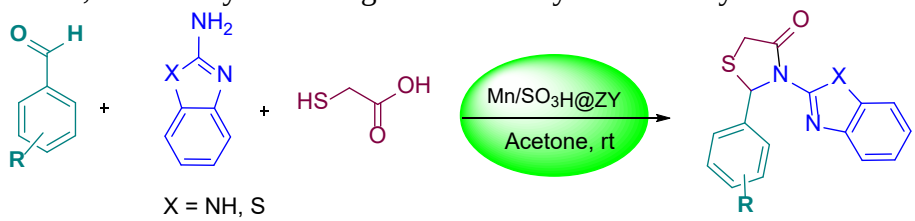

Scheme: The synthetic pathway of 1,3-thiazolidinones using Mn/SO_3H@ZY

References

[1] Li, N.; Huang, B.; Dong, X.; Jiao, F.; Xiao, J.; Qu, Z.; "Bifunctional zeolites-silver catalyst enabled tandem oxidation of formaldehyde at low temperatures." *Nature Commun.*, 2022, *13*, 2209.

[2] Kalhor, M.; Gaeini, R.; Molaei, B.; "Application of a New Bifunctional Nanocatalyst Mn/SO_3H@ zeolite-Y in Rapid Synthesis of 2-Aryl Perimidines." *Org. Prep. Proced. Int.* 2023, 1-11.

[3] Jain, A.K.; Vaidya, A., Ravichandran, V.; Kashaw, S.K.; Agrawal, R.K.; "Recent developments and biological activities of thiazolidinone derivatives. *Bioorg. Med. Chem.*, 2012, *20*, 3378-3395.

Synthesis and Spectroscopic Characterization of O,O,O',O'-tetraethyl butane-1,4-diylbis(phosphoramidothioate) and O,O,O',O'-tetraethyl cyclohexane-1,4-diylbis(phosphoramidothioate)

Yalda Khoshakhlagh Ostad, Mehrdad Pourayoubi*

Department of Chemistry, Faculty of Science, Ferdowsi University of Mashhad, Mashhad, Iran, y.khoshakhlagh@gmail.com, pourayoubi@um.ac.ir.

Keywords: Bisphosphoramidothioate, NMR spectroscopy, Synthesis.

Structural characteristics have been studied for phosphoramides [1] and thiophosphoramides [2]. These compounds have been attracted attention due to their biological activity and flame retardancy properties [3,4]. In this research, we report the syntheses of $(EtO)_2P(S)[NH(CH_2)_4NH]P(S)(OEt)_2$ (I), and $(EtO)_2P(S)[trans\text{-}1\text{-}(NH)C_6H_{10}\text{-}4\text{-}(NH)]P(S)(OEt)_2$ (II), belonging to bisphosphoramidothioate family, and the characterization by IR, NMR (^1H, ^{13}C, and ^{31}P), elemental analysis, and Mass spectroscopy. In the Mass spectra, the molecular ion peaks are revealed (*m*/*z* = 392 for (I) and 418 for (II)). The phosphorus signals for (I) and (II) appear at 71.68 and 70.33 ppm, respectively. The N—H proton of (I) appears as a singlet at 3.07 ppm, and a similar proton of (II) appears at 3.02. In the IR spectra, the bands centered at 3304 cm^{-1} for (I) and at 3310 cm^{-1} for (II) are attributed to the NH stretching frequencies, and the P=S stretching bands appear at 790 and 787 cm^{-1}, respectively.

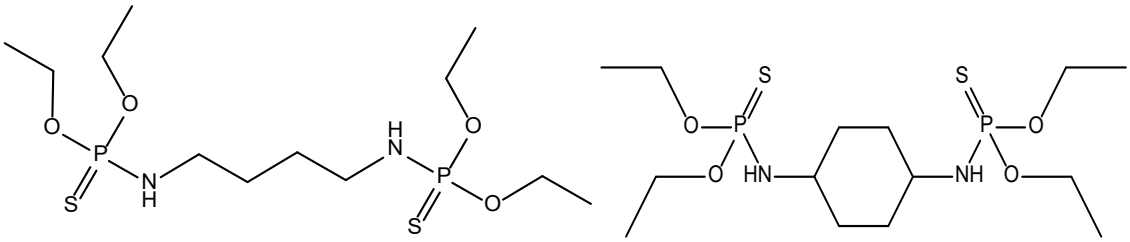

Scheme: Chemical structures of (I) (left) and (II) (right).

References:

[1] Pourayoubi, M., Toghraee, M., Divjakovic, V., van der Lee, A., Mancilla Percino, T., Leyva Ramírez, M. A. & Saneei, A. Analysis of N—H· ·O hydrogen bonds in new C(O)-NH-P(O)-based phosphoric triamides and analogous structures deposited in the Cambridge Structural Database. *Acta Cryst.* 2013, *B69*, 184–194.

[2] Pourayoubi, M., Abrishami, M., Eigner, V., Nečas, M., Dušek, M. & Delavar, M. Two new thiophosphoramide structures: N,N',N''-tricyclohexylphosphorothioic triamide and O,O'-diethyl (2-phenylhydrazin-1-yl)thiophosphonate. *Acta Cryst.* 2014, *C70*, 1147–1152.

[3] Levchik, S. V. & Weil, E. D. Flame retardancy of thermoplastic polyesters-a review of the recent literature, *Polym. Int.* 2005, *54*, 11–35.

[4] D. E. C. Corbridge, Phosphorus: chemistry, biochemistry and technology, CRC *press*, *Boca Raton*.

Investigating and determining the residual concentration of some organochlorine and organophpsphorus pesticides in the Caspian sea waters of Anzali Bandar

Hadi Babaei *, **Siamak Baghari and Hojjat Mohsenpour**

Agricultural Research, Education and Extension Organization (AREEO), Iranian Fisheries Science Research Institute, Inland Waters Aquaculture Research Center, Anzali Bandar, Iran, babaeiha@yahoo.com

Keywords: Gas chromatography, Organochlorine, Organophosphorus, Caspian Sea, Anzali Bandar

Today, the residue of organochlorines and organophosphates is known as an important environmental pollutant, including soil and surface and underground water sources [1]. In this way, a large number of people around the world have been exposed to all kinds of diseases, including all kinds of cancers, abnormalities, genetic mutations, and neurological disorders by using substances contaminated with chemical poisons.In this research, the residual amount of diazinon, malathion, parathion, chlordane, heptachlor, endosulfan, butachlor, lindane, and fibronil in spring and summer in the coastal waters of the Caspian Sea in Bandar Anzali region of Gilan province in the year 2021 was determined.Sampling was done using dark glass bottles, and the samples were separated and extracted according to the ISIRI-1053 standard method, and the concentration was determined using a gas chromatography-mass spectrometer (GC/MS).The results showed that the amount of fibronil, ethion, malathion and lindane toxins was not observed in the investigated samples in the two sampling seasons and the maximum concentration measured was 26.435 µ/l in the spring season belonging to Aldrin poison and the concentration of diazinon toxins in the summer samples and the concentration of endosulfan in the spring samples was not detectable by the gas chromatography mass spectrometer.This study showed that the residual amount of studied poisons in the studied samples was higher in the spring season than in the summer season, which is due to the presence of agricultural fields on the edge of the Anzali lagoon and due to the excessive consumption of toxins in the spring season, which eventually It has affected the coastal waters through the outlet of the lagoon.

Parathion Endosulfan Aldrin Heptachlor

Scheme: The structure of some pesticides measured in this research

References

[1] Sobhanardakani,S. Determination of some organochlorine and organophosphorus pesticide residues in water of Gargar River, J. Env. Sci. Tech., 2017, 19, 4, Spring 2017.

Measurement of polyaromatic petroleum compounds (PAHs) in the water of Neor lake (Ardebil province)

Hadi babaei *, **Hosin Sabri and Hojjat Mohsenpour**

Agricultural Research, Education and Extension Organization (AREEO), Iranian Fisheries Science Research Institute, Inland Waters Aquaculture Research Center,Bandar Anzali, Iran, babaeiha@yahoo.com.

Keywords: Petroleum compounds (PAHs), Gas chromatography, Neor Lake, Ardabil

Polycyclic aromatic hydrocarbons (PAHs) are a group of organic compounds that contain two or more benzene rings. These compounds have been noticed by researchers due to their carcinogenic and mutagenic properties, as well as their stability in marine systems [1]. In this study, three study stations were selected for sampling in the entire water area of Neor Lake and samples were taken using dark glass containers, and according to the EPA 625 standard method and using dichloromethane solvent, the steps of separation and extraction were carried out. The samples were taken. The concentrated samples along with the relevant standards were injected into the GC/MS gas chromatography mass spectrometer and the concentration of each of the petroleum compounds (PAHs) was determined by spectrometry of the samples and drawing a calibration curve based on the injected standards. The results of the analysis of 16 polyaromatic petroleum compounds (PAHs) in the water of Lake Neor showed that due to the lack of sources of these types of compounds in the study area, only two compounds were observed in the investigated samples, the average concentration of phenanthrene and anthracene in the lake water, respectively 2.7±1.27, 1.0±1.04 µ/l were recorded. The ratio of phenanthrene to anthracene was calculated to be less than 10 [2]. Based on this, it can be concluded that the PAHs petroleum compounds in Neor Lake have a pyrolytic source and the entry of these compounds into the lake is from fuel sources such as benzene, diesel consumption due to boat activity and floats are in the lake.

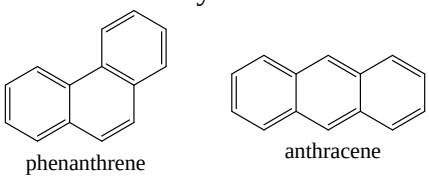

Scheme: The structure of petroleum compounds measured in this research.

References

[1] Ismaili Sari, A. Health and standard pollutants in the environment, Naqsh Mehr Publications, 2002, 769.

[2] Baumard, P.; Budzinski, H.; Garrigues, P.Polycyclic aromatic hydrocarbons in sediments and mussels of the western Mediterranean sea. *Environ. Toxicol. Chem.*,1998.17: 765–776.

Study of the Industrial Production of Biurea Filler in the Pilot Phase and Its Industrial Application in Inhibitors

A. Behboudi Amlashi [a*], A. Musavi Azar [b] and E. Niknam Asl [c]

a) Chem. and Chemical Eng. Complex, Ph.D. student, University of Malek-e-Ashtar, Tehran, Iran, ab.behbudi@gmail.com
b) Analytical Chemistry Lab., Faculty of Chemistry, University of Malek-e-Ashtar, Isfahan, Iran
c) Organic Chemistry Lab., Faculty of Chemistry, University of Shiraz, Shiraz, Iran

Keywords: Smokeless Inhibitors, Biurea, Biurea Production

Low smoke production is especially important for penetrators that are guided by laser, radio or infrared waves, because due to the high smoke, the guidance signal is largely distorted, ineffected and damped in the smoke channel of the engine. Therefore, one of the requirements of the engines is that the smoke production reaches its minimum value. One of the main sources of smoke production is inhibitor. The best way to achieve inhibitor with low smoke is to use inhibitor with a high percentage of oxygen so that the ratio of oxygen to carbon in the inhibitor is at least 1 to 3 [1]. Hydrazodicarbonamide (Biurea) is one of the derivatives of hydrazine, which is commercially important as a raw material or intermediate for the synthesis of azodicarbonamide (blowing agent) and on the other hand, as an organic filler in the production of inhibitors without smoke is used. In this article, the review and introduction of various methods of industrial production of biurea compound, identification of this compound and optimization of its production method in order to achieve a purity of more than 99% have been discussed. The use of cost-effective production method in terms of production efficiency and minimum cost is the priority of this research. The method in which the biuret compound is used as a raw material for the production of biurea is a suitable method for the production of biurea, but on the other hand, the economic aspect and availability of biuret should be considered [2].

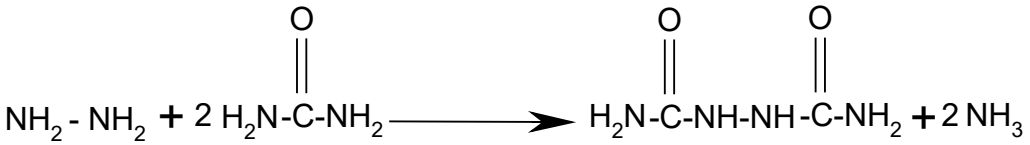

Scheme: The reaction of Biurea Production by Formation of Biureat Intermediate

References

[1] Louis Mehr and et al., Manufacture of Biurea, United State Patent 3227753, 1966.
[2] Jean Pierre Schirmann and et al., Method for manufacturing hydrazodicarbonamide, United State Patent 4049712, 1977.

Study and Optimizing the Synthesis Methods of Energetic Plasticizer BTTN in Experimental Scale and Its Industrial Application

A. Behboudi Amlashi [a*], A. R. Hassanpour Golshani [b] and M. Ebrahimi [c]

a) Chem. and Chemical Eng. Complex, Ph.D. student, University of Malek-e-Ashtar, Tehran, Iran, ab.behbudi@gmail.com
b) Physical chemistry Lab., Faculty of Chemistry, Sharif University of Technology, Tehran, Iran
c) Faculty of Chemistry, Imam Hossein (PBUH) University, Tehran, Iran

Keywords: Energetic Plasticizer, BTTN, DB composits

Plasticizer compounds are very wide compounds due to industrial application and have special importance in various industries. Plasticizer compounds such as BTTN and NG are used with GAP binding agent to strengthen the performance of DB composites. The plasticizer compound butantriol trinitrate (BTTN) as a type of energetic nitrate ester has very wide applications in the industries. This energetic compound is one of the main components of high explosives such as dynamites used in drilling oil wells and DB powder. Energetic plasticizer BTTN has better properties than NG and use as an alternative NG today [1]. The optimal synthesis of this compound is possible through the process of nitration of butanetriol compound and using a mixture of sulfuric acid and nitric acid (65:35) with temperature control up to 20 degrees Celsius in a period of about 20 minutes. In the optimal synthesis method of this compound, the reaction efficiency was about 91%. This compound has been used as a plasticizer in DB composits used in Eastern Bloc countries and in polyethylene glycol base composits as safe and low-sensitivity composits compared to HTPB composits [2,3].

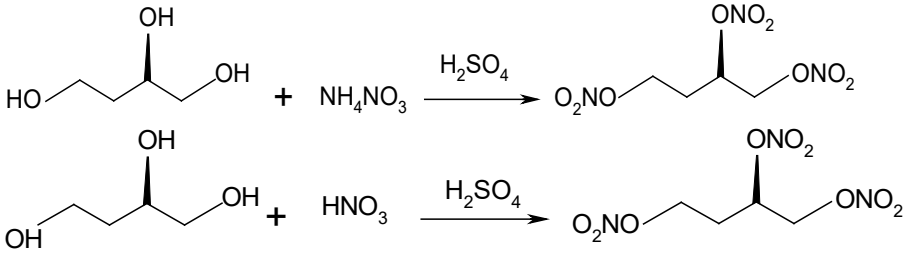

Scheme: production of BTTN according to nitration reactions

References

[1] F. Guranlo, I. Kohsari, Synthesis and Charactrization of 1,2,4- Butanetrioltrinitrate, Asian Journal of Chemistry, Vol. *22*, No. *6*, 2010, 4221-4228.
[2] Copperhead Chemical Company, Butanetriol trinitrate (BTTN), Product Information Bulletin, Rev., May 2011.
[3] M. Rahmani, M.R. Mahmudinezhad, A. Behbudi Amlashi, Design and production of new propellant based on PEG binder, The first national conference on energetics materials and the 7th national conference on P.E.P., Malek-e- Ashtar University, Tehran, Iran, 2014.

Assessing detergent performance after replacing surfactants with enzymes

Kolsoom Najafzadeh*, Fahimeh Sadat Hoseini

Quality Control Laboratory, Pharco Chiemie Company, Lia Industrial City, Qazvin, Iran, kolsoomnajafzadeh0@gmail.com, hosseini.fahime@gmail.com

Keywords: Surfactant, Enzyme, Detergent

Enzymes are naturally occurring substances that are effective at low concentrations, break down rapidly in the environment, and have low toxicity. Enzymes, when combined with other detergent ingredients, enhance wash performance by breaking down stains and removing dirt [2]. In this study, half a gram of enzyme was replaced with 50% of the surfactant in the enzyme-rich detergent. All other detergent ingredients were left unchanged, and the cleaning performance of the two detergents was compared. The results show that the overall wash performance, measured as total reflectance, especially for specific stains such as milk, chocolate, grass, and starch stain, increases when enzymes are replaced by surfactants in the detergent [1].
In addition, to save energy, the wash temperature can be reduced to a lower level with almost the same or better overall wash performance.

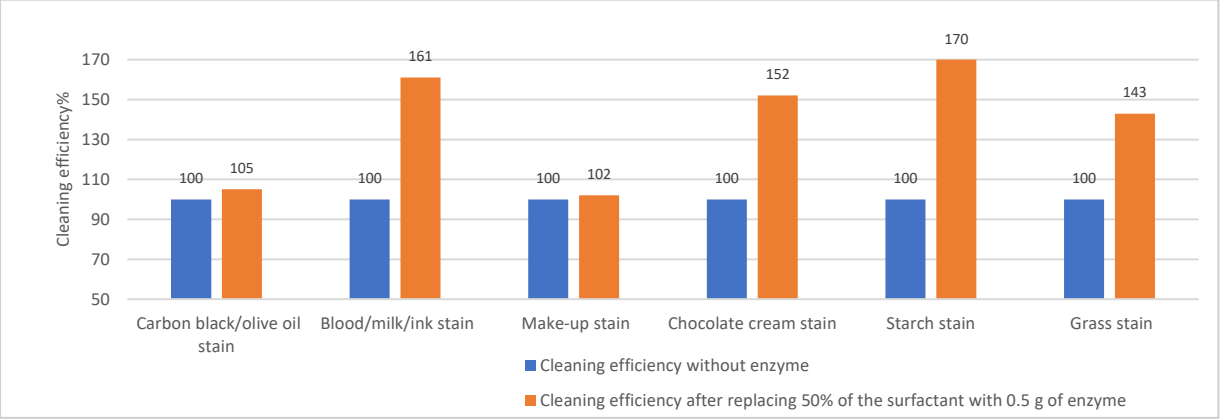

Scheme: Comparison of cleaning performance of enzyme-rich and non-enzymatic detergent

References

[1] Skagerlind. P; Yuanzhao. Y, Excellent stain removal with enzymatic washing powders. *Soaps, Detergents & Toiletries 2018, July* ,28-30

[2] Niyonzima, F.N.; More, S.S. Coproduction of detergent compatible bacterial enzymes and stain removal evaluation. *J. Basic Microbiol. 2015, 55*, 1149–1158

Industrial Production Process and Optimization of Stabilizer 2,4-Dinitrophenoxy Ethanol and its Industrial Application in Inhibitors

A. Behboudi Amlashi [a*], E. Masudi [b], M.R. Babaei[c] and M.R. Morshedi [d]

a) Chem. and Chemical Eng. Complex, Ph.D. student, University of Malek-e-Ashtar, Tehran, Iran, ab.behbudi@gmail.com
b) Polymer Chemistry Lab., Faculty of Chem. and Chemical Eng., University of Tehran, Tehran, Iran
c) Analytical chemistry Lab., Faculty of Chemistry, University of Khajeh Nasir Toosi, Tehran, Iran
d) Faculty of Chemistry, University of Tarbiat Dabir Shahid Rajaei, Tehran, Iran

Keywords: 2,4 Dinitrophenoxy Ethanol, Inhibitors, DB Composits

Chemical stabilizers are used in inhibiting formulations in order to prevent inhibition fatigue in different environmental and storage conditions. 2,4-dinitrophenoxy ethanol (DNPE) or 2,4-dinitrophenyl beta-hydroxy ethyl ether is considered as an excellent stabilizer for composits based on ammonium nitrate and inhibitor based on cellulose acetate [1]. The production and supply of this compound has been done with the purpose of plasticizing of cellulose acetate used in inhibitor merely. The classic method of synthesis of DNPE is the reaction between dinitrochlorobenzene and ethylene glycol in the presence of sodium hydroxide solution. In this method, a minimum amount of 1,2-bis-NPE isomer produce along with the main product [2]. Normally, it is expected that the side product of this reaction to produce bis-DNPE is about 5% of the reaction product. In general, the production efficiency of DNPE is about 95% by weight in the best conditions after crystallization and purification. In this research, the reaction efficiency is about 92%. Considering that one of the important issues in the design of inhibitor for penetrators is the amount and type of smoke resulting from the inhibitor combustion products, it is very important to use compounds that can create the minimum amount of smoke [3].

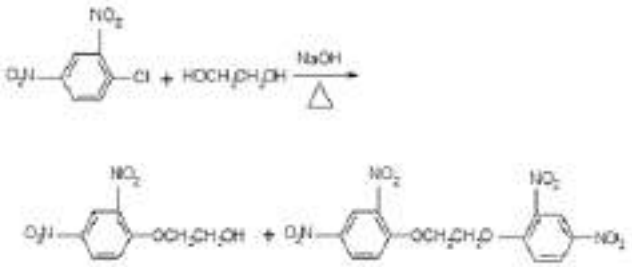

Scheme: The optimized reaction of DNPE Formation

References

[1] A. Musavi Azar, M.H. Keshavarz, M. Hayati, Ayyub Kazemi, Synthesis, Charactrization and Thermal behavior of DNPE as a suitable plasticizer for propellants formulations, TAC, 2016.
[2] Kenneth W. Mc Fie et al., Dinitrophenoxy ethanol Process, US Patent, 2988571- June 1961.
[3] S. M. Akbari, A. Aref Azar, M. R. Mahmudinezhad, Investigating the Baking Conditions and Formulation of DB Inhibitors, 2d A.I.O. conference, Iran, 2002.

Introducing and Evaluating the Safety Parameters of NTO-HMX Based Safe Energetics Compound and its Application in Formed Penetrators

A. Behboudi Amlashi [a*], A. A. Mohammadi[b] , M. Abedin Moghanaki[c]

a) Chem. and Chemical Eng. Complex, Ph.D. student, University of Malek-e-Ashtar, Tehran, Iran, ab.behbudi@gmail.com
b) Appl. Chemistry Lab., Faculty of Chemistry, University of Shahin Shahr Malek-e-Ashtar,Isfahan, Iran
c) Mechanics Engineering. Lab., Faculty of Technology and Engineering, Tabriz, Iran

Keywords: NTO-Based Compound, Insensitive Munitions (IM)

Today, various applications of Insensitive munitions (IM) have increased. Owing to its non-sensitive properties, heterocycle nitrocompond 3- nitro- 1,2,4- triazol- 5- one (NTO) is one of the main compounds in IM formulations [1]. For example, one series of NTO-based IM formulations called XF and XP have been developed [2]. Considering the reproducible performance of this type of compounds in formed penetrators, as well as the characteristics of pressability and very high strength of the pressed energetics compound, its use in some of the formed penetrators of a number of flight systems has been investigated and the results of reproducible penetration depth has been presented as the most important result expected from the performance of these penetrators [3]. Also, the results related to proving the safe performance of NTO-HMX energetics compounds and finally its morphology are presented as one of the interesting cases in the field of safety [3]. The results of these investigations show the safety of this charge and have confirmed this claim.

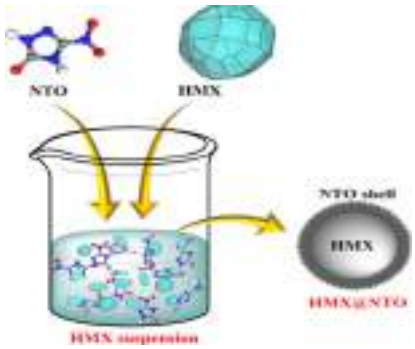

Scheme: Coating Process of HMX with NTO and NTO-HMX Energetics compound Formation

References

[1] J.C. Li et al, Explosive performance of HMX-NTO co-crystal, 2018 IOP Conf. Ser.: Mater. Sci. Eng. 292012032
[2] Matthew W. Smith and Matthew D. Cliff, NTO- Based Explosive Formulations: A Technology Review, WSD, A.M. Research Laboratory, DSTO-TR-0796, 1999.
[3] Li- xiaosong Du, Shao-hua Jin, Qing-hai Shu, Li-jie Li, Kun Chen, Ming-lei Chen, Jun-feng Wang, The Investigation of NTO-HMX based plastic-bonded explosives and its safety performance, 2021.

Optimizing polyglycidyl nitrate elastomer synthesis using various diamines as curing agents

Masoud Mohamadi Vala [a]*, Yadollah Bayat[b] and Mohamad Bayat[a]

a) Department of Chemistry, Faculty of Science Imam Khomeini International University, Qazvin, Iran, masoudmohamadivala@gmail.com
b) Department of Chemistry, Malek Ashtar University of Technology, Tehran, Iran, y_bayat@mut.ac.ir

Keywords: Polyglycidyl nitrate, Elastomer, Diamines

Energetic binders are polymers that contain functional groups such as nitro, nitrato, and azido, etc., and release high energy during combustion and so increase the performance of solid composite propellants [1]. The amount of energy is one of the important parameters for solid propellants, so the development of energetic binders is an important research topic. Among energetic binders, PGN is the most energetic binder (explosion heat: 2616 kJ/kg) but its mechanical properties is not suitable [2]. PGN can be cured rapidly with polyfunctional isocyanates, but the cured sample of PGN will self-decompose after one to two years. In recent years, there have been numerous efforts to modify end-functional group binders. In this study, PGN was modified to form the poly glycidyl nitrate binder with the epoxy end group (e-PGN) under mild conditions.

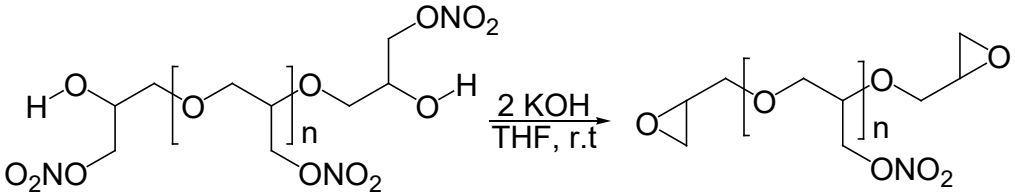

Scheme: Synthesis of e-PGN energetic binder.

Elastomers were also prepared using various diamine agents (aromatic and aliphatic diamines), and their mechanical properties were assessed. Stress-strain testing results indicate that the ideal diamine curing agent is 1,2-cyclohexane diamine.

References

[1] Badgujar, D. M.; Talawar, M. B.; Zarko, V. E.; Mahulikar, P. P. New directions in the area of modern energetic polymers: An overview. *Combust. Explos. Shock Waves* 2017, *53*, 371-387.
[2] Bayat, Y.; Razaghi, M. A.; Ghorbani, M.; Ghadiri, A.; Mossahebi, M. M.; Dehghani, H. Synthesis of Tri-Block Polycaprolactone-Poly Glycidylnitrate Polycaprolactone as Polyol Propellant Binder. *J. Energ. Mater* 2015, *10*, 25-34.

Synthesis, Characterization, and Application of a Novel Palladium(II) Complex of α-Keto Arsonium Ylide in Suzuki−Miyaura Cross-Coupling Reactions

Majid Jamshidi Lotf and Seyyed Javad Sabounchei *

Department of Organic Chemistry, Faculty of Chemistry, Bu-Ali Sina University, Hamedan, Iran, jsabounchei@yahoo.co.uk

Keywords Arsonium ylide, Homogenization, Pd(II) complex, Suzuki-Miyaura reactions

The new Palladium(II) complex with the α-keto stabilized arsonium ylide ligand, represented by the general formula $[Pd(\mu\text{-}Cl)(Ph_3AsCHC(O)C_{10}H_7)]_2$, has been synthesized and investigated as a performance catalyst for the palladium(II)-catalyzed Suzuki-Miyaura reaction (Figure 1). This reaction involves the coupling of arylboronic acid with aryl bromides and has been widely utilized in various C-C coupling reactions for over three decades, including Heck, Sonogashira, Suzuki, Kumada, Negishi, Hiyama, and others [1-3].

The Suzuki-Miyaura reaction is particularly attractive due to its environmentally friendly nature, high tolerance to diverse functional groups, ready availability of starting materials, and excellent stability of the substrates employed. It finds extensive applications in the synthesis of natural products, biologically active pharmaceuticals, and agrochemicals [4].

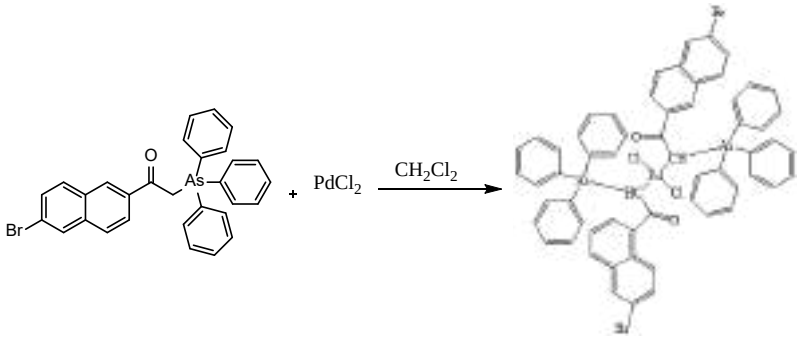

Figure 1. Synthesis of palladium complex

References:

[1] Jakob, A.; Milde, B.; Ecorchard, P.; Schreiner, C.; Lang, H; Palladiumdichloride (ferrocenylethynyl)phosphanes and their use in Pd-catalyzed Heck-Mizoroki-and Suzuki-Miyaura carbon-carbon cross-coupling reactions. *J. Organomet. Chem.* 2008, *693*, 3821–3830.

[2] Albano, G.; and Aronica, L. A.; Potentiality and Synthesis of O-and N-Heterocycles: Pd-Catalyzed Cyclocarbonylative Sonogashira Coupling as a Valuable Route to Phthalans, Isochromans, and Isoindolines. *EurJOC*, 2017, *48*, 7204-7221.

[3] Zhang, L., and Wu, J. Palladium-catalyzed Hiyama cross-couplings of aryl arenesulfonates with arylsilanes. *J. Am. Chem. Soc*., 2008, *130*, 12250–12251.

[4] Baran, T., Sargin, I., Kaya, M., and Menteş, A. An environmental catalyst derived from biological waste materials for green synthesis of biaryls via Suzuki coupling reactions. *J. Mol. Catal. A Chem.*, 2016, *420*, 216–221.

Curcumin derivatives: A brief review of anti-cancer and anti-diabetic properties

Hadi Adibi*

Pharmaceutical Sciences Research Center, Health Institute, Kermanshah University of Medical Sciences, Kermanshah, Iran, hadi.adibi@yahoo.com

Keywords: Curcumin, Anti-cancer, Anti-diabetic, Synthesis, Multi-component

Diabetes is one of the most common metabolic diseases in humans, being a major health problem in the world today due to its high prevalence. Therefore, in this study, curcumin-based hexose derivatives (L2-4) were synthesized and used as influential agents in the treatment of diabetes with inhibitory properties against two carbohydrate-hydrolyzing enzymes α-glucosidase (α-Gls) and α-amylase (α-Amy) which are known to be significant therapeutic targets for the reduction of postprandial hyperglycemia. In many studies, also the anti-cancer effect of curcumin and its derivatives has been proven. In this study, curcumin derivatives based on 4-phenylchromene were synthesized and assayed to investigate the anti-cancer effect and their possible interaction with DNA.

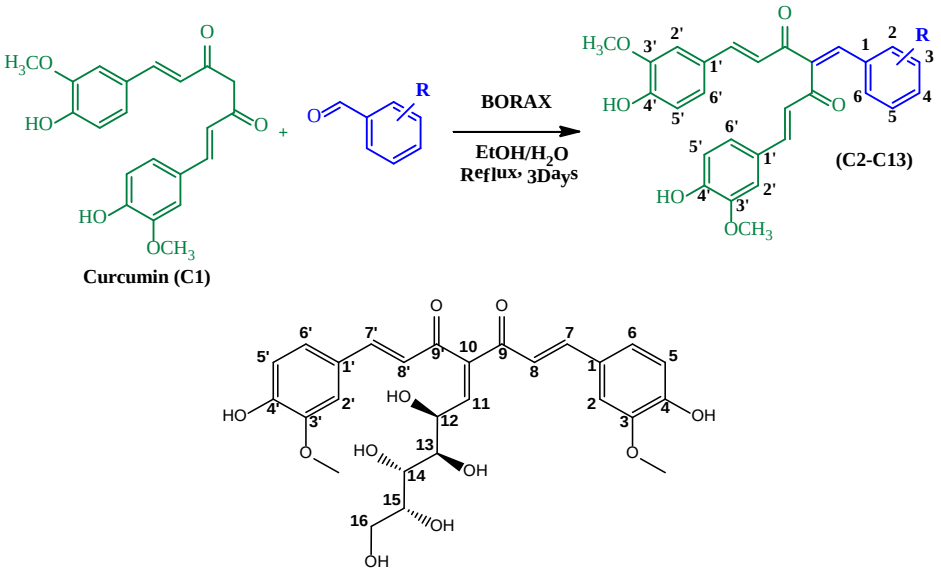

Curcumin (C1)

Scheme: Synthesis of curcumin derivatives

[1] O.K. Arjomandi, S. Almasi, L. Hosseinzadeh, M. Kavoosi, H. Adibi, Preparation, Characterization and In-vitro Biological Evaluation of Novel Curcumin Derivatives as Cytotoxic and Apoptosis-Inducing Agents., Anticancer. Agents Med. Chem. **2021**, *21* (10), 1309-1322.

[2] S. Esmaeili, N. Ghobadi, D. Nazari, A. Pourhossein, H. Rasouli, H. Adibi, R. Khodarahmi, Curcumin-based antioxidant and glycohydrolase inhibitor compounds: Synthesis and in vitro appraisal of the dual activity against diabetes, Med. Chem. **2021**, *17* (7), 677-698.

A Meta-synthesis approach to designing a conceptual framework for environmental health effects of coenzyme B_{12} models

Elahe Keshavarz*

Department of Chemistry Education, Farhangian University, P. O. Box 14665-889, Tehran, Iran, keshavarz@cfu.ac.ir

Keywords: Coenzyme B_{12} models, Environmental effects, Meta-synthesis

In the past decades a serious effort has been assigned to the synthesis and characterization of simple cobalt complexes containing a stable Co-C bond and systematic investigations have been made to understand the ligands function in cobaloximes. Cobaloximes are a set of pseudo-macrocyclic bis(diglyoximato)cobalt complexes that show good models of vitamin B_{12} since they share many of their chemical properties, and each of them shows vital functions, which are essential for life [1]. Considering the structural importance of cobaloxime complexes in vital functions, the present study aims to identify the applications of these compounds and provide a comprehensive model. The research methodology is a meta-synthesis approach according to Sandelowski and Barroso's seven steps [2] (Fig. 1).

Step 1	Specifying the research goal (Determining the study question)
Step 2	Systematic review of research literature
Step 3	Search for keywords and selection of relevant articles
Step 4	Extraction of information from articles
Step 5	Analysis and integration of findings from qualitative studies
Step 6	Quality control
Step 7	Presentation of the conceptual model (results)

Figure 1: Stages of Sandelowski & Barroso meta-synthesis method

This research synthesizes 22 years of studies on cobaloximes. An electronic search of published articles in PubMed, Scopus, Proquest, Sciencedirect and Google Scholar was conducted using a combination of subject headings and keywords relating to cobaloxime and human health effects. After content analysis of the data, the potential challenges as well as the prospects of the research about environmental health effects of cobaloximes were elucidated. The findings showed many interrelated main dimensions for the proposed framework of environmental health effects of coenzyme B_{12} models.

References

[1] Singh, G.; Malik, S.; Pawan; Mohit; Diskit, T.; Kaur, H.; Khurana, S.; Mithun; Kaur. A. Synthesis and structural characterization of new schiff base probe: A conformation modulator for Co-C bond cleavage in coenzyme B_{12}-dependent enzymes. *J. Mol. Struct.* 2023, 1293, 136279.

[2] Keshavarz, E.; Moshkbid, F. Identifying the conceptual model of design thinking in basic science using a meta synthesis approach. *Educ Strategy Med Sci* 2023, Accepted Article.

Synthesis of Bifunctional Compounds and their Potential for the Construction of Heterocyclic Backbones

Saeed Balalaie*

Peptide Chemistry Research Institute, K. N. Toosi University of Technology, P. O. Box 15875-4416, Tehran, Iran, Balalaie@kntu.ac.ir

Keywords: Bifunctional Compounds, Heterocyclic Backbones, Catalytic Reactions.

The discovery of new approaches that can generate complex organic molecules or bioactive heterocyclic backbones is central to advances in the life sciences.
In this regard, using of bifunctional compounds have essential role to access the functionalized heterocyclic backbones. In this lecture, a set of small organic molecules will be introduced that could be used for designing of novel reaction to construct heterocyclic backbones.The development of reactions that convert bifunctional compounds to heterocyclic skeletons have explored the construction of heterocycles using catalytic reactions involved metal catalysts to activate triple bonds. The details of reaction for the synthesis of heterocycles will be presented.

References

1. Nikbakht, A., Ebrahimi Valdani, A., Zahedian Tejeneki, H., Abbasi Kejani, A., Alavijeh, N.S., Bauer, F., Darvish, F., Breit, B. and Balalaie, S., (2023) A Diastereoselective Cascade Annulation Approach to Bridged Polycyclic Heterocycles Involving an Unexpected Rearrangement. *Org. Lett.* **2023**, *25*, 1, 16–20.
2. Rezaei-Gohar,M.; Amiri, K.; Aghaie, K.; Nayebzadeh, B.; Ariafard, A.; Shiri, F.; Rominger, F.; Dar'in, D.; Krasavin, M.; Balalaie, S. Domino Cyclization Reaction of *o*-diisocyanoarenes for the Synthesis of Imidazo[1,2-*a*]pyridinobenzimidazole Backbones, *Org. Lett.* **2023**, 25, 5682-5686.
3. Saeifard, L.; Amiri, K.; Rominger, F.; Müller,T.J.J.; Balalaie, S. (2023) Synthesis of Polysubstituted Pyrimidines through Palladium-Catalyzed Isocyanide Insertion to 2*H*-Azirines, *J. Org. Chem.* **2023**, 88, 12519-12525.
4. Amiri, K.; Nayebzadeh, B.; Kamangar, M.; Babazadeh, M.; Ariafard, A.; Shiri, F.; Rominger, F.; Balalaie, S. (2023) Synthesis of Fused N-Bridged [3.3.1]nonadiquinoline Multicyclic Skeleton via Metal-Free Formal [4+2] Cycloaddition/ Mannich/ Dearomatization Domino Reaction *Green Chem.* **2023**, https://doi.org/10.1039/D3GC03026A

Novel Metallodrugs: Synthesis, Anticancer Potency, and the Crucial Role of Central Atoms and Organic Ligands

Samad Khaksar*

Department of Pharmaceutical Chemistry, School of Science and Technology, The University of Georgia, Tbilisi, Georgia

Keywords: Metallodrugs; Extra-nuclear cation; Cytotoxicity; Apoptosis; Autophagy

Two Ga(III) complexes, derived from pyridine-2,6-dicarboxylic acid and aminopyridine derivatives, share a common structure but differ in extra-nuclear cations. The complexes feature ($pydc^{2-}$) units bound to Ga(III), forming a distorted octahedral geometry, while $(apyH)^{+}$ units act as extra-nuclear cations. This combination results in enhanced electrostatic interactions and overall stability of the crystal structure, supported by various interaction types. Thermal analysis (TGA) shows both compounds remain stable up to 135°C.

In cancer cell lines, the complexes exhibit distinct IC_{50} values, attributed solely to the NH_2 substitution position in the aminopyridine-derived extra-nuclear cations. This emphasizes the profound impact of small extra-nuclear cation variations on the cytotoxicity of metal complexes. Cellular penetration differences are likely due to distinct noncovalent interactions between the extra-nuclear cation and the anionic complex, contributing to varying IC_{50} values.

Notably, these complexes exhibit potent inhibitory effects on A431 cells. Mechanistic investigation through expression assays of apoptosis and autophagy-related proteins suggests bimodal cell death, involving mitochondria-mediated apoptosis and autophagy, in A431 cells treated with both complexes. (**Scheme**).

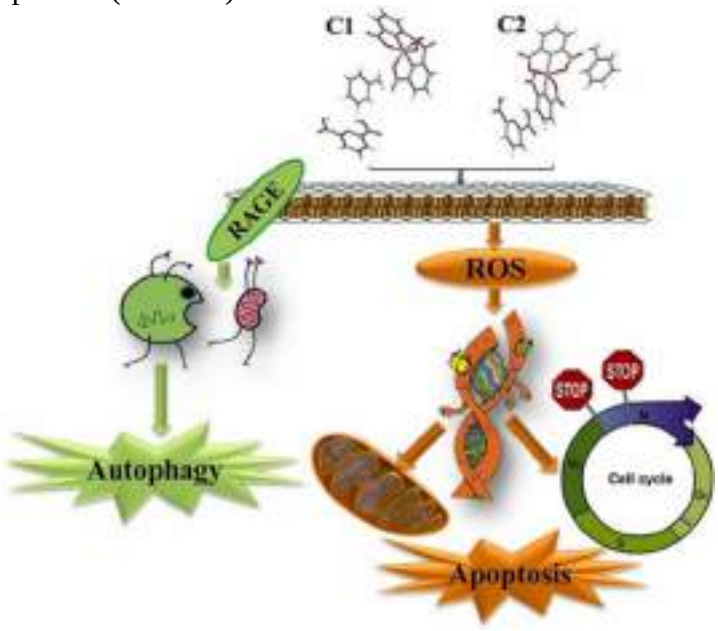

Single atom catalysis for renewable green applications

Esmail Doustkhah*

Koç University Tüpraş Energy Center (KUTEM), Department of Chemistry, Koç University, 34450, Istanbul, Turkey

H_2, as a fuel, could be the last resort for the production of sustainable energy sources. Nowadays, many efforts have been made to investigate catalytic and photocatalytic approaches to develop sustainable and economical processes for H_2 production. The utilization of nanomaterial architecture can be a rational solution for sustainable and efficient H_2 production in all these H_2 production approaches. Nanoarchitechture of materials can be obtained either by top-down or bottom-up synthesis approaches, such as templated materials synthesis. Chemically, nanomaterials for H_2 production can be nitrides, oxides, sulfides, carbides, and carbon-based. A fraction of these nanomaterials is naturally abundant, while others can be developed from abundant nanomaterials and precursors. In theory and sometimes in the experimental analysis, Nanostructures should possess a high surface area. However, they are usually unfavorably less active or inactive in the natural form. For example, in the case of layered materials, their interlayer nanospace and surfaces are inaccessible to catalytic reactions. As a result, these layered nanomaterials require additional post-modifications (e.g., exfoliation or functionalization) to invoke their great physio-chemical potentials in the photocatalytic/electrocatalytic/catalytic H_2 production. Single atom loading on layered materials is essential for green hydrogen generation as it enhances catalytic efficiency, minimizing resource consumption and pollution in the sustainable production of this clean energy source. Therefore, breakthroughs in competitive catalytic H_2 production mandates developing new layered nanomaterials and frameworks that supersede traditional layered nanomaterials' boundaries.

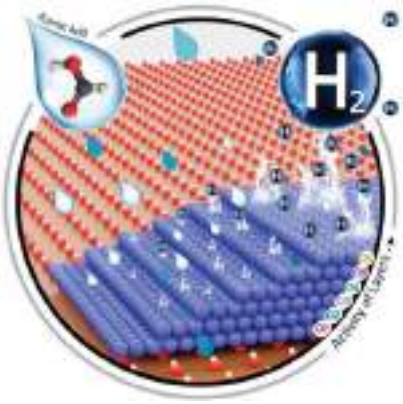

References

[1] Doustkhah, E., et al. "Pd Thickness Optimization on Silicate Sheets for Improving Catalytic Activity" *Adv. Mater. Interfaces, 2022, 10 (4), 2202368.*

[2] T. Ustunel, Y. Ide, S. Kaya, E. Doustkhah, Single-atom Sn-loaded exfoliated layered titanate revealing enhanced photocatalytic activity in hydrogen generation, *ACS Sust. Chem. Eng.*, 2022, 1, 3306-3315.

Microporous and mesoporous organic-inorganic hybrid nanoreactors for photo/catalysis aiming

Sadegh Rostamnia *

Organic and Nano Group (ONG), Department of Chemistry, Iran University of Science and Technology, Tehran 16846-13114, Iran. srostamnia@gmail.com & rostamnia@iust.ac.ir.

Keywords: Microporous, Mesoporous, Nanoreactors, Photo/catalysis.

Microporous nanomaterials such as metal-organic frameworks (MOFs) and covalent organic frameworks (COFs) are new class of porous nanostructures. These materials, as well as mesoporous materials such as SBA-15, can act a good host for the reaction of substrates with catalytic process. In this speech we try to discuss collect review on recent progress of these nanoporous catalyst for organic process. Herein we try to focuses on our achievement in catalyst preparation and organic reaction expanding. [1, 2]. Synthesis and post-synthesis of nanoporous materials and modification of that are our aim in this lecture. (**Scheme 1**).

Scheme 1: Nanoporous materials as the catalysis.

References

[1] Gholipour, B,; Shojaei, S.; Rostamnia, S.; Naimi-Jamal, M.R.; Kim, D.; Kavetskyy, T.; Nouruzi, N.; Jang, H.; Varma, R.; Shokouhimehr. M. Metal-free nanostructured catalysts: sustainable driving forces for organic transformations. *Green Chem.*, **2021**, 23, 6223-6272.

[2] Taghavi, R.; Rostamnia, S.; Farajzadeh, M.; Karimi-Maleh, H.; Wang, J.; Kim, D.; Jang, H.; Luque, R.; Varma, R.; Shokouhimehr. M. Magnetite Metal-Organic Frameworks: Applications in Environmental Remediation of Heavy Metals, Organic Contaminants, and Other Pollutants. *Inorg. Chem.* **2022**, 61, 15747-15783.

Materials Functionalization and Modification *via* Multicomponent Reactions and Their Applications in Shaabani's Research Group

Ahmad Shaabani*

Department of Organic Chemistry, Shahid Beheshti University, Daneshjou Boulevard Street, Tehran, 1983969411, Iran, a-shaabani@sbu.ac.ir

Keywords: Multicomponent reactions, Materials, Functionalization, Biomedical platform

Recently, the preparation of neoteric functional materials with multicomponent reactions strategy has interestingly enhanced the union of materials chemistry. The main components (amine, carboxylic, or carbonyl groups) of MCRs are usually present in the materials structure or can be easily announced on their surfaces. Hence, materials can contribute in MCRs for the greatly talented modified/functionalized materials synthesis.[1-3] In view of our interests in design of combinatorial MCRs and functionalization of nano-materials, in this MCR conference, the design and functionalization/modification of nano-materials and natural polymers with application in the catalytically chemical transformations and materials biomedical platform will be presented.

References

[1] S. Javanbakht, A. Shaabani, Multicomponent reactions-based modified/functionalized materials in the biomedical platforms, ACS Appl. Bio Mater., **2020**, 3, 156-174.
[2] R. Afshari, A. Shaabani, Materials functionalization with multicomponent reactions: state of the art, ACS Combinatorial Science, **2018**, 20 (9), 499-528.
[3] S. Javanbakht, T. Nasiriani, H. Farhid, M. T. Nazeri & A. Shaabani, Sustainable functionalization and modification of materials via multicomponent reactions in water, Frontiers of Chemical Science and Engineering, **2022**, 16, 1318–1344.

Synthesis of Novel Noscapinoids with Promising Anticancer Properties

Peyman Salehi*, Morteza Bararjanian, Zahra Davarzani, Faezeh Nemati, Maryam Mohebbi, Kosar Babanezhad Harikandei, Farzaneh Karimi, Zahra Hassanpour and Fatemeh Famarini

Department of Phytochemistry, Medicinal Plants and Drugs Research Institute, Shahid Beheshti University, Evin, 1983963113 Tehran, Iran, p-salehi@sbu.ac.ir

Keywords: Alkaloid, Anti-tumor activity, Natural product, Semi-synthesis, Cytotoxicity

Noscapine, an alkaloid originally found in *Papaver somniferum*, has gained approval from the Food and Drug Administration (FDA) as a cough suppressant. It has attracted significant attention due to its notable anticancer properties associated with low toxicity. Moreover, multiple pieces of evidence have substantiated the efficacy of noscapine and its derivatives against various cell lines. Our research group, has successfully synthesized a wide range of noscapine derivatives that exhibit remarkable cytotoxicity and outstanding anti-tumor activity [1,2]. Most of these compounds have been obtained through modification of C-6 position of noscapine (**Scheme**) which involves the attachment of a 1,2,3-triazole ring as well as creating a propargylamine group through an A^3-coupling reaction. Furthermore, amino acid conjugation, attachment of a β-amino carbonyl group through Mannich reaction and bile acid conjugation have also been employed.

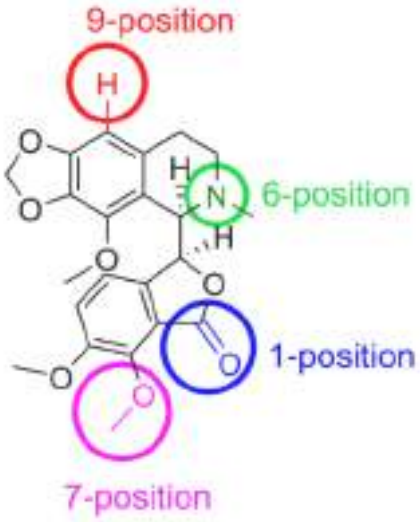

Scheme: Noscapine and its modification sites.

References

1. Nemati, F., Salehi, P., Bararjanian, M., Hadian, N., Mohebbi, M., Lauro, G., Ruggiero, D., Terracciano, S., Bifulco, G., Bruno, I.: Discovery of noscapine derivatives as potential β-tubulin inhibitors. *Bioorg. Med. Chem. Lett*. 30, 127489 (2020).

2. Nemati, F., Bischoff-Kont, I., Salehi, P., Nejad-Ebrahimi, S., Mohebbi, M., Bararjanian, M., Hadian, N., Hassanpour, Z., Jung, Y., Schaerlaekens, S., Lucena-Agell, D., Oliva, M.A., Fürst, R., Nasiri, H.R., Identification of novel anti-cancer agents by the synthesis and cellular screening of a noscapine-based library. *Bioorg. Chem*. 115, 105135, (2021).

Nitroepoxides as efficient intermediates in Organic Synthesis

Azim Ziyaei Halimehjani*

Department of Chemistry, Sharif University of Technology, P. O. Box 11155-9516, Tehran, Iran, azim.ziyaei@sharif.edu

Keywords: Nitroepoxides, Biselectrophile, *N*,*S*-nucleophiles , Heterocyclic compounds

Nitroepoxides have attracted the attention of organic chemists in recent years because of their unique and interesting reactivity in organic transformations. These molecules have particular characteristics including two potential vicinal electrophilic centers which makes them as efficient *mono*- and *bis*-electrophiles for the synthesis of various *N*,*N*- and *N*,*S*-heterocycles and substituted phenyl-2-propanone (P2P) derivatives [1]. In this presentation, I will talk about the recent advances on the application of nitroepoxides as synthetic intermediates for the synthesis of heterocyclic and α-functionalized carbonyl compounds developed by my research group during the years 2017-2023 [2] (**Scheme**).

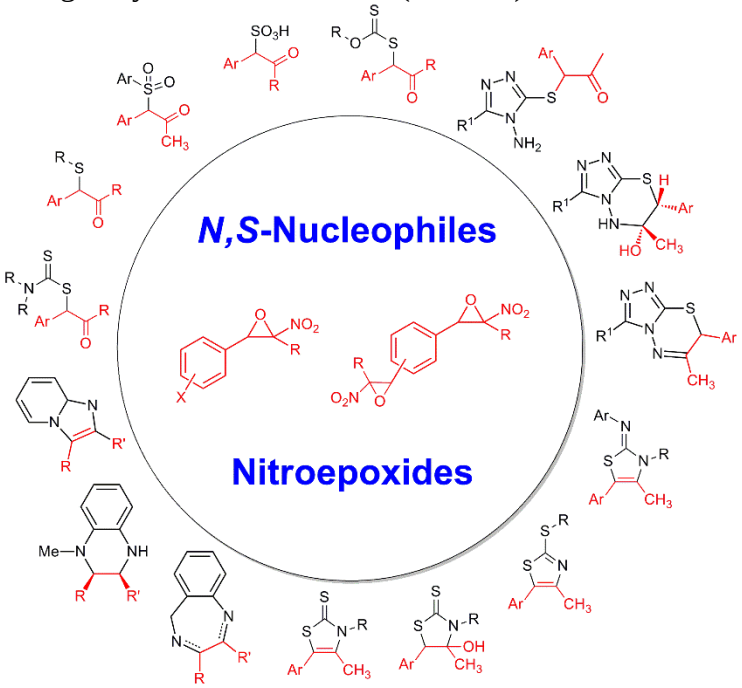

Scheme: nitroepoxides in organic synthesis.

References

[1] (a) Guo, X.; Chen, W.; Chen, B.; Huang, W.; Qi, W.; Zhang, G.; Yu, Y. *Org. Lett*. **2015**, *17*, 1157-1159. (b) Guo, X.; Shao, J.; Liu, H.; Chen, B.; Chen, W.; Yu, Y. *RSC Adv.* **2015**, *5*, 51559-51562. (c) Vidal-Albalat, A.; Rodríguez, S.; González, F. V. *Org. Lett.* **2014**, *16*, 1752-1755. (d) Ibrahim, M. M.; Grau, D.; Hample, F.; Tsogoeva, S. B. *Eur. J. Org. Chem.* **2014**, 1401-1405

[2] (a) Badali, E.; Rahimzadeh, H.; Sharifi, A.; Habibi, A.; Halimehjani, A. Z. *Org. Biomol. Chem*. **2020**, *18*, 4983-4987. (b) Ziyaei Halimehjani, A.; Lotfi Nosood, Y. *Org. Lett*. **2017**, *19*, 6748-6751 and others.

Organic Linker Functionalization and Mechano-synthesis of Metal-Organic Frameworks

Ali Morsali *

Department of Chemistry, Faculty of Sciences, Tarbiat Modares University, P.O. Box 14115-4838, Tehran, Iran, morsali_a@modares.ac.ir

Keywords: Metal-organic framework, Solvothermal methods, solid-state reaction

Metal-organic frameworks are built from metal ions or metal clusters linked together by organic ligands. A key characteristic of MOFs should be their crystallinity for structure determination together with proven (micro-)porosity. An important feature of MOFs over other porous materials such as zeolites and porous carbons is the ability to widely design the physiochemical inner surface properties, and thereby establish a large variety in topologies and structures by the deliberate design and selection of organic and inorganic molecular building blocks. Despite of the impressive progress in MOFs synthesis via conventional solvothermal methods, the large-scaled production of these materials is limited due to the non-green, non-economic and complex synthesis routs. Applying the mechanical force to perform a solid-state reaction is a multipurpose greener alternative to conventional synthetic methods, leading to a fast, scalable, energy-efficient, and environmentally-friendly processes which are necessary for development of commercialization processes as well as providing the more possibility to control over the topology and dimensionality of MOF assemblies. This presentation provides an overview on recent advances on organic linker functionalization and MOFs synthesis via mechanochemical methods highlighting the synthetic challenges as well as the advantageous of mechanochemical synthesis methods. The underlying mechanisms and the characterization methods are also discussed. Based on the important aspects in the fabrication of MOFs assemblies this presentation provides a remarkable information for a wide range of chemists, scientists and engineers.

References

[1] F. Afshariazar, A. Morsali, The unique opportunities of mechanosynthesis in green and scalable fabrication of metal–organic frameworks, *J. Mater. Chem. A* 10 (2022), 15332-15369.

Electrochemistry as an environmentally friendly tool in organic synthesis

Davood Nematollahi*

Faculty of Chemistry, Bu-Ali-Sina University, Hamedan 65174-38683, Iran

Keywords: Electrosynthesis, Green chemistry

Organic electrosynthesis is a method that can fulfil several important environmental problems caused by conventional methods of organic synthesis. There are several features of electrosynthesis that are often cited as being environmentally favourable. Electrons are considered to be clean reagents to effect on oxidation and reduction reactions that under usual circumstances, require potentially polluting metal based reagents. Such procedures have considerable waste streams which require downstream remediation. In addition, electrosynthesis is characterized by high selectivity, good atom economy, readily available starting materials, low-temperature and energy consumption, low costs for reagents and material failure. Furthermore, the electrodes may be regarded as heterogeneous catalysts that are easily separated from the products. So, it can be concluded that, electrosynthesis is a green tool for organic synthesis. The results have shown that at least 11 of the 12 principles of green or sustainable chemistry are implemented in organic electrosynthesis [1].

References

[1] Frontana-Uribe, B. A.; Little, R. D.; Ibanez, J. G.; Palma, A.; Vasquez-Medrano, R. Organic electrosynthesis: A promising green methodology in organic chemistry. *Green Chem.* 2010, *12*, 2099-2119.

Organic Electrochemistry: *Electrifying Synthesis*

Issa Yavari * **and Sina Shaabanzadeh**

Department of Chemistry, Tarbiat Modares University, P.O. Box 14115-175, Tehran, Iran, yavarisa@modares.ac.ir

Keywords: Electrochemistry, *β*-ketonitriles, Hydrazone

Electrochemistry has been used as a tool to drive chemical reactions for over two centuries. With the help of an electrode and a power source, infinite redox range renders electrochemistry capable of oxidizing or reducing some of the most tenacious compounds. A control over the electrode potential allows for the chemo selective differentiation of functional groups with minute differences in potential. These features make electrochemistry an attractive technique for the discovery of new modes of reactivity and transformations that are not readily accessible with chemical reagents alone. Indeed, many of the largest industrial synthetic chemical processes are achieved in a practical way using electrons as a reagent.

We wish to discuss examples of our recent studies in electrochemical synthesis of *β*-ketonitriles,[1a] *β*-ketosulfones,[1b] hydrazones,[1c] cyclobutanes,[1d] and 3*H*-1,2,4-triazol-3-ones.[1e] Various features of these electrochemical transformation will be presented and discussed.

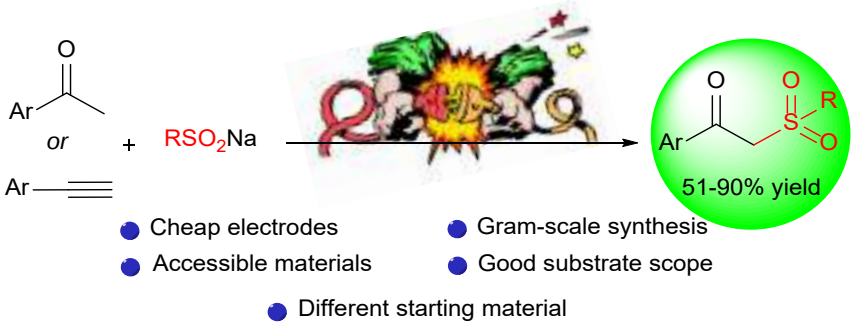

References

[1] a) I. Yavari, S. Shaabanzadeh, S. Sheikhi, *ChemistrySelect* **2020**, 5, 564-568; b) I. Yavari, S. Shaabanzadeh, *Org. Lett.* **2020**, *22*, 464−467; c) I. Yavari, S. Shaabanzadeh, *J. Org. Chem.* **2022**, *87*, 15077-15085; d) I. Yavari, S. Shaabanzadeh, *J. Org. Chem.* **2023**, *88*, 9257−9264; e) I. Yavari, S. Shaabanzadeh, F. Golmoradi, *ChemistrySelect* **2023**, *8*, e202302673.

Synthesis and catalytic application of magnetic metal ferrite nanoparticles in organic reactions

Firouz Matloubi Moghaddam*

Laboratory of Organic Synthesis and Natural Products, Department of Chemistry, Sharif University of Technology, Azadi Street, PO Box 111559516, Tehran, Iran, matloubi@sharif.edu.

Keywords: Bimetallic nanoparticles, Spinel oxides, Ferrites, Coupling reactions

Bimetallic nanoparticles are a class of nanomaterials with new physical and chemical properties resulting from synergistic effects between the two metals. MFe_2O_4, where M is a divalent transition metal, is the formula of one important family of these bimetallic compounds called metal ferrites. These structures crystallize in the spinel form showing superparamagnetic properties originating from the moment of antiparallel spines between ferric ions at tetrahedral sites and M^{2+} ions at octahedral sites. Ferrites used in catalytic applications are generally synthesized by low temperature co-precipitation methods. Further, co-precipitation methods generate Bronsted acid sites in different cationic environment in addition to Lewis sites, which makes the catalyst active and effective for many organic transformations such as aromatic alkylation, acylation, etc. During the last couple of years, application of different types of these magnetic catalysts has shown in various organic transformations by our group [1-2].

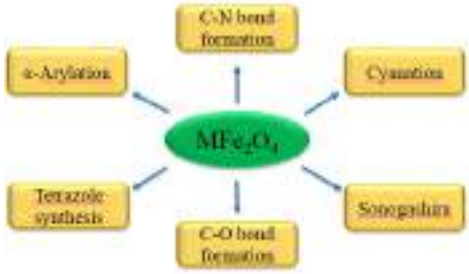

References:

1 F. M. Moghaddam, R. Pourkaveh, M. Ahangarpour, Nano $CoCuFe_2O_4$ catalyzed coupling reaction of acid chlorides with terminal alkynes: A powerful toolbox for palladium-free ynone synthesis. *Catal. Commun.*, 2017, 102, 71-75.

2 F. M. Moghaddam, R. Pourkaveh, Nano cobalt ferrite catalyzed coupling reaction of nitroarene and alkyl halide: An odorless and ligand-free rout to unsymmetrical thioether synthesis. *Catal. Commun*., 2017, 94, 33-37.

29TH IRANIAN ORGANIC CHEMISTRY CONFERENCE
1_3 NOV, 2023
UNIVERSITY OF QOM, IRAN

Evaluating the Mixing Progress in the Compounding of a rubber mixture

Somayyeh Mohammadian-Gezaz, Abbas Khoshhal*

Department of Chemical Engineering, Payame noor University, Tehran, Iran, P. O. Box. 19395-3697.
s.mohammadian@pnu.ac.ir

Abstract

The effect of mixing time on the viscoelastic properties of the tire tread compound was investigated by RPA and the obtained data were compared with the torque variations during mixing. The results showed that changes in the shear elastic modulus (G') were similar to the torque behavior in the internal mixer before and after Black Incorporation Time.

1. Introduction

The aim of mixing process is to produce a homogenate compound that has the uniform dispersion of ingredients to give the required properties for the application. There are four physical steps during the mixing cycle: incorporation, dispersion, distribution, and plasticization [1,2]. In this work, dispersion of carbon black in a SBR compound at various steps of mixing was studied using disperse grader images. Quality of mixing was investigated by measuring G' via RPA and the results compared with the torque variations during mixing.

2. Experimental

The master formulation of a tire tread compound based on styrene-butadiene rubber (table (1)) was mixed using the internal mixer (SYS 90HIB, HAAKE Co.) at 100 °C and 40 rpm. A Rubber Process Analyzer (RPA) is a torsional dynamic instrument to test the rheological behavior of the gum and rubber compounds which consists a biconical geometery [3, 4]. Frequency sweep tests were performed at 1%, 100 °C using RPA2000, Alpha Co.. The photographs of compounds were taken by Disperse Grader (DisperGrader 1000NT) at the magnification of 100 times.

Table **1**- Master formulation of compound.

Ingredients	Phr	Supplier Co.
SBR 1500	37	BIPC
SBR 1712	86.6	BIPC
Black N115	15	Doodeh Pars
Black N375	63	Doodeh Pars
ZnO	3.1	Rangineh Pars
Stearic Acid	2.5	Unichema Int.
Wax	1.25	Unichema Int.
6PPD	1.25	Bayer
Aromatic Oil	14	Behran Oil

3. Results and Discussion

Fig (1) expresses the torque time curve of the mixer schematically and fig (2) shows the photographs of carbon black dispersion (as the white particles) at several mixing times which is related to the marked points of fig (1). As the photographs show, for mixing times larger than BIT (C, D and E) dispersity is improved and with increasing the mixing time, distribution of carbon black was progressed. As expected, deformation of elastomer and breaking down into the small pieces and finally dispersion are taken place during the BIT and then, carbon black distribution in the rubber is begun. At the end of the BIT, torque reaches a maximum value and then decreases gradually until it gets a plateau. The agglomorates of carbon black is clearly observed in image (2A). With increasing the mixing time these agglomorates are broken down and wetting occurs. In the final photograph, a good dispersion of carbon black in the rubber matrix can be seen.

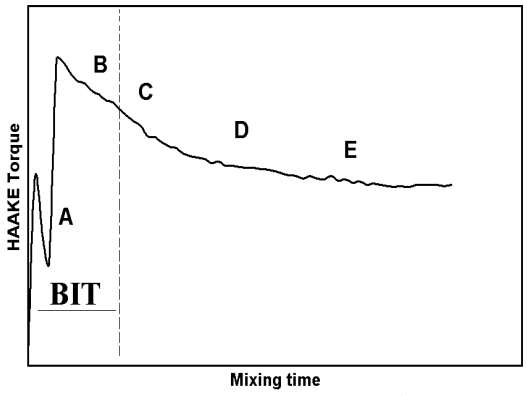

Fig **1** - Schematic torque-time curve of mixer.

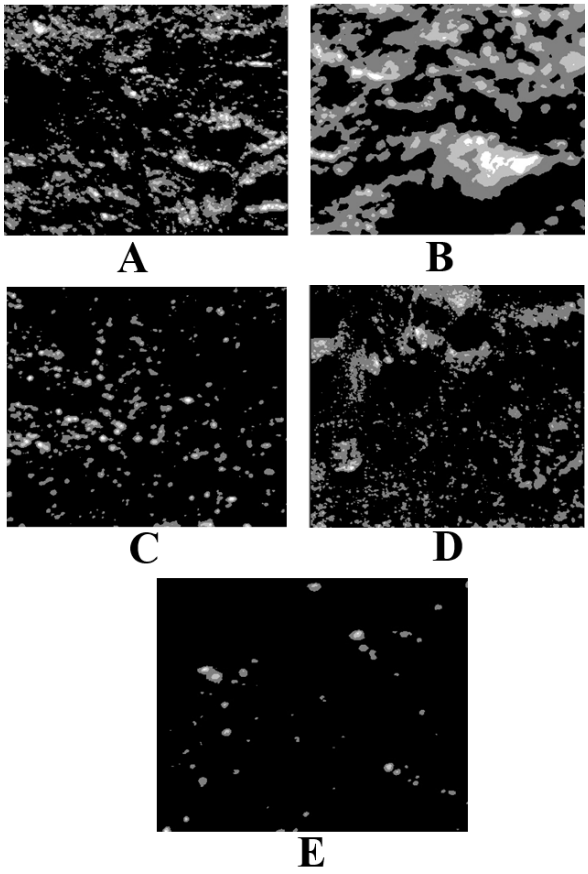

Fig **2** - Photographs of sample at mixing intervals.

The complex dynamic shear modulus (G*) devided to the elastic (G') and viscous modulus (G") by the equetion (1).

$$G^* = \sqrt{(G'^2 + G''^2)} \qquad (1)$$

Fig (3) shows the variation of G' against mixing time at the constant frequency of 1 rad/sec. First, G' curve shows two maximums and then decreases and reaches a plateau or constant value. This curve has a interest similarity to the torque curve versus mixing time during mixing. In fact, elastic modulus is an effective factor on the required shear force for mixing. Thus it is expected that the measured torque and the elastic modulus have the same behavior with mixing time.

Fig (4) expresses the influence of mixing time on the elastic modulus at different frequencies. Regarding to fig (3), to compare the mixing time effect, larger frequencies data selected to draw fig (4). This graph exhibits the same trend of G' variation such as figure (3) for all frequencies.

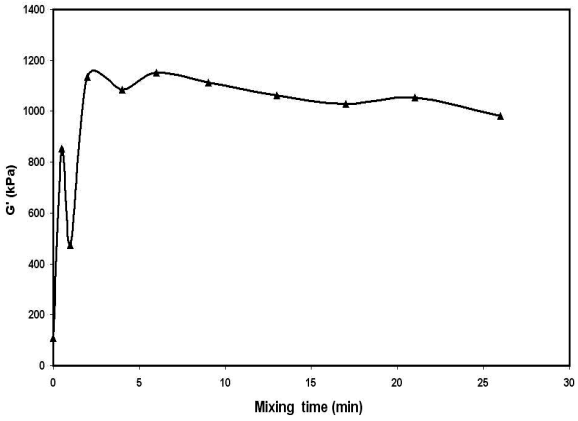

Fig **3** – G' versus mixing time at frequency of 1 rad/sec.

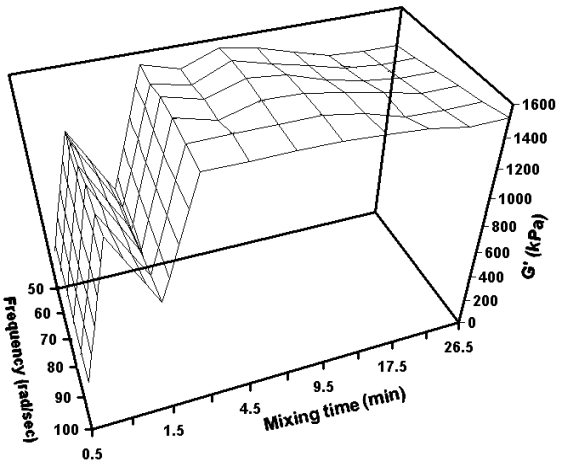

Fig **4**– G' versus mixing time at different frequencies.

4. Conclusion

Samples were prepared at several mixing times. Disperse Grader photographs obviously recognized the different steps of mixing and the influence of mixing time on carbon black dispersion. The results of frequency sweep tests from RPA were compared with the torque-time curve of the internal mixer during mixing. The elastic modulus versus mixing time, at first showed two peaks and after passing the BIT decreased and reached a plateau. This variation is similar to the torque behavior of the internal mixer during mixing.

4. References

[1] N.P. Cheremisinoff, Encyclopedia of fluid mechanics, Polymer flow Engineering, Gulf Pub. Co., 1st ed., 1990.
[2] S. Mohammadian-Gezaz, and M. Karrabi, J. Prog. in Rub. Plas. and Rec. Tech.33 (2017) 261-280.
[3] S. Mohammadian-Gezaz, and M. Karrabi, J. Rubb. Res. 20 (2017) 20-32.
[4] M. Barghamadi, M. Karrabi, M.H.R. Ghoreishy and S. Mohammadian-Gezaz, J.Appl. Polym. Sci. 136 (2019) 1-14.

29TH IRANIAN ORGANIC CHEMISTRY CONFERENCE
1_3 NOV, 2023
UNIVERSITY OF QOM, IRAN

Synthesis of 4H-benzo[h]chromene three-component derivatives in the presence of efficient DFNS/Ag nanocatalyst.

Fatemeh Amarloo[1], *Rahele Zhiani*[*1,2], *Alireza Motavalizadehkakhky*[1,3] *and Malihesadat Hosseiny*[1]

[1]*Department of Chemistry, Neyshabur Branch, Islamic Azad University, Neyshabur, Iran, fatemehamarloo@yahoo.com*
[2]*New Materials Technology and Processing Research Center, Department of Chemistry, Neyshabur Branch, Islamic Azad University, Neyshabur, Iran, r_zhiani2006@yahoo.com*
[3]*Advanced Research Center for Chemistry, Biochemistry & Nanomaterial; Neyshabur Branch, Islamic Azad University, Neyshabur, Iran.*

Abstract - Chromenes are very important due to many industrial, pharmaceutical and biological uses. 4H-benzo[h]chromene reaction is one pot multistep reaction. The aim of this research is the synthesis of Ag nanoparticles supported on dendritic fibrous nanosilica (DFNS/Ag) and the synthesis of 4H-benzo[h]chromene derivatives in the presence of DFNS/Ag nano catalyst. Also, the reaction of 4H-benzo[h]chromene was investigated at different temperatures, the amount of catalyst and different solvents. The results showed that the reaction of 4H-benzo[h]chromene in ethanol solvent, temperature of 75°C and 0.03 g of catalyst had the best efficiency. DFNS/Ag catalyst has a high and efficient contact surface due to its dandelion shape.

1. Introduction

When materials are brought to the nanoscale, many of their properties change, properties such as electrical, optical, magnetic properties, etc., and the appearance of the following three characteristics are also among these changes: very small size, very high surface-to-volume ratio, and increasing the number of atoms on the surface. These three factors are the most important reasons for the emergence of catalytic properties in nanomaterial [1-3]. Nanoparticles have a very high surface energy and are highly active, and it is said that the surface atoms are in a physically unstable and chemically active state and are prone to many chemical reactions. Today, catalysts are widely used in the production of chemicals, pharmaceuticals, etc. The use of nanomaterial in the preparation of nanocatalysts has increased widely. Also, many important reactions are catalyzed by nanomaterial, and these nanocatalysts increase product production efficiency dramatically. Even nano catalysts play an important role in accelerating the reaction [4-6]. A heterogeneous catalyst is not in the same phase as the reactants. The size and characteristics of the heterogeneous catalyst particles are so that they are not easily dissolved in the reaction medium; Therefore, its activity is limited (the overall yield of the reaction decreases). Unlike homogeneous catalysts, heterogeneous catalysts are easily separated from the reaction mixture (with less cost, time and materials) and do not cause impurities in the products [7-10]. In order to compensate for the lack of active surface in such compounds, it is necessary to use a substrate as a catalyst support. The substrate is usually a porous structure with a high active surface [11]. Multicomponent reactions are a useful method to obtain small molecules with diverse structures are, which have been considered economically and practically. In this type of reactions, from the condensation of three or more reactive compounds, products are formed at the same time, which include the main parts of all raw materials [12-14]. One of the important multicomponent reactions is the synthesis of chromium derivatives, which have attracted a lot of attention due to their different chemical and biological properties. Compounds with this ring system have various medicinal applications [15, 16]. In this study, DFNS/Ag heterogeneous nanocatalysis was synthesized. Its effect on the reaction performance of 4H-benzo[h]chromene and the optimal conditions were investigated. This catalyst is easily recovered and reused several times.

Synthesis of DFNS/Ag NPs [17]: 1- Solution number 1: add 0.3 grams of urea to 30 ml of water and put it in the ultrasonic for one hour. Solution number 2: We dissolve one gram of acetylpyridinium bromide (CPB) in 30 ml of cyclohexane and add 1.5 ml of 1-pentanol. Then we add solution number 1 to solution number 2 and then slowly add 2.5 grams of tetraethyl orthosilicate (TEOS) and place it on stirrer for one hour and then reflux for 5 hours and then centrifuge. We wash the sediment obtained with water and acetone and put it in the oven to dry.

2- DFNS (1 g) and 0.2 g of APTES were mixed in toluene (100 ml) and diluted by heating for 12 hours

in a nitrogen environment. Thus, it was centrifuged, washed with ethanol and finally dried under vacuum.
3- H_2N-DFNS (0.5 g) was ultrasonically dispersed in H_2O (50 mL) and then 0.1 g $AgNO_3$ was added. After about 30 minutes, some $NaBH_4$ solution was added drop wise. Then it was centrifuged and finally dried at 60°C.
Synthesis of 4H-benzo[h]chromene: 1 mmol of aromatic aldehyde was added to 5 ml of solvent, and then 1mmol of 1-naphthol was added along with 1mmol of malononitrile and 0.05 of the catalyst. It was placed in an oil bath with a temperature of 75 °C. The reaction was checked for completion by TLC (Scheme 1).

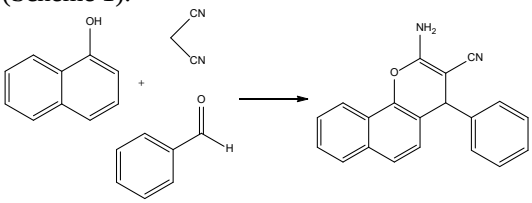

Scheme 1. 4H-benzo[h]chromene reaction

2. Results and Discussion

Morphology and sizes of DFNS/Ag nanocatalyst were determined using SEM. Nanoparticles have been synthesized uniformly. DFNS/Ag nanoparticles contain spheres of uniform size and show wrinkled radial structure. Nanoparticles have been synthesized as a uniform fabric (Fig. 1).

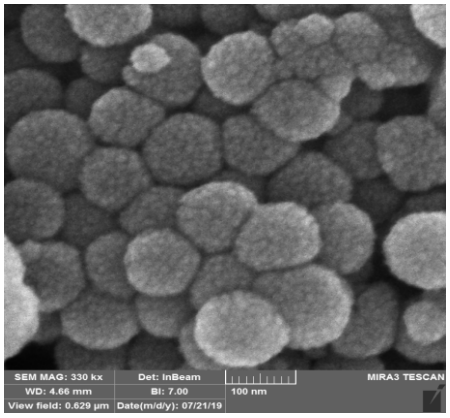

Fig. 1. SEM images of DFNS/Ag

In order to obtain suitable conditions for the reaction of 4H-benzo[h]chromene, different temperature values, the amount of catalyst and different solvents were investigated.
The reaction of 4H-benzo[h]chromene was investigated at different temperatures (Fig. 2).
In order to optimize the temperature, the reaction of 4H-benzo[h]chromene was investigated at different temperatures, and the efficiency increases with increasing temperature, and the best temperature for this reaction is 75°C.

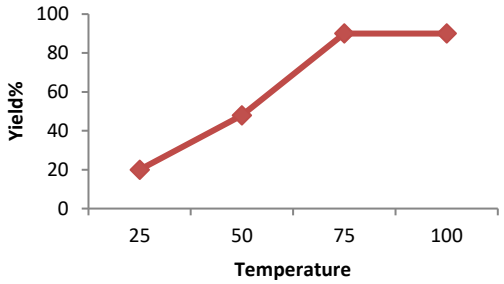

Fig. 2. Optimizing the reaction temperature of 4H-benzo[h]chromene in the presence of DFNS/Ag catalyst

The reaction of 4H-benzo[h]chromene was investigated with different amounts of DFNS/Ag catalyst, and the efficiency increased with the increase of the amount of catalyst. The best amount of catalyst is 0.03g, which did not have a positive effect on the reaction process more than 0.03g. 4H-benzo[h]chromene reaction has 15% efficiency in the condition without catalyst (Fig. 3).

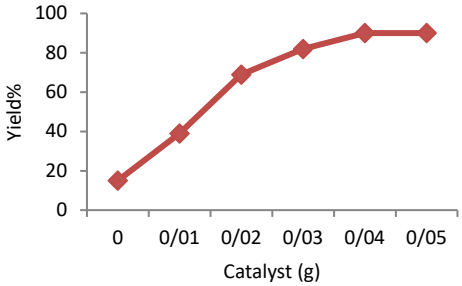

Fig. 3. The reaction of 4H-benzo[h]chromene with different amounts of DFNS/Ag catalyst

The reaction of 4H-benzo[h]chromene was investigated in ethanol, water, methanol, DMSO, THF, water/ethanol solvents. The best solvent for the reaction of 4H-benzo[h]chromene ethanol, which has 90% efficiency in less time. The reaction of 4H-benzo[h]chromene in solvent-free conditions has 52% product (Fig. 4).

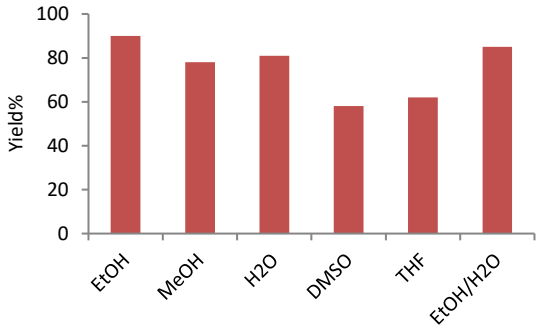

Fig. 4. 4H-benzo[h]chromene reaction in different solvents

The reaction of 4H-benzo[h]chromene was investigated in the presence of various aldehyde derivatives. After optimizing the test conditions, for

the general study of this method, the reactivity of different types of aromatic aldehydes, malonitrile and 1-naphthol was investigated and the results It was observed in (Table 1) that aromatic aldehydes containing two electron-absorbing and electron-donating groups reacted successfully within one hour, and 78 to 90% were related to 4H-benzo[h]chromene reaction derivatives, respectively.

Table 1- Different aldehyde derivatives in the presence of DFNS/Ag catalyst

Entry	Ar-X	Product	Yield (%)
1	4-OMe	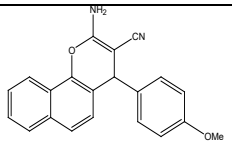	78
2	4-NO_2	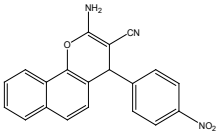	86
3	4-Cl	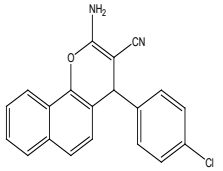	90

3.Conclusion

Nanocatalysts significantly increase the speed of reactions due to the size of the particles and the large accessible surface. In this research, the reaction of 4H-benzo[h]chromene was synthesized in the presence of DFNS/Ag nanocatalyst and had a good yield. Also, the reaction in the presence of ethanol solvent and 4-Clrobenzaldehyde substrate had a high performance compared to other derivatives. The results show that the DFNS/Ag nanocatalyst performs the 4H-benzo[h]chromene reaction with high efficiency and short duration due to its high active surface and excellent selectivity.

4. References

[1] L. Fan, J. Wang, X. Zhang, S. M. Sadeghzadeh, R. Zhiani, M. Shahroudi, F. Amarloo, Catalysis Letters. 149 (2019) 3465.

[2] R. Zhiani, A. Es-haghi, F. Shamsa, F. Amarloo, M. Shahroudi, S. M. Sadeghzadeh. Silicon. 12 (2020) 2005-2015.

[3] S. Wang, C. Xi, Chem. Soc. Rev. 48(2019) 382-404.

[4] L. Sun, J.H. Ye, W.J. Zhou, X. Zeng, D.G. Yu, Org. Lett. 20 (2018) 3049-3052.

[5] L. Zhu, J.H. Ye, M. Duan, X. Qi, D.G. Yu, R. Bai, Y. Lan, Org. Chem. Front. 5(2018)633-639.

[6] R. Yousefi, T.J. Struble, J.L. Payne, M. Vishe, N.D. Schley, J.N. Johnston, J. Am. Chem. Soc. 141(2019) 618-625.

[7] Z. Zhang, T. Ju, J.H. Ye, D.G. Yu, Synlett. 28 (2017) 741.

[8] L. Song, Y.X. Jiang, Z. Zhang, Y.Y. Gui, X.Y. Zhou, D.G. Yu, Chem. Commun. 56 (2020) 8355-8367.

[9] T.B. Nguyen, Adv. Synth. Catal. 359 (2017) 1066-1130.

[10] T.B. Nguyen, Asian J. Org. Chem. 6 (2017) 477.

[11] H. Xie, J. Cai, Z. Wang, H. Huang, G.J. Deng, Org. Lett. 18 (2016) 2196-2199.

[12] H. Chen, P. Li, R. Qin, H. Yan, G. Li, H. Huang, ACS Omega. 5 (2020) 9614.

[13] M. Hulla, M.A. Chamam, G. Laurenczy, S. Das, P.J. Dyson, Angewandte Chemie International Edition. 56 (2017) 10559.

[14] J. Gao, L. He, C. Miao, S. Chanfreau, Tetrahedron. 66 (2018) 4063.

[15] A. M. El-Agrody , A. H. Halawa, A. M. Fouda, A. M. Al-Dies, J. Saudi Chem. Soc. 21(2017) 82-90.

[16] M. J. Mendoza-Castro, N. Linares, J. García-Martínez, Catal. Today, 419 (2023) 114152.

[17] C. Hongtao, C. Jiaqi, Y. Dong, Y. Miao, L. Qing and Z. Jingru, RSC Adv. 11 (2021) 13446-13457.

The effect of nano layered silicate on the linear viscoelastic region of Styrene Butadiene Rubber nanocomposites

*Somayyeh Mohammadian-Gezaz**

Department of Chemical Engineering, Payame noor University, Tehran, Iran, P. O. Box. 19395-3697.
s.mohammadian@pnu.ac.ir

Abstract

This paper considers the rheological behaviour of Styrene Butadiene Rubber (SBR) compounds filled with various nano clay concentrations. Compounds having different levels of nano clay were prepared and the dispersion and the strain dependency of SBR nanocomposite were examined. Desirable dispersion in samples was achieved and the results showed that the viscoelastic properties have been affected strongly by the nano filler content. As the nano clay amount increased in compounds, the linear viscoelastic region became shorter, the elastic modulus increased, and critical strain decreased. At higher nano clay content, higher tan δ was observed.

1. Introduction

Many attempts have been made to the description of the enhancement of the properties by incorporation of nano filler into the polymers [1–2], especially for the rubber-organoclay nano composites. Since the rheological behavior has a vital role in designing processing apparatus, basic understanding of rheological melt properties is necessary. It is well known that the rheological property is depended to morphology of the compound. Some efforts have been done to correlate the viscoelastic properties to the morphology in elastomeric compounds [3-4]. Depending to polymer matrix, type and concentration of nano filler, different morphologies can be obtained in rubber based nanocomposite which can affected the obtained properties. The main objective of this study is to investigate the strain dependency of SBR nanocomposite. Compounds having different levels of nano clay were prepared and the dispersion in nanocomposite and the rheology were examined.

2. Experimental

The information about materials and formulations of samples have been depicted in table (1). Compounding was carried out in HAAKE internal mixer (SYS 90, USA) with a Banbury blade, at mixing times of 12 minutes and temperature of 100ºC. Wide-angle X-ray diffraction (XRD) measurements were done at room temperature on a D5000, Siemens, Germany. The rheological properties were determined by a rubber processing analyzer (RPA 2000) using strain sweep tests at temperature of 50°C, Strain of 1-100% and frequency of 1.68 Hz
.

Table **1**. Materials used in this study

Material	Supplier	Amount
SBR	SBR1500 (Bandar Imam Co.)	100 phr
nanoclay	Cloisite 10A Southern Clay, TX, USA	varied
zinc oxide	Rangineh Pars	5 phr
Stearic Acid	Unichema int.	1.5 phr
Sulfur	Rangineh Pars	1.5 phr
CBS	Bayer	1.5 phr

3. Results and Discussion

Table (2) shows XRD results for various nano clay levels. The peak of organoclay at 2ɵ=4.59° corresponds to1.952 nm inter gallery distance. While in nanocomposites, diffraction peak shifts to the lower 2ɵ values, because of dispersion process; the peak of organoclay is weaker and the distance between layers is greater.

Table **2**. XRD results

Nano amount (phr)	2θ (º)	d (A)
3	1.3	67.7
6	2.1	42.2
9	2.8	31.1
Pure NanoClay	4.59	19.2

Dynamic mechanical properties of compounds were investigated by the strain sweep tests using RPA. Figure (1) give the changes in elastic modulus (G') of compounds against the strain. As can be seen, firstly, there is a region where the elastic modulus is independent of shear strain, which is named the linear viscoelastic region (LVER). As the nano clay amount increases in compounds, the linear viscoelastic region becomes shorter and the elastic modulus increases. At higher nano filler loading, G' is more sensitive to the shear strain. The fall of the G' curve after the linear viscoelastic region (LVER) is due to the breakdown of the filler-rubber networks, and the amount of formed networks is more at higher nano clay content. In all cases, linear viscoelastic behaviour of

compounds corresponds to an elastic modulus independent to deformation which can be observed at small amplitudes.

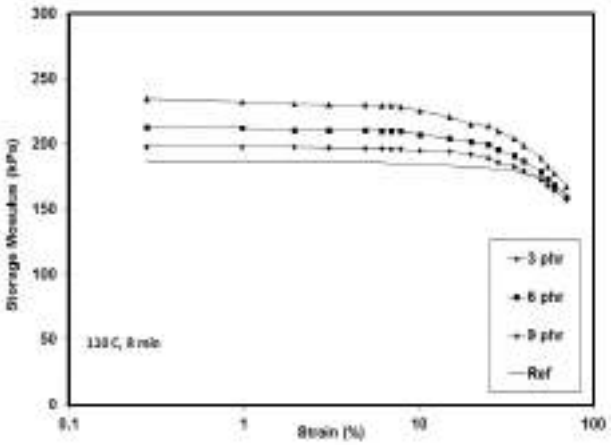

Fig. **1**. Elastic modulus (G') of compounds versus strain

Figure (2) shows the strain of linear viscoelastic zone (critical strain) and the modulus at the plateau (initial modulus) calculated from strain sweep curves. As mentioned, with increasing nano clay critical strain decreases, and the modulus increases.

The curves of damping factor (tan δ) versus strain are shown in figure (3). Tan δ is the ratio of the viscous modulus (G") to the elastic modulus (G'). The elastic modulus is related to the filler-rubber network which falls with increasing shear strain, while the viscous modulus is attributed to the dissipated energy during the deformation, for example with the molecular slippage, increasing by strain. As the shear strain increases, networks are destructed, and molecular slippage becomes greater, therefore, tan δ rises. That is more obvious at higher nano clay content, so tan δ increases slightly with increasing the content.

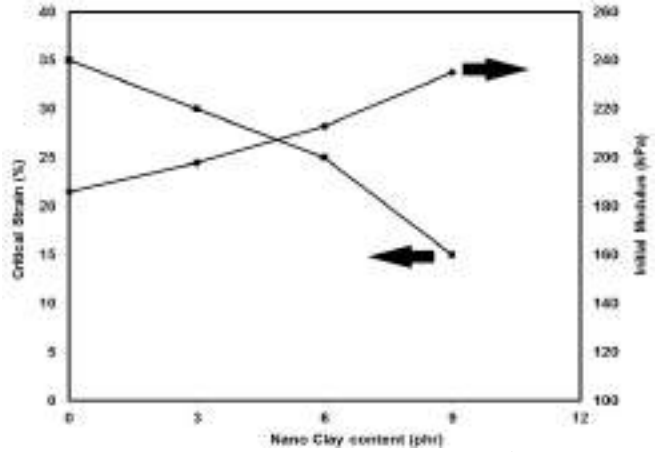

Fig. **2**. Critical strain and initial modulus versus nano filler content

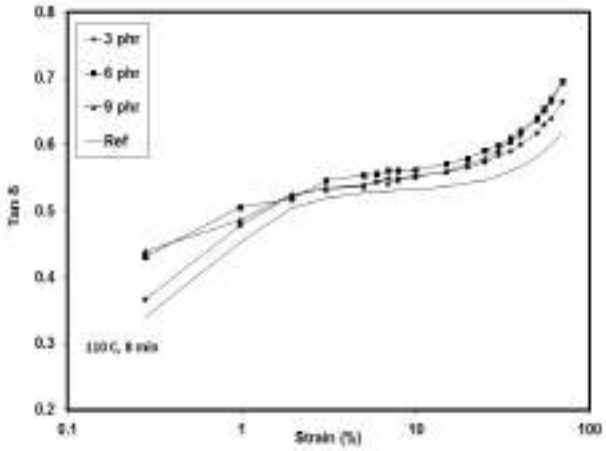

Fig. **3**. Damping factor (tan δ) of compounds versus strain

4. Conclusion

1. In nanocomposites, diffraction peak shifted to the lower 2ɵ values and the distance between layers was greater.
2. As the nano clay amount increased in compounds, the linear viscoelastic region became shorter, the elastic modulus increased, and critical strain decreased.
3. At higher organoclay content, higher tan δ was observed.

4. References

[1] S. Mohammadian-Gezaz, and M. Karrabi, J. Prog. in Rub. Plas. and Rec. Tech.33 (2017) 261-280.
[2] S. Mohammadian-Gezaz, and M. Karrabi, J. Rubb. Res. 20 (2017) 20-32.
[3] M. Karrabi and S. Mohammadian-Gezaz, Iranian Polymer Journal 2011, 20, 15-27.
[4] M. Barghamadi, M. Karrabi, M.H.R. Ghoreishy and S. Mohammadian-Gezaz, J.Appl. Polym. Sci. 136 (2019) 1-14.

29TH IRANIAN ORGANIC CHEMISTRY CONFERENCE
1_3 NOV, 2023
UNIVERSITY OF QOM, IRAN

Synthesis of $FeNi_3/SiO_2/Cu$ Recyclable Nanocatalyst and its Performance on Suzuki Reaction.

Fatemeh Amarloo[1], *Rahele Zhiani*[*1,2], *Alireza Motavalizadehkakhky*[1,3] *and Malihesadat Hosseiny*[1]

[1]*Department of Chemistry, Neyshabur Branch, Islamic Azad University, Neyshabur, Iran, fatemehamarloo@yahoo.com*

[2]*New Materials Technology and Processing Research Center, Department of Chemistry, Neyshabur Branch, Islamic Azad University, Neyshabur, Iran, r_zhiani2006@yahoo.com*

[3]*Advanced Research Center for Chemistry, Biochemistry & Nanomaterial; Neyshabur Branch, Islamic Azad University, Neyshabur, Iran.*

Abstract - Nowadays, nanomaterials are widely used in the preparation of nanocatalysts. Many important reactions are catalyzed by nanomaterials and these nanocatalysts dramatically increase product production efficiency. The aim of this research was to analyze the synthesis of $FeNi_3/SiO_2/Cu$ magnetic nanocatalyst and its performance in the Suzuki coupling reaction. Using $FeNi_3/SiO_2/Cu$ magnetic nanocatalyst, Suzuki reaction was tested under different temperature conditions, amount of catalyst, substrate, solvents and bases, optimal conditions were obtained for each of them. The results show that the Suzuki reaction with 1g of catalyst, in the presence of DMSO solvent, with K_2CO_3 base and at a temperature of 100°C had the best efficiency (92%). The heterogeneous $FeNi_3/SiO_2/Cu$ catalyst is easily separated from the reaction and used several times.

1. Introduction

Nanoparticles exhibit completely new or developed characteristics based on specific characteristics (size, dispersion, morphology, phase, etc.) in comparison with the bulk sizes of these particles [1-3]. When materials are brought to the nanoscale, many of their properties change, properties such as electrical, optical, magnetic properties, etc. The appearance of the following three characteristics is also among these changes: 1- Very small size, 2- Surface to Very high volume, and 3- increasing the number of atoms on the surface. These three factors are the most important reasons for the emergence of catalytic properties in nanomaterials [4,5]. Catalysts are divided into two categories: homogeneous and heterogeneous [6]. A heterogeneous catalyst is not in the same phase as the reactants. The size and characteristics of the heterogeneous catalyst particles are so that they are not easily dissolved in the reaction medium; Therefore, its activity is limited (the overall yield of the reaction is reduced). Unlike homogeneous catalysts, heterogeneous catalysts are easily separated (with less cost, time and materials) from the reaction mixture and do not cause impurity in the products [7]. In order to compensate for the lack of active surface in such compounds, it is necessary to use a substrate as a catalyst support. The substrate is usually a porous structure with a high active surface [8]. In magnetic materials, its constituent molecules and atoms have magnetic properties. In simpler terms, elements such as iron, cobalt, nickel and their alloys that are attracted by a magnet are called magnetic materials [9]. The Suzuki reaction is a type of coupling reaction in which a boronic acid and an aryl (or vinyl) halide are coupled with each other in the presence of a palladium catalyst. It was discovered in 1979 [10-11]. The development and expansion of efficient and useful methods for the formation of carbon-carbon bonds plays a very important role in the synthesis of organic compounds and biologically active compounds. The fact that biaryls are important structural components in polymers, agricultural chemical compounds, natural products and pharmaceutical intermediates has made this method an important and common tool in the synthesis of organic compounds. Various methods, such as acetyl coupling reactions, etc., have been presented for the synthesis of biaryl compounds. Suzuki reaction is known as a main and general method for the synthesis of these compounds [12-18]. The main advantages of Suzuki coupling reactions in comparison with other carbon-carbon coupling reactions include performing the reaction in mild conditions, its insensitivity to Water and functional groups are the non-toxicity of the waste and the ease of separation of the products [19]. Recently, coupling reactions such as Suzuki have been investigated with different catalysts, and in most of these reactions, catalyst recovery has faced problems. In this project, an attempt is made to make these reactions with better efficiency by using heterogeneous nano catalysts with the ability to easily recover from the reaction mixture.

Synthesis of $FeNi_3/SiO_2/Cu$ nanoparticles (0.01 mol of $FeCl_3.4H_2O$ and 0.03 mol of $NiCl_2.6H_2O$ in 200 ml of deionized water and then add 1 g of polyethylene

glycol (6000MW, 0.1gr). Gradually add sodium hydroxide to the solution until the pH of the solution is in the range of 12-13. Add 1 ml of hydrazine hydrate (N_2H_4.H2O, 80%) to the suspension. The reaction is stirred at room temperature for 24 hours until complete. During this period, the pH should be controlled with NaOH in the range of 12-13. Finally, wash the formed FeNi3 nanoparticles several times with deionized water and dry them. Dissolve 0.02 mol of FeNi3 nanoparticles in 80 mL of ethanol, 20 mL of deionized water, and 2 mL of ammonia ($NH_3.H_2O$, 28%wt), then 0.20 g of tetraethyl orthosilicate (TEOS) add. After stirring for 24 hours, wash the suspension several times with deionized water and put it in the oven at 60 degrees Celsius to dry. 0.5 g of $FeNi_3/SiO_2$ nanoparticle, 0.01 g of $Cu(OAc)_2$ and 10 ml of acetonitrile into the flask and place it in ultrasonic for 30 minutes. Then add 1 ml of freshly prepared $NaBH_4$ solution (with a concentration of 0.2 M) to the balloon. Centrifuge the product and wash it several times with deionized water and ethanol and dry it.)

See the Suzuki synthesis in Scheme 1 (1 mmol of benzene halides, 1.2 mmol of bronic acid, 2 mmol of base and 1g of $FeNi_3/SiO_2$/Cu catalyst into the flask. Then add 3 ml of DMSO solvent and reflux at 100°C.)

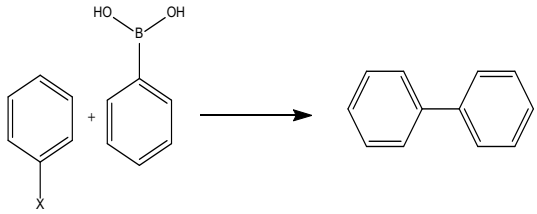

Scheme 1 - Suzuki reaction with $FeNi_3/SiO_2$/Cu catalyst

2. Results and Discussion

The morphology and structure of $FeNi_3/SiO_2$/Cu were characterized by FE-SEM. As shown in Figure 1, FeNi3/SiO2/Cu has uniform spheres with uniform and unified structure.

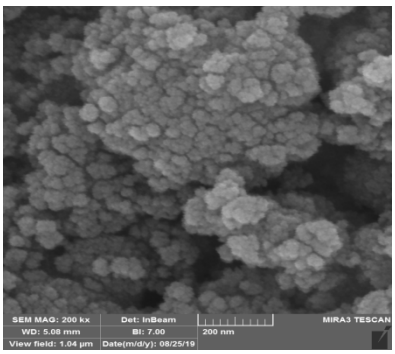

Figure 1- SEM images of $FeNi_3/SiO_2$/Cu

In order to obtain suitable conditions, for the Suzuki and Sonogashira reactions, different temperature values, the amount of catalyst and different solvents were investigated in each reaction and the following results were obtained. According to Figure 2, the reaction has not progressed at ambient temperature, but with the increase in temperature, the reaction has been carried out at a faster rate and the efficiency of the reaction has increased. The best temperature for the Suzuki reaction is 100 ℃. A further increase in temperature does not have a positive effect on the reaction process.

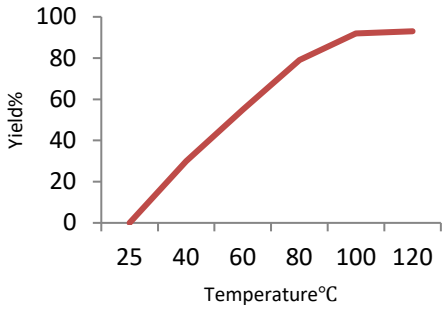

Figure 2- Suzuki reaction in the presence of $FeNi_3/SiO_2$/Cu catalyst at different temperatures.

The Suzuki reaction was investigated with different amounts of catalyst. According to Figure 3, by increasing the amount of catalyst from 0.1 to 1 gram in a period of 1.5 hours, the reaction efficiency has increased from 22% to 92%. Therefore, by increasing the amount of catalyst in this reaction, the efficiency of the reaction increases.

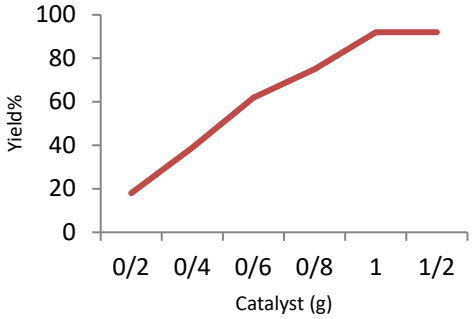

Figure 3- Suzuki reaction with different amounts of $FeNi_3/SiO_2$/Cu catalyst

The reaction must be carried out in the presence of an opener and will not progress without an opener. In this reaction, it was investigated in the presence of 7 different bases such as Na_2CO_3, KOH, K_2CO_3, Cs_2CO_3, NaOH, $NaHCO_3$ and Et_3N. According to Figure 4, the best solution is K_2CO_3, which has yielded 92% efficiency in 1.5 hours.

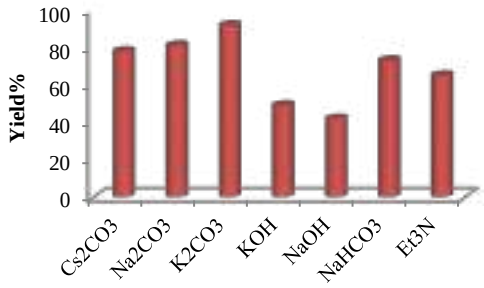

Figure 4- Suzuki reaction with different bases.

Figure 5 shows the reaction of Suzuki with different solvents. Various polar and non-polar solvents such as methanol, ethanol, water, tetrahydrofuran, etc. have been used in this reaction. The most suitable solvent that has brought the highest efficiency in the shortest time is the non-polar solvent DMSO.

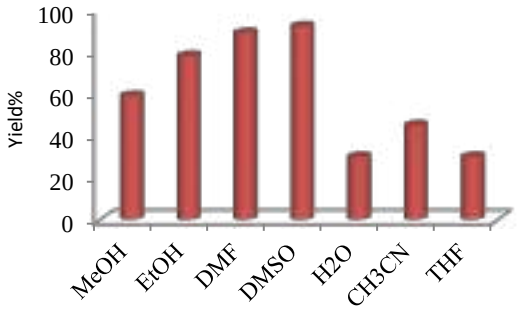

Figure 5- Suzuki reaction with different solvents

Suzuki reaction in the presence of aryl halide I, Br, Cl was also investigated (Table 1). As can be seen, iodized compounds have better efficiency in less time. The reason for this is that Iodine is a better cracker than Br and Cl.

Table 1- Different substrate

Entry	Ar-X	Yield (%)
1	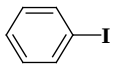	92
2	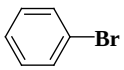	84
3	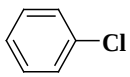	65

3. Conclusion

Catalysts are compounds that, when used in chemical reactions, cause a significant increase in reaction speed. Magnetic nanocatalysts are superior to non-magnetic nanocatalysts due to their magnetic properties. By using this property, they can be easily removed from the reaction environment and reused. $FeNi_3/SiO_2/Cu$ magnetic nanocatalyst has been synthesized and investigated on the Suzuki reaction. The obtained results show that the Suzuki reaction is carried out in the vicinity of this magnetic nanocatalyst due to the high active surface and excellent selectivity with high efficiency and short duration.

4. References

[1] R. Zhiani, M. Shahroudi, F. Amarloo, J. Chem. Res. 43 (2019) 149-151.

[2] F. Amarloo, R. Zhiani, A. Motavalizadehkakhky, M. Hosseiny, J. Ind. Catal. (2023).

[3] R. Zhiani, A. Es-haghi, F. Shamsa, F. Amarloo, M. Shahroudi, Silicon 12 (2020) 2005-2015.

[4] R. Singh, R. Bapat, L. Qin, H. Feng, V. Polshettiwar, ACS Catal. 6 (2016) 2770–2784.

[5] Z. Sun, H. Li, D. Guo, J. Sun, G. Cui, Y. Liu, Y. Tian, S. Yan, J. Mater. Chem. C 3 (2015) 4713–4722.

[6] K. Yu, X. Zhang, H. Tong, X. Yan, S. Liu, Mater. Lett. 106 (2013) 151–154.

[7] Z. Dong, X. Le, C. Dong, W. Zhang, X. Li, J. Ma, Appl. Catal. B 162 (2015) 372–380.

[8] Z. Dong, X. Le, X. Li, W. Zhang, C. Dong, J. Ma, Appl. Catal. B 158–159 (2014) 129–135.

[9] O. Vasylkiv, O. Bezdorozhev, Y. Sakka, J. Ceram. Soc. Jpn. 124 (2016) 489-494.

[10] N. Miyaura, K. Yamada, A. Suzuki, Tetrahedron Lett. 20 (1979) 3437-3440.

[11] N. Miyaura, A. Suzuki, J. Chem. Soc., Chem. Commun. 19 (1979), 866-867.

[12] A. Balanta, C. Godard, C. Claver, Chem. Soc. Rev. 40 (2011) 4973-4985.

[13] S. Kotha, K. Lahiri, D. Kashinath, Tetrahedron 58 (2002) 9633-9695.

[14] R.K. Borah, A. Mahanta, A. Dutta, U. Bora, A.J. Thakur, Appl. Organomet. Chem. 31 (2017) e3784.

[15] R. Jana, T.P. Pathak, M.S. Sigman, Chem. Rev. 111 (2011) 1417-1492.

[16] P. Gautam, M. Dhiman, V. Polshettiwar, B.M. Bhanage, Green Chem. 18 (2016) 5890-5899.

[17] a) H. Veisi, M. Ghorbani, S. Hemmati, Mat. Sci. Eng. C 98 (2019) 584-593; b) H. Veisi, P. Safarimehr, S. Hemmati, Mat. Sci. Eng. C 96 (2019) 310-318.

[18] M.R. Yadav, M. Nagaoka, M. Kashihara, R.L. Zhong, T. Miyazaki, S. Sakaki, Y. Nakao, J. Am. Chem. Soc. 139 (2017) 9423-9426.

[19] C. Zhang, R. Zhang, S. He, L. Li, X. Wang, M. Liu, W. Chen, ChemCatChem 9 (2017) 980-986.

Condensation synthesis and investigation of the structure of some ligands containing imine bond and preparation of inorganic complexes

Babak Mirtamizdoust, Mostafa Kiamehr* and Haniyeh Behzadi*

Department of Chemistry, Faculty of Science, University of Qom, Qom, Iran, babakm.mirtamizdoust@gmai.com, m.kiamehr@qom.ac.ir, haniebehzadi75@gmail.com.

Abstract - Schiff bases are a vast group of compounds characterized by the presence of a double bond linking carbon and nitrogen atoms, the versatility of which is generated in the many ways to combine a variety of alkyl or aryl substituents. Compounds of this type are both found in nature and synthesized in the laboratory. For years, Schiff bases have been greatly inspiring to many chemists and biochemists. In this article, we attempt to present a new take on this group of compounds, underlining of the importance of various types of Schiff bases. Among the different types of compounds that can be classified as Schiff bases, we chose hydrazides, dihydrazides, hydrazones and mixed derivatives such as hydrazide–hydrazones. For these compounds, we presented the elements of their structure that allow them to be classified as Schiff bases. While hydrazones are typical examples of Schiff bases, including hydrazides among them may be surprising for some. In their case, this is possible due to the amide-iminol tautomerism.

1. Introduction

Schiff bases derived from aromatic amines and aromatic aldehydes are widely used in the fields of biology, inorganic chemistry and analytical chemistry [1-2] to use very new analytical devices. The presence of organic reagents is required as essential components of the measurement system. They are used in electrochemical and optical sensors as well as various chromatographic methods and are able to reveal increased selectivity and sensitivity [3]. They are simple and traditional flexibility that provide the design of appropriate structural properties [4]. Schiff bases are widely used in analytical determination, including, in the condensation reactions of first-type amines and carbonyl compounds that form an azomethine bond (determination of compounds with a amine or carbonyl group); in complex formation reactions (determination of amines, carbonyl compounds, and metal ions); or changes in spectroscopic characteristics caused by changes in pH and solvent (pH (solvent polarity indicators)) are used [5].

Schiff bases are important organic intermediates for the production of certain chemicals such as drugs and resins. These compounds are also used as an amine protecting group in organic synthesis. Some Schiff bases are in the form of basic units in certain colors, while some are used as liquid crystals [4].
According to the recommendation of IUPAK, Schiff bases are defined as chemical compounds (imines) [1].

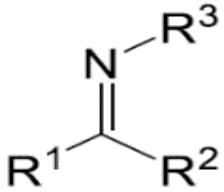

Fig. 2. Schiff base structure

Schiff base structure where R are alkyl or mostly aryl groups. R^1 and R^2 may also be hydrogen atoms [2].
In the future research, new compounds will be synthesized and analyzed by various methods, including NMR, fluorescence, FT-IR, and CHN spectrum. With the expansion of the scope of research, some of the physical and chemical activities of this group of compounds will be studied. The new aspect of these compounds is that they are synthesized for the first time in the world, and with their synthesis, analysis and introduction, a new door is opened to explore the applications of new materials. Examining the structure of new mineral complexes with ligands containing imine bonds, in addition to being new due to having aromatic groups in the ligand and the existence of weak interactions that cause the structure to self-assemble, and also, the modes of the metal coordination sphere will be very interesting.

2. Experimental part

In the current research, the primary goal is to creat a ligad containing an imine bond, whose formation equation is as follows. Fig. 2

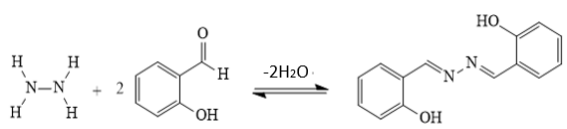

Fig. 2 Ligand synthesis reaction

In this research, the ultimate goal is to create a complex with a ligand containing an imino bond and lead (II) acetate trihydrate.

According to the results of the CHN test analysis, the equation of its formation is suggested below. Fig. 3

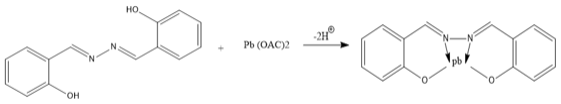

Fig. 3 Synthesis complex reaction

2.1. Synthesis ligand, complex E-1 E-2 E_2

The materials needed to make the desired ligand include hydrazine 80% made by Merck Germany, salicylaldehyde 99.9% made by Merck Germany, acetic acid made by Merck Germany, Pb(C2H3O2)2.3H2O made by Merck Germany, NaQH made by Germany's Merck and Methanol are made by Iran's Dr. Majalli Company.

0.756 grams (0.025 mmol) of 80% hydrazine hydrate was separated with a syringe and a few drops of methanol were added for dilution. Then 617.5 grams (0.046 mmol) of salicylaldehyde was separated with a syringe and a few drops of acetic acid were added to activate Haldehyde and methanol to homogenize. Next, the balloon containing salicylaldehyde was fixed on the stirrer and stirred. Then, within half an hour, 80% hydrazine hydrate was added drop by drop to the flask while stirring. Then the obtained solution was stirred for two hours until the reaction was completed and a temporary red color appeared, and then we left the solution in the previous state for one day. Then the sediments were filtered and washed with a few drops of methanol to remove aldehyde and imine, then dried. Next, FTIR, NMR and fluorescence spectra were taken from it.

Gram (0.4 mmol) of ligand was poured into the flask and 15 ml of ethanol was added and stirred, while stirring for 5-6 hours at a temperature of 90-100 degrees Celsius, it was refluxed to dissolve the contents of the flask. Then 0.17 g (0.4 mmol) of Pb(C2H3O2)2.3H2O was dissolved with 2 ml of ethanol and 10 ml of water at low temperature. After dissolution, the metal salt and ligand reached the boiling temperature and metal salt was added to the ligand at a low speed and stirred for 10 hours at the highest temperature and refluxed during this process. Later, the sediments became smooth and dry. Next, the FTIR spectrum was taken from it

0.09 g (0.4 mmol) of ligand was poured into the flask and a few drops of NaOH and 15 ml of ethanol were added and stirred, and while stirring, it was refluxed for 5-6 hours at a temperature of 90-100 degrees Celsius until the contents inside the flask be resolved Then 0.17 grams (0.4 mmol) of Pb(C2H3O2)2.3H2O was dissolved with 2 ml of ethanol and 10 ml of water at a low temperature and added to the ligand at a low speed and stirred for 10 hours at the highest temperature. Got reflux while doing this process. Later, the sediments became smooth and dry. Next, the FTIR spectrum was taken from it.

0.09 g (0.4 mmol) of ligand was poured into the flask and a few drops of NaOH and 15 ml of ethanol were added and stirred, and while stirring, it was refluxed for 5-6 hours at a temperature of 90-100 degrees Celsius until the contents inside the flask be resolved Then 0.17 grams (0.4 mmol) of Pb(C2H3O2)2.3H2O was dissolved with 2 ml of ethanol and 10 ml of water at a low temperature and added to the ligand at a low speed and stirred for 10 hours at the highest temperature. Got reflux while doing this process. Later, the sediments became smooth and dry. Next, the FTIR spectrum was taken from it.

3. Results and discussion

Based on the obtained results, the Ha proton is related to d splitting, which is created at 7.65744ppm (1H). Peak 7.36431 ppm ((1H) corresponds to Hc proton with t splitting, peak 11.11489 ppm (1H) corresponds to He proton with s splitting. In this ligand, instead of 6 peaks, 5 peaks are observed, because the peak corresponding to Hb proton with double splitting in 6.92862ppm area is merged with Hd proton with triplet splitting in 6.9502ppm area and it is observed as a m peak. It should be noted that the peak corresponding to the imine group (Hf proton with d splitting) is observed in 8.96719ppm (1H) area. This problem shows that the Schiff-opening ligand with the imine agent has been completely synthesized.

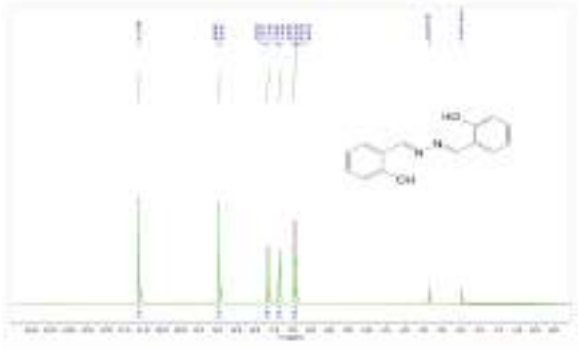

Fig. 4. ^{1}HNMR spectrum for the synthesized ligand

Based on the results presented in the research of Silva et al. (2013), the peak created at 55.116 ppm corresponds to C3 carbon, the peak created at 20.118 ppm corresponds to C1 carbon, the peak created at 61.119 ppm corresponds to C5 carbon, the created peak At 88.130 ppm corresponds to C6 carbon, the peak created at 24.133 ppm corresponds to C4 carbon, the peak created at 68.158 ppm corresponds to imine carbon and finally the peak created at 83.162 ppm corresponds to C2 carbon. The observation of 7 different types of peaks is a confirmation of the formation of a symmetric synthetic Schiff-base ligand

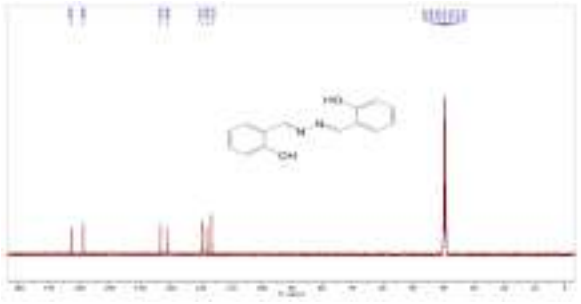

Fig.5. ^{13}CNMR spectrum for the synthesized ligand

The peak indicates the formation of the imine group in the region. 1623 cm-1 appeared, which confirms the formation of the Schiff-opening ligand. The weak peaks seen in the region of 2600-3043 cm-1 are related to imine and aromatic C-H stretching vibrations. In this spectrum, the frequency of C-O group is seen in the area of 1198 cm-1, the frequency of N-N in the area of 1276 cm-1 and finally the frequency of the C=C group is seen in the area of 1486 cm-1.

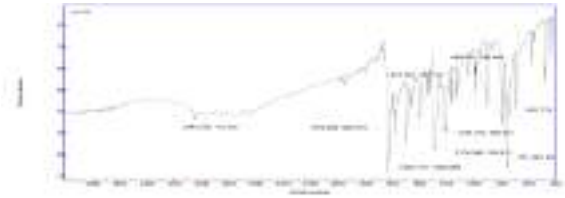

Fig. 6. FTIR spectrum for the synthesized ligand

Due to the increase of ligand emission in DMSO solvent and also the less toxicity of this solvent, the fluorescence test of ligand was performed in this solvent. The first peak created is the standard peak of DMSO solution and after that a strong emission has occurred in the region of 550 nm, which is confirmed according to the research conducted by Levai (2016) in the range of 530-560 nm for the Schiff-open ligand with an imine agent.

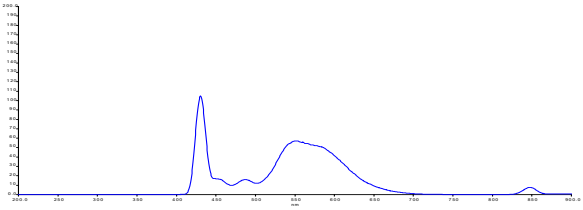

Fig.7. fluorescence spectrum for the synthesized E-1 E-2 complexes

The peak indicates the formation of the imine group in the region. 1623 cm-1 appeared, which confirms the formation of the Schiff-opening ligand. The weak peaks seen in the region of 2600-3043 cm-1 are related to imine and aromatic C-H stretching vibrations. In this spectrum, the frequency of C-O group is seen in the area of 1198 cm-1, the frequency of N-N in the area of 1276 cm-1 and finally the frequency of the C=C group

According to the FTIR spectrum of the complex, which is almost similar to the RTIR spectrum of the ligand, this problem shows that there is a ligand with an imine agent in the structure of the complex.

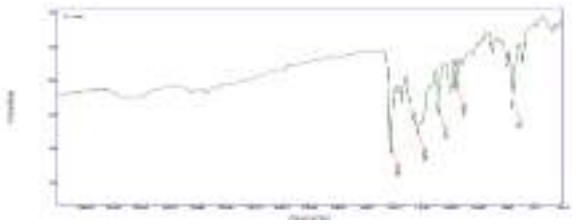

Fig. 8. FTIR spectrum for the synthe E-1 E-2 E2 complex

4. Conclusion

All the studies based on NMR (chemical shifts, coupling constants, deuterium-induced chemical shifts differences and others) are based on average signals and interpolation methods that need values for both tautomers usually corresponding to model compounds. Here, for the first time, the signals of both tautomers were observed in solution, and the tautomeric equilib-rium constant directly measured. Our results may be useful to help understanding the case of more complex situations such as of the azo-hydrazone tautomerism of C3-symmetric trisazo dyes and other dyes, as well as the effect of proton-ation, complexation with metals and excited states, over the equilibria discussed in the present paper.

4. References

[1] A. M. Silva, V. L.Silva, R. M. Claramunt, D. S. María, M. B. Ferraro, Magnetic Resonance in Chemistry, 2013, 530-540.
[2] C. Camp, L. Chatelain, V. Mougel, J. Pecaut, M. Mazzanti, Inorg. Chem (54). 2015, 5774–5783.
[3] W.A. Zoubi, Int. J. Org. Chem (3). 2013, 73–95.
[4] A. Donzelli, I. Metushi, P.G. Potvin, Inorg. Chem (51). 2012, 5138–5145.
[5] N.K. Chaudhary, P. Mishra, Bioinorg. Chem. Appl. 2017.

Effect of temperature on solubility and thermal stability of Triamterene drug in subcritical water

Maryam Khajenoori[*], *Mina Delkhani*, *and Ali Haghighi Asl*

Department of Chemical Engineering, Faculty of Chemical, Petroleum and Gas Engineering, Semnan University, Semnan, Iran, m_khajenoori@semnan.ac.ir, mina.delkhani@semnan.ac.ir

Abstract - Subcritical water at temperatures less than 374°C has the property of constant dielectric adjustment, which turns water into a green and safe solvent for poorly soluble drugs. In this research, the effect of temperature on the solubility of Triamterene (a diuretic drug) in subcritical water was investigated by a static method. The experiments were performed under a constant pressure of 30 bar and at temperatures between 383.15-443.15 K. With increasing temperature, the mole fraction solubility of the drug increased from 0.782×10^{-4} to 1.399×10^{-4}.

1. Introduction

Thousands of tons of medicinal substances are produced and consumed annually to treat diseases. The low aqueous solubility of drugs and their low bioavailability has been one of the main problems in the pharmaceutical industry for their development and clinical use [1]. Therefore, improving the aqueous solubility of drugs is important to increase efficiency or reduce side effects. Water at ambient temperature is a strong polar solvent despite strong hydrogen bonding and high dielectric constant. As the temperature increases, the polarity of water decreases and the solubility of organic compounds such as drugs increases significantly [2-4]. Improving the solubility of organic compounds in water at high temperatures allows it to be used as a green solvent to extract and produce pharmaceutical nanoparticles [5-7]. Today, due to technological advances and environmental safety issues, researchers pay special attention to green and environmentally friendly processes [8,9]. To solve the problems related to the bioavailability of pharmaceutical substances that have challenged the pharmaceutical industry, subcritical fluid technology has attracted the attention of researchers as a green alternative method that is less dangerous, more efficient, and more economical in terms of cost and space [9].

Subcritical water is water above the boiling temperature and below the critical temperature that is in a liquid state under high pressure. As the water temperature increases in subcritical conditions, the hydrogen bond network is weakened and causes a decrease in the dielectric constant of water. As a result, water changes from polar to non-polar [10]. Information on the solubility of drugs in subcritical water is the basis for improving subcritical water processing for organic nanoparticles [11].

In the present study, the effect of temperature on the solubility of the diuretic drug Triamterene in subcritical water was investigated. Triamterene, with the molecular structure of Fig. 1, prevents excessive absorption of salt and excessive reduction of potassium in the body of patients with blood pressure [12]. Also, this drug is generally used to reduce swelling [13,14]. Despite the poor aqueous solubility of this drug, limited research has been reported on improving its solubility. The study of improving the solubility of Triamterene is important for scientists because of the low bioavailability of this drug. Therefore, the solubility of this drug in subcritical water was investigated in the temperature range of 298.15 K to 443.15 K and constant pressure of 30 bar.

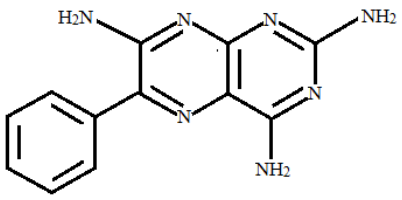

Fig. 1. Chemical structure of Triamterene.

2. Experimental

2.1. Materials: Raw Triamterene was obtained from Tehran Darou, methanol from Merck, and nitrogen from Sabalan Co. Deionized double distilled water was obtained from a Milli-Q deionizing unit (Millipore, Bedford, MA, USA).

2.2. Apparatus and method: Fig. 2 shows the schematic of the experimental device. At first, an excess amount of Triamterene was placed inside the solubility cell along with distilled water and a magnetic magnet. The cell was equipped with a magnetic stirrer. Valves 1 and 2 were opened and nitrogen flowed into the solubility cell, and valve 2 was closed after the

nitrogen bubbles came out. The system pressure was set to 30 bar and the temperature was set to the desired temperature with the help of an electric heater. By turning on the magnetic stirrer, the contents of the solubility cell were mixed for 5 minutes. Then valve 3 was opened and the Triamterene solution and subcritical water were transferred to the collection cell by passing through a 1 µm filter. The solution was transferred to a glass vial and dried in an oven. Finally, the solute powder was dissolved in methanol and analyzed with a UV-Vis spectrophotometer.

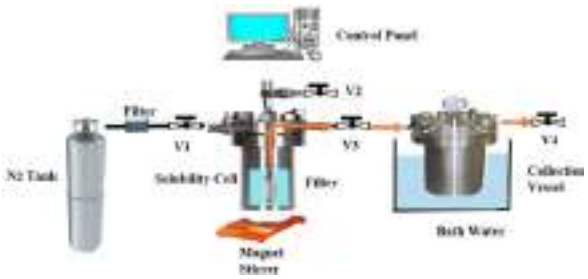

Fig.2. Experimental device for determining solubility in subcritical water [3].

3. Results and discussion

3.1. Solubility and thermal stability results: Fig. 3 shows the solubility of Triamterene in subcritical water solvent at temperatures between 383.15 K and 443.15 K and constant pressure of 30 bar. With the increase of temperature in subcritical conditions, the solubility of Triamterene increased exponentially, which is due to the effect of temperature on the structure of hydrogen bonds of water. In this case, water acts similarly to organic solvents, which can dissolve water-insoluble hydrophobic compounds such as drugs. Therefore, it can be concluded that temperature has a direct effect on solubility.

Investigating the thermal behavior of Triamterene in subcritical water showed that this drug started to melt at a temperature of 324 °C and started to lose mass at a temperature of 215 °C. Therefore, at the experimental temperatures, the drug had thermal stability and did not melt or degrade in this temperature range.

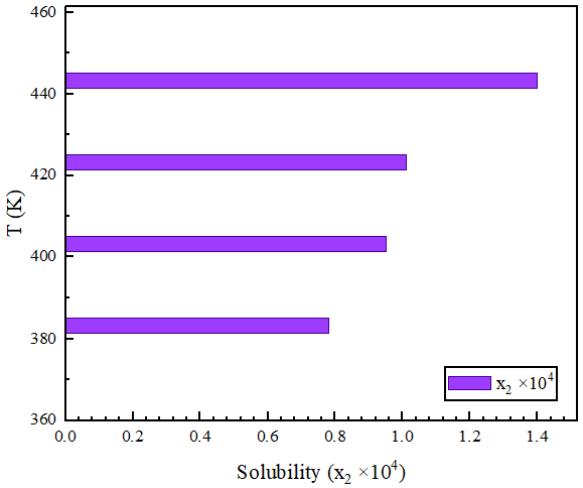

Fig. 3. Experimental mole fraction solubility of Triamterene at different temperatures of subcritical water.

4. Conclusion

In this work, the effect of temperature on the solubility of Triamterene in subcritical water was determined by the static method. Solubility in mole fraction unit was determined at 383.15-443.15 K and at a constant pressure of 30 bar. The mole fraction solubility of Triamterene increased from the temperature of 298.15 K to 443.15 K from the value of 0.782×10^{-4} to 1.399×10^{-4}. Therefore, it can be concluded that solubility in subcritical water is directly affected by temperature. The thermal behavior of the material showed stability and non-degradation in the experimental temperature range.

5. References

[1] H. Chen, C. Khemtong, X. Yang, X. Chang, J. Gao, Drug discov. today, 16 (2011) 354-360.
[2] B. Kayan, Y. Yang, E. J. Lindquist, A. M. Gizir, J. Chem. Eng. Data, 55 (2010) 2229-2232.
[3] H. S. Mohammadi, A. H. Asl, M. Khajenoori, J. Mol. Liq. 362 (2022) 119679.
[4] D. J. Miller, S. B. Hawthorne, A. M. Gizir, A. A. Clifford, J. Chem. Eng. Data, 43 (1998) 1043-1047.
[5] P. Mottahedin, A. Haghighi Asl, M. Khajenoori, J. Food Process. Preserv. 41 (2017) e13095.
[6] A. H. Asl, M. Khajenoori, Subcritical water extraction, In book: Mass transfer advances in sustainable energy and environment oriented numerical modeling, InTech, Rijeka, 2013.
[7] H. S. Mohammadi, A. H. Asl, M. Khajenoori, J. Drug Deliv. Sci. Technol. 67 (2022) 102949.
[8] D. Wang, J. Qian, F. Cai, S. He, S. Han, Y. Mu, Nanotechnology, 23 (2012) 245701.
[9] Y. Pu, X. Wen, Y. Li, D. Wang, N. R. Foster, J.-F. Chen, Powder Technol. 305 (2017) 125-131.
[10] Y. Yang, S. Bowadt, S. B. Hawthorne, D. J. Miller, Anal. Chem. 67 (1995) 4571-4576.
[11] H. S. Mohammadi, A. H. Asl, M. Khajenoori, Korean J. Chem. Eng. 38 (2021) 2304-2312.
[12] B. J. Materson, Am. heart j. 106 (1983) 188-208.
[13] T. Osdene, P. B. Russell, L. Rane, J. Med. Chem. 10 (1967) 431-434.
[14] A. S. Al-Kady, F. I. Abdelmonem, Sen. Actuators B Chem. 182 (2013) 87-94.

29TH IRANIAN ORGANIC CHEMISTRY CONFERENCE
1_3 NOV, 2023
UNIVERSITY OF QOM, IRAN

Investigating the solubility of Curcumin in subcritical water as a green solvent

Maryam Khajenoori, Alireza Simiari and Ali Haghighi Asl*

Department of Chemical Engineering, Faculty of Chemical, Petroleum and Gas Engineering, Semnan University, Semnan, Iran, m_khajenoori@semnan.ac.ir, alirezasimiari3@gmail.com

Abstract – Curcumin is an anticancer drug with low water solubility. In the present study, the solubility of Curcumin drug in subcritical water was investigated by a static method. Solubility was measured under constant pressure of 15 bar and temperatures between 363.15 K and 423.15 K. The results showed that the mole fraction solubility of Curcumin increases with the increase in subcritical water temperature. The mole fraction solubility values were obtained in the range of $0.017\times10^{-4} < x_2 < 0.101\times10^{-4}$.

1. Introduction

Every year, millions of people around the world are diagnosed with cancer and many of these patients die. Curcumin is a yellow powder (Fig. 1) and a polyphenol extracted from Curcuma longa [1]. As an anti-inflammatory [2], anti-cancer [3], antioxidant [4], anti-fungal [5], and anti-spasm drug [6], this substance has wide applications in medicine today. Despite the extensive properties of Curcumin, the use of this drug and the benefit of its anti-cancer properties are limited due to its low solubility in water. Curcumin's low aqueous solubility results in low oral bioavailability and low cellular uptake [7]. Low water-soluble drugs require high doses to reach the optimal blood concentration. Drug solubility information enables scientists to improve drug aqueous solubility in environmental conditions by creating physical and chemical modification conditions [8].

Today, pollution caused by toxic and harmful solvents has drawn researchers' attention to green processes and solvents. Under normal conditions, water is a polar solvent with a high dielectric constant [9]. The main reason for the high polarity of water at ambient temperature is the strong hydrogen bond network of this solvent [10]. With increasing temperature in subcritical conditions, this hydrogen bond network is weakened and as a result, the dielectric constant of water decreases [11,12]. Therefore, in these conditions, the dielectric constant of water is similar to toxic organic solvents, which can dissolve a wide range of polar and non-polar organic substances [13]. Water with a temperature higher than the boiling point and lower than the critical point and under high pressure (to maintain the liquid state) is known as subcritical water, which is considered a green solvent due to its high dissolving power [11]. Subcritical water solvent has the advantages of being readily available, non-toxic, cost-effective, and environmentally friendly. Therefore, this solvent can be a good alternative to toxic solvents in the pharmaceutical industry [14].

In the present study, the solubility of Curcumin in subcritical water green solvent has been investigated. The solubility of Curcumin in subcritical water at 363.15-423.15 K and under the constant pressure of 15 bar was measured by a static method.

Fig. 1. Molecular structure of Curcumin

2. Materials and Method

2.1. Materials: Crude Curcumin was obtained from Bio Basic and ethanol from Merck with maximum purity. Double distilled water was obtained from the Mili-Q deionizer unit. Nitrogen gas was supplied by Sabalan company.

2.2. Method: The schematic of the subcritical water solubility device is shown in Fig. 2. In each experiment, additional Curcumin and 50 ml of double-distilled water with a magnetic magnet were embedded in the equilibrium cell. A magnetic stirrer was placed outside the cell. First, valves 1 and 2 were opened and valve 2 was closed after ensuring the removal of air

from the system. The equilibrium cell pressure was set at 15 bar using the pressure gauge installed on the cell. After the system reached the desired temperature with the help of an electric strip heater, the contents of the equilibrium cell were mixed for 5 minutes by a magnetic stirrer, and equilibrium was established. Then, by opening valve 3, solutions passed through the filter and transferred to the collection vial. The collected solution was dried in a separate container in an oven with a temperature of 323.15 K. Dried Curcumin powder was dissolved in a certain amount of ethanol and the concentration was determined using a UV-Vis spectrophotometer.

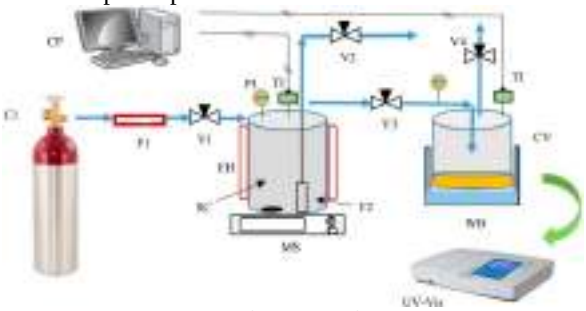

Fig. 2. Schematic diagram of the device for measuring solubility in subcritical water. [15]

3. Result and Discussion

3.1. Solubility results: The strength of hydrogen bonding of water molecules at ambient temperature depends on the presence of bonds around each other. By increasing the temperature and making a slight change in the hydrogen bond, it is also transferred to other bonds. By changing the structure of hydrogen bonds, the dielectric constant of water also changes. Therefore, the weakening of the strength of hydrogen bonds at high temperatures causes intermolecular interactions between water and solutes [10]. As a result, the solubility of hydrophobic compounds in water increases at high temperatures [15-17]. This issue was also observed in the case of Curcumin. Mole fraction solubility values of Curcumin in subcritical water are shown in Fig. 3. When the temperature increased from 363.15 K to 423.15 K, the solubility enhanced significantly. Therefore, it can be concluded that the solubility of Curcumin in subcritical water has a great dependence on temperature.

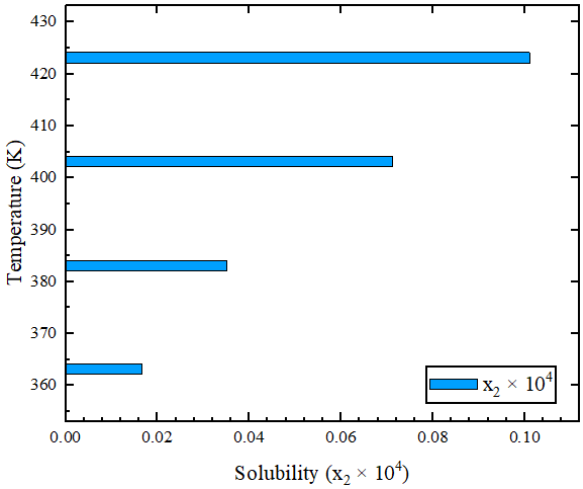

Fig. 3. Experimental solubility of Curcumin in subcritical water at different temperatures.

4. Conclusion

In this study, the aqueous solubility of the anticancer drug Curcumin was investigated in subcritical water conditions. Solubility was measured at a constant pressure of 15 bar and temperatures between 363.15 K and 423.15 K. The results showed that solubility is directly affected by temperature. Therefore, by increasing the temperature from 363.15 K to 423.15 K, the mole fraction solubility of Curcumin in subcritical water increased from 0.017×10^{-4} to 0.101×10^{-4}.

5. References

[1] S.C. Gupta, S. Patchva, W. Koh, B.B. Aggarwal, Clin. Exp. Pharmacol. Physiol. 39 (2012) 283-299.
[2] B.B. Aggarwal, K.B. Harikumar, Int. J. Biochem. Cell Biol. 41(2009) 40-59
[3] L.E Wright, J.B Frye, B. Gorti, B.N Timmermann, J.L Funk, Curr. Pharm. Des. 19 (2013) 6218-6225.
[4] A.J. Ruby, G. Kuttan, K.D. Babu, K. Rajasekharan, R. Kuttan, Cancer lett. 94 (1995) 79-83.
[5] A. Apisariyakul, N. Vanittanakom, D. Buddhasukh, J. Ethnopharmacol. 49 (1995) 163-169.
[6] C. Itthipanichpong, N. Ruangrungsi, W. Kemsri, A. Sawasdipanich, J. Med. Assoc. Thai. 86 (2003) S299-309.
[7] P. Anand, A.B. Kunnumakkara, R.A. Newman, B.B. Aggarwal, Mol. Pharm. 4 (2007) 807-818.
[8] K.T. Savjani, A.K. Gajjar, J.K. Savjani, ISRN Pharm. 2012 (2012) 1-11.
[9] A.G. Carr, R. Mammucari, N. Foster, Chem. Eng. J. 172 (2011) 1-17.
[10] S. Akay, Y. Yang, B. Kayan, J. Chem. Eng. Data 66 (2021) 2550-2560.
[11] H.S. Mohammadi, A.H. Asl, M. Khajenoori, J. Mol. Liq. 362 (2022) 119679.
[12] A. H. Asl, M. Khajenoori, Subcritical water extraction, In book: Mass transfer advances in sustainable energy and environment oriented numerical modeling, InTech, Rijeka, 2013.
[13] D. J. Miller and S. B. Hawthorne, Anal. Chem. 70 (1998) 1618-1621.
[14] X. Liang, Q. Fan, J. Mater. Sci. Chem. Eng. 1 (2013) 1-6.
[15] H. S. Mohammadi, A. H. Asl, M. Khajenoori, Chin. J. Chem. Eng. 28 (2020) 2620-2625.
[16] D. J. Miller, S. B. Hawthorne, J. Chem. Eng. Data 45 (2000) 315-318.
[17] H. S. Mohammadi, A. H. Asl, M. Khajenoori, J. Drug Deliv. Sci. Technol. 67 (2022) 102949.

Green Synthesis and Biological Evaluation of New Substituted Benzofuran-based Compounds as acetylcholinesterase inhibitors

Behjat Pouramiri *

[1]*Department of Organic Chemistry, Qom University of Technology, Qom, Iran, b.pouramiri.chem@gmail.com*

Abstract - A series of benzofuran derivatives (3a–d) have been designed, synthesized and biologically evaluated as potential inhibitors of acetylcholinesterases (AChE). The chemical structures of all final compounds were confirmed by spectroscopic methods. *In vitro* anti acetylcholinesterase activities of these novel compounds were evaluated and showed low to moderate results. Among them, compounds 3a moderately inhibited AChE activities with 68.12 % values.

1. Introduction

Alzheimer's disease (AD) is a complex neurodegenerative disorder that influences the life quality of the elderly population of the world [1]. The patomechanism of AD has not been clearly recognized, the typical pathological marks are amyloid-β (Aβ) deposits, oxidative stress, and decreased levels of acetylcholine (ACh) in the brain [2]. ACh is an important neurotransmitter responsible for memory. Acetylcholinesterase (AChE) and butyrylcholinesterase (BChE) are responsible enzymes for the metabolic hydrolysis of ACh at the cholinergic synapses [3]. Acetylcholinesterase (AChE) inhibitor drugs involving donepezil, rivastigmine and galantamine have been widely used for the treatment of AD [4]. Among the large variety of anti-acetylcholinesterase compounds, benzofurans play an important role in the increasing the levels of acetylcholine [5]. In addition, benzofuran derivatives are observed as an essential building block in bioactive substances [6] with broad range of biological and pharmaceutical activities such as anticancer [7], antiviral (1) [8], antimicrobial (2) [9], anti-inflammatory [10], and angiogenesis [11] (Fig. 1).

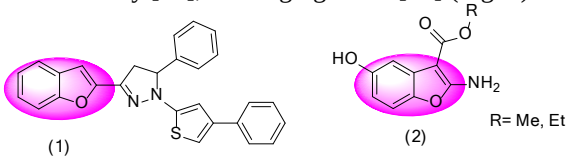

Fig. 1. Biologically active compounds containing benzofuran framework.

The formation of C−C bonds is one of the most common transitions in all areas of organic and drug synthesis [12-13]. Direct C–H bond activation reaction has become an efficient and clean strategy for C-C coupling because of its conciseness and atom economy according to the concepts of "green chemistry" [14,15]. Today, palladium or palladium complexes is commonly used in various coupling reactions [16-19]. Herein, we decided to synthesis novel benzofurans *via* direct C−H activation reaction, with hopes to possess better anti acetylcholinesterase potencies.

2. Results and Discussion

The coupling reaction of 1-(4-(benzofuran-2-yl)benzyl)piperidine (1 mmol), and bromobenzen (1.5 mmol) in the presence of $Pd(OAc)_2$ was chosen as a model reaction . The catalysed-reaction was optimized by the various ligand, base and solvents, described in Table 1.

It was observed that the reaction proceeded efficiently using $Pd(OAc)_2$ in the presence of NH_4OAc in DMF: H_2O (3:2) and resulted in good yield of the desired product (70-78 %). Additionally, we have attempted different ratios of $Pd(OAc)_2$ (3, 5, 10, 12, and 15 mol%) and observed that 10 mol% was suitable for the optimum conversion. The increase in the molar ratio of $Pd(OAc)_2$ also did not improve the yield of reaction.

After the optimization of reaction conditions, we synthesized several di-substituted benzofuran by the reaction of various substituted benzofurans with aryl halides via the coupling reaction. The results are presented in Fig. 2.

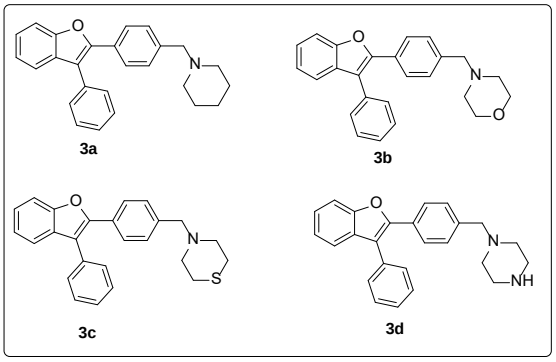

Fig. 2. synthesis of various substituted benzofurans.

In following, the newly synthesis compounds 3a-d were evaluated for their AChE inhibitory activities using modified colorimetric Ellman's method [20] and compared with donepezil as the reference drug, reported in Table 2. Compounds 5a with piperidine substituent, exhibited better activities. No improvements were observed in thiomorpholine, morpholine and piperazine derivatives (Table 2).

Conclusion

In summary, we have designed and synthesized novel benzofuran derivatives via carbon-carbon coupling reaction. The preliminary biological activities screening tests indicated that these synthesized derivatives 3(a-d) were identified as moderate anti-acethylcolinestrase active. These researches showed the key role of benzofuran scaffold in AChE inhibition.

Table 1. Screening solvent, ligand and base conditions synthesis of the synthesis of 1-(4-(3-phenylbenzofuran-2-yl)benzyl)piperidine

En.	[Pd] (mol%)	Ligand	Base (equiv)	Solvent	Time (h)	Yield[b] (%)
1	$Pd(OAc)_2$ (10)	PPh_3	K_2CO_3	Dioxane	12	50
2	$Pd(OAc)_2$ (10)	PPh_3	K_2CO_3	Dioxane	14	55
3	$Pd(OAc)_2$ (5)	PPh_3	Na_2CO_3	Dioxane: H_2O	12	50
4	$Pd(OAc)_2$ (5)	1,10-Phenanthroline	K_2CO_3	DMF	24	20
5	$Pd(OAc)_2$ (10)	1,10-Phenanthroline	Na_2CO_3	DMF:H_2O	24	30
6	$Pd(OAc)_2$ (5)	PPh_3	Cs_2CO_3	DMA	24	40
7	$Pd(OAc)_2$ (10)	10-Phenanthroline	Cs_2CO_3	DMF	24	30
8	$Pd(OAc)_2$ (15)	PPh_3	NH_4OAc	Dioxane	24	60
9	$Pd(OAc)_2$ (10)	PPh_3	NH_4OAc	DMF: H_2O	12	80
10	$Pd(OAc)_2$ (5)	PPh_3	NH_4OAc	DMF: H_2O	14	70
11	$Pd(OAc)_2$(10)	PPh_3	NH_4OAc	DMA	12	80

[a]Reaction condition: 1 (1 mmol), 2 (2.5 mmol), and $Pd(OAc)_2$ (5 mol%).
[b]Yields refer to pure isolated yields

4. References

General procedure for the synthesis of disubstituted benzofuran:

A mixture of 1-(4-(benzofuran-2-yl)benzyl)derivatives 1(a-d) (1.0 equiv), $CsCO_3$ (3.0 equiv), aryl halide (2.5 equiv) and $Pd(OAc)_2$(10 mol%) in DMA: H_2O (1:1, 5 mL) was heated to 100 °C for 3 h. The reaction progress was monitored by TLC using hexane/ ethyl acetate (4:2) as an eluent. After completion of the reaction, the mixture was cooled to room temperature and then H_2O (4 mL) was added. The solid product was filtered, washed with cold water (3 mL) to obtain essentially pure products. The crude product was purified by flash chromatography on silica gel. The structure of all the products was characterized by IR, ^1H and ^{13}C NMR spectra along with elemental analysis data.

Biological Activity Assays

AChE (E.C.3.1.1.7, Type VeS, from Electric eel), Ellman's reagent (DTNB), and acetylthiocholine (ATC) were purchased from Sigma-Aldrich. Donepezil (Sigma) was used as reference drug for AChE inhibition. The AChE inhibitory activities of compounds **3(a-d)** were determined by using previously reported method [20].

[1] N.C. Berchtold, C.W. Cotman, Neurobiol. Aging. 19 (1998) 173-189.
[2] W. Thies, L. Bleiler Alzheimer's Dement 9 (2013) 208-245.
[3] H. Feorstl, A. Kurz Eur Arch Psychiatry Clin Neurosci. 249 (1999) 288-290.
[4] A. Mack, A. Robitzki, Prog. Neurobiol. 60 (2000) 607.
[5] L.L. Shen, G.X. Liu, Y. Tang, Acta Pharmacol Sin; 28 (2007) 2053-2063.
[6] F. Baharloo, M.H. Moslemin, H. Nadri, A. Asadipour, M. Mahdavi, S. Emami, L. Firouzpour, R. Mohebat, A. Shafiee, A. Foroumadi, Eur. J. Med. Chem. 93 (2015) 196-201.
[7] H. Khanam, Eur. J. Med. Chem. 97 (2015) 483-504.
[8] W.C. Wan, W. Chen, L.X. Liu, Y. Li, L.J. Yang, X.Y. Deng, H. Bin Zhang, X.D. Yang, Med. Chem. Res. 23 (2014) 1599-1611.
[9] A. Ozdemir, M.D. Altintop, Z. Canturk, Z.A. Kaplancikli, Lett. Drug Des. Discov. 12 (2015) 607-611
[10] P. Yadav, P. Singh, A.K. Tewari, Bioorg. Med. Chem. Lett. 24 (2014) 2251-2255.
[11] Y. Chen, S. Chen, X. Lu, H. Cheng, Y. Oua, H. Cheng, G.C. Zhou, Bioorg. Med. Chem. Lett. 19 (2009) 1851-1854.
[12] J. P. Corbet and G. Mignani, Chem. Rev. 106 (2006) 2651-2658.
[13] C. C. C. Johansson Seechurn, M. O. Kitching, T. J. Colacot and V. Snieckus, Angew. Chem., Int. Ed. 51 (2012) 5062
[14] S. E. Kazzouli, J. Koubachi, N. E. Brahmi and G. Guillaumet, RSC Adv., 2015, 5, 15292.
[15] N. Winterton, Green Chem. 3 (2001) 73-79.
[16] A. Suzuki, Pure Appl. Chem. 57 (1985) 1749.
[17] K. Sonogashira, J. Organometal. Chem. 653 (2002) 46.
[18] R. F. Heck, Org. React. 27 (1982) 345.
[19] Y. Nakao, T. Hiyama, Chem. Soc. Rev. 40 (2011) 4893.
[20] M. Pohanka, M. Hrabinova, K. Kuca, J.P. Simonato, Int. J. Mol. Sci. 12(2011) 2631-2640.

29TH IRANIAN ORGANIC CHEMISTRY CONFERENCE
1_3 NOV, 2023
UNIVERSITY OF QOM, IRAN

The modified-black phosphorus nanosheets with enhanced photocatalytic activity

Shadi Asgari[1], *Ghodsi Mohammadi Ziarani*[1*] *and Alireza Badiei*[2]

[1]*Department of Organic Chemistry, Faculty of Chemistry, Alzahra University, Tehran, P.O. Box 1993893973, Iran, gmohammadi@alzahra.ac.ir, sh_asgari@alzahra.ac.ir*
[2]*School of Chemistry, College of Science, University of Tehran, Tehran, Iran.*

Abstract
Surface modification is an effective technique for enhancing photocatalytic activity and ambient stability of black phosphorus (BP). The black phosphorus nanosheets (BPNs) decorated with silver (Ag) and gold (Au) nanoparticles as well as graphene oxide (GO) were successfully synthesized, and characterized with powder X-Ray diffraction (PXRD) technique. The photocatalytic activity of BPNs before and after the surface modification was investigated by photodegradation studies deploying cationic and anionic organic dyes. The dyes degradation was obtained in the trend of BPNs@GO>BPNs@Au>BPNs@Ag>BPNs for methyl orange (MO) and in the trend of BPNs@GO>BPNs@Ag>BPNs@Au>BPNs for methylene blue (MB). Considering the results obtained from trapping experiments, $O_2^{\cdot-}$ and $^{\cdot}OH$ were distinguished as the main species for the dyes photodegradation.

1. Introduction

Black phosphorus (BP) has a layered 2D structure and visible-NIR photocatalytic activity, in which the lone pair electrons on its phosphorus atoms can react with oxygen and water molecules, leading to weakening its photocatalytic activity and ambient stability [1]. Finding an effective method to enhance the photocatalytic activity and ambient stability of BP is very highly challenging. Surface modification techniques including covalent and non-covalent functionalization and metal-ion modification are known as the effective methods dedicated to supplementing the ambient stability and photocatalytic activity of BP [2]. In the metal-ion modification, the noble metals for example Ag and Au can be chemically adsorbed on BP by making cation-p interactions. Actually, BP acts as a reducing agent by losing its electrons and binds to the surface of metal ions [2, 3]. The noble metals show excellent features of strong light absorption, vigorous nature, recyclability, and high surface area, which make them good photocatalytic candidates [4]. BP can also partially reduce oxygen-containing functional groups of graphene oxide (GO) by the production of the covalent bonds (P-C and P-O-C) or distribution on the surface of GO [5, 6]. GO shows excellent mobility and low recombination of the photogenerated electron-hole carriers that increases its photocatalytic activity [7]. Accordingly, it is expected that modifying BPNs with Ag/Au nanoparticles (NPs) and GO enhances both, the photocatalytic activity and ambient stability of BPNs.

2. Experimental

2.1. Synthesis of BPNs@Ag

An aqueous solution of $AgNO_3$ (1 mg. mL^{-1}) was slowly added to a dispersion of as-prepared BPNs in deionized water and stirred for 24 h. Centrifugation was used to collect the product.

2.2. Synthesis of BPNs@Au

The synthesis procedure was similar to the synthesis procedure of BPNs@Ag, whereas an aqueous solution of $HAuCl_4$ was used instead of an $AgNO_3$ solution.

2.3. Synthesis of BPNs@GO

GO powder was added slowly to a dispersion of BPNs in DMF and subjected to ultrasonication within 3 h with working for 5 s and intervals of 2 s. The product was collected with a centrifuge. Fig. 1 indicates the schematics of BPNs@Au, BPNs@Ag, and BPNs@GO.

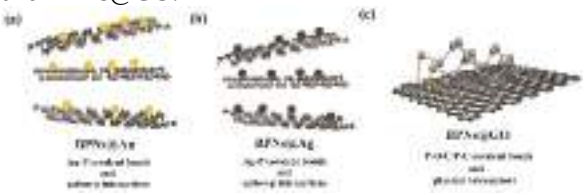

Fig. 1. The schematics of BPNs@Au (a), BPNs@Ag (b), and BPNs@GO (c).

3. Results and Discussion

Modification of BPNs with Au and Ag NPs and GO was confirmed with PXRD (Fig. 2). Red phosphorus (RP) shows a sharp reflectance at $2\theta = 15.7°$ which is related to the amorphous structure of RP. The reflections located at 17.0°, 26.7°, 34.3°, 52.5°, 56.2°, and 56.8° are attributed to the (020), (021), (040), (060), (151) and (061) planes of BPNs, respectively. The diffraction pattern of BPNs@Ag displayed the reflections of Ag at 38.2°, 44.4°, 64.6°, and 77.6° consistent with the (111), (200), (220), and (311)

planes, respectively, and the reflections of Au were observed at 38.2°, 44.6°, 64.7°, and 77.8° which are attributed to (111), (200), (220), and (222) planes, respectively. The diffractogram of BPNs@GO shows the main reflectance of reduced GO at 26.6°.

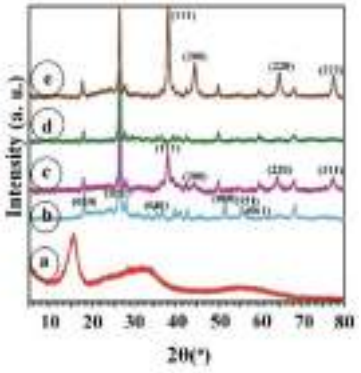

Fig. 2. PXRD patterns of RP (a), BPNs (b), BPNs@Ag (c), BPNs@GO (d), and BPNs@Au (e).

Methylene blue (MB) and methyl orange (MO) were selected as the models of cationic and anionic dyes with the maximum absorbances located at 664 nm and 475 nm, respectively. The MO and MB photodegradation results over the synthesized photocatalysts are presented in Fig. 3. The highest MO degradation was observed for BPNs@GO. BPNs@Ag and BPNs@Au displayed more MO degradation in comparison with the BPNs. The results of MB degradation were found approximately similar to the results obtained for MO degradation.

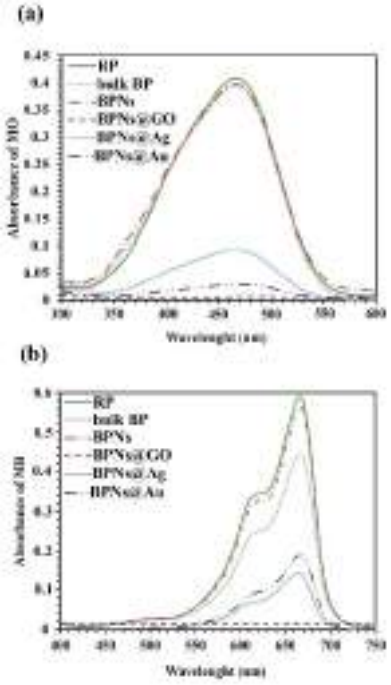

Fig. 3. The photodegradation behavior of photocatalysts over MO (a) and MB (b).

4. Conclusion

The modified BPNs, i.e., BPNs@Au, BPNs@Ag, and BPNs@GO with enhanced photocatalytic activity were successfully prepared and characterized. The following sequences were observed for the degradation of dyes:
BPNs@GO>BPNs@Au>BPNs@Ag>BPNs for MO and BPNs@GO>BPNs@Ag>BPNs@Au>BPNs for MB.

5. References

[1] T. Zhang, Y. Wan, H. Xie, Y. Mu, P. Du, D. Wang, X. Wu, H. Ji, L. Wan, Degradation Chemistry and Stabilization of Exfoliated Few-Layer Black Phosphorus in Water, Journal of the American Chemical Society, 140 (2018) 7561-7567.
[2] S.Y. Lei, H.Y. Shen, Y.Y. Sun, N. Wan, H. Yu, S. Zhang, Enhancing the Ambient Stability of Few-Layer Black Phosphorus By Surface Modification, RSC advances, 8 (2018) 14676-14683.
[3] Z. Guo, S. Chen, Z. Wang, Z. Yang, F. Liu, Y. Xu, J. Wang, Y. Yi, H. Zhang, L. Liao, Metal-Ion-Modified Black Phosphorus with Enhanced Stability and Transistor Performance, Advanced Materials, 29 (2017) 1703811.
[4] S. Moschetto, A. Ienco, G. Manca, M. Serrano-Ruiz, M. Peruzzini, A. Mezzi, M. Brucale, M. Bolognesi, S. Toffanin, Easy and Fast In situ Functionalization of Exfoliated 2D Black Phosphorus with Gold Nanoparticles, Dalton Transactions, 50 (2021) 11610-11618.
[5] T. Zhou, H. Ni, Y. Wang, C. Wu, H. Zhang, J. Zhang, A.P. Tomsia, L. Jiang, Q. Cheng, Ultratough Graphene–Black Phosphorus Films, Proceedings of the National Academy of Sciences, 117 (2020) 8727-8735.
[6] L. Huo, X. Shi, S. Chen, Surface Modification and Stability Performance of Black Phosphorus Nanosheets Based on Metal Ions/Graphene, AIP Advances, 12 (2022).
[7] S.H. Alwan, K.H. Salem, H.A. Alshamsi, Visible Light-Driven Photocatalytic Degradation of Rhodamine B Dye onto TiO_2/rGO Nanocomposites, Materials Today Communications, 33 (2022) 104558.
[8] D. Li, D. Wang, K. Rui, Z. Ma, L. Xie, J. Liu, Y. Zhang, R. Chen, Y. Yan, H. Lin, Flexible Phosphorus Doped Carbon Nanosheets/Nanofibers: Electrospun Preparation and Enhanced Li-Storage Properties as Free-Standing Anodes for Lithium Ion Batteries, Journal of Power Sources, 384 (2018) 27-33.

The photocatalytic nanofibers containing ferrocene-modified graphitic carbon nitride for wastewater treatment

Shadi Asgari[1], *Ghodsi Mohammadi Ziarani*[1*] *and Alireza Badiei*[2]

[1]*Department of Organic Chemistry, Faculty of Chemistry, Alzahra University, Tehran, P.O. Box 1993893973, Iran, gmohammadi@alzahra.ac.ir, sh_asgari@alzahra.ac.ir*

[2]*School of Chemistry, College of Science, University of Tehran, Tehran, Iran.*

Abstract

To resolve the contaminated water-related issues and high degradation of organic dyes from the aqueous media, a photocatalytic nanofibrous system was prepared through 1) modification of graphitic carbon nitride (g-C_3N_4) with ferrocene to produce Fc-g-C_3N_4, 2) incorporation of Fc-g-C_3N_4 into a conductive nanofibrous matrix of polyaniline (PANi) in blending with polyacrylonitrile (PAN), and 3) fabrication of the photocatalytic nanofibers (NFs) through blending electrospinning. The morphologies of the particular form of photocatalyst, Fc-g-C_3N_4, and the photocatalytic NFs were recorded by FE-SEM. The dyes photodegradation experiments showed more MB degradation than MO over both the particular form and nanofibrous form of photocatalyst.

1. Introduction

Water pollution caused by organic dyes has become a serious alarm for many years [1]. Photocatalysis has been introduced as an effective and non-toxic method for the elimination of dyes working by their degradation [2]. Graphitic carbon nitride, g-C_3N_4, is a two-dimensional π-conjugated photocatalyst with visible-light and highly effective photocatalytic activity, chemical stability, low cost, and reusability, which is widely used for photocatalytic degradation of organic pollutants [3]. g-C_3N_4 nanosheets show better photocatalytic activities than g-C_3N_4 in bulk morphology especially when they are prepared as porous structures [4]. Ferrocene contains Fe^{II} and two cyclopentadienyl ligands located in a rigid sandwich structure which can undergo one-electron reversible oxidation to the ferrocenium cation at different potentials [5, 6]. The particular form of photocatalysts can be aggregated, thus, their incorporation into conductive polymeric nanofibers (NFs) may be an effective strategy for both enhancing the photocatalytic activity and reducing aggregation [7, 8]. This research is dealt with designing a photocatalyst based on PANi/PAN NFs embedded with Fc-g-C_3N_4.

2. Experimental

2.1. Synthesis of ferrocene-modified g-C_3N_4 nanosheets (Fc-g-C_3N_4)

The precursors of melamine and ammonium carbonate were mixed and sealed inside a crucible, and then heated at 550 ˚C with a heating rate of 1.67 ˚C/min and more heated at 570 ˚C with the same heating rate. A yellow powder was received as the g-C_3N_4 product. The product was then modified with ferrocene.

2.2. Fabrication of photocatalytic NFs

The spinning solution of Fc-g-C_3N_4 in the PANi/PAN matrix was prepared by its dispersing in DMF and mixing with PANi/PAN. The electrospinning was carried out at 16.5 kV. The NFs were dried at room temperature after peeling off from the aluminum foil. Fig. 1 indicates the fabrication of the photocatalytic NFs by the electrospinning technique.

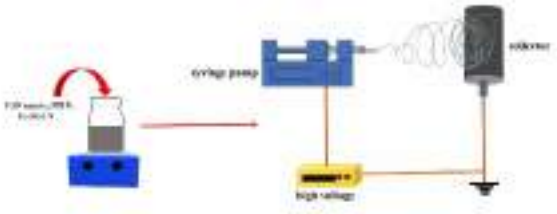

Fig. 1. Fabrication of the photocatalytic NFs through electrospinning technique.

3. Results and Discussions

The morphology of the particulate form and the nanofibrous form of photocatalyst was studied by FE-SEM. Fig. 2 indicates a sheet-like structure for Fc-g-C_3N_4 and a number of protrusions for the photocatalytic NFs.

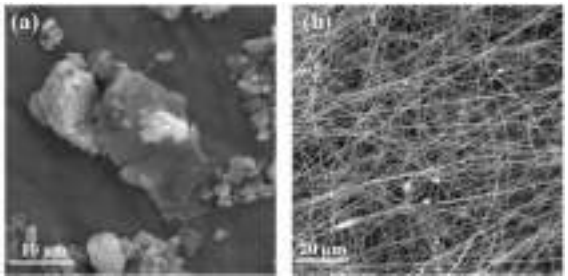

Fig. 2. FE-SEM images of Fc-g-C_3N_4 (a) and photocatalytic NFs (b).

The MB photodegradation efficiencies were received in the sequence of Fc-g-C_3N_4>g-C_3N_4 and photocatalytic NFs> pure PAN NFs. These sequences are showing a higher photocatalytic activity of g-C_3N_4 when it is attached to ferrocene compared to the g-C_3N_4 alone.

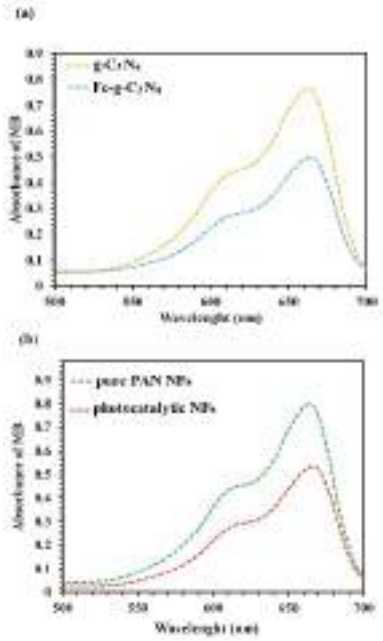

Fig. 3. MB photodegradation curves over particulate form of photocatalyst (a) and nanofibrous form of photocatalyst (b).

4. Conclusion

We successfully synthesized a photocatalytic nanofibrous system by incorporation of the ferrocene-modified g-C_3N_4 into the conductive nanofibrous matrix of PANi/PAN, followed by blending electrospinning. g-C_3N_4 attached with ferrocene showed higher MB photodegradation compared to the g-C_3N_4 alone.

5. References

[1] K.Y.A. Lin, J.T. Lin, Ferrocene-functionalized graphitic carbon nitride as an enhanced heterogeneous catalyst of Fenton reaction for degradation of Rhodamine B under visible light irradiation, Chemosphere, 182 (2017) 54-64.

[2] S. Asgari, G.M. Ziarani, A. Badiei, F. Ajalloueian, Y. Vasseghian, Electrospun composite nanofibers as novel high-performance and visible-light photocatalysts for removal of environmental pollutants: A review, Environmental Research, (2022) 114296.

[3] H. Zhang, X. Zuo, H. Tang, G. Li, Z. Zhou, Origin of photoactivity in graphitic carbon nitride and strategies for enhancement of photocatalytic efficiency: insights from first-principles computations, Physical Chemistry Chemical Physics, 17 (2015) 6280-6288.

[4] C. Wang, G. Zhang, H. Zhang, Z. Li, Y. Wen, One-pot synthesis of porous g-C_3N_4 nanosheets with enhanced photocatalytic activity under visible light, Diamond and Related Materials, 116 (2021) 108416.

[5] P. Chellan, P.J. Sadler, Enhancing the activity of drugs by conjugation to organometallic fragments, Chemistry–A European Journal, 26 (2020) 8676-8688.

[6] A. Togni, T. Hayashi, Ferrocenes: Homogeneous Catalysis, Organic Synthesis, Materials Science, 1 (1995).

[7] J. Yu, J. Li, X. Zhu, X. Zhang, K. Jia, W. Kong, P. Wei, H. Chen, X. Shi, A.M. Asiri, Structured polyaniline: an efficient and durable electrocatalyst for the nitrogen reduction reaction in acidic media, ChemElectroChem, 6 (2019) 2215-2218.

[8] C. Dai, B. Liu, Conjugated polymers for visible-light-driven photocatalysis, Energy & Environmental Science, 13 (2020) 24-52.

29TH IRANIAN ORGANIC CHEMISTRY CONFERENCE
1_3 NOV, 2023
UNIVERSITY OF QOM, IRAN

Investigating the performance of persulfate and hydrogen peroxide oxidants in the degradation of ciprofloxacin using perovskite catalysts

Mohammadali Jalali, Seyed Mahdi Mousavi and Moslem Setoodehkhah*

Department of Applied Chemistry, Faculty of Chemistry, Kashan University, Kashan, Iran,
mj921661@gmail.com, mousavi.smahdi@kashanu.ac.ir

Abstract - Removal of toxic organic substances is one of the important tasks in wastewater treatment. Recently, heterogeneous catalysts are used for the activation of peroxymonosulfate and hydrogen peroxide in advanced oxidation processes based on sulfate radicals and hydroxyl radicals to remove these substances. The present work reports an ideal system for the degradation of organic matter from the environment. For this purpose, perovskites are used as an efficient catalyst to activate peroxymonosulfate and oxygen water to degrade ciprofloxacin. Perovskites have attracted increasing attention due to their controllable oxidation state and the formation of oxygen vacancies, which accelerates the cycle of redox pairs. Electron paramagnetic resonance suggests that both sulfate and hydroxyl radicals play an important role in advanced oxidation processes.

1. Introduction

The increase in water pollution around the world has reinforced the importance of efficient and new strategies in water waste treatment. To meet this need, advanced oxidation processes (AOPs) based on the activation of common oxidants to produce highly active radicals have been successfully investigated for chemical and microbial substances [1-2]. In general, oxidizers based on species highly reactive oxygen radicals, such as hydroxyl radicals (OH) or sulfate (SO4), which can destroy and even mineralize resistant organic pollutants [3]. In advanced oxidation, two homogeneous and heterogeneous systems are used. Homogeneous activator system with Catalysts suffer from unfavorable loss of dissolved metal ions and difficult reuse. To overcome these drawbacks, heterogeneous activation systems have been used. In recent years, perovskite-type oxides have been intensively investigated. and have been developed for many applications. Apart from solar panel production, [4] oxygen separation [5] and construction of solid oxide fuel cell cathode [6], their photoelectric thermochemical properties are increasingly investigated in water splitting and purification [7-10]. Perovskites have the general formula ABO3, which is placed in the A position of alkali metals, alkaline earth metals, and lanthanum and in the B position of transition metals [11]. You can see the structure of perovskite catalyst in Fig. 1.

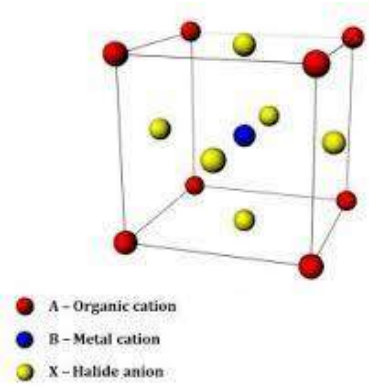

Fig.1. Perovskite catalyst structure

Perovskites, due to their optical and dielectric properties, Superconductivity, high potential, high excitability and synthesis at low temperature are used as suitable catalysts in the oxidation process of medicinal pollutants [12-13]. and then using it, we investigate the performance of persulfate and hydrogen peroxide on the degradation of ciprofloxacin in aqueous environment.

2. Materials and test methods

2.1. Test material: Lanthanum nitrate hexahydrate, cobalt nitrate hexahydrate, nickel nitrate hexahydrate, manganese nitrate tetrahydrate, iron nitrate ninehydrate, citric acid, ciprofloxacin, potassium persulfate, hydrogen peroxide, methanol

2.2. Test Method: For the synthesis of LaCoO3, stoichiometric amounts of raw materials such as lanthanum nitrate hexahydrate, cobalt nitrate hexahydrate were weighed and dissolved in ionized water. Then, citric acid was added to the solution with a molar ratio of 1:1 compared to the total amount of metal ions. The mixture was stirred at a temperature of 150 degrees Celsius, which was constantly stirred by a magnetic current. After the complete evaporation of water and the formation of a spongy solid, the sample was placed in an oven at a temperature of 75 degrees for 24 hours, and then It was calcined at 300 and 750

degrees for 1 and 5 hours. Finally, a soft black LaCoO3 powder was obtained. For the synthesis of three perovskites LaMnO3, LaNiO3, LaFeO3, the same method is used, with the difference that instead of using cobalt nitrate, iron, nickel and manganese nitrates are used for each perovskite.

2.3. Destruction of Ciprofloxacin: First, we prepare a drug solution with a concentration of PPm100. For this purpose, we dissolve 10 mg of the drug in 100 ml of water. In the next step, we take 10 ml of this solution and add it to the volume. Then we add /۱ *gram* of desired perovskite to it. After mixing and forming a suspension, we add /27g of persulfate to it. With the addition of persulfate, the drug removal process begins. Samples are taken at different time intervals and each sample is added to a specific amount of methanol to complete the reaction process. Finally, we filter the solution and absorb it. Now we do the test again with hydrogen peroxide instead of persulfate and record the results.

3. Discussion and results

3.1. X-Ray diffraction: The XRD pattern of the synthesized perovskites is shown in Fig. 2.

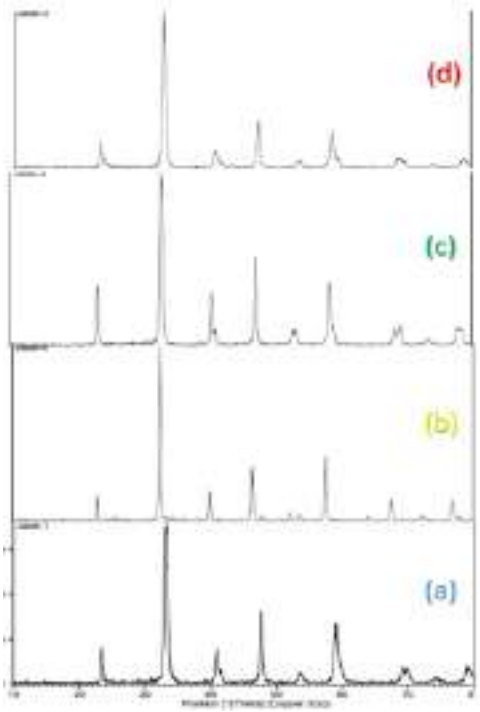

Fig.2. X-ray diffraction pattern of perovskites a) lanthanum cobalt b) lanthanum iron c) lanthanum manganese d) lanthanum nickel

As can be seen in Figure 2-a, the peaks obtained from the X-ray diffraction of the lanthanum cobalt sample correspond well with the standard model with the code (010840848). This model has a cubic phase. Figure 2-b is related to iron lanthanum perovskite. which corresponds to the standard model (010742203). Figure 2-c is related to lanthanum manganese, which corresponds to the model The standard corresponds to code (000511515). Figure-2-d is lanthanum nickel, which corresponds to standard code (000330711). The results show that the prepared perovskites with a high degree of crystallization have formed a phase. The XRD pattern for the prepared perovskites shows clear sharp peaks, which indicate the good tabulation of the samples and the formation of single-phase perovskite structures.

3.2. Performance of different oxidants: The performance of persulfate and hydrogen peroxide oxidants was investigated using perovskites prepared with sol-gel complexing agent citric acid in an aqueous medium with neutral pH and ambient temperature in the process of oxidation of medicinal pollutant ciprofloxacin. In this process, the aqueous solution of the antibiotic ciprofloxacin with a concentration of 10 ppm was used as the test solution. The performance of oxidants on perovskite catalysts was studied separately. To measure the concentration of the drug in the desired samples, a UV/VIS transmission spectrometer is used at the maximum wavelength of ciprofloxacin (275 nm). The results of the degradation and removal of ciprofloxacin from each perovskite with the oxidizing agent persulfate and hydrogen peroxide are shown in Figures 3 and 4, respectively.

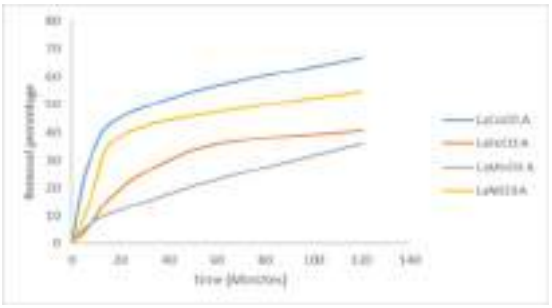

Fig.3. Performance results of different perovskites with persulfate

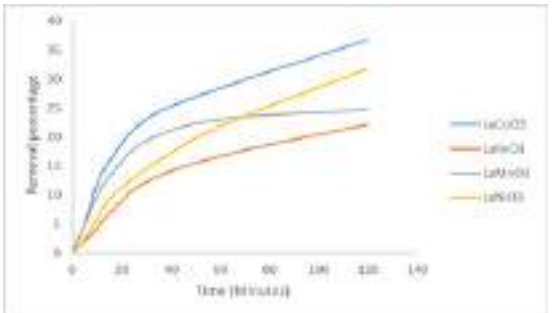

Fig.4. Performance results of different perovskites with hydrogen peroxide

Figure 3 shows the performance results of lanthanum-based cobalt, iron, nickel and manganese perovskites in the removal of ciprofloxacin with persulfate oxidizing agent. The maximum removal of ciprofloxacin for these perovskites is 66%. According to this figure, the superior performance of lanthanum

cobalt perovskite prepared by sol-gel method compared to other prepared perovskites has been clearly identified. Figure 4 shows the performance results of the mentioned perovskites in the removal of ciprofloxacin with the oxidizing agent hydrogen peroxide, and the maximum removal of the drug is related to lanthanum cobalt with a degradation of about 36%. With a general review of the performance results of the prepared perovskites, it is clear that the prepared lanthanum cobalt perovskite had a better performance in the process of catalysing the removal of pharmaceutical pollutants.

4. Conclusion:

In summary, the intended catalysts were successfully prepared by sol-gel method with citric acid complexing agent and were used as a suitable and efficient catalyst for the degradation of ciprofloxacin in food waste water. Sulfate radical and hydroxyl radical production were used. Among the prepared perovskites, lanthanum cobalt has the highest percentage of destruction with both oxidizing agents. Now, in a general comparison between the oxidizing agents of persulfate and hydrogen peroxide, we come to the conclusion that the destruction with persulfate agent is far more than hydrogen peroxide. One of the reasons for the superiority of persulfate over hydrogen peroxide is its high redox potential and longer lifespan, while hydroxyl radicals may remain as radicals and cause toxicity, but persulfate radicals are released as ions after the process is completed. It does not have a simit [14-15].

5. References

[1] Y. Deng, R. Zhao, Advanced oxidation processes (AOPs) in wastewater treatment, Curr. Pollut. Rep. 1 (2015) 167–176.

[2] S. Giannakis, S. Liu, A. Carratalà, S. Rtimi, M. Bensimonc, C. Pulgarin, Effect of Fe(II)/Fe(III) species, pH, irradiance and bacterial presence on viral inactivation in wastewater by the photo-Fenton process: kinetic modeling and mechanistic interpretation, Appl. Catal. B: Environ. 204 (2017) 156–166.

[3] Ren F., Zhu W., Zhao J., Liu H., Zhang X., Zhang H., Wang B., Nitrogen-doped graphene oxide aerogel anchored with spinel CoFe2O4 nanoparticles for rapid degradation of tetracycline. Sep. Purif. Technol.,2020,241,116690.

[4] J.M. Ball, M.M. Lee, A. Hey, H.J. Snaith, Low-temperature processed meso-superstructured to thin-film perovskite solar cells, Energy Environ. Sci. 6 (2013) 1739–1743.

[5] A. Leo, S. Smart, S. Liu, J.D. da Costa, High performance perovskite hollow fibres for oxygen separation, J. Membr. Sci. 368 (2011) 64–68.

[6] N. Ai, N. Li, W.D. Rickard, Y. Cheng, K. Chen, S.P. Jiang, Highly stable Sr-free cobaltite-based perovskite cathodes directly assembled on a barrier-layer-free Y2 O3-ZrO2 electrolyte of solid oxide fuel cells, ChemSusChem 10 (2017) 993–1003.

[7] Y.L. Zhu, W. Zhou, Y. Zhong, Y.F. Bu, X.Y. Chen, Q. Zhong, M.L. Liu, Z.P. Shao, A perovskite nanorod as bifunctional electrocatalyst for overall water splitting, Adv. Energy Mater. 7 (2017) 1602122.

[8] E. Grabowska, Selected perovskite oxides: characterization, preparation and photocatalytic properties—a review, Appl. Catal. B: Environ. 186 (2016) 97–126

[9] P. Kanhere, Z. Chen, A review on visible light active perovskite-based photocatalysts, Molecules 19 (2014) 19995–20022

[10] S. Yin, H. Tian, Z. Ren, X. Wei, C. Chao, J. Pei, X. Li, G. Xu, G. Shen, G. Han, Octahedral-shaped perovskite nanocrystals and their visible-light photocatalytic activity, Chem. Commun. 50 (2014) 6027–6030.

[11] Kour R., Arya S., Verma S., Gupta J., Bandhoria P., Bharti V., Datt R., Gupta V., Potential Substitutes for Replacement of Lead in Perovskite Solar Cells: A Review. Global Challeng.,2019,3(11),1900050.

[12] Müller K A., and Kool T W., Properties of Perovskites and Other Oxides, World Scientific., 2010, 546, 22-36.

[13] Kim H S., Lee C R., Lee J H., Moehl K B., Marchioro T., Moon A., Humphry B S J., Yum R., Moser J H., Eetal J., Lead Iodide Perovskite Sensitized All-Solid-State Submicron Thin Film Mesoscopic Solar Cell with Efficiency Exceeding 9%. Sci. Rep.,2012,591-598.

[14] Y.C. Du, W.J. Ma, P.X. Liu, et al., Magnetic CoFe2O4 nanoparticles supported on titanate nanotubes (CoFe2O4/TNTs) as a novel heterogeneous catalyst for peroxymonosulfate activation and degradation of organic pollutants, J. Hazard. Mater. 308 (2016) 58–66.

[15] P.D. Hu, M.C. Long, Cobalt-catalyzed sulfate radical-based advanced oxidation: a review on heterogeneous catalysts and applications, Appl. Catal. B 181 (2016) 103–117.

29TH IRANIAN ORGANIC CHEMISTRY CONFERENCE
1_3 NOV, 2023
UNIVERSITY OF QOM, IRAN

The effect of deep eutectic solvent on the antifouling performance of ultrafiltration membrane

Azar Asadi and Mohammad Amin Heidari*

Department of Applied Chemistry, Faculty of Gas and Petroleum, University of Yasouj, Gachsaran, Iran, a.asadi@yu.ac.ir

Abstract

In this research, a deep eutectic solvent (DES) based on Choline chloride (ChCl):1,5-Diphenylcarbazide (DPC) has been synthesized and applied into PVDF membrane matrix. The performance of the bare membrane and the DES-incorporated membrane had been evaluated in the terms of filtering dry milk powder solution with 10000 mg/l of concentration. Based on the results, the modified membrane showed higher pure water flux and also permeate flux over pure water and dry milk solution filtration compared with the bare membrane. This outcome showed that DES could be considered as a proper additive to enhance membranes' hydrophilicity and antifouling properties.

1. Introduction

Hydrophilicity is a key factor in developing membranes to industries. Various additives to enhance the hydrophilicity of membranes have been applied and investigated over years[1, 2].

PVDF is composed of semi-crystalline repeating units of $-(CH_2CF_2)_n-$. It has great mechanical strength, outstanding chemical and thermal stability, and exceptional aging resistance, all of which are required for real membrane separation industrial applications[3]. DES as an ionic liquid composed of hydrogen bond acceptor (HBA) as well as one hydrogen bond donor (HBD) is used in the recent years for different applications like catalysis and filtration process and biosensors[4]. DES could be synthesized in an easy way by heating a molar ratio of HBA and HBD. In this research, DES was synthesized by mixing Choline chloride (ChCl) as HBA and :1,5-Diphenylcarbazide (DPC) as HBD. Then the obtained DES was embedded in mixed matrix of PVDF membrane to promote its hydrophilicity properties. The antifouling properties of the bare and modified membranes was evaluated by filtering dry milk solution as organic foulant.

2. Materials and Methods

Choline chloride and 1,5-Diphenylcarbazide (as the respective HBA and HBD molecules) were mixed at a 1:2 molar ratio in an inert environment (50 ml of distilled water) and stirred while heating to 80 ℃ (353.15 K) until a homogenous, transparent liquid was formed. To produce membrane sheet, phase inversion method was used so that for preparing casting solution 20 wt.% PVDF and 1 wt.% PVP were dissolved in NMP with 0.7% of DES (this amount of additive was considered based on the previous work)[5]. To evaluate the performance of the obtained membrane dry milk solution with 10000 mg/l of concentration was used as an organic foulant and passed through a dead-end setup as shown in Fig.1.

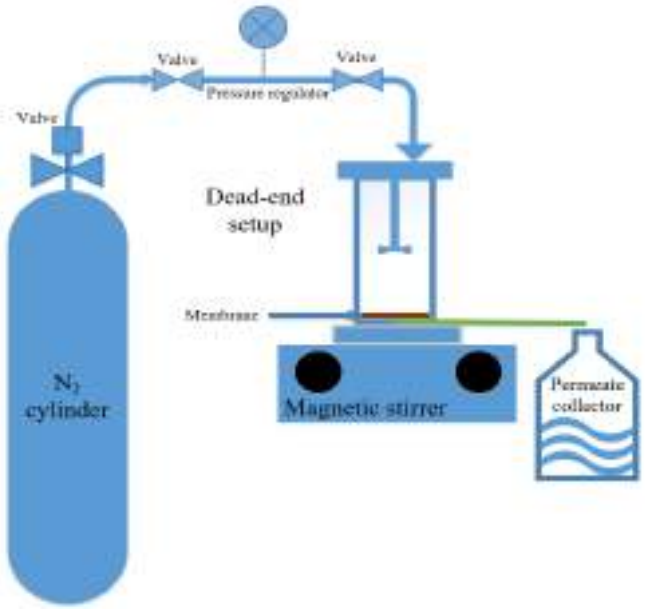

Fig. 1. Schematic of dead-end setup.

3. Results and discussion

To evaluate the effect of embedding of the synthesized DES on the PVDF membrane's performance, dry milk solution with 10000 mg/l of concentration was passed

through a dead-end setup under pressure of 4 bar. a three step filtration was selected to assess pure water flux and antifouling properties of the bare and modified membranes. In this manner, a three step filtration was designated including the first distillated water, dry milk solution, and the second distillated water. The obtained data for both the bare and modified membranes was drawn and shown in Fig.1. based on the figure, the modified membrane showed higher pure water flux compared with the bare one, indicating an enhancement in membrane's hydrophilicity. On the other hand, the permeate flux of the bare membrane illustrated a main reduction after filtering dry milk solution so that its flux was reduced from 80 to 2 kg/ m2.h after 20 min of filtration, however, the modified membrane's flux presented a slight reduction trend. This observation verified upper antifouling properties of the modified membrane confronting of organic foulants, this result could be attributed to higher hydrophilic property influenced by embedding DES which could create a hydration layer near the membrane surface. The hydration layer act as a barrier for preventing the adhesion of foulant molecule on the surface and then the occurrence of water channel blocking will be delayed[6]. After 250 min of dry milk filtration, the membranes were washed with distilled water completely and located in distilled water for 20 min.

The second distilled water filtration represented a significant difference on flux recovery of the studied membranes. The DES-incorporated membrane's flux was recovered significantly after washing, however bare membrane showed lower pure water flux in the second distilled water filtration.

In overall, the amended membrane was able to provide high and stable flux over filtration and it could be concluded that DES as ionic liquid improves hydrophilicity and water flux of the bare membrane.

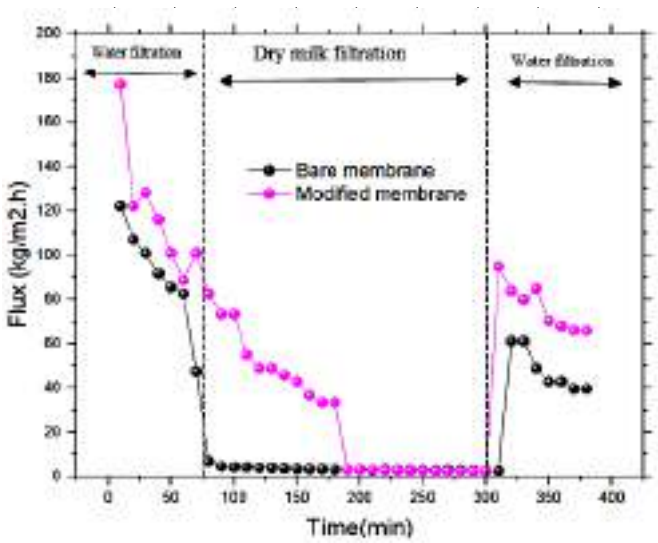

Fig. 2. Three step filtrations of the bare and modified membranes.

4. Conclusion

In this research, a new type of ionic liquids which made of two parts including hydrogen bond donner (HBD) and hydrogen bond acceptor (HBA) has been added to membrane matrix. DES was synthesized by mixing Choline chloride (ChCl):1,5 Diphenylcarbazide. DES-incorporated membrane showed higher pure water flux and permeate flux after passing through dry milk solution with 10000 mg/l concentration compared to the bare membrane.

4. References

[1] A. Asadi, S. Nazari, F. Gholami, M. Dolatshah, Facile and effectual surface modification of polyacrylonitrile (PAN)-based ultrafiltration membranes via manipulating the synergistic interaction of dopamine and enzymes, Journal of Water Process Engineering 52 (2023) 103562.

[2] A. Asadi, F. Gholami, A. Zinatizadeh, H. Jaberi, Application of novel nanofiltration membranes embedded with mesoporous carbon based nanoparticles for desalination and dye removal, Chemical Papers 76(3) (2022) 1349-1363.

[3] G.-d. Kang, Y.-m. Cao, Application and modification of poly (vinylidene fluoride)(PVDF) membranes–a review, Journal of membrane science 463 (2014) 145-165.

[4] M. Taghizadeh, A. Taghizadeh, V. Vatanpour, M.R. Ganjali, M.R. Saeb, Deep eutectic solvents in membrane science and technology: Fundamental, preparation, application, and future perspective, Separation and Purification Technology 258 (2021) 118015.

[5] A. Asadi, F. Gholami, S. Nazari, M. Dolatshah, Improved filtration performance of polyvinylidene fluoride nanocomposite membranes embedded with deep eutectic solvent: Application towards MBR, Desalination 543 (2022) 116088.

[6] A. Asadi, F. Gholami, S. Nazari, M. Dolatshah, Preparation of antifouling and antibacterial polyvinylidene fluoride membrane by incorporating functionalized multiwalled carbon nanotubes, Journal of Water Process Engineering 49 (2022) 103042.

29TH IRANIAN ORGANIC CHEMISTRY CONFERENCE
1_3 NOV, 2023
UNIVERSITY OF QOM, IRAN

Cu (II) Complex Immobilized on Hybrid Nanomaterial as a Catalyst for Synthesis of Benzopyrans and Pyranopyrimidinones

Mohammd Ali Bodaghifard[1] *, *Somayeh Safari*[2]

[1] *Department of Chemistry, Faculty of Science, Arak University, 38156-88138, Arak, Iran, mbodaghi2007@yahoo.com; m-bodaghifard@araku.ac.ir.*
[2] *Institute of Nanosciences and Nanotechnology, Arak University, 38156-88138, Arak, Iran.*

Abstract - In this work, a surface-modified magnetic solid support with the Cu (II) complex tags was prepared. The structure of newly prepared nanostructure was characterized by FT-IR, XRD, TGA/DTG, VSM, FE-SEM, EDS, and ICP/OES techniques. The catalytic activity of prepared hybrid nanomaterial was evaluated in the synthesis of tetrahydrobenzo[*b*]pyran and pyrano[2,3-*d*]pyrimidinone derivatives. Some advantages of this method are high yields, short reaction times, green solvent and conditions, easy workup procedure, negligible copper leaching, reusability without a significant diminish in catalytic efficiency and simple separation of nanocatalyst by using an external magnet alongside the environmental compatibility and sustainability.

1. Introduction

The multicomponent reactions are a good way to produce complex and diverse combinations with high interest rates [1]. The MCRs have many advantages as low reaction times, diminished work-up procedures, high efficiency, cheapness, high selectivity, low environmental impact compared to different methods of classical chemistry [2].
The magnetic nanoparticles (MNPs) have high surface area and can be easily separated by using an external magnetic field and do not have tedious separation procedures which resulted from the small sizes of nanoparticles [3]. MNPs are usually coated with a polymeric or inorganic matrix [4]. Among inorganic compounds, SiO_2 can be a suitable candidate for protecting the surface of MNPs due to its high chemical and thermal stability and most importantly its easy modification by a wide range of functional groups, which increase chemical and colloidal stability of these compounds [5].

Metal complexes have been used as homogenous catalysts in the wide range of organic reactions. However, most of them are precious and expensive and have drawbacks such as tedious separation and decreasing of catalytic activities with time. To overcome some of these issues, several metal complexes have been immobilized onto inorganic supports. So many works have been reported in the literature for grafting and immobilization of metal complexes on magnetic nanosized inorganic supports that benefit from excellent catalytic activity, high selectivity and easy separation [5].

Tetrahydrobenzo[*b*]pyrans and pyranopyrimidinone derivatives are important classes of heterocyclic scaffolds in the field of drugs and pharmaceuticals. These compounds are widely used as antitumor, antibacterial, antihypertensive, hepatoprotective, vasodilator, antiallergic, antifungal, antimalarial and herbicide anti-coagulant, and diuretic agents [6, 7]. There are many reported methods for synthesis of these compounds. However, these methods have many defects such as long reaction times, the use of quantitative amounts of catalysts, expensive and non-recyclable catalysts, use of volatile and harmful solvents contradictory to green chemistry, and difficult separation of the products. So, the development of simpler and high yield approaches and milder reaction conditions toward this valuable nucleus is very desirable.
As part of our continuous effort to develop efficient heterogeneous magnetic nanocatalysts and green organic reactions to gain the valuable heterocyclic compounds [5, 8-10], herein we have reported the preparation of a novel heterogeneous copper complex-supported hybrid nanostructure [$CoFe_2O_4$@SiO_2@BIMA@Cu] as an impressive catalyst for synthesis of tetrahydrobenzo[*b*]pyrans and pyrano[2,3-*d*]pyrimidinones (Scheme 2).

2. Results and Discussion

The magnetic hybrid nanoparticles were prepared sequentially as depicted in Scheme 1. Firstly, $CoFe_2O_4$ prepared easily by the co-preparation method from chemical reaction of Co^{2+} and Fe^{3+} ions in the base conditions [11]. Then, $CoFe_2O_4$ nanoparticles were coated with silica layer using the stöber method [11]. The chloropropyl-modified silica-coated $CoFe_2O_4$

nanoparticles were prepared by reaction of $CoFe_2O_4@SiO_2$ with (3-chloropropyl)triethoxisilane (CPTES) which can bind covalently to the free-OH groups at the particles surface and afforded the $Fe_3O_4@SiO_2$-PrCl. The reaction of (1*H*-benzo[*d*]imidazol-2-yl)methanamine with $CoFe_2O_4@SiO_2$-PrCl resulted to construction of $CoFe_2O_4@SiO_2@BIMA$ nanostructure. Finally, $Cu(OAc)_2$ was stabilized on the modified magnetic nanoparticles. The resulting precipitate was washed with ethanol and dried in the vacuum oven to gain the final hybrid nanomaterial [$CoFe_2O_4@SiO_2@BIMA@Cu$]. The Fourier transform infrared (FT-IR) spectroscopy, X-ray powder diffraction (XRD), field emission scanning electron microscopy (FE-SEM), energy dispersive X-ray spectroscopy (EDS), thermogravimetric analysis (TGA/DTG), vibrating sample magnetometr (VSM) and inductively coupled plasma optical emission spectrometry (ICP/OES) were employed to identify and characterize the prepared hybrid nanostructure.

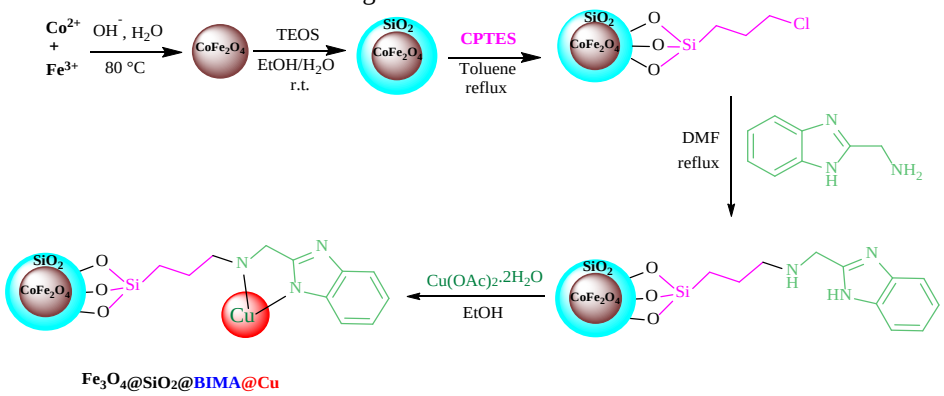

Scheme 1: Schematic steps for the construction of CoFe2O4@SiO2@BIMA@Cu hybrid nanostructure

The size and morphology of the $CoFe_2O_4@SiO_2@BIM@Cu$ particles was investigated by the field emission scanning electron microscopy (Figure 1). The SEM image shows $CoFe_2O_4@SiO_2@BIMA@Cu$ particles are nearly spherical shapes with mean diameter 30 nm. The electron dispersive X-ray spectrum (EDS) confirms the presence of carbon (C), silicon (Si), nitrogen (N), oxygen (O), cobalt (Co), iron (Fe), and copper (Cu) elements in $CoFe_2O_4@SiO_2@BIMA@Cu$ nanostructure.

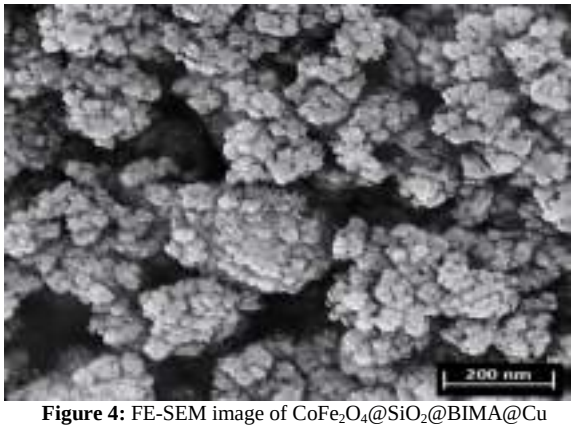

Figure 4: FE-SEM image of $CoFe_2O_4@SiO_2@BIMA@Cu$ nanomaterial

After the successful preparation and characterization of $CoFe_2O_4@SiO_2@BIMA@Cu$, its catalytic activity was considered in the synthesis of tetrahydrobenzopyrans and pyranopyrimidinones. The parameters affecting the reaction yields such as temperature, solvent, catalyst amount, and the solvent-free conditions were investigated. Using the $CoFe_2O_4@SiO_2@BIMA@Cu$ as a catalyst, H_2O/EtOH as a solvent, and conventional heating at 50 °C is the efficient and best condition. It was found that this reaction did not proceed significantly without catalyst and heating, even in a long time.

With the optimized conditions in hand, a mixture of aromatic aldehyde 1, malononitrile 2, dimedone 3 or barbituric acid 5 in H_2O/EtOH at 50 °C was stirred in the presence of a catalytic amount of $CoFe_2O_4@SiO_2@BIMA@Cu$ (20 mg) to afford the 4H-benzo[*b*]pyrans and pyrano[2,3-*d*]pyrimidinones in high yields (87-95%) in relatively short reaction times, without byproducts. Arylaldehydes with electron-donating or electron-withdrawing groups could lead to favorite products with no reasonable difference in their reactivity. The structure of products was confirmed by FT-IR, ^{1}H-NMR, ^{13}C-NMR spectroscopies and comparison with those reported in the literature. The comparison of the $CoFe_2O_4@SiO_2@BIMA@Cu$ nanostructure as catalyst with some previously reported catalysts for the synthesis of 4H-benzo[*b*]pyran and pyrano[2,3-*d*]pyrimidinone derivatives, confirm that the $CoFe_2O_4@SiO_2@BIMA@Cu$ is a comparable, suitable and efficient catalyst for synthesis of these compounds. Based on the literature survey, it is proposed that the Cu (II) ions act as Lewis acids and activate the carbonyl and nitrile functional groups and facilitate the condensation reactions. The porosity and high surface area of hybrid nanostructure

($CoFe_2O_4$@SiO_2@BIMA@Cu) providing suitable support for the chemical reactions and increase the catalytic performance of the prepared hybrid nanomaterial.

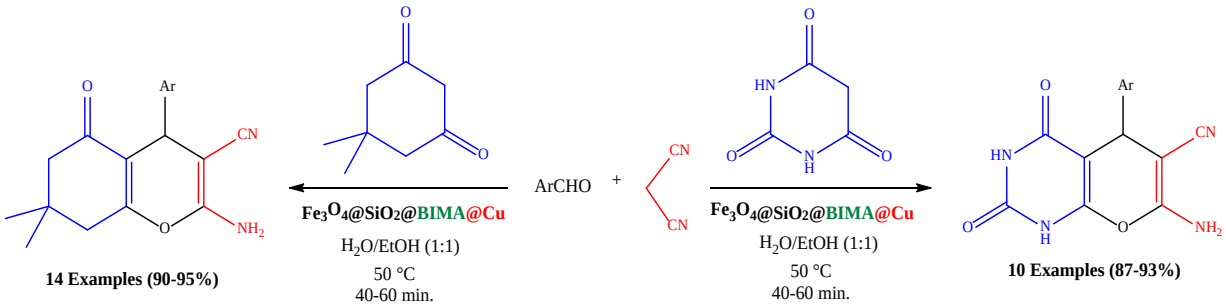

Scheme 2: Synthesis of 4*H*-benzo[*b*]pyran and pyrano[2,3-*d*]pyrimidinone derivatives in the presence of $CoFe_2O_4$@SiO_2@BIMA@Cu hybrid nanocatalyst

3. Conclusion

In this work, a surface-modified magnetic nanoparticles were functionalized with the Cu (II) complex tags. The novel Cu-complex decorated hybrid nanostructure ($CoFe_2O_4$@SiO_2@BIMA@Cu) was characterized successfully using various techniques and its catalytic activity was considered in the synthesis of 4*H*-benzo[*b*]pyran and pyrano[2,3-*d*]pyrimidinone derivatives. The desired products were synthesized by three component reaction of dimedone or barbituric acid, arylaldehydes, and malononitrile in high yields within short reaction times. This strategy offers several key characteristics such as high yield and purity of products, easy work-up and eco-friendly process, and simple separation of catalyst. It is noteworthy that the Cu grafting with organic functional groups on inorganic support efficiently limit Cu leaching and particle growth, which permit this hybrid nanocatalyst to be reused several times with only a slight diminish in its activity.

Acknowledgements

The authors acknowledge the financial support of the Research Council of Arak University.

4. References

[1] J. Zhu, Q. Wang, M.-X. Wang. Multicomponent Reactions in Organic Synthesis. 1nd Edition, Wiley-VCH, Weinheim, Germany, 2015.

[2] H. Bienayme, K. Bouzid. Angew. Chem., Int. Ed. 37 (1998) 2234.

[3] W. Injumpa, P. Ritprajak, N. Insin. J. Magn. Magn. Mater. 427 (2017) 60.

[4] S.H. Araghi, M.H. Entezari. Appl. Surf. Sci. 333 (2015) 68.

[5] M.A. Bodaghifard, M. Hamidinasab, N. Ahadi. Curr. Org. Chem. 22 (2018) 234.

[6] K. Singh, J. Singh, H. Singh, *Tetrahedron* **1996**, *52*, 14273–15280.

[7] D. Heber, C. Hebers, U. Ravens, *Pharmazie* **1993**, *48*, 537–541.

[8] M.A. Bodaghifard, Z. Faraki, A.R. Karimi, Curr. Org. Chem. 20 (2016) 1648.

[9] A. Mobinikhaledi, S. Asadbegi, M.A. Bodaghifard, Mol. Div. 20 (2016) 461.

[10] N. Ahadi, M.A. Bodaghifard, A. Mobinikhaledi, Appl. Organomet. Chem. 33 (2019) e4738.

[11] Z. Mahhouti, H. El Moussaoui, T. Mahfoud, M. Hamedoun, M. El Marssi, A. Lahmar, A. El Kenz, A. Benyoussef. J. Mater. Sci. Mater. Electron. 30 (2019) 14913.

29TH IRANIAN ORGANIC CHEMISTRY CONFERENCE
1_3 NOV, 2023
UNIVERSITY OF QOM, IRAN

FORMATION OF SPIRO[BENZOPYRRLOTHIAZOLE-THIOAZLACTONE] CONJUGATES FROM ERLENMEYER THIOAZLACTONES AND AZOMETHINE YLIDES.

Hamideh Shirazi[1], *Issa Yavari*[2]*

Department of Chemistry, Tarbiat Modares University, Tehran, Iran, yavarisa@modares.ac.ir

Abstract - Pyrrolidines are privileged heterocyclic structures in permitted drugs, and their broad biological applications suggest this skeleton to be an advantaged structure in drug discovery. Spiropyrrolidine, as a branch of the pyrrolidine molecule, has several special biological activities and it is considered an attractive synthetic target. We have developed an operational approach for a diastereoselective synthesis of functionalized spiro[benzopyrrolothiazole-thioazlactone] conjugates from Erlenmeyer thioazlactones and azomethine ylides, which features that four stereogenic centers were simultaneously created with excellent diastereoselectivity. Thus, the azomethine ylides, generated *in situ* from reaction of 3-(2-oxo-2-arylethyl)benzo[*d*]thiazol-3-ium bromides, were seized by 5-alkenylrhodanins featuring exocyclic double bonds that enables the diastereoselective formation of polyfunctionalized spiroheterocycles in good yields. Clear evidence for the stereochemistry of a typical product was obtained from single crystal X-ray analyses.

1. Introduction

Pyrrolidines are privileged heterocyclic structures in many pharmaceuticals and natural bioactive molecules.[1,2] Natural pyrrolidine alkaloids possess potent antiviral, antidiabetic, and anticancer activities.[3] Representative examples of synthetic (**A**)[4] and natural (**B**–**D**)[5] bioactive compounds, together with drugs (**E**–**G**) bearing pyrrolidine skeletons are shown in Figure 1. The synthesis of the pyrrolidine ring has attracted attention because of its prevalence and wide utility as a building block and intermediate in organic synthesis.[6]

The molecular assembly of two or more bioactive motifs in one molecular skeleton has been widely studied as a favorite method for the design of new drugs.[7] In this respect, much effort has been devoted to the development of efficient methods toward these privileged skeletons.[8] The synthesis of hybrid molecules and their evaluation as a diverse range of pharmacological agents and as potent drugs has been steadily increasing over the past two decades. Merging the two classes of strategic heterocyclic motifs (namely, pyrrolidine and thioazlactone) through a spiroquaternary stereogenic carbon atom would rebuild structurally novel spiro[pyrrolidine-thioazlactone] derivatives (see Table 1). These spiroheterocycles may afford some unique benefits to medicinal chemistry, with the anticipation of finding valuable applications in drug discovery.

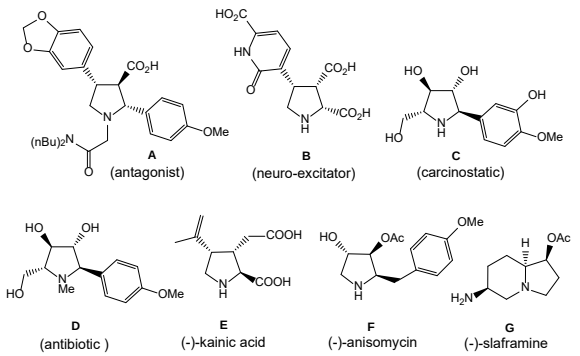

Fig. 1. Representative examples of synthetic (**A**), natural (**B**–**D**) bioactive molecules, and drugs (**E**–**G**) bearing a pyrrolidine core

2. Results and Discussion

We began our investigation using the model reaction of 3-(2-oxo-2-phenylethyl)benzo[*d*]thiazol-3-ium bromide (**1a**) with 4-benzylidene-2-(benzylthio)thiazol-5(4*H*)-one (**2a**)[9] in the presence of Et_3N in MeCN (Table 1). The mixture was stirred at room temperature, and TLC monitoring showed that the reaction was completed in about 3 hours. After workup, the desired product 1-benzoyl-2′-(benzylthio)-2-phenyl-2,3a-dihydro-1*H*,5′*H*-spiro[benzo[*d*]pyrrolo[2,1-*b*]thiazole-3,4′-thiazol]-5′-one (**3a**) was obtained in 82% yield (entry 1). The ^1H NMR spectrum of the reaction mixture showed only one diastereoisomer; therefore, the diastereoselective ratio (*dr*) was estimated to be ≥19:1. Various reaction parameters such as the base, solvent, temperature, and time were subsequently screened. As shown in Table 1, when the temperature was raised to 70 °C, the yield of product **3a** was slightly reduced (entry 2). Increasing the reaction time to 5 hours did not improve the yield

of **3a** (entry 3). Then, a survey of solvents such as CH_2Cl_2, THF, toluene, and dioxane was made. According to Table 1 (entries 4–7), the yields (56–77%) were lower than those obtained in MeCN. Finally, we turned to bases such as K_2CO_3, $EtN(iPr)_2$, DBU, and DABCO, but yields were much lower than those obtained in the presence of Et_3N (entries 8–11). As shown in Table 1, the diastereoselective ratios for entries 1–11 were estimated to be ≥19:1. Therefore, the optimal reaction condition used was equimolar amounts of **1a**, **2a**, and Et_3N in MeCN at room temperature.

Table 1 Optimization of Reaction Conditions for the Synthesis of Spirocyclic Compound 3a at 25 °C[a]

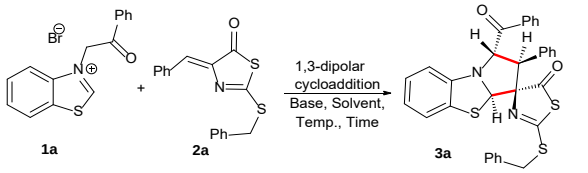

Entry	Base	Solvent	Yield (%)[b]	Selectivity[c]
1	Et_3N	MeCN	82	*dr* ≥ 19:1
2[d]	Et_3N	MeCN	78	-
3[e]	Et_3N	MeCN	83	-
4	Et_3N	CH_2Cl_2	74	*dr* ≥ 19:1
5	Et_3N	THF	77	-
6	Et_3N	Toluene	56	-
7	Et_3N	Dioxane	62	-
8	K_2CO_3	MeCN	52	-
9	$EtN(^iPr)_2$	MeCN	76	-
10	DBU	MeCN	65	-
11	DABCO	MeCN	68	-

[a] Reaction conditions: **1a** (1 mmol), **2a** (1 mmol), base (1 mmol), solvent (5 mL), at 25 °C. [b] Yield of isolated product **3a**. [c] The diastereoselectivity was estimated by ^{1}H NMR spectroscopic analysis of the reaction mixtures. [d] At 70 °C. [e] After 5 hours.

The compatibility and generality of the present method were further investigated using a range of precursors **1** and **2**. As shown in Scheme 1, these reactions led to the formation of spiro[benzopyrrolothiazole-rhodanine]s **3a**–**o** in good yields. The reaction products possess four stereogenic carbon centers, thus eight diastereoisomers are expected (see Table 1 and Scheme 1). However, the ^{1}H NMR spectra of the reaction mixtures only showed the major diastereoisomer **3**. The aryl fragments (Ar^1 and Ar^2) attached to the starting materials **1** and **2**, respectively, were tested. The method worked well especially for benzoyl group and its 3- chloro- and 3-bromo-derivatives (Scheme 1). The electronic properties of the substituents on the benzene ring directly attached to **2** appear to have a significant effect on the reaction. Thus, an electron-releasing functional group at the *para*-position (e.g., 4-methoxy-, and 4-methyl-) showed lower efficiency compared to 4-chloro- and 4-bromo derivatives. The highest yields (90–92%) were achieved for the 4- nitrophenyl derivative.

The structures of products **3a**–**o** were deduced from their IR, ^{1}H NMR, and ^{13}C NMR spectroscopic data. For example, the 1H NMR spectrum of **3a** exhibited characteristic signals for methine and methylene protons. The ^{13}C NMR spectrum of **3a** exhibited 26 signals, in agreement with the proposed structure. The mass spectrum of **3a** displayed the molecular ion peak at *m*/*z* 644. The NMR spectra of compounds **3b**–**j** are similar to those of **3a**, except for the substituents, which showed characteristic signals in the expected regions of the spectra.

The stereochemical features of this cycloaddition reaction was characterized by the X-ray crystal structure.[10] of product **3j**, the ORTEP presentation of which is shown in Figure 2. According to the torsion angles, the pyrrolidine ring adopts the envelope conformation.

Fig. 2. X-ray crystal structure of compound 3j (CCDC 2060493). Nitrogen atoms are shown in blue, oxygen atoms in red, and sulfur atoms in yellow.

The formation of spiro[benzopyrrolothiazole-thioazlactone] derivatives **3** can be explained by a plausible mechanism depicted in Scheme 2. The initial event may be the formation of azomethine ylides **I**, which undergoes 1,3-dipolar cycloaddition reaction with the exocyclic carbon–carbon double bond of Erlenmeyer thioazlactones **2** to afford products **3**. The facial selectivity of the transition-state geometry of this process is shown as structure **II**.

3. Conclusions

In summary, we have developed an operational approach for the diastereoselective synthesis of functionalized spiro[benzopyrrolothiazole-thioazlactone] derivatives from Erlenmeyer thioazlactones and azomethine ylides. Thus, the azomethine ylides, generated in situ from 3-(2- oxo-2-arylethyl)benzo[*d*]thiazol-3-ium bromides, were seized by 5-alkenyl rhodanins featuring exocyclic double bonds that enables the diastereoselective formation of polyfunctionalized spiroheterocycles in good yields.

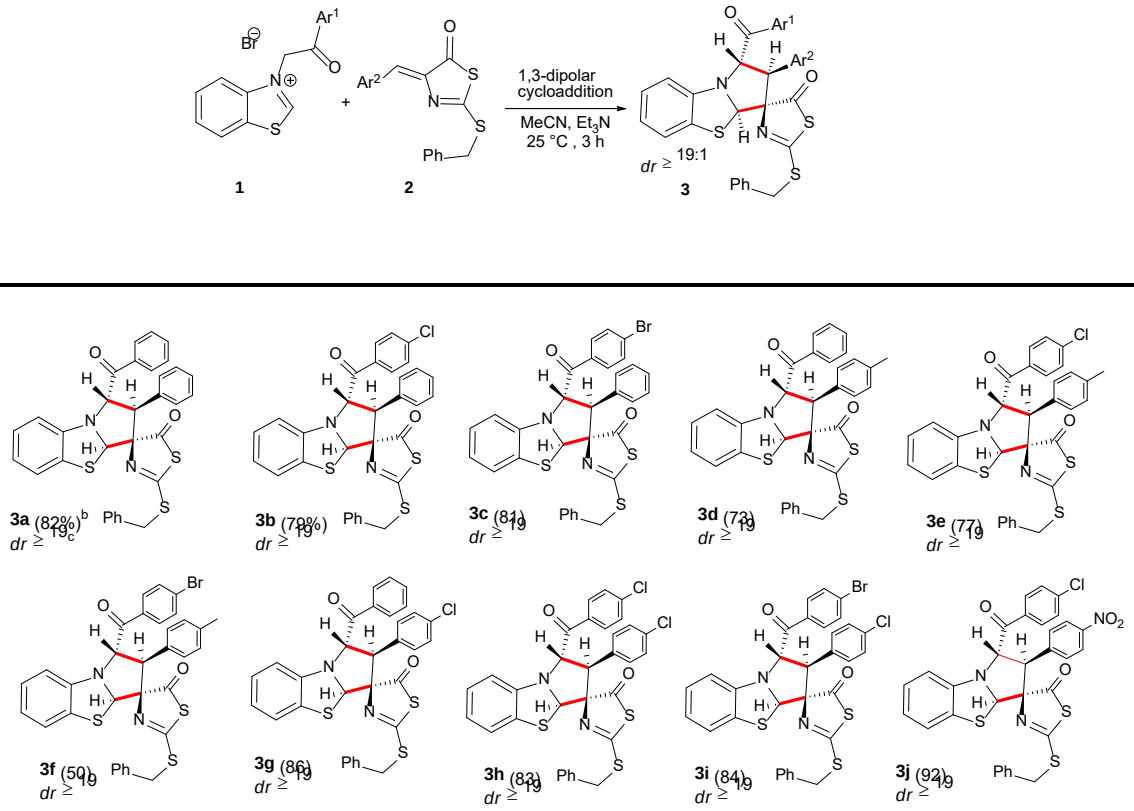

Scheme 1. Diastereoselective Synthesis of Spirocyclic Compounds 3a–j. *Reagents and conditions*: 1 (1 mmol), 2 (1 mmol), Et_3N (1 mmol), MeCN (5 mL), reflux. a Yield of isolated product 3. b The diastereoselective ratio was estimated by ^1H NMR spectroscopic analysis of the reaction mixtures.

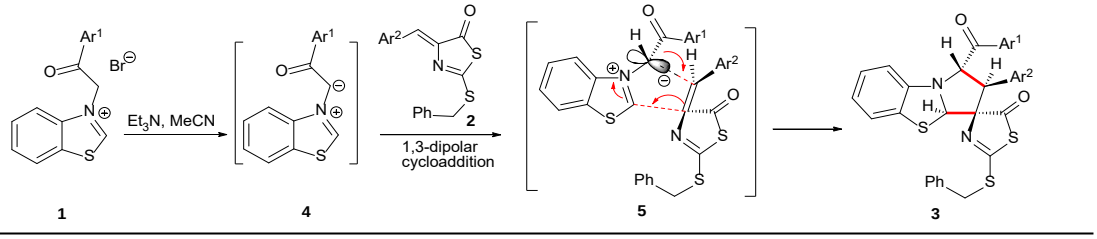

Scheme 2. A plausible mechanism for the formation of product 3

Supporting Information

Supporting information for this article is available online at https://doi.org/10.1055/s-0041-1738398

4. References

[1] R. D. Taylor, M. MacCoss, A. D. G. Lawson, J. Med. Chem. 57 (2014) 5845.

[2] J. P. Michael, Nat. Prod. Rep. 25 (2008) 139.

[3] (a) P. Greimel, J. Spreitz, A. Stutz, T. Wrodnigg, Curr. Top. Med. Chem. 3 (2003) 513. (b) H. Fiaux, F. Popowycz, S. Favre, C. Schütz, P. Vogel, S. Gerber-Lemaire, L. Juillerat-Jeanneret, J. Med. Chem. 48 (2005) 4237.

[4] A. A. Chiappori, E. Haura, F. A. Rodriguez, D. Boulware, R. Kapoor, A. M. Neuger, R. Lush, B. Padilla, M. Burton, C. Williams, G. Simon, S. Antonia, D. M. Sullivan, G. Bepler, Clin. Cancer Res. 14 (2008) 1464.

[5] E.-L. Tsou, S.-Y. Chen, M.-H. Yang, S.-C. Wang, T.-R. R. Cheng, W.-C. Cheng, Bioorg. Med. Chem. 16 (2008) 10198.

[6] (a) W. Notz, F. Tanaka, C. F. Barbas, Acc. Chem. Res. 37 (2004) 580. (b) W. H. Pearson, A. Dietz, P. Stoy, Org. Lett. 6 (2004) 1005. (c) C. Bhat, S. G. Tilve, RSC Adv. 4 (2014) 5405.

[7] A. C. Flick, H. X. Ding, C. A. Leverett, R. E. Jr. Kyne, K. K. C. Liu, S. J. Fink, C. O'Donnell, J. J. Med. Chem. 60 (2017) 6480.

[8] (a) Y. You, W.-Y. Lu, Z.-H. Wang, Y.-Z. Chen, X.-Y. Xu, X.-M. Zhang, W. C. Yuan, Org. Lett. 20 (2018) 4453.

[9] (a) S. Chandrasekhar, V. M. Rao, J. Heterocycl. Chem. 51 (2014) 172. (b) A. Ziyaei-Halimehjani, M. Khoshdoun, J. Org. Chem. 81 (2016) 5699.

[10] X-ray crystal structure determination of 3j. CCDC 2060493. www.ccdc.cam.ac.uk/structures.

29TH IRANIAN ORGANIC CHEMISTRY CONFERENCE
1_3 NOV, 2023
UNIVERSITY OF QOM, IRAN

Assessing Boron Carbide Nanotubes Theoretically as Non-Enzymatic Glucose Sensors

Nastaran Abudnejad, Mahboobeh Salehpour and Zohreh Saadati*

[1]*Department of Chemistry, Omidiyeh Branch, Islamic Azad University, Omidiyeh, Iran., nastaran2701n@gmail.com*

Abstract - Potential applicability of pristine and Al-doped boron carbide nanotube (BCN and Al-BCN) as glucose (GLU) sensor is investigated using density functional theory. Adsorption of GLU on top of pristine BCN leads to adsorption energy (Eads), enthalpy (ΔH), and Gibbs free energy (ΔG) of -14.82, -14.35, and -0.97 kcal.mol-1, respectively. While the corresponding values for Al-BCN are calculated to be -23.29, -24.17, and -11.03 kcal.mol-1, respectively. The detection power of Al-BCN is considerably higher than that of BCN. The required time for desorption of GLU from BCN and Al-BCN is 7.04 × 10-6 and 1.12 × 101 s, respectively.

1. Introduction

Diabetes is a metabolic disease that is characterized by high blood glucose (GLU) levels and if left untreated can lead to complications including blindness, kidney failure, heart attack, stroke, and amputation. Recently, nanomaterial-based sensors as non-enzymatic biosensors have attracted special attention. The various types of materials used as non-enzymatic GLU sensors are conductive polymers, metal-based nanostructures, molecularly imprinted polymers (MIPs), carbon nanotubes, and graphene derivatives [1-3] .

Carbon nanotubes (CNTs) with sp^2 carbon atoms are the most popular 1D nanomaterials used repeatedly as chemical sensors. However, carbon nanotubes have a small energy gap, thus, interact weakly with various chemicals and do not act as a suitable sensor. For this reason, many methods have been proposed to solve this problem, such as doping or adding impurity atoms to the nanotube, functionalizing, and creating defects. BCN nanotubes are the most common type of boron carbide nanotubes used in sensors, ion batteries and catalysts, H_2 storage, and drug delivery. In this study, we intend to use density functional theory (DFT) calculations to investigate whether a BCN nanotube can be proposed as a GLU sensor and if not, how to increase its sensitivity to GLU [4-6].

2.Computational details

All calculations in our study were performed using the DFT method, which is shown to give highly accurate results with an optimum computational cost. The M06-2X and B3LYP functionals in conjunction with 6-31G(d) and 6-311G(d) basis sets were implemented in Gaussian 09 software to perform calculations. Noncovalent interactions were taken into consideration using the correction term of Grimme DFT-D3, and the data have been updated considering the basis set superposition error (BSSE) calculated by the counterpoise approach [7-10]. The structure of BCN and GLU nanotubes was plotted using GaussView 5.0 software [11]. To reduce the edge effects, the carbon and boron atoms at the end of the nanotube were capped with hydrogen so that the final structure of the nanotube had the molecular formula of $B_{40}C_{120}H_{20}$. Vibrational frequency calculations were also carried out at the same theoretical level to ensure that the optimized molecule is at true local minima on the potential energy surface and is not saddle points or transition states. Also, by performing vibrational frequency calculations, zeropoint energy (ZPE) corrections and thermochemical quantities such as enthalpy changes (ΔH) and Gibbs free energy changes (ΔG) can be obtained. Enthalpy changes due to GLU adsorption on the BCN surface at 298 K and 1 atm were calculated using the following equation:

$$\Delta H = H_{(Al)BC_3:GLU} - H_{(Al)BC_3} - H_{GLU} \quad (1)$$

In equation (1) $H_{(Al)BC_3:GLU}$, $H_{(Al)BC_3}$ and H_{GLU} show the enthalpy changes of the complex (Al) BCN:GLU (Al is used for nanotubes doped with aluminum), (Al)BCN nanotube and GLU molecule, respectively. Gibbs free energy changes (ΔG) caused by the complex formation between GLU molecule and BCN nanotube (E_{ads}) were calculated using the corresponding data under the same temperature and pressure. Also, the effect of implicit solvent was determined through the self-consistent reaction field (SCRF) approach and utilizing the polarizable continuum model (PCM) considering the water dielectric constant (ε = 78.36).

To better understand the charge transfer process between (Al)BCN and glucose molecules and to have a deeper insight into the charge distribution and stabilizing energies of the (Al)BCN:GLU complex, we performed natural bond orbital (NBO) calculations. The energy gap (E_g) between the highest occupied

molecule orbital (HOMO) and the lowest unoccupied molecular orbital (LUMO) of (Al)BCN before and after the complex formation is calculated using the following equation:

$$E_g = E_{LUMO} - E_{HOMO} \qquad (2)$$

3. Results and discussion

Adsorption of GLU on the pristine BCN

The structure of the BCN nanotube used in this study is a zigzag (10,0) model consisting of 120 carbon and 40 boron atoms; also, to reduce the edge effects, unsaturated bonds of BCN were capped with 20 hydrogen atoms. The BCN model has a diameter and length of about 8.2 and 16.3 Å (excluding terminal hydrogens), respectively. Two types of bonds are found in the structure of BCN: C—C and B—C, whose average lengths are 1.42 and 1.57 Å, respectively. As can be seen, the bond length of C—C is in agreement with the previously reported bond lengths for graphene (1.42 Å) [27] and carbon nanotubes (1.42-1.46 Å) [28]. Also, two classes of hexagonal rings are observed in the BCN structure: C6 and B2C4. The energy of the highest occupied molecular orbital (HOMO) and the lowest unoccupied molecular orbital (LUMO) of the nanotube are -6.04 eV and -3.61 eV, respectively, resulting in an energy gap (Eg) of 2.43 eV; therefore, BCN can be classified as a semiconductor. The HOMO and LUMO energy levels are in good agreement with the literature [29-31]. The optimized structure, electrostatic potential map (MEP), and frontier molecular orbitals (i.e. HOMO and LUMO) of BCN and GLU are shown in Figures 1 and 2, respectively.

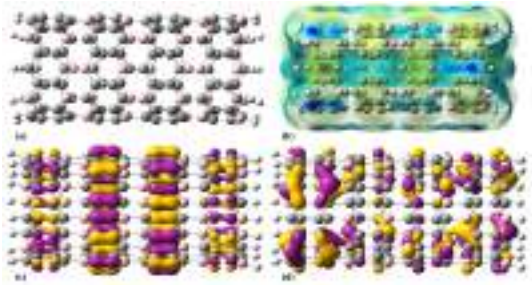

Figure 1. (a) Optimized structure of BCN (b) computed molecular electrostatic potentials (MEP) plot of BCN (The surfaces are defined by the 0.0004 electrons/b3 contour of the electronic density. Color ranges, in a.u.: blue, more positive than 0.010; green, between 0.010 and 0; yellow, between 0 and -0.010; red, more negative than -0.010); (c) HOMO and (d) LUMO profiles of BCN.

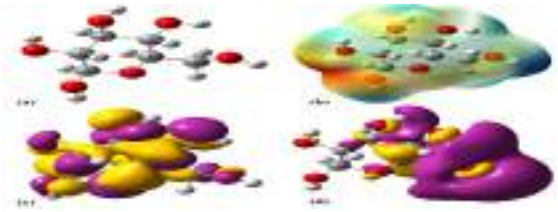

Figure 2. (a) Optimized structure, (b) MEP plot, (c) HOMO, and (d) LUMO profiles of GLU molecule.

Table 1. Calculated energetic data (ΔH, ΔG, and E_{ads} in kcal.mol^{-1}), minimum and maximum modes of vibrational frequencies (ν_{min} and ν_{max}, cm^{-1}) for BCN:GLU complex.

Method	ΔH	ΔG	E_{ads}	E_{BSSE}	ν_{min}	ν_{max}*
M06-2X/6-31G(d)	-14.00	-0.72	-14.10	1.49	13	3745
B3LYP/6-31G(d)	-16.50	-1.10	-16.90	2.05	8	3762
M06-2X/6-311G(d)	-14.35	-0.97	-14.82	1.97	13	3749
B3LYP/6-311G(d)	-16.73	-1.24	-16.97	2.16	11	3770

*ν_{max} indicates the stretching vibrational mode of O5—H23 of GLU.

Adsorption of GLU on the Al-doped BCN

The optimized structure Al-BCN along with the MEP plot and frontier molecular orbitals profile are illustrated in Figure 4. The mean value of C—C, B—C, and Al—C bond lengths are about 1.42, 1.57, and 1.92 Å, respectively. Four types of hexagonal rings can be distinguished in the structure of Al-BCN, which are as follows: (a) C_6, (b) B_2C_4, (c) Al_2C_4, and (d) $AlBC_4$. As can be seen, the Al_2C_4 hexagon is stretched out, which can be attributed to the larger atomic radius of Al compared to the B atom. The HOMO and LUMO energy levels of Al-BCN are calculated to be -5.90 and -3.11 eV, respectively, resulting in an energy gap (E_g) of 2.79 eV. Therefore, Al-BCN could be considered a semiconductor, like BCN. The GLU molecule was also adsorbed horizontally on the Al-BCN surface. After optimizing all the structures and performing the vibrational frequency calculations, we found that the complex in which the GLU molecule binds to the Al atom through the O6—H24 group has the lowest energy level (Figure 5).

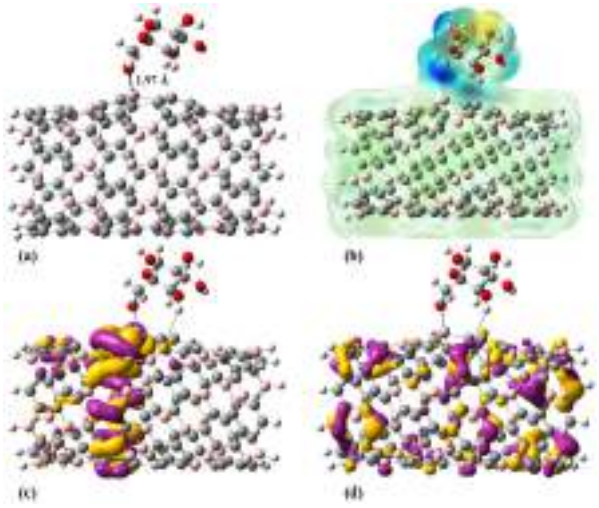

Figure 5. (a) Optimized structure, (b) MEP plot, (c) HOMO, and (d) LUMO profiles of Al-BCN:GLU complex.

Conclusions

We studied the ability of the pristine boron carbide nanotube (BCN) and its Al-doped analog to detect glucose (GLU) molecule with the help of the density functional theory (DFT) method. All calculations including geometry optimization, vibrational frequencies, and natural bond orbital (NBO) were performed using M06-2X and B3LYP functionals with 6-31G(d) and 6-311G(d) basis sets. Adsorption of GLU on top of pristine BCN leads to an E_{ads}, ΔH, and ΔG of -14.82, -14.35, and -0.97 kcal.mol^{-1}, respectively. The E_g value of BCN decreases by only about 3.85%; thus, the electronic properties of the pristine nanotube do not change in the presence of GLU molecules. The electrical conductivity of BCN increases by 5.76 times upon GLU adsorption. To measure the effectiveness of the doping method on the sensitivity of BCN regarding GLU, two boron atoms were replaced by Al ones. The adsorption energy associated with the most stable Al-BCN:GLU complex is about -23.29 kcal.mol^{-1}. The enthalpy and Gibbs free energy changes resulting from the GLU adsorption on the Al-BCN surface are -24.17 and -11.03 kcal.mol^{-1}, respectively. The E_g of Al-BCN shows a decrease of 20.26% after adsorption showing that the electronic properties of Al-BCN are more sensitive to the presence of GLU molecule. The detection power of Al-BCN is higher than that of pristine BCN. The required time for desorption of GLU from pristine and doped BCN is about 7.04×10^{-6} and 1.12×10^{1} s, respectively.

4. References

[1] F. Hill-Briggs, N.E. Adler, S.A. Berkowitz, M.H. Chin, T.L. Gary-Webb, A. Navas-Acien, P.L. Thornton, D. Haire-Joshu, Social determinants of health and diabetes: a scientific review, Diabetes care 44 (2021) 258-279.

[2] Q. Dong, H. Ryu, Y. Lei, Metal oxide based non-enzymatic electrochemical sensors for glucose detection, Electrochimica Acta 370 (2021) 137744.

[3] J. Zhu, S. Liu, Z. Hu, X. Zhang, N. Yi, K. Tang, M.G. Dexheimer, X. Lian, Q. Wang, J. Yang, Laser-induced graphene non-enzymatic glucose sensors for on-body measurements, Biosensors and Bioelectronics 193 (2021) 113606.

[4] Y. Cao, S. Alamri, A.A. Rajhi, A.E. Anqi, M. Derakhshandeh, The capability of boron carbide nanotube as a nanocarrier for fluorouracil anticancer drug delivery; DFT study, Materials Chemistry and Physics 275 (2022) 125260.

[5] S. Bazyari-Delavar, F. Badalkhani-Khamseh, A. Ebrahim-Habibi, N.L. Hadipour, Investigation of host-guest interactions between polyester dendrimers and ibuprofen using density functional theory (DFT), Computational and Theoretical Chemistry 1189 (2020) 112983.

[6] F. Badalkhani-Khamseh, A. Ebrahim-Habibi, N.L. Hadipour, M. Behmanesh, PEGylated PAMAM dendrimers as eptifibatide nanocarriers: An atomistic view from molecular dynamics simulations, Chemical Engineering Science 267 (2023) 118283.

[7] B. Civalleri, C.M. Zicovich-Wilson, L. Valenzano, P. Ugliengo, B3LYP augmented with an empirical dispersion term (B3LYP-D*) as applied to molecular crystals, CrystEngComm 10 (2008) 405-410.

[8] H. Hirao, Which DFT functional performs well in the calculation of methylcobalamin? Comparison of the B3LYP and BP86 functionals and evaluation of the impact of empirical dispersion correction, The Journal of Physical Chemistry A 115 (2011) 9308-9313.

[9] X. Wu, J. Dai, Y. Zhao, Z. Zhuo, J. Yang, X.C. Zeng, Two-dimensional boron monolayer sheets, ACS nano 6 (2012) 7443-7453.

[10] S.F. Boys, F. Bernardi, The calculation of small molecular interactions by the differences of separate total energies. Some procedures with reduced errors, Molecular Physics 19 (1970) 553-566.

[11] R. Dennington, T. Keith, J. Millam, GaussView, version 5, (2009).

Preparation of Regenerated Cellulose film using Green Organic Solvents

Shaya Mahmoudian[1,2]*, *Mat Uzir Wahit*[3]

[1]*Department of Textile Engineering, Kashan Branch, Islamic Azad University, Kashan, Iran.*
[2]*Machine-made Carpet Research Centre, Kashan Branch, Islamic Azad University, Kashan, Iran, shmahmoudian2@gmail.com.*
[3]*School of Chemical and Energy Engineering, Faculty of Engineering, Universiti Teknologi Malaysia, Johor Bahru, Johor, Malaysia*

Abstract - Cellulose is the most abundant natural polymer in nature and it is currently one of the most promising polymeric resources. Cellulose has to be regenerated prior to use. However, cellulose regeneration is difficult to achieve and most of conventional cellulose solvents have some drawbacks such as toxicity, volatility, side reactions and high cost. Recently, Ionic liquids have been developed as organic green cellulose solvents. In this research, mixture of three kind of ionic liquid were used to dissolve cellulose in one step. High percentage of cellulose could be dissolved by using this method which is effect on regenerated cellulose structure and properties. Morphological properties of produced regenerated cellulose film were studied. FTIR results indicated that crystal transformation of cellulose I to cellulose II had occurred during regeneration which is evidence of complete dissolution of cellulose during regeneration. The SEM micrographs showed that the preparation methods used in this research was suitable for the preparation of a regenerated cellulose dense and homogenous structure which is due to the appropriate preparation method as well as the high cellulose concentration.

1. Introduction

Biopolymers have attracted much attention in recent years as an alternative material for petroleum based polymers due to increasing environmental concerns and decreasing fossil resources. Non-biodegradable petroleum-based plastics have become a threat to the environment. Therefore, an increasing attention has been paid on the development of natural bio-based materials. Biopolymers like cellulose, starch and proteins have been considered as alternatives for non-biodegradable petroleum-based polymers because of their abundance, renewability, low cost, and good biodegradability [1-3].

Cellulose is a complex carbohydrate and the most abundant biopolymer on Earth. It is composed of repeating units of glucose molecules linked together by β-1,4-glycosidic bonds. These glucose units form long chains that are interconnected through hydrogen bonding, resulting in a highly stable and rigid structure. Cellulose has many attractive properties such as, biodegradability, renewability, biocompatibity, nontoxicity, and low cost [4].

However, only about 2 % of cellulose renewed annually are used as raw material in manufacture of cellulose material and goods. The major setback to the more extensive use of cellulose is the lack of suitable solvent for cellulose since this natural polymer is neither meltable nor soluble in water and common solvents. Cellulose has to be regenerated prior to use. Cellulose regeneration is difficult to achieve, because of its stiff molecules and close chain packaging via strong hydrogen bonding between molecules [5,6].

For more than one century, polluting viscose process was the main technique for cellulose regeneration and it is still applied for the production of regenerated cellulose fibers and films. However, the environmental pollution caused by the side products has become a major challenge that needs to be resolved [7]. Several cellulose solvents such as LiCl/N,N-dimethyl acetamide (DMAc), NaOH/urea aqueous solution, LiCl/1,3-dimethyl-2-imidazolidinone(DMI), N-methylmorpholine-N-oxide (NMMO) have been developed for cellulose processing. However these solvents have some drawbacks such as toxicity, volatility, side reactions and high cost [8-10].

Recently, room temperature ionic liquids have been used as ‘green’ solvents for cellulose regeneration due to their attractive properties such as good chemical and thermal stability, low flammability, low melting point and ease of recycling, which make them environmental friendly solvents. Ionic liquids are defined as organic salts that melt below about 100 °C. They are composed entirely of ions, typically large organic cations and small organic anion [11-13]. Swatloski, et al. [14] reported for the first time that ionic liquids having the imidazolium structure can be used as non-derivatizing solvents for cellulose. The greatest solubility was achieved with 1-butyl-3-methylimidazolium chloride which could dissolve up to 25 wt. % of cellulose under microwave irradiation. Hermantuze et al. [15] reported

that the use of ionic liquids as solvent for cellulose is easier and safer than the dissolution of cellulose with NMMO as well as viscose process.
In this research mixture of three kind of ionic liquid solvents were used to dissolve cellulose in one step and morphological properties of produced regenerated cellulose film were studied.

2. Experimental

2.1. Materials: Microcrystalline cellulose, a commercial reagent from Sigma with average powder size 50 µm, Avicel type was used. Ionic liquids, 1-buthyl-3-methylimidazolium chloride (BMIMCl), 1-Ethyl-3-methylimidazolium acetate (EMIMAc) and 1-allyl-3-methylimidazolium chloride (AMIMCl) were supplied by Sigma Aldrich.
2.2. Preparation: regenerated cellulose films were prepared according to the following procedure; cellulose was dissolved in the mixture of ionic liquid using magnetic stirring for 4 h at 85 ˚C to get a homogenous solution with cellulose concentration of 15 wt%. After degassing the solution in vacuum oven, it was casted on a glass plate with thickness of about 0.3 mm and immersed immediately into a distilled water bath at room temperature for 24h. The obtained films were washed with running water and dried in vacuum oven at 30°C for 3h.
2.3. Characterization: Fourier Transform Infrared Spectroscopy (FTIR) spectra were recorded by a Perkin-Elmer 180 with resolution of 2cm-1 for 16 scans over wave number range of 4000-600 cm-1. Scanning Electron Microscopy (SEM) was performed on a Philip XL 40 SEM with acceleration voltage of 20 kV. The regenerated cellulose films were frozen in liquid nitrogen, cryo-fractured, and vacuum dried. The fracture surface of the films was coated with gold prior to analysis.

3. Results

3.1. Fourier Transform Infrared Spectroscopy (FTIR): FTIR spectra of microcrystalline cellulose (MCC) and regenerated cellulose (RC) films are shown in Fig.1. It can be seen that although the absorption peak values fluctuated greatly, no new peak appeared in RC and compared to MCC and three spectra are quite similar. The results indicate that no chemical reaction occurred during the dissolution and regeneration process of cellulose and proves that ionic liquids were direct solvents for cellulose. The main wavenumber and assignments for MCC and RC are listed in Table 2. The broad peak at 3356 cm $^{-1}$ in MCC is corresponds to O-H stretching intramolecular hydrogen bonds of crystalline cellulose I. This peak shifted to 3403 cm^{-1} in RC, which are assigned to O-H stretching intramolecular hydrogen bonds of crystalline cellulose II. This result indicated that crystal

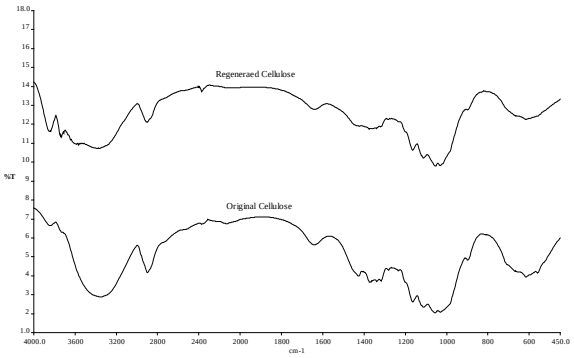

Fig.1.FTIR spectra of (a) MCC, (b) RC, (c) RCG, and (d) GNP

transformation of cellulose I to cellulose II had occurred during regeneration In MCC, the peak at 1431 cm-1 is assigned to CH_2 in plan bending vibration The CH_2 peak at 1431 cm^{-1} is one the typical peaks for crystalline cellulose I and the absence of this peak in RC indicates a predominance of crystalline II in this materials [16]. The transformation of crystalline cellulose I to crystalline cellulose II can be the evidence of complete dissolution of cellulose during regeneration. Crystalline transformation of cellulose I to cellulose II was also reported by Chen et al. [17] for the regeneration of wheat straw using BMIMCl. According to NMR studies on BMIMCl and EMIMAc, the mechanism of dissolution of cellulose in these ionic liquids is based on the formation of hydrogen bonding interactions between the hydroxyl groups of cellulose and both anion and cation of ionic liquid, which disrupt hydrogen bonding in cellulose and lead to dissolution. It was reported that the sites of imidazolium cation-cellulose interaction [18]

3.2. Scanning Electron Microscopy (SEM):
Fig. 2 shows the cross-sectional SEM image of RC films. SEM results showed smooth fractured surface.

Table 1 FTIR absorption band assignments for the MCC and RC

Wavenumber (cm^{-1}) range of maxima	Peak origin (assignment) [220-222]	MCC	RC
3200-3600	O-H stretching	3356	3403
2850-2940	Symmetric CH_2 valence vibration	2899	2889
1600-1650	Carbonyl stretching	1638	1648
1400-1450	CH_2 bending vibrations	1431	-
1365-1375	C-H bending	1372	1371
1315-1317	C-H rocking vibration	1318	1318
1150-1200	C-O stretching	1164	1165
1115-1120	C–C stretching	1115	1117
1015-1060	C–O valence vibration	1059	1060
1030-1035	C–O stretching	1032	1035
890-900	C-O-C symmetric vibration	896	893
670	C–OH out-of-plane bending mode	663	669

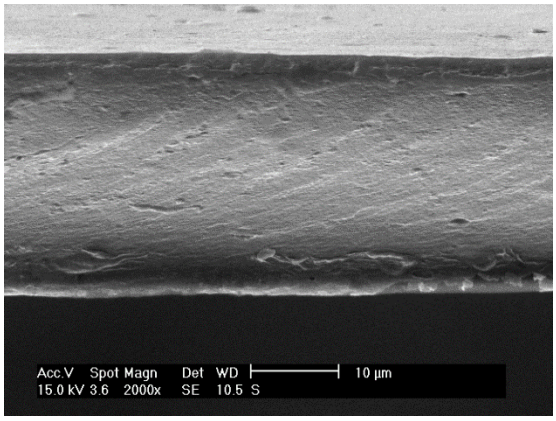

Figure 4.7 SEM micrographs cross sectional view of regenerated cellulose film

It can be seen that the RC films regenerated from mixture of ionic liquids display a dense and homogenous structure Formation of a dense structure is due to the appropriate preparation method as well as the high cellulose concentration Previous studies have shown that the cellulose concentration of lower than 6 wt. % resulted in a porous structure for RC. [19]. Moreover the coagulation conditions affect the structure of the RC. Li et al. [20] and Liu et al. [21] studied the different coagulation temperatures and reported that the coagulation temperature strongly affect the morphology and structure of the RC. They reported that the best temperature for coagulation bath to get denser structure of RC was between 20-24 °C. The SEM images demonstrated that the preparation method used in this research was suitable to obtain homogenous and dense structure for RC film.

References

[1] Rai P, Mehrotra S, Priya S, Gnansounou E, Sharma SK. Recent advances in the sustainable design and applications of biodegradable polymers. Bioresource technology. 2021;325:124739.

[2] Yaashikaa P, Kumar PS, Karishma S. Review on biopolymers and composites–Evolving material as adsorbents in removal of environmental pollutants. Environmental Research. 2022;212:113114.

[3] Vroman, I. and Tighzert, L., Biodegradable Polymers. Materials. 2009. 2(2): 307-344.

[4] Klemm, D., Heublein, B., Fink, H. P., and Bohn, A., Cellulose: Fascinating Biopolymer and Sustainable Raw Material. Angewandte Chemie International Edition. 2005. 44(22): 3358-3393.

[5] Shen H, Sun T, Zhou J. Recent Progress in Regenerated Cellulose Fibers by Wet Spinning. Macromolecular Materials and Engineering. 2023:2300089.

[6] Bredereck, K. and Hermanutz, F., Man–made cellulosics. Review of Progress in Coloration and Related Topics. 2005. 35(1): 59-75.

[7] Wang S, Lu A, Zhang L. Recent advances in regenerated cellulose materials. Progress in Polymer Science. 2016; 53:169-206.

[8] Li, R., Zhang, L., and Xu, M., Novel regenerated cellulose films prepared by coagulating with water: Structure and properties. Carbohydrate Polymers. 2011. 87(1): 95-100.

[9] Sayyed AJ, Deshmukh NA, Pinjari DV. A critical review of manufacturing processes used in regenerated cellulosic fibres: viscose, cellulose acetate, cuprammonium, LiCl/DMAc, ionic liquids, and NMMO based lyocell. Cellulose. 2019;26:2913-2940.

[10] Rosenau, T., Hofinger, A., Potthast, A., and Kosma, P., On the conformation of the cellulose solvent N-methylmorpholine-N-oxide (NMMO) in solution. Polymer. 2003. 44(20): 6153-6158.

[11] Rogers, R. D. and Seddon, K. R., Chemistry: Ionic Liquids--Solvents of the Future? Science. 2003. 302(5646): 792-793.

[12] Shamsuri AA, Abdan K, Jamil SNAM. Properties and applications of cellulose regenerated from cellulose/imidazolium-based ionic liquid/co-solvent solutions: A short review. e-Polymers. 2021;21(1):869-880..

[13] Liu Z, Sun X, Hao M, Huang C, Xue Z, Mu T. Preparation and characterization of regenerated cellulose from ionic liquid using different methods. Carbohydrate polymers. 2015;117:99-105.

[14] Swatloski, R. P., Spear, S. K., Holbrey, J. D., and Rogers, R. D., Dissolution of Cellose with Ionic Liquids. Journal of the American Chemical Society. 2002. 124(18): 4974-4975.

[15] Hermanutz, F., Gähr, F., Uerdingen, E., Meister, F., and Kosan, B., New Developments in Dissolving and Processing of Cellulose in Ionic Liquids. Macromolecular Symposia. 2008. 262(1): 23-27.

[16] Higgins, H. G., Stewart, C. M., and Harrington, K. J., Infrared spectra of cellulose and related polysaccharides. Journal of Polymer Science. 1961. 51(155): 59-84.

[17] Chen, H. Z., Wang, N., and Liu, L. Y., Regenerated cellulose membrane prepared with ionic liquid 1-butyl-3-methylimidazolium chloride as solvent using wheat straw. Journal of Chemical Technology and Biotechnology. 2012.

[18] Zhang, J., Zhang, H., Wu, J., Zhang, J., He, J., and Xiang, J., NMR spectroscopic studies of cellobiose solvation in EmimAc aimed to understand the dissolution mechanism of cellulose in ionic liquids. Physical Chemistry Chemical Physics. 2010. 12(8): 1941-1947.

[19] Chen, H. Z., Wang, N., and Liu, L. Y., Regenerated cellulose membrane prepared with ionic liquid 1-butyl-3-methylimidazolium chloride as solvent using wheat straw. Journal of Chemical Technology and Biotechnology. 2012.

[20] Li, R., Zhang, L., and Xu, M., Novel regenerated cellulose films prepared by coagulating with water: Structure and properties. Carbohydrate Polymers. 2011. 87(1): 95-100.

[21] Liu, S. and Zhang, L., Effects of polymer concentration and coagulation temperature on the properties of regenerated cellulose films prepared from LiOH/urea solution. Cellulose. 2009. 16(2): 189-198.

Synthesis of polytetrahydrofuran

Alireza Banan*, Seyedmojtaba Keshavarz

[1]*Department of Chemistry, Faculty of Imam Hossein Comprehensive University, Tehran, Iran, bananjahromi@yahoo.com, mojtabakeshavarz66@gmail.com*

Keywords: polytetrahydrofuran**,** heteropolyacid**,** Acetic anhydride**,** polymerization.

High molecular weight poly tetrahydrofuran (PTHF) was prepared in the bulk polymerization at ambient temperature by using Acetic anhydride as initiator. The experimental results show that poly tetrahydrofuran is a semi crystalline polymer with a melting temperature of 35 °C. The degradation study revealed that PTH F degrades both in solution and in bulk. The degradation kinetics was studied by using various kinetic methods and product analysis. The results showed that the degradation proceeds via a random chain scission process. The random chain scission occurs primarily at the ether linkages. Under thermo-oxidative degradation conditions, the random chain scission may proceed via the weak side links of hydroperoxide groups formed in the presence of oxygen, which results in a low activation energy. Under thermal degradation conditions, the ether linkages are thermally broken by the random chain scission process, which leads to a high activation energy. Oxygen plays a very important role in the degradation of PTHF. The presence of oxygen changes the degradation process from endo thermic to exothermic and accelerates the degradation. The use of acetic anhydride increases the possibility of adjusting the molecular weight to an acceptable level. The cationic ring opening polymerization reaction of tetrahydrofuran at 20 ºC was catalyzed by $H_3PW_{12}O_{40}\cdot 13H_2O$ as solid acid catalyst. The effect of the proportions of acetic anhydride and catalyst, reaction time and support on the polymerization reaction was investigated. It has been found that the yield and the viscosity of the polymer depend on the proportion of acetic anhydride, the presence of the latter in the reactant mixture being required for the ring-opening. The catalytic activity of the heteropolyacid results showed that Brønsted acid sites are more effective than Lewis ones for the cationic ring-opening polymerization.

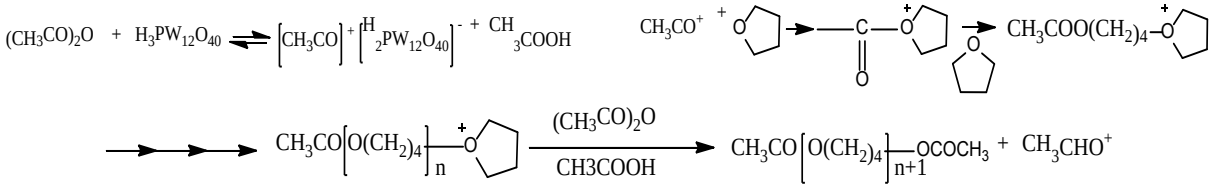

Scheme: Polytetrahydrofuran polymerization reaction in the presence of acetic anhydride.

References

[1] Jayakannan, M.; Ramakrishnan, S. Recent Developments in Polyether Synthesis. *Macromol. Rapid Commun*. 2001, 22, 1463–1473.

[2] Kozhevnikova, E.F.; Kozhevnikov, I.V. A calorimetric study of the acidity of bulk and silica supported heteropoly acid $H_3PW_{12}O_{40}$. *J. Catal*. 2004, 224, 164–169.

[3] Bardin, B.B.; Davis, R.J. Effect of water on silica-supported phosphotungstic acid catalysts for 1-butene double bond shift and alkane skeletal isomerization. *Appl. Catal. A: Gen* 2000, 857-868.

Synthesis of poly tetramethylene glycol containing hydroxyl end-groups

Alireza Banan*, Seyedmojtaba Keshavarz, Mohammad Javanmardi

Department of Chemistry, Faculty of Imam Hossein Comprehensive University, Tehran, Iran, bananjahromi@yahoo.com, mojtabakeshavarz66@gmail.com, mohammadjavanmardi1998@gmail.com

Keywords: Poly tetramethylene glycol, Propylene oxide, Heteropolyacid**.**

Polytetramethylene ether glycol (PTMEG) is an important polymer in the polymer industry, which is widely used as a soft segment in the production of polyurethane and polyester elastomers. PTMEG is synthesized via cationic ring-opening polymerization of tetrahydrofuran (THF). So far, various compounds have been utilized as initiators for the polymerization of THF, but only a limited number of them have been suitable for the production of PTMEG. Considering the growing importance of PTMEG in polymer industries, it is essential to introduce an efficient method for the production of this material. In this research, PTMEG with hydroxyl end-groups was synthesized in the presence of tungstophosphoric acid as a catalyst and propylen oxide as a reaction initiator. The polymerization reaction of tetrahydrofuran was carried out in two steps. In the first step, acetate-terminated PTMEG was obtained from ring-opening polymerization of tetrahydrofuran (THF). In the second step, the acetate end-groups were hydrolyzed and hydroxyl groups were produced at the end of polymer chains. The synthesis of PTMEG is depicted in **Scheme 1**. The results showed that PTMEG with hydroxyl end groups was synthesized with a very good efficiency in mild conditions. The heteropolyacid catalyst can be recycled and reused for several cycle of reactions.

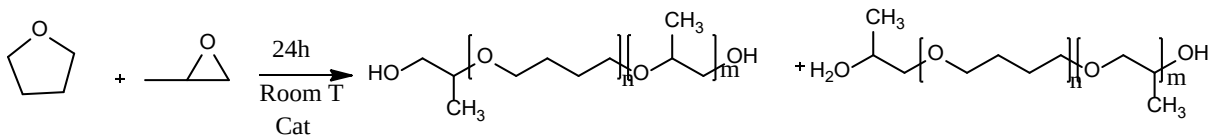

Scheme 1. Synthesis of PTMEG Co propylene oxide.

References

[1] Zhang, A., Zhang, G., & Zhang, H. (1999). Effective promotion of tetrahydrofuran polymerization initiated with heteropolyacid. *J. Appl. Polym. Sci.* 73(12), 2303-2308.

[2] Aouissi, A., Al-Deyab, S. S., & Al-Shahri, H. (2010). The cationic ring-opening polymerization of tetrahydrofuran with 12-tungstophosphoric acid. Molecules, 15(3), 1398-1407.

[3] Dickinson, L. A. (1962). New elastomers derived from copolymers of tetrahydrofuran and propylene oxide. *J. Polym. Sci.* 58(166), 857-868.

29TH IRANIAN ORGANIC CHEMISTRY CONFERENCE
1_3 NOV, 2023
UNIVERSITY OF QOM, IRAN

Direct amidation of the Date seed oil as bio-renewable feedstock for fatty acid amide synthesis

*Samaane Taghvaei nia, Mir Mohammad Alavi nikje**

Department of Chemistry, Faculty of Science, Imam Khomeini International University, P.O. Box 34149-1-6818, Qazvin, Iran, samaa.taghvaei@gmail.com, alavi@sci.ikiu.ac.ir

Abstract – The aim of this study was amidation of Date seed oil to make fatty acid amide. The first step was to extract the oil from date seed powder (as a waste and renewable feedstock) using the soxhlet extraction method with n-hexane as solvent. The second step was to monitor formation of fatty acid amide using FTIR and ^{1}HNMR spectroscopy.

1. Introduction

Vegetable oils have been used in the preparation of fatty acid amides, alcohols, and nitriles. These products can be used to prepare a variety of products [1]. A variety of applications for fatty acid amides exist, such as surfactants, foam-control agents, lubricants, water repellents, cosmetics, fungicides, shampoos, detergents, corrosion inhibitors, and anti-blocking agents in plastics processing and biodiesel development technologies [2].

Date (Phoenix dactylifera L.) has been a key role in the social and economic life of people in arid and semi-arid regions of the world, providing nourishment and economic growth. There are more than sixty varieties of date fruit reported worldwide. Approximately 10-18% of its weight comes from the seeds alone. Date seed oil had the following chemical properties: an acid value of 8.5 mg KOH/g, an iodine number of 49 gI_2/100 g, and a saponification value of 210 mg KOH/g. The primary fatty acid in date seed oil (Zahidi type) was oleic acid, which was followed by fair levels of lauric, myristic, and palmitic acid, which ranged from 43.23%, and 21.08%, and 13.85%, and 12.38%, respectively [3, 4].

2. Materials and methods

2.1. Oil extraction:

Date seeds (Zahidi type) was washed carefully, and dried in room temperature, then the dried seeds were powdered and oil extracted with soxhlet system. n-hexane was used as solvent. After oil extraction, n-hexane was removed by a rotatory evaporator at 80℃, and date seed oil was stored at 6℃.

Several parameters such as temperature, particle size of date powder, solvent to seed ratio (mL of solvent to grams of date seed powder), oil extraction time evaluated on oil yield.

2.2. Amidation reaction:

DSO (7.7805g, 9.9 mmol), Diethanolamine (DEA) (3.3645g, 32 mmol), $NaOCH_3$ as catalyst (0.027g, 0.5 mmol)

Diethanolamine and $NaOCH_3$ (1.5 mol% to DEA) were heated at 80 ℃ for 10 minutes in nitrogen atmosphere. Date seed oil was added dropwise to a glass flask and reacted with diethanolamine. The reaction was carried out in an inert atmosphere. This process was monitored by TLC (with only ethyl acetate used as the mobile phase) and another way to monitor the reaction was by dissolving it in ethanol (volume ratio 1:1). If the mixture reaction was dissolved in ethanol, it was the end of amidation. After the completion of the reaction, it was cooled, and washed with NaCl solution (0.1M) and ethyl acetate (three times). The upper layer was separated from the glycerol layer using a separating funnel and dried over anhydrous $MgSO_4$. The solvent was removed using vacuum rotary evaporator.

Date seed oil/Diethanolamide (DSO/DEA) was analyzed by FTIR and NMR spectroscopy

3. Results and Discussion

3.1. Oil extraction:

Date seed oil (14-15%yield) FTIR (cm^{-1}, KBr window): 3446.85 (OH stretching), 2923.67 and 2853.54 (asymmetrical and symmetrical stretching of C–H of long fatty acid chain), 1746.21 (–C=O stretching (ester)), 1627.93 (–CH_2–), 1465.89 (-C-H (CH_2)), 1377.66 (–CH_3 bend), 1161.96 (C–O), 1115.02 (C–O stretching (ester)), 722.21 (C–O stretching). ^{1}HNMR (300 MHz, $CDCl_3$) (δ, ppm): 5.32 (–CH=CH–), 5.29 (glycerin methylene protons), 4.41 and 4.06 (–CH_2–O–), 2.76 (–CH_2–COOR), 2.30 (–CH_2–C=C), 1.93 (–CH_2–CH_2–COOR), 1.60 and 1.27 (–CH_2– of the long fatty acid chain), 0.87 (–CH_3). ^{13}CNMR (75MHz, $CDCl_3$) (δ, ppm): 174.22 and 172.15 (–C=O), 130.57 and 127.44 (–CH=CH–), 69.45 and 62.28 (–CH_2–O–), 35.65-21.27 (–CH_2– of the long fatty acid chain), 14.49 (CH_3).

Oil extraction process was detected by FTIR spectroscopy (Fig.1).

Oil extraction yield was calculated by bellow formula:

$$\text{yield (\%)} = \frac{\text{Final weight of Oil (g)}}{\text{Weight of Date seed powder (g)}} \times 100$$

When the temperature was raised from 80℃ to 100℃, the seed oil yield increased by 45%, but when the temperature was raised from 100℃ to 120℃, only a minor difference was observed at 120℃.

As a result, the optimal conditions for extracting date seed oil were found to be 100℃, with an average particle size of 0.5 mm, a solvent to seed ratio of 6:1 (ml:g), and an extraction time of 6 hours. The maximum date seed oil yield reached under these conditions (Fig.2).

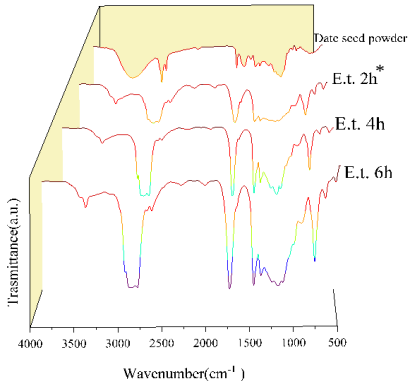

*Oil Exraction time (E.t.)

Fig.1. Monitoring the oil extraction process with FT-IR spectrum

3.2. Amidation reaction

DSO/DEA (>96% yield) FTIR (cm^{-1}, KBr window): 3385.91 (OH stretching), 2923.37 and 2853.45 (asymmetrical and symmetrical stretching of C–H of long fatty acid chain), 1744.12 (–C=O stretching (ester)), 1623.56 (-C=O stretching (amide)), 1466.59 (=C–H bend–), 1365.62 (–CH_3 bend), 1170.76 (C–N stretching), 1052 (-C-O), 859.16 (=CH_2), 721.91 (-$(CH_2)_n$-, -HC=CH- (cis)). ^{1}HNMR (300 MHz, $CDCl_3$) (δ, ppm): 5.32 (–CH=CH–), 3.90 and 3.39 (N–$(CH_2)_2$–OH), 2.74 (–CH_2–CONR), 2.19 (–CH_2–C=C), 2.01 (–CH_2–CH_2–CONR), 1.58 and 1.25 (–CH_2– of the long fatty acid chain), 0.72 (–CH_3). ^{13}CNMR (75MHz, $CDCl_3$) (δ, ppm): 176.21 (–N–CO–CH_2–), 130.23-126.62 (–CH=CH–), 61.21 (–CH_2–O–), 53.2-51.94 (N–$(CH_2)_2$–OH), 34.67-21.40 (–CH_2– of the long fatty acid chain), 14.64 (–CH_3).

The scheme of reaction mechanism is shown in (Fig.3). $NaOCH_3$ catalyst used for the direct amidation with diethanolamine as a reaction under mild conditions.

The conversion interval was calculated from the ^{1}HNMR spectrum by integrating the peaks corresponding to the diethanol amide and the glycerol group protons using the following equation:

$$\text{Conversion (\%)} = \frac{A_{3.90-3.39}}{A_{3.90-3.39}+A_{4.41-4.06}} \times 100$$

Where $A_{3.90-3.39}$ is the integral of the diethanol amide group protons and $A_{4.41-4.06}$ is the integral of the glycerol group protons.

Optimal conditions for amidation of date seed oil are 110℃ and 24 hours (Table1).

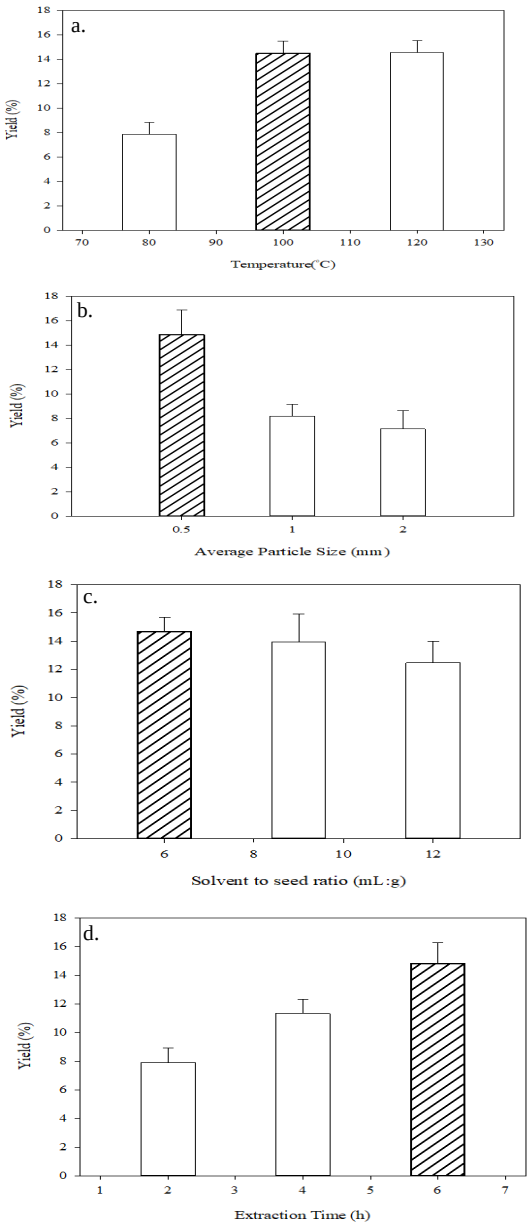

Fig.2. Effect of the main parameters on yield of oil extraction: Temperature (a), Average particle size of date seed powder (b), Solvent to seed ratio (c), Extraction time (d)

In the FTIR spectrum, after the complete conversion of triglyceride to fatty acid amide, a new band at 1623.56 cm^{-1} was observed, which was the C=O stretching of the amide functional group (Fig.4).

In the ^{1}H-NMR spectrum, the appearance of a multiplet at 3.90 and 3.39 ppm due to N–$(CH_2)_2$–OH

protons and the disappearance of characteristic glyceride protons at 4.41 and 4.06 ppm supported the conversion of date seed oil to the corresponding fatty acid amide (Fig.5).

Table 1 Effect of time and temperature on conversion

NO.	Catalyst (mol %)	Time/Temperature (h/℃)	Conversion (%)
1	-	6/110	7
2	1.5	6/110	23
3	1.5	12/110	68
4	1.5	24/80	31
5	1.5	24/110	96
6	1.5	24/140	75

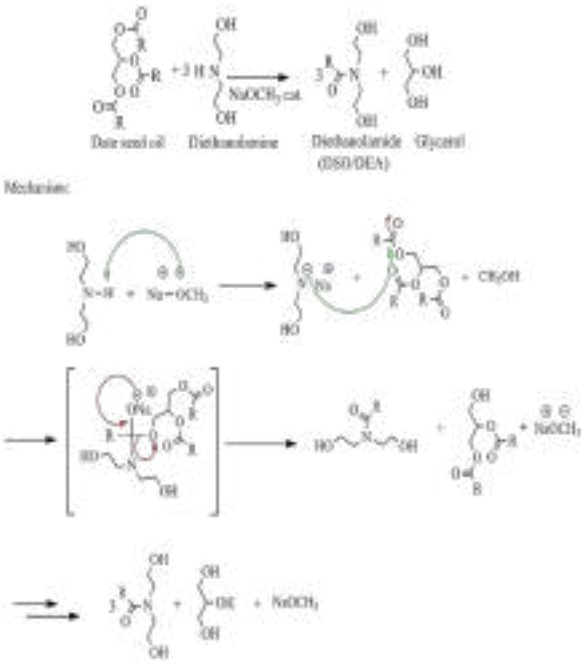

Fig.3. Mechanism of amidation Date seed oil catalyzed by $NaOCH_3$

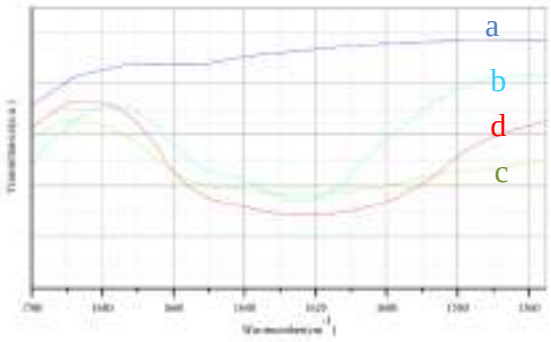

Fig.4. FTIR spectrum (1550-1700cm^{-1}): Date seed oil (a), DSO/DEA after 6 hours (b), DSO/DEA after 12 hours (c), DSO/DEA after 24 hours (d)

4. Conclusions

Although date seeds are considered waste, this study has shown potential for them to be used in fatty acid amide synthesis. In the present study, amidation of date seed oil was conducted. The maximum yield of the reaction was 96% at 110℃, calculated using ^{1}HNMR spectrum. Additionally, date seed oil was used as a renewable feedstock and eco-friendly material, and the direct amidation method, a solvent-free and one-pot reaction, was used for fatty acid amide synthesis.

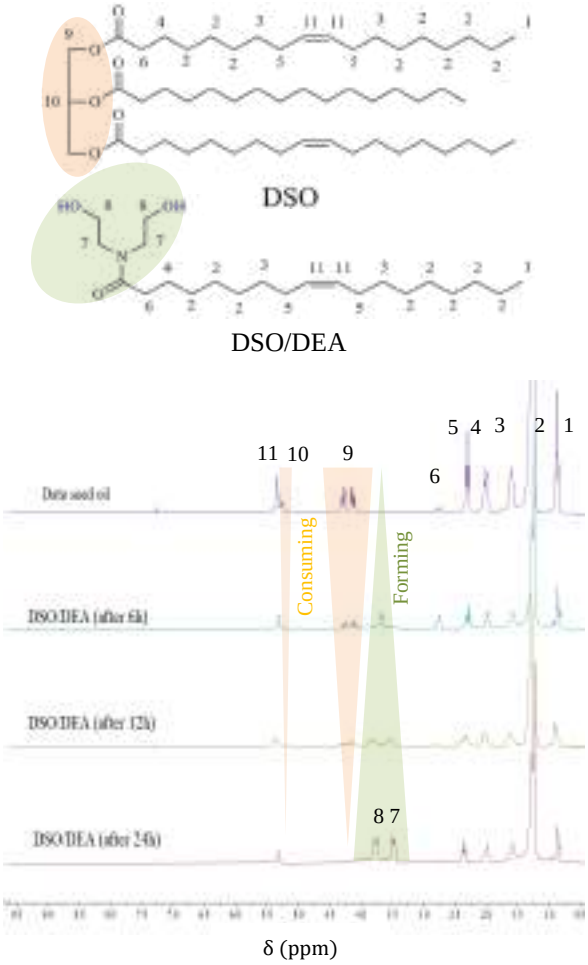

Fig.5. Monitoring the reaction with ^{1}HNMR spectrum

5. References

[1] U. Biermann, W. Friedt, S. Lang, W. Lühs, G. Machmüller, and J. O. Metzger, "New Syntheses with Oils and Fats as Renewable Raw Materials for the Chemical Industry," *Angew Chem Int Ed*, 2000.

[2] Kumar, Park, and Kim, "One-Pot Solvent-Free Synthesis of N,N-Bis(2-Hydroxyethyl) Alkylamide from Triglycerides Using Zinc-Doped Calcium Oxide Nanospheroids as a Heterogeneous Catalyst," *Catalysts*, vol. 9, no. 9, p. 774, Sep. 2019, doi: 10.3390/catal9090774.

[3] S. Besbes, C. Blecker, C. Deroanne, G. Lognay, N.-E. Drira, and H. Attia, "Heating effects on some quality characteristics of date seed oil," *Food Chem.*, vol. 91, no. 3, pp. 469–476, Jul. 2005, doi: 10.1016/j.foodchem.2004.04.037.

[4] H. A. Allami, M. Tabasizadeh, A. Rohani, H. Nayebzadeh, and A. Farzad, "Effect of ultrasonic irradiation on the properties and performance of biodiesel produced from date seed oil used in the diesel engine," *Ultrason. Sonochem.*, vol. 60, p. 104672, Jan. 2020, doi: 10.1016/j.ultsonch.2019.104672.

29TH IRANIAN ORGANIC CHEMISTRY CONFERENCE
1_3 NOV, 2023
UNIVERSITY OF QOM, IRAN

Terpyridine Copper(I) Complex as an Efficient Catalyst in the Ullmann Carbon-Carbon Coupling Reaction in the Presence of a New Deep Eutectic Solvent

Akbar Mobaraki[1] *, *and Zhila Hosseinzadeh*[2]

[1] *Department of Organic Chemistry and Polymer, Faculty of Chemistry, Kharazmi University, Tehran, Iran, akbar.mobaraki@khu.ac.ir*

[2] *Department of Chemistry, K. N. Toosi University of Technology, Tehran, Iran, j.hosseinzadeh44@gmail.com*

Abstract - An efficient protocol for the Cu-catalyzed carbon-carbon Ullmann coupling reaction of aryl halides has been developed for the synthesis of various biaryl products in good to excellent yields. For this purpose, 4′-(4-methoxyphenyl)-2,2′:6′,2″-terpyridine as a ligand, CuI as a catalyst and a mixture of *N*,*N*-dimethylethylenediamine (DMED) and tetrabutylammonium bromide (TBAB) as green Deep Eutectic Solvent (DES) have been used. In the studied reaction, this new DES has been used to act as both a base and a reaction promoter in addition to its main role as a solvent.

1. Introduction

Regarding both industrial and synthetic point of views, transition-metal catalyzed carbon-carbon coupling reaction is a fundamental and challenging process since substitution reactions can occur on planar centers [1]. Carbon-carbon coupling reactions are included broadly in the synthetic procedures of valuable compounds such as various polymers, agrochemicals, dyes, organic conductors/semi-conductors and pharmaceutical intermediates [2,3]. Among carbon–carbon coupling reactions, the Ullmann coupling of aryl halides offers ingenious ways to construct large-scale biaryl compounds in some industrial processes [4,5]. Some progress has been made in this field by using various transition metal catalysts [4,6]. Nevertheless, considerable attention is still devoted to the development of new catalytic systems for this process with efficient activity. Since leachability of the transition metal catalysts is an important factor in catalytic processes [7], the design and/or utilization of organic ligands with carefully-placed binding sites offer great potential for the manufacture of complexes with novel architectures. In this regard, several chelators such as diamines, amino acids, 1,10-phenantrolines, diols and other nitrogen-, phosphorusand oxygen-containing ligands are of a high interest because of their complexation and the chelation affinity [4]. Therefore, using electron-rich ligands in order to anchor the transition-metal particles is an important factor. In this regard, in order to identify a robust and easily prepared system to catalyze carbon-carbon bond-forming reaction, we have used 4′-(4-methoxyphenyl)-2,2′:6′,2″-terpyridine (Mtpy) [8] as a ligand and CuI as a catalyst and investigate its applicability in Ullmann carbon-carbon coupling reaction (Scheme 1). Utilization of a simple and electron-rich terpyridine tridentate ligand keep any leaching of the copper active sites from happening. In other words, the three N of the pyridine rings act as very good electron-donating coordination sites with great affinities for transition metal particles, which create a very stable complex and a more potent catalytic system. To develop environmentally friendly processes the past decade witnessed emergence of new types of green and sustainable solvents similar to ionic liquids called Deep Eutectic Solvents (DESs). Due to the many green properties of DESs, they have been considered in several fields of chemistry for practical applications as promising alternatives to traditional solvents [9]. DESs are binary mixtures comprising one hydrogen bond donor (HBD) such as amines, amides, carboxylic acids, and alcohols and one hydrogen bond acceptor (HBA) such as organic halide salts, which are strongly associated with each other via hydrogen bond interactions. When mixed in the proper molar ratio, DESs have much lower melting points than either of the individual components by forming a eutectic mixture. DESs are effectively and progressively replacing often hazardous and Volatile Organic Compounds (VOCs) in many areas of scientific processes [9]. Therefore, in this paper we use mixture of *N*,*N*-dimethylethylenediamine (DMED) and tetrabutylammonium bromide (TBAB) as a novel DES with triple action (as solvent, base and reaction promoter) in Cu-catalyzed Ullmann carbon-carbon coupling reaction (Scheme 1).

2. Results and Discussion

For the beginning of this study, to find the best reaction conditions, the Ullmann carbon-carbon

coupling reaction was investigated between 2 mmol of iodobenzenes molecules in the presence of our

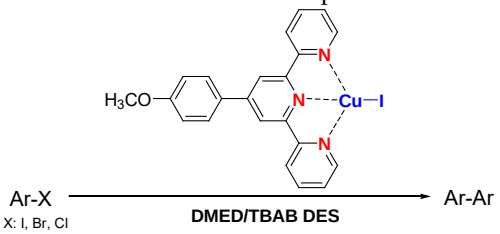

Scheme 1. Schematic representation of our catalytic system in Cu-catalyzed Ullmann carbon-carbon coupling reaction.

novel DMED/TBAB (4: 1) DES (3 mL), 4′-(4-methoxyphenyl)-2,2′:6′,2″-terpyridine (Mtpy) and CuI (5 mol%) as a model reaction at 100 °C for 10 h, thus affording 76% isolated yield for Biphenyl (Table 1, entry 1). To probe the effect of various conditions, the effect of different mol% of Mtpy and CuI and temperature was screened (Table 1). First, the effect of different loadings of the catalytic system was investigated (Table 1, entries 2-4); among them, 10 mol% of the catalytic system showed excellent performance (Table 1, entry 3). More increasing the amount of the catalyst did not have any significant impact on the product yield (Table 1, entry 4). To evaluate the effect of Mtpy ligand in the complexation and stabilization of CuI, the reaction was investigated in the absence of Mtpy, a lower yield of the desired product was obtained under the same reaction conditions (Table 1, entry 8). Finally, the reaction was investigated in the absence of the catalytic system (Mtpy ligand and CuI active sites), which showed no product yield (Table 1, entry 9). Therefore, these results clearly show the significant effect of the catalytic system on the progress of the reaction.

Under similar reaction conditions, to investigate the effect temperature on the reaction rate, the model reaction was accomplished at lower temperatures. It was revealed that reducing the reaction temperature from 100 °C to lower temperatures (80, 50 °C and r.t.) had a negative effect on the product yield (Table 1, entries 5–7). It was concluded that the optimized condition for this reaction is 10 mol% of the catalytic system, 3 mL of DMED/TBAB (4 : 1) DES as the base, reaction promoter and solvent at 100 °C for 10 h (Table 1, entry 3).

With the optimized reaction conditions in hand, the efficiency of the procedure was further extended by coupling various aryl halides (Table 2). As anticipated, the coupling reaction of both electron-donating as well as electron-withdrawing substituted aryl iodides progressed very smoothly to give the desired products in excellent yields (Table 2, entries 1-5). Under the same reaction conditions used for aryl iodides, bromobenzene and *para*-bromoacetophenone with an electron-withdrawing group in the *para* position were more reactive in comparison to those

Table 1 Optimization of the reaction temperature and amount of the Mtpy and CuI catalytic system in the Ullmann reaction of iodobenzene.[a]

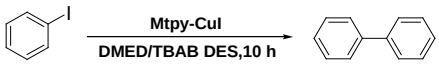

Entry	CuI (mol%)	Mtpy (mol%)	Temperature (°C)	Yield (%)[b]
1	5	5	100	76
2	7.5	7.5	100	84
3	10	10	100	93
4	12.5	12.5	100	95
5	10	10	80	88
6	10	10	50	71
7	10	10	r.t.	47
8	10	-	100	32
9	-	-	100	N.R.

[a] Reaction was carried out using 2 mmol of iodobenzene in the presence of DMED/TBAB (4 : 1) DES (3 mL) for 10 h. [b] Yields refer to the isolated pure products.

With an electron-donating group, *para*-methoxybromobenzene (Table 2, entries 6-8) and gave good yields. These results clearly verify the role of tetrabutylammonium bromide (TBAB) as a promoter of the reaction mixture that was present as a part of our new DES. We then turned our attention on more challenging aryl chlorides. Due to the less reactivity of aryl chlorides, they showed reasonable activity with lower yields of the corresponding products. Therefore, we performed the reaction with higher mol% of Mtpy and CuI, temperature and reaction time. The expected products were successfully obtained in good yields, indicating that the method is successful for various alkyl halides (Table 2, entries 9–11).

Table 2 Cu-catalyzed Ullmann carbon-carbon coupling reactions of various aryl halides.[a]

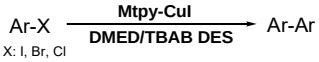

Entry	Aryl halide	Yield (%)[b]
1	Iodobenzene	93
2	*para*-Iodoacetophenone	94
3	*para*-Iodobromobenzene	92
4	*para*-Iodobenzonitrile	95
5	*para*-Methoxyiodobenzene	91
6	Bromobenzene	89
7	*para*-Bromoacetophenone	90
8	*para*-Methoxybromobenzene	92[c]
9	Chlorobenzene	88[d]
10	*para*-Chloroacetophenone	90[d]
11	*para*-MethoxyChlorobenzene	86[e]

[a] Reaction was carried out using 2 mmol of aryl halides, 3 mL of DMED/TBAB (4 : 1) DES in the presence of 10 mol% of Mtpy and CuI at 100 °C for 10 h. [b] Yields refer to the isolated pure products and structures of the products were confirmed by ^{1}H NMR, and ^{13}C NMR spectral data [10]. [c] Reaction was carried out using 12.5 mol% of Mtpy and CuI. [d] Reaction was carried out using 12.5 mol% of Mtpy and CuI at 115 °C. [e] Reaction was carried out using 12.5 mol% of Mtpy and CuI at 115 °C for 15 h.

3. Conclusions

In conclusion, we have developed a general and efficient Cu-catalyzed procedure for the synthesis of biaryls using Tetrabutylammonium bromide (TBAB) and *N*,*N*-Dimethylethylenediamine (DMED) as a new deep eutectic solvent, 4′-(4-methoxyphenyl)-2,2′:6′,2″-terpyridine as a ligand and CuI as catalytic active sites.

So far we have come to this conclusion that the used novel catalytic system in this report is a multipurpose alternative system for performing Cu-catalyzed carbon-carbon Ullmann coupling reaction due to its key features, highlighted as follow:

–The use of a tridentate electron-rich ligand prevents any leaching in the copper active sites.

– The employed DES with triple action acts as both base and promoter, beside its major role as solvent in the Cu-catalyzed carbon-carbon Ullmann coupling reaction is a novel approach in the application of DESs in this catalytic systems.

– The hydrophobic/hydrophilic balance of employed DES, enables easier association of reaction partners in the course of the reactions.

– The capability of using a variety of aryl halides especially more challenging aryl bromides and chlorides with good to excellent efficiency in the Cu-catalyzed carbon-carbon Ullmann coupling reaction.

Acknowledgment

The authors greatly acknowledge Kharazmi University research council for the financial support of this work.

4. References

[1] L. Yin, J. Liebscher, Chem. Rev. 107 (2007) 133–173.

[2] (a) A.F.P. Biajoli, C.S. Schwalm, J. Limberger, T.S. Claudino, A.L. Monteiro, J. Braz. Chem. Soc. 25 (2014) 2186–2214; (b) Q. Yang, H. Jin, Y. Xu, P. Wang, X. Liang, Z. Shen, Z. Chen, D. Zou, X. Fan, Q. Zhou, Macromolecules 42 (2009) 1037–1046; (c) V.L. Budarin, P.S. Shuttleworth, J.H. Clark, R. Luque, Curr. Org. Synth. 7 (2010) 614–627.

[3] (a) C. Torborg, M. Beller, Adv. Synth. Catal. 351 (2009) 3027–3043; (b) T.-S. Jo, S.H. Kim, J. Shin, C. Bae, J. Am. Chem. Soc. 131 (2009) 1656–1657.

[4] (a) I.P. Beletskaya, A.V. Cheprakov, Coord. Chem. Rev. 248 (2004) 2337–2364; (b) S.V. Ley, A.W. Thomas, Angew. Chem. Int. Ed. 42 (2003) 5400–5449; (c) K. Kunz, U. Scholz, D. Ganzer, Synlett (2003) 2428–2439; (d) F. Monnier, M. Taillefer, Angew. Chem. Int. Ed. 47 (2008) 3096–3099; (e) G. Evano, N. Blanchard, M. Toumi, Chem. Rev. 108 (2008) 3054–3131; (f) A. Klapars, X. Huang, S.L. Buchwald, J. Am. Chem. Soc. 124 (2002) 7421–7428; (g) J.C. Antilla, A. Klapars, S.L. Buchwald, J. Am. Chem. Soc. 124 (2002) 11684–11688; (h) F.Y. Kwong, S.L. Buchwald, Org. Lett. 5 (2003) 793–796; (i) D. Ma, Q. Cai, H. Zhang, Org. Lett. 5 (2003) 2453–2455; (j) B. de Lange, M.H. Lambers-Verstappen, L.S. de Vondervoort, N. Sereinig, R. de Rijk, A.H.M. de Vries, J.G. de Vries, Synlett (2006) 3105–3109; (k) A. Shafir, S.L. Buchwald, J. Am. Chem. Soc. 128 (2006) 8742–8743; (l) A. Ouali, J.-F. Spindler, A. Jutand, M. Taillefer, Organometallics 26 (2007) 65–74.

[5] (a) C. Sambiagio, S.P. Marsden, A.J. Blackera, P.C. McGowan, Chem. Soc. Rev. 43 (2014) 3525–3550; (b) H. Lin, D. Sun, Org. Prep. Proced. Int. 45 (2013) 341–394; (c) S. Monda, ChemTexts 17 (2016) 1–11.

[6] (a) B.W. Crabbe, O.P. Kuehm, J.C. Bennett, G.L. Hallett-Tapley, Catal. Sci. Technol. 8 (2018) 4907–4915; (b) A. Gao, H. Liu, L. Hu, H. Zhang, A. Hou, K. Xie, Chin. Chem. Lett. 29 (2018) 1301–1304; (c) N. Marina, A.E. Lanterna, J.C. Scaiano, ACS Catal. 8 (2018) 7593–7597; (d) N.K. Ojha, G.V. Zyryanov, A. Majee, V.N. Charushin, O.N. Chupakhin, S. Santra, Coord. Chem. Rev. 353 (2017) 1–57; (e) B. Zhu, L.K. Yan, L.S. Yao, H. Ren, R.H. Li, W. Guan, Z.M. Su, Chem. Commun. 54 (2018) 7959–7962.

[7] (a) A. Corma, H. Garcia, Top. Catal. 48 (2008) 8–31; (b) L.D. Pachon, G. Rothenberg, Appl. Organomet. Chem. 22 (2008) 288–299; (c) A. Corma, H. Garcia, Adv. Synth. Catal. 348 (2006) 1391–1412; (d) H. Li, P.S. Bhadury, B. Song, S. Yang, RSC Adv. 2 (2012) 12525–12551; (e) H.R. Sonawane, J.V. Deore, P.N. Chavan, ChemistrySelect 7 (2022) e202103900; (f) D. Cantillo, C.O. Kappe, ChemCatChem 6 (2014) 3286–3305.

[8] J. Wang, G.S. Hanan, Synlett, 8 (2005) 1251–1254.

[9] (a) F.M. Perna, P. Vitale, V. Capriati, Curr. Opin. Green Sustain. Chem. 21 (2020) 27–33; (b) B.B. Hansen, S. Spittle, B. Chen, D. Poe, Y. Zhang, J.M. Klein, A. Horton, L. Adhikari, T. Zelovich, B.W. Doherty, B. Gurkan, E.J. Maginn, A. Ragauskas, M. Dadmun, T.A. Zawodzinski, G.A. Baker, M.E. Tuckerman, R.F. Savinell, J.R. Sangoro, Chem. Rev. 121 (2021) 1232–1285; (c) E.L. Smith, A.P. Abbott, K.S. Ryder, Chem. Rev. 114 (2014) 11060–11082; (d) T. El-Achkar, H.G. Gerges, S. Fourmentin, Environ. Chem. Lett. 19 (2021) 3397–3408; (e) C. Florindo, F. Lima, B.D. Ribeiro, I.M. Marrucho, Curr. Opin. Green Sustain. Chem. 18 (2019) 31–36; (f) W. Xu, Y. Ma, X. Wei, H. Gong, X. Zhao, Y. Qin, Q. Penga, Z. Hou, New J. Chem. 46 (2022) 15712–15722; (g) M. Shaibuna, M.J.K. Kuniyil, K. Sreekumar, New J. Chem. 45 (2021) 20765–20775; (h) T.P. Cao, C.N. Hang, H.V. Quang, D.M. Kabtamu, S. Kumar, V.C. Nguyen, X.T. Cao, New J. Chem. 46 (2022) 3786–3793; (i) L. Pan, L. Qi, T. Yongyou, M. Cuiluan, C. Haoyu, A. Yunlong, H. Yu-Cai, Ind. Crops Prod. 186 (2022) 115203–115204; (j) Q. Li, J. Di, X. Liao, J. Ni, Q. Li, Y.C. He, C. Ma, Green Chem. 23 (2021) 8154–8168; (k) M. Wu, J. Di, L. Gong, Y.C. He, C. Ma, Y. Deng, Chem. Eng. J. 452 (2023) 139320–139321; (l) H.T. Nguyen, T.V. Le, P.H. Tran, J. Environ. Chem. Eng. 9 (2021) 105228–105236.

[10] Spectral data of biaryls, *Biphenyl*: ^{1}H-NMR (400 MHz, $CDCl_3$): δ(ppm) = 7.63-7.65 (m, 4H), 7.46-7.51 (d, 4H), 7.37-7.41 (m, 2H); ^{13}C NMR (100 MHz, $CDCl_3$): δ (ppm) = 141.2, 128.8, 127.3, 127.2; *4,4'-Dibromobiphenyl*: ^{1}H-NMR (400 MHz, $CDCl_3$): δ(ppm) = 7.57-7.61 (m, 4H), 7.42-7.46 (m, 4H); ^{13}C NMR (100 MHz, $CDCl_3$): δ (ppm) = 138.9, 132.0, 128.5, 121.9; *4,4'-Dicyanobiphenyl*: ^{1}H-NMR (400 MHz, $CDCl_3$): δ(ppm) = 7.80-7.82 (d, 4H, *J*= 8), 7.71-7.73 (d, 4H, *J*= 8); ^{13}C NMR (100 MHz, $CDCl_3$): δ (ppm) = 143.5, 132.9, 127.9, 118.4, 112.4; *4,4'-Diacetylbiphenyl*: ^{1}H-NMR (400 MHz, $CDCl_3$): δ(ppm) = 8.08-8.11 (dt, 4H), 7.74-7.77 (m, 4H), 2.69 (s, 6H); ^{13}C NMR (100 MHz, $CDCl_3$): δ (ppm) = 197.6, 144.3, 136.5, 129.0, 127.4, 26.7; *4,4'-Dimethoxybiphenyl*: ^{1}H-NMR (400 MHz, $CDCl_3$): δ(ppm) = 7.49-7.53 (m, 4H), 6.97-7.01 (m, 4H), 3.88 (s, 6H); ^{13}C NMR (100 MHz, $CDCl_3$): δ (ppm) = 158.7, 133.5, 127.7, 114.1, 55.3.

[11] General procedure for the Ullmann reaction: A mixture of aryl halide (2.0 mmol), Mtpy and CuI (10 mol%) in 3 mL DMED/TBAB (4 : 1) DES were stirred at 100 °C for an appropriate time (Table 2). The progress of the reaction was monitored by TLC. After completion of the reaction, the mixture was cooled to room temperature and poured into H_2O (10 ml), and extracted with CH_2Cl_2 (2 × 5 ml) to separate the DMED/TBAB DES from the product. After extraction, the

organic layer was dried over anhydrous Na_2SO_4 and concentrated under reduced pressure; the residue was subjected to column chromatography on silica gel (ethyl acetate and hexane as eluent) to yield the expected pure product. All products were characterized by ^{1}H and ^{13}C spectra.

29TH IRANIAN ORGANIC CHEMISTRY CONFERENCE
1_3 NOV, 2023
UNIVERSITY OF QOM, IRAN

The green Synthesis of papaverine one of opium alkaloids in water

Ali Hossein Amini[1,2], *Yaghoub Sarrafi*[1,*], *Khosrow Jadidi*[3], *Masoumehossadat Hosseini*[2,3] ,*Valid Taheri*[2,3] , *Rana Amini*[4]

[1] *Department of Organic Chemistry, Faculty of Chemistry, University of Mazandaran, Babolsar,47416-95447, Iran, alihossein97777@gmail.com*

[2] *Soroush Mana Pharmed, Golrang Pharmaceutical Investment Co (GPI), Golrang Industrial Group (GIG), Tehran, Iran*

[3] *Faculty of Chemistry and Petroleum Sciences, Department of Chemistry, Shahid Beheshti University, Tehran, Iran*

[4] *Department of Chemistry, University of Zanjan, Zanjan, Iran.*

Abstract - Opium mixture serves as a vital source of alkaloids, including significant medicinal compounds used in the pharmaceutical industry. One such compound is papaverine (6), a benzylisoquinolinic alkaloid found in opium mixture, possessing distinct medicinal properties. This artcle addresses the limitations associated with extracting substances from natural compounds by focusing on the synthesis of papaverine in four comprehensive steps. The synthetic route employs 2-(4,3-dimethoxyphenyl) acetic acid (1), which undergoes transformation to yield methyl 2-(4,3-dimethoxyphenyl) acetate (2). Through the binding of compound (2) with commercially available 2-(4,3-dimethoxyphenyl) ethane amine (3), amide (4) is obtained. Subsequently, ring closure of compound (4) is efficiently achieved using polyphosphoric acid (PPA) in refluxing toluene, leading to the formation of 1-(4,3-dimethoxy-benzyl)-7,6-dimethoxy-4,3-dihydroisoquinoline (5). The next crucial step involves the hydrogenation of compound (5) with Pd/C in a water-solvent medium, successfully yielding the desired product, papaverine (6), with an impressive efficiency of 58.7%. Characterization of the formed products is carried out using FTIR, ^{1}H NMR, ^{13}C NMR, and Mass spectrometry techniques, confirming their chemical identities. By developing a synthetic approach to produce papaverine, this study offers valuable insights into the efficient synthesis of this important medicinal compound, potentially paving the way for its widespread application in the pharmaceutical industry.

Keywords: Opium, Isoquinoline, Papaverine, Chemical synthesis.

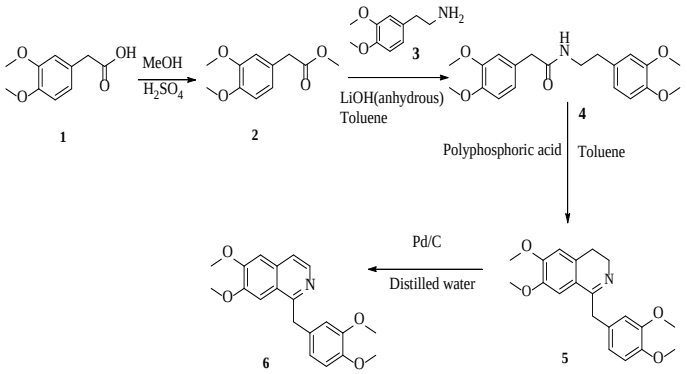

1. Introduction

Alkaloids, naturally occurring compounds that incorporate nitrogen into their molecular structure, derive their name from their alkaline properties. They are synthesized by a diverse range of organisms, including bacteria, microorganisms, plants, fungi, and other organisms. Several alkaloids have found applications in the pharmaceutical industry due to their medicinal effects. One of the most extensively studied alkaloids in this context is the opium alkaloid group [1, 2, 3]. Opium contains a multitude of alkaloids, with over 20 types reportedly isolated from various sources of opium poppy worldwide [4]. These alkaloids are conventionally classified based on their abundance, distinguishing between those with an abundance of more than one percent and those with less than one percent. Among the alkaloids with higher abundance, papaverine stands out significantly. As a member of the benzylisoquinoline category, papaverine has garnered particular attention in the pharmaceutical industry. Remarkably, it is not classified as a narcotic and faces fewer restrictions, making it an appealing

choice for medicinal applications. Papaverine's vasodilation properties, enabling the relaxation of blood vessels, have led to its use in treating male sexual aversion. Administered by injecting a small amount at the base of the male penis, papaverine facilitates erection effectively. There are two primary methods for obtaining papaverine: extraction from the opium mixture and chemical synthesis. However, due to limited sources of alkaloids in natural opium, researchers have focused on chemical synthesis to produce papaverine in higher quantities. The history of synthetic research on papaverine dates back many years, with numerous breakthroughs achieved by scientists worldwide. Notably, the first synthesis of papaverine took place in 1909 by Pictet and Goms, utilizing specific compounds in their method [5]. Subsequent researchers made significant advancements, uncovering new synthetic routes and refining the process [6, 7]. Additionally, in 2010, a biosynthetic pathway for papaverine was proposed, further broadening the scope of research in this area [8].

2. Result and discussion:

Papaverine, as one of the opium alkaloids, has attracted the attention of scientists and researchers. The historical background that shows the importance of papaverine synthesis by chemical method goes back many years. Among the recent studies on the synthesis of papaverine, we can mention the research team's study in 2020, a research team in China achieved the synthesis of papaverine hydrochloride in a different way. They synthesized papaverine in one pot. Based on the claims of these researchers, papaverine hydrochloride has been synthesized in one pot during the five steps [9]. They start from 2-(3,4-dimethoxyphenyl) acetic acid for papaverine synthesis. According to the laboratory experiences in this article, the method proposed by the Chinese research team in 2020 has ambiguity and weaknesses, some of which are discussed below. The most recent studies conducted by researchers for the purpose of papaverine synthesis were reported in 2022 [10]. In this study papaverine had synthesized by biosynthesis of tetrahydropapaverine and so on semisynthesis of papaverine in yeast. The overall yield reported from this method is 15%. All the mentioned syntheses from 1909 until today have many strengths and weaknesses, and in this article, the proposed synthetic path is an effective step for the synthesis of papaverine and the very useful intermediates of this drug. The aim of this research in this article is the synthesis of papaverine, one of the opium alkaloids, which was obtained using available chemicals, papaverine with a total efficiency of 58.7%. In general, Table 2-1 compares the studies done in the past until today, as well as the study done in this article.

Table 2-1: Studies conducted in order to synthesize papaverine

Year of publication	Yield %
1909	1
2020	65
2022	15
Our study	58.7

According to the material mentioned in this article, we decided to synthesize papaverine synthetically from the steps mentioned in the following. Since the natural resources available for the supplier of papaverine in the world are limited and the extraction methods of this compound have many challenges, therefore, the synthesis of papaverine by chemical method is of great importance, and as a result, our mission in this article was to investigate the optimal synthetic route of papaverine synthesis. The advantages of this study compared to other studies reported to date include the use of available and cheap raw materials, the use of green reagents in the reaction steps, relatively high yield in each step, performing the amidation step by bonding between amine and ester for first time, and the most important strength in the study conducted in this article is performing the aromatization step in green and safe water solvent with relatively high yield. Here we report papaverine synthesis in water solvent for first time. In addition, another significant point that has been investigated in this article is that in the amide formation stage, the effects of two important parameters, the presence of water and the cation ion pair [11], have been studied. At this stage, in order to compare other cationic ion pairs and also the presence of water in the reaction and their effect on the reaction process, sodium hydroxide and potassium hydroxide salts were also tested as catalysts, and the results are reported in the table 2-2, 2-3.

Table 2-2: Comparison of catalyst ion pairs

Catalyst	**Yield**
LiOH (anhydrous)	**90%**
NaOH	**60%**
KOH	**51%**

Table 2-3: Comparison of the presence of water in the catalyst

Catalyst	Yield
$LiOH.H_2O$	**30%**
NaOH	**60%**
KOH	**51%**

3. Experimental:

3.1. Synthesized compounds:

In this article, taking into account the methods used in previous studies and the efficiency obtained from these methods, we decided to introduce a new path for the synthesis of papaverine drug from safer methods with higher efficiency. In the new synthetic route introduced in this article, compounds methyl 2-(4,3-dimethoxyphenyl) acetate (compound 2), N-(4,3-dimethoxyphenyl)-2-(4,3-dimethoxyphenyl) Acetamide (compound 4), 1-(4,3-dimethoxybenzyl)-7,6-dimethoxy-4,3-dihydroisoquinoline (compound 5) and finally papaverine compound (compound 6) by the methods described in the continuation of this article has been discussed and they were synthesized.

3.1.1. Synthesis of methyl 2-(4,3-dimethoxyphenyl) acetate:

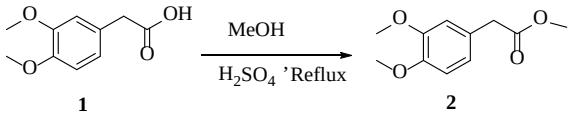

1 2

Scheme 3-1: Synthetic route of methyl 2-(4,3-dimethoxyphenyl) acetate

In a 250 ml flask equipped with a reflux condenser, 0.1 mol (20 g) of 2-(4,3-dimethoxyphenyl) acetic acid (compound 1) and 100 ml of methanol were added as reaction solvent after 5 minutes After stirring 0.01 mol (0.55 ml) of 98% sulfuric acid was added to the reaction flask and the reaction temperature was adjusted in methanol reflux mode. After 19 hours at the reflux temperature, the reaction ended. It should be noted that to ensure the completion of the reaction, the reaction was tracked on TLC paper every few hours. Then the reaction temperature was cooled down to room temperature and after the completion of the reaction in order to neutralize the possible 2-(4,3-dimethoxyphenyl) acetic acid left in the reaction as well as the sulfuric acid present in the reaction, 0.1 mol (8.4) grams of sodium bicarbonate was added to the reaction vessel at room temperature (pH = 8) and stirred for 1 hour, then methanol was removed from the reaction vessel. The salts present in the reaction were separated in such a way that the synthesized ester was dissolved in the toluene phase and the salts present in the aqueous phase. Next, the toluene phase containing the ester was separated by a decanter and dried by dry sodium sulfate to ensure the absence of water in the separated solution. Next, toluene was removed from the reaction vessel by distillation condenser and a clear liquid was obtained, this obtained liquid has been synthesized methyl 2-(4,3-dimethoxyphenyl) acetate (compound 2). The obtained weight is 20.8 grams practically and the reaction efficiency was 99%.

Methyl 2-(3, 4-dimethoxyphenyl) acetate: ^{1}H NMR (300 MHz, $CDCl_3$): δ_H (ppm) 3.57 (3H s), 3.69 (3H s), 3.86 (3H s), 6.82 (3H Ar, s), **^{13}C NMR** (75 MHz, CDCl3): δ_C (ppm) = 40.7, 52.0, 55.8, 55.8, 111.1, 112.3, 121.3, 126.4, 148.1, 148.8, 172.3. **IR** (KBr) ν 1735 (C=O Ester).

3.1.2. Synthesis of N-(4,3-dimethoxyphenyl)-2-(4,3-dimethoxyphenyl) acetamide:

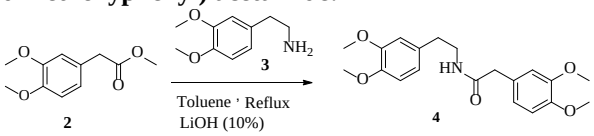

2 3 4

Scheme 3-2: Synthetic route of N -(4,3-dimethoxyphenyl)-2-(4,3-dimethoxyphenyl) acetamide

In a 250 ml flask equipped with a reflux condenser, 0.095 mol (20 g) of methyl 2-(4,3-dimethoxyphenyl) acetate (compound 2) was poured into the flask, then 100 ml of toluene was added to the reaction vessel. Then 2-(4,3-dimethoxyphenyl) ethane amine (compound 3) 0.19 mol (2.36 grams) was added to the reaction, then 0.0095 mol (0.227 grams) of lithium hydroxide was added. The temperature of the reaction was adjusted to toluene reflux and after 72 hours, the reaction ended according to scheme 3-2. After the reaction temperature reached room temperature, in order to separate the excess amine, present in the reaction, 80 ml of distilled water was added to the reaction container, then the amine present in the reaction was separated as a salt in the aqueous phase by acetic acid. After 1 hour, a precipitate was formed. which is N -(4,3-dimethoxyphenyl)-2-(4,3-dimethoxyphenyl) acetamide (compound 4) was filtered, the sediment was left to dry in an oven at 65°C and the sediment was weighed It is 30.9 grams practically and the reaction efficiency was 90.4%. The second method of the synthetic path of N -(4,3-dimethoxyphenyl)-2-(4,3-dimethoxyphenyl) acetamide is as follows:

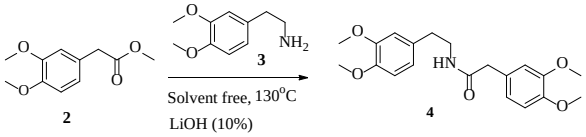

2 3 4

Scheme 3-3: The synthetic route of N-(4,3-dimethoxyphenyl)-2-(4,3-dimethoxyphenyl) acetamide by the second method

In this method, in a 50 ml flask equipped with a reflux condenser, 0.0047 mol (1 g) of methyl 2-(4,3-dimethoxyphenyl) acetate was added in the reaction vessel, then it was added to the amount of 0.01 mol (1.81 g) of 2-(4,3-dimethoxyphenyl) ethane amine was added, then 0.0005 mol (0.012 g) of lithium hydroxide was added to the reaction, then the reaction

temperature was set to 130 °C, then After 1 hour, the reaction was completely completed (see scheme 3-3). The sediment was placed in the oven at a temperature of 65ºC for drying, and the weight of the obtained sediment is 1.53 grams practically, and the efficiency at this stage was 90%.

N-(3,4-dimethoxyphenethyl)-2-(3,4-dimethoxyphenyl)acetamide: ^{1}H NMR (300 MHz, $CDCl_3$): δ_H (ppm) 2.66-2.68 (2H t, *J* = 3 Hz), 3.37 (2H m), 3.47 (2H s), 3.82 (3H s), 3.83 (3H s), 3.85 (3H s), 3.88 (3H s), 5.4 (1H NH, s), 6.50-6.80 (6H Ar, m), **^{13}C NMR** (75 MHz, CDCl3): δ_C (ppm) = 34.9, 40.7, 43.3, 55.8, 55.8, 55.8, 111.0, 111.3, 111.6, 112.3, 120.5, 121.5, 127.0, 130.9, 147.5, 148.2, 148.9, 149.2, 171.4. **IR** (KBr) ν 1641.61 (C=O Amide).

3.1.3. Synthesis of 1-(4,3-dimethoxy-benzyl)-7,6-dimethoxy-4,3-dihydroisoquinoline:

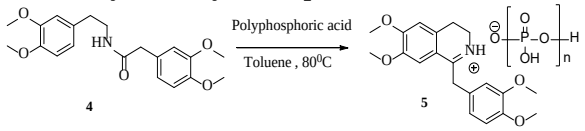

Scheme 3-4: The synthetic route of 1-(4,3-dimethoxy-benzyl)-7,6-dimethoxy-4,3-dihydroisoquinoline

In a 250 ml flask equipped with a reflux condenser, N -(4,3-dimethoxyphenyl)-2-(4,3-dimethoxyphenyl) acetamide (compound 4) 0.0139 mol (5 g) in the reaction vessel then the reaction solvent, 50 ml of toluene, was poured into the reaction vessel. Next, 2.5 times the weight of acetamide and 12.5 grams of polyphosphoric acid were added to the reaction vessel, and then the reaction temperature was set to 80ºC. At this stage, the synthetic compound 1-(4,3-dimethoxybenzyl)-7,6-dimethoxy-4,3-dihydroisoquinoline phosphate (compound 5) according to scheme 3-4 is stable, while after the completion of the reaction and converting the compound from the phosphate salt state and so-called basing it, the compound is very unstable. After 1 day at 80ºC, according to the trace of the reaction on the TLC paper, the amide in the reaction was approximately 25%. In order to isolate the remaining amide in the reaction, first the toluene solvent was overflowed, then after reducing the ambient temperature, 50 ml of water was added to it. After dissolving gum-like substances, 50 ml of ethyl acetate was added to the aqueous phase to separate the remaining amide. In this step, amide was separated from the product. The residue at pH = 1 was obtained as the phosphate salt of the product. Then, in order to neutralize the excess of phosphoric acid, potassium hydroxide solution was added to that solution to the amount of 6 grams dissolved in 30 ml of water and to pH = 5. In this case, the product was directly prepared for the next step. The yield of this step was 80%. Since some of the amide was left in the reaction, ethyl acetate was used to remove it, and the amount of unreacted amide was obtained by concentrating the ethyl acetate phase. In fact, it was subtracted from the total amount of the input raw material and the reaction efficiency was obtained.

Proof of formation of intermediate 1-(4,3-dimethoxy-benzyl)-7,6-dimethoxy-4,3-dihydroisoquinoline:

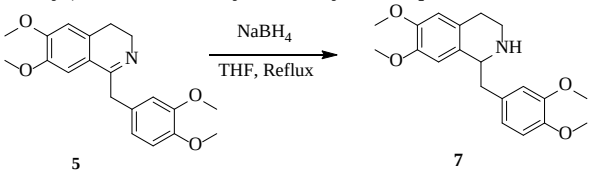

Scheme 3- 5: The synthetic route of reduction of 1-(4,3-dimethoxy-benzyl)-7,6-dimethoxy-4,3-dihydroisoquinoline

In a 50 ml flask equipped with a reflux condenser, 1-(4,3-dimethoxybenzyl)-7,6-dimethoxy-4,3-dihydroisoquinoline (compound 5) 0.011 mol (3.83 g) was added in the reaction vessel, then the reaction solvent, tetrahydrofuran, was poured into the reaction in the amount of 20 ml. Next, 0.033 mol (1.25 g) of sodium borohydride was added to the reaction vessel and then the reaction temperature was adjusted to the reflux temperature of tetrahydrofuran. After 1 day at the reflux temperature, according to the trace of the reaction on the TLC paper, the raw material, was almost finished, and after distilling the reaction solvent, the remaining sodium borohydrides were slowly neutralized with methanol. And then methanol was concentrated and added to the reaction of water and dichloromethane to remove mineral salts, the two phases of water and dichloromethane were separated. The formed amine product (compound 7) was concentrated in the dichloromethane phase and purified with a plate to separate a small amount of impurity. As a result, the experimental evidence and analysis results gave a stamp of approval on the structure of the synthesized unstable imine.

1-(3,4-dimethoxybenzyl)-6,7-dimethoxy-1,2,3,4-tetrahydroisoquinoline: ^{1}H NMR (300 MHz, $CDCl_3$): δ_H (ppm) 2.74-2.78 (2H t, *J* = 6 Hz), 2.91-3.00 (2H m), 3.12-3.25 (2H m), 3.40 (1H NH, s), 3.78-3.86 (12H OMe, s), 4.19-4.23 (1H m), 6.57-6.83 (5H Ar, m), **IR** (KBr) ν 3321 (NH Amine).

3.1.4. Synthesis of papaverine:

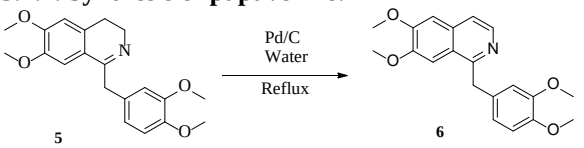

Scheme 3-6: Aromatization pathway of papaverine

In a 250 ml flask equipped with a reflux condenser, the aqueous solution obtained from the previous step (compound 5) containing 0.011 mol (3.75 g) of 1-(4,3-dimethoxybenzyl)-7,6 -dimethoxy-4,3 dihydroisoquinoline was added as phosphate salt in the reaction vessel. Then it was adjusted to pH=5 with potassium hydroxide solution. Then the reaction temperature increased to the reflux temperature. The

reaction was stirred for 48 hours under these conditions. After monitoring the reaction using TLC technique, the reaction was complete (Scheme 3-6). In this step, the reaction temperature decreased to the ambient temperature. Then its pH was adjusted to pH=8 with sodium hydroxide solution. In this condition, 50 ml of dichloromethane was added to the reaction mixture. After mixing and complete dissolution of the materials in the organic phase to separate Pd/C, the reaction solution was filtered. Then two organic and aqueous phases were separated and the organic phase containing papaverine product (compound 6) was concentrated. The amount of crude sediment was 3 grams with an efficiency of 82%.

Extracted papaverine: ^{1}H NMR (300 MHz, $CDCl_3$): δ_H (ppm) 3.78 (3H s), 3.83 (3H s), 3.92 (3H s), 4.01 (3H s), 4.55 (2H s), 6.75-6.84 (3H Ar, m), 7.06 (1H s), 7.36 (1H s), 7.44-7.46 (1H d, *J* = 6 Hz), 8.37-8.39 (1H d, *J* = 6 Hz), **^{13}C NMR** (75 MHz, CDCl3): δ_C (ppm) = 41.9, 55.8, 55.8, 55.8, 56.0, 104.2, 105.3, 111.0, 111.8, 118.86, 120.4, 122.9, 131.9, 133.6, 140.4, 147.5, 149.0, 149.9, 152.6, 157.6. **IR** (KBr) ν 1509.56 (C=N Ar).

Synthetic Papaverine: ^{1}H NMR (300 MHz, $CDCl_3$): δ_H (ppm) 3.78 (3H s), 3.82 (3H s), 3.91 (3H s), 4.00 (3H s), 4.56 (2H s), 6.74-6.85 (3H Ar, m), 7.05 (1H s), 7.36 (1H s), 7.44-7.46 (1H d, *J* = 6 Hz), 8.36-8.38 (1H d, *J* = 6 Hz), **^{13}C NMR** (75 MHz, CDCl3): δ_C (ppm) = 40.6, 55.8, 55.9, 56.0, 56.2, 104.3, 105.4, 111.1, 111.9, 119.4, 120.5, 122.7, 131.0, 134.3, 137.5, 147.7, 149.1, 150.5, 153.6, 156.7. **IR** (KBr) ν 1513.25 (C=N Ar), **MS** (m/z %): 338.2 (M^{-1}), 339.2 (M), 340.2 (M^{+1}).

4. Conclusion:

This article delved into the four-step synthesis of papaverine. As stated earlier, various methods have been documented for papaverine synthesis. Our primary goal in this study was to develop safer synthetic routes with higher yields, utilizing environmentally friendly solvents like water, making our approach more advantageous than previous methods. By employing these synthetic steps for papaverine production, we initiated the conversion of carboxylic acid into an ester, departing from the traditional path of transforming it into an acyl halide, which could introduce potential hazards during the synthesis. As a result, our proposed method ensures higher safety at this stage, achieving an impressive 99% conversion efficiency of the ester intermediate. In the subsequent step, the ester generated in the first stage undergoes nucleophilic attack by the amine, leading to the formation of an amide intermediate. The ensuing step involves ring formation using polyphosphoric acid, which boasts a relatively high yield. Finally, in the ultimate stage, dehydrogenation or aromatization is accomplished with a commendable yield in water solvent. The highlight of our study lies in this phase, specifically the use of a green and environmentally friendly solvent—water. Based on the aforementioned explanations, we can conclude that our study focused on obtaining papaverine through a cost-effective and safer approach. The proposed synthetic route presented in this article can serve as a suitable complementary and auxiliary method for papaverine synthesis, alongside the conventional extraction techniques used for this compound. By prioritizing safety and sustainability, our research contributes to the ongoing efforts in optimizing papaverine synthesis, paving the way for further exploration and utilization of this valuable compound in pharmaceutical applications.

5. References:

[1] Small LF, Lutz RE. Chemistry of the opium alkaloids: US Government Printing Office; 1932.

[2] Schiff PL. Opium and its alkaloids. American Journal of Pharmaceutical Education. 2002;66(2):188-96.

[3] Demirkapu MJ, Yananli HR. Opium Alkaloids. Bioactive Compounds in Nutraceutical and Functional Food for Good Human Health. 2020.

[4] Carlin MG, Dean JR, Ames JM. Opium alkaloids in harvested and thermally processed poppy seeds. Frontiers in Chemistry. 2020; 8:737.

[5] Guthrie DA. Studies on the synthesis of papaverine. 1952.

[6] Burger A. The benzylisoquinoline alkaloids. The Alkaloids: Chemistry and Physiology. 4: Elsevier; 1954. p. 29-75.

[7] Buck JS. 1, 2-Dihydropapaverine and modified syntheses of papaverine and papaveraldine (xanthaline). Journal of the American Chemical Society. 1930;52(9):3610-4.

[8] Han X, Lamshöft M, Grobe N, Ren X, Fist AJ, Kutchan TM, et al. The biosynthesis of papaverine proceeds via (S)-reticuline. Phytochemistry. 2010;71(11-12):1305-12.

[9] Yu W-S, Wu Z-N, Qiu Z-F, Zhao C-J, Zhang F-L, Yang Z-Z. One-Pot Synthesis of Papaverine Hydrochloride and Identification of Impurities. Russian Journal of Organic Chemistry. 2020;56(7):1295-9.

[10] Jamil OK, Cravens A, Payne JT, Kim CY, Smolke CD. Biosynthesis of tetrahydropapaverine and semisynthesis of papaverine in yeast. Proceedings of the National Academy of Sciences. 2022;119(33): e2205848119.

[11] Miller SA, Leadbeater NE. Direct, rapid, solvent-free conversion of unactivated esters to amides using lithium hydroxide as a catalyst. RSC advances. 2015;5(113):93248-51.

29TH IRANIAN ORGANIC CHEMISTRY CONFERENCE
1_3 NOV, 2023
UNIVERSITY OF QOM, IRAN

Mixed Metal Organic Frameworks as Adsorbents

Romina Roozbeh, Narjes Keramati and Mehdi Mousavi Kamazani*

Department of Nanotechnology, Faculty of New Sciences and Technologies, Semnan University, Semnan, Iran, rominaaa4988@gmail.com, narjeskeramati@semnan.ac.ir

Abstract - Water is polluted by many factors, among which industrial wastes are the most important. Adsorption is a mass transfer process that is an effective way to remove waste. The properties of adsorbents are quite specific and depend on their composition. Adsorbent compounds are mainly responsible for removing any specific pollutants from wastewater. Therefore, investigating the effect of different adsorbent properties on the absorption rate is vital. Absorption can be affected by the concentration of organic and inorganic compounds. The adsorption process is strongly influenced by the mixture of many compounds commonly present in water and wastewater. Factors affecting the adsorption process are surface area, nature and initial concentration of adsorbent, solution pH, temperature, interfering substances, and nature and concentration of adsorbent. MOFs are metal-organic frameworks that contain at least two different metal ions as their framework nodes. Although still in their infancy, several applications for multi metallic MOFs (MM-MOFs) are emerging that improve upon conventional monometallic MOFs. In the field of gas absorption and storage, especially the stability and affinity towards the target gases can be greatly improved by introducing the second metal ion.

1. Introduction

The water is one of the most important natural resources for the life and sustainability of the environment. Currently, the intensification of human activities and the rapid development of modern industry have led to water pollution with various organic pollutants, including hormones, pesticides, dyes, phenol, and personal and health care products, which represents an important environmental problem. Therefore, the development of purification technologies that enable the removal of these organic pollutants and guarantee the quality of purified water is of great importance. Various methods such as membrane separation, adsorption, Fenton oxidation, coagulation and photodegradation have been used for wastewater treatment. In the meantime, due to its efficiency, low cost and simplicity, adsorption using porous materials as adsorbents have been proposed as one of the methods to remove water pollution. Various porous solids such as zeolites, activated carbon, silica-based mesoporous materials and hydrotalcites have been evaluated. Organic pollutants are absorbed by these materials through various mechanisms, including hydrophobic interactions, electrostatic interactions, hydrogen bonding, acid-base interactions, or a combination of them[1].

Metal-organic frameworks (MOFs) are porous crystalline coordinated compounds based on the coordination of metal ions or clusters with organic bonds to form one, two or three dimensional networks. Due to the high porosity and surface area, suitable chemical functions, flexibility and adaptability, they have been investigated as adsorbents for the extraction of various pollutants. MOFs have already been used as precursors to obtain advanced porous carbons with uniform pores of different sizes and with new structures and properties. MOF-derived carbons exhibit high porosity and active sites, with the advantage of being more chemically stable than precursor [1, 2].

2. Results and discussion

Due to the large amount of metals, along with the possibility of their chemical functionalization and the introduction of more than one metal (MM-MOFs), organic linker, or a mixture of both, MOFs are becoming a family of nano porous materials that are growing rapidly. Because Cr3+ is relatively neutral but Fe3+ is highly reactive, researchers used the less reactive Fe0 to slow down the reaction rate. Later, the same group reported on another method to ensure high control of the metal ratio in MM-MOFs and obtain frameworks with the predicted architecture. They used the SBU method to obtain MIL-127 bimetallic materials. In the first step, neutral mixed acetate building blocks with the general formula FeIII 2 MIIO(H2O)2-[O2C-CH3]6 nH2O with M = Co, Ni or Mg were synthesized. In contrast, the direct synthesis method with the corresponding metal chloride salts was unsuccessful under the same reaction conditions and led to the creation of amorphous materials or crystallization of materials. Since environmentally friendly solvents were employed, the researchers demonstrated for the first time the preparation of mixed Fe/Ni, Fe/Co or Fe/Mg MOFs with space-time

efficiency. Often the one-step synthesis strategy leads to a more or less homogeneous dispersion of cations. But in this study, it was shown that depending on the synthesis method, when MOFs were synthesized, core heterostructures could be synthesized [2].

Different bimetallic structures of CoxMg1-x-MOF-74, x): zero, 0.12, 0.30, 0.57, 0.78, 1) were synthesized using the thermal dissolution method. The adsorption tendency to normal hexane and 1-hexane and the selection of 1-hexane over normal hexane were evaluated by static adsorption test along with computer simulation. The bimetallic structure of MOF-74 is almost the same structure crystalline but retain higher porosity than their monometallic counterparts. Both the adsorption capacity and selectivity of the bimetallic samples strongly depend on their metal compositions. In particular, Co0.30Mg0.70-MOF-74 shows the highest 1-hexane adsorption capacity (152.7 mg/g) and the highest 1-hexane/N-hexane selectivity with 9.74, which is more than It is monometallic[3].

The morphology of the synthesized MOF-74 samples was observed from SEM images (Figure 1). The samples show remarkably distinct crystal morphologies. In particular, it is shown that the MgMOF-74 crystal exhibits a petal-like morphology and the crystal size is 5–10 μm. Meanwhile, the Co-MOF-74 crystal has a spherical structure composed of rod crystal branches and its average size is about 8 μm. In CoxMg1-x-MOF-74 samples, their transformed morphology changes from a petal-like structure for Co0.12Mg0.88 MOF-74 to a hexagonal prism-like structure. In addition, these samples show an increase in crystal dimensions with Co/Mg ratio. In the case of the Co0.78Mg0.22-MOF-74 sample with a relatively high Co/Mg molar ratio (nCo/nMg = 3.5), the average particle size is approximately 13 μm[4].

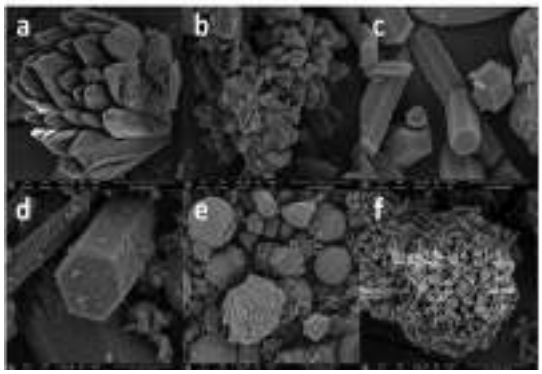

Fig.1.SEM images of synthesized MOF-74 samples. (a) Mg-MOF-74, (b) Co0.12Mg0.88-MOF-74, (c) Co0.30Mg0.70-MOF-74, (d) Co0.57Mg0.43-MOF-74, (e) Co0.78Mg0.22-MOF-74, (f) Co-MOF-74 [4]

The improved absorption in MM MOFs is probably due to the increased enthalpy of binding of H2 to unsaturated metal sites after exchange. The binding enthalpy increases due to the higher charge density of the metal ions, and the unsaturated metal sites strongly polarize H_2, which provides primary binding sites for H2 inside the Cu-BTC pores and subsequently enhances the gravimetric adsorption of the material. The synthetic strategy of MM-MOFs provides a way to improve the gravimetric storage capacity of known MOFs [5].

In another research, Mg-Ni-MOF-74 and Mg-Cd-MOF-74 were studied to gain insight into metal mixing. Calculations predict that metal mixing is energetically preferred in these materials. Mg-Ni-MOF-74 shows a much higher surface area in the presence of water than Mg-MOF-74. To investigate this effect, the adsorption of H2O in Mg-Ni-MOF-74 was studied and it was found that the adsorption energy and electronic structure do not change significantly in metal sites compared to Mg-MOF-74 and Ni-MOF-74, respectively. Therefore, the increased stability of Mg-Ni-MOF-74 is the result of a distortion of the M-O bond length in mixed metal MOF-74, which is consistent with recent work on the stability of MOF-74 exposed to water[6].

Another work conducted on mixed metal (MM-MOF-74) and then studied the effects of metal mixing and observed that adding less than 16 mol% of Ni to Mg-MOF-74 can dramatically increase the percentage of surface area retained after exposure to water compared to Mg-MOF-74. The first of these effects is the lattice constant mismatch and the potential to strain the metal oxide backbone by introducing heterometallic impurities due to the different sizes of the metal ions. Mg-MOF-74 and Ni-MOF-74 have very close lattice constants due to the comparable size of the metal ions, so the strain effects of mismatch are minimized in these mixed metal materials. In contrast, Mg-MOF-74 and Cd-MOF-74 have lattice constants that are significantly different, which allows comment on how this energy affects the mixing energy in Mg-Cd-MOF-74 materials compared to Mg-Ni MOF-74. The second effect is magnetic spin ordering for metal ions that contain unpaired electron spins. Since both Mg and Cd ions have no unpaired spins, spin order effects are absent in Mg-Cd-MOF-74 materials[7].

Various amounts of Co and Ni were substituted in the metal-organic framework Mg-MOF-74 through a one-step thermal dissolution reaction, and the effects of these substitutions on CO2 adsorption and water stability properties were investigated. Co and Ni are more favorably introduced from solution into the MOF-74 framework than Mg. Furthermore, the reaction temperature strongly affects the final metal composition in these MOF74 structures with mixed metal up to the composition of the reaction solvent. Adsorption isotherms show that the CO2 adsorption properties can be tuned by partial substitution of the metal.Mg-Ni-MM-MOF-74 shows a large increase in water stability[8].

A MOF prepared with two different metal nodes has been used for potential absorption chiller applications.

The nickel salt precursor was partially replaced during the synthesis with a relatively cheap zinc salt. Bimetallic MOF-74 containing only a fraction of Ni was shown to provide efficient H2O adsorption performance, while the use of cheaper zinc salts significantly reduced material costs for synthesis/industrial-scale applications[9].
MOF74 with different concentrations of Ni and Zn metal nodes in the framework were synthesized in order to understand the adsorption performance while trying to reduce costs (compared to pure Ni-MOF-74). These NixZn100-x materials show significant changes in H2O adsorption isotherms, which provide better performance and lower cost by using a small amount of nickel in Zn-MOF74. The physical properties show modified morphologies with different metal concentrations while maintaining the structural integrity of the crystalline MOF. Implementation of this mixed-metal strategy in MOFs can have significant effects on absorption, stability, and recyclability to enable the identification of feasible industrial materials for applications such as absorption cooling. Figure 2 shows the PXRD patterns for the synthesized materials where a unique MOF-74 crystalline phase was obtained for all materials[10].

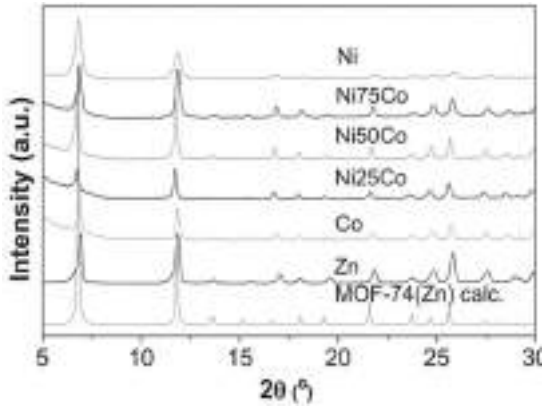

Fig.2. PXRD patterns of obtained materials [10]

3. Conclusions

MOFs are still in their infancy. Using a combination of advanced spectroscopic techniques, several materials have been proven beyond doubt to be true MM-MOFs, i.e., a coherent material with two or more metal ions as nodes. Characterization techniques can also clarify the distribution of metal centers, and in many cases it was found that metals are randomly distributed on the nodes. However, ions sometimes cluster in domains of the same metal nodes, and the presence of this associated disorder gives rise to new specific features of the framework. In the field of gas adsorption and gas storage, the most important advantage of MM-MOFs is to control the affinity of MOFs to a particular gas by adjusting the metal concentration. This can lead to greater stability (e.g. by making the material more hydrophobic or introducing more "noble" metals into the nodes) or to increased affinity.

4. References

[1] M. del Rio, Chem. Eng. J., 428 (2022) 131147.
[2] S. Abednatanzi, Chem. Soc. Rev., 48 (2019) 2535-2565.
[3] S.J. Alesaadi, F. Sabzi, Int. J. Hydrog. Energy, 40 (2015) 1651-1656.
[4] H. Sun, Microporous Mesoporous Mater., 284 (2019) 151-160.
[5] A.M.P. Peedikakkal, I.H. Aljundi, ACS omega, 5 (2020) 28493-28499.
[6] M. Kaykhaii, M. Sasani, and S. Marghzari, Chem. Mater. Eng, 6 (2018) 31-35.
[7] J.D. Howe, J. Phys. Chem. C, 121 (2017) 627-635.
[8] Y. Jiao, Ind. Eng. Chem. Res., 54 (2015) 12408-12414.
[9] J. Liu, Eur. J. Inorg. Chem., 7 (2018) 885-889.
[10] J.A. Villajos, Int. J. Hydrog. 40 (2015) 5346-5352.

29TH IRANIAN ORGANIC CHEMISTRY CONFERENCE
1_3 NOV, 2023
UNIVERSITY OF QOM, IRAN

Effect of Hydrogenation on mechanical properties of HTPB-based polyurethanes

Ali Chanaani, Yasin Kaykha*

Chemical Engineering Department, Imam Hossein University, Tehran, Iran, 110kanaani@ihu.ac.ir, ykaykha@ihu.ac.ir

Abstract

Hydroxyl-terminated polybutadiene double bonds (HTPB) are susceptible to modification processes, including hydrogenation, due to their high reactivity. Hydrogenation of HTPB strongly affects the microstructure and consequently, the mechanical properties of polyurethanes based on this prepolymer, so partial hydrogenation is a useful tool to adjust the mechanical properties of HTPB-based polyurethanes. In this article, an attempt has been made to comprehensively explain the effect of HTPB hydrogenation on the mechanical properties of polyurethanes based on this prepolymer. The results show that the hydrogenation of HTPB generally increases the tensile strength, initial modulus, and hardness of polyurethanes based on this prepolymer and slightly reduces the elongation.

1. Introduction

Polyurethanes based on Hydroxyl-terminated polybutadiene (HTPB) are used in many industries as coatings, adhesives, sealants, etc [1, 2]. Polyurethanes based on HTPB have found widespread use as a binder in composite solid propellants owing to their excellent combination of rheological, and mechanical properties and their very high solids loading (approximately 90%) in composite formulation [3, 4]. Mechanical properties are one of the most important properties of polyurethanes and especially composite propellants. Hydrogenation is a common method to modify and improve the mechanical properties of HTPB-based polyurethanes. Hydrogenation describes the reduction of double bonds or other reactive groups [5]. This process is usually performed by dissolving the unsaturated compounds in an organic solvent, generally toluene or cyclohexane, then hydrogen gas enters the reactor at the desired temperature and pressure [6, 7]. In this way, a wide range of mechanical properties can be accessed in a controlled manner through the hydrogenation process [8]. In fact, the hydrogenation of unsaturated bonds is a method to improve the aging properties and thermal stability of HTPB, as well as to preserve more of its elastomeric properties [9, 10]. In the following sections, firstly, the effect of hydrogenation on the cross-linking density of HTPB-based polyurethanes, which is the most important factor affecting the mechanical properties, is Been investigated, and then the effect of this process on the mechanical properties of HTPB-based polyurethanes is investigated.

2. Effect of hydrogenation on the crosslinks density

crosslinks density is the most important feature of the polyurethane network, which is directly related to the curing, and mechanical properties of the final product, so its investigation is very necessary [11]. To investigate the effect of hydrogenation of HTPB on cross-linking density, HHTPB is added to HTPB in different proportions and then cured. crosslinks density increases steadily with increasing HHTPB content. Theoretically, since HTPB and HHTPB have almost the same functionality distributions and close solubility parameters, the networks are expected to have similar crosslink density values. However, As shown in Table 1, wide variations in cross-linking density values are observed, which may be due to the resistance of HHTPB to swelling in the solvent. Also, crystalline regions in HHTPB may act as cross-linkers. Sol content represents the fraction of the polymer that is not part of the cross-linking network. Sol content remains constant in all samples regardless of HHTPB fraction. Sastri's [12] study about the effect of functionality distribution on the crosslinks density shows that part of HTPB chains is without functionality. Since hydrogenation does not change the functionality distribution, it is easy to imagine that the sol content originates from non-functionalized HTPB and HHTPB moieties that are unable to participate in network formation [8].

Table. 1. Effect of HHTPB fraction on network properties of copolyurethanes

HHTPB Content (%)	Sol Content (%)	Swell Ratio	CLD (mol/M^3)
0	9	7.8	60
5	9	6.0	92
10	11	5.6	97
20	9	4.9	118
25	10	4.6	119
100	8	1.9	300

3. Effect of hydrogenation on mechanical properties

Hydrogenation of HTPB strongly affects the microstructure and consequently, the mechanical properties of polyurethane systems based on this prepolymer. To investigate the effect of HTPB hydrogenation on the mechanical properties of polyurethanes, Hydrogenated Hydroxyl-terminated (HHTPB) is added to HTPB in different proportions and then cured. The addition of HHTPB to HTPB generally increases the tensile strength, modulus, and stiffness and decreases the elongation values. As shown in Fig 1, adding 5% HHTPB to the system causes a strong increase in the modulus and hardness and a slight decrease in the elongation values. After that, the addition of 20% HHTPB results in relatively smaller changes in mechanical properties, but the addition of 25% HHTPB causes significant increases in modulus and hardness. The tensile strength increases linearly with the increase of HHTPB.

The above observation can be justified by the fact that HHTPB chains are significantly stiffer compared to HTPB chains because the activation energy for rotation of the sp^3-sp^3 single bond is about 3 (kcal/mol) higher than that of the sp^3-sp^2 single bond. Therefore, HHTPB chains are likely to be stiffer than HTPB chains. For this reason, it is possible to have crystals in HHTPB. These crystals may act as a solid filler that is chemically bonded to the polyurethane network. Therefore, the stiffness of the chains together with the formation of the crystal causes the strength of the networks and increases the modulus. It is interesting to note that the glass transition temperature increases slightly with the increase of HHTPB content, which is evidence of the increase in stiffness in these systems with the increase of HHTPB content. The sharp increase in modulus in the region of more than 20% is probably due to phase separation. Also, elongation shows fewer changes than other properties because the functionality distribution of HTPB and HHTPB is almost the same, and functionality distribution is the most important parameter that affects elongation [8]. Considering that NCO/OH ratio also strongly affects the mechanical properties. Therefore, by changing the amount of hydrogenation and NCO/OH ratio, systems with different mechanical properties can be produced according to needs. In other words, by adjusting the NCO/OH ratio, polyurethane systems with the same elongation and different tensile strength can be obtained, and vice versa [13]. It should be mentioned that the mechanical properties of solid propellants with different ratios of HHTPB show that the tensile strength and modulus increase with the increase of HHTPB content in the copolyurethane binder. However, elongation and hardness are less affected. It is clear that the HHTPB prepolymer leads to stiffer grains [8].

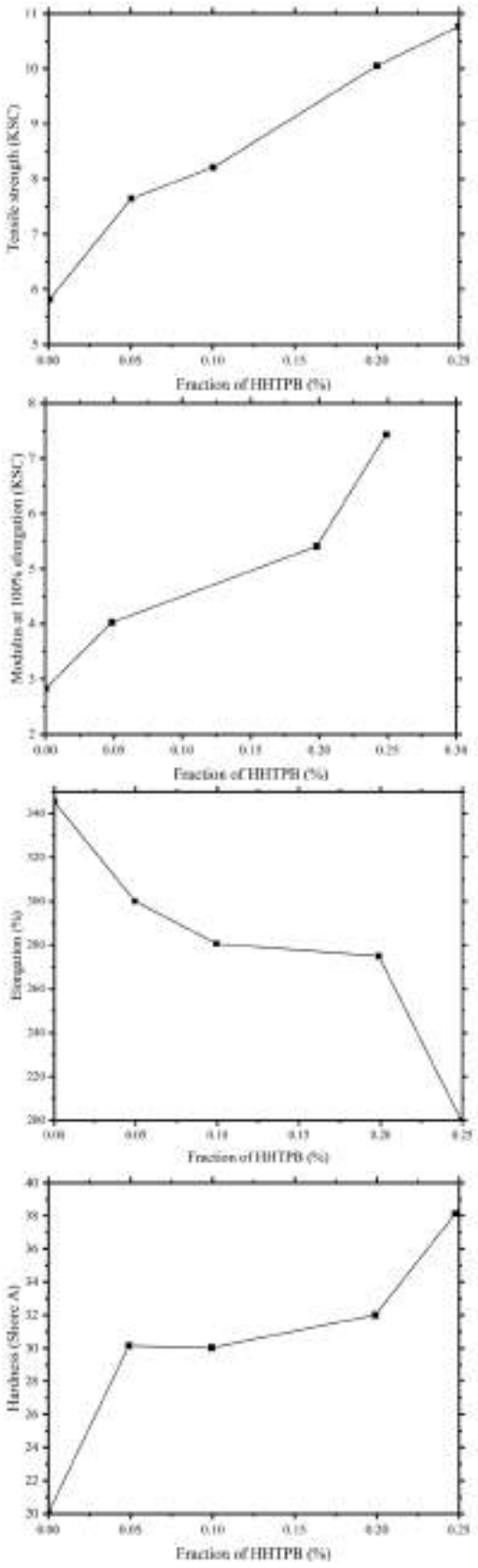

Fig.1. Effect of HHTPB fraction on mechanical properties of copolyurethane

The results of Cyclic Instron tests on two segmented polyurethane samples (one sample with HTPB and the other sample with HHTPB) are shown in Fig 2, that in both samples, First, the stress levels after each series of strain increases are lower than the previous maximum, and second, at strain levels higher than those previously reached, the stress levels are apparently unaffected by pre-straining. In other words, it can be concluded that partial hydrogenation does not affect the elastic recovery of HHTPB-based polyurethanes [14]. The only significant difference is that HHTPB-based polyurethanes show less stress, which is a characteristic behavior of phase-separated materials, and for which there are various interpretations, including disruption of the polymer structure and of the reinforcing mechanism, chain slippage, and chain breakage [15].

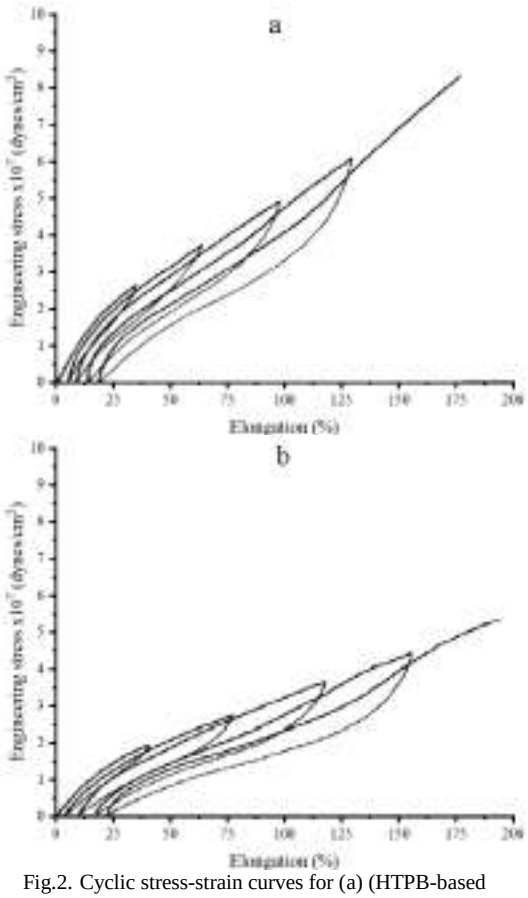

Fig.2. Cyclic stress-strain curves for (a) (HTPB-based polyurethanes); and (b) (HHTPB-based polyurethanes)

4. Conclusions

This study shows that hydrogenation of HTPB significantly affects the mechanical properties of HTPB-based polyurethane networks. In general, hydrogenation increases the tensile strength, initial modulus, and hardness and slightly decreases the elongation. Hydrogenated HTPB chains are stiffer than HTPB chains. By adjusting the NCO/OH ratio, polyurethane systems with the same elongation and different tensile strength can be obtained, and vice versa.

5. References

[1] J. C. Thomas and E. L. Petersen, "HTPB Heat of Formation: Literature Survey, Group Additive Estimations, and Theoretical Effects," *AIAA Journal*, vol. 60, no. 3, pp. 1269-1282, 2022.

[2] D. M. French, "Functionally terminated butadiene polymers," *Rubber Chemistry and Technology*, vol. 42, no. 1, pp. 71-109, 1969.

[3] C. Lira, L. Nicolini, M. Dolinsky, C. Oliveira, and A. Gomes, "Determination of the Hydrogenation Degree of Telechelic Polybutadiene by 1H NMR," *Ann. Magn. Reson*, vol. 5, p. 22, 2006.

[4] J. C. Quagliano Amado, P. G. Ross, L. Mattos Silva Murakami, and J. C. Narciso Dutra, "Properties of Hydroxyl-Terminal Polybutadiene (HTPB) and Its Use as a Liner and Binder for Composite Propellants: A Review of Recent Advances," *Propellants, Explosives, Pyrotechnics*, vol. 47, no. 5, p. e202100283, 2022.

[5] J. C. Uther, "Partly hydrogenated and functionalized polybutadiene rubber," Staats-und Universitätsbibliothek Hamburg Carl von Ossietzky, 2018.

[6] S. Sabata and J. Hetflejs, "Hydrogenation of low molar mass OH-telechelic polybutadienes catalyzed by homogeneous Ziegler nickel catalysts," *Journal of applied polymer science*, vol. 85, no. 6, pp. 1185-1193, 2002.

[7] M. Menossi, A. Ciolino, L. M. Quinzani, M. S. Zabaloy, and J. M. Milanesio, "Hydrogenation of polybutadiene at high pressure," *Industrial & Engineering Chemistry Research*, vol. 61, no. 1, pp. 236-248, 2021.

[8] V. Sekkar, V. Krishnamurthy, and S. Jain, "Mechanical and Swelling Properties of Copolyurethanes based on Hydroxy-Terminated Polybutadiene and its hydrogenated analog," *Propellants, explosives, pyrotechnics*, vol. 22, no. 5, pp. 289-295, 1997.

[9] P. S. Gopala Krishnan, K. Ayyaswamy, and S. Nayak, "Hydroxy terminated polybutadiene: Chemical modifications and applications," *Journal of Macromolecular Science, Part A*, vol. 50, no. 1, pp. 128-138, 2013.

[10] J.-P. Dilcher, H. Jürgens, and G. A. Luinstra, "Sequential post-modifications of polybutadiene for industrial applications," *Multi-component and sequential reactions in polymer synthesis*, pp. 163-201, 2015.

[11] V. Sekkar, A. S. Alex, V. Kumar, and G. Bandyopadhyay, "Theoretical evaluation of crosslink density of chain extended polyurethane networks based on hydroxyl terminated polybutadiene and butanediol and comparison with experimental data," *Journal of Energetic Materials*, vol. 36, no. 1, pp. 38-47, 2018.

[12] K. Sastri, M. R. Rao, and M. Singh, "Modelling the effect of functionality distribution on the crosslinking characteristics of hydroxy-terminated polybutadiene liquid prepolymers," *Polymer*, vol. 35, no. 21, pp. 4555-4561, 1994.

[13] R. Manjari, V. Joseph, L. Pandureng, and T. Sriram, "Structure-property relationship of HTPB-based propellants. I. Effect of hydroxyl value of HTPB resin," *Journal of applied polymer science*, vol. 48, no. 2, pp. 271-278, 1993.

[14] C. Brunette, S. Hsu, W. MacKnight, and N. S. Schneider, "Structural and mechanical properties of polybutadiene-containing polyurethanes," *Polymer Engineering & Science*, vol. 21, no. 3, pp. 163-171, 1981.

[15] G. Estes, S. Cooper, and A. Tobolsky, "Block polymers and related heterophase elastomers," *Journal of Macromolecular Science—Reviews in Macromolecular Chemistry*, vol. 4, no. 2, pp. 313-366, 1970.

29TH IRANIAN ORGANIC CHEMISTRY CONFERENCE
1_3 NOV, 2023
UNIVERSITY OF QOM, IRAN

Meglumine sulfate as an effective catalyst for the preparation of some indeno[1,2-b]indole-9,10-dione derivatives

*Azam Moazeni Bistgani, Leila Moradi**

Department of Organic Chemistry, Faculty of Chemistry, University of Kashan, 87317-51167, Kashan, Iran.
moazeniazam1999@gmail.com, l_moradi@kashanu.ac.ir

Abstract - In this work, in line with the development of green chemistry, meglumine sulfate was synthesized and identified through the Fourier transform infrared (FT-IR) and elemental analysis (CHNS). Meglumine sulfate was used as a homogeneous catalyst in the green and fast synthesis of Indeno[1,2-b]Indole-9,10-dione. A wide variety of Indeno[1,2-b]Indole-9,10-dione compounds were successfully synthesized through the catalytic process. The use of meglumine sulfate in the synthesis of these compounds showed several advantages, including excellent yields, low cost, short reaction time, and ease of purification of the products.

1. Introduction

Green chemistry is an important science in chemistry and an efficient tool for pollution prevention[1]. In organic reactions, the choice of inappropriate solvent leads to poisoning and pollution. Water is a natural solvent, available, neutral, cheap, mild, and environmentally friendly. These properties make it a suitable green solvent for organic reactions[2].

One of the most important synthetic processes in modern chemistry is multicomponent reactions. Multicomponent reactions are cost-effective, environmentally friendly, and a suitable alternative to sequential syntheses[3].

Indenoindoles are heterocyclic frameworks that contain a collection of 6-5-5-6 membered rings[4]. These compounds have many biological and medicinal properties. Indenoindoles are effective in diseases such as nervous disorders, breast cancer, and viral infections. Also, these compounds are potassium channel openers, protein kinase inhibitors, powerful lipid peroxidation, etc[5].

Following the development of green chemistry, efforts to replace expensive and environmentally harmful catalysts with cheap, safe, and environmentally friendly catalysts have increased. Meglumine is a derivative of sugar alcohol in which an OH group has been replaced by an $NHCH_3$ group[6]. Meglumine has amazing properties such as being cheap, stable against moisture and air, low toxicity, biodegradable, non-corrosive, available, etc. It has two hydroxyl groups and one amino group, thus it activates electrophilic and nucleophilic parts by donating electron pairs and establishing hydrogen bonds[7]. In this research, we chose a simple, convenient, and efficient method for the preparation of Indeno[1,2-b]Indole-9,10-diones in water solvent and thermal conditions (Scheme 1).

2. Experimental

2.1 Preparation of meglumine sulfate: 1 g of meglumine was poured into a 50 ml flask and 20 ml of dry chloroform was added to it and the mixture was stirred at a temperature of 75°C by a magnetic stirrer. Then, 0.6 ml chlorosulfonic acid was added drop by drop for one hour and mixed for 5 hours. Finally, the solution was filtered and washed 3 times with ethanol and dried at 90 °C in an oven for 5 hours. The results of the elemental analysis confirm the sulfation of meglumine: (C: 24%, H: 5.3%, N: 4.3%, S: 17%) (Scheme 2).

2.2. Synthesis of indeno[1,2-b]indole-9,10-diones: In a test tube, 1 mmol of aromatic amine, 1 mmol of dimedone or 1,3-cyclohexanedione, and 0.009 g of meglumine sulfate were mixed in 4 mL of water at 75 °C to produce the intermediate 1. After that, 1 mmol of ninhydrin was added. The progvess of the reaction was monitored by TLC, and after the completion of the reaction, the solid product was filtered, washed with water, and purified by recrystallization from ethanol.

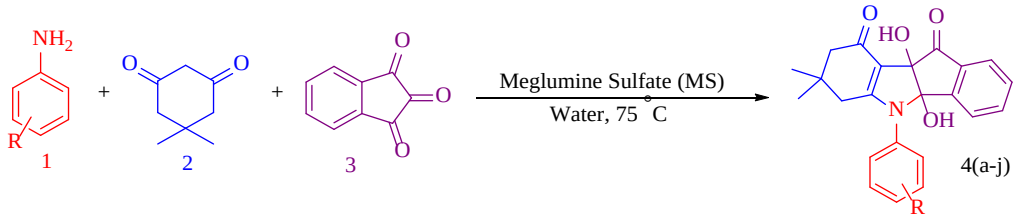

Scheme 1. preparation of indeno[1,2-b]indole-9,10-diones using Meglumine sulfate

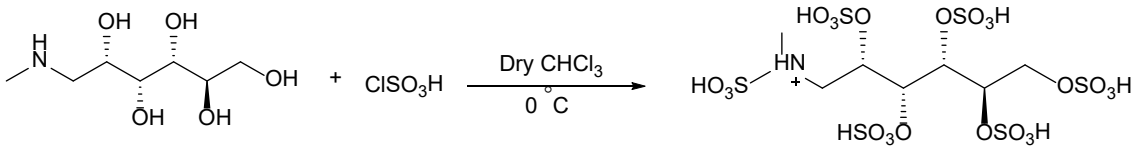

Scheme 2. Synthesis of meglumine sulfate (MS).

3. Results and discussion

3.1. Structural characterization of meglumine sulfate:

Meglumine sulfate catalyst was synthesized according to the method described in the experimental part and was analyzed by Fourier transform infrared (FT-IR) and elemental analysis (CHNS) in order to prove its structure.

By examining the infrared spectra of meglumine, the characteristic absorptions related to OH and NH groups can be identified. These absorptions can be seen in the region of 3100 cm^{-1} to 3400 cm^{-1}. After the sulfonation the absorptions related to the sulfonic acid group, can be well observed in the spectrum of meglumine sulfate. The broadening in absorption in the region of 3364 cm^{-1} indicates the presence of acidic OH. The sharp and intense absorption observed at 1256 cm^{-1} is related to the S=O group and also the absorption at 649 cm^{-1} can be attributed to S-O (Figure 1).

3.2. Synthesis of indeno[1,2-b]indole-9,10-diones derivatives in the presence of meglumine sulfate:

In this research, in order to find the optimal conditions for the reaction, such as temperature, type of solvent, amount of catalyst, investigations have been carried out. Based on optimum conditions, Indeno[1,2-b]Indole-9,10-dione derivatives were synthesized in the presence of 0.03 g of meglumine sulfate at a temperature of 75 ℃ in water solvent (Table 1). All derivatives were synthesized without no by-products and with high yield. Investigations show that aromatic amines with electron-donating groups have higher yields than aromatic amines with electron-withdrawing groups.

3.2. Proposed mechanism: In the first step, the catalyst plays a major role in the condensation of dimedone and aromatic amine by activating dimedone in order to produce an enaminone intermediate through Knoevenagel condensation.

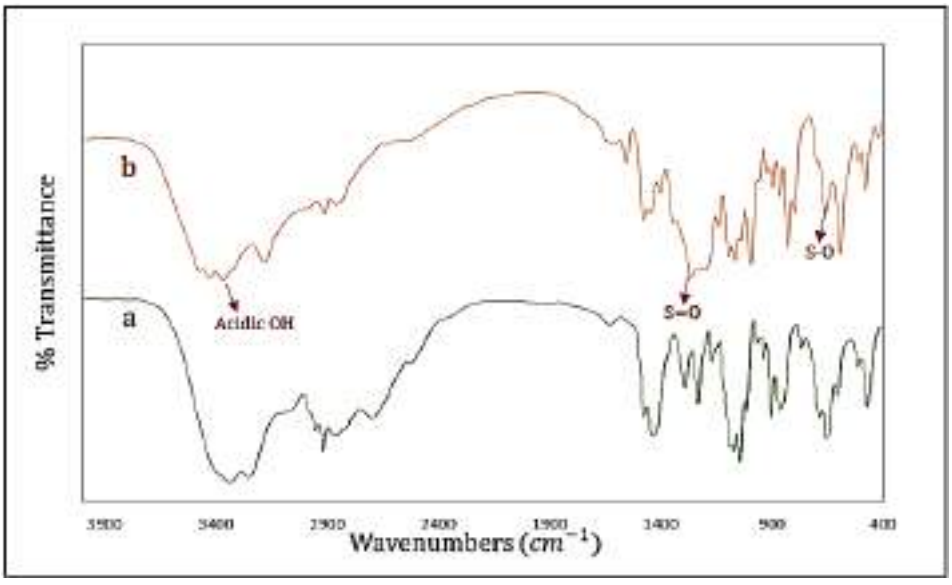

Figure 1. FT-IR of meglumine (a) and meglumine sulfate (b).

Table 1. Synthesis of indeno[1,2-b]indole-9,10-diones catalyzed by meglumine sulfate.

Entry	Product	R	R	Time (mine)	Yield (%)
1	4a	CH_3	3-Cl	75	89
2	4b	CH_3	4-Cl	85	86
3	4c	H	3-CH_3	70	94
4	4d	CH_3	4-NO_2	90	86

5	4e	CH_3	2-Cl	80	86
6	4f	H	2-Cl	80	85
7	4g	CH_3	4-Br	70	91
8	4h	CH_3	3-NO_2	85	88
9	4i	CH_3	3-Cl-4-F	80	85
10	4j	H	3-Cl-4-F	80	84

Reaction conditions: ninhydrin (1 mmol), dimedone (1 mmol), aniline (1 mmol), meglumine sulfate (0.03 gr).

In continuation, the reaction of enaminone and ninhydrin produces intermediate II. Finally, the desired product was synthesized through intramolecular electrophilic cyclization (Scheme 3).

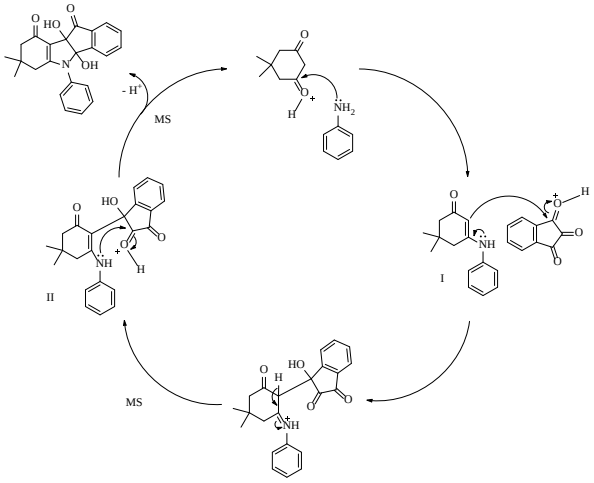

Scheme 3. Reaction mechanism for the preparation of indeno[1,2-b]indole-9,10-diones using meglumine sulfate.

4. Conclusion

In this work, meglumine sulfate was synthesized and identified through Fourier transform infrared (FT-IR) and elemental analysis (CHNS). Methods and used as a homogeneous catalyst in the one-pot multicomponent synthesis of indeno-indoles. A variety of indeno-indole compounds were successfully synthesized through the catalytic process. The use of meglumine sulfate in the synthesis of indeno indoles showed several advantages, including excellent yield, low cost, mild reaction conditions, short synthesis time, and ease of purification of the products.

5. References

[1] P. Anastas, N. Eghbali, Chem. Soc. Rev. 39 (2010) 301-312.

[2] K. Shanab, C. Neudorfer, E. Schirmer, H. Spreitzer, Curr. Org. Chem. 17 (2013) 1179-1187.

[3] T. Zarganes-Tzitzikas, A. L. Chandgude, Chem. Rec. 15 (2015) 981–996.

[4] C. Bal, Biochem. Pharmacol. 68 (2004) 1911–1922.

[5] M. Zare, L. Moradi, Polycycl. Aromat. Compd. 42 (2022) 6647–6661.

[6] D. L. Cassimiro, C. A. Ribeiro, M. S. Crespi, M. V. Capela, J. Therm. Anal. Calorim. 105 (2011) 405–410.

[7] R. Y. Guo, ACS Comb. Sci. 15 (2013) 557–563.

Adsorptive Removal of Organic Reactive Dye from Aqueous Solution using Activated Carbons Prepared from Apricot Seed Shell

Shaya Mahmoudian[1,2]*

[1]*Department of Textile Engineering, Kashan Branch, Islamic Azad University, Kashan, Iran*
[2]*Machine-made Carpet Research Centre, Kashan Branch, Islamic Azad University, Kashan, Iran*
shmahmoudian2@gmail.com

Abstract - Organic dyes, a type of high toxic and carcinogenic chemicals that present severe threats to human and aquatic life, are the most commonly seen organic pollutants in wastewater of industries such as textile, rubber, cosmetic industry etc. Adsorption has proven to be a facile and promising approach for the removal of organic dyes in wastewater. In this study, activated carbon from apricot seed shell was prepared by chemical activation with $ZnCl_2$ and its capacity to remove anionic reactive dye; reactive blue 19, from aqueous solution was reported. The effectiveness of apricot seed shell activated carbon to remove reactive blue 19 was examined at different initial dye concentrations, adsorbent dosage and pH. Results reveal that the equilibrium was attained within 60 min having 1 g/L adsorbent at pH of 4 and initial dye concentration of 40 ppm and the maximum equilibrium capacity was observed 132.8 mg/g. It can be concluded that the apricot seed shell as a low coast agricultural waste can have a great potential for textile waste water treatment.

1. Introduction

The rapid industrialization has significantly transformed our life. However, the unsustainable development also caused severe environmental problems. Various industries, such as rubber, textile, cosmetics leather, gasoline, pharmaceutical, and food, have employed numerous kinds of dyes in the production of various goods. The remediation of wastewater polluted by organic dyes is an important environmental goal. It is estimated that the annual consumption of dyes and pigment is about 7×10^5 tons worldwide, among which approximately 100 tons/year is discharged into wastewater. Consequently, a considerable amount of colored effluent from these industries is discharged into natural environment. Dye molecules consist of chromophores and auxochromes, which are the two key components. Their existence in the hydrosphere presents a serious threat to both human and aquatic life [1-3].

There are a number of useful technologies to eliminate these organic dyes from wastewater such as coagulation, chemical oxidation, membrane separation, solvent extraction, photo catalytic degradation and adsorption, etc., Although the development of wastewater treatment technology is rapidly advanced, 'it is still of changes in the discovery of more cost-effective and highly efficient technologies for the removal of dyes at commercial scale. Various techniques have their advantages and disadvantages in the eradication of contaminants [4]. Among these technologies, adsorption is an attractive option for the removal of dyes due to its low cost, environmental friendly nature, scaling up, and the possibility of using a countless number of potential adsorbents. During the recent decades, numerous adsorbents have been synthesized and modified for the adsorption of organic dyes [5, 6].

Agricultural and food-canning industry wastes, such as various fruit kernels have a wide application in the capacity of adsorbents for inorganic and organic compounds. Granular activated carbon has great importance as adsorbents in the wastewater treatment. Activated carbons are universal adsorbents for the removal of organic and inorganic pollutants from wastewater and drinking water. Carbon sorbents are usually obtained from the natural precursors of organic origin such as bituminous coals, brown coals, wood, cellulose, peat, fruit stones, and peels in the processes of physical or chemical activation [7, 8].

Apricot, Prunus armeniaca L., is a member of the Rosaceae plant family which is widely cultivated in Iran. It has been noted that the world production of apricots made up over 4 mln tons, with over 300 thousand tons being produced in Iran. Many years ago these by-products were used as a fuel in rural areas but now the preparation of activated carbon is considerably encouraged [9, 10]. Apricot seed shell is a cheap precursor for activated carbon source. Therefore, it is important to evaluate its performance as adsorbent. The adsorption of gold ions from industrial wastewater and removal of Ni(II) ions from aqueous solution using activated carbon derived from apricot shells has been studied by several authors. The application of activated carbon in the adsorption process is mainly depends on

the surface chemistry and pore structure of porous carbons [3, 11-13].
This study deals with the adsorption ability of apricot seed shell activated carbon (AAC) for the removal of reactive blue 19 (RB19) from synthetic aqueous solutions. The influences of the operating parameters such as initial dye concentration, pH and adsorbent dosage was explored.

2. Experimental

2.1. Materials: Activated carbon from apricot stone shell. The commercial textile dye, reactive blue 19, was obtained from a textile company and was used without additional purification. Table 1 shows the chemical structure of reactive blue 19. All chemicals used in this study were of analytical-laboratory grade, being purchased from Merck.

2.2. Preparation of activated carbon:
Local apricot seed, a by-product of food processing, were collected and washed in distilled water two times prior to separating the peels. The apricot shells were crushed and ground in a laboratory. In the first step of activation, the starting material was mixed with ZnCl2 at the $ZnCl_2$/starting material weight ratio of 1:1 and the mixture was kneaded with adding distilled water. The mixture was then dried at 110 ◦C to prepare the impregnated sample. In the second step, the impregnated sample was placed on a quartz dish, which was then inserted in a quartz tube. The impregnated sample was heated up to activation temperature (500 ◦C) under N_2 flow at the rate of 10 ◦C min^{-1} and hold at the activation temperature for 1 h. After activation, the sample was cooled down under N^2 flow and 0.5N HCl was added on to activated sample. Activated sample was washed sequentially several times with hot distilled water to remove residual chemical until it did not give chloride reaction with $AgNO_3$. The washed sample was dried at 110 ◦C to prepare activated carbon.

2.3. Adsorption studies
The batch equilibrium experiment was typically carried out to investigate the adsorption behavior. In each adsorption experiment, an amount of the adsorbent was added into the dye solution (50 mL) at the different concentrations (5–100 mg L^{-1}). The solution was stirred at room temperature to obtain a uniform adsorbent dispersion with the different dosages (0.5–2 g L^{-1}). The desired dye solutions pH (2-12) were achieved through adjustment with 0.1 M of HCl and 0.1 M of NaOH. The solutions and solid phase were separated by centrifugation at 7000 rpm for 5 min in a Sigma 3-30k centrifuge. The dye concentration was determined on a double beam UV-Vis spectrophotometer by measuring absorbance at a maximum absorbance wavelength (λ_{max}). Each set of experiments was performed three times.

Table 1. Physicochemical characteristics of reactive blue 19.

Characteristics	Value
Molecular structure	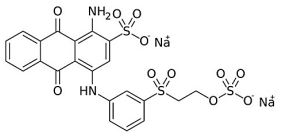
C.I.generic name	C.I. reactive blue 19
Synonym	Remazol brilliant R
Production	DyStar, Germany
Molecular formula	$C_{22}H_{16}N_2Na_2O_{11}S_3$
Molecular weight	626.5 g/mol
λ_{max}	592 nm

The dye adsorption capacity at equilibrium, q_t (mg/g), was calculated using the following equation:

$$q_t = \frac{(C_0 - C_t)V}{M} \quad (1)$$

Where C_0 and C_t (mg L^{-1}) were the dye concentrations at the initial and equilibrium conditions, respectively. V (L) was the dye solution volume and M (g) was the mass of the adsorbent used.

3. Results

3.1 Effect of initial dye concentration on adsorption
The Effect of different dye concentrations on the adsorption is illustrated in Fig.1. With raising the initial RB19 concentration from 5 to 100 mg/L, the amount of RB19 adsorbed increases from 14.2 to 132.8 mg/g. This may be attributed to an increase of the driving force due to the concentration gradient with increasing the dye anion concentration in order to overcome the mass transfer resistance of ions between the aqueous and solid phases. Therefore, a higher initial dye concentration increase the adsorption capacity. In addition, increase of initial dye concentration increases the number of collisions between dye anions and adsorbent, which enhances the sorption process.
The results also shows that removal percentage decreased as the dye concentration increased. The decline in the uptake percentage of dyes is due to the excessive number of pollutants that exceeded the number of available adsorption sites. The AAC showed the best uptake capacity for removing RB19 at concentrations of 40 ppm.

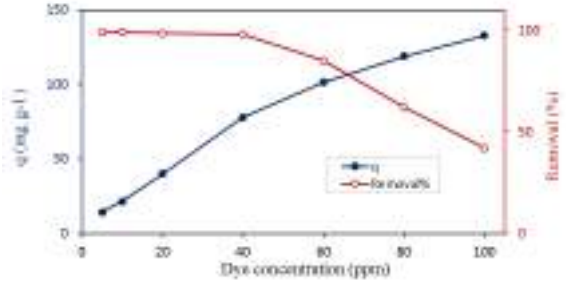

Fig. 1. Effect of initial RB19 concentration on dye adsorption capacities and removal efficiencies**.**

3.3. Effect of adsorbent dose

Adsorption of dye is strongly influenced by the quantity of the adsorbent. Adsorption of RB19 onto AAC was investigated by changing the amount of adsorbent from 0.1– 2 g/L at a constant stirring rate for 60 min using a dye concentration of 10 and 40 mg/L. It was observed from Fig. 2 that with increasing AAC concentration, adsorption of RB19 was enhanced up to an optimum quantity of adsorbent. The highest removal percentage for the solutions with 10 and 40 ppm of dye concentration was attained when the dosage of AAC was 1 and 1.5 g/L alternatively. Increased adsorbent concentration implies a greater surface area of adsorbent and, consequently, a greater availability of the binding sites on the surface area. Additional increase of the amount of adsorbent did not furthermore enhance adsorption that remained constant

3.4. Effect of pH

The pH of the solution plays an important role in the adsorption process and particularly on the uptake capacity. The pH of the solution influences the surface charge of the adsorbent and the ionization of the adsorbate. Fig. 3 shows the effect of pH in the range of 2–12 on the adsorption of RB19 onto AAC. It could be observed that a maximum adsorption uptake of 99 percent was achieved at pH4. RB19 is negatively charged. The attraction forces between an aqueous solution with low pH (high value of H+ charge) and the negatively charge RB19 dye is high, causing the adsorption efciency to increase. Two mechanisms in the process of adsorption is: π-π interaction between the basal planes of the AAC and aromatic rings of the dyes. Also the hydrogen bonds between oxygen and the amino groups of RB19, oxygen, and the hydroxyl groups of the adsorbent. The condition with the lowest point of the surface charge of the adsorbent (pH 4) allows the ionization and protonation of the adsorbent's functional groups to reach their maximum rate, contributing to the highest adsorption uptake of RB19. At higher pH, the competition between RB19 and excess OH- ions obstructed the adsorption process, but a decrease in the anion concentration with decreasing pH favored the reaction.

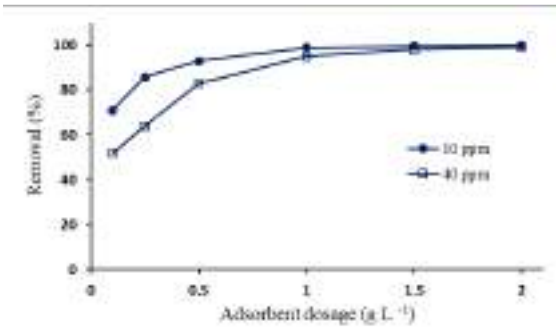

Figure 2. Effect of adsorbent dose on the removal of RB19 by AAC

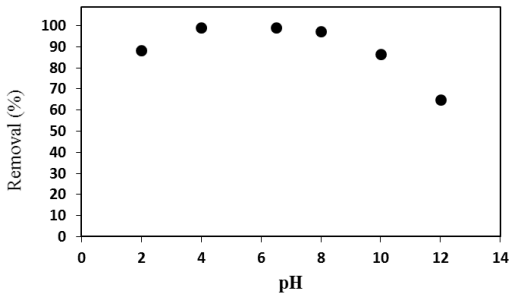

Fig. 3. Effect of pH on removal of RB19 by AAC

References

[1] M. F. Hanafi and N. Sapawe, "A review on the water problem associate with organic pollutants derived from phenol, methyl orange, and remazol brilliant blue dyes," *Materials Today: Proceedings*, 31, A141-A150, 2020.

[2] M. Ismail, K. Akhtar, M. Khan, T. Kamal, M. A. Khan, A. M Asiri, J. Seo, and S. B. Khan, "Pollution, toxicity and carcinogenicity of organic dyes and their catalytic bio-remediation," *Current pharmaceutical design*, 25, 3645-3663, 2019.

[3] A. Hashem, C. O. Aniagor, O. M. Morsy, A. Abou-Okeil, and A. Aly, "Apricot seed shell: an agro-waste biosorbent for acid blue193 dye adsorption," *Biomass Conversion and Biorefinery*, 1-14, 2022.

[4] R. D. Saini, "Textile organic dyes: polluting effects and elimination methods from textile waste water," *Int J Chem Eng Res*, vol. 9, pp. 121-136, 2017.

[5] D. Lan, H. Zhu, J. Zhang, S. Li, Q. Chen, C. Wang, T. Wu, and M. Xu, "Adsorptive removal of organic dyes via porous materials for wastewater treatment in recent decades: A review on species, mechanisms and perspectives," *Chemosphere*, 293, 133464, 2022.

[6] F. J. Alguacil and F. A. Lopez, "Adsorption processes in the removal of organic dyes from wastewaters: very recent developments," *Promising techniques for wastewater treatment and water quality assessment. Intechopen*,. 17-32, 2021.

[7] N. U. M. Nizam, M. M. Hanafiah, E. Mahmoudi, A. A. Halim, and A. W. Mohammad, "The removal of anionic and cationic dyes from an aqueous solution using biomass-based activated carbon," *Scientific Reports*, 11, 8623, 2021.

[8] S. Husien, R. M. El-taweel, A. I. Salim, I. S. Fahim, L. A. Said, and A. G. Radwan, "Review of activated carbon adsorbent material for textile dyes removal: Preparation, and modelling," *Current Research in Green and Sustainable Chemistry*,. 5, 100325, 2022.

[9] J. Cañellas, A. Femenia, C. Rosselló, and L. Soler, "Chemical composition of the shell of apricot seeds," *Journal of the Science of Food and Agriculture*, 59, 269-271, 1992.

[10] V. Halysh, J. M. Romero-García, A. M. Vidal, T. Kulik, B. Palianytsia, M. García, and E. Castro, "Apricot Seed Shells and Walnut Shells as Unconventional Sugars and Lignin Sources," *Molecules*,. 28, 1455, 2023.

[11] O. L. Norboevna, H. T. Narzulloevich, and H. R. Rustamjonovich, "Obtaining activated carbon from the shells of apricot and peach seeds," *International journal on orange technologies*, 2, 33-36, 2020.

[12] I. Shaikhiev, K. Shaykhieva, S. Sverguzova, E. Fomina, Y. Vinogradenko, R. Fediuk, M. Amran, A. P. Svintsov, A. R. G. d. Azevedo, and M. Gunasekaran, "Removing Pollutants from Sewage Waters with Ground Apricot Kernel Shell Material," *Materials*, 15, 3428, 2022.

[13] M. Abbas, S. Kaddour, and M. Trari, "Kinetic and equilibrium studies of cobalt adsorption on apricot stone activated carbon," *Journal of Industrial and Engineering Chemistry*, l. 20, 745-751, 2014.

29TH IRANIAN ORGANIC CHEMISTRY CONFERENCE
1_3 NOV, 2023
UNIVERSITY OF QOM, IRAN

Copolymerization of biodiesel with acrylic acid to remove crude oil pollution from aqueous media

*Mohammad Sadegh Aghili and Hassan Zali boieni**

Department of Chemistry, Faculty of Chemistry, University of Isfahan, Esfahan, Iran,
aghili.sadegh@yahoo.com, h.zali@chem.ui.ac.ir

Abstract - One of the biggest challenges for humanity is water pollution from factors such as crude oil spills, heavy metals, and cooking oil waste, which endangers the health of humans. By removing pollutants from aqueous media, it is possible to have beneficial effects on the health of humans and living organisms. In this research, first, cooking oils were converted into biodiesel by transesterification method, and then copolymerization with acrylic acid monomers and unsaturated biodiesel was synthesized in order to absorb crude oil from the aqueous media. Emulsion copolymerization of biodiesel with acrylic acid was set for 30 minutes at 80 °C at 3 factors with 4 levels in 16 steps. Then factors such as monomer ratio, solution electrolyte, and amount of radical initiator were investigated. Optimizing the synthesis of B-CO-AA adsorbent by the Taguchi method revealed that with a 2:1 ratio of acrylic acid to biodiesel and 1.36 M NaCl solution, the radical initiator amount of 3% by weight is the optimal value for the desired copolymer synthesis. According to the results of the Taguchi method, the first effective factor is the monomer ratio, the second is the soluble electrolyte, and the third is the amount of radical initiator.

1. Introduction

The issue of water pollution has been considered since the establishment of the International Maritime Organization (IMO) and with the rapid increase in sea pollution due to the leakage of crude oil from ships, etc. into the waters. Some of these hydrocarbons in crude oil cause changes in the food chain of aquatic animals and, as a result, humans. [1] Among other factors that pollute the environment, we can mention cooking oil waste, which is produced in a significant amount in the world, and one of the ways to control this pollution is to convert it into biodiesel. Biodiesel is very important due to its high biodegradability and renewable nature. [2-4] The most common process for converting WCO to biodiesel is the transesterification process because this process can produce biodiesel of good quality. [5-6] Replacing fossil fuel-based monomers with renewable monomers such as unsaturated biodiesel is one of the desirable options for producing sustainable polymers. Polymers based on fatty acids are biodegradable, environmentally friendly, and non-toxic. [7] Free radicals polymerization reactions usually start with the thermal decomposition of peroxides. Oxygen strongly affects the polymerization of free radicals and can quench the initiators [8] Therefore, oxygen can be removed by blowing nitrogen gas. [9] One of the things done was the functionalization of methyl oleate monomer for polymerization. In this research, the addition of bromine and acrylate to the double bond of methyl oleate was done in one step. [10] In the first step, the homo polymerization reaction was performed, and a low-quality product and low yield when used. In the next step, this monomer was copolymerized with vinyl acetate by the bulk polymerization method, and the product was in the form of a very viscous liquid. [11] Recently, one-step synthesis of a new vinyl monomer, (acryloyl amino) ethyl soyate, via the direct transesterification reaction of soybean oil-derived biodiesel with N-(hydroxyethyl) acrylamide was reported. [12-13] Solvent-free radical polymerization seems to be a simple method to prepare various biopolymers from FA, but most of the solvents that are suitable for FA-based monomers and their derived polymers are toxic solvents. In addition, the purification of FA-based polymers is usually done with methanol or hexane, both of which are environmentally unfriendly solvents. [14-16] It is very difficult to polymerize very poorly water-soluble monomers, such as FA-based monomers, through the conventional emulsion process because water-soluble monomers are required. These observations are related to the low solubility of AMO in water, which reduces the nucleation of particles and, as a result, greatly reduces the total number of radicals. This problem was overcome by using higher initiator concentrations but resulted in lower molecular weight copolymers being induced [17]. Another group investigated the effect of electrolytes such as NaCl and its effect on the reaction behavior of polymerization. Several researchers observed the positive effect of the presence of electrolytes on emulsion stabilization. [18-19] Taguchi's method is one of the most powerful methods to improve products and reduce costs. [20] The cause of this research is the design and synthesis of B-CO-AA absorbent using the free radical emulsion

copolymerization process based on unsaturated biodiesel monomers and acrylic acid with cross-links.

2. Experimental

2.1. Synthesis of biodiesel: 100 ml of feed along with 450 ml of methanol into a 1-liter flask, then add 2 ml of 98% sulfuric acid and 0.5 g of para-toluene sulfonic acid and heat for 7 hours at a temperature of 90 degrees Celsius under Reflux conditions were established. After washing and separating, the obtained biodiesel was dried with MgSO4.

2.2. Synthesis of B-CO-AA adsorbent: 150 mg of SDS, 7.5 ml of 1 M salt water solution, and 1 g of biodiesel were combined and heated on a heater stirrer. Then 50 mg of K2S2O8 was added to it, and after complete mixing, 2 g of acid was added. Acrylic was added to it. The product was obtained after 30 minutes.

2.3. Optimization of the synthesis of B-CO-AA adsorbent: experimental design by Taguchi method: To optimize the Taguchi method for minimizing other errors, oleic acid was used as the starting material for biodiesel synthesis. Based on the conducted studies and screening tests, factors such as the weight ratio of monomers, the amount of reaction initiator, and the presence of electrolyte species in the reaction environment are efficacious for the final product. Other factors such as pressure, temperature, type and amount of emulsifier, type of initiator, and pH of the environment can also be an effect, which was not investigated in this research. This study aims to synthesize B-CO-AA adsorbent based on unsaturated biodiesel with acrylic acid; the higher the weight of the product, the better. For optimization, four levels were considered for each effect factor. After entering the factors and levels into the software according to Table 1, an array of 16 was obtained for testing. Finally, after conducting the tests, the results were analyzed by Qualitek-4 software to find the optimal parameters and the importance of each factor.

Table 1: Table 1. Effect factors in the synthesis of B-CO-AA adsorbent and the levels of each of them

Entry	Factors	Abbreviation symbol	Level			
			1	2	3	4
1	The ratio of acrylic acid to biodiesel	A	1:1	2:3	1:2	2:5
2	Molarity of NaCl (solvent electrolyte)	B	0.68	1.36	2.04	2.37
3	The weight ratio of reaction initiator to monomer weight (%)	C	1.5	3	4.5	6

3. Result and Discussion

To confirm the synthesis of B-CO-AA adsorbent, the following analysis was performed

3.1. Identification of B-CO-AA adsorbent using FT-IR: As seen in the IR spectrum (Fig. 1), a broad peak is observed in the range of 3000-3500 cm+, which indicates the OH of acrylic acid

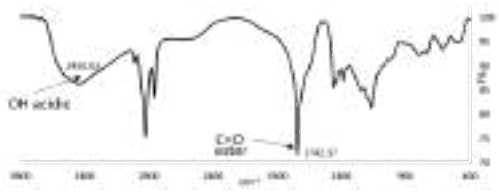

Figure 1: IR spectrum of B-CO-AA absorber synthesized methyl oleate with acrylic acid

3.2. Thermogravimetric Analysis (TGA): The TGA analysis of the synthesized B-CO-AA adsorbent can be seen in Fig. 2, starting from the initial mass of the sample in the device. The horizontal flow of the graph indicates that the substance is pure and does not contain impurities or moisture. From the temperature of 210 °C to the temperature of 293.93 °C, 35.187% of the original sample was destroyed, which was found to be related to small molecules (dimers and trimers) and the weight loss in the temperature range of 293.15 to 4.503 °C the amount of 34.55% of the original sample was destroyed, which is related to the decomposition of long polymer chain molecules.

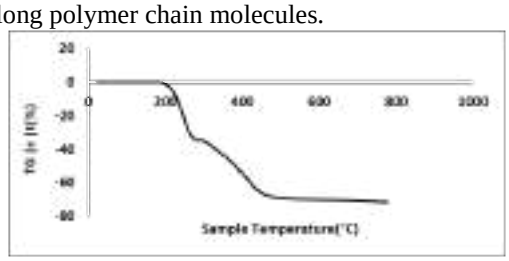

Figure 2: TGA analysis

3.3. Identification of the structure of linseed oil biodiesel using 13C-NMR analysis: In the 13C-NMR spectrum of the above compound, the peaks appearing at 128.01, 128.15, 129.83, and 130.08 ppm are in the C=C groups. (Fig. 3)

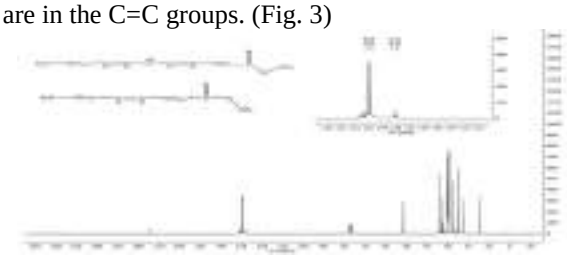

Figure 3: The 13C-NMR spectrum of biodiesel prepared from linseed oil in CDCl3 solvent

3.4. Optimization of B-CO-AA adsorbent synthesis: The final results are as follows (Table 2):

1- The DOF column shows the degree of freedom of each factor.

2- The %P column shows the influence of each factor.

3- In the error column, random errors and other factors that have not been checked include the amount of surfactant, temperature, pressure, etc.

Table 2: Final results obtained from Qualitek-4 software and other parameters

Factor	DOF (f)	Variance (V)	F - Ratio (F)	Percent (%)
1 A	3	6.636	25.06	70.443
2 B	3	2.101	71.274	22.094
3 C	3	0.581	19.734	5.89
Other Errors	6	0.029	-	1.573
Total	15	-	-	100

3.5. Predicting product weight at the optimal point: According to the different levels of each factor, it was found that factor A at level 3, factor B at level 2 and factor C at level 2 are optimal conditions, so the prediction of the product weight at the optimal point is 1.296 grams. According to the optimal points obtained, B-CO-AA adsorbent was synthesized using different biodiesels and after washing and drying, the results are shown in Table 3.

Table 3: Synthesis of B-CO-AA adsorbent from different sources of biodiesel

Biodiesel feed	Iodine value	Weight of B-CO-AA adsorbent (g)
waste cooking oil	100-130	1.255
linseed	170-204	1.302
oleic acid	90	1.245

Based on the obtained results, the highest weight of the synthesized adsorbent is related to the use of linseed oil biodiesel, which can be predicted according to the iodine value of any type of oil that can be used in the preparation of biodiesel.

3.6. The absorption rate of crude oil by B-CO-AA adsorbent: Considering that there is no method to measure the amount of crude oil absorption by B-CO-AA adsorbent, the gravimetric method before (W1) and after absorption (W2) was used (Table 4).

Table 4: Crude oil absorption by B-CO-AA adsorbent

W_1 (g)	W_2 (g)	Absorbed amount (g)	Relative percentage (%)
0.5	0.839	0.339	67.8

5. Conclusion

In this research, B-CO-AA adsorbent was synthesized and its ability to remove crude oil from the water surface was investigated. By examining the obtained results, we can conclude:

1. The synthesized adsorbent B-CO-AA can be used to remove oil pollutants on the surface of the seas and the pH of the environment.
2. Due to its lower density than seawater, after absorbing the crude oil, it can float on the surface of the water and be easily removed from the water.
3. Due to the use of renewable resources and the use of environmental pollutants such as WCO, these absorbents can be a suitable option to prevent the wastage of natural resources.

4. References

[1] Maddikeri, G. L., Pandit, A. B., & Gogate, P. R. (2012). Intensification approaches for biodiesel synthesis from waste cooking oil: a review. Industrial & Engineering Chemistry Research, 51(45), 14610-14628.

[2] Patil, P. D., Gude, V. G., & Deng, S. (2009). Biodiesel production from Jatropha curcas, waste cooking, and Camelina sativa oils. Industrial & Engineering Chemistry Research, 48(24), 10850-10856.

[3] Stiefel, S., & Dassori, G. (2009). Simulation of biodiesel production through transesterification of vegetable oils. Industrial & Engineering Chemistry Research, 48(3), 1068-1071

[4] Math, M. C., Kumar, S. P., & Chetty, S. V. (2010). Technologies for biodiesel production from used cooking oil—a review. Energy Sustain Dev 14 (4): 339–345.

[5] Lotero, E., Liu, Y., Lopez, D. E., Suwannakarn, K., Bruce, D. A., & Goodwin, J. G. (2005). Synthesis of biodiesel via acid catalysis. Industrial & engineering chemistry research, 44(14), 5353-5363.

[6] Akoh, C. C., Chang, S. W., Lee, G. C., & Shaw, J. F. (2007). Enzymatic approach to biodiesel production. Journal of agricultural and food chemistry, 55(22), 8995-9005.

[7] Liu, S., Chua, L., Shamsabadi, A. A., Corcoran, P., Patra, A., Grady, M. C., ... & Rappe, A. M. (2021). Oxygen-Initiated Free-Radical Polymerization of Alkyl Acrylates at High Temperatures. Macromolecules, 54(17), 7925-7930.

[8] Eren, T., & Kusefoglu, S. H. (2005). Synthesis and polymerization of the acrylamide derivatives of fatty compounds. Journal of applied polymer science, 97(6), 2264-2272.

[9] Roberge, S., & Dubé, M. A. (2016). Infrared process monitoring of conjugated linoleic acid/styrene/butyl acrylate bulk and emulsion terpolymerization. Journal of Applied Polymer Science, 133(26).

[10] Tarnavchyk, I., Popadyuk, A., Popadyuk, N., & Voronov, A. (2015). Synthesis and free radical copolymerization of a vinyl monomer from soybean oil. ACS Sustainable Chemistry & Engineering, 3(7), 1618-1622.

[11] Eren, T., & Küsefoğlu, S. H. (2004). Synthesis and characterization of copolymers of bromoacrylated methyl oleate. Journal of applied polymer science, 94(6), 2475-2488.

[12] O'Shaughnessy, B., & Yu, J. (1994). Autoacceleration in free radical polymerization. 1. Conversion. Macromolecules, 27(18), 5067-5078.

[13] Tarnavchyk, I., Popadyuk, A., Popadyuk, N., & Voronov, A. (2015). Synthesis and free radical copolymerization of a vinyl monomer from soybean oil. ACS Sustainable Chemistry & Engineering, 3(7), 1618-1622.

[14] Eren, T., & Kusefoglu, S. H. (2005). Synthesis and polymerization of the acrylamide derivatives of fatty compounds. Journal of applied polymer science, 97(6), 2264-2272.

[15] Kohut, A., Voronov, S., Demchuk, Z., Kirianchuk, V., Kingsley, K., Shevchuk, O., ... & Voronov, A. (2020). Non-Conventional Features of Plant Oil-Based Acrylic Monomers in Emulsion Polymerization. Molecules, 25(13), 2990.

[16] Yamak, H. B. (2013). Emulsion polymerization: effects of polymerization variables on the properties of vinyl acetate based emulsion polymers. In Polymer science. IntechOpen.

[17] Bunker, S. P., & Wool, R. P. (2002). Synthesis and characterization of monomers and polymers for adhesives from methyl oleate. Journal of Polymer Science Part A: Polymer Chemistry, 40(4), 451-458.

[18] Jensen, A. T., de Oliveira, A. C. C., Gonçalves, S. B., Gambetta, R., & Machado, F. (2016). Evaluation of the emulsion copolymerization of vinyl pivalate and methacrylated methyl oleate. Journal of Applied Polymer Science, 133(45).

[19] Sharma, T., & Sangwai, J. S. (2015). Effects of electrolytes on the stability and dynamic rheological properties of an oil-in-water pickering emulsion stabilized by a nanoparticle–surfactant–polymer system. Industrial & Engineering Chemistry Research, 54(21), 5842-5852.

[20] Karna, S. K., & Sahai, R. (2012). An overview on Taguchi method. International journal of engineering and mathematical sciences, 1(1), 1-7.

29TH IRANIAN ORGANIC CHEMISTRY CONFERENCE
1_3 NOV, 2023
UNIVERSITY OF QOM, IRAN

INVESTIGATING THE KINETICS OF REMOVAL WASTEWATER CONTAINING ANILINE IN THE FENTON REACTION THROUGH CHEMICAL OXYGEN DEMAND

Mohsen Sargordan fard Arani, Mehdi Ghavidel*

Department of Chemistry, Faculty of Science, Yadgar-e-Imam Khomeini (RAH) Shahre Rey Branch, Islamic Azad University, Tehran, Iran, mohsenfardarani@gmail.com

Abstract
Industrial wastewater treatment with low concentration of pollutants is possible only in the presence of high activity hydroxyl radicals. The Fenton reaction allows the formation of hydroxyl radicals in high turbidity wastewater. Hydrogen peroxide reacts with two radical hydroxyl mechanisms and molecular oxygen with contaminants. Due to the relative contribution of each mechanism, the amount of hydrogen peroxide consumed is determined. In response to aniline, the optimal amount of hydrogen peroxide consumed is half the amount of stoichiometry obtained, indicating the contribution of the radical response to aniline degradation. The increase in the level of hydrogen peroxide and iron sulfate prevents the recombination of hydroxyl radicals and thus the efficiency of the reaction increases. Also, in this study, the optimal ratio of iron sulfate to hydrogen peroxide was obtained and the reaction speed and reaction equation were extracted without measuring the changes in the concentration of contaminants over time with using Chemical Oxygen Demand(COD) method.
Keywords: Advanced Oxidation, Fenton Process, Radical Hydroxyl, Aniline, COD

Introduction

Nowadays, several biological decomposition processes such as aerobic, anoxic and anaerobic processes can be used individually or in combination to treat wastewater with biodegradable pollution. Heat-resistant organic compounds, due to their toxicity, have serious effects on the health of all living species in nature. After being transferred from industrial environments to urban environments, hazardous organic compounds enter the food chain through infiltration of underground water and cause various complications such as mutations in different genes and carcinogenesis Aniline is one of the toxic pollutants found in wastewater, which is mainly the result of chemical processes of paint, rubber industry, pesticide production and pharmaceutical sectors. This chemical substance is classified as hazardous and carcinogenic waste. It is impossible to purify water contaminated with aniline using chemical oxidation methods, even with high costs. Due to the low percentage of the pollutant in the mixture, the oxidation and decomposition reaction of the pollutant can only be done in the presence of strong and highly active oxidants.

Advanced oxidation processes (AOPs) are a suitable alternative for the decomposition of hazardous organic materials. These processes are based on the production and use of hydroxyl and oxygen radicals, which are very strong oxidants with very high activity [1]. The division of these processes is based on the method and mechanism of radical production. Hydroxyl radical production is done as a result of reaction with inorganic salts or in the presence of ultraviolet light, which are known as Fenton and Photofenton reactions. The Fenton process is one of the advanced oxidation processes, which is known as an alternative for the decomposition of resistant and toxic organic compounds. The Fenton process has been widely used in the decomposition of stable organic compounds in water [2]. In transparent solutions without suspended solid particles, the photofenton process is used [3]. If there are suspended solid particles in the system or if the pollutants absorb ultraviolet rays, the scattering of radiation is greatly increased and the efficiency of radical formation is greatly reduced.

In such a situation, using the reaction of mineral salts with hydrogen peroxide in an acidic environment will be a suitable and economical solution. Aniline decomposition methods include Fenton technology (dark Fenton, electro-Fenton, Photo-Fenton process and photo-electro-Fenton) [4].

The Fenton reaction mechanism includes the formation of hydroxyl free radicals, which has E° = 2.8 V. As a result of the reaction of hydrogen

peroxide with iron ion, hydroxyl radical is produced which can convert almost all the carbons of the organic compound into harmless compounds such as CO2 and H2O through oxidation and mineralization [10] Walling et al. and [5]. However, its use is limited due to the production of an excessive amount of iron hydroxide sludge, which requires a separation and disposal process [6].

In short, it can be said that the key reagents of Fenton's method include hydrogen peroxide and iron salts. Fenton's process is usually more effective in acidic environment and pH=2-4, which is determined by conducting experiments [7]. At higher pH, iron salt is precipitated as iron hydroxide and loses its catalytic properties. The reaction of iron (II) with hydrogen peroxide is carried out spontaneously in the absence of light. As a result of this reaction, iron (II) is oxidized to iron (III) and hydroxyl radical is formed [8].

$$Fe^{2+} + H_2O_2 \longrightarrow Fe^{3+} + OH^- + HO^{\bullet} \quad (1)$$

In addition to reaction (1), other reactions are also carried out in the Fenton process, which are described as reactions (2) to (6):

$$Fe^{3+} + H_2O_2 \longrightarrow Fe^{2+} + HO_2^{\bullet} + H^+ \quad (2)$$

$$Fe^{2+} + HO^{\bullet} \longrightarrow OH^- + Fe^{3+} \quad (3)$$

$$H_2O_2 + HO^{\bullet} \longrightarrow HO_2^{\bullet} + H_2O \quad (4)$$

$$Fe^{2+} + HO_2^{\bullet} + H^+ \longrightarrow Fe^{3+} + H_2O_2 \quad (5)$$

$$Fe^{3+} + HO_2^{\bullet} \longrightarrow Fe^{2+} + O_2 + H^+ \quad (6)$$

The above reactions show that iron is a catalyst. The rate of reduction of iron (III) is much slower than the rate of oxidation of iron (II), as a result, iron ions in the solution are mainly in the form of (III) ions. By using the Fenton process, organic pollutants are converted into water and carbon dioxide, as well as mineral ions, and the mineralization process is completed. At the same time, there are a large number of chemical compounds that prevent the Fenton process or resist further oxidation until reaching water and carbon dioxide. Performing the Fenton process in the presence of these compounds causes their incomplete oxidation, reduces their toxicity and makes them more susceptible to biological degradation [9].

in 2006, the reaction rate equations were calculated based on changes in the concentration of hydrogen peroxide, iron and aniline, in such a way that the concentration of one of the parameters was changed and the other parameters were considered constant, and the speed equation obtained for each parameter was included in the general equation. have put [1]. In this research, we optimized the amount of hydrogen peroxide and iron sulfate and obtained the kinetics of the reaction without measuring the changes in the concentration of the pollutant with respect to the changes of time and through the change of the initial

concentration of the pollutant and in a certain period of time and also by using the amount of COD (Chemical Oxygen Demand).

Experimental

Pour 100 cc of the solution into Erlenmeyer flask and set its pH to about 2-3 using concentrated sulfuric acid and pH meter paper and put it on a magnetic stirrer and add 0.180 mmol of iron sulfate and then 14.71 mmol of hydrogen. We added peroxide (30% of the stoichiometric value) to the sample in three steps with an interval of 10 minutes and allowed the corresponding reaction to take place in 60 minutes and then adjusted the pH of the solution to 7 (neutral) using sodium hydroxide and pH meter paper. After smoothing the sample, we observed the amount of COD by spectrophotometer.

Results and discussion

According to the test method, we repeated the test for iron sulfate values from 0.189 to 0.360 mmol and hydrogen peroxide from 32% to 61% stoichiometry COD results in mg/liter are given in figure 1 observed the amount of COD by spectrophotometer

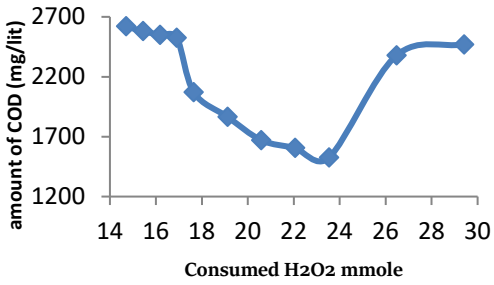

Fig1- The diagram of COD changes of different sample concentrations based on hydrogen peroxide

Based on the obtained results, the optimal amount of hydrogen peroxide consumed is equal to 50% of the stoichiometric value and equal to 23.53 mmol (figure 1).in order to investigate the kinetics and obtain the reaction rate equation, considering the constant time (60 minutes), samples of different concentrations of wastewater containing aniline (to a volume of 100 cc, 80, 60, 40 and 20% of The effluent containing

aniline with distilled water) was subjected to the Fenton reaction. The results are given in figure 2.

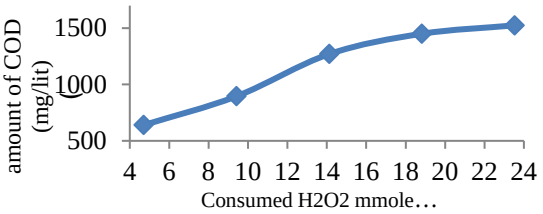

fig 2: The amount of cod changes of different sample concentrations based on hydrogen peroxide concentrations

Now, according to the above data and the calculation of COD of different concentrations of the sample as well as equation (7) (assuming complete mixing reactors), we completed Table ١ and obtained the reaction rate equation (r) and the rate constant value (K).

$$-r_A = \frac{COD_{A_0} - COD_{A_f}}{T} \quad (7)$$

Table1- Calculations related to reaction speed based on COD

$-r_A(\frac{mg}{min})$	Time(min)	$COD_{A_f}(\frac{mg}{lit})$	$COD_{A_0}(\frac{mg}{lit})$	Amount of aniline in the effluent	row
385.83	60	1525	24675	4.38	1
304.83	60	1450	19740	3.50	2
225.58	60	1270	14805	2.63	3
149.58	60	895	9870	1.75	4
71.58	60	640	4935	0.88	5

To calculate the constant value of K and obtain the kinetics of the reaction using the above data and relations (8) and (9) (assuming complete mixing reactors), Table 2 is obtained.

$$-r_A = K\ COD^{n} \quad (8)$$

$$Ln(-r_A) = \ln k + n \ln COD \quad (9)$$

Table2: COD reaction rate calculation

$\ln COD_{A_f}(\frac{mg}{lit})$	$\ln(-r_A)$	$COD_{A_f}(\frac{mg}{lit})$	$-r_A(\frac{mg}{min})$	row
7.33	5.95	1525	385.83	1
7.28	5.72	1450	304.83	2
7.15	5.42	1270	225.58	3
6.80	5	895	149.58	4
6.46	4.27	640	71.58	5

Now using Table ٢ and equation (9) where $\ln(-r_C) \rightarrow Y \quad \ln K \rightarrow \alpha \quad n \rightarrow \beta \quad \ln COD \rightarrow X$ are considered, from Through linear regression (according to diagram 3) and putting the relevant numbers in equation (8), the kinetics of the reaction is obtained as equation (10).

$$-r_A = 0.00072\ COD^{1.79} \quad (10)$$

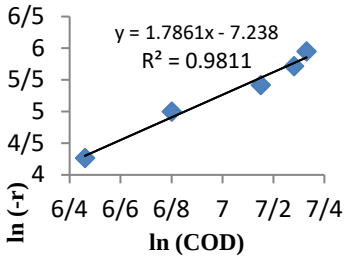

Fig 3- Linear regression of reaction speed based on COD

$$-r_A = \frac{C_{A_0} - C_{A_f}}{T} \quad (11)$$

The obtained rate equation is in mg/min, as a result, we convert it to mol/lit unit and get the rate equation based on mol/min, then Table ٣ using equation (11) (assuming complete mixing reactors) is completed where $\mathbf{C_{A0}}$ is the initial aniline concentration, $\mathbf{C_{Af}}$ is the final aniline concentration, **T** is the required reaction time and r_A is the reaction speed.

Table 3: Reaction rate calculators in terms of concentration of moles per litre

$-r_A(\frac{mol}{min})$	Time (min)	$C_{A_f}(\frac{mol}{lit})$	$C_{A_0}(\frac{mol}{lit})$	m mole aniline	row
0.0041	۶۰	0.016	0.26	4.38	1
0.0032	۶۰	0.015	0.21	3.50	2
0.0023	۶۰	0.013	0.15	2.63	3
0.0017	۶۰	0.0096	0.11	1.75	4
0.00072	۶۰	0.0096	0.05	0.88	5

To calculate the constant value of K and obtain the kinetics of the reaction based on the concentration, using the above data and relations (12) and (13) (assuming complete mixing reactors), Table 4 is obtained

$$-r_A = K\ C^{n} \quad (12)$$

$$Ln(-r_A) = Ln\ K + n\ Ln\ C \quad (13)$$

Table 4: Calculations of logarithm of reaction rate and concentration

$-\ln(C_{A_f})$	$-\ln(-r_A)$	$C_{A_f}(\frac{mol}{lit})$	$-r_A(\frac{mol}{min})$	row
4.13	4.49	0.016	0.0041	1
4.19	5.74	0.015	0.0032	2
4.34	6.07	0.013	0.0023	3
4.64	6.37	0.0096	0.0017	4
4.97	7.23	0.0069	0.00072	5

As a result, based on previous calculations and fig 4, the kinetic equation was obtained based on mol/min and in the form of equation (14) (assuming complete mixing reactors and based on the amount of hydrogen peroxide and iron sulfate optimized).

$$-r_A = 9.91\ C^{1.9} \qquad (14)$$

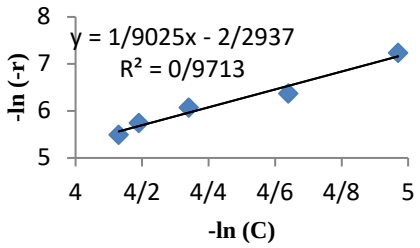

Fig 4- Linear regression of reaction speed based on concentration

Conclusion

By using Fenton's method, the amount of chemically required oxygen in wastewater containing aniline was reduced by 23,000 units, which shows a 94% decrease. The half-life of hydroxyl radicals is low, and if they do not react with the pollutant immediately after their formation, there is a possibility of their recombination or inactivation as a result of hitting the reactor wall, therefore, a stepwise increase of hydrogen peroxide and iron sulfate was used to speed up production and consumption. Hydroxyl radicals are controlled and the reaction efficiency is increased. Also, due to the exothermic nature of the Fenton reaction, the multi-stage increase of hydrogen peroxide and iron sulfate prevents the decomposition of hydrogen peroxide as a result of increasing temperature. In this research, the pollutant removal kinetics has been investigated without measuring the concentration of the pollutant with respect to time changes and through the value of COD and assuming a complete mixing reactor. Also, the concentration of hydrogen peroxide and iron sulfate consumed has been optimized and with a specific ratio in The kinetics of the reaction have been investigated, as a result, the kinetics of the reaction was calculated and the degree of reaction equal to 1.9 (based on concentration) was obtained

References

[1] J. Anotai, M.C.Lu, P.Chewpreecha, .Elzevier Ltd , 40(9) (2006) 1841-1847.

[2] M. Hajian, S. A. Mirbagheri, A.H. Javid, Desalination and Water Treatment, 109 (2018) 132–138.

[3] P. Simon, IWA Publishing. (2004).

[4] E.Brillas, Casado, J. Applied Catalysis B: Environmental, 16(1998) 31–42.

[5] W.H. Glaze, J.W. Kang, R.H. Chapin, Ozone Science and Engineering. 9(1987) 335-352.

[6] P.H. Chang, Y.H. Huang, C.L. Hsueh, M.C. Lu, G.H. Huang, Water Science and Technology 49(4) (2004) 213-218.

[7] M.L.Rodriguez, V.I.Timokhin, S.Contreras, E.Chamarro, S.Esplugas, Advances in Environmental research 7 (2003) 583-595.

[8] J. Anotai, C.C. Su, Y.C. Tsai, M.C. Lu, Journal of Environmental Engineering. 137(5) (2011) 363-370.

[9] F.J. Beltran, M. Gonzalez, J. Javier Rivas And B.Acedo, Water Environ. Res. 72(6) (2000) 689-697.

Strengthening effect of graphene quantum dots as UV blocker for wood-polyester nanocomposite coating

Abbas Madhi[1*], *Amir Hossein Madhi*[2],
[1]*Color Technology Incubator, Institute for Color Science and Technology, Tehran, Iran, abbas.madhi@semnan.ac.ir*
[2]*Faculty of Natural Resources and Environment, Islamic Azad University Science and Research Branch, Tehran, Iran, amirmadhi99@gmail.com*

Abstract - UV radiation from the sun is one of the reasons for wood weathering. Wood constructions weathering in addition to this renewable resource wasting entails environmental and economic losses. Therefore, there is a big need to use nano-additives with a feature of strengthening the coatings of wood surface against harmful UV rays. The main purpose of the present work is to examine the strengthening effect of graphene quantum dots (GQDs) in polyester-wood nanocomposite coating against UV radiation from the sun. To achieve this, graphene quantum dots 0.2wt% nanocomposite was added to unsaturated polyester (UP) resin, and following the radical polymerization process, UP-GQDs nanocomposite coating was prepared. Afterwards, fluorescence effect and UV-blocking behavior in the blank UP and UP-GQDs coatings were evaluated through photoluminescence and UV-visible spectroscopy methods. Adding GQDs 0.2wt% to the polymer matrix resulted in absorption of UV rays within 300-400 nm range and emission of blue fluorescence. Moreover, by adding GQDs to the UP matrix, pull-off adhesion strength of the nanocomposite was raised compared to the blank coating.

Keywords: Wood-polyester nanocomposite coating, graphene quantum dots, UV-blocker, pull-off adhesion strength

1. Introduction

Wood is a natural and renewable substance usable for furniture and construction industries. Apart from great features such as beautiful appearance, good strength, low density and insulation property, wood possesses some weak points including humidity absorption, flammability and surface destruction caused by weathering. Weathering consists in gradual destruction of wood surface occurred through combination effect of UV from sunlight, oxygen and water [1]. Hence, weathering annually brings about irreparable environmental and economical aftermath. Color change like yellowing is the first indication of complex chemical reactions on the wood surface that begins to appear by UV rays from the sun. UV rays owing to holding high energy can break the bonds among polymer molecules of wood and create photochemical reactions leading to lignin polymerization in the cell walls of wood. Amongst the cells of wood wall, lignin offers higher reactivity with UV rays in the 300-400 nm range. Because, following the reaction with UV, phenol hydroxyl groups turn into free phenoxy radicals that this leads to yellowing and photochemical destruction of wood [1,2]. Unsaturated polyester resins (UPs) have features such as high-speed curing and long shelf life at room temperature. UPs are widely applied in construction, wood and furniture, automotive and electronic industries. Due to good mechanical properties and optimal adhesion strength, unsaturated polyester resins are used to produce protective coatings for metal, wooden and stone surfaces against weathering factors. GQDs is a carbon nanomaterial-based substance synthesized by various methods of hydrothermal, microwave-assisted, acid oxidation and et cetera [1,3]. With less than 20 nm size, this compound offers excellent optical characteristics, capability of UV ray absorption, and biocompatible and nonpoisonous fluorescence emission. Production of fluorescent and UV-absorbent polymers has developed in recent years by mixing different resins like epoxy, polyester and polyurethane with graphene quantum dots [4].

In this research, UP-GQDs nanocomposite coatings were obtained through blending the unsaturated polyester resin with GQDs 0.2wt%. After that, fluorescence emission properties and blocking the UV rays (as major causes of wood weathering) were studied. Additionally, pull-off adhesion strength of the blank coating to the wood surface was analyzed relative to the strengthened coating with GQDs.

2. Experimental

2.1. Materials and methods

Dimethylformamide (DMF) solvent was purchased from Merck company. Unsaturated polyester resin BUP 617 (including 30 mass percent of styrene), cobalt naphthenate as an accelerator and methyl ethyl ketone peroxide as a catalyst (hardener) were bought from

Bonyan Kala Shimi company, BKC, Iran. 15×10×2 cm beech wood pieces were prepared from a local market. GQDs nanocomposite synthesized in the previous work was used for this research [5]

In order to evaluate the fluorescence characteristic and protective effect of UP-GQDs nanocomposite coating against UV radiation, photoluminescence spectroscopy (Perkin Elmer LS 55) and UV-visible spectroscopy (Specord 250) were taken into account. Pull-off adhesion testing was performed by Defelsko ASTM D4541 to assess the Pull-off adhesion strength of the samples to the wood surface. The beech wood pieces were prepared before performing surface operations.

2.2. Preparation of UP-GQDs nanocomposite

First, 0.05 g of GQDs was poured into a small beaker and 2 mL DMF was loaded to the beaker. This mixture was dispersed during 15 minutes using an ultrasonic probe and then for 45 minutes by a magnetic stirrer. For the next step, this compound was poured into a beaker containing 25 g of unsaturated polyester resin. A separate beaker was also used to loading only 25 g of unsaturated polyester resin to prepare the blank sample. The mixture containing GQDs was stirred for 4 hours with 600 rpm at 45°C. After that, 0.1 g cobalt naphthenate was separately added to the beaker containing GQDs and the beaker containing blank UP. After 1 minute stirring and then adding 0.4 g of MEKP to both of beakers, the two mixtures were again agitated for 3 minutes. Next, many 0.2 mm thick films were prepared on casting molds and flat beech wood surfaces. In order to complete the curing process and remove the solvent, the samples were left at ambient temperature for 36 hours and then placed in an oven at 65°C for 45 minutes. At last, UP-GQDs and UP (blank) coatings were prepared. It is worth mentioning that polymerization reaction of UP-GQDs nanocomposite formation makes progress through a radical mechanism [2]. Figure 1 exhibits the polymerization mechanism of UP-GQDs nanocomposite.

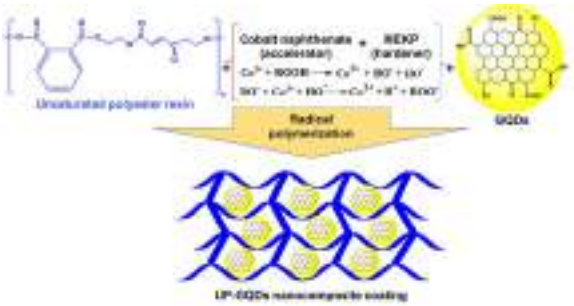

Fig. 1. Polymerization mechanism of UP-GQDs nanocomposite.

3. Results and discussion

3.1. Fluorescence and UV-blocking properties

Figure 2 displays the photoluminescence (PL) spectra of the samples. UP coating offered no significant fluorescence emission, while in the UP-GQDs coating, excitation wavelength and emission peak were respectively observed at 373 nm and 445 nm (blue region). Electron excitement of C=C and C=O groups resident in GQDs resulted in extensive visible radiations. Figure 3 indicates function of UP and UP-GQDs coatings exposed to UV radiation. The observed absorption peak at 300-400 nm confirms that UP-GQDs nanocomposite offers a good performance for absorption of UV rays, however, UP (blank) has no capability of the UV absorbance or blocking in the mentioned region. The appeared absorption peak at 300-400 nm could be pertained to $\pi \rightarrow \pi^*$ electron transferring of C=C bonds and $n \rightarrow \pi^*$ electron conveying of C=O bonds existing in functional groups of GQDs [6,7]. Blocking mechanism of UV rays, blue fluorescence emission from UP-GQDs nanocomposite and protection of wood surface against UV radiation are schematically represented in Figure 4.

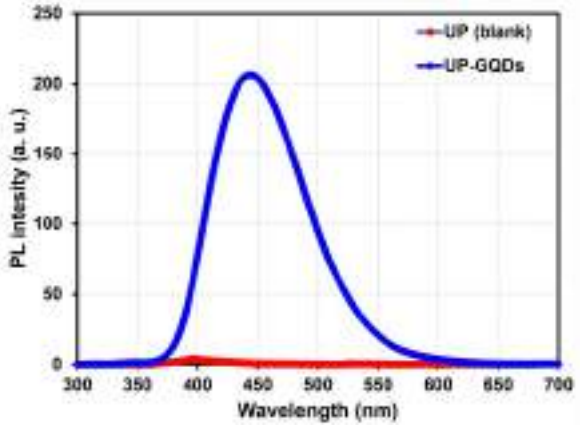

Fig. 2. PL spectra of the coatings

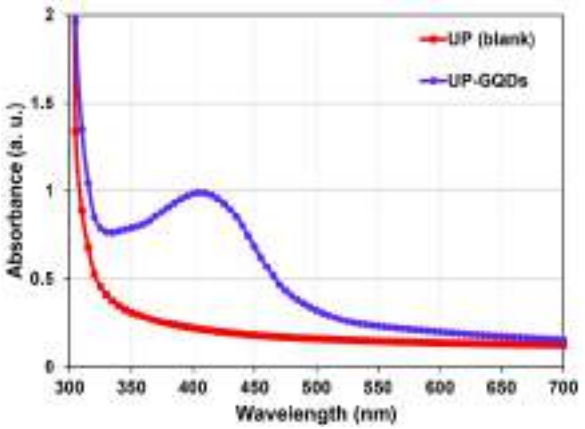

Fig. 3. UV-visible absorbance curves for the nanocomposite coatings.

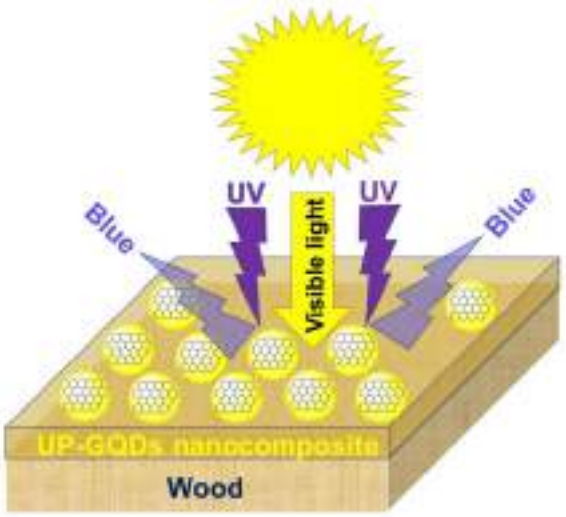

Fig. 4. Schematic image of UV-blocking mechanism and fluorescence emission of UP-GQDs nanocomposite coating.

3.2. Pull-off adhesion strength for the coatings

Pull-off adhesion in the joint surfaces of UP-wood and GQDs-UP-wood was studied after surface operations. The results of the investigation on Pull-off adhesion strength performance are shown in Figure 5. According to the results, pull-off adhesion strength in the nanocomposite-wood joint surface of UP-GQDs nanocomposite is higher than that of blank sample. Adding GQDs to the polymer matrix led to an increase in the Pull-off adhesion strength between wood surface and nanocomposite film. The reason is that adhesion forces are often a kind of physical bonds which increase adhesion strength through mechanical interlocking, hydrogen bonds and Van der Waals forces [8]. Homogenous dispersion of GQDs nanoparticles throughout the polyester matrix and creating physical and chemical interactions in the nanocomposite-wood joint surface enhanced Pull-off adhesion strength.

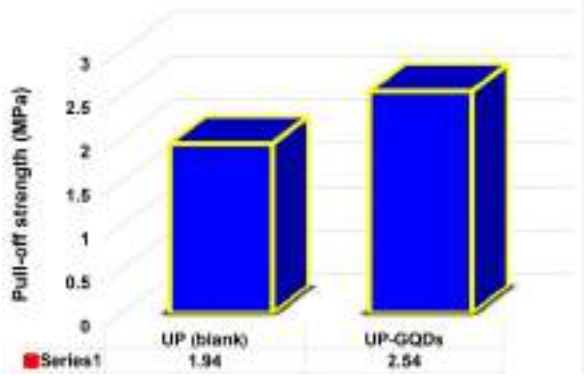

Fig. 5. Pull-off adhesion strength of the coatings.

4. Conclusion

In this project, to increase the wood durability against UV radiation from the sun, UP-GQDs nanocomposite coating was prepared by mixing the unsaturated polyester resin and 0.2wt% GQDs. The strengthening effect of GQDs in this nanocomposite was entirely obvious, so that it was capable of blocking the UV rays within 300-400 nm range and blue fluorescence emission. Additionally, the polymer coating containing GQDs offered higher pull-off adhesion strength in comparison with the blank sample. Use of UP-GQDs nanocomposites as protective coating of wooden surfaces could be an executable and operational idea for various applications in the facade of buildings, and wood and furniture industry.

References

[1] H. Sadeghifar, A. Ragauskas, Polymers. 12 (2020) 1134
[2] A. Madi, J. Compos. Mater. 57 (2023) 2437-2450
[3] A. Madi, B. Shirkavand Hadavand, J Compos Mater. 56 (2022) 2201-2210
[4] A. Madi, B. Shirkavand Hadavand, J. Appl. Chem. 41 (2022) 2202-2212
[5] A. Madi, B. Shirkavand Hadvand, Iran. J. Chem. Chem. Eng. 41 (2022) 2202-2212
[6] A. Madi, B. Shirkavand Hadavand, Polym-plast. Tech. Mat. 61 (2022) 117-130
[7] A. Madhi, B. Shirkavand Hadavand, A.H. Madhi, Fuller. Nanotub. Carbon. Nanostructures. DOI: 10.1080/1536383X.2023.2226272
[8] A. Madi. Polym-plast. Tech. Mat. 62 (2023) 403-418

29TH IRANIAN ORGANIC CHEMISTRY CONFERENCE
1_3 NOV, 2023
UNIVERSITY OF QOM, IRAN

The atmospheric reaction $CH_3CONH_2 + HO_2$: A computational investigation

Soheila Jamali, Fahimeh Khouini and Morteza Vahedpour*

Department of Chemistry, University of Zanjan, PO Box 38791-45371, Zanjan, Iran,
female.jamali1369@gmail.com, khouini_f@znu.ac.ir

Abstract - Acetamide is a simple hydrophilic amide, has been classified as the most dangerous pollutant by the Environmental Protection Agency (EPA). On the basis of M062X/6-31g(d,p) techniques, : Hydrogen abstraction reaction of the CH_3CONH_2 by HO_2 in the gas phase is theoretically studied. all stationary locations along the path have their energy parameters estimated. Finally, thermochemical properties such as energy, enthalpy, Gibbs free energy, and entropy of the product have been predicted based on M062X/6-31g(d,p) method.

Keywords: CH_3CONH_2, HO_2, Theoretically

1. Introduction

The International Agency for Research on Cancer (IARC) has divided acetamide as a Group 2B probable human carcinogen [1]. Acetamide is a significant industrial chemical having several uses in a variety of industries. It is used as a solvent in the production of many organic compounds, including pharmaceuticals, dyes, and plastics. It is also used as an intermediate in the synthesis of other chemicals, such as acetanilide and acrylamide [2]. acetamide is a versatile and important chemical with a wide range of applications in industry and scientific research. Its simple structure and interesting properties make it a valuable tool for chemists and other researchers working in a variety of fields. Consequently, it mostly published to the atmosphere by mentioned activities.

2. Methodology

Under investigation reaction studied based on DFT method by the Gaussian 09 program. The geometry of the stationary points are optimized using the M062X method along with the double zeta basis set, 6-31g(d, p). Complex reactants, transition states, post reactive complexes, and products are the stationary points in the reaction path and are, respectively, indicated by the letters R, CR, TS, CP, and P. Harmonic frequencies are calculated for all species at the level of theory M062X /6-31g(d, p). The reaction's potential energy surface (PES), which is contained by the M062X/6-31G(d,p) level, is then reached.

3. Result and Discussion

3.1. Figures and Tables

The plotted PES is calculated using the M062X/6-31g(d,p) method, as showed in Figure 1. Table 1 compiles the estimated energies at M062X/6-31g(d,p) methodologies. Table 2 is a list of the product's thermodynamic properties.

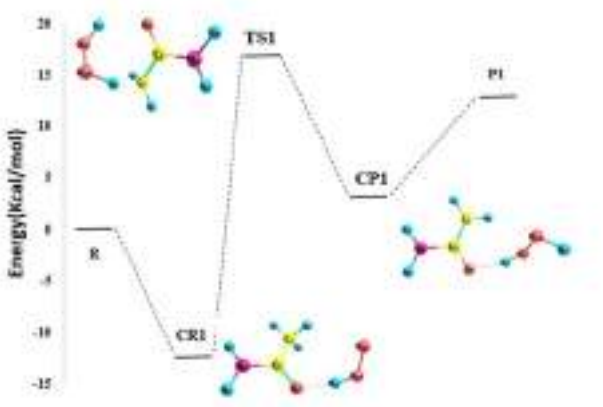

Fig.1. the potential energy surface of the $CH_3CONH_2 + HO_2$ at MO62X/6-31G(d,p) level of theory.

Table1: Computed energies at M062X/6-31G(d,p) Methods

Species	E(Hartree)	ΔE(kcal/mol)
R	-359.98	0.00
CR	-360.00	-12.41
TS	-359.95	16.86
CP	-359.97	3.19
P	-359.95	12.85

Table2: Thermodynamic parameters (in kcal/mol) of the product at MO62X/6-31G(d,p) Method.

Species	ΔE°	ΔH°	ΔG°	ΔS°
R	0.00	0.00	0.00	0.00
CR	-95.68	-98.06	-89.57	-0.02
TS	-67.36	-4.49	-59.02	-0.03
CP	-80.81	5.16	-75.17	-0.02
P	14.81	13.02	12.95	0.0002

3.2. Reaction mechanism

In the doublet state, the reaction mechanism is investigated. The reaction begins with the pre-reactive complex, or CR, as can be shown in Fig. 1. The relative energy of CR is -12.41 kcal /mol. The projected TS has a barrier energy of 29.27 kcal mol-1 and connects CR and CP. After TS, the relative energy of 3.19 kcal /mol generates the post-reactive complex. The last step involves CP releasing all of the remaining adducts. Thermodynamic analysis is used to examine the product formation. Thermodynamically, the CH_2CONH_2 +H_2O_2 adducts have the Gibbs free energy and enthalpy of the reaction with the values of 12.95and 13.02 kcal /mol, respectively.

4. Conclusion

In atmosphere circumstances, we investigated the hydrogen abstraction reaction mechanism of the $CH_3CONH2 + HO_2$ reaction. The mechanism of the reaction $CH_3CONH2 + HO_2$ is investigated using M062X/6-31G(d,p). The resultant product is thermodynamically examined.

References

[1] R. Vismeh, D. Haddad, J. Moore, C. Nielson, B. Bals, T. Campbell, A. Julian, F. Teymouri, A. D. Jones, and V. Bringi. 2018. Exposure assessment of acetamide in milk, beef, and coffee using xanthydrol derivatization and gas chromatography/mass spectrometry. J. Agric. Food Chem. 66:298–305.

[2] M. M. Moore, B. Gollapudi, R. Nagane, N. Khan, M. Patel, T. Khanvilkar, A. M. Roy, E. Ramesh, B. Bals, F. Teymouri, R. Nault, V. Bringi, The food contaminant acetamide is not an in vivo clastogen, aneugen, or mutagen in rodent hematopoietic tissue, Regulatory Toxicology and Pharmacology, Volume 108, 2019, 104451, ISSN 0273-2300.

29TH IRANIAN ORGANIC CHEMISTRY CONFERENCE
1_3 NOV, 2023
UNIVERSITY OF QOM, IRAN

Synthesis and characterization of Ag.ZnO nanocomposite loaded with catechin

*Farideh Khoshsokhan, Azadeh Meshkini**

[1]*Department of Chemistry, Faculty of Science, Ferdowsi University of Mashhad, Mashhad, Iran, f74khoshsokhan@gmail.com, a.meshkini@um.ac.ir*

Abstract

In this study, Ag.ZnO nanocomposite was synthesized and used as a platform for delivery of a natural antioxidant, catechin (Cat). The final nanocomposite was characterized by FESEM, FTIR, and zeta potential. Based on FESEM images the nanocomposite was spherical and FTIR and zeta potential confirmed the successful synthesis of nanocomposite and loading of antioxidant. Catechin loaded nanocomposite showed higher antioxidant activity than bare nanocomposite and catechin alone. Based on these results, Ag.ZnO.Cat could be used in biomedical and food industries.

1. Introduction

Antioxidants interact with free radicals, terminating the adverse chain reactions and converting them to harmless products. Antioxidants thus minimize the oxidative stress and play a crucial role in the treatment of free radicals-induced diseases [1]. Also, nanoparticles that have antioxidant properties have good potential in cancer treatment[2]. Nano zinc oxide (ZnO) is one of the compounds that has received attention due to its non-toxicity, photocatalytic activity, anticancer, and antimicrobial activities [3] Composition of silver and ZnO (Ag.ZnO) in the nanoscale are widely used in various fields such as medicine, pharmacy, physics, and chemistry by researchers due to good conductivity, chemical stability, and catalytic activity [4]. Previous studies have pointed that ZnO nanoparticles has antioxidant activity [5]. Therefore, it could be an appropriate platform for delivery of antioxidant, showing synergistic effects. Medicinal plants are the richest source of bioactive compounds that have wide applications in modern medicine. Catechin hydrate (Cat), as a secondary metabolite of plants, is one of the most important natural flavonoids, which has received attention due to its therapeutic activities as well as its potential biological effects [6]. In this study, Ag.ZnO nanocomposite was synthesized and then catechin was loaded on the surface of nanocomposite (scheme). Final construct was characterized by FESEM, FTIR, and zeta potential. The antioxidant activity of Ag.ZnO.Cat was evaluated using DPPH assay.

Scheme. Structure of catechin and Ag.ZnO.Cat nanocomposite

2. Materials and methods

2.1. Synthesis of silver.zinc oxide nanocomposite (Ag.ZnO)

KOH solution (0.04 M) was added to $Zn(Ac)_2$ (0.01 M). Then, $AgNO_3$ solution was added to the above mixture. After 30 min stirring, the mixture was centrifuged and the precipitate was Ag.ZnO nanocomposite. Catechin solution was added to nanocomposites and the reaction continued for 5 h. Finally, the mixture was centrifuged and the precipitate was Ag.ZnO.Cat nanocomposite.

2.2. Investigation of antioxidant properties.

In order to investigate the antioxidant property of Ag.ZnO.Cat nanocomposite, 1,1-diphenyl 2-picrylhydrazyl (DPPH) was used. Briefly, 1 mL of the the Ag.ZnO.Cat and Ag.ZnO nanocomposite and free catechin was added to 1 mL of a DPPH solution (0.2 mM in ethanol) as the free radical source and kept for 30 minutes at room temperature and read at the end of absorption. Samples were read at wavelength 490 using an ELISA reader. The percentage of radical scavenging capacity was calculated as follows:

Scavenging capacity (%) = $[1-(A_s/A_c)\times100]$

where As is the absorbance of sample and Ac the absorbance of control [7, 8].

3. Results and Discussion

3.1. Characterization of nanoparticles and nanocomposites

As shown in Fig 1, the morphology of Ag.ZnO.Cat nanocomposite was evaluated by FESEM. The average size of nanocomposite was calculated to be 70 nm.

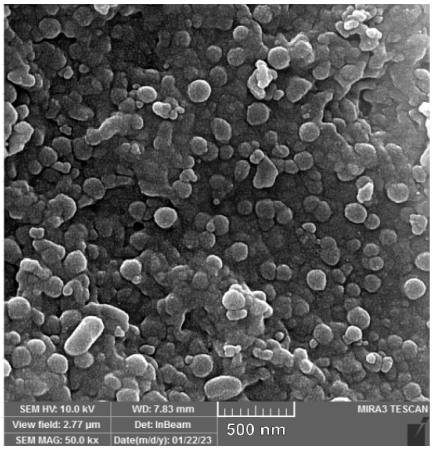

Fig.1. FE-SEM image of Ag.ZnO.Cat

As shown in Fig 2, intermolecular interactions in fabricated nanocomposites were investigated by FT-IR. Broad bands in the region of 3400 cm^{-1} were observed in all the prepared spectra, which related to the stretching vibration of O-H group of nanocomposites. In all samples, the band in the region of 580 cm^{-1} is related to the transverse stretching of Zn-O. The bands in the range of 800 cm^{-1} to 1000 cm^{-1} were attributed to the C=C aromatic stretching in catechin moiety, which observed in catechin-loaded nanocomposite (Fig. 2(c)), indicating the successful loading of antioxidant on nanocomposite surface [9-11].

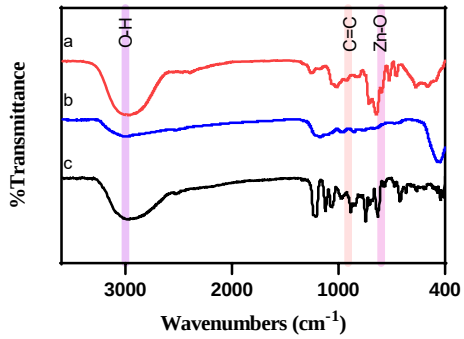

Fig.2. FT-IR spectra of:
(a) catechin standard sample, (b) ZnO, (c) Ag.ZnO.Cat.

To find the surface charge and potential stability of nanoparticles in the colloidal suspension, the zeta potential of the nanocomposite was evaluated. The results of zeta potential measurement show that the surface charge of ZnO nanoparticles was -25±1.8 mV due to the presence of OH- groups. Ag.ZnO nanoparticles also had a negative charge of -31±1.5 mV [6]. Due to the presence of catechin, the zeta potential of nanocomposite moved toward positive values (-26 mV) at physiological pH [12]. Antioxidant activity of nanocomposite was evaluated by DPPH assay. Ag.ZnO.Cat and Ag.ZnO nanocomposite and free catechin have 97%, 51% and 94% antioxidant properties, respectively.

4. Conclusions

In this study, Ag.ZnO nanocomposite was successfully synthesized as a platform for loading of catechin as a natural antioxidant. The results of the studies showed that the synthesized nanocomposite had high antioxidant properties. Accordingly, the Ag.ZnO.Cat nanocomposite can be used in various industries such as biomedicine, cosmetics and pharmaceuticals.

5. References

[1] Hall-Stoodley, L., J.W. Costerton, and P. Stoodley, Bacterial biofilms: from the natural environment to infectious diseases. Nature reviews microbiology, 2004. 2(2): p. 95-108.

[2] Bankier, C., et al., Synergistic antibacterial effects of metallic nanoparticle combinations. Scientific reports, 2019. 9(1): p. 16074.

[3] Sun, J., et al., Multifunctional bionanocomposite films based on konjac glucomannan/chitosan with nano-ZnO and mulberry anthocyanin extract for active food packaging. Food Hydrocolloids, 2020. 107: p. 105942.

[4] Khatami, M., et al., Applications of green synthesized Ag, ZnO and Ag/ZnO nanoparticles for making clinical antimicrobial wound-healing bandages. Sustainable Chemistry and Pharmacy, 2018. 10: p. 9-15.

[5] Parsa, M., M.H. Entezari, and A. Meshkini, Sono-synthesis approach improves anticancer activity of ZnO nanoparticles: reactive oxygen species depletion for killing human osteosarcoma cells. Nanomedicine, 2021. 16(8): p. 657-671.

[6] Kaur, R., et al., Synthesis, characterization and evaluation of antioxidant properties of catechin hydrate nanoparticles. Journal of Drug Delivery Science and Technology, 2017. 39: p. 398-407.

[7] Naemi, S. and A. Meshkini, Phytosynthesis of graphene oxide encapsulated selenium nanoparticles using Crocus Sativus petals' extract and evaluation of their bioactivity. Journal of Drug Delivery Science and Technology, 2023. 81: p. 104286.

[8] Meshkini, A. and M. Tahmasbi, Antiplatelet aggregation activity of walnut hull extract via suppression of reactive oxygen species generation and caspase activation. Journal of acupuncture and meridian studies, 2017. 10(3): p. 193-203.

[9] Zhang, J., et al., Dual-sensitive graphene oxide loaded with proapoptotic peptides and anticancer drugs for cancer synergetic therapy. Langmuir, 2019. 35(18): p. 6120-6128.

[10] Zhao, B., et al., Green synthesis, characterization and antibacterial study on the catechin-functionalized ZnO nanoclusters. Materials Research Express, 2021. 8(2): p. 025006.

[11] Liu, J., et al., pH-sensitive and antibacterial films developed by incorporating anthocyanins extracted from purple potato or roselle into chitosan/polyvinyl alcohol/nano-ZnO matrix: comparative study. International Journal of Biological Macromolecules, 2021. 178: p. 104-112.

[12] Zhang, J., et al., Synthesis of water-soluble γ-aminopropyl triethoxysilane-capped ZnO: MgO nanocrystals with biocompatibility. CrystEngComm, 2012. 14(2): p. 613-619.

29TH IRANIAN ORGANIC CHEMISTRY CONFERENCE
1_3 NOV, 2023
UNIVERSITY OF QOM, IRAN

α-Fe_2O_3@MoS_2@$SnCl_2$ as a Highly Efficient Nano Catalyst for Solvent-Free Esterification of Aromatic Carboxylic Acids

*Mohammad Abdollahi, Behzad Khalili**

Department of Chemistry, Faculty of Sciences, University of Guilan, P.O. Box 41335-1914, Rasht, Iran, mohammadabdollahichem@gmail.com, B.khalili@guilan.ac.ir

Abstract - In this study, we investigate the use of a novel catalyst, α-Fe_2O_3@MoS_2@$SnCl_2$ (FMS) nanoparticles (NPs), for enhancing the efficiency of the esterification reaction. The catalyst was characterized using various techniques such as XRD, SEM and EDX. The catalytic activity of FMSNPs was evaluated by conducting esterification reactions under different reaction conditions. The results showed that the presence of the catalyst significantly improved the conversion rate and yield of the desired esters. Furthermore, the catalyst exhibited excellent stability and could be easily recovered and reused without significant loss in activity. Overall, this study demonstrates the potential of FMSNPs as an efficient catalyst for the esterification of benzoic acid and its derivatives with ethanol, offering promising opportunities for industrial applications in the production of ester-based compounds.

1. Introduction

Esterification is a widely used chemical reaction that involves the formation of esters from carboxylic acids and alcohols in the presence of a catalyst. This reaction is of great importance in various industries, such as the production of plastic and coatings [1], biofuels [2], paints and varnishes [3], herbicides [4], and pharmaceuticals [5]. To enhance the efficiency and selectivity of esterification reactions, catalysts are often employed. The catalyst plays a crucial role in enhancing the reaction rate and improving the overall efficiency of esterification processes. In recent years, significant research efforts have been focused on developing efficient and environmentally friendly catalysts for esterification reactions. These catalysts aim to improve reaction selectivity, reduce energy consumption, minimize waste generation, and enhance overall process sustainability. Several studies have reported promising results using various types of catalysts such as acids, bases, enzymes, metal complexes, zeolites, and solid acids. Acidic catalysts are commonly used for esterification reactions due to their ability to protonate the alcohol or acid molecules, facilitating their reaction with each other. Sulfuric acid (H_2SO_4) [6], p-toluenesulfonic acid (PTSA)[7], and super acids [8] are some examples of commonly employed acidic catalysts in esterification processes. On the other hand, enzymatic catalysis has gained significant attention in recent years due to its high selectivity, mild reaction conditions, and biodegradability. Lipases, a type of enzyme, have shown promising results as catalysts for esterification reactions [9]. In addition to acidic and enzymatic catalysts, ion exchange resins [10], zeolites [11], heteropolyacids [12] and supported chlorides [13]. Metal oxides [14] have also been employed in esterification reactions.

The choice of catalyst depends on various factors such as reaction conditions, desired selectivity, and the nature of the reactants. Each catalyst offers its own advantages and limitations, making it crucial to select the most suitable one for a specific esterification reaction. In present work, we have utilized FMSNPs as a catalyst for the esterification reaction. This catalyst is a nanocomposite material consisting of iron oxide (α-Fe_2O_3), molybdenum disulfide (MoS_2), and tin oxide ($SnCl2_2$). The FMSNPs catalyst has shown great potential in enhancing the efficiency of the esterification reaction. The combination of iron oxide, molybdenum disulfide, and tin oxide provides unique catalytic properties, including high surface area, strong acid-base interactions, and excellent stability. Moreover, the nanoscale structure of this catalyst allows for better dispersion and accessibility of active sites, leading to improved catalytic performance. The presence of molybdenum disulfide also enhances the catalytic activity by providing additional active sites for the reaction.

2. Results and Discussion

The catalytic activity of FMSNPs was evaluated by performing esterification reactions between benzoic acid and ethanol. The reaction was carried out under various conditions including different reaction temperatures, catalyst loadings, and reaction times. The results showed that FMSNPs exhibited excellent catalytic activity for the esterification reaction. At an

optimized reaction temperature of 80°C, a catalyst loading of 0.2 gr, and a reaction time of 45 min, a conversion rate of over 99% was achieved. The enhanced catalytic performance can be attributed to several factors. Firstly, the core-shell structure provides a large surface area for effective contact between reactants and catalysts. Secondly, α-Fe_2O_3 acts as a Lewis acid, promoting the activation of carboxylic acids. Thirdly, MoS_2 and $SnCl_2$ act as Brønsted acids, facilitating the protonation of alcohols. The synergistic effect of these components leads to improved catalytic efficiency.

To optimize the reaction conditions for the esterification of benzoic acid with ethanol in the presence of FMSNPs as catalyst, a model reaction was chosen. The reaction involved the use of benzoic acid and ethanol as reagents. Initially, various amounts of FMSNPs catalyst were tested under different synthetic conditions. As shown in Table 1, Entry 8, optimal conditions were obtained

Table 1. Optimization of synthetic conditions for the preoaration of ethyl benzoate [a].

Entry	Catalyst (gr)	Temperature (°C)	Time (min)	Yield (%) [b]
1	-	reflux	120	trace
2	1	50	50	70
3	1	60	50	78
4	1	70	50	81
5	1	reflux	45	96
6	0.5	reflux	45	99
7	0.3	reflux	45	99
8	**0.2**	**reflux**	**45**	**99**
9	0.1	reflux	45	90

[a] Reaction conditions: benzoic acid (1 mmol), ethanol (2 mmol); [b] Isolated yields.

These optimized results prompted further investigation into the scope of this reaction for synthesizing various substituted carboxylic acids derivatives. This study investigates the esterification reaction of benzoic acid derivatives containing electron-withdrawing and electron-releasing groups. Encouraged by the result, the capability of this synthetic protocol was more studied with the reaction of various aromatic carboxylic acids containing electron-releasing or withdrawing groups with ethanol at the optimized reactions conditions. Table 2 shows the general trend and versatility of this synthetic method. As seen, all reactions were carried out successfully in the presence of the FMSNPs (0.2 g) within 38-90 min to afford the products esters in high yields (93-99 %). The table also shows that the effect of substitutions on aromatic rings is noteworthy. Electron-withdrawing groups accelerated the rate of esterification reaction (Table 2, Entry 6,7) and in contrast releasing substitutions prolonged the reaction times (Table 2, Entry 4,5).

Table 2. Esterification of carboxylic acids with ethanol in the presence of FSM system[a]

Entry	Substrate	Product	Time (min)	Yeild (%[b])
1			45	99
2	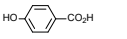	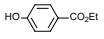	64	98
3	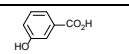	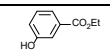	68	95
4	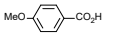	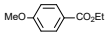	75	94
5	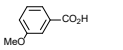	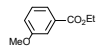	90	93
6	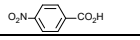	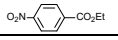	38	98
7	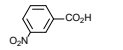	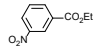	40	97
8	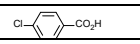	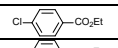	48	99
9	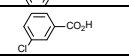	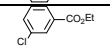	52	99
10	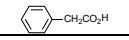	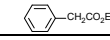	43	99
11	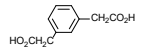	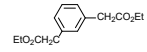	55	98

[a]All reactions were carried out with 1 mmol of carboxylic acid in the presence of FSM (0.2 gr) [b]Isolated yields

2.1 XRD analysis

The XRD analysis of FMSNPs is demonstrated in figure 1. The XRD spectrum shows diffraction peaks at around 2θ= 15.7°, 34.6°, 38.9° and 60.1° which are related to the Molybdenum disulfide (JCPDS card No. 37-1492). Diffraction peaks at around 2θ = 33.6°, 34.7°, 39.7°, and 50.8° are also related to the α-Fe_2O_3 (JCPDS File No. 79-0007). The average size of the nanoparticles was calculated to be about 70 nm using the Scherrer equation.

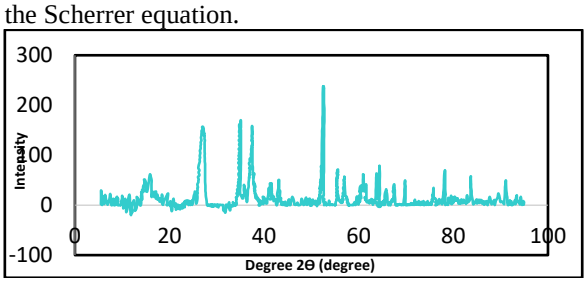

Figure 1. XRD spectrum of FMSNPs

2.2 EDX analysis

According to Figure 2, the EDX analysis of FMSNPs confirmed the existence of Iron, Molybdenum, Sulfur, Oxygen and Tin atoms in the nanoparticles structure.

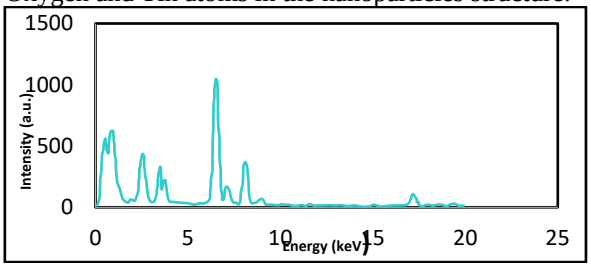

Figure2. EDX spectrum of FMSNPs

2.3 Scanning electron microscope (SEM)

The SEM image of the FMSNPs catalyst reveals a highly intricate and well-structured composition. The catalyst consists of three distinct layers, each contributing to its unique catalytic properties. The SEM image showcases a well-dispersed distribution of these three components throughout the nano catalyst structure. This increased surface area facilitates better contact between reactants, leading to improved reaction kinetics (Figure 3).

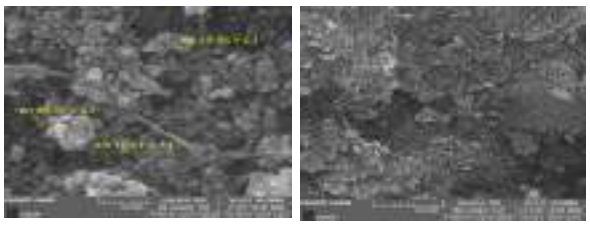

Figure3. SEM image of FMSNPs

In present work, we explore the effectiveness and efficiency of various catalysts used in esterification reactions, with a specific focus on the FMSNPs catalyst. According to table 3, the FMSNPs catalyst exhibits a high reaction rate. By comparing the performance of the FMSNPs catalyst with other commonly used catalysts, it becomes evident that this novel catalyst offers superior reaction rates and high yield of products.

Table 3. Comparison table of various catalysts in esterification of benzoic acid with ethanol

Entry	Catalyst	Quantity	T (ºC)	Time (h)	Yeild (%)
1	silica sulfuric acid	0.02 gr	74	64	28 [15]
2	[PSPy]HSO4	5 mmol	85	3	92 [16]
3	SO4 2−/Ti3AlC2	0.195	120	34	80.4 [17]
4	IL [CP][CH3SO3]	4 mmol	60	8	84 [18]
5	4Å molecular sieve	10 gr	110	12	Trace [17]
6	FSM	0.2	reflux	45 min	99

The study found that FMSNPs is a highly stable and reusable catalyst in the reaction of benzoic acid with ethanol. The catalyst can be easily separated from the reaction mixture and washed for efficient recovery. It maintained its efficiency even after 8 successive runs, with an average yield of 97% for the desired product. This high level of reusability makes FMSNPs economically viable and reduces costs associated with catalyst production and disposal.

3. Experimental

Initially, α-Fe_2O_3@MoS_2 [19] is stirred in ethanol to form suspension 1. Then, a solution of $SnCl_2$ dissolved in distilled water is prepared and NH_3 is added until the solution becomes clear, forming solution 2. Solution 2 is mixed with suspension 1 and refluxed for 1 hour. The resulting product is separated using a magnet, washed with warm water, and dried at 100 °C to obtain FMSNPs. In the catalytic esterification reaction of benzoic acid with ethanol, a round-bottom flask equipped with a reflux condenser and magnetic stirrer is used. Benzoic acid is dissolved in ethanol, and the synthesized FMSNPs catalyst is added under constant stirring. The reaction mixture is heated to reflux temperature and maintained for a specific reaction time. The progress of the reaction is monitored using thin-layer chromatography. After completion of the reaction, the mixture is cooled, and the catalyst is separated by filtration and washed before reuse in subsequent reactions.

4. Conclusion

In conclusion, the esterification of carboxylic acid with ethanol in the presence of FMSNPs catalyst has proven to be an efficient and effective method for synthesizing esters. The use of FMSNPs as a catalyst offers several advantages, including high conversion rates, mild reaction conditions, and easy separation of the catalyst from the reaction mixture.

Refereces

[1] C.S. Pereira, V.M. Silva, A.E. Rodrigues, Green Chem. 13 (2011) 2658– 2671.
[2] B.R. Moser, Biodiesel production, properties, and feedstocks, in: Biofuels, Springer, 2011.
[3] J. L. Kendall, D.W.Kendall (2009). U.S. Patent Application No. 12/315,208.
[4] X. Tang, E.Y.-X. Chen, Chem 5 (2) (2019) 284–312.
[5] A.d.N. de Oliveira, et al, React. Kinet. Mech. Catal 130 (2020) 633-653.
[6] G. Jyoti, A. Keshav, J. Anandkumar, Int. J. Chem. Reactor Eng. 14 (2) (2016) 571–578.
[7] R. Nagahata, T. Nakamura, Y. Mori, K. Takeuchi, Natural Science 9 (2017) 110-122.
[8] S. Ardizzone, C.L. Bianchi, V. Ragaini, Catal Lett 62 (1999) 59–65.
[9] I.G. Rosset et al, Catal. Lett 143 (9) (2013) 863–872.
[10] M.-J. Lee, J.-Y. Chiu, H.-M. Lin, Ind. Eng. Chem. Res 41 (2002) 2882–2887.
[11] I. Hoek, T.A. Nijhuis, A.I. Stankiewicz, J.A. Moulijn, Appl. Catal. A Gen. 266 (2004) 109–116.
[12] F.M. Zhang, J. Wang, C.S. Yuan, X.Q. Ren, Sci. China Ser. B 49 (2006) 140–147.
[13] M. Salavati-Niasari, T. Khosousi, S. Hydarzadeh, J. Mol. Catal. A Chem 235 (2005) 150–153.
[14] C.S. MacLeod, A.P. Harvey, A.F. Lee, K. Wilson, Chem. Eng. J 135 (2008), 63–70.
[15] N. Ahmadi, A. Ramazani, S. Rezayati, F. Hosseini, Eurasian Chemical Communications 2(8) (2020) 862-874.
[16] H. Xing, T. Wang, Z. Zhou, Y. Dai, Industrial & engineering chemistry research 44(11) (2005) 4147-4150.
[17] M. Wu, J. Guo, Y. Li, Y. Zhang, Ceramics International 39(8) (2013) 9731-9736.
[18] H. Zhou, J. Yang, L. Ye, H. Lin, Y. Yuan, Green Chemistry 12(4) (2010) 661-665.
[19] K. Uma, E. Muniranthinam, S. Chong, T.C.K. Yang, J.H. Lin, Crystals 10 (5) (2020) 356.

29TH IRANIAN ORGANIC CHEMISTRY CONFERENCE
1_3 NOV, 2023
UNIVERSITY OF QOM, IRAN

Mechanical Properties of Sago Starch film Incorporated with Phycocyanin Extract of Spirulina Platensis

Fatemeh Sadeghi Erami ***

Department of Chemistry, Sari Branch, Islamic Azad University, Sari, Iran, Fatemesadeghi96d@gmail.com

Abstract - The mechanical and barrier properties of sago starch film incorporated with different percentage of phycocyanin (0.2, 0.4, 0.6, 0.8 and 1.0) were evaluated. With regard to mechanical properties, tensile strength and Youngs modulus decreased when the percentage of extract Elongation at break (%) increased. and increased with increasing percentage of extract from 0.2 to 1/0.

Keywords: Tensile Strength, Elongation at Break, Youngs Modulus

1. Introduction

The use of plastics is increasing dramatically in the world and it has an approximately 5% growth annually [1–3]. Some synthetic packaging materials like Polyethylene terphthalate (PET), polyvinylchloride (PVC), etc., have been very popular [4] because of their low cost, good mechanical properties like tensile strength and elongation, good barrier properties to water, oxygen, aroma compounds and carbon dioxide, heat seal ability and so on. In spite of good properties, their use should be restricted due to their non-biodegradability [5]. Increasing use of synthetic packaging films will contribute to environmental problems. In recent years, biodegradable polymers, such as starch, have been studied extensively as a potential packaging film with good physical, mechanical, and barrier properties [6]. Indeed for some foods, for example fresh foods, biodegradable polymers can be more suitable [7-9]. The popularity of starch is primarily related to it being renewable and abundant [10–12], and relatively low cost. However, starch alone as a packaging material has many limitations due to its hydrophilic nature and poor mechanical properties (for example brittleness). Therefore, starch is often modified Starch-based films have no color, odor, and taste and in comparison with plastic films that have good barrier properties [1,6,13,14] and have good mechanical and barrier properties [13]. The oxygen barrier property of fresh products such as fruits, meats, and salads has an important role on their preservation. Starch films have a selective permeability to some substances such as oxygen which can make it as a very good modified atmosphere packaging (MAP) [14,15]. The water vapor barrier shows the volume of water vapor that pass from a packaging material. It is very important to prevent dehydration in fresh foods [16]. Mechanical properties of films such as tensile strength and elongation at break are important for proper function of packaging materials and may be influenced by interaction between polymer and chemical compounds [17]. Most food contaminations exist on the food surface; therefore packaging has an important role to control food contamination [18-20]. To the best of our knowledge, there is no publication in the literature related to mechanical properties of edible films incorporated with phycocyanin. Therefore, the objectives of this research was to characterize the mechanical and barrier properties of sago starch-based film incorporated with phycocyanin

2. Materials and Methods

2.1. Purification of phycocyanin: Spirulina platensis were cultured in Caspian Reserch Center and phycocyanin purification by this method [21].

2.2. Chemicals and reagents: Sago starch with approximately 12% moisture, glycerol, sorbitol and the other chemicals were supplied by Sigma-Aldrich.

2.3. Film preparation:

2.3.1 Sago starch –based film was explained (Jafarzadeh et al., 2020): First 4% (w/w) sago starch was added to distilled water and followed by heating to 90 ◦C for gelatinization of starches and stirred continuously for 45 min to complete homogeneity and gelatinization in solution. A mixture of plasticizer (sorbitol: 3/glycerol: 1) that previously reported by as the best heat seal ability at 40%, also added. This mixture was cooled to 40–45 ◦C. Different amount of suspension Phycocyanin dissolve in water (0. 2, 0. 4, 0. 6, 0. 8 and 1 w/V) was added into the mixture Phy1,Phy2,Phy3, Phy4,Phy5 films respectively. Film without the addition of Phy (Phy0) was served as control. Each suspension was cast on Perspex plates and fitted with rims to yield a 16 cm × 16 cm film-forming area. Then the films were dried in the oven at 40 ◦C for 20 h and peeled off after drying, and kept at 23 ± 2 ◦C and the dried and peeled off film was put into a desiccator with 50% relative humidity until further analyses.

2.4. Mechanical properties

The mechanical properties of the films was determined using ASTM D882 [22-24] with a slight modification. Film strips cut into 100 mm × 20 mm sections and were kept for 48 h at 23 ◦C and 53% RH to be conditioned. The mechanical properties were then measured using a universal testing machine(SANTAM)in an initial grip separation with crosshead speeds of 50 mm/s and 1 mm/s. Deformation and force were recorded by the software during extension and expressed in graph format. Elongation and tensile strength at breaking as well as Young's modulus were calculated. At least five replicates were carried out for each sample.

3. Results and Discussion

3.1. Tensile strength, elongation at break and Youngs modulus: Tensile strength (TS) expresses the maximum force per area that the film can tolerance before breaking, while elongation at break (EB), elongation shows flexibility of the film when subjected to mechanical stress and tension and Young's modulus (YM) [25].

Fig. 1 indicates that increasing the phycocyanin increased tensile strength from 0.98±0.05 MPa to 41.96±0.125 MPa, but decreased to control.

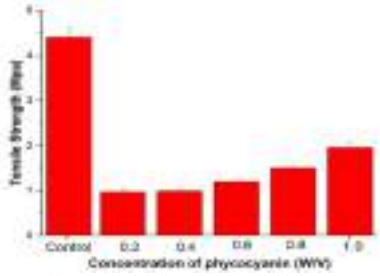

Fig. 1 Tensile strength of sago starch films incorporated phycocyanin Bars represent mean (n = 10) ± SD.

Fig.2 while decreased the percentage of elongation at break from 43.98±0.07 to 25.12±0.705, increased to control increase flexibility of films.This result is consistent with several reports [26].

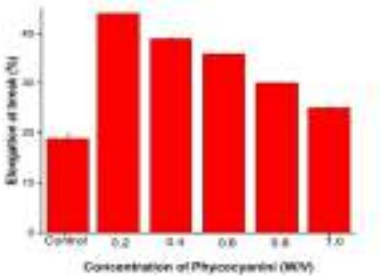

Fig. 2. Elongation at break of sago starch films incorporated phycocyanin. Bars represent mean (n = 10) ± SD.

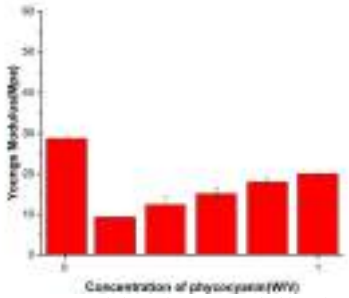

Fig. 3. Young's modulus of sago starch films incorporated phycocyanin. Bars represent mean (n = 10) ± SD.

Results showed that by increasing the amount of phycocyanin to film structure TS and YM significantly decreased and EB of the sago starch films significantly increased. It is likely phycocyanin plays a role as plasticizing agent and improves the flexibility of the starch films. Such behavior of other EOs reported by other researchers [27].

4. Conclusion

The results demonstrated that films containing phycocyanin (0.2, 0.4, 0.6, 0.8 and 1.0) had a good tensile strength and Youngs modulus decreased and elongation at break increased when percentage of incorporated extract in the film increased

5. References

[1] F.E. Ehivet, B. Min, M.K. Park, J.H. Oh, Journal of Food Science 76 (2011) C178–C184.

[2] V. Siracusa, P. Rocculi, S. Romani, M.D. Rosa, Trends in Food Science and Tech- nology 19 (2008) 634–643.

[3] G. Robertson, State-of-the-art biobased food packaging materials, in: E.Chiellini (Ed.), Environmentally Compatible Food Packaging, Woodhead Publishing, Cambridge, UK, 2008, pp. 3–28.

[4] G. Davis, J.H. Song, Industrial Crops and Products 23 (2006) 147–161.

[5] A. Sorrentino, G. Gorrasi, V. Vittoria, Trends in Food Science and Technology 18 (2007) 84–95.

[6] C.N. Cutter, Meat Science 74 (2006) 131–142.

[7] S. Imam, G. Glenn, B.-S. Chiou, J. Shey, R. Narayan, W. Orts, Types, Production and Assessment of Biobased Food Packaging Materials, in: E. Chiellini (Ed.), Environmentally Compatible Food Packaging, Woodhead Publishing, Cambridge,UK, 2008, pp. 29–62.

[8] M. Maizura, A. Fazilah, M.H. Norziah, A.A. Karim, Journal of Food Science 72(2007) C324–C330.

[9] J. Lorcks, Polymer Degradation and Stability 59 (1998) 245–249.

[10] D. Lourdin, G.D. Valle, P. Colonna, Carbohydrate Polymers 27 (1995)261–270.

[11] Y. Takahashi, T. Kumano, S. Nishikawa, Macromolecules 37 (2004) 6827–6832.

[12] Y. Zhang, Z. Liu, J. Han, Starch-based edible films, in: E. Chiellini (Ed.), Environ- mentally Compatible Food Packaging, Woodhead Publishing, Cambridge, UK,2008, pp. 108–136.

[13] M.O. Nisperos-Carriedo, Edible coatings and films based on polysaccharides, in:J.M. Krochta, E.A. Baldwin, M.O. Nisperos-Carriedo (Eds.), Edible Coatings and Films to Improve Food Quality, Technomic Publishing Company, Inc., Lancaster,1994, pp. 305–335.

[14] J. Rankin, I. Wolff, H. Davis, C. Rist, Industrial and Engineering Chemistry Chemical and Engineering Data Series 3 (1958) 120–123.

[15] C. Pagella, G. Spigno, D.M. De Faveri, Food and Bioproducts Processing 80 (2002)193–198.
[16] F. Debeaufort, J.-A. Quezada-Gallo, A. Voilley, Critical Reviews in Food Scienceand Nutrition 38 (1998) 299–313.
[17] S. Quintavalla, L. Vicini, Meat Science 62 (2002) 373–380.
[18] F.B. Ahmad, P.A. Williams, J.-L. Doublier, S. Durand, A. Buleon, CarbohydratePolymers 38 (1999) 361–370.
[19] M.N. Abdorreza, M. Robal, L.H. Cheng, A.Y. Tajul, A.A. Karim, LWT – Food Sciencea and Technology 46 (2012) 135–141.
[20] M. Aminian, A.M. Nafchi, M. Bolandi, A.K. Alias, Starch/Stärke 65 (2013)686–693.
[21] R. Bhat, M.-T. Liong, M.N. Abdorreza, A.A. Karim, International Journal of Food Properties 16 (2012) 1371–1379.
[22] M.N. Abdorreza, L.H. Cheng, A.A. Karim, Food Hydrocolloids 25 (2011) 56–60.
[23] M. Anker, M. Stading, A.M. Hermansson, Journal of Agricultural and Food Chemistry 47 (1999) 1878–1886.
[24] ASTM, Annual book of ASTM standards, 2010, Philadelphia, PA.
[25] A. Mohammadi Nafchi, A.A. Karim, Journal of Nano Research 25 (2013) 90–100.
[26] ASTM, Annual book of ASTM standards, 2009, Philadelphia, PA.
[27] A.M. Nafchi, R. Nassiri, S. Sheibani, F. Ariffin, A.A. Karim, Carbohydrate Polymers 96 (2013) 233–239.

29TH IRANIAN ORGANIC CHEMISTRY CONFERENCE
1_3 NOV, 2023
UNIVERSITY OF QOM, IRAN

Anti-corrosive eco-friendly UV-curable polyurethane acrylate/carbon quantum dots coating

Abbas Madhi[1], Shima Bahrami[2], Amir Hossein Madhi[3]*

[1]*Color Technology Incubator, Institute for Color Science and Technology, Tehran, Iran, abbas.madhi@semnan.ac.ir*
[2]*Non-Communicable Disease Research Center, Shiraz University of Medical Sciences, Shiraz, Iran, bahramishima31@gmail.com*
[3]*Faculty of Natural Resources and Environment, Islamic Azad University Science and Research Branch, Tehran, Iran, amirmadhi99@gmail.com*

Abstract - One of the major applications of the polymer nanocomposite coatings is to protect the metal surfaces against corrosion prosses and prevent them from harmful effects of this phenomenon. The main goal of this research was the synthesis of UV-curable polyurethane acrylate/carbon quantum dots (PUA/CQDs) coating and the investigation of the corrosion resistance properties of the resulting nanocomposite. To perform this, carbon quantum dots 0.5wt% was added to urethane acrylate resin and PUA/CQDs 0.5wt% nanocomposite coating was prepared. For the step subsequent to this, anti-corrosive features of the pure polymer coating and the coating with CQDs were evaluated by salt spray test. The results confirmed the improved corrosion resistance of the resulting nanocomposite.

Keywords: Polyurethane acrylate, eco-friendly polymer, nanocomposite coatings, anti-corrosion

1. Introduction

Polymer coatings are applied to metal substrates to prevent the harmful effects of corrosion. The anti-corrosion efficiency of polymer coatings depends on factors such as adhesion to metal, cross-linking density, type and amount of nanofiller. The use of these coatings increases the durability of the metal surfaces modified with them by protecting against the triggers of metal destruction and resisting top corrosion. These compounds reduce the rate of metal corrosion by creating a protective coating on steel surfaces. Anti-corrosion polymer coatings are most widely used in the oil, gas, petrochemical, and power plant industries to protect the installations of these industries from damage caused by chemicals and corrosive environmental factors and prevent the leakage of compounds into the environment [1].

Polyurethanes are used in making transparent and flexible coatings, adhesives, and various applications due to their excellent properties such as high mechanical, chemical, and thermal resistance. In recent years, the use of UV-curable polyurethanes has attracted the attention of industries and researchers due to the high speed of the process, removal of dangerous organic solvents and compatibility with the environment, high speed of curing at low temperature, and energy saving [2].

CQDs are zero-dimensional particles with a diameter of less than 20 nm, which are prepared from the oxidation of carbon sources such as fluorine, starch, citric acid, and graphite by various methods such as acid oxidation, pyrolysis, and electrochemistry. CQDs can have various applications due to properties such as solubility in water, biocompatibility, and excellent optical properties such as the ability to absorb ultraviolet rays [3,4]. Smart coatings have the properties of corrosion protection, resistance to acids, and photo-responsive properties [5]. The use of CQDs in the synthesis of polymer nanocomposites can be a suitable idea for the production of smart coatings as nano fillers to improve the performance of the polymer coating against corrosion factors [6,7].

In this research, castor oil was used as a natural and environmentally friendly polyol for synthesis of UV-curable polyurethane acrylate resin. Also, by adding CQDs to polyurethane resin and UV-curing method, a eco-friendly nanocomposite with the ability of resistance to corrosive agents was made.

2. Materials and Methods

2.1. Materials and methods

Isophorone diisocyanate (IPDI), 2-hydroxyethyl methacrylate (HEMA), dibutyltin dilaurate (DBTDL), triethanolamine (TEA), dimethylformamide (DMF), benzophenone, and acetone were all supplied from Merck. Trimethylpropanetriacrylate (TMPTA) was purchased from Sigma Aldrich. Castor oil (CO) was bought from a local market.

In order to perform the corrosion testing, the coatings were put in a salt spray device with ASTM B117 standard for 300 h.

2.2. Synthesis of PUA/CQDs nanocomposite

CQDs was synthesized using citric acid and prepared according to the method mentioned in reference [8,9]. Synthesis and characterization of UV-curable urethane acrylate oligomer using IPDI, CO, and HEMA monomers were done according to the previous work [8]. An amount of 0.1 g of CQDs was added to 3 mL of DMF solvent in a beaker. This mixture was dispersed for 20 min by an ultrasonic probe and 1 h by magnetic stirrer. In two beakers, a mixture of 7 g of urethane acrylate oligomer and 3 g of TMPTA as a diluent was added separately.

The aforementioned CQDs mixture was added to one of these beakers and the other beaker remained free of CQDs as the blank sample. The reaction mixture was stirred for 2 hours at room temperature. Next, 0.05 g of benzophenone and 0.05 g of triethanolamine were added to each of the reaction containers and stirred for 5 minutes at room temperature. Then, films with a thickness of 0.2 mm were molded by a film applicator. To remove the solvent, the molds were placed at room temperature for 12 hours. Then, each of the molds was exposed to the ultraviolet lamp (Hg, 1000W) for 2 min at room temperature and the curing process was done. According to the content of CQDs, the resulting films were coded as PUA/CQDs 0wt% (blank), and PUA/CQDs 0.5wt%. Figure 1 presents the synthesis steps of PUA/CQDs nanocomposite coating.

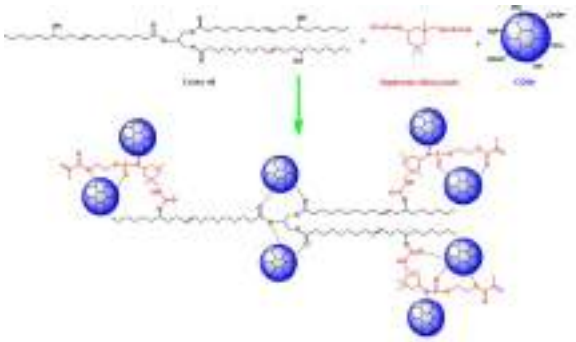

Fig. 1. Synthesis steps of PUA/CQDs nanocomposite coating.

3. Results and Discussion

3.1. Corrosion protection performance

The Anti-corrosive behavior of the coatings was assessed dependent on the degree of rusting and scribe failure on the basis of ASTM standards with D1654-05 for evaluation the scribe failure intensity including a range of 0-10 that 10 symbolizes the coatings without scribe and 0 stands for the coatings undergoing highest degree of scribe failure, and ASTM D610-01 to analyze the rusting intensity.

The results obtained from the salt spray test are shown in Figure 2 and Table 1. In the blank film, visual evaluation of the photographic reference standards indicated an increase in the amount of rust at the rusting scratched surface compared to the film reinforced with CQDs.

The filling of holes in the polymer matrix by CQDs and the establishment of hydrogen bonds and van der Waals forces at the steel/polymer interface cause strong adhesion. Also, CQDs can trap and reduce the oxygen dispersed in the damaged area of the coating, thus preventing the development of corrosion phenomenon in the scratched area. In the blank film, corrosive agents such as chloride ions penetrate through the coating to a high degree, and as a result, the corrosion rate increases. Figure 3 displays schematically the anti-corrosive mechanism of the PUA/CQDs coating against corrosive agents.

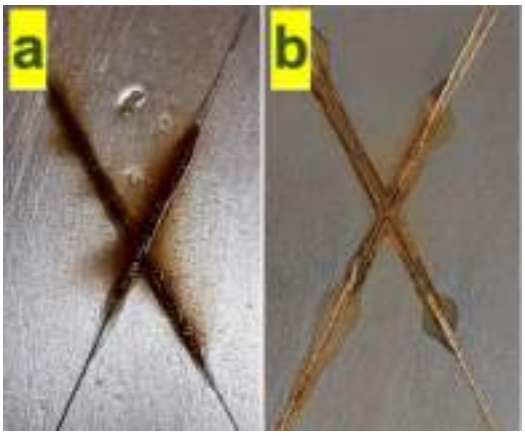

Fig. 2. Corrosion resistance results images for: (a) blank films and (b) PUA/CQD coatings.

Table 1. Corrosion resistance properties of blank and PUA/CQDs coating

Coatings	Scribe failure (rating number)	Rust grades
PUA (blank)	4	4
PUA/CQDs	6	6

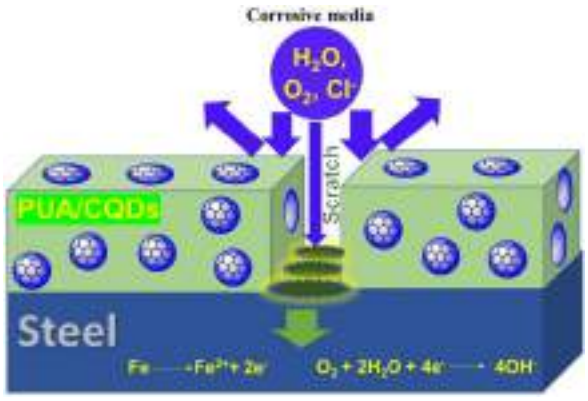

Fig. 3. Schematic mechanism of anti-corrosion PUA/CQD coatings.

4. Conclusion

The main goal of this work was to produce a eco-friendly UV-curable polyurethane acrylate nanocomposite reinforced with CQDs and to

investigate the resistance properties of this coating against corrosive agents. The obtained results showed that CQDs in the role of a nano-strengthening agent increased the resistance of the nanocomposite coating against corrosive agents. This coating with its capabilities can have special applications in the electronics, aircraft, automotive, and construction industries.

References

[1] A. Madi. Polym-plast. Tech. Mat. 62 (2023) 403-418
[2] A. Madhi, B. Shirkavand Hadavand, J Compos Mater. 54 (2020) 101-110
[3] A. Madi, J. Compos. Mater. 57 (2023) 2437-2450
[4] A. Madi, B. Shirkavand Hadavand, Polym-plast. Tech. Mat. 61 (2022) 117-130
[5] A. Madi, B. Shirkavand Hadavand, J. Appl. Chem. 41 (2022) 2202-2212
[6] A. Madhi, B. Shirkavand Hadavand, A.H. Madhi, Fuller. Nanotub. Carbon. Nanostructures. DOI: 10.1080/1536383X.2023.2226272
[7] A. Madi. Polym-plast. Tech. Mat. 62 (2023) 403-418
[8] A. Madi, B. Shirkavand Hadavand, J Compos Mater. 56 (2022) 2201-2210
[9] A. Madi, B. Shirkavand Hadvand, Iran. J. Chem. Chem. Eng. 41 (2022) 2202-2212.

29TH IRANIAN ORGANIC CHEMISTRY CONFERENCE
1_3 NOV, 2023
UNIVERSITY OF QOM, IRAN

The Interaction of Imidazolium and Ammonium-Based Ionic Liquids (ILs) with Fluorographene (FG) Surface: A DFT Study

Mehdi Shakourian-Fard[1], Hamid Reza Ghenaatian[2] and Vali Alizadeh[3]*

[1]*Department of Chemical Engineering, Birjand University of Technology, Birjand, P.O. Box 97175/569, Iran.*
[2]*Department of Physics, Jahrom University, Jahrom, P.O. Box 74135-111, Iran, Ghenaat@jahromu.ac.ir.*
[3]*Department of Petroleum Engineering, Faculty of Engineering, University of Garmsar, PO Box:3581755796, Garmsar, Iran.*

Abstract

In this work, the interaction of imidazolium and ammonium-based ionic liquids (ILs) with fluorographene (FG) surface is studied using density functional theory (DFT) calculations. The binding energy (ΔE_b) values for adsorption of these ILs on the FG surface are calculated and compared with those on the graphene and hexagonal boron nitride surfaces. Furthermore, the charge transfer values in the FG…IL complexes and the reactivity parameters of FG surface and its complexes with the ILs are investigated.

1. Introduction

Fluorographene (FG) is a fluorocarbon derivative of graphene: all carbon atoms are sp^3 hybridized through the incorporation of polar C-F bonds [1]. Fluorographene can be used as a tunnel barrier and as a high-quality insulator or barrier material for organic electronics. It can also act as a wide-gap semiconductor in light-emitting diodes (LEDs) and displays [1]. Fluorographene can be readily prepared from graphene oxide *via* photochemical fluorination or plasma treatment [2]. Liquid-phase exfoliation of 2D materials is one of the most promising routes for their production on a large scale. Recently ionic liquids (ILs) have been used to mediate exfoliation as they also improve the electronic behaviour of the resulting nanosheets and so can be used as both an exfoliant during manufacture, and as a coating for the eventual application [1]. The interactions at the interfacial layers between ionic liquids and nanomaterials is of paramount importance for the synthesis (exfoliation) of these 2D sheets [1], and for determining their optoelectronic appropriateness for emerging energy applications including supercapacitors, ionic-liquid gated transistors, light-emitting diodes (LEDs) and displays [1,3]. Therefore, in the present report, we determine the specifics of the interaction of ionic liquids with fluorographene and compare the affinities of different ionic liquids (both 1-butyl-3-methylimidazolium $[Bmim]^+$, and butyltrimethylammonium $[Btma]^+$-based ILs) for the fluorographene surface using density functional theory (M06-2X/cc-pVDZ) method (Fig. 1). Finally, the emergent properties obtained in this study are compared with those we have previously calculated for graphene and boron nitride surfaces [4,5] to show the complementarity of these three systems for developing innovative materials for 2-D semiconductor applications.

2. Computational details

$C_{54}F_{72}$ was chosen as a suitable initial model for fluorographene (FG). This FG model contains 54 carbon and 72 fluorine atoms. The edge carbon atoms are passivated with fluorine atoms. All geometries of the FG model, ionic liquids (ILs; [Bmim][Y] and [Btma][Y] (Y = BF_4^-, PF_6^-, and Tf_2N^-) and the resulting FG…IL complexes were optimized with M06-2X/cc-pVDZ level of theory. The binding energies (ΔE_b) were calculated using equation 1:

$$\Delta E_b = E_{FG...IL} - (E_{FG} + E_{IL}) + E_{BSSE} \qquad \text{(Eq 1)}$$

Where E_{FG}, E_{IL} and $E_{FG...IL}$ denote the total energies of the FG model, ILs and $E_{FG...IL}$ complexes, respectively. For optimized structures, the last term ($E_{FG...IL}$) was corrected according to basis set superposition error (BSSE) through the counterpoise procedure.

The ChelpG charge analysis was carried out to quantify the charge transfer between FG model and ILs. All the calculations were carried out using the Gaussian 09 suite of programs [6]. The quantum theory of atoms in molecules (QTAIM) was used to characterize the strength of interaction between FG model and ILs. Finally, the global molecular descriptors such as HOMO-LUMO energy gap (E_g; $E_g = \varepsilon_{(LUMO)} - \varepsilon_{(HOMO)}$), Fermi energy level ($E_{FL}$), electronic chemical potential (μ; $\mu = (E_{HOMO} + E_{LUMO})/2$), chemical hardness ($\eta$; $\eta = (E_{LUMO} - E_{HOMO})/2$), and electrophilicity index (ω; $\omega = \mu^2/2\eta$) were calculated for the FG model and then the effect of IL adsorption on these parameters was investigated.

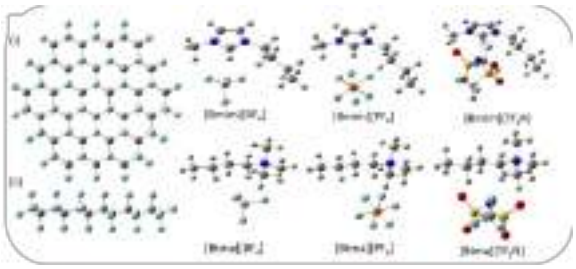

Fig. 1. Optimized geometries of fluorographene (FG) model and ionic liquids at M06-2X/cc-pVDZ level: (i) top view and (ii) side view.

3. Results and discussion

To find the most stable geometries of FG…IL complexes, the optimized ILs were allowed to approach the FG surface through all possible binding modes. Then, these structures were optimized at the M06-2X/cc-pVDZ level of theory. Finally, the lowest energy geometries for each FG…IL complex were identified and introduced as the most stable complexes in Fig. 2.

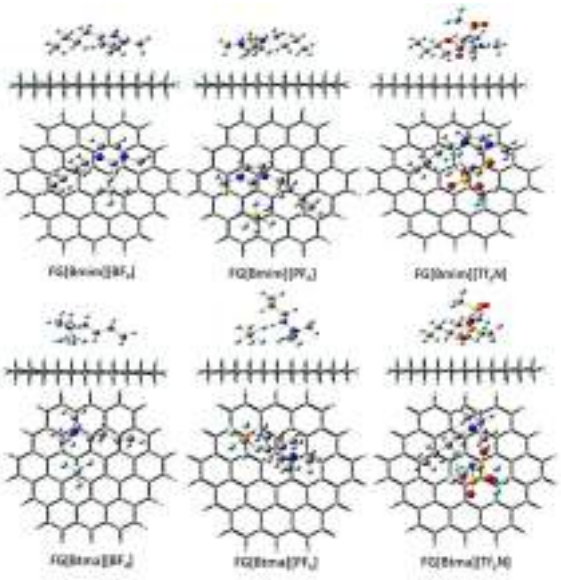

Fig. 2. The most stable geometries of FG…IL complexes.

Lacking graphene's π-system, the interactions with FG are certainly expected to be different from graphene surface and are comprised of a series of weak interactions, including C-H⋯F-C, S=O⋯F-C, C-F⋯F-C and C (IL site)⋯F-C (FG surface) interactions. To obtain more insight into the exact strength of these key interactions, QTAIM analysis was used. The sum of electron density values at the bond critical points (BCPs) between the cations and anions of ILs and FG surface are summarized in Table 1. As seen from Table 1, for FG…[Bmim][Y], the ∑ρ(r) values for the cation are greater than those of anion in all cases; while in the case of FG…[Btma][Y] complexes, ∑ρ(r) values for interaction of the anions are greater than that of the $[Btma]^+$ cation except in the case of the $[Tf_2N]^-$ anion. This discrepancy is due to the stronger affinity of the $[Bmim]^+$ cation than the $[Btma]^+$ cation for the FG surface. Independent of the identity of the cation, the anions show the same order of affinity ($[PF_6]^- > [BF_4]^- > [Tf_2N]^-$).

As seen from Table 1, the ΔE_b values for adsorption of [Bmim][Y] (Y = BF_4^-, PF_6^-, and Tf_2N^-) ILs on the FG surface is higher than those of [Btma][Y] (Y = BF_4^-, PF_6^-, and Tf_2N^-) ILs. However, the rank order of adsorption of [Bmim][Y] and [Btma][Y] (Y = BF_4^-, PF_6^-, and Tf_2N^-) ILs on the FG surface is similar and as follows: [Y][Tf_2N] > [Y][PF_6] > [Y][BF_4] (Y = $Bmim^+$ and $Btma^+$).

Table 1. Thermodynamic parameters of FG surface and FG…IL complexes.

Structure	ΔE_b (kcal/mol)	$\sum\rho(r)_{(cation\ldots FG)}$	$\sum\rho(r)_{(anion..FG)}$
Fluorographene			
FG[Bmim][BF_4]	-2.02	0.0782	0.0558
FG[Bmim][PF_6]	-2.28	0.0825	0.0760
FG[Bmim][Tf_2N]	-2.31	0.0798	0.0544
FG[Btma][BF_4]	-1.68	0.0629	0.0786
FG[Btma][PF_6]	-1.98	0.0556	0.079
FG[Btma][Tf_2N]	-2.18	0.0931	0.0746
Structure	[a]$\Delta q_{(Surface)}$ (e)	E_g (eV)	E_{FL} (eV)
Fluorographene		9.21	-6.25
FG[Bmim][BF_4]	-0.0898	7.55	-5.34
FG[Bmim][PF_6]	-0.0401	7.48	-5.55
FG[Bmim][Tf_2N]	-0.1824	7.0	-5.29
FG[Btma][BF_4]	-0.0843	9.07	-6.03
FG[Btma][PF_6]	0.0294	8.79	-6.19
FG[Btma][Tf_2N]	-0.0022	7.12	-5.38

[a] The charge on the fluorographene (FG) surface is zero before adsorption of ILs.

We also compared the trend of these ILs for adsorption on the FG surface with respect to graphene and hexagonal boron-nitride surfaces reported in our previous works (Fig. 3a). The adsorption of ILs to the surfaces, regardless of IL identity, is generally found to be in order of graphene> hexagonal boron-nitride> fluorographene, indicating that fluorinating the graphene surface strongly decreases the binding energy of ILs. The negative sign of induced charge on the FG surface ($\Delta q_{(Surface)}$) indicates that the charge is transferred from the ILs to the FG surface with the exception of FG…[Btma][PF_6] complex.

Our results indicate that the Fermi energy level of the FG surface rises upon adsorption of ILs. As seen from Fig. 3b, the E_g of the FG surface significantly decreases, meaning leading to an enhancement in electrical conductivity upon adsorption of ILs. The

greater the amount of binding energy, the greater the decrease in the E_g value of the FG surface with adsorption of ILs. According to our results, the FG…[Btma][Y] complexes have bigger E_g values, higher η values and lower reactivities than the FG…[Bmim][Y] complexes. Electronic property calculations show that the adsorption of ILs increases the μ value of FG surface, while the η and ω values of FG surface decrease upon adsorption of ILs.

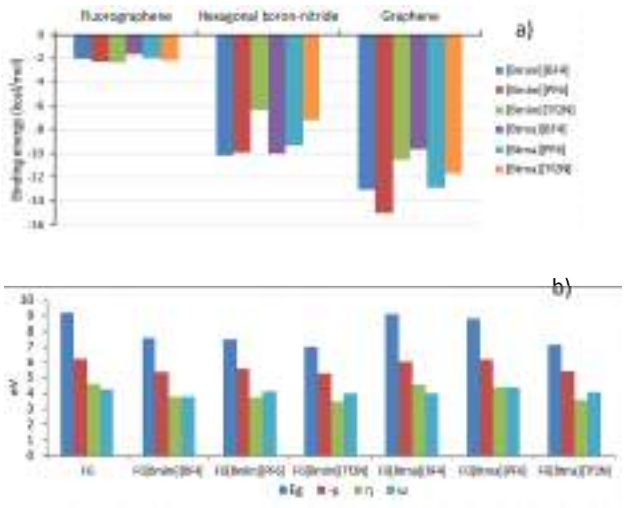

Fig. 3. a) Comparison of binding energies of fluorographene, graphene and hexagonal boron-nitride surfaces with ILs, b) Comparison of E_g, -μ, η, and ω values (in eV) of FG surface and different FG…IL complexes.

4. Conclusions

The adsorption of [Bmim][Y] and [Btma][Y] (Y = BF_4^-, PF_6^-, and Tf_2N^-) ionic liquids (ILs) on the fluorographene (FG) surface and the corresponding changes in the FG electronic structure have been investigated using DFT based methods. Binding energy (ΔE_b) calculations show that the fluorination of graphene surface significantly decreases the adsorption strength of ILs with respect to graphene and hexagonal boron nitride surfaces such that for almost any IL, the binding affinities follow a predictable trend: $\Delta E_{b\,(\text{Graphene…IL})} > \Delta E_{b\,(\text{Hexagonal boron-nitride…IL})} > \Delta E_{b\,(\text{Fluorographene…IL})}$.

Our results show that the HOMO-LUMO energy gap (E_g) of the FG surface significantly decreases, meaning leading to an enhancement in electrical conductivity upon adsorption of ILs. The greater the amount of binding energy, the greater the decrease in the E_g value of the FG surface with adsorption of ILs. According to our results, the FG…[Btma][Y] complexes have bigger E_g values, higher η values and lower reactivities than the FG…[Bmim][Y] complexes. Electronic property calculations show that the adsorption of ILs increases the μ value of FG surface, while the η and ω values of FG surface decrease upon adsorption of ILs.

5. References

[1] Nair, R.R., Ren, W., Jalil, R., Riaz, I., Kravets, V.G., Britnell, L., Blake, P., Schedin, F., Mayorov, Yuan, S., Katsnelson, M.I., Cheng, H.M., Strupinski, W., Bulusheva, L.G., Okotrub, A.V., Grigorieva, I.V., Grigorenko, A.N., Novoselov, K.S. and Geim, A.K., "Fluorographene: A two-dimensional counterpart of teflon", Small, 6, 2877-2884 (2010).

[2] Gong, P., Wang, Z., Li, Z., Mi, Y., Sun, J., Niu, L., Wang, H., Wang, J. and Yang, S., "Photochemical synthesis of fluorinated graphene via a simultaneous fluorination and reduction route", RSC Adv., 3, 6327-6330 (2013).

[3] Simon, P. and Gogotsi, Y., "Materials for electrochemical capacitors", Nat. Mater., 7, 845-854 (2008).

[4] Shakourian-Fard, M., Kamath, G. and Jamshidi, Z., "Trends in physisorption of ionic liquids on boron-nitride sheets", J. Phys. Chem. C, 118, 26003-26016 (2014).

[5] Shakourian-Fard, M., Jamshidi, Z., Bayat, A. and Kamath, G., "Meta-hybrid density functional theory study of adsorption of imidazolium- and ammonium-based ionic liquids on graphene sheet", J. Phys. Chem. C, 119, 7095-7108 (2015).

[6] Frisch, M.J., et al., Gaussian 09, Revision D. 1, Gaussian, Inc., Wallingford, CT, 2010.

29TH IRANIAN ORGANIC CHEMISTRY CONFERENCE
1_3 NOV, 2023
UNIVERSITY OF QOM, IRAN

Adsorption of Cadmium (Cd), Mercury (Hg), and Lead (Pb) Metal Atoms on the Graphene and Heteroatom Doped Graphene Surfaces: A DFT Study

Hamid Reza Ghenaatian[1], Mehdi Shakourian-Fard[2], and Vali Alizadeh[3]*

[1]*Department of Physics, Jahrom University, Jahrom, P.O. Box 74135-111, Iran, Ghenaat@jahromu.ac.ir.*
[2]*Department of Chemical Engineering, Birjand University of Technology, Birjand, P.O. Box 97175/569, Iran.*
[3]*Department of Petroleum Engineering, Faculty of Engineering, University of Garmsar, PO Box:3581755796, Garmsar, Iran.*

Abstract

The adsorption of toxic heavy metals (THMs), including cadmium (Cd), mercury (Hg), and lead (Pb) on the graphene (G) and six sulfur and nitrogen/sulfur co-doped graphene surfaces (G@1N@1S, G@1N@2S, G@2N@1S, G@1S, G@2S, G@3S) has been studied using electronic structure methods. The doping of graphene surface with the nitrogen and sulfur atoms increases the adsorption energies of THMs. The strongest interaction is seen with adsorption of Pb atom on the surfaces, following the order Pb> Cd> Hg and is confirmed by the atoms in molecules (AIM) analysis. The free energy of adsorption calculation shows that the adsorption process of Pb atoms on the surfaces is exothermic and proceeds spontaneously, while the nature of adsorption of Cd and Hg atoms is endothermic. Significant changes in the electronic structure of the surfaces are seen with adsorption of THMs. A significant change in the HOMO-LUMO energy gap (E_g) of the surfaces is observed with adsorption of Pb atoms, in contrast to Cd and Hg atoms counterparts.

1. Introduction

Heavy metals are currently one of the significant environmental pollutants and their toxicity is a serious threat for environment (air, water and soil) and human health [1]. Therefore, the concentration of heavy metals should be controlled below the standard levels. Heavy metals such as cadmium (Cd), mercury (Hg), and lead (Pb) are regarded as a longstanding environmental contaminant, and should be separated from the environment, drinking water, food products and biological fluids.

Recently, graphene, as a two-dimensional (2D) material, has sparked enormous scientific interest in sensing platforms [2] due to its significant characteristics including a large surface area and particular electronic properties, high signal-to-noise ratio and high electron-transfer rate [3]. A major problem of graphene surface towards THMs adsorption is its poor sensitivity [4]. Therefore, in order to obtain an effective adsorption of THMs on the graphene surface, the graphene surface should be functionalized/modified to provide the necessary reactive surface area. Interestingly, irradiation of graphene with electrons or ions can generate point defects during the growth of graphene nanosheet [5]. The presence of defects on the graphene surface enhances chemical reactivity and sensitivity of graphene towards active chemical species. In order to gain more insight into the effect of nitrogen and sulfur doping in the graphene surface on the THMs adsorption, the interaction mechanism between sulfur and nitrogen/sulfur co-doped graphene surfaces (Fig. 1) and THMs (Cd, Hg and Pb) is investigated using density functional theory (DFT) calculations. On the other hand, the main aim of this study is to understand how the Cd, Hg and Pb atoms will affect structural and electronic properties of sulfur and nitrogen/sulfur co-doped graphene surfaces.

2. Computational methods

In this work, all the calculations have been carried out by the density functional theory (DFT) method as implemented in the Gaussian 09 suite of programs [6]. Geometry optimization and property calculations of the graphene (G) and sulfur and nitrogen/sulfur co-doped graphene surfaces (G@1N@1S, G@1N@2S, G@2N@1S, G@1S, G@2S, G@3S) as well as their complexes with THMs were carried out using the M06-2X functional with a 6-311G(d,p) basis set for carbon, nitrogen, sulfur and hydrogen atoms as well as Def2-TZVPP basis set for the THMs. The adsorption energies (E_{ads}) between THMs and the surfaces are calculated according to the following equation:

$$E_{ads} = E_{surface\text{-}metal} - (E_{metal} + E_{surface}) \qquad (1)$$

where $E_{surface\text{-}metal}$ corresponds to the energy of surface-metal systems, $E_{surface}$ corresponds to the energy of graphene and sulfur and nitrogen/sulfur co-doped graphene surfaces and E_{metal} corresponds to the energy of isolated THMs, respectively. The adsorption energies were corrected by basis set superposition errors (BSSEs) calculated with the Boys and Bernardi counterpoise method [7]. The enthalpy of adsorption (ΔH_{ads}) and the free energy of adsorption (ΔG_{ads}) of the surface-THM complexes were calculated at 298.15 K using equation 2:

$$\Delta X_{ads} = X_{(surface\text{-}THM)} - (X_{(THM)} + X_{(surface)}) \qquad (2)$$

X = H (enthalpy) or G (free energy)

where $X_{(surface\text{-}THM)}$ is the enthalpy (or free energy) of the complex of THM with the surface, $X_{(THM)}$ is the enthalpy (or free energy) of the THM atom, and $X_{(surface)}$ is the

enthalpy (or free energy) of the graphene or sulfur and nitrogen/sulfur co-doped graphene surface, respectively. The entropy (S) of adsorption (ΔS_{ads}) was also calculated at 298.15 K using the calculated ΔH_{ads} and ΔG_{ads} values, according to the following equation:

$$\Delta S_{ads} = \frac{(\Delta H_{ads} - \Delta G_{ads})}{298.15} \qquad (3)$$

Hirshfeld charge analysis [8] was done to calculate the charge transfer during complex formation of the surfaces and THMs. The theory of Atoms in Molecules (AIM) [9] was employed to characterize the strength of interaction between the surfaces and THMs using the AIM2000 package [10]. The HOMO-LUMO energy gap of the surfaces and their complexes is defined as Eq. (4):

$$\text{HOMO-LUMO energy gap} = E_{LUMO} - E_{HOMO} \qquad (4)$$

where the E_{HOMO} and E_{LUMO} terms are the energy of the highest occupied molecular orbital (HOMO) and the lowest unoccupied molecular orbital (LUMO) of the surfaces or their complexes, respectively [11].

3. Results and discussion

3.1 Adsorption of Cd, Hg and Pb atoms on the surfaces

In order to investigate the effect of sulfur and nitrogen/sulfur co-doping in the graphene surface on adsorption of toxic heavy metals, six different optimized configurations of sulfur and nitrogen/sulfur co-doped graphene surfaces are built from pristine graphene model and shown in Fig. 1. To construct these configurations, firstly, a perfect graphene model with 54 carbon atoms and 18 hydrogen atoms ($C_{54}H_{18}$) is built as the representation of pristine graphene (G) model. Hydrogen termination is used to saturate the boundaries of graphene model [12, 13]. Then, the vacancy sites in the six configurations are built by removing carbon atoms and replacing nitrogen and sulfur atoms. It should be noted that the G@1N@1S and G@1N@2S surfaces adopts a doublet, while a singlet is taken for theG@2N@1S, G@1S, G@2S and G@3S surfaces. Geometry optimization of these surfaces shows that the sulfur (S) dopant protrudes outside from the surfaces, while nitrogen (N) dopant is retained inside the surfaces. The presence of S atoms outside the defective graphene surfaces could be due to the large size of S atoms and the steric hindrance between them and other atoms at the defect sites, including C, N and S atoms. In fact, other atoms push the S atoms outside the defective graphene surfaces and lead to the sp^3 hybridization of the S dopant. This induces the local structure curvature on the surfaces.

In order to find the equilibrium structures of surface-THM complexes and the adsorption position of THMs, the THMs were placed directly above the center of vacancy site of the sulfur and nitrogen/sulfur co-doped graphene surfaces and then the structures were allowed to fully relax at the M06-2X/6-311G(d,p)/Def2-TZVPP level of theory. It should be noted that the starting coordinates were the same for Cd, Hg and Pb metals in the surface-metal complexes before geometry optimization. Therefore, it is reasonable to assume that adsorption patterns of THMs on the surfaces only originate from the unique metal properties and the specific interaction between surfaces and metals.

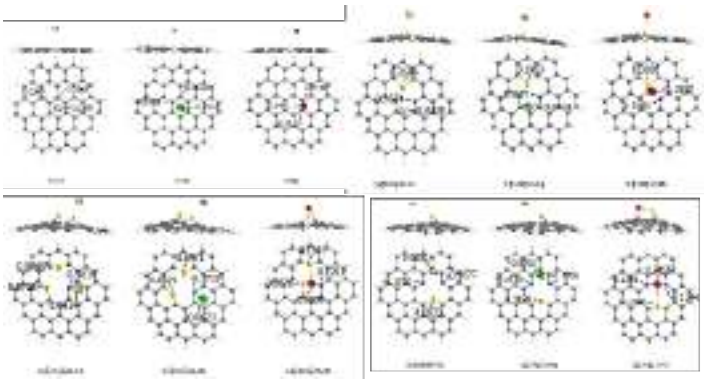

Fig. 1. Optimized structures of pristine graphene and sulfur and nitrogen/sulfur co-doped graphene surfaces.

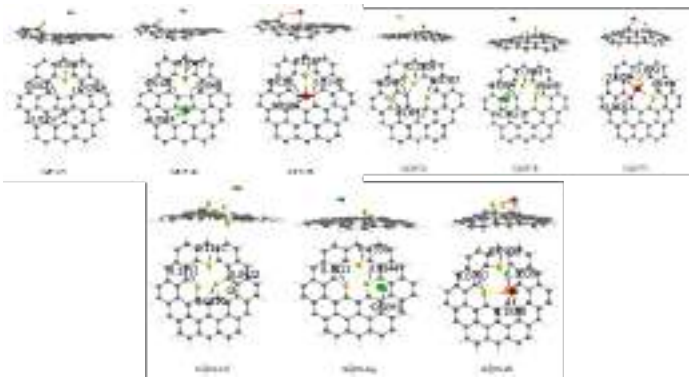

Fig. 2. The most stable structures of surface-THM complexes with the Hirshfeld atomic charges.

The optimized structures of surface-THM complexes are depicted in Fig. 2, and the corresponding geometric properties and adsorption energies are listed in Table 2. As can be seen from Fig. 2, the adsorption of Cd, Hg and Pb atoms on graphene surface suggests no significant structural changes in the graphene surface, due to the weak interaction of THMs with the graphene surface that is predominantly controlled by van der Waals (vdW) interactions. Therefore, the graphene surface retains its planar structure upon adsorption of THMs. Our calculations reveal that the Cd and Hg atoms are adsorbed on the G surface at the center of the hexagonal ring (the hollow site) with the equilibrium distances of 3.31 Å and 3.25 Å, respectively, while the Pb atom is adsorbed above the center of a C–C bond (the bridge site) with the equilibrium distance of 3.0 Å (Table 1). It is interesting to note that the THMs adsorption onto sulfur and nitrogen/sulfur co-doped graphene surfaces induces more buckling into the surfaces (Fig. 2). Table 1 summarizes the calculated dipole moment values of the surfaces and their complexes with THMs. As seen from these values, the creation of defects containing nitrogen and sulfur atoms in the graphene surface increases the dipole moment value of graphene surface. It should be noted that the dipole moment values for the surfaces increase with adsorption of Cd, Hg and Pb atoms and follow the order surface-Pb> surface-Cd> surface-Hg. This is in good agreement with the sum of electron density ($\sum\rho(r)$) achieved from AIM analysis for stronger interaction of Pb atom with the surfaces than Cd and Hg toms (Table 1).

Table 1. HOMO and LUMO energies (E_{HOMO} and E_{LUMO}, respectively, in eV), HOMO-LUMO energy gap (in eV), equilibrium distance (d in Å), dipole moment (in Debye), and the sum of electron density ($\sum\rho(r)$ in a.u.) at the BCPs between the metal atoms and the surfaces.

Structure	E_{HOMO}	E_{LUMO}	HOMO-LUMO gap	d_{C-X} / d_{N-X}	Dipole moment	$\sum\rho(r)$
G	− 6.17	− 1.82	4.35		0.0	
G@3N@3S	− 4.84	− 1.9	2.94		0.0167	
G@3N@2S	− 5.11	− 2.11	3.05		2.9189	
G@2N@3S	− 5.06	− 2.06	3.0		1.4188	
G@2S	− 5.76	− 2.94	2.82		2.1696	
G@3S	− 5.42	− 2.05	3.37		1.0083	
G@3S	− 4.77	− 2.85	1.92		1.3564	
G–Hg	− 6.19	− 1.85	4.34	3.256	0.3370	0.0421
G–Cd	− 6.19	− 1.85	4.34	3.310	0.0015	0.0116
G–Pb	− 4.87	− 1.95	2.16	3.0	0.7956	0.0160
G@3N@3S–Hg	− 4.87	− 1.92	2.95	N(3.788), N(5.735)	1.1650	0.0147
G@3N@3S–Cd	− 4.87	− 1.93	2.94	S (3.977), N(3.887)	1.2070	0.0120
G@3N@3S–Pb	− 5.13	− 2.01	2.52	N(2.969), N(3.861)	1.4195	0.0344
G@3N@2S–Hg	− 5.17	− 2.14	3.05	S(4.088), N(5.391)	1.3085	0.0169
G@3N@2S–Cd	− 5.17	− 2.15	3.02	S(4.124), N(5.488)	1.3489	0.0142
G@3N@2S–Pb	− 4.91	− 2.38	2.53	S(2.681), N(2.488)	4.5624	0.1096
G@2N@3S–Hg	− 5.91	− 2.11	3.8	S(3.783), N(5.566)	2.4461	0.0048
G@2N@3S–Cd	− 5.91	− 2.11	3.8	S(5.871), N(5.679)	2.5226	0.0120
G@2N@3S–Pb	− 4.5	− 2.02	2.48	S(2.653), N(2.291)	6.7437	0.2997
G@3S–Hg	− 5.79	− 2.97	2.82	S(3.941), C(3.609)	2.6075	0.0132
G@3S–Cd	− 5.79	− 2.98	2.81	S(4.076), C(3.806)	2.7920	0.0112
G@3S–Pb	− 5.21	− 2.28	2.94	S(2.791), C(2.458)	4.8905	0.1661
G@2S–Hg	− 5.45	− 2.08	3.37	S(4.055), C(3.456)	2.1774	0.0087
G@2S–Cd	− 5.46	− 2.08	3.38	S(4.270), C(3.612)	2.2710	0.0071
G@2S–Pb	− 4.82	− 2.08	2.74	S(2.671), C(2.290)	2.6570	0.1981
G@3S–Hg	− 4.78	− 2.88	1.9	S(3.930), C(3.499)	1.9137	0.0282
G@3S–Cd	− 4.78	− 2.89	1.89	S(4.017), C(3.634)	1.9841	0.0220
G@3S–Pb	− 5.31	− 1.96	3.35	S(3.023), C(2.431)	2.1143	0.1867

The charge transfer (Q_{CT}) values between the Cd, Hg and Pb atoms and the surfaces were calculated through focusing on the net charge on the metal atoms in the complexes (Table 2).

Table 2. Adsorption energy (E_{ads} in kcal/mol), charge transfer (Q_{CT} in e), enthalpy of adsorption (ΔH_{ads} in kcal/mol), entropy of adsorption (ΔS_{ads} in kcal/mol.K), $T\Delta S_{ads}$ (in kcal/mol) and free energy of adsorption (ΔG_{ads} in kcal/mol).

Structure	E_{ads}	Q_{CT}	ΔH_{ads}	ΔS_{ads}	$T\Delta S_{ads}$	ΔG_{ads}
G-Hg	− 1.87	− 0.0551	− 1.16	− 0.02459	− 7.33151	6.17
G-Cd	− 3.61	0.0380	− 1.10	− 0.01812	− 5.40248	4.30
G-Pb	− 6.16	− 0.1481	− 7.76	− 0.02437	− 7.26592	− 0.49
G@3N@3S-Hg	− 3.48	− 0.0651	− 4.00	− 0.01980	− 5.66793	1.66
G@3N@3S-Cd	− 3.53	0.0338	− 3.84	− 0.01611	− 4.8032	0.97
G@3N@3S-Pb	− 37.53	0.1500	− 38.64	− 0.02212	− 6.59508	− 32.04
G@3N@2S-Hg	− 3.14	− 0.0623	− 4.75	− 0.02059	− 6.13891	1.38
G@3N@2S-Cd	− 4.77	0.0414	− 4.18	− 0.01888	− 5.62907	1.45
G@3N@2S-Pb	− 50.57	0.0809	− 52.81	− 0.02209	− 6.36511	− 44.45
G@2N@3S-Hg	− 3.80	− 0.0765	− 4.51	− 0.02021	− 6.02561	1.51
G@2N@3S-Cd	− 4.05	0.0251	− 4.59	− 0.01951	− 5.81666	1.22
G@2N@3S-Pb	− 46.37	0.2436	− 49.13	− 0.02217	− 9.59149	− 39.54
G@3S-Hg	− 3.89	− 0.0674	− 4.50	− 0.01916	− 5.71258	1.22
G@3S-Cd	− 3.91	0.0357	− 4.34	− 0.01813	− 5.40548	1.07
G@3S-Pb	− 63.04	0.2395	− 65.32	− 0.0207	− 9.15521	− 56.16
G@2S-Hg	− 3.93	− 0.0613	− 4.63	− 0.019	− 5.66485	1.03
G@2S-Cd	− 4.20	0.0422	− 4.59	− 0.01819	− 5.42335	0.84
G@2S-Pb	− 62.86	0.1389	− 65.49	− 0.02039	− 8.46648	− 57.02
G@3S-Hg	− 4.62	− 0.0841	− 5.67	− 0.02057	− 6.13295	0.46
G@3S-Cd	− 4.74	0.0422	− 5.48	− 0.02042	− 6.08927	0.61
G@3S-Pb	− 68.79	0.1580	− 72.01	− 0.02047	− 6.48933	− 65.52

$^{a}Q_{CT}$ is the charge transfer between the THMs and surfaces, obtained through calculation of Hirshfeld charge on the THMs in the surface–THM complexes

A negative value of Q_{CT} indicates that the metal atom gains electrons, while a positive value indicates that the surfaces gains electrons. As seen from Table 2, the charge transfer occurs from the sulfur and nitrogen/sulfur co-doped graphene surfaces to the Hg atoms in the surface-Hg complexes, while it happens from the Cd and Pb atoms to the surfaces in the surface-Cd and surface-Pb complexes. It is interesting to note that the magnitude of charge transfer between the Pb atom and the surfaces is higher than that of Cd and Hg atoms, following the order Pb> Hg> Cd. Furthermore, the greatest change in the HOMO-LUMO energy gap values of the surfaces is observed with adsorption of Pb atoms, while the adsorption of Cd and Hg atoms does not have much effect on the HOMO-LUMO energy gap value of the surfaces.

The negative values of adsorption energies (E_{ads}) listed in Table 2 indicate that the adsorption of Cd, Hg and Pb atoms on the surfaces is energetically favorable. Our results for adsorption of these atoms on the pristine graphene surface show that the Pb atom has the largest adsorption energy, following the order G-Pb (-6.16 kcal/mol)> G-Cd (-3.65 kcal/mol)> G-Hg (-1.87 kcal/mol). Comparison of the E_{ads} values of these atoms on the graphene and sulfur and nitrogen/sulfur co-doped graphene surfaces reveals that sulfur and nitrogen/sulfur co-doping at the defect sites in the graphene surface significantly increases the adsorption of THMs on the graphene surface.

Thermochemistry parameters, including the enthalpy of adsorption (ΔH_{ads}), entropy of adsorption (ΔS_{ads}) and free energy of adsorption (ΔG_{ads}) of THMs on the surfaces are calculated to understand the energetics associated with the adsorption and the possibility of such an adsorption process. The most favourable ΔH_{ads} values are observed for adsorption of Pb atoms, indicating the strong interaction between the Pb atom and the surfaces. Moreover, the ΔG_{ads} values are negative for the surface-Pb complexes, showing that the formation of these complexes is exothermic and proceeds spontaneously. However, the ΔG_{ads} values for the surface-Cd and surface-Hg complexes is positive, indicating that the adsorption process is endothermic in nature.

4. Conclusions

Our results indicate that nitrogen/sulfur co-doped graphene surfaces could be used for the chemical sensing of THMs. These results should encourage in development of defect engineering and functionalization of graphene sheets for selective heavy metal adsorption.

5. References

1. JM Harrison. *Science*, **226**, 11 (1984).
2. NH Bings, A Bogaerts, JAC Broekaert. *Anal Chem*, **78**, 3917 (2006).
3. MR Jamali, Y Assadi, F Shemirani, MRM Hosseini, RR Kozani, M Masteri-Farahani, et al. *Anal Chim*, **579**, 68 (2006).
4. S Agnoli, M Favaro. *J Mater Chem A*, **4**, 5002 (2016).
5. I Shtepliuk, V Khranovskyy, R Yakimova. *emicond Sci Technol*, **31**, 113004 (2016).
6. L Zhang, D Peng, R-P Liang, J-D Qiu. *Trends Anal Chem*, **102**, 280 (2018).
7. I Shtepliuk, NM Caffrey, T Iakimov, V Khranovskyy, IA Abrikosov, R Yakimova. *Sci Rep*, **7**, 3934 (2017).
8. Z Liu, Y Zhang, B Wang, H Cheng, X Cheng, Z Huang. *Appl Surf Sci*, **427**, 547 (2018).
9. I Shtepliuk, R Yakimova. *Phys Chem Chem Phys*, **20**, 21528 (2018).
10. R Yadav, C Dixit. *J Science: Adv Mat Devices*, **2**, 141 (2017).
11. F Banhart, J Kotakoski, AV Krasheninnikov. *ACS Nano*, **5**, 26 (2011).
12. GL Turdean. *Int J Electrochem*, **2011** (2011).
13. S Sahoo, SN Khanna, P Entel. *Appl Phys Lett*, **107**, 043102 (2015).

29TH IRANIAN ORGANIC CHEMISTRY CONFERENCE
1_3 NOV, 2023
UNIVERSITY OF QOM, IRAN

SIMULATION OF CESIUM TIN IODIDE PEROVSKITE SOLAR CELLS WITH P3HT AS A HOLE TRANSPORTING MATERIAL

Fatemeh Abdolah Abyaneh[1] *, *Alireza Mohaghegh Hazrati*[2] *and Javad Beheshtian*[1]

[1]*Department of Chemistry, Faculty of Science, Shahid Rajaee Teacher Training University, Tehran, Iran, abyaneh.fatemeh71@gmail.com*
[2]*Department of Physics, Faculty of Science, Shahid Rajaee Teacher Training University, Tehran, Iran*

Abstract
In the last decade, perovskite solar cells (PSCs) received an impressive attention among the research community due to their sudden increase in the efficiency of the system. However, the toxicity of lead-based perovskites has been a big obstacle in its commercialization. For this purpose, researchers have tried to solve the toxicity problem by removing lead from the absorber layer and replacing it with new materials such as Tin, Cesium, and Germanium. In this research, the effect of using P3HT (poly(3-hexylthiophene-2,5-diyl)) as a hole transport layer (HTL) on the performance of lead-free perovskite solar cells based on $CsSnI_3$ has been investigated. Our proposed device is FTO/n-TiO_2/p-$CsSnI_3$/p-P3HT/Au, consisting of a smooth p-n heterogeneous structure with p-type $CsSnI_3$ as the absorber layer, Titanium dioxide (TiO_2) as the electron transport layer, Fluorine-doped tin oxide (FTO) considered as the buffer layer (anode) and gold (Au) as the cathode. The effect of variation of increasing absorber layer thickness on the photovoltaic parameters investigated. The results show the possibility of using perovskite solar cell without lead and high efficiency by using non-toxic materials such as $CsSnI_3$ as an absorber layer and P3HT as a hole transporting material.

Keywords: Perovskite Solar Cell, P3HT, Hole Transport Layer, SCAPS-1D Software

1. Introduction

Researchers are searching for environmentally friendly, sustainable, and low-cost energy sources that can be a potential alternative to conventional energy. The most common and dominant renewable energy is solar energy, which will undoubtedly become the future energy to meet the ever-increasing global energy demand [1]. To keep up with the current growth of photovoltaic technologies in recent years, researchers are trying to develop efficient solar cells, and in this context, perovskite solar cells are the most popular because of their high absorption coefficient, low excitation energy, adjustable band gap and high load mobility are inevitably the best choices.

The efficiency of perovskite solar cells has improved significantly from 3.8% in 2009 to 25.7% in 2020 [2]. However, major issues hindered the mass production of perovskite solar cells, such as the stability of perovskites, which easily decompose in reaction with moisture, oxygen, light, or heat, and the toxicity of lead halide perovskite cells. Replacement of toxic lead ions (Pb^{2+}) in perovskites with divalent metal ions such as tin (Sn^{2+}) and germanium (Ge^{2+}) does not cause any distortion in the perovskite structure, because the outer shell of Sn and Ge is almost similar to the Pb shell [3]. $CsSnI_3$ is one of the best alternatives for lead-based solar cells because its photovoltaic performance improved due to its ideal band gap of 1.3 eV, high carrier mobility, low binding energy, and high absorption coefficient [4]. Previous studies have shown that perovskite materials based on cesium and tin improved thermal stability and environmental solar cell performance. $CsSnI_3$ has shown the highest recorded efficiency of 10.1% among inorganic perovskite solar cells [5].
A new technique has been introduced in which metallic tin is used to reduce Sn^{2+} oxidation, which leads to increased stability of $CsSnI_3$ [6]. A typical perovskite solar cell has a multilayer structure consisting of a perovskite active layer, an electron transport layer, and a hole transport layer. Since experimental fabrication of different layers of a multilayer perovskite solar cell is time-consuming and costly, computational modeling and simulation studies are important methods to help identify suitable materials for different layers. The use of a suitable electron transporting material that extracts the photoelectrons produced by the perovskite material and the hole transporting material that increases the extraction of holes will increase the efficiency of the absorber. In this project, the photovoltaic performance of a solar cell based on $CsSnI_3$ with a P3HT as a HTL as has been studied. HTL plays an important role in influencing the charge extraction and recombination mechanism in PSCs. P3HT is widely used in electronics due to its distinctive features, including high solubility in various solvents and easy deposition at low temperatures [7].

2. Device simulation details

2.1 How to run the program: Since experiments are sometimes exposed to uncertainties, errors, and different complications, simulations are done to save time and resources. In this research, SCAPS-1D software was used for numerical simulation; This software obtains all the transmission characteristics of a semiconductor piece by solving the one-dimensional Poisson equation and the continuity equations of electrons and holes [8]. The results of this numerical simulation will help the researchers to make low-cost lead-free perovskite solar cells with the appropriate combination of absorber layers, electron transporters, and hole transporters.

2.2. Solar cell structure: We have considered a p-n heterogeneous perovskite solar cell structure for device simulation, which includes $CsSnI_3$ as a p-type absorber layer between TiO_2 as an electron-transporting layer and P3HT as a hole-transporting layer. Fig. 1 shows the schematic structure of the proposed solar cell. The simulation has been done in the presence of 1000 W/m^2 solar energy density equivalent to AM 1.5G.

2.3. Parameters required for simulation: Table 1 shows the input parameters of different layers, which are adapted from previously published data and the Table 2 shows the related defect parameters of interface layer and bulk absorber layer.
The values of the radiative recombination coefficient, Auger electron absorption coefficient, and Auger hole absorption coefficient are 3×10^{-10} cm^3/s, 1×10^{-29} cm^6/s, and 1×10^{-29} cm^6/s respectively in the bulk absorber layer.

Fig. 1. Schematic structure of the proposed perovskite solar cell

Table 1 Input parameters of absorber, ETL, HTL and FTO

Parameters	FTO [9]	TiO_2 [10]	$CsSnI_3$ [11]	P3HT [12]
Thickness (nm)	500	40	200-1000	200
E_g (eV)	3.5	3.2	1.3	2
χ (eV)	4	3.9	3.6	3.2
$_r\varepsilon$	9	9	9.93	4.2
N_C (cm^{-3})	2×10^{18}	2×10^{18}	1×10^{18}	2×10^{21}
N_V (cm^{-3})	1.8×10^{19}	1.8×10^{19}	1×10^{19}	2×10^{21}
μ_n(cm^2/V.s)	20	100	1500	1.8×10^{-3}
μ_p(cm^2/V.s)	10	25	585	1.8×10^{-3}
N_D (cm^{-3})	1×10^{15}	1×10^{16}	0	0
N_A (cm^{-3})	0	0	1×10^{17}	1×10^{19}
N_t(cm^{-3})	1×10^{15}	1×10^{15}	1×10^{15}	1×10^{15}

Table 2 Input parameters of interface defect layers

Interface	FTO/ TiO2	TiO_2/ $CsSnI_3$	$CsSnI_3$/ P3HT	Bulk $CsSnI_3$
Defect type	neutral	neutral	neutral	neutral
Total defect density (cm^{-3})	1×10^{11}	1×10^{11}	1×10^{11}	1×10^{15}
Electron capture cross section (cm^2)	1×10^{-19}	1×10^{-19}	1×10^{-19}	1×10^{-15}
Hole capture cross section (cm^2)	1×10^{-19}	1×10^{-19}	1×10^{-19}	1×10^{-15}
Energy distribution	Gaussi	Gaussi	Gaussi	Gaussi
Reference defect energy level (eV)	0.6	0.6	0.6	0.6

3. Results

3.1. Variation of absorbent layer thickness: The thickness of the absorber layer plays an important role in improving the efficiency and other photovoltaic characteristics of solar cells. In this research, the thickness of the $CsSnI_3$ layer changes from 200 to 1000 nm and the rest of the parameters are constant. Fig. 2 shows the changes in the photovoltaic parameters of the desired cell for different thicknesses of the absorber layer. As can be seen, the photovoltaic parameters have improved with the increase in thickness, only in the open circuit voltage up to the thickness of 400 nm, the value increased and then decreased.

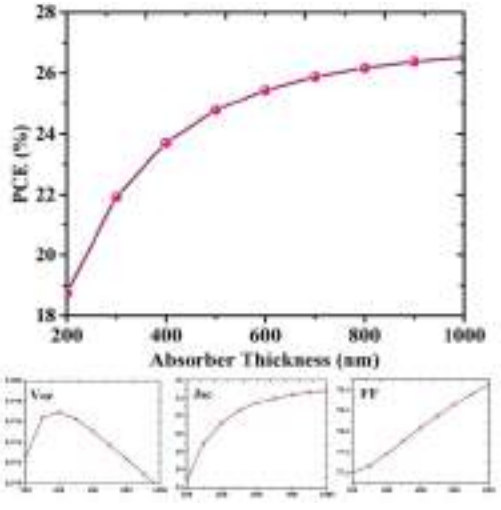

Fig. 2. Variation of absorber thickness on PV parameters

3.2. Variation of temperature: To understand the effect of temperature on the electrical performance of the studied solar cell, the temperature of the simulated system considered to vary from 300 to 400 K. Fig. 3 shows the effect of this parameter on solar cell performance.

As the temperature increases, the short circuit current density, open circuit voltage, and power conversion efficiency decrease. In the first two cases, this decrease is linear, but as the temperature increases, as can be seen, the filling factor first increases and decreases from the temperature of 360 K.

4. Discussion and conclusion

In this project, we have designed and investigated a perovskite solar cell based on $CsSnI_3$ with $FTO/TiO_2/CsSnI_3/P3HT/Au$ structure and P3HT as the hole transport layer using SCAPS-1D numerical simulation software. Fig. 4 shows the Current- Voltage and the Quantum Efficiency curves for the simulated device.

The influence of increasing the absorber thickness on the photovoltaic parameters of the system have been investigated.

Our simulation results with the main photovoltaic parameters, power conversion efficiency 26.17%, fill factor 78.26%, open circuit voltage 0.97V. and short circuit current 34.40mA/cm^2 show an excellent performance for our proposed device with P3HT as a hole transporting layer.

Therefore, this proposed perovskite solar cell can be a benchmark for making lead-free perovskite solar cells with high efficiency, stability, and low cost.

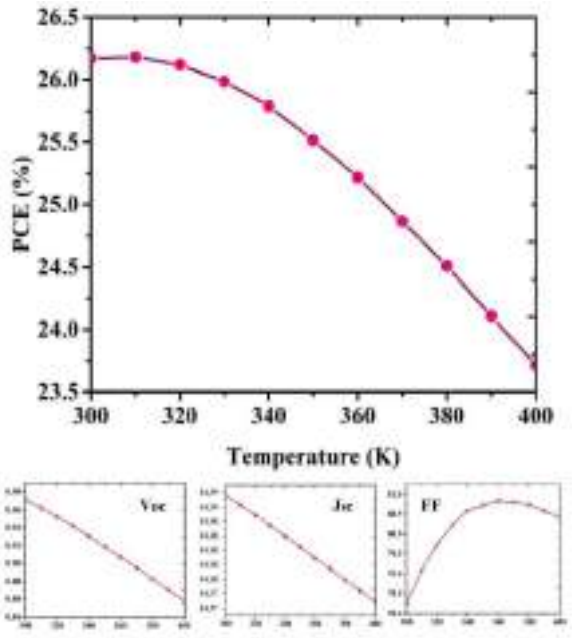

Fig. 3. Variation of system temperature on PV parameters

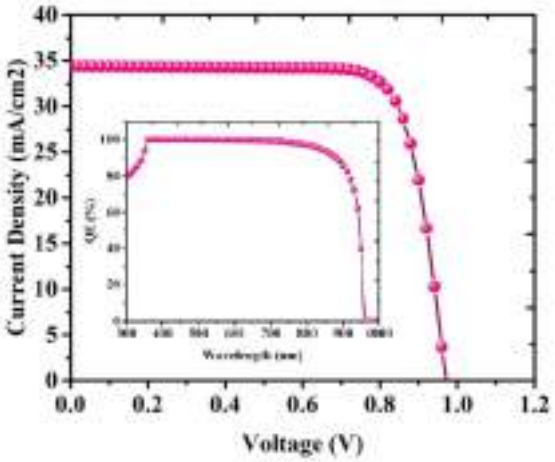

Fig. 4. J-V and QE curves for simulated device

5. References

[1] Suresh Kumar, N., Naidu, C.B., K., 2021. A review on perovskite solar cells (PSCs), materials and applications. J. Materiomics 7 (5), 940–956

[2] Ye, T., Wang, K., Hou, Y., Yang, D., Smith, N., Magill, B., Yoon, J., Mudiyanselage, R.R., Khodaparast, G.A., Wang, K., 2021. Ambient-air-stable lead-free CsSnI3 solar cells with greater than 7.5% efficiency. J. Am. Chem. Soc. 143 (11), 4319–4328

[3] Zhao, S., Cai, W., Wang, H., Zang, Z., Chen, J., 2021. All-Inorganic Lead-Free Perovskite (-Like) Single Crystals: Synthesis, Properties, and Applications. Small Methods 5 (5), 2001308

[4] Krishnamoorthy, T., Ding, H., Yan, C., Leong, W.L., Baikie, T., Zhang, Z., Sherburne, M., Li, S., Asta, M., Mathews, N., 2015. Lead-free germanium iodide perovskite materials for photovoltaic applications. J. Mater. Chem. A 3 (47), 23829–23832.

[5] Sabbah, H., 2022. Numerical Simulation of 30% Efficient Lead-Free Perovskite CsSnGeI3-Based Solar Cells. Materials 15 (9), 3229

[6] Jiang, M., Tang, J., 2021. Simulated development and optimized performance of narrowbandgap CsSnI3-based all-inorganic perovskite solar cells. J. Phys. D: Appl. Phys., 54

[7] Wang, Q., Shao, S., Xu, B., Duim, H., Dong, J., Adjokatse, S., Portale, G., Hou, J., Saba, M., Loi, M.A., 2020. Impact of the Hole Transport Layer on the Charge Extraction of Ruddlesden-Popper Perovskite Solar Cells. ACS Appl. Mater. Interfaces 12 (26), 29505–29512

[8] Sharma, Shiva &Mehra, Rajesh, Perovskite Solar Cell design using Tin Halide and Cuprous Thiocyanate for Enhanced Efficiency, International Journal of Engineering and Advanced Technology(IJEAT),2019, Volume 6 (8), 2249 8958.

[9] Deepthi Jayan, K., 2022. Design and Comparative Performance Analysis of HighEfficiency Lead-Based and Lead-Free Perovskite Solar Cells. Phys. Status Solidi (a) 219 (7), 2100606.

[10] Liu, X., Hu, Y., 2022. Investigation of TiO2 as the buffer layer in wide bandgap chalcopyrite solar cells using SCAPS. J. Mater. Sci. Mater. Electron. 33 (9), 6253–6261.

[11] Srivastava, S., Singh, A.K., Kumar, P., Pradhan, B., 2022. Comparative performance analysis of lead-free perovskites solar cells by numerical simulation. J. Appl. Phys. 131 (17), 175001.

[12] Mohandes, A., Moradi, M., Nadgaran, H., 2021. Numerical simulation of inorganicCs2AgBiBr 6 as a lead-free perovskite using device simulation SCAPS-1D. Opt. Quant. Electron. 53 (6), 319.

29TH IRANIAN ORGANIC CHEMISTRY CONFERENCE
1_3 NOV, 2023
UNIVERSITY OF QOM, IRAN

Preparation of ZIF-8@GO@$CoFe_2O_4$: a Novel Ternary Catalyst for the Synthesis of Pyrazole-Based Pyrido[2,3-d]pyrimidine-diones

Boshra Mirhosseini-Eshkevari [1,2], *Mohammad Ali Ghasemzadeh* [1]*

[1]*Department of Chemistry, Qom Branch, Islamic Azad University, Qom, I. R. Iran, Mbsme@yahoo.com, qasemzade.a@gmail.com*
[2]*Department of Chemistry, North Tehran Branch, Islamic Azad University*

Abstract- An efficient and stable $CoFe_2O_4$ nanoparticles incorporated in zeolitic imidazolate framework-8 supported on graphene oxide (GO) was synthesized. Using the achieved heterogeneous catalyst including ZIF-8@GO@$CoFe_2O_4$, various pyrazolo[4',3':5,6]pyrano[2,3-d]pyrimidine-dione derivatives were synthesized through the one-pot five-component reaction of hydrazine hydrate, ethyl acetoacetate, 1,3 dimethyl barbituric acid, ammonium acetate, and aryl aldehydes in the absence of any solvent. Furthermore, it was found that such a new heterogeneous catalyst was simply recyclable and separable. This research introduces a green and suitable versatile to synthesize a class of organic compounds by simple work-up, facile recycling system, excellent yields, utilizing non-toxic materials, as well as short reaction times. Scanning electron microscopy (FE-SEM), energy-dispersive X-ray spectroscopy (EDX), Furrier transforms infrared spectroscopy (FT-IR) and X-ray diffraction spectroscopy (XRD) analysis were used to characterization and structure elucidation of the catalyst.

1. Introduction

Graphene oxide is a kind of nanomaterial with edge/surface functional groups that has great features and chemical structures which make it an ideal support for different metal nanoparticles (NPs) [1-3]. Metal-organic frameworks (MOFs) are another group of nanomaterials that employ to support the growth of nanoparticles and also prevent their aggregation. These frameworks provide an excellent platform for integration of different functionalities within a single framework, which represents notable features including high surface area, abundant catalytic sites, high adsorption affinity, and broad tenability [4-6]. Zeolitic imidazolate framework-8 with a crystalline structure and outstanding features is a subgroup of MOFs which has been great attention in recent years [7]. Fused pyrazolopyranopyrimidines containing biologically active pyranopyrazole and pyranopyrimidine offer broad spectrum of pharmacological and biological properties [8].
herein, we report a facile one-pot five-component protocol for the synthesis of a series of pyrazolo[4',3':5,6]pyrano[2,3-d]pyrimidine-dione derivatives in the presence of a ZIF-8@GO@$CoFe_2O_4$ nanocomposite as catalyst under solvent-free conditions (Scheme 1).

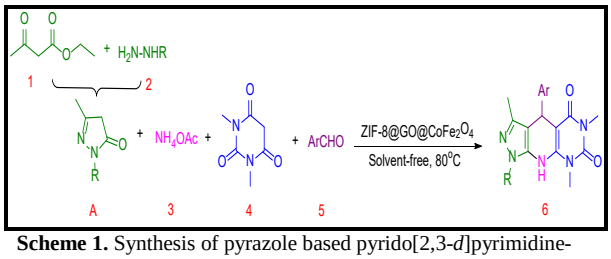

Scheme 1. Synthesis of pyrazole based pyrido[2,3-*d*]pyrimidine-diones using ZIF-8@GO@$CoFe_2O_4$

2. Experimental

2.1. Preparation of $CoFe_2O_4$ nanoparticles

0.1 g of $CoSO_4$ and 0.34 g of $FeCl_3$ $6H_2O$ were dissolved in 100 ml of deionized water. 20 ml of NaOH solution (1M) was then slowly added to the solution until reaching pH to around 10. A brown precipitate was then centrifuged and rinsed with distilled water. Finally the obtained solution was remained at 80 °C and its color goes from brown to black [9].

2.2. Preparation of ZIF-8@$CoFe_2O_4$

In a backer, $CoFe_2O_4$ NPs (0.5 g) and $Zn(NO_3)_2.6.H_2O$ (0.6 g) were mixed in methanol (10 mL). In another vessel, 2-methyl imidazole (1.3 g) was poured in methanol (10 mL) and then the mixture was stirred vigorously. Then, two vessels were mixed together and the solution was mixed completely for 30 min. The obtained residue was separated by centrifugation method and was washed several times with methanol. Eventually, the product was dried at 100°C for 24 h.

2.3. Synthesis of ZIF-8@GO@$CoFe_2O_4$

Initially, GO was prepared with oxidation of graphite utilizing the modified Hummer's method [10]. Then, a mixture of 0.1 g of ZIF-8@$CoFe_2O_4$ nanocomposite and GO (0.5 g) was dispersed in DMF (35 mL) under ultrasonic irradiations and then the mixture was conducted into a Teflon-lined stainless-steel autoclave at 110 °C for 12 h. When the reaction was ended, the obtained residue was separated and washed three several times with dimethyl formamide, DI water and ethanol, respectively. Lastly, the prepared ZIF 8@GO@$CoFe_2O_4$ was dried at 50 °C for overnight (Scheme 2).

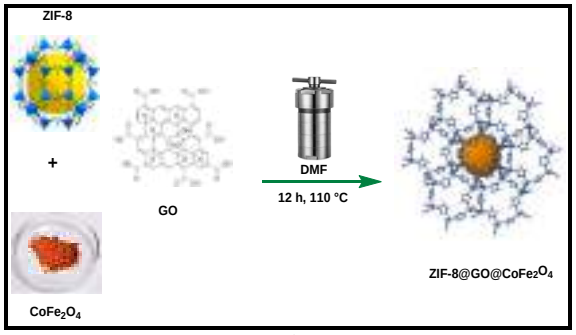

Scheme 2. Synthesis of ZIF-8@GO@$CoFe_2O_4$

2.4. General process to synthesize pyrazolo[4',3':5,6]pyrano[2,3-d]pyrimidine-dione derivatives

1.1 mmol of hydrazine hydrate or phenyl hydrazine was added dropwise to an aqueous solution of ethyl acetoacetate to produce 3-methyl-pyraxole-1-one as a white precipitate. Then, aryl aldehyde (1 mmol), catalytic amount of ZIF-8@GO@$CoFe_2O_4$ (0.005 g), 1,3-dimethyl barbituric acid (1 mmol), and ammonium acetate (1.2 mmol) was added to the mixture and the reaction vessel was heated at 80°C under solvent-free circumstances. With the completion of the reaction, indicated by TLC (n-hexane: ethyl acetate, 4:1), the reaction mixture was dissolved in dichloromethane and the catalyst was then magnetically separated. With evaporating of the solvent and then recrystallizing of the residue from ethanol.

3. Results and discussion

Initially, the catalytic performance of the ZIF-8@GO@$CoFe_2O_4$ was evaluated in the preparation of pyrazolo[4',3':5,6]pyrano[2,3-d]pyrimidine-diones. Thus, the five-component condensation between ethyl acetoacetate (1 mmol), 1,3-dimethyl barbitueic acid (1 mmol), hydrazine hydrate (1.1 mmol), ammonium acetat (1.2 mmol), and 4-chlorobenzaldehyde (1 mmol) was considered as a model study to optimize the effect of different solvents, various temperatures and diverse amounts of the catalyst (Scheme 3).

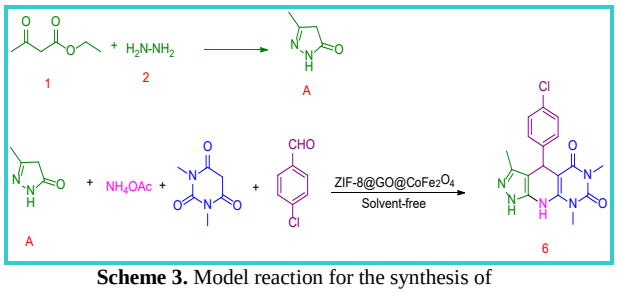

Scheme 3. Model reaction for the synthesis of pyrazolo[4',3':5,6]pyrano[2,3-d]pyrimidine-dione

The significance of this research was revealed when we compared the catalytic activity of the ZIF-8@GO@$CoFe_2O_4$ with other catalysts such as CuI, MgO, Co_3O_4, $MgFe_2O_4$, GO and ZIF-8. In accordance with the obtained results from Fig 1, the best outcomes (98% yield within 20 min) belong to ZIF-8@GO@$CoFe_2O_4$ under solvent-free conditions (Fig. 1).

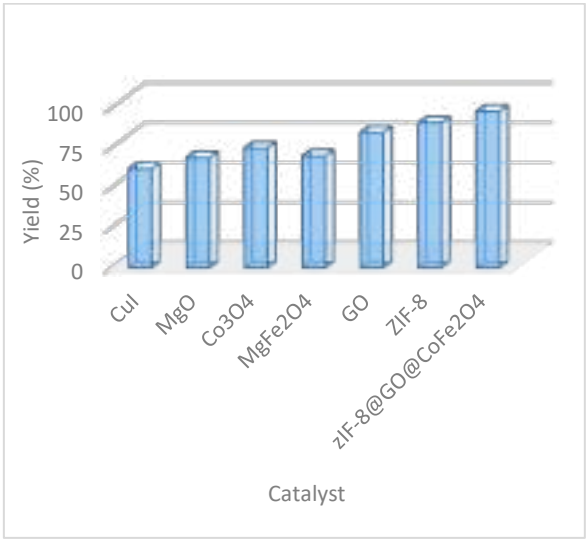

Fig 1. The effect of various catalysts on the model reaction

SEM analysis was studied to distinguish the particle size and surface morphology of the synthesized ZIF-8@GO@$CoFe_2O_4$. FE-SEM micrograph of the as-synthesized ZIF-8@GO@$CoFe_2O_4$ (Fig.2) representing a characteristic spherical shape form.

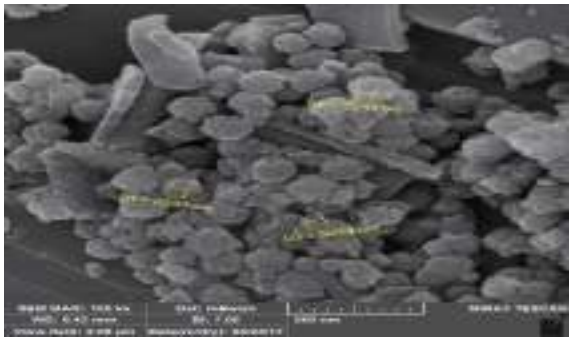

Fig. 2. FE-SEM images of ZIF-8@GO@$CoFe_2O_4$.

Figure 3 demonstrates the elemental analysis of ZIF-8@GO@$CoFe_2O_4$ obtained from EDX. The results confirm the existence of C, O, N, Co, Fe and Zn as the only elementary components of ZIF-8@GO@$CoFe_2O_4$ (Fig. 3).

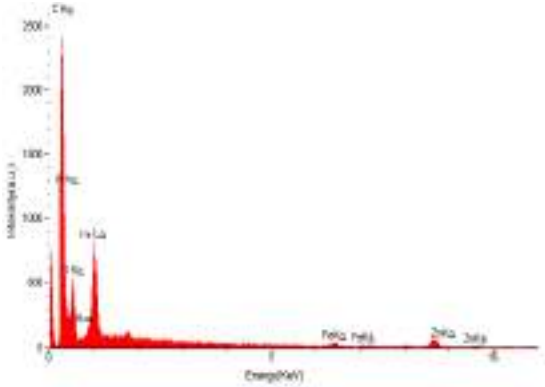

Fig. 3. EDX spectrum of ZIF-8@GO@$CoFe_2O_4$

Figure 4 displays the FT-IR spectrum of ZIF-8@GO@ $CoFe_2O_4$ which approves the existence of each component in the structure. The stretching vibrations of Co-O and Fe-O in $CoFe_2O_4$ NPs are shown at 438 and 564 cm^{-1}.

Moreover, the main absorption bonds in ZIF-8 structure are appeared at 2965, 1522 and 475 cm^{-1} due to stretching vibrations of C-H, C=N and Zn-N bonds, respectively [11]. The peak at 3328 cm^{-1} is related to the OH groups in grapheme oxide. The absorption bonds at 1718 cm^{-1}, 1025 cm^{-1}, and 1282 cm^{-1} is related to the stretching vibration of carbonyl group, and C-O bonds in the structure of GO [12].

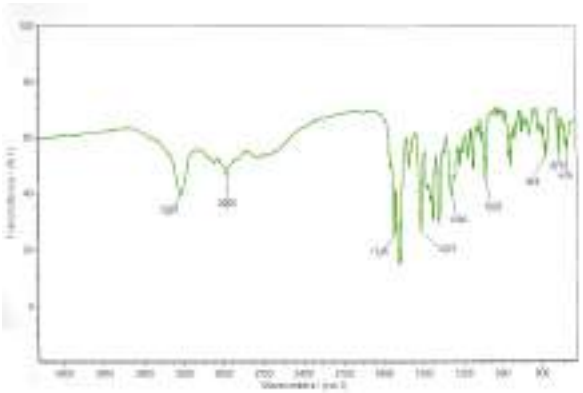

Fig. 4. FT-IR spectra of ZIF-8@GO@$CoFe_2O_4$

X-ray diffraction pattern of ZIF-8@GO@$CoFe_2O_4$ nanocomposite is depicted in Figure 5. The difraction peaks of synthesized nanocomposite showed 2θ values of 30.15°, 35.34°, 36.78°, 42.82°,53.36°and 56.71° of synthesized $CoFe_2O_4$ nanocomposite. Also, the presence peaks at 7.6°, 12.4°, and 18° (2θ°) show the formation of the ZIF-8 frameworks, as well as, the peaks at 9.3° and 11.3° (2θ°) indicate the construction of the GO [13] which confirms the formation of the nanocomposite.

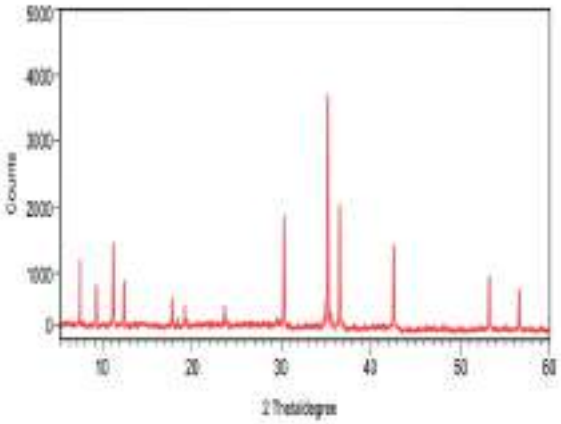

Fig. 5. XRD pattern of ZIF-8@GO@$CoFe_2O_4$

4. Conclusion

A novel ternary nanocomposite including ZIF-8@GO@$CoFe_2O_4$was successfully synthesized and then the structure elucidation of it was fully conducted by various spectroscopy techniques including SEM EDX, FT-IR and XRD analysis. An excellent catalytic activity of this ternary hybrid nanocatalyst has been examined for the multi-component preparation of pyrazolo[4',3':5,6]pyrano[2,3-d]pyrimidine-diones.

The main features of this research were simple reaction work-up, reusability of the catalyst, and satisfactory yields of the products within short reaction times.

5. References

[1] H. Li, Z. Song, X. Zhang, Y. Huang, S. Li, Y. Mao, H. J. Ploehn, Y. Bao, M. Yu, Science. 342 (2013) 95-98.

[2] B. Mi, Materials science. Science. 343 (2014) 740-742.

[3] P. Babaei, J. Safaei-Ghomi, Mater. Chem. Phys. 2021 (267) 124668-124680.

[4] V. I. Isaeva, L. M. Kustov, Petro. Chem. 50 (2010) 167-180.

[5] V. Pascanu, G. G. Miera, A. K. Inge, B. M. J. Am. Chem. Soc. 141 (2019) 7223-7234.

[6] A. Nikseresht, S. Ghasemi, S. Parak, Polyhedron, 151 (2018) 112-117.

[7] L. Liu, X. Zhou, Y. Yan, J. Zhou, W. Zhang, X. Tai, Polymers. 10 (2018) 1089-1104.

[8] S. R. Mandha, S. Siliveri, M. Alla, V. R. Bommena, M. R. Bommineni, S. Balasubramanian, Eco-friendly synthesis and biological evaluation of substituted pyrano[2,3-c]pyrazoles, Bioorg Med Chem Lett. 22 (2012) 5272-5278.

[9] K. Hedayati, S. Azarakhsh, D. Ghanbar, J. Nanostruct. 6 (2016) 127-131

[10] S. William, J. Hummers, R. E. Offeman, J. Am. Chem. Soc. 80 (1958) 1339-1339.

[11] M. Akbari, M. A, Ghasemzadeh, M. Fadaeian, Chemistry Select. 5 (2020)14564-14571.

[12] D. Huang, Q. Xin, Y. Ni, Y. Shuai, S. Wang, Y. Li, H. Ye, L. Lin, X. Dinga, Y. Zhang, RSC Adv. 8 (2018) 6099-6109.

[13] R. mozafari, M. ghadermazi, RSC Adv. 10 (2020) 15042-15064.

29TH IRANIAN ORGANIC CHEMISTRY CONFERENCE
1_3 NOV, 2023
UNIVERSITY OF QOM, IRAN

Effect of acid pre-treatment on the yield, chemical compounds, and antioxidant activity of *Oliveria decumbens* essential oil

Saeed Mollaei and Mina Mohammadi*

Department of Chemistry, Faculty of Sciences, Azarbaijan Shahid Madani University, Tabriz, Iran, smollayi@ymail.com

Abstract - *Oliveria decumbens*, an annual herb, belongs to the Apiaceae family and distributes in Syria, south-east Anatolia, Iraq, and Iran. In this study, the influence of acid pre-treatment prior to hydrodistillation on the yield and antioxidant activity of the *O. decumbens* essential oil was investigated. Hydro-distillation method was used for isolating the essential oils from the air-dried powdered flowers (10 g) which was treated with acid solution. Then, yield and antioxidant activity of the essential oils were calculated. The obtained results indicated that the pre-treatment with high acid concentration (0.6 mM HCl) increased essential oil yield from 5.0 to 7.16%, compared to the conventional method. Acid solution could hydrolyze the cell wall and then releases secondary metabolites out of the cells. Also, thymol and carvacrol were the major constituent with up to 60% obtained through both methods, and the acid pre-treatment could not change the amount of them, significantly. However, no significant changes were observed in the antioxidant property of the essential oil. Therefore, it may be suggested that, if high yield is required, the *O. decumbens* flowers could be distilled from acid medium**.**

Keywords: Antioxidant; Essential oil; *Oliveria decumbens; Pre-treatment*

1. Introduction

Oliveria decumbens, belongs to *Apiaceae* family, is an endemic medicinal plant of Iran. It is the only species of *Oliveria* genus which is grown through subtropical areas of Iran including Ilam, Kermanshah, Khuzestan, Fars, and Kohgiluyeh and Boyer-ahmad provinces [1].

Oliveria decumbens have been applied as remedies for inflammation, febrifuge and digestive, cancer, infections, abdominal pains, fever, indigestion, and diarrhea [2, 3]. Furthermore, its insecticidal, anti-tumour, anti-cholinesterase, anti-Helicobacter pylori, antioxidant, and antibacterial activities have been studied [4].

O. decumbens is a good source of essential oil. The flowering stages of this plant begin in June and change with three color phases as green, pink-purple and white. The maximum amount of essential oil and its major constituents have been studied, and the results indicated that *p*-cymene, γ-Terpinene, carvacrol, and thymol are the main compounds. Also, the biological activities of the essential oil of *O. decumbens* can be related to the presence of these compounds [5, 6]. Hajimehdipoor et al., (2010) stated that 10 compounds were detected in the *O. decumbens* essential oil, and the main compounds were thymol, γ-terpinene, ρ-cymene, myristicin, and carvacrol [7].

Up to our knowledge, the influence of acid pre-treatment prior to hydrodistillation (A-HD) on the yield, chemical compounds, and antioxidant activity of essential oil from *O. decumbens* flowers has not been studied so far. Thus, the present work aimed to isolate essential oil from *O. decumbens* flowers using A-HD, and then their yield, chemical compounds, and antioxidant activity were studied.

2. Material and Methods

2.1. Plant materials: The flowering aerial parts of *O. decumbens* Vent were gathered from its wild habitat in July 2022 in the northen regions of Kermanshah province, Iran. After identifying, voucher specimen was placed in the Azarbaijan Shahid Madani University Herbarium. The plant was dried in a shade at 25°C, and kept at 4°C.

2.2. Acid pre-treatment prior to hydrodistillation (A-HD): 200 mL distilled water were added to a one-liter round flask, and then 1 mL of 0.6 mM HCl was added. Ten grams of powdered *Oliveria decumbens* flowers was added to above solution and refluxed for 10 minutes.

2.3. Conventional Hydrodistillation (HD): After acid pre-treatment of the *O. decumbens* flowers, the flask connected to a Clevenger apparatus, and hydrodistillation method was applied for the essential oil extraction from the air-dried powdered flowers (10 g, 200 mL of distilled water, 3h) based on the procedure mentioned in British Pharmacopoeia. The isolate essential oil was dehydrated by sodium sulfate and kept at -25°C for further analysis.

2.4. Antioxidant activity: The antioxidant activity of the *O. decumbens* essential oil was studied using

DPPH assay. 200 microliter of the DPPH solution (1.0 mM) was added to various amounts of essential oil. The obtained mixture was incubated for 30 min in the dark, at room temperature. Then the absorbance of the sample was read at 517 nm. Finally, the radical scavenging activity (%) was calculated.

2.5. GC chromatography: The analysis of essential oil was done using an Agilent 6890 N GC-FID system equipped with a fused capillary column DB-5 (30 m × 0.25 mm, 0.25 µm film thickness). Nitrogen with a flow rate of 1.0 mL/min was used as the carrier gas. The ionization voltage and splitting ratio were 70 eV and 1:100, respectively.

3. Result and Discussion

3.1. Effect of Acid pretreatment on the yield: The influence of acid concentration on the essential oil yield of *O. decumbens* was studied. To evaluate the effect of acid concentration on the extraction yield of essential oil, pre-treatments were conducted at different concentrations (0.30, 0.45, 0.60, and 0.75 mM). The yields were shown at Fig. 1. According to the results, the increment of acid concentration from 0.030 to 0.060 mM indicated an increase of essential oil yield, and then decreased essential oil yield by increasing acid concentration from 0.60 to 0.75 mM. Acid solution could hydrolyze the cell wall and then releases secondary metabolites out of the cells.

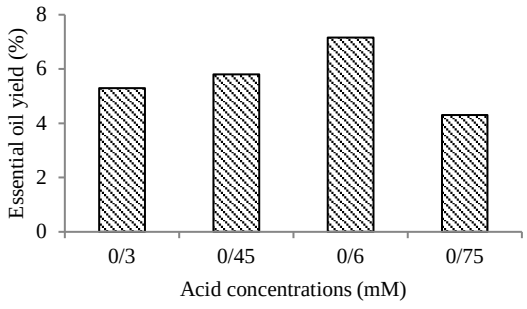

Fig.1. The effect of acid pretreatment on the essential oil yield of *O. decumbens*

3.2. Effect of acid pretreatment on the antioxidant activity: Based on the analysis of antioxidant activities of different samples, it was determined that the inhibitory activity of the essential oil was concentration dependent, and the inhibitory percentage increased with increasing concentration. Figure 2 illustrates the IC_{50} values of essential oil obtained by conventional hydrodistillation and acid pretreatment-hydrodistillation methods. The results were compared with the IC_{50} value of ascorbic acid as standard. According to the results, no significant changes were observed in the antioxidant activity of the essential oil.

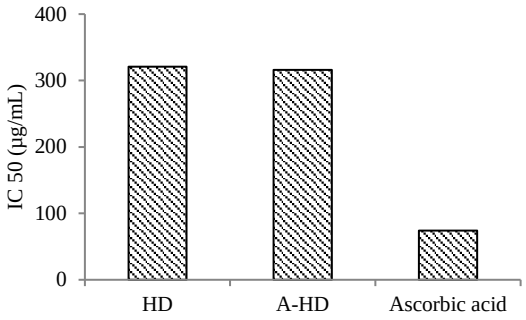

Fig.2. The effect of different methods on the antioxidant activity of essential oil. HD: conventional hydrodistillation; A-HD: acid pretreatment-hydrodistillation

3.3. Effect of acid pretreatment on the essential oil compounds: In the essential oil extracted using HD and A-HD methods, 8 major constituents were identified, yielding up to 96% of the essential oil (Table 1). The results showed that the main constituents were myristicine, carvacrol, thymol, γ-terpinene, and p-cymene. Thymol and carvacrol were the major constituent with up to 60% obtained through both methods. Also, the acid pre-treatment could not change the amount of them, significantly.

Table 1 The chemical composition of essential oils from *O. decumbens* obtained by HD, and A-HD methods.

No	Components	[a]Retention index	Methods	
			HD (%)	A-HD (%)
1	β-Pinene	975	1.5	1.1
2	β-Myrcene	990	1.2	2.2
3	p-Cymene	1023	14.0	11.8
4	Limonene	1026	2.5	2.4
5	γ-Terpinene	1057	12.4	12.6
6	Thymol	1292	29.4	31.1
7	Carvacrol	1298	32.5	30.6
8	Myristicin	1522	3.1	4.3
	Monoterpene hydrocarbons		30.4	30.1
	Oxygenated monoterpenes		61.9	61.7
	Phenyl propene		3.1	4.3
	Total		96.6	96.1

HD: Hydrodistillation.
US-HD: Ultrasonic pre-treatment prior to hydrodistillation
[a]Retention index of each compound calculated in DB-5 column by retention time with that of n-alkanes (C8–C26).

4. References

[1] V. Mozaffarian, Flora of Ilam. Farhang Moaser Publication, Tehran, Iran, 2008.

[2] B.A. Behbahani, F.T. Yazdi, A. Vasiee, S.A. Mortazavi, Oliveria decumbens essential oil: Chemical compositions and antimicrobial activity against the growth of some clinical and standard strains causing infection, Microbial Pathogenesis, 114 (2018)., 449–452.

[3] T. Jamali, G. Kavoosi, S.K. Ardestani, In-vitro and in-vivo anti-breast cancer activity of OEO (Oliveria decumbens Vent. essential oil) through promoting the apoptosis and

immunomodulatory effects, Journal of Ethnopharmacology, 248 (2020) 112313.
[4] M. Eftekhari, M.R.S. Ardekani, M. Amin, F. Attar, T. Akbarzadeh, M. Safavi, E. Karimpour-razkenari, M. Amini, M. Isman, M. Khanavi, Oliveria decumbens, a bioactive essential oil: Chemical composition and biological activities, Iranian Journal of Pharmaceutical Research, 18 (2019) 412–421.
[5] E.D.S. da Silva Moura, L.R. D'Antonino Faroni, F.F. Fernandes Heleno, A.A.Z. Aparecida Zinato Rodrigues, L.H. Figueiredo Prates, M.E. Lopes Ribeiro de Queiroz, Optimal extraction of Ocimum basilicum essential oil by association of ultrasound and hydrodistillation and its potential as a biopesticide against a major stored grains pest, Molecules, 25 (2020) 2781.
[6] A. Karami, T. Khoushbakht, H. Esmaeili, F. Maggi, Essential oil chemical variability in Oliveria decumbens (Apiaceae) from different regions of Iran and its relationship with environmental factors, Plants, 9 (2020) 680.
[7] M.H. Hajimehdipoor, N. Samadi, V. Mozafarian, N. Rahimifard, S. Shoeybi, H.M. Pirali, Chemical composition and antimicrobial activity of Oliveria decumbens volatile oil from West of Iran, Journal of Medicinal Plants, 9 (2010) 39-44.

Investigating The Kinetics Of Polyurethane Formation Based On HTPB-IPDI By Chemorheological Method

*Abolfazl Moein, Abbas Kebritchi**

Chemical Engineering Department, Imam Hossein Comprehensive University, Tehran, Iran, fazl_moein@ihu.ac.ir, A.Kebritchi@ippi.ac.ir

Abstract - Kinetics of polyurethane formation based on HTPB (Hydroxyl-terminated polybutadiene) - IPDI (Isophorone diisocyanate) was investigated using Arrhenius and Ehring equations. The method of calculating kinetic data was based on chemorheological studies. In this method, the criterion of reaction speed is changes in viscosity. According to the studies, the reaction kinetics between HTPB prepolymer and IPDI curing agent is two-step. The activation energy rate constant, activation entropy and reaction activation enthalpy were calculated for each step. The results show that the first stage of the reaction is faster than the second stage. According to the kinetic data extracted from the reaction, a reaction mechanism between curing agent and prepolymer was proposed.

1. Introduction

Polyurethane is a synthetic resin compound, often abbreviated as PU or PUR. PU is a network polymer formed by the addition reaction between alcohols (diols or polyols) and isocyanates (di-isocyanate or poly-isocyanate). This reaction creates urethane bonds (–NHCOO–) in polymer chains. Since PU contains two types of monomers that are polymerized one after the other, they are classified as alternating copolymers. The isocyanate segments include the hard segment, and the diol part includes the soft segment. The hard segment is responsible for increasing the hardness, resistance, strength, and thermal stability of PU. The soft segment is responsible for increasing the flexibility, elasticity, impact, and rubbery behavior of PU. The kinetics of PU network formation is important to understand and control the properties and performance of PU materials [1]. Therefore, by understanding the kinetics and factors affecting the formation of urethane bonds, it is possible to synthesize a polymer with desirable properties (mechanical, physical, thermal, and process). There are different methods to check the kinetics of PU formation, which are [2, 3]:

- **Differential Scanning Calorimetry (DSC):**
- **Nuclear Magnetic Resonance Spectroscopy (NMR)**
- **Fourier Transform Infrared Spectroscopy (FT-IR)**
- **Measuring Viscosity:** Chemo-rheological studies are key to understanding polymerization and cross-linking in PU. In the field of PU research, viscosity measurement serves as a practical method to investigate polymerization kinetics. By monitoring changes in the viscosity of a reaction mixture over time, scientists can estimate the degree of polymerization and cross-linking in PU materials. During the formation of the PU network, two key events occur:

I. **Increasing molecular weight**: by forming urethane bonds between isocyanate and polyol, the molecular weight of the polymer increases.

II. **Creation of crosslinks:** due to the functionality of more than 2 HTPB during the curing process, in addition to increasing the length of polymer chains, crosslinks are also created between polyols.

These two events lead to an increase in viscosity during polymerization. By measuring viscosity during the curing process, scientists can track changes at any point relative to previous steps. This valuable insight helps unravel the mystery of the structure and behavior of PU formation [4]. Our desired method in this laboratory work is to use changes in viscosity in terms of time to determine the kinetics of the formation of urethane bonds between the IPDI (Isophorone diisocyanate) curing agent and the HTPB (Hydroxyl-terminated polybutadiene) prepolymer.

2. Materials and Methods

2.1. Materials

HTPB (number-average molecular weight = 3019 g/mol, hydroxyl value = 0.76 mmol/g) was obtained

from the industry (Iran). Curing agents, Isophorone diisocyanate (IPDI), were supplied from Merck (Germany). The curing catalyst, Dibutyltin dilaurate (DBTDL), was supplied from Sigma Aldrich (USA).

2.2. Preparation of urethane elastomers

According to Table 1, the formulation was prepared. Before starting the work, the material was removed from water vapor using a vacuum oven. First, HTPB is mixed with POSS using a double-blade mixer in a water bath. Then the curing agent is added and mixed for 30 seconds at 1000 rpm.

Table 1 PU formulation

resin	Isocyanate	Catalyst(wt%)	T(C°)	NCO/OH
HTPB	IPDI	DBTDL(0.003)	50 55 60	0.81

2.3. Kinetic and thermodynamic studies

To understand the kinetics of PU formation, a mathematical model is needed to show the relationship between viscosity and time. Important thermodynamic parameters that are required to study the reaction kinetics include Activation energy (Ea), activation enthalpy (ΔH‡), and activation entropy (ΔS‡). These parameters can be calculated for a chemical reaction and help in the optimization of the polymerization process.

2.3.1. Arrhenius Relationship

- **Determination of Rate Constant**

As the curing process progresses, the viscosity of the binder system increases exponentially with the reaction time, which can be simulated using the Arrhenius model

$$\eta(t)\frac{T}{\eta 0}(T) = e^{k\eta(T)t}$$

where η(t)T is the binder system viscosity at temperature T and at any given time t, η0(T) is the initial system's viscosity at temperature T, kη(T)is the rate constant for viscosity build-up (min^{-1}) at the temperature T and t are curing time.

To determine the rate constants, the natural logarithm of the Arrhenius model is considered, where the slope of the line represents the rate constant of the reaction [5].

$$\ln(\eta(t)T) = \ln(\eta 0\,(T)) + k\eta(T)t$$

- **Determination of Activation Energy**

Using the Arrhenius equations, the Ea of each step of the reaction can be obtained.

$$\mathrm{LnK} = -\frac{\mathrm{Ea}}{\mathrm{RT}} + \mathrm{LnA}$$

In this equation, Ea is the activation energy (KJ/mol), R is the global gas constant, A is the exponential constant, and T is the reaction temperature [6]. Based on this equation, the Ea of the reaction can be measured by plotting the regression of constant changes in the reaction rate in terms of 1/T. In this work, three temperatures of 50, 55, and 60 °C were chosen, and a comparison was made between the reaction Ea of pure PU and HTPB containing 1% POSS.

2.3.2. Eyring Relationship

Using Eyring's equation, it is possible to establish a relationship between the kinetic parameters obtained from the Arrhenius equation and the thermodynamic parameters.

$$\mathrm{Ln}\frac{\mathrm{K}}{\mathrm{T}} = -\frac{\Delta \mathrm{H}\ddagger}{\mathrm{RT}} + \frac{\Delta \mathrm{S}\ddagger}{\mathrm{R}} + \mathrm{Ln}\frac{\mathrm{R}}{\mathrm{Nh}}$$

Where ΔH‡ is the enthalpy of activation (KJ/mol), ΔS‡ is the entropy of activation ($KJ.k^{-1}$), N is Avogadro's number, and h is Planck's constant [7].

3. Results and Discussion

IPDI is known as a cyclic aliphatic diisocyanate. Therefore, in terms of reaction kinetics, diols are more inactive than aromatic diisocyanates. The industrial product of IPDI is a mixture of cis and trans isomers. The spatial form of IPDI has various configurations that are constantly changing. IPDI can be boat or chair-shaped. Due to the lower Ea, the dominant configuration is its chair shape. There are thus four stereoisomers in IPDI, with two chair configurations readily interconverting [8] (Fig 2). There are two types of isocyanate with different reactivity in IPDI, which are:

- **secondary isocyanate group (NCOsec) linked to the cyclohexane**
- **Primary isocyanate group (NCOprim) linked to methyl**

Due to the steric hindrance of the cyclohexane ring and the alpha substituent, the reactivity of the NCOprim group is much lower than that of the NCOsec group. Therefore, first NCOsec and then NCOprim react with diol [9]. These two steps cannot be measured with a

viscometer because they do not cause substantial changes in the molecular weight of the polymer. After the formation of urethane bonds between IPDI and polyol, a bond with the second isocyanate group of the curing agent must be formed. This step increases the molecular weight and viscosity of the polymer. According to the diagram, there are three stages in the reaction between HTPB/IPDI, which are (Fig 1):

- **First stage:** In this stage, due to less spatial crowding, the trans isomer reacts first
- **Second step:** When the concentration of the trans isomer in the reaction medium decreases, the cis isomers also start to react with the polyol. At this stage, both isomers are creating PU.
- **Third step:** In this step, all trans isomers have reacted, and the only reaction is between cis IPDI and polyol. The cis isomer is less reactive than the trans isomer due to more steric crowding (Table 2)

A comparison between the rate constants extracted through the Arrhenius equation indicates that the rate of the first step is more than four times that of the second step (Table 2), much higher than the TDI rate constants. Kinetic constants according to Arrhenius and Ehring equations are drawn in Figure 2 and compiled in Table 3. Due to the complexity and high spatial density of the IPDI structure, the rate difference between the two stages is very significant.

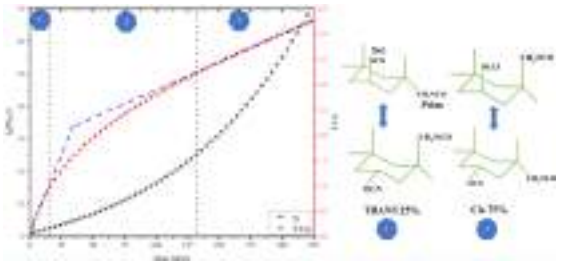

Fig. 1 Formation stages of PU based on HTPB-IPDI from the Rheokinetic point of view

Table 2 Rate constants and pot-life for of HTPB-IPDI

Pot-life	**K_1**	**K_2**	**K_1/K_2**
224	0.04567	0.01081	4.22

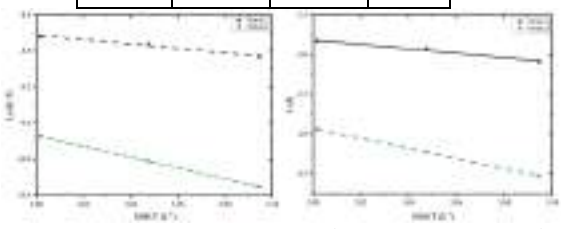

Fig. 2 Arrhenius and Eyring diagram for the curing reaction of the HTPB-IPDI

Table 3 Thermodynamic parameters for the curing reaction of the HTPB-IPDI

ΔE_1	**A_1**	**$\Delta H‡_1$**	**$\Delta S‡_1$**
22.95	237.46	20.20	-208.51
ΔE_2	**A_2**	**$\Delta H‡_2$**	**$\Delta S‡_2$**
52.63	e^{15}	49.8	-129.033

4. Conclusion

In this study, the curing reaction of HTPB-based binder system with IPDI curing agent has been investigated through rheological viscosity test. The rheological reaction rate constants and pot life of HTPB-IPDI binder system have been obtained. The reaction kinetics of polyurethane formation based on HTPB-IPDI is a two-step reaction, the first step of which is faster than the second step. The reason for the two-stage reaction can be attributed to the different isomers of IPDI. By examining the reaction kinetics of polyurethane formation, the pot life of the system can be calculated. The pot life of the binder system is a critical parameter in industrial production. This feature is undoubtedly significant in improving the performance of the resulting products.

5. References

[1]. Guo, J., Chai, T., Liu, Y., Cui, J., et al., “Kinetic research on the curing reaction of hydroxyl-terminated polybutadiene based polyurethane binder system via FT-IR measurements”, Coatings. 8, 175, 2018.

[2]. Ma, H., Liu, Y., Guo, J., Chai, T., et al., “Catalyzed HTPB/HDI-trimer curing reactions and influence on pot life”, Coatings. 10, 1073, 2020.

[3]. Kazachenko, A.S., Akman, F., Abdelmoulahi, H., Issaoui, N., et al., “Intermolecular hydrogen bonds interactions in water clusters of ammonium sulfamate: FTIR, X-ray diffraction, AIM, DFT, RDG, ELF, NBO analysis”, Journal of Molecular Liquids. 342, 117475, 2021.

[4]. Sekkar, V. and Raunija, T.S.K., “Hydroxyl-terminated polybutadiene-based polyurethane networks as solid propellant binder-state of the art”, Journal of Propulsion and Power. 31, 16-35, 2015.

[5]. Halley, P.J. and Mackay, M.E., “Chemorheology of thermosets—an overview”, Polymer Engineering & Science. 36, 593-609, 1996.

[6]. Lee, S., Choi, J.H., Hong, I.-K., and Lee, J.W., “Curing behavior of polyurethane as a binder for polymer-bonded explosives”, Journal of Industrial and Engineering Chemistry. 21, 980-985, 2015.

[7]. Zalewski, K., Chyłek, Z., and Trzciński, W.A., “Rheokinetic studies on the curing process of energetic systems containing RDX, HTPB with high content of 1, 2-vinyl groups and hydantoin-based bonding agent”, Polymer Testing. 111, 107611, 2022.

[8]. Lucio, B. and De La Fuente, J.L., “Rheokinetic analysis on the formation of metallo-polyurethanes based on hydroxyl-terminated polybutadiene”, European polymer journal. 50, 117-126, 2014.

[9]. Ma, H., Liu, Y., Chai, T., Yu, Y., et al., “The Effect of Single Curing Agents on the Curing Reactions of the HTPB-based Binder System”, Coatings. 12, 1090, 2022.

Remediation of wastewater containing 4-nitrophenol by reduction to 4-aminophenol using gold nanoparticles decorated on mesoporous carbon

*Maryam Zirak**

Department of Chemistry, Payame Noor University, Tehran, Iran, m.zirak@pnu.ac.ir.

Abstract - Gold nanoparticles decorated mesoporous carbon (Au@MC) was synthesized by carbonization of egg biomass, followed by decorating Au nanoparticles by reduction of Au(III) salts using hydrazine. Synthesized Au@MC was characterized using XRD, SEM, TEM, EDS, and BET analysis, revealing the successful decoration of Au nanoparticles on the surface of mesoporous carbon. Au@MC exhibited high catalytic activity for the remediation of 4-nitrophenol contaminant from wastewater by reduction to 4-aminophenol. Reusability test indicated that the recycled catalyst can be reused for five runs without considerable changes in the catalytic activity.

Keyword: 4-Nitrophenol, Au Nanoparticles, Mesoporous carbon.

1. Introduction

Nitroaromatics are toxic and generally distributed to the environment by different industries, which can affect the human and animals health, especially marine animals life. So, the removal of nitroaromatic compounds is of interest from an environmental point of view. However, there are different methods for the removal of nitroaromatic pollutants from wastewater, including adsorption, photocatalytic degradation, biodegradation, etc. but reduction of nitroaromatic compounds into the corresponding anilines is one of the best method for the treatment of nitroaromatic polluted water [1, 2]. because, reduction products of nitroaromatics, amines are versatile and useful intermediates in the synthesis of a wide range of biologically active products, drugs, pharmaceuticals, polymers, sensors, corrosion inhibitors, cosmetics, etc [3].

4-nitrophenol (4-NP), one of the most important nitro aromatic derivative, due to its high solubility and stability in water [4], is a highly toxic pollutant for aquatic ecosystem and human life, which could be discharged into the environment from various textile industries [5, 6].

In recent decades, supported metal nanoparticles [7] have been widely reported for the reduction of 4-nitrophenol [8, 9]. The reduction of nitroaromatics to the corresponding aniline derivatives in the presence of metal nanoparticles including Ag [10-12], Rh [13], Au [14], Pd [15], Co [12], Ni [16], Pt [17], etc. has grown considerably. Therefore, the development of new approaches and catalytic systems for the reduction of 4-nitrophenol is of great interest.

Herein we report preparation of gold nanoparticles supported on mesoporous carbon, and its catalytic activity toward the reduction of 4-nitrophenol to 4-aminophenol.

2. Results and Discussion

The mesoporous carbon (MC) material was synthesized by carbonization of egg biomass in the presence of sucrose at 700 ºC under N_2 atmosphere, followed by decorating Au nanoparticles on the surface of MC by reduction of $NaAuCl_4$ using hydrazine to give catalyst, Au@MC. Then, the prepared Au@MC was characterized by XRD, SEM, TEM, EDS, and BET analyses.

SEM and TEM technique were used to study the morphology and textural properties of the prepared Au@MC. The TEM image of Au@MC exhibited the formation of Au spherical nanoparticles with average diameters of 8 nm on the surface of MC materials (Figure 1a). Also, SEM image of Au@MC showed the successful decoration of spherical gold nanoparticle on the surface of mesoporous carbon material (Figure 1b). Also, the presence of Au in the Au@MC was approved by EDX analysis.

XRD pattern of the Au@MC is shown if Figure 2, in which peaks at around 25.7° and 44.2°, are related to the graphitic structure of MC material. Additionally,

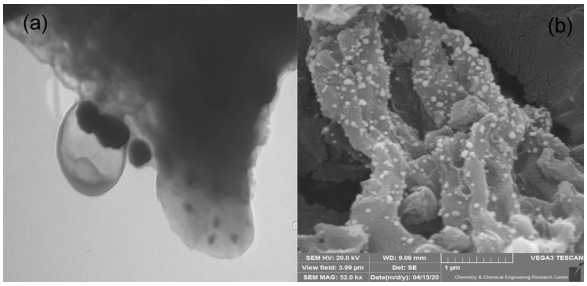

Fig.1. (a) TEM and (b) SEM images of Au nanoparticles decorated mesoporous carbon material.

38.1°, 44.8° and 64.5° diffraction peaks are related to the crystal structures of Au.

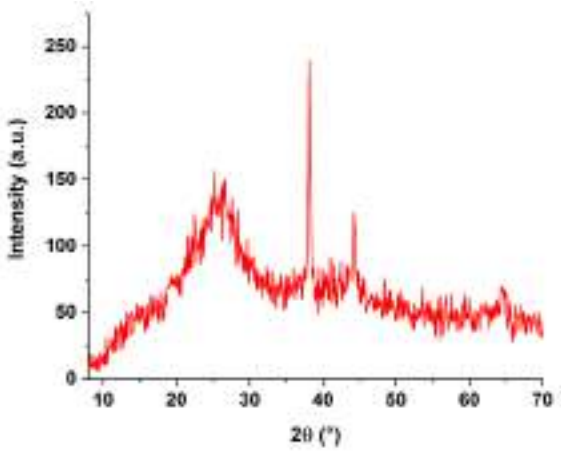

Fig.2. XRD pattern of Au nanoparticles decorated mesoporous carbon material.

BET analysis was used to determine the surface area and pore volume of the synthesized Au@MC. As indicated in Figure 3, N_2 adsorption-desorption isotherm of Au@MC catalyst exhibited a type IV isotherm, indicating the formation of mesostructure carbon.

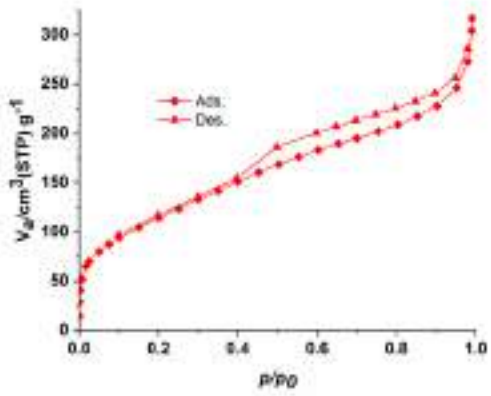

Fig.3. N_2 adsorption-desorption isotherm of Au nanoparticles decorated mesoporous carbon material.

Then, the catalytic activity of the Au@MC toward the reduction of 4-nitrophenol (4-NP) to 4-aminophenol (4-AP) was studied under different conditions. After optimization of the reaction conditions, heating an aqueous solution of 5 mg of 4-NP in 2 mL of water in the presence of 50 mg of $NaBH_4$ and 2 mg of Au@MC at 55 °C, led to the full reduction of 4-NP to 4-AP in 15 min.

The UV spectra of the reduction of 4-NP catalyzed with Au@MC by time is shown in Figure 4. Typically, a mixture of 4-NP and $NaBH_4$ exhibited an absorbance at 400 nm, relating to the formation of 4-nitrophenolte ion.[18] By addition of Au@MC, 4-NP started to reduce, and the absorbance at 400 nm was decreased gradually by the time, and a new absorbance at 300 nm, relating to the formation of 4-aminophenol, was appeared, and increased by time. Turning the color of reaction mixture from yellow to colorless could be considered as a visual witnessof the complete reduction of 4-NP.

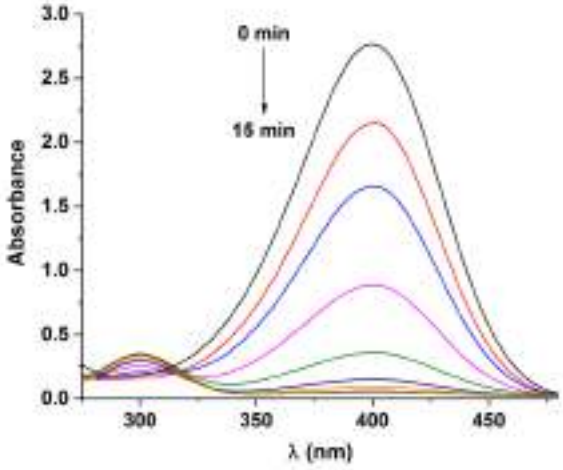

Fig.4. UV-Vis spectra of the reduction of 4-NP catalyzed with Au@MC by time.

Also, the kinetic of the reduction of 4-NP using Au@MC was studied. Because an excess amount of $NaBH_4$ was used, pseudo-first-order kinetic was applied to study the reduction kinetic by plotting $\ln(A_t/A_0)$ vs. time as expressed by equation (1).

$$\ln\left(\frac{A_t}{A_0}\right) = -kt \qquad (2)$$

Where, A_t and A_0 are the absorbance at 400 nm at time t and time 0 (min) of the reaction, respectively, and k was the kinetic constant.

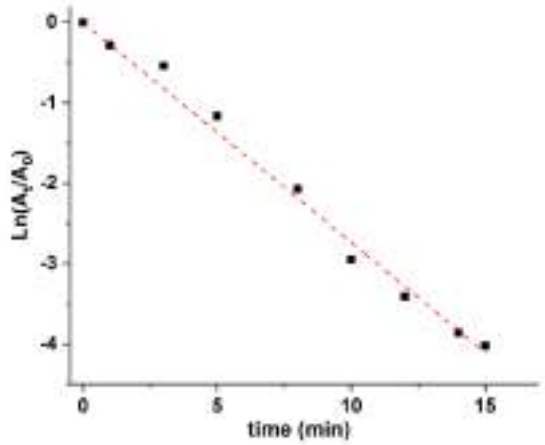

Fig.5. Pseudo-first-order kinetic of the reduction kinetic by plotting $\ln(A_t/A_0)$ vs. time.

As shown in Figure 5, the kinetic of the reduction follows pseudo-first-order kinetic, in wich *k* value was calculated to be 0.2736 s^{-1}, with r^2 value of 0.9965.

Recyclability of Au@MC catalyst was studied by separation of catalyst from reaction medium by centrifuge and then washing and drying at 70 °C. Recovered catalyst was treated with the fresh solution of 5 mg of 4-NP in 2 mL of water in the presence of 50 mg of $NaBH_4$ and heated at 55 °C. Results revealed that the Au@MC could be recycled and reused for 5 runs.

3. Conlusion

In summary a novel heterogenous nanocatalysts, gold nanoparticles decorated mesoporous carbon material was synthesized via carbonization of egg biomass followed by decoration of gold nanoparticles by chemical reduction of Au(III) salt with hydrazine. The prepared Au@MC was characterized using SEM, TEM, EDX, XRD and BET analysis. The results reveald the succesfull decoration of Au nanoparticles on the surface of mesoporous carbon material. Then the catalytic activity of the prepared Au@MC toward reduction of 4-nitrophenol to 4-aminophenol was studied. Kinetic study revealed that the Au@MC-catalyzed reduction of 4-nitrophenol followed pseudo-first-order kinetic model.

. The investigation of catalytic performance of Ag@HNTs-ILs and Co@HNTs-ILs nanocatalysts for 4-NP redaction reaction demonstrated high catalytic activity of the nanocatalysts under mild reaction conditions. The

4. References

[1] K.-S. Ju, R.E. Parales, Microbiol. Mol. Biol. Rev. 74 (2010) 250-272.

[2] I.D. Entwistle, A.E. Jackson, R.A. Johnstone, R.P. Telford, J. Chem. Soc., Perkin Trans. 1 (1977) 443-444.

[3] M. Shokouhimehr, Catalysts 5 (2015) 534-560.

[4] M.I. Din, R. Khalid, Z. Hussain, T. Hussain, A. Mujahid, J. Najeeb, F. Izhar, Critic. Rev. Anal. Chem. 50 (2020) 322-338.

[5] Z. Dong, X. Le, X. Li, W. Zhang, C. Dong, J. Ma, Appl. Catal. B: Environ. 158 (2014) 129-135.

[6] R. Begum, K. Naseem, E. Ahmed, A. Sharif, Z.H. Farooqi, Colloid. Surf. A: Physicochem. Eng. Asp. 511 (2016) 17-26.

[7] A. Akbari, M. Amini, A. Tarassoli, B. Eftekhari-Sis, N. Ghasemian, E. Jabbari, Nano-Struct. Nano-Objects 14 (2018) 19-48.

[8] S. Navalón, M. Álvaro, A. Dhakshinamoorthy, H. García, Molecules 24 (2019) 3050.

[9] Y.R. Mejía, N.K.R. Bogireddy, RSC Adv. 12 (2022) 18661-18675.

[10] I. Sargin, Int. J. Biol. Macromol. 137 (2019) 576-582.

[11] K. Yavari, B. Eftekhari-Sis, A. Akbari, Nano 16 (2021) 2150089.

[12] A. Akbari, A. Naderahmadian, B. Eftekhari-Sis, Polyhedron 171 (2019) 228-236.

[13] A. George, D. Selvan, S. Mandal, Chem. Select 2 (2017) 9718-9721.

[14] B. You, Y. Tian, B. Wang, G. Zhu, Catalysts 12 (2022) 588.

[15] A.Y. Khormi, B.M. Al-Shehri, F.A. Al-Zahrani, M.S. Hamdy, A. Fouda, M.R. Shaaban, Catalysts 13 (2023) 445.

[16] Y. Qu, G. Xu, J. Yang, Z. Zhang, Appl. Catal. A: Gen. 590 (2020) 117311.

[17] C.H. Campos, K. Shanmugaraj, T.M. Bustamante, E. Leal-Villarroel, V. Vinoth, R. Aepuru, R.V. Mangalaraja, C.C. Torres, Catal. Today 394 (2022) 510-523.

[18] F. Kazeminava, N. Arsalani, A. Akbari, Appl. Organomet. Chem. 32 (2018) e4359.

29TH IRANIAN ORGANIC CHEMISTRY CONFERENCE
1_3 NOV, 2023
UNIVERSITY OF QOM, IRAN

Nickel immobilized on ZPD as an efficient and reusable nanocatalyst for organic transformations

Pouya Taheri, Fatemeh Golmiri, Mahmood Tajbakhsh*

Department of Chemistry, Faculty of Chemistry, University of Mazandaran, Mazandaran, Iran, fatemehgolmiri76@gmail.com, pooyataheri90@yahoo.com

Abstract

ZPD as one type of MOF is based on zinc ions, in the structure of which 2,5 pyridine dicarboxylic acid (pydc) ligand is present. A heterogeneous catalyst containing nickel nanoparticles (NPs) loaded on $Zn_4(pydc)_4(DMF)_2 \cdot 3DMF$ support (Ni@ZPD) was synthesized by incipient wet impregnation procedure and its catalytic activity in the Biginelli reaction was investigated. Ni@ZPD has some significant benefits such as high surface area and porosity, high thermal stability, and good tolerance for air and moisture. Using inductively coupled plasma-optical emission spectroscopy (ICP-OES), the content of Ni loaded into the Ni@ZPD nanocatalyst was obtained at nearly 3% wt. The heterogeneous catalyst could be used six times without losing its catalytic activity. The catalyst is easily separated from the reaction products without a significant decrease in the catalytic activity and reaction yield which makes it suitable for practical applications.

1. Introduction

The metal-organic framework is a new category of crystalline hybrid material made from the bonding of metal ions with organic ligands and has specific organic sections or topologies [1]. In the last decade, MOFs have received much attention due to considerable properties such as their topology, high specific surface area, suitable microporous pores, and regular and uniform pores [2-4]. These compounds as a new type of porous material have many applications such as gas storage, separation, optical properties, drug delivery, and catalysts [5]. Post-synthetic modification (PSM) of MOF has recently been an incredible feature for the production of functionalized catacatalysts achieving an ideal porous composition. In this method, the nature of MOF cavities is changed after synthesis, and thus high-sensitivity cavities are provided to the guest molecules [6]. Over the past few decades, MCR reactions have expanded rapidly. There are various types of MCR reactions, such as the reactions involving ethyl acetoacetate (Huntzsch, Biginelli reaction) and the reactions involving isocyanide coupling reaction of ugi and tetrahydrochromene [7] Polyfunctionalized dihydropyrimidines (DHPMs) are a group of valuable heterocyclic compounds that are essential in synthesis of organic compounds. These valuable chemical compounds are used to synthesize biologically active molecules because of their attractive pharmacological effects, including anti-tumor, antibacterial, antiviral, and anti-HIV agents [8]. These combinations are commonly synthesized through a one-pot three-component cyclo condensation reaction between dimedone, aryl aldehydes, and Urea in the presence of various catalysts including LiBr, Phenylboronic acid, l-proline, HBF_4, CuO, and Mo/γ-Al_2O_3 [9]. $Zn_4(PYDC)_4(DMF)_2 \cdot 3DMF$ (ZPD) has a three-dimensional lattice consisting of two types of zinc atoms. Primary zinc atoms are six-coordinated with five oxygen and one nitrogen atom from four pyridines dicarboxylic acid and one DMF ligand. The second type of zinc atom is coordinated with four Oxygen and one nitrogen atoms enamel of three pyridine dicarboxylic acid pyridoxine ligands where disturbed solvent DMF molecules are engrossed in a space-filling style [10].

ZPD with suitable surface area, sufficient porosity, and thermal stability is suitable for modifying and making efficient catalysts. In this study, after the successful preparation of ZPD, it was modified with Ni NPs to prepare the Ni@ZPD nanocatalyst. The catalytic activity of the Ni@ZPD NPs heterogeneous catalyst was studied in the Biginelli reaction. The results show that the catalyst can catalyze the reaction for producing a product with high efficiency, and the catalyst can also be used several times for synthesis.

2. Results and Discussion

2.1. Characterization of Ni@ZPD

In the ZPD FTIR spectra displayed in **Fig. 1**, the bands at 1620 cm^{-1} are allocated to carbonyl groups (C=O) of the dicarboxylate ligand. There is a characteristic peak at 1041-1175 cm^{-1} associated with the tensile vibration of (C-O) in the ligand, 2,5-pyridine dicarboxylic acid, and the peak at 3400 cm^{-1} is related to the tensile vibration of the hydroxyl group. These spectra indicate that the MOF structure is preserved after Ni loading.

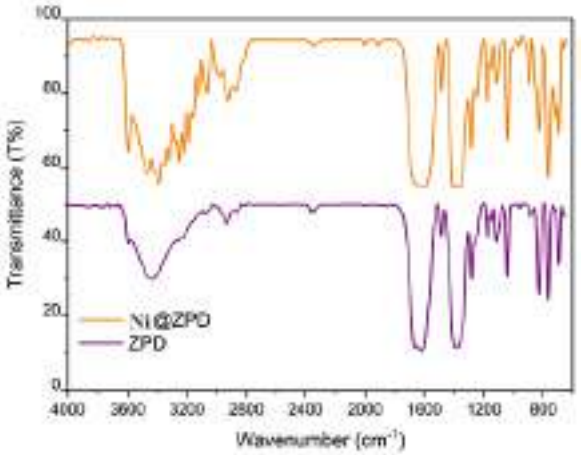

Fig. 1. The FT-IR curves of (a) ZPD and (b) Ni@ZPD

The X-ray patterns of ZPD and Ni@ZPD are displayed in **Fig. 2**. In the XRD pattern of, ZPD some peaks appeared at 2θ of 7.79, 17.09, 23.39, 25.24 and, 31.34°. After the formation of Ni in the structure of the ZPD, the index peaks at 2θ of 7.79, 17.09, 23.39, 25.24, and 31.34° were maintained. The characteristic peak of Ni can be observed at 2Θ=45, 55° related to plane (**JCPDS card no**. **01-078-7533**).

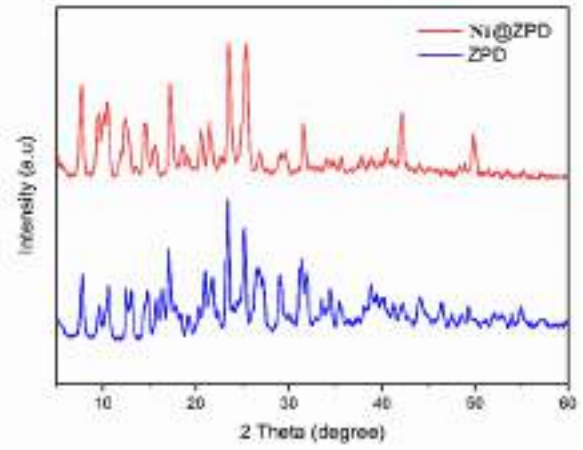

Fig. 2. The XRD curves of ZPD and Ni@ZPD

The ICP-OES technique was also used to determine the accurate content of Ni on the surface of MOF. The calculated value is 3% wt. which confirms the immobilization of Ni onto the catalyst surface.

In order to measure the surface area and the size of the pores, the BET method was used. Nitrogen adsorption isotherms were measured for ZPD and Ni@ZPD. According to ZPD's BET surface area (SBET), and micropore volume (cm^3), they are respectively 384 m^2 g^{-1} and 0.189 cm^3 g^{-1}. In Ni/ZPD, the BET surface area (SBET), and micropore volume are 54 m^2 g^{-1} and 0.052 cm^3 g^{-1}, respectively. Ni@ZPD has a significantly reduced surface area and pore volume compared to ZPD, as shown in **Table 1**. This decline in pore volume and surface area may be because Ni nanoparticles occupy ZPD pores.

Table 1. The BET analysis for ZPD, and Ni@ZPD

Samples	Specific surface area (m^2 g^{-1})	Average pore volume (cm^3 g^{-1})	Average pore diameter (nm)
ZPD	384	0.189	1.6
Ni@ZPD	54	0.052	4.9

The curves of the ZPD samples consist of three-step of mass reductions (**Fig. 3**). The first mass reduction in the range of 100-200 °C is related to the removal of H_2O molecules from the structure of the ZPD. The second mass reduction at 200-300 °C is related to the removal of DMF molecules from the structure of the ZPD. The third mass reduction at 300-450 °C is assigned to the release of carbon dioxides from the structure of the ZPD or decomposition of the frameworks for both ZPD and Ni/ZPD. The presence of Ni in the nanohybrid increases the stability compared to ZPD, and the thermal loss for ZPD at 600 °C is 22 % more than that for Ni/ZPD.

.

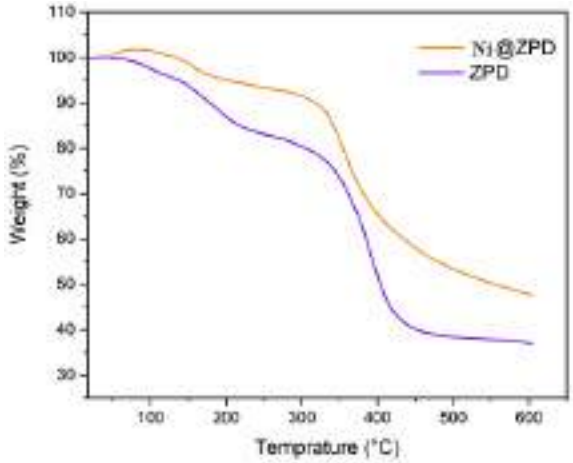

Fig. 3. The TGA curves of ZPD and Ni@ZPD

2.2. Evaluating Ni@ZPD NPs catalytic activity in the Biginelli reaction

Ni@ZPD NPS was studied in this study as a heterogeneous catalyst in the Biginelli reaction. Initially, for optimization of the reaction conditions, benzaldehyde (1 mmol), urea (1 mmol) and ethyl acetoacetate were selected as a model reaction to explore the catalytic activity of Ni@ZPD nanocatalyst. In order to optimize the reaction conditions, the reaction parameters Such as solvent, temperature, and amount of catalyst were investigated. In order to obtain a suitable solvent, different solvents were used to perform the reaction. EtOH was the best solvent for the reaction compared to other solvents. As a result of the use of solvents such as water and H_2O/EtOH, the reaction rate and yield have been reduced. In addition, MeOH and THF provided moderate yields, while Toluene, Chloroform, and CH_3CN led to lower yields. In order to select the appropriate amount of catalyst for the Biginelli reaction, benzaldehyde, urea, and ethyl acetate were reacted in the presence of different

amounts of Ni@ZPD catalyst in ethanol solvent. According to the obtained results, the optimal amount of the Ni@ZPD catalyst was 0.015 g. Utilization of the lower amount of catalyst decreased the product yield. When the amount of catalyst increased to 0.02 g, no significant change was observed in the yield and reaction time. The reaction was also investigated in the absence of the catalyst. However, no products were formed. To optimize the temperature for the Biginelli reaction, the reaction in ethanol solvent at different temperatures was performed. Based on the obtained results, the optimum temperature for the reaction is 70 °C. However, when the temperature was 80 °C, there was no noticeable change in the yield and reaction time.

2.3. Check the catalyst recyclability

To explore the catalytic activity and reusability of the Ni@ZPD catalyst in the Biginelli reaction, the reaction of aldehyde, dimedone, and urea was used as a patterning process for the Biginelli reaction. After the reaction was complete, the catalyst was separated via filter paper and then washed with EtOH (3×10 mL) and the solids were dried at 80 °C for 12 h in vacuum conditions. So, it was ready to be used in the next round under the same conditions without any more purification. According to test results, the heterogeneous catalyst can be recycled and reused six times to perform the reaction without a significant decrease in catalytic activity and reaction yield.

4. Conclusions

In summary, Ni@ZPD nanocatalyst has been prepared, and its catalytic activity was explored in the synthesis of diphenylacetylene derivatives under mild and green reaction conditions. Some crucial advantages of the catalyst, such as high surface area and porosity, and high thermal stability, were examined, the catalytic activity of Ni@ZPD NPs heterogeneous catalyst was studied in the Biginelli reaction, and the results showed that the efficiency of the process is enhanced in the presence of the catalyst in comparison to the condition in which no catalyst is present in the reaction vessel. The catalyst is easily removed from the reaction products without significantly decreasing the catalytic activity and reaction yield. The catalyst was recovered six times, the structure of the catalyst was also preserved, and a low amount of Ni was lost. This means the high stability of catalysts during the recycling process. The obtained results confirmed that the proposed catalyst has a high potential to be used in catalyzing different reactions.

5. Experimental

5.1. Synthesis of Cu@ZPD

To prepare Ni@ZPD, 100 mg of ZPD was dissolved in 5 mL of EtOH at room temperature. Then, $NiCl_2$ (30 mg) was added to the suspension. The mixture was dispersed with ultrasound for 10 minutes, then a 10 mL aqueous solution of sodium borohydride (0.2 M) was slowly injected into the mixture. After 60 min of sterilization, the final product was collected and centrifuged in 8000 r.p.m for 20 minutes, washed three times with methanol (3×10 mL), and then placed in a vacuum oven at 60 °C for 6 h to obtain gray powder product.

5.2. The general producer for performing the Biginelli reaction

In a typical experimental procedure, a mixture of aldehyde (1 mmol), a β-dicarbonyl compound (ethyl acetoacetate, or dimedone) (1 mmol), urea (1.5 mmol), in the presence of 3 mL of EtOH solvent was prepared. 0.015 g of Ni@ZPD catalyst was added to the above mixture. The resulting mixture was stirred at 78°C. The progress of the reaction was evaluated by thin-layer chromatography (TLC) using (n-hexane/ethyl acetate, 2:3.) As soon as the reaction was complete, the reaction mixture was cooled to room temperature, followed by filtration to separate the catalyst from the reaction mixture. A solution of ethanol was used to dissolve the precipitate, which was then crystallized using ice cubes added to the reaction mixture.

6. References

[1] Y. S. Kang, Y. Lu, K. Chen, Z Y. hao, P. Wang, W. Y. Sun, Metal-organic frameworks with catalytic centers: from synthesis to catalytic application, Coor. Chem. Rev. 378 (**2019**) 262-280.

[2] M. Zhong, L. Kong, N. Li, Y.Liu, Y., Zhu, J., Bu, X. H.. Synthesis of MOF-derived nanostructures and their applications as anodes in lithium and sodium-ion batteries. Coor.Chemi. Rev. 388 (**2019**) 172-201.

[3] J.Wang, N. Li, Y. Xu, H. Pang, Two-dimensional MOF and COF nanosheets: synthesis and applications in electrochemistry, Chemistry–A European Journal, 26 (**2020**) 6402-6422.

[4] R. Sacourbaravi, Z. Ansari-Asl, M. Kooti, V. Nobakht, E. Darabpour, Fabrication of Ag NPs/Zn-MOF Nanocomposites and Their Application as Antibacterial Agents, Journal of Inorganic and Organometallic Polymers and Materials, 30(11) (**2020**) 4615-4621.

[5] A. Bavykina, N. Kolobov, I. S. Khan, J. A. Bau, A. Ramirez, J.Gascon, Metal-organic frameworks in heterogeneous catalysis: recent progress, new trends, and future perspectives. Chemical Reviews, 120 (**2020**), 8468-8535.

[6] M. Kalaj, S. M. Cohen, Postsynthetic modification: an enabling technology for the advancement of metal-organic frameworks, ACS central science, 6(**2020**) 1046-1057.

[7] Sharma UK, Ranjan P, Van der Eycken E V., You S-L. Sequential and direct multicomponent reaction (MCR)-based dearomatization strategies. Chem Soc Rev, 49 (**2020**), 21–48.

[8] Lal J, Gupta SK, Thavaselvam D, Agarwal DD. Design, synthesis, synergistic antimicrobial activity and cytotoxicity of 4-aryl substituted 3,4-dihydropyrimidinones of curcumin. Bioorg Med Chem Lett 22 (**2012**), 2872–2876.

[9] Kouachi K, Lafaye G, Pronier S, Bennini L, Menad S. Mo/γ-Al2O3 catalysts for the Biginelli reaction. Effect of Mo loading. J Mol Catal A Chem 395(**2014**), 210–216.

DFNS/IL/Ru nanoparticles as efficient catalyst for the quinazoline-2,4(1*H*,3*H*)-diones

Farzaneh Shamsa[1], *Alireza Motavalizadehkakhky*[1*], *Rahele Zhiani*[1,2], *Jamshid Mehrzad* [3], *Malihe Sadat Hosseiny* [1]

[1] *Department of Chemistry, Neyshabur Branch, Islamic Azad University, Neyshabur, Iran, farzane.shamsa@yahoo.com.*
[2] *New Materials Technology and Processing Research Center, Neyshabur Branch, Islamic Azad University, Neyshabur, Iran*
[3] *Department of Biochemistry, Neyshabur Branch, Islamic Azad University, Neyshabur, Iran*

Abstract - The transmutation of waste into valuable materials has a special place in green chemistry. Herein, we reported chemical composition of 2-iodoaniline, isocyanides, and carbon dioxide to prepare quinazoline-2,4(1H,3H)-diones in the presence of Ru NPs stably placed on the surface of dendritic fibrous nanosilica by ionic liquid (DFNS/IL-Ru) as a catalyst. This is a great economic strategy to create three bonds in one-pot multicomponent reaction step employing functional groups. With the aim of preparing the catalyst, the dendritic fibrous nanosilica surface was first activated using IL to be employed as a substrate to support Ru NPs. IL acts as a stabilizing and reducing agent for Ru nanocatalyst and eliminates the need for a reducing agent. The highest amount of quinazoline-2,4(1H,3H)-diones was obtained under ideal situations in the presence of 5 mg of DFNS/IL-Ru under carbon dioxide (1 atm) utilizing a balloon set at 70 ºC for 3 hours. Thus, allowing its being potentially applicable for green and economic production of quinazoline-2,4(1H,3H)-diones especially from the low-cost feedstocks.

1. Introduction

Recently, the scientific circles have shown great interest in the employment of non-venomous, recyclable, available, and cost-effective CO_2 to produce valuable organic composites [1]. Remarkable progress has been made in the area, mostly by d-block metal-catalyzed reactions. However, the preparation of heterocyclic composites like phenyl-annulated heteroarenes via the introduction of CO_2 has been less investigated [2-5].

Isocyanides have been mainly employed as significant synthons in modern synthetic organic chemistry, especially for N-containing heterocyclic composites synthesis through chemical transformations, like multi-component reactions [6-9]. Today, different transition metals (such as Cu [10], and Ag [11]) catalyzed reactions have been announced, in which isocyanides were deployed to generate N-containing heterocyclic molecules. Quiznazoline-2,4(1*H*,3*H*)-diones are key anatomical sub-moiety of a wide range of commercial medicines as well as biological molecules. They are the main framework of anti-hypertensive medicines like pelanserin, [12] ketanserin [13] as well as anti-psychotic medicines like tioperidone [14] and belaperidone [15].

Combining isocyanide and CO_2 through a multi-element reaction to produce N_3-substituted 2,4(1*H*,3*H*)-quinazolinediones may seem an interesting approach. However, in the presence of transition metal catalysts, this sort of multi-element reaction is yet underdevelopment [16]. The reason is that the solubility of carbon dioxide in organic solvents is very low, and this low solubility reduces with enhancing temperature. Furthermore, isocyanides are solids/liquids entirely solvable in organic solvents. Hence, combining CO_2 and isocyanides in a multi-element reaction is not easy.

The group of North employed chromium and aluminum salphen compounds with TBAB to produce cyclic carbonates [17]. Bimetallic Co(II), Cu(II), and Ni(II) compounds combined with TBAI for the CO_2 coupling under moderate reaction situations were announced by Kumar et al [18].

In the view of the above, we decided to provide a heterogeneous catalyst with immobilized *Ru* NPs stably placed on the surface of dendritic fibrous nanosilica (DFNS) by ionic liquid (IL), and examine its catalytic attributes in an efficient three-component reaction to create valuable 2,4(1*H*,3*H*)-quinazolinediones through the deployment of atmospheric carbon dioxide (Scheme 1).

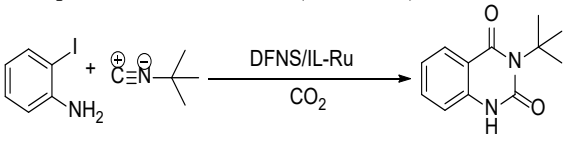

Scheme 1 Importance and preparation of quinazoline-2,4(1*H*,3*H*)-diones.

The synthesis of DFNS/IL-Ru catalyst and the reaction of N3-substituted 2,4(1H,3H)-quinazolinediones were carried out according to the method [19] and [20] respectively.

2.Results and discussion

The DFNS/IL-Ru catalyst was investigated in the binding reaction between CO_2 insertion into isocyanides and 2-iodoaniline. To meet the best reaction state, the impact of various parameters like a solvent, temperature, catalyst quantity, and reaction time on the development of the binding reaction between CO_2 insertion into isocyanides and 2-iodoaniline was investigated deploying the catalyst. First, the influence of temperature on the reaction efficiency was examined (Fig.1.). Results showed that the reaction temperature (30-80 °C) and the cyclic carbonate efficiency are directly related together. Finally, the quinazoline-2,4(1*H*,3*H*)-dione synthesis reactions were done at 70 °C.

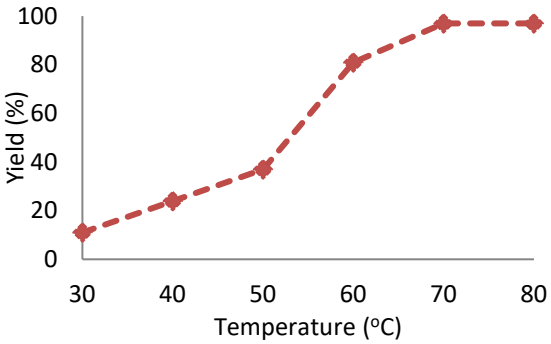

Fig.1. Impact of temperature on the synthesis efficiency of quinazoline-2,4(1*H*,3*H*)-dione.

Illustrates the impact of solvent on catalytic progress. The reaction did not begin under toluene or solvent-free situations and demonstrated low conversion in polar protic solvents, including ethanol, methanol, and *i*-PrOH. CH_2Cl_2 and $CHCl_3$ resulted in 64% and 51% yield. The cross-coupling product showed a relatively average-to-good yield with CH_2Cl_2 and $CHCl_3$ as the polar aprotic solvents. DMF considered as the finest solvent for reactions and generated a high efficiency of 96%. The solvent had deeply influenced the catalytic activity of DFNS/IL-Ru NPs towards the synthesis of quinazoline-2,4(1*H*,3*H*)-dione derivatives. Therefore, DMF was selected as a cost-effective solvent.

The impact of reaction duration on the yield of quinazoline-2,4(1*H*,3*H*)-dione under equivalent reaction situations (at 70 °C and 3 MPa CO_2) is illustrated in Fig. 2. It was discovered that increasing the reaction time positively affects the product's yield. In practice, the binding reaction reached 96 % within 3 hours; therefore, 3 hours was determined as the optimal time.

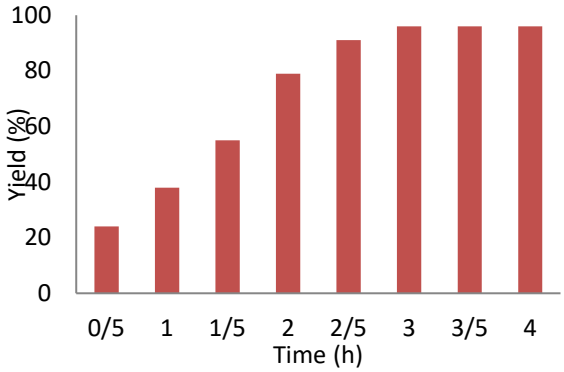

Fig. 2. Impact of reaction time on the synthesis function of quinazoline-2,4(1*H*,3*H*)-dione.

Fig.3. depicts the impact of catalyst quantity on the transformation of raw materials into products. Although increasing the catalyst quantity increased the yield percentage, this increase was not significant. Therefore, the finest catalyst value of 5 mg was determined.

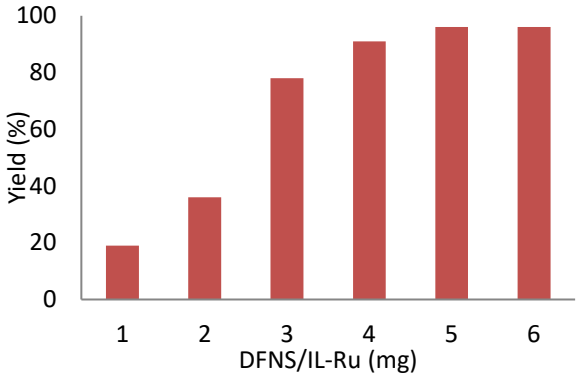

Fig.3. Impact of catalyst quantity on the synthesis performance of quinazoline-2,4(1*H*,3*H*)-dione.

Under the best reaction situations, we examined the bed range of different derivatives of o-iodoanilines (Table 1). The Methyl group, as an electron donor group containing 2-iodoanilines, provides > 90% of the isolated efficiency of the product. When mild electron-with drawing groups like cyano, chloro, or fluoro substituted o-iodoanilines were replaced to the reaction, moderate to very fine isolated yields (81–98%) were achieved. In addition, the substituted 2-iodoaniline derivative for electron-NO_2 adsorption substituted also generated 86% of the quinazolinedione product yield.

Table 1 Synthesis of quinazoline-2,4(1*H*,3*H*)-dione derivatives in the participation of DFNS/IL-Ru NPs.

Entry	Substrate	Product	Yield (%)
1	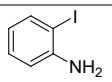	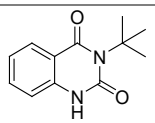	92
2	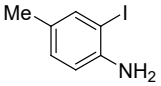	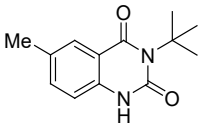	96
3	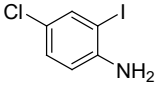	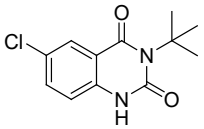	88

3-*tert*-butyl-6-chloroquinazoline-2,4(1*H*,*3H*)-dione White solid, m.p.: > 300 °C (lit.: > 300 °C), IR (KBr, ν, cm^{-1}): 3347, 3315, 3076, 2978, 2812, 1698, 1639, 1432, 1278, 1234, 820, 774, 712, 648, 511. ^{1}H NMR ($CDCl_3$, 400 MHz) δ = 11.19 (s, 1H), 7.73 (dd, *J* = 2.5, 0.5 Hz, 1H), 7.64 (dd, *J* = 8.7, 2.5 Hz, 1H), 7.12 (dd, *J* = 8.6, 0.5 Hz, 1H), 1.63 (s, 9H) ppm. ^{13}C NMR ($CDCl_3$, 400 MHz) δ = 163.0, 150.6, 137.9, 134.1, 126.7, 125.8, 117.4, 116.2, 60.3, 29.5 ppm.

For a more precise assessment of the efficiency of the catalyst, a number of control investigations were conducted (Table 2). The reaction performed utilizing dendritic fibrous nanosilica revealed that no quantity of the quinazoline-2,4(1*H*,3*H*)-dione was generated after 3 hours (Table 2, enrty 1). The findings revealed that the synthesis of quinazoline-2,4(1*H*,3*H*)-dione is fundamentally catalyzed employing DFNS/IL-Ru. Nanoparticles enhanced the activity of the catalyst on account of the increase in surface area to volume. Therefore, they remarkably enhanced the sensitivity between the catalyst and the reactants and functioned as a homogeneous catalyst (Table 2, enrty 3).

Table 2 Influence of different catalysts for the preparation of quinazoline-2,4(1*H*,3*H*)-dione.

Entry	Catalyst	Yield (%)
1	DFNS	-
2	DFNS/IL	90
3	DFNS/IL-Ru	96

3.Conclusions

DFNS/IL-Ru through a facile and sustainable reduction technique, without any reducing agent to create a separable catalyst. We have developed the first three-component reaction to synthesize valuable 3-*tert*-butylquinazoline-2,4(1*H*,3*H*)-dione from carbon dioxide, tert-butyl isocyanide, and o-iodoaniline. This strategy has advantages such as ease of access to raw materials, wide range of substrate, and good functional group tolerance that allow access to a wide range of 3-*tert*-butylquinazoline-2,4(1*H*,3*H*)-dione derivatives. Therefore, other sustainable NPs with features such as high efficiency and reusability can be developed in the future by following the techniques suggested in this study.

References

[1] M. Cokoja, C. Bruckmeier, B. Rieger, W.A. Herrmann, F.E. Kühn, Angew. Chem., Int. Ed. 50 (2011) 8510-8537.
[2] S.M. Sadeghzadeh, R. Zhiani, M. Khoobi, S. Emrani, Microporous and Mesoporous Materials. 257 (2018) 147-153.
[3] Q.W. Song, Z.H. Zhou, L.N. He, Green Chem. 19 (2017) 3707-3728.
[4] S.M. Sadeghzadeh, R. Zhiani, S. Emrani, RSC advances. 7(2017) 24885-24894.
[5] S. Wang, C. Xi, Chem. Soc. Rev.48(2019) 382-404.
[6] L. Sun, J.H. Ye, W.J. Zhou, X. Zeng, D.G. Yu, Org. Lett., 20(2018)3049-3052.
[7] L. Zhu, J.H. Ye, M. Duan, X. Qi, D.G. Yu, R. Bai, Y. Lan, Org. Chem. Front.5(2018) 633-639.
[8] R. Yousefi, T.J. Struble, J.L. Payne, M. Vishe, N.D. Schley, J.N. Johnston, J. Am. Chem. Soc. 141(2019) 618-625.
[9] L. Song, Y.X. Jiang, Z. Zhang, Y.Y. Gui, X.Y. Zhou, D.G. Yu, Chem. Commun. 56(2020) 8355-8367.
[10] T.B. Nguyen, Adv. Synth. Catal.359(2017) 1066-1130.
[11] T.B. Nguyen, Asian J. Org. Chem. 6(2017) 477.
[12] Y. Liao, Y. Peng, H. Qi, G.J. Deng, H. Gong, C.J. Li, Chem. Commun. 51(2015) 1031-1034.
[13] F. Chen, G. Liao, X. Li, J. Wu, B.F. Shi, Org. Lett. 16(2014) 5644-5647.
[14] L. Meng, T. Fujikawa, M. Kuwayama, Y. Segawa, K. Itami, J. Am. Chem. Soc. 138(2016)10351-10355.
[15] H. Xie, J. Cai, Z. Wang, H. Huang, G.J. Deng, Org. Lett. 18(2016) 2196-2199.
[16] W. Lu, J. Ma, J. Hu, J. Song, Z. Zhang, G. Yang, B. Han, Green Chem. 16(2014) 221-225.
[17] W.B. Wang, G.B. Hammond, B. Xu, Journal of the American Chemical Society. 134(2012) 5697.
[18] L. Guczi, A. Beck, Z. Paszti, Catalysis Today. 181(2012)26-32.
[19] Y. Li, S. Song, S. M. Sadeghzadeh, Catalysis Letters.153(2023)95–103.
[20] F. Shamsa, A. Motavalizadehkakhky, R. Zhiani, J. Mehrzad, M.S. Hosseiny, RSC Adv. 11(2021) 37103-37111.

29TH IRANIAN ORGANIC CHEMISTRY CONFERENCE
1_3 NOV, 2023
UNIVERSITY OF QOM, IRAN

Biogenic CuO nanoparticles for CO_2 hydrogenation

Farzaneh Shamsa[1], *Alireza Motavalizadehkakhky*[1*], *Rahele Zhiani*[1,2], *Jamshid Mehrzad* [3], *Malihe Sadat Hosseiny* [1]

[1] *Department of Chemistry, Neyshabur Branch, Islamic Azad University, Neyshabur, Iran, farzane.shamsa@yahoo.com*
[2] *New Materials Technology and Processing Research Center, Neyshabur Branch, Islamic Azad University, Neyshabur, Iran*
[3] *Department of Biochemistry, Neyshabur Branch, Islamic Azad University, Neyshabur, Iran*

Abstract- After being exposed to toxic metal ions, microorganisms produce metal nanoparticles. Despite the possibility of using these biological processes to steadily improve vital metals (like copper oxide), the catalytic performance of biosynthesized metal nanoparticles has not been studied. This strategy has superb advantages like high economic efficiency and tolerance of functional groups. In this study, biogenic copper oxide nanoparticles were produced by the *Desulfovibrio alaskensis* to reduce carbon dioxide for the preparation of formate salts in an aqueous medium. The effect of various parameters such as volumes of water, temperature, time, amount of catalyst process was investigated. The results showed that had the highest efficiency in the presence of 5mg catalyst at 70°C for 8 h with 15 ml water.

1. Introduction

Nonrenewable carbon resources have recently given rise to a variety of industrial techniques, and carbon dioxide has taken the place of C1 raw materials. Processes are stabilized by CO_2, a material that is accessible, plentiful, and secure [1-2]. One of the major issues in sectors where catalysis is important, such as industry and academia, is the transformation of CO_2 into advanced commodities. The study of epoxide reactions [3-12], where easily prepared cobalt catalysts are active, is one of the most comprehensive areas of study for the use of carbon dioxide. It also aids in the hydrogenation of CO_2 to formic acid or methanol, cyclic carbonates, or polycarbonates through CO_2/ electrolylation of organometallic derivatives [13-16], and the production of carboxylic acids through reductive methylation. The generation of green synthesis nanoparticles by fungi, bacteria, algae lead, and plants to the large-scale creation of pure metal oxide particles [17, 16]. Various chemical and physical steps are broadly employed to synthesize metal oxide NPs and allow the acquisition of particles with desired properties. Nanoparticle synthesis techniques employing microbes provide stronger dimension control through segmentation in the periplasmic space and vesicles. The rate of intracellular particle generation and thus, the nanoparticle dimension can be partially changed by monitoring factors like temperature, pH, substrate concentration, and exposure time of the substrate [18]. In addition, nanoparticles synthesized by microorganisms are fixed by peptides like phytochelatins, which prevents their accumulation [19]. These peptides are synthesized due to the stress of heavy metals and are a universal mechanism for the separation of metal ions in fungi, plants, and bacteria [20].

The current study reports that biogenic CuO nanoparticles created by *Desulfovibrio alaskensis* are active catalysts for catalytic depletion of CO_2 for the synthesis of formate salt under environmental situations. The reaction has a wide range, can accelerate dramatically in membrane related to TPGS micelles, and act better than other heterogeneous NP catalysts created microbially or by chemical synthesis. Overall, this represents a unique character of the metal depletion path in *Desulfovibrio spp*. That is particularly suitable for the production of highly active metal nanoparticles catalysts (for utilization in organic synthesis).

Synthesis of DaCuO NPs through microwave technique

Freshly made $Cu(CH_3COO)_2{\cdot}2H_2O$ stock solution (40 mM in H_2O) was released in the cell suspension to *D. alaskensis* cells of 2 mM. The centrifuge tubes were incubated in an anaerobic chamber at 45 ˚C for 20 hours. The biogenic nanoparticles (*Da*CuO NPs) were centrifuged for 15 min and cleansed with 40% acetone in H_2O.

Catalytic hydrogenation of CO_2

1M KOH solution (15 mL) and *Da*CuO NPs (5 mg) were added to a 100 mL high-pressure stainless steel reactor vessel. Next, the reactor vessel was pressurized with CO_2 and H_2 gases (10:10, CO_2/H_2).

The reactor vessel was warmed up to 60 °C and stirred at 400 rpm for eight hours. Upon the completion of the reaction, the reactor was cooled at environment temperature. Finally, the reactor was depressurized, the reaction mass was collected in a sample vial, and centrifuged to eliminate *Da*CuO NPs.

2. Results and discussion

Fig. 1. exhibits the impression of heat on the yield and selectivity of the ultimate good. Taking into account the sensitivity of the catalytic activity to the heat of the reaction, the potency of the ultimate product escalated with risinghe at from 50 °C to 60 °C. Nevertheless, temperatures above 70 °C didn't changed performance.

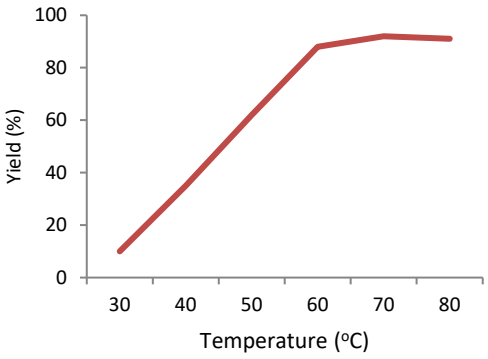

Fig. 1. The effect of temperature on the depletion of CO_2.

The sensitivity of the potency to the reactiontime at 60 °C is depicted in Fig. 2. As can be seen, increasing the reaction time enhanced the potency, and 92 % CO_2 was converted within 8 h.

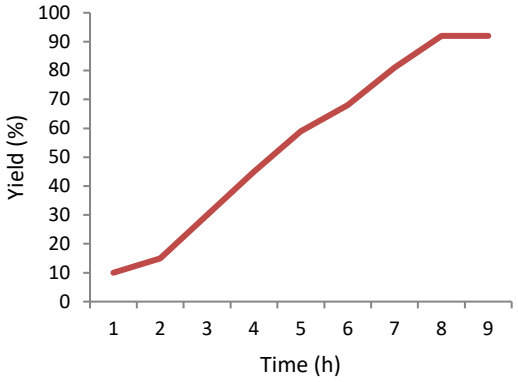

Fig.2. The effect of time on the depletion of CO_2.

Therefore, *Da*CuO NPs were considered suitable nanocatalysts for the hydrogenation of carbon dioxide to formate. Fig.3. depicts the impression of volumes of water on the potency of the ultimate product in the partnership of *Da*CuO NPs. The potency of the ultimate product enhanced to 92% in 15 mL of water.

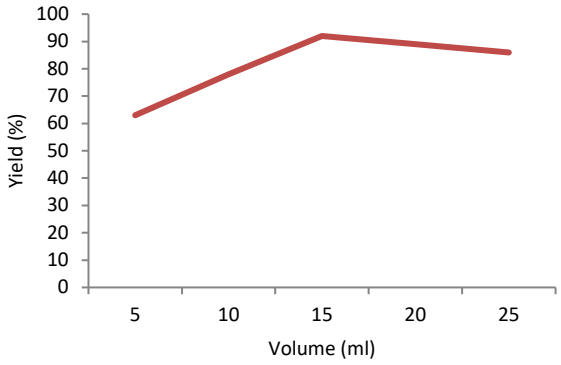

Fig.3.The effect of volumes of water on the depletion of CO_2.

In addition, the impression of the mass of *Da*CuO NPs as a catalyst on the reaction was probed under several situations. The potency escalated to 69% upon the addition of 4.0 mg *Da*CuO NPs (Fig.4.). When the mass of *Da*CuO NPs elevated to 5.0 mg, the potency of the product enhanced to 92%.

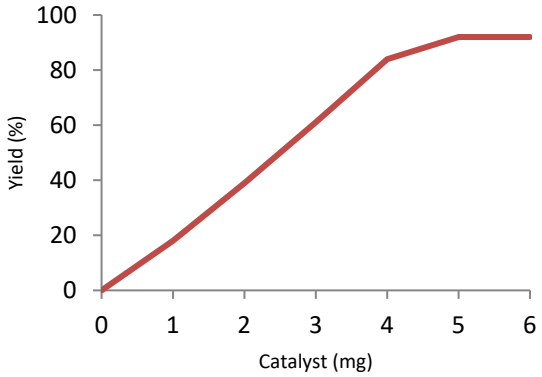

Fig.4. The effect of catalyst amount on the depletion of CO_2.

Convenient recovering and isolation are two crucial attributes of a heterogeneous catalyst. The catalyst recoverability was probed for the fabrication of the product. The *Da*CuO NPs was eliminated from the amalgam after each run. The *Da*CuO NPs were eluted with H_2O and EtOH, and vacuum-dried. As Fig.5. depicts, the catalyst preserved its potency after ten continual runs.

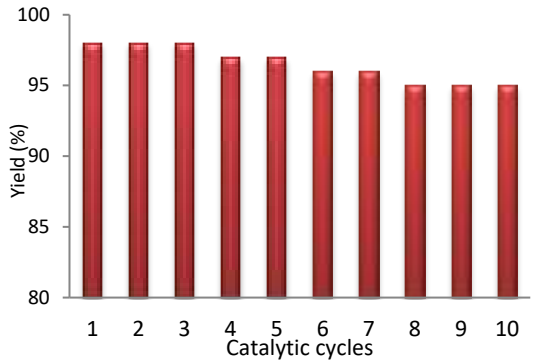

Fig.5. Reproducibility and recyclability of the catalytic system.

3. Conclusions

To sum up, we showed that CuO nanoparticles synthesized by Desulfovibrio alaskensis are very active heterogeneous catalysts for the hydrogenation of carbon dioxide to formate. These biological catalysts can be easily generated from bacterial cell culture employing high-efficiency Cu salts. We demonstrated that the reactions catalyzed by these nanoparticles could be improved by employing designer micelles to co-localize substrates at the cell membrane. The focus of future studies will be on the genetic engineering of D. alaskensis to generate "designer NPs" by increasing reactivity and extending the process to use industrial waste streams as a metal source.

References

[1] A. Dibenedetto, A. Angelini, P. Stufano, J. Chem. Technol. Biot. 89 (2014) 334–353.
[2] J.X. Low, B. Cheng, J.G. Yu, Appl. Surf. Sci. 392 (2017) 658–686.
[3] V.S. Thoi, C.J. Chang, Chem. Commun. 47 (2011) 6578-6580.
[4] S. Biju, J. Gallo, M. Bañobre-López, B.B. Manshian, S.J. Soenen, U. Himmelreich, L.V. Elst, T.N. Parac-Vogt, Chem. Eur. J. 24 (2018) 7278-7297.
[5] A. Kudo, Y. Miseki, Chem. Soc. Rev. 38 (2009) 253-278.
[6] Y. Qu, X. Duan, Chem. Soc. Rev. 42 (2013) 2568-2580.
[7] J. Eppinger, K.W. Huang, ACS Energy Lett. 2 (2017) 188-195.
[8] K. Mandal, D. Bhattacharjee, S. Dasgupta, Int. J. Hydrogen Energy 40 (2015) 4786-4793.
[9] W. Wang, Y. Himeda, J.T. Muckerman, G.F. Manbeck, E. Fujita, *Chem. Rev.* 115 (2015) 12936-12973.
[10] P. Rios, A. Rodriguez, J. Lopez-Serrano, ACS Catal. 6 (2016) 5715-5723.
[11] Y. Kuwahara, Y. Fujie, H. Yamashita, ChemCatChem. 9 (2017) 1906-1914.
[12] M.E. Boot-Handford, J.C. Abanades, E.J. Anthony, M.J. Blunt, S. Brandani, N. Mac Dowell, J.R. Fernandez, M.C. Ferrari, R. Gross, J.P. Hallett, R.S. Haszeldine, P. Heptonstall, A. Lyngfelt, Z. Makuch, E. Mangano, R.T.J. Porter, M. Pourkashanian, G.T. Rochelle, N. Shah, J.G. Yao, P.S. Fennell, Energy Environ. Sci. 7 (2014) 130–189.
[13] G. Devens, T.A. Moore, A.L. Moore, Acc. Chem. Res. 42 (2009) 1890-1898.
[14] A.J. Morris, G.J. Meyer, E. Fujita, Acc. Chem. Res. 42 (2009) 1983-1994.
[15] T. Morimoto, C. Nishiura, M. Tanaka, J. Rohacova, Y. Nakagawa, Y. Funada, K. Koike, Y. Yamamoto, S. Shishido, T. Kojima, T. Saeki, T. Ozeki, O. Ishitani, J. Am. Chem. Soc. 135 (2013) 13266-13269.
[16] R. Yuvakkumar, J. Suresh, A.J. Nathanael, M. Sundrarajan, S.I. Hong, Mater. Sci. Eng. C. 41 (2014) 17-27.
[17] M. Gericke, A. Pinches, Hydrometallurgy. 83 (2006) 132-140.
[18] S. Kang, K.N. Bozhilov, N.V. Myung, A. Mulchandani, W. Chen, Angew. Chem. Int. Ed. 47 (2008) 5186-5189.
[19] D. Pages, J. Rose, S. Conrod, S. Cuine, P. Carrier, T. Heulin, W. Achouak, PLoS ONE. 3 (2008) e1539.
[20] L. Guimaraes-Suares, C. Pascoal, F. Cassio, Ecotoxicol. Environ. Saf. 66 (2007) 36.

29TH IRANIAN ORGANIC CHEMISTRY CONFERENCE
1_3 NOV, 2023
UNIVERSITY OF QOM, IRAN

Electrochemical Oxidation and Antioxidant Activity of Ethanolic Extract of *Stachys lavandulifolia Vahl.*: A Herb-drug interaction in Treatment of Barbiturate Poisoning

Ameneh Amani *

Nahavand Higher Education Complex, Bu-Ali Sina University, Hamedan Iran, 65178-38683,
amani.iran@gmail.com

Abstract - Electrochemical oxidation of ethanolic extract of *Stachys lavandulifolia Vahl.* has been studied in the absence and presence of barbituric acid at the biological pH, using cyclic voltammetry method. The results showed that the electrochemically generated compounds in extract of *Stachys lavandulifolia Vahl.*, participate in the chemical reaction with barbituric acid. Based on our results, the extract of *Stachys lavandulifolia Vahl.* has a high antioxidant activity in comparison of galic acid, salicylic acid and quercetin as standard antioxidants and simultaneous can be useful for the treatment of barbiturate poisoning before starting clinical treatments.

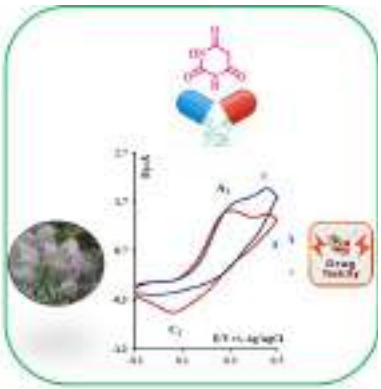

1. Introduction

Millions of people today use herbal therapies along with prescription and nonprescription medications. Although considered natural, many of these herbal therapies can interact with other medications, causing either potentially dangerous side effects and / or reduced benefits from the medications. Currently, there is very little information published on herb-drug interactions whilst the use of herbs is progressively growing across the world [1,2]. As the use of herbs is getting popular, interactions between herbs and allopathic drugs need to be addressed and reviewed properly. Certain herbal supplements can cause potentially dangerous side effects when taken with prescription drugs. The use of alternative therapy is mostly not supervised by physicians or alternative therapy practitioners resulting in increased harm to patients, especially if they are using herbal and prescription medicines that have latent interactions. These interactions can go unnoticed until a patient is hurt or a serious life-threatening event has occurred [3,4]. Barbiturates are a leading cause of acute poisoning. The poisoning is characterized by stupor or coma, are flexia and in late cases, severe respiratory depression and cardiovascular insufficiency. Although today because of the replacing of these class of drugs with the other safety drugs, mortality rates associated with barbiturate toxicity is less than 2% but it is very important for each person to know how to manage this toxicity before the starting each clinical treatment [4-7]. On the other hand, the dietary intake of antioxidants plays an important role in the protection of the human organism against free radicals. Radical reactive species (ROS) generated by our body by various endogenous systems by exposure to different physiochemical conditions or pathological states. A balance between free radicals and antioxidants is necessary for proper physiological function [7-10].

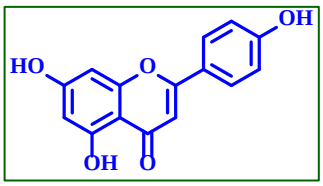

Figure 1. The picture of *Stachys lavandulifolia Vahl.* and the structure of main compound in its extract.

Stachys lavandulifolia Vahl is an herbaceous wild plant native to Iran which is used in Iranian folk medicine as a mild sedative tea for reducing anxiety and for treatment of gastrointestinal disorders. The genus *Stachys* is one of the largest genera in the flowering plant family of Lamiaceae with about three hundred species distributed in Europe, Asia, Africa, Australasia, and North America [11]. In this study at first the electrochemical oxidation of ethanolic extract of *Stachys lavandulifolia Vahl* investigated. Because of the electrochemical oxidation very often parallels

cytochrome P450 catalyzed oxidation in liver microsomes and the hepatic metabolism is the main route of endogenous clearance of all barbiturates [12], it is interesting to study the electrooxidation of ethanolic extract of *Stachys lavandulifolia Vahl* in the presence of barbituric acid. Our results showed that ethanolic extract of *Stachys lavandulifolia Vahl.* has high antioxidant activity and the products of their oxidation entered in the chemical reaction with barbiturates. This reaction reduces the concentration of the active form of the barbiturates and indicates an effective herb-drug interaction. Also the antioxidant activity of this extract compaired with galic acid, salicylic acid and quercetin as standard antioxidants.

2.1. Experimental procedure

2.1.1. Materials and Apparatus

All the reagents and chemicals utilized in the present study were of analytical reagent grade and purchased from E. Merck (Darmstadt, Germany). They were applied without any further purification.

2.1.2. Preparation of the ethanolic extract of Stachys lavandulifolia Vahl.

Stachys lavandulifolia Vahl. were collected from the Nahavand city. They were then washed and dried at room temperature for 72 h. After proper drying, these herbs were ground in to a fine powder. In order to prepare the extract, 0.2 g of the powder was mixed with 50 ml of ethanol, then warmed to 50 °C, and finally maintained at room temperature for 15h. After that, the mixture was filtered with Whatman filter paper number 1 and allowed to be cooled. These extracts were considered as the ethanolic extract of *Stachys lavandulifolia Vahl.*

3.1. Results and discussion

3.1.1. Electro-oxidation of the ethanolic extract of *Stachys lavandulifolia Vahl.* and evaluation of Antioxidant Activity

The cyclic voltammogram of the ethanolic extract of *Stachys lavandulifolia Vahl.* (3mL) in water (phosphate buffer, at the biological pH of 7.0, c = 0.2 mol/L) is illustrated in Figure 2 (curve a). According to Figure 2, there is an anodic peak (A_1) and a cathodic peak (C_1), which are related to the oxidation of phenolic compounds (the main phenolic compound in Fig.1) in these extracts to the corresponding product and *vice versa*, by a quasi-reversible process. As can be observed, proportional to the increase of the potential sweep rate (Fig. 2, curves b), the heights of the A_1, C_1, and the peak current ratio (I_p^{C1}/ I_p^{A1}) rise (Fig. 2). This observation revealed that A_1 and C_1 are counterpart and related together.

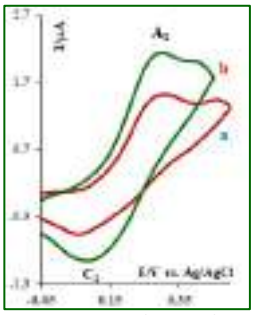

Figure 2. Cyclic Voltammograms of 3mL of the ethanolic extract of *Stachys lavandulifolia Vahl.* at scan rates of (a) 100, and (b)150 mV/s on a glassy carbon electrode in an aqueous solution (phosphate buffer, c = 0.2 mol/L, pH = 7.0).

The cyclic voltammograms of gallic acid, quercetin, and salicylic acid as standard antioxidants were recorded, and the E_p^A values were used to determine the antioxidant activity [8,9]. A relationship between the oxidation potential in cyclic voltammetry and ferric reducing antioxidant power (FRAP) can be observed. An increase in the antioxidant activity caused a decrease in E_p^A and an increase in the number of hydroxyl groups on the aromatic ring [8,9]. Based on the results in Figure 2,3 *Stachys lavandulifolia Vahl.* extract exhibit acceptable antioxidant activity compared with gallic acid, salicylic acid, and quercetin as standard synthetic antioxidants (Fig.3).

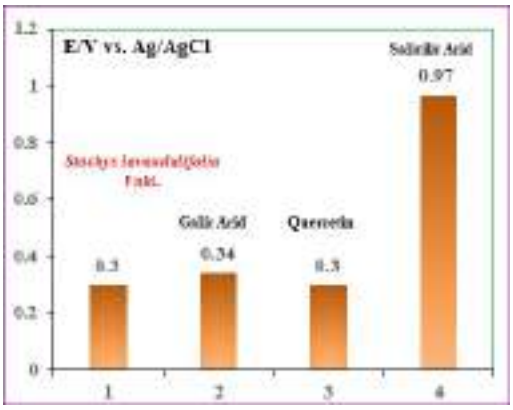

Figure 3. Comparison of the antioxidant activity (*EpA*) of the ethanolic extract of *Stachys lavandulifolia Vahl.* with gallic acid, salicylic acid, and quercetin.

3.1.2. Electrooxidation of ethanolic extract of *Stachys lavandulifolia Vahl.* in the presence of barbituric acids

The oxidation of ethanolic extract of *Stachys lavandulifolia Vahl.* in the presence of barbituric acid (1.0 mmol/L) was studied in some detail. Figure 4, curve b, shows the cyclic voltammogram obtained for 3 mL solution of ethanolic extract of *Stachys lavandulifolia Vahl.* in the presence of barbituric acid (1.0 mmol/L). As can be seen the anodic peak A_1 increases and the cathodic peak (C_1) decreases.

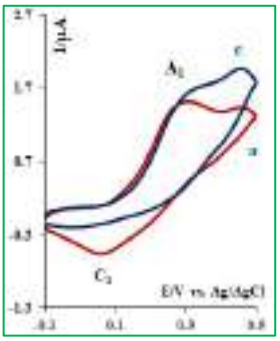

Fig. 4: (a) Cyclic voltammogram of 3mL ethanolic extract of *Stachys lavandulifolia Vahl*. (1), in the absence, (b) in the presence of barbituric acid (1 mmol/L) at a glassy carbon electrode in aqueous solution (phosphate buffer, c = 0.2 mol/L, pH 7.0). Scan rate: 50 mV/s. T = 25±1°C.

The existence of a subsequent chemical reaction between electrochemically generated compounds of *Stachys lavandulifolia Vahl.* extract and barbituric acid is supported by the following evidences (a) Decreasing of *I*pC1 during the reverse scan and increasing of Ip^{A1} in the presence of barbituric acid (Fig. 4, curve b). This could be indicative of the fact that electrochemically generated compounds in ethanolic extract *of Stachys lavandulifolia Vahl.* are removed partially from surface electrode by chemical reaction with barbituric acid. (b) Dependency of peak current ratio (Ip^{C1}/ I_p^{A1}) on potential sweep rate. In this case, for lower sweep rates, the peak current ratio (Ip^{C1}/ Ip^{A1}) is nearly zero and increases with increasing sweep rate. This is indicative of departure from intermediate reign and arrival to diffusion reign with increasing sweep rate. The results of cyclic voltammetry show that the electro generated compounds of oxidation this extract is stable and can react and reduce the concentration of barbituric acid. Our results indicate that the ethanolic extract of *Stachys lavandulifolia Vahl.* can be used as antidote in barbiturate poisoning before the start of clinical treatments. It can be seen clearly synergism between antioxidant activity and treatment of barbiturate poisoning with the ethanolic extract of *Stachys lavandulifolia Vahl.*

4. Conclusion

The results of this work show that the ethanolic extract of *Stachys lavandulifolia Vahl.* has acceptable antioxidant activity in comparison with some of synthesis antioxidants. The components produced by the oxidation of them are effective antidotes for barbiturate poisoning before starting clinical treatments. In the other words, we think our results are a report about the effectiveness of the herb-drug interaction.

5. References

[1]. K.J. Gohil, J. A. Patel, Indian J Pharmacol., 39 (2007) 129-139.
[2] A. Fugh-Berman, Lancet 2000, 355, 134-38.
[3] B. J. Gurley, E. K. Fifer, Z. Gardner, Planta Med. 78 (2012) 1490.
[4] T. CheCh, Z. J. Wang, M. S. S. Chow, C. W. K. Lam, Molecules 18 (2013) 5125.
[5] K. Shashi, B. C. Nandini, Indian J. Anaesth. 46 (2002) 480.
[6] A.A. Izzo, Med. Princ. Pract. 21 (2012) 404.
[7] R. Mactier, M. Laliberte, J. Mardini, M. Ghannoum, V. Lavergne, R. S. Gosselin, antioxidant.
[8] S. Chatterjee, Z. Niaz, S. Gautam, S. Adhikari, P.S. Variyar, A. Sharma, Food Chem, 101 (2007) 515.
[9] A. Simić, D. Manojlović, D. Šegan, M. Todorović, Molecules 12 (2007) 2327.
[10] Duh Pin-Der, J. Am. Oil Chem. Soc. 75 (1998) 455.
[11] S. E. Sajjadi, S. M. Ghanadian, M. Rabbani, F. Tahmasbi, Iran. J. Pharm. Res. 16 (2017) 58-63.
[12] R. Mactier, M. Laliberte´, J. Mardini, M. Ghannoum, V. Lavergne, S. Gosselin, R. S. Hoffman, T. D. Nolin, Am. J. Kidney Dis. 64 (2014) 347

29TH IRANIAN ORGANIC CHEMISTRY CONFERENCE
1_3 NOV, 2023
UNIVERSITY OF QOM, IRAN

Structural and electrochemical properties study of the 1,4,5,8-Naphthalenetetracarboxylic diimide (NTCDI) molecule and its polymers for the use in lithium-ion batteries using density functional theory (DFT) calculations

Nabaa Al_timimi, Alireza Abbassi*

Department of Chemistry, Faculty of Science, University of Qom, Qom, Iran, altimiminabaa@gmail.com

Abstract -
Density functional theory calculation was used to study the structure and electrical properties of NTCDI and its polymers and their reaction with Lithium atoms for the use in the Lithium-Ione batteries. Using the quantum chemical parameters and the calculated thermodynamic data, we have concluded that the polymerization is an appropriate way of developing the properties of the basement organic molecules for the use in Li-Ione batteries. Hence the emf of 1.7 volt for NTCDI-Li increases to 2.3 volt for NTCDI-trimer-Li.

1. Introduction

Lithium-ion batteries have achieved significant success in use in small electronic devices due to their density and high cycle number of energy storage. These batteries are based on the reaction of lithium compounds. Lithium ions move between two reactive electrodes. In these batteries, a negative graphite electrode is connected by a non-aqueous liquid to a positive electrode made of metal oxides, which usually create a potential difference of 4 volts. Since the use of these metal oxides has limitations such as toxicity, high cost of preparation and production, rarity and high price of the metals used, scientists have thought of using organic sources instead of these mineral sources [1-11].

2. Work

1,4,5,8-Naphthalenetetracarboxylic diimide (NTCDI) is an organic substance with semiconducting properties. Due to the carboxylic groups and the aromatic skeleton (Fig. 1) this molecule has received considered attention in the Lithium-Ion batteries as a basement in cathode electrode [].

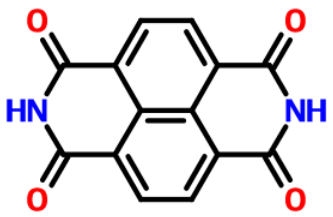

Fig. 1: The structure of NTCDI molecule

In this work we used density functional theory calculation using B3LYP hybrid functional and 6_311g(d, p) bases sets and the Gaussian 03 package for the calculations. At first, the structure of NTCDI was fully optimized using the mentioned theory level. The frequency calculations were done to understand the through minima and the Gibbs free energies.
Then, two and three NTCDI were connected from the nitrogen part to make NTCDI dimer and trimer. These molecules were fully optimized using the same level of theory.
In the next step, two lithium atoms were added to the optimized molecules. The calculations show that Li atoms like to connect to the carbonyl oxygens in the trans structure, as depicted in Fig. 2.

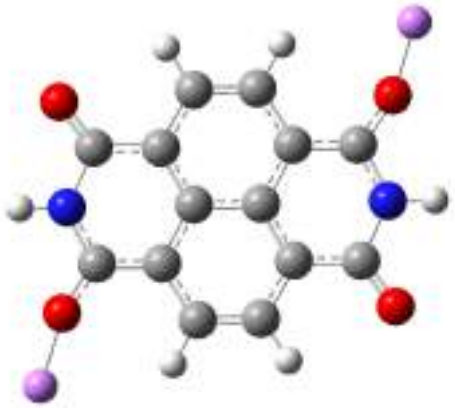

Fig. 2: The structure of NTCDI-Li_2

We can write the reaction of NTCDI and two Li atoms as: NTCDI + 2Li → NTCDI-Li_2 and the Gibbis free energy of this reaction can be obtained using the following equation.

$$\Delta G = G_{NTCDI-Li2} - G_{NTCDI} - 2G_{Li}$$

The battery emf was also calculated using the below equation.

$$emf = -\frac{\Delta G}{nf}$$

where, n is the number of transferring electrons which is 2 here as each Li atom transfer one electron and f is Faraday number.

For the NTCDI dimer and trimer one Li atom was connected to one terminal carbonyl oxygen and the second one was connected to central or terminal carbonyl oxygen. Therefore, for the dimer and trimer we have varieties of structures with Li. The Gibbs free energies and the emf of the calculated structures of mono, di and trimer are summarized in Table1.

Table 1: ΔG and emf of all the optimized structures of NTCDI mono, di and trimer

Structure	ΔG(kJ/mol)	Emf (volt)
NTCDI	-332.828	1.72
NTCDI-dimer (A)	-407.612	2.11
NTCDI-dimer (B)	-280.637	1.45
NTCDI-dimer (C)	-424.92	2.20
NTCDI-trimer (A)	-451.725	2.34
NTCDI-trimer (B)	-110.641	0.57
NTCDI-trimer (C)	-312.765	1.62

It can be seen from the data of Table 1 the emf of NTCDI monomer is 1.72 volt. For dimer and trimer three possible structures were studied. The best (the highest) emf for dimer and trimer are 2.20 and 2.34 respectively. So, we can find the emf increase by increasing the number of monomers in the polymer. The emf of the dimer increasing bout 0.5 volt with respect to the monomer and emf of the trimer is 0.14 volt larger than dimer. Hince, we expect shifting to larger number of monomers do not trilby influence the emf for the number of monomers larger than three.

In conclusion, using DFT calculations, we have studied the effect of the polymerization of the organic molecule i.e., NTCDI in the Li-ion batteries. The results show that the emf increase by adding more NTCDI molecule to the polymer. The emf are arranged as 2.34 > 2.20 > 1.72 for mono, di and trimer respectively.

4. References

1. Manthiram, A. (2011). Materials Challenges and Opportunities of Lithium Ion Batteries. The Journal of Physical Chemistry Letters, (2), 176–184.
2. Whittingham, M. S., (1976). Electrical energy storage and intercalation chemistry. Science, 192 (4244), 1126–1127.
3. Poizot, P., Dolhem, F., and Gaubicher, J., (2018). Progress in all-organic rechargeable batteries using cationic and anionic configurations: toward low cost and greener storage solutions? Current Opinion in Electrochemistry, (9), 70–80.
4. Gracia, R., and Mecerreyes, D., (2013). Polymers with redox properties: materials for batteries, biosensors and more. Polymer Chemistry, (4), 2206–2214.
5. Novák, P., Müller, K., Santhanam, K. S. V., and Haas, O., (1997). Electrochemically active polymers for rechargeable batteries. Chemical Reviews, (97) 1, 207–282.
6. Deng, W., Shen, Y., Qian, J., Cao, Y., and Yang, H. (2015). A Perylene Diimide Crystal with High Capacity and Stable Cyclability for Na-Ion Batteries. Applied Material and Interfaces, (7), 21095-21099.
7. Wu, D., Jing, F., Xi, X., Ma, L., Lu, D., Yang, P., and Liu, R., (2019). An Organic Solvent-free Approach towards PDI/Carbon Cloth Composites as Flexible Lithium-Ion Battery Cathodes. Journal of Colloid and Interface Science, (538), 597-604.
8. Alt, H.; Binder, H.; Köhling, A.; and Sandstede, G., (1972). Investigation into the use of quinone compounds-for battery cathodes. Electrochimica. Acta, (17), 873.
9. Kim, D. J.; Je, S. H.; Sampath, S.; Choi, J. W.; and Coskun, A., (2012). Effect of N-substitution in naphthalenediimides on the electrochemical performance of organic rechargeable batteries. RSC Advances., (2), 7968
10. Labasan, K. B., Lin, H. J., Baskoro, F., Togonon, J. J. H., Wong, H. Q., Chang, C. V., Arco, S. D., and Yen, H. J. (2021). Dicyanotriphenylamine-Based Polyimides as High-Performance Electrodes for Next Generation Organic Lithium-Ion Batteries. ACS Applied Materials & Interfaces, (13), 15, 17467-17477
11. Lyu, H.; Sun, X.-G.; and Dai, S. (2021) Organic Cathode Materials for Lithium-Ion Batteries: Past, Present, and Future. Advanced Energy and Sustainability Research. (2), 2170001.

29TH IRANIAN ORGANIC CHEMISTRY CONFERENCE
1_3 NOV, 2023
UNIVERSITY OF QOM, IRAN

Effect of iron chloride catalyst on the reaction yield and product composition of benzene chlorination

Mohammad Mehdi Shams Nateri, Morteza Ghafoori, Sajad Asadi and Hamid Alimohammadi*

Department of Chemical Engineering, Faculty of Engineering, Imam Hossein Comprehensive University, Tehran, Iran. mohammadmehdi.shams1999@gmail.com, Dr.mghafoori@gmail.com sajad.asadi67@gmail.com

Abstract

Chlorobenzenes are widely used in chemical reactions as precursor for manufacture of chemicals, pigments, pesticide or solvents for oil, wax, resin, rubber. They are prepared in various methods, liquid phase or gas phase. The gas phase is less common in industry due to its high temperature and low efficiency because it makes the reaction uncontrollable and leads to higher chlorobenzene formation. The choice of a catalyst can affect not only on the rate of a chemical reaction but sometimes can also control the nature of the products. In this research, experimental studies on the liquid phase of benzene chlorination in batch wise process are carried out. The effect of the amount of catalyst with constant mass flow on the efficiency of chlorination products was investigated . It was observed that of the amount of 0.65 grams, by increasing the amount of the catalyst up to 1.3 grams, the yield of the product (chlorobenzene) and the percentage of the progress of the reaction It gradually increases and After That decreases.

1. Introduction

Benzene chlorination is of considerable commercial importance as raw material or solvent in chemicals manufacture and has therefore received wide attention. These compounds are currently used and important additives in the production of insecticides, fungicides, herbicides, paints, pharmaceuticals, disinfectants, rubber, plastics, textiles and high quality electrical goods[1]. Chlorobenzene is used as a raw material in the production of the energetic material 2,4-dinitroanisole (DNAN) and new safe explosives based on 2,4-dinitroanisole and dichlorodiphenyl-trichloro-ethane (DDT) pesticides [2]

There is a considerable number of chemical reactions which occur between gases and liquids for example: hydrohalogenation of alcohols and the alkylation and halogenation of aromatics. These gas/liquid reactions are usually carried out by utilizing some type of contacting device such as a packed tower, and are homogeneous in that conversion occurs only after the gas has been transferred to the liquid phase .An example of these reactions is substitution between chlorine and benzene [3].

The electrophilic aromatic substitution reaction is one of the most common organic reactions. Fig.1 depicts the generally accepted mechanism of electrophilic substitution reactions for aromatic compounds, which is described in most of the organic chemistry textbooks [4].

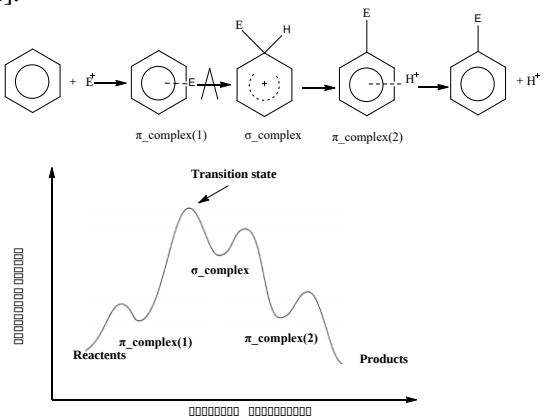

Fig 1: The general reaction mechanism and speculative potential energy curve for electrophilic aromatic substitution reaction.

Chlorinated benzenes are generally manufactured in a liquid phase batch process although continuous liquid phase plants and high temperature gas phase plants have also been used. The most common catalyst used is sublimed ferric chloride, Anhydrous aluminum chloride, tin-tetrachloride, molybdenum, pentachloride, metallic iron or aluminum, metal silicates and ferric oxide have also been used. The progress of the reaction can be followed by density measurements [1].

Chlorobenzenes are prepared industrially by reaction of liquid benzene with gaseous chlorine in the presence of a catalyst at moderate temperature and atmospheric pressure. Hydrogen chloride is formed as a byproduct. Generally, mixtures of isomers and compounds with varying degrees of chlorination are obtained, which any given chlorobenzene can be further chlorinated up to the stage of hexachlorobenzene. In addition, Because of the substitution in the benzene ring by chlorine atoms it is possible to obtain 12 compounds,

monochlorobenzene(MCB), three isomeric forms of dichlorobenzene(diCB), three isomers of trichloro-benzene(triCB), three isomers of tetrachloro-benzene(tetraCB), pentachlorobenzene (pentaCB), and hexachlorobenzene(hexaCB) [5 ,6] The rate of chlorination for an individual chlorine compound depends on the compound's structure and, because of this, both the degree of chlorination and also the isomer ratio change continuously during the reaction. By altering the reaction conditions and changing the catalyst, one can vary the ratios of the different chlorinated products within certain limits.

The choice of a catalyst for the liquid phase chlorination of benzene depends operating conditions, and cost. Also,The choice of a catalyst can affect not only the rate of the chemical reaction but sometimes can also control the nature of the products [٧]. Many different catalysts have been used in laboratory studies of the reaction. Iron filings, iron turnings, or anhydrous ferric chloride has been preferred for industrial processes because of the high product yields and low catalyst cost. Lewis acids ($FeCl_3$, $AlCl_3$, $SbCl_3$, $MnCl_2$, $MoCl_3$, $SnCl_4$, $TiCl_4$) are used as principal catalysts. The optimum reaction temperature depends on the desired degree of chlorination. Mono and dichlorination are carried out at 20 – 80°C [3].

The accepted theory for the mechanism of the catalytic halogenation of benzene in the liquid phase was originated by Schluerderburg. His theory was refined by Pfeiffer and Wizinger who suggested the formation of an intermediate ionic complex. They concluded that the catalyst polarized the halogen molecule and formed an ionic intermediate as shown Fig. 2: [3]

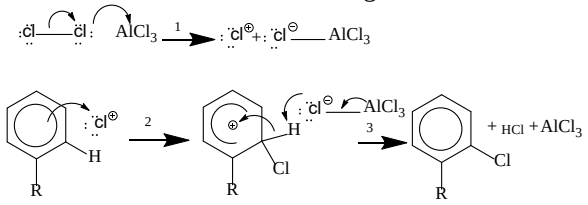

Fig 2 :Reaction mechanism

.

Experimental

The synthesis of chlorobenzene was carried out in a half-liter round-bottomed flask with four openings, equipped with a stirrer, thermometer, chlorine injection, condenser and a sample collection device. The reaction flak was immersed in a water bath to keep the reaction temperature constant. Fig 3 shows the equipment setup which is used.

.

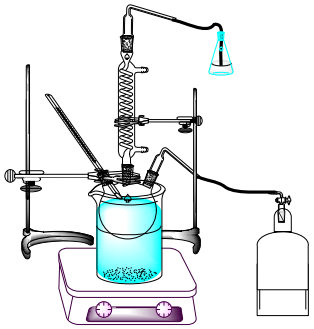

Fig 3 Equipment used in the experiment

The chlorination reaction of benzene occurred in the liquid phase at atmospheric pressure, in the temperature range between 50 and 55°C, using iron chloride ($FeCl_3$) as a catalyst. Chlorine gas was injected into a flask containing benzene through a tube with a constant Mass flow rate. The reaction time was 1 hour. For investigating the effect of the amount of catalyst on the yield of the main product(chlorobenzene), and composition of total product, iron chloride in 0.65, 1.3, 0.98 and 1.9 grams were weighed and added to reactants. After completion of reaction the whole of content of the reaction flask discharged and was analyzed by gas chromatography and mass spectrometry (GC_MS).

Results and discussion

GC_MS spectrum was taken from the extracted product samples. By applying 0.65 grams of iron chloride as catalyst of chlorination reaction, the chromatogram of resulted product showed: chlorobenzene in the retention time of 3.6 was appeared with a purity of 49.94%. Also, benzene appeared at the retention time of 2.1 and dichlorobenzene at 5.7 and 5.8(Fig. 4).

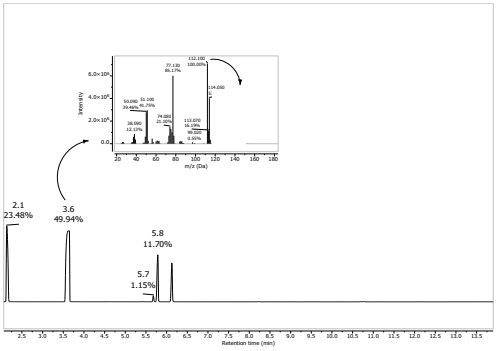

Fig 4: GC_MS chromatogram for value 0.65g

Fig 5 showed the chromatogram of resulted product for applying 0.98 grams of iron chloride as catalyst of chlorination, chlorobenzene in the Retention time of 3.6 It appeared with a purity of 51.72%.Also, benzene appeared at the retention time of 2.1 and dichlorobenzene at 5.7 and 5.8.

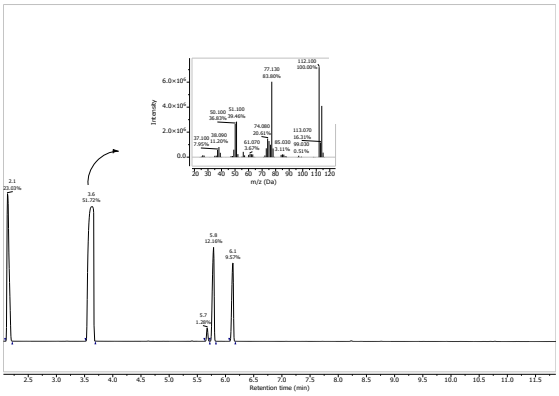

Fig 5: GC_MS chromatogram for value 0.98g

Fig 6 showed the chromatogram of resulted product for applying 1.3 grams of iron chloride as catalyst of chlorination, chlorobenzene in the Retention time of 3.6 It appeared with a purity of 51.69%.Also, benzene appeared at the retention time of 2.1 and dichlorobenzene at 5.7 and 5.8.

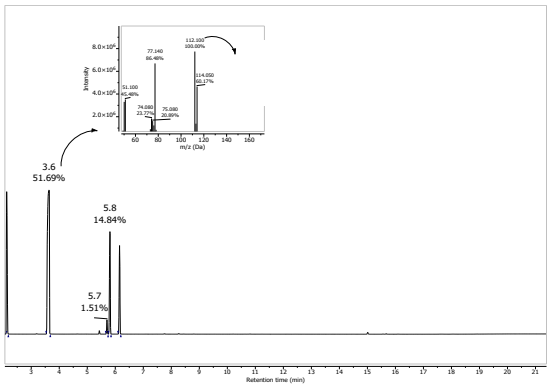

Fig 6: GC_MS chromatogram for value 1.3g

In the last sample, by applying 1.9 grams of iron chloride as catalyst of chlorination, the chromatogram of resulted product showed: chlorobenzene appeared at a retention time of 3.6 with a purity of 48.49%, benzene appeared at the retention time of 2.1 and dichlorobenzene at 5.7 and 5.8 (Fig. 7).

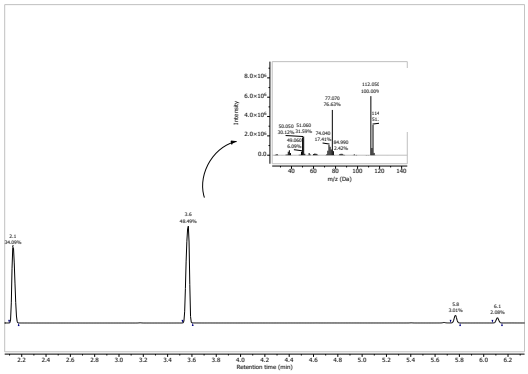

Fig 7: GC_MS chromatogram for value 1.9g

The summery of obtained results from GC_MS spectra are of benzene chlorination products are given in Table 1.

Table 1: Analysis of chromatogram spectra of final product

Catalyst (g)	Final products compositions			Benzene conversion %	Yield of chlorobenzene %
	Benzene %	MCB %	DCB %		
0.65	23.33	49.94	12.85	72.29	41.6%
0.98	23	51.72	23.01	72.89	42.30%
1.3	20.06	51.69	16.35	75.62	42.91%
1.9	34.09	48.49	5.09	60.61	38.3%

According to Table 1, the following results were obtained:

1. When producing chlorobenzene, there is still some unreacted benzene and the by-product, dichlorobenzene.
2. From the amount of 0.65 grams, the reaction yield increases with the increase of the amount of the catalyst up to the amount of 1.3 grams, and then it decreases after 1.3 grams.
3. It was observed that by increasing the amount of catalyst from 0.65 grams, the percentage of reaction progress gradually increases and decreases from 1.3 grams onwards.
4. The highest purity of chlorobenzene in the amount of catalyst is 0.98 grams with 51.72%.

References

[1] L. E. Beck Uwe, "Chlorinated benzenes and other nucleus-chlorinated aromatic hydrocarbons," *Ullmann's Encyclopedia of Industrial Chemistry*, 2000.

[2] D. J. W. Anthony, "The Liquid Phase Chlorination Of Benzene ", Princeton, Proquest Dissertations, 1966.

[3] B. Silberstein, H. Bliss, and J. Butt, "Kinetics of Homogeneously Catalyzed Gas-Liquid Reactions. Chlorination of Benzene with Stannic Chloride Catalyst," *Industrial & Engineering Chemistry Fundamentals*, vol. 8, no. 3, pp. 365-374, 1969.

[4] Y. Osamura, K. Terada, Y. Kobayashi, R. Okazaki, and Y. Ishiyama, "A molecular orbital study of the mechanism of chlorination reaction of benzene catalyzed by Lewis acid," *Journal of Molecular Structure: THEOCHEM*, vol. 461, pp. 399-416, 1999.

[5] B. Silberstein, *Kinetics of Homogeneously Catalyzed Reactions Between Gases and Liquids with and Without Diffusional Effects*. Yale University, 1968.

[6] L. Wolska, P. Konieczka, A. Jastrzebska, and J. Namieśnik, "Analytical procedure for the determination of chlorobenzenes in sediments," *Journal of chromatographic science*, vol. 41, no. 2, pp. 53-56, 2003.

[7] J. T. Stock, "Arthur Slator And The Chlorination Of Benzene," *Bull. Hist. Chem*, vol. 28, p. 6, 2003.

29TH IRANIAN ORGANIC CHEMISTRY CONFERENCE
1_3 NOV, 2023
UNIVERSITY OF QOM, IRAN

Free, esterified, and bound phenolic acids in *Artemisia vulgaris*

Saeed Mollaei and Mina Mohammadi*

Department of Chemistry, Faculty of Sciences, Azarbaijan Shahid Madani University, Tabriz, Iran, smollayi@ymail.com

Abstract - *Artemisia vulgaris* L. is one of the best-known species of this genus, which belongs to Asteraceae family, and has a widespread distribution in the natural habitats worldwide, and exhibits antioxidant, hypolipidemic, hepatoprotective, antispasmolytic, analgesic, estrogenic, cytotoxic, antibacterial, antifungal, and broncholytic properties. In this study, the amount of free, esterified and bound phenolic acids exiting in *A. vulgaris* has not been studied was investigated. In the first level, the phenolic acids were extracted, and then the amounts of them were studied using HPLC. The obtained results showed that the bound phenolic acid extract had the highest yield with the amount of 3.44%. The analysis of phenolic acids indicated that rosmarinic acid, salicylic acid, m-coumaric acid and caffeic acid were the main free phenolic acids with the amounts of 68.77, 21.05, 10.21, and 5.09 mg/g extract, respectively. Caffeic acid, m-coumaric acid, and gallic acid with the amounts of 8.37, 3.36, and 1.14 mg/g extract, respectively, were the main of esterified phenolic acid. Therefore, it may be suggested that, *Artemisia vulgaris* is a source of phenolic acid compounds.

Keywords: *Artemisia vulgaris*, Caffeic acid, Phenolic acid, Rosmarinic acid.

1. Introduction

Artemisia is one of the largest genera of the Asteraceae (Compositae) family. *Artemisia* genus has more than 500 species, and grows widely in all the world, and is the most widespread plant in Asia [1-3]. The species of *Artemisia* genus grow perennial, biennial, or annual plant, which are subshrub or shrubs and usually aromatic herbs, with alternative and smooth-edged leaves. The stems of the *Artemisia* genus plants are upright or ascending, sometimes decumbent and the flowers of this genus are all tubular and narrow with brown, yellow and red color. These plants also have panicle, sometimes racemose, more nearly spike-like, or almost capitate inflorescence [5, 6]. According to the phytochemical study, the Artemisia genus have mainly terpenoids, acetylenes, and phenolic compounds such as coumarins, flavonoids, caffeoylquinic acids, and sterols [6]. The plants of the *Artemisia* genus have an important position in traditional and modern medicine. They have some biological properties such as anti-inflammatory, anti-malaria, anti-cancer, anti-fungal, anti-bacteria, and antiviral [4-6].

Artemisia vulgaris L. (common mugwort) is one of the best-known species of this genus, which has a widespread distribution in the natural habitats worldwide (Europe, Asia, North and South America, and Africa). For many centuries, this species has been mainly used for treating gynecological ailments and gastrointestinal diseases. Recently, researches have proved that this species exhibits antioxidant, hypolipidemic, hepatoprotective, antispasmolytic, analgesic, estrogenic, cytotoxic, antibacterial, antifungal, hypotensive, and broncholytic effects. The different applications of this plant species have been possible due to its rich chemical composition, which especially includes essential oils, flavonoids, sesquiterpene lactones, phenolic acids, coumarins, and other groups of metabolites [6-8].

Up to our knowledge, the amount of free, esterified and bound phenolic acids exiting in *A. vulgaris* has not been studied so far. Thus, in this study, free, esterified and bound phenolic acids exiting in *A. vulgaris* were studied.

2. Material and Methods

2.1. Plant materials: The aerial parts of *A. vulgaris* were collected from Sahand, Tabriz. The voucher specimen was deposited at Herbarium of Azarbaijan Shahid Madani University.

2.1. Extraction of Phenolic Acids: Phenolic acids were extracted from the extract according to several previously described methods with little changes. The plant (4 g) was extracted three times with 40 mL of 80% methanol and assisted by ultrasonic at room temperature. Then, it was centrifuged at 5000 rpm for 5 min. The combined supernatant was evaporated under vacuum at 40 °C to about 4 mL. The aqueous suspension was adjusted to pH 2 (2 M HCl) and centrifuged. The clear supernatant was extracted five times with ethyl acetate/diethyl ether (1:1, v/v) at a solvent to water phase ratio of 1:1 to obtain the free phenolic acid [9].

The ether/ethyl acetate extracts were dehydrated with anhydrous sodium sulfate, filtered, and evaporated to dryness under vacuum at 30 °C. The dry residues

were dissolved into 10 mL of methanol. The aqueous phase was first treated by alkaline hydrolysis (2 M NaOH) for 4 h under a nitrogen atmosphere at room temperature. After acidification to pH 2 using 6 M HCl, phenolic acids released from the soluble esterified were extracted as described above. Afterward, 10 mL of 2 M HCl was added, and the medium was placed under a nitrogen atmosphere and hydrolyzed for 1 h at 85°C. Then phenolic acids released from soluble glycosides were extracted as described above. The residues from the 80% methanol extractions were hydrolyzed directly with 10 mL of 2 M NaOH and treated as the esterified. This fraction was methanol insoluble ester-bound phenolic acids [9].

2.2. Isolation and identification of phenolic compounds: High performance liquid chromatography (HPLC) (Knauer, Berlin, Germany) was used to isolate and identify phenolic compounds of the extracts. 20 µL of the sample was injected to the reverse phase Welch Ultisil XB-C18 column (150 mm, 4.6 mm and 5 µm). Methanol (Solvent A) and acidic water (solvent B) as gradient elution were used at a flow rate of 0.5 mL/min. This process was done at room temperature at a wavelength of 280 nm [10]. Finally, the amount of each phenolic compound was obtained using the calibration equation of the standard solution.

3. Result and Discussion

In this article, free, esterified and bound phenolic acids exiting in *A. vulgaris* were extracted, and the kind of phenolic acids were studied. As shown at figure 1, the bound phenolic acid extract had the highest yield with the amount of 3.44%.

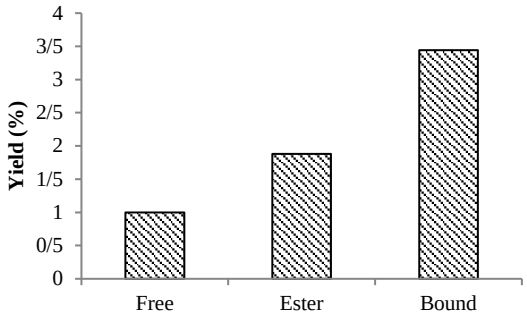

Fig. 1. The Yield of free, esterified and bound phenolic acids exiting in *A. vulgaris*

Table 1 shows the amount of free, esterified and bound phenolic acids in the extract of *A. vulgaris*.

Table 1 The amount of free, esterified, and bound phenolic acids (mg/g extract) in the extract of *A. vulgaris.*

		Free	Esterified	Bound
1	Cinnamic acid	trace	N.D.	trace
2	m-Coumaric acid	10.21	3.36	3.24
3	Salicylic acid	21.05	N.D.	N.D.
4	Ferulic acid	N.D.	0.60	trace
5	p-Coumaric acid	0.21	trace	N.D.
6	Rosmarinic acid	68.77	trace	trace
7	Caffeic acid	5.09	8.37	6.31
8	Vannilic acid	trace	trace	N.D.
9	p-hydroxy benzoic acid	0.31	0.48	0.55
10	Gallic acid	N.D.	1.14	1.33
	Total	**105.64**	**13.95**	**11.43**

Analysis of free phenolic acid extract of *A. vulgaris* indicated that rosmarinic acid, salicylic acid, m-coumaric acid and caffeic acid were the main phenolic acids with the amounts of 68.77, 21.05, 10.21, and 5.09 mg/g extract, respectively. Also, ferulic acid and gallic acid were not found in the extract. Cinnamic acid and vannilic acid were trace in the sample.

According to the analysis of esterified phenolic acid extract, the largest phenolic acids were caffeic acid, m-coumaric acid, and gallic acid with the amounts of 8.37, 3.36, and 1.14 mg/g extract, respectively. Cinnamic acid and salicylic acid were not detected in the sample. m-Coumaric acid, rosmarinic acid, and vannilic acid were trace in the sample.

The results of bound phenolic acids indicated that caffeic acid, m-coumaric acid, and gallic acid were the main phenolic acids with the amounts of 6.31, 3.24, and 1.33 mg/g extract, respectively. Salicylic acid, p-coumaric acid, and vannilic acid were not identified in the sample.

Therefore, according to the results obtained to identify and determine the amount of phenolic acids in the extracted extracts, it can be said that meta-coumaric acid and para-hydroxybenzoic acid are present in all the extracts, while cinnamic acid and vannilic acid were not detected in any extract. Salicylic acid and para-coumaric acid were detected only in the extract of free phenolic acids.

Figure 1 indicates the amount of total free, esterified, and bound phenolic acids in the extract. As shown, a free phenolic acid with the amount of 105.64 mg/g extract was the main studied phenolic acids.

Fig. 1. The amount of total phenolic acids in the extract of *A. vulgaris*.

4. Conclusion

In this study, the amount of free, esterified and bound phenolic acids exiting in *A. vulgaris* has not been studied was investigated. The obtained results showed that the bound phenolic acid extract had the highest yield. The analysis of phenolic acids indicated that rosmarinic acid, salicylic acid, m-coumaric acid and caffeic acid were the main free phenolic acids. Caffeic acid, m-coumaric acid, and gallic acid were the main of esterified phenolic acid. Therefore, it may be suggested that, *Artemisia vulgaris* is a source of phenolic acid compounds.

5. References

[1] A. Rustaiyan, A. Faridchehr, A review on constituents and biological activities of further Iranian Artemisia species, International Journal of Pharmaceutical, Chemical, and Biological Sciences, 3 (2014) 6-14.

[2] A. Rustaiyan, S. Masoudi, Chemical constituents and biological activities of Iranian Artemisia species, Phytochemistry Letters, 4 (2011) 440-447.

[3] C. H. Oberieler, R. Vogt, L. E. Watson, The Families and genera of vascular plants. Sperniger. 2004. vol. VIII, pp.358-359.

[4] P. Janaćkovića, N. Rajčevića, M. Gavrilovića, J. Novakovića, A. Giwelib, D. Stešević̀c, P. D. Marin, Essential oil composition of five Artemisia (Compositae) species in regards to chemophenetics, Biochemical Systematics and Ecology, 87 (2019) 103960.

[5] A. Taleghani, S. A. Emami, Z. Tayarani-Najaran, Artemisia a promising plant for the treatment of cancer, Bioorganic & Medicinal Chemistry, 28 (2020) 115180.

[6] L. Holm, J. Doll, E. Holm, J. Pnacho, J. Herberger World Weeds: Natural Histories and Distribution. John Wiley and Sons; New York, NY, USA: 1997.

[7] A. Chevallier The Encyclopedia of Medicinal Plants: A Practical Reference Guide to more than 500 Key Medicinal Plants and Their Uses. DK Publishing; New York, NY, USA: 1996.

[8] J.N. Barney, A. DiTommaso, The biology of Canadian weeds. 118. Artemisia vulgaris L. Canadian Journal of Plant Science, 83 (2003) 205–215.

[9] K. Krygier, F. Sosulski, L. Hogge, Free, esterified, and insoluble-bound phenolic acids. 1. Extraction and purification procedure. Journal of Agricultural and Food Chemistry, 30 (1982), 330-334.

[10] S. Mollaei, M. Eslami, M. Ebadi, Investigation of phenolic compounds and biological properties of vegetative organs of Lepdium vesicarium L. Applied Biology, 35 (2022), 110-126.

29TH IRANIAN ORGANIC CHEMISTRY CONFERENCE
1_3 NOV, 2023
UNIVERSITY OF QOM, IRAN

Study the Effect of Temperature Reaction on the Liquid-phase Chlorination of Benzene

Hamid Alimohammadi, Morteza Ghafoori, Sajad Asadi and Mohammad Mehdi Shams Nateri*

Department of Chemical Engineering, Faculty of Engineering, Imam Hossein Comprehensive University, Tehran, Iran, hamidalimohammadi4552@ihu.ac.ir, Dr.mghafoori@gmail.com.

Abstract

Chlorobenzenes are used as a precursor in the manufacturing of chemicals. Chlorination of benzene is done by various methods, including continuous and discontinuous chlorination process and in the liquid phase or vapor phase and usually by direct reaction of benzene with gaseous chlorine in the presence of a catalyst. In order to study the effect of temperature on the reaction yield and products composition, benzene chlorination was done at three temperatures: at 45℃ yield production of monochlorobenzene was higher, the conversion of benzene and the formation of dichlorobenzene increased at 55℃, and by increasing the tmperature to 65℃, benzene conversion, formation of monochlorobenzene and dichlorobenzene decreases.

1. Introduction

The term "nuclear chlorinated aromatic compounds" refers to a substance in which at least one of the ring carbons has chlorine instead of hydrogen. Laboratory work on the compounds of this group has been started for a long time. For example, Laurent reported in 1833 that he obtained wax-like compounds during the chlorination of naphthalene. However, their construction and industrial use was delayed until the first third of the 20th century [1]. Chlorobenzenes are used as a precursor for chemicals manufacturing such as insecticides, fungicides, herbicides, paints, pharmaceuticals, disinfectants, rubbers, plastics, textiles, nitrochlorobenzenes and phenols [1, 2].

Most of chlorobenzenes are currently produced from benzene and chlorine in factories that work continuously [1]. The continuous process of chlorobenzene production produces several products and is a multi-product operation. Only limited control can be exercised over product proportions. Benzene (BZ), monochlorobenzene (MCB), para and ortho dichlorobenzene (p-DCB and o-DCB), trichlorobenzene (TCB) and hydrochloric acid (HCl) are the products of this operation [3, 4].

There are various methods and processes through which benzene chlorination can be done:

A) Raschig process: In this process, benzene is chlorinated by chlorine produced in the reactor by the catalytic oxidation of hydrogen chloride. A preheated mixture of benzene vapor, air, steam, and HCl is contacted with a copper oxide catalyst at normal pressure and at a temperature of 220-260 ℃. The disadvantage of this process is that the high temperature greatly favors the high rate of combustion of benzene and the reaction may become uncontrollable. In addition, the high costs of this process (vapor phase chlorination) compared to other existing processes, makes it very uneconomic to produce chlorobenzene and thus makes it obsolete [3, 5].

B) Loser and Schmidt: In this process, a mixture of benzene vapor, hydrochloride and air is reacted at a temperature of 150 to 300℃ in contact with the copper hydroxide-alumina catalyst (in the form of a fluid bed). This process may be considered as a type of Raschig process [3, 5].

C) Quartz tube process: Chlorination of benzene is done in a quartz tube at a temperature of 400 to 500℃, here the main product obtained is chlorobenzene with minor amounts of dichlorobenzene [5].

Gas phase chlorination is done at about 250-300℃. It has recently been shown that by adding a suitable initiator such as $CCl_3SO_2CCl_3$, measurable rates can be obtained even at around 170℃ [6].

The disadvantages of all these processes are low efficiency and high temperature, which may make the reaction uncontrollable and lead to higher chlorobenzene formation [5].

Based on all the above considerations, the continuous liquid phase chlorination of benzene at a temperature of about 40℃ is suitable for the production of large quantities of monochlorobenzene in industry. This process is also economically viable, making it the most popular process used in industry to make

monochlorobenzene worldwide. Chlorobenzene and o- and p-dichlorobenzene are the main products [3, 5, 7]. Liquid phase chlorination of benzene is an ideal example of a series of sequential reactions with different rates from the monochlorinated molecule to the fully chlorinated molecule containing six chlorines. If chlorobenzene (mono) is the desired product, controlling the ratio of dichlorobenzene to chlorobenzene is primarily done by controlling the amount of chlorination [1].

Ferric chloride and iron Raschig rings are usually used as catalysts [2]. In actual practice in industry, only chlorobenzene and small amounts of dichlorobenzene are formed. By using selective catalysts and modifying the reaction conditions, the amount of dichlorobenzene and higher substituted chlorobenzene formed can be reduced [5].

Depending on the chosen ratio of benzene to chlorine, it is possible to achieve a low rate of benzene conversion and low formation of dichlorobenzene, or almost complete conversion of benzene with a higher amount of dichlorobenzene formation. Which of the two options is desirable depends on the profitability calculation, in which the distillation costs due to dichlorobenzenes should be taken into account [1].

Elevated temperatures in substitution reactions favor the introduction of a second chlorine atomin the ortho and meta positions, whereas para substitution is favored if cocatalysts and lower temperatures are used. The optimal reaction temperature depends on the desired degree of chlorination. Mono and dichlorination are carried out at 20–80 ℃. In the production of hexachlorobenzene by chlorination of benzene, however, temperatures of about 250℃ are needed toward the end of the reaction [1].

In this article, in order to investigate the effect of temperature on benzene conversion percentage, chlorination reaction products and monochlorobenzene production yield, experimental tests were performed at three different temperatures.

4. Experimental

First, 250g of industrial grade benzene was poured into a three-hole flask and 1.3g of anhydrous iron chloride was added to it. In order to keep the temperature constant, the balloon was placed in a water bath on a heater and the chlorine gas feeding tube was placed inside the balloon. A thermometer was placed inside the balloon to control the temperature. Chlorine was flowed into benzene at a constant mass flow rate and the solution was stirred throughout the reaction. Due to the exothermic nature of the reaction, the temperature of the reaction was constantly rising, and the temperature of the solution inside the balloon was kept constant by cold water in the water bath. The flow of chlorine gas was stopped after one hour and the weight of the solution was measured and then analysed by gas chromatography. The described process was carried out identically for three temperatures of 45, 55 and 65℃.

5. Results and discussion

The results of gas chromatography of three experiments were reported as follows:

1. The result of gas chromatography for reaction products for testing at 45℃, in the form of different retention times for different compounds is shown in Figure 1. In this reaction temperature, benzene conversion was 64.76%, and the chlorination products contained 35.24% unreacted benzene, 54.49% monochlorobenzene and 10.27% dichlorobenzene.

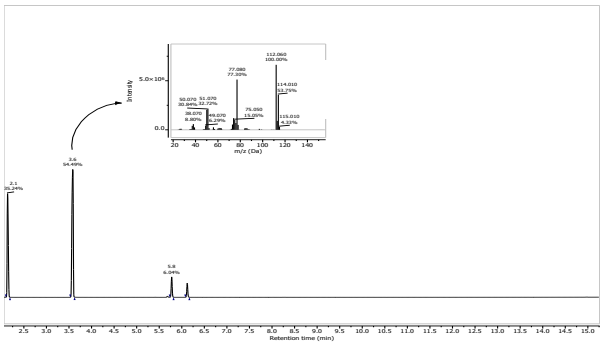

Figure 1: The result of gas chromatography for testing at 45℃

2. In the test conducted at 55℃, 80.00% of benzene was converted and the chlorination products contained 20.00% unreacted benzene, 52.00% mono-chlorobenzene and 28.00% dichlorobenzene. The result of gas chromatography for testing at 55℃, in the form of different retention times for different compounds is shown in Figure 2.

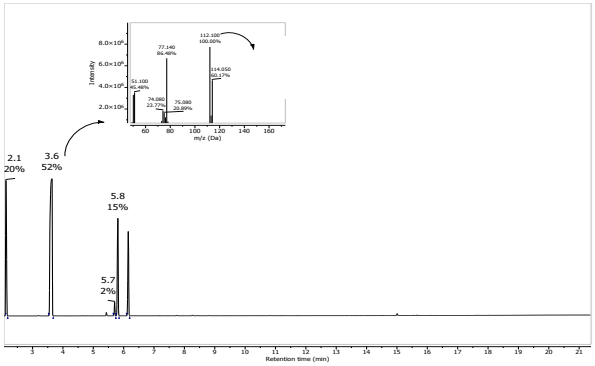

Figure 2: The result of gas chromatography for testing at 55℃

3. In the test conducted at 65℃, 50.01% of benzene was converted and the product contained 49.99% unreacted benzene, 44.13% monochlorobenzene and 5.88% dichlorobenzene. The result of gas chromatography for testing at 65℃, in the form of different retention times for different compounds is shown in Figure 3.

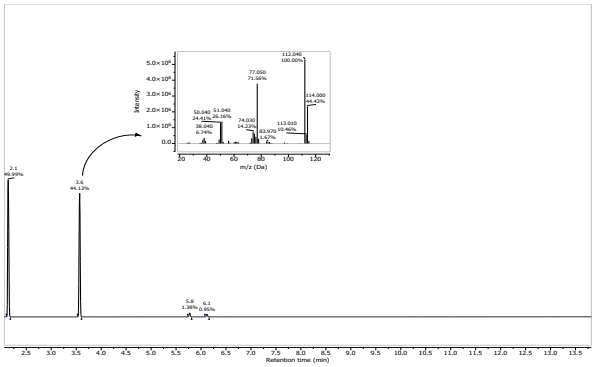

Figure 3: The result of gas chromatography for testing at 65℃

The results of gas chromatography analyzes are summarized in Table 1.

Table1: Gas chromatography results at different temperatures

Temperature (℃)	Final products compositions			benzene conversion(%wt)	Yield of chlorobenzene %
	Benzene %	MCB %	DCB %		
45	35.24	54.49	10.27	64.76	44.54
55	20.00	50.00	28.00	80.00	41.24
65	49.99	44.13	5.88	50.01	33.38

As shown in the table, as the temperature increases, the percentage of chlorobenzene in the final product decreases, and its efficiency decreases. The rate of benzene conversion is high at 55 and 80% of the initial benzene has participated in the reaction. At a temperature of 65, the production rate of dichlorobenzene is very low and is reported to be around 6%. The graph of Figure 4 shows the changes in benzene conversion, percentage of monochlorobenzene and dichlorobenzene with respect to temperature.

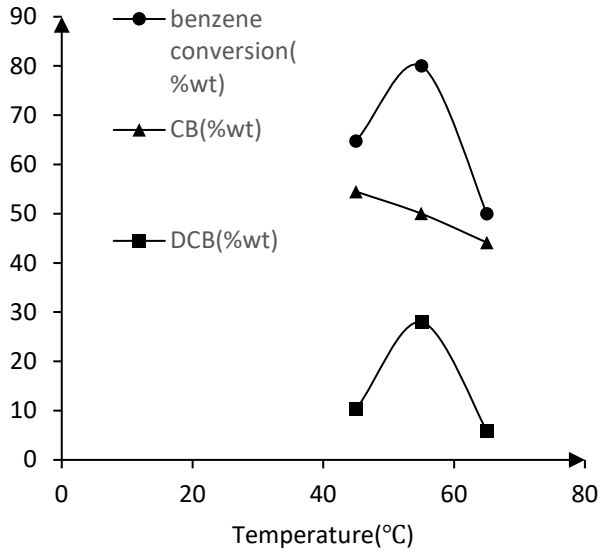

Figure 4: Graph of changes in the benzene conversion, MCB and DCB in the product with respect to temperature.

According to the analysis, the following results are obtained:

1- Reaction temperature at 45℃ favors the yield production of monochlorobenzene.

2- By increasing the tmperature to 55℃, the conversion of benzene and the formation of dichlorobenzene also increased.

3- Increasing the tmperature above the 55℃, decreases all of the benzene conversion reaction, monochloro-benzene production yield, and formation of dichlorobenzene are.

4- Depending on the desireed products composition reaction, the optimal temperature should be chosen.

6. References

[1] Ullmann F, Ullman's Encyclopedia of Industrial Chemistry, Wiley-vch, Seventh Edition, 483-520, 2011.

[2] Kalooo K.S, Production of Chlorobenzene from Benzene and Chlorine, Institute of Chemical Technology, Mumbai, 2020.

[3] Othmer K, Encyclopedia of Chemical Technology, Wiley-vch, Fourth Edition, Volume 6, 46-52, 2004.

[4] Yoshio N, T. Biegler L, Demand-based Optimization of a Chlorobenzene Process With High-fidelity and Surrogate Seactor Models Under Trust Region Strategies, Chemical Engineering, Carnegie Mellon University, Pittsburgh, Pennsylvania, Alche Journal, 2020.

[5] Mishra A, Simulation of Chlorobenzene Plant in Aspen Plus, Department of Chemical Engineering Deenbandhu chhotu Ram University of Science And Technology Murthal, Sonipat-131039, 2015.

[6] Dorreppal W, Louw R, The Mechanism of the Vapor-Phase Chlorination of Benzene Derivatives, International Journal of Chemical Kinetics, 249-275, Gorlaeus Laboratories, University of Leiden, Leiden, The Netherlands, 1978.

[7] Wang E, Simulation and optimization of chlorobenzene distillation process, College of Chemistry and Chemical Engineering, University of Chinese Academy of Sciences, Beijing, China, 2013.

29TH IRANIAN ORGANIC CHEMISTRY CONFERENCE
1_3 NOV, 2023
UNIVERSITY OF QOM, IRAN

Aerobic photocatalytic oxidation of 2-naphthol under visible light using NH_2-MIL-125(Ti)

Hoda Mollabagher[1]*, *Seyed Amir Hossein Seyed Mousavi*[2] *and Salman Taheri*[1]*

*[1]Chemistry and Chemical Engineering Research Center of Iran, PO Box 14115-186, Tehran, Iran
[2]Process Engineering Department, Faculty of Chemical Engineering, Tarbiat Modares University, Tehran, Iran

Abstract

2-Naphthol has undergone a specific oxidation process, leading to the formation of 2-hydroxy-1,4-naphthoquinone, a compound also recognized as Lawsone. In this research, NH_2-MIL-125(Ti) was employed as a potent catalyst for photocatalytic reactions in conjunction with H_2O_2. The impact of NH_2-MIL-125(Ti) on the reaction efficiency was prominently observed, leading to noticeable enhancements in the reaction yield.

1. Introduction

Lawsone, extracted from the henna plant, is among the most widely employed natural compounds in the synthesis of bioactive molecules [1]. In recent years, researchers have published numerous articles regarding the utilization of this compound in multicomponent reactions to obtain compounds with pharmaceutical properties [2-4]. Additionally, it finds application as a hair dye and serves as an ultraviolet filter in the formulation of sunscreens [5]. Based on reported articles, despite the significant importance of Lawsone, limited research has been conducted in the field of synthesizing this compound. One of the methods for synthesizing lawsone involves the selective oxidation of 2-naphthol [6].
Conventional oxidizing agents like $KMnO_4$, CrO_3, Br_2, and tert-butyl hydroperoxide are typically toxic, corrosive, or costly [7].
Utilizing a selective catalyst with low cost oxidant that is ultimately recoverable not only results in energy and cost savings but also demonstrates environmental compatibility, contributing to fewer ecological pollutants [8].
In recent times, MOFs have attracted attention for their dual composition, intertwining metallic ions and organic ligands in a single complex. This dual composition flexibility enables the manipulation of organic ligands and metallic ions to achieve varied efficiencies and yields [8-10]. Furthermore, the significant porosity of these structures empowers them as potent nano-reactors for chemical reactions [11, 12].
By appropriately selecting the cluster and linker pair, the tunable design of MOFs can decrease the solid's band gap, leading to heightened absorption of solar light and facilitating photoactivation within the visible spectrum [13, 14].
In this research, we present an effective catalytic system for the selective synthesis of lawsone from 2-naphthol. This process employs NH_2-MIL-125(Ti) as the catalyst and hydrogen peroxide as the oxidant in an aqueous solution.

2. Experimental

2.1. Materials and reagents

All starting materials were purchased from Sigma-Aldrich and Merck companies and used without additional purification. All reactions were carried out in double distilled deionized water.
Spectrophotometric measurements were conducted using a Shimadzu UV-Vis Spectrometer. Infrared spectra were recorded employing a Perkin-Elmer 1420 spectrophotometer through the KBr disc technique.

3.1 Preparation of NH_2-MIL-125(Ti)

Into a solution comprising 9 mL of DMF and 1 mL of dry MeOH, 2-Aminoterephthalic acid (0.54 g, 3 mmol) and Tetra-n-butyl titanate (0.26 mL, 0.75 mmol) were introduced and stirred for 30 minutes at room temperature. Subsequently, the prepared solution was transferred to a 50 mL Teflon-lined stainless steel autoclave (Amatis Ara Shimi, model AR 100). The synthesis was carried out without agitation in an oven at 150°C for a duration of 3 days. Upon completion of the synthesis, the resulting suspension was filtered, washed separately with DMF and MeOH, subjected to extraction using a Soxhlet extractor with MeOH, and ultimately dried to yield a yellow solid product.

3.2 Catalytic oxidation of 2-naphthol

A solution of 2-naphthol (1.0 mmol), NaOH (100 mmol), and NH_2-MIL-125(Ti) (0.01 g) dissolved in 25 mL of water was stirred at 25°C, and then hydrogen peroxide (0.8 mL) was introduced into the mixture.
Upon the addition of H_2O_2, an orange colour emerged. The reaction mixture was left to stand at room temperature for 15 minutes. Subsequently, the resultant mixture was neutralized using 0.1 M HCl. The precipitate was filtered, washed with water, vacuum-dried, and subsequently recrystallized using ethanol. The product's melting point was determined to be 192°C.
The influence of various reaction parameters on the yield of the reaction product was evaluated using the UV-vis technique. The isolated reaction product was dissolved in 50 ml of 0.1 N NaOH and quantitatively assessed by measuring the absorbance at 453 nm, a characteristic wavelength for sodium salt of lawsone.

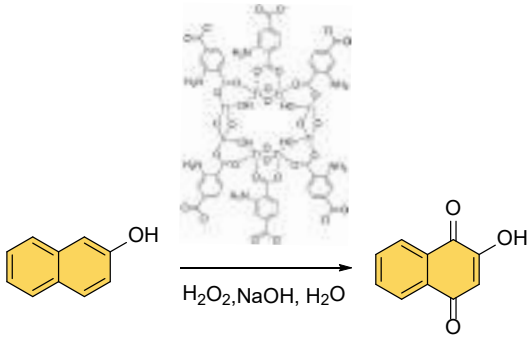

Scheme 1. Oxidation of 2-naphthol to lawsone by applying NH_2-MIL-125(Ti) as catalyst.

4. Results and discussion.

To further examine the morphological and facet changes of all samples over time, scanning electron microscopy (SEM) images were acquired. (Fig 1)

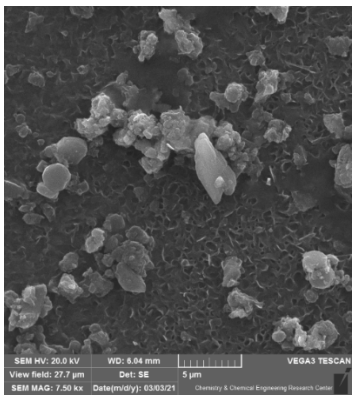

Fig 1. SEM of NH_2-MIL-125(Ti)

The potential reusability of NH_2-MIL-125(Ti) as a catalyst for the synthesis of lawsone was investigated. To achieve this objective, the catalyst was isolated via a simple filtration process next to the initial reaction cycle. Following isolation, the catalyst washed with ethanol and then dried under vacuum conditions.
Then, the recovered catalyst was used again for the next run of the reaction for 4 times and no significant difference in the catalyst's efficiency was observed.
The FT-IR spectra before and after catalyst utilization indicate that no significant changes have occurred in the functional groups of the catalyst.

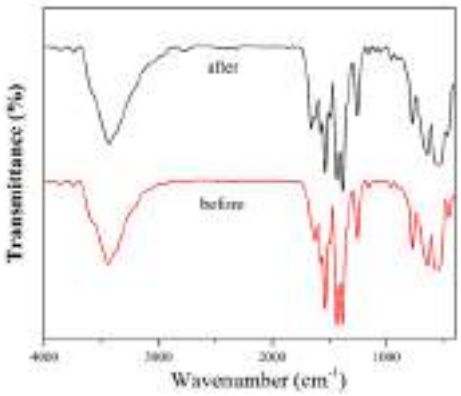

Fig 2. FT-IR of NH_2-MIL-125(Ti) before and after photocatalytic reaction

The powder X-ray diffraction (PXRD) patterns of the synthesized samples are depicted in Figure 2, affirming a strong resemblance between the samples and the NH2-MIL-125(Ti) reported previously[15].

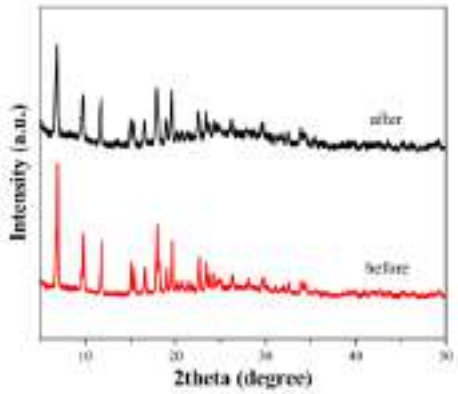

Fig 3. PXRD of NH_2-MIL-125(Ti) before and after photocatalytic reaction.

5. Conclusions

The catalytic oxidation system using NH_2-MIL-125(Ti) in conjunction with hydrogen peroxide (H_2O_2), under mild reaction conditions, demonstrates efficient selective conversion of 2-naphthol to 2-hydroxy-1,4-naphthoquinonewith high yield.
The catalyst was recovered for 4 time and there is no change in efficiency and structure of catalyst.

6. References

1. Zhao, Y.; Cai, W.; Chen, J.; Miao, Y.; Bu, Y., A highly efficient composite catalyst constructed from NH_2-MIL-125 (Ti) and reduced graphene oxide for CO2 photoreduction. *Frontiers in chemistry* **2019,** *7*, 789.
2. Chandrakar, K.; Patel, J. L.; Vedula, R. R.; Virendra, R.; Mahapatra, S. P.; Penta, S.; Varma, R. S., Recent Developments in Multi-component Synthesis of Lawsone Derivatives. *Current Organic Synthesis* **2023,** *20* (3), 278-307.
3. Mohammadi Ziarani, G.; Mollabagher, H.; Gholamzadeh, P.; Badiei, A.; Yazdian, F., Synthesis of the biologically active henna based benzochromene derivatives using ionic liquid functionalized SBA-15 as a nanoreactor. *Iranian Journal of Catalysis* **2018,** *8* (1), 59-67.
4. Mohammadi Ziarani, G.; Mollabagher, H.; Lashgari, N.; Badiei, A., One-pot solvent-free synthesis of pyranonaphthoquinone-fused spirooxindoles catalyzed by SBA-IL. *Scientia Iranica* **2018,** *25* (6), 3295-3304.
5. Sankar, J.; Kini, M.; Sangle, P., Estimation of Lawsone Release from Lawsonia inermisLeaf Powder and Dye Uptake on the Hair. **2023**.
6. Jordao, A. K.; Vargas, M. D.; Pinto, A. C.; da Silva, F. d. C.; Ferreira, V. F., Lawsone in organic synthesis. *RSC advances* **2015,** *5* (83), 67909-67943.
7. Sedelmeier, J.; Ley, S. V.; Baxendale, I. R.; Baumann, M., KMnO4-mediated oxidation as a continuous flow process. *Organic letters* **2010,** *12* (16), 3618-3621.
8. Taheri, S.; Mollabagher, H.; Seyed Mousavi, S. A. H., Metal organic framework Cu-BDC as an efficient and reusable catalyst for one-pot synthesis of benzophenazine derivatives. *Polycyclic Aromatic Compounds* **2022,** *42* (9), 6523-6536.
9. Pirouzfar, V.; Moghaddam, S. N.; Mousavi, S. A. H. S.; Dehaghani, A. H. S.; Mollabagher, H.; Su, C.-H., Investigation of light aromatics removal from industrial wastewater using nano metal organic framework. *Journal of Contaminant Hydrology* **2022,** *249*, 104048.
10. Mollabagher, H.; Taheri, S.; majid Mojtahedi, M.; Seyedmousavi, S., Cu-metal organic frameworks (Cu-MOF) as an environment-friendly and economical catalyst for one pot synthesis of tacrine derivatives. *RSC advances* **2020,** *10* (4), 1995-2003.
11. Li, Z.; Hu, M.; Liu, J.; Wang, W.; Li, Y.; Fan, W.; Gong, Y.; Yao, J.; Wang, P.; He, M., Mesoporous silica stabilized MOF nanoreactor for highly selective semi-hydrogenation of phenylacetylene via synergistic effect of Pd and Ru single site. *Nano Research* **2022**, 1-10.
12. Wang, A.; Ni, J.; Wang, W.; Liu, D.; Zhu, Q.; Xue, B.; Chang, C.-C.; Ma, J.; Zhao, Y., MOF Derived Co− Fe nitrogen doped graphite carbon@ crosslinked magnetic chitosan Micro− nanoreactor for environmental applications: Synergy enhancement effect of adsorption− PMS activation. *Applied Catalysis B: Environmental* **2022,** *319*, 121926.
13. Gao, Y.; Yi, X.-H.; Wang, C.-C.; Wang, F.; Wang, P., Effective Cr (VI) reduction over high throughput Bi-BDC MOF photocatalyst. *Materials Research Bulletin* **2023,** *158*, 112072.
14. Shan, C.; Zhang, X.; Ma, S.; Xia, X.; Shi, Y.; Yang, J., Preparation and application of bimetallic mixed ligand MOF photocatalytic materials. *Colloids and Surfaces A: Physicochemical and Engineering Aspects* **2022,** *636*, 128108.
15. Muelas-Ramos, V.; Belver, C.; Rodriguez, J.; Bedia, J., Synthesis of noble metal-decorated NH2-MIL-125 titanium MOF for the photocatalytic degradation of acetaminophen under solar irradiation. *Separation and Purification Technology* **2021,** *272*, 118896.

29TH IRANIAN ORGANIC CHEMISTRY CONFERENCE
1_3 NOV, 2023
UNIVERSITY OF QOM, IRAN

Nickel (II) anchored on graphene oxide functionalized glutamine as a high-performance supercapacitor electrode

Samira Mohammadi, S. Morteza Mousavi-Khoshdel *

Industrial Electrochemical Research Laboratory, Faculty of Chemistry, University of Science and Technology, Teheran, Iran, samira.mo1371@gmail.com, mmousavi@iust.ac.ir

Abstract - In this work, a novel composite was prepared with a two-step method as an electrode material for a supercapacitor using graphene oxide (GO) and nickel stabilized on glutamine (GO-G@ Ni). The composite was analyzed by Fourier-transform infrared (FT-IR) spectroscopy, energy dispersive X-ray (EDX) analysis, and scanning electron microscopy (SEM) techniques. Also, electrochemical properties were measured using a three-electrode system. The specific capacitance of 1136 F g^{-1} was obtained at a current density of 2 A g^{-1} in 6 M KOH aqueous electrolyte.

1. Introduction

Non-renewable resources such as oil, gas, and coal are running out and the use of these resources creates environmental problems such as global warming. Considering the environmental considerations and the need for independence from these sources of energy, the attention of researchers has been drawn to finding clean and efficient sources of energy. In addition to energy production, energy storage is another challenge facing human societies. Therefore, energy storage devices have been more attractive [1-3]. Supercapacitors are among the most important electrical energy storage devices, due to their high stability, wide operating temperature range, and high power density which have been used in applications such as satellite applications, uninterruptible power sources, clinical instrumentation, transportation, and memory backup systems [4,5]. Supercapacitors are divided into two categories based on the charge storage mechanism: 1. electric-double layer capacitors (EDLC) 2. pseudo capacitors. EDLC-type involves the storage of physical charge, which makes long-term stability and fast charge-discharge and is mainly based on carbon materials, while the pseudo capacitance type is based on the faradaic redox reaction mechanism that includes transition metal oxides and conducting polymers and leads to high energy density. The combination of EDLC and pseudo capacitance in materials has significantly increased the capacitance and efficiency of supercapacitors [6-8].

Among the graphene compounds, graphene oxide has recently received more attention than graphene due to its simple preparation and fine dispersing compared to graphene for application supercapacitors. On the other hand, glutamine is an amino acid that is involved in the control of cancer stem cells, and many biosynthetic, regulatory, and energy production processes [9,10], and nickel is a transition metal due to rapid faradaic redox reactions at the electrode surface than EDLC materials have better capacitive performance [11].

In this work, GO-G @Ni is synthesized through a green method as the new electrode for supercapacitors. Glutamine as a non-toxic amino acid compound through an amide reaction was placed on the surface of graphene oxide and then anchored by nickel. The assembled GO-G @Ni electrode has shown a high specific capacitance of 1136 F g^{-1} at a current density of 2 A g^{-1} within a potential window of 0–0.5 V. Our research presents a non-toxic, efficient, cheap, novel, and hybrid material that is applied to supercapacitors.

2. Experimental section

A novel composite was prepared with a two-step method as an electrode material for a supercapacitor using graphene oxide (GO) and nickel stabilized on glutamine (GO-G@ Ni). To evaluate the electrochemical properties of the synthesized GO-G @Ni, a 3-electrode system including a saturated calomel electrode as reference electrode, platinum rod as counter electrode, and foam nickel coated with the active material as working electrode with 6 M KOH as electrolyte solution was used. In order to prepare the working electrode, the active material, carbon black, and polytetrafluoroethylene with the ratio of 80:15:5 were first mixed and then dispersed in an ethanol solution. The suspension was homogenized for 20 min in an ultrasonic bath. Then, the resultant mixture was coated with a brush on foam nickel substrates and dried for 24 h at 80 °C. Then, the resultant mixture was coated with a brush on foam nickel substrates and dried for 24 h at 80 °C. After placing the working electrode in the 3-electrode cell, Electrochemical impedance spectroscopy (EIS), galvanostatic

charge/discharge(GCD), and cyclic voltammetry (CV) tests were performed.

3. Results and Discussion

Fig. 1 shows the FT-IR spectra of composite GO-G @Ni. The absorption bands in the 3400 cm^{-1} are related to N–H and O–H groups. Also, the adsorption band at 2925 cm^{-1} belongs to C–H aliphatic bonds in glutamine. The adsorption band at 1640 cm^{-1} is corresponding to the amide (HN-C=O) groups. In addition, the adsorption band at 1717 cm^{-1} belongs to an acid carbonyl group. The absorption band in the range of 600–900 cm^{-1} is related to nickel metal [12-14].

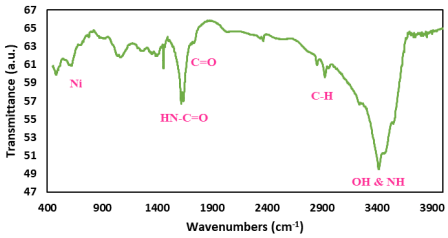

Fig. 1: FTIR spectra of GO-G@ Ni.

EDX analysis shows the presence of C (57.62%), O (27.66%), N (11.08%), and Ni (3.64%) elements, which confirms the structure of the composite GO-G@ Ni successfully (**Fig. 2**).

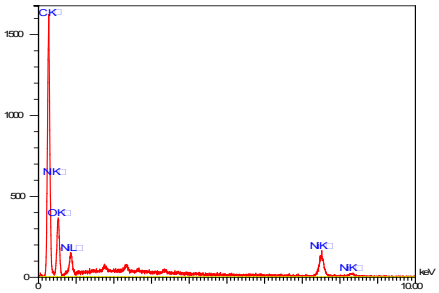

Fig. 2: EDX spectra of GO-G@ Ni.

SEM images of composite GO-G@ Ni are illustrated in **Fig. 3**. Graphene oxide has a planar and regular state [15]. In these images, the graphene oxide has gone out of the planar and regular state and has turned into an interwoven form, which indicates the placement of the desired functional groups on its surface and the formation of the final composite.

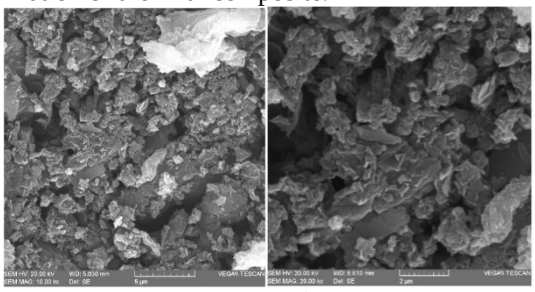

Fig. 3 SEM images of GO-G@ Ni.

Fig. 4 shows the cyclic voltammetry profile of the GO-G@ Ni electrode at six different sweep rates ranging from 0.01 to 0.06 Vs^{-1} and 0-0.5 V potential range. The quasi-rectangular shape CV profiles with redox peak (oxidation and reduction) [1,16]. The reversible Faradaic redox reaction at the electrode-ion electrolyte interface can be represented by the following equation (**1, 2**):

$$Ni^{2+} + OH^- \leftrightarrow Ni\,(OH)_2 \quad (1)$$

$$Ni\,(OH)_2 + OH^- \leftrightarrow NiOOH + H_2O + e^- \quad (2)$$

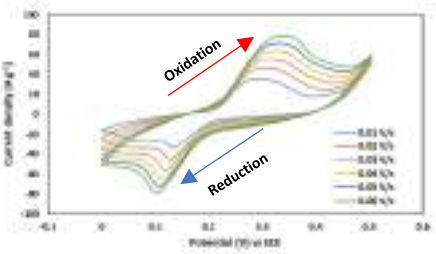

Fig. 4. CV curves of GO-G@Ni.

Fig. 5 displays galvanostatic charge/discharge profiles of the composite GO-G@ Ni electrode in 0-0.5 V potential range and current density 2 to 5 A g^{-1}. The shape of the curves is not triangular. In addition, a pair of peaks appeared on the graph which showed pseudo capacitive behavior. The specific capacitance of the composite GO-G@ Ni was obtained 1136 F g^{-1} at a current density of 2 A g^{-1}.

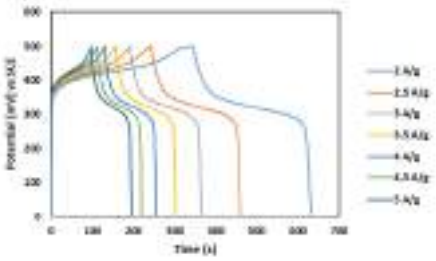

Fig. 5: GCD diagram of GO-G@ Ni.

The cycle stability of the GO-G@ Ni composite electrode was evaluated by repeating the GCD measurements between 0 to 0.5 V at a current density of 10 A g^{-1} for 12000 cycles, after 12000 cycles retain 78.33% of the initial capacitance (**Fig. 6**).

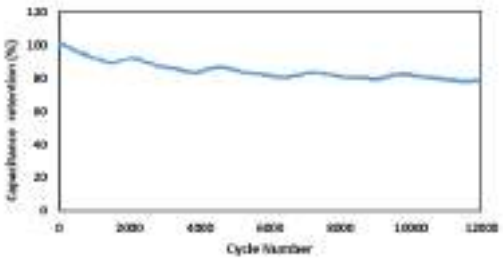

Fig. 6. cycling stability of GO-G@ Ni.

Fig. 7 shows the Nyquist plot at high frequencies of electrode GO-G@ Ni, in which the imaginary part of the impedance (Z") is drawn versus the real part (Z) in a range between 0.01 Hz to 100 kHz. The Randles model is used as an equivalent electric circuit. Their values the solution resistance and charge transfer resistance for the composite are presented in 5.31 and 6.10 Ω, respectively that higher conductivity due to the semicircle in the high frequency and better capacitive behavior, indicated by the straight line in the low frequency [17,18].

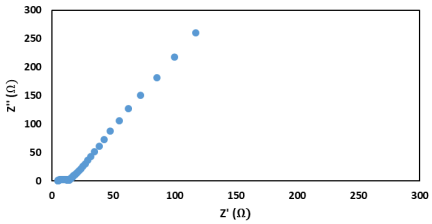

Fig. 7. Nyquist plots of GO-G@ Ni.

4. Conclusions

The graphene oxide and nickel stabilized on glutamine as an electrode material for supercapacitors was synthesized with a two-step method. The GO-G@ Ni electrode exhibited a specific capacitance of 1136 F g^{-1} at a current density of 2 A g^{-1} in a 6 M KOH electrolyte at a potential range of 0 to 500 mV. The significant increase in capacity can be attributed to the existence of both pseudo-capacitive and EDLC mechanisms to store charges and the dispersion of glutamine-functionalized graphene oxide sheets that increase the area of graphene oxide. Moreover, the GO-G@ Ni electrode exhibited excellent electrochemical stability after 12000 cycles at a current density of 10 A g^{-1} retaining 78.33% of the initial capacitance.

5. References

[1] X. Zhang et al., "P-induced oxygen-deficient P-Ni2MnO4−x@rGO with enhanced energy density for supercapacitor," J. Alloys Compd., vol. 937, p. 168321, 2023.

[2] A. Paul, S. Ghosh, H. Kolya, C. W. Kang, N. Chandra Murmu, and T. Kuila, "Synthesis of nickel-tin oxide/nitrogen-doped reduced graphene oxide composite for asymmetric supercapacitor device," Chem. Eng. J., vol. 443, no. February, p. 136453, 2022.

[3] A. F. Alem et al., "Ag doped Co3O4 nanoparticles for high-performance supercapacitor application," Heliyon, vol. 9, no. 2, p. e13286, 2023.

[4] B. Xu et al., "Reduced graphene oxide as a multi-functional conductive binder for supercapacitor electrodes," Energy Storage Mater., vol. 12, no. December 2017, pp. 128–136, 2018.

[5] S. Rajeevan, S. John, and S. C. George, "Polyvinylidene fluoride: A multifunctional polymer in supercapacitor applications," J. Power Sources, vol. 504, no. January, p. 230037, 2021.

[6] C. Xiang, M. Li, M. Zhi, A. Manivannan, and N. Wu, "A reduced graphene oxide/Co3O4 composite for supercapacitor electrode," J. Power Sources, vol. 226, pp. 65–70, 2013.

[7] S. Sundriyal, M. Sharma, A. Kaur, S. Mishra, and A. Deep, "Improved electrochemical performance of rGO/TiO2 nanosheet composite based electrode for supercapacitor applications," J. Mater. Sci. Mater. Electron., vol. 29, no. 15, pp. 12754–12764, 2018.

[8] V. Sharavath, S. Sarkar, and S. Ghosh, "One-pot hydrothermal synthesis of TiO2/graphene nanocomposite with simultaneous nitrogen-doping for energy storage application," J. Electroanal. Chem., vol. 829, pp. 208–216, 2018.

[9] F. Pacifico, A. Leonardi, and E. Crescenzi, "Glutamine Metabolism in Cancer Stem Cells: A Complex Liaison in the Tumor Microenvironment," Int. J. Mol. Sci., vol. 24, no. 3, p. 2337, 2023.

[10] L. Pochini, M. Scalise, M. Galluccio, and C. Indiveri, "Membrane transporters for the special amino acid glutamine: Structure/function relationships and relevance to human health," Front. Chem., vol. 2, no. August, pp. 1–23, 2014.

[11] A. Ganiyat Olatoye, W. Li, E. Oluwaseyi Fagbohun, X. Zeng, Y. Zheng, and Y. Cui, "High-performance asymmetric supercapacitor based on nickel-MOF anchored MXene//NPC/rGO," J. Electroanal. Chem., vol. 928, no. November 2022, p. 117036, 2023.

[12] N. Ghanbari and H. Ghafuri, "Preparation of novel Zn – Al layered double hydroxide composite as adsorbent for removal of organophosphorus insecticides from water," Sci. Rep., pp. 1–15, 2023.

[13] D. R. Rout, P. Senapati, H. Sutar, D. C. Sau, and R. Murmu, "Graphene Oxide (GO) Supported Palladium (Pd) Nanocomposites for Enhanced Hydrogenation," Graphene, vol. 08, no. 03, pp. 33–51, 2019.

[14] H. Ghafuri, N. Joorabchi, A. Emami, and H. R. Esmaili Zand, "Covalent Modification of Graphene Oxide with Vitamin B1: Preparation, Characterization, and Catalytic Reactivity for Synthesis of Benzimidazole Derivatives," Ind. Eng. Chem. Res., vol. 56, no. 22, pp. 6462–6467, 2017.

[15] W. W. Liu, S. P. Chai, A. R. Mohamed, and U. Hashim, *Synthesis and characterization of graphene and carbon nanotubes: A review on the past and recent developments*, vol. 20, no. 4. The Korean Society of Industrial and Engineering Chemistry, 2014.

[16] E. M. Almutairi, M. A. Ghanem, A. Al-Warthan, M. R. Shaik, S. F. Adil, and A. M. Almutairi, "Chemical deposition and exfoliation from liquid crystal template: Nickel/nickel (II) hydroxide nanoflakes electrocatalyst for a non-enzymatic glucose oxidation reaction," Arab. J. Chem., vol. 15, no. 1, p. 103467, 2022.

[17] S. Mohammadi, E. Targholi, and S. M. Mousavi-Khoshdel, "Metal–organic framework-derived cobalt hydroxide microparticles as supercapacitor electrode materials," J. Iran. Chem. Soc., vol. 18, no. 8, pp. 2115–2122, 2021.

[18] H. Banna, M. Emrooz, M. S. Hosseini, S. Mohammadi, and S. M. Mousavi-khoshdel, "One-step green synthesis of meso-microporous carbons by self-activation of lemon wastes for high-performance supercapacitors," J. Energy Storage, vol. 56, no. PA, p. 105989, 2022.

29TH IRANIAN ORGANIC CHEMISTRY CONFERENCE
1_3 NOV, 2023
UNIVERSITY OF QOM, IRAN

Design, synthesis and in vitro evaluation of antibactrial activity of some new pyrano-pyrimidine compounds

Nasrin Saberi Harooni[a*], *Fatemeh Dehghani Tafti*[b], *Nazanin Moghadam*[c], *Parisa Azarang*[d], *Hossein Naeimi*[a] *and Aazar Tahghighi*[a]

[1]*Department of Organic Chemistry, Faculty of Chemistry, University of Kashan, Kashan, 87317, I.R. Iran, nasrinsaberi72@gmail.com, naeimi@kashanu.ac.ir*
[2]*Medicinal Chemistry Laboratory, Department of Clinical Research, Pasteur Institute of Iran, Tehran, Iran*

Abstract - A series of new pyrano[2,3-d]-pyrimidines were synthesized using Cu/Cu/Ni/MWCNTs as a catalyst to reduce various aldehydes. The synthesized compounds were confirmed by ^{1}HNMR and FTIR. In addition, the target molecules were their antibacterial activity was screened against Klebsiella pneumoniae, Staphylococcus aureus, Escherichia coli and Bacillus subtilis. Molecule 4a showed good antifungal activity.

1. Introduction

Pyrano[2,3-d] pyrimidine can be prepared by the one-pot multicomponent synthesis of 1,3-diethyl barbituric acid, various aldehydes, and malononitrile **[1-4].** The different pyrano[2,3-d] pyrimidine derivatives constituting so far indicate interesting anti-tumor, cardiotonic, anti-bronchitis, and hepatoprotective. Moreover, polyfunctionalized pyrano[2,3-d] pyrimidine formatives are joint constructive subunits of actual intrinsic products **[5-10].**

2. Experimental section

2.1. General procedure for the synthesis of pyrano]2,3-d[pyrimidine

Aromatic aldehyde (1 mmol), malononitrile (1.2 mmol), and 1,3-diethyl barbituric acid (1 mmol) were transferred to the 25 mL Round-bottom flask and added Cu/Co/Ni/MWCNTs (0.005 g) as a catalyst. Then, 5 mL of the water was added to the mixture as a solvent. The mixture was stirred at room temperature, and the reaction progress was monitored by thin-layer chromatography (TLC) technique. After the completion of the reaction, the sediments were filtered and washed with ethanol. Then, with the help of ethyl acetate, the catalyst was separated from the reaction mixture. The recovered catalyst was washed with ethanol and water and dried at 80 °C for reuse. The crude product was recrystallized in ethanol after evaporation of the ethyl acetate. As needed, the compounds were purified with the help of column chromatography.

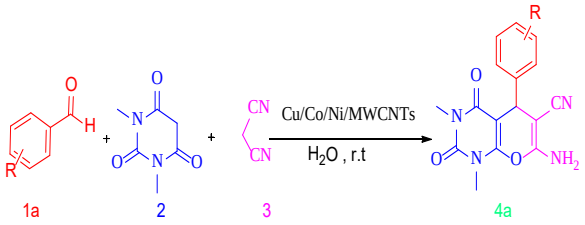

Fig 1. Synthesis of pyrano]2, 3-d[pyrimidine derivatives

Biological assay

2.2. Antimicrobial studies

The antimicrobial activity of the novel synthesized molecules was screened in vitro bacterial strains against Escherichia coli, Klebsiella pneumonia, Bacillus subtilis, and Staphylococcus aureus by disc diffusion method. All the compounds were dissolved in dimethyl sulfoxide (DMSO) solvent at concentrations of 50 and 100 µg/mL and a standard inoculum (1-2 × 107 c.f.u./mL 0.5 McFarland) were presented on to the surface of sterile agar plates and a sterile glass spreader was utilized for uniform dissemination of the inoculums. Ampicillin and levofloxacin were used as the reference drugs for antibacterial respectively. The plate was incubated for 24 h at 37°C.

3. Results and discussion

The Cu/Co/Ni/MWCNTs catalyst is prepared in three-step described in Fig 1. At first, the MWCNTs are activated by H_2SO_4 and HNO_3. As a result, the hydroxyl and carboxylic groups are formed on the surface of the MWCNTs and activating them. In the second step, the Cu is stabilized on the activated MWCNTs with the help of these organic groups created in the previous step through creating bonds. Then Cu^{2+} is reduced to Cu^0 by using the formaldehyde. Finally, the Co and Ni metals are fixed on the Cu/MWCNTs.

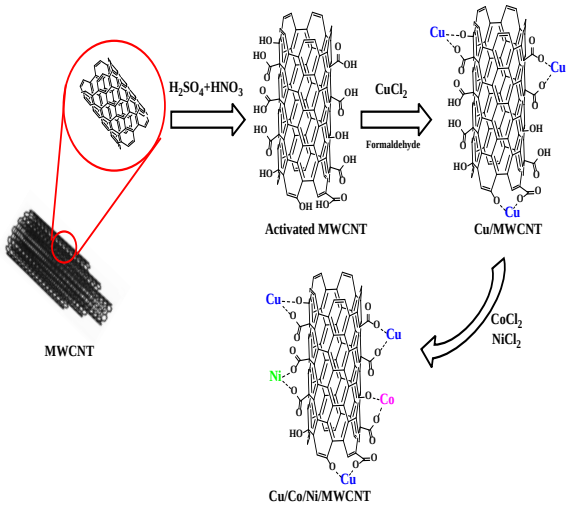

Fig. 2. Preparation of Cu/Co/Ni/MWCNTs catalyst

Biological assay

The synthesized molecules (4a-v) were evaluated for their in vitro antibactrial activity and all the results were described in Tables 1.Various compounds were displaying the best antimicrobial activity when compared with Ampicillin and levofloxacin .The novel molecules (4a-v) proved the better effective as an antimicrobial activity to against Gram (+) bacteria: Bacillus subtilis, Staphylococcus aureus, and Gram (-) bacteria: Klebsiella pneumoniae, Escherichia coli, Salmonella typhi. The anti-bacterial activity shown that all the screened compounds exhibited good zone of inhibition against several tested microbial strains compared to the reference. Compound 4a exhibited excellent antibacterial activity against all tested cell lines because the group contains a nitro group at position 2 of the pyranopyrimidine ring, which shows good antibacterial activity. Generally, increase of electron contributing group (Me, MeO) strength on phenyl ring on pyranopyrimidine reduces antibacterial activity Table1.

Table 1 Antibacterial activity of compounds

	Sample Name	*E.coli ATCC:29232* (-)	*S.aureus ATCC:29223* (+)	*B.Subtillus ATCC:* (+)	*K.pnumonia ATCC: 9997* (-)	*S.Typhi* (-)	*Strep A ATCC:19615* (+)	*p.aeruginosa 27853* (-)
		MIC(µg/ml)	*MIC(µg/ml)*	*MIC(µg/ml)*	*MIC(µg/ml)*	*MIC(µg/ml)*	*MIC(µg/ml)*	*MIC(µg/ml)*
1	4a	<7.8	<7.8	<7.8	62.5	31.25	31.25	250
2	4b	1000	1000	>1000	1000	>1000	1000	1000
3	4c	1000	1000	1000	100	>1000	>1000	>1000
4	4d	1000	1000	>1000	1000	>1000	>1000	>1000
5	4e	1000	1000	1000	1000	>1000	>1000	>1000
6	4f	1000	1000	1000	1000	>1000	>1000	>1000
7	4g	1000	1000	1000	1000	>1000	>1000	>1000
8	4h	1000	1000	1000	1000	>1000	>1000	>1000
9	4i	1000	1000	1000	1000	>1000	>1000	>1000
10	4j	1000	1000	1000	1000	>1000	>1000	>1000
11	4k	1000	1000	1000	1000	>1000	>1000	>1000
12	4l	1000	1000	1000	1000	>1000	>1000	>1000
13	4m	>1000	1000	1000	1000	>1000	>1000	>1000
14	4n	1000	1000	1000	1000	>1000	>1000	>1000
15	4o	>1000	1000	1000	1000	>1000	>1000	>1000
16	4p	>1000	>125	500	250	1000	>1000	>1000
17	4q	>1000	500	1000	1000	1000	>1000	1000
18	4r	1000	1000	1000	1000	>1000	>1000	>1000
19	4s	1000	1000	500	250	>1000	>1000	>1000
20	at	1000	1000	1000	1000	1000	1000	>1000

21	4u	1000	62.5	1000	500	1000	250	>1000
22	4v	1000	250	250	1000	1000	250	>1000
C+	Ampicillin	4	-	-	-	4	-	4
C+	levofloxacin	<0.3	<0.3	<0.3	<0.3	<0.3	<0.3	<0.3
	DMSO	10% v/v	>10% v/v	10% v/v	10% v/v	10% v/v	10% v/v	10% v/v

4. Conclusion

In conclusion, we have amplified, prepared and tested a series of pyranopyrimidines in vitro for antibacterial activity and studied the structure-activity relationship. Two molecules (4a and 4v) showed excellent activity in all cell lines tested, having electron-withdrawing (nitro) groups on the phenyl ring and furan linked to the pyranopyrimidine.

4. References

[1] Y. Rajinder, M. Gupta, J. Kour (2019) J. Iran. Chem. Soc.16, 1977.
[2] M. Abaszadeh, S. J. Roudbaraki, M. Ghashang (2019) Org. Prep. Proced. Int. 51, 255.
[3] G. Brahmachari, K. Nurjamal (2019) Tetrahedron Lett.60, 1904.
[4] M. Daraie, M. M. Heravi, T. Tamoradi (2019) ChemistrySelect. 4,10742.
[5] D. Azarifar, R. Nejat-yami, F. Sameri, Z. Akrami (2012) Lett. Org. Chem. 98, 435.
[6] J. A. Angulwar, G. S. Khansole, V. N. Bhosale (2018) Int. J. Chem. Phys. Sci. 7, 2319.
[7] M. C. Bagley, D. D. Hughes, M. C. Lubinu, E. A. Merritt, P. H. Taylor, N. C. O. Tomkinson (2004) QSAR Comb. Sci.23, 859.
[8] M. N. Elinson, A. I. Ilovaisky, V. M. Merkulova, T. A. Zaimovskaya, G. I. Nikishin, (2011) Mendeleev Commun. 21, 122.
[9] S. Beheshti, V. Safarifard, A. Morsali (2018) Inorg. Chem. Commun. 94, 80.
[10] J. A. Valderrama, P. Colonelli, D. Vásquez, M. F. González, J. A. Rodríguez, C. Theoduloz (2008) Bioorg. Med. Chem. 16, 10172.

29TH IRANIAN ORGANIC CHEMISTRY CONFERENCE
1_3 NOV, 2023
UNIVERSITY OF QOM, IRAN

Green synthesis of 3,4-dihydropyrimidin-2(1H)-ones via Cobalt (II) schiff-base complex immobilized mesoporous silica as heterogenous catalyst

Fatemeh Janati *

Department of Chemistry, Payam Noor University, Tehran, Iran, fsjanati@pnu.ac.ir

Abstract - A Cobalt (II) Schiff-base complex immobilized mesoporous silica material (COSC@MCM-41) was prepared using the ultrasonication method. The formation of material with expected morphological and structural features was confirmed with various characterization techniques including UV-D, FTIR, SEM, EDAX and TEM analyses. Furthermore, the COSC@MCM-41 catalyzed Biginelli reaction has performed under an eco-friendly solvent approach at room temperature, achieving high product yield. The exhibition of excellent catalytic activity towards 3,4-dihydropyrimidone derivatives with high product yield in a short time at room temperature proved that the COSC@MCM-41 is a more effective heterogeneous catalyst toward the Biginelli reaction compared to other catalysts.

1. Introduction

In this context, heterogeneous metal complexes modified solid supports such as polymers, zeolites, silica, graphene, metalorganic frameworks, biochar, carbon nanotubes, and metal oxide nanoparticles have received considerable attention [1]. Among these, Mesoporous silica materials (MCM-41) have garnered significant attention in contemporary science due to their outstanding applications in various fields, including catalysis, drug delivery systems, adsorption, extraction, energy, sensing, and gas storage [2]. Also, MCM-4 represents the most desirable solid support due to its greater surface area, which increases the probability of interaction and, consequently, catalytic activity. Moreover, the silica architecture is renowned for its stability and simple functionalization, where the presence of more silica groups on the surface of MCM-41 provides a strong binding site for metal complexes and facilitates the immobilization of suitable functional groups [3]. The Biginelli reaction is a prominent example of a multicomponent reaction in which three or more aldehydes, urea, and ethyl acetoacetate react to form a new compound.
Schiff-base complex utilized as outstanding catalysts in Biginelli reaction. The exhibition of excellent catalytic activity towards 3,4-dihydropyrimidone derivatives with high product yield in a short time at room temperature proved that the COSC@MCM-41 is a more effective heterogeneous catalyst toward the Biginelli reaction compared to other catalysts (Scheme1).

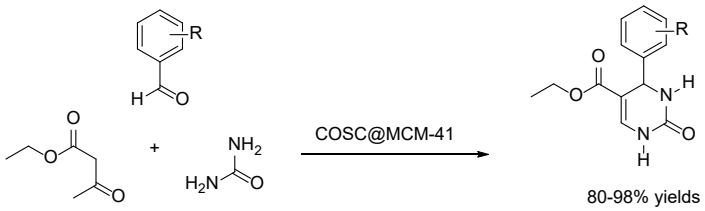

Scheme 1. The Biginelli synthesis of DHPM.

2. Results and Discussion

The electronic transitions of prepared MCM-41, Schiff-base ligand, Cobalt complex, and COSC@MCM-41 were studied using UV-DRS spectra. As shown in Fig. 1a, the purified MCM-41 spectrum does not display any absorption peak in the UV-DRS, which can be attributed to the absence of p and n-electrons and its non-reactive nature. On the other hand, the Schiff base ligand (C=N) produces absorption maxima at 222 nm and 318 nm due to the n- n* and n- n* transitions, respectively [4]. In the Cobalt Schiff-base compound, the presence of ligand-to-metal charge trans produces significant peaks at 345 and 480 nm.

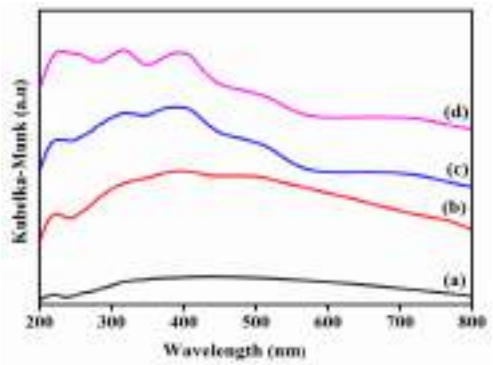

Fig. 1. The UV-DRS spectra of (a) MCM-41, (b) Schiff-base ligand, (c) Cobalt complex, and (d) COSC@MCM-41.

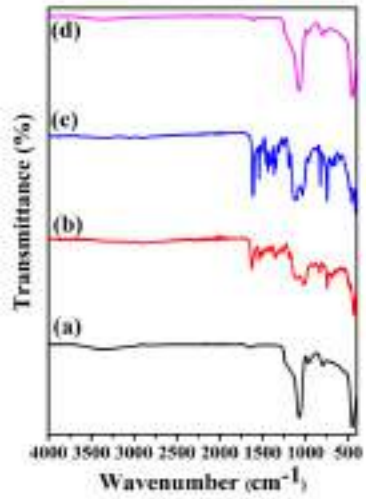

Fig. 2. Infrared Spectra of (a) MCM-41, (b) Schiff base ligand, (c) Cobalt complex, and (d) COSC@MCM-41.

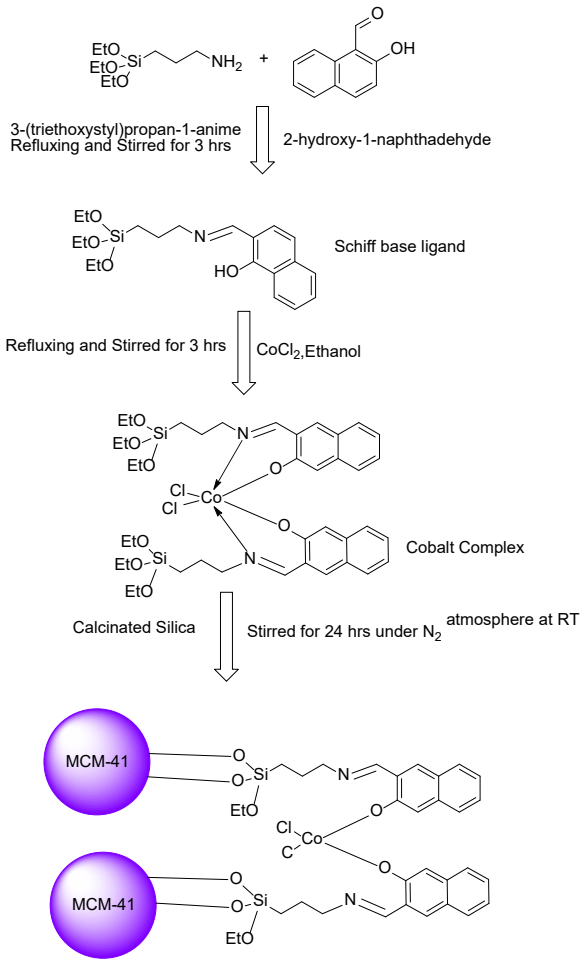

CoSC@MCM-41

Scheme2. The synthesis of CoSC@MCM-41.

The FT-IR spectra of Co-SBand COSC@MCM-41 are displayed in Fig. 2, where the Co-N and Co-O peaks for both complexes show less intense peaks at ~ 595cm-1 and 456cm-1, indicating the successful coordina ion of the Cobalt ion to the ligand moieties. Additionally, the distinct Si-O-Si bands are observed at ~ 1067 cm-1 and 803 cm-1 due to their asymmetric and symmetric stretching vib at ons [5]. A peak at 3366 cm-1 in Co-SB is related to the ligand bands, which shifted to lower wavenumber regions after the complex formation. In COSC@MCM-41, the observed overlapping bands at ~3354 cm-1 is ascribed to the (Si-OH) of MCM-41 and Cobalt compl x s, indicating the effective functionalization of the Cobalt complex on the mesoporous surface [6-7]. Furthermore, the concomitant shift obtained in a peak at ~ 1625 cm-1, which corresponds to the azomethine stretching, also confirms the Schiff base functionalization over MCM-41.

The XRD patern of MCM-41 exhibits a single dominant peak (d100) at ~ 1.9 θ, which is well-matched with the previously reported XRD pattern of mesoporous silica (Fig. 3). After the complex formation, the intensity of the above-said peak is decreased due to the complete coverage of exposed MCM-41surface plane by Co(II) Schiff base complex

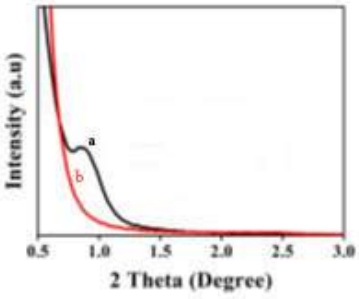

Fig. 3. Low angle diffraction peaks of MCM-41(a) and COSC@MCM-41(b).

3. Conclusion

The successful preparation of COSC@MCM-41 using 2-hydroxy-1-naphthaldehyde is reported in this study. The catalyst displayed exceptional catalytic activity in the Biginelli reaction for the synthesis of 3,4-dihydropyrimidone derivatives. Compared to other heterogeneous catalysts, the prepared catalyst showed superior catalytic efficiency. Furthermore, the catalyst showed excellent catalytic performance at ambient temperature with short reaction times, leading to a high yield of products.

4. References

[1] Bharathi M, Indira S, Vi oth G, Shanmuga Bharathi K. J Porous Mater (2019), 26:1377–90.
[2] Palania an M, Selvaraj D, Kandasamy S, Kahng YH, Narayanan M, Rajendran R, et al.
Environ Res (2022); 215:114325.
[3] Sharma RK, Sharma S, Dutta S, Zboril R, Gawande MB.. Green Chem 2015;17 :3207–30.

[4] Chetna Dhand, a Molamma P. Prabhakaran, b Roger W. Beuerman, ac R. Lakshminarayanan ac ND and SR. RSC Advances. RSC Adv n.d.

[5] Anbarasu G, Malathy M, Karthikeyan P, Rajav l R. J Solid State Chem (2017) ;253:305–12.

[6] Moorthy M, Govindaraj A, Madheswaran B, Kannan B, Rangappan R. J Porous Mater (2017);24:1395–407.

[7] Muthusami R, Kesavan A, Ramachandran V, Vasudevan V, Irena K, Rangappan R. Microporous Mesoporous Mater (2020), 294:109910.

29TH IRANIAN ORGANIC CHEMISTRY CONFERENCE
1_3 NOV, 2023
UNIVERSITY OF QOM, IRAN

The Biginelli reaction promoted by choline chloride based deep eutectic solvents for the synthesis of 3,4-dihydropyrimidin-2(1H)-ones.

Fatemeh Janati *

Department of Chemistry, Payam Noor University, Tehran, Iran, fsjanati@pnu.ac.ir

Abstract - Biginelli condensation of β-keto ester, benzaldehyde and urea catalyzed by L-proline in the choline chloride -based deep eutectic solvents was achieved. High yields are up to 93.6%. Mild reaction conditions, enhanced rates, improved yields, recyclability of deep eutectic solvents containing L-proline, and reagents' reactivity which is different from that in standard organic solvents are the remarkable features observed in deep eutectic solvents. The deep eutectic solvents containing catalyst was recycled in three subsequent runs with no decrease in activity.

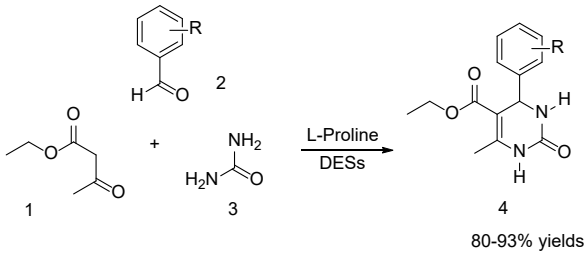

Scheme1.

1. Introduction

3,4-Dihydropyrimidin-2(1H)-ones (DHPMs) and their derivatives have attracted increasing interest due to their diverse therapeutic and pharmacological activities, such as calcium-channel blocking, antihypertensive, antifungal, antibacterial, antiviral, anti-inflammatory, and anticancer properties.[1-3] Some of them have been successfully used as calcium-channel blockers, antihypertensive agents, and α1a-antagonists.[4, 5] Several alkaloids isolated from marine sources whose molecular structures contain the dihydropyrimidinone unit also exhibit interesting biological activities. The Biginelli reaction involves a three component, one-pot condensation of benzaldehyde, β-keto ester, and urea under strongly acidic conditions. However, some methods often require harsh conditions, long reaction times, expensive catalysts, and volatile organic solvent.[5]The search for new, efficient, and green catalysts is still being actively pursued.

Deep eutectic solvents (DESs) are similar to ILs, with low melting point, low volatility, and high thermal stability. In addition, DESs are biodegradable, nontoxic, cheap, and easy to prepare. Therefore, DESs are also called "green solvent." DESs first came to the public vision in 2001 [6]. Since then, the research on deep eutectic solvent has been developing rapidly in extraction, organic synthesis, biocatalysis, and other fields [7-10]. In this paper, an effective and green preparation method that is proline catalyzed Biginelli condensation in choline chloride based DESs was established for the first time (Scheme 1). Obviously, the chirality of the catalyst is not necessary for the described procedure, but the cheapness of L- proline in comparison with the corresponding racemic amino acid makes it the catalyst of choice

2. Results and Discussion

It is well-known that the reaction medium has a great influence on the activity, stability, and possible stereostructure of the catalyst. Thus, the infuence of DESs on L-proline-catalyzed Biginelliel condensation was investigated in this study. Based on our previous researches [8], Biginellie l condensation between benzaldehyde ethyl acetoacetate and urea was used as a model reaction. The initial experiments were performed in nine pure DESs (Table 1, entries 3–11) at 60 °C for 24 h. As shown in Table 1, the composition and proportion of DES greatly affected the reaction yield. The yield in ChCl/Gly and ChCl/EG were all higher than that in ChCl/ Urea. Furthermore, in ChCl/Gly and ChCl/EG reaction system, when ChCl/Gly(1:1) and ChCl/EG(1:3) were used as a medium in the model reaction, the yields were very high, 93.0% and 91.0%, respectively (Table 1, entries 3 and 8). But when the composition proportion of ChCl/Gly and ChCl/ EG changed, the yield decreased. According to our previous research, the yield in ChCl/Gly(1:1) and ChCl/EG(1:3) is higher than that in organic solvent and IL [bmim][BF-4] [10]. In order to prove the promotion of L-proline-catalyzed Biginelli condensation by DESs, some control experiments were performed under the same conditions. The yield is only 65.5% under solvent free condition (Table 1, entry 1),

indicating that ChCl/Gly and ChCl/EG can greatly promote the catalytic activity of L-proline. The yield is only 16.9% in the presence of water without DESs (Table 1, entry 2). More than this, when water was added to ChCl/Gly and ChCl/EG, respectively, the yield was also greatly reduced (Table 1, entries 12–13). The probable reason for these observations is that the poor water solubility of the reactant and the solubility of catalyst L-proline in water make the reactant and catalyst unable to contact, which leads to the reduction of reaction yield. So we chose ChCl/Gly(1:1) and ChCl/EG(1:3) as the reaction medium for further reaction investigations.

We investigated the influence of reaction time on the model reaction. As shown in Fig. 1, the yield was increasing with the extension of reaction time from 12 to 24 h. When the reaction time was 24 h, the yield was highest in both ChCl/Gly(1:1) and ChCl/EG(1:3). Then, when the reaction time continues to be extended to 24 h and 34 h, the yield decreased. The probable reason for these observations is also that the reaction reached equilibrium when the reaction time was 24 h, while the by-products increased when the reaction time was prolonged. So, 24 h was selected as the optimal reaction time for Biginellie condensation.

Then, the influence of reaction temperature on the model reaction was examined. The model reaction was performed at four different temperatures that ranged from 40 to 80 °C for 24 h. As shown in Table 2, the yield increased with the increase of temperature at first. The reaction at 60 °C for 24 h offered the best result with yields up to 93.6% and 94.6% in ChCl/Gly(1:1) and ChCl/EG(1:3), respectively. Then, when the reaction temperature continues to rise to 60 °C and 70 °C, the yield decreased. According to the reaction mechanism [8], we speculated that temperature plays an important role on the stability of the intermediate. The intermediate was easy to be formed at the optimum temperature. To obtain the best yield, the reaction temperature of 60 °C is chosen for L-proline catalyzed Biginelli condensation. L-proline was used to catalyze the Biginelli reaction to prepare 3,4-dihydropyrimidin-2(1H)-one (DHPM) under conventional heating and for the first time (Scheme 2).

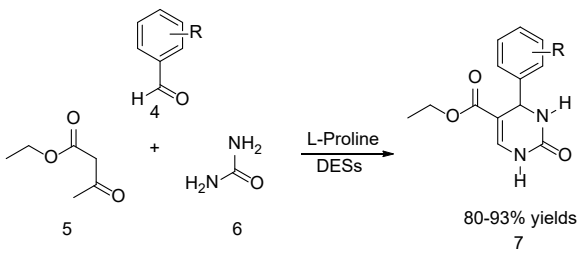

Scheme 2. The Biginelli synthesis of DHPM.

Initially, we began our investigation by using benzaldehyde (4), ethyl acetoacetate (5), and urea (6) for the model reaction.

Table 1 The effect of DES on the L-proline-catalyzed Biginelli condensation

Entry	Solvent	Yield%[b]
1	Blank	65.5
2	deionized water	16.9
3	ChCl/Gly(1:1)	93.0
4	ChCl/Gly(1:2)	85.7
5	ChCl/Gly(1:3)	90.7
6	ChCl/EG(1:1)	92.6
7	ChCl/EG(1:2)	83.4
8	ChCl/EG(1:3)	91.0
9	ChCl/Urea(1:1)	63.7
10	ChCl/Urea(1:2)	68.8
11	ChCl/Urea(1:3)	45.2
12	ChCl/Gly(1:2):deionized water=50:50	16.7
13	ChCl/EG(1:2):deionized water=50:50	21.7

Conditions: benzaldehyde (6.5 mmol), ethyl acetoacetate (10.25 mmol), urea and L-proline (0.70 mmol) in DES (1.0 mL), DES with deionized water (1.0 ml, DES/water, v/v) at 60 °C for 24 h.

Table 2. The effect of temperature on the L-proline-catalyzed Biginelli condensation.

Entry	Temperature(ºC)	solvent	Yield%[b]
1	30	ChCl/Gly(1:1)	34.5
2	40	ChCl/Gly(1:1)	62.4
3	50	ChCl/Gly(1:1)	96.6
4	60	ChCl/Gly(1:1)	29.3
5	70	ChCl/Gly(1:1)	32.5
6	30	ChCl/EG(1:3)	17.8
7	40	ChCl/EG(1:3)	49.1
8	50	ChCl/EG(1:3)	95.6
9	60	ChCl/EG(1:3)	51.9
10	70	ChCl/EG(1:3)	38.4

Conditions: benzaldehyde (7.5 mmol), ethyl acetoacetate (11.25 mmol), urea and L-proline (0.75 mmol) in DES (1.0 mL) at 60 °C for 24 h.

With the optimized conditions in hand, a variety of aldehydes were investigated. The results are summarized in Table 3. Both electron-withdrawing and electron-donating groups on the aldehyde aryl ring were investigated and found to be reactive.

Table 3. Synthesis of DHPMs catalyzed by L-proline under solvent conditions[a]

Entry	Product	R	Time (min)	Yield (%)[b]	Mp (ºC)	
					Found	Ref.
1	7i	3-Br	10	89	184-186	185-18633
2	7j	4-Br	10	88	224-225	225-22610
3	7k	4-NO2	10	97	209-211	210-21132
4	7l	4-Me	10	89	213-215	213-2159
5	7m	4-MeO	10	86	200-202	200-2029
6	7n	3-OH	10	92	184-186	184-18632
7	7o	3-MeO-4-OH	10	87	238-240	239-24032

[a]Reaction conditions: aldehyde (2.5 mmol), ethyl acetoacetate (2.5 mmol), L-proline (0.75 mmol) in DES (1.0 mL) at 60 °C for 24 h.

3. Conclusions

L-proline-catalyzed Biginelli reaction between aromatic aldehydes and, β-keto ester, and urea catalyzed by L-proline was promoted by DESs in the

present work. It was more meaningful to find that ChCl/ Gly and ChCl/EG system had decisive infuence on the catalytic activity of L-proline. The reactions could be performed smoothly between a wide range of aromatic aldehydes, β-keto ester and urea in DESs, and good to excellent yields were obtained. These results create a “green” Biginelli-like reaction in which the solvent and catalyst can be recycled at least four times. As a green and efficient synthesis method, L-proline and DESs not only expand the application fields, but also are expected to become a potential synthesis method with industrial application

4. References

1. S. Sheik Mansoor, S. Syed Shafi, S. Zaheer Ahmed, Arab. J. Chem. (2016), 9,S846–S851
2. da Silva, L. V. Modolo, *J. Adv. Res.* 2015, *6*, 363–373.
3. H. Nagarajaiah, A. Mukhopadhyay, J. N. Moorthy, Tetrahedron Lett. (2016), 57, 5135–5149.
4. B. Mohammadi, F. K. Behbahani, Mol. Diversity. (2018), 22, 405–446.
5. R. V. Patil, J. U. Chavan, D. S. Dalal, V. S. Shinde, A. G. Beldar, ACS Comb.Sci. (2019), 21, 105–148.
6. N. Yao, M. Lu, X. B. Liu, J. Tan, Y. L. Hu, J. Mol. Liq.(2018), 262, 328–335.
7. Dalil Heirati, S. Z.; Shirini, F.; Shojaei, A. F. RSC Adv. (2016), 6, 67072.
8. S. ben Moussa, A. Mehri, B. Badraoui, J. Mol. Struct. (2020), 1200, 127111
9. Charushin, Mendeleev Commun. (2018), 28, 357–358.
10. N. Azizi, M. Edrisi, J. Mol. Liq.(2020), 300, 112263

29TH IRANIAN ORGANIC CHEMISTRY CONFERENCE
1_3 NOV, 2023
UNIVERSITY OF QOM, IRAN

Sulfonic acid heterogeneous nanocomposite for Conversion of fructose into 5-hydroxymethylfurfural

Pouya Ghamari Kargar, Afsaneh Yousefi Monfared, and Ghodsieh Bagherzade**

Department of Chemistry, Faculty of Sciences, University of Birjand, Birjand 97175-615, Iran, P.ghamari71@gmail.com; gbagherzade@gmail.com

Abstract - A novel magnetically recoverable solid acid catalyst was synthesized by immobilization of sulfonic acid groups on g-C_3N_4-modified magnetic nanoparticles. The structure and composition of the synthesized catalyst were characterized by energy-dispersive X-ray (EDX) spectroscopy, elemental mapping, X-ray diffraction (XRD), transmission electron microscopy (TEM). The catalytic performance of the catalyst was evaluated for the conversion of fructose as carbohydrate to 5-hydroxymethylfurfural (5-HMF) in solvent free condition as green and environmentally benign reaction media. Thus, this catalyst system would open up a novel opportunity for the efficient production of 5-HMF under solvent-free conditions. Moreover, the catalyst could be simply separated from the reaction mixture by using a magnetic field and recycled up too many times without incredible loss in its activity.

1. Introduction

Recently, lignocellulosic biomass, which is acknowledged as the world's most abundant renewable carbon resource, has attracted great attention as a satisfactory substitution of the diminishing fossil fuel reserves for industrial culture [1]. One important platform molecule produced from biomass feedstock is 5-hydroxymethylfurfural (5-HMF) which has been listed in the top ten value-added biochemicals by the U.S. Department of Energy [2]. It is a key structural unit in the synthesis of pharmaceuticals, agrochemicals, plastics, and polymers [3]. 5-HMF can also be converted into various high value-added fine and fuel chemicals like 1,6-hexanediol, 2,5-furandicarboxylic acid, 2,5-dimethylfuran, 2,5-dihydroxymethylfuran, levulinic acid, caprolactam, and caprolactone [4]. The main strategy for the synthesis of 5-HMF is the dehydration of fructose in the presence of acid catalysts [5,6]. To date, different homogeneous and heterogeneous Lewis and Brønsted acid catalysts like H_2SO_4, HCl, H_3PO_4, organic acids, zeolites, heteropoly acids, and Amberlyst-15 resins were used for 5-HMF production from fructose [7,8]. In terms of industrial applications, heterogeneous acid catalysts are preferred owing to their long-term stability, simple separation and recycling [9]. Hence, recent attention has been directed towards the immobilization of homogeneous acid catalysts onto various solid supports in order to improve their recovery and recycling features [10]. In particular, considerable research efforts have been focused on the modification of different solid supports with sulfonic acid groups due to their outstanding reactivity in fructose dehydration reaction [11].

During few past years, carbon-based nanomaterials, for instance, graphene, carbon nanotubes (CNTs), graphite carbon nitride (g-C_3N_4), ordered porous carbon and carbon aerogels, have concerned excessive attention due to its wide potential applications in catalysis, adsorption, gas separation, drug delivery and energy storage [12]. Among the carbon-based nanomaterials, graphitic carbon nitrides (g-C_3N_4) are inspiring great research efforts because they exhibit several desirable performances, such as resistant to acidic or basic media, low toxicity and high stability as well as unique structure which gives it worthy photocatalytic activity [13]. Recently, significant effort has been placed on the design and fabrication of nanostructure to achieve high catalytic activity by adjusting the size and surface morphology of the g-C_3N_4 nanostructure [14]. In addition, doping g-C_3N_4 with metal and/or nonmetal ions, copolymerization with organic molecules and modification with carbon materials appeared and showed significant improvement in their catalytic activity [15]. However, bare g-C_3N_4 suffers from active sites and less specific surface area and to expand the reactivity, the functionalization of g-C_3N_4 with acidic, basic or ionic groups is an excellent method to modify their electronic and optical properties which improve the catalytic activity of g-C_3N_4 [16]. However, the major problem associated with g-C_3N_4 based catalysts is the requirement of high time- and energy consumption separation techniques like filtration or centrifugation for their separation and recovery [17]. This problem causes severe restrictions in using them for practical and industrial applications. The introduction of magnetic nanoparticles on g-C_3N_4 nanosheets, which allows its efficient magnetic separation and recovery, is regarded as an effective

strategy to solve this problem [18]. Thus, in recent years, magnetic graphite carbon nitride nanocomposite as catalysts or catalyst supports have been extensively used in various organic reactions with a high level of activity [19]. Though there are few reports about the application of sulfonic acid-modified g-C_3N_4 for the conversion of fructose into 5-HMF [20], as far our awareness reach, there is no any report on the application of magnetic graphite carbon nitride-supported sulfonic acid groups for this reaction.

Consequently, we decided to design a heterogeneous acid catalyst by modifying the surface of magnetic g-C_3N_4 with sulfonic acid groups. The prepared catalyst was successfully used as a magnetically recoverable heterogeneous catalyst for the dehydration of fructose into 5-HMF.

2. Result and Discussion

The g-C_3N_4 coated magnetic nanoparticles (Fe_3O_4@ g-C_3N_4) were prepared according to the literature method [21]. Also, adding the acidic group can be referred to the past literature [22]. The schematic of Fe_3O_4@g-C_3N_4@$(CH_2)_4$-SO_3H is presented in Fig. 1.

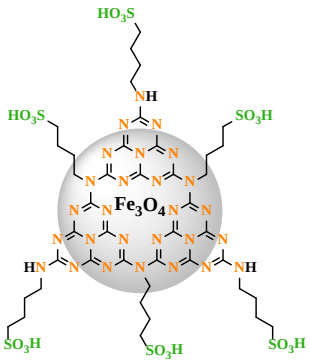

Fig.1. Schematic of Fe_3O_4@g-C_3N_4@$(CH_2)_4$-SO_3H nanocomposite

Energy-dispersive X-ray (EDX) spectroscopy analysis was carried out to examine the elemental composition of the catalyst.

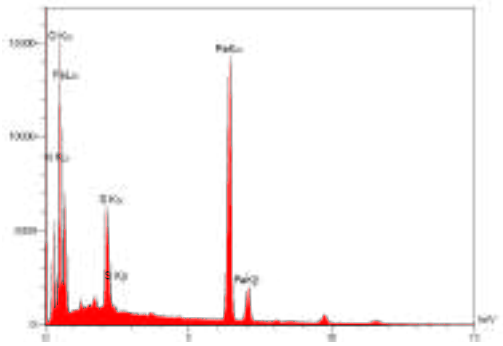

Fig.2. EDX spectrum of Fe_3O_4@g-C_3N_4@$(CH_2)_4$-SO_3H nanocomposite

EDX pattern of Fe_3O_4@g-C_3N_4@ $(CH_2)_4$-SO_3H (Fig. 2) clearly confirmed the presence of C, N, O, S, and Fe elements in the catalyst structure. The crystalline phase of the prepared samples was verified by X-ray diffraction (XRD) analysis. The XRD pattern of Fe_3O_4@g-C_3N_4@$(CH_2)_4$-SO_3H is given in Fig. 3. The XRD pattern of nanocomposite exhibited 2θ peaks at 30° (220), 36° (311), 43° (400), 54° (422), 57° (511), and 63°(440). All of these peaks were also detected in the XRD pattern of Fe_3O_4@ g-C_3N_4@$(CH_2)_4$-SO_3H, demonstrating that the crystalline phase of Fe_3O_4@g-C_3N_4 nanoparticles was not destroyed during the synthesis of the catalyst.

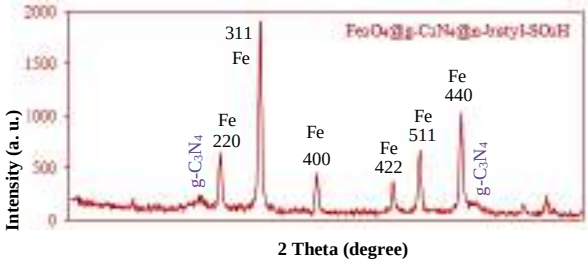

Fig.3. XRD spectrum of Fe_3O_4@g-C_3N_4@$(CH_2)_4$-SO_3H nanocomposite

To gain a better understanding of the morphology and structure of the samples, transmission electron microscopy (TEM) analysis was also performed. The TEM image of Fe_3O_4@g-C_3N_4@ $(CH_2)_4$-SO_3H is presented in Fig. 4. Clearly, the TEM image of nanocomposite demonstrated that the magnetic nanoparticles were spherical in shape with average diameters of 27-35 nm and structured as core−shell.

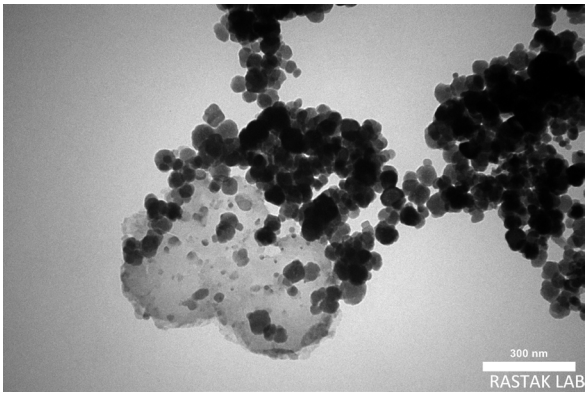

Fig.3. TEM image of Fe_3O_4@g-C_3N_4@$(CH_2)_4$-SO_3H nanocomposite

After the initial characterization of Fe_3O_4@g-C_3N_4@ $(CH_2)_4$-SO_3H, the prepared nanocomposite was evaluated as a solid acid catalyst in the conversion of fructose into high value-added chemical 5-HMF. The catalyst could efficiently promote this reaction to obtain 90% of 5-HMF at 80 ºC for 60 min in solvent free (S.F.) condition as an environmentally friendly reaction medium (Fig. 4). Besides, the catalyst could

be conveniently recovered by a magnetic bar and reused for five times with no significant loss in its activity.

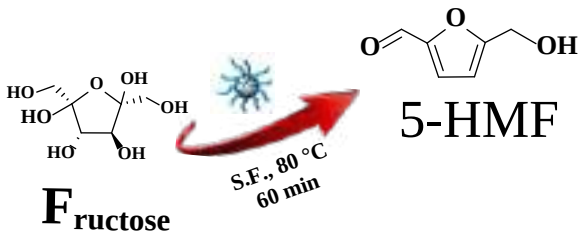

Fig.4. Schematic diagram of 5-HMF preparation

3. Conclusion

A new magnetically retrievable solid acid catalyst was synthesized by g-C_3N_4-coated magnetic nanoparticles in combination with the immobilization of sulfonic acid groups. The synthesized catalyst could effectively catalyze the conversion of carbohydrates into 5-HMF with a high yield in solvent free condition as reaction media. Specifically, the catalyst revealed a remarkable activity in the conversion of fructose that acted as a substrate for 5-HMF production. Therefore, the reaction was performed under solvent-free conditions which are very important from the green chemistry point of view. The numerous reaction parameters including the reaction temperature, catalyst amount, and reaction time were optimized to achieve a maximum yield of 5-HMF. Moreover, the catalyst was easily recovered from the reaction mixture by an external magnet and could conserve its catalytic activity during five consecutive cycles. Altogether, the possibility to perform the reaction under solvent-free conditions, and at the same time the simple separation of the catalyst by a convenient magnetic separation technique, makes this protocol a valid candidate toward the goal of green chemistry.

4. References

[1] Q. Hou, X. Qi, M. Zhen, H. Qian, Y. Nie, C. Bai, S. Zhang, X. Bai, M. Ju, Biorefinery roadmap based on catalytic production and upgrading of 5- hydroxymethylfurfural, Green Chem. 23 (2021) 119e231.

[2] J.J. Bozell, G.R. Petersen, Technology development for the production of biobased products from biorefinery carbohydratesdthe US Department of Energy's "Top 10" revisited, Green Chem. 12 (2010) 539e554.

[3] X. Liu, X. Min, H. Liu, Y. Cao, Y. Liu, M. Han, Z.M. Sun, S. Ji, Efficient conversion of cellulose to 5-hydroxymethylfurfural catalyzed by a cobalt-phosphonate catalyst, Sustainable Energy Fuels 4 (2020) 5795e5801.

[4] X. Zou, C. Zhu, Q. Wang, G. Yang, Catalytic dehydration of hexose sugars to 5-hydroxymethylfural, Biofuel, Bioprod. Bior. 13 (2019) 153e173.

[5] D. Wu, S. Zhang, W.Y. Hernandez, W. Baaziz, O. Ersen, M. Marinova, A.Y. Khodakov, V.V. Ordomsky, Dual metal-acid Pd-Br catalyst for selective hydrodeoxygenation of 5-hydroxymethylfurfural (HMF) to 2,5-dimethylfuran at ambient temperature, ACS Catal. 11 (2021) 19e30.

[6] C. Thoma, J. Konnerth, W. Sailer-Kronlachner, P. Solt, T. Rosenau, H.W.G. Herwijnen, Current situation of the challenging scale-up development of hydroxymethylfurfural production, ChemSusChem 13 (2020) 3544e3564.

[7] R. Tomer, P. Biswas, Dehydration of glucose/fructose to 5-Hydroxymethylfurfural (5-HMF) over an easily recyclable sulfated Titania (SO_4 2-/TiO_2) catalyst, New J. Chem. 44 (2020) 20734e20750.

[8] A. Mittal, H.M. Pilath, D.K. Johnson, Direct conversion of biomass carbohydrates to platform chemicals: 5 hydroxymethylfurfural (HMF) and furfural, Energy Fuels 34 (2020) 3284e3293.

[9] G.P. Perez, M.J. Dumont, Production of HMF in high yield using a low cost and recyclable carbonaceous catalyst, Chem. Eng. J. 382 (2020), 122766.

[10] S. Karimi, H. Shekaari, A.Z. Halimehjani, M. Niakan, Solvent-Free production of 5-hydroxymethylfurfural from deep eutectic substrate reaction mixtures over a magnetically recoverable solid acid catalyst, ACS Sustain. Chem. Eng. 9 (2021) 326e336.

[11] L. Wang, L. Zhang, H. Li, Y. Ma, R. Zhang, High selective production of 5-hydroxymethylfurfural from fructose by sulfonic acid functionalized SBA-15 catalyst, Compos. B Eng. 156 (2019) 88e94.

[12] C. Cha, S. Ryon Shin, N. Annabi, M.R. Dokmeci, A. Khademhosseini, Cha, C., Shin, S. R., Annabi, N., Dokmeci, M. R., & Khademhosseini, A. (2013). Carbon-based nanomaterials: multifunctional materials for biomedical engineering. ACS Nano 23, (2013) 2891–2897.

[13] W.J. Ong, L.L. Tan, Y. Hau, N.S.T. Yong, S.P. Graphitic carbon nitride (g-C_3N_4)-based photocatalysts for artificial photosynthesis and environmental remediation: are we a step closer to achieving sustainability. Chai, Chem. Rev. 116, (2016) 7159–7329.

[14] A. Thomas, A. Fischer, F. Goettmann, M. Antonietti, J.O. Muller, R. Schlogl, J.M. Carlsson, J. Graphitic carbon nitride materials: variation of structure and morphology and their use as metal-free catalysts. Mater. Chem. 18, (2008) 893–4908.

[15] X. Zhang, H. Song, C. Sun, C. Chen, X. Li, Photocatalytic oxidative desulfurization and denitrogenation of fuels over sodium doped graphitic carbon nitride nanosheets under visible light irradiation. Mater. Chem. Phys. 226 (2019) 34–43.

[16] K. Prakash, S. Karuthapandian, S. Senthilkumar, Zeolite nanorods decorated g-C3N4 nanosheets: a novel platform for the photodegradation of hazardous water contaminants. Mater. Chem. Phys. 221 (2019) 34–46.

[17] Y. Xu, L. Zhang, J. Chen, J. Fu, X. Wang, Synthesis of nano-Ag-assisted attapulgite/g-C_3N_4 composites with superior visible light photocatalytic performance. Mater. Chem. Phys. 221 (2019) 447–456.

[18] M., Edrisi, & N. Azizi, Sulfonic acid-functionalized graphitic carbon nitride composite: a novel and reusable catalyst for the one-pot synthesis of polysubstituted pyridine in water under sonication. Journal of the Iranian Chemical Society. 17 (2020) 901-910.

[19] B. Bhuyan, D. Jyoti Koiri, M. Devi, S. Sankar Dhar, A novel $MnFe_2O_4$/graphitic carbon nitride (g-C_3N_4) nanocomposites as efficient magnetically retrievable catalyst in crossed aldol condensation. Mater. Lett. 218 (2018) 99–102.

[20] M. Zhu, S. Kim, L. Mao, M. Fujitsuka, J. Zhang, X. Wang, T. Majima, Metal-free photocatalyst for H_2 evolution in visible to near-infrared region: black phosphorus/graphitic carbon nitride. J. Am. Chem. Soc. 139 (2017) 13234–13242.

[21] Xiong, C., Ren, Q., Liu, X., Jin, Z., Ding, Y., Zhu, H., ... & Chen, R. Fenton activity on RhB degradation of magnetic g-C_3N_4/diatomite/Fe_3O_4 composites. Applied Surface Science, 543 (2021) 148844.

[22] Sansano, J. M. A new bifunctional heterogeneous nanocatalyst for one-pot reduction-Schiff base condensation and reduction–carbonylation of nitroarenes. RSC advances, 9(3) (2019) 1362-1372.

Recent advances of perovskite halides

Mohammadali Jalali[1], *Seyed Mahdi Mousavi*[2*] *and Moslem Setoodehkhah*[3]

[1] *Senior Student of Inorganic Chemistry, Kashan University, Kashan, Iran, mj921661@gmail.com.*
[2] *Department of Applied Chemistry, Faculty of Chemistry, Kashan University, Kashan, Iran, mousavi.smahdi@kashanu.ac.ir.*
[3] *Department of Inorganic Chemistry, Faculty of Chemistry, Kashan University, Kashan, Iran, Setoodehkhah@kashanu.ac.ir.*

Abstract - Halide based perovskite materials have fascinated strong attention for being a hopeful candidate for optoelectronic device applications. Single-crystalline halide perovskites exhibit no grain boundaries and possess low trap densities; and are therefore likely to show superior optoelectronic performances in comparison to their polycrystalline film counterparts. In spite of this, their basic perceptive of physico-chemical properties are however controversial to the scientific society. In this review article, the properties and applications of perovskite halides are investigated. On account of advanced characteristics like long carrier recombination lifetime and exciton diffusion length, wide-ranging visible to NIR absorption, high charge mobility, controllable optoelectronic properties etc., hybrid halide perovskites have emerged to be a tough challenger in the optoelectronic research area in comparison to the purely inorganic halide perovskites and have consequently been paid much attention.

Keywords: Perovskite, Halides, Solar cells, Single crystal

1. Introduction

Perovskite is basically the structure of mineral calcium titanate (CaTiO3) that was first discovered in 1839 by Gustav Rose who was a Russian scientist and later on named by Count Lev Aleksvich von Perovski, a Russian mineralogist. Thus, perovskites are defined as the materials with the same crystal structure as that of CaTiO3 or having the formula ABX3 [1,2]. Currently, metal halide perovskites with the same crystal structure as that of CaTiO3 or having the formula ABX3, where A is $CH3NH^{3+}$, $CH(NH2)^{2+}$ or Cs^{+} , B is Pb^{2+}, Bi^{2+}, Sn^{2+} or Ge^{2+}, and X is I^{-} , Br^{-} or Cl^{-} , have become a limelight in the field of optoelectronics and photonics [3]. The successful application of these metal halide perovskites, that have been studied for several decades, strongly depends upon the synthesis of high-quality perovskites with well-developed qualities like high carrier mobility, low trap density, and longer diffusion lengths etc. These perovskites can be grown in various forms like single crystals, nanostructures, and polycrystalline films, etc by adopting different growth methods [4,5]. Even though, the polycrystalline perovskite thin films show good performance in energy harvesting applications, but due to the morphological chaos, structural defects and the deterioration of the film surface in ambient atmosphere, their practical commercialization is sternly impeded by the severe instabilities and the long-term stability issues faced by them [6]. In ball-stick model of cubic ABX3 perovskite unit cell (Fig. 1), B is a divalent metal, A is the cation and X is halide. In the past years, metal halide-perovskite structures have gained considerable popularity due to their unique optical and electrical properties for use in the manufacture of neurovoltaic components such as solar cells and light emitting diodes [7].

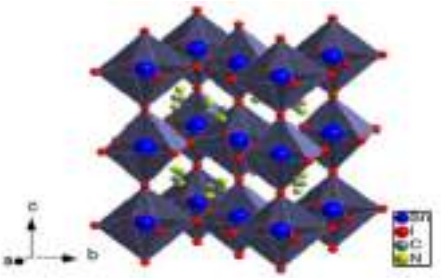

Fig.1. Structure of perovskite halide

2. Electronic Properties

Single crystal perovskites are superior to polycrystalline thin-film perovskites due to the presence of a lesser number of defects and grain boundaries in single crystals than the thin film counterpart. However, to promote the development of devices incorporating single crystal perovskites, it is essential to have the knowledge about the effect of defects and advanced procedures that would engineer the surface imperfections for an enhanced photoluminescence in single crystal perovskites. Ding et al. [5] investigated the role of surface defects in MAPbI3 single crystals. They saw by improving the crystalline quality and grain size, an extended PL decay was observed. This was due to the presence of surface imperfections that benefited the charge carrier

trapping as well as recombination, which in turn resulted in an improved PL emission. In consequence, the surface imperfections played a crucial role in boosting the photoluminescence emission in MAPbI3 single crystals. Thus, in order to design an appropriate device for a particular perovskite, it is very important to understand its fundamental properties. The fundamental electronic properties like trap density, carrier mobility, carrier concentration, carrier lifetime and diffusion length that should be considered while designing a device are explained below [8].

2.1. Carrier mobility: Carrier mobility is a very important factor to determine the performance of a device. This parameter characterizes how rapidly the carriers (electrons and holes) can move through a metal or semiconductor, under the presence of an applied electric field. Researchers have used several techniques for calculating carrier mobility of charge carriers such as Hall effect, time of flight (TOF) and space charge limited current (SCLC) .[9,10]

2.2. Carrier lifetime: Carrier lifetime finds a significant function in the optoelectronic device application, especially for photovoltaics. Various methods can be used to determine the carrier lifetime of single crystal perovskites such as transient absorption, impedance, photoluminescence decay, transient photovoltage decay, etc [11,10]. Further, the carrier lifetime also depends upon the nature, purity, and dimension of the material. Hence, the carrier lifetime of single-crystal perovskite is much longer than that of the polycrystalline thin film indicating fewer defects in single crystal [12,13].

2.3. Carrier Diffusion length: The diffusion length of perovskite single crystal is much larger in comparison to polycrystalline thin film [9,14,15]. For instance, polycrystalline films of MAPbI3 showed diffusion length in the range of 0.30 to 2.74 μm [16]. In addition, longer carrier diffusion length of single-crystal perovskites also finds direct applications primarily in photodetection, radiation energy harvesting, x-ray sensing, gamma-ray sensing etc.

3. Optoelectronic applications

Among various kinds of single crystal perovskites, organic-inorganic hybrid halide perovskites possess superior optoelectronic properties and therefore demonstrate potential applications in lasers, solar cells, light-emitting diodes, photodetectors, etc. Some typical applications are summarized below.

3.1. Solar Cells: The perovskite-based thin film solar cell has attracted much attention as a promising technology to receive and convert sunlight into effective electricity [17]. For the first time in 2008, Masaka's group used organic-inorganic perovskites as sensitizers in pigment solar cells and achieved a yield of 3.8%. This efficiency was later increased to 6.5% by Im and his colleagues by optimizing the electrolyte. In both cases, the stability of the cells was very low due to the rapid dissolution of perovskites in the liquid electrolyte. This problem was solved by using spiramide as a solid-state cavity carrier. Kim and his colleagues achieved a yield of 9% using spiramide. The efficiency of these cells in laboratory dimensions has recently reached 22% [17].

3.2. High-Energy ray detector: A device that converts high energy X-ray and γ-ray to charges is known as a high energy ray detector. This device can be used in various fields like industrial material inspection, medical imaging, security inspection, etc. [18]. When X-ray falls on a crystal, the photons are collected by the crystal layer and the generation of charges takes place. Thus, for a highly sensitive X-ray detector, carrier lifetime and carrier mobility are two very important parameters. Lead halide perovskites contain large atomic number elements Pb, Br or I and exhibit outstanding carrier transport properties. Therefore, lead halide perovskites are a promising material for detecting X-rays [19].

3.3. Lasers: For lasing applications, hybrid perovskites exhibit high optical gain as a result of low defect density, slow auger recombination rate, high absorption coefficient, long carrier diffusion length, high photoluminescence quantum yield, etc. For the first time, Deschler et al. demonstrated laserlink operation using a perovskite halide [20]. After that, Liao et al. designed square single crystal MAPbBr3 microdiscs for lasers.[13] After that, Zhizhchenko and colleagues designed microlasers based on MAPbBrxIy using femtosecond laser beams [21].

3.4. Photodetectors: Photodetectors detect the electromagnetic waves and convert them into electrical signals. Photodetectors with high sensitivity and rapid response have implementations in medical diagnosis, information transportation, biological sensing, camera imaging, automatic control systems and communications, etc [22]. The photodetectors can be further classified into two types: photovoltaic detector and photoconductive detector, depending on the utilization of generated carriers. A photovoltaic detector is basically a solar cell device, where photon generated carriers are collected by the built-in electric field caused due to the presence of asymmetrical electrodes. Photoconductive photodetectors consist of symmetrical electrodes with structure like Ag/material/Ag, ITO/material/ITO; Au/material/Au, etc. By the application of voltage bias on the electrodes, which is necessary for this type of detector, the device current is monitored that determines the performance of the photoconductive detector [14.23].

3.5. Light-Emitting Diodes (LEDs): In comparison to conventional fluorescent tubes or incandescent bulbs, light-emitting diodes are emerging as a key research technology for wide-ranging lighting applications and are considered significantly efficient. As a result of excellent photoluminescence efficiency along with

high color purity and weak Auger recombination, single-crystal halide perovskites are recognized as an ultimate emitting source [24]. Single crystal hybrid perovskites show outstanding luminescent properties like strong luminescence, narrowband emission and high stability and are therefore considered as a highly promised material for application in LEDs [25]. Moreover, it was reported that perovskite based LEDs exhibit high quantum yields.

4. Conclusion:

In this work, a comprehensive picture about the properties of perovskite crystals and optoelectronic applications was described. Single crystal perovskites have been found to be a much better candidate for optoelectronic applications than the analogous polycrystalline thin-film counterparts. Almost every technique that has been used for the synthesis of halide based single-crystal perovskites involves either liquid or solid state reactions. To facilitate the profound understanding of the fundamental characteristics and device physics of hybrid perovskites, more consideration should be given to their growth processes and defects. Consequently, good quality single crystal perovskites will provide a means for the understanding of their fundamental characteristics. Further, the devices utilizing these single-crystalline perovskites having different dimensions would possibly come out as a significant research field.

5. References

[1] Poglitsch, A. and Weber, D., 1987. Dynamic disorder in methylammoniumtrihalogenoplumbates (II) observed by millimeter-wave spectroscopy. The Journal of chemical physics, 87(11), pp.6373-6378.

[2] Kour, R. Arya, S. Verma, S. Gupta, J. Bandhoria, P. Bharti, V. Datt, R. Gupta, V. Potential Substitutes for Replacement of Lead in Perovskite Solar Cells: A Review. Global Challenges, 3(11), 1900050, 2019.

[3] Kay, H.F. and Bailey, P.C. Structure and properties of CaTiO3. Acta Crystallographica, 10(3), pp.219-226, 1957.

[4] Stoumpos, C.C. and Kanatzidis, M.G., Halide Perovskites: Cao, M. Tian, J. Cai, Z. Peng, L. Yang, L. and Wei, D. Perovskite heterojunction based on CH3NH3PbBr3 single crystal for high-sensitive self-powered photodetector. Applied Physics Letters, 109(23), p.233303, 2016.poor Man's high-performance semiconductors.Advanced Materials,28(28), pp.5778-5793, 2016.

[5] Ding, J. Lian, Z. Li, Y. Wang, S. and Yan, Q. The role of surface defects in photoluminescence and decay dynamics of high-quality perovskite MAPbI3 single crystals. The journal of physical chemistry letters, 9(15), pp.4221-4226, 2018.

[6] Murali, B., Kolli, H.K., Yin, J., Ketavath, R., Bakr, O.M. and Mohammed, O.F., Single Crystals: The Next Big Wave of Perovskite Optoelectronics. ACS Materials Letters, 2020.

[7] Yin W. J., Shi T., Yan Y., " Unusual defect physics in CH3NH3PbI3 perovskite solar cell absorber", Applied Physics Letters 104 (2014)063903 .

[8] Babu, R.Giribabu, L. Recent Advances in Halide-Based Perovskite Crystals and Their Optoelectronic Applications. Crystal Growth & Design,18(4), pp.2645- 2664, 2018.

[9] Dong, Q., Fang, Y., Shao, Y., Mulligan, P., Qiu, J., Cao, L. and Huang, J., Electron-hole diffusion lengths> 175 μm in solution-grown CH3NH3PbI3 single crystals. Science, 347(6225), pp.967-970, 2015.

[10] Weber, D., CH3NH3SnBrxI3-x (x= 0-3), ein Sn (II)-System mit kubischer Perowskitstruktur/CH3NH3SnBrxI3-x (x= 0-3), a Sn (II)-system with cubic perovskite structure. Zeitschrift für Naturforschung B, 33(8), pp.862-865, 1978.

[11] Bi, Y., Hutter, E.M., Fang, Y., Dong, Q., Huang, J. and Savenije, T.J., Charge carrier lifetimes exceeding 15 μs in methylammonium lead iodide single crystals. The journal of physical chemistry letters, 7(5), pp.923-928, 2016.

[12] Yang, Y., Yan, Y., Yang, M., Choi, S., Zhu, K., Luther, J.M. and Beard, M.C., Low surface recombination velocity in solution-grown CH 3 NH 3 PbBr 3 perovskite single crystal. Nature communications, 6, p.7961, 2015.

[13] Liao, Q., Hu, K., Zhang, H., Wang, X., Yao, J. and Fu, H., Perovskite microdisk microlasers self-assembled from solution. Advanced materials, 27(22), pp.3405-3410, 2015.

[14] Saidaminov, M.I., Abdelhady, A.L., Murali, B., Alarousu, E., Burlakov, V.M., Peng, W., Dursun, I., Wang, L., He, Y., Maculan, G. and Goriely, A., High-quality bulk hybrid perovskite single crystals within minutes by inverse temperature crystallization. Nature communications, 6(1), pp.1-6, 2015.

[15] Wei, H., Fang, Y., Mulligan, P., Chuirazzi, W., Fang, H.H., Wang, C., Ecker, B.R., Gao, Y., Loi, M.A., Cao, L. and Huang, J., Sensitive X-ray detectors made of methylammonium lead tribromide perovskite single crystals. Nature Photonics, 10(5), p.333, 2016.

[16] Lim, J., Hörantner, M.T., Sakai, N., Ball, J.M., Mahesh, S., Noel, N.K., Lin, Y.H., Patel, J.B., McMeekin, D.P., Johnston, M.B. and Wenger, B., Elucidating the long-range charge carrier mobility in metal halide perovskite thin films. Energy & Environmental Science, 12(1), pp.169-176, 2019.

[17] J-H. Im, C-R. Lee, J-W. Lee, S-W. Park, "6.5% Efficient Perovskite Quantum-Dot-Sensitized Solar Cell, Nanoscale'', vol. 3,pp. 4088-4093. 2011.

[18] Náfrádi, B., Náfrádi, G., Forró, L. and Horváth, E., Methylammonium lead iodide for efficient X-ray energy conversion. The Journal of Physical Chemistry C, 119(45), pp.25204-25208, 2015.

[19] Heiss, W. and Brabec, C., X-ray imaging: Perovskites target X-ray detection. Nature Photonics, 10(5), p.288, 2016.

[20] Deschler, F., Price, M., Pathak, S., Klintberg, L.E., Jarausch, D.D., Higler, R., Hüttner, S., Leijtens, T., Stranks, S.D., Snaith, H.J. and Atatüre, M., High photoluminescence efficiency and optically pumped lasing in solution-processed mixed halide perovskite semiconductors. The journal of physical chemistry letters, 5(8), pp.1421-1426, 2014.

[21] Zhizhchenko, A., Syubaev, S., Berestennikov, A., Yulin, A.V., Porfirev, A., Pushkarev, A., Shishkin, I., Golokhvast, K., Bogdanov, A.A., Zakhidov, A.A. and Kuchmizhak, A.A., Single-mode lasing from imprinted halide-perovskite microdisks. ACS nano, 13(4), pp.4140-4147, 2019.

[22] Cao, M., Tian, J., Cai, Z., Peng, L., Yang, L. and Wei, D., Perovskite heterojunction based on CH3NH3PbBr3 single crystal for high-sensitive self-powered photodetector. Applied Physics Letters, 109(23), p.233303, 2016.

[23] Liu, Y., Sun, J., Yang, Z., Yang, D., Ren, X., Xu, H., Yang, Z. and Liu, S., 20-mm-Large Single-Crystalline Formamidinium-Perovskite Wafer for Mass Production of Integrated Photodetectors. Advanced Optical Materials, 4(11), pp.1829-1837, 2016.

[24] Palazon, F. Di Stasio, F. Krahne, R. Prato, M. and Manna, L. Polymerfree films of inorganic halide perovskite nanocrystals as UV-to-white color-conversion layers in LEDs. Chemistry of Materials, 28(9), pp.2902-2906, 2016.

[25] Lian, X., Wang, X., Ling, Y., Lochner, E., Tan, L., Zhou, Y., Ma, B., Hanson, K. and Gao, H., Light Emitting Diodes Based on Inorganic Composite Halide Perovskites. Advanced Functional Materials, 29(5), p.1807345, 2019.

29TH IRANIAN ORGANIC CHEMISTRY CONFERENCE
1_3 NOV, 2023
UNIVERSITY OF QOM, IRAN

Preparation of ZIF-8/$ZnFe_2O_4$ nanocomposite as a heterogeneous catalyst for the synthesis of quinoline derivatives

Maryam Mahdavi[1], *Mohammad Ali Ghasemzadeh* [*,1], *Ali Javadi* [2]

[1] *Department of Chemistry, Qom Branch, Islamic Azad University, Qom, Iran, maryam.mahdavi1990@gmail.com, m.a.qasemzade@gmail.com.*
[2]*Department of Medical Sciences, Faculty of Medicine, Qom Medical Sciences, Islamic Azad University, Qom, Iran.*

Keywords: Quinoline, Catalyst, ZIF-8/$ZnFe_2O_4$ nanocomposite, Metal-organic Frameworks, Heterocycle.

Abstract: In this report, we synthesized quinoline derivatives by the multicomponent reaction of aniline, aldehydes and malononitrile in the presence of ZIF-8/$ZnFe_2O_4$ nanocomposite under reflux conditions. The fabrication of the synthesized structure was established using various spectral techniques such as scanning electron microscopy (SEM), energy dispersive X-ray spectroscopy (EDX), Fourier transform infrared (FTIR). The present method offers various advantages such as increasing the efficiency of the results, easy separation of the catalyst, excellent results of the products in a short reaction time.

1. Introduction

Heterocyclic compounds are widely distributed in nature and have biological and industrial importance [1]. Also due to their antiviral [2], anti-inflammatory [3], antitumor [4] and antihypertensive effects [5] are of interest to researchers.
Metal organic frameworks (MOFs) have attracted the attention of many researchers because they are rapidly developing and are characterized by high porosity and abundant properties. The diversity of MOF topologies (eg, pore shapes and sizes) makes MOFs attractive for a wide variety of applications. These materials were widely used in various fields such as drug delivery, sensing, catalyst, etc. [6]. In addition, the use of ZIF in industrial applications such as water purification from heavy metals and organic dyes [7]. Magnetic nanoparticles are an important substrate for linking inorganic and organic catalysts. This can lead to major advances in the growth of various nanocatalytic systems through the immobilization of homogeneous catalysts on magnetic nanoparticles. Then, magnetic nanoparticles can be considered attached to organometallic frameworks, which provide enhanced surface area and grow up feedback rate [8].

In this study, considering the importance of heterogeneous catalysts, ZIF-8 and magnetic nanoparticles, it is considered to produce ZIF-8/$ZnFe_2O_4$ nanocomposite as a strong and reusable catalyst for the production of quinoline derivatives (Scheme 1).

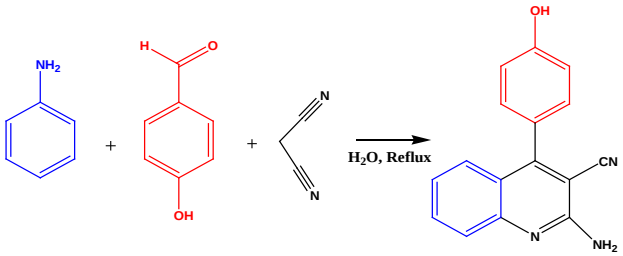

Scheme 1. Synthesis of quinoline using ZIF-8/$ZnFe_2O_4$ as catalyst.

2. Experimental

2. 1. Preparation of $ZnFe_2O_4$ nanoparticles
Initially, $FeCl_3.6H_2O$ (0.2 M) and $ZnCl_2.6H_2O$ (0.1 M) were dissolved individually in 75 mL of distilled water. Next, NaOH (2 M) was poured dropwise to the $FeCl_3$ solution till the pH of the solution reach to 10. Then, $ZnCl_2$ solution was added to another mixture. Next, the temperature of the reaction was increased to 80°C for 3 hours to gain a brown residue. The earned residue was washed several times with distilled water and ethanol via centrifugation and then kept at room temperature for 24 hours. Finally, $ZnFe_2O_4$ nanoparticles were obtained in the furnace at 500 °C for 5 hours [9].
2.2. Synthesis of ZIF-8/$ZnFe_2O_4$
A mixture of ZIF-8 (0.2 g), and $ZnFe_2O_4$ (0.1 g) were mixed in methanol (20 mL) and the mixture was placed in the autoclave at 100°C for 24 hours. The final precipitate was washed twice with DMF and methanol and then dried overnight at room temperature [10,11].

2.4. Preparation method for the synthesis of quinoline derivatives

The mixture of aniline (1 mmol), aldehyde (1 mmol) and malononitrile (1 mmol) It was refluxed in water for 30 minutes with ZIF-8/$ZnFe_2O_4$ as catalyst (0.005 g). The progress of the reaction was monitored by TLC (n-hexane:ethyl acetate 5:1). After the completion of the reaction, the heterogeneous catalyst was separated through a magnet, and then the precipitate was filtered and recrystallized from ethanol.

3. Results and discussion

3. 1. FT-IR spectroscopy

The structure of ZIF-8/$ZnFe_2O_4$ was considered via FT-IR spectroscopy (Fig. 1). As shown, the peak at 3428 cm^{-1} is due to the stretching vibration of OH groups in the structure. and at 2853 cm^{-1} stretching vibration of C-H bond is appeared, while the adsorption band at 1484 cm^{-1} is due to C=N bond. In addition, the peak at 1384 $cm^{-1}$are related to the stretching vibration of C-O bond, Moreover, the peaks at 757 cm^{-1}, and 616 cm^{-1} are relevant to the Zn–N and Zn–O bonds, and the peak at 458 cm^{-1} are relevant to the Fe-O.

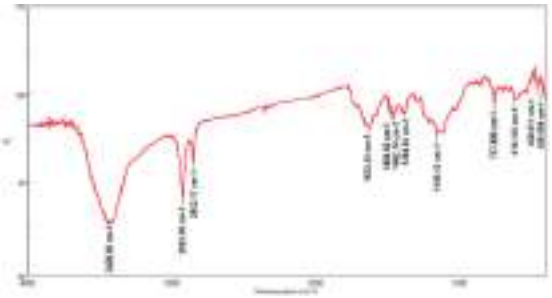

Fig. 1. FT-IR spectrum of ZIF-8/$ZnFe_2O_4$

3. 2. SEM analysis

The morphology and particle size for ZIF-8/$ZnFe_2O_4$were looked over via Field-emission electron microscopy analysis. The results illustrate that the prepared nanostructure has a uniform and particle size of 45-50 nm (Fig. 2).

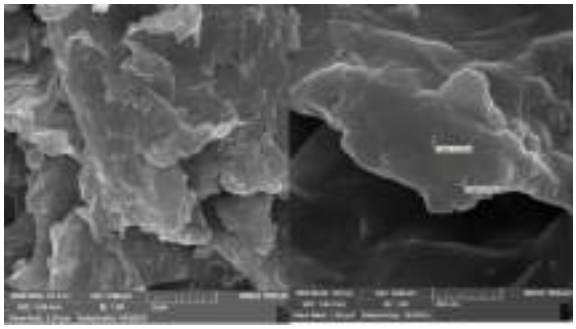

Fig. 2. The SEM images of ZIF-8/$ZnFe_2O_4$

3. 3. EDX analysis

The chemical purity of the sample was tested using energy dispersive X-ray spectroscopy (EDX). Fig. 3 shows the EDX spectrum of ZIF-8/$ZnFe_2O_4$. As shown sample contains O, Zn, C and Fe elements.

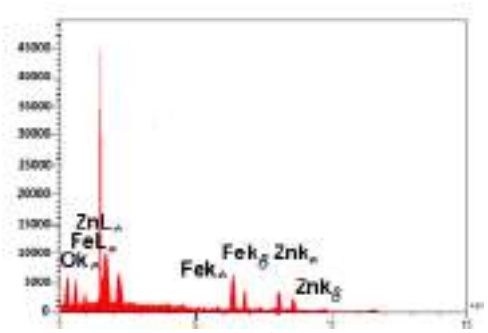

Fig. 3. EDX spectra of ZIF-8/$ZnFe_2O_4$

In order to compare the present catalyst with other catalysts, the model reaction was carried out by various catalysts having acidic or basic properties. The results are shown in Fig. 4. In the investigation of different catalysts, 0.01 g of each catalyst was used and the performance of the reaction was checked through TLC. The best performance corresponds to the ZIF-8/$ZnFe_2O_4$ catalyst, which has several acidic sites in the structure.

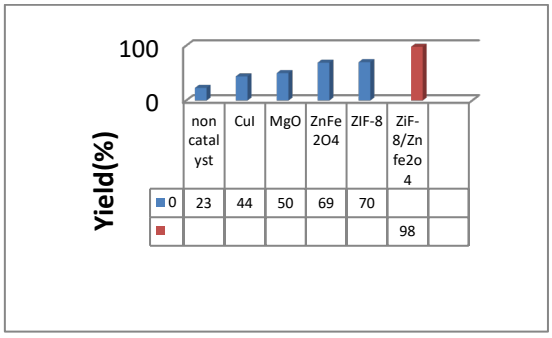

Fig. 4. The effect of various catalysts and the absence of a catalyst in the preparation of quinolines

3. 4. Reusing and recycling the catalyst

The recyclability of the ZIF-8/$ZnFe_2O_4$ catalyst was investigated under the optimal conditions of the model study. Due to the heterogeneity and magnetic properties of the catalyst, it was simply divided from the crude via an external magnet and were used for six cycles, as shown in Fig. 5.

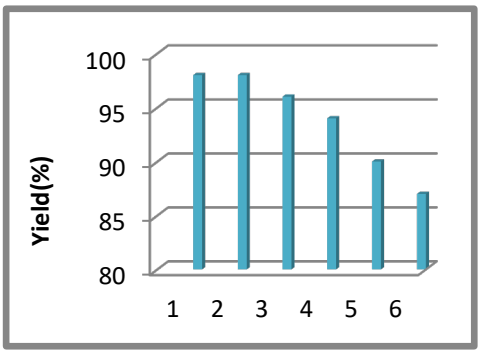

Fig. 5. The reusability of ZIF-8/$ZnFe_2O_4$

4. Conclusion

In this study, a reasonable synthesis method for the preparation of quinoline compounds using ZIF-8/$ZnFe_2O_4$ as an efficient catalyst is reported. The acidic nature of the catalyst makes it more efficient regarding less time-consuming within excellent yields in comparison with other catalysts. The properties of the produced heterogeneous catalyst were examined via different methods including EDX, SEM and FT-IR analysis. The catalyst was simply retrieved and reused for six cycles with any notable loss of its catalytic activity. The utilize of this catalyst is suggested as a green and reasonable method for the synthesis of quinoline derivatives under green reaction conditions.

References

[1] A. U. Czaja, N. Trukhan, U. Müller, Industrial applications of metal–organic frameworks. Chem. Soc. Rev. 38 (2009) 1284-1293.

[2] C. O Kappe. Highly versatile Solid phase synthesis of biofunctional 4-aryl-3,4-dihydropyrimidines using resin-bound isothiourea building blocks and multidirectional resin cleavage. Bioorg. Med. Chem. Lett. 10 (2000) 49–51.

[3] E. Palaska, G. Şahin, P. Kelicen, N. T. Durlu, G. Altinok, Synthesis and anti-inflammatory activity of 1-acylthiosemicarbazides , 1,3,4-oxadiazoles, 1,3,4-thiadiazoles and 1,2,4-triazole-3-thiones. Il Farmaco, (2002) 101-107

[4] Grover, Gary J.; Dzwonczyk, Steven; McMullen, Diane M.; Normandin, Diane E.; Parham, Charles S.; Sleph, Paul G.; Moreland, Suzanne. Pharmacologic Profile of the Dihydropyrimidine Calcium Channel Blockers SQ 32,547 and SQ 32,946. J. Cardiovasc. Pharmacol. 26 (1995) 289-294.

[5] C. Oliver Kappe. 100 years of the biginelli dihydropyrimidine synthesis. Tetrahedron. 49 (1993) 6937–63.

[6] A. J. Howarth, A. W. Peters, N. A. Vermeulen, T. C Wang, J. T. Hupp, O. K. Farha, "Best Practices for the Synthesis, Activation, and Characterization of Metal–Organic Frameworks, Chem. Mater. 29 (2016) 26–39.

[7] S. Bibi, E. Pervaiz, M. Ali, Synthesis and applications of metal oxide derivatives of ZIF-67: a mini-review. Chem. Pap. 75 (2021) 2253–2275.

[8] E. Doustkhah, S. Rostamnia.Covalently bonded sulfonic acid magnetic graphene oxide: Fe_3O_4@GO-Pr-OSO_3H is a powerful hybrid catalyst for the synthesis of imidazolophthalazinetriones. J. Colloid Interface Sci. 478 (2016) 280–287.

[9] P. P. Upare, D.-Y. Hong, J. Kwak, M. Lee, S. K. Chitale, J.-S. Chang, D. W. Hwang, Y. K Hwang. Direct chemical conversion of xylan into furfural over sulfonated graphene oxide. Catal. Today, 324 (2019) 66–72.

[10] P. A. Vinosha, L. A. Mely, J. E. Jeronsia, S. Krishnan, S. J. Das. Synthesis and properties of spinel $ZnFe_2O_4$ nanoparticles by facile co-precipitation route. Optik, 134 (2017) 99–108.

[11] J. Shi, L. Zhang, N. Sun, D. Hu, Q. Shen, F. Mao, Q. Gao, W. Wei. Facile and Rapid Preparation of Ag@ZIF-8 for Carboxylation of Terminal Alkynes with CO_2 in Mild Conditions. ACS Appl. Mater. Interfaces. 11 (2019) 28858–28867.

29TH IRANIAN ORGANIC CHEMISTRY CONFERENCE
1_3 NOV, 2023
UNIVERSITY OF QOM, IRAN

One pot synthesis of dibenzodiazepine and its derivatives using PEG-SO3H as acid catalyst

Fatemeh Norozi, Setareh Habibzadeh and Afshin Sarvary*

Department of Chemistry, Faculty of Basic Science, Babol Noshirvani University of Technology, Babol, Iran, fatemehnorozi877@gmail.com, habibzadeh@nit.ac.ir, asarvary61@gmail.com

Abstract –A highly efficient, simple and rapid method for the preparation of various dibenzodiazepine and other dibenzodiazepine derivatives using a catalytic amount of poly (ethylene glycol)-bound sulfonic acid (PEG-SO_3H) is described. PEG-SO_3H is found to be an economical and reusable catalyst with low catalytic loading. The percent yield was found to be satisfactory, experimental set up and purification of products are facile and easy.

1. Introduction

Benzodiazepines (BDZ's) is privileged heteroaromatic molecule and from an important class of pharmaceutically active compounds and their synthesis is of great importance for medicinal chemists and pharmacists in the field of medicinal and pharmaceutical chemistry owning to their application as analgesic, anticonvulsant, anti-inflammatory, sedative and hypnotic activity.[1]For example, the use of 1-H-1,5-benzodiazepines has been extended to various diseases such as cancer, viral infection, and cardiovascular disorders.[2]

Benzodiazepines are principally synthesized by the condensation of o-phenylenediamine with ketones[3]and aldehydes,[4] respectively, in the presence of conventional or Lewis acid catalyst. Different reagents such as BF_3-etherate, polyphosphoric acid, $NaBH_4$, MgO/$POCl_3$, Yb(OTf)$_3$, Ga(OTf)$_3$, lead nitrate, L-proline, acetic acid under microwave conditions, molecular iodine, and ionic liquids have also been used for the synthesis of benzodiazepines.[5,6] Recently the synthesis of benzodiazepines has also been reported using different solid acid catalysts such as sulfated zirconia, Al_2O_3/P_2O_5, $Ag_3PW_{12}O_{40}$, PVP-$FeCl_3$, and zeolite catalysts.[7,8] Unfortunately, many of these catalysts suffer from one or more limitations, such as long reaction times, occurrence of several side reactions, drastic reaction conditions, low yields, and tedious workup procedure. In addition, the solid oxide catalyst used previously had poor textural parameters such as low surface area and pore volume which do not support a better performance in the synthesis of benzodiazepines. These factors stimulate the search for a better catalyst, which should offer a high activity for the synthesis of 1,5-benzodiazepines under mild reaction conditions. In recent years, mesoporous materials with different structure and tunable pore diameters have been receiving much attention. However, it is found that many of the reagents suffer from one or more drawbacks due to drastic conditions such as long reaction times, harsh reaction conditions, formation of undesired side product or occurrence of many side reactions, tedious work-up procedure and low yields of the product. In addition, the previously used solid phase catalysts showed low surface area and low pore volume which do not prove to be more efficient for performance because of not effective adsorption on the surface and hence poor yield benzodiazepines.

Benzodiazepines have been the subject of previous reviews. Recently, Varvounis et al., published a review describing the synthesis of pyrrolo[2,1-c][1,4]benzodiazepines, whereas Sathish et al. reviewed the synthesis and biological activities of benzodiazepam derivatives[9,10] Mantaj et al. published a review describing the developments from anthramycin to pyrrolobenzodiazepine (PBD)-containing antibody-drug conjugates as anticancer agents[11]. However, these reviews considered limited aspects of their medicinal chemistry reports and did not address the comprehensive advances that have taken place in the past few years. Although the benzodiazepine ring system is critical in medicinal chemistry including organic synthesis and many advances including a number of breakthrough studies in their biological activities have been reported, an authoritative review describing the recent advancements in the synthetic and pharmacological perspective of these candidates has not been published.

2. Materials and methods

2.1. Preparation of poly ethylene glycol (PEG)-bond sulfonic acid catalyst

To a solution of poly(ethylene glycol)-6000(1mmol) in dichloromethane (15ml) was added chlorosulfonic acid (10mmol) at cold temperature (0-8°C). The resulting solution was stirred mechanically at 20°C for 16h, and the concentrated under reduced pressure. Diethyl ether was added and the precipitated product was washed three times to give PEG-SO_3H(Fig. 1). The obtained product was identified by NMR spectrum and the pure product efficiency of this reaction is 95%.

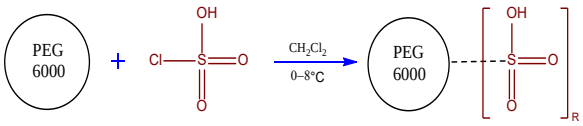

Fig. 1 Diagrammatic representation of synthesis of poly(ethylene glycol)-bound sulfonic acid (PEG-SO_3H)

2.2. General procedure for the synthesis of dibenzodiazepine(Fig. 2) derivatives

A mixture of 1,2-phenylenediamine (0.5 mmol), 1,3-cyclohexanedione (0.5 mmol), and catalyst (0.03 g) was prepared in a crucible under solvent-free conditions. They were ground at 60°. After 10 minutes, chlorobenzaldehyde (0.5 mmol) was added to the reaction mixture. The progress of the reaction was investigated by thin layer chromatography (TLC) using a solvent tank of hexane-ethyl acetate in a ratio of 2:3. After the reaction was completed, ethanol (10 ml) was added to the reaction mixture and the catalyst was separated by centrifugation. And the solvent was evaporated with a vacuum evaporator. The obtained crude product was recrystallized with methanol-water for further purification, and the obtained crude product was identified using ^{13}CNMR, ^{1}HNMR, melting point and IR spectroscopy. The efficiency of the pure product obtained from this reaction is 80-97%(Table 1).

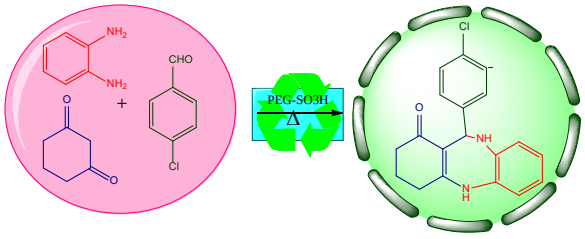

Fig. 2 Synthesis of substituted dibenzodiazepine derivatives from s1,2-phenylendiamine and 1,3-cyclohexadione and 4-chlorobenzaldehyde

Table 1 Benzodiazepine synthesis using different aldehydes in solvent-free conditions

Entry	1,2-diamine	Aldehyde	Product	Yield
1	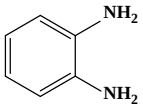	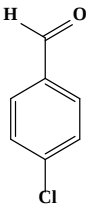	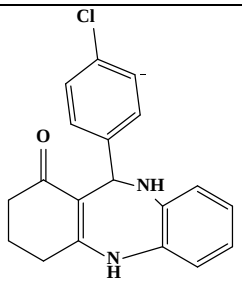	97
2	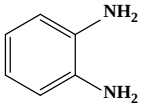	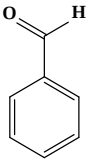	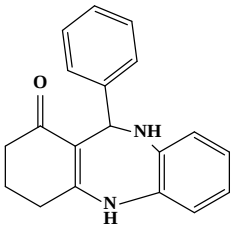	94
3	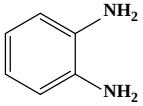	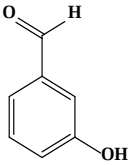	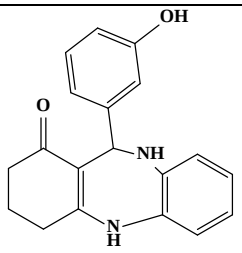	89

2.3. Synthesis of dibenzodiazepine in water solvent under ultrasonic irradiated(Fig. 3)

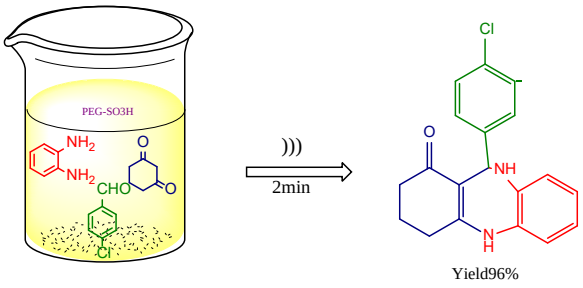

Fig. 3 synthesis of dibenzodiazepine in ultrasonic device.

A mixture of 1,2-phenylendiamine(0/5mmol),1,3-cyclohexanedione(0/5mmol),chlorobenzaldehyde(0/5 mmol),catalyst PEG-SO_3H(0/03g) and 10 ml water were placed into Pyrex-glass open vessel and irradiated in water bath under silent condition by ultrasound(45kHz) at room temperature for required reaction times(1-5min).The progress of the reaction was monitored by Thin Layer chromatography(TLC)(Hexane: ethyl acetate 2:3).Then the reaction mixture was filtered to separate the product and recrystallized from EtOH. The pure product were collected in90-98% yield(Table 2).

Table 2 Dibenzodiazepine synthesis under ultrasonic waves (45 kHz) at room temperature

Entry	Aldehyde	Product	Time (min)	Yield
1	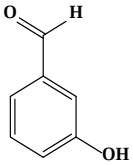	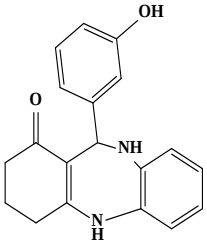	3	90
2	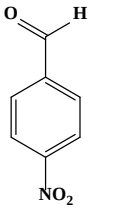	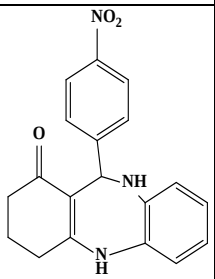	1	93
3	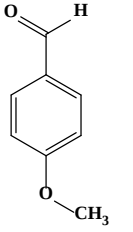	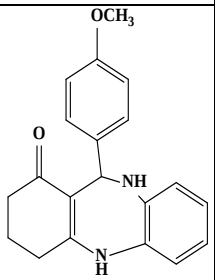	1	96

3. Result and Discussion

In optimal conditions, we carried out the reaction from 0.0004% by weight of the catalyst and 0.07% by weight of 1,2-phenylenediamine in the ratios of 1:1 and 2:1 to the solvent at room temperature and 60°C, and the progress of the reaction was investigated by thin layer chromatography(TLC) it placed(Table 1)

Table 3 Different ratios of catalyst to 1,2-phenylenediamine at different temperatures

Solvent	Catalyst to diamine ratio	Temp	Time (min)
water	1:1	25°	150
ethanol	1:1	60°	60
water	1:1	60°	60
water	2:1	25°	60
water	2:1	60°	80

4. References

[1] Christian and Demeunynck, 2007; Pathak et al., 2007; Moody et al., 2007; Barrett et al., 2007; Puodziunaite et al., 2000.

[2] (a) Di Braccio, M.; Grossi, G.; Roma, G.; Vargiu, L.; Mura, M.; Marongiu, M. E. Eur. J. Med. Chem. 2001, 36, 935; (b) Glick, G. D.; Opipari, A. W. U.S. Pat. 2003119029, 2001.

[3] For the synthesis of benzodiazepines see: (a) Pan, X.-Q.; Zou, J.-P.; Huang, Z.-H.; Zhang, W. Tetrahedron Lett. 2008, 49, 5302; (b) Varala, R.; Enugala, R.; Adapa, S. R. J. Braz. Chem. Soc. 2007, 18, 291; (c) Sivamurugan, V.; Deepa, K.; Palanichamy, M.; Murugesan, V. Synth. Commun. 2004, 34, 3833; (d) Chen, W. Y.; Lu, J. Synlett 2005, 1337; (e) Pozarentzi, M.; Stephanidou-Stephanatou, J.; Tsoleridis, C. A. Tetrahedron Lett. 2002, 43, 1755; (f) Kuo, C.-W.; More, S. V.; Yao, C.-F. Tetrahedron Lett. 2006, 47, 8523; (g) Chari, M. A.; Shobha, D.; Syamasundar, K. J. Heterocycle. Chem. 2007, 44, 929; (h) Balakrishna, M. S.; Kaboudin, B. Tetrahedron Lett. 2001, 42, 1127; (i) Curini, M.; Epifano, F.; Marcotullio, M. C.; Rosati, O. Tetrahedron Lett. 2001, 42, 3193.

[4] For the synthesis of benzimidazoles see: (a) Perumal, S.; Mariappan, S.; Selvaraj, S. ARKIVOC 2004, viii, 46; (b) Trivedi, R.; De, S. K.; Gibbs, R. A. J. Mol. Catal. A: Chem. 2006, 245, 8; (c) Oskooie, H. A.; Heravi, M. M.; Sadnia, A.; Behbahani, F. K.; Jannati, F. Chin. Chem. Lett. 2007, 18, 1357; (d) Landge, S. M.; Török, B. Catal. Lett. 2008, 122, 338; (e) Varala, R.; Nasreen, A.; Enugala, R.; Adapa, S. R. Tetrahedron Lett. 2007, 48, 69; (f) Jacob, R. G.; Dutra, L. G.; Radatz, C. S.; Mendes, S. R.; Perin, G.; Leandro, E. J. Tetrahedron Lett. 2009, 50, 1495.

[5] Herbert JAL, Suschitzky H. Syntheses of heterocyclic compounds. part xxix. substituted 2,3-dihydro-1h-1,5-benzodiazepines. *Journal of the Chemical Society.* 1974:2657–2661.

[6] Jarikote DV, Siddiqui SA, Rajagopal R, Thomas D, Lahoti RJ, Srinivasan KV. Room temperature ionic liquid promoted synthesis of 1,5-benzodiazepine derivatives under ambient conditions. *Tetrahedron Letters.* 2003;44(9):1835–1838.

[7] Reddy BM, Sreekamth PM, Reddy VR. Modified zirconia solid acid catalysts for organic synthesis and transformations. *Journal of Molecular Catalysis A.* 2005;225:71–78.

[8] Hegedüs A, Hell Z, Potor A. A simple environmentally-friendly method for the selective synthesis of 1,5-benzodiazepine derivatives using zeolite catalyst. *Catalysis Letters.* 2005;105(3-4):229–232.

[9] G. Varvounis, An update on the synthesis of pyrrolo[1,4]benzodiazepines, Molecules, 21 (2016), 154.

[10] S. Kumar, H. Kavitha, S. Arulmurugan, B.R. Venktaraman, Review on synthesis of biologically active diazepam derivatives, Mini Rev Org Chem. 9 (2012), 285-302.

[11] J. Mantaj, P.J. Jackson, D.E. Thurston, From Anthramycin to Pyrrolobenzodiazepine (PBD)-Containing Antibody-Drug Conjugates (ADCs), Angew. Chem. Int. Ed. Engl. 56 (2017), 462-488.

29TH IRANIAN ORGANIC CHEMISTRY CONFERENCE
1_3 NOV, 2023
UNIVERSITY OF QOM, IRAN

Use of green and efficient catalysts for knoevenagel condensation

Sabah Salahvarzi, Fatemeh Behzadpour*

Department of Chemistry, Faculty of Science, Khorramabad Branch, Islamic Azad University, Khorramabad, Iran. sabahsalahvarzi@yahoo.com

Abstract - Knoevenagel condensation is one of the most useful reactions in organic chemistry because the products of this reaction are suitable intermediates in the preparation of heterocyclic compounds and compounds with biological activity. In this research, knoevenagel condensation reaction was performed using various aromatic aldehydes and active methylene compounds in the presence of renewable catalyst. In the present research, the interaction of aldehydes with active methylenes with molar ratios (1:1) was carried out in the presence of Water Extract of Banana (WEB) and Water Extract of Orange Fruit Peel Ash (WEOFPA) (green catalysts). The resulting products were identified with the help of FT-IR and HNMR methods. The use of green catalysts created products with higher efficiency. The method used in terms of greenness, simplicity, use of available raw materials, reduction of reaction time, good to excellent yield of products, single-stage reaction and easy product extraction, from an economic and environmental point of view for the synthesis of organic compounds, is very It is noticable.

Keywords: knoevenagel condensation, Water Extract of Banana (WEB), Water Extract of Orange Fruit Peel Ash (WEOFPA), green catalyst.

1. Introduction

knoevenagel condensation is one of the most common methods used in organic chemistry, which was first discovered by Emil knoevenagel [1-2], which includes a well-known carbon-carbon bond formation reaction in organic chemistry [3]. Generally, this condensation occurs between aldehydes or ketones and active methylene compounds in the presence of ammonia or other amines as catalysts in organic solvents [4,5]. Many catalysts are used in Knoevenagel condensation reactions, amines, ammonia or sodium ethoxide in organic solvents [6], Lewis acids [7], surfactants [8], zeolites [9], heterogeneous catalysts [10], ionic liquids [11] and... the feasibility of some reactions requires the application of extreme conditions [12-14] and some are performed under ultraviolet [15], ultrasonic or microwave conditions.

The use of nanocatalysts also has a special place in the condensation of novel. Magnetic nanocatalysts are widely used in various organic reactions due to their separation and recycling properties. [16]. Meanwhile, the use of recycled catalysts also has countless advantages. [17] In the meantime, the use of green catalysts has a special place and the results of this research can be a new window in the Knoevenagel condensation and the production of anti-cancer drugs. [17] Using renewable and natural catalysts of banana peel extract, knoevenagel condensation reaction between aromatic and also heteroaromatic aldehydes with malononitrile has been reported.

In this research, knoevenagel condensation reaction was used using various aromatic aldehydes and active methylene compound in the presence of renewable catalyst (agricultural waste such as Water Extract of Banana (WEB) and Water Extract of Orange Fruit Peel Ash (WEOFPA) as a catalyst). IR and HNMR were performed. The method used in terms of being green, reducing energy consumption in the process of producing products, operating simplicity, using available raw materials, reducing reaction time, having good to excellent yield of products, single-stage reaction and easy product extraction from an economic point of view and the environment is important for the synthesis of organic compound.

2. Experimental

In this research, it was tried to carry out the knoevenagel condensation reaction of different compounds using green catalysts. In this method, green catalysts such as Water Extract of Banana (WEB) and Water Extract of Orange Fruit Peel Ash (WEOFPA) were used. Each time, 7 aldehydes including: benzaldehyde, 4-methylbenzaldehyde, 4-nitro benzaldehyde, cinnamaldehyde, vanillin, salicyl aldehyde, and malononitrile were used and a total of 7 samples were made. Finally, a total of 14 products were obtained from the reaction of 7 aldehydes and malonitrile with two types of catalysts.

2.1. Prepare Water Extract of Banana (WEB) and Water Extract of Orange Fruit Peel Ash (WEOFPA):

First, orange or banana peels were washed with distilled water and dried under the sun for about a week. Each of the dry skins was completely crushed using an electric grinder, and then the dry powders were passed through a fine sieve to make the particles

uniform. The resulting powder was heated. It should be noted that for oranges, its color should change from orange to light brown, and for bananas, it was heated a little to make it a little darker than dark brown. Then, 10 grams of orange peel ash or banana peel ash was taken and poured into an Erlenmeyer flask, 100 ml of distilled water was added to it, and then it was stirred for one hour with a magnetic stirrer. Then, the contents of Arlene were filtered and the Water Extract of Orange Fruit Peel (WEOFPA) was obtained in orange color and the water extract of banana peel (WEB) was obtained in light brown color.

2.2. Knoevenagel condensation:

In the method of using green catalyst ((WEOFPA) or (WEB)), in a 25 ml Erlenmeyer flask, 1 mmol of aldehyde and 1 mmol of active methylene and 3 ml of aqueous extract (catalyst) It was poured and stirred at room temperature with the help of a magnetic stirrer. At the time of 5, 10, 15 and 20 minutes, TLC was taken from the contents of erlen. Examining the results showed that the optimal time to complete the reaction is 15 minutes. Then, 10 ml of frozen distilled water was added to the contents of the beaker, the contents of the beaker were filtered, the sediment was dried and weighed. To purify the product, the sediment was recrystallized with methanol solvent, after filtering and drying, the obtained sediment was weighed, and then the efficiency before and after the recrystallization operation was calculated, and a total of 21 samples were made with the help of each catalyst. Also, the method of using the orange peel catalyst was exactly the same as the banana peel catalyst.

3. Result and Discussion:

From the reaction of 7 aldehydes and diethylmalonate (active methylene) in each method, 7 types of products were obtained, which are given below along with the results of HNMR and FT-IR spectra (table1). The general form of Knoevenagel condensation reaction for the interaction of different aldehydes with malononitrile is given in figure (1). All synthesized compounds using orange peel catalyst and banana peel catalyst with extensive chemical formula, efficiency, color and melting point of the products before and after recrystallization are listed in Table 1. IR spectra were taken from all the products and raw materials, but due to the large volume of the spectra, only the data of the products made in the presence of orange peel were evaluated in the steps of FT-IR and HNMR spectroscopy to identify the structure. The summary of the results of IR and HNMR spectra of the synthesized compounds is also given in Table 1. Based on the obtained results, the use of banana peel or orange peel as a catalyst has increased the efficiency of the product. While in 57.14% of the cases, the product efficiency was higher in the banana peel method and in 42.86%, the product efficiency was higher using the orange peel. In summary, the use of aqueous extract of orange or banana peel as a green catalyst has increased product efficiency. The results are given in Table 2.

.

4. Conclusion:

The aim of this research was the synthesis of Knoevenagel condensation using various aromatic aldehydes and active methylene compounds in the presence of renewable catalyst. The method used in terms of being green, reducing energy consumption in the process of producing products, operating simplicity, using available raw materials, reducing reaction time, having good to excellent yield of products, single-stage reaction and easy product extraction from an economic point of view and Environment has been considered for the synthesis of some organic compounds. After examining the efficiency of the products, it was concluded that the use of green catalysts ((WEB) and (WEOFPA)) has created products with higher efficiency. It is suggested to investigate and study the anticancer effects of the derivatives made on cell lines and antibacterial effects. It is also suggested that the effects of cytotoxicity of the derivatives made in vivo on rats should be investigated, and other aromatic and heteroaromatic derivatives should also be made using the mentioned methods, and their biological effects should also be studied and investigated.

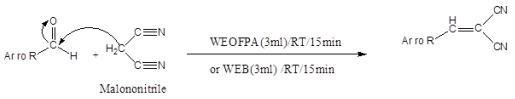

Fig.1 Knoevenagel condensation reaction for the interaction of different aldehydes with malononitrile

Table 1 -Spectral data of the synthesized compounds

Name of product	Spectra result
2- Benzylidene malononitrile	IR(CM^{-1}): 2930.66-3205.13 ,2223.00 ,1608.57 ,1491.56 -1590.78, 1042.50 .HNMR(400MHZ ,DMSO) : 2.477-3.324(PPM) ,8.531(PPM) ,6.641-7.947(PPM)
2- (4-Methylbenzylidene) malononitrile	IR(CM^{-1}): 2960.30-3205.04 ,2224.79 ,1606.07 , 1413.43-1588.44 ,1040.28 . HNMR(400MHZ ,DMSO): 2.473-3.331(PPM) ,1.01(PPM) ,2.07-2.26(PPM) ,2.383(PPM) .
2-(4-nitrobenzylidene)malononitrile	IR(CM^{-1}): 2929.29-3204.66 ,2231.46 ,1605.86 ,1414.62 - 1580.40 ,1008.67 ,1344.41 ,1521.21 . HNMR(400MHZ,DMSO): 2.476-3.317(PPM), 8.689(PPM) ,8.098-8.421(PPM) .
trans-2-(3-phenylallylidene) malononitrile	IR(CM^{-1}): 2599.28-3204.68 ,2090 ,1609.26 ,1681.11 ,1 417.03-1590.31 ,1042.27 . HNMR(400MHZ ,DMSO): 2.476-3.326 (PPM) ,6.639(PPM) ,6,670(PPM) ,9 .1(PPM) ,7-7.382(PPM)

2-(4-hydroxy-3-methoxybenzylidene) malononitrile	IR(CM^{-1}): 2691.21-3305.58 ,2227.71 ,1665.82 ,1455.45 -1587.46 ,1027.36 ,3427.73 . HNMR(400MHZ ,DMSO): 8.219(PPM) ,6.571-7.949(PPM) ,3.783(PPM) ,9.747(PPM) .
2-(Diphenylmethylene) malononitrile	IR(CM^{-1}): 2928.41-3205.68 ,1649.91 ,1416.09-1592.49 ,1040 . HNMR(400MHZ ,DMSO): 2.474(PPM) ,3.304(PPM) ,7.533-7.721(PPM) .
2-(2-Hydroxybenzylidene) malononitrile	IR(CM^{-1}): 2937.20-3335.63 ,2195.01 ,1643.54 ,1423.27 -1605.10 ,1048.86 ,3457.07 . HNMR(400MHZ ,DMSO): 2.476-3.324(PPM) ,7.094-7.807(PPM) ,8.336(PPM) ,8.8(PPM) ,4.562(PPM) ,5.043(PPM)

Table2- Melting point and yield of products

Name of product	WEOFPA	WEB
2- Benzylidene malononitrile 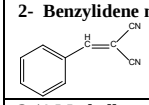	90.90 % 84 ºC	84.41% 84 ºC
2-(4-Methylbenzylidene) malononitrile 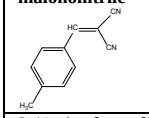	89.28 % 138 ºC	89.28% 138 ºC
2-(4-nitrobenzylidene) malononitrile 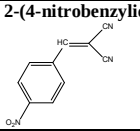	92.96 % 160 ºC	80.40% 160 ºC
trans-2-(3-phenylallylidene) malononitrile 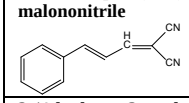	80.55 % 235 ºC	88.88% 235 ºC
2-(4-hydroxy-3-methoxybenzylidene) malononitrile	95 % 129 ºC	90 % 129 ºC
2-(Diphenylmethylene)malononitrile 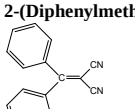	90.04 % 48 ^{oC}	86.95% 48 ^{oC}
2-(2-Hydroxybenzylidene) malononitrile 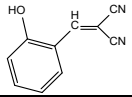	64.23 % 145 ^{oC}	88.23% 145 ^{oC}

4. References

[1] E. Knoevanagel, Condensation von malonsäuremit-aromatischen aldehyden durch ammoniakund amine. Ber. Deut. Chem. Ges. 31 (1898) 2596-2619

[2] A. Debache, R. Boulcina, A. Belfaitah, S. Rhouati, B. Carboni, One-pot synthesis of 1,4- dihydropyridines via a phenylboronic acid catalyzed hantzsch three-component reaction. Synlett (2008) 509-512.

[3] N. Aramini, , J.M. Yu, M.W. Germann, , Z. Huang, TetrahedronLett. 41 (2000) 6993-6996.

[4] O. Attanasi, , P. Fillippone, A. Mei, Synth. Commun. 13 (1983) 1203. F. Bigi, L. Chesini, R. Maggi, G.Sartori, J.Org. Chem. 64 (1999) 1033.

[5] K. Nasri, C. Chtara, C. Hassen, M. Fiallo, P. Sharrock, A. Nzihou, H. El Feki, Recrystallization of industrial triple super phosphate powder, Ind. Eng. Chem. Res. 53 (2014) 14446–14450.

[6] B. Boonchom, Parallelogram-like microparticles of calcium dihydrogen phosphate monohydrate (Ca(H2PO4)2·H2O) obtained by a rapid precipitation route in aqueous and acetone media, J. Alloys Compd. 482 (2009) 199–202.

[7] B. Boonchom, C. Danvirutai, The morphology and thermal behavior of calcium dihydrogen phosphate monohydrate (Ca(H2PO4)2•H2O) obtained by a rapid precipitation route at ambient temperature in different media, J Optoelectron Biomed Mater. 1 (2009) 115–123.

[8] J. B. M. de ResendeFilho, G. P. Pires, J. M. G. de Oliveira Ferreira, E. E. S. Teotonio, J. A. Vale, Knoevenagel condensation of aldehydes and ketones with malononitrile catalyzed by amine compounds-tethered Fe3O4@SiO2 nanoparticles, Catal. Lett. 147 (2017) 167–180.

[9] H. M. A. Hassan, R. F. M. Elshaarawy, S. K. Dey, I. Simon, C. Janiak, Microwave-assisted hydrothermal fabrication of magnetic amino-grafted graphene oxide nanocomposite as a heterogeneous knoevenagel catalyst, Catal. Lett. 147 (2017) 1998–2005.

[10] N. Zohreh, M. Tavakolizadeh, S. H. Hosseini, A. Pourjavadi, C. Bennett, Tungstate-loaded triazine-based magnetic poly(bis-imidazolium ionic liquid): an effective bi-functional catalyst for tandem selective oxidation/knoevenagel condensation in water, Polymer. 112 (2017) 342–350.

[11] S. M. Islam, A. S. Roy, R. C. Dey, S. Paul, Graphene based material as a base catalyst for solvent free aldol condensation and knoevenagel reaction at room temperature, J. Mol. Catal. Chem. 394 (2014) 66–73.

[12] I. Bahammou, A. Esaady, S. Boukhris, R. Ghailane, N. Habbadi, A. Hassikou, A. Souizi, Direct use of mineral fertilizers MAP, DAP, and TSP as heterogeneous catalysts in organic reactions. Mediterr. J. Chem. 5 (2016) 615–632.

[13] J. RichaKhare, Pandey.; Smritiand Ruchi Rupanwar. The Importance and Applications of Knoevenagel Reaction (Brief Review), OJCHEG. 35 (2019) 423-429.

[14] X. Zhang, X. He, S. Zhao, Preparation of a novel Fe3O4@SiO2@propyl@DBU magnetic core–shell nanocatalyst for Knoevenagel reaction in aqueous medium. Green Chemistry Letters and Reviews. 14 (2021) 85–98.

[15] B. Krishnappa, Badiger and Kantharaju Kamanna. Knoevenagel condensation reaction catalysed by agro-waste extract as a greener solvent catalyst. Org. Commun. 14 (2021) 81-91.

[16] K.B. Badiger, K. Kamanna., Knoevenagel condensation reaction catalysed by agro-waste extract as a greener solvent catalyst. Org. Commun. 14 (2021) 81-91.

[17] K. Kantharaju, P.B. Hiremath, S.Y. Khatavi, WEB: A green and an efficient catalyst for Knoevenagel condensation under grindstone method. Indian Journal of Chemistry. 58 (2019) 706-713.

29TH IRANIAN ORGANIC CHEMISTRY CONFERENCE
1_3 NOV, 2023
UNIVERSITY OF QOM, IRAN

Investigation of New Approaches and Methods of Thermal Stability of PVC Plastisol

Hamidreza Ejraee, Abbas Kebritchi and Nasser Karimi*

Chemical Engineering Department, Imam Hossein Comprehensive University, Tehran, Iran, Hamidejraee1998@ihu.ac.ir, A.Kebritchi@ippi.ac.ir, Ms.karimi.m@gmail.com

Abstract - Thermal stability of PVC plastisol is one of the most important topics in the plastics industry. Plastisol PVC is one of the plastics that is used in many industries such as automotive, electronics, clothing and packaging, etc. Thermal stability means the material's resistance to changing its shape and characteristics at high temperatures. In this article, new methods of thermal stability of PVC plastisol are investigated. In this context, the effect of temperature and time on thermal stability, methods of evaluating thermal stability and methods of improving the thermal stability of PVC plastisol have been investigated. Research results show that the thermal stability of PVC plastisol is strongly influenced by temperature and time. Some methods of improving thermal stability include increasing resistance to high temperature, using additives, etc. In general, thermal stability in PVC plastisol is very important, and it is very important to observe this issue for its industrial applications.

1. Introduction

PVC plastisol is a plastic that is used in many industries because of its lightness, corrosion resistance, electrical insulation, and easy processing. It is made of PVC and other plastic materials to improve its properties. It has various applications such as car interior parts, electronic parts, building materials, water and sewage pipes, clothing parts, food packaging, and medical parts. Thermal stability is an important feature of PVC plastisol that means how well it can resist high temperatures. Thermal stability affects the performance and quality of products made from PVC plastisol. It also affects the health risks of PVC plastisol. Thermal stability can be improved by changing some factors such as the type and amount of plasticizer, stabilizer, filler, and pigment. Thermal stability can also be measured by different methods such as thermogravimetric analysis, differential scanning calorimetry, and dynamic mechanical analysis. Therefore, thermal stability is a very important issue for PVC plastisol in various industries [1].

2. Results and Discussion

Definition of thermal stability

Thermal stability means how well a material resists changes at high temperatures. Thermal stability is very important for construction materials, such as plastics and metals, that may be exposed to high temperatures and may experience deformation, failure or other changes if they do not have high thermal stability [2].

Factors affecting thermal stability in PVC plastisol

Factors affecting thermal stability in PVC plastisol the thermal stability of PVC plastisol is affected by various factors, such as:

- Type of resin, filler, polymer material and base material used in the production of PVC plastisol
- Processing method and conditions to produce PVC plastisol
- Internal structure of PVC plastisol

These factors can be effective in combination and to improve the thermal stability of PVC plastisol, attention should be paid to all these factors in the process of production and use of this material [3].

Thermal stability evaluation methods

Thermal stability evaluation methods Thermal stability means how well a material resists changes at high temperatures. There are two types of methods to evaluate the thermal stability of plastics: experimental and analytical.

- Experimental methods: These methods test how the physical and chemical characteristics of plastic samples change over time under certain conditions, such as temperature and time. Some examples of experimental methods are DSC, TGA, DMA and FTIR.
- Analytical methods: These methods analyze the structure and chemistry of the plastic material. Some examples of analytical methods are Raman spectroscopy, UV-Vis spectroscopy, and SEM.

Evaluating the thermal stability of plastics can help to improve their characteristics, increase their useful life and improve the efficiency of plastic products [4].

Effect of temperature on thermal stability:

- Temperature can cause chemical and physical changes in plastics, thereby reducing their thermal stability. For example, high temperature can cause

decomposition, change in physical properties, and change in hardness of plastics.

- To increase the thermal stability of plastics, various additives such as fillers, softeners and thermal protectors can be used, which reduce the effects of temperature on plastics [5].

Effect of temperature on the thermal stability of PVC plastisol

High temperatures may cause the decomposition of PVC plastisol, and the use of suitable additives and control of the processing temperature can help its thermal stability. Several researches have shown that the thermal stability of PVC plastisol decreases with increasing temperature, and different factors such as thermal stabilizers and zinc ions can affect this decrease. Several studies have been conducted on the thermal stability of PVC and the effect of temperature on it. In these studies, the effect of different additives and temperature on the thermal stability of PVC has been investigated. In the following, we refer to some of the results of these studies and their comparison with each other: In a study conducted in 2018 by a group of researchers in China, the effect of different fillers on the thermal stability of PVC was investigated. In this study, samples of PVC with different amounts of calcium carbonate, talc and microsilica fillers were prepared and examined in terms of thermal stability at different temperatures for 30 minutes. The results showed that the use of different fillers can help the thermal stability of PVC and calcium carbonate filler can provide the best thermal stability for PVC. In another study conducted in 2020 by a group of researchers in South Korea, the effect of processing temperature on the thermal stability of PVC was investigated. In this study, samples of PVC were processed at different temperatures (from 150 degrees Celsius to 200 degrees Celsius) and their thermal stability was investigated. The results showed that as the processing temperature increases, the thermal stability of PVC decreases and appropriate additives should be used to increase the thermal stability. In another study conducted in 2017 by a group of researchers in Japan, the effect of the type of thermal stabilizer on the thermal stability of PVC was investigated. In this study, samples of PVC were prepared using different thermal stabilizers and were examined in terms of thermal stability at different temperatures (from 80 degrees Celsius to 200 degrees Celsius) for 30 minutes. The results showed that the use of suitable thermal stabilizers can help the thermal stability of PVC and the use of a more suitable thermal stabilizer can improve the thermal stability of PVC. In another study conducted in 2015 by a group of researchers in Italy, the effect of different additives on the thermal stability of PVC was investigated. In this study, samples of PVC were prepared using different additives, including heat stabilizers, fillers, and dyes, and were checked for thermal stability at different temperatures for different periods of time (from 10 minutes to 3 hours). The results showed that the use of suitable additives can help the thermal stability of PVC and the use of thermal stabilizer and calcium carbonate filler can provide the best thermal stability for PVC.

Therefore, the results of various studies on the thermal stability of PVC and the effect of temperature on it show that the use of suitable additives and control of the processing temperature can help the thermal stability of PVC. Also, the use of calcium carbonate filler and suitable thermal stabilizer can provide the best thermal stability for PVC [6].

Effect of time on thermal stability

Over time, the strength and thermal stability of polymer materials decrease, and this issue can become more important at high temperatures or for long-term purposes. For example, over time, PVC may decompose and change its mechanical strength and chemical structure, which reduces its thermal stability. The thermal stability of polymer materials can be increased by using certain methods such as improving the production process, modifying the chemical structure, using fillers and additives, and using advanced technologies. These methods can reduce the effects of time on polymer materials and increase their resistance to heat and decomposition. The results and their comparison with other studies Various studies have been conducted on the thermal stability of PVC plastisol, which have shown different results. However, in some similar studies, they have agreed with the results of the previously mentioned reviews. In the following, we examine the results of some of these studies [7]:

1. In a study conducted in 2014, the effect of time on the thermal stability of PVC plastisol was investigated. Samples of PVC plastisol with a thickness of 1.5 mm were prepared and kept at 80°C for 5000 hours. Then the thermal stability of these samples was investigated using the TGA method. The results showed that with the passage of time, the thermal stability of PVC plastisol decreases drastically.

2. In another study conducted in 2016, the effect of adding calcium carbonate nanoparticles on the thermal stability of PVC plastisol was investigated. In this study, samples of PVC plastisol were prepared by adding calcium carbonate nanoparticles with different concentrations. Then the thermal stability of these samples was investigated using the TGA method. The results showed that the thermal stability of PVC plastisol was improved by adding calcium carbonate nanoparticles.

3. In another study conducted in 2019, the effect of adding graphene oxide nanoparticles on the thermal stability of PVC plastisol was investigated. In this study, samples of PVC plastisol were prepared by adding graphene oxide nanoparticles with different concentrations. Then the thermal stability of these

samples was investigated using the TGA method. The results showed that by adding graphene oxide nanoparticles, the thermal stability of PVC plastisol improved.

Therefore, various results have been obtained in various investigations that have been conducted on the thermal stability of PVC plastisol. But according to the studies reviewed, it seems that adding nanoparticles to PVC plastisol can improve its thermal stability. Of course, more results are needed to validate and it is better to conduct more studies in this field. Also, compared to other studies in the field of materials, the thermal stability of PVC plastisol has been used due to its good characteristics such as mechanical and chemical properties [8].

Methods to improve thermal stability:

- Thermal stability means the material's resistance to damage and temperature and thermal changes. Various methods such as adding nanostructured materials, using additives, using different processing methods, and using protective coatings can improve the thermal stability of materials.
- PVC plastisol is a material used in various industries and its thermal stability is important. To improve the thermal stability of PVC plastisol, methods such as adding graphene nanoparticles, using polyamide as additives, using ceramic coatings, using different processing methods, and using materials with better properties can be used.

the advantages and disadvantages of each method to improve the thermal stability of materials:

- Adding nanostructured materials to the material: This method can improve the thermal stability, mechanical and electrical properties of the material, but it may also cause problems such as changes in the behavior of the material, quality control and high cost.
- Use of additives: This method can improve the thermal stability, mechanical and electrical properties of the material, but it may also cause changes in the behavior of the material and be expensive.
- Using different processing methods: This method can improve the thermal stability of the material and reduce production costs and time, but it may also cause changes in the properties of the material and environmental pollution.
- Use of protective coatings: This method can improve the thermal stability and protection of the material, but it may also increase the weight and volume of the material and have a high cost.

To choose an appropriate method to improve the thermal stability of a material, one should consider the specific characteristics of the material and the application conditions. Also, a combination of different methods may be used to obtain the best result.

3. Conclusion:

In the field of improving the thermal stability of materials, several researches and studies have been done. Some of the most important results and studies are:

1. Adding nanomaterials to polymer materials can improve their thermal stability. For example, adding silica nanoparticles to polyester and polycarbonate plastics can improve their thermal stability.

2. The use of ceramic coatings can improve the thermal stability of materials. Some ceramic coatings such as aluminum oxide and silicon oxide can help protect the material against high temperatures.

3. The use of additives can improve the thermal stability of the material. For example, using polyamide as an additive can improve the thermal stability of plastics.

4. Using different processing methods can improve the thermal stability of materials. For example, heat pressing can improve the thermal stability of diamonds.

5. Using materials with better characteristics can improve the thermal stability of materials. For example, the use of heat-resistant plastics can improve the thermal stability of materials.

From these results, it can be concluded that the use of additives, ceramic coatings, different processing methods and materials with better characteristics can improve the thermal stability of materials. Each of these methods has its own advantages and disadvantages, which should be chosen according to the conditions and characteristics of the material [8].

4. References

[1]. K. K. Pant and S. K. Nayak, "Improving thermal stability of polymers using nano-fillers: A review," Journal of Applied Polymer Science, vol. 132, no. 10, 2015.

[2]. S. M. Lee et al., "Thermal degradation behavior and mechanism of poly(butylene succinate) nanocomposites with organically modified layered double hydroxides," Polymer Degradation and Stability, vol. 97, no. 6, 2012.

[3]. A. A. Alshammari et al., "Thermal stability of polyamide 6 and its nanocomposites with clay and carbon nanotubes," Polymer Degradation and Stability, vol. 96, no. 9, 2011.

[4]. J. J. Watkins et al., "High-temperature stability of diamond," Nature, vol. 410, no. 6829, pp. 970-971, 2001.

[5]. C. Gao et al., "Enhanced thermal stability of polyophenylenesulfide by graphene oxide modification," Applied Surface Science, vol. 496, pp. 143646, 2019.

[6]. W. W. Zhang et al., "Thermal stability and degradation of polyimide nanocomposites containing core-shell structured SiO2@TiO2 nanoparticles," Polymer Degradation and Stability, vol. 177, pp. 109-119, 2020.

[7]. J. C. Liao et al., "Thermal stability improvement of high-temperature polymer matrix composites by SiC coating," Composites Part A: Applied Science and Manufacturing, vol. 109, pp. 165-171, 2018.

[8]. X. Huang et al., "Thermal stability of polypropylene foam modified with organoclay and polyamide," Polymer Degradation and Stability, vol. 147, pp. 1-9, 2018.

29TH IRANIAN ORGANIC CHEMISTRY CONFERENCE
1_3 NOV, 2023
UNIVERSITY OF QOM, IRAN

Preparation of Co_3S_4 nanoparticles derived from Co-BDC as an electrochemical sensor for the determination of acetaminophen in real samples

*Seyed Mohammad Amin Daei Naseri**, *Fariba Fotouki*[2]

Department of Chemistry, Faculty of Chemistry, University of Mazandaran, Babolsar, Iran, m.a.daeinaseri@gmail.com, ariba.fotouki.77@gmail.com

Abstract
Acetaminophen (AP) is one of the common drugs that is used as a pain reliever, but its excessive use causes irreparable effects. Herein, an electrochemical sensor based on Co_3S_4 nanoparticles derived from CO-BDC was prepared. The prepared sensor showed a very good activity in the electrochemical determination of acetaminophen with LOD 4nM.
Keywords: Acetaminophen, Nanoparticles, Sulfide, Electrochemical sensor

1. Introduction

Acetaminophen (N-acetyl-p-aminophenol;) is an antipyretic that is specifically used in the combination of Chinese and Western medicine. This medicine is made in the form of tablets, syrups, ampoules and suppositories, and the form of tablets is more convenient. AP is well tolerated and does not have many side effects like aspirin, and since it does not require a doctor's prescription to buy and consume AP, it is easily available. This medicine is usually used to treat fever, headache, and mild pain. If AP is used together with non-steroidal anti-inflammatory drugs, it can be significant in the treatment of severe pain. AP is usually used in higher doses to treat colds and flu. With this excessive consumption, it can lead to daily poisoning and even death [1].
Metal-organic frameworks (MOFs) are functional materials composed of organic ligands and metal ions. These compounds can be converted into materials with micro/nano architecture, such as carbon and its hybrids, which have porous materials with a crystalline structure and have recently attracted much attention. Due to their high surface area and permanent porosity, MOFs have been used to load or encapsulate catalytically active metal nanoparticles, which can effectively prevent the re-aggregation of metal nanoparticles and facilitate catalytic efficiency. Also, MOFs of the first transition metals have become ideal electrochemical intermediate materials due to their low cost, non-toxicity, and especially electrochemical oxidation-reduction properties, and they can be used as materials for electrode surface modification. Different combinations of MOF crystals, for example (metal oxides/sulphides/carbides) and their nanocomposites can be obtained in controllable size, shape and composition from the combination of desired metal ions and organic ligands after preparing MOFs. These MOF-derived materials (porous carbon, hollow structures, etc.) can have the advantages of precursor MOFs, especially their high surface area and suitable porosity. MOFs as precursors or templates for the design of functional porous materials have become an expanding research field in recent years. Most MOFs have poor electrical conductivity, so they cannot be used directly as electrocatalysts. However, the decomposition of these materials with the help of controlled heat in different atmospheres turns them into very conductive carbons. Metal nanoparticles formed after burning MOFs can include metal oxide, phosphide, or sulfide, which have high potential, high pore volume, and many active sites for electrochemical reactions [2].
Transition metal sulfides, as an important classification of minerals, can be used as electrode materials for a variety of electrochemical energy storage devices, sensors, etc. [3] .Cobalt is a common metal element and can form various sulfides such as CoS, CoS_2, Co_3S_4 and Co_9S_8. Some of these sulfides have attracted a lot of attention due to their high specific capacity, good electrical conductivity, high energy density, abundant chemical reaction sites, low preparation cost, non-toxicity, etc. [4, 5]. Due to the lower electronegativity of sulfur compared to oxygen, TMSs show higher electrical conductivity and electrochemical activity than metal oxides and hydroxides [6]. In this study, we used Co_3S_4 nanoparticles derived from Co-BDC as an electrode material to prepare a high-performance Co_3S_4/GCE electrochemical sensor for AP determination.

2. Results and discussion

2.1. XRD

In Figure 1 (A) the peaks at positions 8, 9, 14, 17, 18, 27.14, 29, 30.84, 32.75, 49.69° related to planes (200), (110), (001), (201), (400), (312), (422), (420), (013) and (123) formation of the pure and crystalline phase of Co-BDC according to the standard card (CCDC-1430630) confirm. Also, the diameter of the crystals

was 27 nm. The XRD pattern of the Co_3O_4 sample after calcination is presented in Figure 1 (B). The presence of peaks in the positions of 9.19, 31.5, 37, 38.4, 45, 56, 59, 65 and 77.5 related to pages (111), (220), (311), (222), (400), (422), (511), (440) and (533) according to standard card number (JCPDS 01-074-1656) confirm the formation of crystalline structure and cubic phase of Co_3O_4. In addition, the diameter of the crystals was equal to 28.4 nm. The XRD pattern of Co_3S_4 sample is given in Figure 1 (C). Sample has peaks with positions in 16.8, 31, 39, 47.4, 54.4, 55, 58, 63 and 75° corresponding to the plates (111), (311), (400), (422), (511), (440), (531), (620) and (642), which proves the crystalline and cubic structure of the sample according to the standard card number (JCPDS 01-047-1738). In addition, the diameter of the crystals was equal to 11 nm.

The crystal size of the samples is calculated by the Debye-Scherer equation:

$$D_{hkl} = \frac{\kappa\lambda}{\beta_{hkl}\, cos\theta} \quad (1)$$

Fig.1 XRD pattern of (A) Co-BDC, (B) Co_3O_4 and (C) Co_3S_4.

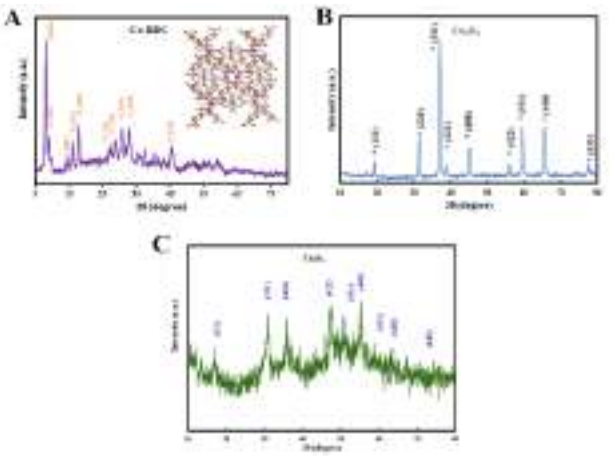

2.2. FT-IR

In Figure 2 (A), the peaks in the range of 3600 cm^{-1} are related to the acidic O-H group of BDC ligand or ethanol remaining in the structure. The C-H sp^3 vibrational peak appeared in the region of 2900 cm^{-1} and the C-H sp^2 vibrational peak appeared in the region of 3100 cm^{-1}. The peak at 2360 cm^{-1} is related to the stretching vibration of carbon dioxide in the air absorbed on the surface of the sample. The peak at 1650 cm^{-1} shows the C = C asymmetric bond. The asymmetric bond C = O appeared at 1580 cm^{-1}. In addition, the peak at 1500 cm^{-1} related to C = C symmetric bonds. The 1380 cm^{-1} peak is probably related to the C = O symmetric stretching vibration. The vibrations corresponding to 1104, 1015 and 805 cm^{-1} belong to CH aromatic stretching vibrations. Also, the peaks in the range below 700 cm^{-1} are related to metal-ligand bonds [7]. In Figure 2 (B), the peak in the region of 3500 cm^{-1} is related to the OH stretching vibrations of water molecules. C-H sp^3 vibration peak appeared in the 2900 cm^{-1} region and sp^2 C-H stretching vibration peak appeared in the 3100 cm^{-1} regions. The peak observed in the region of 2360 cm^{-1} is related to the asymmetric vibrations of CO_2 absorbed in the environment on the surface. The peak that appeared in the region of 1635 and 1629 cm^{-1} is related to the C = C double bond of the benzene ring, which shows It shows that after calcination, the linking benzene ring is largely broken. The peak in the region and 1103 cm^{-1} are related to C-H vibrations of the remaining benzene group in the sample. Two sharp peaks in the fingerprint area are related to the bonding of metal with oxygen, the peak at 660 cm^{-1} is related to Co^{2+} and the peak at 576 cm^{-1} is for Co^{3+} [8]. Figure 2 (C) shows the FT-IR spectrum of Co_3S_4 sample. The broad peak in the region of 3600 cm^{-1} is related to the stretching vibration of the OH group as well as the C = N group. C-H sp^3 stretching vibration peak appeared in 2900 cm^{-1} region and C-H sp^2 stretching vibration peak appeared in 3100 cm^{-1} regions. The peak of 2280 cm^{-1} corresponds to CO_2 present in the air absorbed on the sample surface. The peak in the 1628 cm^{-1} region is related to the C = C double bond of the benzene ring. In the following, the peak observed in the 1400 cm^{-1} region is related to the stretching vibration of the C-N bond and the sharp peak in the 1100 cm^{-1} region are related to the asymmetric stretching vibration of the sulfone group, which has well proven the sulphuration of the sample. In the fingerprint region, at 468 cm^{-1} it shows the Co-S bond [9].

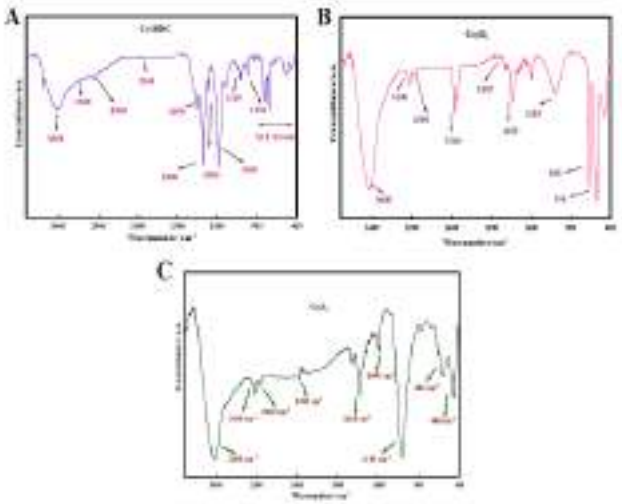

Fig.2 FT-IR of (A) Co-BDC, (B) Co_3O_4 and (C) Co_3S_4.

3. Electrochemical analysis

3.1. CV

Evaluating the electrochemical behavior of the prepared electrodes using the CV fan is an important matter for the preparation and evaluation of electrochemical sensors. For this purpose, GCE, GCE/Co-BDC, GCE/Co_2O_3 and GCE/Co_3S_4 were prepared and prepared in 0.1 M PBS solution with pH=7 and in the presence of AP 0.5 mM at a scan rate 50 mVs^{-1} in the potential range of 0 to 0.6 V were investigated. As can be seen, an irreversible peak related to AP oxidation has been seen for GCE with a potential of 0.43 V. While for GCE/Co_3O_4, GCE/Co-BDC and GCE/Co_3S_4, respectively, a strong and irreversible response has appeared at more negative potentials than GCE. The highest current and the lowest peak potential of GCE/Co_3S_4 are equal to 45 µA and 0.4 V. Therefore, it can be concluded that GCE/Co_3S_4 shows the best performance for AP electrocatalysis due to the presence of many active sites for electrochemical reactions.

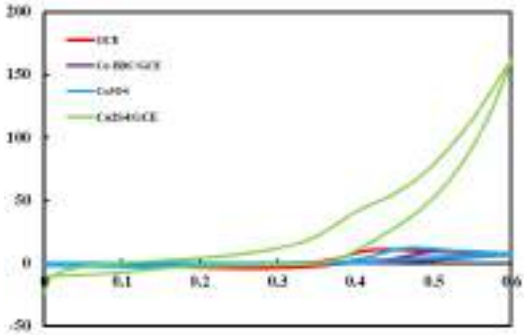

Fig.3 CV curves of GCE, Co-BDC/GCE, Co_3O_4/GCE, Co_3S_4/GCE for electrochemical behavior of AP.

Figure. 4 shows the effect of AP concentration using the chronoamperometric and applying a potential of 0.55 V in the concentration range of 7 to 141 nM. with the increase in AP concentration, the oxidative current response increases strongly, the reason for this is the transfer of electrons between the analyte and the electrode. Also, the linear graph of oxidation peaks according to concentration is shown in Figure 4 with a correlation coefficient of 0.98. The calculated value of LOD was equal to 4 nM. Therefore, it can be concluded that the proposed GCE/Co_3S_4 sensor has a very good ability to detect AP at low concentrations.

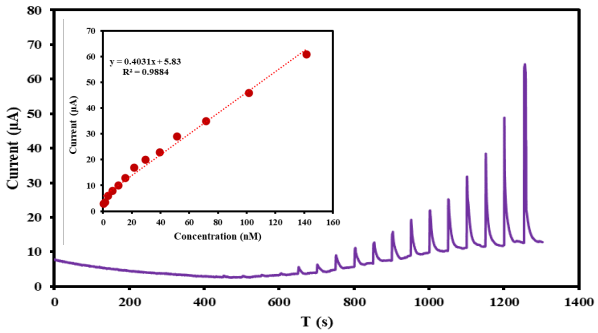

Fig.4 Amperometric response of GCE/Co_3S_4 to successive increases in AP in PBS stirring solution.

4. Conclusion

In the present study, Co_3S_4 nanoparticles were synthesized using thioacetamide. Next, the formation of nanostructure with crystalline and cubic structure was confirmed by XRD and FT-IR analysis. Also, using cyclic voltammetry and amperometry techniques, the electrochemical performance of the prepared sensor was analyzed for AP detection in real and phosphate buffer samples. The obtained data showed that the fabricated electrode has a very good LOD 4 nm and significant stability. The developed sensor is cheap and readily available. This method is a good alternative for detecting different drugs in real samples, for this reason, in the future, it is possible to develop an electrochemical sensor with different types of nanoparticles.

5. References

1. Guo, L., et al., *Metal-organic framework precursors derived Ni-doping porous carbon spheres for sensitive electrochemical detection of acetaminophen.* Talanta, 2021. 228: p. 122228.
2. Zhang, H., et al., *MOF-derived nanohybrids for electrocatalysis and energy storage: current status and perspectives.* Chemical Communications, 2018. 54(42): p. 5268-5288.
3. Shen, L., et al., *$NiCo_2S_4$ nanosheets grown on nitrogen-doped carbon foams as an advanced electrode for supercapacitors.* Advanced Energy Materials, 2015. 5(3): p. 1400977.
4. Huang, Z.X., et al., *Synthesis of self-assembled cobalt sulphide coated carbon nanotube and its superior electrochemical performance as anodes for Li-ion batteries.* Electrochimica Acta, 2015. 167: p. 388-395.
5. Zhang, D., et al., *Mesoporous anion-cation-codoped Co_9S_8 nanorings for enhanced electrocatalytic oxygen evolution reactions.* Nanotechnology, 2020. 31(33): p. 334001.
6. Buckley, A.N., et al., *Electronic environments in carrollite, $CuCo_2S_4$, determined by soft X-ray photoelectron and absorption spectroscopy.* Geochimica et Cosmochimica Acta, 2009. 73(15): p. 4452-4467.
7. Sivam, T., et al., *Tunable electrochemical behavior of dicarboxylic acids anchored Co-MOF: Sensitive determination of rutin in pharmaceutical samples.* Colloids and Surfaces A: Physicochemical and Engineering Aspects, 2021. 622: p. 126667.
8. Jagadale, A., V. Kumbhar, and C. Lokhande, *Supercapacitive activities of potentiodynamically deposited nanoflakes of cobalt oxide (Co_3O_4) thin film electrode.* Journal of colloid and interface science, 2013. 406: p. 225-230.
9. Tabrizi, A.G., et al., *Growth of polyaniline on rGO-Co_3S_4 nanocomposite for high-performance supercapacitor energy storage.* international journal of hydrogen energy, 2018. 43(27): p. 12200-12210.

29TH IRANIAN ORGANIC CHEMISTRY CONFERENCE
1_3 NOV, 2023
UNIVERSITY OF QOM, IRAN

EXTRACTION AND PURIFICATION OF PHENOLIC COMPOUNDS FROM POMEGRANATE HUSK

Mahdi Fatehi Marj, Hale Ghanei*

Department of Chemistry, Faculty of Science, University of Kashan, Kashan, Iran, mahdifatehi.313@gmail.com

Abstract - Pomegranate (*Punica granatum* L.) fruits are widely cultivated and consumed in Iran. There are some by-products in pomegranate processing industries, among which pomegranate husk can be mentioned. Pomegranate husk is a source of hydrolysable tannins called ellagitannins. Considering the low price of the raw material of this extraction and the large amount of this by-product, this will be a cost-effective practice. This article presents different methods for extraction and purification of ellagitannins such as punicalin and punicalagin, ellagic acid and phenolic acids mostly hydroxy benzoic acids. Due to the fact that ellagitannins show the potential of anti-cancer, anti-arteriosclerosis and antioxidant properties, these extracts are very suitable and affordable for the preparation of medicines and food supplements. In this way, we can directly extract phytochemicals from available and cheap sources and use them in medicines and food supplements that prevent common diseases.

1. Introduction

Pomegranate (*Punica granatum* L.) is widely produced in Iran. After India and China, Iran is the third producer of pomegranate in the world; so, there's a wide, low-price number of by-products that are available for extraction of phytochemicals such as polyphenols like ellagitannins (ETs) that are endowed with potent anti-inflammatory, anti-cancer and anti-atherosclerotic biological properties. Tannins are high molecular weight plant polyphenols divided into two chemically and biologically distinct groups: condensed tannins or proanthocyanins and hydrolysable tannins or ellagitannins (ETs). In the pomegranate juice (PJ) industry we normally have these compounds extracted in (PJ) because of solubility in water and its polyphenols including punicalagin can reach levels >2 g/L juice, depending on the fruit cultivar and processing methods. We can use vacuum-aspirated columns to rapidly purify an aqueous extract of pomegranate husk to afford total pomegranate tannins (TPT) in substantial yields (58–60 g TPTs/kg husk; time <1 h). Using analytical HPLC and tandem LC-ES/MS, evaluation of TPT showed that it contains the major fruit husk ET, punicalagin (80–85% w/w) and ellagic acid (EA; 1.3% w/w). A rapid and large-scale separation method of punicalin from pomegranate husk was established, using medium pressure liquid chromatography (MPLC). Punicalin, has been reported to have potential in anti-hepatotoxic, antibacterial, anti-cancer, and anti-HIV replication activities. [4]

Preparative separation of punicalin from waste water of hydrolyzed pomegranate husk can be performed by macroporous resin and preparative high-performance liquid chromatography. Pulsed ultrasound-assisted extraction (PUAE) is one of the most effective extraction techniques. The application of an efficient technique for extraction of natural antioxidants (like phenolic compounds) from pomegranate peel can be very useful and efficient. PUAE can provide higher efficiency than the conventional extraction methods. It requires shorter time, lower energy, chemicals and solvents than the conventional methods.

This article explains the mentioned methods to extract and purify these compounds in detail.

2. Methods and materials

2.1. A rapid large scale column chromatography method under vacuum:

This method has industrial applications because it can be scaled-up and is cost-effective due to low price husk.[1]

2.1.1. Reagents: All solvents should be HPLC grade. Ellagic, formic and acetic acids, Sephadex Lipophilic LH-20 and Amberlite XAD-16 resins are used in this method.[1]

2.1.2 Purification of total pomegranate tannins: After washing and cleaning pomegranate fruits to yield their husk, the husk (1 kg, fresh weight) should be percolated with water (5 L) for 1 h, squeezed by hand and blended. Then the puree will be filtered and squeezed dry to gain a dark brown aqueous extract. The XAD-16 resin column was prepared for chromatography by pre-washing in methanol then pre-equilibrating in water for 12 h. The aqueous extract was divided into 200 mL portions and adsorbed onto a vacuum aspirated column of Amberlite XAD-16 resin (500 g). The optimal loading volumes of the aqueous extract varied from 200 ± 10 mL per 500 g of preconditioned XAD-16 resin per column. Each column was eluted with copious amounts of distilled water (4 L) until the sugary pale-yellow eluate was

clear in color. Remaining water was removed from the resin by vacuum aspiration and the adsorbed tannins were eluted with MeOH (2 × 400 mL) to yield a dark brown solution. The time taken to complete one cycle per column was <15 min. Methanol was removed by rotary in vacuum at low temperature (37 ◦C) to yield total pomegranate tannins (TPT) as a dark brown powder (58–60 g/kg husk). The XAD-16 column was regenerated by washing with water and can be reused (over 100 times) in this processing method.[1]

2.1.3. Purification of punicalagin for quantification studies of TPT: Total phenolic tannins (300 mg) were adsorbed onto a Sephadex-LH-20 column that was pre-equilibrated with H_2O: MeOH (8:2, v/v) and eluted with increasing amounts of MeOH. LC-ES/MS analyses revealed that the 50% MeOH fraction was enriched in two compounds, both corresponding to the molecular weight for punicalagin (M − H m/z 1083). This fraction (273 mg) was evaporated in vacuum and chromatographed, this time pre-equilibrating the column with EtOH. Elution with increasing amounts of H_2O and Me2CO to EtOH: H_2O: Me_2CO (6:3:1, v/v/v) and finally EtOH: Me_2CO (1:1, v/v) yielded a fraction which was evaporated in vacuum to afford a yellow amorphous powder (34 mg). This was identified as a mixture of alpha and beta punicalagin anomers by ^{1}H and ^{13}C NMR spectral data.[1]

2.1.4. HPLC: All samples were analyzed on a C-18 column under linear gradient condition and it proved the existence of punicalagins and all other compounds.

2.1.5 LC-ES/MS analyses: Tannins were detected by use of Symmetry C-18 column, solvent: A 2% HCOOH/H_2O, B 2% HCOOH/MeOH; gradient% A in B: initial: 99%, 30 min: 80%, 45 min: 60%, 60 min: 5%; run time 60 min; flow rate 0.15 mL/min; injection volume 20L; MS parameters: Ionization mode, electron spray (ES) negative mode; scan range: 120–1500 amu; scan rate: 1 scan/s; cone voltage: 17 eV, source temperature: 275 ◦C. Peaks were identified as: punicalagin (m/z 1083); punicalin (m/z 781;); gallagic acid (m/z 601) and EA (m/z 301). EA-glycosides correlated with literature and were identified as EA-hexoside (m/z 463), EA-rhamnoside (m/z 447) and EA-pentoside (m/z 433). [1]

2.2. An optimized method of pulsed ultrasound assisted extraction of Phenolics:

2.2.1 Reagents: Pure standards of punicalagin (≥ 97%) and ellagic acid (≥ 97%). Phenol reagent, 2,2-diphenyl-1- 132 1 picrylhydrazyl (DPPH), gallic acid (98%), and sodium carbonate. Ethanol, acetonitrile, methanol, phosphoric acid and hydrochloric acid (analytical and HPLC grade).[2]

2.2.2. Pulsed ultrasound-assisted extraction of phenolic compounds: After washing and peeling the pomegranate fruits**,** 18 kg Fresh peels were immediately air-dried for approximately 7 days at 20 ± 2 ˚C. Then, the dried peels (~8 kg) were put in the moisture proof bottles, then covered with parafilm. Finally, the bottles were closed and kept at -20 ± 2 °C prior to extraction. The dried pomegranate peels were ground by a grinder, then sieved (180 μm mesh size). The extraction was performed by means of an ultrasound at a constant frequency of 24 kHz. The ultrasound processor was attached to a probe with an area of 1.53 cm2 at different intensity levels up to 105 W/cm2. The operation was carried out under the pulsed mode. In order to apply PUAE, 10.0 g of pomegranate peel powder was mixed with 100 ml of the ethanol (70%). Phenolic compounds were extracted from pomegranate peel by using different solvents such as methanol, acetone, water and ethanol-water. The extraction was carried out under the following experimental condition: Extraction time (2,6, and 10 min); Duty cycle (50, 70, and 90%); Intensity level (53, 79, and 105 W/cm2).[2]

2.2.3. Optimization and validation procedures:

In order to achieve the exact optimum point of each PUAE variable the response optimizer plot was drawn. The multiple numerical optimizations predicted that the most desirable pomegranate peel extract can be obtained by extraction for 10 min at 50% duty cycle and intensity level of 105 W/cm2. Under the suggested optimum ultrasound extraction condition, the following predicted values were expected to be achieved: 41.14% of extraction yield, 318.71 mg GAE/g total phenolic content, 5.50 μg/ml DPPH radical scavenging activity, 146.58 mg/g punicalagin, 20.66 mg/g ellagic acid and 0.053 mg/g gallic acid. [2]

2.3. A fast, cost-effective method for preparation of punicalin from hydrolyzed pomegranate husk waste water by H-103 macroporous resin and preparative HPLC:

2.3.1. Apparatus and reagents: Preparative high-performance liquid chromatography equipment used was equipped with a fluid handling unit (pump heads), controller (for solvent gradient, flow rate, external events, and sparging process), a 2487 dual-wavelength absorbance detector with a preparative cell, an Empower workstation and a reversed phase C18 column (19 300 mm, 7 lm, Symmetry). Methanol used for macroporous resin column chromatography was of analytical grade; Trifluoracetic acid (TFA) used for HPLC analysis and preparative liquid chromatography was of chromatography grade. Methanol used for HPLC analysis and preparative liquid chromatography was of chromatography grade. [3]

2.3.2. Preparation of sample and Selection of macroporous resins: Pomegranate husk was hydrolyzed to produce ellagic acid, and wastewater was neutralized with NaOH solution. After filtration, the liquid was submitted to the resin-based column chromatography. The macroporous resins S-8, NKA, SP-850, AB-8, H-103, HP-20, and HPD-600 were used in this study. 1 ml of pretreated resin was put into three air-tight Erlenmeyer flasks respectively. 100 ml sample liquid was added into each flask. The flasks

were then shaken at 120 rpm for 12 h, at a constant temperature of 298 K. The solutions after adsorption were analyzed by HPLC. After adsorption equilibrium was reached, the resin was desorbed with 100 ml of methanol solution. After adsorption equilibrium was reached, the flasks were shaken at 100 rpm for 12 h, at constant temperature of 298 K. The desorption solutions were analyzed by HPLC. Among the seven resins investigated, H-103 resin offered the best separation power for punicalin from waste water of hydrolyzed pomegranate husk. [3]

2.3.3. Separation by H-103 resin-based column chromatography and HPLC: The resin-based column chromatography was performed on a low-pressure glass chromatographic column (200 10 mm ID) filled with H-103 macroporous adsorption resin (PDVB, non-polar, 0.315–1.25 mm particle size). Such a resin-based column needed to be pretreated prior to use. The resin was washed once with 95% ethanol for 2 h, then successively once with 4% HCL and 4% NaOH solution, and finally washed with distilled water to neutral pH. 120 Microliters of sample liquid were loaded onto the pretreated column and adsorbed at a flow rate of 0.2 ml/min. After adsorption, the column was eluted with redistilled water. Then, the punicalin rich extract was eluted with 150 ml of 50% (v/v) methanol solution at a flow rate of 0.3 ml/min and this fraction was carefully collected. At last, 100% methanol was used to elute the hydrophobic compounds. The punicalin rich portion was concentrated and dried by rotary evaporator. It was redissolved with 50 ml of 10% (v/v) methanol solution. Finally, this concentrated extract was submitted to the preparative HPLC. The preparative HPLC separation was performed as follows: the solvent system consisted of 0.1% (v/v) TFA in water as fluid phase A and methanol as fluid phase B (90:10, v/v). The flow rate was 8 ml/min while the detection wavelength was 378 nm. The injection volume was 10 ml. The peak fraction of punicalin was collected according to the chromatogram.[3]

3. Figures:

3.1. Figure 1: PUAE optimization for extracting [2]

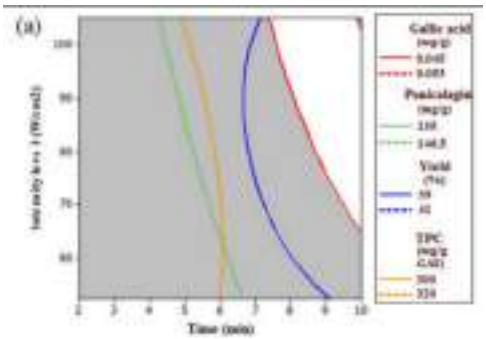

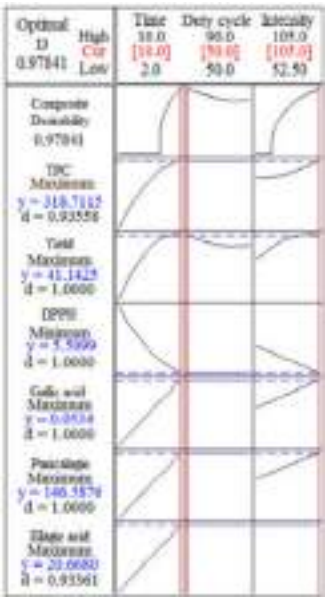

4. Conclusion:

After examining different methods, we realize that each of them has its own advantages and disadvantages, but in general,the cheapness and abundance of the raw material of this extraction make it very affordable and with high efficiency, and due to the usage field of the extracted materials, the ideal method can be choosed.

4. References

1. Seeram, N., R. Lee, M. Hardy, and D. Heber, *Rapid large scale purification of ellagitannins from pomegranate husk, a by-product of the commercial juice industry*. Separation and purification technology, 2005. **41**(1): p. 49-55.
2. Kazemi, M., R. Karim, H. Mirhosseini, and A.A. Hamid, *Optimization of pulsed ultrasound-assisted technique for extraction of phenolics from pomegranate peel of Malas variety: Punicalagin and hydroxybenzoic acids.* Food chemistry, 2016. **206**: p. 156-166.
3. Zhou, H., Q. Yuan, and J. Lu, *Preparative separation of punicalin from waste water of hydrolysed pomegranate husk by macroporous resin and preparative high-performance liquid chromatography.* Food chemistry, 2011. **126**(3): p. 1361-1365.
4. Wang, Y., H. Zhang, H. Liang, and Q. Yuan, *Purification, antioxidant activity and protein-precipitating capacity of punicalin from pomegranate husk.* Food chemistry, 2013. **138**(1): p. 437-443.

29TH IRANIAN ORGANIC CHEMISTRY CONFERENCE
1_3 NOV, 2023
UNIVERSITY OF QOM, IRAN

Effects of solvent presence and intra-structure rotation on structural stability of zwitterionic sarcosine amino acid, in DFT theoretical study

*Azimeh Davarpanah and Amir Abdolmaleki**

Department of Chemistry, College of Science, University of Shiraz, Shiraz, Iran, abdolmaleki@shirazu.ac.ir

Abstract - We used DFT theoretical calculations to show that the zwitterionic form of sarcosine amino acid (*N*-methylglycine) has structural stability only under an external force such as polar solvents. Also, by DFT relaxed-scan theoretical calculations on the rotation of carboxylate and amide's nitrogen intra-structure, an abnormal stable conformer was discovered in addition to normal trans and cis conformers of zwitterionic sarcosine.

Keywords: DFT, Relaxed-scan, Zwitterion, Sarcosine, Amino acid

1. Introduction

N-Methylglycine or sarcosine ($C_3H_7NO_2$) is an *N*-methyl derivative of glycine non-proteinogenic amino acid [1,2]. This compound has been found in muscles and other human body tissues, starfish, and sea urchins [1].

Sarcosine has acted as a noninvasive biomarker for prostate cancer progression and there have been studies on its performance against schizophrenia and sarcosinemia [1,2].

Sarcosine zwitterionic form usually exists in a polar solution or crystalline phase [1].

Much attention is paid to computational chemistry methods in predicting and developing the performance of chemical structures, nowadays. The robust density functional theory (DFT) calculation method has unique features and advantages in structural optimization, fabrication process, and performance evaluation of organic compounds compared to other calculation methods such as Hartree-Fock [1,3].

For investigation of the effects of solvent presence and conforms' difference of sarcosine zwitterion on its structural stability, the theoretical quantum study was executed in this work based on DFT theory using Gaussian 09 suite of programs [4], B3LYP method, and 6-311++G(d,p) basis set [1].

2. Results and discussions

By structural energy and geometries optimization of both acidic and zwitterionic chemical forms of sarcosine, the first part of theoretical calculations was performed in the gas (isolated monomolecular) and solution (including solvent effects) phases. The conductor-like polarizable continuum model of water (CPCM/Water) has been used as a solvent in solution phase calculations. The presented results in **Scheme 2** indicated that in both phases, the acidic form of sarcosine could not be transformed to zwitterionic without any external force from out of its own structure (Such as interactions with other acidic compounds or even its own molecules). Also, it has clearly demonstrated that zwitterionic sarcosine is not stable in the gas phase but stable in the solution phase due to the solvent stabilizing of this structure and prevents the free transforming of zwitterionic to acidic form by limiting intra-structural hydrogen transfer between amide's nitrogen and carboxylate's oxygen. This solvent effect may be related to hydrogen bonding in the interaction between solvent and zwitterionic sarcosine. Therefore, the zwitterionic form of sarcozine needs an external stabilizer such as a solvent to be stable and does not transform to acidic form freely.

Scheme 1. The structure of acidic and zwitterionic chemical forms of sarcosine. "α" and "β" are the dihedral angles of the indicated bonds.

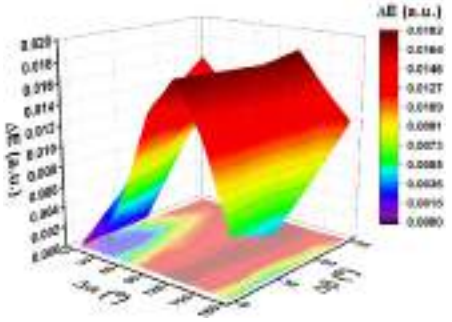

Figure1. DFT/B3LYP/6-311++G(d,p) relaxed-scan 3D curve of structural total energy variation (ΔE(a.u.)) due to dihedral angles variation of "α" and "β" (Δα and Δβ (°))

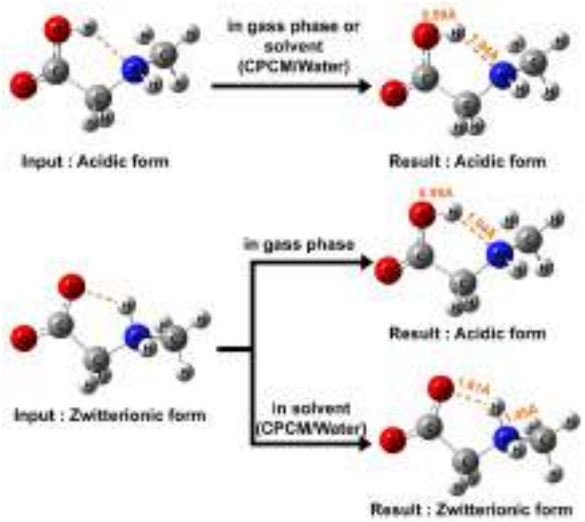

Scheme 2. Both acidic and zwitterionic forms' structural energy and geometric optimization of sarcosine in gas or solvent (CPCM/Water) phases by DFT/B3LYP/6-311++G(d,p).

In the second part of theoretical calculations, we tried to investigate the effect of increasing "α" and "β" as the bonds' dihedral angles of the zwitterionic structure of sarcosine (**Scheme 1**) on its structural stability by relaxed-scan calculations of dihedral angles "α" and "β" variation (Δα and Δβ) in 6 and 3 steps of 30°, respectively.

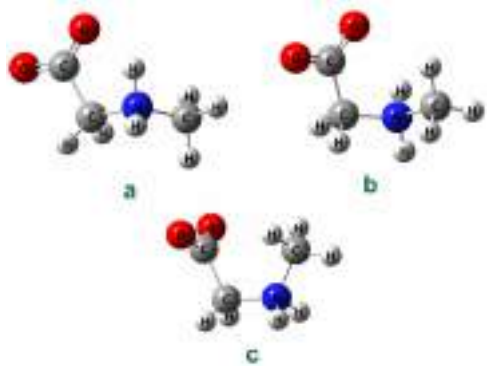

Scheme 3. Three different zwitterionic sarcosine's conformers calculated during DFT/B3LYP/6-311++G(d,p) relaxed-scan theoretical calculations.

The results of this theoretical calculations based on DFT/B3LYP/6-311++G(d,p) are presented in **Figure 1** as a **3D** curve of structural total energy variation (ΔE) due to dihedral angles variation of "α" and "β" (Δα and Δβ), **Scheme 3** and **Table 1**.

Table 1. Three different zwitterionic sarcosine's conformers calculated during DFT/B3LYP/6-311++G(d,p) relaxed-scan theoretical calculations

	Zwitterionic conformers of sarcosine		
	a	**b**	**c**
α (°)	-117.171	62.829	2.829
b (°)	-0.897	29.103	89.103
E_0 (a.u.)	-323.781327	-323.777303	-323.763174
Δα (°)	0	180	120
Δβ (°)	0	30	90
ΔE(a.u.)	0.000000	0.004024	0.018153

According to **Figure 1**, the most stable geometric form of zwitterionic sarcosine was observed when Δα and Δβ were equal to 0° (α=-117.171° and β=-0.897°) where the structural total energy (E_0) was -323.781327 a.u. (**Scheme 3-structure "a"** and **Table 1- entry a**). Also, the most unstable geometric forms of zwitterionic sarcosine were observed when Δα and Δβ were equal to 120 and 90 degrees, respectively (α=2.829° and β=89.103°) that the structural total energy calculated as -323.763174 a.u. (**Scheme 3-structure "c"** and **Table 1- entry c**). Although the trans conformer of zwitterionic sarcosine (**Scheme 3-structure "a"**) is more stable than its cis conformer (**Scheme 3- structure "c"**), the structural energy level difference between the two (ΔE) is only about 0.018153 a.u. (11.391182 kcal/mol), therefore all resulted conformers from this relaxed-scan calculations can be presented in the bulk of zwitterionic sarcosine at room temperature. The results of accurate studies in the second part of the theoretical calculations (Figure 1) indicated that when Δα and Δβ were equal to 180° and 30°, respectively (α=62.829° and β=29.103°), the structural total energy was calculated as -323.777303 a.u. (**Table 1-entry b**) and the conformer "b" (**Scheme 3**) was observed in a very close level of structural stability to trans conformer "a".

3. Conclusions

The form of sarcosine is so important and affects the performance of this compound in several usages, especially in medical applications. The zwitterionic form of sarcosine has structural stability only under external forces such as polar solvents. Also, the acidic form of sarcosine is not able to transform to zwitterionic form freely and intra-structure self alone. This is in full agreement with experimental references that emphasize, the hydrogen bonding is an important stabilizing force both in aqueous as well as crystal phases, and packing forces play an important role in producing significant effects on the geometries of the molecule and their complexes [1]. The trans (a) and cis (c) conformers of zwitterionic sarcosine are the most stable and unstable conformers of this structure, respectively. Although, it has several conformers that can exist in its bulk. We also discovered one abnormal stable conformer of zwitterionic sarcosine presented as conformer "b" in this work.

4. References

[1] P. Sharma, D.K. Singh, V. Gupta, B.P. Asthana, P.C. Mishra, R.K. Singh, Spectrochim. Acta - Part A Mol. Biomol. Spectrosc. 116 (2013) 74–83.

[2] N. Cernei, Z. Heger, J. Gumulec, O. Zitka, M. Masarik, P. Babula, T. Eckschlager, M. Stiborova, R. Kizek, V. Adam, Int. J. Mol. Sci. 14 (2013) 13893–13908.

[3] A.H. Mazurek, Ł. Szeleszczuk, D.M. Pisklak,

Pharmaceutics 12 (2020) 415.
[4] M. Frisch, G.W. Trucks, H.B. Schlegel, G.E. Scuseria, M.A. Robb, J.R. Cheeseman, G. Scalmani, V. Barone, B. Mennucci, Ga. Petersson, (2009).

29TH IRANIAN ORGANIC CHEMISTRY CONFERENCE
1_3 NOV, 2023
UNIVERSITY OF QOM, IRAN

Synthesis of low-cost semiconductor based on aniline and anthraquinone for perovskite solar cells

*Hosein Ahangar, Mostafa Moslempoor and Esmaeil Sheibani**

Department of Chemistry, Faculty of Science, University of Isfahan, Isfahan, Iran,
mostafa.moslempoor@gmail.com, e.sheibani@sci.ui.ac.ir

Abstract

In this research work, a cost-effective organic Hole-Transporting Material (HTM) was developed utilizing readily available starting materials, including aniline and anthraquinone. This material was designated with the proprietary code "HTM-37". The synthesized compound demonstrates favorable solubility and thermal stability, along with the capacity to form an acceptable morphology on the surface of perovskite layers. The inherent π-conjugated system in the structure, functioning as an electron donor-acceptor motif, enhances charge transport mobility while concurrently reducing the necessity for chemical additives. The resultant Perovskite Solar Cell (PSC) device incorporating HTM-37 was characterized through photovoltaic analyses, revealing preliminary photovoltaic parameters: a short-circuit current of 15.49 mA/cm², an open-circuit voltage of 0.67 V, a fill factor of 0.56, and a Power Conversion Efficiency (PCE) of 5.84%, all under additive-free conditions. These findings prompt optimism for further enhancement in efficiency through the optimization of operating conditions in the future.

1. Introduction

Organic HTM have emerged as pivotal components in the rapidly evolving landscape of solar cell technology. These materials serve as conduits for facilitating the movement of positively charged holes generated by the absorption of light within the active layer of the solar cell. The imperative for enhanced energy conversion efficiencies and the quest for sustainable energy solutions have driven the exploration and utilization of organic HTMs in various solar cell architectures, including novel contenders such as PSC [۳-۱]. PSC, have reached an efficiency of 25.7% in recent years despite facing challenges in terms of stability [4]. As mentioned, One of the integral constituents within PSC systems is the HTM, which plays a pivotal role in hole transport [5]. HTMs are categorized into various types based on their constituent materials, including inorganic, organic, and polymeric compositions. However, only a subset of these HTMs exhibit sufficient stability and are capable of fulfilling their role effectively within solar cells [6, 7]. In this investigation, a proprietary small organic molecule denoted as 37 was employed as the HTM. This molecule boasts several advantageous attributes, including favorable solubility, cost-effective and accessible precursors such as anthraquinone and aniline, as well as thermal stability. Furthermore, it circumvents the need for specific conditions or hazardous reagents. The structure of the hole transporting layer is presented in Figure 1, and its authenticity has been affirmed through a meticulous array of analytical methodologies. These methodologies encompassed Cyclic Voltammetry (CV), Ultraviolet/ Visible (UV) absorption, and emission spectroscopy, as well as nuclear magnetic resonance (NMR) spectroscopy. This comprehensive analytical endeavor corroborated the chemical attributes, compositional purity, and definitive identification of this layer. Notably, this investigative scrutiny was conducted under conditions devoid of any supplemental components, ensuring an evaluation grounded solely in the intrinsic characteristics of the material. In continuation, for the fabrication of the device, initially, a layer of Fluorine-doped Tin Oxide (FTO) was deposited onto a glass substrate. Subsequently, a layer of Titanium dioxide (TiO_2) was coated onto the FTO, followed by the deposition of the perovskite, also known as the active layer, via spin-coating. Finally, the HTM layer was deposited atop this structure, and subsequently, then a thick Ag back contact was deposited onto it by thermal evaporation.

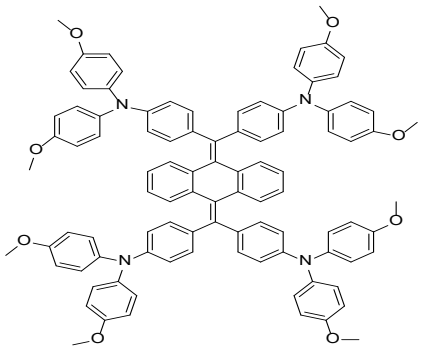

Fig.۱. Structure of HTM-37.

2. Results and Discussion

2.1. Cyclic voltammetry (CV):

CV is a scientific and powerful technique employed for characterizing quantitative and qualitative electrochemical properties of soluble substances and deposits on conductive surfaces. In this method, while measuring the current at the working electrode, the potential of the working electrode cyclically and linearly changes upwards and downwards at a controlled rate. CV measurements were initiated by preparing solutions of compounds in 10 mL volumetric flasks, utilizing a 50 mL reference solution and a 100 mL tetra-butyl ammonium hexafluorophosphate salt bridge. Subsequently, the measurements were conducted within a three-electrode cell configuration consisting of a carbon-glass working electrode, a silver/silver chloride reference electrode, and a platinum auxiliary electrode. Cyclic voltammetry curves were recorded in dry dichloromethane solvent along with the tetra-butyl ammonium hexafluorophosphate electrolyte, scanning at a rate of 50 millivolts per second. By identifying the first oxidation point from the cyclic voltammetry plot, the HOMO and LUMO energy levels were computed in terms of electron volts. Here, Eg ($E_g = \frac{(h.c)/e}{\lambda}$) corresponds to the energy gap obtained by dividing 1240 electron volt-ampere by the wavelength of the absorption-emission crossover point.

According to Figure 2, the cyclic voltammetry curve of Compound 37 is reversible, indicating a high electrochemical stability of the compound. The HOMO and LUMO energy levels of this compound are reported in Table ١. in addition, the compound exhibits several oxidation peaks, with the first peak appearing at 805 mV.

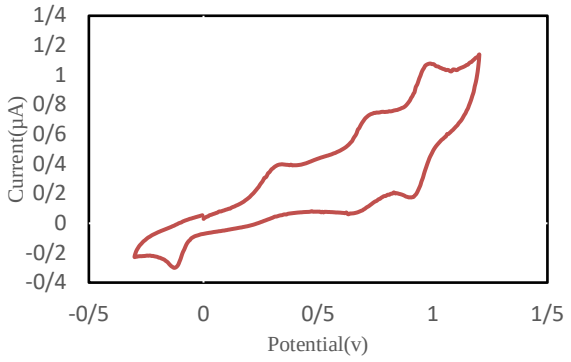

Fig.2. Cyclic voltammetry of HTM-37.

Table 1. Results obtained from cyclic voltammetry HTM-37.

Compound	HOMO (ev) vs NHE (mv)	HOMO (ev) vs vacuum	LUMO (ev) vs vacuum
HTM-37	805	-5/21	-2/16

2.2. Thermogravimetric Analysis (TGA):

Thermal analysis is employed to investigate the thermal properties and stability of high-temperature materials. By providing insight into thermal degradation pathways, it offers quantitative information regarding mass changes and critical temperature ranges. This assists in making informed decisions regarding material selection, optimization, and encapsulation strategies to enhance performance in solar cells. TGA shown the decomposition temperature of compound 37 at 450 degrees Celsius in a nitrogen (N_2) atmosphere (Figure 3). Consequently, the cell fabricated using the 37 as HTM can exhibit a notable stability under high-temperature conditions, showcasing a prolonged resistance to temperature-induced alterations.

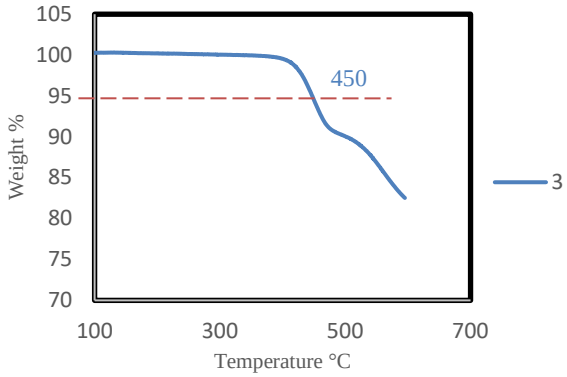

Fig.3. Results obtained from cyclic thermogravimetric analysis of HTM-37.

2.3. Ultraviolet/Visible absorption spectrum and fluorescence emission:

Compound 37 was dissolved in dichloromethane solvent, and its absorption and emission spectra were measured. The maximum absorption wavelength of this compound is situated in the ultraviolet region within the wavelength range of 314 nanometers. This absorption is attributed to π→π* electronic transitions within the aromatic system. The compound exhibits little absorption in the visible region, a distinctive hallmark of an efficient HTM for perovskite systems. In this context, the maximum energy in this region is absorbed by the perovskite, leading to the generation of more excitons and facilitating charge extraction from the perovskite surface. In addition, the energy gap of this compound falls within the range of 3.05 electron volts.

As depicted in Figure 4, the dark curve represents the absorption peak of Compound 37, while the red curve illustrates its emission peak.

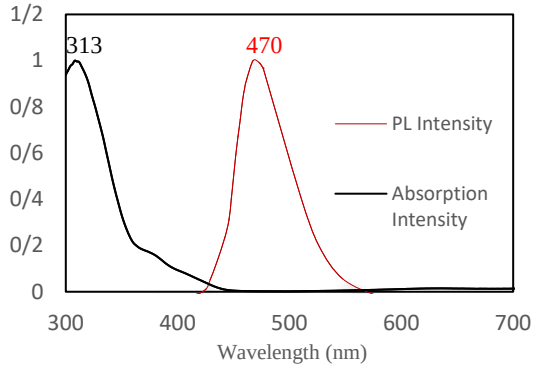

Fig.4. Absorption and emission spectrum of HTM-37.

2.4. Nuclear Magnetic Resonance (NMR) Spectral Data:

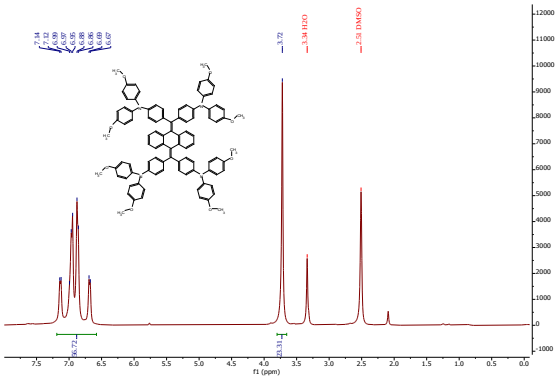

Fig.5. ^{1}H NMR Spectrum of Compound 5 in DMSO Solvent.

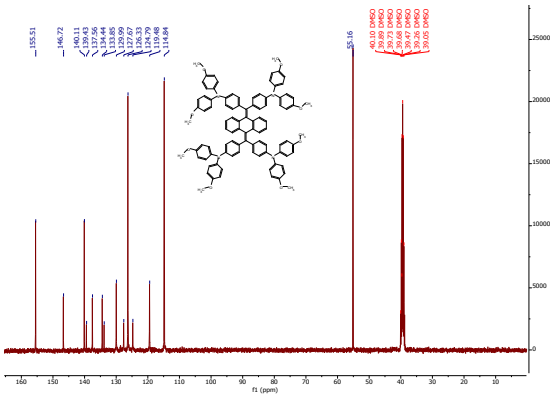

Fig.6. ^{13}C NMR Spectrum of Compound 5 in DMSO Solvent.

2.٥. Photovoltaic Performance of Hole-Transporting Material 37:

Under additive-free conditions, a photovoltaic efficiency of 5.84% was achieved using Compound 3٧ as a HTM in a photovoltaic cell. This compound exhibited a current density of 15.49 mA/cm², an open-circuit voltage of 0.67 V, and a fill factor of 0.56 as a promising HTM for the fabrication of stable perovskite solar cells in the absence of moisture-absorbing additives that can degrade the perovskite layer. By optimizing the conditions, highly favorable efficiency results can be expected in additive-free conditions.

Table 2. photovoltaic analyses of HTM-37.

Compound	V_{OC} (V)	J_{SC} (mAcm2)	FF	Efficiency (%)
HTM-37	0.67	15.49	0.56	5.84

3. Conclusions

In this research, utilizing cost-effective starting materials including aniline and anthraquinone, the small organic molecule 37 was synthesized as an efficient semiconductor species. The final compound was characterized by employing both electrochemical techniques and NMR spectroscopy for validation of its chemical attributes, compositional purity, and unequivocal identification. This molecule was subsequently employed as a HTM within perovskite solar cells. Furthermore, the thermal properties and stability of the compound at elevated temperatures were evaluated using thermal gravimetric analysis, providing insights into its endurance and suitability for high-temperature conditions. In addition, the favorable solubility and thermal stability, along with the capacity to form an acceptable morphology on the surface of the perovskite layer, are the characteristics of this compound, which can make it an ideal semiconductor for PSC fabrication.

4. References

[1] E. Sheibani, L. Yang, and J. Zhang, "Recent Advances in Organic Hole Transporting Materials for Perovskite Solar Cells," Solar RRL, vol. 4, no. 12, 2020.

[2] X. Li et al., "A Multifunctional Small-Molecule Hole-Transporting Material Enables Perovskite QLEDs with EQE Exceeding 20%," ACS Energy Letters, vol. 8, no. 3, 2023, pp. 1445-1454.

[3] B. Xu et al., "Carbazole-based hole-transport materials for efficient solid-state dye-sensitized solar cells and perovskite solar cells," Adv Mater, vol. 26, no. 38, Oct 2014, pp. 6629-34.

[4] J. Park et al., "Controlled growth of perovskite layers with volatile alkylammonium chlorides," Nature, vol. 616, no. 7958, 2023, pp. 724-730.

[5] E. Sheibani, M. Amini, M. Heydari, H. Ahangar, R. Keshavarzi, J. Zhang, and V. Mirkhani, "Hole transport material based on modified N-annulated perylene for efficient and stable perovskite solar cells," Solar Energy, vol. 194, 2019, pp. 279-285.

[6] D. Molina et al., "Molecularly Engineered Low-Cost Organic Hole-Transporting Materials for Perovskite Solar Cells: The Substituent Effect on Non-fused Three-Dimensional Systems," ACS Applied Energy Materials, vol. 5, no. 3, 2022, pp. 3156-3165.

[7] E. Sheibani, M. Moslempoor, and F. Arami Ghahfarokhi, " Investigation of Hole Transporting Materials Based on p-type Polymers in Invert Perovskite Solar Cells (In press)," Iranian Journal of Polymer Science and Technology, vol. 1, 2023.

29TH IRANIAN ORGANIC CHEMISTRY CONFERENCE
1_3 NOV, 2023
UNIVERSITY OF QOM, IRAN

DFT Study on Cyclic and Linear Germylene Ligands

*Somayeh Rahmati and Mohamad Z. Kassaee**
Department of Chemistry, Faculty of Science, University of Tarbiat Modares, Tehran, Iran,
t88_rahmati@yahoo.com, kassaeem@modares.ac.ir

Abstract
Following our previous surveys on group 14 divalents, we report new series of N-heterocyclic germylenes (NHGe) and their analogs which are regarded as cyclic (1_C-10_C) and linear (1_L-10_L) forms. Their thermodynamic and structural parameters are compared and contrasted, at the B3LYP/6-311++G** level of theory. The complexation of these NHGe with Cu metal is investigated. The results indicate that there are strong interactions between the metal-ligand bonds with a high contribution of π-back donation. Every linear germylene demonstrates a higher ability of σ-donation and π-acceptation. Our scrutinized germylenes turn out as remarkable ligands to the Cu which can be applied in several types of catalysis.

Keywords: Germylene, DFT, Ligand, Cooper and Nucleophilicity.

1. Introduction

Divalent carbenes, silylenes and germylenes are of significant interest in applied chemistry [1–10]. These group 14 analogs show the different electronic and structural properties [11–18]. Carbene usually prefers the triplet ground state (T) whereas heavier group 14 analogs such as germylene favor the singlet ground state (S) [19–21].Theoretical studies show a significant electronic effect of different substituents on the S-T energy gap ($\Delta E_{S\text{-}T}$) [22–24]. Electronegative atoms or electron-withdrawing groups (EWGs) increase the $\Delta E_{S\text{-}T}$, whereas electropositive atom or electron-donating groups (EDGs) decrease the $\Delta E_{S\text{-}T}$ [25] and π-donor or π-acceptor substituents stabilize S and T, respectively. The steric effects appear as a determining factor to predict the magnitude of $\Delta E_{S\text{-}T}$. The S becomes more unstable upon widening of the divalent bond angle ($\widehat{A}$). On the other extreme, the T turns out as a more stable state. Germylene prefers to keep its nonbonding electrons in 4s orbital which leads to a higher p-character of covalent bonds next to the divalent center. Consequently, the lower $\widehat{A}$ is seen in a linear germylene compared to its corresponding silylene or carbene analogs. Germylenes are suitable ligands for the synthesis of transition metal complexes that are used in homogeneous catalysis. The ability of germylenes to serve as σ-donor and π-acceptor ligands is less developed than their corresponding group 14 analogs [26–28]. Herein, we report new series of stable cyclic (1_C-10_C) and linear (1_L-10_L) germylenes which can be categorized as N-heterocyclic germylenes (NHGe), using the DFT method. We compare and contrast their thermodynamic and structural parameters and their ability to act as ligands to the Cu metal (Scheme 1).

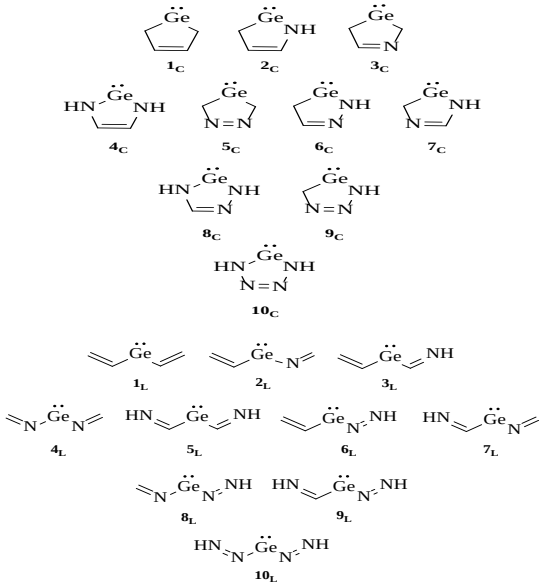

Scheme 1. New series of stable cyclic (1_C-10_C) and linear (1_L-10_L) germylenes

2. Results and discussions

The ΔEs-t which is described as E_S-E_T implies the multiplicity statuses of divalent germylenes where the ES and ET are the sum of electronic and thermal energies of the S and T, respectively. The negative obtained values indicate that our scrutinized germylenes mostly prefer the S then T (Table 1). Every linear germylene displays a lower ΔEs-t which tends to less negative values. For instance, structures 1C and 1L show the ΔEs-t values of -35.58 and -27.84 kcal/mol, respectively. It is worth mentioning that the ΔEs-t increases through cyclization by stabilizing the S and destabilizing the T [29]. Furthermore, during cyclization, the hybridization of inner orbitals gains more p-character while the outer orbitals achieve more s-character which favors the lower $\widehat{A}$ values. Therefore, the s-character may be held responsible for

the choice of multiplicity. These consequences can be observed for 10C with the lowest Â (77.07o) and the highest ΔEs-t (-63.03 kcal/mol).

Absolutely, the thermodynamic features play a significant role to determine the multiplicity. The proximity and number of electronegative atoms such as nitrogens to the divalent Ge increases the $\Delta E_{s\text{-}t}$. For example, **3C** (with a non-attached N to Ge) and **4C** (with two attached N to Ge) demonstrate the noteworthy difference of $\Delta E_{s\text{-}t}$ values (-33.54 and -46.67 kcal/mol) (Figure 1).

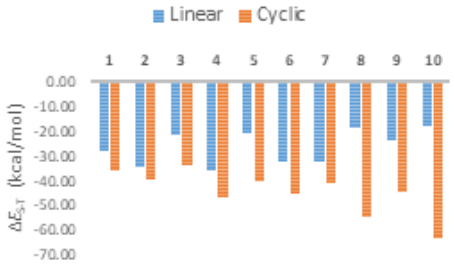

Figure 1. Comparison between the $\Delta E_{S\text{-}T}$ values (kcal/mol) of cyclic and linear germylenes.

Table 1. Calculated $\Delta E_{S\text{-}T}$ values (kcal/mol) of **1C-10C** and **1L-10L**, at the B3LYP/6-311++G** level of theory.

Structures	$\Delta E_{S\text{-}T}$
1_C	-35.58
1_L	-27.84
2_C	-39.31
2_L	-34.60
3_C	-33.54
3_L	-21.51
4_C	-46.67
4_L	-35.90
5_C	-40.41
5_L	-20.75
6_C	-45.22
6_L	-32.12
7_C	-40.51
7_L	-32.26
8_C	-54.51
8_L	-18.23
9_C	-44.53
9_L	-23.14
10_C	-63.03
10_L	-17.99

2.1 Complexation energies

To further study on the nature of Ge-Cu bond, the complex quantum-mechanical wave functions are simplified into the perceptible Lewis formalisms. Each orbital is known as a donor (Lewis) or acceptor (non-Lewis) which involves in the donor-acceptor interaction [30]. This kind of interaction may describe the strength of a bond or a charge transfer. The overlap of the lone pair (LP) of Cu with the vacant LP^* of Ge causes a change in energy which is called the stabilization energy (*E*2). The calculated *E*2 values of $LP_{Cu} \rightarrow LP_{Ge}^*$ interactions may reflect the magnitude of π-back donation from the 3*d* orbital of Cu to the 4*p* orbital of Ge (Scheme 2).

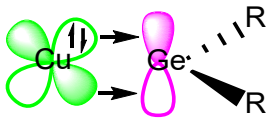

Scheme 2. The π-back bonding from 3*d* of Cu to the 4*p* of Ge.

The complexation energies are calculated *via* $\Delta E_{Com} = E_{Complex} - [E_{Germylene} + E_{Cu}]$ where the $E_{Complex}$, $E_{Germylene}$, and E_{Cu} are the energies of the optimized complex, germylenes (**1C-10C** and **1L-10L**), and Cu (Table 4). Structures **5C** and **10C** show the highest and lowest values of ΔE_{com} in cyclic series, respectively (-118.72 and -93.15 kcal/mol). In linear series, **5L** and **4L** establish the strongest and weakest complexes with ΔE_{com} values of -159.80 and -128.13 kcal/mol, respectively. Every linear germylene shows a higher value of ΔE_{com} than its corresponding cyclic isomer. For instance, **3C** and **3L** demonstrate ΔE_{com} values of -115.57 and -155.11 kcal/mol, respectively (Table 2).

Table 2. The complexation energies (ΔE_{com}, kcal/mol) of **1C-10C** and **1L-10L** with Cu.

Structures	ΔE_{Com}
1_C	-112.47
2_C	-101.90
3_C	-115.57
4_C	-98.48
5_C	-118.72
6_C	-105.24
7_C	-109.77
8_C	-100.80
9_C	-108.75
10_C	-93.15
1_L	-154.42
2_L	-139.39
3_L	-155.11
4_L	-128.13
5_L	-159.80
6_L	-152.44
7_L	-148.65
8_L	-133.23
9_L	-142.5
10_L	-135.61

3. Conclusions

In this investigation, we have scrutinized novel series of NHGe and their linear analogs (**1C-10C** and **1L-10L**, respectively), at the B3LYP/6-311++G** level of theory. The calculations indicate that every linear germylene is more nucleophilic than its corresponding cyclic isomer. In addition, a linear germylene displays a lower $\Delta E_{S\text{-}T}$ value which favors the T. Structures **5C** and **5L** turn out as the most nucleophilic germylenes which strongly bond to Cu. Every linear germylene shows wider Â than cyclic due to its higher *p*-character of valence orbitals. All calculations show consistency. The obtained results verify the strength of the Ge-Cu

bond with a high contribution of π-back donation. The overall orders of the strength of ligands for cyclic and linear germylenes appear as **5**$_C$>**3**$_C$>**1**$_C$>**7**$_C$>**9**$_C$>**6**$_C$>**2**$_C$>**8**$_C$>**4**$_C$>**10**$_C$ and **5**$_L$>**3**$_L$>**1**$_L$>**6**$_L$>**7**$_L$>**9**$_L$>**2**$_L$>**10**$_L$>**8**$_L$>**4**$_L$, respectively. It can be concluded that our studied germylenes are noteworthy ligands to the Cu which can be used in various fields of organocatalysis and industry.

4. References

[1] M. Ayoubi-Chianeh, M. Z. Kassaee, S. Ashenagar, J. Phys. Org. Chem. 32, (2019) e3956.
[2] M. Ayoubi-Chianeh, M. Z. Kassaee, J. Phys. Org. Chem. 32 (2019), e3988.
[3] M. Ayoubi-Chianeh, M. Z. Kassaee, J. Phys. Org. Chem. 32 (2019) e4007.
[4] M. Ayoubi-Chianeh, M. Z. Kassaee, Res. Chem. Intermed. 45 (2019) 4677.
[5] B. Tumanskii, P. Pine, Y. Apeloig, N. J. HillWest, , J. Am. Chem. Soc. 127 (2005) 8248.
[6] A. J.Arduengo III, R. L. Harlow, M. Kline, J. Am. Chem. Soc. 113 (1991) 361.
[7] L. Pause, M. Robert, J. Heinicke, O. Kühl, J. Chem. Soc. Perkin Trans. 2 No. 8 (2001) 1383.
[8] A. J. Arduengo III, H. Bock, H., M. Chen, D. A. DenkDixon, J. C. Green, W. A. Herrmann, N. L. Jones, M. Wagner, R. West, J. Am. Chem. Soc. 116 (1994) 6641.
[9] C. Mohapatra, Scharf, L. T. T.Scherpf, B. Mallick, K. Feichtner, C. Schwarz, V. H. Gessner, Angew. Chemie Int. Ed. 58 (2019) 7459.
[10] M.-D.Su, S.-Y. Chu, J. Am. Chem. Soc. 121 (1999) 4229.
[11] M. Ayoubi-Chianeh, M. Z. Kassaee, J. Chinese Chem. Soc. 67 (2020) 1544.
[12] M. Ayoubi-Chianeh, M. Z. Kassaee, (2020) 1.
[13] M. Ayoubi-Chianeh, M. Z. Kassaee, J. Chinese Chem. Soc. 67 (2020) 692.
[14] M. Ayoubi-Chianeh, M. Z. Kassaee, J. Chinese Chem. Soc. 68 (2021) 541.
[15] M. Ayoubi-Chianeh, M. Z. Kassaee, 13(2021) 939.
[16] M. Ayoubi-Chianeh, M. Z. Kassaee, Phys.Org.Chem. 33 (2020) e4074.
[17] M. Ayoubi-Chianeh, M. Z. Kassaee, J. Struct. Chem. 61 (2020) 1017.
[18] M. Ayoubi-Chianeh, M. Z. Kassaee, Struct. Chem. 31(2020) 2041.
[19] A. Sekiguchi, T.Tanaka, M. Ichinohe, K. Akiyama, S. Tero-Kubota, J. Am. Chem. Soc. 125 (2003) 4962.
[20] P. Jiang, P. P. Gaspar, J. Am. Chem. Soc. 123 (2001) 8622.
[21] Y. Apeloig, T. Mueller, J. Am. Chem. Soc. 117 (1995) 5363.
[22] M. C. Holthausen, W. Koch, Y.Apeloig, , J. Am. Chem. Soc. 121 (1999) 2623.
[23] B. A. S. Mohamed, M. Kikuchi, H. Hashimoto, K. Ueno, H. Tobita, H. Ogino, Chem. Lett. 33 (2004) 112.
[24] L. Nyulászi, A. Belghazi, S. K. Szétsi, T. Veszprémi, J. Heinicke, J. Mol. Struct. THEOCHEM 313 (1994) 73.
[25] P. R. Schreiner, H. P. Reisenauer, W. D. Allen, K. W. Sattelmeyer, Org. Lett. 6 (2004) 1163.
[26] C. Boehme, G. Frenking, Organometallics. 17 (1998) 5801.
[27] D. Gallego, A. Brück, E. Irran, F. Meier, M. Kaupp, M. Driess, J. F. Hartwig, J. Am. Chem. Soc. 135 (2013) 15617.
[28] N. Deak, O. T. Du Boullay, , I.T.Moraru, S.Mallet-Ladeira, D. Madec, G. Nemes, Dalt. Trans. 48 (2019) 2399.
[29] M. Z. Kassaee, M. R. Nimlos, K. E. Downie, E. E.Waali, Tetrahedron. 41 (1985) 1579.
[30] C. R. Landis, E. D. Glendening, Int. Rev. Phys. Chem. 35 (2016) 399.

29TH IRANIAN ORGANIC CHEMISTRY CONFERENCE
1_3 NOV, 2023
UNIVERSITY OF QOM, IRAN

Pervaporate desulfurization of fuel by ionic liquid

*A. Abdolmaleki *, S. Kafash*

Department of Chemistry, School of Sciences, Shiraz University, abdolmaleki@shirazu.ac.ir, smnkafash@gmail.com.

Abstract

The present research work reports the synthesis of an ionic liquid (IL) based on acidic pyridinium ionic liquid [CMDMAPy]Br. Full characterization of [CMDMAPy]Br was then performed using 1H NMR, 13C NMR, FTIR. [CMDMAPy]Br was then used in the mild oxidative desulfurization of a model oil (1000 ppm). The results confirm the great efficiency of IL in oxidative desulfurization.

Keywords:
Acidic Ionic liquids, Oxidative desulfurization, Fuel.

1. Introduction

The sulfur present in fuel causes the emission of greenhouse gases SOx in the combustion process. Therefore, desulfurization of these fuel compounds plays a significant role in reducing air pollution [1]**.** In industry, desulfurization is done by the hydrodesulfurization (HDS) method which is under high temperature and pressure. To deal with the problems of HDS, other desulfurization methods such as extractive desulfurization (EDS), oxidative desulfurization (ODS) [2], bio desulfurization, and adsorptive desulfurization [3] have been developed. Among these methods, ODS attracts special attention because it does not require hydrogen. In addition, the reaction conditions of ODS are mild and effective for removing aromatic sulfur compounds. On the other hand, ionic liquids (ILs) are a kind of molten salt that have unique properties such as low melting point, chemical and thermal stability, and high solubility for organic materials and are used as a novel method for desulfurization of fuel that uses ionic liquid as a solvent for dissolving and separating sulfur compounds from fuel instead of organic solvents [4].

2. Experimental

The ionic liquid [CMDMAPy]Br was synthesized according to the Scheme 1. In a 50 mL round-bottom flask, 50 mmol of bromoacetic acid was added to 5 mL of ethanol and 50 mmol of DMAP were added to the flask. Then the reaction was refluxed for 6 hours. As the reaction completed, white precipitate crystals were formed.

Finally, the fuel containing 1000 ppm of initial sulfur in n-octane was prepared and then desulfurized by ionic liquid and hydrogen peroxide.

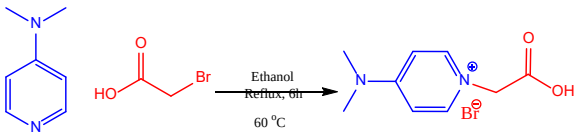

Scheme (1): Synthesis procedures of [CMDMAPy]Br.

3. Results

The synthesized ionic Liquid [CMDMAPy]Br was characterized by 1H-NMR, 13C-NMR, and FT-IR (Figures 1-3). The 1H-NMR spectrum of the ionic liquid, shows the methylene protons (-CH2) at 4.5-5.0 ppm, due to being between the electron-withdrawing groups of carboxylic acid and the positive aromatic ring. The methyl group hydrogens (-CH3) appeared in lower fields at 3.1 ppm due to the positive charge, compared to pure DMAP.

Figures (1): ^{1}H-NMR spectrum of [CMDMAPy]Br

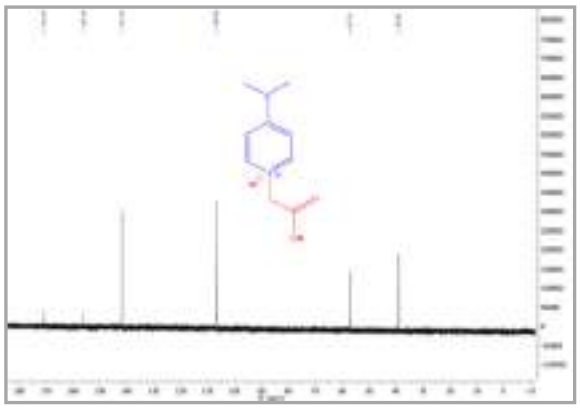

Figures (2): 13C-NMR spectrum of [CMDMAPy]Br

The presence of the carboxylic acid functional group in the synthesized ionic liquid was confirmed by FT-IR, which was appeared as a broad peak at 3300 cm-1. The peak at 1706 cm-1 is related to the carbonyl group of the ionic liquid.

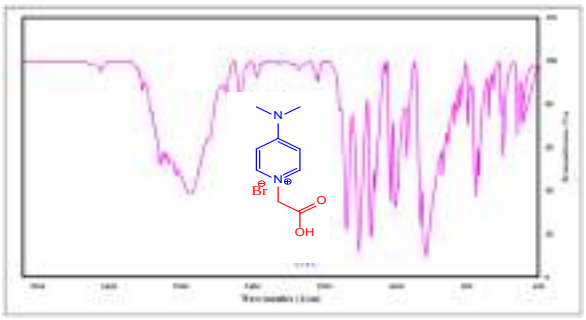

Figures (3): FTIR spectrum of [CMDMAPy]Br.

4. Conclusion

Finally, the ionic liquid was used as the solvent and cheap catalyst in fuel desulfurization by oxidation method under mild conditions. The results confirm great efficiency of the IL in oxidative desulfurization.

5. Reference

[1] X. Wang, S. Wang, C. Liu, J. Li, F. Liu, X. Tian, H. Chen, T. Mao, J. Xu, Z. Wang, Cage-like cross-linked membranes with excellent ionic liquid retention and elevated proton conductivity for HT-PEMFCs, Electrochimica Acta 283 (2018) 691-698.

[2] D. Julião, F. Mirante, S.O. Ribeiro, A.C. Gomes, R. Valença, J.C. Ribeiro, M. Pillinger, B. de Castro, I.S. Gonçalves, S.S. Balula, Deep oxidative desulfurization of diesel fuels using homogeneous and SBA-15-supported peroxophosphotungstate catalysts, Fuel 241 (2019) 616-624.

[3] L.L. Mguni, Y. Yao, X. Liu, Z. Yuan, D. Hildebrandt, Ultra-deep desulphurization of both model and commercial diesel fuels by adsorption method, J. Environ. Chem. Eng. 7 (2019) 102957.

[4] A.S. Ogunlaja, O.S. Alade, Catalysed oxidation of quinoline in model fuel and the selective extraction of quinoline-N-oxide with imidazoline-based ionic liquids, Egypt. J. Pet. 27 (2018) 159-168.

29TH IRANIAN ORGANIC CHEMISTRY CONFERENCE
1_3 NOV, 2023
UNIVERSITY OF QOM, IRAN

Synthesis of dihydroxy acenaphtho [1,2-b] indolone derivatives in the presence of HKUST-1 MOF as a good catalyst with high efficiency

Mahdiye Abdollahi, Leila Moradi*

Department of Organic Chemistry, Faculty of Chemistry, University of Kashan, 87317-51167, Kashan, Iran, mah.abdollahi99@gmail.com, l-moradi@kashanu.ac.ir.

Abstract - In this work, HKUST-1 as a (MOF) was synthesis at room temperature and characterized by analytical methods. The efficiency of this heterogeneous catalyst was studied for the synthesis of some dihydroxy acenaphtho [1,2-b] indolone derivatives by multicomponent reaction in H_2O/EtOH solvent. Products were obtained with good to high yields and reaction was completed at short times. All of derivatives were characterized by spectroscopic and analytical methods.

1. Introduction

Multicomponent reaction (MCR) is a chemical reaction where three or more compounds reacted to form a single product [1]. There are a lot of MCRs but the first reaction that was known as a MCRs, is Strecker synthesis in 1850. There are another examples of multicomponent reactions like Mannich, Passerini, Ugi, Asinger and etc [2]. Products of these reactions were obtained very fast in shortest time and highest efficiency.

Acenaphthoquinone is a 1, 2- diketo compound with two aromatic rings. So, is very active for the nucleophilic substitution reactions. Acenaphthoquinone is prepared by oxidation of acenaphthene by potassium dichromate. This structure is a yellow solid and is insoluble in water [3,4].

Nanoporous materials are consisted of an organic or inorganic bulk phase with nanometric pore size of 100 nm or less. These structures can be used as gas storages, which are important for environment, energy and drug delivery applications [5]. There are a lot of nanoporous materials which were used as catalyst or catalyst supports in organic synthesis reactions.

Metal–organic frameworks (MOFs) are a class of compounds consisting of metal clusters (also known as SBUs) coordinated to organic ligands to form one-, two-, or three-dimensional structures [6]. Generally, MOFs are used as a heterogeneous catalyst due diversity in metal, high surface area and tunable porosity. In this study, we have introduced green and new routes for synthesis of dihydroxy acenaphtho[1,2-b] indolone derivatives in the presence of the HKUST-1 MOF as green and reusable catalyst.

HKUST-1 is produced with Cu^{2+} and H_3BTC (benzentricarboxylic acid) ligand. This structure can be used as an efficient catalyst to increase the velocity of organic reactions. The advantages of presented method are recyclable and highly efficient catalyst, short reaction times, easy workup and green solvent.

2. Experimental

2.1 Synthesis of HKUST-1:

HKUST-1 was synthesised at room temperature. 0.60 g of Cu $(CH_3COO)_2.H_2O$ was dissolved in 50 mL of water and 0.42 g of H_3BTC was dissolved in 50 mL of ethanol, respectively. After they were completely mixed, another mixture of 10 mL of cyclohexane and 0.85 mL of triethylamine was added dropwise. Then, blue solids formed and precipitated afterwards. The reaction was allowed to stand for 24 h before the solids were centrifuged and washed with DDW (double distilled water) and ethanol, sequentially. The obtained product was dried in vacuum for 12 h at 50˚C [7].

2.2 Synthesis of the dihydroxy acenaphtho [1,2-b] indolone at the presence of the HKUST-1:

A mixture of aniline (1.0 mmol), 1,3-dicarbonyl compound (dimedone or cyclohexane-1,3-dione) (1.0 mmol), and HKUST-1 (10 mol%) were stirred in 5 mL of H_2O/EtOH at 70 ˚C. After 30 min, 1,2-dicarbonyl compound (acenaphthenequinone) (1.0 mmol) was added (Scheme 1). After completion of the reaction (determined using thin-layer chromatography (TLC)), solvent was removed by filtration. After that, the obtained precipitated was dissolved in chloroform and the catalyst was separated of product by filtration. Eventually, the products were dried at 80˚C in oven.

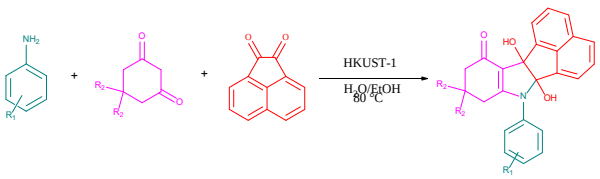

Scheme 1. Synthesis of the dihydroxy acenaphtho [1,2-b] indolone in the presence of the HKUST-1.

3. Result and discussion

3.1 Structural characterization of HKUST-1:

HKUST-1 catalyst was synthesized according to the method in the experimental section. This catalyst characterized with X-ray diffraction (XRD) analysis (Figure1). The strong peaks at 2Θ of 6.38, 9.14, 11.26 and 13.08˚ were corresponded to the regular (002), (022), (222) and (004) planes of HKUST-1, respectively. (111) plane shows existence of Cu^{2+} at 40-50 position. Other peaks at 2Θ of 18.66, 25.58, 28.94, 34.78 and 38.78, also matched well with the planes of (044), (355), (555), (377) and (559), respectively. The result confirmed that the prepared HKUST-1 possessed a similar structure to the reported data.

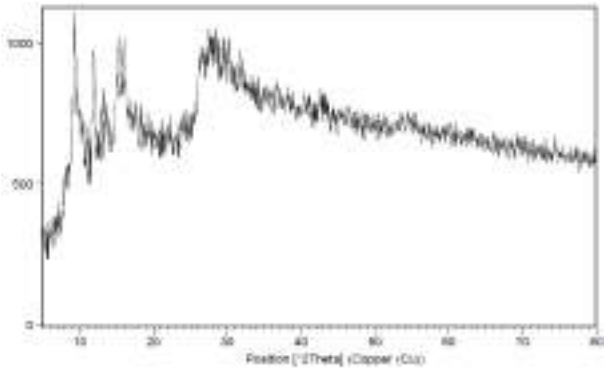

Figure 1. XRD pattern of the HKUST-1

Table 1. Synthesis of dihydroxy acenaphtho [1,2-b] indolone at the presence of the HKUST-1

Entry	R_1	R_2	Time	Yield
1	4-OMe	CH_3	2 h	92%
2	4-Et	CH_3	2.5 h	89%
3	3-Cl-4-F	CH_3	2h	90%
4	4-Cl	CH_3	3h	80%
5	4-Br	CH_3	3h	77%
6	H	H	3h	80%
7	3-Me	CH_3	3h	85%
8	4-I	H	4h	73%
9	H	CH_3	3h	82%
10	3-Cl-4-F	H	2.5h	89%

Reaction condition: Dimedone (1 mmol), aniline (1mmol), Acenaphthoquinone (1mmol), HKUST-1 (0.02g), 5 ml of H_2O/EtOH.

3.2 Synthesis of the dihydroxy acenaphtho [1,2-b] indolone derivatives in the presence of the HKUST-1:

Table 1 shows the information of synthesized derivatives using various aniline derivatives, dimedone and 1,3-cyclohexadione in reaction with acenaphthoquinone. The best amount of catalyst was 0.02 g in the presence of The H_2O/EtOH solvents at 80 ˚C, which was determined through the reaction of dimedone, 4-methoxy aniline and acenaphthoquinone as model reaction.

3.3 Mechanism for synthesis of a dihydroxy acenaphtho[1,2-b] indolone:

The mechanism is shown at the schemes 2. At the first step, the HKUST-1 catalyst is linked with carbonyl group of the dimedone or cyclohexadione. After that, nitrogen of aromatic amin was attacked to the carbonyl group and enaminone (3) was formed. This compound was reacted with acenaphthoquinone (4) as important material in this study and then, acenaphtho indolone product is formed (6) (scheme 2).

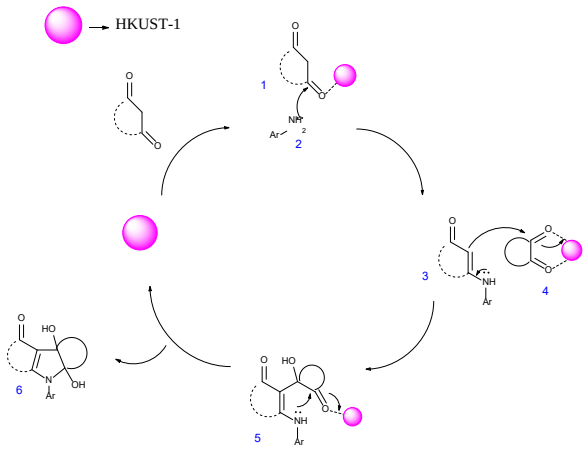

Scheme 2. Mechanism for the synthesis of dihydroxy acenaphtho [1,2-b] indolone.

4.Conclusion

In summary, HKUST-1 is used as an excellent and applied heterogeneous catalyst for the synthesis of acenaphtho indolones. The yield of reactions by using HKUST-1 was good to high and time of the reactions was short. Also, HKUST-1 has properties like gas storage that can be used for a lot of industrial applications.

5. References

[1] R. W. Armstrong, A. P. Combs, P. A. Tempest, S. D. Brown, T. A. Keating, ACR., 29(3) (1996) 123-131.
[2] R. Melo, L, W. A Silva, Curr. Green Chem., 3(2) (2016) 120-132.
[3] C. F. H. Allen, J. A. VanAllan, Org. Synth., (1944).
[4] O. Tsuge, I. Shinkai, OPPI., 4(4) (1944) 159-168.
[5] R. E. Morris, P. S. Wheatley, Angew. Chem. Int. Ed., 47(27) (2008) 4966-4981.
[6] S. R. Batten, N. R. Champness, X. M. Chen, J. Garcia-Martinez, S. Kitagawa, L. Öhrström, J. Reedijk, Pure Appl. Chem., 85(8) (2013) 1715-1724.
[7] T. Shen, T. Liu, H. Mo, Z. Yuan, F. Cui, Y. Jin, X. Chen, RSC Adv., 10(39) (2020) 22881-22890.

29TH IRANIAN ORGANIC CHEMISTRY CONFERENCE
1_3 NOV, 2023
UNIVERSITY OF QOM, IRAN

A new one-pot synthesis of 5,5-Dimethylhydantoin

Ebrahim Khalilzadeh[1]*, *Ali Mehrafarine*[2], *Keyvan Nosrat Zadegan*[2] , *Amin Mehrzad*[2]

[1]*Department of Organic Chemistry, Faculty of Chemistry, University of Tarbiat Modares, Tehran, Iran, ebekhalilebe@gmail.com*
[2]*Department of Organic Chemistry, Faculty of Chemistry, University of Razi Kermanshah, Kermanshah, Iran.*

Abstract:
The hydantoin scaffold is a versatile structure that has shown potential in various medicinal applications, including as androgen receptor modulators, anticonvulsants, [1] antidiabetic agents, and anticancer agents. This makes it an important target for synthetic chemists looking to develop new drugs. [2, 3] In this study, we focused on developing an efficient method for the synthesis of 5,5-disubstituted hydantoin. We used a reaction between a ketone compound and ammonium carbonate, along with potassium cyanide as a catalyst-free system. By optimizing the reaction conditions, we were able to achieve good yields of the desired hydantoin derivatives. The absence of a catalyst simplifies the synthetic procedure and reduces costs associated with catalysts. This research contributes to the further development of synthetic protocols for hydantoin derivatives, which potentially leads to the production of drugs on an industrial scale.

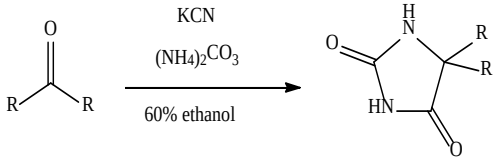

R: Methyl , Phenyl

1. Introduction:

The Bucherer-Bergs reaction is a commonly used method for the synthesis of hydantoins. This reaction starts with an aldehyde or a ketone, which are readily available compounds. [4, 5] Due to the wide range of pharmaceutical applications of hydantoins, many derivatives have been identified as anticonvulsants, antimuscarinics, antiulcers, antiarrhythmics, antivirals, antidiabetics, serotonin and fibrinogen receptor [6] antagonists, inhibitors of the glycine binding site of the NMDA receptor [7], and antagonists of leukocyte cell adhesion acting as allosteric inhibitors of protein-protein interaction. Among these derivatives, 5,5-dimethylhydantoin (DMH) is particularly important and widely used as an anticonvulsant and cardiac antiarrhythmic compound. Here, we development of a new one-pot hydantoin synthesis that overcomes solubility problems associated with water and ethanol. (fig1) The inclusion of ammonium carbonate can cause sublimation issues, requiring the reaction to be conducted in a sealed tube or acid digestion bomb. we found that using an excess amount of ammonium carbonate increases the yield of the product to some extent. However, using less than 3 times the amount of ammonium carbonate decreases reaction efficiency, while using more than 3 times does not affect efficiency. Therefore, the optimal amount is determined to be 3 times ammonium carbonate. (Table1).

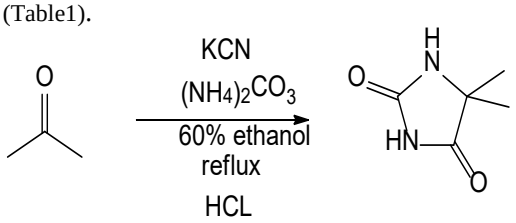

Fig1: Synthesis of 5, 5-di methyl hydantoin

Table 1. Comparison for the Synthesis of 5, 5-di methyl hydantoin

sample	Aceton (mmol)	Potassium cyanid (mmol)	Ammonium carbonate (mmol)	Yield %
1	2.5	.5	2.5	66%
2	2.5	.5	5	73%
3	2.5	.5	7.5	91%
4	2.5	.5	15	91%

The reaction yield was calculated based on the limiting starting material (Potassium Cyanide).

The proposed mechanism for the one-pot reaction to form hydantoins consists of steps. (fig2)

1.The first step involves the condensation of ammonium carbonate with acetone. In this step, the amine group of ammonium carbonate attacks the carbonyl carbon of acetone, resulting in the formation of an imine intermediate.

2. The second step is the attack of an isocyanide on the imine intermediate, leading to the formation of an aminonitrile.

3. The third step involves the nucleophilic addition of the aminonitrile to carbon dioxide (CO_2), resulting in the formation of cyanocarbamic acid.

4. The next step is the intramolecular ring closing of cyanocarbamic acid, forming 5-imino-oxazolidin-2-one.

5. Lastly, there is a rearrangement of 5-imino oxazolidin-2-one to form the hydantoin product via an isocyanate intermediate.

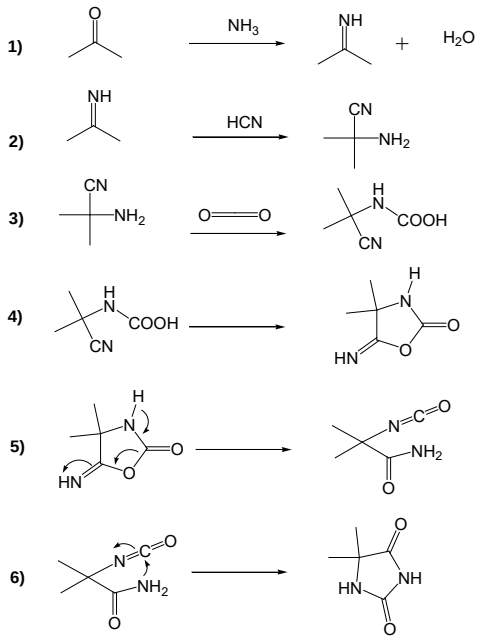

Fig2: Mechanism 5, 5-di methyl hydantoin

Overall, this mechanism involves condensation, cyclization, tautomerization and nucleophilic addition reactions to form 5,5-dimethylhydantoin from imine and ketone.

2. Conclusion

That is an impressive technological achievement! The ability to prepare 5,5-disubstituted hydantoins from ketones and potassium cyanate without the need for excess reagents or purification steps is not only environmentally friendly but also efficient. It is particularly remarkable that this methodology has been successfully applied in the preparation of an antiepileptic drug, as it opens up new possibilities for the safe and eco-friendly synthesis of pharmaceutically important drugs on a large scale. Such advancements are crucial for the development of sustainable approaches in the pharmaceutical industry.

3.Experimental Methods:

The ketone (2.5 mmol) and ammonium carbonate (288mg) were placed in a 100-mL round bottom flask. Potassium cyanide (65mg) was dissolved in ethanol (60%) and added to the reaction flask. The reaction mixture was heated on an oil bath at 90°C. After completion of the reaction (TLC), Then, separate the condenser from the balloon and heat it for 20 minutes under a Laboratory hood at a temperature of 90°C until impurities such as ammonium carbonate and cyanide are removed, the mixture was cooled to room temperature and acidified using concentrated HCl The resulting precipitates were filtered (The acidification step is done under the Laboratory hood to remove the residual gases from the reaction of potassium cyanide and acid to be prevented). The precipitates were filtered and recrystallized from ethanol/water to give a pale yellow product.

Yellow powder, m.p.:178 °C; yield: (89%). IR (KBr) (ν_{max}, cm^{-1}): 3220, 2051, 1770,1700. ^{1}H NMR (300 MHz, DMSO): δ_H: 10.53 (s, 1H), 7.95 (s, 1H), 1.23 (d, J = 1.9 Hz, 6H).

^{13}C NMR (75 MHz, DMSO): δ_C: 179.23(C=O), 156.01(C=O), 58.93(C), 24.66(CH_3), 24.41(CH_3).

4. Refrence:

[1] Meusel, M.G., M. Org. Prep. Proced. Int. 2004, 36, 391.

[2] Dhanawat, M.B., A.G. Med. Chem. Res. 2012, 21, 2807.

[3] Iqbal, Z.A., S.; Iqbal, J.; Abbas, Q.; Qureshi, I.Z.; Hameed, S. Bioorg. Med. Chem. Lett. 2013, 23, 488.

[4] J.C. Thenmozhiyal, P.T.H.W., W.K. Chui, J. Med. Chem. 2004, 1527–1535.

[5] C.W. Bazil, T.A.P., Annu. Rev. Med. 1998, 49, 135– and N.R. 162; b) M.S. Luer, 20, 178–182.

[6] M. Jansen, H.P., C. Brandt, W. Löscher, G. Dannhardt, and J. Med. Chem. 2003, 64–73.

[7] K. Last-Barney, W.D., M. Cardozo, L.L. Frye, C.A., et al.

29TH IRANIAN ORGANIC CHEMISTRY CONFERENCE
1_3 NOV, 2023
UNIVERSITY OF QOM, IRAN

Efficient reduction of nitroarenes catalyzed by reusable polyoxometalate supported on graphene oxide

Ali Zarnegaryan and Soghra Hossinimotlagh*

Department of Chemistry, College of Sciences, Yasouj University, Yasouj, 75918-74831, Iran, zarnegaryana@yu.ac.ir, shosseini@yu.ac.ir

Abstract

In the present study, Anderson-type polyoxometalate was immobilized on amino-modified magnetic graphene oxide, and employed as a new catalyst in a reduction of nitroarenes. The results indicated that our catalyst was quite active in reduction of nitroarenes to their corresponding in the presence of hydrazine. The synthesized catalyst can be easily separated from the reaction medium and reused for 4 consecutive runs without a significant reduction in reaction efficiency.

Keywords: Anderson-type polyoxometalate, Graphene oxide, Reduction of nitroarene.

1. Introduction

Aromatic amines are important organic pollutants widely used as starting materials and key intermediates in the synthesis of photographic chemicals, additives, surfactants textile auxiliaries, chelating agents, dye stuffs, agricultural chemicals, and pharma [1]. The most commonly used method to produce aromatic amines is reduction of corresponding aromatic nitro nitroarenes. One of the customary and interesting methods for reduction of the nitro group is catalytic transfer hydrogenation. In this context, metal nanoparticle catalysts based on noble metals displayed high potential for the facile reduction of nitroarenes using numerous reducing compounds, including hydrazine hydrate, formic acid, ammonium format, H_2, and sodium borohydride [2-4].

Graphene oxide (GO) sheets are an appealing class of microporous materials with well-organized structures. Graphene oxide, a new type of carbon nanomaterial composed of a monolayer of sp^2 carbon atoms, is prominent owing to its exclusive chemical and physical properties. GO is a fascinating material for catalytic applications due to its unique properties, such as high mechanical properties and high surface area. It provides a template for immobilization of inorganic and organic species like catalysts and synergistic interactions between them; these and graphene oxide can result in improved yields. GO is an exclusive candidate for a polyoxometalate support material to overcome challenges of the high solubility of POMs, low surface area, and hybrid catalyst [5].

Polyoxometalates (POMs), transition metal-oxygen anion exhibits various electronic and chemical properties and various topologies. POMs display very strong Brønsted acidity, reversible multi-electron redox transformations, and fast making them efficient catalysts for different reactions such as hydrolysis, esterification, oxidation of sulfides, epoxidation of olefins and for the oxidation of alcohols [6-8]. Heteropolyacids, with a general formula of $[XM_{12}O_{40}]^{n-}$, where M = (mainly Molybdenum and Tungsten) and X = Si^{4+}, $P^{5+,}$ As^{5+}or Ge^{4+} have been widely utilized as catalysts for different organic reactions owing to their individual excellent chemical and physical properties. Amongst the Keggin-type polyoxometalate of these solid acids, phosphotungstic acid $(PW_{12}O_{40})^{3-}$ was received considerable attention and is a target catalyst in recent times because of its solid acidity is its facile fabrication [9-12].

Herein we report the design of a new nanocatalyesd amine-functionalized graphene oxide immobilized with Anderson-type POM clusters, which feature a well-defined structure and stability and show promising catalytic performance as a catalyst for reduction of nitroarenes.

Results and discussion

2.1. Synthesis of the GO/[$FeMo_6$]

To immobilize $[FeMo_6O_{18}(OH)_6]$ on the GO, a stirred solution of GO-NH_2 (0.30 g) in CH_3CN solvent (15 mL) at 70 °C, a solution of $FeMo_6$ (0.15g) in CH_3CN (15 mL) was added dropwise. The reaction mixture was vigorously stirred at reflux for 24 h. The composite material was then isolated by vacuum filtration, and it subsequently sonicated in CH_3CN solvent for 8h. Finally, the material was washed entirely with C_2H_5OH two times and it was dried at 45 °C.

Fourier transform infrared (FT-IR) analysis is utilized for the chemical structure of POM, GO, and GO/[$FeMo_6$] catalyst (Fig. 1) Peaks at 1049 and 1121.7 cm^{-1} (Fig. 1 a) illustrate the presence of Si–O–C and Si–O–Si bonds, respectively. The characteristic peak of Anderson-type POM (Fig. 1b) appeared at 946 (Mo=O) and 645 (Mo-O-Mo) cm^{-1}. However, the nano-catalyst showed peaks at 941, and 676 cm^{-1} (Fig. 1c).

The significance of the interaction between GO and [$FeMo_6$] can be analyzed by the changes in the carbon framework by Raman spectra. Raman spectra with characteristic G and D, bands sensitive to disorder, carbon grain size, and defects, have extensively been used to characterize carbon materials. The Raman spectra of GO and GO/[$FeMo_6$] are shown in Fig. 2. The position of the D band is almost the same before and after the chemical modifications. However, the G band shifts from 1614 for GO to 1618 cm^{-1} for GO/[$FeMo_6$] catalyst. This may be attributed to the attachment of the polyoxometalate on GO, causing an increased defect density in graphene sheets.

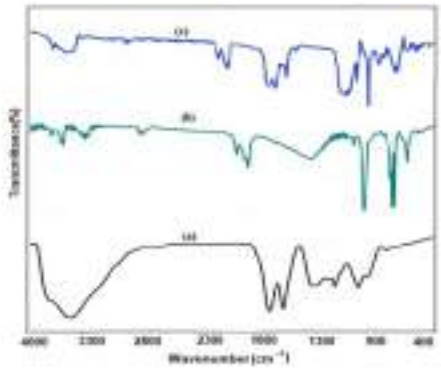

Figure 1. FT-IR spectra of (a) GO (b) POM and (c) GO/[$FeMo_6$]

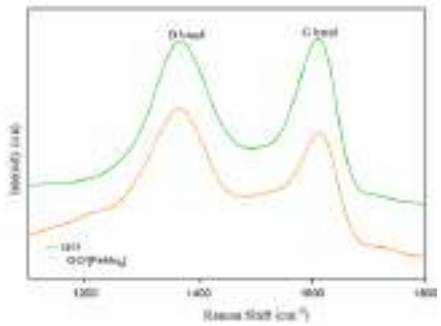

Figure 2. Raman spectra obtained on the GO and GO/[$FeMo_6$]

The thermal behavior of catalyst was investigated by thermal gravimetric analysis (TGA), as illustrated in Figure. 3. The thermal gravimetric analysis plot of the catalyst demonstrates a three-step mass loss around 25–650 ºC. The first 4.82 % weight loss at 100 °C can be accounted for solvent associated with the compound[59]. The weight loss starting at 220 °C of 46.80 % corresponds to the loss of the organic cations and the ligands[60]. At about 570 °C, the decomposition of the metal oxide starts.

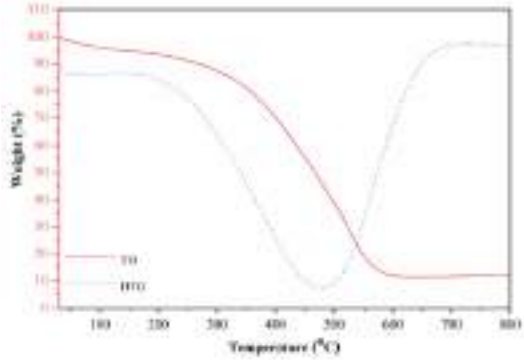

Figure 3. TG analysis of the GO/[$FeMo_6$]

3.1. Catalytic activity of GO/[$FeMo_6$]

The catalytic activity of the prepared GO/[$FeMo_6$] catalyst has been tested as a catalyst for the reduction of nitroarenes. The catalytic activity of the GO/[$FeMo_6$] for the hydrogenation of nitroarenes (Fig. 1) was evaluated using hydrazine hydrate as a hydrogen and electron donor. Hydrazine is an attractive choice because of the high hydrogen content (8.0mass%), simply separable by-products (only hydrogen and nitrogen) and scalable synthesis from ammonia. Reaction optimization using 15 mg of the GO/[$FeMo_6$] catalyst showed that at 1h with 0.6mmol of hydrazine afforded the product (aniline) at 100% yield and selectivity, using 0.1mmol of the nitrobenzene substrate.

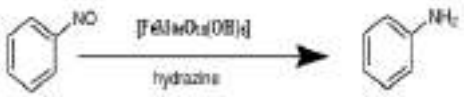

Schme 1. Catalytic reaction study. Reduction of nitrobenzene using GO/[$FeMo_6$]

3.2. Recycling of the GO/[$FeMo_6$]

To further determine the stability of the GO/ [$FeMo_6$] nano-catalyst, the catalytic activity of the recovered catalyst was evaluated in the treduction of nitroarenes. under similar conditions, and the results are given in Fig. 4. The results demonstrated that after five consecutive runs, the catalytic activity has no significant changes and that the catalyst is active and stable after recycling.

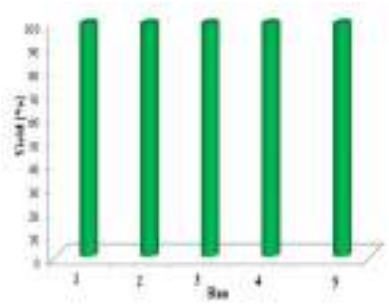

Figure 5. Recycling experiments of the GO/ [$FeMo_6$]

4. Conclusion

In summary, a new, efficient and recyclable catalyst was prepared successfully and used for the treduction of nitroarenes. The atalyst, GO/[$FeMo_6$], made immobilized on graphene oxide-supported polyoxometalate, was easily synthesized. Moreover, the recyclability test exhibited that it could be reused for five consecutive runs without appreciable loss in catalytic efficiency. The additional advantages of the present nanocatalyst include simplicity, yield, cost, reaction time, and selectivity as compared to other catalysts available in the literature for the same organic transformation. Furthermore, easy catalyst recovery, faster synthesis, recyclability and inexpensive reactants make this methodology a potential candidate for sustainable synthesis.

References

[1] J. R. H. Ross, Contemporary Catalysis: Fundamentals and Current Applications (Elsevier, 2019).

[2] N. A. Romero, & D. A. Nicewicz, Organic photoredox catalysis. Chem. Rev. 116 (2016)10075–10166

[3] H. B. Blaser. Selective hydrogenation for fne chemicals: recent trends and new developments. Adv. Synth. Catal. 345 (2003) 103–151

[4] A. Corma, & P. Serna, Chemoselective hydrogenation of nitro compounds with supported gold catalysts. Science. 313 (2006) 332–334

[5] S. Kargar, D. Elhamifar, A. Zarnegaryan, Core–shell structured Fe3O4@ SiO2-supported IL/[Mo_6O_{19}]: A novel and magnetically recoverable nanocatalyst for the preparation of biologically active dihydropyrimidinones. J. Phys. Chem. Solids, 146(2020) 109601.

[6] A. Zarnegaryan, A. S. Beni, Immobilization of hexamolybdate onto carbon-coated Fe3O4 nanoparticle: A novel catalyst with high activity for oxidation of alcohols. J. Organomet. Chem. 953 (2021)122043

[7] M. Neysi, A. Zarnegaryan, D. Elhamifar, Core–shell structured magnetic silica supported propylamine/molybdate complexes: an efficient and magnetically recoverable nanocatalyst. *New J. Chem.* 43, (2019) 12283-12291.

[8] A. Zarnegaryan, M. Moghadam, S. Tangestaninejad, V. Mirkhani, I. Mohammadpoor-Baltork, Synthesis and characterization of a novel polyoxometalate–Cu (II) hybrid catalyst for efficient synthesis of triazols, *Polyhedron*, 115, 61-66 (2016).

[9] R. Keshavarz, M. Farahi, B. Karami, P. Gheibipour, A. Zarnegaryan, TiO_2-coated graphene oxide-molybdate complex as a new separable nanocatalyst for the synthesis of pyrrole derivatives by Paal-Knorr reaction. *Arab. J. Chem.*15, (2022*)* 103736

[10] R. Nemati, D. Elhamifar, A. Zarnegaryan, Shaker, M. Core-shell structured magnetite silica-supported hexatungstate: A novel and powerful nanocatalyst for the synthesis of biologically active pyrazole derivatives. *Appl. Organomet. Chem.* 35(2021) e6409.

[11] S. Abaeezadeh, A. S Beni, Zarnegaryan, A., Nabavizadeh, M. Immobilization of Polyoxometalate onto Modified Magnetic Nanoparticles: A New Catalyst for the Synthesis of Dihydropyranopyrazole Derivatives. *ChemistrySelect*, 6(2021). 11039-11046

[12] R. Tajgardoon, A. Zarnegaryan, D. Elhamifar, A Lindqvist type hexamolybdate [Mo_6O_{19}]-modified graphene oxide hybrid catalyst: Highly efficient for the synthesis of benzimidazoles. *J. Photochem. Photobiol.* 430 (2022)113960

29TH IRANIAN ORGANIC CHEMISTRY CONFERENCE
1_3 NOV, 2023
UNIVERSITY OF QOM, IRAN

MOF-derived Binary Metal Sulfide for Electrocatalysis of OER

Nasrin Mohseni[1], Shahram Ghasemi [1], Niaz Monadi[2], and Farimah Mousavi[1]*

[1]*Department of Applied Chemistry, Faculty of Chemistry, University of Mazandaran, Babolsar, Iran, mohseni.n1992@gmail.com, sghasemi@umz.ac.ir and sghasemimir@yahoo.com*
[2]*Department of Inorganic Chemistry, Faculty of Chemistry, University of Mazandaran, Babolsar, Iran,*

Abstract - Developing high-performance and cost-efficient catalysts for oxygen evolution reaction (OER) has remained a challenging task due to its sluggish kinetics. In this work, a cobalt-copper metal-organic framework (CoCu-MOF) was prepared by a simple co-precipitation method using corresponding metal salts and a 2-methylimidazole ligand. Further, Co_2CuS_4 nanostructure was derived from CoCu-MOF, using thioacetamide. The product was characterized by X-ray diffraction (XRD) technique, and the crystallite diameter was calculated as 28 nm. The glassy carbon electrode (GCE) was further modified by the Co_2CuS_4 nanostructures, and was studied by linear voltammetry (LSV) technique. The modified electrode has shown excellent catalytic performance toward oxygen evolution reaction (OER) with low overpotential of 352 mV at a current density of 10 mA cm^{-2}, maximum current density of 391 mA cm^{-2}, and low Tafel slope of 58 mV dec^{-1} in 1 M KOH. The study suggests the high potential of MOF-derived binary metal sulfides for water-splitting systems or metal-air batteries.

1. Introduction

There is still an ongoing effort to search for sustainable, clean and highly efficient energy generation to satisfy the energy needs of modern society. Electrochemical water splitting is among the most promising approach that can be utilized to ameliorate the energy problems, due to its cleanliness, safety, and simplicity of the process [1,2]. They are two-electrode systems, where the cathode part involves hydrogen evolution reaction (HER) or oxygen reduction reaction (ORR), and the anode part proceeds with oxygen evolution reaction (OER) or oxidation of some chemical fuels [2]. In the past several decades, the electrocatalysis of OER has been extensively studied and various catalysts have been designed to improve electrode kinetics and stability under different electrolyte environments [3].

Metal-organic frameworks (MOFs) have attracted the attention of researchers in many fields such as gas storage and isolation, sensing, biomedical applications, energy conversion and storage devices, as well as in electro catalysis. Many features such as low cost, availability of organic linkers and transition metals [2], facile synthetic scheme, robust nature [3], high porosity [4,5], chemical and thermal stability [6,7], huge surface area and conductive nature make MOFs a promising candidate for electrocatalytic applications [4,5]. Recently, the incorporation of second metal ions into the nodes of frameworks for the synthesis of bimetallic MOFs has been proposed to boost the catalytic, electronic, and luminescence properties [6]. These particular types of MOFs involve the integration of two dissimilar metal ions into the same structure, to form bimetallic MOFs, which imparted MOFs, an enhanced structural stability and improved performance [7,8]. Furthermore, sulfur-containing nanomaterials, have gained a great reputation in the electrochemical sensing field owing to their good electrical conductivity and rich redox species [9].

In this work, MOF-derived Co_2CuS_4 nanostructures have prepared and studied for electrochemical catalysis of OER in alkaline environment.

2. Experimental

2.1. Materials

Cobalt(II) nitrate hexahydrate (Merck, 98%), copper(II) acetate (Merck, 99%), potassium hydroxide (Merck, 99%), 2-methylimidazole (Sigma, 99%), thioacetamide (Merck, 99%), and double-distilled water have used in this work.

2.2. Instruments

SAMA 500 potentiostate-galvanostate (Iran), Sharif Solar iRASOL EIS-27 (Iran), and Philips PW1730 X-ray diffractometer with Cu Kα radiation (The Netherlands) have employed in this research.

2.3. Methods

2.3.1. Synthesis of CoCu-MOF

First, 439.063 mg of cobalt(II) nitrate hexahydrate along with 108.97 mg of copper(II) acetate were mixed with 25 mL of methanol (solution A). As well, 985.2 mg of 2-methylimidazole was mixed with 25 mL of methanol (solution 2). Then solution A was dropwise added to solution B and the purple colored suspension

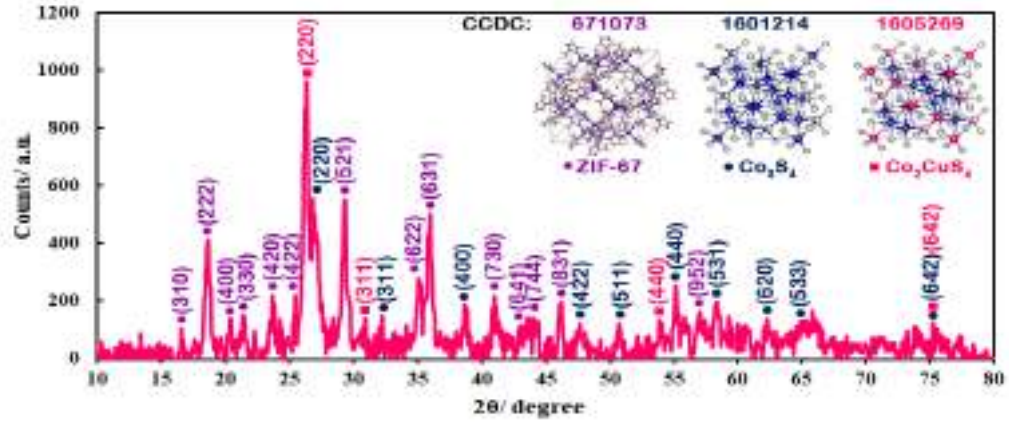

Fig. 1. XRD pattern of MOF-derived Co_2CuS_4.

was stirred under a magnetic stirrer for 24 h at room temperature. The product was collected by centrifugation, washed with water, and dried at 60 °C for 1 h.

2.3.2. Synthesis of MOF-derived Co_2CuS_4

Sulfidation was taken place in a reflux system. First, 44 mg of CoCu-MOF was dispersed in 15 mL of ethanol and sonicated for 2 min (solution 1). Simultaneously, 200 mg of thioacetamide dispersed in 5 ml of double-distilled water (solution 2). Then, solution 1 was added to solution 2, and was refluxed for 12 min. The obtained sediment was centrifuged, washed with ethanol, and dried at 60 °C for 1 h.

2.3.3. Electrode preparation and electrochemical measurements

Glassy carbon electrode (GCE) was modified by as-synthesized Co_2CuS_4 nanomaterials and was used as the working electrode. In this regard, 2 mg Co_2CuS_4 was dispersed in 1 mL distilled water and was sonicated for 1 h. Then, 3 μL of the suspension was drop-casted on GCE and dried at room temperature. The electrochemical studies were performed in a three-electrode cell containing Ag/AgCl (KCl_{sat}) as reference electrode, Pt wire counter electrode, and 0.1 M KOH electrolyte. All the reference potentials were converted into the reversible hydrogen electrode (RHE), using equation (1):

$$E_{RHE} = E_{(Ag/AgCl)} + 0.059 \times pH + 0.197\ V \quad (1)$$

and the overpotential (η) was calculated by equation (2):

$$\eta = E_{RHE} - 1.23\ V \quad (2)$$

without iR compensation correction.

3. Results and discussion

MOF-derived Co_2CuS_4 was characterized by X-ray diffraction (XRD) technique. According to Fig. 1, the XRD pattern of Co_2CuS_4 matches the reference patterns of Co_2CuS_4 (CCDC 1605269) with crystalline planes reflected at 2θ of 26.3° (220), 30.8° (311), 53.8° (440), and 75.3° (642). Since the resource MOF contained 4:1 molar ratio of Co:Cu ions in the ingredients, it is acceptable to find Co_3S_4 in the corresponding MOF-derived sulfide material. The crystalline planes of Co_3S_4 have appeared by peaks at 26.7° (220), 32.2° (311), 38.6° (400), 47.6° (422), 50.7° (511), 53.8° (440), 58.3° (531), 62.2° (620), 65.1° (533), 75.3° (642), CCDC 1601214 [10]. The pattern has also shown that not all the MOF resource has converted into sulfides in the synthetic conditions, and an amount of it has remained in the final product. The reflection peaks at 16.5° (310), 18.6° (222), 20.3° (400), 21.3° (330), 23.6° (420), 25.4° (422), 29.2° (521), 35.0° (622), 35.9° (631), 40.9° (730), 43.0° (641), 43.6° (744), 46.2° (831), 57.0° (952) belong to the ZIF-67 crystal structure (CCDC 671073) [11], so-called Co-MOF.

According to the Scherrer's equation [12]:

$$D_{hkl} = \frac{K\,\lambda}{\beta\,Cos\theta} \quad (3)$$

where, K, λ, β, and θ are crystalline shape coefficients (0.9), Cu Kα irradiation wavelength (1.5406 Å), FWHM, and the Bragg's angle, respectively. The crystallite diameter (D_{hkl}) of Co_2CuS_4 was calculated about 28 nm along the (220) plane.

The as-prepared MOF-derived Co_2CuS_4 was further dispersed in water and drop-casted on GCE to enhance its electrocatalytic behavior toward OER in 0.1 M KOH. In this regard, Fig. 2A shows the linear sweep voltammograms of GCE and GCE/Co_2CuS_4. The study has shown that the electrocatalytic performance of GCE has hugely enhanced after modification by Co_2CuS_4. The corresponding electrode has shown the lowest overpotential of 352 mV at the current density of 10 mA cm^{-2}. The electrode has provided the highest maximum current density of 391 mA cm^{-2}, benefiting from the high porosity and large surface area of the MOF precursor (e.g., ZIF-67), as well as the optimized electronic properties by copper

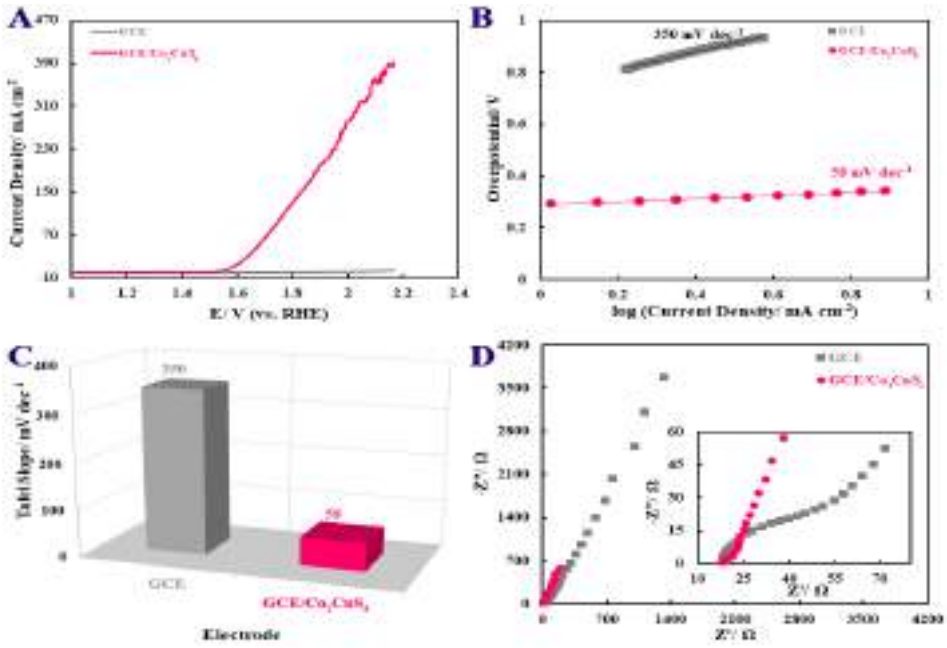

Fig. 2. (A) LSV curves, **(B)** Tafel plots, **(C)** Tafel slope comparing graph, and **(D)** Nyquist plots of GCE and GCE/Co_2CuS_4 in 0.1 M KOH electrolyte.

doping [13]. To evaluate the OER kinetics, Tafel plots (Fig. 2B) were obtained from the linear region of the corresponding LSV curves, according to the Tafel equation:

$$\eta = b \log j + a \quad (4)$$

where *j* stands for the current density and the b signifies the slope of the Tafel plot. Typically, the smaller b is, the faster j grows [13]. The column graph in Fig. 2C compares the great difference in the Tafel slope of bare and modified GCE, where GCE/Co_2CuS_4 with the lowest Tafel slope of 58 mV dec^{-1} shows 83% superior performance.

Electrochemical impedance spectroscopy (EIS) was carried out in the frequency range from 100 kHz to 0.1 Hz at the electrodes in KOH medium. The Nyquist plots in Fig. 2D reveal that the $CoCuS_4$ nanostructure decreases the resistance of GCE. As shown in Fig. 2D inset, the semicircle in the high-frequency reagon of GCE plot, relating to the value of charge transfer resistance (R_{CT}), was broader than that of GCE/Co_2CuS_4. This implies the improved electron transfer rate at the interface of electrode/electrolyte by the MOF-derived binary metal sulfide, further approving the enhanced electrocatalytic activity toward OER.

4. Conclusions

In this work, Co_2CuS_4 nanostructures have used to modify GCE for the electrocatalysis of the water oxidation process. Taking CoCu-MOF as a template, the Co_2CuS_4 nanostructures were synthesized by a facile reflux strategy. The product was further subjected to electrochemical studies for modification of GCE. The Co_2CuS_4 electrode provided the overpotential of 352 mV at 10 mA cm^{-2}, the maximum current density of 391 mA cm^{-2}, and the Tafel slope of 58 mV dec^{-1}, which were 83% better than the bare GCE performance for electrocatalysis of OER. The study indicates that the Co_2CuS_4 nanostructures reduce the charge transfer resistance of GCE, suggesting its high potential for application in water-splitting systems or metal-air batteries.

5. References

[1] N.-T. Suen, S.-F. Hung, Q. Quan, N. Zhang, Y.-J. Xu and H. M. Chen, Chem. Soc. Rev. 46 (2017) 337-365.

[2] H. Shi, Y.-T. Zhou, R.-Q. Yao, W.-B. Wan, X. Ge, W. Zhang, et al. Nat. Commun. 11 (2020) 2940.

[3] R. Frydendal, E. A. Paoli, B. P. Knudsen, B. Wickman, P. Malacrida, I. E. Stephens, et al. ChemElectroChem 1 (2014) 2075-2081.

[4] Q. Shao, J. Yang, X. Huang, Chem. Eur. J. 24 (2018) 15143-15155.

[5] X. Li, Y. Liu, J. Wang, J. Gascon, J. Li, B. Van der Bruggen, Chem. Soc. Rev. 46 (2017) 7124-7144.

[6] X. Yang, Q. Xu, Cryst. Growth Des. 17 (2017) 1450-1455.

[7] Y. Jiao, J. Pei, D. Chen, C. Yan, Y. Hu, Q. Zhang, et al. J. Mater. Chem. A 5 (2017) 1094-1102.

[8] M. Y. Masoomi, A. Morsali, A. Dhakshinamoorthy, H. Garcia, Angew. Chem. 131 (2019) 15330-15347.

[9] L. Wang, J. Wang, L. Yan, Y. Ding, X. Wang, X. Liu, et al. ACS Sustain. Chem. Eng. 10 (2022) 17230-17240.

[10] D. Lundqvist, A. Westgren, Z. anorg. allg. Chem. 239 (1938) 85-88.

[11] R. Banerjee, A. Phan, B. Wang, C. Knobler, H. Furukawa, M. O'Keeffe, O.M. Yaghi, Science 319 (2008) 939-943.

[12] P. Scherrer, Nachr. Ges. Wiss. Göttingen. 2 (1918) 98−100.

[13] D. Liu, X. Hui, W. Cheng, S. Hongyuan, Y. Rui, W. Yuan, L. Jie, L. Xingchi, D. Yukou, Inorg. Chem. 60 (2021) 5882-5889.

29TH IRANIAN ORGANIC CHEMISTRY CONFERENCE
1_3 NOV, 2023
UNIVERSITY OF QOM, IRAN

One-pot Synthesis of 1,3,5,7-tetracetyl-1,3,5,7-octahydroazocine (TAT) using Simple and Available Methodes

*Mostafa Amiri**

Department of Chemistry, Faculty of Science, University of Sayyed Jamaleddin Asadabadi (SJAU), Asadabad, Hamadan, Iran, m_amiri1360@yahoo.com.

Abstract - Energetic materials, including explosives, propellants, gunpowder and so on, have attracted more and more attention and been widely used in military and civil fields. Despite intensive research for possible replacements, TAT (1,3,5,7-tetracetyl-1,3,5,7-octahydroazocine) is still considered to be one of the most important energetic materials because of its versatile application. Due to the high demand for TAT, optimization of synthesis and development of new methods are of great interest to both academia and industry. Therefore, in this work, the synthesis of TAT via the intermediate DAPT (1,5-diacetyl-1, 3, 5, 7-tetraazabicyclo (3,3,1) nonane) was investigated as a possible alternative industrial production methods. TAT (1,3,5,7-tetracetyl-1,3,5,7-octahydroazocine) is an intermediate in a noval process for the production of the important military explosive HMX (1,3,5,7-tetranitro-1,3,5, 7-octahydro- tetazocine)[4-5]. This paper reports a new procedure for preparing TAT from hexamine in a one-step process without the separation of DAPT (1,5-diacetyl-1, 3, 5, 7-tetraazabicyclo (3,3,1) nonane).

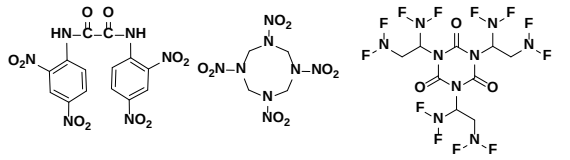

Fig.1. Some explosive materials

1. Introduction

The use of high-energy materials, especially explosives in the military and civilian fields, and as a result, the exposure of these materials to various initiators and the possibility of their explosion is inevitable [1-4. The need to develop energetic materials with high performance and greater stability to heat has made thermally stable explosives materials to the priority of research for the development of energetic materials. Heat resistant explosive materials in today's application programs In the field, military, civilian, space, etc., they are safer, more reliable and more stable at higher temperatures. For example; TNO stands for 2,4,2,4-tetranitro-oxanilide. This substance is fairly stable, being able to resist shock, friction, and heat. It is primarily used as a component in pyrotechnical devices or in gunpowder formulations. It was first prepared in 1892 when A.G. Perkins heated oxanilide powder in nitric acid [5]. DTT This explosive seems somewhat complected to synthesize because of the necessity for a pressurized reaction vessel, it can be done however. This material is insensitive to friction and heat as well as being rather hard to detonate from shock. This substance has found uses as both an explosive and as a rocket propellent. One of the nifty things about this material when it is being used as a propellent is the ability for the motor to be stopped and restarted when needed, this is usually the domain of liquid propellents.

The use of explosives in the field of deep-earth oil well drilling is limited due to the internal heat of the earth and the heat resulting from friction and as a result a sudden explosion. Also, in the aerospace industry and air-to-ground missiles, on the contrary, due to the friction and heat produced, the explosives are activated and do not work properly. Therefore, these industries need explosives with higher thermal stability such as TNO, DTT and HMX (fig.1). Based on this, the need to use explosives for high-speed missile warheads, drilling oil and gas wells, avalanche control, seismic tests and fire extinguishing has led to the production of a group of explosives called heat-resistant explosives.

The purpose of this research project was to develop novel synthetic approaches to 1,3,5,7-tetraacetyl-l,3,5,7-octahydrotetrazocine abbreviated "TAT" [5-8]. TAT is an effective intermediate for preparing HMX. It is nitrolyzed to HMX in good yields[5-6]. Among various improved methods, the nitration of 1,3,5,7-tetraacetyl-1,3,5,7-tetraazacyclooctane (TAT) attracts a great deal of attention due to its high yield and product purity [6c,7]. TAT was first prepared in 1940s [7], by heating DAPT with acetic anhydride containing a small amount of acetyl chloride as the catalyst, but the yield was very poor.

Since 1970s, many new processes for preparing HMX have been developed, the synthesis of TAT has again become a project for people to explore. As a result, many reports about it have constantly been published

[8]. Among others, the procedure suggested by V. I. Siele [6,7] is comparatively practicable..

2. Results and discussion

In a continuation of our interest in the application of 1,3,5,7-tetraacetyl-l,3,5,7-octahydrotetrazocine abbreviated (TAT) [5-8], in energetic materials synthesis, [1-12], we wish to report here a facile and improved protocol for the preparation of TAT using hexamine (Scheme 1, 2)

One-pot Synthesis of TAT form Hexamine

The predicted results were obtained by our experiments and the procedure is also considerably simplified. Further, in order to reduce the consumption of acetic anhydride and increace the yield as well as purity of TAT, we furthermore studied the reactions of TAT formation from hexamine (scheme 1) and that of TAT from DAPT (scheme 2).

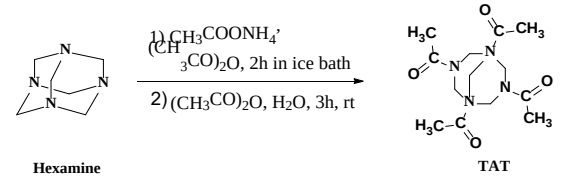

Scheme 1.

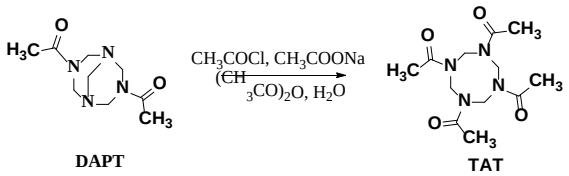

Scheme 2.

TAT Formation from DAPT

We have developed a new procedure for preparing TAT from hexamine without separation of DAPT. By our procedure TAT has been prepared in a higher yield, higher purity and lower consumption of acetic anhydride. The reaction mechanism shows that the reactions in preparing TAT from DAPT undergo in different ways under an anhydrous or aqueous condition. In the presence and absence of water the reaction is shown in scheme 3.

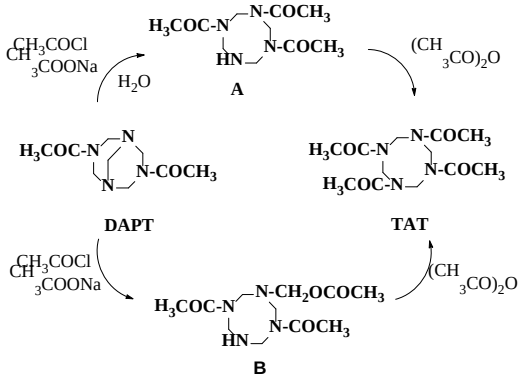

Scheme 3.

From these reactions, it is known that the reaction of TAT from DAPT would form an intermediate A or B, both of which have different structures, in spite of the presence or absence of water. The determination of reaction rate shows that the rates of both reactions are controlled by the stage of TAT formation. In the presence of water, TAT is formed from A, through the acetylation of secondary amine with higher reaction rate: and in the absence of water TAT is formed from B through acetolysis with lower reaction rate. About 2-3 days are required for completing the later reaction. Thus, in the TAT preparation from DAPT water is a necessary reagent to hasten the reaction.

If a certain amount of water is added during the course of reaction, it may be possible for part of acetic anhydride to be hydrolysed and the amount of acetic anhydride used is greater. The effect of amount of acetic anhydride used on the yield of TAT was obtained by our experiments and the results are shown in table 1.

Table 1: The effect of amount of acetic anhydride in the presence of water used on the yield of TAT

No:	DAPT: $(CH_3CO)_2O$ mol (%)	TAT yield (%)	TAT m.p. (ºC)
1	1: 5	98.0	161
2	1: 4	84.5	159-160
3	1: 3	70.5	160
4	1: 2	70.0	160-161
5	1: 1	55.0	159-161

It can be seen from table 1 that the yield is significantly decreased as the amount of acetic anhydride used is lowered. We have also found that when CH_3COONH_4 is used instead of water, the reaction rate can be promoted in a similar manner as that in the presence of water. NMR spectra show that CH_3COONH_4 has the tendency to combine with methylene fragments dissociated from DAPT to form new molecules of DAPT again, which provides a new approach for making better use of methylene group.

The reaction can be carried out in the absence of water when CH_3COONH_4 is employed and the amount of $(CH_3CO)_2O$ used is thus greatly lowered. In the presence of CH_3COONH_4, the effect of the amount of $(CH_3CO)_2O$ used on the yield of TAT is shown in table 2.

Table 2. The effect of amount of acetic anhydride in the presence of amonium acetate used on the yield of TAT

No:	DAPT: $(CH_3CO)_2O$ (mol%)	T(min)	TAT yield (%)	TAT m.p. (ºC)
1	1: 5	120	95.0	159-161
2	1: 4	120	90.0	158-159
3	1: 2	120	88.0	156-158
4	1: 2	120	88.0	159-160
5	1:1	120	88.0	158-159

It can be seen from table 2, in the presence of CH_3COONH_4, the reduction of the amount of

$(CH_3CO)_2O$ has very little effect on the yield of TAT. What's more, as there is no water in the reaction system, the excess of $(CH_3CO)_2O$ can be recovered by distillation and thus the practical amount of $(CH_3CO)_2O$ used is further lowered.

3. Conclusions

General procedure for synthesis of 1,3,5,7-tetraacetyl-l,3,5,7-octahydrotetrazocine (TAT)

28g (0.2 mol) of hexamine, 31g (0.4 mole) of ammonium acetate, 52 g (0.64 mole) of anhydrous sodium acetate and 80 ml of acetic acid are charged into a 100 ml round bottomed three necked flask, and the contents are cooled between 5-10 °C with an icebath. To the stirred mixture 50-60 ml of acetic anhydride are added dropwise at 10°C . The resulting mixture is stirred for 90 min and 0.6 mole of acetyl chloride and 70 ml of acetic anhydride are then added dropwise with vigorously stirred. The reaction continues while stirring for 2 hours at 20°C and then 2 ml distilled water was added to the mixture reaction. The filtrate is distilled and the residue is washed with a little water and dried, giving 60 g of TAT, yield 98%, m.p. 160-161 °C.

General procedure for synthesis of DAPT (1,5-diacetyl-1, 3, 5, 7-tetraazabicyclo (3,3,1) nonane) (DAPT)

Measure out 28g (0.2 mol) of 98% hexamine into a round bottomed 500 mL Florence flask. Place the flask into a salt-ice bath to provide cooling. While stirring rapidly, slowly add 31 g (0.4 mol) of ammonium acetate, while the temperature is maintained below 10 °C. After the addition of the ammonium acetate is completed (addition should take 90 min), the agitation is continued for 30 minutes, then 52 g (0.64 mole) of anhydrous sodium acetate and 80 ml of acetic acid are add into mixture reaction round bottomed three necked flask, and the contents are cooled between 5-10 °C with an icebath. The flask is now transferred to a water bath where the temperature is then raised to 50 °C over a period of 1 hour and maintained at 80-85 °C for 3 hours. The reaction mixture thus obtained was agitated at 5°-10°C. for 45 minutes and then filtered to remove chloroform insolubles. The filtrate was evaporated on a steam bath to an oil, and the oil was dissolved in 50 ml. of water and mixed with sufficient Na_2CO_3 to produce a solid mass. The solid was extracted with 300 ml. of chloroform and the extract was dried with anhydrous magnesium sulfate, filtered and evaporated to dryness. 10.8 grams of TAT melting at 159±2°C. were obtained, corresponding to 95% of theory yield. The DAPT is washed with 100 ml acetonitrile, then acetonitrile, dried in the air, and finally dried at 100-110 °C. Yield is 90-97% of the theoretical.

References:

[1] M.S. Klenov et al. Toward the synthesis of tetrazino-tetrazine 1,3,6,8-tetraoxide (TTTO): an approach to non-annulated 1,2,3,4-tetrazine 1,3-dioxides Eur. J. Org. Chem. (2015). Volume 2015, Issue 28, October 2015, Pages 6170-6179.

[2] Q. Ma et al. Pyrazol-triazole energetic hybrid with high thermal stability and decreased sensitivity: facile synthesis, characterization and promising performance Chem. Eng. J. (2020), Volume 379, 1 January 2020, 122331.

[3] X. Nie et al. Methylation of a triazole-fused framework to create novel insensitive energetic materials Energ. Mater. Front. (2020). Energetic Materials Frontiers Volume 1, Issues 3–4, December 2020, Pages 165-171.

[4] S.-B. Feng et al. Comparative study on 1,2,3-triazole based azo- and triazene-bridged high nitrogen energetic materials Energ. Mater. Front. (2021). Energetic Materials Frontiers Volume 2, Issue 2, June 2021, Pages 125-130.

[5] A.G. Perkins heated oxanilide powder in nitric acide, 1982; W. E. Bachmann, E. L. Jenner, 1-Acetoxymethyl-3,5,7-trinitro-1,3,5,7-tetrazacyclooctane and its Reactions. Significance in the Nitrolysis of Hexamethylenetetramine and Related Compounds, J. Am. Chem. Soc.¬ 1951, 73, 2773–2775.

[6] M. H. Xi, Preparation of HMX from DPT by using Polyphosphoric Acid, Chin. J. Energ. Mater. 1996, 4, 57–61.

[7] Linstead, R. P., O.S.R.D. 950, October, 1942.

[8] C. L. Coon, Preparation of Octahydro-1,3,5,7-tetraalkanoyl-1,3,5,7-tetrazocines, US Patent 3978046, The United States of America as Represented by the Secretary of the Army, Washington, DC, USA, 1976.

[9] Q. X. Li, P. Wang, Z. L. Lou, Y. Liu, Z. H. Meng, Z. B. Xu, M. Xue, Separation of Key Intermediates in the Synthesis of 1,3,5,7-Tetranitro-1,3,5,7-tetrazocine by Semi-preparative High Performance Liquid Chromatography, Chin. J. Org. Chem. **2012**, 32, 165–168.

[10] M. Kaiser, HPLC Investigation of Explosives and Nitroaromatic Compounds with a Cyanopropyl Phase, Propellants Explos. Pyrotech. **1998**, 23, 309–312.

[11] Z. L. Lou, Z. H. Meng, W. J. Meng, P. Wang, Separation of TAT and TRAT Using HPLC, Chin. J. Energ. Mater. 2010, **18**, 226–228.

[12] B. Dejaegher, D. Mangelings, Y. V. Heyden, Method Development for HILIC Assays, J. Separation Sci. 2008, **31**, 1438–1448; b) M. Xue, Z. Lu, Y. Wu, S. K.

29TH IRANIAN ORGANIC CHEMISTRY CONFERENCE
1_3 NOV, 2023
UNIVERSITY OF QOM, IRAN

Solvent-free synthesis of novel adamantane-containing dihydropyrimidines derivatives

Adeleh Moshtaghi Zonouz, Mina Abkar Aras*

Department of Chemistry, Faculty of Science, Azarbijan Shahid Madani University, Tabriz, Iran, adelehmz@yahoo.com, m86.abkar@gmail.com

Abstract Dihydropyrimidines incorporating an adamantane motif have been synthesized using three-component Biginelli reaction of adamantane-containing β-keto amide N-1-adamantyl acetoacetamide as active methylene compound, thiourea, and aromatic aldehydes under solvent-free conditions with high yields. The structures of the synthesized compounds were confirmed by spectral data (FT-IR, ^{1}H and ^{13}C NMR).

1. Introduction

Diamondoids, which resemble parts of the diamond lattice, are cage saturated hydrocarbon molecules that can be described as hydrogen-terminated nanodiamonds [1]. Adamantane, $C_{10}H_{16}$, is the smallest diamondoid that isolated in 1933 from crude oil and synthesized chemically for the first time in 1941 by Prelog and Steinwerth. Then Schleyer reported simple and inexpensive Lewis acid-catalyzed rearrangement of *endo*-trimethylenenorbornane to adamantane [2]. After Schleyer's synthesis, the study of adamantane and its functionalization became widely available, and syntheses of adamantane derivatives started fueling pharmaceutical studies thereof. 1-Aminoadamantane (Amantadine), a well-known antiviral drug, has been used to treat type A *Influenza* [3]. Antiviral activity of this amine was found gainst *Rubella* viruses thereafter [4]. Amantadine and the aminoadamantane antivirals constitute the birth of medicinal chemistry of adamantane derivatives. Other targets for pharmaceuticals featuring this symmetrical "bullet" hydrocarbon were successfully identified. Until now eight drugs incorporating the adamantane moiety have been approved and are existing in the pharmaceutical market (Fig. 1). These drugs are used for treatment of acne [5], Parkinson [6], Alzheimer [7], influenza A and diabetes' s disease [8]. Today adamantane motif is used mainly as an "add-on" to known pharmaceuticals for modification of known drugs. The incorporation of the adamantyl moiety into the known pharmacologically-active molecules resulted in many cases improving pharmacological properties of these compounds, without increasing their toxicity. So "add-On" strategy resulted in many promising drug candidates incorporating an adamantane moiety [9]. Size, lipophilicity, rigidity and biocompatibility of this spherical paraffine make it special for modification of known drugs. On the other hand, the trend of larger molecules being exploited as pharmaceuticals.

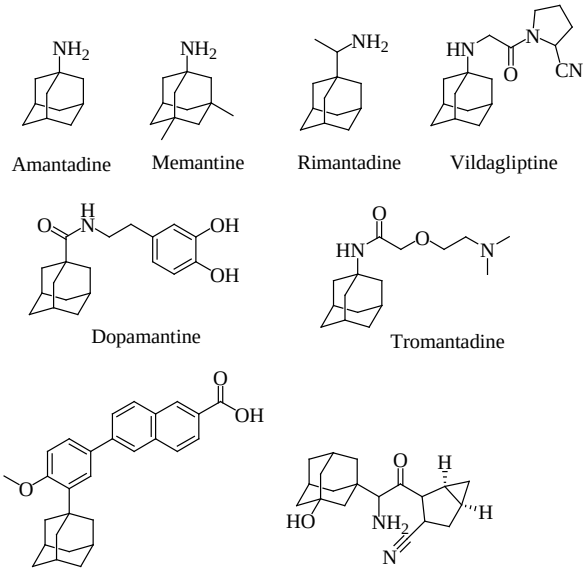

Fig.1.The eight drugs incorporating the adamantane motif.

The synthesis of dihydropyrimidinone derivatives (DHPMs) was first reported in 1893 by Italian chemist Pietro Biginelli via acid-catalyzed three-component reaction of aromatic aldehydes, ethyl acetoacetate and urea or thiourea in protic solvents (Scheme 1) [10]. This reaction is known as Biginelli pyrimidone synthesis or Bigenelli reaction.

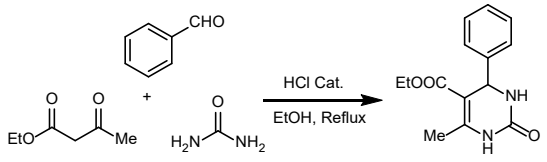

Scheme **1.** Classical Biginelli reaction

The Biginelli products, namely dihydropyrimidones (DHPMs), are regarded as one of the most important groups of drug-like scaffolds. A

number of dihydropyrimidinone derivatives are medicinally important as calcium channel blockers [11], antihypertensive agents [12], α_{1a}-adrenergic antagonists, mPGES-1 inhibitors, A_{2B} receptor antagonists [13]. Other biological activities associated with DHPM derivatives are antiviral, antibacterial [14], antifungal, anti-inflammatory[15], antitumour, antiparasitic, antimalarial [16], antidiabetic, antitubercular, antiepileptic, antimuscarinic, antileishmanial, antithyroidic, hypolipidemic, antiproliferative activities. The pharmacological activities associated with DHPM derivatives were recently thoroughly reviewed. DHPMs are also found in bioactive natural products such as marine alkaloids including crambescidins, batzelladines, and monanchocidins.

Because of the incorporation of the adamantyl moiety into the known pharmacologically-active molecules resulted in many cases improving pharmacological properties of these compounds, we are interested to praper adamntane-containing Biginelli products. Synthesis of C-5 and C-6 adamantylated pyrimidines have been previously reported. C-5 Adamantylated pyrimidines have been synthesized through adamantylation of aminopyrimidine, barbituric acid , and thiobarbituric acid in boiling trifluoroacetic acid [17] and C-6 adamantylated pyrimidine derivatives have been prepared based on the Traube reaction of 3-(adamantan-1-yl)-3-oxopropionic acid ethyl ester with urea, thiourea, guanidine and acetamidine, respectively[18]. Despite these findings, to the best of our knowledge, due to the sensitivity of the Bigenelli reaction to the sterically hindered reagents, there is only one report in which adamantane-containing active methylene compounds have been used in the Biginelli reaction. Lashmanova et al. have been obtained adamantylated Biginelli products with the poor yields of 6-35 % using trimethylsilyl chloride promoted Biginelli reaction of adamantane 3-oxonitrile and adamantane 1,3-dicarbonyl compounds, as active methylene compounds, aromatic aldehydes, and thiourea [19].

Nowadays, the green process for preparing biologically active materials from small and commercially available compounds is one of the ultimate goals and challenges in ecofriendly synthetic methodologies.

Many organic solvents are potentially toxic to the ecosystem, and their use should be minimized as far as possible or even replaced with green solvents.

We describe here the synthesis of Biginelli products incorporating an adamantane motif using a three-component Biginelli reaction of adamantane-containingβ-keto amide as active methylene compound, thiourea, and aromatic aldehydes with high yields under solvent-free conditions.

2. Results and Discussion

According to the Biginelli reaction, N-adamantyl substituted ureas/thioureas, or adamantyl-containing active methylene compounds could be used to introduce the adamantyl pharmacophore to the 3,4-dihydropyrimidin-2(1H)-one structure of Biginelli products.

We decided to employ adamantane-substituted active methylene compound as substrate. Accordingly, *N*-1-adamantyl β-keto amide **1** was prepared in 95 % yield by nucleophilic amidation of ethyl acetoacetate with 1-adamantylamine in the presence of a catalytic amount of triethylamine in refluxing toluene under an argon atmosphere (Scheme 2) [20]. The structure of N-1-adamantyl acetoacetamide was confirmed by spectral data (FT-IR, ^{1}H and ^{13}C NMR). Absence of the ester carbonyl frequency in IR spectrum provided definite proof for the amidation of ester group.

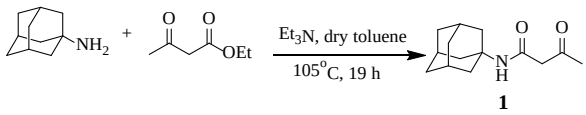

1

Scheme 2. Synthesis of N-(adamantan-1-yl) acetoacetamide

Moreover, the amide carbonyl (amide I band) appeared as a strong absorption band at lower wave number (1640 cm^{-1}) due to the resonance in the amide functional group, and also N-H stretching vibration give absorption band at 3315 cm^{-1}. The ^{1}H NMR spectrum of this compound confirmed amidation by the disappearance of ethoxy proton signals of ethyl acetoacetate and appearance of adamantyl proton signals at 1.60 (s, 6H, Ad), 1.92 (s, 6H, Ad), 1.95 (s, 3H, Ad) ppm, and the NH signal at 7.56 ppm.The ^{13}C NMR spectrum further confirmed the product by the presence of adamantyl carbon signals at 28.71, 36.01, 40.87, 52.29 ppm, and two carbonyl signals at 203.36 (C=O) and 165.33 (NH-C=O) ppm.

Then, three-component reaction of N-1-adamantyl acetoacetamide **1**, benzaldehyde derivatives, and thiourea was investigated.

To the mixture of N-(adamant-1-yl) acetoacetamide (235 mg, 1 mmol), benzaldehyde (0.1 mL, 1 mmol), and thiourea (76 mg, 1 mmol) was added TFA (4 μL, 2 mol %). The mixture was stirred at 50 ºC until completion of the reaction as indicated by TLC. The crude solid product was washed with water and recrystallized from EtOH (Scheme 3) [21].

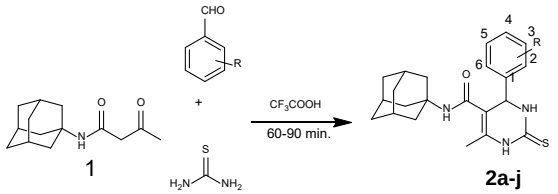

Scheme 3. Synthesis of 5-(1-adamantylcarbamoyl)−6-methyl-4-aryl-3,4-dihydropyrimidin-2(1H)-thiones **2** via Biginelli reaction

The structures of novel compounds were confirmed by ^{1}H NMR, ^{13}C NMR, and IR spectroscopy. For example, FT-IR spectrum of 5-(1-adamantylcarbamoyl)-6-methyl-4-phenyl-3,4-dihydropyrimidin-2(1H)-thione 2a confirmed the presence of the functional groups NH at 3396, 3244, 3173 cm^{-1}, the amide carbonyl (NH-C=O) as a strong absorption band around 1619 cm^{-1}, and C=S at 1203 cm^{-1}. The ^{1}H NMR spectrum of 5a displayed adamantane protons at 1.57 (s, 6H, Ad), 1.84 (s, 6H, Ad), 1.95 (s, 3H, Ad) ppm, the three NH protons at 9.73, 9.18, 7.01ppm, the C-H(4) and CH_3 protons at 5.21, and 1.94 ppm, respectively. The ^{13}C NMR spectrum further confirmed the product by the presence of amide carbonyl signal at 165.52 and C=S at 174.08 ppm. Presence of C=C signals at 108.48 and 143.16 ppm was another reason for confirming the formation of this product. The results are summarized in Table 1. Electronic effects of the substituents on the aromatic aldehydes have little influence on this reaction, and benzaldehydes with both the electron-withdrawing groups and electron-donating groups were well tolerated (compare entries 5-8 with entries 9, 10).

Table 2. Synthesis of pyrimidines **2** incorporating an adamantane moiety

Entry	R	product	Yield (%)	MP (°C)
1	H	**2a**	78	234-235
2	2-Me	**2b**	87	258
3	3-Me	**2c**	81	256
4	4-Me	**2d**	77	233
5	2-OMe	**2e**	78	234
6	3-OMe	**2f**	79	259
7	2-OH	**2h**[a]	85	>250
8	3-OH	**2i**	80	183-185
9	3-NO_2	**2g**	88	>270
10	2-Cl	**2j**	88	186-189

[a] **2h** is 8-oxa-10,12-diazatricyclo[7.3.1.0^{2,7}]tridecatriene derivative

3. Conclusion

In summary, we have developed for the first time a convenient and highly efficient add-on strategy to generate pyrimidines incorporating adamantane moiety. In order to introduce adamantane moiety in the pyrimidine skeletone, adamantylateted active methylene compound **1** was used in the three-component Biginelli reaction. We hope the size, rigidity and approximately spherical shape of adamantane as a lipophilic bullet can influence and modify the physico–chemical features of these pymidine-based scaffolds.

4. References

[1] A. A. Fokin, B. A. Tkachenko, P. A. Gunchenko, D. V. Gusev, P. R. Schreiner, Eur. J. Chem. 11 (2005) 7091.
[2] R. Von, P. Schleyer, J. Am. Chem. Soc. 79 (1957) 3292.
[3] W. Davies, R. Grunert, R. Haff, J. McGahen, E. Neumayer, M. Paulshock, J. Watts, T. Wood, E. Hermann, C. Hoffmann, Science. 144 (1964) 862.
[4] H. F. Maassab, K. W. Cochran, Science. 145(1964) 1443.
[5] S. Piskin, E. Uzunali, Ther. Clin. Risk Manag. 3 (2007) 621.
[6] R. S. Schwab, A. C. England, D. C. Poskanzer *et al*., *Jama*, 208 (1969) 1168-1170.
[7] S. A. Lipton, Nat. Rev. Drug Discov. 5 (2006) 160.
[8] A. Barnett, Int. J. Clin. Pract. 60 (2006) 1454.
[9] L. Wanka, K. Iqbal, P. R. Schreiner, Chem. Rev. 113 (2013) 3516.
[10] P. Biginelli, P. Gazz, Gazz. Chim. Ital. 23 (1893) 360.
[11] C. O. Kappe, Eur. J. Med. Chem. 35 (2000) 1043.
[12] K. S. Atwal, B. N. Swanson, S. E. Unger, D. M. Floyd, S. Moreland, A. Hedberg, B. C. O'Reilly, J. Med. Chem. 34 (1991) 806.
[13] R. Chikhale, R. Bhole, P. Khedekar, K. Bhusari, Eur. J. Med. Chem. 44 (2009) 3645.
[14] A. El Maatougui, J. Azuaje, M. Gonzalez-Gomez, G. Miguez, A. Crespo, C. Carbajales, L. Escalante, X. García-Mera, H. Gutierrez-de-Teran, E. Sotelo, J. Med. Chem. 59 (2016) 1967.
[15] T. N. Akhaja, Raval, J. P. Eur. J. Med. Chem. 46 (2011) 5573.
[16] S. S. Bahekar, D. B. Shinde, Bioorganic Med. Chem. Lett. 14 (2004) 1733.
[17] N. October, N. D. Watermeyer, V. Yardley, T. J. Egan, K. Ncokazi, K. Chibale, ChemMedChem: Chemistry Enabling Drug Discovery. 3 (2008)1649.
[18] B. Orzeszko, Z. Kazimierczuk, J. K. Maurin, A. E. Laudy, B. J. Starościak, J. Vilpo, L. Vilpo, J. Balzarini, A. Orzeszko, A. Farmaco Sci. 59 (2004) 929.
[19] E. A. Lashmanova, V. B. Rybakov, A. K. Shiryaev, Synthesis. 48 (2016) 3965.
[20] M. Abkar Aras, A. Moshtaghi Zonouz, Journal of Sulfur Chemistry. 4 (2023) 361-76.
[21] Typical Procedure: To a mixture of N-(adamant-1-yl)acetoacetamide **1** (235 mg, 1 mmol), benzaldehyde (0.1 mL, 1 mmol), and thiourea (76 mg, 1 mmol) was added TFA (4 µL, 2 mol %). The mixture was stirred at 50 ºC until completion of the reaction as indicated by TLC (60-90 min). The crude solid product was washed with water and recrystallized from EtOH. 5-(1-adamantylcarbamoyl)-6-methyl-4-phenyl-3,4-dihydropyrimidin-2(1H)-thione **2a**; mp 234-235 °C; IR (KBr): ῡ= 3396, 3244, 3173 (NH), 2906, 2848 (C-H), 1619 (C═O), 1331 (C-N), 1203 (C=S) cm^{-1}; ^{1}H NMR (DMSO-d_6, 500 MHz): δ = 1.57 (s, 6H, Ad), 1.84 (s, 6H, Ad), 1.94 (s, 3H, C=C-CH_3), 1.95 (s, 3H, Ad), 5.21 (CH), 7.10 (s, 1H, NH-C=O), , 7.20 (d, *J*= 8 Hz, 2H arom), 7.25 (t, *J*= 7.5 Hz, 1H arom), 7.33 (t, *J* =7.5 Hz, 2H arom), 9.18 (s, 1H, NH), 9.73 (s, 1H, NH) ppm. ^{13}C NMR (DMSO-d_6, 125 MHz): δ=16.2 (C=C-CH_3), 28.8 (3C-Ad), 36.0 (3C-Ad), 40.9 (3C-Ad), 51.2 (C-Ad), 55.4 (CH), 108.5 (=C), 143.2 (=C), 126.3 (C_2, C_6), 127.5 (C_4), 128.4 (C_3, C_5), 132.6 (C_1), 165.5 (C=O), 174.1 (C═S) ppm.

29TH IRANIAN ORGANIC CHEMISTRY CONFERENCE
1_3 NOV, 2023
UNIVERSITY OF QOM, IRAN

Polyoxometalate immobilized on graphene oxide as catalyst for the epoxidation of olefins

*Seyedeh Soghra Hossini Motlagh and Ali Zarnegaryan**

Department of Chemistry, College of Sciences, Yasouj University, Yasouj, 75918-74831, Iran, shosseini@yu.ac.ir, zarnegaryana@yu.ac.ir.

Abstract

The development of effective catalytic epoxidation processes that are an alternative to stoichiometric non-selective oxidation routes is important to meet environmental sustainability goals. In this work, a new, recoverable and heterogeneous catalyst was prepared by covalent attachment of the Polyoxometalates onto graphene oxide via the amide linkages. The catalytic activity of this catalyst was investigated in the epoxidation of olefins with tert-butyl hydroperoxide. The catalyst is of great reusability and stability in the epoxidation reactions. The result shows that hybrid catalyst base graphene oxide performed high activity in the benzimidazoles owing to the unique state of support of GO and the polyoxometalate.

Key words: Graphene oxide, Epoxidation of olefins, Anderson-type polyoxometalate

1. Introduction

Polyoxometalates (POMs) delegate an important class of anionic metal-oxide clusters typically architected from early transition metal polyhedra in corner-, edge- or face-sharing manners, with diverse nuclearities, sizes and shapes which encompass unique physicochemical properties (unique ligand properties, thermal stability, remarkable redox abilities, high negative charges) in catalysis, magnetism, medicine, magnetism, nanotechnology, materials science, etc and have been developed ingenious material candidates as an emerging class of molecular systems[1]. Polyoxometalates (POMs) are public oxidation catalysts that have received wide interest as a result of high activity in the presence of air or oxygen. The advantage of polyoxometalates as aerobic oxidation catalysts over other systems is their multifunctional active center, containing protons, atoms of oxygen, and metals. The use of POMs as catalysts in ODS has been formerly reported Polyoxometalates have six basic structures . As one of them, Anderson clusters can be functionalized with the tris(hydroxymethyl)aminomethane (TRIS) directly and then provide a platform for covalent modification with organic molecules with various functions. The Anderson-type heteropolyanions with the general formula $[H_y(XO_6)M_6O_{18}]n-$ (X is a transition-metal atom such as Ni, Co, Mn or Cr in a central octahedral cavity of the crown by edge-sharing six octahedral MO_6 and M is W or Mo), have received great interest because of their potential catalytic applications in selective oxidation . When X is Co or Ni, Anderson-type heteropolyanions has been the efficient catalysts in the hydrodesulfurization reaction [2].

Graphene and its derivatives have their own unique advantages and can be used in many domains such as energy storage, biosensing, optoelectronics, flexible electronics, electrochemical sensing, robotics, textile industry, and so on applying different techniques, such as self-assembly technique, solution dispersion technique, thermal chemical vapor deposition (CVD), spin coating, thermal decomposition, vacuum filtration, and chemical decomposition polymer processing technique [3]. The excellent electrical, mechanical, and optical properties of graphene as well as the ease of functionalization of its derivates have enabled graphene to become an attractive candidate for the construction of flexible devices. Graphene with a thickness of a single carbon atom is arranged in a honeycomb lattice. There is no bandgap in graphene, and it has poor water solubility, which greatly limits its application in some areas [3]. For example, treating graphite with strong oxidants will add epoxy groups, carboxyl group, and hydroxyl groups on the basal plan of graphite layers, thus producing graphene oxide (GO). GO is an oxidised form of graphene containing hydrophilic functional groups allowing for its easier solution processability in large quantities at low costs. These polar oxygen-containing functional groups make GO highly hydrophilic. This allows GO to have excellent dispersibility in many solvents, especially in water. Some of the most important advantages of using GO are its ability to be used as an additive during the fabrication of nanocomposite materials where pristine graphene cannot be used directly. Graphene, when used directly, undergoes considerable restacking mediated by π-π and hydrophobic-hydrophobic interactions between the sheets which results in

detrimental phase separation of graphene within the nanocomposite. The oxygen-containing functional groups (carboxyl, hydroxyl, carbonyl and epoxy) on GO provide ample stability to the sheets to allow improved incorporation and uniform distribution within the nanocomposite.

Alkene epoxidation is an momentous class of oxidation reactions that provides valuable chemical intermediates in the production of commodity chemicals, drug intermediates, perfumes, food additives and agrochemicals, among others that are considered one of the most critical intermediate chemicals in the field of industrial chemistry because of their high commercial importance. In the global market, the production of propylene oxide achieves 8 million tons per year with an expected yearly increase of 5%. Due to the industrial relevance of catalytic oxidation of olefins to fine chemicals, numerous studies have been devoted to the progress of impressive heterogeneous and homogeneous catalysts. Catalytic epoxidation of olefins in the presence of green oxidants is one of the most important methods for epoxidation of olefins. Due to this reason, various catalysts based on transition metal coordination compounds have been used for this transformation and among them high valent metal-oxido catalysts have possessed worthy attention by considering their high activity in catalytic oxidation reactions[4].

In this work, a new Anderson type POM $[(C_4H_9)_4N]_2[CrMo_6O_{18}]$ were synthesized and immobilized on the surface of GO to generate a supported catalyst via an easy synthesis method (Scheme 1). The hybrid catalyst was characterized and used for the epoxidation of olefins.

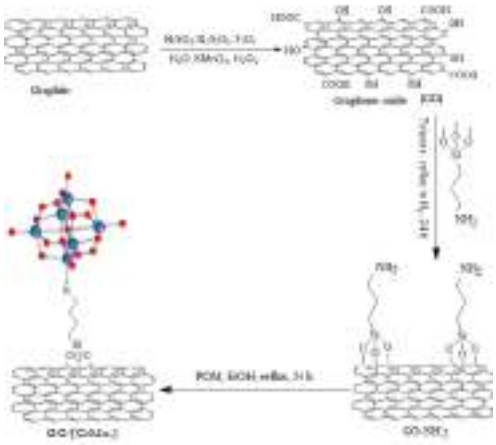

Scheme 1 Synthetic strategy for GO/$[CrMo_6]$

2. Results and discussion

Preparation and characterization of catalyst in brief, graphene oxide (GO) was prepared from oxidation of graphene powder by modified Hummer's method. Prior to the immobilization of the polyoxometalate catalyst, the POM was treated with TRIS. The GO- was reacted with polyoxometalate.

The thermal behavior of the GO/$[CrMo_6]$ was investigated by thermal gravimetric analysis (TGA), as illustrated in Figure. 1. The TGA plot of the catalyst demonstrates a three-step mass loss the around 25–650 ºC. The mass loss below 100 ºC is related to the removal of adsorbed water. The mass loss in the temperature at around 240 to 580 ºC has been attributed to the decomposition of aminopropyl functions and corresponds to removing residual organic groups.

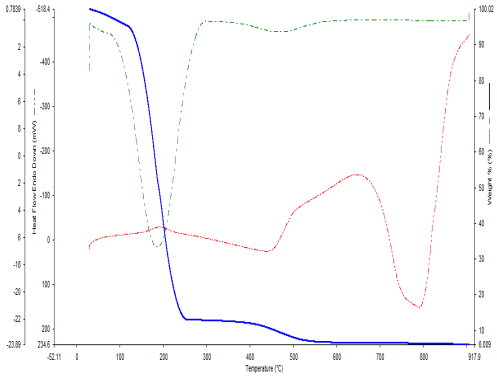

Figure 1. TG analysis of the GO/$[CrMo_6]$

3.1. Investigation of catalytic activity of GO/$[CrMo_6]$ in the epoxidation of olefins

Initially, the catalytic activity of the prepared catalyst was investigated in the epoxidation of cyclooctene using TBHP as a model reaction under different conditions. To find optimum reaction conditions, the influence of different factors that may affect the conversion and selectivity of the cyclooctene epoxidation was investigated. For choosing the reaction media, the model reaction was carried out in different. water and water using 0.5 mol% of the heterogeneous catalyst. The effect of reaction temperature was also investigated in the model reaction. The temperature showed remarkable effect on the epoxide yield. For optimization of the catalyst amount, different amounts of catalyst were used in the model reaction (Scheme 2).

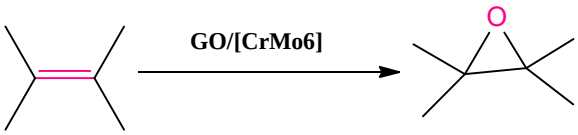

Scheme 2. Alkene epoxidation catalyzed by GO/$[CrMo_6]$

3.2. Recycling of the GO/$[FeMo_6]$

The reusability of catalyst was investigated in the sequential epoxidation of cyclooctene with TBHP. In

this manner, after each run, the catalyst was separated from the reaction mixture by simple filtration and washed with acetonitrile and ethanol, dried at 40 ^{o}C and used with fresh cyclooctene and TBHP. The results, showed that the catalyst could be reused four consecutive times without loss of its catalytic activity.

4. Conclusion

A novel heterogenized catalyst was prepared by covalent attachment of molybdenum Schiff base complex on the GO surface, and its properties were investigated. This catalyst was heterogeneously and effectively employed in epoxidation of olefins derivatives under reaction conditions. Other advantages of this catalytic system were the use of short reaction times, low catalyst loading, and the use of green solvent, easy recoverability, and high catalyst stability under applied conditions.

References

[1] S. Yanbin, Z. Jianfeng, X. Jiajia, Y. Kaixuan, Z. Zhiguo,S. Ting, G. Hui, R. Wanzhong, L. Hongying, An Anderson-type polyoxometalate triggers aerobic oxidation of 5-hydroxymethylfurfural to 2,5-diformylfuran, Fuel. 315 (2022) 123226

[2] J. Peng, W Huijuan , Z. Limin , W. Donghui, W. Yiqiang , Z. Bin, W. Xiangyu, L. Baojun, Anderson-type polyoxometalate as excellent catalyst for green synthesis of adipic acid with hydrogen peroxide, Mol. Catal, 510 (2021) 111705

[3] R. Aamir*, B. Faiza, Z. Xiaoxiao, P. Raffaello, S. H. M. Jafri, L. Hu, Review on Graphene-, Graphene Oxide-, Reduced Graphene Oxide-Based Flexible Composites: From Fabrication to Applications, Materials. 2022, 15(3) 1012

[4] H. M. A. Hassan, M. A. Betiha , E. A. El-Sharkawy, R. F. Elshaarawy , N. B. El-Assy, A. A. Essawy , A. M. Tolba , A. M. Rabie, Highly selective epoxidation of olefins using vanadium (IV) schiff base- amine-tagged graphene oxide composite, Colloids Surf, 591(2020) 124520

29TH IRANIAN ORGANIC CHEMISTRY CONFERENCE
1_3 NOV, 2023
UNIVERSITY OF QOM, IRAN

Activation of a carbonyl of H_2CO in Diels-Alder reaction by pnicogen bond donor

*Fereshteh Yaghoobi**

Nahavand Higher Education Complex, Bu-Ali Sina University, Hamedan, Iran, f.yaghoobi@basu.ac.ir.

Abstract - Density functional theory calculations have been used to study whether the AsS_2Br or PS_2Br as pnicogen-bond donors are capable of activating a neutral organic substrate. Therefore, the effect of AsS_2Br or PS_2Br on the Diels-Alder (DA) cycloaddition reaction between the H_2CO and cis-1,3−butadiene have been investigated. The effect of AsS_2Br or PS_2Br on the DA reaction via interaction between As or P atoms with O atom of H_2CO have been also studied. The relative Gibbs free energies for the reaction between the H_2CO and butadiene molecules in the presence and absence of AsS_2Br or PS_2Br were calculated. The results showed that the AsS_2Br decrease the activation energies of DA reaction studied here by 12.99 kcal/mol. The activation strain model (ASM) was used to more analyze the influence of the AsS_2Br and PS_2Br on the studied reaction.

1. Introduction

The noncovalent interactions including, hydrogen bonding, chalcogen bonding, halogen bonding and pnicogen bonding, can be able to activate organic substrates via relatively strong interactions, in Diels-Alder cycloaddition reactions. The pnictogen bonding, one of the newest members of noncovalent interactions is an attractive interaction between an electrophilic pnictogen atom (e.g., P or As) and a negative atom that in the last decades, has attracted the attention of researchers [1-3]. In recent years, several theoretical-investigations have been done on effect of pnictogen bonding in organocatalysis on Diels-Alder reactions. In 2017, Schmauck and Breugst reported the first theoretical study on applications of pnictogen bond in catalysis on Diels-Alder reactions, and showed that pnicogen-bond-donor catalyst might be comparable to halogen-bond-donor catalysts [4]. Also, Matile and colleagues in 2018 studies the catalytic activity of some noncovalent bonding and showed that catalytic activity from main group VII to V from row 3 to 5 increases in the periodic table [5]. Matile and colleagues reported pnictogen-bonding catalysis of Sb(V), Sb(III) and Bi, in 2020 [6]. Sun Zeng, and colleagues carried out the theoretical computation on catalytic activity of pnicogen bonds and showed that catalytic activity of pnicogen bonds are more than chalcogen bonds and halogen bonds. [7]. However, compared with the other noncovalent bonds, only limited studies have been performedon application and effect of pnictogen bonds in organo catalysis in Diels-Alder reactions. In our previous works we show that $PHCl_2$ and as well as the PO_2X (X=F, Cl, OH) as pnictogen bond donor, can act as a catalyst in activating the Hetro−Diels−Alder reaction [8,9]. In this work, we investigate the effect of AsS_2Br and PS_2Br on the free energy of Diels Alder reaction. The model DA reaction investigated in this work, in the presence of AsS_2Br shown in Fig.1.

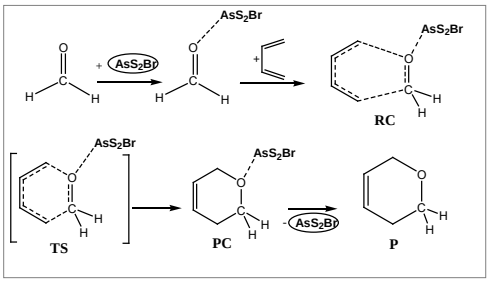

Fig.1. Model DA reaction used in this investigation in the presence of AsS_2Br.

2. Computational details

All the calculations were carried out using the Gaussian 09 package [10] at the M06-2X level of theory [11] using the TZVP basis set and also Chem3D Ultra software was used to draw the initial 3D structures of the optimized geometries. The harmonic vibrational frequency calculations for the optimized structures confirmed that the reactants and products structures do not have imaginary frequencies, and transition states have one imaginary frequency. The distortion-interaction energies of transition states using the activation strain model (ASM) [12] at M06-2X/TZVP level of theory were evaluated.

3. Results and Discussion

In order to investigation the effect of AsS_2Br or PS_2Br as pnicogen-bond donor in activating the H_2CO as a neutral substrate, DA reaction between H_2CO and cis-1,3-butadiene (Cbut) in the absence and the presence of AsS_2Br or PS_2Br was investigated. As can be seen in Fig.2, the H_2CO and Cbut interact with each other through the formation C…O and C…C bonding. In the presence of AsS_2Br or PS_2Br, the first step is the

formation of the interaction between AsS_2Br or PS_2Br and H_2CO via pnicogen bonding. After the formation of initial complex, the second step is the addition of Cbut molecule and then the reaction passes through the transition state and finally generates the six membered ring as product. The value of bond distances at the formed structures have been showed in Figure 2. The comparison of the above bond lengths for TS structures shows that in the presence of AsS_2Br or PS_2Br, the C…C bond lengths are relatively have decreased. In contrast, the C…O distance in TS complex in in the presence of AsS_2Br or PS_2Br have increased.

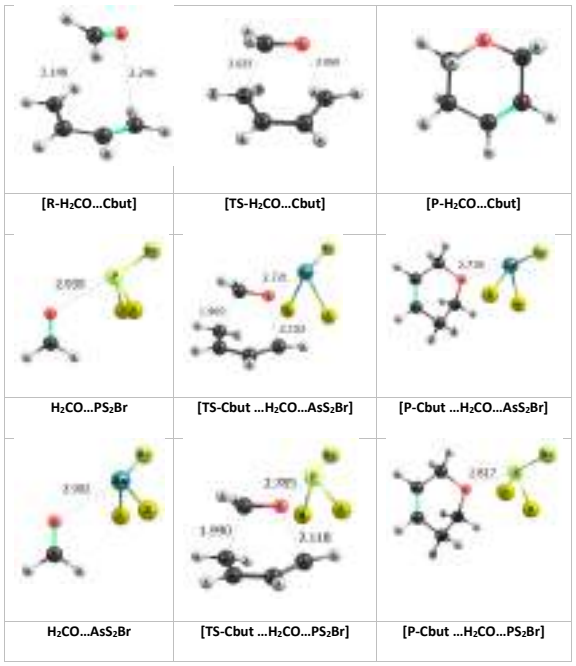

Fig.2. Optimized structures of the reactant complex, transition state and product between H_2CO and Cbut in the presence and absence of AsS_2Br or PS_2Br.

3.1. Energy Diagrams

In order to better understand the effects of AsS_2Br or PS_2Br on the DA reaction studied here, the pathways and relative Gibbs free energies were investigated. The pathways for the DA reactions in the absence of AsS_2Br or PS_2Br and relative Gibbs free energy profiles were displayed in Figure 3, in which the Gibbs free energies of [H_2CO + Cbut]were set to 0.0 kcal/mol as a reference. As can be seen, the reaction in the absence of pnicogen bond donors proceeds through the high-energy transition state (+33.86 kcal/mol) which can be expected for the combination of the H_2CO and Cbut. In the presence of AsS_2Br, the binding of the AsS_2Br to the O atom of the H_2CO lead to the stabilization of formed pair and the value of energy about -10.05 kcal/mol is released, but for the PS_2Br, this step is endothermic (+5.51 kcal/mol). In the next stage, the process of forming the TS for all structures are endothermic. Therefore, the process of forming the TS need to overcome an energy barrier of +20.87 and +37.41 for the AsS_2Br or PS_2Br respectively. The values of released energies upon the forming of the [P-Cbut…H_2CO…AsS_2Br] and the [P-Cbut…H_2CO…PS_2Br] are -48.52 and -49.24 kcal/mol, respectively. The final step, as can be seen in Fig.3, the formation of the product from the [P-Cbut…H_2CO…AsS_2Br] complex, is endothermic, but for the PS_2Br this step is exothermic.

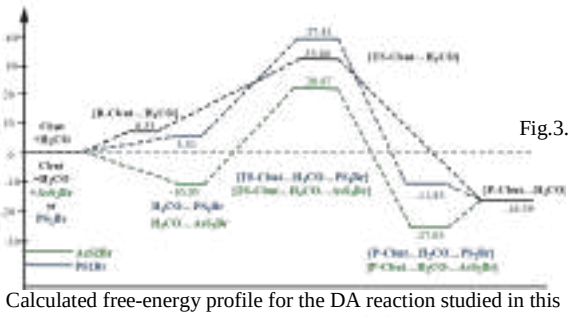

Fig.3. Calculated free-energy profile for the DA reaction studied in this work, in the absence and the presence of of AsS_2Br or PS_2Br.

3.2. Activation−strain analysis

We have analyzed the DA reaction studied here using the activation-strain model (ASM). In Fig.4, the blue and red arrows, demonstrate the interaction ($\Delta E^{\ddagger}_{int}$) and activation ($\Delta E^{\ddagger}$) energies, respectively. It is worth mentioning that the deformation (distortion) energies ($\Delta E^{\ddagger}_{dis}$) are broken into the distortion energies for Cbut, H_2CO and Pnicogen bond donor (AsS_2Br or PS_2Br), and are shown in black, orange and green colors. As can be seen in Fig.4, the lower activation energy is the result of a lower deformation energies that for AsS_2Br is -14.16.

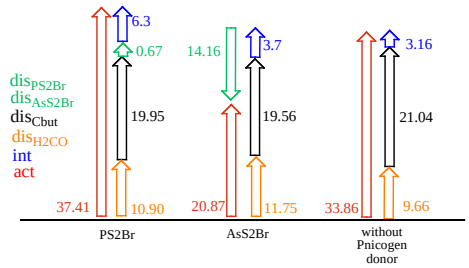

Fig.4. Plots of the distortion, interaction, and activation energies for the transition states of the DA reactions; orange, distortion energy of H_2CO; black, distortion energy of Cbut; green, distortion energy of AsS_2Br or PS_2Br; blue, interaction energy; red, activation energy.

.

4.Conclusion

The results show that in the presence of AsS_2Br the activation energiy of DA reaction studied here has decreased and in the presence of PS_2Br, activation energy has increased. The results of analyses using the activation strain model (ASM) showed that in the case of As as pnicogen bond donor, there is the negative deformation energy. Thus, the reaction proceeds

through the minimum amount of activation energy.

5. References

[1] S. Zahn, R. Frank, E. Hey-Hawkins, B. Kirchner, Pnicogen bonds: a new molecular linker? Chem. Eur. J. 17 (2011) 6034–6038.

[2] L. Guan, Y. Mo, Electron transfer in pnicogen bonds, J. Phys. Chem. A 118 (2014) 8911–8921.

[3] G. Sánchez-Sanz, C. Trujillo, M. Solimannejad, I. Alkorta, J. Elguero, Orthogonal interactions between nitryl derivatives and electron donors: pnictogen bonds, Phys. Chem. Chem. Phys. 15 (2013) 14310–14318.

[4] J. Schmauck, M. Breugst, The potential of pnicogen bonding for catalysis–a computational study, Org. Biomol. Chem. 15 (2017) 8037–8045.

[5] S. Benz, A.I. Poblador-Bahamonde, N. Low-Ders, S. Matile, Catalysis withpnictogen, chalcogen, and halogen bonds, Angew. Chem. 130 (2018) 5506–5510.

[6] A. Gini, M. Paraja, B. Galmés, C. Besnard, A.I. Poblador-Bahamonde, N. Sakai,A. Frontera, S. Matile, Pnictogen-bonding catalysis: Brevetoxin-type polyether cyclizations, Chem. Sci. 11 (2020) 7086–7091.

[7] Y. Li, L. Meng, C. Sun, Y. Zeng, Organocatalysis by halogen, chalcogen, and pnictogen bond donors in halide abstraction reactions: an alternative to hydrogen bond-based catalysis, J. Phys. Chem. A 124 (2020) 3815–3824.

[8] F. Yaghoobi, M. Sohrabi-Mahboub, Theoretical study on the Aza–Diels–Alder reaction catalyzed by $PHCl_2$ Lewis acid via pnicogen bonding, J. Phys. Chem. A 122 (2018) 2781–2791.

[9] F. Yaghoobi, S. Salehzadeh, Catalysis of the Nitroso–Diels–Alder cycloaddition reaction between $CH_3N{=}O$ and cis-1,3-butadiene by pnictogen bonding, a theoretical study, J. Mol. Graph. Model. 125 (2023) 108583.

[10] M. Frisch, G. Trucks, H. Schlegel, G. Scuseria, M. Robb, J. Cheeseman, G. Scalmani, V. Barone, B. Mennucci, G. Petersson, et al., Gaussian 09 Revision A. 1, 2009, Vol. 66, Gaussian Inc, Wallingford CT, 2009.

[11] Y. Zhao, D.G. Truhlar, The M06 suite of density functionals for main group thermochemistry, thermochemical kinetics, noncovalent interactions, excited states, and transition elements: two new functionals and systematic testing of four M06-class functionals and 12 other functionals, Theor. Chem. Acc. 120 (2008)215–241.

[12]D.H. Ess, K. Houk, Distortion/interaction energy control of 1, 3-dipolar cycloaddition reactivity, J. Am. Chem. Soc. 129 (2007) 10646–10647.

29TH IRANIAN ORGANIC CHEMISTRY CONFERENCE
1_3 NOV, 2023
UNIVERSITY OF QOM, IRAN

Chitosan Based Molecular Imprinted Polymer for Oxaliplatin Release

Fahimeh Farshi Azhar, Maryam Ahmadi and Leila Khoshmaram*

Department of Chemistry, Faculty of Basic Sciences, Azarbaijan Shahid Madani University, Tabriz, Iran, fahimeh.farshi@gmail.com,

Abstract - A selective chitosan-based molecular imprinted polymer (MIP) system was prepared for oxaliplatin using glutaraldehyde as a crosslinker. Also, graphene quantum dot (GQD) was synthesized by the pyrolysis of citric acid and incorporated into chitosan through electrostatic interactions and H-bonding. The CS MIP (without GQD) and nonimprinted polymer systems (NIPs) were prepared and used as controls. The synthesized systems were characterized by FTIR, XRD, and SEM. Then, the kinetic, isotherm and drug release studies were evaluated. According to the results, the first-order kinetic model and the Langmuir isotherm showed better agreement with the experimental data. The comparison of drug release in different pH (1.2, 7.4 and 10) showed that the CS-GQD MIP system is pH-sensitive and maximum release was obtained at acidic pH, where the accumulative release amount of drug was up to 80% within 8 h.

1. Introduction

In recent years, due to the prominent advantages, such as recognition ability, mechanical and chemical stability, and relatively ease and low cost of preparation, molecularly imprinted polymers (MIPs) have attracted much attention and have been used for several different applications, including solid-phase extraction, chemical sensors, drug delivery and biological antibodies. MIPs fully respond to the modern drug delivery system (DDS) requirements due to their ability to sustain the release of a therapeutic agent, enhance the loading capacity, intelligently release the therapeutic by responding to the environment, reduce systemic side effects, and improve the drug efficacy [1].

MIPs are synthetic materials with specific spatial structure and strength that are prepared through the molecular template technique (MIT). In this method, a template molecule is introduced into a mixture of monomer and crosslinker dissolved in a solvent and it is converted into a three-dimensional polymer matrix. After removing the template from the prepared polymer, the permanent holes of the main template produced in the polymer matrix are formed according to the shape, size and direction of the template molecules, which can selectively reconnect to the template molecules. A smart MIP-DDS can be achieved by using functional materials, including magnetic, pH-sensitive, temperature-sensitive, light-sensitive, and bio-macromolecule-sensitive materials [2].

Safety and biocompatibility considerations of MIP-based DDS are very important. Acrylic and methacrylic monomers have been widely used in various MIP applications. Zheng et al. [3] prepared a MIP system based on graft copolymer of chitosan with methyl methacrylate (MIP-CS-g-PMMA) by free radical polymerization with 5-fluorouracil (5-FU) as template molecule. However, the long-term toxicity of methacrylate needs further investigation. To avoid the risk of long-term toxicity, the use of natural biodegradable polymers can be considered [4]. Recently, chitosan has attracted the attention of researchers.

Chitosan, a biopolymer obtained by deacetylation of chitin, is the most abundant naturally occurring amino polysaccharide, possess several advantages such as non-toxicity, bioavailability, and biocompatibility. The presence of hydroxyl and amine groups in chitosan facilitates its modification. It can react with various crosslinking agents, such as aldehyde (glutaraldehyde), epoxide (epichlorohydrin) and acids (sulfuric acid), provides flexibility for the preparation of MIPs [5].

In the past decades, carbon-based materials have been widely used in biomedical fields. Among these materials, graphene quantum dots (GQDs) are attractive due to their biocompatibility, low toxicity, large surface area with delocalized electrons, and unique fluorescence properties [6]. Amjadi et al. [7] prepared MIP based on nitrogen-doped graphene quantum dots (MIP@NGQDs) and used them to detect the anticancer drug, doxorubicin. When potassium permanganate was injected into the MIP@NGQD solution, strong chemiluminescence (CL) emission was observed. While, in the presence of DOX, CL intensity was significantly reduced.

In this study, based on the molecular imprinting technique, a novel oxaliplatin delivery system has been successfully developed using CS-GQDs as matrix and oxaliplatin as the template. The synthesized MIPs were

thoroughly characterized. Moreover, kinetic, isotherm and in vitro drug release studies were evaluated.

2. Results and Discussion

2.1. Characterization

The results of FTIR analysis for pure and synthesized samples are shown in Fig. 1.

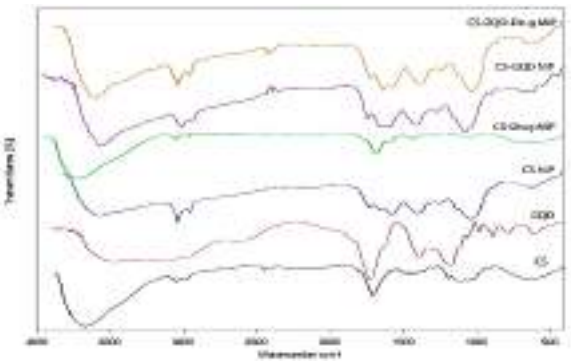

Fig. 1. FTIR spectra of samples

According to the results, in the FTIR spectrum of chitosan, the broad peak around 3600 cm^{-1} is related to NH and OH stretching vibrations. The bands at 2990 and 2881 cm^{-1} correspond to stretching vibrations of aliphatic CH, 1650 and 1560 cm^{-1} correspond to bending vibrations NH, 1423 and 1380 cm^{-1} correspond to CH methylene and methyl bending vibrations. In GQD spectrum, the band at 2925 cm^{-1} corresponds to C-H, 1766 cm^{-1} corresponds to C=O, 1577 cm^{-1} corresponds to C=C, and the band in 1384 cm^{-1} are related to O-H of oxygenated functional groups. In the spectra of CS-GQD composites, there is a weak peak around 1211 cm^{-1}, which is related to the formation of amide bond between graphene quantum dot and chitosan molecules. The spectra of CS NIP and CS MIP samples are similar and the spectra of CS-GQD MIP and CS-GQD NIP are similar and without drug characteristic peaks.

X-ray diffraction technique was performed on synthesized samples and the results are shown in Fig. 2.

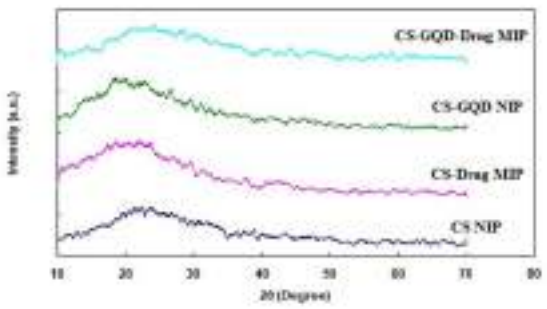

Fig. 2. XRD patterns of samples

According to literatures, GQD have a broad peak in the range of 2θ=15-25°. Also, there is a peak at 2θ=10° and a broad peak at 2θ=20° in the pattern of chitosan. In the XRD patterns of the synthesized samples, the broadness of the peaks and the decrease in their intensity indicate the formation of amorphous composites due to the interactions of graphene quantum dot and chitosan.

The results of the scanning electron microscope for the synthesized samples are shown in Fig. 3.

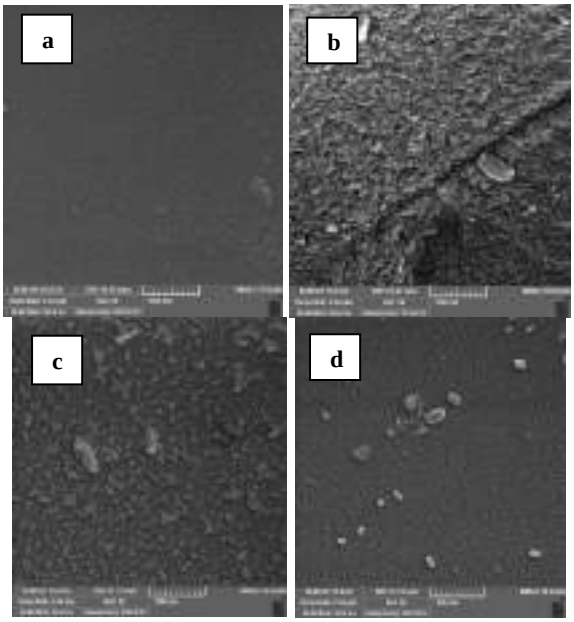

Fig. 3. SEM images of (a) CS NIP, (b) CS MIP, (c) CS-GQD NIP, (d) CS-GQD MIP

According to the CS NIP image, the surface of the sample is smooth and free of porosity, which shows that no drug has entered into the chitosan matrix. From CS MIP image, lumpy surfaces are observed, which indicates the interaction between chitosan and the drug and the release of the drug after washing. In the SEM image of the CS-GQD NIP sample, the presence of graphene quantum dot nanoparticles in the chitosan substrate is evident. The CS-GQD MIP sample show a smoother surface.

2.2. Adsorption studies

2.2.1. Kinetic

In this project, three first-order, pseudo-second order and second-order kinetic models were investigated, and the results are shown in Fig. 4.

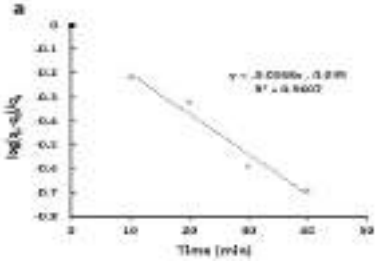

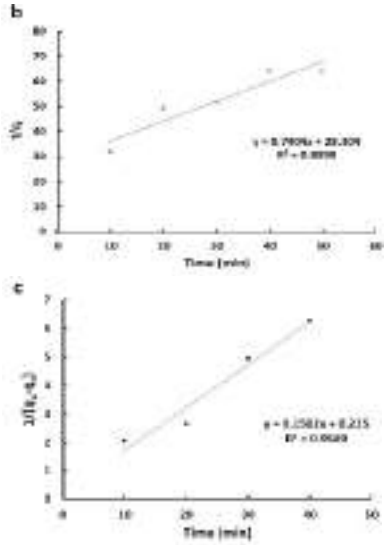

Fig. 4. Kinetic plots (a) first order, (b) pseudo-second order, (c) second order for adsorption of oxaliplatin by CS-GQD MIP

The results show that the kinetic data for CS-GQD MIP show better agreement with the first-order kinetic model. The correlation coefficient (R^2) and kinetic constant obtained are 0.9607 and 0.038, respectively.

2.2.2. Isotherm

The adsorption isotherm model is significantly important to investigate the interaction between the adsorbent and the adsorbate. Fig. 5 shows the adsorption equilibrium isotherm data using Langmuir and Freundlich isotherm models.

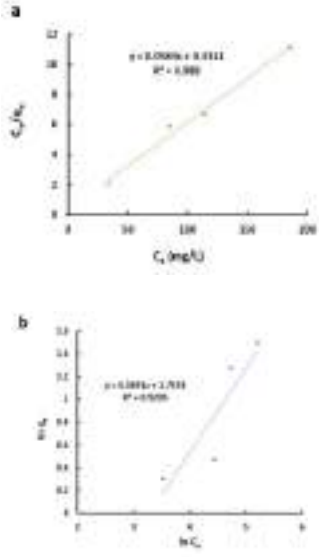

Fig. 5. Isotherm plots (a) Langmuir, (b) Freundlich, (c) for adsorption of oxaliplatin by CS-GQD MIP

According to the results, the appropriate isotherm model is the Langmuir model and the R_L value obtained from the Langmuir model is $0 < R_L < 1$ which confirmed the optimal absorption process.

2.3. In vitro drug release behavior

The pH-dependent drug release from the MIPs is very important in the clinical application, because cancer tissues, intracellular lysosomes and endosomes have an acidic environment, and the pH-dependent release behavior is for the local release of molecules. The profile of oxaliplatin release in different pHs (1.2, 7.4 and 10) are given in Fig. 6.

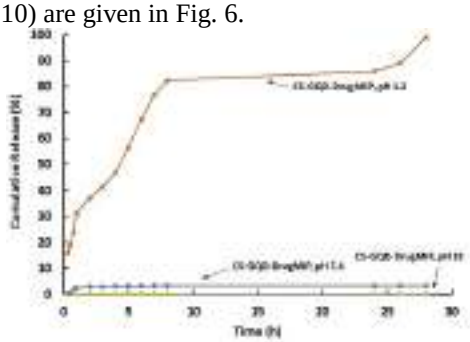

Fig. 6. The in vitro release profile of oxaliplatin from CS-GQD MIP at different pH

The results showed that the drug release did not take place at pH 7.4 and 10, but at pH 1.2 a controlled release was obtained (80% release within 8 h). The trapping of the drug in the mentioned system at neutral and alkaline pH is due to the interaction between different functional groups such as amine, hydroxyl and carboxyl, which limits the release of the drug. As a result, it is possible to use this sensitivity to pH in the body and deliver drugs to cancer cells through the CS-GQD MIP system.

3. Conclusion

In summary, CS-GQD were successfully fabricated by molecularly imprinting method using CS and GQDs as matrix and oxaliplatin drug as template. The adsorbability of CS-GQD MIP was much better than CS MIP and NIPs. The adsorption isotherms of CS-GQD MIP indicated that the adsorption behavior fitted better to the Langmuir model, which showed that the adsorption process was monomolecular layer. The results of in vitro drug release studies demonstrated that CS-GQD MIP exhibited an excellent controlled oxaliplatin release profile without burst release at acidic pH. Therefore, the application of pH-sensitive CS-GQD MIP in new intelligent drug delivery system will have a broad prospect.

4. References

[1] H. Chen, W. Zhang, N. Yang, C. Chen, M. Zhang, Appl. Biochemi. Biotechnol. 185 (2018) 370-384.
[2] S. He, L. Zhang, S. Ba, H. Yang, Z. Cui, X. Zhang, Y. Li, Eur. Polym. J. 143 (2021) 110179.
[3] X. F. Zheng, et al. Sci. Rep. 6 (2016) 21409.
[4] R. Liu, A. Poma, Molecules, 26 (2021) 3589.
[5] A. Karrat, A. Lamaoui, A. Amine, J. M. Palacios-Santander, L. Cubillana-Aguilera, Chem. Africa, 3 (2020) 513-533.
[6] Y. Sheng, et al. Mate. Sci. Eng. C, 112 (2020) 110888.
[7] M. Amjadi, R. Jalili, RSC Adv. 6 (2016) 86736-86743.

29TH IRANIAN ORGANIC CHEMISTRY CONFERENCE
1_3 NOV, 2023
UNIVERSITY OF QOM, IRAN

Thin-layer chromatography analysis for biostability assay of PEG-Maleimide/polyamidoamine/Au drug

Simin Janitabar Darzi[1]*, *Leyla Moghaddam Banaem*[1], *Reza Rezaei*[2]

[1]*Nuclear Science & Technology Research Institute, Nuclear Fuel Research School, Tehran, Iran, P.O. Box: 14395-836, sjanitabar@aeoi.org.ir.*

[2]*Department of Biochemistry, Faculty of Science, Zanjan University, 45371-38791, Zanjan, Iran.*

Abstract - In this research, folate moitiey was conjugated to PEG-Maleimide/ polyamidoamine/^{198}Au compound in order to approach a selective radio-drug. The prepared drugs were characterized by means of Fourier transform infrared spectroscopy (FT-IR) and Transmission electron microscopy (TEM). The average particle size distribution of the ^{198}Au/P-MPEG-FA nanoparticles were estimated by Minitab statistical software to be 17.95 nm. Radiochemical stability tests using instant thin-layer chromatography (ITLC) analysis was performed which determines what percentage of the sample has retained its formula by spend time after incubation in PBS or human serum is acceptable. DLS analysis exhibited that particles with an average size of 67.48 nm were the most common after prolonged storage.

Keywords: PEG-Maleimide, Polyamidoamine (PAMAM), ^{198}Au, ITLC analysis, DLS

1. Introduction

Radio-labeled drugs could fight cancer by delivering targeted radiation to specific receptor-bearing cells. Radioactive gold (^{198}Au) ($t_{1/2}$=2.7 days) decays, dominantly by beta-radiation (99%, 0.96 MeV), which has an efficient radius of about 1 mm in tissue. Firstly, micron scale composites of radioactive gold particles and Polyamidoamine (PAMAM) dendrimers having PEG grafts were used for interstitial brachytherapy for treatment of prostate cancer [1]. PAMAM dendrimers with abundant surface amino groups are used for many nanotechnology applications, especially in biology and medicine including drug and gene delivery, imaging, and inhibition of amyloid aggregation. PEG-attached PAMAM dendrimers are also excellent candidates as Au nanoparticles carriers. PEGylation of PAMAM does not merely yield modified dendrimers with better solubility and low toxicity; but it may also address the problem of precipitation via the PEGylation-induced steric stabilization phenomenon [2]. The aim of this study is preparation of chemically stable radio-labeled drug containing ^{198}Au for effective dose delivery to cancer cells. There are very few examples of gold nanoparticles being actively investigated in clinical trials [3] and its anticancer efficiency remain largely unexplored although a few studies focused on gold nanoparticles. So, it is necessary that its particle size and radio-chemical stability be carefully considered. Chemical stability of the radiolabeled system in the physiological environment should always be well-addressed before applications. However, there is no defined standard for radiochemical stability condition of drugs containing radioactive Au. Therefore, lack of sufficient information in this field gave us incentives to prepare ^{198}Au/P-MPEG-FA as a new radioactive gold containing composite and evaluate its stability using instant thin-layer chromatography analysis.

2. Experimental

2.1. Synthesis and characterization techniques

1-(3-dimethylaminopropyl)-3-ethylcarbodiimide (EDC), PAMAM dendrimer, FA, and dialysis tubing membrane (M_w cut off 12,000) were obtained from (Sigma-Aldrich). Hydrogen tetrachloroaurate ($HAuCl_4.3H_2O$), sodium borohydride ($NaBH_4$), sodium hydroxide, DMSO and DMF were received from (Merck). Maleimide PEG Succinimidyl Carboxymethyl ester (MAL-PEG7500-NHS) was from (jenkem technology).

For modifying PAMAM dendrimer with Maleimide PEG Succinimidyl Carboxymethyl ester, (85 mg, 1.1×10^{-5} mol) of MAL-PEG7500-NHS was added to a solution of (71 mg, 5.15×10^{-6} mol) PAMAM in 15 mL of DMSO and stirred for 72h at room temperature. After that, the mixture was dialyzed in deionized water for 48h and finally, it was subsequently lyophilized to obtain PEGylated PAMAM. The prepare mater marked as (P-MPEG). PEGylated PAMAM (120 mg, 5.5×10^{-7}mol) was added to 5 mL of water while vigorously stirred. Then 5 mL of an aqueous solution of $HAuCl_4$ (27 mg, 6.85×10^{-5}) was added to the above solution. After that, the solution was vigorously stirred for further 45 min followed by addition of a basic aqueous solution of sodium borohydride (25 mM

sodium borohydride in 0.3 M NaOH). The light-yellow solution of the compound turned to red-brown, indicating the formation of colloidal gold in the P-MPEG polymer. The stirring was continued for one more hour to complete the reaction. The reaction mixture was then extensively dialyzed against phosphate buffered saline (PBS) as (Three times, 4L) and water (six times, 4L) for 1 day to remove the excess reactants. At this stage ^{197}Au/P-MPEG is prepared. For producing of ^{198}Au containing nanocomposites, a sample of ^{197}Au/P-MPEG was prepared and poured in the quartz vials. After that the vials were sealed and then inserted in the aluminum cans. The samples were bombarded in the core-face location of Tehran Research Reactor (TRR) with a thermal neutron of 1×10^{11} neutrons/cm^2/sec for 2h. For preparation of FA conjugated nanocomposites, 14 mg of FA (32 folds of molar ratio to PAMAM) was dissolved in 4 ml of DMSO and 12 ml of DMF (with 1:3 ratio). After that, 90 mg of EDC.HCl (14 folds of molar ratio to FA) as a FA activator was added to the above solution and stirred for 3h in dark and under nitrogen atmosphere. The activated FA solution was added dropwise to ^{197}Au/P-MPEG and vigorously stirred at room temperature for 3 days under nitrogen atmosphere. The ^{197}Au/P-MPEG-FA solution was filtered and dialyzed against PBS (Three times, 4L) and water (six times, 4 L) for 48h to remove excess of unreacted FA. Radioactive ^{198}Au/P-MPEG-FA was prepared with the same method using ^{198}Au/P-MPEG sample.

Spectroscopic analysis was performed using a Fourier transform infrared spectroscopy (FT-IR Perkin–Elmer 843). Transmission electron microscopy (TEM) Philips-EM208S was applied for morphological studies. The average particle size distribution was estimated by means of a microstructure measurement program and Minitab statistical software. The dynamic light scattering (DLS) analysis was performed by (Malvern, U.K) with a red diode laser at 633 nm. The stability of the ^{198}Au/P-MPEG-FA was analyzed by instant thin-layer chromatography (ITLC) using Whatman chromatography paper, and methanol (70%). Biostability tests using ITLC analysis determines what percentage of the sample has retained its formula by spend time after incubation in PBS or human serum.

3. Results and discussion

3.1. Characterization of nanocomposite

Fig. 1 shows the FT-IR spectra of FA, P-MPEG and ^{198}Au/P-MPEG-FA nanocomposite. Considering the spectrum of P-MPEG, the broad transmittance band at 3459 cm^{-1} shows the stretching vibration of the –NH– groups of PAMAM. The band at 1657 cm^{-1} is due to the C=O stretching of carbonyl groups of PAMAM internal amides or MPEG–PAMAM amide bonds, and the band at 1102 cm^{-1} is indicative of –CH_2–O–CH_2– etheric bonds of PEG molecules. The observed bands prove incorporation of PEG groups into the PAMAM. According to Narmani report [2], absorption peaks at 1643 cm-1 (–C=O stretch); 2887 cm^{-1} (C–H stretch); 3408 cm-1 (N– H stretch of amide) and 1734 cm-1 (C=O stretch of carbonyl group) are revealed formation of P-MPEG conjugate. From 1145 to 554 cm^{-1}, the C–O and C–C groups' vibration modes are present and the carbohydrates show their bands.

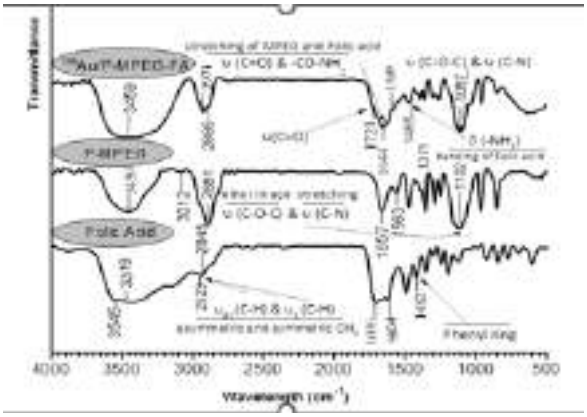

Fig. 1. FT-IR spectra of FA, P-MPEG and ^{198}Au/P-MPEG-FA

FT-IR spectrum of pure FA shows the stretching vibration peak of C=O appeared at 1696cm^{-1}and the band at 1604cm^{-1} related to the bending mode of NH vibration. As shown in FT-IR spectrum of FA, the bands between 3400 - 3600cm^{-1} are due to the hydroxyl stretching of glutamic acid and NH of pterin ring. The bands between 1482-1511cm^{-1} are attributed to absorption of the phenyl and pterin rings. For ^{198}Au/P-MPEG-FA, important peaks of FA were at 3545 and 3415 cm^{-1} (N–H stretch of primary amine and amide); 3328 cm^{-1} (alkyl C–H and C=C stretch); 1695 cm^{-1} (aromatic C=C bending and stretching); 1492 cm^{-1} (CH–NH–C=O amides bending); 837 cm^{-1} (aromatic C–H bending and benzene 1,4-disubstitution).

3.2. Bio-stability study

Radiochemical stability test of ^{198}Au/P-MPEG-FA was performed to evaluate quantity of drug during incubation in PBS or human serum and monitor the probable degradation or probable impurities by means of (ITLC). Bio-stability of the radiolabeled system in the physiological environment should always be well-addressed before applications [8]. Radiochemical stability of ^{198}Au/P-MPEG-FA in the PBS and in the human blood serum was checked at 37°C by (ITLC) in vitro at pH~7.5. Radiochemical stability tests were performed in order to evaluate quantity of drug with desired formula during incubation in PBS or human serum and monitor the probable degradation products

or other impurities. The stability studies were conducted based on the previous studies performed for other radiolabeled compounds. First, a 100µL (32MBq) of the ^{198}Au/P-MPEG-FA compound was added to the human blood serum and then incubated at 37°C. After that, at different time intervals of incubation (2, 8, 24, 48 h), 5 µl of the sample was added to 1 cm at the bottom point of Whatman No. 1 paper. The spot was allowed to dry for 5-10 min. The paper was then placed into an ITLC tank containing methanol 70% solvent and allowed to develop to the 7.0-cm line (about 15 min). After drying, the paper was cut with scissors at the 4.5-cm mark. The activity on each piece of the plate was counted using a gamma counter. The top portion of the paper contained the ^{198}Au/P-MPEG-FA and the bottom portion contained all radio-impurities. The radiochemical purity (RCP) was calculated using the equation (1).

$$\text{RCP (\%)} = \frac{\text{The activity of the top piece}}{\text{Total activity}} \text{x100} \quad \text{Equation (1)}$$

Where the activity of the top piece is related to activity of ^{198}Au/P-MPEG-FA and total activity is summation of activities of all pieces of TLC paper. Each experiment was performed in triplicates, and the RCP data were plotted as mean ± standard deviation (S.D.) at different times of incubation in PBS or serum at 37 or 4°C. The same procedure was repeated, incubating the ^{198}Au/P-MPEG-FA nanocomposite in PBS sample. In vitro stability studies data at 37°C and 2, 8, 24 and 48 h post incubation in serum and PBS are shown in Fig. 2a. According to the Fig. 2a, the ^{198}Au/P-MPEG-FA stabilities were determined as 83.34±1.23% and 83.97±2.47% in PBS and serum after 2h. Moreover, stability studies exhibited RCP at about 73.37±2.3% in serum at 37°C after 48 h of incubation and was 75.98±5.8%% in PBS. ^{198}Au/P-MPEG-FA showed good stability up to 48 h in both of the media. However, since a 48-hour stability data could not be used as an indication of immaculate storage, further studies were devised by storing the final solution of prepared ^{198}Au/P-MPEG-FA at 4°C for 14 days (almost 5 times of physical half-life) in PBS and performing frequent ITLC analysis to determine radiochemical stability. Fig. 2b shows the ^{198}Au/P-MPEG-FA stabilities data at times 24, 48, 72, 140, 210 and 336 h after incubation at 4°C. As seen in the Fig. 2b, on the average 87.8±4.52% of the compound has retained its formula after 336 h post incubation in the PBS. It means ^{198}Au/P-MPEG-FA revealed good radiochemical purity and these conditions were suitable for ^{198}Au/P-MPEG-FA nanocomposite storage and applications. DLS analysis was conducted at the end of the 14-day incubation to evaluate aggregation of nanocomposite during prolonged storage (336 h) at 4°C.

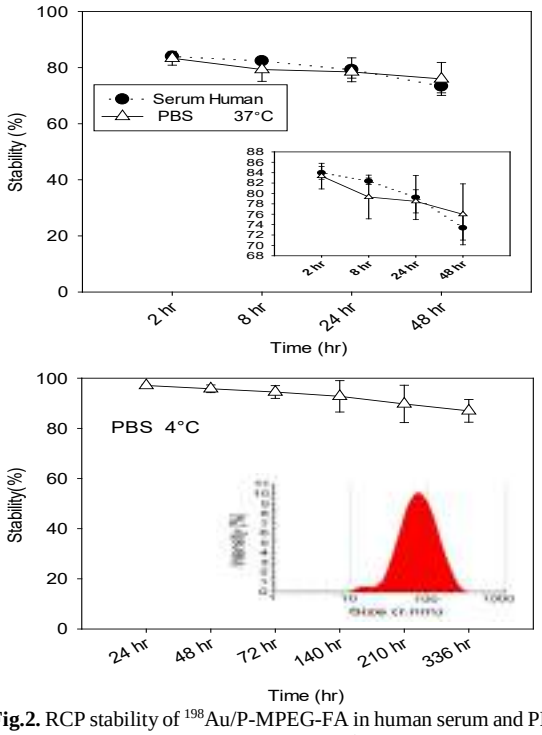

Fig.2. RCP stability of ^{198}Au/P-MPEG-FA in human serum and PBS, plotted as mean±(S.D.) at various time after incubation (a) - RCP stability data of ^{198}Au/P-MPEG-FA in PBS at times 24, 48, 72, 140, 210 and 336 h after incubation at 4°C (b), and the inset: DLS analysis of ^{198}Au/P-MPEG-FA in PBS (336 h after incubation at 4°C).

The result is presented as an inset in the Fig. 2b. The result of DLS analysis at intensity mode is presented as an inset in the Fig. 2b. DLS analysis exhibited that particles with an average size of 67.48 nm were the most common. The polydispersity index of the analysis was 0.266.

4. Conclusion

Radioactive gold containing nanocomposite was synthesized by Folic acid, Polyamidoamine dendrimer (PAMAM) and NHS ester of Maleimide-Polyethylene glycol (MPEG) organic starting materials. ITLC analysis results showed that ^{198}Au/P-MPEG-FA revealed good radiochemical purity confirming the presented conditions in this research were suitable for ^{198}Au/P-MPEG-FA nanocomposite storage and applications. According to DLS analysis, there is almost a single size population and we could say the sample is relatively stable as aggregation point of view.

5. References

[1] M. Valladares, A.Gonzalez-Fernandez,. Assessment of the evolution of cancer treatment therapies. Cancers3 (2011) 3279-3330.

[2] A. Narmani, M. Arani, J. Mohammadnejad, A.Vaziri, S. Solymani, K. Yavari, F. Talebi, S. Janitabar-Darzi, Breast Tumor Targeting with PAMAM-PEG-5FU-99mTc As a New Therapeutic Nanocomplex: In In-vitro and In-vivo studies. Biomed Microdevices. 25 (2020) 31-38

[3] J. Deng; M. Yao, C. Gao, Cytotoxicity of gold nanoparticles with different structures and surface-anchored chiral polymers. Acta Biomater.53 (2017) 610-618.

29TH IRANIAN ORGANIC CHEMISTRY CONFERENCE
1_3 NOV, 2023
UNIVERSITY OF QOM, IRAN

Prediction of some biological activities of the series of crystal structures of Schiff bases derived from hydrazide by PASS software

Pardis Roozbahani[1], *Ali Reza Akbarzadeh*[2*]

[1]*Department of Chemistry, Faculty of Science, Semnan University, P.O. Box: 35195-363, Semnan, Islamic Republic of Iran, p.roozbahani11@gmail.com*
[2] *Department of Chemistry, Iran University of Science and Technology, P.O. Box: 16846-13114, Tehran, Islamic Republic of Iran*

Abstract - Schiff bases derivatives especially those having hydrazide-hydrazone fragment have been reported by researchers. These compounds are very attractive compounds due to their wide range of biological activities. Here the series of crystal structures of Schiff bases derived from hydrazide have been collected. To investigate some of the biological properties of the mentioned compounds the PASS software was used.

1. Introduction

Schiff base derivatives are an important class of organic compounds that play an important role in the development of coordination chemistry. Recently, the importance of Schiff bases, especially those with hydrazide-hydrazone moiety [-(C=O)NHN=CH], is essential for the preparation and development of new drugs with better mechanism of action and structure-activity relationship .The contributions of these bases are widely used in various applications such as anticancer, anti-HIV, anti-radical, anti-bacterial, anti-fungal, anti-microbial, anti-seizure, anti-inflammatory ,antifungal DNA cleavage etc.[1-3]. Also During the time-consuming processes of drug discovery and development, a large number of molecular structures are evaluated with different parameters. The ultimate goal of these processes is to identify the best quality chemicals. Therefore, to study the essential pharmacokinetic properties of compounds, in silico methods are a valid alternative to primary experiments and a reasonable way to reduce labour and associated costs [4, 5]. In this study, some crystal structures of Schiff bases derived from hydrazide have been collected. The biological activities (antituberculosic, antinociceptive, antibacterial, andantiviral (Picornavirus)) are studied by the Prediction of Activity Spectra for Substances (PASS) software to anticipate better Schiff from the viewpoint of biochemistry. PASS algorithm was used to predict the biological activities of Schiff bases derived from hydrazide with two parameters: probability activity (P_a) and probability inactivity (P_i). P_a and P_i values for biological activities are between 0 and 1. The mentioned parameters report the activity or inactivity of a specific property of compounds. The PASS prediction is based on the Multiple Neighbourhood Atom (MNA) method. The MNA method means that each atom in a compound is influenced by its neighbouring atoms, leading to an increase or decrease in biological activities with Pa and Pi [6, 7].

2. Results and Discussion

Four biological activity spectra of the Schiff bases, with hydrazide moiety were studied by PASS software According to Table 1, compounds 6 and 9 have the maximum p_a antibacterial activities (0.467 and 0.428 respectively). Furthermore, the maximum probability of antituberculosic activities is shown in compounds 9 and 10, respectively. Also antinociceptive activity of compounds 1and 5 are higher than other compounds. Moreover, antiviral activity (Picornavirus) with the highest p_a related to compound number 10.

3. Conclusion

In the present study, some crystal structures of Schiff bases derived from hydrazide which are highly efficient in biological activities have been collected. We have specifically focussed on four biological activities including antituberculosic, antinociceptive, antibacterial, and antiviral (Picornavirus) of mentioned compounds by using PASS software. For a given compound activity, whenever the $P_a > P_i$, the predicted biological activity can be pursued experimentally. Therefore, based on the results of the PASS prediction, these compounds are attractive candidate, which can be recommended to the experimental study.

Table1. Pass investigation for Schiff bases derived from hydrazide

Compounds	Antibacterial		Antituberculosic		Antinociceptive		Antiviral (Picornavirus)		Ref
	p_a	p_i	p_a	p_i	p_a	p_i	p_a	p_i	
1	0.389	0.033	0.675	0.004	0.562	0.013	0.555	0.031	[1]
2	0.413	0.027	0.808	0.003	0.561	0.013	0.642	0.012	[9]
3	0.385	0.034	0.807	0.003	0.462	0.062	0.402	0.108	[10]
4	0.307	0.058	0.617	0.005	0.441	0.077	0.375	0.132	[2]
5	0.361	0.040	0.498	0.013	0.614	0.007	0.514	0.045	[11]
6	0.428	0.024	0.891	0.002	0.502	0.035	0.662	0.009	[13]
7	0.414	0.027	0.796	0.003	0.509	0.031	0.678	0.008	[13]
8	0.410	0.028	0.784	0.003	0.484	0.046	0.651	0.010	[13]
9	0.467	0.020	0.909	0.002	0.472	0.055	0.601	0.019	[13]
10	0.403	0.029	0.915	0.009	0.408	0.103	0.708	0.005	[12]
11	0.398	0.030	0.664	0.004	0.462	0.061	0.385	0.122	[14]
12	0.219	0.102	0.633	-	-	0.044	0.452	0.074	[3]

4. References

4.1. In text citation:

[1] RM. Ramadan, SM. El-Medani, A. Makhlouf, H. Moustafa, MA. Afifi, M. Haukka, A. Abdel Aziz, Applied Organometallic Chemistry, 2021.

[2] SM. El-Medani, AA. Makhlouf, H. Moustafa, M. A. Afifi , M.Haukka , Ra. M. Ramadan, Journal of Molecular , 2020 .

[3] F. Faye, A. Guèye, PS Camara, AA Gaye, FB Tamboura, N Gruber, M Gaye, American Journal of Applied Chemistry, 2021.

[4] G. Kapoor, D. Pal Pathak, R.Bhutani, A.Husain, S.Jain , Md. Azhar Iqbal, Bioorganic Chemistry, March 2019.

[5] JN. Sangshetti, FAK. Khan, RH. Patil, SD. Marathe, W. N. Gade , D B. Shinde, Bioorganic & Medicinal , 2015 .

[6] EA. Kurashov, EV. Fedorova, JV. Krylova, GG. Mitrukova, Scientifica, 2016.

[7] A. Lagunin, A.Zakharov,D.Filimonov, V.Poroikov, Molecular informatics, 2011

[8] AK. Singh, S. Kumari, KR. Kumar, B. Sridhar, TR. Rao - Polyhedron, 2008.

[9] O.Pouralimardan, AC.Chamayou, C. Janiak, H.Hosseini-Monfared, Inorganica chimica acta, 2007.

[10] NS. Gwaram, HM. Ali ,MA. Abdulla ,MJC. Buckle ,S D.Sukumaran ,LY. Chung,R.Othman ,AA. Alhadi ,WA. Yehye, AHA. Hadi , P.Hassandarvish ,H. Khaledi ,SI. Abdelwahab, Molecules. 2012

[11] K. Tiwari, M. Mishra, VP. Singh, RSC advances, 2013.

[12] M.Shankar, AD. Raj, M. Jeeva, R. Purusothaman, M. Vimalan , I. V. Potheher, Materials Letters, 2018..

[13] J. Pisk, I. Đilović, T. Hrenar, D. Cvijanović, G. Pavlović, V. Vrdoljak, RSC advances, 2020.

[14] F. Diouf, EA. Fall, FB. Tamboura, M. Gaye, N. Gruber, A. Jouaiti, IOSR Journal of Applied Chemistry, 2022.

29TH IRANIAN ORGANIC CHEMISTRY CONFERENCE
1_3 NOV, 2023
UNIVERSITY OF QOM, IRAN

A new fluorescein-based chemical sensor for selective identification of Cu^{2+} and Hg^{2+}

Sepideh Pourrohani, Yaghoub Sarrafi, Saied Shafiei Navid and Mahmood Tajbakhsh*

Department of Organic Chemistry, Faculty of Chemistry, University of Mazandaran, 47416-95447 Babolsar, Iran, sepideh.pourrohani@gmail.com

Abstract – In this research, fluorescein-based chemical sensors were designed and synthesized through the Schiff base reaction to identify Cu^{2+} and Hg^{2+} cations. For this purpose, at first SP1 and SP2 sensors were synthesized and their structures were investigated and confirmed by ^{1}HNMR and MS spectroscopy methods. Then, their properties as chemical sensors for some metal cations were investigated by fluorescence emission spectroscopy and ultraviolet-visible spectroscopy (UV-Vis). The obtained results indicated that the SP1 and SP2 acted selectively and also showed a color change for Cu^{2+} and Hg^{2+} cations, respectively. The reversibility studies in the presence of EDTA show that the fluorescence was turned on with the addition of the extra amount of the mentioned cations. Also, the data obtained from Job's graph and fluorescence titration determined that both sensors form complexes with cations in a ratio of 1:1. Since the structures of both SP1 and SP2 are rigid, the fluorescence turned on with a plausible CHEF mechanism.

1. Introduction

In general, a tool that has the ability to convert the chemical characteristics of a component of a sample into a signal for quantitative measurement is called a chemical sensor. The reason for producing this signal is the interaction between the target element and the sensor, and as a result, the changes in the energy level of the sensor. A chemical sensor is a chemical molecule that consists of two parts: a central part and a part for binding to the guest species [1].

Cations play a very important and sometimes vital role in our daily life. So that their lack or excess are both very dangerous and cause various diseases and generally endanger the health of the environment. Therefore, identification of cations is very important for biologists, chemists, and environmentalists. For example, copper is a very essential element for the body's functioning and helps to make red blood cells or too much of it can cause liver damage. In addition, in the list of dangerous compounds, mercury ranks sixth among the most toxic chemicals and can cause problems such as Alzheimer's, bronchitis, dementia, blurred vision, and breathing problems [2]. In this study, fluorescein, which is usually used in forensic medicine to detect blood stains, has been used as a fluorophore part for the synthesis of a new sensor [3]. Two new fluorescein-based sensors were synthesized successfully through the Schiff base reaction in the presence of different aldehydes to obtain SP1 (with salicylaldehyde) and SP2 (thiophene-2-carbaldehyde) for the identification of metal ions [4].

2. Results and discussion

2.1. Synthesis and characterization of sensors SP1 and SP2: Both sensors SP1 and SP2 were synthesized through a Schiff base reaction (Scheme 1) with two different aldehydes in an acidic medium. The ^{1}HNMR spectrum showed that the NH_2 protons completely disappeared (4.49 ppm) and the new -CH=N- signals at 9.34 and 9.23 ppm showed the successful synthesis of SP1 and SP2 sensors, respectively (Fig. 1). MS-ESI-positive: SP1, calculated: 746.1, found 746.2. SP2, calculated: 736.3, found 736.1.

2.2. Colorimetric and UV-Vis studies of sensors with metal cations: To investigate the interactions between sensors and metal cations, the calculated amount of metal cations in solvent (10^{-6} M in water/ethanol (1:1)) were added to the sensor solution with the same concentration and then the spectra were recorded. As seen in the UV-Vis spectrum of SP1 (Fig. 2a), the sensor has an additional absorbance at 490 nm

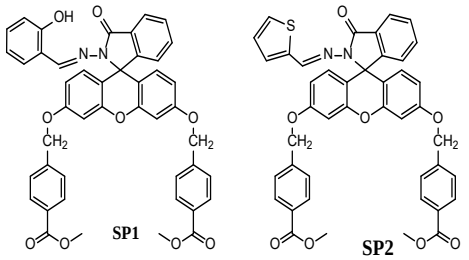

Scheme 1. The chemical structures of SP1 and SP2.

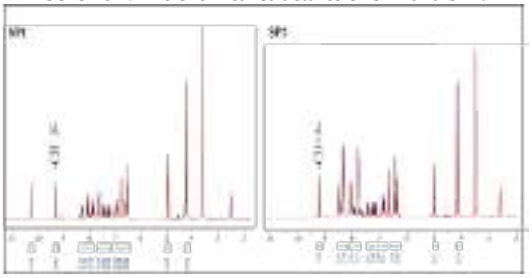

Fig.1. The ^{1}HNMR spectra of SP1 and SP2 in DMSO-d_6.

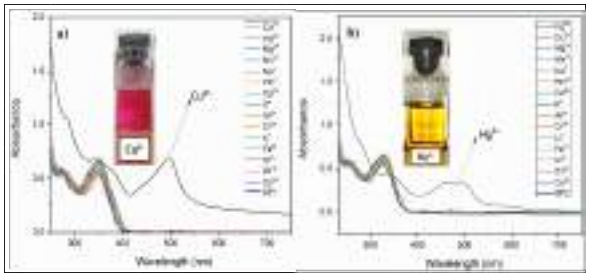

Fig. 2. Colorimetric and UV-Vis spectra of sensors with different metal cations (10^{-6} M).

in the presence of Cu^{2+} ions. Also, by creating a bathochromic shift, Cu^{2+}-complex has moved to the visible area and changed color (pink), while other cations did not show this color change. Similarly, the SP2 sensor (Fig. 2b) also has another two-peaked absorption at 485 nm in the presence of Hg^{2+} ion, and only in the presence of Hg^{2+} ion did a color change occur in the visible area (yellow) [5].

2.3. Fluorescence emission spectroscopy studies of sensors: According to the maximum excitation wavelength (UV-Vis), first the fluorescence emission of the sensors with a certain concentration (10^{-6} M) was investigated and since no emission was observed, it was determined that both sensors are on-off. After that, the fluorescence emission spectrum of the sensor was recorded in the presence of each metal (10^{-6} M), the results of which are given in Fig. 3a and 3b. According to Fig. 3, sensors SP1 and SP2 acted selectively for Cu^{2+} and Hg^{2+} cations, respectively, because the sensor is turned on only in the presence of these cations.

2.4. Investigation of the stoichiometric ratio of sensors and cations: Job's graph is used to check the stoichiometric ratio of the sensor with the analyte [6]. In this way, different mole fractions of sensors and cations were studied using the fluorescence emission technique. In the next step, the graph of mole fractions in each solution was drawn in relation to its fluorescence emission intensity, which is shown in Fig. 4. Based on the results obtained from Job's graph, SP1 (Fig. 4a) and SP2 (Fig. 4b) sensors form complexes with Cu^{2+} and Hg^{2+} cations, respectively, with a ratio of 1:1. Although in similar researches, diester groups showed proper coordination ability, but in this research, the results show that the diester part was not involved in the complex formation process [7]. Therefore, it can be said that the coordination interactions between the Schiff-base part in the sensors with cations overcome the interactions of the diester part, and for this reason, this group is not involved in the formation of the complex. The addition of ester groups also helps to better understand the mechanism of sensing.

2.5. study of the responsiveness of sensor detector in the presence of interfering ions: To prove the selectivity of the sensor and to confirm its selective response to the target ions in the presence of interfering ions, first the fluorescence emission spectrum of the

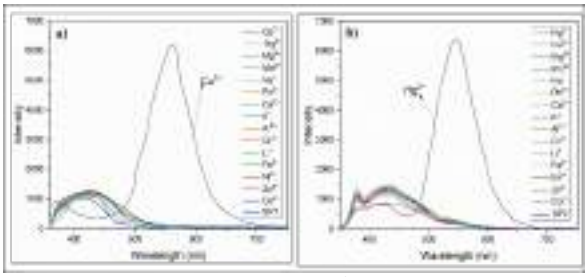

Fig. 3. Fluorescence emission spectra of SP1 and SP2 sensors in the presence of different metal cations.

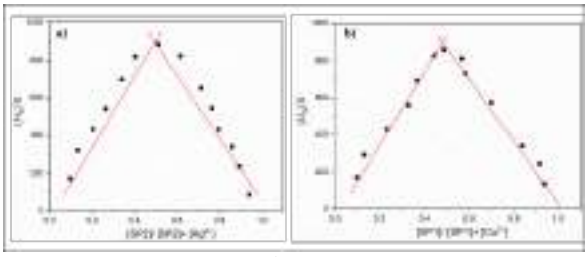

Fig. 4. Job's graph for SP1 and SP2 sensors.

sensors were measured. Then, solutions of interfering ions with a specific concentration (2 eq.) were added. Their fluorescence emission was recorded, and at the end, Cu^{2+} or Hg^{2+} ions were added to this solution and its fluorescence emission spectrum was recorded (Fig. 5). As can be seen, the sensors by themselves and in the presence of interfering ions did not show significant fluorescence emission. However, by adding the target cations, a strong fluorescence emission was observed in the region of 400-600 nm. These results, which are consistent with the results of previous measurements, showed that SP1 and SP2 sensors selectively detect Cu^{2+} and Hg^{2+} ions, respectively, even in the presence of interfering ions.

2.6. Reversibility of the sensors in the presence of EDTA: One of the most important parameters studied about the sensors is the reversibility of the studied sensor, for this purpose, EDTA salt (10^{-4} M) was used. First, the fluorescence emission spectrum of the sensors was recorded in the presence and absence of the target cations. To check the reversibility of the sensors, an aqueous solution of EDTA salt was added to the sensor/cation solution and its fluorescence emission spectrum was recorded. The results showed that EDTA salt destroys coordination bonds between the sensors and target cations [8]. Next, excess amounts of target cations were added to this solution and its fluorescence emission spectrum was recorded (Fig. 6). The results showed that in the presence of additional amounts of Cu^{2+} and Hg^{2+} ions, the fluorescence of SP1 and SP2 sensors was turned on, respectively. These observations indicate the reversibility and reusability of the sensors.

2.7. Plausible mechanism of sensing cations by sensors: In similar studies, it was believed that the sensing mechanism is based on the resonance of fluorescein hydroxyl groups and ring openings. Since

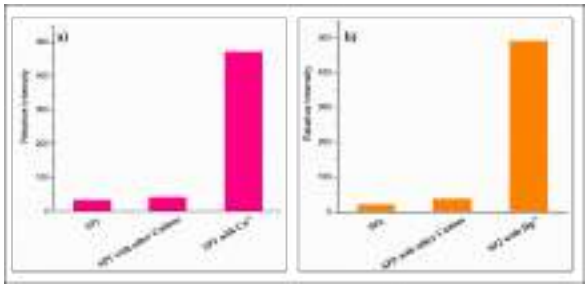

Fig. 5. Job's graph for SP1 and SP2 sensors.

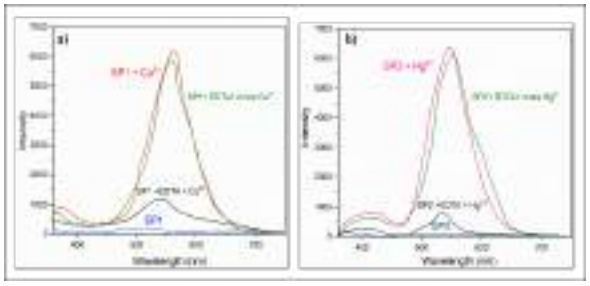

Fig. 6. Reversibility and reusability of SP1 and SP2 sensors in the presence of EDTA.

in this research the hydroxyl groups have been functionalized and still both sensors are sensing the cations, the plausible mechanism is shown in Fig. 7. The PET in both SP1 and SP2 sensors is on, so that the isomerism of the imine group and its free rotation cause the PET to be on and the fluorescence to be off. When the solution of metal cations is added to sensors, the nitrogen atom (Schiff-base group) is coordinated with the cation, and this rotation no longer occurs and makes the system more rigid. As a result of increasing the rigidity of the system, the fluorescence of the complex is turned on by the CHEF [9] mechanism or by increasing the fluorescence intensity through chelation.

2.8. Study of the formation constants of complexes: According to the results obtained from the fluorescence titration, the constant rate of complex formation (Ka) and the limit of detection (LOD) for both sensors are tabulated in Table 1. The obtained values indicate the high ability of both sensors to form complexes with the target cations. Also, according to the data obtained from LOD, the ability of these sensors to sense these metal cations in very low concentrations is proven. The selectivity of these sensors can be due to the appropriate interactions and the size of the target metal.

3. Conclusion

As discussed, the purpose of this research was to synthesize and identify fluorescein-based sensors for sensing metal cations. The results obtained from various techniques such as ^{1}HNMR and MS spectroscopy that SP1 and SP2 sensors were successfully synthesized. The obtained results from UV-Vis and fluorescence emission spectroscopy confirmed that SP1 and SP2 sensors can selectively sense Cu^{2+} and Hg^{2+} cations, respectively. Also, the

Table 1 The Ka and LOD values for SP1-Cu^{2+} and SP2-Hg^{2+} complexes

Complexes	Ka (M^{2-})	LOD (M)
SP1-Cu^{2+}	2.84×10^{10}	1.47×10^{-8}
SP2-Hg^{2+}	4.35×10^{10}	1.01×10^{-8}

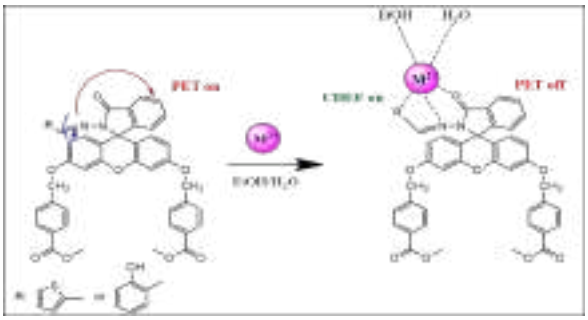

Fig. 7. The plausible sensing mechanism of SP1 and SP2 sensors.

colorimetric results proved that both SP1 and SP2 sensors show color change only with Cu^{2+} and Hg^{2+} cations, respectively. So, these sensors can be used as a practical tool for metal identification even with the naked eye. The fluorescence titration results showed these sensors could sense target cations at low concentrations. Considering the complex formation constant and fluorescence emission intensity for SP1 and SP2 sensors, both can be used to check the concentration of mentioned cations in different aqueous and organic environments. Because of the diester groups, the synthesized sensors can be applied for the identification of small molecules such as amino acids or phenolic compounds which is our next research purpose.

4. References

[1]. J. Janata, Anal. Chem. 64 (1992) 196-219.

[2]. A. Kumar, M. Saini, B. Mohan, M. Kamboj, Microchem. J. (2022) 107798.

[3]. H. Schiff, Ann. Chem. Suppl. 3 (1864) 343-9.

[4]. K. A Maher, S. R Mohammed, Int. J. Curr. Res. 7 (2015) 6.

[5]. P. Chaquin, D. Costa, C. Lepetit, M. Che, J. Phys. Chem. A 105 (2001) 4541-4545.

[6]. C. Hao, X. Guo, Q. Lai, Y. Li, B. Fan, G. Zeng, Z. He, J. Wu, Inorganica. Chim. Acta. 1 (2020) 523.

[7]. J. Konczyk, A. Nowik-Zajac, CA. Kozlowski, Sep. Sci. Technol. 51 (2016) 2394-410.

[8]. HY. Lin, PY. Cheng, CF. Wan, AT. Wu, Analyst. 137 (2012) 4415-7.

[9]. L. Xue, Q. Liu, H. Jiang, Org. Lett. 11 (2009) 3454-7.

Experimental: SP1 and SP2 were synthesized on a gram-scale through a Schiff-base reaction between amino fluorescein (1 mmol) and aldehydes (2 mmol) by using a catalytic amount of acetic acid in ethanol. Both sensors were purified via recrystallization in ethanol and were obtained as milky-white crystals.

29TH IRANIAN ORGANIC CHEMISTRY CONFERENCE
1_3 NOV, 2023
UNIVERSITY OF QOM, IRAN

Application of new techniques for extraction of the volatile components and essential oils

Sayedeh Mansoureh Memarzadeh[1]*, *Abdollah Ghasemi Pirbalouti*[2], *Ali Gholmi*[3], *Sayed Ahmad Nourbakhsh*[4], *Farita Nourizadeh*[5]

[1]*Food and Drug Deputy, Shahrekord University of Medical Sciences, Shahrekord, I.R. Iran. Memarzadeh.m@skums.ac.ir, memarzadeh8291@gmail.com*
[2] *Research Center for Medicinal Plants, Shahr-e-Qods Branch, Islamic Azad University, Fath Highway, P.O. Box 37541-374, Tehran, Iran,*
[3]*Department of Analytical Chemistry, Faculty of Chemistry, University of Kashan, Kashan, Iran.*
[4]*Student and Cultural Deputy, Shahrekord University of Medical Sciences, Shahrekord, I.R. Iran.*
[5]*eHealth Deputy, Shahrekord University of Medical Sciences, Shahrekord, I.R. Iran*

Abstract

The conventional methods for the essential oil extraction (hydro-distillation and steam distillation) have some disadvantages. Losses of some volatile constitute, low extraction efficiency, degradation of unsaturated or ester compounds through thermal or hydrolytic effects and toxic solvent residue in the extract may be encountered using these extraction methods. The development of new extraction techniques for the food and herbal drugs industries has received a lot of attention lately due to the environmental restrictions and the need for minimizing the energy costs. In order to reduce the extraction time, and the operation costs and possibly improve the oil yield and the quality of the essential oil, new approaches such as microwave-assisted extraction, supercritical fluid extraction, and ultrasound-assisted extraction have also been sought. Results of our study indicated that the changes in yield of the volatile oil during extraction depended on extraction method and temperature, type constituent and the biological characteristics of the plants. Extraction methods had significant effects on aroma quality of the dried samples in Iranian herbs. In conclusion, extraction of the essential oil from some Iranian medicinal and aromatic plants with microwave-assisted hydro-diffusion was better in terms of extraction time, phenolic and aroma fractions, and product quality.

Keywords: Medicinal and aromatic plants; Chemical composition; Essential oil yield; Novel techniques.

1. Introduction

Herbs are rich genetic resources and one of the most valuable national capital of each country. Iran is one of the 8 most important countries with a diverse flora medicinal plants in the world [9]. The genus *Satureja* L. (Savory) belongs to the Lamiacea family and contains 200 species of herbs and Shrubs, often aromatic, widely distibiuted in the Asian and Mediterranean areas [6]. The essential oil of *S.bachtiarica* that is isolated from aerial parts of plant has antibacterial, antifungal and antioxidant properties [18] and also includes the kinds of phenolic compounds, monoterpenes and sesquiterpenes.The main compounds of *S.bachtiarica* essential oil are Thymol, Carvacrol, γ-terpinene and ρ-cymene and it can be used as food preservative in the food industry [3], hygienic and cosmetic procurement, such as deodorants, toothpastes and mouthwashes [5]. The extraction methods of essential oil from medicinal plants are divided in two models: Conventional methods include hydrodistillation , steamdisrillation, steam and water distillation and extraction with organic solvents and Innovative methods include supercritical fluid extraction, microwave-assisted extraction, ultrasound-assisted extraction [15].

The problems of coventional extraction methods contain: loss of volitle compounds, low extraction efficiency, degridation of esteric and unsaturated compoundes through the thermalling and hydrolysing effects. Because the essential oil compounds are very sensitive, in the conventional methods,toxic solvent residue, the longtime of the extraction and the direct heating maybe encountered chemical changes and polymerization in the essential oils [10,11,21].

The new methods of essential oil extraction are considered not only high quality and quantity of essential oil but also organic solvent free, speed, low

energy and water consumption [16, 20]. Because the extraction methods are affective on the efficiency, types and contents of chemical compounds of the essential oils and their propertis, according to the benefits of the modern extraction and disadvantages of coventional extraction also over the years some of the traditional process and other thermal extraction techniques have been replaced with the procdure base on microwave extraction and some recently studies have successfully utilized a microwave oven for the essential oil extraction from herbs [10, 17, 13, 19, 20]. However , base on authors searches no work has been published on the microwave - assisted of Savory species . In this study we compared antioxidant activity (DPPH procedures), total phenolic compounds of *Satureja bachtiarica* Bunge essential oils obtained from diferent extractions methods in order to find the most adventageous in term of extraction methods with high protective antioxidant capacity.

2. Materials and methods

2.1.Plant material

The fresh aerial parts (up to ~ 5cm,100g) of *Satureja bachtiarica* Bunge. were gathered from Chaharmahal va Bakhtiari province in the southwestern of Iran about 2200 m above sea level in june 2021.The plant was confirmed by vocher specimens (no.1999) that have been placed at Research institute of Forests and Rangland Herbarium, Shahrekoard, Iran . The fresh aerial parts of Bakhtiari savory were dried at dark room in (30±5ºC) temperature for six days and then Endecott food processor was used to produce the tiny powder and 16 mesh sieve was used for removing large pieces of debris.

2.2. chemicals

Homologous series of C_5-C_{24} n-alkanes, β-Carotene, DPPH (Sigma-Aldrich , Steineheim, Germany) and Anhydrous sodium sulphate, Folin-ciocalteu, Gallic acid, BHT, Sodium carbonate, Linoleic acid, Tween 40, Ascorbic acid , Diethyl ether, Methanol, Ethanol, Chloroform HPLC grade (Merck Co. Darmstadt, Germany)

2.3..Conventional methods

The coventional methods consisted of hydrodistillation and traditional steam and water distillation .

2.3.1..Hydrodistillation(HD_{BP} and HD_{RIFR})

Hydrodistillation method was performed by two clevenger –types apparatus: British pharmacopia (HD_{BP}) and Research Institute of Forests and Raglans of Iran (HD_{RIFR}) (fig.1), 100 g of plant with 1L of water for 4 h was extracted at least triplicate .

The essential oils obtained from all of the different extraction methods were dried by anhydrous Na_2SO_4 and transferd to sealed dark vials and stored at 4ºC until analysis.

2.3.2.Steam and water distillation (SWD)

In this procedure thespecial innovative flask (designed by Memarzadeh and Ghasemi Pirbalouti patent no.89031 in Iran) was used . The vapor produced by 1L water from lower part of flask passed through the 100 g essential oil rich plant material before being codensed into a receiving Clevenger-type apparatus (British pharmacopia approach) for 4 h and at least triplicate .

Fig1. Hydrodistillation of Research Institute of Forests and Raglans of Iran metod (HD_{RIFR})

Fig2. Innovative steam distillation method ($SD_{innovative}$)

Fig3. Microwave- assisted steam hydro-diffusion method (MSHD)

2.4.Innovative methods (Apparatus and Procedure)

The innovative methods consist of steam distillation (SD_{innove}), Microwave- assisted hydro-diffusion (MHD)and Microwave- assisted steam hydro-diffusion (MSHD)

2.4.1. Innovative steam distillation (SD_{innove})

In an innovative steam distillation technique (SD_{innove}) that was designed by Memarzadeh and Ghasemi Pirbalouti (fig.2) the vapour was produced by the simple steam generator and then steam was transferred from the tube that was embedded in the lower part of 1L special flask and passed through the 100 g essential oil rich plant material before being codensed into a receiving Clevenger-type apparatus (British pharmacopia approach) for 4 h.

2.4.2. Microwave- assisted steam hydro-diffusion ($MSHD_{400 \text{ and } 800W}$)

As an energy source, a domestic microwave oven (MG-4012WM/00, LG, Korea) was modifiedin two methods MSHD and MHD.100 g of Bakhtiari savory that had been macerated in 1L distilled water for 30 min was placed on the lattice surface in the middle of 1L special flask and the lower part of this flask containing 1L of dionized water.The flask was set up within the microwave oven cavity and condenser was used on the top (outside the oven) to collect the extracted essential oil. The vapour that produced by the microwave oven passed through the essential oil rich plant material before being condenced in to a receiving Clevenger type apparatus (fig.3). The microwave oven was operated at two power level 400W and 800W for a period of 30 min. This period was sufficient to extract all the essential oil from the samples. During 30 min, the collected essential oils were decanted from the condensate in 10 min intervals.

2.4.3. Microwave-assisted hydro-diffusion ($MHD_{400 \text{ and } 800 W}$)

This method were done base on part 2.4.2 with the difference that the bottem of the special flask was empty.

2.5. Determination of essential oil yelid

Essential oil content was determined using the Europian Pharmacopea on basis of dry matter carried out in triplicates. Essential oil yelid (%) was measured using the following formula [36].

$$\text{EO yield}(\%) = \frac{\text{mass of EO obtained(g)}}{\text{mass of dry matter(g)}} \times 100$$

2.6. Determination of total phenolic contents

The total phenolic content (TPC) in each extract was determined using the Foline-ciocalteu procedure [21 with minor modifications]. Briefly , 500µL of 1000 µg/mL (solution essential oil in Methanol) was mixed with 5 mL of the Foline-Ciocateu' reagent (1:10 diluted with distilled water) and shaken slowly for 5 min , then 3 mL of 2% Sodium carbonate solution was added in the tube test and shaken well for 1 min. The mixture was maintained at laboratory temperature for 1 hour until making blue color in solution. Then, the absorbance of the mixture was measured at 760 nm using an ultraviolet and visible (UV-Vis) spectrophotometer (Varian- Cary100 conc). A blank sample consisting of water and reagents was used as the refrence. Gallic acid equivalents (GAE) were used as the refrence standard and TPC was expressed as mg of GAE per gram of each extract on the essential oil. Buthylatedhdroxytoluene (BHT) and Ascorbic acid were used as the positive refrence standards. Each test was performed at least three times and the results were reported as mean ± SD of triplicates [14].

2.7. Antioxidant activity

2.7.1. DPPH Radical scavenging Assay

Brifely, 100 µL of the sample of each essential oil was blended at chosen concentrations (500,250,125,62.5µg/mL) with 3.9 mL from 25mg/L methanol DPPH solution.The mixture was shaken vigorously and allowed to stand at dark room temperature for 30 min. The absorbance of the samples was measured at 517 nm using a spectrophotometer UV-Vis (Varian- Cary100 conc). The methanol used as at the blank and a control (A_B Control) including methanol and DPPH solution was also measured. BHT and Ascorbic acid were used as the positive refrence standards. Each test was performed at least three times.The inhibition percentage of the samples was calculated accordingto the following formula:

% inhibitation = ($1-A_A/A_B$) × 100

A_A and A_B are the absorbance values of the DPPH radical in the presence of the essential oil samples and the control, respectively [2]

The inhibition percentage was plotted versus the essential oil samples concentration and 50% of the inhibitory concentration (IC_{50}) of the DPPH value was determined by linear regression analysis .

percentages were reported as mean ± SD of triplicate.

2.8. Statistic analysis

All the tests were carried out in three replications; in order to analyze the data , SPSS software ,version 20, was used. The means comparision was carried out using One way ANOVA and Duncan´s multiple range test ($p \leq 0.05$).

3. Resuts and discussion

3.1. Effect of extraction methods on the essential oil yield

Results indicated that different extraction methods had a significant effect on essential oil yield of *Satureja bachtiarica* Bunge. ($p \leq 0.05$), HD_{BP} and $MSHD_{400w}$ methods had the highest essential oil yield (v/w on dry weight basis) and the lowest essential oil yield obtained by HD_{RIFR} and MHD_{400w} methods (Table 1). HD_{BP} showed 1.4±0.01 mL EO/100 g dry plant in 4h extraction time and $MSHD_{400w}$ showed 1.37±0.06 mL EO/100 g dry plantin 30 min extraction

time, these methods reached to maximal yields but $MSHD_{400w}$ was faster than HD_{BP} in the extraction time, an approved refrence method for quantificating of essential oils butthe heat transfer speed in MSHD is more than HD and microvawe rapidly delivers energy to extractant and plant matrix [22]. Results of a study by [10] on the *Thymus vulgaris* L. showed that microvawe -assisted hydrodistillation decomposed the glands of leaves in 30 min but the traditional hydrodistillation ruined the essential oil glands in 75 min . These results confirm this literature, other microvawe assisted methods does not have possitive effect on the maximum yeild but has positive effect on the time saving.

Table 1. Effect of extraction methods on the essential oil yield

E. method	yield ± SD
$HD_{(BP)}$	1.400 ± 0.010 **a**
$SWD_{(BP)}$	1.270 ± 0.076 **c**
$SD_{(innove)}$	1.283 ± 0.029 **bc**
$HD_{(RIRF)}$	1.060 ± 0.040 **e**
MHD_{400w}	1.033 ± 0.058 **e**
MHD_{800w}	1.167 ± 0.058 **d**
$MSHD_{400w}$	1.370 ± 0.060 **ba**
$MSHD_{800w}$	1.167 ± 0.058 **d**
ANOVA	**p≤ 0.05**

Note : Significant different at 5% level probability with Duncan test have been indicated with different letters ($p \leq 0.05$).

3.2. Relationship betweentotal phenolic contents and antioxidant activities of

Saturejabachtiarica Bunge essential oil under different extraction methods

3.2.1. Total phenolic contents of essential oils

TPC (Total Phenolic Contents) is the one of main keys indicators widely employed to display the overall antioxidant activity in the samples [21] The results detected significant diffrences ($p \leq 0.05$) TPC values of Bakhtiari savory essential oils under different extraction methods. The results reported in mg (GAE: Gallic Acid Equivalent) per g of essentialoil (Table 2). The highest TPC value was found by $MSHD_{800w}$ (268 ± 6.34 mg GAE/g EO) on the other hand , the lowest TPC value was recorded for SD_{innove} (205.91 ± 2.5mg GAE/g EO). Phenolic compounds were able to scavenge the reactive oxygene intermediates without invoking further oxidative reactions [2] BHT, Carvacrol were used as positive control with TPC values (327.72± 2.30, 259.04 ± 0.57 mg GAE/g) respectively.The results in the present study accorded to the literature on *Satureja Hortensis* [11] and due to ghanges in some evironmental factors such as origin and elevatio of the sea,TPC value equal 185.5 mg GAE/g EO on *Satureja Coneifolia* Ten [16] was different with this study**.**

3.2.2.Antioxidant activity

3.2.2.1.DPPH scavenging activity

Anioxiant activity is most usually estimated by DPPH scavenging activity test [4]. In this study ,different extraction methods were campared to determin the ability of their essentials to scavenge the DPPH free radical, BHT was positive control.The IC_{50} values were found to range from 1.95 ± 0.13 to 4.34 ± 0.18 mg/mL.The results detected significant diffrences ($p \leq 0.05$) in the IC_{50} values of Bakhtiari savory essential oils under different extraction methods. The essential oil of MHD_{800w} exhibited the highest antioxidant activity (the lowest IC_{50} value: 1.95 ± 0.13mg/mL),while the essential oil of SD_{innove} showed the weakest antioxidant activity (the highest IC_{50} value :4.34 ± 0.18mg/mL) (Table.1). Comparison of the TPC and IC_{50} valueresults from essential oils under different extraction methods showed that TPC has reverse
relation with IC_{50} value and direct relationship with the antioxidant activity these results are agreement with two studies [8, 12].

Table 2. Total phenolic contents TPC) and antioxidant activity of essential oil under different extraction method

E. method	DPPH	TPC
	IC50 (mg/ml)	**(mg GA/g)**
HD_{BP}	3.44 ± 0.76 **ed**	249.52 ± 3.64 **c**
SWD_{BP}	2.74 ± 0.57 **d**	258.37 ± 9.13 **c**
SD_{innove}	3.25 ± 0.69 **d**	205.91 ± 2.55 **f**
HD_{RIFR}	3.27 ± 0.20 **d**	255.12 ± 5.10 **c**
MHD_{400w}	4.34 ± 0.18 **f**	229.35 ± 5.27 **d**
MHD_{800w}	3.16 ± 0.37 **d**	219.14 ± 1.60 **e**
$MSHD_{400w}$	4.03 ± 0.48 **fe**	226.67 ± 2.99 **de**
$MSHD_{800w}$	1.95 ± 0.13 **b**	268.22 ± 6.34 **b**
BHT	0.13 ± 0.00 **a**	327.72 ± 2.30 **a**
Carvacrol	2.73 ± 0.08 **d**	259.04 ± 0.57 **c**
ANOVA	**p≤ 0.05**	**p≤ 0.05**

Note : Significant different at 5% level probability with Duncan test have been indicated with different letters ($p \leq 0.05$)

4. Conclusion

Extraction of secondary methabolits from medicinal plants is very vital and important. Essential oils are one of the most valuable secondary metabolites that inclouded Polyphenols, terpenoids, alkaloids and phenylpropanoids. In this study extraction time, yield, total phenolic contents, antioxidant activity of essential oils obtained from 8 different extraction methods in two models conventional (HD_{BP}, HD_{RIFR}, SWD_{BP}) and innovative methods (SD_{innove}, MHD_{400w},

MHD_{800w},$MSHD_{400w}$, $MSHD_{800w}$) were compared. Reduce extraction time [40 min against 4h for conventional methods], high oil yield (1.2 ml/100 g dry plant), natural odor (similar smell to the original savory), high antioxidant activity and total phenol content were caused that ($MSHD_{800w}$)was the best extracrion method of the *Satureja bachtiarica* Bunge essential oil. In conclusion, the microwave – assisted extraction "was green technology" in terms of lower extraction time, high essential oil yield,good quality of obtained essential oil and was a promising tool for the extraction of essential oil from medicinal plants and aromatic herbs in use pharmaceutical , food industry , cosmetics , hygienics and aromatherapy.

Acknowledgements
The authors are grateful to University of Kashan for supporting this work.

4. References

[1] Al-Abed, N.M., Nor.Z M., Mansor, M., Azhar, F., Hasan, M. S.,&Kassim, M. Antioxidant, antibacterial activity, and phytochemical characterization of Melaleucacajuputi extract, BMCCompiementary and Alternative Medicine,15 (2015) 385-398.
[2] Ang, L. Z. P., Hashim, R., Sulaiman, S. F., Coulibaly, A. Y., Sulaiman, O., Kawamura, F.,&Salleh, K. M. In vitro antioxidant and antidiabetic activities of Glutatorquata. Industrial Crops and Products, 76 (2015) 755–760.
[3] Babadi, ES., GhasemiPirbalouti, A., Nourafcan, H., Hamedi,B. Bioactivity of essential oil of *bakhtiari savory* (Lamiaceae). Electronic Journal of Biology, 8(4) (2012) 73-8.
[4] Baharfar, R., Azimi, R., &Mohseni, M. Antioxidant and antibacterial activityof flavonoid-, polyphenol-and anthocyanin-rich extracts from Thymus kotschyanusboiss&hohen aerial parts. Journal of Food Science and Technology. 52 (2015) 6777–6783.
[5] Costa, p., Medronho, B., Goncalves, S., & Romano, A. Cyclodextrines enhance the antioxidant activity of essential oils from three Lamiaceaspecies. Industrial Crops and Products. 70 (2015) 341-346.
[6] Cronquist, A. The Evolution and Classification of Flowering Plants, TheNewYork. Botanical Garden, New York, USA, (1988).
[7] Fathi, A., Sahari, MA., Barzegar, M., Naghdi Badi, H. Antioxidant activity of *Saturejahortensis*L. essential oil and its application in safflower oil.Journal of Medical Plants. (2013) 12 45 51-67.
[8] Gharibi, S., Tabatabaei, B. E. S., &Saeidi, G. Comparison of essential oil composition, flavonoid content and antioxidant activity in eight Achillea species. Journal of Essential Oil Bearing Plants. 18 (2015) 1382–1394.
[9] Ghasemi, A. Medicinal and Aromatic plants. Shahrekoard Islamic Azad University. (2010) 32 ,10.
[10] Golmakani,MT.,Rezaei,K. Comparison of microwave-assisted hydrodistillation with the traditional hydrodistillation method in the extraction of essential oils from *Thymus vulgaris* L. Food Chememistry Journal. 109,4 (2008) 925-30.
[11] Gupta, D., Shah, M.,Shrivastav, P. Microwave-Assisted Extraction of Eucalyptus Citriodora Oil and Comparison with Conventional Hydro Distillation. Middle-East. Journal of Science Research. 16,5 (2013) 702-5.
[12] Hashemi, M., Niakousari, M &Saharkhiz, M. Antioxidant activity of *Saturejabachtiarica*Bunge essential oil in rapeseed oil irradiated with UV rays. European Journal of Lipid Science and Technology. 113 (2011) 1132–1137.
[13] Lucchesi, M.E., Smadja, J., Bradshaw, S., Louw, W., Chemat, F. Solvent freemicrowave extraction of Elletariacardamomum L.: a multivariate study of anew technique for the extraction of essential oil. Journal of Food Engineering . 79 (2007) 1079–1086.
[14] Memarzadeh,S.M.,GhasemiPirbalouti, A., Adibnejad, M.Chemical composition and yield of essential oils from Bakhtiari savory (*Saturejabachtarica*Bunge.) under different extraction methods.Journal of Industrial Crops and Products. 76 (2015) 809-816.
[15] Meshkatalsadat,M. ,Rabiei, K.,Shabaninejad,Y. Chemical characterization of volatile oils of different parts of *Saturejabachtarica*Bunge. Journal of Advances in Chemistry .(2013) 5,2,678-684.
[16] Oke F, Aslim B, Ozturk S, Altundag S. Essential oil composition, antimicrobial and antioxidant activities of *Saturejacuneifolia*Ten. Journal of Food Chemistry.112 (2009) 874–879.
[17] Pare, J., Belanger, J. Instrumental Methods in Food Analysis. Elsevier, Amsterdam. (1997).
[18] Périno-Issartier, S., Ginies, C., Cravotto, G., Chemat, F. A comparison ofessential oils obtained from Lavandin via different extraction processes: ultrasound, microwave, turbo hydrodistillation, steam and hydrodistillation. Journal of Chromatography. A .1305 (2013) 41–47.
[19] Stashenko, E.E., Jaramillo, B.E., Martı´ınez, J.R. Comparison of differentextraction methods for the analysis of volatile secondary metabolites of Lippiaalba (Mill.) NE Brown, grown in Colombia, and evaluation of its in vitroantioxidant activity. Journal of Chromatography. A. (2004) 93–103.
[20]. Tigrine-Kordjani, N., Meklati, B.Y., Chemat, F. Microwave 'dry' distillation asan useful tool for extraction of edible essential oils.International Journal Aromatherapy. 16 (2006) 141–147.
[21] Tohidi, B., Rahimmalek, M., Arzani, A. Essential oil composition ,totalphenolic,flavonoidcontents,and antioxidant activity of Thymus species collected from different regions of Iran.Journal of Food Chemistry. 220 (2017) 153-161.
[22] Zhang, H.F., Yang, X.H., Wang, Y. Microwave assisted extraction of secondarymetabolites from plants: current status and future directions. Trends in Food Science and Technology journal. 22(2011) 672–688.

29TH IRANIAN ORGANIC CHEMISTRY CONFERENCE
1_3 NOV, 2023
UNIVERSITY OF QOM, IRAN

The effect of TPP concentration on levothyroxin release from nanoclay/chitosan nanocomposite

*Nastran Baghfar and Elham Rostami**
Department of Chemistry, Faculty of Science, Shahid Chamran University of Ahvaz, Ahvaz, Iran,
e.rostami@scu.ac.ir, e.rostami@scu.ac.ir

Abstract - A nanoparticle polymer has been developed as a potential platform for drug delivery. Chitosan nanoparticles were prepared with tripolyphosphate (TPP) by the ionic crosslinking method. The particle size of chitosan nanoparticles was in the range of 190-250 nm and encapsulation efficiencies of levothyroxine were 85%. The particle size was determined by photon correlation spectroscopy (PCS). Shape and surface morphology were determined by transmission electron microscopy (TEM) and scanning electron microscopy (SEM). They revealed fairly spherical shape of nanoparticles. A non-invasive way to deliver drugs to the deepest parts of the human body is ultrasound. To study how ultrasound causes levothyroxine to be released from chitosan nanoparticles, cumulative release was examined. In this report, we explore the effect of ultrasound and tripolyphosphate (TPP) concentration on release behavior of levothyroxine from chitosan nanoparticles. The drug release from chitosan nanoparticles was enhanced using the ultrasound wave.

1. Introduction

Chitosan is a neutral polysaccharide polymer which is widely applied in pharmaceutical products. This biopolymer is composed of β-2-amino-2-deoxy-D-glucopyranose (glucosamine units). Monomer units are combined by β (1-4) glycosidic linkages. Chitosan has unique properties such as biocompatibility, biodegradability, safety and mucoadhesivity. Due to its biocompatibility may not cause allergic reactions and rejection. Moreover, as stated above it is biodegradable which gradually degrades to safe products (amino sugars), which are completely absorbed by the human body. Pharmaceutical usage of chitosan is due to the amino groups on its chain. Chitosan application as a biomaterial to provide controlled release systems has received much attention [1-4]. Ultrasound has a promising role in the delivery of therapeutic agents including genetic material, proteins, and chemotherapeutic agents. Cavitating gas bodies such as microbubbles are the mediators through which the energy of relatively non-interactive pressure waves is concentrated to produce forces that are able to increase cell membrane permeability and may shear the drug-carrying vesicles. The size of the bubbles can be affected by passing pressure wave through the media [5, 6]. In the presence of microbubbles, delivery of drug material is seriously improved using ultrasound [6]. Ultrasound affects the degradation rate of bioerodible polymers [1-3]. In this work we studied the effect of ultrasound and TPP concentration on levothyroxine release, as a drug model, which is loaded in chitosan nanoparticles. We reported that release percent of levothyroxine from chitosan nanoparticles (polymeric matrix) can be repeatedly modulated from an external position to the environment by ultrasonic energy.

2. Materials and Methods

2.1. Matrilas: Materials. Chitosan was purchased from Sigma–Aldrich (USA) with a MW of 60*103 and the degree of deacetylation was 93%. Levothyroxine sodium was obtained as a gift from the Iran Hormone Company. Tripolyphosphate (TPP), polysorbate 80 (Tween 80), acetic acid and other reagents were purchased from Merck.

2.2. Prepartion of nanocomposite chitosan/Nanoclay: Preparation of TPP-Chitosan nanoparticles. Chitosan solution was prepared by dissolving it in 1% acetic acid and polysorbate 80, as an emulsifier, (2% v/v) was mixed into the chitosan solution. Levothyroxine, poorly soluble drug in water, was dissolved in DMSO (2:10) and then this oil phase was mixed with aqueous phase (chitosan solution) by probe sonication applying 20 kHz frequency for 10 min. TPP (2% w/v) solutions were dropped by spray gun into the chitosan solution. Then, nanoparticles were washed with distilled water repeatedly followed by vacuum drying for 12 h [4].

In vitro release of levothyroxine from chitosan nanoparticles. The experiment was conducted by a static horizontal Franz diffusion cell to evaluate the amount of released levothyroxine sodium. The receptor medium was 50 mL in volume and composed of an aqueous solution of physiological saline, phosphate buffer solution, which stirred by a magnetic stirrer at 100 rpm to homogenize the medium (pH=7.4). A 2 ml of chitosan nanoparticles was separately loaded onto the donor compartment. 1 ml of the release medium was sampled using a syringe

needle and the same volume of fresh receptor medium was replaced at certain time intervals. The samples were analyzed using a spectroscopic method as described previously [5].

Morphological characterization of chitosan nanoparticles. Size and zeta potential were measured by photon correlation spectroscopy (PCS) (Nano ZS4700 nanoseries, Malvern Instruments, UK). To capture the transmission electron microscopy (TEM) (Zeiss-EM 10C- Germany) microphotographs, the nanoparticles samples stained with 2% (w/v) phosphotungstic acid were employed. Investigation of surface morphology of nanoparticles was performed by scanning electron microscopy (SEM, KYKY-EM3200, China).

3. Results and discussion

3.1. Characterization of nanocomposite: Characterization of chitosan nanoparticles. SEM image of the samples containing drug loaded chitosan nanoparticle is shown in Fig. 1. The image showed spherical shape and smooth surface with a particle size in nanometric scale. The particle size of levothyroxine-loaded chitosan nanoparticle showed SEM images are in agreement and the result of PCS (Fig. 2). Fig. 2 showed a narrow size distribution with a poly dispersity index of 0.232, indicating chitosan nanoparticle mono dispersity, with an average diameter of 225 nm. All applied techniques are indicative of circular shape and no aggregation of the nanoparticles. The average diameter determined by both SEM and TEM was found to be around 200 nm which is approximately the same as that of obtained by PCS.

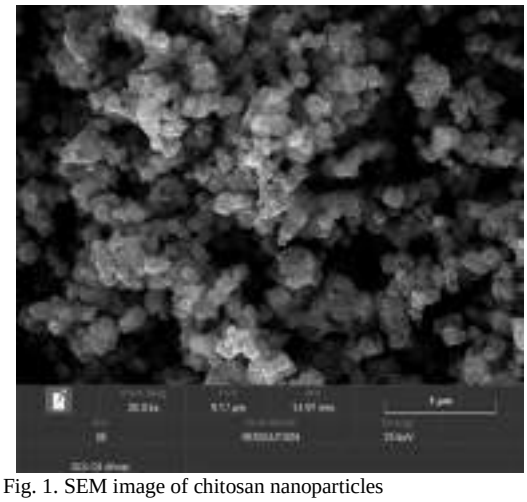

Fig. 1. SEM image of chitosan nanoparticles

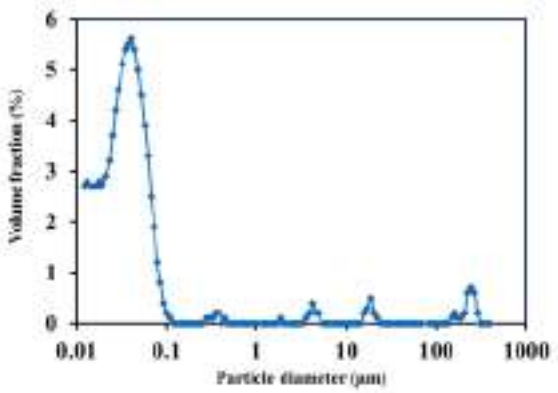

Fig. 2. Size distribution of chitosan nanoparticles

3.2. Effect of Ultrasound on release of Levothyroxine:
The effect of ultrasound on drug release. The results of drug release have been shown in Fig. 4. Ultrasound influenced the degradation rate of chitosan nanoparticles. Ultrasound increased the amount drug release of nanoparticles. Cavitating gas, which is created by ultrasound, is a moderator through which the energy of relatively non-interactive pressure waves is concentrated to produce forces that unstable cell membranes and shear the drug containing vesicles. Thus the presence of microbubbles immensely increases delivery of the drug [5].

3.2.Effect of TPP concentration on release of Levothyroxine:
The effect of TPP concentration and ultrasound on drug release profile. In this study TPP/Chitosan nanoparticles were fabricated by the virtue of ionic interaction between positively charged amino groups of chitosan and the negatively charged counter ions of TPP.

3.4. Conclusion: uring the last decade, nanomedicine has provided a promising new field in medicine to apply nanoscale materials for drug delivery. Chitosan nanoparticles were prepared with tripolyphosphate (TPP) by ionic crosslinking method. The size and morphology of chitosan nanoparticles were determined by TEM and SEM that obtained in the range of 190-250 nm. Encapsulation efficiencies of levothyroxine were measured to be 85%. The efficiency of drug delivery was enhanced by the application of directed energy, e.g. ultrasound. Ultrasound increased the amount of levothyroxine molecules diffused from the polymer matrix at a higher rate, up to 90%.

4. References

[1] 1. V Mourya, N.N. Inamdar,. Reactive and Functional polymers, 68 (2008) 1013-1051.

[2] 2. R. Shepherd, S. Reader, and A. Falshaw, Glycoconjugate journal, 14 (1997) 535-542.
[3] 3. F.A. Razmi, et al. Journal of cleaner production, 23 (2019) 98-109.
[4] 4. Ren, L., et al., International journal of biological macromolecules, 135 (2019) 898-906.
[5] 5. Q.Luo, et al. International journal of biological macromolecules, 139 (2019) 521-530.
[6] 6. F. Taher., et al., International journal of biological macromolecules, 126 (2019) 478-487.

29TH IRANIAN ORGANIC CHEMISTRY CONFERENCE
1_3 NOV, 2023
UNIVERSITY OF QOM, IRAN

Ethanol-Drop Grinding Approach: CuI-Graphene Nanocomposite Catalyzed Synthesis of Chromene Derivatives

Simin Janitabar-Darzi[1]*, *Shahrzad Abdolmohammadi*[2]*

[1]*Nuclear Science & Technology Research Institute, Nuclear Fuel Research School, Tehran, Iran, P.O. Box: 14395-836, sjanitabar@aeoi.org.ir*

[2]*Department of Chemistry, South Tehran Branch, Islamic Azad University, Tehran, Iran, sh.abdolmohammadi@iau.ac.ir*

Abstract - This paper presents an applicable and high-yield protocol for the preparation of 7-aryl-6*H*,7*H*-chromeno[4,3-*b*][1,3]dioxolo[4,5-*g*]chromen-6-ones under ethanol-drop grinding at room temperature. The use of effective grinding manner as a simple and inexpensive method a long with the simple operation, reusability of catalyst, short reaction time, and high product yields are the prominent features of this procedure.

Key words: Synthesis, Chromene Derivatives, CuI-Graphene Nanocomposite, Catalyst

1. Introduction

Among the various number of natural and unnatural bio-active heterocycles discovered heretofore, chromene based molecules are assumed privileged scaffolds due to their versatile biological profiles [1]. Compounds bearing the chromene motif exhibit numerous efficacious biological activities, such as antimicrobial [2], antiviral [3, 4], mutagenicitical [5], antitumoral [6], antioxidants [7], central nervous system (CNS) activities [8], and enzyme inhibitors [9]. In the present work we encouraged to develop the utility of CuI-graphene nanocomposite as an efficient heterogeneous catalyst for a facile synthesis of novel 7-aryl-6*H*,7*H*-chromeno[4,3-*b*][1,3]dioxolo[4,5-*g*]chromen-6-ones (**4**) by the cyclocondensation reaction of 4-hydroxycoumarin, aromatic aldehydes, and 3,4-methylenedioxyphenol under ethanol-drop grinding at room temperature (Scheme 1).

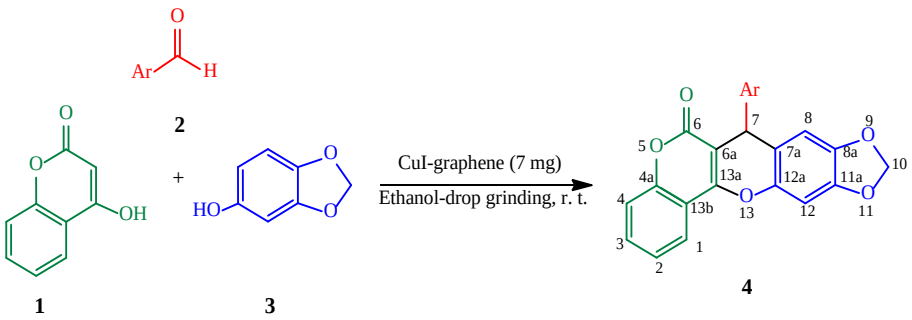

Figure 1. Chromene based derivatives obtained from natural origin with cell damage potential.

2. Results and Discussion

First, the nanocomposite was synthesized *via* the co-precipitation method reported by Sslavati et al. [10].
To get the detailed information of the surface state and morphology of the CuI-graphene nanocomposite, the SEM image of nanocomposite is depicted in Figure 2. The SEM study of the nanocomposite reveals that the CuI nanoparticles are spherical in shape with the average diameter between 40-50 nm. Most of the CuI NPs are coated onto the graphene sheets, with best distribution. Moreover, most of the graphene nanosheets existed in the composite are curled and entangled with a layered structure.
XRD and SEM-EDS techniques were used to demonstrate the morphology and purity of the nanocomposite.

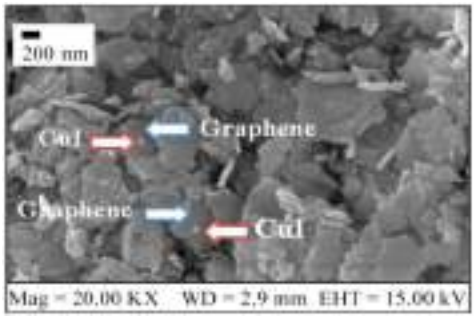

Fig.2. SEM image of the CuI-graphene nanocomposite.

The XRD pattern of the synthesized CuI-graphene nanocomposite is shown in Figure 3. All reflection peaks can be readily indexed to the planes of the pure cubic phase nanocomposite with Fd3m space group (JCPDS 82-2111).

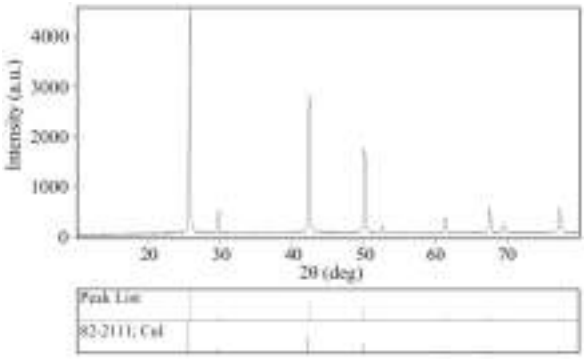

Fig.3. Powder XRD pattern of the CuI-graphene nanocomposite.

In our next endeavor, we have studied on a model reaction between 4-hydroxycoumarin, benzaldehyde, and 3,4-methylenedioxyphenol to find suitable reaction conditions (Table **1**). The best results are obtained from conditions of entry 3.

Table 1 Screening of the optimized reaction conditions in the synthesis of 7-phenyl-6*H*,7*H*-chromeno[4,3-*b*][1,3]dioxolo[4,5-*g*]chromen-6-ones (4**a**).

Entry	Nanocatalyst (mol%)	Tim (min)	Yield (%)[b]
1	No catalyst	40	trace
2	CuI-graphene (5 mg)	15	83
3	CuI-graphene (7 mg)	15	95
4	CuI-graphene (10 mg)	15	95
5	HCl (10 mol%)	30	70
6	*p*-TSA[a] (10 mol%)	30	72
7	CuI-graphene (7 mg)	10	90
8	CuI-graphene (7 mg)	20	96

[a]*p*-TSA: *p*-Toluenesulfonic acid.
[b]Isolated yield.

After determining the optimized reaction conditions, the condensation of various aromatic aldehydes with 4-hydroxycoumarin and 3,4-methylenedioxyphenol in the presence of CuI-graphene was studied. As shown in Table 2, reactions proceeded smoothly under the optimized reaction conditions, and led to the high yields of desired products.

Table 2 CuI-graphene catalyzed synthesis of 7-aryl-6*H*,7*H*-chromeno[4,3-*b*][1,3]dioxolo[4,5-*g*]chromen-6-ones **4**(**a-e**)

Products	Ar	Time (min)	Yield (%)[a]
4a	C_6H_5	15	95
4b	4-BrC_6H_4	12	97
4c	4-NCC_6H_4	15	98
4d	3-HOC_6H_4	15	94
4e	3-$O_2NC_6H_4$	10	96

[a]Isolated yield.

3. Experimental Section

General procedure for the synthesis of compounds 4a-e: A mixture of 4-hydroxycoumarin (**1**, 1 mmol), arylaldehyde **2** (1 mmol), 3,4-methylenedioxyphenol (**3**, 1 mmol), and and CuI-graphene (7 mg) were grinded in a mortar at room temperature, in the presence of catalytic drops of ethanol, for 10-15 minutes. The progress of the reaction was monitored with TLC in 2:1 ethyl acetate/n-hexane as TLC solvent. Upon completion of the reaction, the reaction mixture was dissolved in hot ethanol (3 mL), and the mixture was centrifuged at 2000-3000 rpm, for 5 min to remove the catalyst for reusing after washing several times with ethanol and drying. The pure product was obtained by cooling the ethanol solution to room temperature, diluted with 1 mL H_2O and allowed to crystallize.

7-Phenyl-6H,7H-chromeno[4,3-b][1,3]dioxolo[4,5-g]chromen-6-one **(4a):** White powder; yield: 0.352 g (95%), m.p. 278-280 ˚C. IR (KBr): ν_{max} = 3060, 2727, 2605, 1702, 1657, 1606, 1562, 1345, 1305, 1267, 1205, 1096 cm^{-1}. – ^1H NMR (500 MHz, DMSO-d_6): δ = 6.05 (1 H, d, J = 1.1 Hz, H-10), 6.10 (1 H, d, J = 1.1 Hz, H-10'), 6.40 (1 H, s, H-7), 7.17 (3 H, m, HAr), 7.24 (2 H, m, HAr), 7.35 (2 H, brt, J = 7.4 Hz, HAr), 7.38 (1 H, brs, HAr), 7.40 (1 H, brs, HAr), 7.70 (1 H, brt, J = 7.7 Hz, HAr), 7.93 (1 H, brd, J = 7.9 Hz, HAr) ppm. – ^{13}C NMR (125 MHz, DMSO-d_6): δ = 35.5, 98.7, 104.7, 108.0, 115.5, 117.3, 123.4, 123.5, 125.2, 126.2, 127.5, 128.5, 128.8, 131.4, 134.1, 139.2, 140.1, 151.7, 164.3, 164.5, 169.6 ppm. – Analysis calcd for $C_{23}H_{14}O_5$ (370.36): C 75.59, H 3.81; found C 75.69, H 3.65%.

4. References

[1] R. Pratap, V. J. Ram, Natural and Synthetic Chromenes, Fused Chromenes, and Versatility of Dihydrobenzo[h]chromenes in Organic Synthesis, Chem. Rev. 114 (2014) 10476–10526.

[2] M. M. Khafagy, A. H. F. A. El-Wahas, F. A. Eid, A. M. El-Agrody, Synthesis of halogen derivatives of benzo[h]chromene and benzo[a]anthracene with promising antimicrobial activities, Farmaco, 57 (2002) 715-722.

[3] W. P. Smith, L.S. Sollis, D. P. Howes, C. P. Cherry, D. I. Starkey, N. K. Cobley, Dihydropyrancarboxamides Related to Zanamivir: A New Series of Inhibitors of Influenza Virus Sialidases. 1. Discovery, Synthesis, Biological Activity, and Structure−Activity Relationships of 4-Guanidino- and 4-Amino-4H-pyran-6-carboxamides, J. Med. Chem. 41 (1998)787- –797.

[4] Martinez-Grau, J. L. Marco, Friedländer reaction on 2-amino-3-cyano-4H-pyrans: Synthesis of derivatives of 4H-pyran [2,3-b] quinoline, new tacrine analogues, J. Bioorg. Med. Chem. Lett. 7 (1997) 3165-3170.

[5] K. Hiramoto, A. Nasuhara, K. Michiloshi, T. Kato, K. Kikugawa, DNA strand-breaking activity and mutagenicity of 2,3-dihydro-3,5-dihydroxy-6-methyl-4*H*-pyran-4-one (DDMP), a Maillard reaction product of glucose and glycine , Mutat. Res. 395 (1997) 47-56.

[6] S. J. Mohr, M. A. Chirigos, F. Fuhrman, J. W. Pryor, Pyran Copolymer as an Effective Adjuvant to Chemotherapy against a Murine Leukemia and Solid Tumor, *Cancer Res*. 35 (1975) 3750–3754.

[7] K. Mukai, K. Okabe, H. Hosose, Synthesis and stopped-flow investigation of antioxidant activity of tocopherols. Finding of new tocopherol derivatives having the highest antioxidant activity among phenolic antioxidants, *J. Org. Chem*, 54(1989) 557-560.

[8] F. Eiden, F. Denk, [Synthesis of CNS-activity of pyran derivatives: 6, 8-dioxabicyclo (3,2,1) octane]. Arch. Pharm. 324 (1991) 353-354.

[9] T. Ishikawa, Anti HIV-1 Active Calophyllum Coumarins: Distribution, Chemistry, and Activity, Heterocycles 53 (2000) 453.

[10] F. Tavakoli, M. Salavati-Niasari, A facile synthesis of CuI-graphene nanocomposite by glucose as a green capping agent and reductant, J. Ind. Eng. Chem, 20 (2014) 3170-3174.

29TH IRANIAN ORGANIC CHEMISTRY CONFERENCE
1_3 NOV, 2023
UNIVERSITY OF QOM, IRAN

Simultaneous Removal of Chromium and Congo Red from Water Using Zeolite-Based Nanocomposite

Fahimeh Farshi Azhar, Zahra Pasandeh and Leila Khoshmaram*

Department of Chemistry, Faculty of Basic Sciences, Azarbaijan Shahid Madani University, Tabriz, Iran, fahimeh.farshi@gmail.com

Abstract - Heavy metal ions, aromatic compounds and organic dyes are the major pollutants in water resources and removal of them from wastewaters is currently one of the most important environmental tasks for research. For this purpose, in this study, the synthesis of a nanocomposite based on natural zeolite (clinoptilolite, Clin) for the simultaneous removal of Cr (VI) ions and concord dye (CR) was performed. The synthesized material was identified by FTIR, XRD, and FESEM. Also, the simultaneous removal studies of Cr (VI) and CR were modelled and optimized with the response surface methodology, and in the optimal state, the maximum simultaneous removal percentage of Cr (VI) and CR was obtained 100% and 88%, respectively. Examination of the isotherm models showed best agreement with the Langmuir model. Also, the kinetic data had a better match with the pseudo-second order model. Evaluation of the stability and recovery of the adsorbent by performing five consecutive cycles of adsorption and desorption process, showed the high capability of the adsorbent for reuse.

1. Introduction

The expansion of industries has caused the entrance of various pollutants, including heavy metals and organic dyes into water sources. Because of the environmental and life risks caused by these pollutants, strict laws have been passed by the World Health Organization and national organizations. Arsenic, barium, cadmium, mercury, lead, and chromium have been recorded as the most toxic heavy metals for human's life. Also, organic dyes, due to their high consumption in industries, include a large volume of effluents. The mentioned pollutants cause various diseases due to their non biodegradability and tendency to accumulate in the body of living organisms. Therefore, wastewater treatment is very important to remove these pollutants [1].

There are various chemical and physicochemical methods for wastewater treatment, such as membrane filtration, chemical oxidation, coagulation and flocculation, biological treatment, adsorption, ion exchange, etc. Absorption is one of the low-cost, efficient and environmentally friendly technologies in the field of wastewater treatment. The basic challenge in the adsorption process is the synthesis of adsorbents with high adsorption capacity, selectivity, fast adsorption kinetics, reusability and cost-effectiveness [2].

Adsorbents are generally synthetic or natural materials with amorphous or microcrystalline structures. The most important adsorbents used in the process of removing pollutants from water are activated carbon, zeolites, clays, alumina, cheap adsorbents including agricultural products, biomass, polymers (natural and synthetic) and bioadsorbents (algae, fungus, bacteria, plants, grasses, compost).

In recent years, natural biodegradable polymers such as chitosan, starch, alginate, cyclodextrin, etc. have attracted special attention due to their biocompatibility, biodegradability, and accessibility. However, because of some limitations, such as low surface area, poor mechanical properties and low porosity, there is a need for their chemical or physical modification [3]. Zeolites, belong to the group of alumina silicates which consist of open frameworks with channels and pores of very different sizes and shapes containing water molecules. Clinoptilolite, as one of natural zeolites, due to its large surface area, valuable ion exchange capability and low cost has widely been used in removal of pollutants from water [4]. One of the polymers that has recently received attention in combination with natural polymer composites for pollutant removal applications is polyaniline. Due to its inherent advantages such as ease of synthesis, high stability, reversible redox properties, monomer cheapness, polyaniline is the most widely used conductive polymer. In polyaniline, due to the presence of amine and imine functional groups and benzoid and quinoid rings, there are an ability to forming a complex with some metal ions or electrostatic interaction with organic pollutants [5]. Therefore, taking into account the above-mentioned materials, in this research work, for the first time, a nanocomposite system is designed based on natural polymer, natural zeolite, and polyaniline, which is used

as an absorbent for simultaneous removal of Congo red dye and chromium from water.

2. Results and Discussion

2.1. Characterization

The results of FTIR analysis for pure and synthesized samples are shown in Fig. 1. Clin spectrum shows a broad peak at 3449 cm^{-1} due to the OH stretching vibration in (Al–OH–Al) and (Si–OH–Si). Also, the peaks at 1638 cm^{-1} and 1080 cm^{-1} are related to the H–O–H bending and Si–O (Si), (Al) stretching vibrations, respectively. The two distinct peaks at 793 cm^{-1} and 607 cm^{-1} are related to the Si–O(Si) and Si–O(Al) stretching bridges, respectively. The characteristic bands of PANI were observed at 3414 cm^{-1} (N–H stretching vibration), 1550 cm^{-1} (C=C stretching of the quinoid ring), 1460 cm^{-1} (C=C stretching of the benzenoid ring),1230 and 1286 cm^{-1} (C–N stretching), and 790 cm^{-1} (C–H stretching). The FT-IR spectrum of Alg exhibited the absorption bands at 3418 cm^{-1} (O–H stretching), 2926 cm^{-1} (CH_2 stretching), 1640 cm^{-1} (COO asymmetric stretching) and 1419 cm^{-1} (COO symmetric stretching). The bands at 900-1200 cm^{-1} were due to the O–C–O stretching of ether groups and the C–O stretching of alcoholic groups. In the FTIR spectrum of Clin-Alg/PANI nanocomposite, lower wavenumbers indicate some physicochemical interactions, such as hydrogen bonding between components, as well as the presence of

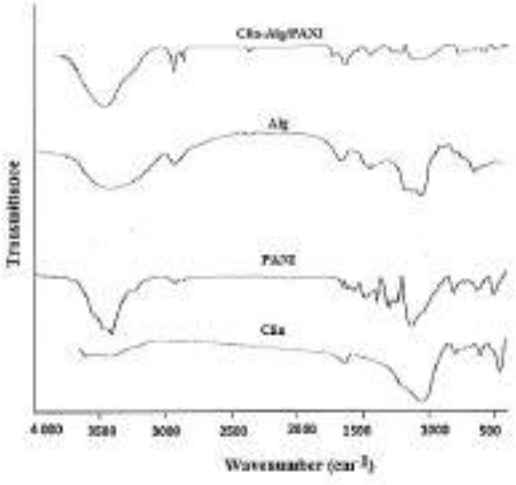

Fig. 1. FTIR spectra of samples.

X-ray diffraction technique was performed on samples and the results are shown in Fig. 2. In Clin pattern, the diffraction peaks appeared at 2θ=9°, 11° and 22° corresponding to the Miller indices of [020], [200] and [400], respectively, indicates its crystalline structure. The diffraction peaks of Alg were at 2θ=19°, 31°, 33° and 45°. The XRD pattern of PANI indicated its less crystalline structure. The diffraction peaks at 2θ=10°, 25° and 30° were assigned to the emeraldine polyaniline. In the XRD pattern of the Clin-Alg/PANI, the presence of specific peaks of all components and their broadness indicate the formation of amorphous composites.

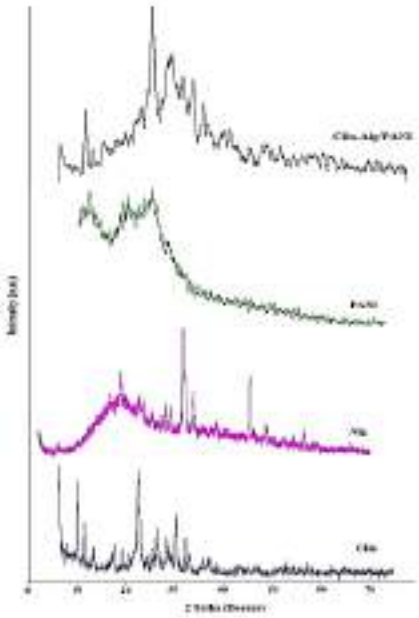

Fig. 2. XRD patterns of samples.

The results of the scanning electron microscope for the samples are shown in Fig. 3. SEM image of polyaniline showed a globular morphology. The image of Clin shows its uneven and porous structure. In Clin, holes have different shapes and sizes. It is also evident that there are open channels between the holes. In the Clin-Alg/PANI nanocomposite, the accumulation of polyaniline on the surface of the nanocomposite is clearly observed. The morphology of polyaniline is in the form of nanofibers with a diameter of 30-40 nm.

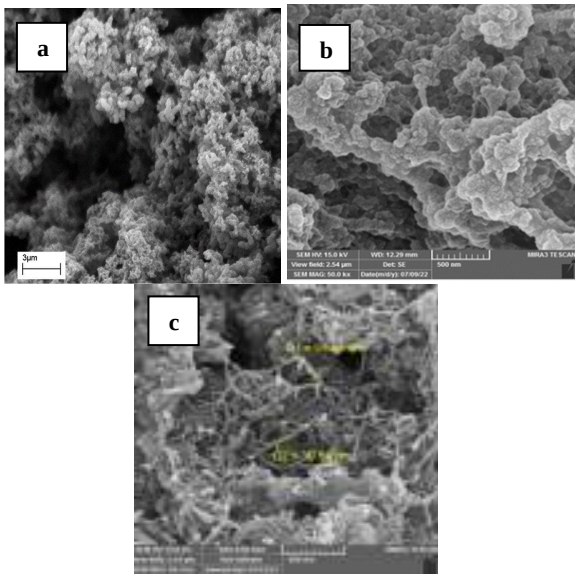

Fig. 3. SEM images of (a) PANI, (b) Clin, (c) Clin-Alg/PANI.

2.2. Removal studies

2.2.1. Effect of contact time

The effect of contact time between the Clin-Alg/PANI nanocomposites and Cr (VI)-CR solution was studied. Results indicated that the removal efficiency was increased within 2 min and remains almost constant even up to 20 min.

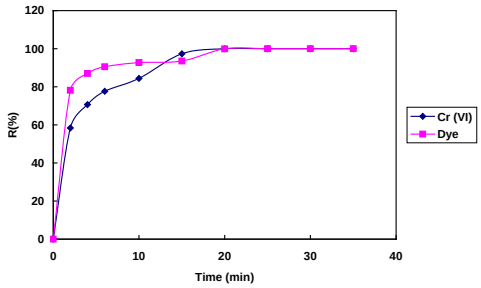

Fig. 4. Effect of contact time on the simultaneous removal of Cr(VI) and CR by Clin-Alg/PANI [Cr(VI)=20 mg l^{-1}, CR=40 mg l^{-1}, pH=6, adsorbent dose= 0.06 g/50 ml), T=25°C, 120 rpm].

2.2.1. Kinetic

In this project, pseudo-first-order, pseudo-second order, Elovich and intraparticle diffusion models were investigated. Results (Table 1) showed that the kinetic data fitted best into pseudo-second order model.

Table 1- Values of the parameters of kinetic models.

Elovich	Intraparticle diffusion	Pseudo-second order	Pseudo-first order	
β=0.328	K_p= 2.25	K_2= 0.024	K_1 = 0.196	**Cr (VI)**
α= 35.68	I= 6.97	Q_e = 18.41	Q_e = 11.83	
R^2= 0.9759	R^2 = 0.9917	R^2 = 0.9933	R^2 = 0.9029	
β=0.394	K_p= 1.81	K_2 = 0.045	K_1= 0.082	**CR**
α=49.58	I = 24.77	Q_e= 33.33	Qe= 5.78	
R^2= 0.8969	R^2= 0.8314	R^2= 0.997	R^2= 0.7434	

2.2.2. Isotherm

The adsorption isotherm is significantly important to investigate the interaction between the adsorbent and the adsorbate. Table 2 shows the adsorption equilibrium isotherm data using Langmuir, Freundlich and Temkin isotherm models. According to the results, the appropriate isotherm model is the Langmuir model and the R_L value obtained from this model is $0<R_L<1$ confirmed the optimal absorption process.

Table 2- Values of the parameters of isotherm models.

Temkin	Freundlich	Langmuir	
K_T = 245.24	K_f = 23.69	Q_m= 28.90	**Cr (VI)**
B = 1.9048	n = 14.45	k= 4.49	
R^2 = 0.9656	R^2 = 0.9585	R_L= 0.0044-0.0074	
		R^2 = 0.992	
K_T= 172.4	K_f = 22.83	Q_m= 35.21	**CR**
B= 4.4039	n = 6.29	k= 1.27	
R^2= 0.9231	R^2= 0/9351	R_L= 0.015-0.0026	
		R^2= 0.9958	

2.2.3. Reusability

To make the adsorbent economically competitive, the prepared nanocomposite should be reused for "n" number of cycles. The removal decreased nominally per cycle up to five cycle suggesting very high efficiency of the adsorbent. In the last cycle, 79% for Cr (VI) and 76% for CR adsorption was feasible.

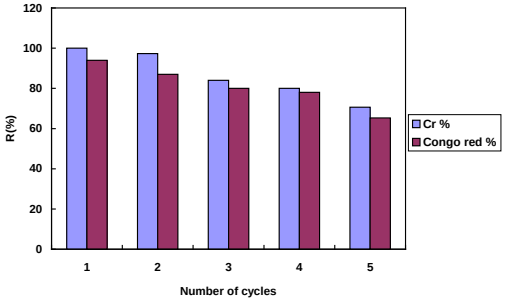

Fig. 5. Adsorption/desorption cycles of the simultaneous removal of Cr (VI) and CR by Clin-Alg/PANI nanocomposite.

3. Conclusion

The synthesis of Clin-Alg/PANI nanocomposite was performed by chemical oxidative polymerization of aniline in the presence of Clin-Alg nanocomposite dispersion. The application of prepared nanocomposite was investigated as an adsorbent for the simultaneous removal of Cr (VI) and CR from aqueous solutions. The batch sorption kinetics was tested and the pseudo-second order kinetic model was able to best describe the adsorption kinetic. The adsorption isotherms indicated that the adsorption behavior fitted better to the Langmuir model, which showed that the adsorption process was monolayer. Finally, the novel nanocomposite designed in this study is distinguished by significantly higher removal rate, reusability and stability, making it an industrially viable, economical and successful product to simultaneous removal of Cr (VI) and CR from solutions.

4. References

[1] M. K. Goswami, A. Srivastava, R. K. Dohare, A. K. Tiwari, A. Srivastav, Environ. Sci. Poll. Res. 30 (2023) 73031-73060.

[2] S. Jadoun, J. P. Fuentes, B. F. Urbano, J. J. Yáñez, J. Environ. Chem. Eng. 11 (2023) 109226.

[3] I. Jahan, L. Zhang, J. Polym. Environ. 30 (2022) 1709–1729.

[4] L. R. Rad and M. Anbia, J. Environ. Chem. Eng. 9 (2021) 106088.

[5] M. M. Talukder, M. M. R. Khan, M. K. Amin, S. Afr. J. Chem. Eng. 44 (2023) 276-282.

29TH IRANIAN ORGANIC CHEMISTRY CONFERENCE
1_3 NOV, 2023
UNIVERSITY OF QOM, IRAN

Interaction of Carmustine anticancer drug with Adenine, Cytosine, and Guanine nucleobases: By density functional theory, localized lector orbitals and atom in molecule theory

M. Rezaei Sameti[*], *A. Bagheri* and *L. Hosseiny Nejad*

Department of Applied Chemistry, Faculty of Science, Malayer University, Malayer, 65174, Iran,
ashkanbagherichemist@gmail.com, mrsameti@malayeru.ac.ir

Abstract

In this work, the interaction of Carmustine (CAM) anticancer drug with Adenine, Cytosine, and Guanine nucleobases is scrutinized at the B3LYP/6-31G (d, p) level of density functional theory by using Gaussian 09 software. The results of adsorption energy and deformation energy of all studied complexes are exothermic. The electrical properties of all studied complexes alter significantly from original states.

Keywords: Carmustine drug, Adenine, Cytosine, Guanine, Density functional theory

1. Introduction

Carmustine drug is used as an alkylating agent to treat several types of brain cancer including glioma, glioblastoma ultiforme, medulloblastoma and astrocytoma, multiple myeloma, and lymphoma (Hodgkin's and non-Hodgkin [1]. Biochemical research has shown that deoxyribonucleic acid or DNA plays a very important role in the body of living organisms and the transmission of hereditary codes that are required for the synthesis of all enzymes, proteins and affect cell function. It is found that DNA is the first target for the interaction of various therapeutic drugs, including antibiotics and anti-cancer drugs [2–5]. For this purpose in this study, we decided to investigate the interaction of Carmustine anticancer drug with Adenine, Cytosine, and Guanine nucleobases.

2. Computational section

In this study, all several of configuration of Carmustine anticancer drug with Adenine, Cytosine, and Guanine nucleobases are considered and all structures are optimized at the B3LYP/6-31G (d, p) level of density functional theory by using Gaussian 09 software. From optimized structures (see Fig. 1) the interaction energy, deformation energy, thermodynamic parameters, localized orbital lector, HOMO-LUMO energies, density of states plots (DOS), and atom in molecule (AIM) topological parameters are calculated for all considered structures.

3. Results discussion

The calculated results reveal that the adsorptions process of CAM-drug with Adenine, Cytosine, and Guanine nucleobases are exothermic, and spontaneous. The adsorption energies results demonstrate that the binding of Carmustine drug with adenine and guanine is strong. The density of states (DOS) plots (Fig.2) disclosed that the electrical properties of CAM-drug&adenine and guanine change significantly, so the effects of drug on adenine and guanine is more tangible, the reactivity of studied complexes increase.

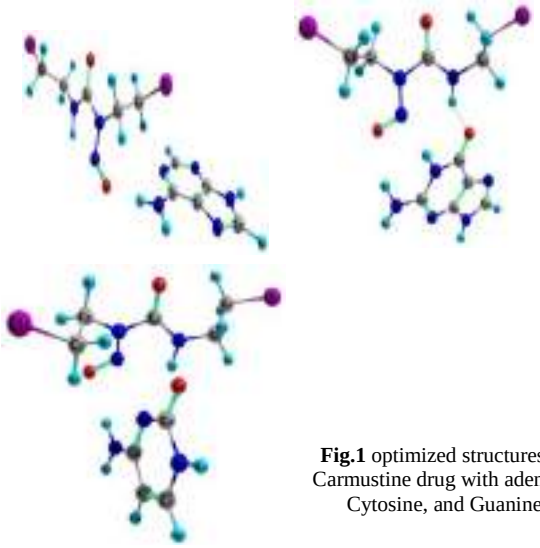

Fig.1 optimized structures of Carmustine drug with adenine, Cytosine, and Guanine

The AIM and LOL topological parameters (see Fig. 3) confirm that the type of bonding between drugs with these nucleobase is hydrogen bond or electrostatic type.

In the LOL plots the most electron density is concentrated around drug, this properties are important for treatment effects of drug in biological system.

4. Conclusion

The results of this study prove that Carmustine drug gives a stronger bond with the adenine and guanine part of DNA and affects the cell structure more. These results can help pharmaceutical experts in predicting how the drug works in the target cells.

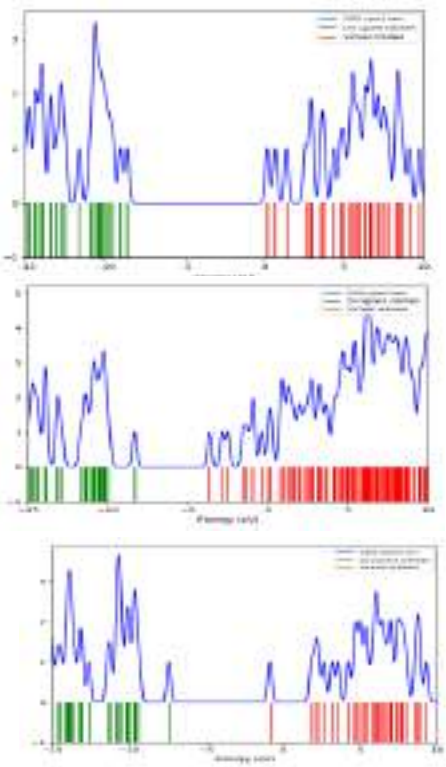

Fig. 2 The DOS plots of Carmustine drug with adenine, Cytosine, and Guanine

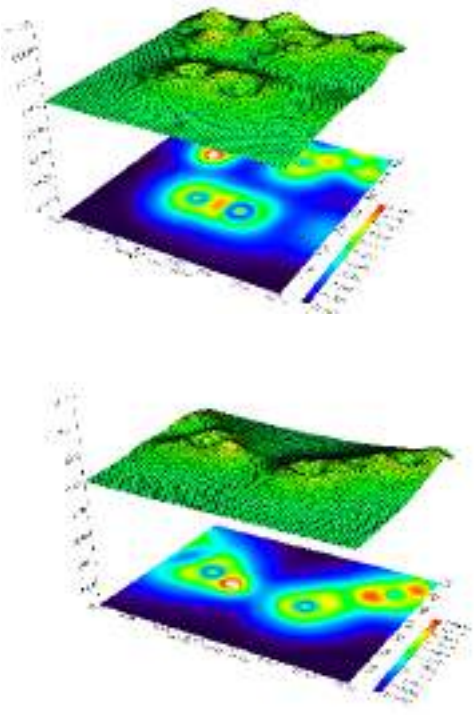

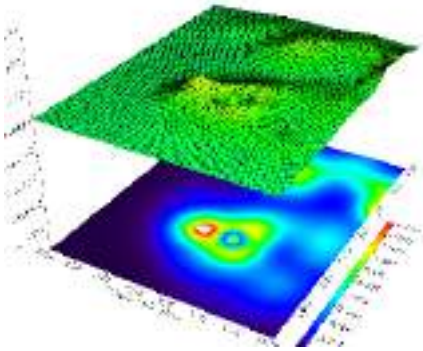

Fig.3 The LOL plots of Carmustine drug with adenine, Cytosine, and Guanine

References

[1] J. Rider Barbara, S.J. Enna, Bylund, B. David B. (eds.), Comprehensive Pharm. Referenc. 4(2022)1–4,

[2] D. B. Longley, D.P. Harkin, P.G. Johnston, 3 (2003) 330–338.

[3] R. Khorram, H., Raissi, M. Shahabi, M. Structural Chemistry (2018)1165-1172.

[4] A. Richards, A. Rodger, Chemical Sciety Reviews, 36(3) (2006) 471-483.

[5] M. Rezaei Sameti, H. Zanganeh, Physical Chemistry Research, 8(3) (2020) 511-527.

29TH IRANIAN ORGANIC CHEMISTRY CONFERENCE
1_3 NOV, 2023
UNIVERSITY OF QOM, IRAN

The computational study of interaction and adsorption of Mercaptopurine drug with adenine nucleobase of DNA: By DFT, TD-DFTT AIM methods

M. Rezaei Sameti[*], *A. Bagheri* and *M. Maleki*

Department of Applied Chemistry, Faculty of Science, Malayer University, Malayer, 65174, Iran, mrsameti@malayeru.ac.ir, ashkanbagherichemist@gmail.com.

Abstract

In the current study, we decided to investigate the interaction of Mercaptopurine (MEC) drug with adenine, thymine, guanine and cytosine nucleobase of DNA at ωB97XD/6-311G (d, p) level of density functional theory by using Gaussian 16 software. The thermodynamic results indicate that interaction of MEC drug with DNA nucleobase exothermic and favorable in the thermodynamic view. The results of the results can be used for detecting the nature of MEC drug with nucleobase of DNA.

Keywords: Mercaptopurine drug, DNA, DFT, AIM, Interaction

1. Introduction

The main motivation of this study to investigate the interaction of Mercaptopurine (MEC) drug with DNA nucleobases. Mercaptopurine drug is specifically used to treat acute lymphocytic leukemia (ALL), acute promyelocytic leukemia (APL), Crohn's disease, and ulcerative colitis [1]. The MEC anti-cancer drug adsorb to the DNA nucleobases of cancer cells and prevents their uncontrolled growth, so investigating its interaction can be theoretically important. In recent years, the interaction of anticancer drugs with various types of nanoparticles and DNA has attracted the attention of many pharmaceutical and chemical experts [2–5].

2. Computational section

In the current work by using density functional theory at the ωB97XD/6-311G (d,p) level of theory the interaction of MEC drug with adenine, thymine, guanine and cytosine nucleobases of DNA is scrutinized with Gaussian 16 software. The optimized geometrical structures, thermodynamic parameters, adsorption energy, quantum parameters such as global HOMO-LUMO energies, gap energy and global hardness, electrochemical potential atom in molecule (AIM) and reduced density gradient (RDG) parameters are computated.

3. Results discussion

The computational results indicate that due to the interaction of the drug with the adenine, cytosine, thymine nucleotide bases, the geometrical parameters of the drug and nucleobases alter significantly from pure state, so the electrical properties of all the MEC& nucleobases complexes alter. The adsorption energy and enthalpy values of all studied complexes are negative and the adsorption process is exothermic. The quantum parameters such as global hardness and electrochemical potential of all studied complexes reveal that the reactivity and stability of MEC@ nucleobases increase significantly from original state and this property is suitable for understanding the mechanism of drug interaction. The HOMO-LUMO results reveal that the most density of HOMO and LUMO orbital localized on the surface of adenine and other nucleobases, so this surface is suitable for electrophilic and nucleophilic interactions (see Fig.1). The density of plots (DOS) (Fig.2) results indicate that the number of peaks in the HOMO and LUMO region after adsorbing MEC drug increase, therefore the electrical and optical properties of all studied complexes increase.

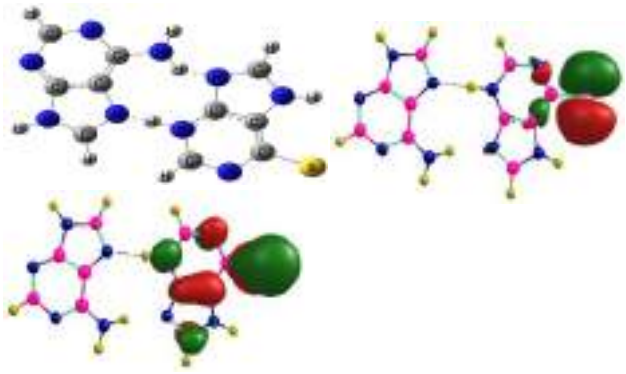

Fig.1 The optimized structures and HOMO-LUMO of Mercaptopurine with adenine

For detecting the MCE& nucleobase complexes the IR and Uv-visible spectrum of all studied complexes are calculated (see Fig. 3). These results can be used as a valuable method to detect the location of the drug in the vicinity of the target cells. Which can be important

in determining the effectiveness of the drug. The atom in molecule theory (AIM), and reduced density gradient (RDG) results confirm that the interaction of drug with adenine, cytosine, and thymine is non covalent or electrostatic type. (Fig. 3)

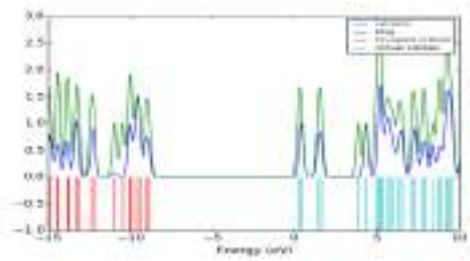

Fig.2 The DOS plot of Mercaptopurine with adenine

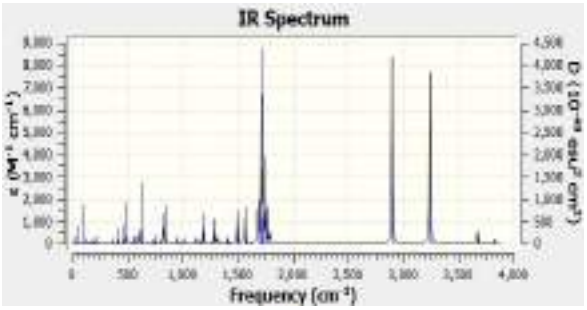

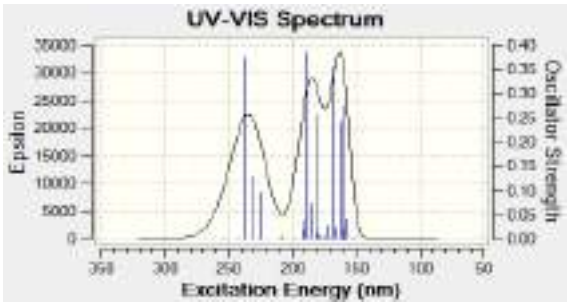

Fig. 3 The IR and Uv-visible Mercaptopurine with adenine

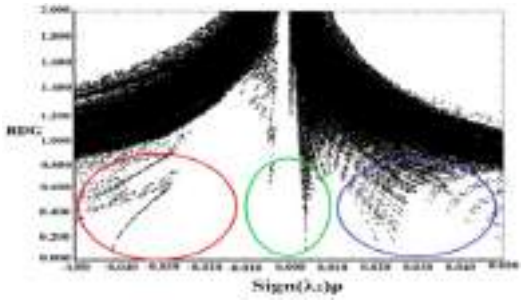

Fig. 4 The RDG plots Mercaptopurine with adenine

4. Conclusion

In this study by using computational methods the interaction of MEC drug with various nucleobases of DNA are investigated. The results this study demonstrate that the MEC drug with strong electrostatic or hydrogen bond adsorb on the surface of adenine and thymine nucleobases and the electrical properties of MEC& nucleobase change significantly from original state. This property is important in the treatment effects of drug in body. On the other hand by using the electrical and thermodynamic properties of all studied MEC&nuclobase complexes can be predicted the mechanism of drug reaction with DNA, these results can useful for pharmaceutical experts to predict how the drug works in the target cells.

References

[1] The American Society of Health-System Pharmacists. Archived from the original on 20 December (2016).
[2] M. Rezaei Sameti, Chemical Methodologies 4 (2020) 494–451
[3] M. Rezaei Sameti, J. Molecular Stru. 1248 (2020) 131478–82.
[4] N. Okulik, A. H. Jubert, .J. Molecular Design, 4 (2005) 17–30
[5] J.J. Lee JJ, J.H. Beumer, E. Chu, Cancer Chemother Pharmacol. 447(2016)447–464

29TH IRANIAN ORGANIC CHEMISTRY CONFERENCE
1_3 NOV, 2023
UNIVERSITY OF QOM, IRAN

Synthesis of Thiazolylaminomethyl-2-naphthols using Glucose-Choline Chloride Deep Eutectic Solvent

Ali Esmaeili[1], Hamzeh Kiyani[1,2] and Jalal Albadi[1]*

[1]*Department of Chemistry, Faculty of Science, Shahrekord University, Shahrekord, Iran, hkiyani@sku.ac.ir.*
[2]*School of Chemistry, Damghan University, Damghan, Iran, hkiyani@du.ac.ir.*

Abstract – The deep eutectic solvent was prepared from mixing glucose and choline chloride. The deep eutectic solvent was then employed in a one-pot, three-component reaction for the synthesis of some Betti base derivatives. The reactions were implemented using 2-naphthol, aryl/heteroaryl aldehydes, and 2-aminothiazole (or sulfathiazole drug) under solvent-free conditions at 60 ºC. The approach has the merits of good to high reaction yields, short reaction times, easy work-up, environmentally friendliness, atom economy, pot-, and step-economy.

1. Introduction

In synthetic and medicinal chemistry, multicomponent reactions (MCRs) are highly valuable and useful chemical transformations involving three or more reactants, which lead to the formation of the product in one-pot operation. These reactions are widely used for the synthesis of pharmaceuticals, agrochemicals, and other eye-catching organic molecules with structural diversity. MCRs allow faster synthesis of complex molecules and are also compatible with the goals of green and sustainable chemistry [1-4]. The Betti reaction, which includes a one-pot, three-component reaction between aldehydes, amine/ammonia and 2-naphthols to synthesize Beti bases, is of great importance [5]. Betti bases have various biological applications such as antibacterial [6], antitumor [7], antioxidant [8], anti-Alzheimer [9], antimicrobial, anthelmintic, anti-inflammatory, and blood pressure lowering activities. Fig. 1 shows some representative Betti bases (1-(α-aminoalkyl)-2-naphthols) and derivatives with pharmaceutical potential. In addition, the synthesis of aminothiazolyl naphthol derivatives according to Betti's method is a beneficial research field due to the formation of C-C bond under mild experimental conditions [10-12]. As we know, deep eutectic solvents (DESs) can be simply synthesized by mixing hydrogen bond acceptors (HBAs) and hydrogen bond donors (HBDs) molecules, usually under heating. DESs often exhibit a eutectic point. They are often low toxicological effects, low-priced, environmentally friendly, low volatility, safe, nonflammable, and more synthetically accessible. These new bio-renewable and biodegradable low-transition temperature mixtures have been employed as green reaction media or catalysts in a variety of chemical transformations and have applications in various fields such as nanomaterials, lubricants, pharmaceuticals, and separation techniques [13,14]. Several methods are available in literature for the one-pot synthesis of Betti bases using different reagents, catalysts, and supports, such as silica sulfuric acid [6], kaolin [8], porcine pancreatic lipase (PPL) [9], (+)-camphor-10-sulfonic acid [11], Fe_3O_4@MCM-41@$ZrCl_2$ [15], nano-[Ni-4-MSP]$(NO_3)_2$ [16], $FeCl_3$•$6H_2O$ [17], choline chloride/urea [18], sodium dodecyl sulfate (SDS) [19], NaCl [20], ZnO nano-micelles [21], etc. [22]. Based on the above facts, an efficient and green protocol for the synthesis of aminothiazolyl naphthols from aldehydes, 2-naphthol, and aminothiazoles in the presence of glucose-choline chloride (Gu-ChCl) deep eutectic solvent (DES) at 60 ºC under solvent-free conditions (Scheme 1).

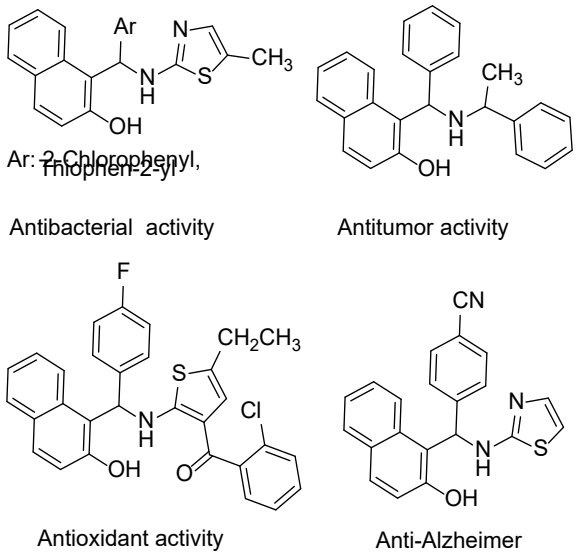

Fig.1. Representative examples of biologically active Betti bases.

2. Results and Discussion

To find the best optimal conditions, we have explored the synthesis of 1-(phenyl(thiazol-2-ylamino)methyl)-naphthalen-2-ol (**4a**) from the one-pot three-component condensation of 2-naphthol (**1**),

benzaldehyde (**2a**), and 2-aminothiazole (**3a**) under various reaction conditions. The optimization of reaction conditions was studied using diverse solvents, catalyst loading, reaction temperatures, and the time of the reaction were explored (Table 1).

Table 1 Optimization of reaction conditions

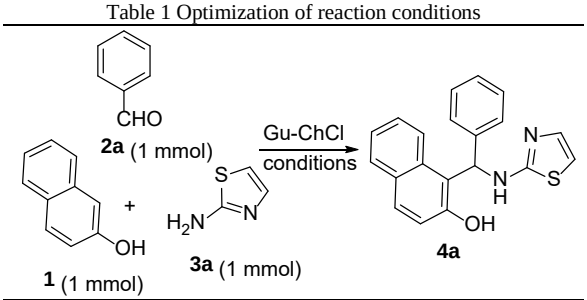

Entry	Catalyst (mol%)	Solvent	Temp. (ºC)	Time (min)/ yield (%)
1	-	H_2O	RT	75/64
2	-	EtOH	RT	75/trace
3	-	*n*-Hexane	RT	75/trace
4	-	EtOH	40	75/trace
5	-	EtOH	60	75/trace
6	1	H_2O	RT	75/68
7	1	EtOH	RT	75/trace
8	1	*n*-Hexane	RT	75/trace
9	1	H_2O	60	30/72
10	1	H_2O	reflux	30/75
11	1	-	40	15/68
12	1	-	50	15/72
13	1	-	55	5/80
14	1	-	60	5/86
15	1	-	65	5/82
16	1	-	70	5/80
17	2	-	60	5/87
18	3	-	60	5/89
19	4	-	60	5/91
20	**5**	-	**60**	**5/97**
21	6	-	60	5/88
22	7	-	60	5/80
23	-	-	RT	60/38

As shown in Table 1, three solvents including water, ethanol, and *n*-hexane were investigated in the absence the catalyst at various reaction temperatures (Table 1, entries 1-5). With the exception of the water solvent, which yielded 65% of the desired product (**4a**) in 75 min, the reaction in other solvents did not give satisfactory results, and after 75 min from the start of the reaction, only trace amounts were obtained. Also, the same reaction was carried out using 1 mol% catalyst in the same solvents, but the product was obtained in trace amounts in ethanol, and *n*-hexane (Table 1, entries 7 and 8), while it was slightly improved in water (Table 1, entry 6). Carrying out the reaction in the presence of 1 mol% of the catalyst in the water solvent at 60 ºC and under reflux conditions did not result in significant changes in yields, but the reaction time was reduced (Table 1, entries 9 and 10). Moreover, using 1 mol% of the catalyst, under solvent-free conditions, the model reaction was checked in the temperature ranging 40-70 ºC (Table 1, entries 11-16). The best result in terms of reaction time and yield was obtained at 60 ºC. The loading of catalyst was evaluated in 2, 3, 5, 6, and 7 mol% (Table 1, Entries 17-22) at 60 ºC, thus confirming that the optimal amount was actually 5 mol% (Table 1, Entry 20). Finally, the reaction was also carried out at room temperature and under solvent and catalyst-free conditions (Table 1, Entry 23). The reaction proceeds with very low product yield of 38% after 60 min. The reaction at other temperatures did not have significant results, and for this reason, other results were not mentioned in the Table.

After finding the best reaction conditions, the scope and generality of this organic transformation was evaluated. In this regard, various 2-naphthol (**1**), substituted benzaldehydes (**2a**-**h**), and 2-aminothiazole (**3a**), were employed to synthesizing a series of derivatives of Betti bases.[23] The results are shown in Table 2.

Table 2 synthesized Betti base derivatives catalyzed by Gu-ChCl

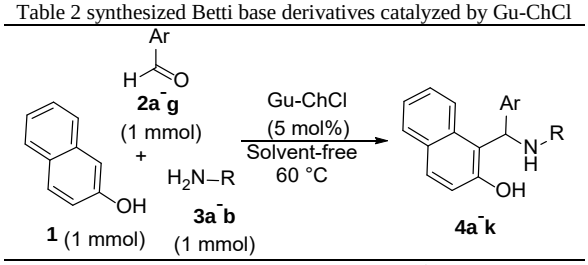

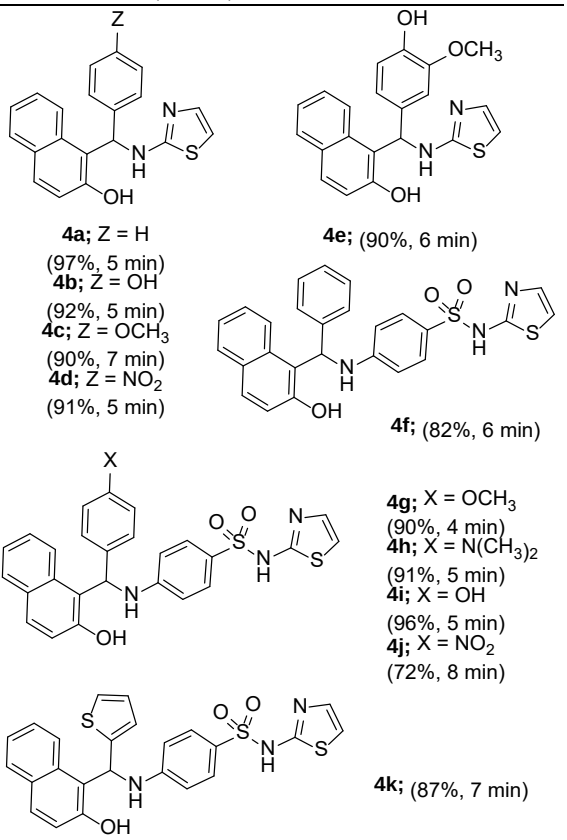

It was found that both electron-donating and electron-accepting benzaldehydes could be transformed to the

corresponding 1-(α-aminoalkyl)-2-naphthols (**4a**-**e**) in the presence of Gu-ChCl DES (5 mol%) at 60 ºC in the time range of 5-7 min and excellent isolated yields of the reactions (90-97%). Moreover, the aminothiazole component was changed to sulfathiazole drug in the three-component reaction and the synthesis of the corresponding Betti bases was explored. The reactions proceeded smoothly when sulfathiazole was used as the amine substrate. Under the same reaction conditions, the desired products (**4f**-**j**) were obtained in 72-96% yield in 4-8 min. Also, when thiophene-2-caboxaldehyde was used as a heteroaryl aldehyde, the three-component reaction proceeded well and the expected Betti base product (**4k**) was obtained in 87% reaction yield after 7 min.

3. Conclusions

A deep eutectic solvent (DES) was obtained from glucose and choline chloride at 50-60 ºC and used as the efficient and environmentally friendliness catalyst to synthesizing various 1-(α-aminoalkyl)-2-naphthols. Different amounts of DES catalyst were loaded in the model reaction and the results indicated that 5 mol% gave the best results. Also, the better results could be obtained at 60 ºC. The reaction was carried out in various solvents and under solvent-free conditions. The collected data led us to the conclusion that the better yields were obtained under solvent-free conditions and organic transformations occurred in the shortest reaction times. This method has the advantages of environmentally benign, pot-, atom-, and step-economy (PAS-economy).

4. References

[1] A. Domling, Chem. Rev. 106 (2006) 17-89.
[2] S. Kamalifar, H. Kiyani, Curr. Org. Chem. 23 (2019) 2626-2634.
[3] H. Kiyani, Curr. Org. Synth. 15 (2018) 1043-1072.
[4] Y.E. Ryzhkova, A.N. Fakhrutdinov, M.N. Elinson, Tetrahedron Lett. 81 (2021) 153336.
[5] A. Olyaei, M. Sadeghpour, RSC Adv. 9 (2019) 18467-18497.
[6] S.N. Dandekar, O.A. Lotlikar, M.M. Ramana, S.V. Rathod. Russ. J. Bioorg. Chem. 47 (2021) 874-881.
[7] R. Mallamaci, M.A.M. Capozzi, C. Cardellicchio, Appl. Sci. 12 (2022) 7779.
[8] I. Yellapurkar, S. Shaikh, M.G. Pavale, S. Bhabal, M.M.V. Ramana, Res. Chem. Intermed. 47 (2021) 4067-4082.
[9] S. Shaikh, M.M.V. Ramana, Res. Chem. Intermed. 47 (2021) 2731-2750.
[10] Z. Li, X. Mao, Heterocycl. Commun. 17 (2011) 219-222.
[11] E. Pelit, Z. Turgut, J. Chem. 2016 (2016) Article ID 9315614.
[12] O. Özbek, M.B. Gürdere, Phosphorus, Sulfur, Silicon, Relat. Element. 196 (2021) 444-454.
[13] D.A. Alonso, A. Baeza, R. Chinchilla, G. Guillena, I.M. Pastor, D.J. Ramon, Eur. J. Org. Chem. 2016 (2016), 612-632.
[14] A. Monem, D. Habibi, H. Goudarzi, Polycycl. Aromat. Compod. (2023) DOI:10.1080/10406638.2023.2254900
[15] R.P. Kisomi, F. Shirini, M. Golshekan, Appl. Organomet. Chem. 35 (2021) e6212.
[16] H. Goudarziafshar, A.R. Moosavi-Zare, E. Khazael, Polycycl. Aromat. Compd. 42 (2022) 3606-3621.
[17] I. Ramsha, Z.F. Ameer, A. Sajjad, H. Atta, N. Shazia, Curr. Org. Synth. 19 (2022) 569-577.
[18] (a) A. Bahrani, Z. Karimi-Jaberi, Indian J. Heterocycl. Chem. 29 (2019) 337-344; (b) N. Azizi, M. Edrisi, Res. Chem. Intermed. 43 (2017) 379-385.
[19] A. Kumar, M.S. Rao, V.K. Rao, Aust. J. Chem. 63 (2010) 1538-1540.
[20] K.N. Venugopala, M. Krishnappa, S.K. Nayak, B.K. Subrahmanya, J.P. Vaderapura, R.K. Chalannavar, R.M. Gleiser, B. Odhav, Eur. J. Med. Chem. 65 (2013) 295-303.
[21] J. Mou, G. Gao, C. Chen, J. Liu, J. Gao, Y. Liu, D. Pei, RSC Adv. 7 (2017) 13868-13875.
[22] (a) R. Iftikhar, M. Kamran, A. Iftikhar, S. Parveen, N. Naeem, N. Jamil, Mol. Divers. 27 (2023) 543-569; (b) S. Khandelwal, Y.K. Tailor, M. Kumar, J. Mol. Liq. 215 (2016) 345-386.
[23] Synthesis of Betti base compounds (**4a**-**k**). To a mixture of 2-naphthol (1 mmol), aldehydes (), and amine precursors (1 mmol) in a round bottom flask, 5 mol% of DES catalyst was added and stirred at 60 ºC for appropriate times. After completion of the reaction as monitored using thin layer chromatography (TLC), the reaction vessel was cooled to room temperature and precipitates began to settle. The precipitates were separated by simple filtration. The crude products purified by recrystallization from ethanol. The products were characterized by conventional spectroscopic techniques. Data for 1-((4-nitrophenyl)(thiazol-2-ylamino)methyl)naphthalen-2-ol (**4d**). ^{1}H NMR (300 MHz, DMSO-d_6) δ 6.69 (d, J = 3.6 Hz, 1H, $H_{thiazole}$), 7.07 (d, J = 3.6 Hz, 1H, $H_{thiazole}$), 7.27-7.34 (m, 3H, $H_{benzylic}$, Ar-H), 7.42 (t, J = 7.2 Hz, 1H, Ar-H), 7.55 (d, J = 8.4 Hz, 2H, Ar-H), 7.85 (d, J = 8.4 Hz, 2H, Ar-H), 7.92 (d, J = 7.2 Hz, 1H, Ar-H), 8.19 (d, J = 8.7, 2H, Ar-H), 8.53 (s, 1H, NH), 10.32 (s, 1H, OH); ^{13}C NMR (75 MHz, DMSO-d_6) δ 59.9 ($C_{benzylic}$), 107.9 ($C_{thiazole}$), 118.8, 118.9, 123.1, 123.8, 127.1, 127.8, 129.0, 129.1, 130.4, 132.5, 138.8 ($C_{thiazole}$), 146.4, 152.1, 153.7 (C-OH), 169.1 ($C_{thiazole}$).

29TH IRANIAN ORGANIC CHEMISTRY CONFERENCE
1_3 NOV, 2023
UNIVERSITY OF QOM, IRAN

Physicochemical evaluation of the effect of natural zeolite modification on the adsorption of dye

Hajar Farhadi, *Narjes Keramati* ***

Department of Nanotechnology, Faculty of New Sciences and Technologies, Semnan University, Semnan, Iran, Farhadi_hajar@semnan.ac.ir, narjeskeramati@semnan.ac.ir

Abstract Adsorption process is used in removing dye from wastewater due to its high efficiency, low cost, convenience and simplicity. In the present study, clinoptilolite (CP) zeolite was modified using the NaOH. The XRD pattern and FT-IR spectrum show that the CP is properly modified. The adsorption of methylene blue (5 ppm) by natural and modified clinoptilolite zeolite (0.3 g/L) was investigated for 20 and 40 minutes. The removal efficiency with the modified zeolite is higher than the original raw sample.
Keyword: Adsorption, clinoptilolite zeolite, chemical tretment, methylene blue

1. Introduction

Water pollution by industries such as textile and petrochemical, agricultural pesticides is one of the biggest problems in the world. One of the main sources of water pollution is dyes such as methylene blue (MB). It is widely used in textiles, leather, printing, paint, plastic and medicine. In recent years, various processes such as adsorption, ion exchange, sedimentation, reverse osmosis, filtration and oxidation have been used to remove pollutants. Among them, absorption is used due to its high efficiency, low cost, and simplicity [1].
Zeolites are porous alum inosilicates, which include elements such as Na, K, Mg, and Ca [2]. Their three-dimensional structures include silicon and aluminum atoms connected to oxygen, which are arranged in tetrahedral units, and are placed in a crystal structure. They include channels and cavities that have fine pores [3]. The adsorption capacity of natural zeolites varies depending on their source. For example: the absorption capacity of Clinoptilolite (CP) obtained from Manisa-Demirci, Turkey is more than other regions of Turkey and Greece. Also the adsorption capacity of zeolite depends on the characteristics of it, including composition, size and distribution of pores and crystal structure. However, unmodified natural zeolites have lower adsorption capacity than modified zeolites [4].
In order to be able to use zeolites as effective adsorbents [2], they can be modified by thermal treatment or a combination of heating and chemical modification using acids, bases and inorganic salts. Chemical and thermal treatment in zeolite may lead to cation migration and thus affect cation localization and pore opening. The adsorption characteristics of each zeolite depend on the precise chemical and structural properties of the adsorbent [3]. Desilication of zeolite is an effective method to improve its structure. It works through the selective extraction of silicon from the framework without significant changes in acidity and crystal structure [2]. Chemical modification methods were used to improve the efficiency of raw natural zeolite. Composition, Si/Al ratio, cation type, number and location also affect the efficiency of zeolite [3]. Also, the type of cation may affect the pore diameter. If zeolite contains one of potassium (K^+), sodium (Na^+) and calcium (Ca^{+2}) cations, their effective pore diameter will be approximately 3A°, 4A° and 5A° respectively [2]. Modification with acids and bases, and surfactant saturation with ion exchange are among the common methods used to modify the properties and change the hydrophilic/hydrophobic properties of zeolites.
In this research, clinoptilolite zeolite was modified by chemical modification method by using NaOH, and the results indicated that the adsorption capacity and its performance in adsorbing methylene blue has been compared with the unmodified sample.

2. Materials and Method

In order to remove natural zeolite impurities, it was washed with distilled water for one hour and then dried in an oven at 70 °C for one hour and named as CP. In order to modify natural zeolite, 2 g of CP were mixed with 60 ml of 0.2 M NaOH at 338 °K for 30 minutes, the zeolite was washed until it reached pH =7, and then dried at 373 °K for 12 hours. XRD and FT-IR analyzes were used to investigate the accuracy of the modification. Adsorption containing 100 ml of methylene blue solution (5 ppm) with 0.03 g of adsorbent were investigated in 20 and 40 minutes. The removal efficiency (R) of methylene blue was calculated using the equation 1. In Equation 1, C_i is the initial concentration of the MB (mg/L) and C_t is the concentration of the MB at time t (mg/L).

$$R\ (\%) = \frac{(C_i - C_t)}{C_i} \times 100 \quad (1)$$

3. Results and Discussion

Figure 1 shows the comparison of XRD patterns of natural and modified zeolites. The XRD pattern of natural zeolite shows that it mainly contains significant amounts of clinoptilolite, hollandite, biotite, and feldspar and quartz phases. Therefore, in addition to the clinoptilolite phase, there are other phases in the material. But the dominant phase in zeolite is clinoptilolite [5]. The peaks of clinoptilolite index have appeared at the angles of 9.8, 11.24, 17.4, 20.8, 22.4, 26.7, 30 and 33 degrees [6-8]. There are changes in some of the modified clinoptilolite peaks that are attributed to the zeolite modification processes and are caused by changes in the Si/Al of the modified materials [3].

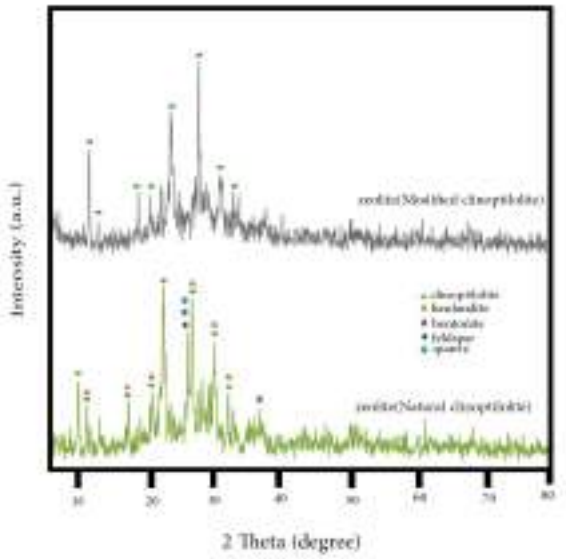

Fig.1. XRD pattern of natural and modified CP zeolite

FT-IR analysis was used to analyze the chemical structures of the samples. The FT-IR spectra of natural and modified clinoptilolite samples are shown in Figure 2.

In the FT-IR spectrum study of natural clinoptilolite, the peaks observed in the range of 3750-2900 cm^{-1} are attributed to OH.

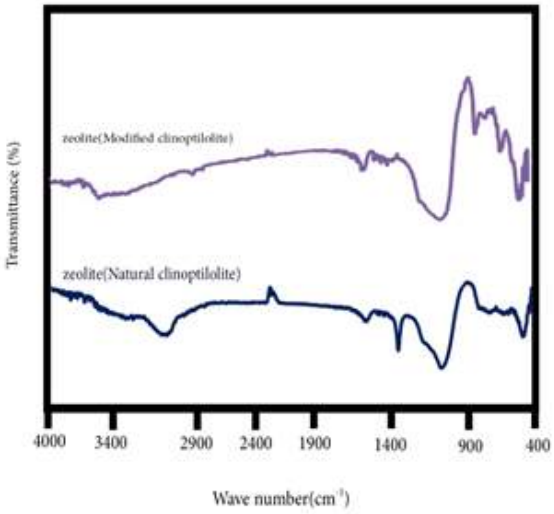

Fig.2. FTIR spectra of natural and modified CP

The peak at 3408 cm^{-1} is attributed to the reaction of OH- bound to oxygen ions. The sharp peak at 13620 cm^{-1} is assigned to the stretching vibration of OH dissociated from water. The bending vibration of H_2O is observed at 1627 cm^{-1}. The sharp peak at 1013 cm^{-1} is related to Al atoms [9, 10]. All the peaks related to natural clinoptilolite were also observed in the modified clinoptilolite, which confirms the correctness of the synthesis.

The efficiency and adsorption capacity of natural and modified clinoptilolite were investigated and compared. As can be seen in Table 1, the efficiency of modified clinoptilolite has increased from natural clinoptilolite.

Table 1 Removal efficiency and adsorption capacity of natural and modified CP

Sample	Time (min)	R (%)
Natural CP	20	91.1
	40	93.5
Modified CP	20	96.5
	40	100

4. Conclusions

In order to increase the methylene blue adsorption efficiency, natural clinoptilolite was modified using NaOH. The results of adsorption efficiency of natural and modified clinoptilolite showed that the alkaline modification of clinoptilolite caused desilicification and as a result the Si/Al ratio decreased and due to the higher negative charge in the framework, the tendency of modified clinoptilolite to adsorb methylene blue increased. Also, accordance to XRD

and FT-IR results, it was observed that the natural clinoptilolite was properly modified.

5. References

[1] FARHADI, Hajar; KERAMATI, Narjes. Investigation of kinetics, isotherms, thermodynamics and photocatalytic regeneration of exfoliated graphitic carbon nitride/zeolite as dye adsorbent. Scientific Reports, (2023), 13.1: 14098.

[2] DIGNOS, E. C. G., et al. The comparison of the alkali-treated and acid-treated naturally mined Philippine zeolite for adsorption of heavy metals in highly polluted waters. In: IOP Conference Series: Materials Science and Engineering. IOP Publishing, (2019). p. 012030.

[3] DE SOUZA, Vanessa Castro, et al. Basic treatment in natural clinoptilolite for improvement of physicochemical properties. Minerals,(2018), 8.12: 595.

[4] ATES, Ayten. Effect of alkali-treatment on the characteristics of natural zeolites with different compositions. Journal of colloid and interface science, (2018), 523: 266-281.

[5] ALOTAIBI, Abdulrahman Masoud; ISMAIL, Aznan Fazli. Modification of clinoptilolite as a robust adsorbent for highly-efficient removal of thorium (IV) from aqueous solutions. International Journal of Environmental Research and Public Health,(2022), 19.21: 13774.

[6] MERSIN, Gülşah; AÇIKEL, Ünsal; LEVENT, Menderes. Efficient adsorption of Basic Blue 41 from textile wastewaters by natural and magnetically modified Manisa-Gördes clinoptilolite. Chemical Engineering and Processing-Process Intensification, (2021), 169: 108632.

[7] ADAM, Mohd Ridhwan, et al. Influence of the natural zeolite particle size toward the ammonia adsorption activity in ceramic hollow fiber membrane. Membranes, (2020), 10.4: 63.

[8] HAMID, Mohd Azhar Abd, et al. Optimization and analysis of zeolite augmented electrocoagulation process in the reduction of high-strength ammonia in saline landfill leachate. Water, (2020), 12.1: 247.

[9] NOORI, Maryam; TAHMASEBPOOR, Maryam; FOROUTAN, Rauf. Enhanced adsorption capacity of low-cost magnetic clinoptilolite powders/beads for the effective removal of methylene blue: Adsorption and desorption studies. Materials Chemistry and Physics, (2022), 278: 125655.

[10] MERSIN, Gülşah; AÇIKEL, Ünsal; LEVENT, Menderes. Efficient adsorption of Basic Blue 41 from textile wastewaters by natural and magnetically modified Manisa-Gördes clinoptilolite. Chemical Engineering and Processing-Process Intensification,(2021), 169: 108632.

29TH IRANIAN ORGANIC CHEMISTRY CONFERENCE
1_3 NOV, 2023
UNIVERSITY OF QOM, IRAN

How fluorine functionalization influence on 1,4,5,8-Naphthalenetetracarboxylic diimide (NTCDI) molecule in the reaction with lithium atoms: A density functional theory (DFT) study.

Roya Alzoha, Alireza Abbassi*
Department of Chemistry, Faculty of Science, University of Qom, Qom, Iran, ruaaibrahim199@gmail.com.

Abstract -
Density functional theory calculation was used to study the structure and electrical properties of 2,6-difuloro 1,4,5,8-Naphthalenetetracarboxylic diimide and its dimer. and their reaction with Lithium atoms for the use in the Lithium-Ione batteries. Using the quantum chemical parameters and the calculated thermodynamic data, we have concluded that the fluorine functionalization can improve the properties of NTCDI molecules for the use in Li-Ione batteries. Hence, the emf of 1.7 volt for NTCDI-Li increases to 2.5 volt for NTCDI-F_2-Li.

1. Introduction

Lithium-ion batteries have achieved significant success in use in small electronic devices due to their density and high cycle number of energy storage. These batteries are based on the reaction of lithium compounds. Lithium ions move between two reactive electrodes. In these batteries, a negative graphite electrode is connected by a non-aqueous liquid to a positive electrode made of metal oxides, which usually creates a potential difference of 4 volts. Since the use of these metal oxides has limitations such as toxicity, high cost of preparation and production, rarity and high price of the metals used, scientists have thought of using organic sources instead of these mineral sources [1-5].

2. work

1,4,5,8-Naphthalenetetracarboxylic diimide (NTCDI) is an organic substance with semiconducting properties. Due to the carboxylic groups and the aromatic skeleton (Fig. 1 a) this molecule has received considered attention in the Lithium-Ion batteries as a basement in cathode electrode [6].
In this work we used density functional theory calculation using B3LYP hybrid functional and 6_311g(d, p) bases sets and the Gaussian 03 package for the calculations. At first, the structure of NTCDI was fully optimized using the mentioned theory level. The frequency calculations were done to understand the through minima and the Gibbs free energies.
Then two Florine atoms were added to the 2 and 6 positions as it shown in Fig. 1 b. This structure was fully optimized using the theory level as discussed before.

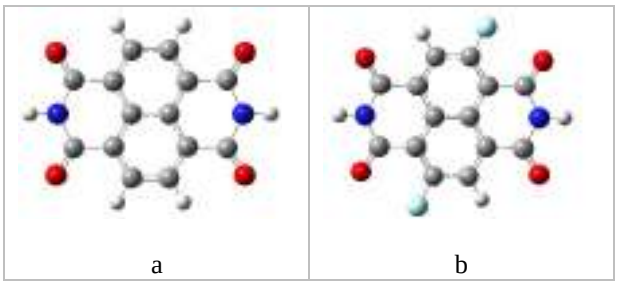

Fig. 1. The model structures of NTCDI (a) and NTCDI-F_2 (b)

In the next step, we studied the interaction of these molecules with two lithium atoms. The optimized structures are shown in Fig. 2. In NTCDI molecule (Fig. 2. a) Li atoms directly connected to oxygens, while in NTCDI-F_2 lithium are bonded to oxygen and fluorine (Fig. 2. b).

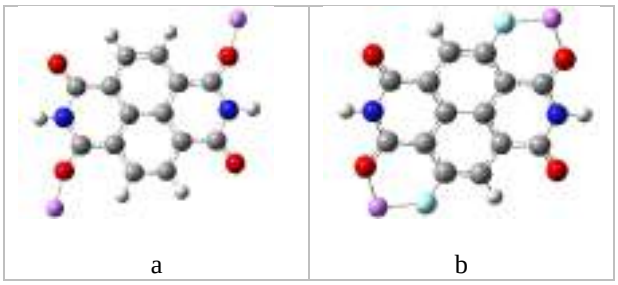

Fig. 2. The model structures of NTCDI-Li (a) and NTCDI-F_2-Li (b)

We can write the reaction of NTCDI and two Li atoms as: NTCDI + 2Li → NTCDI-Li_2 and the Gibbis free energy of this reaction can be obtained using the following equation.

$$\Delta G = G_{NTCDI-Li2} - G_{NTCDI} - 2G_{Li}$$

The calculated ΔG for fluorine functionalized NTCDI is -488.28 kJ/mol that is 155 smaller than Gibbs free energy of NTCDI-Li. Hence, the interaction of Li atoms with NTCDI-F_2 is more stable than NTCDI.
We used the calculated Gibbs free energies to obtain emf of the butteries using the following equation.

$$emf = -\frac{\Delta G}{nF}$$

where n is the number of transferring electrons which is 2 here as each Li atom transfers one electron and F is the Faraday number.

The obtained emfs are 1.72 and 2.53 for NTCDI and NTCDI-F_2 respectively. The higher value for the functionalized NTCDI shows that fluorine functionalization improves the battery functionality.

In the next step, two NTCDI-F_2 were connected from the nitrogen part to make dimer (Fig. 3). The dimer also was fully optimized using the same level of theory.

Fig. 3. The model structures of NTCDI-F_2 dimmer

For the NTCDI dimer one Li atom was connected to one terminal carbonyl oxygen and the second one was connected to central or terminal carbonyl oxygen. Therefore, for the dimer we have varieties of structures in the interaction with Li. The Gibbs free energies and the emf of the calculated structures are summarized in Table1.

Table 1: ΔG and emf of all the calculated structures of NTCDI-F_2-Li

Structure	ΔG(kJ/mol)	Emf (volt)
NTCDI-F_2	-488.28	2.53
NTCDI-F_2-dimer (A)	-498.61	2.58
NTCDI-F_2-dimer (B)	-496.55	2.57
NTCDI-F_2-dimer (C)	-430.62	2.23

Table 1 shows that the emf of dimer is about 0.05 volt larger than monomer. Therefore, the polymerization has a very small effect on the battery functionality from the emf point of view. This is contrary to NTCDI which polymerization influences a lot on the emf battery.

In conclusion, using DFT calculations, we have studied the effect of the polymerization of the organic molecule i.e., NTCDI in the Li-ion batteries. The results show that the emf increases by adding fluorine atom.

4. References

1. A. Manthiram, J. Phys. Chem. Let. 2 (2011) 176–184.
2. M. S. Whittingham, Science. 192 (1976), 192 (4244), 1126–1127.
3. P. Poizot, F. Dolhem, J. Gaubicher, Current Opinion in Electrochem. 9 (2018) 70-80.
4. R. Gracia, D Mecerreyes, Polym. Chem. 4 (2013). 2206–2214.
5. P. Novák, K. Müller, K.S.V. Santhanam, O. Haas, Chem. Rev. 97 (1997) 207–282.
6. S. Geeta, et.al. Chem. Mate. 26 (2014) 7151–7157

29TH IRANIAN ORGANIC CHEMISTRY CONFERENCE
1_3 NOV, 2023
UNIVERSITY OF QOM, IRAN

Synthesis of 2-amino-3-cyanopyridine derivatives using superparamagnetic and recyclable nanocatalyst Fe_3O_4@THAM-Mercaptopyrimidine

Elham Mir *, *Nourallah Hazeri*

Department of Chemistry, Faculty of Science, University of Sistan and Baluchestan, Zahedan, Iran, miss.mir68@gmail.com, nhazeri@chem.usb.ac.ir, n_hazeri@yahoo.com

Abstract - Due to the importance and many applications of nano catalysts in various pharmaceutical, petroleum, food industries, etc., they are one of the important applications in new technologies. In this research, Fe_3O_4@THAM-Mercaptopyrimidine magnetic nanocatalyst [1] was used for the synthesis of 2-amino-3-cyanopyridine derivatives [2] in solvent-free conditions at 70°C. Among the advantages of this method are easy separation using an external magnet and reusability, high stability, compatibility with the environment and high yield synthesized products, and the structure of the products was identified using melting point and IR and ^{1}H NMR spectroscopy.

1. Introduction

Nanotechnology is the ability to make, control and use materials in nanometers. In recent years, nanomaterials have had many applications in chemistry, biology, pharmaceuticals and even medicine.

In this research, magnetic nanocatalyst Fe_3O_4@THAM-Mercaptopyrimidine [1] has been used, which is a magnetic nanocatalyst in the group of green nanocatalysts.

Among the heterocyclic compounds, pyridines play an important role in biological, medicinal, anticancer, antimicrobial, and analgesic activities. For this reason, their synthetic methods are very important, and by using magnetic nanocatalysts, the speed and efficiency of synthetic reactions can be increased. increased pyridine.

The importance of the synthesis of 2-amino-3-cyanopyridine derivatives using the Fe_3O_4@THAM-Mercaptopyrimidine nanocatalyst, the high activity of the nanocatalyst surfaces and the ability to recycle and easy separation, the short reaction time in the synthesis of 2-amino-3-cyanopyridine derivatives and High efficiency and productivity. The ability to separate easily makes the final product have a high percentage of purity.

For the synthesis of 2-amino-3-cyanopyridine through a four-component reaction, a one-pot mixture of aromatic aldehydes, acetophenone derivatives, malononitrile and ammonium acetate was investigated in the presence of Fe_3O_4@THAM-Mercaptopyrimidine magnetic nanocatalyst [2].

2. Results and discussion

2.1. General: The melting point of pure products was collected by Electrothermal 9100 and infrared (IR) spectrum was collected on JASCO-460 plus. Nuclear magnetic resonance spectrum (^{1}H NMR) was taken on BRUKER DEX 300 device. All chemicals and solvents used are from Aldrich and Merck, which are prepared with high purity. The completion of the reaction was monitored using thin layer chromatography (TLC).

2.2. Synthesis of Fe_3O_4 magnetic nanoparticles: The synthesis of iron oxide nanoparticles (Fe_3O_4) has been carried out by chemical co-precipitation method. At first, for the synthesis of Fe_3O_4 nanoparticles, a mixture of $FeCl_2.4H_2O$ (2.5 mmol) and $FeCl_3.6H_2O$ (5 mmol) was dissolved in 100 ml of double distilled water at room temperature in the reaction vessel. After that, ammonium hydroxide solution was added to make the reaction medium alkaline. The black suspension was stirred at 1000 rpm for one hour at room temperature. Then the obtained nanoparticles were dried after several times of washing with water and ethanol.

2.3 Coating of Fe_3O_4 magnetic nanoparticles: The synthesized Fe_3O_4 nanoparticles were first dispersed in 100 ml of water and ethanol solution, and then trihydroxymethylaminomethane (THAM) (2 g) was added to the mixture and refluxed for 24 hours. Finally, the obtained magnetic nanoparticles were washed with water and ethanol and dried at 70 degrees Celsius.

2.4 Synthesis of Fe_3O_4 @THAM—CH_2CH_2–Cl magnetic nanoparticles: Synthesized Fe_3O_4 @THAM nanoparticles were dispersed in 50 mL of CH_3CN for 15 minutes, and then dichloromethane (1 mL) and triethylamine (0.1 mL) were added to the reaction mixture and the resulting mixture was stirred for 24 The clock is refluxed. Finally, the obtained nanoparticles were washed with water and ethanol and dried at 70 degrees Celsius.

2.5 Synthesis of Fe_3O_4 @THAM-Mercaptopyrimidine: Synthesized Fe_3O_4 @THAM--CH_2CH_2-Cl nanoparticles were added to 50 ml of toluene and dispersed for 15 minutes, and 2-mercaptopyrimidine (2 g) was added to the reaction mixture and refluxed for 24 hours. Finally, after washing the nanocatalyst with water and ethanol and drying at 70 degrees Celsius, the magnetic nanocatalyst Fe_3O_4 @THAM-Mercaptopyrimidine was obtained.

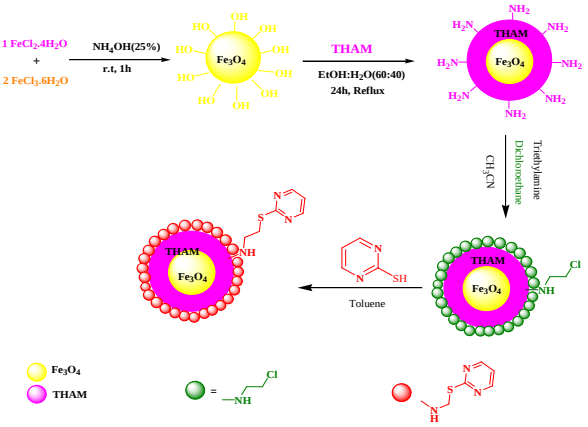

Fig.1. Preparation of Fe3O4@THAM-Mercaptopyrimidine

2.6. Investigation of reaction conditions to obtain optimal conditions for the synthesis of 2-amino-3-cyanopyridine derivatives: At first, a mixture of 4-chlorobenzoaldehyde (1 mmol), 4-chloroacetophenone (1 mmol), malononitrile (1 mmol) and ammonium acetate (1 mmol) and the amount of catalyst Fe_3O_4 @THAM-Mercaptopyrimidine (0.005 g)) at a temperature of 70°C and 5 mL of different solvents, the reaction was performed and the best yield was obtained in solvent-free conditions. Then the reaction was investigated in different amounts of Fe_3O_4 @THAM-Mercaptopyrimidine nano catalyst and the best efficiency was obtained in 0.005 g of nano catalyst. In the next step, the reaction was checked at different temperatures and 70 degrees Celsius was chosen as the optimal temperature.

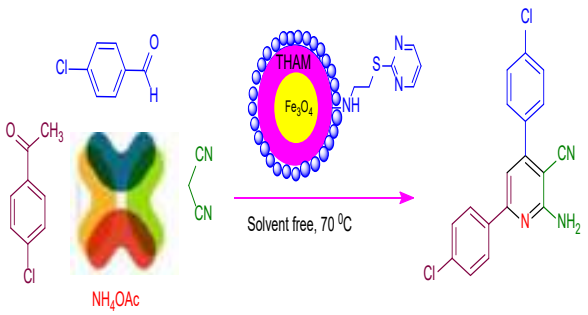

Fig.2. Model reaction for reaction conditions in the synthesis of 2-amino-3-cyanopyridine derivatives

2. 7. General working procedure for the synthesis of 2-amino-3-cyanopyridine in the presence of 0.005 g of nano-catalyst and temperature conditions of 70 degrees Celsius and without solvent: First, a mixture of different acetophenone derivatives (1 mmol), benzaldehyde derivatives (1 mmol), malononitrile (1 mmol) and ammonium acetate (1 mmol) was added to the reaction vessel in the presence of 0.005 g of magnetic nanocatalyst Fe_3O_4 @THAM-Mercaptopyrimidine and stirred at 70 degrees Celsius. The completion time of the reaction was monitored by thin layer chromatography (TLC). After the completion of the reaction, the reaction mixture was dissolved in hot ethanol and the magnetic nanocatalyst was separated by an external magnet and washed for reuse. The remaining precipitate was dried after filtration and the pure product was obtained.

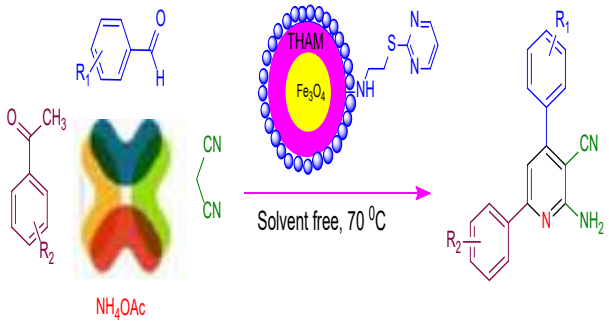

Fig.3. General procedure for the synthesis of 2-amino-3-cyanopyridine derivatives

Table 1 Synthesis of 2-amino-3-cyanopyridine derivatives under optimal conditions

Entry	R_1	R_2	Time (min)	Yield (%)	M.p (°C)
1	4-Cl	H	10	97	237-238
2	4-Me	4-Cl	10	86	173-175
3	4-NO_2	H	10	76	211-213
4	H	H	10	75	182-184
5	4-Cl	H	15	75	187-188
6	3-Br	4-Cl	20	86	232-233
7	4-F	H	15	97	148-150
8	4-Me	H	10	91	136-138
9	H	4-Me	15	81	172-173
10	4-NO_2	4-Me	20	76	198-200
11	4-F	4-Cl	20	86	181-182
12	3-NO_2	4-Cl	25	87	278-279

2.8 Selected spectral data

2.8.1. 2-amino-4,6-bis(4-chloro phenyl) nicotine nitrile: FT-IR(KBr): 2206, 3501, 3645 cm^{-1}; ^1H NMR (300 MHz, DMSO): δ (ppm) 7.12 (s, 2H, NH_2), 7.33 (s,1H, Ar-H), 7.58-7.74 (m, 6H, Ar-H), 2.04 (d, 2H, j=8.1, Ar-H).

2.8.1. 3-(2-amino-3-cyano-6- (p-tolyl) pyridine -4- yl) phenyl nitrate: FT-IR(KBr): 2217, 3364, 3480

cm^{-1}; ^1H NMR (300 MHz, DMSO): δ (ppm) 2.38 (s, 3H, CH_3), 7.12-8.15 (m,11H, Ar-H, NH_2).

3. Investigating the recyclability of nanocatalyst Fe_3O_4@THAM-Mercaptopyrimidine

Magnetic nanocatalyst Fe_3O_4@THAM-Mercaptopyrimidine entered the reaction of 4-chlorobenzaldehyde, 4-chloroacetophenone, malononitrile, ammonium acetate in least 6 times (4). After the end of each reaction, the catalyst was isolated and after washing with ethanol, it was dried and reused. The obtained results are shown in figure (4). The obtained results showed that the Fe_3O_4 @THAM-Mercaptopyrimidine catalyst retained its catalytic properties and magnetic properties after 6 reuses.

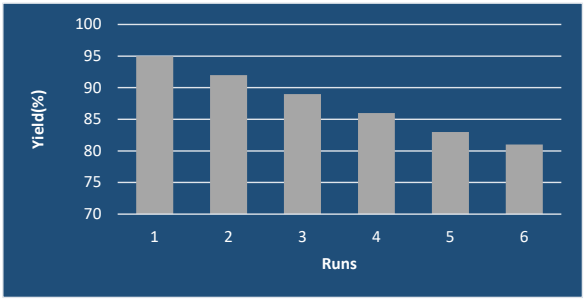

Fig. 4. Reusability of Fe_3O_4@THAM-Mercaptopyrimidine MNPs as a catalyst in the synthesis 2-amino-3-cyanopyridine

4. Conclusion

In summary, by using a green and simple method, the Fe_3O_4 @THAM-Mercaptopyrimidine magnetic nanocatalyst was synthesized and this magnetic nanocatalyst has a very high efficiency due to its high surface-to-volume ratio, easy separation by an external magnetic magnet, and the ability to recycle for reuse. in the synthesis of medicinal compounds.
In this research, this Fe_3O_4 @THAM-Mercaptopyrimidine magnetic nanocatalyst was used in the synthesis of 2-amino-3-cyanopyridine derivatives. Among the advantages and features of this research are not using a solvent, the ability to recycle the nanocatalyst at least six times without losing selectivity, performing the reaction in a one-pot manner, high stability, short reaction time, and high efficiency.

4. References

[1] Mir, E.; Hazeri, N.; Faroughi Niya, H.; Fatahpour, M. Synthesis, identification and application of Fe_3O_4@THAM-Mercaptopyrimidine nanoparticles as a novel and highly recyclable nanocatalyst in one-pot multicomponent synthesis of 1,8-dioxo-octahydroxanthenes and polyhydroquinolines. *Research on Chemical Intermediates* 2023, *49*, 1439−1462.

[2] Faroughi Niya, H.; Hazeri, N.; Maghsoodlou, M.T.; Fatahpour, M. Synthesis, characterization, and application of $CoFe_2O_4$@TRIS@sulfated boric acid nanocatalyst for the synthesis of 2-amino-3-cyanopyridine derivatives. *Research on Chemical Intermediates* 2021, *47*, 1315−1330.

Modified Species of the Natural Rubber

*Mehri Nadiri Niri**

Research laboratory, Tanin Peak Sabalan Company (Beta), No. 2 Industrial Zone, Ardabil, Iran

Abstract – Natural rubber (NR) is a valuable material of natural origination with growing demand worldwide. Natural rubber was the subject of intensive investigation with respect to its chemical reactions and the preparation of commercially useful derivatives. One of the biggest disadvantages of NR is low resistance to aging, ozone, and saturated hydrocarbons. The reason is the high chemical activity of the isoprene unit in the NR molecule. To overcome this disadvantage, effective modification techniques for NR property improvement are continuously developed. Some products obtained from modification reactions are depolymerized rubber, cyclized rubber, chlorinated rubber, rubber hydrochloride, epoxidized rubber, and deproteinated rubber. All the natural rubber derivatives mentioned earlier are useful types and have specific applications. This article deals particularly with methods of chemical modification of NR and wide applications of these valuable materials.

Keywords: Natural rubber, High chemical activity, Derivatives, Modification reactions, Applications.

1. Introduction

Natural rubber has had commercial value for hundreds due to its advantages such as high tensile strength, elasticity, good dynamic properties, and low head build-up. Despite these advantages, the high chemical activity of NR causes NR disadvantages such as low thermal and ozone resistance. So, there is a need for modification reactions in order to improve NR properties. With chemical modification, many NR derivatives with new functional groups and new properties may be formed.

In the molecular structure of NR for every five carbon atoms in the chain, there is one olefin double bond and the activity of this double bond is similar to the double bond in alkene, therefore chemical reactions that may occur to alkene also apply to NR, such as electrophilic addition at C=C bond or substitution at the allylic position. Chemical modifications of NR may be classified as follows:

- Changing the molecular structure or reducing the molecular mass without introducing new atoms or molecules into the NR chain. Examples of this kind of reaction are cyclization, isomerization, or depolymerization.

- Functionalization of NR by introducing the new atoms or functional groups with specific physicochemical characters into the NR chain

- Modification of allylic carbon by grafting other monomers or polymers.

Examples of reactions of the first group are cyclization and chain decomposition. The products obtained from these reactions have some commercial applications. Chain decomposition formes liquid NR (LNR) with low molecular mass and is easy to dissolve and process. In LNR may be functional groups containing oxygen due to the reaction of oxygen with radicals formed during chain scission [1]. LNR may be used as a sealant or viscosity-controlling agent during processing. Some of the modification reactions are discussed further in more detail.

2. Results and Discussion

2.1. Some Products Obtained from Modification Reactions and their Applications

2.1.1. Depolymerized Rubber: The polymer is degraded whenever raw rubber is exposed to temperatures of 120 °C or higher for several hours. Under these conditions, rubber becomes liquid and its molecular weight decreases significantly. These rubbers can be converted into soft or hard rubbers by using of the vulcanization process [2].

2.1.2. Cyclized Rubber: Natural rubber becomes a resin-like material in the presence of acidic catalysts and heat, and its saturation level is greatly reduced. In this case, the specific weight of rubber increases to 99% and its softening point reaches about 90 to 120 ^{0}F. This kind of rubber is divided into two categories, which are [2]:

2.1.2.1. Thermoprenes: These rubbers are prepared using acidic catalysts such as sulfuric acid, p-toluenesulfonic acid, phosphoric acid, and trichloroacetic acid. The procedure is that the mixture is heated for 1 to 4 hours at a temperature of 125 to 145 ^{0}C. These rubbers are used in cases such as protecting metals against corrosion and improving the adhesion of metal to rubber. It should be noted that the

cyclization reaction can be also carried out in leachate [2].

2.1.2.2. Amphoteric Halides: Heavy metal chlorides such as tin, antimony, iron, aluminum, or titanium form complex substances when added to rubber solutions. These materials are precipitated by alcohol or separated by solvent distillation. The obtained white amphoteric powder is used as a material for molding [2].

2.1.3. Chlorinated Rubber: Natural rubber easily reacts with chlorine with substitution and addition mechanisms. Although chlorine can also be added to the leachate, the best method is to chlorinate the rubber solution in inert solvents such as carbon tetrachloride at a temperature of 180 ^{0}C. After that, a white powder of chlorinated rubber is obtained by separating the solvent through distillation. The fully chlorinated rubber (65% chlorine) has a specific gravity of 1.63 to 1.66 and is soluble in aromatic hydrocarbons and chlorinated solvents. The chlorinated rubber is used in the preparation of chemically resistant paints and also for bonding rubber to metals due to ineffectiveness [3].

2.1.4. Rubber hydrochloride: Rubber hydrochloride can be obtained by passing dry hydrogen chloride gas through the rubber solution. After that, the desired substance can be obtained both through precipitation using an anti -solvent and distillation method. Rubber and isoprene polymers readily add hydrogen chloride in benzene or chloroform solution. In carbon tetrachloride, the reaction is much slower and incomplete. Rubber hydrochloride has been marketed for a number of years as Pliofilm and has found widespread use as a film material, particularly in the food packaging field. This material is also used to bond rubber to metals. To prevent the decomposition and corrosion of this material, anti-acid stabilizers are added to it. Rubber hydrochloride (containing 28 to 30% chlorine) has a specific gravity of 1.16 and a refractive index of -1.532. This rubber is mostly crystalline and melts at a temperature of 115 ^{0}C [3].

2.1.5. Oil-Extended Natural Rubber: Since 1950, when it was found that the compounds prepared with oil-expanded rubber provide good wear characteristics and improve the sliding resistance of tires, the huge movement of using oil-expanded SBR began in tires. Process oils as plasticizers are essential for the production of rubber compounding and mixing. They are used during rubber mixing to improve production and advance rubber performance. Their presence affects the lowering of the cohesive forces between polymer chains and therefore, an increase of the chain mobility. Overall, this causes an enhancement in the deformability and flexibility of the rubber. It is very important to note that the main criteria for choosing the right oil are based on its compatibility with rubber. The Hansen solubility parameter (HSP) has recently been used as the main criterion to select the right process oil by predicting its solubility. This method divided Hildebrand's energy into three characteristic groups: dispersion energy, polar, and hydrogen bonding, which take into account intermolecular forces, in order to better pronounce and clarify the interactions between oil and rubber [3].

2.1.6. Epoxidized Natural Rubber: In this reaction, the epoxidation agent interacts with the double bond C=C to form an oxirane group. The epoxidation agent may be hydroperoxide or organic peracids [4-6]. Organic peracid also may be formed *in situ* by a reaction of H_2O_2 and suitable organic acid. Epoxidation of NR occurs as follows [7]:
The existence of the epoxy group in the NR chain makes the properties of NR such as oil or aging resistance and damping improve. However, this effect is notable only with a high content of epoxy. ENR10 with 10%mol of epoxy content is not different from NR. That is why mostly ENR with 25 %mol of epoxy content and more is used for many applications
Note, that in the epoxidation process, some side reactions may occur. These reactions tend to form groups containing oxygen such as tetrahydrofuran, hydroxyl, and carbonyl ether. The higher the reaction temperature, the more side reactions, and when the reaction temperature exceeds 25 ^{o}C, side reactions may overpass the epoxidation reaction.
ENR has improved properties in comparison with NR. For example, ENR adhesion to steel or nylon is higher than that of NR. In [6] has been shown that the damping properties of ENR rised along with epoxy content while mechanical properties such as tensile strength, tear resistance, and compression set remained at a level of that of NR. Also, oil resistance, gas permeability, or abrasion resistance of ENR remarkably enhanced in comparison with NR [8-11].

2.1.7. Deproteinated Natural Rubber: Like low-nitrogen natural rubber, this rubber is also produced for applications where the presence of rubber impurities is harmful. Rubber protein can be removed through enzymatic proteolysis or alkaline hydrolysis. Then alpha globulin, which is insoluble in rubber, is removed by solubilization with glycerol. The cured mixture of the purified rubber has very good mechanical properties, good resistance against thermal erosion, low heat generation, and low swelling against water [12].

3. References

[1] P. Phinyocheep, Chemistry, Manufacturing and Application of Natural Rubber, Woodhead Publishing Ltd., p. 68-81, 2014.

[2] L. X. Hien, Chemical Conversions of Natural Rubber and Application, Natural Science & Technology Publishing House, 1-50, 2011.

[3] T. Vinh Dieu, B. Chuong, D. Viet Hung, N. H. Tung, N. P. Duy Linh, D. T. Yen Oanh, Vietnam J. Chem. 61 (2023) 269-283.

[4] A. Alimuniar, M. A. Yarmo, M. Z. Rahman, S. Kohjiya, Y. Ikeda, S. Yamashita, Polymer Bulletin 23 (1990) 119-126.

[5] J. L. Le Blanc, H. P. De Livonniere, G. Boccaccio, Prog. Rubb. and Plast. Technol. 8 (1990) 79-113.

[6] R. Sanjoy, B. R. Gupta, Epoxidized Rubbers, in the Book “Elastomer Technology handbook”, CRC press, p. 645-670, 1993.

[7] N. Viet Bac, M. Mihailov, L. Terlemezyan, Eur. Polym. J. 27 (1990) 557-563.

[8] D. R. Burfield, K. L. Lim, K. L. Law, J. Appl. Polym. Sci. 29 (1984) 1661-1673.

[9] V. Tanrattanakul, B. Wattanathai, A. Tiangjunya, P. Muhamud, J. Appl. Polym. Sci. 90 (2003) 261-269.

[10] C. S. L. Baker, I. R. Gelling, R. Newell, Rubber Chem. Technol. 58 (1985) 67-85.

[11] I. R. Gelling, Rubber Chem. Technol. 58 (1985) 86-96.

[12] N. Viet Bac, L. Terlemezyan, M. Mihailov, Eur. Polym. J. 26 (1990) 1055-1060.

29TH IRANIAN ORGANIC CHEMISTRY CONFERENCE
1_3 NOV, 2023
UNIVERSITY OF QOM, IRAN

Brush-coating process of emulsion resin based on acrylic copolymer and TiO_2 nanoparticles composite onto the copper sheet

Sina Nasiri[1,2], *Majid Ahmadlouydarab*[1]* *and Reza Najjar*[2]

[1] *Faculty of Chemical & Petroleum Engineering, University of Tabriz, Iran*, sn7748@gmail.com, *mahmadlouydarab@tabrizu.ac.ir*
[2] *Polymer Research Laboratory, Faculty of Chemistry, University of Tabriz, Tabriz, Iran*

Abstract
Coating on metals refers to the process of applying a protective layer or film on the surface of metal objects. This coating is usually done to improve the appearance of the metal, improve its durability, protect against corrosion, and other functional properties. In this study, the copper sheet was brush-coated with an emulsion resin composite containing titanium dioxide nanoparticles. To determine the structure of the material, infrared spectroscopy analysis (FT-IR) was used, which revealed that, the resin is based on acrylic-styrene copolymer. Scanning electron microscope (SEM) analysis was used to determine the surface morphology and distribution of the sample on the copper sheet surface and it was observed that the distribution of nanoparticles in the polymer matrix is almost homogeneous and no apparent agglomeration of nanoparticles is seen on the surface of the sample. Also, the surface roughness of the coating measured by atomic force microscope (AFM) analysis is 4.31 nm. The results of the investigation indicated that the adhesion and transparency of the coating were suitable; however, the uniformity of coating achieved with this method is not optimal.

Keywords: brush-coating, titanium dioxide nanoparticles, emulsion resin, copper sheet

1. Introduction

In recent years, research has been directed towards the development of very thin coatings, including self-assembled monolayers and polymer brush coatings [1]. The preparation of polymer nanocomposite coatings has been mainly considered due to their various properties such as high thermal and chemical stability, high corrosion resistance, ease of manufacturing, favorable mechanical strength, and cost efficiency [2]. Improving the properties of polymer coatings reinforced with nanoparticles depends on many factors such as chemical nature, particle size, and concentration of nanoparticles in the coating. In addition, the interaction between nanoparticles and polymer matrix is also an important factor [3,4]. Organic coatings or paints are among the most ubiquitous and useful methods of preventing corrosion on steel and other metals [5]. Also, epoxy resins are another widely used coating material that can be applied to both metallic and non-metallic structures for protection or decoration purposes. The performance of epoxy-based coating can be significantly increased by mixing functional fillers, so it can be used for corrosion protection and high durability [6,7]. Titanium dioxide is an oxide material that is widely used as an effective reinforcement for the synthesis of various composites with its chemical stability, environmental friendliness, antibacterial properties, lower production cost, and ease of synthesis [8,9].
In the study by Santos et al., PMMA-TiO_2 and PMMA-ZrO_2 coatings have a high potential to protect the metal surface from corrosion. These two hybrids deposited on carbon steel as thin films with a thickness of (0.5-3 µm) were transparent and had a low surface roughness of (0.4-1.8 nm) [10]. "Chang et al" coated TiO_2 thin films on metal substrates (stainless steel, copper alloy, and aluminum alloy) and polymer substrates (PMMA and PET) by nanoparticle deposition system (NPDS) at room temperature and low vacuum conditions. The results of the investigation showed that the coating has an uneven surface and a large surface area, also, NPDS provides a good coating method for TiO_2 materials for applications that require a large surface area [11]. In the experimental study of "A.Tessa ten Cate et al.", the preparation of hydrophilic and hydrophobic brush coatings on different substrates by using the primer layer of polyacrylic acid has been reported. They found that the resulting brush coatings were stable in the aquatic environment and reduced the adhesion of marine bacteria to the surface [12].
The purpose of this research is to utilize brush-coating with an emulsion resin based on acrylic copolymer and TiO_2 nanoparticles to prepare a coating film with desirable transparency and adhesion on solid copper sheets.

2. Experimental

Copper sheet with a purity above 95% was purchased from Zanjan Copper Company (Zanjan, Iran). Ethanol

(purity>96%) was obtained from Kimia Alcohol Zanjan and acetic acid was obtained from Merck, Germany. Titanium dioxide nanoparticles with a particle size of<20 nm and purity above 99% were purchased from US Nano. emulsion resin based on acrylic copolymer was made by Tehran Kenitex (Tehran, Iran) as a polymer material that contains 53% total solid content.

At first, copper sheets measuring 3 cm × 3 cm were immersed in acetic acid solution (Conc. >99%) and distilled water for 30 seconds, then washed with distilled water and finally dried in the oven at 60 °C. The coating solution was prepared by adding 0.88 mg of TiO_2 to 5 ml of ethanol, which was equivalent to 1% of solid material in 0.5 ml of emulsion resin based on acrylic copolymer and water solution. This solution was dispersed by ultrasonication for 10 hours. After the nanoparticles were completely dispersed, another solution containing 0.5 ml of the resin and diluted water was added to the previous solution, and the final solution was dispersed again for 3 hours. The desired copper sheet was coated with a brush and dried in an oven at 80 °C.

3. Results and Discussion

FT-IR analysis was used to investigate the functional groups and the structure of acrylic lacquer compounds. According to Fig. 1, the absorption bands that appear in the range of 2957 cm^{-1} and 3061 cm^{-1} are attributed to the stretching vibrations of aliphatic and aromatic C-H bonds, respectively. Absorption bands resulting from stretching vibrations of C-O bonds are observed in the range of 1163-1252 cm^{-1}. The absorption peak at 1492 cm^{-1} and 1602 cm^{-1} is assigned to stretching vibrations of C=C bonds. The carbonyl group (C=O) corresponding to the acrylic part of the compound appeared in the range of 1731 cm^{-1}. Also, the overtones of out-of-plane bending vibrations of aromatic C-H bonds were appeared at 1876 - 1951 cm^{-1}.

3.1. Investigation of coated sheet

To prepare the coating film, two separate solutions were used. The first solution contained 0.88 mg of titanium dioxide and 5 ml of ethanol, and the second solution, containing 0.5 ml of a diluted emulsion resin/water mixture, was added to the first after dispersing the nanoparticles. The final mixture was then ultrasonically mixed for three hours to reduce any nanoparticle agglomeration and improve compatibility with the polymeric matrix. As seen in Fig. 2, after the brush-coating process, the resultant coating is completely attached to the surface of the sheet and has desirable transparency and roughness.

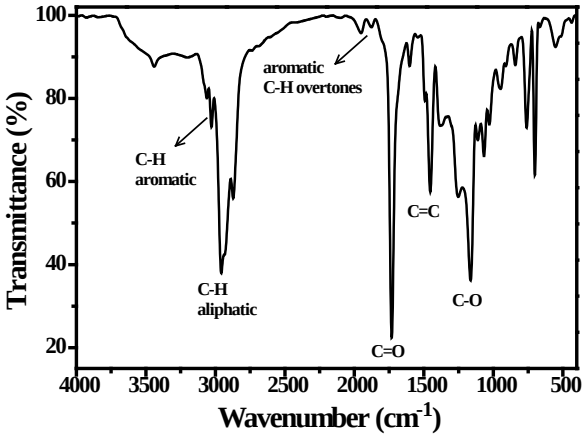

Fig.1. FTIR spectra of emulsion resin based on acrylic copolymer

Fig.2. Copper sheet with brush-coated emulsion resin/TiO_2 nanoparticles film

3.2. SEM and AFM analysis

The surface morphology of the brush-coated sheet was investigated according to SEM images. According to SEM images and their comparison with the mapping pattern, the distribution of TiO_2 nanoparticles in the polymer matrix is almost homogeneous and no significant agglomeration of nanoparticles can be seen on the surface of the sample. Also, the clusters seen in Fig. 3 are due to the air bubbles trapped between the solid surface and the emulsion resin.

AFM analysis was used to evaluate the surface structure and surface roughness of the coated sample. As depicted in Fig. 4, the average surface roughness of the sample after measuring the roughness of different parts is estimated to be about 4211 pm equivalents to 4.21 nm. This is almost equal to the standard deviation of height or root mean square roughness (sq=4.31 nm).

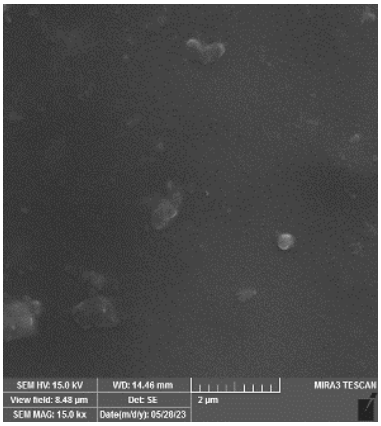

Fig.3. SEM image of the emulsion resin/TiO_2 nanoparticles film brush-coated on the copper sheet

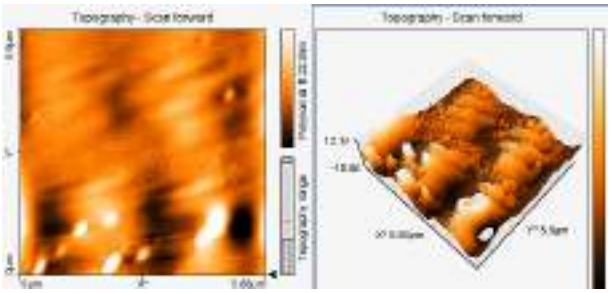

Fig.4. AFM analysis of brush-coated sheet

4. Conclusion

In the current research, the brush-coating technique was used to coat copper sheet with emulsion resin composite based on acrylic and TiO_2 nanoparticles. The results of the investigation confirm the good adhesion and transparency of the polymer film on the surface of the substrate. However, according to SEM and mapping results, the uniformity of coating with this method was not as expected, also, the presence of bubbles trapped between the solid surface and the coating due to the latex property, requires that the employed brush-coating technique needs more investigations to obtain suitable coatings of the present emulsion on the copper sheets.

5. References

[1] Currie, E. P. K., Norde, W., & Stuart, M. C, Adv Colloid Interface Sci, 100 (2003) 205-265.
[2] Li, X. W., Song, R. G., Jiang, Y., Wang, C., & Jiang, D, Appl Surf Sci, 276 (2013) 761-768.
[3] Perera, D. Y, Prog Org Coat, 50.4 (2004) 247-262.
[4] Kotnarowska, D., Przerwa, M., & Szumiata, T, J Mater Sci Res, 3.2 (2014) 52.
[5] Ozcan, U. E., Karabork, F., Yazman, S., & Akdemir, A, Arab J Sci Eng, 44 (2019) 5723-5731.
[6] Wei, H., Xia, J., Zhou, W., Zhou, L., Hussain, G., Li, Q., & Ostrikov, K. K, Compos B Eng, 193 (2020) 108035.
[7] Afzal, A., Siddiqi, H. M., Saeed, S., & Ahmad, Z, Mater Express, 1.4 (2011) 299-306.
[8] Augugliaro, V., Bellardita, M., Loddo, V., Palmisano, G., Palmisano, L., & Yurdakal, S, J Photochem Photobiol C: Photochem Rev, 13.3 (2012) 224-245.
[9] Elsellami, L., Dappozze, F., Fessi, N., Houas, A., & Guillard, C, Process Saf Environ Prot, 113 (2018) 109-121.
[10] Harb, S. V., Trentin, A., Uvida, M. C., Magnani, M., Pulcinelli, S. H., Santilli, C. V., & Hammer, P, Prog Org Coat, 140 (2020) 105477.
[11] Chun, D. M., Kim, M. H., Lee, J. C., & Ahn, S. H, CIRP Ann, 57.1 (2008) 551-554.
[12] Ten Cate, A. T., Reinders, S. A., Turkenburg, D. H., Bruin, A., D'Souza, F., Donnelly, G. T, van Bommel, K. J, Prog Org Coat, 64.2-3 (2009) 221-224.

Investigation of kinetic release of levothyroxin from nanoclay/chitosan nanocomposite

*Nastran Baghfar and Elham Rostami**
Department of Chemistry, Faculty of Science, Shahid Chamran University of Ahvaz, Ahvaz, Iran,
e.rostami@scu.ac.ir

Abstract - In recent decades, research in the field of nanotechnology and its applications in medicine has been carried out extensively. In this regard, this thesis studies the effect of chitosan nanoparticles using tripolyphosphate tertbutylpyrophosphate (TTP) on drug release. A nanoparticle polymer has been developed as a potential platform for drug delivery. In this research, different samples of nanoparticles with different concentrations of TTP were prepared and during a certain period of time, the cell viability was measured. The results show that with increasing TTP concentration, cell viability decreases. Then, zeroorder, first-order, second-order, Higuchi and Peppas kinetic models were used to analyze the data and fit them. The results show that the zero-order model has the best fit with the data and has the ability to adequately describe the effect of TTP concentration on drug release.

1. Introduction

Chitosan is a neutral polysaccharide polymer which is widely applied in pharmaceutical products. This biopolymer is composed of β-2-amino-2-deoxy-Dglucopyranose (glucosamine units). Monomer units are combined by β (1-4) glycosidic linkages. Chitosan has unique properties such as biocompatibility, biodegradability, safety and mucoadhesivity. Due to its biocompatibility may not cause allergic reactions and rejection. Moreover, as stated above it is biodegradable which gradually degrades to safe products (amino sugars), which are completely absorbed by the human body. Pharmaceutical usage of chitosan is due to the amino groups on its chain. Chitosan application as a biomaterial to provide controlled release systems has received much attention [1-4]. Ultrasound has a promising role in the delivery of therapeutic agents including genetic material, proteins, and chemotherapeutic agents. Cavitating gas bodies such as microbubbles are the mediators through which the energy of relatively non-interactive pressure waves is concentrated to produce forces that are able to increase cell membrane permeability and may shear the drugcarrying vesicles. The size of the bubbles can be affected by passing pressure wave through the media [4,5]. In the presence of microbubbles, delivery of drug material is seriously improved using ultrasound [2-3]. Ultrasound affects the degradation rate of bioerodible polymers [2]. In this work we studied the effect of ultrasound and TPP concentration on levothyroxine release, as a drug model, which is loaded in chitosan nanoparticles. We reported that release percent of levothyroxine from chitosan nanoparticles (polymeric matrix) can be repeatedly modulated from an external position to the environment by ultrasonic energy.

2. Materials and Methods

2.1. Materials. Chitosan was purchased from Sigma–Aldrich (USA) with a MW of 60*103 and the degree of deacetylation was 93%. Levothyroxine sodium was obtained as a gift from the Iran Hormone Company. Tripolyphosphate (TPP), polysorbate 80 (Tween 80), acetic acid and other reagents were purchased from Merck.

2.2. Prepartion of nanocomposite chitosan/Nanoclay: Preparation of TPP-Chitosan nanoparticles. Chitosan solution was prepared by dissolving it in 1% acetic acid and polysorbate 80, as an emulsifier, (2% v/v) was mixed into the chitosan solution. Levothyroxine, poorly soluble drug in water, was dissolved in DMSO (2:10) and then this oil phase was mixed with aqueous phase (chitosan solution) by probe sonication applying 20 kHz frequency for 10 min. TPP (2% w/v) solutions were dropped by spray gun into the chitosan solution. Then, nanoparticles were washed with distilled water repeatedly followed by vacuum drying for 12 h [4]. In vitro release of levothyroxine from chitosan nanoparticles. The experiment was conducted by a static horizontal Franz diffusion cell to evaluate the amount of released levothyroxine sodium. The receptor medium was 50 mL in volume and composed of an aqueous solution of physiological saline, phosphate buffer solution, which stirred by a magnetic stirrer at 100 rpm to homogenize the medium (pH=7.4). A 2 ml of chitosan nanoparticles was separately loaded onto the donor compartment. 1 ml of the release medium was sampled using a syringe needle and the same volume of fresh receptor medium was replaced at certain time intervals. The samples were analyzed using a spectroscopic method as described previously [5]. Morphological characterization of chitosan nanoparticles. Size and zeta potential were measured by photon correlation spectroscopy (PCS) (Nano ZS4700 nanoseries, Malvern Instruments, UK). To capture the transmission electron microscopy (TEM) (Zeiss-EM 10C- Germany) microphotographs, the nanoparticles

samples stained with 2% (w/v) phosphotungstic acid were employed. Investigation of surface morphology of nanoparticles was performed by scanning electron microscopy (SEM, KYKYEM3200, China).

3. Results and discussion

3.1. Characterization of nanocomposite: Characterization of chitosan nanoparticles. SEM image of the samples containing drug loaded chitosan nanoparticle is shown in Fig. 1. The image showed spherical shape and smooth surface with a particle size in nanometric scale. The particle size of levothyroxineloaded chitosan nanoparticle showed SEM images are in agreement and the result of PCS (Fig. 2). Fig. 2 showed a release levothyroxine of nanocomposite in 225 nm.

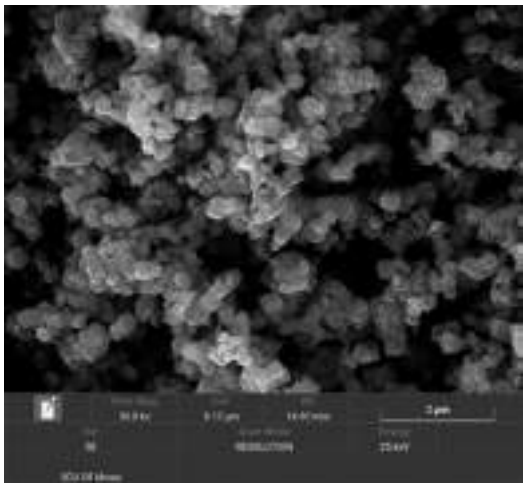

Fig. 1. SEM image of chitosan nanoparticles

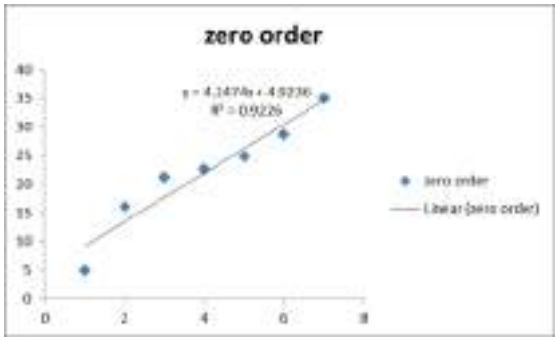

Fig. 2. Kinetic model of nanocomposite (zero order)

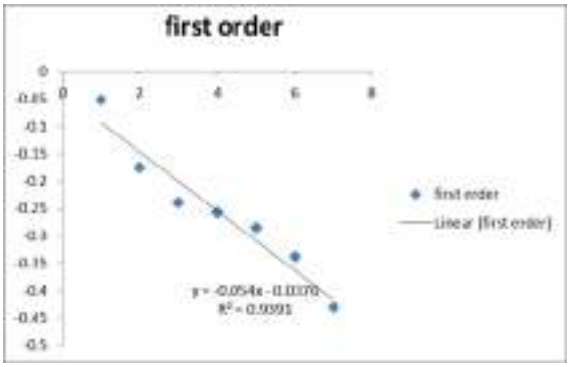

Fig. 3. Kinetic model of nanocomposite (first order)

3.2. Kinetic release of nanocomposite: Chitosan has been developed toward a multifunctional drug delivery system by exploring positively charged properties and modifiable functional groups. Various modifications to the polymer backbone, charge, or functional groups will undoubtedly affect the drug release from CSNPs. The drug release from CSNPs has a significant influence on its therapeutic actions. Our review's objective was to summarize and discuss the relationship between the modification in CSNPs as multifunctional delivery systems and drug release properties and kinetics of the drug release model. Kinetic models help describe the release rate, leading to increased efficiency, accuracy, the safety of the dose, optimizing the drug delivery device's design, evaluating the drug release rate, and improvement of patient compatibility (Fig.2). In conclusion, almost all CSNPs showed bi-phasic release, initial burst release drug in a particular time followed controlled manner release in achieving the expected release, stimuli external can be applied (Fig.3). CSNPs are a promising technique for multifunctional drug delivery systems. 3.3. Conclusion: The effect of TPP concentration and ultrasound on drug release profile. In this study TPP/Chitosan nanoparticles were fabricated by the virtue of ionic interaction between positively charged amino groups of chitosan and the negatively charged counter ions of TPP.

3.3. Conclusion: The effect of TPP concentration and ultrasound on drug release profile. In this study TPP/Chitosan nanoparticles were fabricated by the virtue of ionic interaction between positively charged amino groups of chitosan and the negatively charged counter ions of TPP.

4. References

[1] 1. V Mourya, N.N. Inamdar,. Reactive and Functional polymers, 68 (2008) 1013-1051.

[2] 2. R. Shepherd, S. Reader, and A. Falshaw, Glycoconjugate journal, 14 (1997) 535-542.

[3] 3. F.A. Razmi, et al. Journal of cleaner production, 23 (2019) 98-109.

[4] 4. Ren, L., et al., International journal of biological macromolecules, 135 (2019) 898-906.
[5] 5. Q.Luo, et al. International journal of biological macromolecules, 139 (2019) 521-530.
[6] 6. F. Taher., et al., International journal of biological macromolecules, 126 (2019) 478-487.

29TH IRANIAN ORGANIC CHEMISTRY CONFERENCE
1_3 NOV, 2023
UNIVERSITY OF QOM, IRAN

Preparation and characterization of SiO_2/APTPOSS immobilized on Manganese Ferrite as core–shell nanomagnetic composite for synthesis of spirooxindoles

Samira Moein Najafabadi, *Javad Safaei Ghomi*[*]

Department of Organic Chemistry, Faculty of Chemistry, University of Kashan, Kashan, Iran, moeins5471@gmail.com, safaei@kashanu.ac.ir

Abstract - A polyhedral oligomeric silsesquioxane derivative called Octakis[3-(3-aminopropyltriethoxysilane)propyl]octa-silsesquioxane (APTPOSS) was synthesized and utilized as a pioneering reagent to produce a novel core-shell composite. This composite consisted of $MnFe_2O_4$ nanoparticles as the core and an inorganic-organic hybrid polyhedral oligomeric silsesquioxane as the shell. The confirmation of $MnFe_2O_4$@SiO2/APTPOSS was conducted through various analytical techniques such as Fourier transform infrared spectroscopy, scanning electron microscopy, energy dispersive spectroscopy, dynamic light scattering, thermogravimetric analysis, X-ray diffraction, and vibrating sample magnetometry. These inorganic-organic hybrid polyhedral oligomeric silsesquioxane magnetic nanoparticles were employed as an effective heterogeneous catalyst for the one-pot synthesis of spirooxindoles derivatives. Additionally, these nanoparticles could be easily separated by an external magnet and subsequently reused multiple times without experiencing significant loss in their catalytic activity.

1. Introduction

In the field of academia, magnetic nanoparticles (MNPs) have gained significant interest over the past few decades due to their distinctive characteristics such as simple synthesis, strong stability, minimal toxicity, high activity, effective recoverability, large surface area, and easy separation from mixtures using an external magnet [1]. As a result, numerous MNP-supported catalysts with outstanding catalytic capabilities have been developed and utilized in various organic synthesis processes. These include coupling reactions (C&bond; C, C&bond; N, C&bond; S), hydrogenations, oxidation, photocatalysis, cycloaddition reactions, as well as innovative applications in hydration, asymmetric synthesis, CO_2 cycloaddition, and Knoevenagel condensations [2]. Additionally, MNPs (specifically $MnFe_2O_4$) serve as a versatile support for the functionalization of N-heterocyclic carbenes, metals, organocatalysts, and chiral catalysts [3]. In recent years, there has been significant interest in the use of inorganic-organic hybrid polyhedral oligomeric silsesquioxanes (POSSs) in various fields due to their unique cage-shaped structures, nanometer-sized structures, and potential for chemical modification [4]. These hybrid nanoparticles have found applications in drug delivery, dental materials, medical devices, anti-tumor agents, tissue engineering scaffolds, semiconductors devices, optical devices, binders for ceramics, catalysis, and solar cells [5]. The synthesis of spiro compounds has also been a major area of focus over the past decade due to their wide range of biological and medicinal applications. The core structure of 1H-indole-2,3-diones (isatins) is particularly significant as it can generate a variety of natural and artificial spiroheterocycles that exhibit diverse biological activities such as laxative agents, anti-inflammatory properties, antimicrobial effects, antitubercular activity, antimalarial properties, antitumor effects, antibacterial activity, and anti-HIV activity [6]. Therefore, there is still a need for the improvement of simple methods for synthesizing spirooxindoles in the academic context. As a result, researchers have investigated various techniques for synthesizing oxospiro[indolin-pyrans] compounds by reacting isatins with 1,3 dicarbonyl compounds and malononitrile under mild conditions [7]. However, these methods have limitations including long reaction times, high temperatures, complex procedures, low product yields, and expensive and non-reusable catalysts. Hence, it is highly important to develop an environmentally friendly and straightforward approach for producing oxospiro[indolin-pyrans]. In this study, building upon our recent research on nanoparticle synthesis, we prepared a novel recyclable heterogeneous core–shell nanomagnetic $MnFe_2O_4$@SiO_2/octakis[3-(3aminopropyltriethoxy- silane) propyl]octasilsesquioxane using $MnFe_2O_4$ MNPs as the core and organic–inorganic hybrid silica as the shell. Subsequently, we utilized these inorganic–organic hybrid POSS MNPs as an efficient new heterogeneous catalyst for the one-pot three-component synthesis of spirooxindole derivatives under reflux conditions in ethanol.

2. Results and discussion

Scheme 1 demonstrates the sequential process for immobilizing iron oxide MNPs with a POSS-based organic-inorganic hybrid. Initially, the MNPs ($MnFe_2O_4$) were synthesized using a co-precipitation method in a basic solution. It is known that the surface of the MNPs can be functionalized using various surface modifiers. Subsequently, octakis(3 chloropropyl)octasilsesquioxane was prepared by hydrolyzing 3-chloropropyltrimethoxysilane under acidic conditions. This was followed by reacting ClPOSS with 3-aminopropyltriethoxysilane to produce APTPOSS. The final step involved treating MnFe2O4 with an aminopropyltriethoxysilane derivative and TEOS to form the core-shell composite of $MnFe_2O_4$@SiO_2/APTPOSS (with $MnFe_2O_4$ MNPs as the core and SiO2/APTPOSS as the shell). Characterization of $MnFe_2O_4$@SiO_2/APTPOSS was conducted using TEM, SEM-EDX, VSM, Fourier transform infrared (FT-IR) analyses, TGA, DLS and XRD.

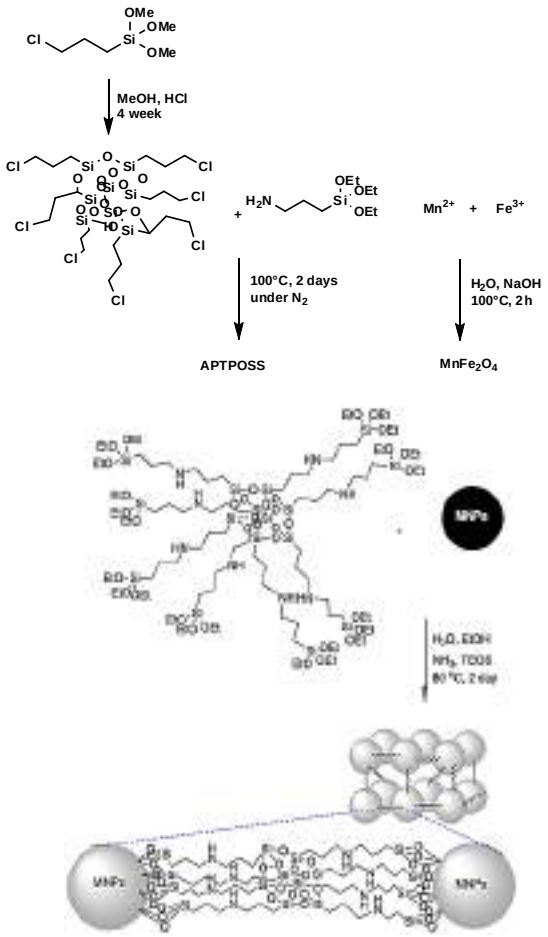

Scheme1. Preparation routes to $MnFe_2O_4$@SiO_2/APTPOSS nanoparticles.

Different solvents were used to examine the reactivity of isatin derivatives, 1,3-dicarbonyl compounds (2a-d), and malononitrile 1. A good yield was achieved when the reaction was conducted in ethanol (EtOH). Subsequently, the reaction was carried out using different catalysts and without a catalyst. It was found that $MnFe_2O_4$@SiO_2/APTPOSS was the most effective catalyst, resulting in a 96% yield of product 4a. The impact of catalyst loading was then investigated using 5 mg and 15 mg of $MnFe_2O_4$@SiO_2/APTPOSS respectively. The experimental findings indicated that the utilization of 10 mg of $MnFe_2O_4$@SiO_2/APTPOSS as a catalyst yielded the most favorable results. Any deviation from this specific catalyst loading, whether it was decreased or increased, led to a decrease in the overall product yield.

Following an optimization process, the outcomes obtained for different types of spiro[chromene-4,3'-indolines], spiro[indoline-3,4'-pyrano[3,2 c]chromene], and spiro[indoline-3,5'-pyrano[2,3-d]pyrimidine] synthesized from various 1,3-dicarbonyl and isatin derivatives in ethanol at a temperature of 80 ℃ were presented in table 1.

Table 2. Synthesis of Spirooxindole Derivatives 3 in the Presence of $MnFe_2O_4$@SiO_2/APTPOSS

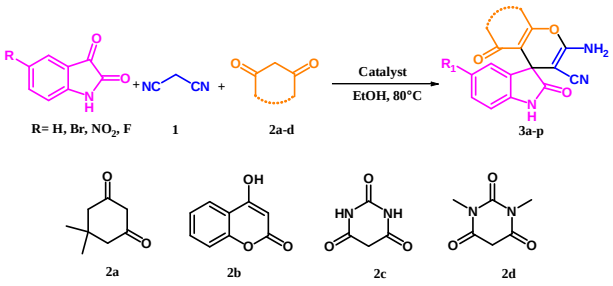

Products	
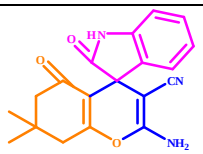 3a	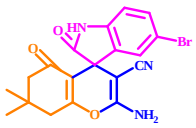 3b
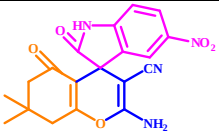 3c	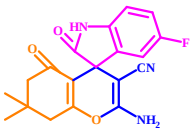 3d
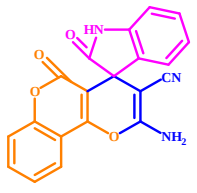 3e	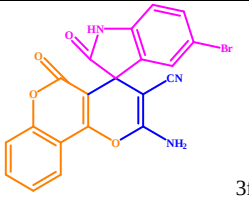 3f

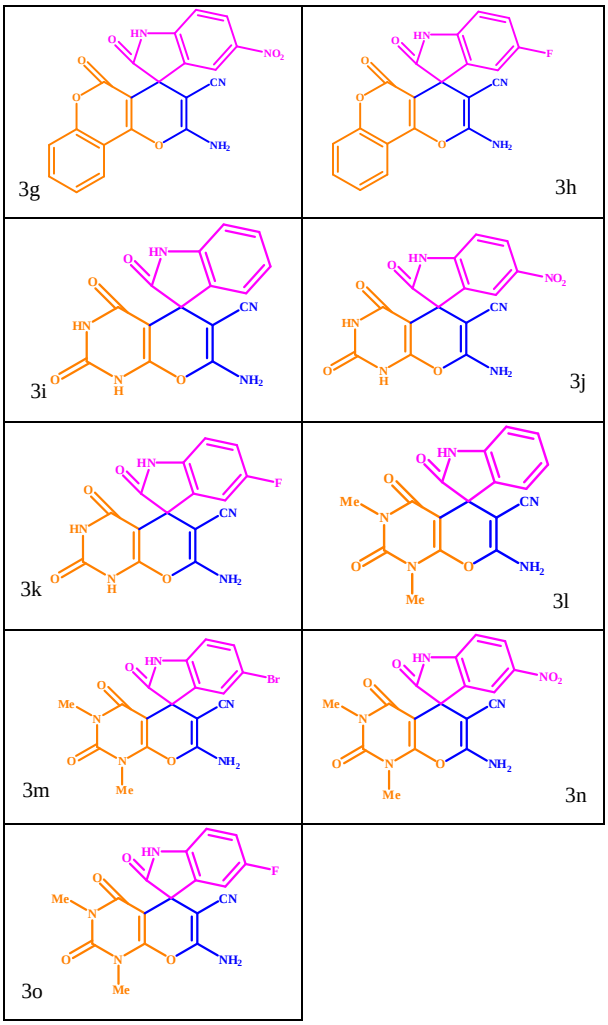

3. Conclusion

In our study, we successfully synthesized new core–shell composite nanoparticles by combining iron oxide MNPs ($MnFe_2O_4$) with APTPOSS for the purpose of producing oxindoles. The reaction was efficiently carried out in a short duration and with minimal catalyst usage. Moreover, the resulting catalyst exhibited numerous benefits including long-term stability, exceptional catalytic activity for this specific reaction, effortless separation of the catalyst through an external magnetic field, and straightforward work-up procedures. Additionally, the catalyst could be conveniently recovered and reused multiple times without experiencing significant decline in its catalytic activity.

The present method is expected to be applicable to the synthesis of libraries with high diversity due to the abundance of isatins and 1,3-dicarbonyl compounds. Therefore, it is anticipated that this method will have widespread application in the field of combinatorial chemistry and drug discovery.

4. References

[1] Sh. Saurabh, R. Khan, and A. Daverey. "Synthesis and characterization of magnetic nanoparticles, and their applications in wastewater treatment: A review." *Environmental Technology & Innovation* 24 (2021): 101924.

[2] B. Karimi, F. Mansouri, and H. M. Mirzaei. "Recent Applications of Magnetically Recoverable Nanocatalysts in C□ C and C□ X Coupling Reactions." *ChemCatChem* 7, no. 12 (2015): 1736-1789.

[3] D. Sriparna, P. Kumar, S. Yadav, R. D. Sharma, P. Shivaprasad, K. S. Vimaleswaran, A. Srivastava, and R. K. Sharma. "Accelerating innovations in CH activation/functionalization through intricately designed magnetic nanomaterials: From genesis to applicability in liquid/regio/photo catalysis." *Catalysis Communications* (2023): 106615.

[4] W. Mingyue, H. Chi, J. KS, and F. Wang. "Progress in the synthesis of bifunctionalized polyhedral oligomeric silsesquioxane." *Polymers* 11, no. 12 (2019): 2098.

[5] B. H. Alshammari, M. M. Lashin, M. Adil Mahmood, F. S. Al-Mubaddel, N. Ilyas, N. Rahman, M. Sohail, A. Khan, Sh. Sh. Abdullaev, and R. Khan. "Organic and inorganic nanomaterials: fabrication, properties and applications." *RSC advances* 13, no. 20 (2023): 13735-13785.

[6] R. S. Cheke, V. M. Patil, S. D. Firke, J. P. Ambhore, I. A. Ansari, H. M. Patel, S. D. Shinde. "Therapeutic outcomes of isatin and its derivatives against multiple diseases: Recent developments in drug discovery." *Pharmaceuticals* 15, no. 3 (2022): 272.

[7] Sh. Nasri, M. Bayat, and F. Mirzaei. "Recent strategies in the synthesis of spiroindole and spirooxindole scaffolds." *Topics in Current Chemistry* 379 (2021): 1-37.

29TH IRANIAN ORGANIC CHEMISTRY CONFERENCE
1_3 NOV, 2023
UNIVERSITY OF QOM, IRAN

Choline chloride-urea as a solvent/catalyst for the synthesis of 2-aminoimidazopyridines

Amin Parvizi Moghadam, Afshin Sarvary, and Negin Dehghan*

Department of Chemistry, Faculty of Science, Babol Noshirvani University of Technology, Babol, Iran, aminparvizimoghaddam@gmail.com, a.sarvary@nit.ac.ir.

Abstract Imidazo[2,1-α] pyridine heterocycle is important in the base of drugs such as Alpidem, Zolpidem and Olprinone. in the present study, the three-component reaction between aldehyde, 2-aminopyridine, and KCN in choline chloride-urea deep eutectic solvent (DES) was used for the synthesis of imidazopyridine. This reaction is completely carried out in a single container in a test tube, and the reaction efficiency is very favourable. Choline chloride-urea is an environmentally friendly solvent/catalyst, which has importance and value in green chemistry.

Keywords Deep eutectic solvent; Imidazopyridine; Choline chloride-urea; Green chemistry.

1. Introduction

In chemistry, solvents occupy a strategic place that to qualified as a green medium, they have to meet different criteria such as availability, non-toxicity, biodegradability, recyclability, flammability, and low price among others. Figure. 1 shows graphically that the use of solvents must be minimized and optimized to enhance the reactions with the minimum environmental and operational concerns [1].

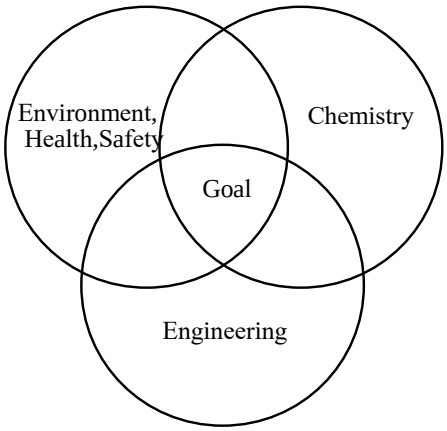

Fig.1. Optimizing energy consumption and avoiding damage to the environment

Over the last two decades, researchers are exploring a new group of solvents so-called deep eutectic olvents (DES). The preparation of DES was first reported in 2003 by Abbott and his workers [2]. DES are undoubtedly new solvents that exhibit great potential to be used for design of eco-efficient processes and their also exhibited simple access to new chemicals [3]. Imidazopyridine, an imidazole moiety fused with a pyridine ring, is an important biologically active compounds (Fig. 2.). The imidazo[1,2-a]pyridine have emerged as versatile biologically active compounds. They have a variety of biological activities such as anticancer, antiviral, antimicrobial, antiparkinson, antimutagenics, antihypoxia, and antinflammatory effects.

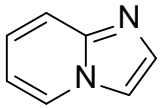

Fig.2. Imidazopyridine

2. Results and Discussion

According to the scientific reports in which DES are used as both solvent and catalyst [4] and also the acidic role of choline chloride. In the present study, choline chloride-urea as solvent and catalyst were investigated in three-component reaction between 2-aminopyridine, benzaldehyde, and cyanide, which is shown in figure 3.

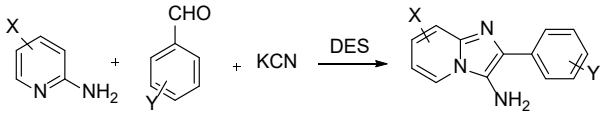

Fig.3. three-component reaction

Thus, initially the DES choline chloride-urea solvent was prepared using choline chloride and urea with molar ratio of 1:1 at 100 °C [5]. After preparing DES solvent, the reaction of 5-methyl-2-aminopyridine (**II**), *para*-chlorobenzaldehyde (**I**) and KCN with molar ratio 1:1:1 in Choline chloride-urea (1 mL) at room temperature was performed.

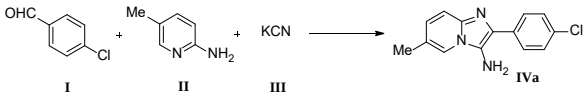

Fig.4. Synthesis of product IVa *via* a three-component reaction

The progress of reaction was monitored by TLC, which was not suitable at room temperature. In order to improve this preliminary finding, the reaction was carried out at 80°C. Fortunately, the reaction was progressed with increasing temperature within 3 h. In order to separate the product, 2 drops of hydrogen chloride 37% were added to the reaction mixture, and then 6 ml distilled water was added to the reaction vessel in two steps. The precipitate formed was separated from the solvent and dissolved in chloroform, after evaporation of chloroform, the reaction product was obtained, which was a dark green compound. The results of spectroscopic methods showed that the intended product was formed. After it was ensured reaction was carried out in choline chloride-urea, the optimization of reaction was carried out to obtain suitable conditions, including amount of solvent, reaction temperature and molar ratio of reactant materials. Finally, the best reaction conditions was identified as: molar ratio 1.2 (**I**): 1 (**II**): 2 (**III**) in choline chloride-urea (1 mL) at 80 °C. As shown in fig. 5 after optimizing the reaction conditions, we tested the various derivatives of aldehydes, and 2-aminopyridin to obtain new derivatives of product.

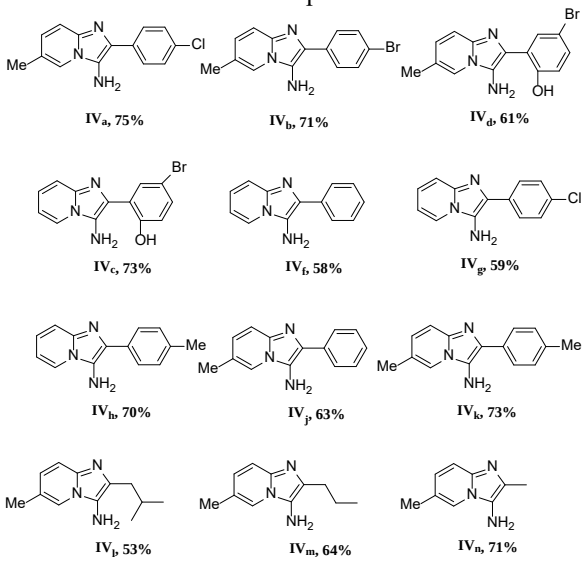

Fig.5. Structure of synthesized derivatives

The mechanism of the synthesis of imidazo[1,2-α]pyridine was presented in figure 6. First, aromatic carbonyl (**I**) was activated with DES as an acidic catalyst, then the activated aldehyde was attacked by the amino group of 2-aminopyridine (**II**) and after proton exchange and loss of one mole of water, the imine intermediate **A** was formed. Then [4+1] cyclization reaction between intermediate **A** and cyanide was carried out at peresent of DES. Finally, during imine-enamine tautomerization, imidazo[1,2-α]pyridine derivatives (**IV)** were obtained [6].

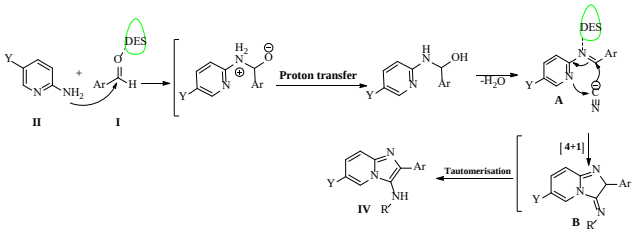

Fig.6. Mechanism of synthesis imidazo[1,2-α]pyridine

3. Conclusions

In conclusion, we reported a three-component reaction leading new valuable pharmaceutical products from simple and readily available reactant and using an eco-friendly and biodegradable deep eutectic solvent based on the choline chloride–urea mixture.

4. References

[1] Q. Zhang, K.D.O. Vigier, S. Royer, F. Jerome, Chem. Soc. Rev. 41 (2012) 7108–7146.
[2] A. Shaabani, S.E. Hooshmand, Tetrahedron Lett. 57 (2016) 310-313.
[3] M. Meenu, V. Bansal, S. Rana, N. Sharma, V. Kumar, V. Aror, M. Garg, Sustain Chem. Pharm. 34 (2023) 101168-101174.
[4] A. Shaabani, A. Maleki, Monatshefte für Chemie-Chemical Monthly. 138 (2007) 51-56.
[5] T. Pavithra, ChemistrySelect, 6 **(**2021) 3548-3552.
[6] A. Hameed, Green Processing and Synthesis, 6 **(**2017) 371-375.

29TH IRANIAN ORGANIC CHEMISTRY CONFERENCE
1_3 NOV, 2023
UNIVERSITY OF QOM, IRAN

Structural and electrochemical properties study of the 2,6-dicyano1,4,5,8-Naphthalenetetracarboxylic diimide (NTCDI(CN)2) molecule and its dimers for the use in lithium-ion batteries using density functional theory (DFT) calculations.

*Zahraa Alsudani, Alireza Abbassi**
Department of Chemistry, Faculty of Science, University of Qom, Qom, Iran, ash869k@gmail.com, a.abbasi@qom.ac.ir

Abstract -
Utilizing density functional theory calculations, an investigation was carried out into the structure and electrical attributes of (NTCDI(CN)2) and its corresponding polymers. Additionally, their interaction with lithium atoms was explored in the context of potential application in lithium-ion batteries. By analyzing quantum chemical parameters and computed thermodynamic data, it was determined that functionalization presents a viable approach for enhancing the characteristics of the foundational organic molecules for the use in Li-ion batteries (LIBs). Consequently, the observed voltage potential, initially measured at 1.7 volts for NTCDI-Li, is improved to 3.0 volts for NTCDI(CN)2-Li.

1. Introduction

As the investment costs of renewable energy (RE) decrease, the world continues its transition toward sustainable energy systems. However, some RE sources are intermittent, and power grids that rely on them would not provide a steady energy supply. These fluctuations can impact the system's frequency and voltage, affecting the overall power quality. Thus, energy storage would be a crucial aspect to supplement the growth of RE since it can offset intermittency. Offsetting intermittency is one of the many energy storage functions in the electric power grid, illustrating the necessity of energy storage to ensure electricity quality, availability, and reliability

Energy storage has different categories: thermal, mechanical, magnetic, and chemical). An example of chemical energy storage is battery energy storage systems (BESS). They are considered a prospective technology due to their decreasing cost and increase in demand. The BESS is also gaining popularity because it might be suitable for utility-related applications, such as ancillary services, peak shaving, and energy shifting. A study also predicted that lithium-ion batteries will increase until 2025.

In the LIBs Lithium ions move between two reactive electrodes. A negative graphite electrode is connected by a non-aqueous liquid to a positive electrode made of metal oxides, which usually create a potential difference of 4 volts. Since the use of these metal oxides has limitations such as toxicity, high cost of preparation and production, rarity and high price of the metals used, scientists have thought of using organic sources instead of these mineral sources [1-5].

2. work

2,6-Dicyano-1,4,5,8-naphthalenetetracarboxylic diimide (NTCDI(CN)2), is a cyanide derivative of 1,4,5,8-naphthalenetetracarboxylate diimide (NTCDI), and is a solid organic compound and the simplest dinaphthalene derivative. This molecule is recognized for its reactivity in reduction reactions, forming a radical anion with a charge of -1. This property has prompted extensive research into NTCDI(CN)2 and its derivatives as potential candidates for lithium-ion batteries [6].

The inclusion of the cyanide functional group may potentially influence the anticipated characteristics of the molecule. In this study, our primary objective is to examine these effects on the electronic structure and electrical properties of the molecule using density functional theory (DFT) calculations. Moreover, we aim to explore its feasibility for application in lithium batteries.

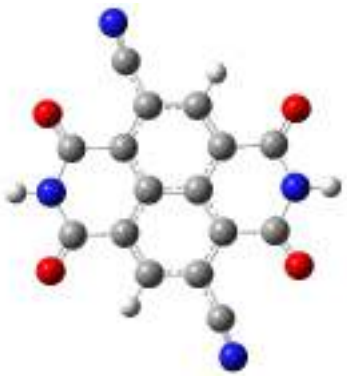

Fig. 1 the molecular structure of NTCDI(CN)2.

In this research, we employed density functional theory calculations with the B3LYP hybrid functional and 6-311g (d, p) basis sets, utilizing the Gaussian 09

package. Initially, we optimized the structure of NTCDI(CN)2 using the mentioned theoretical approach. Frequency calculations were then performed to ascertain the transition states and Gibbs free energies.

Subsequently, dimers of NTCDI(CN)2 were formed by connecting two molecules from the nitrogen terminus. This structure was fully optimized employing the same theoretical level.

The subsequent step involved the addition of two lithium atoms to the optimized molecules. Our calculations indicate a preference for Li atoms to interact with the carbonyl oxygens and cyanide Nitrogens in a trans configuration, as depicted in Fig. 2.

Fig. 2 The structure of NTCDI(CN)2-Li2.

Du to the electronegativity of O and N, Li atom like to bond to these atoms. Hence, Li makes more stranger bond with NTCDI(CN)2 regard to non-functionalized NTCDI.

The reaction of NTCDI(CN)2 with two Li atoms can be expressed as follows:

NTCDI(CN)2 + 2Li → NTCDI(CN)2-Li2.

The Gibbs free energy change (ΔG) for this reaction can be evaluated using the equation:

$$\Delta G = G_{NTCDI-Li2} - G_{NTCDI} - 2G_{Li}$$

Furthermore, the electromotive force (emf) of the battery was calculated using the equation:

$$emf = -\frac{\Delta G}{nf}$$

where "n" represents the number of transferred electrons (in this case, 2 electrons due to the transfer of each Li atom) and "f" is the Faraday constant.

For the NTCDI(CN)2 dimer one Li atom was linked to a terminal carbonyl oxygen, while the second Li atom was connected to a central carbonyl oxygen. The calculated Gibbs free energies and emf values are summarized in Table 1.

It can be seen from the data of Table 1 the emf of (NTCDI(CN)2 monomer is 3.08 volt and for dimer is 2.97. Hence, contradictory to NTCDI, polymerization do not change the emf

Table 1: ΔG and emf of all the optimized structures of (NTCDI(CN)2

Structure	ΔG(kJ/mol)	Emf (volt)
(NTCDI(CN)2	-594.88	3.08
(NTCDI(CN)2 - dimer (A)	-745.248175	3.86
(NTCDI(CN)2 - dimer (B)	-556.196422	2.88
(NTCDI(CN)2 - dimer (C)	-650.745928	3.37

In conclusion, using DFT calculations, we have studied the effect of the cyanide functional group on the functionality of NTCDI(CN)2 in LIBs. The investigation shows the C=N functional group is greatly improving the functionality of NTCDI(CN)2 in the use of LIBs. However, the polymerization does not have visible effect.

4. References

1. A. Manthiram, J. Phys. Chem. Let. 2 (2011) 176–184.
2. M. S. Whittingham, Science. 192 (1976), 192 (4244), 1126–1127.
3. P. Poizot, F. Dolhem, J. Gaubicher, Current Opinion in Electrochem. 9 (2018) 70-80.
4. R. Gracia, D Mecerreyes, Polym. Chem. 4 (2013). 2206–2214.
5. P. Novák, K. Müller, K.S.V. Santhanam, O. Haas, Chem. Rev. 97 (1997) 207–282.
6. S. Geeta, et.al. Chem. Mate. 26 (2014) 7151–7157

29TH IRANIAN ORGANIC CHEMISTRY CONFERENCE
1_3 NOV, 2023
UNIVERSITY OF QOM, IRAN

Synthesis of Imidazo[2,1-*b*][1,3]thiazin-7-imines and Imidazo[2,1-*b*][1,3]thiazin-7-amines with Thiohydantoins, Isocyanides, Acetylenedicarboxylates

Abdolhamid Raeisi[1] *and Mohammad Mehdi Ghanbari*[2]*

[1]*Department of Chemical Industry, Technical and Vocational University (TVU), Tehran, Iran, ahraeisi@tvu.ac.ir*
[2]*Department of Chemistry, Sarvestan Branch, Islamic Azad University, Sarvestan, Iran, m.mehdi.ghanbari@gmail.com*

Abstract - Hydantoin and thiohydantoin derivatives are important core moiety in the design and synthesis of heterocyclic compounds as well as medical products with good biological activity, these derivatives are very useful building blocks for the synthesis of various heterocycles with hypothermic activities, antibacterial, fungicidal activity and other pharmaceuticals properties. The three component reaction of stoichiometric amounts of acetylenedicarboxylates with alkyl isocyanides in the presence of 2-thiophenytoins afforded imidazo[2,1-b][1,3]thiazines as a imine compounds and then these imines produce target amines in the present of catalyst in good overall yields. To choose the best catalyst among various common acidic catalys, PTSA has the best yield in the shortest reaction time. Finally the stereochemistry of the Imidazo[2,1-b][1,3]thiazin-7-imines was studied by NOE spectra. We have developed a simple and useful method for the synthesis of functionalized imidazo[2,1-b][1,3]thiazines in two methods. The present method carries the advantage that not only is the reaction performed under mild conditions, but also the starting materials and reagents can be mixed without any activation or modification.

Keywords: Hydantoin, NOE spectra, Imidazo thiazines, Heterocylic compounds, Antibacterial.

1. Introduction

5,5-Diaryl-2-thiohydantoins are important core moiety in the design and synthesis of heterocyclic compounds as well as medical products, these derivatives are very useful building blocks for the synthesis of various heterocycles such as imidazo[2,1-b][1,3]thiazines, 4,5-dihydro-2-(methylthio)-5-oxoimidazoles, imidazo[2,1-b]thiazoles and imidazo[2,1-b]naphtho[1,2-e][1,3]thiazin-10-ones[1-4].
hypothermic activities, antibacterial, fungicidal activity and other pharmaceuticals properties[5-8].
1,3-Thiazines are of great interest as biologically active compounds. They have strong analgesic, muscle relaxing, and stimulation of the entire sympathetic system. As a part of our current studies in our laboratory on the development of new routes in hydantoin and thiohydantoin derivatives synthesis 1-4 we report the results of our studies involving the reaction of the zwitterionic intermediates derived from alkyl isocyanides 3 and acetylenic esters 2 with 5,5-diaryl-2-thioxoimidazolidin-4-one 1, which constitutes a synthesis of 7-alkylamino-3-oxo-2,2-diaryl-2,3-dihydro-5H-imidazo[2,1-b][1,3]thiazine-5,6-dicarboxylic acid alkyl esters 5 in 80-98% yields (see Scheme 1 and Table I).

2. Experimental

Acetylenic esters and isocyanides were obtained from Fluka and were used without further purification. 5,5-diaryl-2-thiohydantoins was prepared by known methods[9]. Elemental analyses for C, H, N and S were performed using a Heraeus CHN-O-Rapid analyzer. The experimental data were in good agreement with the calculated values. 1H and 13C NMR spectra were measured with a Bruker DRX-300 Avance spectrometer. IR spectra were recorded on a Shimadzu IR-460 spectrometer.

Typical Procedure for the Preparation of Dimethyl 7-(cyclohexylimino)-3,5,6,7-tetrahydro-3-oxo-2,2-diphenyl-2H- imidazo[2,1-b][1,3]thiazine-5,6-dicarboxylate (exemplified by 4a):
To a magnetically stirred solution of 0.536 g 1a (2 mmol) and 0.284 g 2a (2 mmol) in 5 cm3 ether was added dropwise a solution of 0.218 g 3a (2mmol) in 2 cm3 ether at 5ºC over 10 min. After 12 h stirring at room temperature, the product was filtered and washed with cold ether to give 4a.

Typical Procedure for the Preparation of 3-Oxo-2,2-diphenyl-7-[(toluene-4-sulfonylmethyl)-amino]-2,3-dihydro-5H-imidazo[2,1-b][1,3]thiazine-5,6-dicarboxylate (exemplified by 5d):
Two-steps method:
A solution of 2 mmol of the compound 4 in toluene (3 cm3) in the presence of catalytic amount of PTSA was refluxed for 10 h. The solvent was removed under reduced pressure, and the yellowish oil was separated

by silica column chromatography (Merck 230–400 mesh) using hexane/AcOEt as eluent to afford pure imidazo thiazines (5).

One-step method:

To a magnetically stirred solution of 0.536 g 1d (2 mmol) and 0.340 g 2d (2 mmol) in 5 cm3 toluene was added dropwise a solution of 0.390 g 3d (2mmol) in 2 cm3 toluene over 10 min in the presence of catalytic amount of PTSA. After 10 h stirring under reflux condition, the product 5d was achieved.

3. Result and Discution

The reaction of 5,5-diaryl-2-thioxoimidazolidin-4-one 1 with dialkyl acetylenedicarboxylates 2 in the presence of isocyanides proceeded at room temperature in dry diethyl ether, and was complete about 12 hours. 1H and 13C NMR spectra of the crude products clearly indicated the formation of stable dialkyl 7-(alkylimino)-3,5,6,7-tetrahydro-3-oxo-2,2-diaryl-2H-imidazo[2,1-b][1,3]thiazine-5,6-dicarboxylate 4 (Scheme 1).

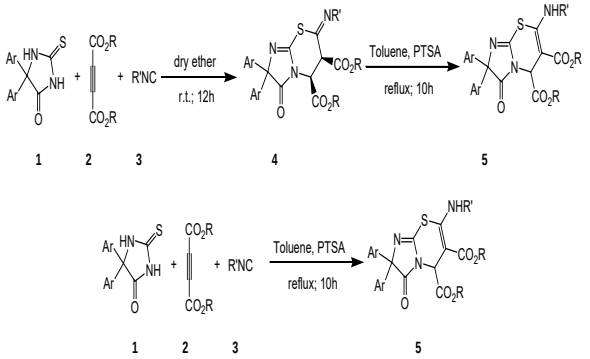

Scheme 1. Synthesis of Imidazo[2,1-b][1,3]thiazines in two-steps method and one-step method, respectively.

The white precipitate 4 left from this stage produce 7-alkylamino-3-oxo-2,2-diaryl-2,3-dihydro-5H-imidazo[2,1-b][1,3]thiazine-5,6-dicarboxylic acid alkyl esters 5 under reflux condition. In the second method imidazo[2,1-b][1,3]thiazines 5 were synthesized directly from 5,5-diaryl-2-thioxoimidazolidin-4-one 1 with dialkyl acetylenedicarboxylates 2 and isocyanides in the presence of p-Toluenesulfonic acid (PTSA or pTsOH) under reflux condition. No other products other than 5 could be detected. The structures of compounds 5a–5h were deduced from their elemental analyses and IR, ^{1}H and ^{13}C NMR spectra. Any initial fragmentation involves loss from, or complete loss of the side chains and scission of the heterocyclic ring system. The structures of compounds 5 were deduced from ^{1}H and ^{13}C NMR and IR data.

Although the relative configuration of CH-CH in compounds 4 is cis,[1] the distance between these two hydrogens (H_5-H_6) in the compound 4a is QUOTE, 2.28 Å while the distance between H_6 and Hydrogen in cyclohexyl is QUOTE, 1.75 Å (figure 1). From the NOE spectra and using the expression $\frac{\mathrm{NOE_{ref}}}{\mathrm{NOE}} = \frac{r_{\mathrm{ref}}^{-6}}{r^{-6}} = \frac{r^6}{r_{\mathrm{ref}}^6}$, the distance between two hydrogen (r) were calculated[10].We now report a simple synthetic procedure for the preparation of imidazo[2,1-b][1,3]thiazines 5 in the presence of PTSA as a catalyst.

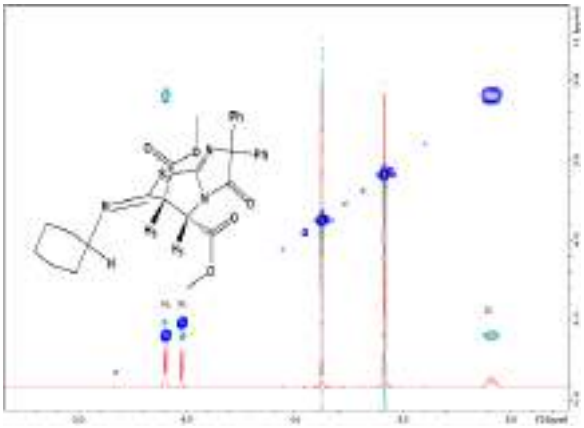

Figure 1. The NOE Spectra of 4a

TABLE I Synthesis of Imidazo[2,1-b][1,3]thiazines

Entry	Ar	R	R'	Product	Yield, %	
					Two steps	One -pot
1	Ph	Me	Cy	5a	91	90
2	Ph	Et	Cy	5b	97	95
3	Ph	Me	TsCH2	5c	95	95
4	Ph	Et	TsCH2	5d	96	96
5	ph	Me	tBu	5e	85	84
6	ph	Et	tBu	5f	80	80
7	ptoly	Me	Cy	5g	98	97
8	ptoly	Et	Cy	5h	87	85

To choose the best catalyst among various common acidic catalyst (Table II), the results showed that PTSA has the best yield in the shortest reaction time.

TABLE II Preparation of 5a in the presence of various Catalysts

Entry	Catalyst	Time, h	Yield, %
1	PTSA	10	91
2	CH3COOH	14	85
3	AlCl3	12	80
4	H3BO3	7	45

Although we have not yet established the mechanism of formation of 5 in an experimental manner, a plausible rationalization for the formation of functionalized imidazo[2,1-b][1,3]thiazines 5a–5h is shown in Scheme 2.

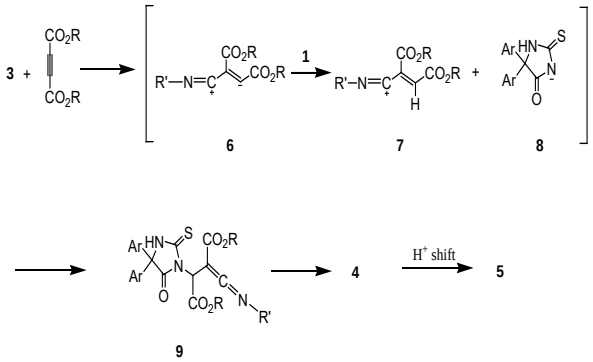

Scheme 2. Proposed mechanism

4. Conclusion

In conclusion, we have developed a simple and useful method for the synthesis of functionalized imidazo[2,1-b][1,3]thiazines in two methods. The present method carries the advantage that not only is the reaction performed under mild conditions, but also the starting materials and reagents can be mixed without any activation or modification.

5. References

[1] M. Ghanbari, I. Yavari, G. Batta, J. Sulfur Chem. 35 (2014) 312.
[2] M. M. Ghanbari, Monatsh Chem. 142 (2011) 749.
[3] M. M. Ghanbari, I. Yavari, A. Emadi, J. Sulfur Chem. 35 (2014) 57.
[4] M. M. Ghanbari, M. Jamali, G. Batta, J. Sulfur Chem. 35 (2014) 394.
[5] J. Han, H. Dong, Z. Xu, J. Wang, M. Wang, Int. J. Mol. Sci. 14 (2013) 19526.
[6]A. A. Magd El-Din, S. A. Elsharabasy, A. Y. Hassan, Phosphorus, Sulfur, and Silico. 180 (2005) 407.
[7] V. J. Ram, P. Srivastava, A. Goel, Tetrahedron. 59 (2003) 7141.
[8] C. Lamberth. F. Querniard, Tetrahedron Lett. 49 (2008) 2286.
[9] J. Safari, H. Naeimi, M. M. Ghanbari, O Sabzi-Fini, Russ. J. Org. Chem. 45 (2009) 477.
[10] G. Batta, T. Barna, Z. Gaspari, S. Sandor, K. Kover, U. Binder, B. Sarg, L. Kaiserer, A. K. Chhillar, A. Eigentler, E. Leiter, N. Hegedus, I. Pocsi, H. Lindner and F. Marx, FEBS Journal. 276 (2009) 2875.

29TH IRANIAN ORGANIC CHEMISTRY CONFERENCE
1_3 NOV, 2023
UNIVERSITY OF QOM, IRAN

Exploring *Achillea* Species Essential Oils: Computer-Based Assessment Against SARS-CoV-2 Main Protease

Maryam Manafi Moghadam[*], *Armin Zarei*, *Ali Ramazani*
Department of Chemistry, Faculty of Science, University of Zanjan, Zanjan, Iran,
m73.manafimoghadam@gmail.com

Abstract - In this study, we identified and analyzed phytochemicals from three different *Achillea* genera to assess their potential as antiviral agents against SARS-CoV-2 and SARS-CoV-1 proteases. We used chemi-informatics tools to investigate the compounds' interactions with the proteases and found that kessanyl acetate, chavibetol (m-eugenol), farnesol, and 7-epi-β-eudesmol bind to the active sites of these viruses. These compounds were shown to inhibit SARS-CoV-2 by blocking its progression, and their low toxicity suggests they could be considered for further preclinical research.

Introduction

Iran is home to a significant share of plant species and endless natural habitats characterized by numerous special plants and centers of local endemic species [1]. A. millefolium, with the common name yarrow, is a member of the Asteraceae family and is a flowering plant [2] comprising 130 species, 19 of which are grow wild in Iran [1].

The *Achillea* genus has a rich history in traditional medicine for various purposes, including anti-inflammatory, diuretic, and sedative effects [3]. These plants produce essential oils with diverse natural compounds that have medicinal properties, including antimicrobial effects. [4, 5]. These essential oils can be extracted from different parts of the plants using various techniques [6]. A recent study suggests that compounds from essential oils (EOs) show potential for combatting COVID-19 by inhibiting the SARS-CoV-2 main protease [7].

In 2019, a novel coronavirus disease (COVID-19) outbreak occurred in Wuhan, China. Since then, this viral disease has spread quickly worldwide, with millions of casualties [8]. This viral disease is caused by SARS-CoV-2 (syndrome acute respiratory CoronaVirus- 2), which belongs to the beta-coronavirus family and shares a similarity of up to 79% to SARS-CoV-1, which underlies the next-generation sequencing technology. The SARSCoV- 2 3C-like protease (3CLpro), or the main protease (Mpro), plays a vital role in the proteolytic processing of coronaviruses and creates other significant proteins for viral replication [9]. Hence, this protease may be the best target for therapeutic repositioning to identify promising antiviral drugs against SARS-CoV-2.

Owing to their long history of folk use in Iranian traditional medicine and because of their low toxicity and excellent pharmacokinetics, the *Achillea* genera, alongside the reported biological activities of three *Achillea* species (A. millefolium, A. wilhelmsii C. Koch, and A. tenuifolia Lam), were the subject of this research. We wanted to address the question of whether the extracted compounds from three different EOs of the *Achillea* species can be the inhibitors, or have the potency to be a possible source of strong and/or effective inhibitors, of the SARS-CoV-2 3CL protease. The antiviral potential of the extractedcompounds (from their EOs) against SARS-CoV-2 3CLpro (and SARS-CoV-1 3CLpro, as a standard) was investigated for the first time. Initially, the EOs of A. millefolium, A. wilhelmsii C. Koch, and A. tenuifolia Lam were obtained. The identified compounds were selected to investigate their antiviral potential against viral targets using AutoDcock 4.2.6. These compounds also showed low toxicity and very good pharmacokinetic properties in the SwissADME and ProTox-II evaluations. The compounds with the lowest binding energies (with the viral targets) were the best antiviral candidates against the viral protease and are worthy of further in vitro and in vivo analyses to clarify their antiviral potential.

Docking Studies of SARS-CoV-2 $3CL^{pro}$

Molecular docking is a potent approach used to elucidate protein and small-molecule interactions. Among the identified compounds from the EOs of the three different types of yarrow tested against SARS-CoV-2 $3CL^{pro}$, four natural inhibitors (Kessanyl acetate, Chavibetol (m-Eugenol), Farnesol, and 7-epi-β-Eudesmol) extracted from the EO of A. millefolium exhibited strong inhibitory effects against the viral target. It was clear that $3CL^{pro}$ (or the main protease) catalyzed the most important maturation cleavage phenomenon and also played a significant role in the viral replication of SARS-CoV-2, signifying its importance as a drug target [10].

As shown in Figure 5A, kessanyl acetate formed three H-bonds with the viral target: two with Ser 144 and one with the important residue Cys 145 (located in domain

II and acting as a nucleophile in the initial step of the hydrolysis reaction in the catalytic region of the enzyme with the assistance of His 41 as a base catalyst) [65]; therefore, the interaction with this residue may have remarkably caused a malfunction in its enzymatic activities. Moreover, the hydrophobic interactions between kessanyl acetate and the important residues located in domains I and II [10], including His 41, Met 49, Leu 141, Asn 142, Gly 143, and Gln 189, can ratify the potent inhibitory effect of this natural product on the active site of the enzyme.

Cys 145 is located in the active site positioned in the oxyanion loop (residues 138–146), which, along with Gly 143, defines an oxyanion hole (via interactions between their amide groups and the carbonyl group of peptides), and, together with the β-strand segment (His163-Pro168), they are highly important for the preparation of active sites and substrate binding. Furthermore, residues near the loop segment play a significant role in expanding the active site [10]. Based on this information, it is worth pointing out that chavibetol (m-eugenol) binds to the active site of $3CL^{pro}$ through five strong hydrogen bonds with the residues Leu 141, Gly 143, Ser 144, and His 163, showing that this natural inhibitor may have high impairment and disruptive effects on the active site, and it may potentially disturb active site formation and accurate substrate binding (Figure 5B).

These disruptive effects on the active site formation and substrate binding of 3CLpro can be seen for the other two remaining natural inhibitors (Farnesol and 7-epi-β-Eudesmol) because each of them form H-bonds with Leu 141 and Ser 144, although the former shows an additional H-bond with His 163. Interestingly, both had hydrophobic interactions with Cys 145 and His 41, showing their strong antiviral effects on the catalytic function of this enzyme (Figure 5 C,D). Taken together, these results show that the binding of the four natural inhibitors (extracted from A. millefolium) to the active site of $3CL^{Pro}$ may disrupt substrate binding and active site formation, thereby impeding catalytic functions.

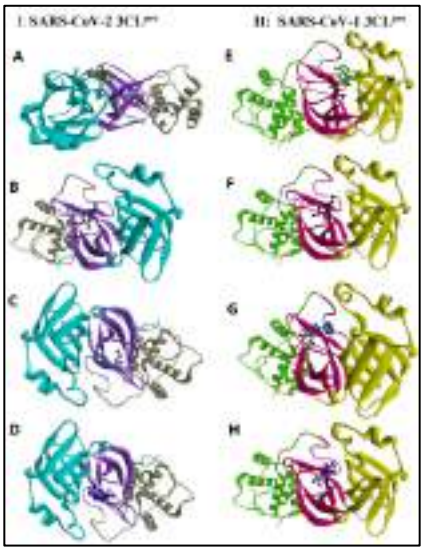

Figure 1. A 3D illustration of the interactions between the candidate compounds and the viral polymerases. (A–D) SARS-CoV-2 3CLpro: 6NUR. (E–H) SARS-CoV-1 3CLpro: 2H2Z. (A) Kessanyl acetate. (B) Chavibetol (m-Eugenol). (C) Farnesol. (D) 7-epi-β-Eudesmol.

Docking Studies of SARS-CoV-1 $3CL^{pro}$

To investigate the potency of the extracted natural products against other major proteases, we selected SARS-CoV-1 $3CL^{pro}$ by using the same docking procedure. Based on the docking data, it could be asserted that four of the tested ligands showed higher binding energies (as they did against SARS-CoV-2 $3CL^{pro}$). The 3CL proteases of SARS-CoV-1 and SARS-CoV-2 share approximately 96% sequence identity, indicating that they are similar to each other [66], and SARS-CoV-1 $3CL^{pro}$ also possesses the three main domains, I, II, and III, and its catalytic dyad is composed of His 41 and Cys 145, in which its substrate-binding pocket is located in the cleft between I and II [11]. Interestingly, kessanyl acetate binds to this viral receptor through three H-bonds with Gly 143, Ser144, and Cys 145, which, in turn, may hinder the catalytic site and cause strong disorganization in the enzymatic function of the protease. In addition, hydrophobic interactions with other residues located in the active site (Leu 141 and Asn 142) can prove its high preventive effects on the catalytic site (Figure 5E). As shown in Figure 5F, all interacting residues were located at the active site. Moreover, Chavibetol (m-eugenol) formed five strong hydrogen bonds with amino acid residues located in the catalytic region of domain II (Gly 143, Gly 143, Ser144, and His 163), and the active site entry may have been impaired [11], and the catalytic activities of such enzymes can be remarkably diminished. With regard to the interaction of SARS-CoV-2 $3CL^{pro}$ with Farnesol and 7-epi-β-Eudesmol, it can be mentioned that both have formed H-bonds with Leu 141 and Ser 144, along with hydrophobic interactions with the significant catalytic dyad residues His 41 and Cys 145, indicating that these

two natural inhibitors may possess highly potent activity for hindering the catalytic region of the protease, and they can potentially disrupt its enzymatic function (Figure 5G,H). Thus, these four natural inhibitors may have strong inhibitory effects on the active site of SARS-CoV-1 $3CL^{pro}$ and could have a preventive and momentous disruptive impact on its catalytic function.

The four selected natural products were pharmacokinetically investigated using SwissADME. Interestingly, all four natural inhibitors satisfied the drug-likeliness properties, indicating a high bioavailability score. Remarkably, none of them served as P-glycoprotein (P-gp) substrates, showing excellent oral availability of these ligands and indicating that they have no inhibitory or inductive effect on metabolizing enzymes [12, 13]. More importantly, all showed high gastrointestinal absorption and could cross the blood–brain barrier, indicating that passing the cell membrane is vital for the components to enter the cells infected with SARS-CoV-2 and obtain successful access to the viral $3CL^{pro}$ of SARS-CoV-2. Consistent with our results, it should be noted that kessanyl acetate and farnesol possessed better pharmacokinetic characteristics, such as pharmacological and drug-likeliness properties. Although Kessanyl acetate did not interact with other medications, Farnesol and Chavibetol (m-eugenol) showed inhibitory effects on CYP1A2, which can be anticipated to interact with the metabolism of some typical anxiety or dispersive disorder drugs. Considering all of these properties, it can be postulated that these four naturally occurring compounds may be effectively absorbed, distributed, and diffused within the body. Finally, the toxicities of the four compounds were predicted using the ProTox-II online tool. All compounds exhibited modest or light toxicity, and Farnesol and Kessanyl acetate showed higher LD50 values. Based on the results obtained in this study, it can be asserted that all four natural compounds (particularly kessanyl acetate and farnesol) may be the most desirable candidates for further in vitro and in vivo investigations of SARS-CoV-2.

Conclusions

We computationally assessed the antiviral potential of compounds extracted from three *Achillea* types against SARS-CoV-2 and SARS-CoV-1 proteases using Autodock 4.2.6. Among these compounds, those extracted from A. millefolium (Kessanyl acetate, Chavibetol, farnesol, and 7-epi- -Eudesmol) showed the strongest binding energies and cluster numbers, indicating their potential to disrupt protease activity by forming hydrogen bonds with key amino acid residues (CYS 145 and HIS 41). Additionally, we evaluated the pharmacokinetic properties and found that kessanyl acetate and farnesol have favorable drug characteristics. Based on the findings of the present study, it should be mentioned that kessanyl acetate and farnesol are more potent inhibitors of 3CL-proteases than the other studied natural compounds, and they may be applied in future experimental studies to identify effective anti-SARS-CoV-2 compounds.

References

1. Mirdavoudi, H., et al., *Ecological Niche Modelling and Potential Distribution of Artemisia sieberi in the Iranian Steppe Vegetation.* Land, 2022. **11**(12): p. 2315.
2. Magiatis, P., et al., *Chemical composition and in-vitro antimicrobial activity of the essential oils of three Greek Achillea species.* Zeitschrift für Naturforschung C, 2002. **57**(3-4): p. 287-290.
3. Saeidnia, S., et al., *A review on phytochemistry and medicinal properties of the genus Achillea.* DARU: Journal of Faculty of Pharmacy, Tehran University of Medical Sciences, 2011. **19**(3): p. 173.
4. Ammarellou, A., et al., *Ammarellou A, Yousefi AR, Heydari M, Uberti D, Mastinu A. Biochemical and Botanical Aspects of Allium sativum L. Sowing. BioTech. 2022; 11 (2): 16. https://doi. org/10.3390/biotech11020016*. BIOTECH, 2022.
5. Jam, B.J., et al., *Impact of silicon foliar application on the growth and physiological traits of Carthamus tinctorius L. exposed to salt stress.* Silicon, 2023. **15**(3): p. 1235-1245.
6. Mohammadhosseini, M., *Essential oils extracted using microwave-assisted hydrodistillation from aerial parts of eleven Artemisia species: Chemical compositions and diversities in different geographical regions of Iran.* Records of natural products, 2017. **11**(2): p. 114.
7. Strub, D.J., et al., *Evaluation of the anti-SARS-CoV-2 properties of essential oils and aromatic extracts.* Scientific reports, 2022. **12**(1): p. 14230.
8. Rane, J.S., et al., *Targeting SARS-CoV-2 spike protein of COVID-19 with naturally occurring phytochemicals: an in silco study for drug development.* 2020.
9. Vuong, W., et al., *Feline coronavirus drug inhibits the main protease of SARS-CoV-2 and blocks virus replication.* Nature communications, 2020. **11**(1): p. 4282.
10. Suárez, D. and N. Díaz, *SARS-CoV-2 main protease: A molecular dynamics study.* Journal of chemical information and modeling, 2020. **60**(12): p. 5815-5831.
11. Xue, X., et al., *Production of authentic SARS-CoV Mpro with enhanced activity: application as a novel tag-cleavage endopeptidase for protein overproduction.* Journal of molecular biology, 2007. **366**(3): p. 965-975.
12. Sun, J., et al., *Multidrug resistance P-glycoprotein: crucial significance in drug disposition and interaction.* Medical science monitor: international medical journal of experimental and clinical research, 2004. **10**(1): p. RA5-14.
13. Ribaudo, G., et al., *Computational and experimental insights on the interaction of artemisinin, dihydroartemisinin and chloroquine with SARS-CoV-2 spike protein receptor-binding domain (RBD).* Natural product research, 2022. **36**(20): p. 5358-5363.

29TH IRANIAN ORGANIC CHEMISTRY CONFERENCE
1_3 NOV, 2023
UNIVERSITY OF QOM, IRAN

g-C_3N_4/$H_3PW_4Mo_8O_{40}$ nanohybrid as catalyst for synthesis of 2,3-dihydroquinazolin-4(*1H*)-ones

*Razieh Nejat**

Chemistry Department, Faculty of Science, Kosar University of Bojnord, Iran. Bojnord, Iran. P.O. Box 9415615458, organochem.nejat@kub.ac.ir

Abstract - g-C_3N_4/$H_3PW_4Mo_8O_{40}$ nanohybrid was explored as an effective catalyst to effect the three-component condensation reactions of aromatic aldehydes with isatoic anhydride and amines. 2,3-dihydroquinazolin-4(*1H*)-ones were produced from these reactions in EtOH/H_2O (1:1) at room temperature in high yields. The easy preparation and recycling of the catalyst, easy reaction procedure and work up, and also use of EtOH/H_2O as environmentally benign solvent are the main advantages of this protocol.

1. Introduction

Recently tungesto- and molybo-phosphoric acids draw attention in photocatalytic reactions. For example, Fazlali et al. [1] explored Keggin hetero polyacid supported on BN and C_3N_4 as an efficient catalyst in the methanol photocatalytic dehydration reaction. Also, the ion-exchange in Keggin type HPAs (W and Mo) lead to improve the catalytic properties of the catalysts because the substitution of these atoms changes their acid and redox properties [2-4]. Unfortunately, low charge separation and high solubility in polar media hinder its practical utilization at a large scale. Recent studies have shown that the recombination of photogenerated electrons and holes can be controlled by coupling HPAs with an ideal substrate [5, 6]. In this perspective, for the anchoring of HPAs, graphitic carbon nitride (g-C_3N_4) can be an appropriate candidate because of the presence of various functional groups and their unique properties. Graphitic carbon nitrides as the most stable allotrope of carbon nitride with high chemical and thermal stability and also unique electronic structure, have been standing in the hot research area for their potential applications in photocatalysis [7-9]. Also, g-C_3N_4 has rich surface properties that are attractive for catalysis applications due to the presence of basic surface sites. Multi-component reactions (MCRs) are emerging as useful tools for carbon-carbon and carbon-heteroatom bondformation and for the synthesis of important organic molecules with several degrees of structural diversity. (MCRs) have some advantages over classic divergent reaction strategies, such as lower costs, shorter reaction time,and less side products,as well as environmentally friendlier aspects. Several methods have been reported for the synthesis of 2,3-dihydroquinazolinones. However,these methods suffer from lengthy procedures and/or low yields and vigorous conditions.

2. Materials and method

Chemicals used in this work were purchased from Fluka and Merk chemical companies and used without purification. FT-IR spectra were obtained over the region 400-4000 cm-1 with NICOLET IR100 FT-IR with spectroscopic grade KBr. The phase purity and crystalline structure of samples were analyzed by using Philips X-pert X-ray diffractometer using Cu Kα radiation (α = 0.154056 Å).

2.1. Preparation and characterization of the catalyst

The bulk graphitic carbon nitride (g-C_3N_4) was synthesized by thermal condensation of melamine following a previously published method. HPAs nanoparticles were prepared according to reported reference [4]. For the synthesis of PW_4Mo_8/g-C_3N_4, the g-C_3N_4 (0.5 g) was taken in ethanol (30 ml) and sonicated for 2 h to make the thick slurry. $H_3PMo_8W_4O_{40}$ (0.8 g) was added to the slurry and then sealed and stirred for 20 hours. Afterward, the cap was removed and the solid phase was filtered. Subsequently, it was dried at 75℃.

3. Results and Discussion

A mixture of aromatic aldehyde (1), isatoic anhydride (2), and amine (3) under the catalytic effect of PW_4Mo_8/g-C_3N_4, undergo one-pot reactions in EtOH/H_2O (1:1) at room temperature to afford the corresponding 2,3-dihydroquinazolin-4(*1H*)-ones 4 (Scheme 1).

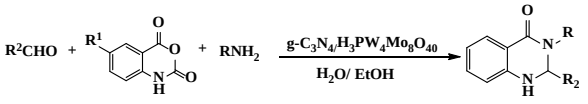

Scheme 1

Table 1. Synthesis of 2,3-dihydroquinazolin-4(*1H*)-ones by $PW_4Mo_8/g\text{-}C_3N_4$

Entry	R^1	R^2	Amine	Time (h)	Yield (%)
1	H	4-(ph)C_6H_4	p-$(CH_3)C_6H_4$	1	95
2	H	2-($C_{10}H_7$)	p-$(CH_3)C_6H_4$	2	90
3	H	2-($C_{10}H_7$)	p-$(OCH_3)C_6H_4$	3	96
4	Cl	2-($C_{10}H_7$)	p-$(OCH_3)C_6H_4$	3	85
5	Cl	2,3-$(Cl_2)C_6H_3$	p-$(CH_3)C_6H_4$	3	86
6	Cl	2,3-$(Cl_2)C_6H_3$	p-$(OCH_3)C_6H_4$	2	96
7	H	2,3-$(Cl_2)C_6H_3$	p-$(OCH_3)C_6H_4$	2	95
8	H	2,3-$(Cl_2)C_6H_3$	p-$(CH_3)C_6H_4$	1	90

The Fourier transform infrared (FT-IR) spectroscopy of (a) the PW_4Mo_8 and (b) PW_4Mo_8 /g-C_3N_4 were also investigated in the range of 500–4000 cm^{-1}. The chief peaks of $PW_4Mo_8/g\text{-}C_3N_4$ located at 1048 and 1020 cm^{-1} (ν P-O), 930–945 cm^{-1} (ν metal=O), 850–890 cm^{-1} (ν Metal-O-metal) and 769 cm^{-1} (ν Metal-O-metal) were observed (Figure 1a). For $PW_4Mo_8/g\text{-}C_3N_4$, the peaks between 3100 and 3300 cm^{-1} are assigned to N-H and OH stretching vibrations. As well as, the bands at 1150-1750 cm^{-1} regions are attributed to aromatic C-N heterocycles. The intensity of the specific bands of $H_3PW_4Mo_8O_{40}$ is low, due to the presence of a small amount of HPA on the g-C_3N_4 (Figure 1b).

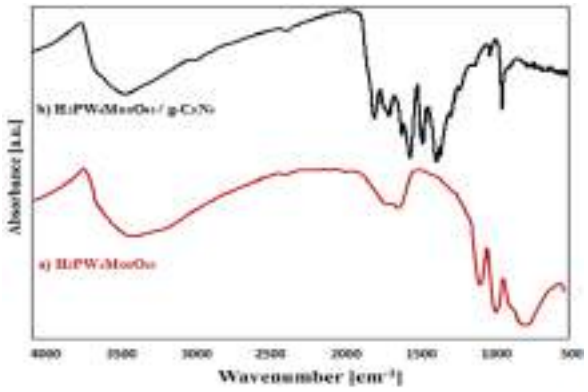

Figure 1. The FT-IR spectra of (a) the PW_4Mo_8 and (b) PW_4Mo_8 /g-C_3N_4.

The XRD measurements were implemented to investigate the presence as well as the crystallinity degree and purity of g-C_3N_4, PW_4Mo_8, and $PW_4Mo_8/g\text{-}C_3N_4$ catalysts (Figure 2). The XRD pattern of g-C_3N_4 showed diffraction peaks at 2θ = 13.1 ° and 27.5 ° correspondings to the reflection planes (100) and (002), respectively (JCPDS No. 87-1526). The intensity of the (100) plane is quite good which confirms the presence of a graphite-like structure. The sample of PW_4Mo_8 exhibits peaks at 7º~10º, 16º~23º, 25º~31º, and 36º~43º corresponding to the peaks of the Keggin structure, which demonstrated that heteropoly acid with Keggin structure had been prepared. Whole these diffraction peaks have remained in the XRD patterns of $PW_4Mo_8/g\text{-}C_3N_4$ compound but with reduced intensity, which can result from the decrease crystallite size. The XRD pattern of both the g-C_3N_4 and PMo_8W_4 /g-C_3N_4 showed a strong diffraction peak at 2θ =27.5°, which indicated the characteristic interlayer stacking of aromatic systems. Thus the XRD pattern of the $PW_4Mo_8/g\text{-}C_3N_4$ exhibits the typical Keggin-type diffraction peaks and g-C_3N_4 diffraction peaks which indicated that PW_4Mo_8 was loaded on g-C_3N_4 successfully.

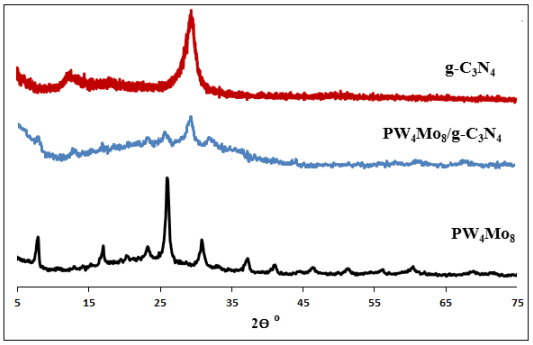

Figure 2. XRD of g-C_3N_4, PW_4Mo_8, and $PW_4Mo_8/g\text{-}C_3N_4$.

Conclusions

In summary, the $PW_4Mo_8/g\text{-}C_3N_4$ nanoparticles were explored as effective and re-usable catalyst for synthesis of 2,3-dihydroquinazolin-4(*1H*)-ones in $EtOH/H_2O$ at room temperature.

Acknowledgment

Financial support of this work by Kosar University of bojnord is gratefully acknowledged.

4. References

[1] F. R. Pomilla, F. Fazlali, E I. García-Lopez, G. Marcì, A. R. Mahjoub, I. Kritsov, L F. Liotta, L. Palmisano, 2020. Keggin heteropolyacid supported on BN and C3N4: Comparison between catalytic and photocatalytic alcohol dehydration, Mater. Sci. Semicond. Process. 112, 104987.

[2] M. Chamack, A.R. Mahjoub, H.Aghayan, Cesium salts of tungsten-substituted molybdophosphoric acid immobilized onto platelet mesoporous silica: Efficient catalysts for oxidative desulfurization of dibenzothiophene, Chem. Eng. J. 255 (2014) 686-694. https://doi.org/10.1016/j.cej.2014.06.054.

[3] R. Wang, G. Zhang, H. Zhao, Polyoxometalate as effective catalyst for the deep desulfurization of diesel oil, Catal. Today. 149 (2010) 117–121. https://doi.org/10.1016/j.cattod.2009.03.011.

[4] H. Wu, M. Zhou, Y. Qu, H. Li, H. Yin, Preparation Chemical Society Reviews and Characterization of tungsten-substituted molybdophosphoric acids and catalytic cyclodehydration of 1,4-butanediol to tetrahydrofuran, Chinese J. Chem. Eng. 17 (2009) 200-206. https://doi.org/10.1016/S1004-9541(08)60194-9.

[5] A. Ucar, M. Findik, I.H. Gubbuk, N. Kocak, H. Bingol, Catalytic degradation of organic dye using reduced graphene oxide–polyoxometalate nanocomposite, Mater. Chem. Phys. 196 (2017) 21-28. https://doi.org/10.1016/j.matchemphys.2017.04.047.

[6] Z. Kang, E. Wang, B. Mao, Z. Su, L. Gao, S. Lian, L. Xu, Controllable fabrication of carbon nanotube and nanobelt with a polyoxometalate-assisted mild hydrothermal process, J. Am. Chem. Soc. 127 (2005) 6534-6535. https://doi.org/10.1021/ja051228v.

[7] X. Wei, J. Cao, F. Fang, A novel multifunctional Ag and Sr2+ co-doped TiO2 @rGO ternary nanocomposite with enhanced p-nitrophenol degradation, and bactericidal and hydrogen evolution activity, RSC Adv. 8 (2018) 31822–31829. https://doi.org/10.1039/C8RA06813E.

[8] X. Wang, K. Maeda, A. Thomas, K. Takanabe, G. Xin, J M. Carlsson, K. Domen, M. Antonietti, A metal-free polymeric photocatalyst for hydrogen production from water under visible light, Nat. Mater. 8 (2009) 76–80. https://doi.org/10.1038/nmat2317.

[9] A. Thomas, A. Fischer, F. Goettmann, M. Antonietti, J.-O. Muller, R. Schlogl, J M. Carlsson, Graphitic carbon nitride materials: variation of structure and morphology and their use as metal-free catalysts, J. Mater. Chem. 18 (2008) 4893–4908.

[10] Hu, T., Dai, K., Zhang, J., Zhu, G., and Liang, C. (2019). One-pot synthesis of step-scheme Bi2S3/porous g-C3N4 heterostructure for enhanced photocatalytic performance. Mater. Lett. 257, 126740

[11] I. Krivstov, E.I. García-Lopez, G. Marcì, L. Palmisano, Z. Amghouz, J.R. García, S. Ordonez, E. Díaz, Selective photocatalytic oxidation of 5-hydroxymethyl-2- furfural to 2, 5-furandicarboxyaldehyde in aqueous suspension of g-C_3N_4, Appl. Catal. B. 204 (**2017**) 430–439. https://doi.org/10.1016/j.apcatb.2016.11.049.

[12] He, F., Meng, A., Cheng, B., Ho, W., and Yu, J. (2020). Enhanced photocatalytic H2-production activity of WO3/TiO2 step-scheme heterojunction by graphene modification. Chin. J. Catal. 41, 9–20.

[13] Mu, J., Teng, F., Miao, H., Wang, Y., and Hu, X. (2020). In-situ oxidation fabrication of 0D/2D SnO_2/SnS_2 novel Step-scheme heterojunctions with enhanced photoelectrochemical activity for water splitting. Appl. Surf. Sci. 501, 143974.

[14] Wang, R., Shen, J., Zhang, W., Liu, Q., Zhang, M., Zulfiqar, H.T., and Tang, H. (2020). Build-in electric field induced step-scheme TiO2/ W18O49 heterojunction for enhanced photocatalytic activity under visible-light irradiation. Ceram. Int. 46, 23–30.

[15] L. Ye, J. Liu, Z. Jiang, T. Peng, L. Zan, Facets coupling of BiOBr-g-C_3N_4 composite photocatalyst for enhanced visible-light-driven photocatalytic activity, Appl. Catal. B. 142-143 (**2013**) 1–7.

[16] Q. Xu, L. Zhang, B. Cheng, J. Fan, J. Yu, S-Scheme Heterojunction Photocatalyst, Chem. 6 (**2020**) 1543-1559**.**

[17] X. Xiao, J. Jiang, L. Zhang, Selective oxidation of benzyl alcohol into benzaldehyde over semiconductors under visible light: The Case of $Bi_{12}O_{17}Cl_2$ Nanobelts, Appl. Catal. B. 142-143 (**2013**) 487-493.

[18] C. Zheng, G. He, X. Xiao, M. Lu, H. Zhong, X. Zuo, J. Nan, Selective photocatalytic oxidation of benzyl alcohol into benzaldehyde with high selectivity and conversion ratio over $Bi_4O_5Br_2$ nanoflakes under blue LED irradiation, Appl. Catal. B. 205 *(***2017***)* 201-210.

[19] A. López-Magano, A. Jiménez-Almarza, J. Alemán, R. Mas-Ballesté, Metal–Organic Frameworks (MOFs) and Covalent Organic Frameworks (COFs) Applied to Photocatalytic Organic Transformations**,** Catalysts. 10 (**2020**)720.

29TH IRANIAN ORGANIC CHEMISTRY CONFERENCE
1_3 NOV, 2023
UNIVERSITY OF QOM, IRAN

Degradation of methyl blue by Polyoxometalate/g-C_3N_4 as an active and recyclable photocatalyst under visible light

*Razieh Nejat**

Chemistry Department, Faculty of Science, Kosar University of Bojnord, Iran. P.O. Box 9415615458;
organochem.nejat@kub.ac.ir

Abstract - A new photocatalyst, Polyoxometalate/g-C_3N_4 (g-C_3N_4/$H_3PW_4Mo_8O_{40}$) was synthesized and characterized. This magnetic catalyst showed high catalytic activity for the degradation of methyl blue (MB) under visible light irradiation. High yield, low reaction times, the use of green solvents and non-toxicity of the catalyst are the main merits of this protocol. The results indicated improved photocatalytic efficiency for the polyoxometalate supported on g-C_3N_4 compared to the pure polyoxometalate. To improve photocatalytic activity, the effect of complex loading and optimal synthesis conditions were investigated. The Catalyst was characterized by Fourier transform infrared spectroscopy (FT-IR) and X-ray spectroscopy (XRD).

1. Introduction

The disposal of various toxic dyes from the textile industry has attracted extensive attention in the field of water pollution prevention and cure. methyl blue (MB) is one of the famous dyes and is widely used as a colorant in foodstuffs and textiles due to its high stability

It is harmful to human beings and animals and causes irritation of the skin, eyes, and respiratory tract. The removal methods of toxic dyes have been considered in recent studies in the literature. These include physical adsorption [1,2], chemical degradation [3], biological degradation [4], photodegradation, or the synergic treatments of different methods.

Recently, much attention has been paid to the photocatalytic degradation of dye pollutants using nanodispersed catalysts TiO_2 [5], SnO_2 [6], and so forth. It uses light energy to initiate chemical reactions in the presence of photocatalysts which are mostly semiconductor materials. Heterogeneous photocatalysis using semiconductors is an effective and rapid technique for the removal of dye pollutants from wastewater [7].

Organic wastewater effluents of textile mills and other dye processing units, because 15% of synthetic textile dyes are believed to get dispersed in wastewater during manufacturing and processing.

Among the best agents for dye degradation are wide band gap semiconductors, in which electron-hole pairs are formed upon photoexcitation. A fraction of these get trapped in shallow defect states and are subsequently available for relatively slow, redox processes.

Most organic photodegradation reactions utilize the oxidizing power of holes and result in the conversion of the organic species at the interfaces into nontoxic end products. An ideal photocatalyst should be stable, inexpensive, nontoxic, and highly photoactive, and the redox potential of the OH/H_2O couple must lie within its band gap.

Photocatalytic activity has been mostly studied using spherical or equiaxed nanoparticles, in which the catalytic efficiency indeed increases with decreasing particle size. However, the recovery of nanoparticulate catalysts from the solution at the end of the reaction cycle may prove to be impractical.

Recently tungesto- and molybo-phosphoric acids draw attention in photocatalytic reactions. For example, Fazlali et al. [8] explored Keggin hetero polyacid supported on BN and C_3N_4 as an efficient catalyst in the methanol photocatalytic dehydration reaction. Also, the ion-exchange in Keggin type HPAs (W and Mo) lead to improve the catalytic properties of the catalysts because the substitution of these atoms changes their acid and redox properties [9-11]. Unfortunately, low charge separation and high solubility in polar media hinder its practical utilization at a large scale. Recent studies have shown that the recombination of photogenerated electrons and holes can be controlled by coupling HPAs with an ideal substrate [12, 13].

The catalyst was characterized and its suitability and efficiency was tested for photocatalytic degradation of methyl blue (MB).

2. Materials and method

Chemicals used in this work were purchased from Fluka and Merk chemical companies and used without purification. FT-IR spectra were obtained over the region 400-4000 cm-1 with NICOLET IR100 FT-IR with spectroscopic grade KBr. The phase purity and

crystalline structure of samples were analyzed by using Philips X-pert X-ray diffractometer using Cu Kα radiation (α = 0.154056 Å).

2.1. Preparation and characterization of the photocatalyst

The bulk graphitic carbon nitride (g-C_3N_4) was synthesized by thermal condensation of melamine following a previously published method. HPAs nanoparticles were prepared according to reported reference [4]. For the synthesis of PW_4Mo_8/g-C_3N_4, the g-C_3N_4 (0.5 g) was taken in ethanol (30 ml) and sonicated for 2 h to make the thick slurry. $H_3PMo_8W_4O_{40}$ (0.8 g) was added to the slurry and then sealed and stirred for 20 hours. Afterward, the cap was removed and the solid phase was filtered. Subsequently, it was dried at 75℃**.**

3. Results and Discussion

The photocatalytic activities of (g-C_3N_4/$H_3PW_4Mo_8O_{40}$) are evaluated by taking 50 mL of reaction mixture of methyl blue (20 mg/L) and 0.005 g of catalyst aqueous medium. First of all, the methyl blue molecular is kept in the dark under magnetic stirring for 60 min to maintain adsorption/desorption equilibrium between the pollutant and the surface of the catalyst. The visible illumination was provided by a 400 W lamp (high-pressure mercury-vapor lamp and λ=546.8 nm and air diffuser (air pump, flow: 3.5 L. min^{-1}) was located at the bottom of the reactor to uniformly disperse air into the solution. The photocatalytic reaction temperature was kept at the room temperature using cooling fans to prevent any thermal catalytic effect. The UV-Visible absorption spectra of the methyl blue degradation is shown in Figure 1.

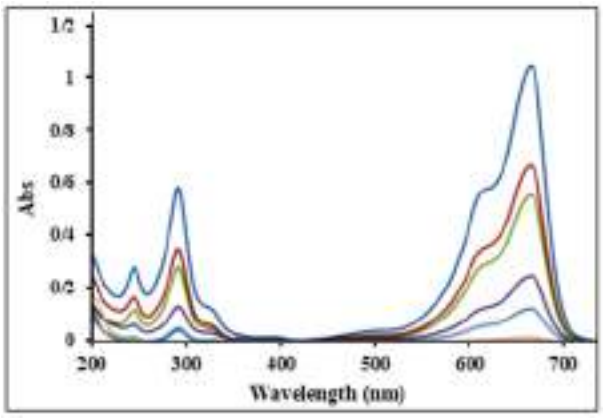

Figure 1.

The Fourier transform infrared (FT-IR) spectroscopy of (a) the PW_4Mo_8 and (b) PW_4Mo_8 /g-C_3N_4 were also investigated in the range of 500–4000 cm^{-1}. The chief peaks of PW_4Mo_8/g-C_3N_4 located at 1048 and 1020 cm^{-1} (ν P-O), 930–945 cm^{-1} (ν metal=O), 850–890 cm^{-1} (ν Metal-O-metal) and 769 cm^{-1} (ν Metal-O-metal) were observed (Figure 1a). For PW_4Mo_8/g-C_3N_4, the peaks between 3100 and 3300 cm^{-1} are assigned to N-H and OH stretching vibrations. As well as, the bands at 1150-1750 cm^{-1} regions are attributed to aromatic C-N heterocycles. The intensity of the specific bands of $H_3PW_4Mo_8O_{40}$ is low, due to the presence of a small amount of HPA on the g-C_3N_4 (Figure 1b)**.**

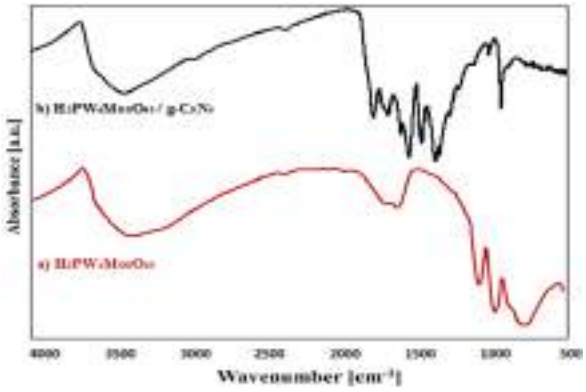

Figure 1. The FT-IR spectra of (a) the PW_4Mo_8 and (b) PW_4Mo_8 /g-C_3N_4.

The XRD measurements were implemented to investigate the presence as well as the crystallinity degree and purity of g-C_3N_4, PW_4Mo_8, and PW_4Mo_8/g-C_3N_4 catalysts (Figure 2). The XRD pattern of g-C_3N_4 showed diffraction peaks at 2θ = 13.1 ° and 27.5 ° correspondings to the reflection planes (100) and (002), respectively (JCPDS No. 87-1526). The intensity of the (100) plane is quite good which confirms the presence of a graphite-like structure. The sample of PW_4Mo_8 exhibits peaks at 7º~10º, 16º~23º, 25º~31º, and 36º~43º corresponding to the peaks of the Keggin structure, which demonstrated that heteropoly acid with Keggin structure had been prepared. Whole these diffraction peaks have remained in the XRD patterns of PW_4Mo_8/g-C_3N_4 compound but with reduced intensity, which can result from the decrease crystallite size. The XRD pattern of both the g-C_3N_4 and PMo_8W_4 /g-C_3N_4 showed a strong diffraction peak at 2θ =27.5°, which indicated the characteristic interlayer stacking of aromatic systems. Thus the XRD pattern of the PW_4Mo_8/g-C_3N_4 exhibits the typical Keggin-type diffraction peaks and g-C_3N_4 diffraction peaks which indicated that PW_4Mo_8 was loaded on g-C_3N_4 successfully.

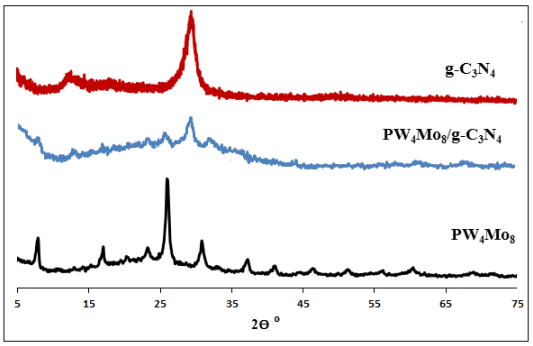

Figure 2. XRD of g-C_3N_4, $PW_4Mo_{8,}$ and PW_4Mo_8/g-C_3N_4.

Conclusions

In summary, the catalyst was characterized and its suitability and efficiency was tested for photocatalytic degradation of methyl blue (MB).

Acknowledgment

Financial support of this work by Kosar University of bojnord is gratefully acknowledged.

4. References

[1] Eftekhari, S. Habibi-Yangjeh A. Sohrabnezhad, S. H., J. Hazard. Mater. 178 (2010) 349–355.
[2] Xue, X. He, X. Zhao, Y. Desalin. Water Treat., 37 (2012) 259–267.
[3] Tehrani-Bagha, A. R. Mahmoodi, N. M. Menger, F. M. Desalination, 260 (2010), 34–38.
[4] Saratale, R. G. Saratale, G. D. Chang, J. S. Govindwar, S. P. Int. Biodeterior. Biodegrad., 21 (2010) 999–1015.
[5] Chen X. Mao, S. S. Chem. Rev., 107 (2007) 2891–2959.
[6] Esen, B. Yumak, T. Sinag, A. Yildiz, T. Photochem. Photobiol., 87 (2011) 267–274.
[7] Colmenares J. C. Luque, R. Chem. Soc. Rev., 43 (2014) 765–778.
[8] F. R. Pomilla, F. Fazlali, E I. García-Lopez, G. Marcì, A. R. Mahjoub, I. Kritsov, L F. Liotta, L. Palmisano, 2020. Keggin heteropolyacid supported on BN and C3N4: Comparison between catalytic and photocatalytic alcohol dehydration, Mater. Sci. Semicond. Process. 112, 104987.
[9] M. Chamack, A.R. Mahjoub, H.Aghayan, Cesium salts of tungsten-substituted molybdophosphoric acid immobilized onto platelet mesoporous silica: Efficient catalysts for oxidative desulfurization of dibenzothiophene, Chem. Eng. J. 255 (2014) 686-694.
[10] R. Wang, G. Zhang, H. Zhao, Polyoxometalate as effective catalyst for the deep desulfurization of diesel oil, Catal. Today. 149 (2010) 117–121.
[11] H. Wu, M. Zhou, Y. Qu, H. Li, H. Yin, Preparation Chemical Society Reviews and Characterization of tungsten-substituted molybdophosphoric acids and catalytic cyclodehydration of 1,4-butanediol to tetrahydrofuran, Chinese J. Chem. Eng. 17 (2009) 200-206.
[12] A. Ucar, M. Findik, I.H. Gubbuk, N. Kocak, H. Bingol, Catalytic degradation of organic dye using reduced graphene oxide–polyoxometalate nanocomposite, Mater. Chem. Phys. 196 (2017) 21-28.
[13] Z. Kang, E. Wang, B. Mao, Z. Su, L. Gao, S. Lian, L. Xu, Controllable fabrication of carbon nanotube and nanobelt with a polyoxometalate-assisted mild hydrothermal process, J. Am. Chem. Soc. 127 (2005) 6534-6535.

29TH IRANIAN ORGANIC CHEMISTRY CONFERENCE
1_3 NOV, 2023
UNIVERSITY OF QOM, IRAN

Apoferritin nanocage for the delivery of epirubicin

Ronak Rafipour[1*], *Hasanain Gomhor J. Alqaraghuli*[2], *Soheila Kashanian*[3,4]

[1] *Department of Chemistry, Kermanshah Branch, Islamic Azad University, Kermanshah, Iran, ronak.rafipour@iau.ac.ir*
[2] *Department of Science, College of Basic Education, Al-Muthanna University, Al-Muthanna, Iraq.*
[3] *Department of Applied Chemistry, Faculty of Chemistry, Razi University, Kermanshah, Iran*
[4] *Nano Drug Delivery Research Center, Kermanshah University of Medical Sciences, Kermanshah, Iran*

Abstract – Epirubicin (Epr) is an effective chemotherapeutic drug; however, the clinical amenability of Epr is limited by its highly toxic interaction with normal cells. This toxicity can be decreased by utilizing nanocarriers and targeted drug delivery systems. This work describes an approach to delivering Epr via encapsulation in the horse spleen apoferritin (HsAFr) cavity. UV–vis spectroscopy, fluorescence spectroscopy, circular dichroism (CD) and transmission electron microscopy (TEM) were utilized for structural characterization of the HsAFr–Epr and HsAFr–Epr–FA complexes.

1. Introduction

Breast cancer is the leading cause of cancer death in women around the world and despite advances in detection and treatment, breast cancer continues to impact patient mortality rates [1]. While prevalent cancer treatments include: surgery, chemotherapy, radiotherapy, immunotherapy and targeted therapies, the success of these strategies are largely impaired by their non-specific toxicity and development of drug resistance, such that new therapeutic strategies are in progress [2]. Protein nanocages have been developed as a new class of targeted drug carriers as one new therapeutic strategy. They can decrease the un-intended toxicity caused by chemotherapeutic drugs [3]. Apoferritin is an example of such a novel drug nanocarrier. HsAFr is another protein nanocage which is comprised of 24 polypeptide subunits, which self-assemble to form a spherical nanocage. HsAFr contains heavy (H) and light (L) subunits, which are highly homologous [4]. The HsAFr cage has 14 hydrophilic and hydrophobic channels, each 3–4Å in diameter, permitting cargo exchange between the protein cage interior and exterior environments. HsAFr contains a cage with an internal diameter of 8 nm and external diameter of 12nm [5]. The drug encapsulation process is based on the response of HsAFr structure to the pH changes of surrounding microenvironment. In acid and alkaline conditions, at pH of 2.0 and 13.0, respectively, HsAFr can be dissociated into subunits while not denatured. HsAFr can then be mixed with small drug molecules and after adjusting pH to 7.4 subunits are reassembled again, thus encapsulating the drug within the HsAFr molecules [6]. Anthracycline drugs are utilized to treat various solid tumours and blood cancers. Anthracyclines, such as doxorubicin, epirubicin (Epr) and daunorubicin, continue to be the most active anticancer drugs used to treat these cancer types [7].

2. Materials and methods

2.1 Chemicals

Horse spleen apoferritin (HsAFr) was purchased from Calbiochem (San Diego, CA). Epirubicin hydrochloride was obtained from Kavosh Gostar Darou Company (Tehran, Iran) (manufactured by Ebewe pharma, Unterach am Attersee, Austria). All other materials were purchased from Merck (Kenilworth, NJ).

2.2 Encapsulation of epirubicin into apoferritin

The initial concentrations of HsAFr and Epr were 1 mg/mL and 0.12 mg/mL, respectively. Epr solution was added to HsAFr solution and the pH mixture was adjusted to 2.0 using HCl (1 M), and then maintaining this pH value for about 20 min at 8 °C. Then, the pH was slowly adjusted to 7.4 using NaOH (1 M). The resulting solution was stirred at 200 rpm under room temperature for 2 h and dialyzed (12 kDa cutoff) against phosphate buffer solution (25 mM, pH 7.4) for 24 h to remove the un-encapsulated Epr.

3. Results and discussion

3.1 UV–Vis spectroscopy

The UV–Vis spectra of the HsAFr and HsAFr–Epr

were determined, as shown in Figure 1. HsAFr displays absorption maxima at 280 nm. Proteins show a broad peak at 251–299nm for aromatic rings of phenylalanine (Phe), tyrosine (Tyr) and tryptophan

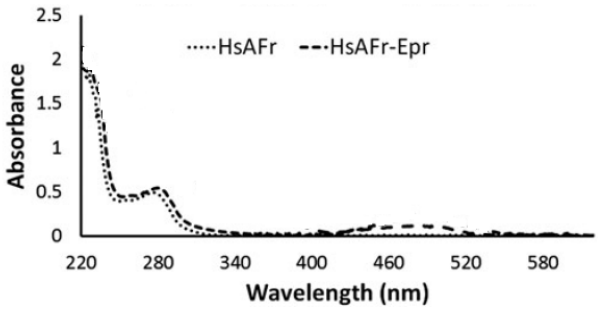

(Trp) residues. Epr demonstrates broad maxima at 480 nm. The UV–Vis spectra of the HsAFr and HsAFr–Epr were determined to examine the encapsulation of Epr in the HsAFr through the absorption showing up at 480 nm.

Figure 1. UV–Vis spectra of the HsAFr and HsAFr–Epr.

3.2 Fluorescence spectroscopy

The Epr fluorescence spectra in the Epr solution, and HsAFr–Epr were determined, as shown in Figure 2. Epirubicin fluorescence emission spectra were recorded at 495–675 nm with the excitation wavelength at 482 nm. The results suggest that the Epr was encapsulated in the HsAFr cages of HsAFr–Epr.

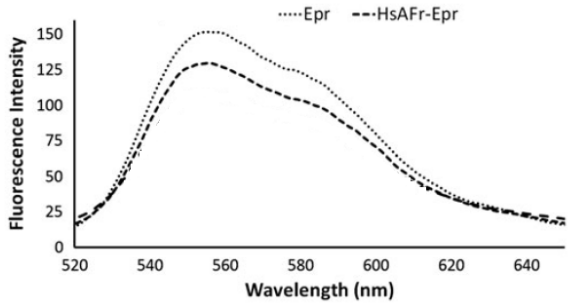

Figure 2. Epirubicin fluorescence spectra in the Epr solution and HsAFr–Epr. The excitation wavelength was set at 482 nm.

3.3 Transmission electron microscopy

When Epr molecules are encapsulated within HsAFr nanocages, we may expect that uranyl acetate would not flow within the cavity of HsAFr. This is because Epr occupied the inner cavity, preventing the uranyl acetate from entering the inner cavity of HsAFr (it has been indicated in black arrows). For HsAFr alone, uranyl acetate can be seen in the cavity (it has been indicated in white arrows) due to uranyl acetate flow into HsAFr cavity via channels after negatively stained with uranyl acetate. Figure 3 demonstrates the TEM image of negatively stained HsAFr–Epr.

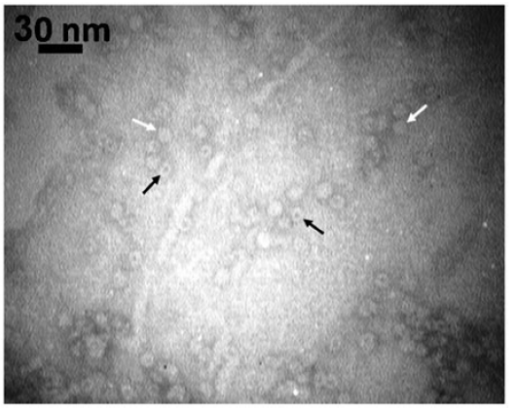

Figure 3. TEM image of negatively stained HsAFr–Epr with uranyl acetate. The presence of HsAFr and HsAFr–Epr has been indicated in black and white arrows.

4. Conclusions

In conclusion, a novel HsAFr protein cage-based drug delivery platform was designed by encapsulating Epr, an anticancer drug, into the cage of HsAFr using the self-assembly/disassembly property of this nanocarrier. The successful preparation of HsAFr–Epr and its characterization weas described in detail and it was found that Epr was loaded successfully in the nanocarrier cage.

5. References

[1] L. A. Torre, F, Bray, R. L. Siegel, et al. CA Cancer J Clin. 65(2015) 87-108.
[2] C. Engblom, C. Pfirschke, M. J. Pittet, Nat Rev Cancer. 16 (2016) 447–462.
[3] M. Karimi, P. S. Zangabad, F. Mehdizadeh, et al. Nanoscale. 9 (2017) 1356–1392.
[4] S. Zanzoni, K. Pagano, M. D'Onofrio, et al. Chem Eur J. 23 (2017) 9879-9887.
[5] L. Zhang, L. Laug, W. Mu€nchgesan, et al. Nano Lett. 10 (2010) 219-223.
[6] X. T. Ji, L. Huang, H.Q. Huang, J Proteomics. 75 (2012) 3145-3157.
[7] J. V. McGowan, R. Chung, A. Maulik, et al. Cardiovasc Drugs Ther.31 (2017) 63-75.

29TH IRANIAN ORGANIC CHEMISTRY CONFERENCE
1_3 NOV, 2023
UNIVERSITY OF QOM, IRAN

The presence effect of Cu(II) on thermal stability of Fe_3O_4@SiO_2 core-shell

*Setareh Rahmatzadeh, Alireza Sardarian**

Department of Chemistry, College of Sciences, University of Shiraz, Shiraz, Iran,
s.rahmatzadeh@shirazu.ac.ir, sardarian@shirazu.ac.ir

Abstract - In this article, we tried to investigate an abnormal chemical phenomenon and provide a scientific explanation for it. Our experimental thermogravimetric analysis (TGA) indicated that copper(II) nanoparticles, which are used to contribute to the catalytic role, improve the properties and also increase the stability of the catalyst structure in the formation of organometallic complexes for a wide range of supported catalysts by Fe_3O_4@SiO_2 core-shell, unlike the oxide of this metal, reduces the thermal stability of the core-shell substrate due to disturbing the integrated crystallography of the SiO_2 shell. This decrease in thermal stability has usually been observed in a higher temperature range than the organometallic catalysts' work-cycle temperature. Therefore, this potential weakness in these compounds will not be considered a catalytic weakness.

Keyword: Thermogravimetric Analysis, Copper(II) Nanoparticles, Fe_3O_4@SiO_2.

1. Introduction:

Nowaday, magnetic iron nanoparticles have drawn a lot of attention in modern catalysis and medical research due to their ability to be recycled and reused. Compared to conventional separation, magnetic separation has emerged as a powerful, efficient, easy, and rapid separation method. Despite having a high surface-to-volume ratio and strong magnetic attractions, nanomagnetite particles suffer from oxidation, aggregation, and corrosion because of their high reactivity and self-aggregation potential.[1]

To fix these weaknesses, the magnetite core's surface should be modified by a shell layer of such materials as polymers, biomolecules, metals, metal oxides, surfactants, etc. One of these shells is silica, which has a controllable thickness, low toxicity, is porous, and is biocompatible. In addition, SiO_2 can be easily joined with organic and inorganic catalysts. In fact, Fe_3O_4@SiO_2 has been recognized as a reliable substrate for improving the properties and performance of the reaction engineering and recycling of organic and inorganic catalysts, including organometalic catalysts.[1]

Other research has indicated so far that the complexing of metal oxides such as Cu_2O and CuO by surface layer of supported organic catalysts with Fe_3O_4@SiO_2 core-shell, in addition to improving the properties and increasing the performance of the catalyst, has increased the thermal stability of this core-shell substrate due to protecting the silica layer.[2]

The interaction of Cu(II) with the SiO_2 shell's surface is shown in **Scheme 1**.[3]

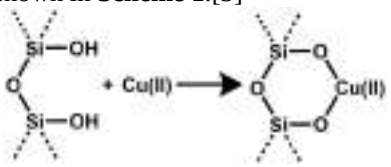

Scheme 1. Intraction Cu(II) nanoparticles with hydroxles of silica

Now the question is: what is the effect of atomic Cu(II) on the thermal stability of Fe_3O_4@SiO_2?

2. Materials and Methodes:

Fe_3O_4@SiO_2 was synthesized based on the method presented in the article by Sardarian et al.[1].

All chemicals with high quality were prepared from Sigma Aldrich, Merck and Alfa Aesar. The reaction accuracy and purity grace was accomplished by thin layer chromatography on silica gel polygram SILG/UV 254 plates and micro melting point apparatus (electrothermal, BUCHI 510). An SDT Q600 V20 9 Build 20 Thermal Gravimeter was used to get Thermal gravimetric analysis(TGA) data in the range of 400-800˚C.

3. Resules and discussion:

We encountered an abnormal phenomenon in one of our experimental studies on TGA curve investigation in which the presence of Cu(II) caused a serious decrease in the thermal stability of the Fe_3O_4@SiO_2 core-shell.

For Fe_3O_4@SiO_2 without Cu(II), as demonstrated in Figure 1, the SiO_2 shell has decomposed in the range of 400 to 800°C.

Therefore, in the absence of Cu(II), the SiO_2 shell prevented the Fe_3O_4 core from disintegrating under 800°C.

Figure 1's comparison of the two graphs clearly demonstrates that the SiO_2 shell's thermal stability in

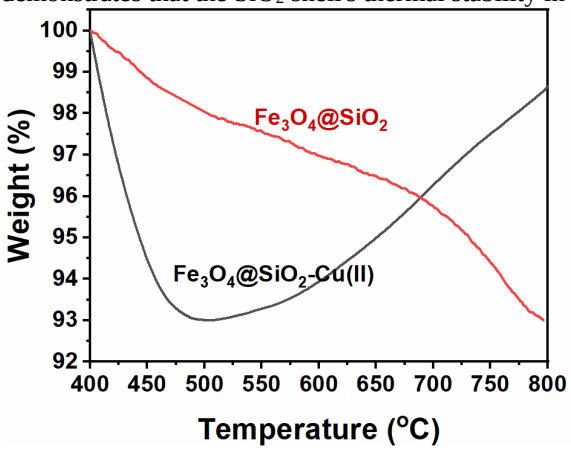

Figure 1. TGA cruves of Fe_3O_4@SiO_2 and Fe_3O_4@SiO_2-Cu(II)

the presence of Cu(II) has significantly decreased to the point where it completely decomposes from 400 to 500°C. So, in the presence of Cu(II), the magnetite core's destruction began at 500°C.

There are now two theories. a: Cu(II) has been oxidized first when exposed to heat. So, based on what was said earlier, this metal oxide should have boosted the thermal stability of this shell by protecting the SiO_2 shell. Therefore, we should not have discovered the start of the destruction of the magnetite core under 800°C. So, this assumption is false clearly. b: Cu(II) has interacted with the SiO_2 shell's outer oxygen atoms first. This may cause a thermal stability decrease in the shell due to the linking of those oxygen atoms and exerting pressure on the integrated crystal structure of the SiO_2 shell, potentially leading to its destruction or cracking in the lower temperature range.

4. Conclusion:

The investigation of an abnormal chemical phenomenon in our experimental thermogravimetric analysis (TGA) indicated that copper(II), unlike the oxide of this metal, reduce the thermal stability of the Fe_3O_4@SiO_2 core-shell substrate due to disturbing the integrated crystallography of the SiO_2 shell. This effect was observed because of the interactions between Cu(II) and oxygen of SiO_2 shell's surface.

The results indicated that if Cu(II) complexes in the surface layer of the supported catalyst by Fe_3O_4@SiO_2 core shell's, it may cause a decrease in the termal stability of this core-shell if, in the decomposition process, it turns to have interaction with the SiO_2 surface. The decrease in thermal stability has been observed in a higher temperature range than the organometallic catalysts' work-cycle temperature. Therefore, this potential weakness in these compounds will not be considered a catalytic weakness.

References:

[1] A.R. Sardarian, M. Kazemnejadi, M. Esmaeilpour, Appl. Organomet. Chem. 35 (2021) e6051.

[2] J.Y. Do, N. Son, J. Shin, R.K. Chava, S.W. Joo, M. Kang, Mater. Des. 198 (2021) 109357.

[3] Z. Bian, W. Zhong, Y. Yu, B. Jiang, S. Kawi, Int. J. Hydrogen Energy 45 (2020) 27078–27088.

29TH IRANIAN ORGANIC CHEMISTRY CONFERENCE
1_3 NOV, 2023
UNIVERSITY OF QOM, IRAN

New synthetic analogs of favipiravir as promising antiviral compounds

Maryam Haghpanah[1*], *Ali Reza Molla Ebrahimlo*[2], *Adeleh Moshtaghi Zonouz*[1]

[1]*Organic Chemistry Laboratory, Department of Chemistry, Faculty of Science, Azarbaijan Shahid Madani University, Tabriz, Iran, Maryam.hag6@gmail.com, Adelehmz@yahoo.com*
[2]*Department of Chemistry, Islamic Azad University, Khoy Branch, Khoy, Iran, mollaebrahimilo@yahoo.com*

Abstract - Viruses have always been the concern of human societies, The threat of emerging RNA-viruses spreading further demands for the development of potent therapeutic agents with activities against a broad range of such pathogens.1,4-Pyrazine-3-carboxamide-based antiviral compounds have been under intensive study for the last 20 years. One of these compounds, favipiravir (6-fluoro-3-hydroxyl pyrazine-2-carboxamide,T-705),that exhibits antiviral activities against a variety of RNA viruses and is approved for use against the influenza infection in a number of countries. In recent years,favipiravir actively used against COVID-19. In order to propose compounds with new antiviral properties, we designed and synthesized a new class of 3-hydroxy-5-aryl-pyrazine-2-carboxamide derivatives using 2-Aminopropanediamide and arylglyoxal derivatives under reflux conditions with a short duration and using green water solvent.The compounds were characterized by ^{13}C NMR, ^{1}H NMR, and IR. Therefore, the development of a short and eco-friendly approach using non-toxic reagents and solvents is highly desirable. The present work proves to new insights for develop new drugs using Based on favipiravir in the treatment of virus.

1. Introduction

Viruses and ways to deal with them have always been a concern of human societies, and as we know, since the end of 2019, the new coronavirus disease has spread everywhere and has caused serious problems in public health. In addition to making great efforts to make new compounds to fight viruses, screening of existing drugs has always been an important way to quickly identify possible pathways in pharmacology. For this purpose, in this research, we investigate the synthesis of Favipiravir antiviral drug analogues and its development methods. Favipiravir is active against a wide range of RNA viruses, including the influenza virus and its different types, which include: H_1N_1, H_5N_1, H_7N_9, but it has no activity against DNA viruses. It is also used to treat human infection caused by Ebola virus, Lassa virus, rabies and fever. Severe thrombocytopenia syndrome has been used. This antiviral drug inhibits the resistance of the influenza virus to a wide range of antiviral drugs, including amantadine,rimantadine,and neuraminidase inhibitors, and shows a synergistic effect in combination with seltamivir(Tamiflu), which is an antiviral drug against influenza. The result of favipiravir in the treatment of influenza is also one of the options that can be developed [1,2,3]. Favipiravir (T-705, 6-fluoro-3-hydroxypyrazine-2-carboxamide) was developed as an antiviral drug and was subsequently approved as an anti-influenza medicine in Japan in 2014. [2]. Favipiravir is a small pyrazine compound containing three substituents (–F, –OH, $–CONH_2$) in place. Due to the hydroxyl group, this compound exhibits acidic properties and could be tautomerized to the keto form, shown in Fig.1.This compound is a prodrug, it is phosphoribosylated in cells to favipiravir triphosphate which inhibits viral replication[4]. Aryl glyoxals are key precursors for the synthesis of a multitude of potential drugs, ranging from anticonvulsive agents [5] to HIV inhibitors[6]and anti-trypanosomal agents [7].

2. Results and discussion

Development of convenient protocols for biologically active pyrazine scaffolds from simple raw materials is a key research area in heterocyclic chemistry and especially drug discovery programs, Because the pyrazine ring, which is the central core of the favipiravir drug, is also considered as a drug intermediate due to its anti-HIV, anti-tuberculosis and anti-bacterial activities. Therefore, the main goal of this work is to introduce a simple one-pot strategy for synthesis of new Different derivatives of 3-hydroxy-5-arylpyrazine-2-carboxamide compounds as new analogs of favipiravir to be prepared using inexpensive and available materials. To approach this goal, we first chose the reaction of phenylglyoxal monohydrate (1a), 2-Aminopropane diamide (2) as model reaction. The arylglyoxal monohydrates were prepared by oxidation of corresponding aryl methyl ketones according to standard literature procedure [8] Scheme1.The intermediate compound 2-amino propanediamide was prepared from the reaction of

diethylaminomalonate hydrochloride salt with 25% ammonia solution in room temperature Scheme 2.

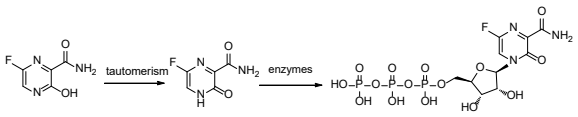

Fig1. Chemical structures of favipiravir (T-705) and T-705 RTP

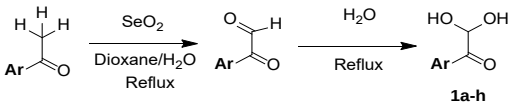

Ar=Ph,4-BrC_6H_4,4-ClC_6H_4,4-FC_6H_4,4-$NO_2C_6H_4$,4-MeC_6H_4, 4-$OMeC_6H_4$,$C_{10}H_7$,$C_{12}H_{10}$

Scheme1.

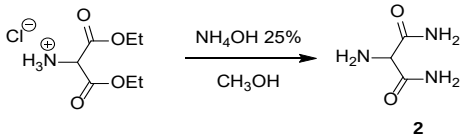

Scheme2.

We was examined the reaction conditions using various solvents such as water, ethanol, H_2O–EtOH (1:1) under different temperature conditions. The results for this model reaction indicated that the solvent and temperature had a significant effect on the synthesis of 3a. When the reaction was attempted in water at above 80°C a product was synthesized, in which the phenyl group is located at the 5 position of the pyrazine ring, and it is considered as the main derivative of the favipiravir drug skeleton. (Scheme 3)

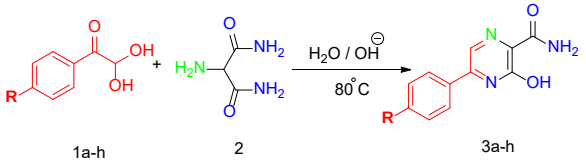

R=H,Cl,Br.F,NO_2,Me,OMe,$C_{10}H_7$,$C_{12}H_{10}$

Scheme3. One pot synthesis of new of 3-hydroxy-5-arylpyrazine-2-carboxamide derivatives

The proposed mechanism of reaction is shown in Scheme 4. In the conditions of this reaction, The most likely to occur would be the one resulting from the condensation of the most nucleophilic group of the 2-amino propanediamide (its amine) on the most electrophilic component of the Aryl glyoxal (its aldehyde) to give intermediate 4.

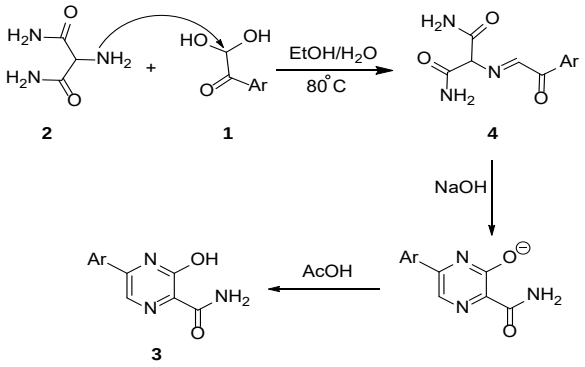

Scheme4.

3. Conclusions

This synthetic method therefore, appears to be generally applicable to the synthesis of heterocycles which are suitable synthetic intermediates for new analogs of favipiravir with possible pharmaceutical applications and could be expected to intercalate with virus.

4. References

[1] K. Izawa, J. L. Aceña, J. Wang, V. A. Soloshonok, H. Liu, Small-Molecule Therapeutics for Ebola Virus (EBOV) Disease Treatment, Eur. J. Org. Chem. ,vol. 1, pp. 8–16, 2016.

[2] Furuta, Y.; Gowen, B. B.; Takahashi, K.; Shiraki, K.; Smee, D. F.; Barnard, D. L, Favipiravir (T-705), a novel viral RNA polymerase inhibitor, Antiviral Res 2013, 100, 446.

[3] Shiraki, K.; Daikoku, T, Favipiravir, an anti-influenza drug against life-threatening RNA virus infections, Pharmacol. Ther 2020, 209,107512.

[4] Guo, Q.; Xu, M.; Guo, S.; Zhu, F. ; Xie, Y.; Shen, J, The complete synthesis of favipiravir from 2-aminopyrazine, Chem. Pap 2019,73, 1043–1051.

[5] Zuliani, V.; Fantini, M.; Nigam, A.; Stables, J. P.; Patel, M. K.; Rivara, M, Anticonvulsant activity of 2,4(1*H*)-diarylimidazoles in mice and rats acute seizure models. Bioorg, Med. Chem. 2010, 18, 7957–7965.

[6] Ettari, R.; Pinto, A.; Micale, Synthesis and anti-HIV activity evaluation of new phenyl ethyl thiourea (PET) derivatives,ARKIVOC 2009, xiv, 227–234.

[7] Reid, C. M.; Ebikeme, C.; Barrett, M. P.; Patzewitz, E.-M.; Müller, S.; Robins, D. J.;Sutherland, A, Synthesis and anti-protozoal activity of C2-substituted polyazamacrocycles, Bioorg. Med. Chem. Lett. 2008, 18, 2455–2458.

[8] H.A. Riley, A.R. Gray. Phenyl glyoxal. Org.synth 1935,15,67.

29TH IRANIAN ORGANIC CHEMISTRY CONFERENCE
1_3 NOV, 2023
UNIVERSITY OF QOM, IRAN

Design and Evaluation of Novel Inhibitors to SARS-CoV-2 Main Protease: An In-silico Approach

Saeid Azimi[*]

Department of Chemistry, Payame Noor University, P. O. BOX 19395-3697, Tehran, Iran, S_azimi@pnu.ac.ir

Keywords: In-Silico approach, SARS-CoV-2-Main protease, Novel inhibitors, ADMET prediction

Abstract - The viral main protease is one of the most attractive targets among all key enzymes involved in the SARS-CoV-2 life cycle [1]. In Silico study and evaluation are applied through virtual screening tools, such as molecular docking simulations and predictions of ADMET-related properties to investigate novel potent inhibitors of SARS-CoV-2 main protease as a target protein. The active site of M^{pro} was studied [2]. The standard inhibitor-target protein interactions were investigated. Using data server's libraries such as *PubChem* similar ligands structures were selected and molecular docking simulation was occurred [3]. Then prediction of ADMET related properties occurred using *ADMETLab 2.0* and prediction results were combined with molecular docking results. Finally, indicated that (1*R*,2*S*,5*S*)-*N*-[(2*S*)-1-amino-3-[(3*S*)-2-oxopyrrolidin-3-yl]propan-2-yl]-3-[(2*S*)-3,3-dimethyl-2-[(2,2,2- trifluoroacetyl)amino]butanoyl]-6,6-dimethyl-3-azabicyclo[3.1.0]hexane-2-carboxamide (Ligand L09) had best results and must be considerate as potent SARS-CoV-2 main protease inhibitor.

1. Introduction

A major viral respiratory disease appeared in Wuhan, Hubei Province, China, in December 2019. The initial cluster of infections known as Coronavirus infected not only animals but also humans. This new corona type virus is known as severe acute respiratory syndrome coronavirus 2 (SARS-CoV-2) since eighty-two percent of similar RNA genome analogous found to the SARS coronavirus (SARS-CoV), and both viruses belong to the Betacoronavirus b gene clade[1]. One of the reasons is that, despite the devastating consequences of SARS for the affected patients, the development of an antiviral drug against this virus would not be commercially viable in view of the fact that the virus has been rapidly contained and did not reappear since 2004[2]. As of January 2023, roughly three years after its initial breakout, COVID-19 continues to pose serious threats to human health and public safety, with more than 762-million confirmed cases and 6.8 million deaths worldwide[3]. SARS-CoV-2 is an enveloped positive-sense single-stranded RNA virus of approximately 30 kb in size, belonging to the genus *Betacoronavirus* of the family Coronaviridae[4, 5]. SARS-CoV-2 M^{pro} represents one of the most attractive therapeutic targets for the development of antiviral therapy for treating COVID-19. Evaluations and studies were performed in order to achieve SARS.CoV-2 M^{pro} inhibitors and some compounds passed clinical phases and acceptable results in inhibition of Mpro. So, design and study as well evaluation of novel potent inhibitors for SARS.CoV-2 M^{pro}, are interesting for researchers and medical chemists. The in-silico approaches in medicinal chemistry are important section in guidelines to the new drugs. This work describes the selection and structure evaluation of some new potent inhibitors using in silico approach.

2. Results and Discussion

2.1. Materials and methods: The three-dimensional structure and crystallographic data of the complex of main protease and *nirmatrelvir* as standard inhibitor were retrieved from Protein Data Bank as Target Molecule and docking receptor (http://www.rcsb.org/pdb; pdb code: 7RFS). The 2D and 3D structure of selected and designed ligands were received from the *PubChem*, as an open chemistry database at the National Institute of Health (NIH)[6]. All SARS-CoV-2 M^{pro} inhibitors were studied and structure of *nirmatrelvir* in complex with main protease enzyme were selected as Macromolecule throughout virtual screening using *PyRx* and *Molegro* platforms[7-9].

2.2. The preparing of target protein: At the first, the pdb format of SARS-CoV-2 M^{pro} was received from protein data bank. The crystal structure of main protease was studied throughout in silico investigation of ligand-target interactions[10-12]. Using *Chimera 1.8.1*, *AutoDock* and *Molegro* all basic preparation processes were performed such as removing non-standard molecules (such as solvent and ion molecules), selection basic protein chain, structure

analysis, finding hydrogen bonds and sequence rechecking (Figure1-a).

2.3. The determination of active site in target molecule: The 3D identification of cavities in target protein was performed using *Molegro virtual Docker* (*MVD*). This process was performed in order to detection of main cavity in active site in target protein. The active site was superimposable with one of the detected cavities using *MVD* software (figure 1-b).

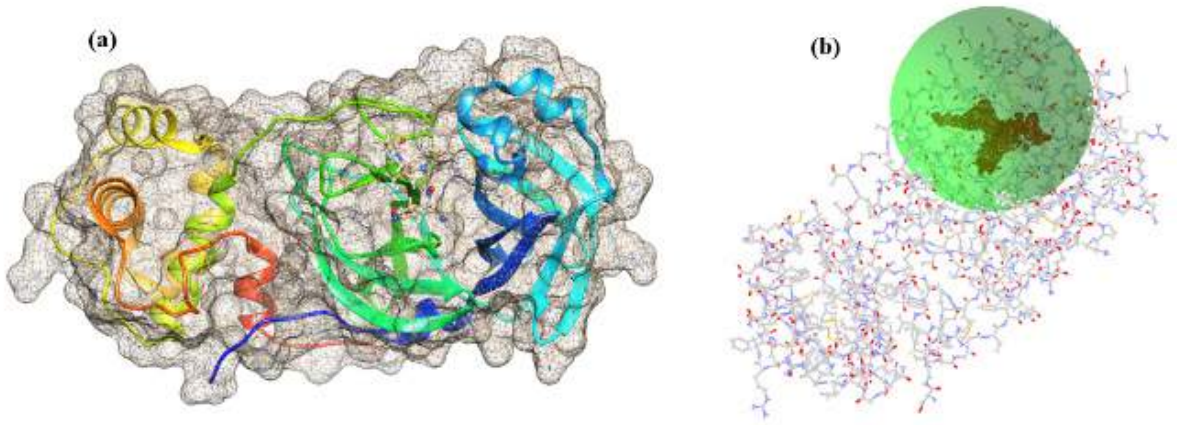

Figure 1. (a) the position of *nirmatrelvir* as standard inhibitor in main protease enzyme as the target molecule. (b). the detection of active site in target protein.

2.4. The preparation of ligands: The selection and investigation of ligands were based on similarity to standard drugs that prescript to inhibition of SARS-CoV-2- M^{pro}. So, the molecular structure of *nirmatrelvir* was studied and the structures of similar ligands were selected from *PubChem* data server using *Tanimoto* scoring on data server[13-17]. The comparisons basis was 90% similarity at the *Tanimoto* threshold. As a result, eleven molecules were identified as similar structures. These eleven molecules (L01-L11) were considered as new ligands and molecular screening was performed using *PyRx* platform. The molecular structure of ligands as well specific code in *PubChem* data server and IUPAC names are summarized in Table1. The structure of *nirmatrelvir* as standard inhibitor ligand showed because of comparisons between structures.

2.4. The molecular docking simulation process: After preparation of target protein and ligands, the docking simulation was performed using *PyRx* as a virtual screening platform for computational drug discovery. All of substance structures were re-checked by *Chem Draw* and *ChemSketch ACD lab*. Then the molecular docking simulation was performed throughout target protein, L1-L11 ligands and *nirmatrelvir* as standard inhibitor. the results and data analysis were obtained. The summary of results was showed in Table 2. The results of molecular docking simulations showed that compounds L09 and L11 have best ranking score and binding affinity rather than other ligands and *nirmatrelvir*. Furthermore, compound L05 has competitive binding affinity rather than *nirmatrelvir* as standard inhibitor.

Table1. The chemical structures, IUPAC names and PubChem codes of selected ligands and *nirmatrelvir*.

Ligand	PubChem CID	IUPAC name	Chemical structures
L01	163421961	(1R,2S,5S)-N-[(2S)-1-amino-1-oxo-3-[(3S)-2-oxopyrrolidin-3-yl]propan-2-yl]-3-[(2S)-3,3-dimethyl-2-[(2,2,2-trifluoroacetyl)amino]butanoyl]-6,6-dimethyl-3-azabicyclo[3.1.0]hexane-2-carboxamide	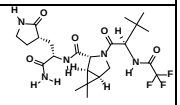
L02	168291677	(1R,2S,5S)-3-[(2S)-3,3-dimethyl-2-[(2,2,2-trifluoroacetyl)amino]butanoyl]-6,6-dimethyl-N-[2-(2-oxopyrrolidin-3-yl)ethyl]-3-azabicyclo[3.1.0]hexane-2-carboxamide	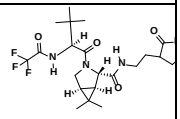
L03	167331639	(1R,2S,5S)-N-[(2S)-1-amino-1-oxo-3-[(3S)-2-oxopyrrolidin-3-yl]propan-2-yl]-3-[(2S)-2-[(2,2-difluoroacetyl)amino]-4-methylpentanoyl]-6,6-dimethyl-3-azabicyclo[3.1.0]hexane-2-carboxamide	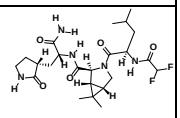

L04	166157215	(1R,2S,5S)-N-[(2S)-1-amino-1-oxo-3-[(3S)-2-oxopyrrolidin-3-yl]propan-2-yl]-3-[(2S)-2-[(2,2-difluoroacetyl)amino]-3,3-dimethylbutanoyl]-6,6-dimethyl-3-azabicyclo[3.1.0]hexane-2-carboxamide	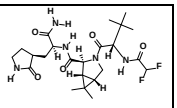
L05	1661572155	(1S,2S,5R)-N-((S)-1-amino-1-oxo-3-((S)-2-oxopyrrolidin-3-yl)propan-2-yl)-3-((2R,3S)-2-amino-3-(trifluoromethyl)pentanoyl)-6,6-dimethyl-3-azabicyclo[3.1.0]hexane-2-carboxamide	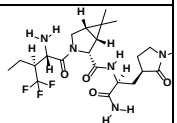
L06	164701757	N-[(2S)-1-amino-1-oxo-3-[(3S)-2-oxopyrrolidin-3-yl]propan-2-yl]-6,6-dimethyl-3-[(2S)-3-methyl-2-[(2,2,2-trifluoroacetyl)amino]butanoyl]-3-azabicyclo[3.1.0]hexane-2-carboxamide	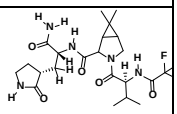
L07	163283387	(1R,2S,5S)-3-[(2S)-2-amino-4,4-difluorobutanoyl]-N-[(2S)-1-amino-1-oxo-3-[(3S)-2-oxopyrrolidin-3-yl]propan-2-yl]-6,6-dimethyl-3-azabicyclo[3.1.0]hexane-2-carboxamide	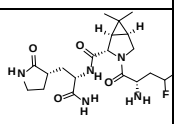
L08	163283371	(1R,2S,5S)-N-[(2S)-1-amino-1-oxo-3-[(3S)-2-oxopyrrolidin-3-yl]propan-2-yl]-3-[2-amino-3-(trifluoromethyl)pentanoyl]-6,6-dimethyl-3-azabicyclo[3.1.0]hexane-2-carboxamide	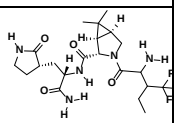
L09	157010397	(1R,2S,5S)-N-[(2S)-1-amino-3-[(3S)-2-oxopyrrolidin-3-yl]propan-2-yl]-3-[(2S)-3,3-dimethyl-2-[(2,2,2-trifluoroacetyl)amino]butanoyl]-6,6-dimethyl-3-azabicyclo[3.1.0]hexane-2-carboxamide	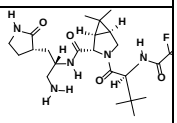
L10	168010016	N-[1-amino-1-oxo-3-(2-oxopyrrolidin-3-yl)propan-2-yl]-3-[3,3-dimethyl-2-[(2,2,2-trifluoroacetyl)amino]butanoyl]-6,6-dimethyl-3-azabicyclo[3.1.0]hexane-2-carboxamide	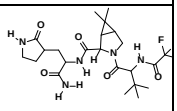
L11	162677687	(1R,2S,5S)-3-[(2S)-2-(tert-butylcarbamoylamino)-3,3-dimethylbutanoyl]-N-[(2S)-1-imino-3-[(3S)-2-oxopyrrolidin-3-yl]propan-2-yl]-6,6-dimethyl-3-azabicyclo[3.1.0]hexane-2-carboxamide	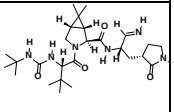
Nirmatrelvir	156621364	(1R,2S,5S)-3-[(2S)-3,3-dimethyl-2-[(2,2,2-trifluoroacetyl)amino]butanoyl]-N-[(2S)-1-imino-3-[(3S)-2-oxopyrrolidin-3-yl]propan-2-yl]-6,6-dimethyl-3-azabicyclo[3.1.0]hexane-2-carboxamide	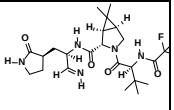

3. Conclusions

In conclusion, the *in-silico* study was performed to investigate and evaluate novel potent inhibitors for SARS-CoV-2 M^{pro}. The crystallographic structure of main protease and active site pockets were studied using Chimera 1.8.1 and MVD. Then preparation of the structure of target protein was performed. Some of the reported ligands were studied and one of them was selected as standard inhibitor. Using data servers' libraries as PubChem, some similar compounds selected and simulation molecular docking has occurred. The results were evaluated and high quantities in binding affinities were selected as candidate ligands. Finally, indicated that (1R,2S,5S)-N-[(2S)-1-amino-3-[(3S)-2-oxopyrrolidin-3-yl]propan-2-yl]-3-[(2S)-3,3-dimethyl-2-[(2,2,2-trifluoroacetyl)amino]butanoyl]-6,6-dimethyl-3-azabicyclo[3.1.0]hexane-2-carboxamide (L09 table1) and (1R,2S,5S)-3-[(2S)-2-(tert-butylcarbamoylamino)-3,3-dimethylbutanoyl]-N-[(2S)-1-imino-3-[(3S)-2-oxopyrrolidin-3-yl]propan-2-yl]-6,6-dimethyl-3-azabicyclo[3.1.0]hexane-2-carboxamide (L11 table1) has best results and must be considerate as novel potent SARS-CoV-2 main protease inhibitors.

Table2.The ligands, binding affinity resulted throughout Molecular Docking simulation.

Entry	Ligand (poses)	Ranking Score (Binding Affinity)	RMSD (Upper bound/ Lower bound)
1	**L09**	**-135.158**	0/0
2	**L11**	**-135.09**	0/0
3	**Nirmatrelvir**	**-127.498**	0/0
4	L05	-124.353	0/0
5	Nirmatrelvir	-121.371	0/0
6	L07	-119.83	0/0
7	L03	-119.673	0/0
8	L06	-119.211	0/0
9	L05	-117.749	0/0
10	L07	-117.731	0/0
11	L07	-116.999	0/0

4. References

[1] A.A. Mamun, F. Akter, M. Khan, S.S. Ahmed, M.G. Uddin, N.T. Tasfia, F.M. Efaz, M.A. Ali, M.U.C. Sultana, M.A. Halim, Identification of potent inhibitors against transmembrane serine protease 2 for developing therapeutics against SARS-CoV-2, J Biomol Struct Dyn, (2021) 1-13.

[2] L. Zhang, D. Lin, Y. Kusov, Y. Nian, Q. Ma, J. Wang, A. von Brunn, P. Leyssen, K. Lanko, J. Neyts, A. de Wilde, E.J. Snijder, H. Liu, R. Hilgenfeld, alpha-Ketoamides as Broad-Spectrum Inhibitors of Coronavirus and Enterovirus Replication: Structure-Based Design, Synthesis, and Activity Assessment, J Med Chem, (2020).

[3] C. Ngo, W. Fried, S. Aliyari, J. Feng, C. Qin, S. Zhang, H. Yang, J. Shanaa, P. Feng, G. Cheng, X.S. Chen, C. Zhang, Alkyne as a Latent Warhead to Covalently Target SARS-CoV-2 Main Protease, Journal of Medicinal Chemistry, 66 (2023) 12237-12248.
[4] C. Pozzi, A. Vanet, V. Francesconi, L. Tagliazucchi, G. Tassone, A. Venturelli, F. Spyrakis, M. Mazzorana, M.P. Costi, M. Tonelli, Antitarget, Anti-SARS-CoV-2 Leads, Drugs, and the Drug Discovery–Genetics Alliance Perspective, Journal of Medicinal Chemistry, 66 (2023) 3664-3702.
[5] C. Wang, L. Zhao, S. Xia, T. Zhang, R. Cao, G. Liang, Y. Li, G. Meng, W. Wang, W. Shi, W. Zhong, S. Jiang, K. Liu, De Novo Design of alpha-Helical Lipopeptides Targeting Viral Fusion Proteins: A Promising Strategy for Relatively Broad-Spectrum Antiviral Drug Discovery, J Med Chem, 61 (2018) 8734-8745.
[6] S. Kim, J. Chen, T. Cheng, A. Gindulyte, J. He, S. He, Q. Li, B.A. Shoemaker, P.A. Thiessen, B. Yu, L. Zaslavsky, J. Zhang, E.E. Bolton, PubChem in 2021: new data content and improved web interfaces, Nucleic Acids Research, 49 (2021) D1388-D1395.
[7] S. Dallakyan, A.J. Olson, Small-molecule library screening by docking with PyRx, Chemical biology, Springer2015, pp. 243-250.
[8] S. Mahdian, M. Zarrabi, A. Moini, M. Shahhoseini, M. Movahedi, In silico evidence for prednisone and progesterone efficacy in recurrent implantation failure treatment, Journal of Molecular Modeling, 28 (2022) 105.
[9] G. Bitencourt-Ferreira, W.F. de Azevedo, Molegro Virtual Docker for Docking, in: W.F. de Azevedo Jr (Ed.) Docking Screens for Drug Discovery, Springer New York, New York, NY, 2019, pp. 149-167.
[10] E.F. Pettersen, T.D. Goddard, C.C. Huang, G.S. Couch, D.M. Greenblatt, E.C. Meng, T.E. Ferrin, UCSF Chimera--a visualization system for exploratory research and analysis, J Comput Chem, 25 (2004) 1605-1612.
[11] S. Azimi, L. Heydari, Design and Evaluation of New Potent G-Protein Coupled Receptor Kinase Inhibitors Using Virtual Screening Methods, Nashrieh Shimi va Mohandesi Shimi Iran, (2023) -.
[12] X. Lian, Z. Xia, X. Li, P. Karpov, H. Jin, I.V. Tetko, J. Xia, S. Wu, Anti-MRSA drug discovery by ligand-based virtual screening and biological evaluation, Bioorganic Chemistry, 114 (2021) 105042.
[13] P. Baldi, R. Nasr, When is Chemical Similarity Significant? The Statistical Distribution of Chemical Similarity Scores and Its Extreme Values, Journal of Chemical Information and Modeling, 50 (2010) 1205-1222.
[14] S. Azimi, B. Mohammadi, S. Babadoust, E. Vessally, In Silico study and design of some new potent threonine tyrosine kinase inhibitors using molecular docking simulation, Molecular Simulation, (2023) 1-8.
[15] K.M. Elokely, R.J. Doerksen, Docking Challenge: Protein Sampling and Molecular Docking Performance, Journal of Chemical Information and Modeling, 53 (2013) 1934-1945.
[16] E. Glaab, Building a virtual ligand screening pipeline using free software: a survey, Brief Bioinform, 17 (2016) 352-366.
[17] G.M. Morris, R. Huey, W. Lindstrom, M.F. Sanner, R.K. Belew, D.S. Goodsell, A.J. Olson, AutoDock4 and AutoDockTools4: Automated docking with selective receptor flexibility, Journal of Computational Chemistry, 30 (2009) 2785-2791.

One-pot, simple, clean and highly efficient green protocol have been developed for regioselective synthesis of linear naphtho[2,3-b]-furan-4,9-diones derivatives using citric acid as a biodegradable catalyst in aqueous-ethanol media

*Mostafa Amiri**

Department of Chemistry, Facualty of Science, Sayyed Jamaleddin Asadabadi University, Asadabad, Iran, m.amiri6694@gmail.com

Abstract Citric acid has been used as a green and efficient catalyst for one-pot, multi-component synthesis of linear naphtho[2,3-b]-furan-4,9-dione derivatives by condensation of 2-hydroxy-1,4-naphthoquinone with cyclohexyle isocyanides and variety of aldehydes at ambient temperature under aqueous-ethanol media. This method has several advantages including use of a nonhazardous and inexpensive catalyst, easy work-up, clean reaction conditions, and high yields.

1. Introduction

In recent years, the search for more environmentally friendly processes constitutes one central theme of research and development in both academic and industrial chemistry. Development of non-hazardous synthetic methodologies for organic synthesis is one of the latest challenges to organic chemists. The growing concern for the environment demands the development of eco-friendly and economic processes wherein even less hazardous byproducts are not desirable. The importance of these heterocyclic compounds is highlighted by the huge number of publications on the total synthesis of natural oxygen derivatives and of other communications dedicated to synthetic derivatives [1]. The chemistry of quinone annulated heterocycles is largely dependent on the substituents being either on the quinonic or on adjacent ring [2]. Among various classes of heterocyclic quinones, naphthofuroquinones have attracted wide-spread interest in view of their presence in natural products, and for their pharmacological activities [3-6]. A great number of naphthofuroquinones are natural products exhibiting a broad spectrum of biological activity. For example, some naphthofuroquinone derivatives as represented by avicequinones [2,7], and maturinones [7] have shown a diversity of biological activities of medical importance, such as anticancer, antibacterial, and anti-inflammatory activities [8]. Also, many synthetic naphthofuroquinones and their phytochemical analogs isolated from the inner bark of Tecoma ipe Mart show antitumor activity [9]. In addition, the chloroform extract of Tabebuia ochracea ssp. neochrysanta that contained six naphthofuroquinone derivatives has shown cytotoxicity against melanoma B16 cells, and antimalarial activity in vitro against strains of Plasmodium berghei [10]. Furthermore, because of their potent activity against the growth of human keratinocytes, some naphthofuroquinone compounds, in particular: naphtho[2,3-b]furan-4,9-diones, appear to be promising as effective antipsoriatic agents [11]. Finally, very recently, naphthofuroquinone were evaluated for inhibitory activities against receptor tyrosine kinases [12]. The diversity of their natural origins and biological activities have motivated efforts toward their syntheses or to find pathways to structural analogs [13-15].

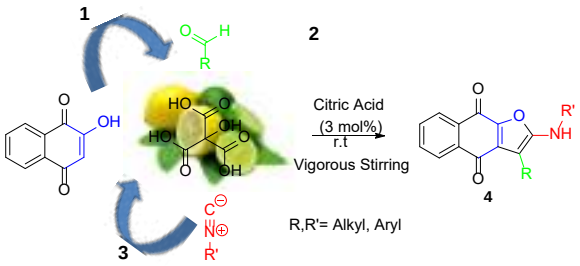

Scheme 1.

2. Results and Discussion

Synthesis of hetrocyclic compounds is one of the most important research topics and has attracted most of the researchers. The use of green catalysts in chemical synthesis can reduce the damage to the environment occurred by the use of hazardous chemicals. Citric acid has been used as a green and efficient catalyst for one-pot, multi-component synthesis of linear naphtho[2,3-b]-furan-4,9-dione derivatives by condensation of 2-hydroxy-1,4-naphthoquinone with cyclohexyle isocyanides and variety of aldehydes at ambient temperature under aqueous-ethanol media. This method has several advantages including use of a nonhazardous and inexpensive catalyst, easy work-up, clean reaction conditions, and high yields.

Herein, we report the use of citric acid as a green and efficient catalyst for one-pot, multi-component synthesis of linear naphtho[2,3-b]-furan-4,9-dione derivatives by condensation of 2-hydroxy-1,4-naphthoquinone with cyclohexyle isocyanides and variety of aldehydes at ambient temperature under aqueous- ethanol media. Initially, we carried out the reaction of 2-hydroxy-1,4-naphthoquinone with benzaldehyde in the presence of 3 mol% of citric acid in H_2O/EtOH (3:2), at room temperature. After 45 min the reaction was completed with good yield (85%). The applicability of the present methodology is further extended by performing the reaction in an aqueous-ethanol media, to our surprise, the reaction was performed well in water and the reaction rates as well as the yields of products are satisfactory. We also investigated the effect of others solvents on this reaction. Citric acid is highly soluble in water and can be easily remove from the reaction mixture by simple filtration. In the case of water as solvent, after evaporation of water, the catalyst was obtained and could be reused in another reaction. However, this process is green, environmental friendly, clean, can perform easily at room temperature and no undesirable side reactions were observed.

Following our recent works [16-18] on the application of isocyanide-based multicomponent reactions in heterocyclic synthesis, in this work, we have introduced the best methodology for synthesis of various substituted naphtho[2,3-b]-furan-4,9-dione skeleton via a three-component condensation reaction of isocyanides with the formation of three bonds by a [3+1+1] furannulation strategy. 2-Hydroxy-1,4-naphthoquinone **1** and various aldehydes **2,** alkyl and aryl isocyanides **3**, in the presence of 3 mol% of citric acid in EtOH undergo an additional reaction at room temperature with vigorous stirring to produce the linear naphtho[2,3-b]-furan-4,9-dione derivatives **4** in good to exellent yields. The reaction can be represented as in Table 1.

Table 1. Synthesis of linear naphtho[2,3-b]-furan-4,9-dione derivatives.

En.	Aldehyde	Isocyanide	Time (min)	Product	Yil. (%)
1		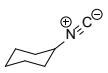	45	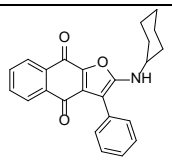	85
2	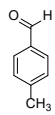	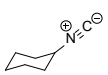	35	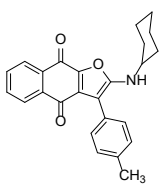	95

Table 1. (*continued*)

En.	Aldehyde	Isocyanide	Time (min)	Product	Yil. (%)
3	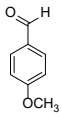	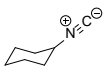	35	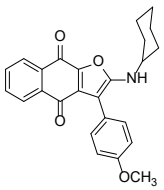	92
4	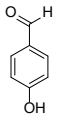	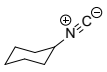	40	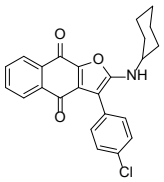	93
5	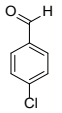	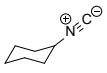	25	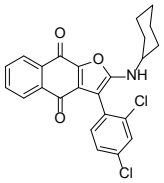	88
6	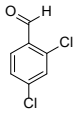	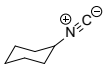	45	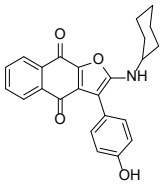	90
7	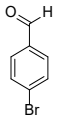	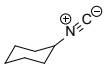	60	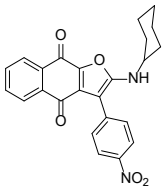	78
8	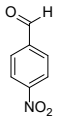	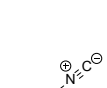	50	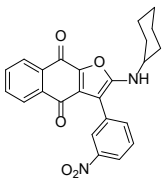	75
9	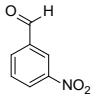	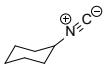	35	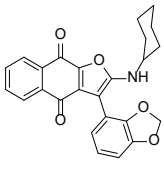	65

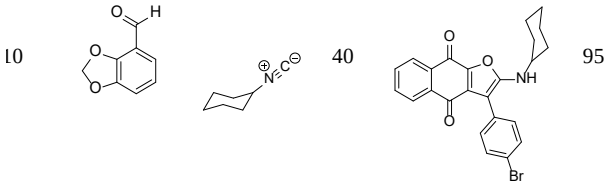

In a model condensation reaction, 2-Hydroxy-1,4-naphthoquinone with a benzaldehyde and cyclohexylisocyanide were stirred at room temperature in the presence of catalytic amount of citric acid anhydrous (10 mol%) in aqueous-ethanol conditions (Scheme 1). To our surprise, the reaction was completed in less than 60 min (TLC). In order to evaluate the optimum concentration of citric acid required for this condensation, the reaction was carried out under varying concentrations of citric acid viz. 1, 3, 5 and 12 mol%, in which we found that 3 mol% citric acid provides the most favorable conditions for the reaction shown in scheme 1. The one-pot three-component condensation reactions of 2-hydroxy-1,4-naphthoquinone **1** with various aldehydes **2** in the presence of alkyl and aryl isocyanides **3** proceeded rapidly in room temperature and were complete after 60 min to afford 2-(alkylamino)-3-alkyl or arylnaphtho[2,3-b]furan-4,9-diones **4** in exellent yields. 1H and 13C NMR spectra of the crude products clearly indicated the formation of fused naphthofuroquinone **4**. All the products were characterized by FTIR, 1H and 13C-NMR spectra. These results promoted us to investigate the scope and the generality of this new protocol for various aldehydes with cyclohexylisocyanide under optimized conditions. As shown in Table 1, a series of aldehydes underwent electrophilic substitution reaction with 2-hydroxy-1,4-naphthoquinone to afford a wide range of substituted naphtho[2,3-b]-furan-4,9-dione derivatives in good to excellent yields. The electron deficiency and nature of the substituents on the aromatic ring effect the conversion rate; aromatic aldehydes having electron-withdrawing groups on the aromatic ring (Table 1, entries 8, 9) react faster than electron-donating groups (Table 1, entries 1-7, 8).

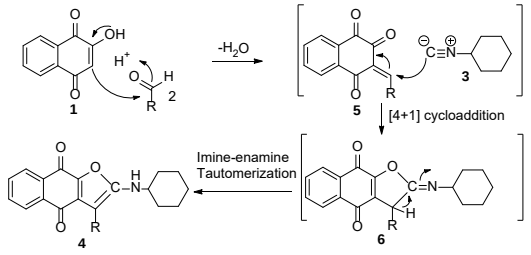

Scheme 2.

Although we have not established the mechanism of the reaction between 2-hydroxy-1,4-naphthoquinone and aldehydes in the presence of isocyanides experimentally, the synthesis of linear naphtho[2,3-b]-furan-4,9-dione derivatives **4** can be rationalized by initial formation of a conjugated electron-deficient enone **5** by a Knoevenagel condensation of the cyclic 2-hydroxy-1,4-naphthoquinone **1** and the aldehyde **2**. The next step of this mechanism could involve a [4+1] cycloaddition reaction of the electron-deficient heterodiene moiety of adduct **5** with the isocyanide to afford an iminolactone intermediate **6**. The subsequent isomerization of iminolactone **6** leads to formation of product **4** (Scheme 2).

3. Experimental

To a magnetically stirred solution of 2-hydroxy-1,4-naphthoquinone (0.174 g, 1.0 mmol), benzaldehyde (0.106 g. 1.0 mmol), cyclohexyl isocyanide (0.110 g, 1.0 mmol), in 25 mL H_2O/C_2H_5OH, 3 mol % Citric acid as catalyst was added quickly. The above reaction mixture was stirred vigorously at room temperature until the completion (by TLC). After usual workup, the crude product was purified by simple filtration then the solvent was removed under reduced pressure, the residue was washed with CH_2Cl_2 (10 mL) and recrystallized from diethyl ether/n-hexane (1:3) to give blue needles (0.315 g). 85%) ; mp 247 °C; FTIR (KBr) (max. cm^{-1}): 3220 (N-H), 1650 (C=O), 1610 (C=C).

In conclusion we have achieved an efficient process for the synthesis of biologically interesting functionalized linear naphtho[2,3-b]-furan-4,9-dione derivatives starting from readily available reagents. The reaction is very simple from the experimental point of view and allows the creation of a fused naphthofuroquinone ring with concomitant formation of two new C-C bonds and one C-O bond in a single operation.

References

[1] Clementina, M.M. Santos.; Artur, M.S. Silva. Progress in Heterocyclic Chemistry, 2020, 31, 533-595.

[2] (a)Spyroudis, S. Molecules 2000, 5, 1291–1330. (b)Tisler, M. Advances in Heterocyclic Chemistry; Katritzky, A. R., Ed.; Heterocyclic Quinones; Academic: London, 1989; Vol. 45, p 37.

[3] Jimei, Li.; Zhang, Jie.; Mingfei, Li.; Zhang, C.; Yuan, Y.; Renhua, Liu. Chem. Commun., 2019, 55, 2348-2351.

[4] Kobayashi, K.;Tanaka, K.; Uneda, T.; Maeda, K.; Morikawa, O.; Konishi, H. Synthesis 1998; 1998(9): 1243-1245.

[5] Shaabani, A.; Maleki, A.; Rezayan, A. H.; Sarvary, A. Molecular Diversity. 2011, 15, 41–68.

[6] Teimouri, M. B.; Khavasi, H.R. Tetrahedron, 2007, 63, 10269-10275.

[7] Ito, C.; Katsuno, S.; Kondo, Y.; Tan, H. T.-W.; Furukawa, H. Chem. Pharm. Bull. 2000, 48, 339–343.

[8] Romo, J.; Joseph-Nathan, P. Tetrahedron 1964, 20, 2331-2337.

[9] Thomson, R. H. Naturally Occurring Quinones III: Recent Advances; Chapman and Hall: London, New York, NY, 1987.

[10] Rao, M. M.; Kingston, D. G. J. Nat. Prod. 1982, 45, 600–604.

[11] Diaz, F.; Medina, J. D. J. Nat. Prod. 1996, 59, 423–424.

[12] Muller, K.; Sellmer, A.; Wiegrebe, W. J. Nat. Prod. 1999, 62, 1134–1136.

[13] Lee, K.-I.; Park, Y.; Park, S.-J.; Hwang, J.-H.; Lee, S.-J.; Kim, G.-D.; Park, W.-K.; Lee, S.; Jeong, D.; Kong, J.-Y.; Kangd, H.-K.; Choc, H. Bioorg. Med. Chem. Lett. 2006, 16, 737–742.
[14] Hooker, S. C. J. Am. Chem. Soc. 1936, 58, 1168–1173.
[15] Kobayashi, K.; Tanaka, K.; Uneda, T.; Maeda, K.; Morikawa, O.; Konishi, H. Synthesis 1998, 1243–1245.
[16] GhorbaniVaghei, R.;. Amiri, M.; Veisi, H. Letters in Organic Chemistry. 2013, 10, 37 – 41.
[17] GhorbaniVaghei, R.;. Amiri, M.; Karimi-Nami, R.; Salimi, Z. RSC Adv., 2013, 3, 25924-25929.
[18] GhorbaniVaghei, R.; Amiri, M.; Karimi-Nami.; Zahra Toghraei-Semiromi, Z.; Ghavidel, M. Mol Divers. 2013, 17, 251–259.

29TH IRANIAN ORGANIC CHEMISTRY CONFERENCE
1_3 NOV, 2023
UNIVERSITY OF QOM, IRAN

Green synthesis Evaluation of silver nanoparticles using Quince (*Cydonia oblonga*) leaf

Nafiseh Annabestani [a], *Nasrin Mollania* [b*]

[a] *Department of Biology, Hakim Sabzevari University, Sabzevar, Iran, Nafise.annabestani@gmail.com*
[b] *Department of Biology, Hakim Sabzevari University, Sabzevar, Iran, n.mollania@hsu.ac.ir*

Abstract
Physical and chemical methods of nanoparticle synthesis have limitations such as poor structure, low production rate, and high cost. The biosynthetic pathway using plant extract was a safe and environmentally friendly method for nanoparticle synthesis using plants and microorganisms for bio-medical applications.
In the process of nanoparticle production for drug delivery, it is essential to control their size and surface properties to achieve the desired release of active pharmaceutical agents. This is important to ensure that the drug functions effectively at the intended location, with the appropriate dosage and timing.
In this research, the shape and size of silver nanoparticles synthesized by leaf extract of *Cydonia oblonga* were investigated. The produced AgNPs had spherical shape and morphology, uniform dispersion and size of 52 nm.

Keywords: Leaf extract of *Cydonia oblonga*, Green synthesis, Silver nanoparticles

1. Introduction

Nanotechnology is the most famous study of material science, and the production of nanoparticles is rapidly increasing all over the world [1].
In the last two decades, because of its applications in various areas of biomedicine, industry, and engineering, nanotechnology has made wide progress to become one of the most intensive research areas.
Nanoparticles and nanomaterials derived from them are widely used in various parts such as food, agriculture, cosmetics, medicine and etc [2-4].
The cooperation between nanotechnology and biology has opened new horizons of nanobiotechnology, combining the use of biological materials in a number of biochemical and physiological processes. This approach has considerably increased the production of nanoparticles without the use of difficult and toxic conditions and chemicals [5, 6].
AgNPs were widely used in the medical field due to their antimicrobial and anticancer effects. furthermore, these nanoparticles can be used in biosensors, drug delivery systems, and medical devices [3].
Some parts of plants, such as leaves, fruits, roots, stalks, and seeds, have been used for the synthesis of various nanoparticles because of the various metabolite content. The chemical compounds in the extract of plants such as terpenoids and polyphenols are responsible for the bio-reduction of metal ions [7, 8].
Cydonia oblonga Mille is a tree of the *Rosaceae* family and contains important medicinal metabolites such as phenolics, flavonoids, carotenoids, organic acids, terpenoids, tannins and other volatile compounds. The phenolic content in the leaf extract of *Cydonia oblonga Mille* tree is more than other parts. Due to the high phenolic content of leaves, more antioxidant activity is expected from the leaves compared to the fruit and seeds [9, 10].

2. Methods

2.1. Plant Extraction:

The additional parts of the tree leaves are removed and the rest is powdered. It is mixed with a ratio of 1:15 plants and solvent (deionized water). It is placed on the heater for 1 hour at a 70 °C to obtain the brewed extract. Then the resulting extract is dried at room temperature.

2.2. AgNPs Biosynthesis:

For nanoparticle synthesis, the powdered plant extract (0.5 g) dissolved in 10 ml of deionized water and pH adjusted to 10.
After that, the AgNO3 was mixed with the extract in such a way that the final sample contained 1.5 mM salt. The reaction mixture was then placed in a shaker incubator at 180 RPM for 24 hours at 50°C. After that, the resulting solution was placed in a centrifuge for 15 minutes at 12,000 RPM, and the brownish sediment was separated.
One of the important goals in investigating nanoparticles is to produce them with appropriate size and shape. Therefore, the characteristics of produced nanoparticles were investigated with different analytical methods such as UV-VIS, DLS, and SEM.

3. Results and Discussion

3.1. Ultraviolet–visible spectroscopy:

According to the articles and sources, the existence of the index peak in the range of 400-450 nm is related to AgNPs. The index peak and the highest absorption rate for silver nanoparticles in optimal synthesis conditions were obtained at 408 nm (Fig. 1). Several repetitions were done to ensure the synthesis of nanoparticles.

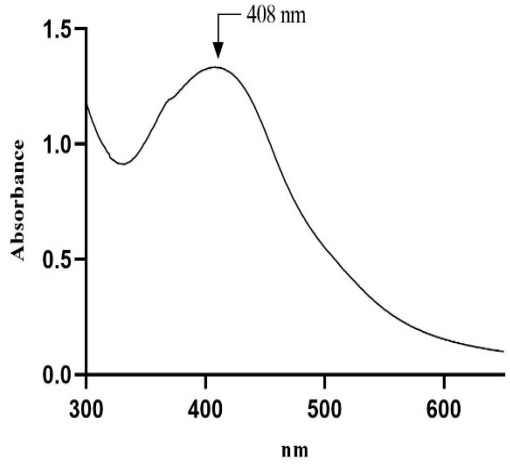

Fig.1: UV–Vis absorption spectra of the synthesized in 1.5 mM silver solution

3.2. Dynamic light scattering (DLS):

Neutron, light, or electron scattering from materials is one of the main techniques for measuring nanoparticle size. DLS is a physical method to determine the distribution of particles in solutions. The average size of produced AgNPs in this protocol was about 52.9 nm (Fig. 2).

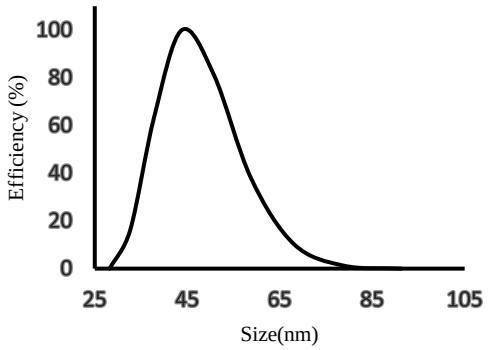

Fig. 2: DLS analysis of the produced silver nanoparticles

3.3. Scanning Electron Microscopy (SEM) with Energy Dispersive X-Ray Analysis (EDX):

Scanning electron microscopy is a powerful technique for imaging the surface of matter with a resolution of less than about 1 nm [11]. The shape, size, morphology, and distribution of the synthesized nanoparticles are determined using SEM. AgNPs are spherical and have a uniform and appropriate size distribution

EDX analysis examines the purity and analytical spectrum of the elements in the sample. The presence of elements of sulfur, carbon, sodium and metals such as gold, etc. can indicate the presence of proteins and peptides along with nanoparticles or due to the materials used in sample stabilization techniques during analysis (Fig. 3).

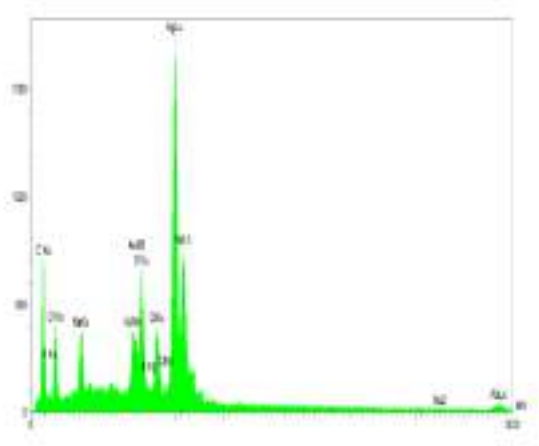

Fig. 3: EDX analysis of the produced nanoparticles

3. Conclusions

The plant leaf extract, with its dual role as a reducing and stabilizing agent, is useful to facilitate the synthesis of nanoparticles. produced Metal nanoparticles have suitable functional groups that allow them to bind with ligands, antibodies, and drugs [2].

One of the challenges of nanoparticle biosynthesis is controlling the size, dispersion and morphology of produced nanoparticles. These problems must be overcome before nanoparticles can be clinically or commercially available; This was one of the goals of this research. The produced AgNPs had spherical shape and morphology, uniform dispersion and appropriate size. These nanoparticles synthesized by plant extracts of Quince (Cydonia oblonga) leaf can be the basis of future research.

4. References

1. Alabdallah, N.M. and M.M. Hasan, Plant-based green synthesis of silver nanoparticles and its effective role in abiotic stress tolerance in crop plants. Saudi Journal of

Biological Sciences, 2021. **28**(10): p. 5631-5639.
2. Chandrakala, V., V. Aruna, and G. Angajala, Review on metal nanoparticles as nanocarriers: Current challenges and perspectives in drug delivery systems. Emergent Materials, 2022: p. 1-23.
3. Dikshit, P.K., et al., Green synthesis of metallic nanoparticles: Applications and limitations. Catalysts, 2021. **11**(8): p. 902.
4. Saleh, T.A., Nanomaterials: Classification, properties, and environmental toxicities. Environmental Technology & Innovation, 2020. **20**: p. 101067.
5. Kamran, U., et al., Green synthesis of metal nanoparticles and their applications in different fields: a revie*w.* Zeitschrift für Physikalische Chemie, 2019. **233**(9): p. 1325-1349.
6. Choudhury, H., et al., Silver nanoparticles: Advanced and promising technology in diabetic wound therapy. Materials Science and Engineering: C, 2020. **112**: p. 110925.
7. Jadoun, S., et al., Green synthesis of nanoparticles using plant extracts*: A review.* Environmental Chemistry Letters, 2021. **19**: p. 355-374.
8. Malik, P., et al., Green chemistry based benign routes for nanoparticle synthesis. Journal of Nanoparticles, 2014. **2014**.
9. Semnani, S.N., N. Hajizadeh, and H. Alizadeh, Antibacterial effects of aqueous and organic quince leaf extracts on gram–positive and gram–negative bacteria. Banat's Journal of Biotechnology, 2017. **8**(16): p. 54-61.
10. Khoubnasabjafari, M. and A. Jouyban, *A* review of phytochemistry and bioactivity of quince (Cydonia oblonga Mill.). Journal of Medicinal Plants Research, 2011. **5**(16): p. 3577-3594.
11. Ijaz, I., et al., Detail review on chemical, physical and green synthesis, classification, characterizations and applications of nanoparticles. Green Chemistry Letters and Reviews, 2020. **13**(3): p. 223-245.

Extraction and measurement of ofloxacin drug in biological samples using electromembrane extraction based on agarose-polyacrylamide-catira gum combined gel

Fatemeh Hamdi*, Ali Zraatkarmoghaddam

Department of Chemistry, Faculty of Science, University of Birjand University, Birjand, Iran, ftmehamdi@gmail.com, a_zeraatkar_m@yahoo.com

Abstract - In this project, for the first time, the extraction and measurement of the drug ofloxacin using the electromembrane extraction method (G-EME), which is a simple method without the use of organic solvents [1], using a combined membrane of agarose-polyacrylamide-Katira gum, green membrane and bio Degradable done. Important chemical parameters were optimized by central composite design (CCD) and response surface method (RSM). The optimal conditions for the drug Ofloxacin are: The concentration of ofloxacin drug is 0.5 mg/liter with a total membrane percentage composition (weight/volume) of 4% and the percentage composition of the membrane components of agarose-polyacrylamide-catira gum respectively (2-1-1) which is as The optimal conditions for the membrane were determined. Under the proposed method, the concentration limit (ppm 0.1-2) of ofloxacin was linear and the values of LOD and LOQ were calculated as 0.023 ppm and 0.076 ppm. Short extraction time, very small amount of sample consumption, fast method and low cost are among the advantages of this method and it is important for the measurement of ofloxacin drug in biological samples.

1. Introduction

Antibiotics include a wide range of powerful drugs, ofloxacin is one of the types of antibiotics. Compared to other available fluoroquinolones, ofloxacin is well tolerated so that there is less chance of clinically relevant drug interactions. Ofloxacin therefore provides a valuable oral therapy for use in a wide range of clinical infections. Its special advantage in severe and chronic infections when broad-spectrum agents are needed saves money and also allows outpatient treatment. Considering that the direct measurement of this drug in biological fluids due to the presence of complex matrices, the use of sample preparation methods before identification and measurement is necessary and unavoidable. Liquid-liquid extraction (LLE) and solid-phase extraction (SPE) methods have often been the methods of choice, but these methods are ineffective due to the use of organic solvents that produce toxic and hazardous wastes.[1, 2] Microextraction methods were considered. Among the types of microextraction methods, electromembrane extraction has received much attention due to its versatility, high efficiency and low solvent consumption. EME is a new approach of HF-LPME in which an electric field is created as a driver of charged analytes across the SLM to accelerate the mass transfer of analytes. The common material used in SLM is propylene HF hollow fiber. Since HF-LPME is difficult to decompose and harmful to the environment, therefore, biological membranes were used [3]. Agarose is a well-known biopolymer with good biodegradable properties. Agarose is a polysaccharide produced from red algae [4]. Structurally, it consists of alternating units of D-galactose and 3,6-anhydro-L-galactopyranose, which form a linear polymer. Polyacrylamide, also called PAM for short, is one of the most widely used types of water-soluble polymers that have a large number of free amide groups in its molecular structure. Amide group has high chemical activity and can form a series of derivatives with different types of compounds. Gum is a kind of substance that is obtained from the sap of trees and has various uses. Katira gum is a viscous, odorless, tasteless and water-soluble mixture of polysaccharides. Mixing some additives during the gel making process creates interesting hybrid materials that improve membrane properties[5]. It reduces the amount of EEO and provides a better extraction process and higher recovery factors. In this project, agarose-polyacrylamide-catira gum composite membrane has been used as a biological and environmentally friendly membrane. This method was evaluated in terms of its ability to extract basic drugs from blood serum and urine samples at different concentration levels.

2. Results and discussion

In order to achieve the highest efficiency for the extraction and measurement of small amounts of ofloxacin drug, the parameters affecting the EME process, including the concentration and ratio of the compounds forming the membrane, the applied voltage, the extraction time, and the pH of the donor and acceptor phases were optimized. Also, the effect of acetic acid concentration on membrane mass transfer efficiency was evaluated.

2.1. Optimizing the percentage of the total set of gel membrane compounds: In order to investigate the effective parameters on the performance of the gel membrane, first the percentage values of the total components of the gel membrane were changed and this was done in the condition that the ratio of the mixed components of agarose (AG), polyacrylamide (PA), and turpentine gum (TG) to prepare the membrane They were fixed The effect of the composition of the total percentage of the combined membrane of agarose, polyacrylamide and catira gum was investigated in the range of 2-6% by weight-volume. For this purpose, 6 gel membranes with fixed ratios of agarose/polyacrylamide/rubber and with different total percentages were prepared and the EME process was performed. The value of 4% was determined as the total percentage of the membrane. (Fig.1)

2.2. Optimizing the ratio of gel membrane forming compounds: In the continuation of investigating the parameters affecting the performance of the gel membrane, different proportions of agarose (AG), polyacrylamide (PA), and castor gum (TG) were investigated to prepare the membrane, so that the total amount of components used in the membrane was 4% by weight. - Do not exceed the volume. For this purpose, 12 gel membranes with different ratios of components were prepared and the EME process was carried out by them. Finally, the percentage ratio (2-1-1) was chosen as the optimal value. (Fig..2)

2.3. The effect of increasing acetic acid: Next, the effect of acetic acid during the preparation of the membrane based on agarose-poly-acrylamide-kathira gum on the extraction efficiency was investigated in the range of zero to 0.2% volume-volume. The value of 0.01 volume-volume percentage was chosen as the optimal value.(Fig.3)

Table.1 Analytical performance of dual G-EME for determination of ophloxacin

Sample	LOQ (ppm)	LOD (ppm)	Linearity (ppm)	Recovery%	RSD %
ophloxacin	0.076	0.023	0.1-2	95.54%	6.9

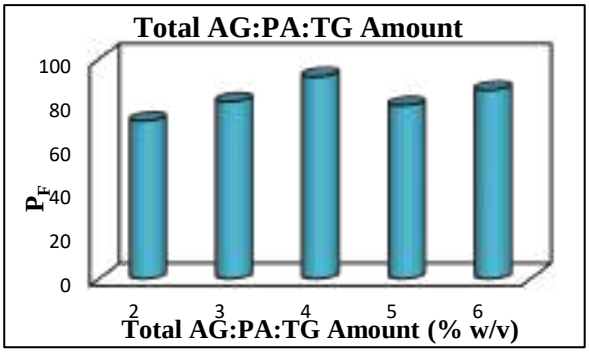

Fig.1 The effects of Optimizing the overall percentage of the gel membrane

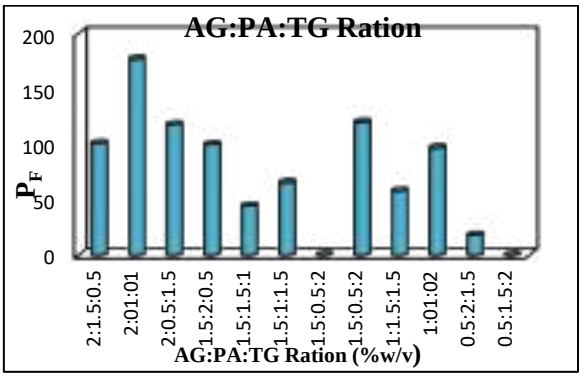

Fig..2 Optimizing the ratio of ingredients that make up the gel membrane

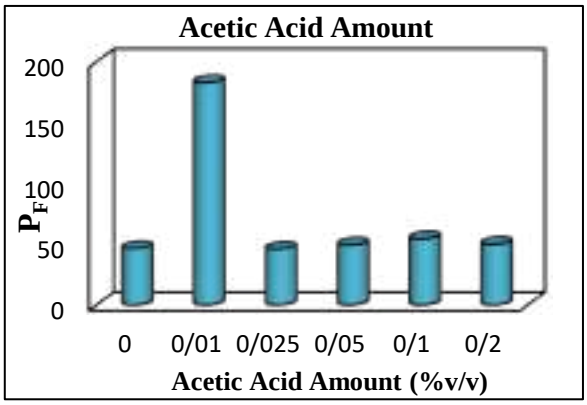

Fig.3 The effect of increasing acetic acid

3. Experiment design

3.1. Statistical analysis and model matching: The factors of applied voltage, extraction time, and pHs of sample solution and receiver solution were considered as effective factors in extraction. It should be noted that the parameters affecting the composition of the gel membrane components were previously optimized by a time variable method. Here, the central composite design was applied directly on the basis of model matching. Therefore, the total number of tests in this

study was considered to be 30 tests for the drug in questionThe ranges have been selected according to laboratory experiences and studies. Also, the experiments were performed under the optimal conditions obtained for combining the components of the gel membrane. Using the statistical design, the optimal model for the desired drug was determined, which is expressed as the following equation:

ER%=+64.0+9.2A-8.7B+2.5C+0.5D+3.8AB-1.7AC+0.7AD+0.07BC-0.7BD+1.9CD-2.9A^2-2.0B^2+1.3C^2 -4.6D^2

The degree of conformity of the equation with the sample data is expressed by a factor called correlation coefficient. The predicted correlation coefficients show the amount of change in the new data expressed by the model. By performing the Backward method, the second degree polynomial agreement with the answer was obtained, which was expressed as follows.

ER%=+65.5+9.2A-8.7B+2.5C+0.5D+3.8AB-3.0A^2-2.2B^2-4.6D^2

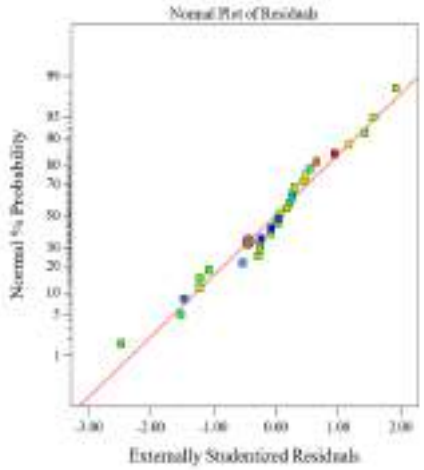

Fig.4 Normal distribution curve of ofloxacin drug

3.2. Three-dimensional surface response curves: In this part, as the pH phaser approaches 9, the color of the graph changes from green to orange, and this means that it has the most efficiency in this part. Regarding the pH of the receiving phase at the point, 3 voltage of 50 volts and time of 30 minutes, the efficiency is more than other points, under these conditions, the highest intensity of the fluorescence signal was observed.

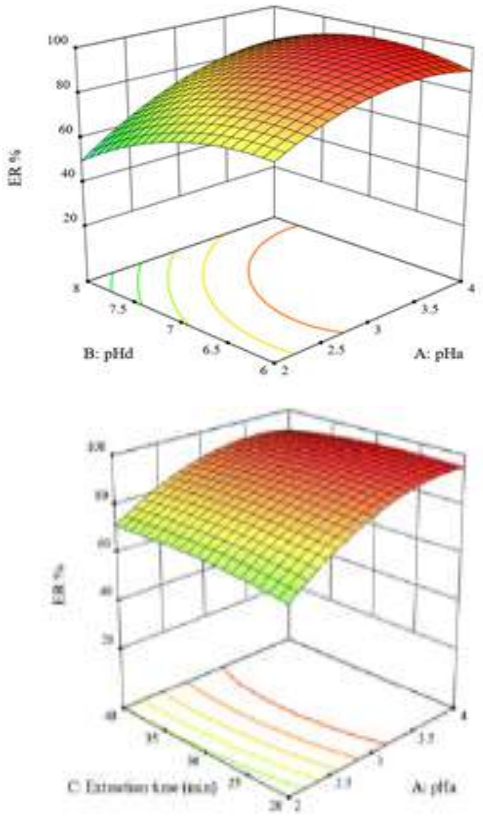

Fig.5 Surface response curves

4. References

1. Carasek, E. and J. Merib, *Membrane-based microextraction techniques in analytical chemistry: a review.* Analytica chimica acta, 2015. **880**: p. 8-25.

2. Płotka-Wasylka, J., K. Owczarek, and J. Namieśnik, *Modern solutions in the field of microextraction using liquid as a medium of extraction.* TrAC Trends in Analytical Chemistry, 2016. **85**: p. 46-64.

3. Tabani, H., et al., *Recent developments in green membrane-based extraction techniques for pharmaceutical and biomedical analysis.* Journal of pharmaceutical and biomedical analysis, 2018. **160**: p. 244-267.

4. Arnott, S., et al., *The agarose double helix and its function in agarose gel structure.* Journal of molecular biology, 1974. **90**(2): p. 269-284.

5. Sambrook, J. and D.W. Russell, *The condensed protocols from molecular cloning: a laboratory manual*. 2006: Cold Spring Harbor Laboratory Press.

STUDYING THE PHYTOCHEMICALS OF *NIGELLA SATIVA*, EXTRACTION AND BIOACTIVITIES

*Mahdi Fatehi Marj**

Department of Chemistry, Faculty of Science, University of Kashan, Iran, mahdifatehi.313@gmail.com

Abstract - *Nigella sativa* (black caraway) known as (Siah Daneh) in Persian, is a plant, native to Iran and some other eastern Europe and western Asia countries and has been used for a long time in cooking and traditional medicine of Iran**.** There are lots of phytochemicals in the seeds of this plant like thymol, carvone, thymoquinone, nigellicimine, nigellicine, dithymoquinone, thymohydroquinone and many others. This article will study some methods of extraction from the seeds and the bioactivity of the extracted compounds. In vivo studies show that this plant has numerous therapeutic properties, including anti-cancer, cardio protecting, anti-diabetes, etc. The medicinal potential of this plant is so high that makes it act like a complex perfect medicine.

1. Introduction

Nigella sativa is an annual flowering plant. It has black seeds which are called Siah Daneh in Iran and these seeds are full of important bioactive phytochemicals. We can gain these compounds through different extraction methods like mechanical oil extraction (cold pressing) or extraction with different solvents. In each method we gain different combination of phytochemicals with different percent of each part. Although we can't introduce all these numerous wide scale phytochemicals here, we decided to consider the most important ones. Despite these large amounts of useful compounds, we are faced with a very high and strange medicinal potential that leads us to prepare medicine from these valuable seeds. Studies show that this plant has anti-oxidant, anti-cancer, Anti-nephrolithiasis, anti-diabetes, anti-sepsis and many other protective effects in the body. This study hopes to draw the attention of people interested in investing in herbal medicines towards this plant by scientifically introducing the medical effects of this plant and its relationship with the metabolites made by the plant.

2. Extraction methods

2.1. Mechanical extraction: In this method we can extract the oil of the seeds with hot or cold pressing. In both methods, the seeds enter the machine and are pressed until the hard texture of the seed is destroyed and it takes a paste-like state, and then it is applied with a heat element that separates the oil from the pressed seed. The difference between hot pressing and cold pressing is that in the hot-pressing method, the seeds are heated before entering the machine, but this does not happen in the cold pressing, and the temperature of the oil when exiting should not be more than 40 degrees Celsius. Also, the temperature of the existing element rises to a maximum temperature of 70 degrees Celsius, which causes the primary and secondary metabolites to decompose less. The advantage of the cold pressing method is that the phytochemicals dissolved in the plant oil are not damaged, and the number of antioxidants and natural vitamins in the oil produced by the cold pressing method is much higher than the oil produced by other methods. Of course, in this mechanical method, hexane solvent can also be used, which improves the extraction efficiency to a great extent, but it should be noted that for medicinal use, the organic solvent must be filtered.

2.2. Solvent extraction:

2.2.1: First method: Powdered *Nigella sativa* seed was macerated in 400ml of petroleum ether, for 24 hrs with occasional shaking. The result was extracted and filtered by using filter paper. The petroleum ether extract was evaporated to dryness in vacuum by using Rota vapor at 40° C to yield 3.5 gm of crude extract (2.8 %W/W). The mark from petroleum ether extract would be socked with 400mLof ethyl acetate for 24hrs. The ethyl acetate would be filtered out connected by using Rota vapor at 40° C to yield 7gm of crude extract (5.6%W/W). The mark from ethyl acetate extract would be socked with 400ml of methanol for 24 hrs. The methanol extract was filtered out and connected to Rota vapor at 40 centigrade to yield crude extract. The mark was socked again with the same amount of methanol for the same period of time. The total weight of crude methanol extract after evaporated using Rota vapor at 40° C to yield 20gm of crude extract (16 %W/W).[1]

2.2.2: Second method: Black cumin seeds were ground (750 mesh) with a domestic electronic grinder and hydro distilled in a Clevenger-type apparatus for 3 hours. A light orange volatile oil, with a characteristic

odor, was obtained with a yield of 1.2%. It was dried over anhydrous sodium sulfate and the sample was stored at 4° C before use. After the isolation of the essential oil, the crude material was oven dried at 50° C for 24 h. Then, 20 g of dried material were loaded on to a Soxhlet apparatus and extraction were carried out with acetone (400 ml) at 90° C for 3 hours. The solvent was removed under reduced pressure.[2]

3. Phytochemicals

There are many ways to extract these compounds from *Nigella sativa* seeds and each method gives us different fractions with different percents. Here we introduce a wide range of extracted compounds through different ways of extraction during the time. A report claims the following proximate nutrient composition for Nigella sativa seeds: 21% protein, 35.5% fat, 5.5% moisture, 3.7% ash and the rest being total carbohydrate. Fatty acid analysis of the extracted oil showed 56% linoleic acid, 24.6% oleic acid, 12% palmitic acid, 3% stearic acid, 2.5% eicosadienoic acid, 0.7% linolenic acid and 0.16% myristic acid. Traces of few unidentified fatty acids were also found. Amino acid analysis of the seed protein hydrolysate of the n-propyl, N-acetyl derivatives showed the presence of 15 amino acids including 9 essential amino acids[3]. The mineral and vitamin analyses showed that black cumin seeds contained iron (105 mg/kg), copper (18 mg), zinc (60 mg), phosphorus (527 mg), calcium (1,860 mg), thiamin (15.4 mg), niacin (57 mg), pyridoxine (5.0 mg) and folic acid (160 m g). [4] *Nigella sativa* seeds contain fixed and volatile oils. Fatty acid composition of the fixed oil of Nigella sativa comprised eight fatty acids: linoleic acid 55.6%, oleic acid 23.4%, palmitic acid 12.5%, stearic acid 3.4%, eicosadienoic acid 3.1%, lauric acid 0.6%, myristic acid 0.5% and linolenic acid 0.4%.[5] The total tocopherol content of *N. sativa* seeds ranged from 9.15–27.92 mg/100 g. The tocopherol profile was shown to be: alpha-tocopherol 0.63–4.80 mg/100 g, alpha-tocotrienol 0.035 mg, beta-tocopherol 0–6.96 mg, gama-tocopherol 0.97–5.53 mg, beta-tocotrienol 8.21–17.91 mg, gama-tocotrienol 0–1.00 mg, delta-tocopherol 0–0.48 mg and delta-tocotrienol 0–0.4%. The profile of sterol in the seeds comprised: cholesterol 0.7–1.25 mg, 24-methylen-cholesterol 1.21–2.36 mg, campesterol 9.88–14.06 mg, campestanol 0.54–0.94 mg, stigmasterol 9.95–18.38 mg, 7-camersterol 0.35–0.72 mg, 5,23 stigmastadienol 0.18–0.21 mg, clerosterol 0.18–0.21 mg, beta-sitosterol 46.68–51.92 mg, sitostanol 2.29–2.78 mg, 5-avenasterol 7.35–16.60 mg, 5,24-stigmastadienol 1.05–1.29 mg, delta 7-avenastenol 1.11–2.38 mg and 7-avenastenol 1.82–2.99 mg. [6] The major fatty acids present in all lipid classes was C18:2n-6 followed by C18:1n-9 and C16:0 acids. The major individual phospholipid classes were found to be phosphatidylcholine (46–48% of total phospholipid) followed by phosphatidylethanolamine, phosphatidylserine and phosphatidylinositol. Phosphatidylglycerol, lysophosphatidylcholine and lysophosphatidylethanolamine were isolated in smaller quantities.[7] Thirty-two constituents were isolated from *N. sativa* seed volatile oil comprising phenyl propanoid compounds 46.1%, monoterpenoid hydrocarbons 26.9%, monoterpenoid ketones 6.0%, nonterpenoid hydrocarbons 4.0%, monoterpenoid alcohols 2.7% and sesquiterpenoid hydrocarbons 1.0%.The major components were trans-anethole (38.3%), para-cymene (14.8%), limonene (4.3%), carvone (4.0%) and alpha-thujene 2.4%. Other minor constituents included estragole 1.9%, dill apiole 1.8%, anisaldehyde 1.7%, n-nonane 1.7%, carvacrol 1.6%, sabinene 1.4%, myristicin 1.4%, beta-pinene 1.3%, alpha-pinene 1.2%, fenchone 1.1%, apiole 1.0%, longifolene 0.7%, terpinen-4-ol 0.7%, alpha-phellandrene 0.6%, thymoquinone 0.6%, gama-terpinene 0.5%, 1,3,5-trimethyl benzene 0.5%,1-methyl-3-propyl benzene 0.5%, para-cymene-8-ol 0.4%, n -decane 0.4%, myrcene 0.4%, alpha-longipinene 0.3%, 3-methyl nonane 0.3%, dihydrocarvone 0.3%, 1-ethyl-2,3-dimethyl benzene 0.2%, n-tetradecane 0.2% and n-hexadecane 0.2%.[5]A total of 47 different compounds comprising quinines, monoterpene hydrocarbons, oxygenated monoterpenes, sesquiterpene hydrocarbons, oxygenated sesquiterpenes, diterpenes, alkane, alkenes, fatty acids and fatty acid esters were identified in *N. sativa* seed oils extracted by supercritical CO2 (SFE 1 and SFE 2) and hydro distillation of SFE 1 (HD SFE)[8]. About 31 compounds were identified in SFE 1 oil, 22 compounds in SFE 2 oil and 23 compounds in HD SFE oil. The major phenolic compounds isolated were thymoquinone (35.05%: SFE1, 33.12%: SFE2, 38.41%: HDSFE), thymohydroquinone (1.17%: SFE1, 1.12%: SFE2, 2.31%: HDSFE) and thymol (7.43%: SFE1, 5.30%: SFE2, 16.95%: HDSFE). Sixteen volatile compounds were reported for the first time namely n-nonane (0.12%: SFE1), alloocimenol (0.11: SFE2), terpinen-1-ol (0.11 for HDSFE), 1,5,8- r -menthatriene (0.43% for SFE1, 0.38 for SFE2), dihydrocarvone (0.37% for SFE1, 2.06 for SFE2), ocimenone (E) (0.54% for SFE1, 1.50 for SFE2), n-octyl isobutyrate (0.12% for HDSFE), citronellyl acetate (0.50% for HDSFE), thymohydroquinone methyl ether (Trace for HDSFE), (Z)-caryophyllene (0.23% for SFE1), thymohydroquinone dimethyl ether (0.12% for SFE1), aromadendrene (1.05% for HDSFE), davanone (0.31% for SFE1), 8-heptadecene (1.23% for SFE1, 1.13% for SFE2, 0.86% for HDSFE), dihydro farnesyl acetate (2.28% for SFE1, 4.68% for SFE2) and pimaradiene (1.23% for SFE1, 2.25% for SFE2). The other known compounds isolated included: tricyclene (trace for SFE1), camphene (1.64% HDSFE), beta-pinene (0.4% for HDSFE), 2,4,(10)-thujadiene (4.74% for SFE1, 0.19% for SFE2),

sabinene (1.05% for SFE1), beta-myrcene (0.31% for SFE1), 1,8cineole (0.98% HDSFE), alpha-terpinene (2.34% for SFE1), limonene (0.18% for SFE1, 0.38% for SFE2, 1.03% for HDSFE), gamma-terpinene (27.46% for SFE1, 13.20% for SFE2, 12.87% for HDSFE), cis -sabinene hydrate (0.38% for SFE2, trace for HDSFE), linalool (0.25% for SFE1, 0.19% for SFE2), terpinolene (trace for HDSFE), trans -sabinene hydrate (0.37% for SFE1), borneol (1.02% for HDSFE), pinocarvone (2.96% for SFE1, 3.00% for SFE2), trans-dihydrocarvone (0.19% for SFE2), carvacrol (1.98% for SFE1, 1.73% for SFE2, 0.81% for HDSFE), 2-undecanone (13.72% for HDSFE), alpha-longipene (0.26% for SFE1), cyclosativene (1.43% HDSFE), alpha-longicyclene (0.43% for SFE1, 5.25% for SFE2), alpha-copaene (1.54% for SFE1, 2.00% for SFE2, 0.41% for HDSFE), alpha-longifolene (0.51% for HDSFE), beta-caryophyllene (2.89% for SFE1, 5.07% for SFE2, 4.80% for HDSFE), palmitic acid (0.18% for SFE1), pimara-8(14),15-diene (0.92% for SFE1), and octadecanoic acid (0.26% for SFE1, 12.31% for SFE2).[8] Alkaloids isolated were nigellicine, nigellimine, nigellimine N-oxide, nigellidine and nigellidine-4-O-sulfite, dolabellane-type alkaloids nigellamines A(1), A(2), B(1) and B(2); A(3), A(4), A(5), and C.[9] [10]. There are also many saponins isolated from this plant[11, 12] that can't be mentioned here due to space limitations.

4. Medicinal effects

Due to the numerous metabolites that the seeds of this plant have, it also shows numerous medicinal effects in in vitro and in vivo studies. Effects like antioxidant, haemeostasis , homeopathic, antidyslipidemic/anti hypercholesterolemic, cardioprotective , antidiabetic, hypotensive/antihypertensive, cytochrome metabolic and analgesic/antinociceptive activities, anti-inflammatory , anti-asthmatic , anti-encephalomyelitis, anti-arthritic , anti-allergic , respiratory stimulant , relaxant/spasmolytic, antineoplastic/anticancer, radioprotective, gastroprotective and nephroprotective activity, anti-nephrolithiasis, hepatoprotective and neuroprotective activity, skin-darkening, skeletal muscle protective , sedative, anxiolytic, anti-oxytocic , anti-sepsis, immunomodulatory, antiplatelet and haemostatic, antiepileptic, antifertility and fertility activity, antimicrobial, testicular protective, anti-sickling, bone healing, antiparasitic and therapeutic activity in opioid tolerance and dependence, cardiac hypertrophic activity, healing allergy problems and it's traditionally used to treat asthma, bronchitis, diarrhoea, dyslipidaemia, diabetes, hyperglycaemia, and related abnormalities headache, dysentery, infections, obesity, back pain, hypertension, gastrointestinal problems, eczema, boils, rheumatism, cancer, fungal infections, diabetes, hypertension, cardiac diseases, haemorrhoids, sexual diseases and as an abortifacient. Each of these effects is related to the category or group of phytochemicals of this seed and due to the limitation of the pages, you can study the relationship of each of the therapeutic effects with the phytochemicals responsible for that effect in the reference.[13]

5. Conclusion:

Nigella sativa currently has five FDA separate patents in the U.S. and one in the UK for the treatment of: diabetes, inhibition of cancer growth, improvement of immune system, viral infections, psoriasis and asthma. Considering that this plant is native to Iran and due to the richness of this plant in natural compounds and its many therapeutic effects, this plant has the potential of investing in the field of herbal medicine production.

6. References

1. Yessuf, A.M., *Phytochemical extraction and screening of bio active compounds from black cumin (Nigella sativa) seeds extract.* American Journal of Life Sciences, 2015. **3**(5): p. 358-364.
2. Singh, G., P. Marimuthu, C.S. de Heluani, and C. Catalan, *Chemical constituents and antimicrobial and antioxidant potentials of essential oil and acetone extract of Nigella sativa seeds.* Journal of the Science of Food and Agriculture, 2005. **85**(13): p. 2297-2306.
3. Babayan, V., D. Koottungal, and G. Halaby, *Proximate analysis, fatty acid and amino acid composition of Nigella sativa L. seeds.* Journal of Food Science, 1978. **43**(4): p. 1314-1315.
4. Takruri, H.R. and M.A. Dameh, *Study of the nutritional value of black cumin seeds (Nigella sativaL).* Journal of the Science of Food and Agriculture, 1998. **76**(3): p. 404-410.
5. Nickavar, B., F. Mojab, K. Javidnia, and M.A.R. Amoli, *Chemical composition of the fixed and volatile oils of Nigella sativa L. from Iran.* Zeitschrift für Naturforschung C, 2003. **58**(9-10): p. 629-631.
6. MatthauS, B. and M.M. ÖzCaN, *Fatty acids, tocopherol, and sterol contents of some Nigella species seed oil.* Czech Journal of Food Sciences, 2011. **29**(2): p. 145-150.
7. Ramadan, M.F. and J.-T. Mörsel, *Analysis of glycolipids from black cumin (Nigella sativa L.), coriander (Coriandrum sativum L.) and niger (Guizotia abyssinica Cass.) oilseeds.* Food Chemistry, 2003. **80**(2): p. 197-204.
8. Tiruppur Venkatachallam, S.K., H. Pattekhan, S. Divakar, and U.S. Kadimi, *Chemical composition of Nigella sativa L. seed extracts obtained by supercritical carbon dioxide.* Journal of food science and technology, 2010. **47**: p. 598-605.
9. Khan, S., et al., *Nigella sativa: From chemistry to medicine*, in *Black Seeds (Nigella Sativa)*. 2022, Elsevier. p. 29-62.
10. Ali, Z., et al., *Nigellidine-4-O-sulfite, the first sulfated indazole-type alkaloid from the seeds of Nigella sativa.* Journal of natural products, 2008. **71**(6): p. 1111-1112.
11. Ansari, A.A., S. Hassan, L. Kenne, and T. Wehler, *Structural studies on a saponin isolated from Nigella sativa.* Phytochemistry, 1988. **27**(12): p. 3977-3979.
12. Taşkin, M.K., et al., *Triterpene saponins from Nigella sativa L.* Turkish Journal of Chemistry, 2005. **29**(5): p. 561-569.
13. Lim, T., *Edible Medicinal and Non-Medicinal Plants: Volume 5, Fruits, Nigella Sativa.* Springer, Netherlands. DOI, 2013. **10**: p. 978-94.

29TH IRANIAN ORGANIC CHEMISTRY CONFERENCE
1_3 NOV, 2023
UNIVERSITY OF QOM, IRAN

Green synthesis of polyhydroquinoline derivatives using superparamagnetic and recyclable nanocatalyst Fe_3O_4@THAM-piperazine

Bahareh Kavasi, Nourallah Hazeri, Elham Mir *

Department of Chemistry, Faculty of Science, University of Sistan and Baluchestan, Zahedan, Iran, nhazeri@chem.usb.ac.ir, n_hazeri@yahoo.com

Abstract - An efficient and environmentally friendly method for the synthesis of polyhydroquinoline derivatives in a one-step and four-component reaction including dimedone, ethyl acetoacetate, ammonium acetate, and aromatic aldehydes in the optimal solvent conditions of water and temperature of 70 degrees Celsius in the presence of nanocatalyst Fe_3O_4@THAM -piperazine was performed, and the synthesized product was obtained with high efficiency; The structure of the product was identified using melting point and IR and NMR spectroscopy.

1. Introduction

Today, heterogeneous magnetic nanocatalysts have played an important role in modern technology and science, especially in organic synthesis. These nanoparticles (NPs) are used in various biological fields and industries, such as drug delivery, bioseparation, hyperthermia, magnetic resonance imaging, and catalytic processes. Magnetic nanoparticles have gained much attention in expanding medical applications. The most widely used magnetic nanoparticles in medical applications are chromium dioxide (CrO_2), iron oxide (Fe_3O_4), maghemite (γ-Fe_2O_3), and cobalt ferrite ($CoFe_2O_4$). Among different magnetic nanoparticles, Fe_3O_4 has different characteristics, including high thermal and mechanical stability, high catalytic activities, high surface area, easy synthesis, and easy magnetic recovery. These nanoparticles contain both Fe_3^+ and Fe_2^+ ions, they have high catalytic activity. In recent years, due to the high capacity of Fe_3O_4 magnetic nanoparticles, it has been widely used in various fields such as bioengineering and biomedicine, such as labeling and sorting cells, magnetic resonance imaging (MRI), separation of biomedical products, and cancer chemotherapy. Fe_3O_4 magnetic nanoparticles were synthesized by various methods, including co-precipitation, ion-thermal, and solvothermal methods. Among all the current methods, the co-precipitation method of this technique is known as a widely used method due to its environmental compatibility, low reaction temperature, and easy operation.

Currently, several heterogeneous magnetic nanocatalysts have high activity and selectivity and are used in multicomponent reactions (MCRs) such as Fe_3O4@THAM-SO3H, MNPs-$PhSO_3H$, Fe_3O_4@TiO_2/Cu_2O, Fe_3O_4NPs@TiO_2NTs, Fe_3O_4/PEG@CPTMS-thioaminophenol@Ni and Fe_3O_4@THAM-piperazine are reported.

Tris(trihydroxyaminomethane) (THAM) was introduced as a cheap and non-toxic buffer solution that is widely used in molecular biology and biochemistry. Tris (trihydroxyaminomethane) is rich in electron donor and acceptor groups due to three CH_2OH groups and one NH_2 functional group, which makes it useful for coating on the surface of Fe_3O_4 NPs and improves the stability of Fe_3O_4 NPs through the interaction of THAM with Fe_2^+ and preventing from its oxidation by air [1].

Multicomponent reactions are one-pot chemical reactions with more than two starting materials, where the final product includes a significant portion of all starting materials. This advanced approach is an efficient approach, affordable Economical, and environmentally friendly, multicomponent reactions have emerged as a sustainable process for chemists in the design, synthesis, and further development toward drug discovery and sustainable production of drugs, catalysts, or advanced materials and food additives [2].

In this research, we report a heterogeneous base nanocatalyst using piperazine as a basic functional group in tris(trihydroxyaminomethane) immobilized in Fe_3O_4 nanoparticles, then the activity of this new and recyclable nanocatalyst for the quasi-quaternary synthesis of derivatives Polyhydroquinoline has been reported from the reaction between derivatives of benzaldehyde, dimedone, ethyl acetoacetate and ammonium acetate [3].

2. Experimental

2.1. General: All chemicals, solvents, and reagents used were obtained from Merck, Germany, and Fluka, Switzerland. The melting point of the products was taken in a BUCHI 510 melting point machine using a capillary tube. IR spectra were taken in FTIR-BRUKER spectrometer, and NMR spectra were taken using BRUKER DEX-300 AVANCE NMR in DMSO solvent. Thin layer chromatography (TLC) was prepared using silica gel 60 GFS254 sheets from Merck, Germany.

2.2. Synthesis of Fe_3O_4 magnetic nanoparticles: For the synthesis of Fe_3O_4 nanoparticles, first, we put a mixture of 10 mmol of $FeCl_3•6H_2O$ and 5 mmol of $FeCl_2•4H_2O$ with 100 ml of deionized water and put a magnet inside the balloon. The balloon containing the mixture is placed on the heater at room temperature until the material is completely dissolved in the next step, ammonium hydroxide (NH_4OH) solution was added dropwise to the solution using a burette and stirred vigorously at a speed of 1000 rpm. After reaching a pH value of 11-12, the resulting mixture was stirred for 1 hour The temperature of the room was strongly stirred. At the end, the synthesized nanoparticles were collected by a strong external magnet and the solution on the nanoparticle was separated. Water and ethanol were used to wash and purify the nanoparticle. And the synthesized nanoparticle was immediately used in the next step.

2.3 Synthesis of Fe_3O_4@THAM MNPs: 50 ml of 96% ethanol was added to the synthesized Fe3O4 and stirred using a bath at room temperature for 30 minutes, and then, THAM (2gr) was added to this, the mixture was suspended and subjected to reflux conditions for 24 hours. After cooling to room temperature, the prepared Fe_3O_4@THAM was separated by an external magnet, washed several times with water and ethanol to completely remove impurities, and dried at 60°C for 24 hours.

2.4 Synthesis of Fe_3O_4@THAM—CH_2CH_2–Cl MNPs: First, 50 mL of CH_3CN was added to the synthesized MNPs (1 g) and stirred for 15 minutes at 80-100. Then, dichloroethane (1 mL, 12.6 mmol) was added to the mixture of Fe_3O_4@THAM- CH_2CH_2-Cl in acetonitrile was added dropwise with triethylamine (0.1 mL) as a proton absorber. After that, the resulting mixture was subjected to reflux conditions, and after 24 hours of reflux, after cooling the final product at room temperature, the synthesized nanoparticles were collected by a strong external magnet, and the solution on the nanoparticles was separated for washing and Water and ethanol were used for nanoparticle purification. For complete drying, the nanoparticle was placed in an oven at 60 degrees Celsius for 24 hours.

2.5 Synthesis of Fe_3O_4@THAM-piperazine: First, we add 50 ml of methanol to 1 g of magnetic nanocatalyst Fe_3O_4@THAM–CH_2CH_2–Cl and it was stirred for 20 minutes at reflux temperature. Then, piperazine (2.0 g) was added dropwise to the reaction mixture and heated at 90 degrees Celsius. It was stirred for 24 hours. The obtained nanoparticles (Fe_3O_4@ THAM-piperazine) were separated by an external magnet and washed several times with ethanol and water to completely remove the unreacted compound and the magnetic nanocatalyst was dried in an oven at 60°C for 24 hours. The complete synthesis of Fe_3O_4@THAM-piperazine magnetic nanocatalyst is shown in scheme 1.

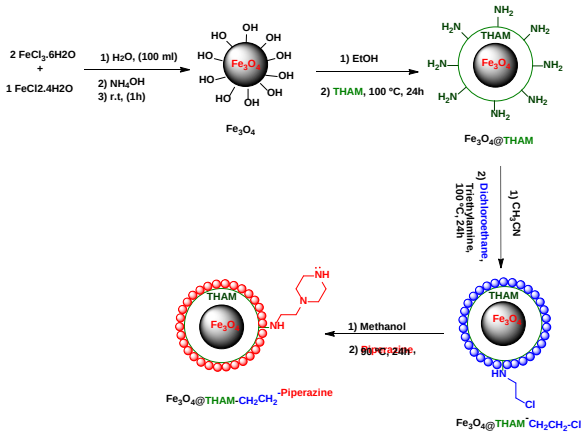

Scheme.1. Preparation of Fe_3O_4@ THAM-piperazine

2.6. Investigating reaction conditions to obtain optimal conditions for the synthesis of polyhydroquinoline derivatives in the presence of Fe_3O_4@THAM-piperazine nanocatalyst: Fe_3O_4@THAM-piperazine nanocatalyst has been used as a highly efficient and heterogeneous nanocatalyst in the synthesis of polyhydroquinoline derivatives.

First, the reaction was carried out in different solvents (water, ethanol, water/ethanol, and solvent-free conditions) and it was observed that the best yield was related to water solvent conditions. In the water solvent, due to the high hydrogen bonding of the water, it is in full contact with the reactants, and the catalyst is well suspended. As a result, in the presence of 4 ml of water, the reaction was performed with the shortest time and the highest efficiency.

Then, the reaction was carried out in different amounts of Fe_3O_4@THAM-piperazine nanocatalyst, and the best case corresponding to the amount of 0.005 grams of Fe_3O_4@THAM-piperazine nanocatalyst was obtained in the shortest time and with the highest efficiency. At the end of checking the reaction conditions, the reaction was carried out at different temperatures and it was observed that the temperature is suitable for this reaction. It is 90 degrees Celsius and was chosen as the optimal temperature.

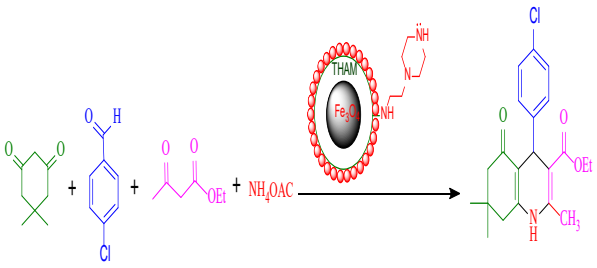

Fig.1. Model reaction for reaction conditions in the synthesis of polyhydroquinoline derivatives

2. 7. General working procedure for the synthesis of polyhydroquinoline in the presence of 0.005 g of nanocatalyst and temperature conditions of 90 degrees Celsius and H_2O solvent: First, a mixture of different benzaldehyde derivatives (1 mmol), dimedone (1 mmol), ethyl acetoacetate (1 mmol) and ammonium acetate (1 mmol) was added to the reaction vessel in the presence of 0.005 g of magnetic nanocatalyst Fe_3O_4@THAM-piperazine and stirred at 90 degrees Celsius. The completion time of the reaction was monitored by thin-layer chromatography (TLC). After the completion of the reaction, the reaction mixture was dissolved in hot ethanol and the magnetic nanocatalyst was separated by an external magnet and washed for reuse. The remaining precipitate was dried after filtration and the pure product was obtained.

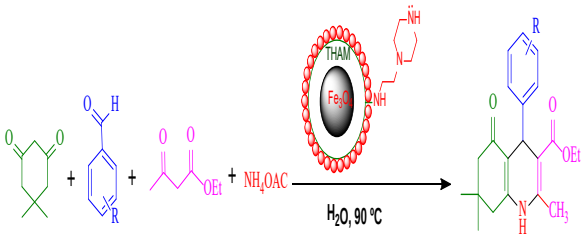

Fig.2. General procedure for the synthesis of polyhydroquinoline derivatives

Table 1 Synthesis of polyhydroquinoline derivatives under optimal conditions

Entry	R	Time (min)	Yield (%)	M.p (°C)
1	H	5	77	202-204
2	4-Me	5	75	260-261
3	4-Cl	5	85	245-246
4	2-Cl	10	78	208-209
5	3-NO_2	20	95	176-177
6	3-OH	5	78	228-229
7	4-OMe	15	82	255-257
8	4-NO_2	15	92	244-246
9	2-NO_2	15	70	206-207

2.8 Selected spectral data

2.8.1. 4-(4-Chloro-phenyl)-2,7,7-trimethyl-5-oxo-1,4,5,6,7,8-hexahydro-quinoline-3-carboxylic acid ethyl ester: FT-IR(KBr): 3274, 3207, 3076, 2959, 1706, 1604, 1488, 1381, 1214, 884 cm^{-1}; ^1H NMR (300MHz, DMSO): δ (ppm) 0.84 (s, 3H, CH_3), 1.02 (s, 3H, CH_3), 1.13 (t, 3H, J = 6 Hz, CH_3), 1.96-2.46 (m, 4H, $2CH_2$), 2.31 (s, 3H, CH_3), 3.98 (q, 2H, J = 6 Hz, OCH_2), 4.85 (s, 1H, CH), 7.17 (d, 2H, J = 6 Hz, ArH), 7.26 (d, 2H, J = 6 Hz, ArH), 9.14 (s, 1H, NH).

3. Results and discussion

A magnetic Fe_3O_4@THAM-piperazine nanocatalyst was synthesized and the structural process of this magnetic nanocatalyst was observed in scheme 1 in 4 steps. In the first step, magnetic nanoparticles (Fe_3O_4) were synthesized by chemical co-precipitation method, and in the second step, the nanoparticles were covered by tris (hydroxymethyl)aminomethane, and in the next steps, by dichloroethane and piperazine, the magnetic nanocatalyst Fe_3O_4@THAM-piperazine was synthesized.

Synthesized nanocatalyst using infrared transformation techniques (FTIR), field emission scanning electron microscopy (FESEM), energy dispersive X-ray spectroscopy (EDS), thermal gravimetry (TGA), vibrating sample magnetometer (VSM) and diffraction. X-rays (XRD).

To evaluate the catalytic activity of Fe_3O_4@THAM-piperazine nanoparticles in the synthesis of polyhydroquinoline derivatives. The four component reaction compounds of 4-chlorobenzaldehyde (1 mmol), dimedone (1 mmol), ethyl acetoacetate (1 mmol), and ammonium acetate (1 mmol) were selected as the model reaction. To achieve this goal, first the reaction conditions with solvent, amount of catalyst, and temperature were optimized. Then derivatization was done using different aldehydes. The best result was obtained in water solvent and catalyst amount of 0.005 g and temperature of 90 degrees Celsius.

According to the optimal reaction conditions, the synthesis of polyhydroquinoline derivatives using different aldehydes was investigated and the products were synthesized in a short reaction time and with a yield of 70-92% (Table 1).

When the synthesis of polyhydroquinoline was carried out without a catalyst, its efficiency was negligible, which is a sign of the efficiency of the Fe_3O_4@THAM-piperazine magnetic nanocatalyst.

4. Conclusion

In this article, we used Fe_3O_4@THAM-piperazine nanocatalyst for the synthesis of polyhydroquinoline derivatives, which is very important in medicinal

chemistry. Magnetic nanocatalyst Fe_3O_4@THAM-piperazine has high efficiency in the synthesis of pharmaceutical compounds due to its properties such as highly active surface, ability to be recycled, and easily separated by an external magnet. Derivatives of this heterogeneous nanocatalyst can be used at least 6 times without losing catalytic activity. In summary, compared to other reported nanocatalysts, the synthesized nanocatalyst has advantages such as the use of green solvent, excellent yield of products, high stability, easy synthesis, and short reaction time among other features of this research.

4. References

[1] Kazemi, M., Based on MFe_2O_4 (M= Co, Cu, and Ni): Magnetically recoverable nanocatalysts in synthesis of heterocyclic structural scaffolds, *Synth. Commun*, 2020, 46, 3651–3666.

[2] Younus, H. A., Al-Rashida, M., Hameed, A., Uroos, M., Salar, U., Rana, S., Khan, K. M. Multicomponent reactions (MCR) in medicinal chemistry: a patent review. *Expert Opinion on Therapeutic Patents*. 2020,31, 267-289.

[3] Ruijter, E., Orru, R.V. Multicomponent reactions–opportunities for the pharmaceutical industry. *Drug Discovery Today: Technologies*, 2013, 10, e15-e20.

29TH IRANIAN ORGANIC CHEMISTRY CONFERENCE
1_3 NOV, 2023
UNIVERSITY OF QOM, IRAN

Synthesis and characterization of calcium-rich biochar from pyrolysis of crustacean waste

Leila Khoshmaram, Sahar Shiri, Fahimeh Farshi Azhar*

Department of Chemistry, Faculty of Science, Azarbaijan Shahid Madani University, Tabriz, Iran, l.khoshmaram@gmail.com, shrshirii1378@gmail.com

Abstract: In this study, a calcium-rich biochar was prepared through pyrolysis of crustacean waste. The prepared biochar was assessed by Fourier transform infrared (FTIR), X-ray diffraction (XRD), Dynamic light scattering (DLS), Zeta potential and Brunauer–Emmett–Teller (BET).

Keywords: crustacean waste, biochar, pyrolysis, Characterization.

1. Introduction

Biochar is the carbon-rich material produced from organic feedstock under certain thermal combustion with limited oxygen. Many organic wastes can be used as feedstock to produce biochar, such as agricultural wastes and municipal solid waste [1]. Various methods have been employed for biochar production, such as combustion, or- refaction, gasification, and pyrolysis (slow and fast types) [2]. Each method results in a yield, heating rate, feedstock residence time and carbon content and yield. Earlier, combustion was used to produce charcoal from woody biomass. However, it resulted in low yields and extreme air pollution. With time, the advancement in technology (endothermic and exothermic processes) allows the maximum energy Combustion and gasification generate heat and gas, respectively, by thermally decomposing organic matter in an oxic environment [3]. However, these processes are less effective and pyrolysis is the most common, oldest, and the most effective process for meeting energy requirements and reducing emissions [4]. Pyrolysis leads to the production of biochar (solid), bio-oil (liquid), and syngas (gas). The generated by products can also be utilized as energy substances to meet the energy crisis. Here, pyrolysis can be classified into slow, intermediate, and fast pyrolysis in accordance with the heating rate, temperature, pressure, and residence time [5]. For high yield of biochar, slow pyrolysis should meet heating rate of 0.1–1◦C min^{-1}, whereas fast pyrolysis and high temperature can result in generation of more liquid and syngas. In addition, the mass fraction range of pyrolysis solid increases with increasing temperature. In case of intermediate pyrolysis where the conditions are between slow and fast pyrolysis, there is a balance yield of biochar and bio-oil yield, but it is rarely approved from a biochar production perspective [6,7]. Various biochar modified methods, including acid or alkali modification, redox modification, load metal ions modification, nanometer modification, magnetic modification and organic modification have been applied [8]. Acid treatment of biochar results in enhanced surface area, better porosity, increased sorption capacity, created charged and hydrophilic surface functional groups, and increased colloidal stability and mobility [9]. The common acids include hydrochloric acid, sulfuric acid, nitric acid, phosphoric acid, oxalic acid and citric acid [10]. One of the approaches for the modification of biochar is HCl treatment resulting in higher adsorption of concomitant organic compounds. This is because functional groups (carboxylic, phenolic, and carbonyl groups) are added to the BC surface after treatment, the ash content is reduced, and the adsorption sites (hydrophobic) are increased [11,12]. The main aim of alkaline modification is to increase the surface area and the oxygen containing functional groups. The common alkaline agents include potassium hydroxide and sodium hydroxide [13]. Since biochar is relatively high in surface area and pore volume, and rich in surface functional groups and minerals, it has attracted increasing attention as sustainable platform for biochar-based materials [14]. However, most biochars are produced from lignocellulosic biomasses; a few is from the crustacean waste that is also one of the most abundant biomass in nature. Crustacean waste, such as crab shell is composed of valuable components, such as proteins (20-40%), chitin (15-40%), and calcite (20-50%) [15]. Traditionally, crustacean waste can be used as a feedstock for the production of chitin, chitosan, and their derivates [16].

In this study, a calcium-rich biochar was prepared through pyrolysis of crustacean waste and characterized the properties of synthesized biochare.

2. Methods

2.1. Preparation of biochar: To prepare biochar, crustacean waste were washed with distilled water. After drying, the oysters were crushed and passed through a sieve. 30 g of crustacean waste were poured into the crucible and placed in the furnace. The

temperature of the furnace started at 300°C and was increased at a rate of 10°C/min until the temperature reached 900°C. When the temperature reached 900 degrees Celsius, it remained at the same temperature for two hours until the pyrolysis process was performed.

2.2. Characterization of biochar: The FTIR spectrum was measured by Bruker TENSOR27. The XRD patterns were characterized by Tongda TD-3700 Advance. The surface area was calculated using BET method with relative pressures of 0.99, the total pore volume and the average pore diameter were derived from the BJH method. Dynamic light scattering and zeta potential analysis were also performed.

3. Results and discussion

3.1. Fourier transform infrared spectroscopy (FTIR) analysis : Figure 1 shows the FTIR spectrum of biochar. In this spectrum, a peak has appeared in the range of 3639.81 cm^{-1}, which indicates that the lime was formed during the pyrolysis process at a higher temperature and converted to $Ca(OH)_2$ in the air with a certain moisture content [17]. The peak at 3451.21cm^{-1} corresponds to the OH bond vibration. The peak with a wave number of 2511.90 cm^{-1} corresponds to the vibration of the C-H bond. Peaks at 1412.94 cm^{-1} and 874.34 cm^{-1} belong to C-O vibration in $CaCO_3$ functional group. The wavenumber of 710.57 cm^{-1} indicates the C-O bond in CaO [18].

3.2. X-ray diffraction (XRD) analysis: Figure 2 shows the XRD spectrum of biochar. In this spectrum, the phase analysis of biochar components was investigated in the range of 2ɵ=5-60. In this pattern, the highest peaks are at the angles of 29.42^0, 34.08^0, 39.42^0, 47.5^0, 48.48^0 and 50.7^0, and the highest peak is related to calcite.

3.3. Brunauer–Emmett–Teller (BET) analysis: Specific surface area, volume and pore size distribution of biochar absorbent were obtained using BET and BJH theory based on adsorption and desorption isotherms of nitrogen gas (at 77 degrees Kelvin). The degassing process was carried out at a temperature of 150^0C for 2 hours by nitrogen gas. The surface area of the biochar absorber is 0.2211 $m^2.g^{-1}$. The average pore size in BJH analysis is equal to 31.01 nm, which is classified as macropore (d>2nm), mesopore (d<50nm>2) and micropore (d>50nm), this adsorbent is in the mesoporous category based on IUPAC classification. The total pore volume in BJH with relative pressure (p/p0=0.99) is equal to 0.006737 $cm^3.g^{-1}$.

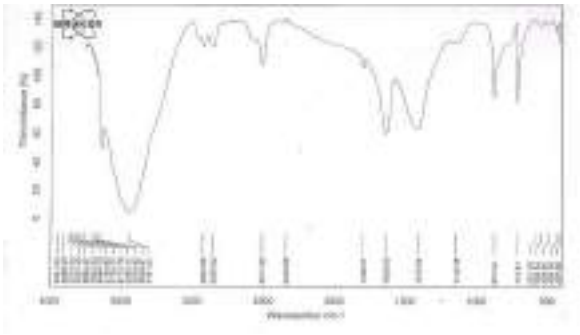

Fig.1. FTIR spectra of biochar

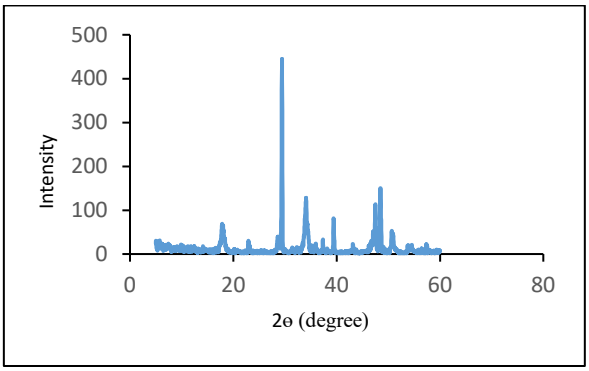

Fig.2. XRD patterns of biochar

3.4. Dynamic Light Scattering (DLS) analysis: Figure 3 shows DLS analysis of biochar. According to Fig. 3, the average hydrodynamic size of biochar is 1115 nm, About 35% of the particles are dispersed and the water-covered radius is 307.6 nm.

3.5. Zeta potential analysis: Figure 4 shows Zeta potential analysis of biochar. According to the zeta potential, the electric charge of biochar was -8.075, which shows that the electric charge of biochar is negative.

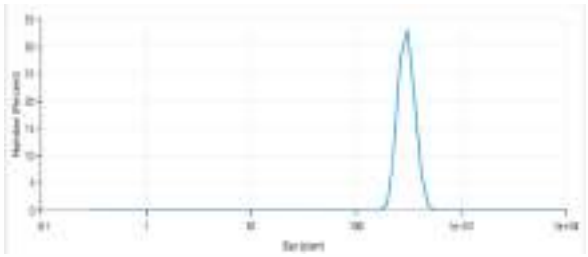

Fig.3. DLS analysis of biochar

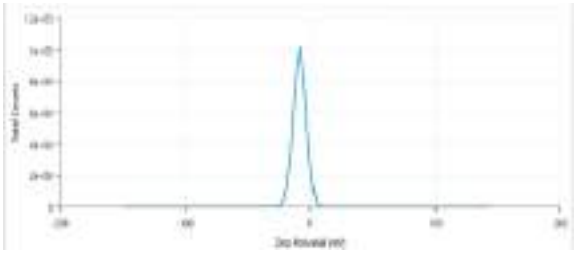

Fig.4. Zeta potential of biochar

4. References

[1] J. Lehmann, Biochar for environmental management: an introduction, Biochar for Environmental Management Science and Technology 25 (2009), 15801-15811.

[2] A. Al- Rumaihi, M. Shahbaz, G. Mckay, H. Mackey, T. Al-Ansari, A review of pyrolysis technologies and feedstock: A blending approach for plastic and biomass towards optimum biochar yield, Renew. Sustain. Energy Rev. 2022, 167, 112715.

[3] C.Z. Zaman, K. Pal, W.A. Yehye, S. Sagadeven, S.T. Shan, G.A. Adebisi, R.B. Johan, Pyrolysis: A Sustainable Way to Generate Energy from Waste; IntechOpen: Rijeka, Croatia, 2017; Volume 1, p. 316806.

[4] W.J. Liu, H. Jiang, H.Q. Yu, Development of biochar-based functional materials: Toward a sustainable platform carbon material. Chem. Rev. 2015, 115, 12251–12285.

[5] S. Goswami, A. Kushwaha, L. Goswami, N.R. Gupta, V. Kumar, U. Bhan, B.S. Reddy, K.M. Tripathi, Nanobiochar-a green catalyst for wastewater remediation. In Bio-Based Nanomaterials; Elsevier: Amsterdam, The Netherlands, 2022; pp. 109–132.

[6] H. Zeghioud, L. Fryda, H. Djela, A. Assadi, A. Kane, A comprehensive review of biochar in removal of organic pollutants from wastewater: Characterization, toxicity, activation /functionalization and influencing treatment factors. J. Water Process Eng. 2022, 47, 102801.

[7] M. Tripathi, J.N. Sahu, P. Ganesan, Effect of process parameters on production of biochar from biomass waste through pyrolysis: A review. Renew. Sustain. Energy Rev. 2016, 55, 467–481.

[8] B. Tang, H. Xu, F. Song, H. Ge, L. Chen, S. Yue, W. Yang, Effect of biochar on immobilization remediation of Cd **-** contaminated soil and environmental quality, Environ Res 204 (Pt A), (2021), 111840.

[9] H.H. Cho, K.Wepasnick, B.A. Smith, F.K. Bangash, D.H. Fairbrother, W.P. Ball, Sorption of aqueous Zn [II] and Cd [II] by multiwall carbon nanotubes: The relative roles of oxygen-containing functional groups and graphenic carbon. Langmuir 2010, 26, 967–981.

[10] A.U. Rajapaksha, S.S. Chen, D.C. Tsang, M. Zhang, M. Vithanage, S. Mandal, B. Gao, N.S. Bolan, Y.S. Ok, Engineered/designer biochar for contaminant removal/ immobilization from soil and water: Potential and implication of biochar modification. Chemosphere 148 (2016), 276-291.

[11] Y. Li, J. Shao, X. Wang, Y. Deng, H. yang, H. Chen, Characterization of modified biochars derived from bamboo pyrolysis and their utilization for target component (furfural) adsorption. Energy Fuels 2014, 28, 5119–5127.

[12] P. Peng, Y.H. Lang, X.M. Wang, Adsorption behavior and mechanism of pentachlorophenol on reed biochars: pH effect, pyrolysis temperature, hydrochloric acid treatment and isotherms. Ecol. Eng. 2016, 90, 225–233.

[13] J. Wang, S. Wang, Preparation, modification and environmental application of biochar: A review, Journ. Cleaner production, 2019, 227, 1002-1022.

[14] W.J. Liu, H. Jiang, H.Q. Yu, Development of Biochar-Based Functional Materials: Toward a Sustainable Platform Carbon Material, Chem. Rev. 115 (2015), 12251-12280.

[15] N. Yan, X. Chen, Sustainability: Don't waste seafood waste, Nature 524 (2015), 155-157.

[16] S. Duan, L. Li, Z. Zhuang, W. Wu, S. Hong, J. Zhou. Improved production of chitin from shrimp waste by fermentation with epiphytic lactic acid bacteria. Carbohydr. Polym. 89 (2012), 1283-1288.

[17] L. Dai, F. Tan, H. Li, N. Zhu, M. He, Q. Zhu, G. Hu, L. Wang, J. Zhao, Calcium-rich biochar from the pyrolysis of crab shell for phosphorus removal, 198 (2017), 70-74.

[18] S. Dampang, E. Durwanti, F. Destyorini, S.B. Kurniawan, S.R. Abdullah, M.F. Imron, Analysis of Optimum Temperature and Calcination Time in the Production of CaO Using Seashells Waste as CaCO3 Source, J. Ecolog. Eng. 22 (2021), 221-228.

29TH IRANIAN ORGANIC CHEMISTRY CONFERENCE
1_3 NOV, 2023
UNIVERSITY OF QOM, IRAN

Modification of thermal properties of polyglycidyl nitrate through copolymerization with ε-caprolactone

Asghar Bodaghi[*]
Department of Chemistry, Faculty of Science, University of Qom, P. O. Box: 37185-359, Qom, Iran, a.bodaghi1347@gmail.com

Abstract - A DAMPGN-co-PCL copolymer containing azido group was synthesized through ring-opening polymerization. Initially, diazido end-functionalized two-arm PGN, $(PGN)_2$-$(N_3)_2$, was synthesized by ROP of glycidyl nitrate monomers. Subsequently, DAMPGN-co-PCL was obtained from the copolymerization between diazido end-functionalized $(PGN)_2$-$(N_3)_2$ polymers and ε-caprolacton as monomer at presence stannous 2-ethylhexanoate ($Sn(Oct)_2$). This copolymer solves problems of PCL (lake of energy) and PGN (high Tg) and can act as a bonding agent, react with reactive plasticizer containing propargyl group. The FT-IR, ^{1}H NMR and GPC studies revealed that DAMPGN-co-PCL was successfully obtained. The thermal behavior of star polymer was investigated by thermogravimetric analysis (TGA) and derivative thermogravimetry. The results show that DAMPGN-co-PCL decomposed at two stages. The first stage is seen at 213°C which related to degradation of $–ONO_2$ group and second stage attributed to degradation of PCL group which is seen at 371°C. Copolymerization of polyglycidyl nitrate reduces the glass transition temperature from -38°C to -48.6°C.

1. Introduction

Poly (ε-caprolactone) (PCL) is one of the most important and widely studied degradable polymers with a history dating back to the very first synthetic polyesters in the 1930s. It is a saturated aliphatic polyester with hexanoate repeat units, and can be classed as semicrystalline with degrees of crystallinity up to 70% depending on weight average molecular weights (*M*w) typically ranging from 3,000 to 800,000 g.mol^{-1}. At higher molecular weights, crystallinity is reduced with increasing molecular weight - due to chain folding, such that at *M*w = 200,000 g.mol^{-1}, 33% crystallinity is observed [1]. PCL has a very low glass transition temperature and shows elastic behaviour at room temperature. In addition, relatively low melting temperatures, of around 60 °C, make PCL materials easy to fabricate or process into highly structured forms such as foams prepared in conjunction with super-critical CO2 [2]. PCL is highly soluble in a range of non-polar solvents and is well known to be soluble with a wide range of other polymers for effective blending [3, 4]. It has a low-melting point (approximately 60 °C); low melts viscosity, and is easy to process [5]. PCL has good water, oil, and chlorine resistance. The PCL chain is flexible and exhibits high elongation at break and low modulus. The elongation at break and tensile strength of PCL films have been reported to be between 450% and 1100% and 25 and 33 MPa, respectively [6]. The main drawback of PCL is its low melting point, which can be overcome by blending it with other polymers or by radiation cross-linking processes, which result in enhanced properties suitable for a wide range of applications [7]. PCL is used mainly in thermoplastic polyurethanes, resins for surface coatings, adhesives, and synthetic leather and fabrics [5].

The energetic binders are prepolymers containing energetic functional groups such as N_3, NO_2, ONO_2, and NF_2. These energetic binders improve energy contain and oxygen balance of the propellants. Since the energetic binders are important components propellant formulation, development of a new and high efficient energetic binder is very important.

PGN is one of the energetic polymers that are high energy output and good compatibility with high energetic oxidizers [8]. However, its poor thermal properties, high glass transition transition (Tg=-35°C) and weak mechanical properties, significantly restricts its application in solid propellants [9].

A good idea to improve the mechanical and thermal properties of PGN is preparation PGN co-polymers with binders such as HTPB [10] and polycaprolactone (PCL) that have good mechanical properties.

In this study, we synthesized a copolymer by means of ROP that has two azido pendant groups. So, the copolymer can act as a bonding aging; react with compounds containing the propargyl group (for example reactive plasticizer [11, 12]) and use in dual curing. This copolymer, on one side, solves the PGN binder problem (high glass transition temperature) and, on the other hand, resolves the PCL problem (lack of energy). Chemical structures of synthesized copolymers were confirmed by FT-IR and ^{1}HNMR spectroscopy and GPC.

2. Experimental

2-1. Materials and methods

ε-caprolactone (CL) (Aldrich), stannous 2-ethylhexanoate ($Sn(Oct)_2$) (Aldrich), 2, 2- bis (bromomethyl)-1, 3-propanediol (Aldrich), Epichlorohydrin (99%, Merck), $BF_3.OEt_2$ (50 %, Merck), Solvents, dichloromethane (CH_2Cl_2), dimethylformamide (DMF), ethanol and tetrahydrofuran (THF) were distilled over drying agents under nitrogen before use.

2.2. Synthesis of 2, 2-bis (azido methyl) propane-1, 3-diol (DAP)

2, 2-bis (bromomethyl) propane-1, 3-diol (25g, 95.5 mmol) were dissolved in 100 ml DMF. Under continuous stirring, sodium azide (25 g, 381 mmol) were added gradually. The reaction mixture was heated to 110 °C and refluxed for 24 h. After cooling to room temperature, the formed precipitate was filtered and washed with 20 ml DMF. 60 ml ethyl acetate was added to the filtrate and water was added until phase separation occurred. The mixture was extracted with ethyl acetate (50 ml×3) and the combined organic phases were washed once with 30 ml water. The organic phase was dried over Na_2SO_4 and evaporated. Solvent residues were removed by vacuum pump at elevated temperatures. The resulting (17.15 g, 80 %).

2.3. Synthesis of diazido end-functionalized poly (glycidyl nitrate) [(PGN)$_2$-(N$_3$)$_2$]

For the synthesis of (PGN) $_2$-$(N_3)_2$, 2, 2-bis (azido methyl) propane-1, 3-diol (DAP) (0.93 g, 0.005 mol) and $BF_3 \times OEt_2$ (1.7 mL, 0.014 mol) were added into a three-neck flask equipped with a magnetic stirrer and thermometer. This mixture was stirred for 1h under N_2 at (0–5) °C. A solution of glycidyl nitrate (30 g, 0.25mol) in CH_2Cl_2 (70 mL) was added dropwise to this reaction mixture; the duration of this process was over 5h. The reaction mixture stirred at (0–5) °C for 1h. Then, the reaction completed by adding saturated NaCl (50 mL) solution. The organic layer was washed with a saturated $NaHCO_3$ solution (50 mL×4), dried over Na_2SO_4, filtered and evaporated in vacuum to produce 23 g of light yellow liquid, with a yield of 75%.

2.4. Synthesis of DAMPGN-co-PCL.

For the synthesis of DAMPGN-co-PCL, 5 g (5 mmol) of DAMPGN with low molecular weight (*M*n = 1020 g/mol) was taken in a three-necked flask fitted with a thermometer and nitrogen inlet. 7.5g (65.8 mmol) ε-caprolactone was added into the reaction mixture. Then, 0.1 g of stannous 2-ethylhexanoate dissolved in 4mL of toluene and 1mL of it injected to the reaction mixture. Thereafter, the reaction was heated at 130 °C for 24 h. Then the reaction mixture was cooled to room temperature. The resulted product was isolated by dissolving in CH_2Cl_2 and washing with n-hexane. The isolated copolymer was dried over sodium sulfate, filtered, and the solvent evaporated off under vacuum to obtained 11.5g of DAMPGN-co-PCL (92% yield).

2.5. Characterization.

The IR spectra recorded on a Nicolet 800 spectrometer in the range 400–4000 cm^{-1}. ^1H NMR spectra recorded on a Bruker DPX-250 instrument operating at 500 MHz and using $CDCl_3$ as a solvent; chemical shifts were reported in δ (ppm) from TMS. Tg was measured by DSC (DSC200F3t-sensor/E, Perkin-Elmer). All tests were performed under a nitrogen atmosphere (20 mL/min) at a heating rate of 10 K/min at the temperature ranging from -100 to 308C. Thermogravimetric analysis (TGA, SDT Q600 V20.9 Build 20) was performed at a heating rate of 10 K/min from 25–500 °C with a argon flow rate of 50 mL/min. Derivative thermal gravimetry (DTG) data were obtained from TGA. Gel Permeation Chromatography (GPC) was conducted using 10 µm PL gel columns using a GPC Agilent 1100 (USA) with refractive index detector using an Agilent PLgel 5 µm mixed-C 300 mm × 7.5 mm column, THF was used as solvent and injected at 30 °C and the rate of 1 mm/min and calibrated by polystyrene as standard.

3. Results and discussion

3.1. Synthesis of diazido end-functionalized poly (glycidyl nitrate) [(PGN)$_2$-(N$_3$)$_2$]

First, 2, 2-bis (bromomethyl) propane-1, 3-diol is transformed to 2, 2-bis (azido methyl) propane-1, 3-diol (DAP) by azidation reactions with sodium azide in DMF at 55 °C. Then, 2, 2-bis (azidomethyl)-1, 3-propanediol with two hydroxyl groups was chosen as the initiator in order to produce diazidomethyl poly (glicidyl nitrate) as seen in Scheme 1. The molar ratios of [GN]/ [2, 2-bis (azidomethyl)-1, 3-propanediol] was taken as 20/1. At least, DAPGN was selected as the initiator in order to preparation of DAPGN-co-PCL. The molar ratio of [CL]/ [DAPGN] was as 17/1. Table 1 summarizes the conditions and results of polymerization of GLYN monomers with 2, 2- bis (azidomethyl)-1, 3-propanediol and ε-caprolacton with DAMPGN to produce DAMPGN-co-PCL.

Table 1. Conditions and results of the DAMPGN [a] and DAMPGN-co-PCL [b].

No	polymer	Temp. (°C)	Conversion (%)	$M_{n\ theo}$ (g/mol)	$M_{n\ H\ NMR}$ (g/mol)	$M_{n\cdot exp}$ (g/mol)	M_w/M_n
1	DAMPGN	0-5	75	-	1376	1020	1.63
2	DAMPGN-co-PCL	130	92	2803	2844	2457	2.75

[a] Prepared by ROP of GN. $[GN]_0$ = 0.25 mol (in bulk), [I]/ [GN] = 1/50.

[b] Prepared by ROP of ε-CL. $[\varepsilon\text{-CL}]_0$ = 0.066 mol (in bulk), [I]/ [ε-CL] = 1/17.

The ^{1}H NMR spectral analyses provided a facile method to calculate the degree of polymerization (DPn) of each polymer arm and the molecular weights ($M_{n\ H\ NMR}$) of the PGN polymers. The DPn of PGN for per polymer arm was found as 5. The DPn for a polymer arm was calculated by comparing the integral ratio of -CH_2-ONO_2 (from PGN) protons in the repeating polymer units to those of terminal -CH_2-N_3 protons based on ^{1}H NMR spectra. $M_{n\ H\ NMR}$ of DAMPGN and DPn of polymer arm could be calculated using the following formulas:

$M_{n\ H\ NMR} = DPn \times M_m \times 2 + M_I$

$DPn = I_P/I_I$

where, DPn is the degree of polymerization of each polymer arm; I_P represents the integral values of the signals of -CH_2- protons in PGN backbone; I_I represents the integral values of the signals of -CH_2- protons in the initiator unit at the DAP; $M_{n\ HNMR}$ is the ^{1}H NMR molecular weight of each polymer, Mm is the molecular weight of GN monomer, M_I represents the molecular weight of initiator unit at the terminal group of DAP. The same calculation carried out for PCL section. The theoretical number average molecular weights ($M_{n\ theo}$) of the resulting DAMPGN-co-PCL was calculated using the following equation:

$M_{n\ theo} = [M]_0/[I]_0 \times M_m \times Conversion + M_I$

Where $[M]_0$ and $[I]_0$ are the initial molar concentrations of monomer (ε-CL) and initiator (DAMPGN); M_m and M_I are the molecular weights of the monomer (ε-CL) and the initiator (DAMPGN). There is a relatively good agreement between the molecular weight distributions (Mw/Mn) and the $M_{n\ theo}$, $M_{n\ H\ NMR}$, and $M_{n\ GPC}$ of the polymer, which are summarized in Table 1.

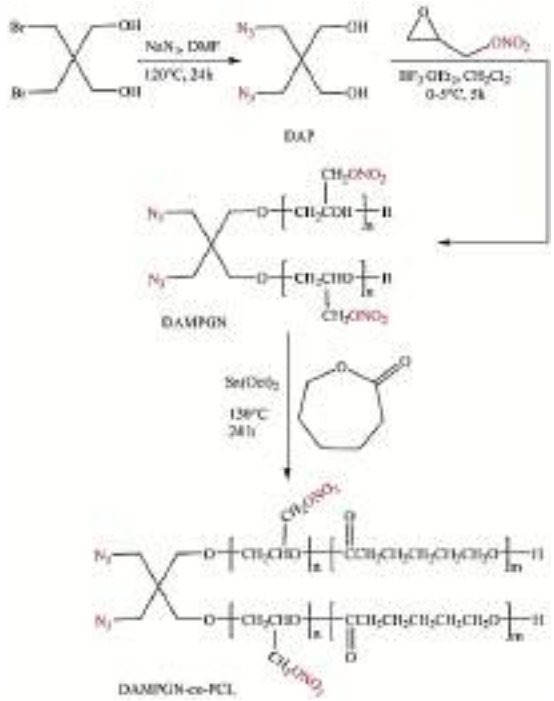

Scheme 1. Synthesis route of DAMPGN-co-PCL

Structural characterization of the DAMPGN and DAMPGN-co-PCL were confirmed by FT-IR and ^{1}H NMR spectroscopic analyses. The FT-IR spectrum of DAMPGN and DAMPGN-co-PCL are shown in Figure 1. At the FT-IR spectrum of DAMPGN, the absorption peaks at 3440, 2105, 1634, 12281, 1117 and 857 cm^{-1} are due to OH, -N_3, NO_2 stretching asymmetric, NO_2 stretching symmetric and O-N stretching vibration respectively. The characteristic ester carbonyl group signal of the PCL section was appeared at 1724cm^{-1} as shown in Figure 1.

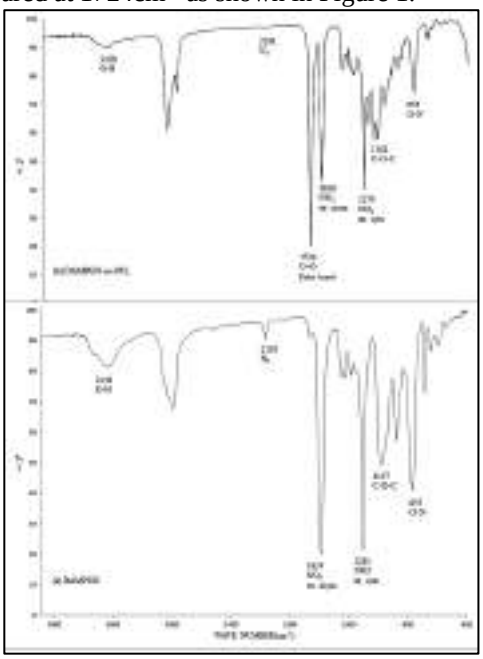

Figure 1. . FT-IR spectra of (a) DAMPGN (b) DAMPGN-co-PCL.

From the ^{1}H NMR spectrum of DAMPGN-co-PCL indicated in Figure 2, the typical signal of the N_3- CH_2- and -CH_2-O protons of the terminal group from the initiator (2,2- bis (azidomethyl)-1,3-propanediol), were clearly detected at 3.41 ppm (1 protons) and at 4.15 ppm (2 protons), respectively. The peaks of -CH_2O- and -CH_2- protons of PCL backbone were also observed at δ4.06-4.03 and δ2.31-2.28, δ1.67-1.60, δ1.40-1.34 respectively. The peak of terminal CH_2 of PCL section (CH_2-OH) appeared at δ3.53. The peaks of –CH_2-ONO_2, O-CH_2 and C-H proton at the chiral center protons of PGN section were observed at δ4.60-4.51 and δ3.77- 3.61 respectively. These evidences indicate successful synthesis of DAMPGN-co-PCL.

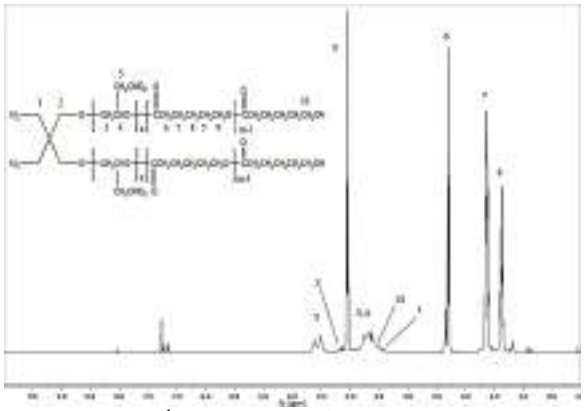

Figure 2. ^{1}H NMR spectra of DAMPGN-co-PCL.

3.2. Thermal Decomposition of DAMPGN-co-PCL

Figure 3 shows the DSC thermograms of the DAMPGN and DAMPGN-co-PCL. The glass-transition temperature (Tg's) of synthesized copolymer is listed in Table 2. As shown in Table 2, the glass transition temperature of the DAMPGN and DAMPGN-co-PCL were -38.0°C, -48.6°C respectively. As shown the copolymerization of DAMPGN with PCL decrease Tg of DAMPGN.

The overall thermal behaviors and decomposition temperatures of copolymer synthesized are summarized in Table 2.

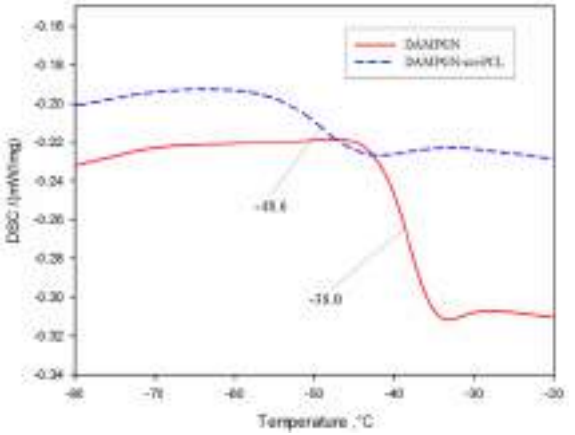

Figure 3. DSC thermogram of DAMPGN and DAMPGN-co-PCL.

Table 2. Thermal properties and decomposition temperatures of polymers

Polymer	T_g(°C)	T_m(°C)	T_{in}[a](°C)	T_{max}[b](°C)
DAMPGN	-38.0	-	175	218
DAMPGN-co-PCL	-48.6	55.5	313	380

[a] The initial decomposition temperature.
[b] The temperature corresponding to the maximum rate weight loss.

Figure 4 shows the DSC thermogram of DAMPGN-co-PCL. The DSC thermogram of the DAMPGN-co-PCL is carried out under argon atmosphere at heating rate of 10˚C.min^{-1} from room temperature to 450˚C. The DSC thermogram of DAMPGN-co-PCL has three peaks. The endothermic peak is seen at around 55.5˚C is attributed to melting point of copolymer, the second peak is exothermic which is seen at 218˚C is attributed to decomposition of nitrato group. The energy liberated at this stage is 559.8 J.g^{-1}. The third peak is endothermic, which is seen at 380°C and related to degradation of PCL with heat absorption which is 135.6J.g^{-1}.

The experimental evidence has been established that thermal decomposition of PCL leads to formation of H_2O, CO_2, 5-hexenoic acid and ε-caprolactone (cyclic monomer) as result of an unzipping depolymerization process [13-15]. So, the broad endothermic peak shown at 380˚C, is related to dehydration reaction. At this temperature, the caprolactone portion is degraded and the caprolactone ring is again formed by releasing the water molecule [16].

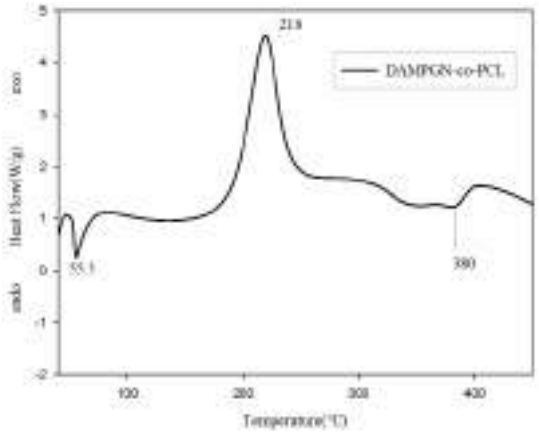

Figure 4. DSC thermogram of DAMPGN-co-PCL.

Figures 5, 6 shows the thermal curves of the DAPGN and DAMPGN-co-PCL recorded at 10°C/min. In the TGA curve of DAMPGN-co-PCL, two specific weight loss steps were observed. The first step started at 175°C, ended at 250°C, and corresponded to the decomposition of $–ONO_2$. The second stage involved the decomposition of the PCL section between 275 and 425°C. These two weight loss stages are clearly depicted in the derivative thermogram (figure 6).

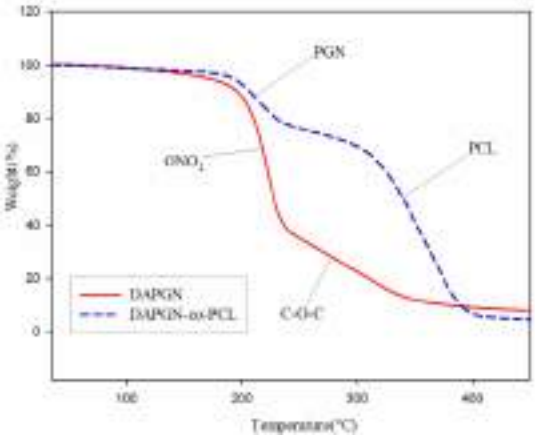

Figure 5. TGA curve of the DAMPGN-co-PCL.

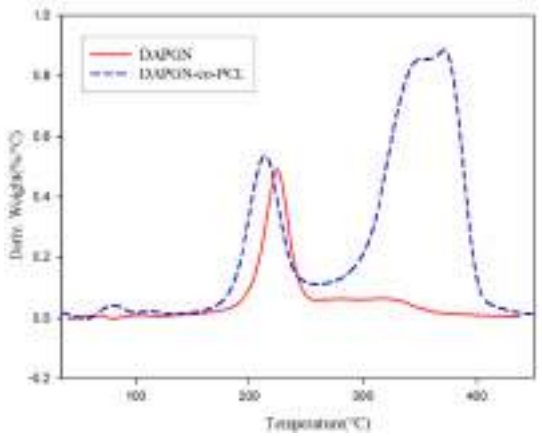

Figure 6. DTG of the DAMPGN-co-PCL.

Conclusion

We synthesized DAMPGN-co-PCL copolymer containing azide (N_3) group by using controlled/living ring opening polymerization. This copolymer can act as a bonding aging; react with compounds containing the propargylic group (for example reactive plasticizer) and use in dual curing. The copolymer, on one side, solves the PGN binder problem (low Tg) and, on the other hand, resolves the PCL problem (Lack of energy). Their structures were characterized by spectral and GPC measurements. The thermal behaviors of the synthesized polymer were investigated by differential scanning calorimetry and thermogravimetric analysis (DSC/TGA). The energetic copolymer decomposes at two stages. The first stage attributed to decomposition of $–ONO_2$ group and the second stage related to decomposition of PCL arms. The peaks of each stage were at 218 and 380°C. The melting point of copolymer is 55.5°C.

References

[1] M. J. Jenkins, K. L.Harrison, The effect of molecular weight on the crystallization kinetics of polycaprolactone. Polym Advan Technol. 17 (2006) 474-478.

[2] M. Karimi, M. Heuchel, T. Weigel, M. Schossig, D. Hofmann, A. Lendlein, Formation and size distribution of pores in poly(ε-caprolactone) foams prepared by pressure quenching using supercritical CO_2. J Supercrit Fluid. 61 (2012) 175-190.

[3] L. S. Nair, C. T. Laurencin, Biodegradable polymers as biomaterials. Progr Polym Sci. 32 (2007**)** 762-798.

[4] B. D. Ulery, L. S. Nair, C. T. Laurencin, Biomedical applications of biodegradable polymers. J Polym Sci Part B Polym Phys. 49 (2011**)** 832- 864.

[5] M. Funabashi, F. Ninomiya, M. Kunioka, Biodegradation of polycaprolactone powders pro- posed as reference test materials for international standard of biodegradation evaluation method. J. Polym. Environ. 15 (2007) 7-17.

[6] M.F.,Koening, S.J. Huang, Biodegradable blends and composites of polycaprolactone and starch derivatives. Polymer. 36 (1995) 1877- 1882.

[7] S. Sinha Ray, M. Bousmina, Biodegradable polymers and their layered silicate nanocompo- sites: in greening the 21st century materials world. Prog. Mater. Sci. 50 (2005) 962- 1079.

[8] M. B. Talawar, R. Sivabalan, T. Mukundan, H. Muthurajan, A. K. Sikder, B. R. Gandhe, R. A. Subhananda, Environmentally Compatible Next Generation Green Energetic Materials (GEMs). J. Hazard. Mater. 161 (2009) 589–607.

[9] A.Provatas, Characterisation and Polymerisation Studies of Energetic Binders. Publisher: Melbourne, Vic. : DSTO Aeronautical and Maritime Research Laboratory, 2001.

[10] M. Ghorbani, Y. Bayat, Synthesis and Characterization of Hydroxyl- terminated Triblock Copolymer of Poly(glycidyl nitrateblock- butadiene-block-glycidyl nitrate) as Potential Energetic Binder. Polymer Sci. B. 57 (2015) 654–658.

[11] A. Bodaghi, M. Shahidzadeh, Synthesis and Characterization of New PGN Based Reactive Oligomeric Plasticizers for Glycidyl Azide Polymer. Propellants Explos. Pyrotech. 43 (2018) 364-370.

[12] M. Ma, Y. Shen, Y. Kwon, C. Chung, J. S. Kim, Reactive Energetic Plasticizers for Energetic Polyurethane Binders Prepared via Simultaneous Huisgen Azide-Alkyne Cycloaddition and Polyurethane Reaction. Propellants Explos. Pyrotech. 41 (2016) 746-756.

[13] C. Vogel, H. W. Siesler, Thermal Degradation of Poly(e-caprolactone), Poly(L-lactic acid) and their Blends with Poly(3-hydroxy-butyrate) Studied by TGA/FT-IR Spectroscopy. Macromol. Symp. 265 (2008) 183–194.

[14] O. Persenaire, M. Alexandre, P. Dege´e, P. Dubois, Mechanisms and Kinetics of Thermal Degradation of Poly(ε-caprolactone). Biomacromolecules, 2 (2001) 288-294.

[15] Y. Aoyagi, K. Yamashita, Y. Doi, Thermal degradation of poly[(*R*)-3-hydroxybutyrate], poly[ε-caprolactone], and poly[(*S*)-lactide]. Poly. Deg. And Stab. 76 (2002) 5359.

[16] G. klančnik, J. Medved, P. Mrvar, Differential thermal analysis (DTA) and differential scanning calorimetry (DSC) as a method of material investigation. RMZ – Materials and Geoenvironment. 57 (2010) 127–142.

29TH IRANIAN ORGANIC CHEMISTRY CONFERENCE
1_3 NOV, 2023
UNIVERSITY OF QOM, IRAN

Fe_3O_4@saponin/Cd a novel magnetic nano-catalyst for the synthesis of β-aminoketone derivatives.

*Hossein Anaraki-Ardakani**
Department of Chemistry, Mahshahr Branch, Islamic Azad University, Mahshahr, Iran,
hosseinanaraki@yahoo.com

Abstract - A novel recyclable Magnetic core-shell nanoparticles Fe_3O_4@saponin/Cd was synthesis by the combination of nano-Fe_3O_4@saponin with cadmium acetate. It was found that the catalyst was active for the synthesis of β-aminoketone derivatives via one-pot three-component Mannich-type reactions of ketones, aromatic aldehydes, aromatic amines under eco-friendly solvent, at room temperature. Furthermore, this catalyst can be easily recovered magnetically and can be reused for other runs without any reduction in the activity.

1. Introduction

The heterogeneous catalysts made out of organic and inorganic materials have recently been introduced by researchers who possess the advantages of both homogeneous and heterogeneous catalysts. Furthermore, the use of MNPs as support in heterogeneous catalysis is a growing field of research. In this area, MNPs appear as an ultimate nanosupport due to their ease of recovery [1]. Fe_3O_4 NPs for their strong magnetic properties, high chemical stability, being abundant, effortless preparation via co-precipitation, and low toxicity are the most common MNPs, have been more extensively studied as the core magnetic support by researchers [2]. Quillaja Saponaria (sapogenin) is a huge evergreen tree, which is native to China, Peru, and the arid zones of Chile. Leaves of this tree are shiny, leathery, and its' bark is thick [8]. Its bark is rich in saponins, plant glycosides, which are widely distributed in the plant and marine animal kingdoms. Chemically, saponins are steroids, or triterpene glycosides, possessing a wide variety of activities, which are cancer-related, anti-inflammatory, anti-allergic, and anti-viral activities with effects on the physiology of the cardiac, and blood systems, as well as molluscicidal activities [4]. The Quillaja saponaria's bark is rich in industrial triterpenoid saponin. Saponin is the general name of this chemical and about 20 to 35 percent of the chemical is composed of sapogenin. Saponin is mainly cellulose, especially the hydroxyl groups in cellulose, which provide active sites for numerous attractive chemical modifications [5]. Therefore cellulose in saponin can be used as an efficient supporting agent for the synthesis of various heterogeneous catalysts [6]. Hence, we report Fe_3O_4@saponin/Cd as a strong and attractive biological heterogeneous nano-catalyst for the synthesis of β-amino ketone derivatives by a three-component reaction of ketones, aromatic aldehydes, and aromatic amines under mild reaction conditions.

2. Results and discussion

Nano-Fe3O4@saponin/Cd was synthesized within two steps. Firstly, nano-Fe3O4 was synthesized by co-precipitation of Fe^{2+} and Fe^{3+} ions, and then it was mixed with saponin. Finally, it was used as a magnetic support to bond cadmium **(Scheme 1)**

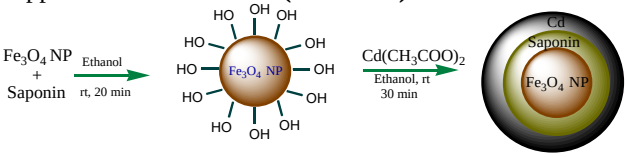

Scheme 1. Preparation of nano-Fe_3O_4@saponin/Cd.

The magnetically heterogeneous nano-catalyst, Fe3O4@saponin/Cd, is characterized by FT-IR spectroscopy, VSM, EDS analysis, XRD, SEM, ICP, BET and TGA.
The catalytic activity of nano-Fe_3O_4@saponin/Cd was investigated for synthesis of β-aminoketones derivatives via one-pot three-component Mannich reaction of aromatic amines, aromatic aldehydes and ketones in ethanol at room temperature. (Scheme 2).

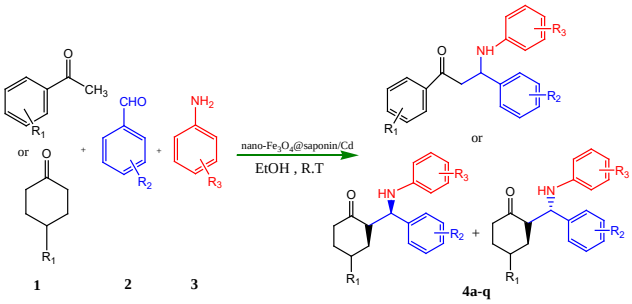

Scheme 2. One-pot Mannich reaction of ketones, aromatic aldehydes and aromatic amines catalyzed by nano-Fe3O4@saponin/Cd at room temperature.

Table1: optimization of condition for condensation of acetophenone (1.1mmol); aniline (1 mmol) and increasing the amount of catalyst from 0.01 g to 0.08 g

Entry	Catalyst	Temp(°C) /Solvent	Time(h)	Weight(g)	Isolated yield[a](%)
1	no catalyst	r.t /EtOH	12	-	trace
2	nano-Fe_3O_4	r.t /EtOH	7	0.09	60
3	nano-Fe_3O_4@saponin	r.t /EtOH	3	0.09	48
4	nano-Fe_3O_4@saponin/Cd	r.t/EtOH.	3	0.08	93
5	nano-Fe_3O_4@saponin/Cd	r.t/ MeOH	3	0.08	65
6	nano-Fe_3O_4@saponin/Cd	r.t /$CHCl_3$	3	0.08	40
7	nano-Fe_3O_4@saponin/Cd	r.t /Xylene	3	0.08	35
8	nano-Fe_3O_4@saponin/Cd	r.t/ DMF	3	0.08	55
9	nano-Fe_3O_4@saponin/Cd	120 ^{0}C/ None	3	0.08	65
10	nano-Fe_3O_4@saponin/Cd	r.t/ CH_3CN	3	0/08	70
''	nano-Fe_3O_4@saponin/Cd	r.t/ Toluene	3	0.08	trace
12	nano-Fe_3O_4@saponin/Cd	r.t/H_2O	3	0.08	trace
13	nano-Fe_3O_4@saponin/Cd	r.t./EtOH	7	0.01	53
14	nano-Fe_3O_4@saponin/Cd	r.t./EtOH	7	0.02	61
15	nano-Fe_3O_4@saponin/Cd	r.t./EtOH	7	0.03	68
16	nano-Fe_3O_4@saponin/Cd	r.t./EtOH	6	0.04	73
17	nano-Fe_3O_4@saponin/Cd	r.t./EtOH	6	0.05	80
18	nano-Fe_3O_4@saponin/Cd	r.t./EtOH	5	0.06	86
19	nano-Fe_3O_4@saponin/Cd	r.t./EtOH	5	0.07	91
20	nano-Fe_3O_4@saponin/Cd	r.t./EtOH	3	0.08	93
21	nano-Fe_3O_4@saponin/Cd	r.t./EtOH	3	0.09	93
22	nano-Fe_3O_4@saponin/Cd	r.t./EtOH	3	0.1	90
23	nano-Fe_3O_4@saponin/Cd	40 /EtOH	3	0.08	93
24	nano-Fe_3O_4@saponin/Cd	60 /Et OH	2.30	0.08	93
25	nano-Fe_3O_4@saponin/Cd	70/EtOH	2.10	0.08	86
26	nano-Fe_3O_4@saponin/Cd	Ref/EtOH	1.30	0.08	80

benzaldehyde (1 mmol). [a]Isolated yields

Firstly, for the optimization of the reaction conditions, the model reaction was carried out by using acetophenone, aniline, and benzaldehyde in the Presence of nano-Fe_3O_4, nano-Fe_3O_4@saponin, and nano-Fe_3O_4@saponin/Cd as catalyst. It was found that nano-Fe_3O_4@saponin/Cd was the most efficient catalyst for the reaction in ethanol at ambient temperature. (Table 2, entry 4). However, only a trace amount of the product was formed in the absence of catalyst (Table 2, entry 1). To improve the yield of the target product, we carried out the test reaction in the presence of various solvents and results are presented in Table 2 As shown in table 2, Ethanol has been found to be the best solvent among other solvents (Toluene, xylene, CH_3CN, MeOH, $CHCl_3$, DMF and H2O). Then, the optimization of nano-catalyst amounts was carried out in the model study by using different amounts of the nano-Fe3O4@saponin/Cd in ethanol at room temperature The higher yield was obtained by (entry 13-21). However, a further increase in catalyst amount from 0.08g to 0.1 g did not significantly increase the yield of the product. Hence, the optimum concentration of nano- Fe_3O4@saponin/Cd was chosen 0.08 g in the model reaction (entry 20). We also investigated the reaction temperature and found out that when the reaction temperature was increased no improved the amount of yield. (Entry 23-26).

In order to demonstrate the effectiveness of this method and to study the scope and generality of the reaction various ketones, aromatic amines and aromatic aldehydes were examined and the results are summarized in Table 2.

Compounds **4n-q** were new and their structures were deduced by elemental and spectral analysis. Other compounds (**4a-m**) were known and their structures were deduced by comparison of melting points and spectral data with authentic samples.

4. Conclusions

In conclusion, we have described the characterization and preparation of nano-Fe3O4@saponin/Cd as a novel core-shell magnetic heterogeneous catalyst in good yields. The catalytic activity of this catalyst was examined in the synthesis of β-aminoketones derivatives through the one-pot three-component reaction of aromatic aldehydes, aromatic amine, and

Reusability of this catalyst are from other advantages of the described protocol.

Table 2. Synthesis of β-aminoketone derivatives by nano-Fe_3O_4@saponin/Cd

ntry	ketone	R_2	R_3	Time (h)	Yield (%)	anti/syn	mp. (◦C)	lit. mp. (◦C)
4a	cyclohexanone	1-naphthyl	H	1	99	99/1	170-172	171-173 [35]
4b	cyclohexanone	2-naphthyl	H	1	99	99/1	127-128	129-131 [36]
4c	cyclohexanone	1-naphthyl	4-CH_3	1.10	94	97/3	135-137	137-139 [37]
4d	cyclohexanone	4-Br	H	50(min)	93	98/2	109-111	109-110 [38]
4e	cyclohexanone	4-Cl	4-CH_3	45(min)	95	98/2	119-121	119-120 [39]
4f	cyclohexanone	3-NO_2	H	1.30	90	93/7	160-162	163-165 [40]
4g	cyclohexanone	4-F	H	1.20	91	82/18	118-120	-
4h	4-methylcyclohexanone	H	H	55(min)	99	95/5	131-133	132-135 [35]
4i	4-methylcyclohexanone	1-naphthyl	H	1	97	97/3	168-170	169-172 [35]
4j	4-methylcyclohexanone	2-naphthyl	H	1	98	99/1	174-176	174-178 [35]
4k	4-methylcyclohexanone	2-Cl	H	1.10	83	99/1	144-146	146-147 [35]
4l	Acetophenone	H	H	3	93	-	166-168	168-169 [41]
4m	Acetophenone	4-OCH_3	4-CH_3	4	89	-	161-162	160-161 [42]
4n	Acetophenone	H	4-Br	3	97	-	177-179	[This work]
4o	Acetophenone	4-Cl	4-Br	3.20	91	-	171-173	[This work]
4p	Acetophenone	4-CH_3	4-Br	3.30	90	-	175-177	[This work]
4q	Acetophenone	4-CH_3	4-NO_2	3.50	87	-	63–165	[This work]

Reaction conditions: ketone (1.1 mmol), amine (1 mmol), aldehyde (1mmol); catalyst (0.08 g).

All reactions were obtained in ethanol at room temperature

4. References

[1] D. Astruc, F. Lu, J.R. Aranzaes, Angew. Chem. Int. Ed., 44 (2005) 7852–7872.

[2] X. Zheng, S. Luo, L. Zhang and J.-P. Cheng, Green Chem., 11 (2009) 455-458.

[3] A.Y. Leung, Encyclopedia of Common Natural Ingredients Used in Foods, Drugs, and Cosmetics, (NY: Weily, 1980).

[4] S. Balakrishnan, A. Rajendran, R. Kulandaivelu, S. Narayanan, T. S. Nellaiappan, Journal of the Australian Ceramic Society., 55 (2019) 953-967.

[5] A. Moslemizadeh, S. Khezerloo-ye Aghdam, Kh. Shahbazi, S. Zendehboudi, Journal of Molecular Liquids., 247 (2017) 269-280.

[6] A. Shaabani and A. Maleki, Applied Catalysis A: General., 331 (2007) 149-151.

Green synthesis of silver nanoparticles using aqueous extract of *Falcaria Vulgaris*

Nadia Beyzaei[1], *Nasrin Mollania*[1]*, *Rasoul Esmaeely Neisiany*[2], *Somayeh Dolatabadi*[1]

[1]*Department of Biology, Faculty of Basic Sciences, Hakim Sabzevari University, Sabzevar, Iran, beyzaei.nadia@yahoo.com, n.mollania@hsu.ac.ir*
[2] *Department of Materials and Polymer Engineering, Faculty of Engineering, Hakim Sabzevari University, Sabzevar, Iran*

Abstract
In recent times, nanotechnology and nanomaterials production has become a rapidly expanding area with various applications in the field of biomedical science. Silver nanoparticles (AgNPs) are a type of nanomaterial that possess antibacterial, antifungal, and antiviral properties. The goal of this study is to synthesize silver nanoparticles using *Falcaria vulgaris* extract and optimize the synthesis conditions. Specific parameters such as pH, biomass, temperature, and reaction time were evaluated for this purpose.
The produced nanoparticles have been studied using various techniques. The UV-Vis peak at 414 nm indicated the presence of silver nanoparticles. The formation of silver nanoparticles with a size of approximately 10 nm was confirmed by the dynamic light scattering (DLS) method. The study found that the mentioned plant extract could be a safe, economical, and eco-friendly substitute for dangerous procedures in the chemical synthesis of this nanoparticle.

Keywords: Silver nanoparticle, Aqueous extract of *Falcaria Vulgaris*, Dynamic light scattering

1. Introduction

Nanotechnology has received the attention of the world due to its rapid development in the fields of science, industry, health, and biomedicine. In nanotechnology, the nanoparticle synthesis between 1 and 100 nanometres has various advantages due to their unique physical and chemical properties (1-2).
Generally, there are two methods (bottom to top and top to bottom) for the synthesis of nanoparticles. In a top-down approach, scientists try to formulate nanoparticles using larger particles to guide their assembly. A bottom-up approach is a process that starts at the molecular level and moves up to a larger and more complex system while maintaining close control of molecular structures (3).

Considering the wide applications of nanoparticles in various fields of industry, however, synthesis of famous metal nanoparticles including silver, gold, copper, and magnetic nanoparticles by classic and routine chemical processes is commonly toxic, expensive, and non-benign for the environment (4).

Among the synthesis of nanoparticles, silver nanoparticles are one of the most popular. Silver nanoparticles contain 20 to 15,000 silver atoms whose diameter is less than one hundred manometers. these nanoparticles due to the large surface-to-volume ratio, have significant antimicrobial and antioxidant activity. Furthermore, silver nanoparticles are cheap and show low cytotoxicity. Silver has been used since ancient times, and silver has been proven to be harmless to human cells in small amounts (5)
Nanomaterials are produced through physical, chemical, or biological methods. Since, environmental pollution could result from physical and chemical synthesis, "green synthesis" through biological methods using plant extracts, bacteria, or fungi was more valuable due to its eco-friendliness and non-toxicity. With this method, there is no need for the application of toxic chemicals, high pressure, energy, or extreme temperatures (6, 7).
Medicinal plants have a wide range of bioactive compounds such as alkaloids, phenolic, and tannins. The presence of these bioactive or biological compounds in plants increases the rate of conversion of metal ions into nanoparticles. Plant parts such as fruits, leaves, stems, seeds, flowers, bark, roots, and rhizomes are used to produce nanoparticles (8)
Falcaria Vulgaris plant contains many antioxidant compounds, all of which play an important role in reducing of metal ions and converting them into Metal atoms in nano-dimensions as well as stabilizing synthesized nanoparticles.

2. Material and methods

2.1 Material

AgNO3 silver nitrate was obtained from Sigma-Aldrich Chemicals. Deionized water was used during the reaction. Chloric acid and soda from Merck were used to adjust the pH of the solutions. Falcaria vulgaris plant was collected from Bowanat City, Fars province.

2.2 Preparation of aqueous extract

Plant samples were collected in the spring and washed with deionized water to remove dust. Then fresh leaves were cut into small pieces and leaves (5g) were added to an Erlenmeyer flask containing 50 ml of deionized water at 80°C. After 30 minutes, the mixture was filtered.

2.3 Synthesis of silver nanoparticles with *Falcaria vulgaris* extract

For AgNP production, the plant extract was combined with silver nitrate. For optimization of AgNPs synthesis, the various parameters were examined. In order to determine the effective salt concentration, the supernatant was initially supplemented with various concentrations of silver nitrate (1mM-5mM). The solution was then left in the dark condition for 140 minutes while being stirred at 180 rpm. The medium color was changed from yellow to brown, indicating the silver reduction and formation of the nanoparticles. Then, the absorption range of 350-650 nm was measured using a UV-visible spectrophotometer.

To determine the optimal temperature, the solution underwent heating to 20°, 45°, and 60 °C for 140 minutes, and the amount of biosynthesis was measured using the UV-Vis method. Throughout the experiment, all parameters such as pH, extract, and time were kept constant to investigate the effect of temperature on the biosynthesis of AgNPs.

The initial pH influence of the supernatant was studied in the synthesis of AgNPs in acidic, neutral, and basic mediums. Furthermore, biosynthesis of nanoparticles was performed at different incubation time.

After optimization of nanoparticle amount, AgNPs were suspended in deionized ultra-pure water and hydrodynamic particle size were determined by measuring the DLS technique.

3. Result and Discussion

The extract showed the best result in 1.8 mM concentration of silver nitrate after 140 min incubation, by brownish suspension formation. These results indicated the ability of plant metabolites to reduce colorless silver anion to elemental AgNPs.

It was found that changes in temperature greatly affected the rate of NPs biosynthesis. As results showed, the optimum temperature for the synthesis of AgNPs was 60 °C.

Since there were probably significant physicochemical interactions between silver ions and different functional groups on the plant extract metabolites. Therefore, the pH of the extract would be a strongly affecting parameter in the biosynthesis process. Fig. 1 showed that optimum nanoparticle synthesis is achieved at pH 10, resulting in nanoparticles with the smallest size distribution.

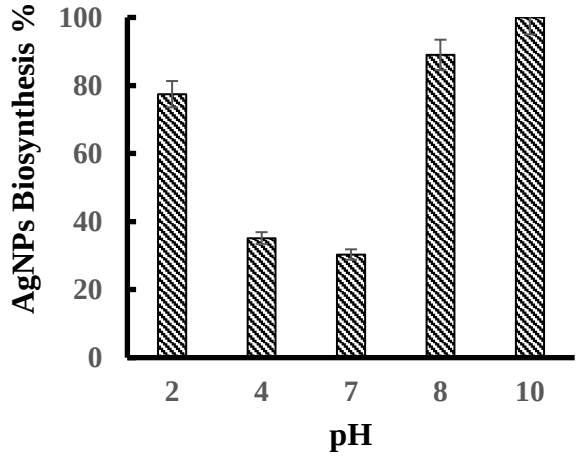

Fig. 1: The effect of pH on nanoparticle biosynthesis

The absorption peak in optimum condition observed at 414 nm confirms the formation of silver nanoparticles (Fig. 2).

Fig. 3 shows the DLS pattern of the biosynthesized AgNPs using *Falcaria vulgaris* aqueous extract. The histogram analysis presented that the average size of synthesized nanoparticles was 10 nm.

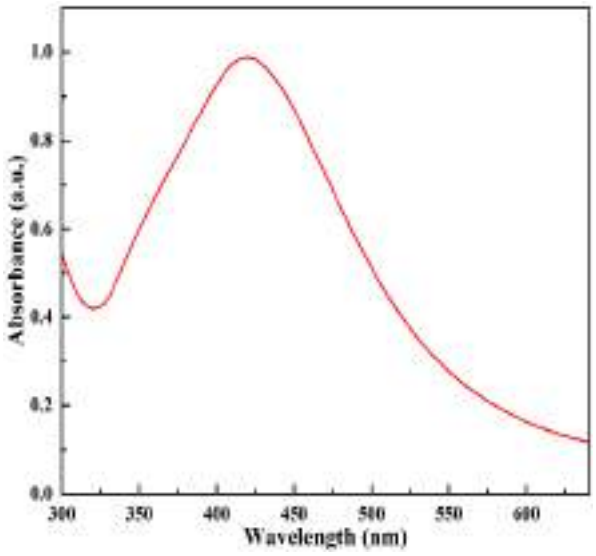

Fig. 2. UV-visible spectra of synthesized Ag nanoparticles

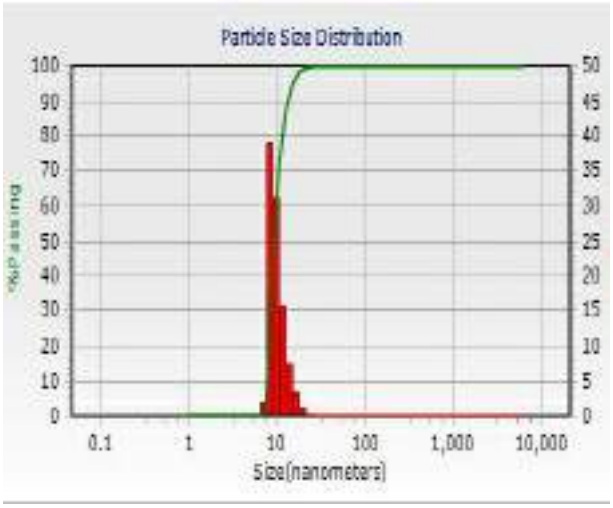

Fig. 3. Particle size distribution of synthesized silver nanoparticles by DLS histogram analysis

4. Conclusion

Based on the aforementioned studies, it is evident that *Falcaria vulgaris* plant possesses numerous medicinal properties and can serve as a viable option for producing nanoparticles. Notably, nanoparticle production by the plants was cost-effective, low-risk, and eco-friendly (9).

5. References

1. Yin IX, Zhang J, Zhao IS, Mei ML, Li Q, Chu CH. The antibacterial mechanism of silver nanoparticles and its application in dentistry. International journal of nanomedicine. 2020:2555-62.
2. Mirda E, Idroes R, Khairan K, Tallei TE, Ramli M, Earlia N, et al. Synthesis of chitosan-silver nanoparticle composite spheres and their antimicrobial activities. Polymers. 2021;13(22):3990.
3. Ramya M, Subapriya MS. Green synthesis of silver nanoparticles. Int J Pharm Med Biol Sci. 2012;1(1):54-61.
4. Barot T, Rawtani D, Kulkarni P. Nanotechnology-based materials as emerging trends for dental applications. Reviews on Advanced Materials Science. 2021;60(1):173-89.
5. Yazdanian M, Rostamzadeh P, Rahbar M, Alam M, Abbasi K, Tahmasebi E, et al. The potential application of green-synthesized metal nanoparticles in dentistry: a comprehensive review. Bioinorganic Chemistry and Applications. 2022;2022.
6. Awad MA, Mekhamer W, Merghani NM, Hendi AA, Ortashi KM, Al-Abbas F, Eisa NE. Green synthesis, characterization, and antibacterial activity of silver/polystyrene nanocomposite. Journal of Nanomaterials. 2015;2015:5-.
7. Yadav J, Tangade P, Jain A, Agrahari P, Chaudhary V. Dental herbs: Ethomedicinal plants in dentistry. 2021.
8. Habeeb Rahuman HB, Dhandapani R, Narayanan S, Palanivel V, Paramasivam R, Subbarayalu R, et al. Medicinal plants mediated the green synthesis of silver nanoparticles and their biomedical applications. IET nanobiotechnology. 2022;16(4):115-44.
9. Mohammadi SS, Ghasemi N, Ramezani M, Khaghani S. Biosynthesis of silver nanoparticles using the Falcaria Vulgaris (Alisma Plantago-Aquatica L.) extract and optimum synthesis. Chemical Methodologies. 2021;5(4):296-307.

29TH IRANIAN ORGANIC CHEMISTRY CONFERENCE
1_3 NOV, 2023
UNIVERSITY OF QOM, IRAN

Origins of the Endo Selectivities in Intramolecular Hetero Diels–Alder Cycloadditions of Benzylidenepyrazoles

*Leyla Mohammadkhania, Majid M. Heravi * and Maryam Anafcheh **

Department of Chemistry, Faculty of Chemistry, Alzahra University, Tehran, Iran, mmh1331@yahoo.com, m.anafcheh@alzahra.ac.ir

Abstract - In this article, we present a study of the endo and exo stereoselectivities of intramolecular hetero Diels−Alder cycloaddition reactions of benzylidenepyrazoles using density functional theory (DFT) calculations. Specifically, we sought to investigate the reasons why the endo cycloadduct with the cis-configured isomer is preferred out that observed experimentally. Our analysis (thermodynamic and kinetic indicators, non-covalent interactions (NCI), and global electron density transfer (GEDT)) indicated that the endo pathway was superior to the exo pathway, consistent with the reported experimental product.

1. Introduction

The discovery of the Diels–Alder reaction in 1928, regarded as one of the most useful ring-forming reactions in organic chemistry, has been a significant topic of interest for synthetic chemists in both theoretical and synthetic studies [1]. This reaction has demonstrated powerful stereochemical control through interactions of oxygen or nitrogen lone pairs with a π-system [2]. The development of six-membered oxygen heterocycles encompassing dihydropyrans, tetrahydropyran, and chroman scaffold has been achieved using the Domino Knoevenagel/hetero Diels–Alder (DKHDA) reactions. The formation of multiple rings in a single synthetic step is a remarkable aspect of chemical synthesis [۳]. Of particular interest in this context is the functionalized 3,4-dihydroquinolone moiety, which is present in various biologically active compounds and natural products and imparts notable cardiovascular effects [٤]. In addition, tetrahydropyranopyrazoles are also a vital core structure ubiquitous in many biological molecules [٥]. Combining established pharmacophoric core structures to create hybrid molecules is a key concept in pharmaceutical chemistry [٦]. In 2019, Kiamehr et al. developed an innovative Diels–Alder reaction to synthesize pyrazolopyranoquinolone structures. They achieved this by utilizing a new and efficient Lewis acid-catalyzed DKHDA reaction of pyrazolones with *N*-acrylated anthranilic aldehydes. The reaction was conducted with $ZnBr_2$ in ethanol at 351.52 K and favored the *endo* cycloadduct over the *cis*-configured isomer (Fig. 1) [٧].

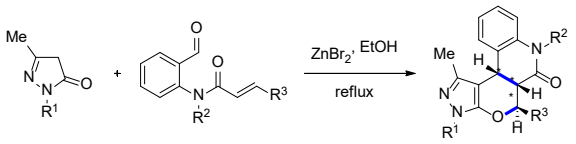

Fig.1. DKHDA reaction of pyrazolones with N-acrylated anthranilic

Kiamehr proposed a possible mechanism for DKHDA reactions, which is outlined in Fig. 2. This mechanism initiates with the Knoevenagel condensation of pyrazolone with aldehyde, facilitated by $ZnBr_2$, generating an intermediate that could exist in both *exo* or *endo* orientation. Notably, it is observed that the stereochemistry of the DKHDA products is reliant on the stereochemical orientation of the dienophile in the transition state (TS). The intramolecular Diels–Alder cycloaddition (IMDAC) selectively occurs via the [4+2] *endo*-TS, leading to the formation of *cis*-configured isomers, which is consistent with the results obtained through ^{1}HNMR analysis.

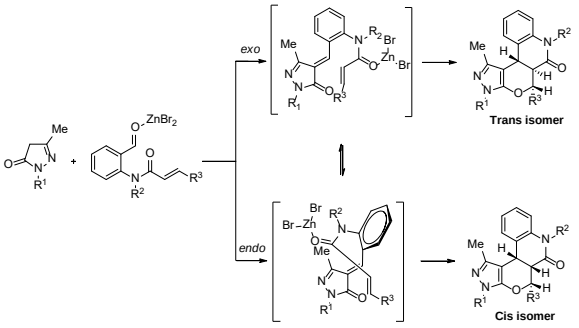

Fig.2. The possible mechanism for the DKHDA reaction of pyrazolones with *N*-acrylated anthranilic

The above experimental results have motivated further investigation into the mechanisms and product selectivity of intramolecular hetero Diels–Alder cycloadditions of benzylidenepyrazoles, using DFT calculations to address the following questions: (i) Why is the *endo* cycloadduct with the *cis*-configuration the most preferable? (ii) Which isomer is preferred in the gas phase or ethanol solvent? (iii) How does $ZnBr_2$ influence the activation energies of the transition structures? (iv) Does the reaction proceed by synchrony?

2. Results and Discussion

2.1. Introduction of Reactants and Reaction

In this study, the nature of the transition state structure in a specific reaction was investigated, and the model is illustrated in Fig. 3. The reaction divided into two general paths called *endo* and *exo* pathways. The reaction involves a starting material referred to as SM1, two transition states denoted as TS1n and TS1x, and two products named P1n and P1x.

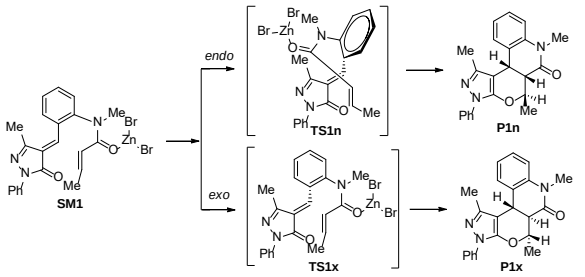

Fig. 3. Numbering of structures in the intramolecular hetero Diels–Alder reaction of benzylidenepyrazole

2.2. The Investigation of Thermodynamic and Kinetic Parameters of the Reaction

In order to determine the optimal energy pathway for the intramolecular hetero Diels–Alder reaction of benzylidenepyrazole, two possible paths were investigated and compared. Using the results of optimization[8] of initial material, TSs, and products, thermodynamic parameters, including activation energy (E_a), Gibbs free energy of activation ($\Delta G^{\ddagger}$), enthalpy of activation ($\Delta H^{\ddagger}$), and entropy of activation ($\Delta S^{\ddagger}$), as well as energy (ΔE_{rxn}), Gibbs free energy (ΔG), enthalpy (ΔH), and entropy (ΔS) of the reaction were determined.

2.3. Thermodynamic Parameters

The thermodynamic parameters of the hetero Diels–Alder reaction of benzylidenepyrazole were systematically investigated in both gas and liquid phases, as well as in the presence of zinc bromide acting as a Lewis acid that shown in Table 1.
Furthermore, the optimized structures of the TSs have been prominently illustrated in Fig. 4, providing valuable insights into the reaction mechanism.

Table 1 The thermodynamic parameters of the hetero Diels–Alder reaction of benzylidenepyrazole

Structure	TS1n	TS1x	TS1n (EtOH)	TS1x (EtOH)	TS1n-cat (EtOH)	TS1n-cat (EtOH)
E_a	15.38	35.42	15.56	37.58	17.08	39.67
$\Delta G^{\ddagger}$	19.24	39.06	18.96	40.79	18.40	38.54
$\Delta H^{\ddagger}$	15.38	35.43	15.56	37.58	17.08	39.67
$\Delta S^{\ddagger}$	-10.94	-10.29	-9.07	-9.08	-3.73	3.28
ΔE_{rxn}	-27.10	-24.02	-25.41	-21.28	-23.079	-17.48
ΔG	-21.3	-18.03	-19.11	-15.23	-17.19	-13.99
ΔH	-27.80	-24.02	-25.41	-21.28	-23.08	-17.48
ΔS	-16.64	-17.08	-17.97	-17.24	-16.79	-9.96

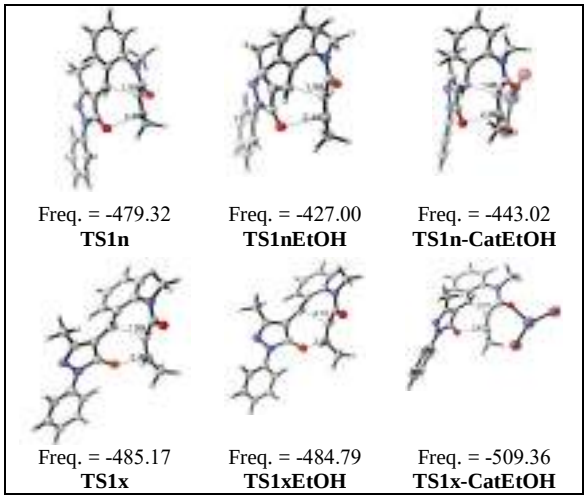

Fig.4. The geometries of the TSs associated with the hetero Diels–Alder reaction of benzylidenepyrazole and their frequency (Freq.)

As indicated in Table 1, the *endo* isomer is more stable than the *exo* isomer and have lower activation energy barrier. This result can be attributed to the presence of stabilizing secondary interactions in the *endo* isomer. Since in [4+2] cyclization reactions, the pathway with a lower activation energy barrier is more favorable, it can be predicted that the *endo* isomer will be the main product in these reactions. The results obtained from Gibbs free energy of activation, enthalpy of activation, and entropy of activation, as well as the energy, Gibbs free energy, enthalpy, and entropy of reaction, confirm the preference for the *endo* pathway over the *exo* pathway. The entropy of reaction is negative for two pathways, indicating a decrease in disorder, which is an unfavorable factor for the reaction. The endo isomer has a slightly smaller value of entropy than another isomer. The Gibbs free energy of reaction is negative for two pathways, indicating that the reactions are spontaneous and thermodynamically favorable. The enthalpy of reaction is negative for two pathways, indicating the exothermic nature of the reactions, which is a favorable factor for the reaction to take place.
The Gibbs free energy diagram in Fig. 5 shows the stability of the products compared to the reactants and the stability of *endo* product compared to *exo* product. The *endo* pathway requires less energy and time for bond breaking and formation compared to the *exo* pathway.

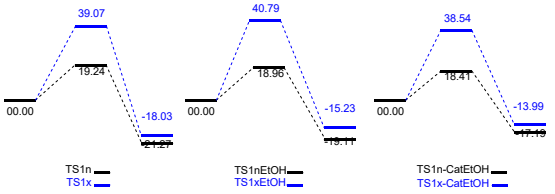

Fig.5. Gibbs free energy diagram for the hetero Diels–Alder reaction of benzylidenepyrazole

2.4. Kinetic Parameters

The kinetic parameters for the hetero Diels–Alder reaction of benzylidenepyrazole in both gas and liquid phases as well as in the presence of zinc bromide were investigated and are presented in Table 2. The results obtained indicate a higher rate constant of *endo*-TS compared to *exo*-TS, which is consistent with thermodynamic results. The Hammond postulate serves as a valuable factor in distinguishing between early and late TSs. The Hammond acceptability range is between 0 and 1, where a value greater than 0.5 signifies a late TS, and a value less than 0.5 signifies an early TS. The results showed the value is less than 0.5, indicating an early TS and a closer similarity to the reactants. The synchronicity index for a TS reflects the relative progress in the formation or breaking of bonds involved in the reaction. One of the most common methods for studying synchronicity is transition state analysis. By comparing the bond lengths during formation, synchronicity can be examined. The ΔR values, which represent the difference in bond-forming atom distances and a measure of synchronicity, are calculated. The results of the ΔR values indicate that the reaction will proceed through a non-concerted asynchronous mechanism in five pathways, except for $TS1x_{EtOH}$.

Table 2. Reaction rate constant, Hammond postulate and ΔR for the hetero Diels–Alder reaction of benzylidenepyrazole

Structure	$k*10^5$	n_T	ΔR
TS1n	19.64	0.322	0.368
TS1x	19.09	0.406	0.501
$TS1n_{EtOH}$	19.64	0.3	0.478
$TS1x_{EtOH}$	19.03	0.365	0.087
$TS1n\text{-}cat_{EtOH}$	19.66	0.340	0.413
$TS1x\text{-}cat_{EtOH}$	19.09	0.423	0.461

2.5. Non-Covalent Interaction Analysis

In order to identify the type of NCI in TSs (in the presence of zinc bromide) and the reasons for the stability and instability of these compounds, 3D NCI analysis was employed,depicted in Fig. 6. By observing the 3D NCI plots, the presence of stabilizing pseudo-hydrogen interactions in bond formations in the TS can be demonstrated (blue surfaces). In TS1n, the accumulation of green surfaces is observed between pyrazolone and zinc bromide, which is absent in another TS, and is due to stabilizing van der Waals interactions that noticeably reduce the energy surface of the TS .

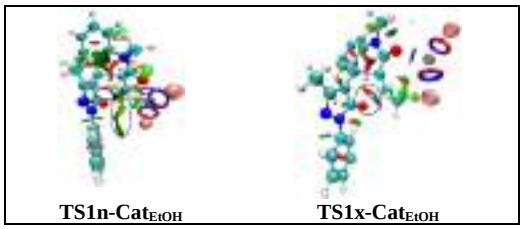

Fig.6. 3D NCI diagrams for $TS1n\text{-}cat_{EtOH}$ and $TS1x\text{-}cat_{EtOH}$ in the presence of zinc bromide

2.6. Charge Transfer

Using GEDT analysis, the $TS1n_{EtOH}$ and $TS1x_{EtOH}$ were examined as shown in Fig. 7. The results indicate a negative value for the diene component and a positive value for the dieneophile component, representing electron transfer from the dieneophile moiety to the diene moiety during the reaction. The electron density and widespread red color in the diene region support the conclusion that the reaction is a inverse-electron-demand hetero-Diels–Alder reaction.

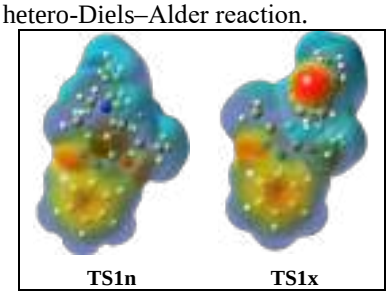

Fig.7. Electrostatic potential map and GEDT for TS1n and TS1x

3. Conclusions

In this study, intramolecular hetero Diels–Alder reactions of benzylidenepyrazoles were investigated via DFT. The results are summarized as follows: (i) The thermodynamic and kinetic parameters for two pathways in the gas and solution phases and in the presence of zinc bromide were examined, indicating the superiority of passing through the transition state TS1n, leading to the production of P1n product, which is in good agreement with experimental results. The reactions were shown to be spontaneous and exothermic by Gibbs free energy and reaction enthalpy analysis. (ii) Hammond's postulate analysis indicated the early occurrence of TSs and their greater similarity to the reactants. (iii) The reaction proceeds through a non-synchronous concerted mechanism. (iv) The NCI analysis revealed that stabilizing pseudo-hydrogen interactions exist in forming bonds in TSs. Additionally, stable van der Waals interactions were identified in TS1n, causing a decrease in its energy surface. (v) The GEDT analysis showed that the reaction was identified as an inverse-electron-demand hetero-Diels–Alder reaction.

4. References

[1] O. Diels, K. Alder, Leibigs Ann. Chem. 460 (1928) 98-122.
[2] M.A. McCarrick, Y.D. Wu, K. Houk, J. Am. Chem. Soc. 114 (1992) 1499-1500.
[3] L.F. Tietze, Chem. Rev. 96 (1996) 115-136.
[4] W. Zhou, L. Zhang, N. Jiao, Tetrahedron 65 (2009) 1982-1987.
[5] R.N. Brogden, Drugs 32 (1986) 60-70.
[6] S. Mishra, P. Singh, Eur. J. Med. Chem. 124 (2016) 500-536.
[7] M. Kiamehr, L. Mohammadkhani, M.R. Khodabakhshi, B. Jafari, P. Langer, Synlett 30 (2019) 1782-1786.
[8] Gaussian 09 software was used at the M06-2X/6-31G(d,p)//IEF-PCMTHF//M06-2X-D3/6-311++G(2df,2pd)//IEFPCMTHF at 351.52 K using the polarizable continuum model.

29TH IRANIAN ORGANIC CHEMISTRY CONFERENCE
1_3 NOV, 2023
UNIVERSITY OF QOM, IRAN

Thermal pyrolysis of polystyrene plastic

*Samira Rahimi, Ali Shahdadi, Mohammad Rostamizadeh**

Faculty of Chemical Engineering, Sahand University of Technology, Sahand New Town, Tabriz, Iran, samira.r9720@gmail.com, Rostamizadeh@sut.ac.ir

Abstract

Pyrolysis of polystyrene is an effective method for recycling this plastic and producing energy. The results showed that polystyrene has a high potential in liquid product production. In an optimal operating condition, this plastic was well decomposed so that 0.72 g of liquid product was produced.

1. Introduction

The accumulation of plastic waste in the environment and the risks caused by them are increasing every year because these plastics do not decompose quickly and can remain in the environment for a long time. Therefore, plastic waste management is considered very important [1]. Although mechanical methods and burning of plastic waste are very common, their use is not recommended. Plastic waste contains different types of plastics. Due to its good durability, strength and lightness, polystyrene is widely used in food packaging, electronics, and construction and medicine sectors. Therefore, plastic waste contains a large amount of polystyrene waste [2]. Among the chemical recycling methods, the pyrolysis method has attracted a lot of attention because it has a very high potential in converting plastic into fuel. The thermal pyrolysis process is an environmentally friendly method that enables the conversion of low-value polymers into gaseous and liquid hydrocarbons [3]. Many studies have been done on the thermal decomposition of polystyrene. Liu et al. [4] performed the thermal pyrolysis of polystyrene in a fluidized bed reactor in the temperature range of 450-700 °C and pressure of 0.31-1.6 MPa. The heating rate was 10 °C min^{-1}. They noted that the highest liquid oil (98.7 wt%) was obtained at 600 °C. William et al. [5] performed the thermal pyrolysis of polystyrene in a mini bench top reactor at 500 °C, they obtained 71 wt% crude oil and 2 wt% gas. Buekens et al. [6] performed the pyrolysis of PS in a batch reactor at 581 °C. They obtained 24.6 wt% liquid and 9.9 wt% gas. In this study, the thermal pyrolysis of polystyrene in a double wall fixed bed reactor and its conversion into valuable hydrocarbons will be investigated.

2. Materials and methods

The feed used in this study is polystyrene plastic. In this work, plastics were placed in a U-shaped tube that was embedded in a fixed bed reactor. The reactor was heated from the ambient temperature to 625 °C with a heating rate of 5 °C min^{-1}. The reaction time was 3 hours. The plastics are decomposed and the produced vapors are directed towards the condenser to turn into a liquid product.

3. Results and Analysis

Table 1 shows the results obtained from thermal pyrolysis of PS at 625 °C. In the pyrolysis process, when the temperature rises, the molecules in polymers can undergo either end-chain or random scission. This process follows a free radical chain mechanism, which involves the initiation, propagation, and termination steps commonly observed in chemical reactions [7]. It has been reported that polystyrene has a high yield in liquid production compared to polyethylene and polypropylene, which is due to its simple structure and simple kinetic mechanism of degradation [8]. Also, high temperature reduces the residence time of lighter hydrocarbons formed during the pyrolysis process. As can be seen in Table 1, a large amount of liquid product (0.72 g) has been produced that can be used as a fuel source.

Table 1 Yield of products obtained from thermal pyrolysis of PS

Feed	Liquid (gr)	gas (ml min^{-1})
PS	0.72	48.6

4. Conclusion

Thermal cracking of polystyrene plastic was investigated in a fixed bed reactor to produce a usable fuel. The feed used in this process showed a high potential for fuel production under optimal operating conditions. The results of reactor tests showed that a high yield of liquid product was obtained (0.72 gr).

5. References

[1] M. Artetxe, G. Lopez, M. Amutio, G. Elordi, J. Bilbao, M. Olazar, Light olefins from HDPE cracking in a two-step thermal and catalytic process, Chemical Engineering Journal, 207 (2012) 27-34.
[2] S.D.A. Sharuddin, F. Abnisa, W.M.A.W. Daud, M.K. Aroua, A review on pyrolysis of plastic wastes, Energy Conversion and Management, 115 (2016) 308-326.
[3] N. Miskolczi, R. Nagy, Hydrocarbons obtained by waste plastic pyrolysis: comparative analysis of decomposition described by different kinetic models, Fuel Processing Technology, 104 (2012) 96-104.
[4] Y. Liu, J. Qian, J. Wang, Pyrolysis of polystyrene waste in a fluidized-bed reactor to obtain styrene monomer and gasoline fraction, Fuel Processing Technology, 63 (2000) 45-55.
[5] P.T. Williams, E. Slaney, Analysis of products from the pyrolysis and liquefaction of single plastics and waste plastic mixtures, Resources, Conservation and Recycling, 51 (2007) 754-769.
[6] A. Buekens, H. Huang, Catalytic plastics cracking for recovery of gasoline-range hydrocarbons from municipal plastic wastes, Resources, Conservation and Recycling, 23 (1998) 163-181.
[7] W. Zeng, W.K. Chow, B. Yao, Chemical kinetics and mechanism of polystyrene thermal decomposition, in: Asia-Oceania Symp. Fire Sci. Technol. Fire Chem, 2007.
[8] N.K. Ciliz, E. Ekinci, C.E. Snape, Pyrolysis of virgin and waste polypropylene and its mixtures with waste polyethylene and polystyrene, Waste Management, 24 (2004) 173-181.

Conversion of high-density polyethylene into fuel

*Samira Rahimi, Ali Shahdadi, Mohammad Rostamizadeh**

Faculty of Chemical Engineering, Sahand University of Technology, Sahand New Town, Tabriz, Iran, samira.r9720@gmail.com, Rostamizadeh@sut.ac.ir

Abstract

Thermal pyrolysis of plastics is a promising technique to reduce plastic waste from the environment and convert it into valuable fuel. In the present study, the thermal pyrolysis of high-density polyethylene and its conversion into fuel have been investigated. The pyrolysis process was carried out in a fixed bed reactor at 625 °C, nitrogen flow rate of 20 ml min $^{-1}$ and ambient pressure. The results showed that the plastics were well decomposed, so that 0.6 grams of liquid product was produced, which can be used as an energy source.

1. Introduction

The consumption of plastics is increasing all over the world due to their various benefits and numerous applications [1, 2]. In 2011, the total plastic waste produced in the world was reported to be about 280 million tons [3]. Among plastics, high-density polyethylene constitutes a high percentage of plastic materials, besides after polyvinyl chloride and polypropylene, it is known as the third largest plastic material in terms of volume [4]. A suitable approach to deal with plastic waste is chemical recycling. Among the chemical recycling methods, the pyrolysis method has attracted much attention for the sustainable management of plastic waste and the production of fuel as an energy source. In the pyrolysis process, long chain hydrocarbons are converted into short chain hydrocarbons at a favorable temperature and produce products with high added value [4]. In this regard, Li et al. [5] performed the thermal pyrolysis of PE in a rotary kiln reactor at a temperature of 800 °C. They obtained 0.46 wt% liquid and 99 wt% gas. Mastral et al. [6] performed thermal pyrolysis of HDPE in a fluidized bed reactor. Their operating temperature range was 640-850 °C. The amount of gas produced was in the range of 33.5-9.1 wt% and the amount of liquid produced was in the range of 68.5-16.2 wt%. The aim of this study is the thermal pyrolysis of polyethylene in a fixed bed reactor under optimal operating conditions to achieve products with high added value.

2. Materials and methods

The plastic used in this work is high-density polyethylene (MFI=4 g.10min^{-1}). Thermal pyrolysis of polyethylene was carried out in a stainless steel fixed bed reactor. The feed was poured into a U-shaped glass tube and placed inside the reactor. A condenser was used to collect the liquid product. The reactor was heated to a temperature of 625 °C with heating rate of 20 °C min^{-1} and remained at this temperature for 180 min. Finally, gaseous and liquid products were obtained.

3. Results and Analysis

Thermal pyrolysis of HDPE in a fixed bed reactor was carried out at 625 °C, which is a suitable temperature for the decomposition of this plastic. According to the structure of this plastic, a temperature higher than 500 °C has been suggested for its decomposition [7]. Pyrolysis of polyethylene occurs by a random-chain scission mechanism, which has several steps, such as initiation, propagation and/or free-radical transfer, and termination [8]. Table 1 shows the liquid and gas products obtained from this process. It has been reported that higher temperatures lead to an increase in light products, so that at temperatures higher than 675 °C, gaseous products dominate [9]. The presence of light hydrocarbons improves the fuel quality, so the obtained fuel can be used as an energy source. Table 1 shows that in these operating conditions, a high and acceptable yield of the product has been obtained.

Table 1 Yield of products obtained from thermal pyrolysis of HDPE

Feed	Liquid (gr)	gas (ml min $^{-1}$)
HDPE	0.6	72.5

4. Conclusion

In the present study, the thermal pyrolysis of high-density polyethylene and its conversion into fuel have been investigated. The pyrolysis process was carried out in a fixed bed reactor at 625 °C and a nitrogen flow rate of 20 ml min $^{-1}$. The results showed that the

plastic was well decomposed so that 0.6 grams of the product became liquid.

5. References

[1] R. Miandad, M. Barakat, A.S. Aburiazaiza, M. Rehan, A. Nizami, Catalytic pyrolysis of plastic waste: A review, Process Safety and Environmental Protection, 102 (2016) 822-838.

[2] P. Lettieri, S.M. Al-Salem, Thermochemical treatment of plastic solid waste, in: Waste, Elsevier, 2011, pp. 233-242.

[3] W. Sriningsih, M.G. Saerodji, W. Trisunaryanti, R. Armunanto, I.I. Falah, Fuel production from LDPE plastic waste over natural zeolite supported Ni, Ni-Mo, Co and Co-Mo metals, Procedia Environmental Sciences, 20 (2014) 215-224.

[4] S. Kumar, R. Singh, Recovery of hydrocarbon liquid from waste high density polyethylene by thermal pyrolysis, Brazilian journal of chemical engineering, 28 (2011) 659-667.

[5] A. Li, X. Li, S. Li, Y. Ren, N. Shang, Y. Chi, J. Yan, K. Cen, Experimental studies on municipal solid waste pyrolysis in a laboratory-scale rotary kiln, Energy, 24 (1999) 209-218.

[6] F. Mastral, E. Esperanza, C. Berrueco, M. Juste, J. Ceamanos, Fluidized bed thermal degradation products of HDPE in an inert atmosphere and in air–nitrogen mixtures, Journal of Analytical and Applied Pyrolysis, 70 (2003) 1-17.

[7] S. Al-Salem, A. Antelava, A. Constantinou, G. Manos, A. Dutta, A review on thermal and catalytic pyrolysis of plastic solid waste (PSW), Journal of environmental management, 197 (2017) 177-198.

[8] A. Marcilla, M. Beltrán, R. Navarro, Thermal and catalytic pyrolysis of polyethylene over HZSM5 and HUSY zeolites in a batch reactor under dynamic conditions, Applied Catalysis B: Environmental, 86 (2009) 78-86.

[9] M. Artetxe, G. Lopez, M. Amutio, G. Elordi, J. Bilbao, M. Olazar, Cracking of high density polyethylene pyrolysis waxes on HZSM-5 catalysts of different acidity, Industrial & Engineering Chemistry Research, 52 (2013) 10637-10645.

29TH IRANIAN ORGANIC CHEMISTRY CONFERENCE
1_3 NOV, 2023
UNIVERSITY OF QOM, IRAN

Synthesis of 9-Phenyl-2,3,7-trihydroxy-6-fluorone

Elham Bastani[*] [1,2], *Esmaeil Sheibani*[1]

[1]*Department of Chemistry, Faculty of Science, University of Isfahan, Isfahan, Iran, ebastani97@gmail.com*
[2]*Department of Chemistry, Faculty of Chemistry, Iran University of Science and Technology, Tehran, Iran*

Abstract

Xanthines and Benzoxanthenes are important classes of heterocyclic compounds that are abundant in biologically active molecules. These compounds have a wide range of medicinal properties such as antibacterial, anti-inflammatory, and anti-viral. These compounds can also be used in pH-sensitive fluorescence materials to identify biological molecules and also because of their spectroscopic properties used in laser technology. 2,3,7-Trihydroxy-fluorones, Derivatives of Xanthine, particular the readily available 9-phenyl derivatives have been used extensively in the spectrophotometric analysis of a wide range of metals.

In this paper, Fluorone black was synthesized in two steps with an efficiency of about 80%. As a crucial step, Fluorone black was obtained with a temperature optimization strategy with acceptable purity in our laboratory. The structure of synthesized Fluorone black was fully confirmed by ^{1}H NMR and ^{13}C NMR.

1. Introduction

Over the last decades, several heterocyclic derivatives compounds have been synthesized or extracted from natural resources and have been tested for their pharmaceutical activities. Xanthene is one of these heterocyclic derivatives. These compounds consist of an oxygen-containing central heterocyclic structure with two more cyclic structures fused to the central cyclic compound. It has been shown that xanthane derivatives are bioactive compounds with diverse activities such as anti-bacterial, anti-fungal, and anti-inflammatory as well as therapeutic effects on diabetes and Alzheimer [1,2]. In particular, the structure of xanthene dione is present in many natural products and is part of colors. Xanthene derivatives form a class of dyes that include fluoresceins, eosins and rhodamines. A large number of xanthine dyes can be prepared from the condensation reaction of phthalic anhydride derivatives with resocinol or 3-aminophenol derivatives. Fluorescein is a synthesized organic compound that is observed as a dark red-orange powder and is soluble in water and alcohol. and was first discovered in 1871 by Adolf von Baer[3].

In this research, one of the derivatives of xanthene, 9-phenyl-2,3,7-trihydroxy-6-fluorone was synthesized from the reaction of triacetoxybenzene and benzaldehyde.

2. Results and Discussion

The results of temperature and time optimization were obtained according to Tables 1 and 2, and based on the results obtained, time of 2.5 hours and temperature of 47˚C were selected as optimal conditions for the synthesis of triacetoxybenzene (Fig. 1).

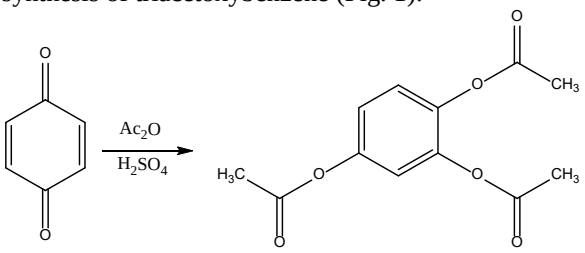

Fig. 1. Synthesis of triacetoxybenzene

Table 1 Temperature optimization

	Temperature(˚C)	Efficiency(%)
1	35	63
2	47	80
3	58	72

Table 2 Time optimization

	Time(h)	Efficiency(%)
1	1	52
2	2.5	81
3	4	68

Next, temperature optimization was done for the synthesis of 9-phenyl-2,3,7-trihydroxy-6-fluorone (Fig. 2), and based on the obtained results (table 3), the temperature of 52˚C was chosen as the optimal temperature. This product was characterized by both ^{1}H-NMR and ^{13}C-NMR (Fig. 3 and 4).

Table 3 Temperature optimization

	Temperature(˚C)	Efficiency (%)
1	40	62
2	52	79
3	65	51

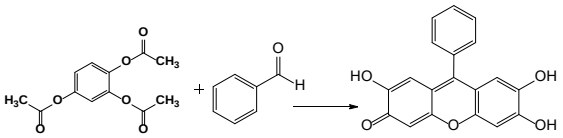

Fig. 2. Synthesis of 9-phenyl-2,3,7-trihydroxy-6-fluorone

^{1}H NMR (400 MHz, d6-DMSO): ð 6.41 (s, 2H), 6.75(s, 2H), 7.49(m, 2H), 7.72(m, 3H)

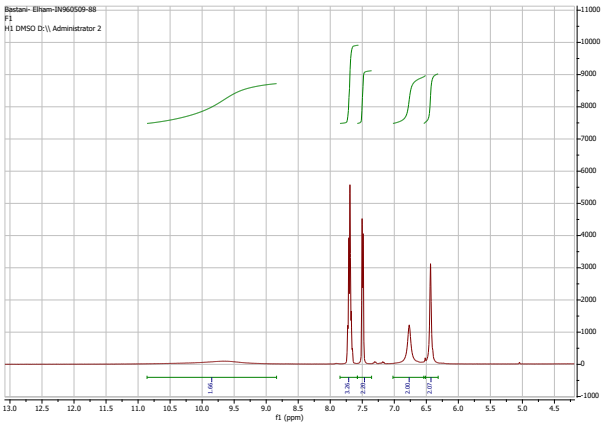

Fig. 3. ^{1}H NMR spectra in DMSO

^{13}C NMR (100.5 MHz, d6-DMSO): ð 102.27, 102.50, 128.64, 128.74, 129.04, 129.10, 129.33, 133.72, 145.57

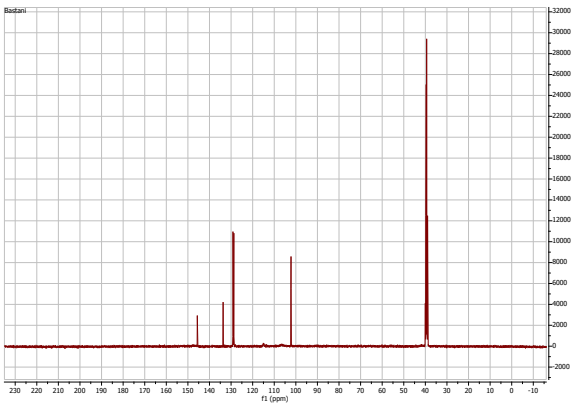

Conclusions

One of the most important and widely used heterocycles in various cases are xanthenes. Due to the importance of these compounds and their use in the pharmaceutical-medical industries and biological research, this class of compounds has attracted the attention of many organic chemists. In this research, one of xanthene derivatives, 9-phenyl-2,3,7-trihydroxy-6-fluorone, was synthesized. This compound is used in the presence of acetylpyridinium chloride for the spectrophotometric determination of copper (II) in blood serum. It is also used for the determination of germanium and molybdenum (VI).

References

[1] Mchedlov-Petrossyan. N. O.; Salamanova N. V.; Vodolazkaya, N.A.G., Yu. A.; Borodenko, V. I. J. Phys. Org. Chem. **2006**, 19,365.

[2] Aref G. Ghahsare.; Zahra S. Nazifi.; Seyed M.R. Nazifi. Current Organic Synthesis, 2019, 16, 1-7.

[3] Sun, W.C.; Gree, K. R.; Klaubert, D. H.; Haugland, R. P. *J. Org. Chem*. **1997**, 62, 6469.

Optimizing the electrocoagulation process by reversing the polarity method and investigating the removal of chromium(VI)

Yadollah Shad[1]*, *Alireza Yaqubzadeh*[2], *Khalilollah Dolatmand*[3] *and Mohammadreza Rokhian*[4]

[1]*Faculty of Chemistry, University of Mazandaran, Babolsar, Iran, shad.chmistry@gmail.com*
[2]*Department of Chemistry, Faculty of Engineering, University of Ferdowsi, Mashhad, Iran*
[3]*Isfahan University of Technology, Isfahan, Iran*
[4]*Department of Chemistry, Payame Noor University, Mashhad, Iran*

Abstract - Electrocoagulation is an effective and reliable method to remove industrial pollutants and this process has been introduced as an effective and economical method to remove heavy metals from water due to its many advantages such as high efficiency and greater compatibility with the environment. The aim of this research is to optimize the process of electrocoagulation for the removal of chromium by using reversing the polarity method in order to reduce the electrical energy consumption. In this research, the reaction time, the input voltage (from 5V to 12.5V) and the amount of electrical energy consumed in two states without reversing the polarity and with reversing the polarity for the optimal removal of chromium(VI) was investigated in different states and the results show that at lower voltages the effect of changing the polarity in the amount of chromium(VI) removal is completely evident and It accelerates the removal of chromium(VI), and at higher voltages, this effect reverses and reduces the purification process of chromium. Also, the results showed that a higher removal value can be achieved by using reversing the polarity method with less electrical energy consumption.

1. Introduction

The extensive use of heavy metals by various industries has caused the discharge of a large amount of these elements into the environment [1 , 2]. The heavy metal chromium is known as a toxic substance that has carcinogenic potential. Chromium compounds are mainly found in nature in two forms, hexavalent and trivalent. Hexavalent chromium enters the environment by various industrial units such as metal plating and polishing industries, chromate production, tanneries and chemical fertilizer production [3].
So far, several methods have been studied to remove chromium from industrial wastewater. Chemical precipitation, ion exchange, stabilization by microbial membrane, membrane processes, electrochemical methods or electrocoagulation (EC) are among these methods (4).
Over the past decades, electrocoagulation has been accepted as an efficient and promising alternative technology in the field of water and wastwater treatment. The electrocoagulation process has been studied as one of the most effective treatment methods due to its features such as scope of operation for the treatment of all types of industrial wastewater, simple system design, low cost of start-up and operation, no need for special chemicals and low production of sludge. Previous studies indicate that electrocoagulation can remove various types of pollutants from water such as suspended solids, colloids, organic matter, color, oil and grease, metals and metalloids, fluoride, phosphate, bacteria, viruses. In general, electrocoagulation can effectively eliminate many macromolecular organics, such as tannic acid and dyes, which are often hydrophobic in nature. In terms of the removal of heavy metals and metalloids, electrocoagulation is considered as a successful technology [5]. Figure 1 shows the electrocoagulation process for the removal of a wide range of pollutants.

Fig.1. Electrocoagulation process for the removal of a wide range of pollutants.

The conducted research shows the success of iron and aluminum electrodes in removing chromium. In

electrochemical systems, the type of electrodes plays an essential role in removing pollutants, and the use of iron electrodes has been reported as the most effective electrode [6-8]. Figure 2 shows the general principles of this method schematically

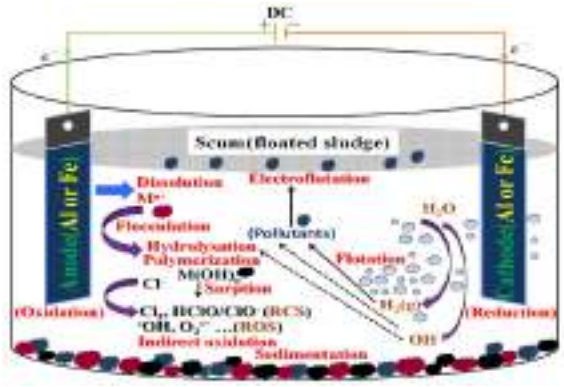

Fig.2. Schematic diagram of electrocoagulation mechanisms.

In the electrochemical process, metal pollutants are deposited as hydroxide clots and are separated, and organic pollutants are also absorbed on the formed hydroxide clots. These two mechanisms help to remove various types of industrial pollutants [9].
Despite the mentioned advantages, this method has disadvantages such as high consumption of electrical energy and loss of electrodes due to corrosion [10]. In recent years, various researches have been conducted to investigate the effect of various parameters on the performance of the electrocoagulation process, but less has been addressed to the issue of reducing the electrical energy used in this process [11]. The purpose of this research is to investigate the effect of the reversing the polarity method on the amount of electrical energy used until the complete removal of chromium(VI) at voltages of 5 to 12.5 volts.

3. Experimental

In this research, the electrocoagulation process reactor was made of Plexiglas with a useful volume of 6000 ml and dimensions of 20 x 15 x 25 cm. The blades used for the electrodes were in the form of mesh and iron with a thickness of 2 mm and dimensions of 10 x 25 cm and were fixed in the form of 10 parallel sheets with a distance of 2 cm from each other and placed inside the reactor. above. A 30 volt 500 amp rectifier with the ability to change output poles was used to supply electrical energy. To prepare the solution containing chromium(VI), the real effluent of a hard chromium plating unit was used. The initial concentration of chromium (VI) in the wastewater sample is equal to 1282 ppm. Sampling was done every 5 minutes until the complete removal of chromium(VI) by the outlet valve installed at the bottom of the reactor, and after filtering with filter paper, the samples were analyzed. In each stage, the electric current was recorded at different times and the act of changing the poles (reversing the polarity) was done every one minute for the state where the polarity change was investigated. An atomic absorption device was used to measure chromium(VI).

4. Results and discussion

The tests were performed at voltages of 5 to 12.5 volts and in two normal modes without changing the polarity and with changing the polarity until the complete removal of chromium(VI) from the wastewater solution and various parameters such as time, voltage, output current of the rectifier were recorded and then using The amount of electrical energy consumed was calculated from the respective formulas. The measured data related to the state without polarity switching are given in Table 1 and the measured data related to the state with polarity switching are given in Table 2.

Table 1, Measured data from performing various tests in the state without changing the polarity

without reversing the polarity						
Voltage (V)	current (A)	total Time (min)	Sampling time (min)	Concentration of chromium(VI) (ppm)	Removal percentage	electrical energy V*I*T (watt)
5	22.5	5	5	825	35.65	562.50
5	23.0	10	5	573	55.30	575.00
5	20.1	15	5	459	64.20	502.50
5	18.9	20	5	364	71.61	471.25
5	16.9	25	5	360	71.92	422.50
5	14.7	30	5	236	81.59	367.50
5	8.8	50	20	5	99.61	875.00
total electrical energy (watt)						**3776.25**
7.5	39.9	5	5	535	58.27	1496.25
7.5	38.5	10	5	417	67.47	1443.75
7.5	31.0	15	5	199	84.48	1162.50
7.5	23.8	20	5	142	88.92	892.50
7.5	21.4	25	5	47	96.33	802.50
7.5	20.0	30	5	1	99.96	750.00
7.5	19.3	35	5	0	100.00	723.75
total electrical energy (watt)						**7271.25**
10	58.4	5	5	457	64.35	2920.00
10	51.0	10	5	174	86.43	2550.00
10	45.0	15	5	0	100.00	2250.00
total electrical energy (watt)						**7720.00**
12.5	79.5	5	5	358	72.07	4968.75
12.5	85.0	10	5	0	100.00	5312.50
total electrical energy (watt)						**10281.25**

Table 2, Measured data from performing various tests in the state with changing the polarity

By reversing the polarity						
Voltage (V)	current (A)	total Time (min)	Sampling time (min)	Concentration of chromium(VI) (ppm)	Removal percentage	electrical energy V*I*T (watt)
5	23.0	5	5	504	60.69	575.00
5	21.0	10	5	391	69.50	525.00
5	20.0	15	5	255	80.11	500.00
5	19.9	20	5	352	72.54	497.50
5	19.6	30	10	51	96.02	980.00
5	20.3	35	5	0	100.00	507.50
total electrical energy (watt)						**3585.00**
7.5	37.0	5	5	504	60.69	1387.50
7.5	40.0	10	5	391	69.50	1500.00
7.5	40.0	15	5	255	80.11	1500.00
7.5	45.0	20	5	0	100.00	1687.50
total electrical energy (watt)						**6075.00**
10	49.5	5	5	487	62.01	2475.00
10	52.0	10	5	294	77.07	2600.00
10	63.0	15	5	109	91.50	3150.00
10	79.0	20	5	0	100.00	3950.00
total electrical energy (watt)						**12175.00**
12.5	72.5	5	5	423	67.00	4531.25
12.5	87.0	10	5	147	88.53	5437.50
12.5	124.0	15	5	0	100.00	7750.00
total electrical energy (watt)						**17718.75**

In this research, the electrocoagulation process was used as a purification technology to remove chromium(VI), and its removal efficiency was investigated under different conditions. Increasing the voltage and time has a similar effect on the removal of chromium(VI), which is due to the increase in the production of iron and hydroxyl ions in the reactor, which is also consistent with other researches [11,12]. On the other hand, the use of the polarity switching technique shows that at low voltages, the use of this technique accelerates the removal process and, as a result, reduces the electrical energy consumption. But at higher voltages, this technique has the opposite effect, which can be due to the fact that at low voltages, due to the low rate of production of metal cations in the anode, some sludge is formed on the anode and causes the anode surface to become inactive and reduce its efficiency, which Changing the polarity, the anode electrode is changed and new metal cations are produced on the opposite electrode, whose surface is more active. but at higher voltages, because the rate of production of metal cations is higher than the rate of formation of sludge resulting from the removal of pollutants, the method of changing polarity on It has no effect and on the contrary, it slows down the production of metal cations and therefore increases the purification time and consequently increases the amount of electrical energy consumed in the electrochemical removal process.

Considering that the electrocoagulation process is an efficient method for removing industrial pollutants, including organic and inorganic pollutants, and its general principles in removing pollutants are similar to each other [5,13]. According to the results of this research, the process of removing organic pollutants can be optimized using this method.

5. Conclusion

The results of this research show that the electrical energy consumed in the process of electrocoagulation using the technique of changing the polarity is much less than the case in which this process is used at high voltages. Also, with this technique, the cost of providing the main equipment such as rectifier can be reduced, because with this technique, the process can be started with a device with a lower power and cheaper.

6. References

[1] M. Hunsom, K. Pruksathorn, S. Damronglerd, H. Vergnes, P. Duverneuil, Water Res. 39 (2005) 610-616.
[2] P. Gao, X. Chen, F. Shen, G. Chen, J. Sep. Purif. Technol. 43 (2005) 117–123.
[3] A. Shafaei, M. Rezayee, M. Arami, M. Nikazar, Desalination. 260 (2010) 23–28.
[4] A. Movahed, A. Dehghan, R. Haji.Hosseini, S. Akbarzadeh, A.A. Zendehboudi, M. Nafisi.Behabadi, M.M. Mohammadi, N. Hajian, F. Pakdel, A. Hefzulla, D. Iranpour, Iran. South. Med. J. 16. (2013) 100-109.
[5] J. Lu, P. Zhang, J. Li, J. Environ. Manage. 296 (2021) 113259.
[6] V.K. Gupta, I. Ali, T.A. Saleh, M.N. Siddiqui, Sh. Agarwal, Environ. Sci. Pollut. Res. 20 (2013) 1261–1268.
[7] H.-Y. Lee, J.-K. Baek, S.-W. Jang, S.-M. Lee, S.-T. Hong, K.-Y. Lee, M.-H. Kim, J. Power Sources. 101 (2001) 206-212.
[8] H. Karadede-Akin, E. Ünlü, Environ. Monit. Assess. 131 (2007) 323–337.
[9] S. Aber, A.R. Amani-Ghadim, V. Mirzajani, J. Hazard. Mater. 171 (2009) 484–490.
[10] M.A. Barakat, Arab. J. Chem. 4 (2011) 361–377.
[11] F. Hashemzadeh, S.M. Borghei, J. Environ. Sci. Technol. 23 (2021) 213-224.
[12] A. Akhondi, A. Khodadadi.Darban, H. Ganjidoust, J. Water. wastewater, 2 (2012) 86-93.
[13] M.-K. Kima, T. Kima, T.-K. Kimb, S.-W. Jooc, K.-D. Zoha, J. Sep. Purif. Technol. 247 (2020) 116911.

29TH IRANIAN ORGANIC CHEMISTRY CONFERENCE
1_3 NOV, 2023
UNIVERSITY OF QOM, IRAN

A new method for the syntheses of bis (1,2,4-triazole-3-thiols)

*Sattar Ebrahimi**
Department of Chemistry, Malayer Branch, Islamic Azad University, Malayer, Iran, seyonesi@iau-malayer.ac.ir

Abstract – A series of bis(4-amino-4H-1,2,4-triazole-3-thiols) 3a-e were prepared by condensation reactions of 2,2'-(phenylmethylene)bis(sulfanediyl)diacetic acids 2a-e with thiocarbohydrazide. The starting diacid 2a-e was prepared by reactions of aromatic aldehydes 1a-e with 2-mercaptoacetic acid. The structures of these newly synthesized compounds are characterized by elemental analysis, and IR and NMR Spectroscopy.
Keywords: bis(4-amino-4H-1,2,4-triazole-3-thiol), thiocarbohydrazide, 1,2,4-triazole, thioacetal, thioglycolic acid.

1. Introduction

The 1,2,4-triazole system has been known to be an important recognition element in biologically active molecules. This moiety was also found in potent agonist or antagonist receptor ligands [1, 2]. 1,2,4-Triazole derivatives have been used as mimics [3, 4] or isosteres [5] of the amide bond in attempts to increase bioavailability of the parent bioactive molecules. They have also been incorporated into peptides as surrogate for cis amide bonds [6].

Different approaches have been reported for the preparation 4-amino-1,2,4-triazol-3-thiones. 1,2,4-triazoles were prepared by reacting nitryl [7], hydrazines and formamide [8] and aryl hydrazines, paraformaldehyde [9]. The amino and thiol groups are ready-made nucleophilic centers for the synthesis of condensed nitrogen and sulfur heterocyclic rings, e.g., triazolothiadiazoles [10-13], triazolothiadiazines [14], macrocycles [15-17] and triazolothiadiazepines [18]

As part of our ongoing studies on the synthesis of triazole drivatives, we report here the synthesis of some novel symmetrical bis(4-amino-4H-1,2,4-triazole-3-thiols).

2. Results and discussion

The synthesis of compounds 2a-e and 3a-e are outlined in Scheme 1 and Scheme 2. Firstly, 2,2'-(arylmethylene)bis(sulfanediyl)diacetic acids were synthesized. Reaction of various substituted benzaldehyde and thioglycolic acid using L-proline as an organocatalyst at 70 ºC under solvent free condition afforded the corresponding compounds 2a-e as shown in scheme 1. The expected compounds were obtained in excellent yields.

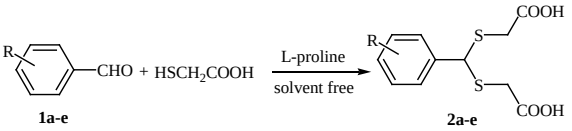

Scheme 1: Synthesis of compound **2a-e**

^{1}H NMR spectra of all synthesized compounds reveal a singlet signal in the region δ = 5.25-5.86 ppm attributed to the resonance of the methine proton (S-CH-S). The appearance of the IR absorptions and 13C-NMR signals due to the carbonyl groups of the synthesized compounds 2a-e, clearly confirmed the formation of 2,2'-(arylmethylene)bis(sulfanediyl)diacetic acids.

Compounds 2a-e were used as key intermediates for the synthesis of novel bis(4-amino-4H-1,2,4-triazole-3-thiol) derivatives. Thus, the novel bis triazole compounds 3a-e were prepared by heating compounds 2a-e with two equivalents of carbonothioic dihydrazide in an oil bath at 150 °C (Scheme 2). The expected compounds were obtained in reasonable yields as reported in Table 1.

Table 1: synthesis of compounds **2a-e** and **3a-e**

Entry	R	Time (min)	Yields (%)
2a	H	15	>99
2b	4-Methyl	15	>99
2c	4-Chloro	12	>99
2d	3-Nitro	10	>99
2e	4-Nitro	10	>99
3a	H	15	65
3b	4-Methyl	15	70
3c	4-Chloro	15	85
3d	3-Nitro	15	87
3e	4-Nitro	15	85

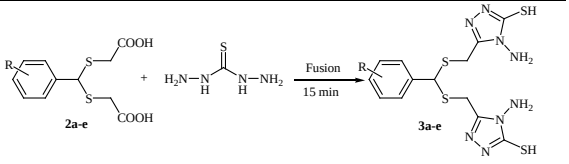

Scheme 2: Synthesis of the bis amino triazole **3a-e**

The structures of new compounds 3a-e were identified by NMR, IR, and elemental analyses. The infrared spectrum of the compounds 2a-e showed two absorption bands, at 1700 cm-1 and 2500-3500 cm-1 due to C=O and OH groups respectively, which were absent in the IR spectra of the bis amino triazole 3a-e. Similarly, the ^{1}H NMR spectrum of compounds 2a-e showed broad singlets at δ ~ 12.60, attributed to the OH groups, which disappeared upon formation of bis

amino triazole 3a-e. The appearance of the IR absorptions and 1H-NMR signals due to the NH2 and SH groups of synthesized compounds 3a-e, clearly confirmed the formation of bis amino triazols.

3. Conclusion

In conclusion, we have described a rapid and highly efficient method for the synthesis of a new series of symmetrical bis amino triazoles. This protocol is characterized by a rapid reaction rate, short reaction time, good yield, and simple purification. Our ongoing efforts for the synthesis of other compounds starting from intermediate 2 and 3 will be reported elsewhere.

Acknowledgement

We are thankful to Malayer Branch, Islamic Azad University for their financial support.

References

[1] C. Chen, R. Dagnino, C. Q. Huang, J. R. McCarthy, D. E. Grigoriadis, Bioorg. Med. Chem. Lett., 11, (2001) 3165–3168.

[2] S. M. Jenkins, H. J. Wadsworth, S. Bromidge, B. S. Orlek, P. A. Wyman, G. J. Riley, J. Hawkins, J. Med. Chem., 35 (1992) 2392–2406.

[3] G. Burrell, J. M. Evans, M. S. Hadley, F. Hicks, G. Stemp, Bioorg. Med. Chem. Lett., 4(1994) 1285–1290.

[4] W. R. Tully, C. R. Gardner, R. J. Gillepsie, R. Westwood, J. Med. Chem. 34(1991) 2060–2067.

[5] Boyd, S. A.; Fung, A. K. L.; Baker, W. R.; Mantei, R. A.; Stein, H. H.; Cohen, J.; Barlow, J. L.; Klinghofer, V.; Wessale, J. L.; Verburg, K. M.; Polakowski, J. S.; Adler, A. L.; Calzadilla, S. V.; Kovar, P.; Yao, Z.; Hutchins, C. W.; Denissen, J. F.; Grabowski, B. A.; Cepa, S.; Hoffman, D. J.; Garren, K. W.; Kleinert, H. D. J. Med. Chem. 37 (1994) 2991–3007.

[6] J. V. Duncia, J. B. Santela, A. Higley, M. K. VanAtten, P. C. Weber, R. S. Alexander, C. A. Kettner, J. R. Pruitt, A. Y. Liauw, M. L. Quan, R. M. Knabb, R. R. Bioorg. Med. Chem. Lett. 8(1998) 775–780.

[7] S. Ueda, H. Nagasawa, J. Am. Chem. Soc., 131 (2009) 15080-15081

[8] N. Yang, G. Yuan, J. Org. Chem., 83 (2018) 11963-11969.

[9] G. M. Shelke, V. K. Rao, M. Jha, T. S. Cameron, A. Kumar, Synlett, 26 (2015) 404-407.

[10] N. Foroughifar, A. Mobinikhaledi, S. Ebrahimi, M. A. Bodaghi Fard, H. Moghanian, J. Chin. Chem. Soc. 56 (2009) 1043-1047.

[11] N. Foroughifar, S. Ebrahimi, A. Mobinikhaledi, R. Mozafari Heterocycl. Commun., 17 (2011) 211–214.

[12] N. Foroughifar, S. Ebrahimi, A. Mobinikhaledi, R. Mozafari S. Afr. J. Chem., 65(2012), 1–4.

[13] N. Foroughifar, S. Ebrahimi, A. Mobinikhaledi, M. Kamali, M. Kazemi, Journal of Sulfur Chemistry 32 (2011), 593-598.

[14] N. Foroughifar, A. Mobinikhaledi, S. Ebrahimi, Synthetic Commun. 40(2010) 2421-2428.

[15] N. Foroughifar, A. Mobinikhaledi, S. Ebrahimi, Synthesis, 15(2009) 2557-2560.

[16] N. Foroughifar, S. Ebrahimi, A. Mobinikhaledi, H. Moghanian, M. A. Bodaghi Fard, M. Kalhor, Tetrahedron Lett. 50 (2009) 836-839.

[17] S. Ebrahimi, H. Moghanian Heterocycl. Commun. 18(2012) 29–31.

[18] G. L. Almajan, S. F. Barbuceanu, I. Saramet, C. Draghici Eur. J. Med. Chem. 45 (2010), 3191-3195.

Exprimental

General

Melting points were determined using an electro thermal digital apparatus and are uncorrected. Purity of the compounds were checked by thin layer chromatography (TLC) using EtOH/n-hexane (1:1 v/v) as an eluent. IR spectra were prepared on a galaxy series FT-IR 5000 spectrophotometer using KBr discs. NMR spectra were recorded on Bruker spectrophotometer (300 MHz) in DMSO-d6 using TMS as an internal standard. C, H, N and S analyses were performed on a Vario EL III elemental analyzer.

General Procedure for the Synthesis of compounds 2a-e:

Aldehydes 1a-e (5 mmol), thioglycolic acid (12 mmol) and L-proline (5% mol) were mixed and the resulting mixture was magnetically stirred at 70 ºC. After completion (controlled by TLC), the reaction mixture slowly was poured into crushed ice with stirring. The solid separated out was filtered and washed with water. The compound so obtained was dried to give the pure products **2a-e.**

2,2'-(phenylmethylene)bis(sulfanediyl)diacetic acid (2a, Table 1):

mp 133-134 ˚C, IR (KBr): (υ, cm^{-1}) = 2520-3420 (OH), 1701 (C=O), 1201 (C-O); ^{1}H NMR (DMSO-d_6, δ, ppm): 12.71 (br, 2H, 2 OH), 7.33-7.39 (br, 5H, $H_{arom.}$), 5.28 (s, 1H, CH), 3.40 (d, 2H, CH_2, *J* = 15.4 Hz), 3.23 (d, 2H, CH_2, *J* = 15.4 Hz); Calcd. for: $C_{12}H_{14}O_4S_2$: C, 48.51; H, 4.44; S, 23.55; Found: C, 48.39; H, 7.35; S, 23.43.

2,2'-(p-Tolylmethylene)bis(sulfanediyl)diacetic acid (2b, table 1):

mp 133-134 ˚C, IR (KBr): (υ, cm^{-1}) = 2450-3430 (OH), 1702 (C=O), 1190 (C-O); ^{1}H NMR (DMSO-d_6, δ, ppm): 12.60 (br, 2H, 2 OH), 7.28 (d, 2H, $H_{arom.}$, *J* = 7.7 Hz), 7.17 (d, 2H, $H_{arom.}$, *J* = 7.7 Hz), 5.25 (s, 1H, CH), 3.37 (d, 2H, CH_2, *J* = 15.3 Hz), 3.23 (d, 2H, CH_2, *J* = 15.3 Hz); Calcd. for: $C_{12}H_{14}O_4S_2$: C, 50.33; H, 4.93; S, 22.39; Found: C, 50.21; H, 4.89; S, 22.29.

2,2'-((4-Chlorophenyl)methylene)bis(sulfanediyl) diacetic acid (2c, table 1):

mp 152-154 ˚C, IR (KBr): (υ, cm^{-1}) = 2500-3450 (OH), 1700 (C=O), 1185(C-O); ^{1}H NMR (DMSO-d_6, δ, ppm): 12.26 (br, 2H, 2 OH), 7.41 (s, 4H, $H_{arom.}$), 5.30 (s, 1H, CH), 3.40 (d, 2H, CH_2, *J* = 15.4 Hz), 3.25 (d, 2H, CH_2, *J* = 15.4 Hz); Calcd. for: $C_{11}H_{11}ClO_4S_2$: C, 43.07; H, 3.61; S, 20.90; Found: C, 42.98; H, 3.58; S, 20.84.

2,2'-((3-Nitrophenyl)methylene)bis(sulfanediyl) diacetic acid (2d, table 1):

mp 120-121 ˚C, IR (KBr): (υ, cm^{-1}) = 2500-3430 (OH), 1705 (C=O), 1532, 1321 (NO_2), 1191 (C-O); ^{1}H NMR (DMSO-d_6, δ, ppm): 12.63 (br, 2H, 2 OH), 7.94 (d, 1H, $H_{arom.}$, *J* = 7.7 Hz), 7.76-7.83 (m, 2H, $H_{arom.}$), 7.58 (d, 1H, $H_{arom.}$, *J* = 7.1 Hz), 5.86 (s, 1H, CH), 3.46 (d, 2H, CH_2, *J* = 15.3 Hz), 3.30 (d, 2H, CH_2, *J* = 15.3 Hz); Calcd. for: $C_{11}H_{11}NO_6S_2$: C, 41.63; H, 3.49; N, 4.41; S, 20.21; Found: C, 41.48; H, 3.42; N, 4.21; S, 20.09.

2,2'-((4-Nitrophenyl)methylene)bis(sulfanediyl) diacetic acid (2e, table 1):

mp 165-168 ˚C, IR (KBr): (υ, cm^{-1}) = 2500-3400 (OH), 1706 (C=O), 1520, 1320 (NO_2), 1199 (C-O); ^{1}H NMR (DMSO-d_6, δ, ppm): 12.74 (br, 2H, 2 OH), 8.23 (d, 2H, $H_{arom.}$, *J* = 8.2 Hz), 7.67 (d, 2H, $H_{arom.}$, *J* = 8.3 Hz), 5.45 (s, 1H, CH), 3.45 (d, 2H, CH_2, *J* = 15.5 Hz), 3.31 (d, 2H, CH_2, *J* = 15.5 Hz); Calcd. for: $C_{11}H_{11}NO_6S_2$: C, 41.63; H, 3.49; N, 4.41; S, 20.21; Found: C, 41.55; H, 3.45; N, 4.48; S, 20.14.

General Procedure for the Synthesis of bis aminotriazole 3a-e

A mixture of thiocarbohydrazide (20 mmol) and diacid **2a-e** (10 mmol) was fused at 150°C in an oil bath for 15 min. After cooling, the reaction mixture was triturated with ethanol. The compound so obtained was dried and crystallized from ethanol to give the pure products **3a-e**.

5,5'-(Phenylmethylene)bis(sulfanediyl)bis (methylene)bis(4-amino-4H-1,2,4-triazole-3-thiol) (3a, table 1):

mp 232-233 ˚C, IR (KBr): (υ, cm^{-1}) = 3290, 3150 (NH_2), 2771 (SH) 1610 (C=N), 1493 (CH_2); ^{1}H NMR (DMSO-d_6, δ, ppm): 13.25 (s, 2H, 2 SH), 7.32-7.40 (m, 5H, $H_{arom.}$), 5.52 (s, 4H, 2 NH_2), 5.37 (s, 1H, CH), 3.92 (d, 2H, CH_2, *J* = 14.5 Hz), 3.70 (d, 2H, CH_2, *J* = 14.4 Hz); ^{13}C NMR (DMSO-d_6, δ, ppm): 25.3, 53.2, 124.6, 128.1, 128.7, 129.1, 150.1, 166.8; Calcd. for: $C_{13}H_{16}N_8S_4$: C, 37.84; H, 3.91; N, 27.16; S, 31.09; Found: C, 37.69; H, 3.85; N, 26.98; S, 30.96.

5,5'-(p-Tolylmethylene)bis(sulfanediyl)bis (methylene)bis(4-amino-4H-1,2,4-triazole-3-thiol) (3b, table 1):

mp 246-247 ˚C, IR (KBr): (υ, cm^{-1}) = 3317, 3170 (NH_2), 2764 (SH) 1614 (C=N), 1485 (CH_2); ^{1}H NMR (DMSO-d_6, δ, ppm): 13.40 (s,

2H, 2 SH), 7.29 (d, 2H, $H_{arom.}$ *J* = 7.2 Hz), 7.14 (d, 2H, $H_{arom.}$ *J* = 7.1 Hz), 5.51 (s, 4H, 2 NH_2), 5.33 (s, 1H, CH), 3.89 (d, 2H, CH_2, *J* = 14.7), 3.68 (d, 2H, CH_2, *J* = 14.9), 2.27 (s, 3H, CH_3); ^{13}C NMR (DMSO-d_6, δ, ppm): 21.2, 25.3, 53.0, 128.0, 129.6, 136.18, 138.1, 150.1, 166.8. $C_{14}H_{18}N_8S_4$: C, 39.42; H, 4.25; N, 26.27; S, 30.07; Found: C, 39.21; H, 4.15; N, 26.08; S, 29.93.

5,5'-((4-Chlorophenyl)methylene)bis (sulfanediyl) bis(methylene)bis(4-amino-4H-1,2,4-triazole-3-thiol) (3c, table 1):

mp 247-278 ˚C, IR (KBr): (υ, cm^{-1}) = 3321, 3191 (NH_2), 2774 (SH) 1602 (C=N), 1490 (CH_2); ^{1}H NMR (DMSO-d_6, δ, ppm): 13.45 (s, 2H, 2 SH), 7.40 (br, 4H, $H_{arom.}$), 5.51 (s, 4H, 2 NH_2), 5.38 (s, 1H, CH), 3.89 (br, 2H, CH_2), 3.74 (br, 2H, CH_2); ^{13}C NMR (DMSO-d_6, δ, ppm): 25.4, 52.4, 129.0, 130.0, 133.2, 138.3, 150.0, 166.8; $C_{13}H_{15}ClN_8S_4$: C, 34.93; H, 3.38; N, 25.07; S, 28.69; Found: C, 34.68; H, 3.26; N, 24.82; S, 28.51.

5,5'-((3-Nitrophenyl)methylene) bis(sulfanediyl) bis(methylene) bis (4-amino-4H-1,2,4-triazole-3-thiol) (3d, table 1):

mp 227-229 ˚C, IR (KBr): (υ, cm^{-1}) = 3281, 3164 (NH_2), 2756 (SH) 1606 (C=N), 1520, 1321 (NO_2), 1495 (CH_2); ^{1}H NMR (DMSO-d_6, δ, ppm): 13.50 (s, 2H, 2 SH), 8.23 (s, 1H, $H_{arom.}$), 8.13 (s, 1H, $H_{arom.}$), 7.85 (s, 1H, $H_{arom.}$), 7.61 (s, 1H, $H_{arom.}$), 5.58 (s, 1H, CH), 5.50 (s, 4H, 2 NH_2), 5.33 (s, 1H, CH), 3.98 (d, 2H, CH_2, *J* = 14.2), 3.80 (d, 2H, CH_2, *J* = 14.1); ^{13}C NMR (DMSO-d_6, δ, ppm): 25.6, 52.2, 122.8, 123.6, 130.6, 134.7, 141.6, 148.0, 149.8, 166.8; $C_{13}H_{15}N_9O_2S_4$: C, 34.12; H, 3.30; N, 27.55; S, 28.03; Found: C, 33.86; H, 3.19; N, 27.74; S, 27.82.

5,5'-((4-Nitrophenyl)methylene)bis(sulfanediyl) bis(methylene)bis(4-amino-4H-1,2,4-triazole-3-thiol) (3e, table 1):

mp 241-242 ˚C, IR (KBr): (υ, cm^{-1}) = 3292, 3171 (NH_2), 2770 (SH) 1600 (C=N), 1520, 1321 (NO_2);^{1}H NMR (DMSO-d_6, δ, ppm): 13.52 (s, 2H, 2 SH), 8.15 (d, 2H, $H_{arom.}$ *J* = 5.2 Hz), 7.65 (d, 2H, $H_{arom.}$ *J* = 5.0 Hz), 5.51 (s, 5H, 2 NH_2, 1CH), 3.98 (d, 2H, CH_2, *J* = 14.0), 3.80 (d, 2H, CH_2, *J* = 14.1 Hz); ^{13}C NMR (DMSO-d_6, δ, ppm): 21.2, 25.3, 53.0, 128.0, 129.6, 136.18, 138.1, 150.1, 166.8; $C_{13}H_{15}N_9O_2S_4$: C, 34.12; H, 3.30; N, 27.55; S, 28.03; Found: C, 33.93; H, 3.21; N, 27.37; S, 27.90.

29TH IRANIAN ORGANIC CHEMISTRY CONFERENCE
1_3 NOV, 2023
UNIVERSITY OF QOM, IRAN

Identification of effective Plants and Metabolites in carbon compound biosynthesis using Systems Biology approaches

Maedeh Barabadi[1], Nasrin Mollania[1], Eisa Kohan Baghkheirati [1], Hamid Mollania[2], Hassan Alehdaghi[1]*

[1]Department of Biology, Faculty of Basic Sciences, Hakim Sabzevari University, Sabzevar, Iran, barabadimaedeh@gmail.com, e.kohan@hsu.ac.ir
[2]Ferdowsi University of Mashhad, Department of Electrical Engineering, Mashhad, Iran.

Abstract

Developing carbon-based compounds with unique characteristics, such as graphene, graphene oxide, and carbon quantum dots, is one of the most effective technical approaches in science and industry. So far, various methods have been used to produce carbon-based compounds, however, from a biotechnological standpoint, using a green, non-toxic, and environmentally friendly approach to synthesize these compounds by using plants and their valuable metabolites is critical. To find a suitable plant, effective plant-metabolites in carbon-based nano-compounds biosynthesis were list through virtual screening. Subsequently, KNApSAcK-Family Database was use to find metabolites related to each plant and the bipartite network of plant-metabolites was created and analysed using Cytoscape software. Finally, the network analyses shown the species of Vitis vinifera is desirable for our goal.

Keywords: KNApSAcK-Family Database, Vitis vinifera, Carbon based nanomaterial.

1. Introduction

The discovery and study of novel forms of carbon are intrinsically tied to scientific and technological achievements. A succession of recent developments in the manufacturing of nanometer-sized carbon-based compounds, such as scaffolds or nanocarbons, have enabled access to a diverse variety of commonly used chemicals in industries such as pharmaceuticals, medicine, and engineering (1). Various types of carbon-based nanomaterials such as carbon nanotubes, nanosheets, and quantum dots have already been synthesized. They have a wide range of applications and play a significant role in biomedicine and industry (2, 3). Various methods have been used for their production, which include physical, chemical, and biological methods, and among these methods, green biosynthesis is one of the most popular due to its high biocompatibility and the absence of toxic waste materials (4). Physical and chemical synthesis methods include mechanical and thermal exfoliation, chemical reduction, chemical vapour deposition (CVD), and epitaxial growth. Although several reports have been published on the synthesis of carbon-based nanomaterial, however, most of these methods need harsh reaction conditions such as elevated temperature, high pressure, and hazardous reagents (5).

The primary challenge in biological synthesis methods techniques is discovering effective plants or metabolites in the synthesis procedure (6). To shorten the laboratory process, powerful computing tools are required. Biological system studies can be useful in this regard.

Data mining is one of the applied fields in system biology, which seeks to extract information from unstructured textual data by identifying and exploring patterns and models (7). The steps used in data mining include: a) retrieval and extraction of data, b) classification, clustering, and normalization of data c) tracking the topic and discovering the relationship between concepts, and d) displaying, analysing, and integrating the information. By adding biological meaning and significance to the results, data mining can provide a powerful tool for generating and analysing systems biology models. Each network has a large number of nodes that are connected through edges (8).

2. Methods

The primary purpose of data mining is to extract small portions of information from massive amounts of textual data without having to read them all. The grid is one of the data presentation systems that can present multiple data sets in a single fabric structure. Information was retrieved from PubMed and Google

scholar databases using the keywords biosynthesis or green synthesis, and plant extract or plant metabolites. Green synthesis of carbon-based compounds, Synthesis of graphene and carbon nanotubes with plant extract were also employed. Then articles related to plants that had an impact on the synthesis of carbon nano-compounds were listed. To identify key metabolites effective on carbon nano-compounds, the list of plant metabolites was taken from the KNApSAcK-Family database (Table 1). The name of the plants was searched in this database and the list of its metabolites was extracted.

The bipartite network of plant-metabolites was created and analysed using 11 network analysing parameters. The metabolites with high ranked selected to introduce best plants for synthesis of carbon based nano-compounds.

Table 1: KNApSKcK-Family database output for *Visit vinifera* plant compounds.

3. Result and Discussion

Data mining and network analysis approaches are utilized in this method to identify plants and metabolites involved in the production of carbon compounds. There were 7489 records found with the keywords synthesis of carbon compounds using plant extract, graphene, graphene oxide, and carbon nanotube synthesis with extract. In this identification, 68 plants were chosen from a total of 186 plants as the finest plants involved in the production of carbon Nano compounds (Table 2).

Table 2: A number of plant species that are involved in the synthesis of carbon compounds and have more than 100 metabolites.

During network analysis using the cytoHubba plugin, it was discovered that certain parameters among 11 parameters were not appropriate for analysis. DMNC and MNC parameters were incapable of distinguishing between nodes and were subsequently removed from the table. Nevertheless, the plugin remains effective in predicting and exploring vital nodes and subnetworks using its remaining parameters that utilize various topological algorithms. In the remaining 9 parameters, the two parameters و Degree and MCC و showed similar values for the node. The other 7 indicators (EPC, Stress, Radiality, Betweenness, Closeness, Eccentricity, and Bottleneck) showed different values for each node (Table 3).

Table 3: Among the 11 parameters, 8 parameters are selected that show different values of the node.

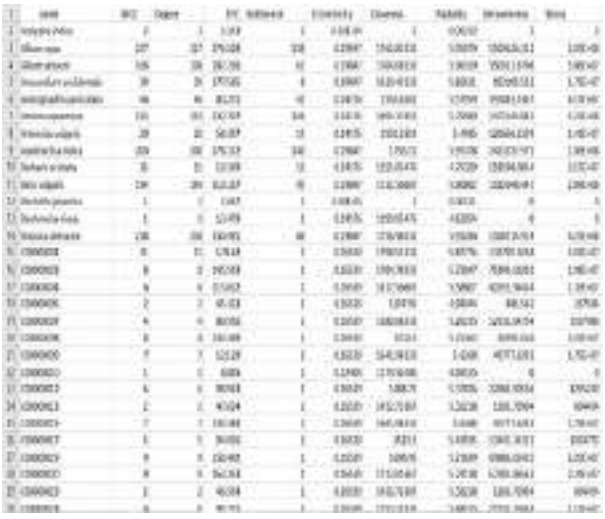

In addition, to identify the top plant and metabolite of each network, 100 top metabolite nodes were selected in each of the 8 parameters, and the sub-network was extracted for each parameter from the parent network. Based on the revers-studies of the keys metabolites, the best plant was grape (*Vitis vinifera*).

4. Conclusion

This study examined 7489 data titles relating to the synthesis of carbon-based compounds. Through a detailed analysis, 168 plant species involved in the process were discovered. These findings revealed the value of using proper keywords while conducting an in-depth review and researching available literature and studies on the synthesis of carbon compounds from plant extracts. The findings demonstrated that creating a bipartite network of plants/metabolites and analysing it with indicators such as degree can aid in identifying key ones. The grape plant leaf was one of the plants studied in the synthesis of carbon compounds. The Cytohubba plugin was a highly efficient technique for locating critical and central hubs in the plant/metabolite network.

5. References

[1] I. A. Stepek, M. Nagase, A. Yagi, K. Itami, Tetrahedron, 123(2022) 132907.

[2] Z. Zdrojewicz, , M. Waracki, B. Bugaj, D. Pypno, K. Cabała, Postepy Hig. Med. Dosw, 69 (2015) 1196-1204.

[3] Y. Ghahramani, F. Fallahinezhad, M. Afsa, J. Adv. Appl. NanoBio Tech, 2 (2021) 54-56.

[4] V. Bressi, A. Ferlazzo, D. Iannazzo, and C. Espro, Nanomaterials (Basel), 11 (2021) 1120.

[5] S. S. Shams, R. Zhang, J. Zhu, Mater. Sci.-Pol, 33 (2015) 566-578.

[6] P. Shubha, K. Namratha, H.S. Aparna, N.R. Ashok, M.S. Mustak, Jit Chatterjee, K. Byrappa, Mater. Chem. Phys, 198 (2017) 66-72.

[7] C. Rygielski, J.C. Wang, and D.C. Yen, Technol. Soc, 24 (2002) 483-502.

[8] M.J. Berry, G.S. Linoff, Data mining techniques: for marketing, sales, and customer relationship management, John Wiley & Sons, 2004:

29TH IRANIAN ORGANIC CHEMISTRY CONFERENCE
1_3 NOV, 2023
UNIVERSITY OF QOM, IRAN

APS catalyzed one-pot three- component synthesis of 2H-Indazolo[2,1-b]phthalazine-triones derivatives

Sattar Ebrahimi[*]

Department of Chemistry, Malayer Branch, Islamic Azad University, Malayer, Iran, seyonesi@gmail.com

Abstract – An efficient and practical method for the synthesis of 2H-indazolo[2,1-b]phthalazine-triones using Ammonium persulfate (APS) as an inexpensive and available catalyst from the three-component condensation reaction of phthalhydrazide, dimedone and aromatic aldehydes at 100 °C is described. Inexpensive of catalyst, high yields, simple product isolation and high atom economy are the noteworthy aspects of the protocols.

Keywords: Ammonium persulfate, APS, phthalazine-triones, phthalhydrazideIntroduction

1. Introduction

Multi-component reactions (MCRs), an important subclass of tandem reactions, are powerful tools in modern medicinal chemistry with greater efficiency and atom economy by generating structural complexity in a single step from three or more reactants. [1] Over the years, the synthesis of new heterocyclic compounds has been a subject of great interest due to their wide applicability in nature and life. Nitrogen heterocycles containing phthalazine moiety show biological and pharmacological activities such as antimicrobial [2], anticonvulsant [3], antifungal [4], anticancer [5], anti-inflammatory activities [6], thus, the syntheses of phthalazine derivatives are an important task in organic reaction. Recently several methods have been reported in the literature for the synthesis of phthalazine-trione derivatives by the condensation of phthalhydrazide, aldehydes, and 1,3-diketones using of different types of catalysts. [7-16] The recent methods show varying degrees of successes as well as limitations, such as formation of by-products, expensive catalyst, harsh reaction conditions, long reaction times, low product yields and large amounts of catalyst.

Herein I report an efficient and convenient approach for the synthesis of 2H-indazolo[2,1-b]phthalazine-1,6,11(13H)-trione by cyclocondensation reaction in the presence of APS as an free radical initiator under solvent free conditions.

2. Results and discussion

In order to achieve the most suitable conditions in this cyclocondesation reaction, a mixture of dimedone (1 mmol), benzaldehyde (1 mmol), and phetalhydrazide (1 mmol) was selected as a model reaction. Preparation of 3,4-dihydro-3,3-dimethyl-13-phenyl-2H-indazolo[2,1-b] phthalazine-1,6,11(13H)-trion (**4b**) was studied at different amounts of APS (ammonium persulfate) as a catalyst (1, 2, 3, and 5, mol%), different time and different temperatures (Table 1). During our optimization studies, various solvents were examined and DMSO was found to be the most optimum in terms of isolated yield and reaction rate.

Table 1: Optimization of conditions

Entry	APS(mol%)	Time(min)	T(°C)	Yields (%)
1	15	10	120	75
2	10	20	120	77
3	5	10	120	99
4	5	20	100	97
5	5	20	120	99
6	5	30	90	65

Some other catalysts such as Fe_3O_4@silica sulfuric acid, PEG-OSO_3H, p-TSA, $Ce(SO_4)_2.4H_2O$, TBBDA and Montmorillonite K-10, exhibited moderate to good catalytic properties. In most of these cases comparative yields of the desired product were obtained. Following the APS catalyzed procedure, the reported methods required expensive catalyst, high catalyst loading, strong acidic conditions, and long reaction times. These results clearly demonstrated that APS is a more efficient catalyst for the synthesis of 2H-indazolo[2,1-b]phthalazine-triones. The results are summarized in Table 2.

Table 2: Influence of different catalysts on the reaction of benzaldehyde (1mmol), dimedone (1mmol) and phthalhydrazide (1mmol)

Entry	Catalyst	Amount (mol%)	Time (min)	Yields (%)
1	(Fe_3O_4@silica sulfuric acid)	2	40	81
2	PEG-OSO_3H	8	13	87
3	$Ce(SO_4)_2.4H_2O$	2.5	6	78
4	p-TSA	30	10	86
5	TBBDA	0.04	14	85
6	Montmorillonite K-10	10	30	65
7	APS	5	20	98

Using these optimized reaction conditions, the scope and efficiency of these procedure were explored for the preparation of a wide variety of substituted phetalazine-trione derivatives. (Scheme 1 and Table 3) In all cases, the reaction afforded the desired phetalazine-triones in good to excellent yields. This method offers significant improvements with regard to the scope of the transformation, green aspects, simplicity and inexpensive catalyst.

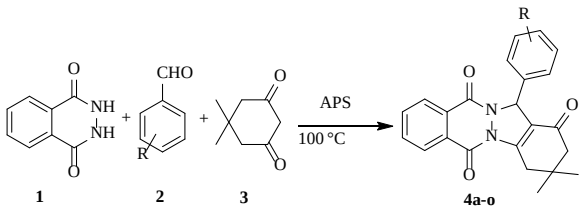

Scheme 1: Synthesis of phthalazine-triones **4a-o** catalyzed by APS

As shown in Table 3, a series of aromatic aldehydes bearing electron-withdrawing or electron-donating substituents gave the corresponding product in good yields. The method tolerates key functional groups such as alkyl, halayde alkoxy, nitro, hydroxyl, and besides the Ortho, Meta and Para positions on the aromatic aldehyde, different functional groups were also introduced to ortho position indicating the method is not sensitive to steric or electronic ortho variation of substituents.

Table 3: APS catalyzed synthesis of phthalazine-trione derivatives **4a-o**

Entry	R	Product	m. p. [lit.]	Yields (%)
1	H	**4a**	209-21 [207-209] [17]	98
2	4-Me	**4b**	227-229 [227-229] [18]	95
3	3-Me	**4c**	228-230	90
4	2- Me	**4d**	240-243 [241-243] [19]	85
5	4-MeO	**4e**	216-219 [220-221] [20]	96
6	3-MeO	**4f**	205-208	85
7	4-Cl	**4g**	262-264 [262-264] [11]	96
8	3-Br	**4h**	220-223	92
9	4-Br	**4i**	261-264 [266-268] [18]	90
10	3-OH	**4j**	275-278 [268-270] [11]	84
11	4-OH	**4k**	294-296 [292-294] [18]	88
12	2-Cl	**4l**	263-265 [264-266] [18]	90
13	$2NO_2$	**4m**	247-249 [238-240] [18]	88
14	$3NO_2$	**4n**	272-275 [268-271] [11]	95
15	$4NO_2$	**4o**	224-226 [220-222] [20]	88

3. Conclusion

In summary, an efficient protocol for the one-pot synthesis of phetalazine trione derivatives by a three-component condensation reaction of phthalhydrazide, dimedone and aromatic aldehydes has been described using APS as a catalyst. Mild reaction conditions, simplicity, inexpensive catalyst and high isolated yields are significant advantages of this protocol.

4. References

[1] X. N. Zhang, Y. X. Li, Z. H. Zhang, *Tetrahedron, 67(2011)* 7426-7430.

[2] A. Pramanik, Tetrahedron Lett. 54 (2013) 3137–3143

[3] L. Zhang, L. P. Guan, X. Y. Sun, C. X. Wei, K. Y Chai, Z. S. Quan, *Chem. Biol. Drug Des. 73*(2009) 313-319.

[4] C.-K. Ryu, R.-E. Park, M.-Y. Ma, J.H. Nho, *Bioorg. Med. Chem. Lett., 17*(2007) 2577-2580.

[5] M.A. Kadhim, A. Sh. Abdullah Alani, M.H. Hussein, Materials Today: Proceedings in press 2021 https://doi.org/10.1016/j.matpr.2021.04.156

[6] J. Sinkkonen, V. Ovcharenko, K. N. Zelenin, I. P. Bezhan, B. A. Chakchir, F. Al-Assar, K. Pihlaja, *Eur. J. Org. Chem*. (2002), 2046-2053.

[7] M. Mousapour, F. Shirini, M. Abedini, Polycyclic Aromat. Comp., 41 (2019) 419-426.

[8] P. M. Pisal, V. T. Kamble, R. Varala, P. B. Gujarathi Org.Commun.13(2020) 194-201

[9] Sayyafi, M.; Seyyedhamzeh, M.; Khavasi, H. R.; Bazgir, A. *Tetrahedron 64*(2008) 2375-2378.

[10] M. Mahmoodi Fard Chegeni, A. Bamoniri, B. F. Mirjalili, Polycycl. Aromat. Comp. 42(2020) 1-9

[11] R. Ghorbani-Vaghei, R. Karimi-Nami, Z. Toghraei-Semiromi, M. Amiri, M. Ghavidel,*Tetrahedron 67*(2012) 1930-1937.

[12] G. Sabitha, C. Srinivas, A. Raghavendar, J. S. Yadav, *Helv. Chim. Acta 93 (2010)*, 1375-1380.

[13] Raghuvanshi, D. S.; Singh, K. N. *Tetrahedron Lett*. **2011**, 52, 5702.

[14] E. Mosaddegh, A. Hassankhani, *Tetrahedron Lett*., 52(2012) 488-490.

[15] S. Nikzad Shalkouhi, H. Kefayati, Sh.Shariati, Iranian J. Cat. 8 (2018) 213-220

[16] A. Shaabani, A. Rahmati, J. Moghimi Rad, *Comptes Rendus Chimie 11(2011)*, 759-764.

[17] H. R. Shaterian, M. Aghakhanizadeh *Comptes Rendus Chimie 15(2012)* 1060-1064.

[18] Hasaninejeda, A.; Rasekhi Kazerooni, M.; Zare, A. *Catalysis Today*, **2012**, *196*, 148.

[19] H. R. Shaterian, A. Hosseinian, M. Ghashang, *Arkivoc* (ii) (2009) 59-67.

[20] X. Wang, W.W. Ma, L. Q. Wu, F. L. Yan, *J. Chin. Chem. Soc*., *57*(2010) 1341-1345.

Experimental

Melting points were determined using an electro thermal digital apparatus and are uncorrected. Purity of the compounds were checked by thin layer chromatography (TLC) using EtOH/n-hexane (3:1 v/v) as an eluent. NMR spectra were recorded on Bruker spectrophotometer (400 MHz) in DMSO-d6 using TMS as an internal standard. Elemental analyses were performed on a Vario EL III elemental analyzer.

General procedure for the synthesis of phthalazine-trione 4a–o

A mixture of phthalhydrazide **1** (1 mmol), aromatic aldehyde **2** (1 mmol), dimedone **3** (1 mmol), DMSO (0.3 mL) and APS (5% mol) was heated at 100 °C for 20 min (TLC). After cooling, the reaction mixture was washed with water (5 ml) and the residue recrystallized from EtOH to afford the pure product **4a-o**.

3,4-Dihydro-3,3-dimethyl-13-(3-methylphenyl)-2H-indazolo[2,1-b]phthalazine-1,6,11(13H)-trione 4c. (Table 3, Entry 3):

Isolated yield 90 %; mp = 228-230 °C; ^{1}H NMR ($CDCl_3$, 400 MHz) δ (ppm): 1.23 (s, 3H, Me), 1.24 (s, 3H, Me), 2.34 (s, 3H, CH_3), 2.35 (s, 2H, CH_2), 3.27 (d, d 1H, *J*=19.0 و 2.4 Hz, CH), 3.45 (d, d 1H, *J* = 19.1, 0.8 Hz CH), 6.42 (s, 1H, CHN), 7.10 (d, 1H, $H_{arom.}$ *J* = 6.4, Hz), 7.20 7.24 (m, 3H, $H_{arom.}$), 7.85-7.87 (m, 2H, $H_{arom.}$), 8.27-8.30 (m,

1H, $H_{arom.}$), 8.36-8.39 (m, 1H, $H_{arom.}$), ^{13}CNMR ($CDCl_3$, 100 MHz) δ (ppm): 21.5, 28.4, 28.7, 34.6, 38.0, 50.9, 65.0, 118.7, 124.0, 127.7, 127.9, 128.0, 128.6, 129.0, 129.1, 129.6, 133.5, 134.5, 136.3, 138.3, 150.7, 154.2, 156.0, 192.1.; Calcd for $C_{24}H_{22}N_2O_3$: C, 74.59; H, 5.74; N, 7.25%; Found: 74.47; H, 5.71; N, 7.14% .

3,4-Dihydro-3,3-dimethyl-13-(3-methoxyphenyl)-2H-indazolo[2,1-b] phthalazin-1,6,11(13H)-trione 4f (Table 3, Entry 6):

Isolated yield 85 %; mp = 205-208 °C; ^{1}H NMR ($CDCl_3$, 400 MHz) δ (ppm): 1.22 (s, 3H, Me), 1.23 (s, 3H, Me), 2.36 (s, 2H, CH_2), 3.26 (d, d 1H, *J* = 19.0, 2.4 Hz, CH), 3.45 (d, d 1H, *J* =19.2, 1.2 Hz CH), 3.80 (s, 3H, OCH_3), 6.44 (s, 1H, CHN), 6.83 (d, d 1H, $H_{arom.}$ *J* = 8.8, 2.0 Hz), 6.96-6.97 (m, 1H, $H_{arom.}$), 7.02 (d, 1H, $H_{arom.}$ *J* = 7.6 Hz), 7.25-7.27 (m, 1H, $H_{arom.}$), 7.86-7.88 (m, 2H, $H_{arom.}$), 8.28-8.31 (m, 1H, $H_{arom.}$), 8.36-8.39 (m, 1H, Harom.), ^{13}C NMR ($CDCl_3$, 100 MHz) δ (ppm): 28.5, 28.6, 34.7, 38.0, 51.0, 55.2, 64.8, 113.1, 113.8, 118.6, 119.4, 127.7, 128.0, 128.9, 129.0, 129.7, 133.5, 134.5, 137.9, 150.8, 154.3, 156.0, 159.7, 192.0.; Calcd for $C_{24}H_{22}N_2O_4$: C, 71.63; H, 5.51; N, 6.96; %; Found: C, 71.45; H, 5.44; N, 6.81 %.

3,4-Dihydro-3,3-dimethyl-13-(3-Bromophenyl)-2H-indazolo[2,1-b] phthalazin-1,6,11(13H)-trion4h (Table 3, Entry 8):

Isolated yield 92 %; mp = 220-223 °C; ^{1}H NMR ($CDCl_3$, 400 MHz) δ (ppm): 1.23 (s, 3H, Me), 1.24 (s, 3H, Me), 2.34(s, 2H, CH_2), 3.26 (d, d 1H, *J*=19.2, 2.4 Hz, CH), 3.43 (d, d 1H, *J* =19.4, 1.2 Hz CH), 6.41 (s, 1H, CHN), 7.23 (t, 1H, $H_{arom.}$ *J* = 8.0, Hz), 7.42-7.45 (m, 2H, $H_{arom.}$), 7.50 (s, 1H, $H_{arom.}$), 7.88-7.90 (m, 2H, $H_{arom.}$), 8.25-8.31 (m, 1H, $H_{arom.}$), 8.37-8.40 (m, 1H, $H_{arom.}$), ^{13}C NMR ($CDCl_3$, 100 MHz), δ (ppm): 28.5, 28.6, 34.7, 38.0, 50.9, 64.2, 117.9, 122.8, 126.3, 127.7, 128.1, 128.9, 129.0 129.7, 130.2, 131.8, 133.7, 134.6, 138.6, 151.2, 154.2, 156.0, 192.0.; Calcd for $C_{23}H_{19}BrN_2O_3$: C, 61.21; H, 4.24; N, 6.21; %; Found: C, 61.03; H, 4.20; N, 6.12; %.

29TH IRANIAN ORGANIC CHEMISTRY CONFERENCE
1_3 NOV, 2023
UNIVERSITY OF QOM, IRAN

Intramolecular rotation effects on IRC: A DFT theoretical study of converting 2,5-bis(iminomethyl)terephthalic acid to an *N*-heterocycle

*Azimeh Davarpanah and Amir Abdolmaleki**

Department of Chemistry, College of Sciences, University of Shiraz, Shiraz, Iran, abdolmaleki@shirazu.ac.ir

Abstract - In this article, we investigated and compared the possible pathways for the conversion reaction of 2,5-bis(iminomethyl)terephthalic acid to pyrrolo[3,4-*f*]isoindole-1,5-dione using theoretical calculations of the intrinsic reaction coordinate, DFT theory, the B3LYP method, and 6-311++G(d,p) basis set. The outcomes of these theoretical studies demonstrated that the formation of zwitterionic intermediates and the reaction coordinate path both are influenced by the rotation of the carboxylic acid substituent group and its orientation relative to the ortho-amino substituent group. It was found that the starting chemical structure exhibits better stability when the acidic OH is positioned close to the amine group, allowing for the formation of a hydrogen bond. Under these conditions, the system tends to form zwitterion intermediate. Therefore, despite the larger energy difference between the starting material and the final product, as well as the lower stability of the final product compared to the starting material in this situation, the reaction primarily proceeds through this coordinated pathway and its subsequent zwitterionic intermediate.

Keywords: 2,5-bis(iminomethyl)terephthalic, DFT, IRC, N-heterocycle, Zwitterion.

1. Introduction

The formation of five-membered *N*-heterocyclic compounds from derivatives of terephthalic acid (TPA) containing amine groups and/or triazole rings has been undergone extensive study due to their, potential applications as biological factors, corrosion inhibitors, pesticides, dyes, acid-base indicators, and other industrial chemicals [1,2].

In this study, we conducted the theoretical quantum research utilizing the DFT theory, B3LYP method, and 6-311++G(d,p) basis set [1,2] through the Gaussian 09 suite of programs [3]. The aim of our investigation was to explore the effects of rotational variations in the carboxylic acid substituent group and its orientation relative to the ortho-amino substituent group on the reaction coordinate paths (IRC) involved in the conversion of 2,5-bis(iminomethyl)terephthalic acid to pyrrolo[3,4-*f*]isoindole-1,5-dione. These aspects have not been addressed in previously reported articles.

2. Results and discussions

The four different conversion pathways from 2,5-bis(iminomethyl)terephthalic acid to pyrrolo[3,4-*f*]isoindole-1,5-dione are presented in **Scheme 1** and summarized in **Table 1**.

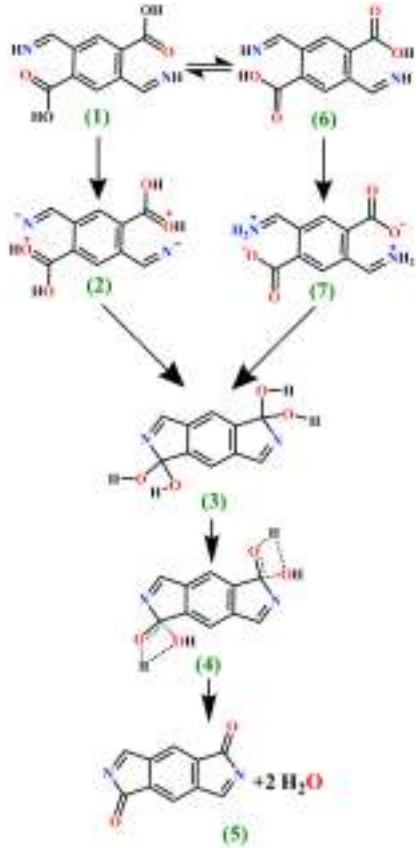

Scheme 1. The reaction paths for 2,5-bis(iminomethyl)terephthalic acid converting to pyrrolo[3,4-*f*]isoindole-1,5-dione.

Table 1. Different paths of reaction coordinate for 2,5-bis(iminomethyl)terephthalic acid converting to pyrrolo[3,4-*f*]isoindole-1,5-dione.

Reaction coordinate path (From entry)-(To entry)	
	→
a:	**1-2-3-4-5**
b:	**1-6-7-3-4-5**
c:	**6-1-2-3-4-5**
d:	**6-7-3-4-5**

Typically, two different forms of 2,5-bis(iminomethyl)terephthalic acid can be distinguished based on the orientation of the acidic group in relation to the ortho-amino substituent.

Table 2. The 2,5-bis(iminomethyl)terephthalic acid converting reaction's coordinate to pyrrolo[3,4-*f*]isoindole-1,5-dione, calculated during DFT/B3LYP/6-311++G(d,p) IRC theoretical calculations.

Reaction coordinate	Theoretical Optimized Structure by Dft/B3Lyp/6-311++G(d,p) ( )	ΔE (kcal/mol)
1	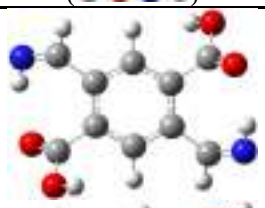	0.000
2		21.989
3		3.930
4		128.289
5		-2.368
6	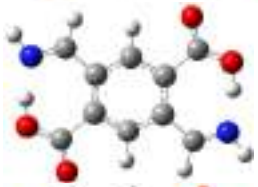	-22.267
7	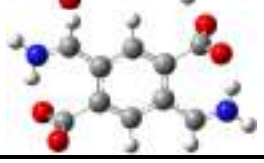	15.080

In the first form, the carbonyl oxygen is exposed to the amine hydrogen (**Scheme 1-Entry 1** and **Table 2-Entry 1**) while in the second form, the acidic H is positioned near the amino nitrogen (**Scheme 1-Entry 6** and **Table 2-Entry 6**). These forms are characterized by intramolecular hydrogen bonding between the acidic and ortho-amino substituent groups.

According to theoretical calculations conducted using DFT/B3LYP/6-311++G(d,p) and considering the ground state energy and geometric optimization of both forms, the second form (**6**) exhibits higher thermal, structural, and geometric stability compared to the first form (**1**) (Table 2). Hence, it is expected that the majority of molecules in the bulk of the starting material for this reaction will be in the form represented by entry "**6**".

According to the classification presented in **Scheme 1** and **Table 1**, all the proposed pathways involve passing through the coordinates of compound "**3**" as an intermediate, compound "**4**" as a transition state, and entry "**5**" as the final products.

Among the paths, only path "a" avoids passing through the coordinate of compound "**6**", while paths "**b**" and "**d**" both involve the zwitterionic intermediate (**7**) in the reaction coordinate. The theoretical optimization calculations for each of these four paths (a, b, c, and d) are provided in Table 2, depicting the results for each step of the reaction.

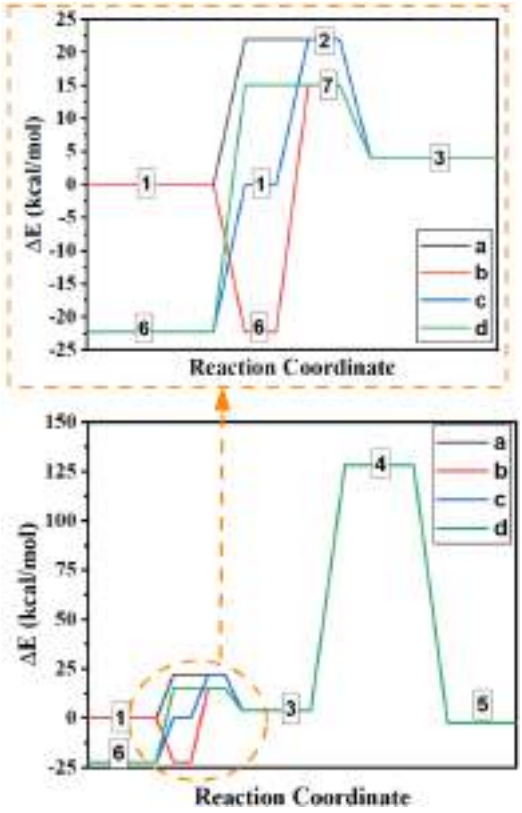

Figure1. IRC curves of four possible reaction path a, b, c and d, of 2,5-bis(iminomethyl)terephthalic acid converting to pyrrolo[3,4-*f*]isoindole-1,5-dione. ΔE =structural total energy variation related to structure of entry "1".

ΔE represents the difference between entry "**1**" and the total energy of each entry, as calculated theoretically.

The intrinsic coordinates of the conversion reaction from 2,5-bis(iminomethyl)terephthalic acid to pyrrolo[3,4-*f*]isoindole-1,5-dione (IRC) for paths a, b, c, and d were determined by using DFT/B3LYP/6-311++G(d,p) quantum theory calculations. **Figure 1** illustrates these four different paths.

Based on **Figure 1** and **Table 2**, it can be observed that if the starting material is in the form represented by entries "**1**" or "**6**," the preferred pathway for the reaction coordinate would be "b" and "d", respectively.

3. Conclusions

Based on the discoveries made in this article, the formation of zwitterionic intermediates and the coordinate path of this reaction, are both affected by the rotation of the carboxylic acid substituent group and its orientation in relation to the ortho-amino substituent group. Additionally, the favourable coordinate paths for the conversion reaction from 2,5-bis(iminomethyl)terephthalic acid to pyrrolo[3,4-*f*]isoindole-1,5-dione always pass through the second form of the starting material (**6**) where the acidic hydrogen forms a hydrogen bond with the amino nitrogen, and its resulting zwitterionic intermediate (**7**).

4. References

[1] M. Karabacak, M. Cinar, Z. Unal, M. Kurt, J. Mol. Struct. 982 (2010) 22–27.

[2] M. Pagacz-Kostrzewa, M. Sałdyka, A. Bil, W. Gul, M. Wierzejewska, D.M. Khomenko, R.O. Doroschuk, J. Phys. Chem. A 123 (2019) 841–850.

[3] M. Frisch, G.W. Trucks, H.B. Schlegel, G.E. Scuseria, M.A. Robb, J.R. Cheeseman, G. Scalmani, V. Barone, B. Mennucci, Ga. Petersson, (2009).

29TH IRANIAN ORGANIC CHEMISTRY CONFERENCE
1_3 NOV, 2023
UNIVERSITY OF QOM, IRAN

Unexpected synthesis of bis(pyrazolyl)methane derivatives from the reaction of ethyl 2-(arylidene)acetoacetates and 3-methyl-1H-pyrazol-5(4H)-one

Adeleh Moshtaghi Zonouz[*], *Mostafa Razban*

Department of Chemistry, Faculty of Science, Azarbijan Shahid Madani University, Tabriz, Iran , adelehmz@yahoo.com, mostafarazban7@gmail.com

Abstract - An interesting three-component reaction of 3-methyl-1H-pyrazol-5(4H)-one, ethyl 2-(arylidene)acetoacetates and ammonium acetate in refluxing ethanol afforded 4,4′-(arylmethylene)bis(3-methyl-1-H-pyrazol-5-ol) derivatives **II** instead of expected fused pyrazolo-1,4-dihydropyridines **I**.

1. Introduction

Pyrazolopyridines and their derivatives have a wide range of biological activities [1]. For example, a number of pyrazolo[3,4-*b*]pyridines exhibit anxiolytic (*e.g.*, tracazolate), antiallergic, antiherpetic, antitubercular, antibacterial, antihypertensive and antifungal activities. Also appropriately substituted pyrazolo- and dipyrazolopyridines as luminescent dyes were evaluated as light-emitting materials in electroluminescent devices [2].
4,4′-(Aryl methylene)bis(1H-pyrazol-5-ol)s have also exhibited a wide range of biological activities [3]. The conventional chemical approach to these compounds involves: 1) the Knoevenagel synthesis of the corresponding arylidenepyrazolones and its base-promoted Michael reaction; 2) the one-pot reaction of arylaldehydes with 2 equiv of 3-methyl-1Hpyrazol-5-ol performed under a variety of reaction conditions [4]; and 3) three-component reaction of ethyl acetoacetate, hydrazine hydrate, and aldehydes in the presence of pyridine trifluoroacetate or acetic acid in water [5].

To the best of our knowledge fused Pyrazolo-1,4-dihydropyridine derivatives **I** have been prepared by the reaction of 5-aminopyrazole derivatives and 2-arylidene acetoacetates in refluxing organic solvents [6]. Reaction of 5-aminopyrazole derivatives with arylidene derivatives of malonodinitrile and ethyl cyanoacetate both in organic solvents and in water have been furnished pyrazolo[3,4-*b*]pyridine derivatives [7,8]. Three-component reaction of 3-methyl-5-aminopyrazole, malononitrile, and substituted aldehydes under ultrasound irradiation has also been afforded pyrazolo[3,4-*b*]pyridine derivatives [9]. On the other hand, fused dipyrazolo-1,4-dihydropyridine derivatives have been synthesized by the three-component reaction of 3-methyl-1H-pyrazol-5(4H)-one or 3-methyl-1-phenylpyrazol-5(4H)-one, aldehydes and ammonium acetate in refluxing organic solvents [10, 11]. Dabiri et al. have described four component reaction of a 1,3-dicarbonyl compounds, an aldehyde, hydrazine and ammonium acetate in ethanol for the synthesis of fused dipyrazolo-1,4-dihydropyridine derivatives [12]. Reaction of 5-amino-3- methyl-1-phenylpyrazole with aldehydes under microwave irradiation and solvent-free conditions have been achieved dipyrazolo[3,4-*b*:4',3'-*e*]pyridines [13].

In continuation of our interest in multicomponent reactions, and in order to the preparation of fused pyrazolo-1,4-dihydropyridines we performed the three-component reaction of easily accessible 3-methyl-1H-pyrazol-5(4H)-one, ethyl 2-(arylidene)acetoacetates and ammonium acetate in refluxing ethanol. Howevere according to the spectral data the results are interesting and unexpected 4,4′-(arylmethylene)bis(3-methyl-1-H-pyrazol-5-ol) deri - vatives **II** were obtained.

2. Results and discussion

To prepare pyrazolo-1,4-dihydropyridines **I**, we initially performed the multi-component reaction of ethyl acetoacetate (2 mmol), aromatic aldehyde (1 mmol), hydrazine hydrate (1 mmol) and ammonium acetate (1.5 mmol) in refluxing ethanol. We anticipated *in situ* preparation of pyrazolone **1** and Ethyl 2-(benzylidene)acetoacetates **2** by the reaction of ethyl acetoacetate with hydrazine hydrate and aromatic aldehydes respectively. Then Michael addition of **1** to **2**, followed by intramolecular cyclization of adduct in the presence of ammonium acetate, both as reactant and catalyst, to afford **I.** But, as indicated by TLC, a mixture of products was obtained. Therefore, pyrazolone **1** was prepared through the condensation reaction of hydrazine hydrate and ethyl acetoacetate under solvent-free condition [14]. Ethyl 2-(arylidene)acetoacetates **2** have been prepared by Knovenagel condensation of ethyl acetoacetate and aromatic aldehydes according to the literature [15].

Then three-component reaction of **1** (1 mmol), **2** (1 mmol) and ammonium acetate (1.2 mmol) was performed in refluxing ethanol [16]. The spectral data of products indicated formation of bis(pyrazolyl)methanes **II** instead of pyrazolo-1,4-dihydropyridine derivatives **I** (Scheme 1).

The ^{1}H and ^{13}C NMR spectral data, as well as IR spectra, are in agreement with the proposed structures. For example, in the IR spectrum of the compound **IIa**, a broad absorption band at 3400-2000 cm^{-1} suggests that the product is predominately in the enol form. Also, the structure **IIa** is confirmed by the absence of ethoxy proton signals of ethyl ester group in the ^{1}H NMR spectrum and the appearance of a singlet at 1.78 ppm for two methyl group, a singlet at 4.93 ppm for C(4)-H, a multiplate at 7.04-7.19 for aromatic protons, and a broad singlet at 11.29 ppm for two NH protons.

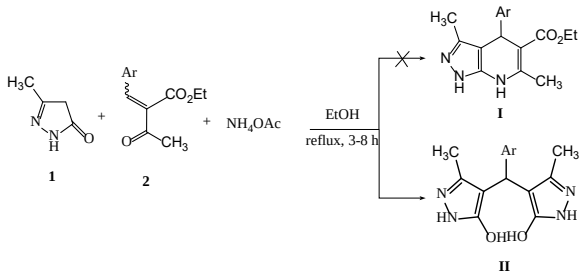

Scheme 1. Three-component reaction of pyrazolone **1**, benzylidene ethyl acetoacetate **2** and ammonium acetate.

The proposed mechanism is shown in Scheme 2. Most likely, the reaction of pyrazolone **1** and ethyl 2-benzylidenacetoacetates **2** leading to arylidene pyrazolones **3** which was further reacted with the second molecule of pyrazolone **1** to form **II**. Finally, reaction of **3** with ammonium acetate followed by cyclization affords the final dipyrazolo-1,4-dihydropyridine derivatives **II**.

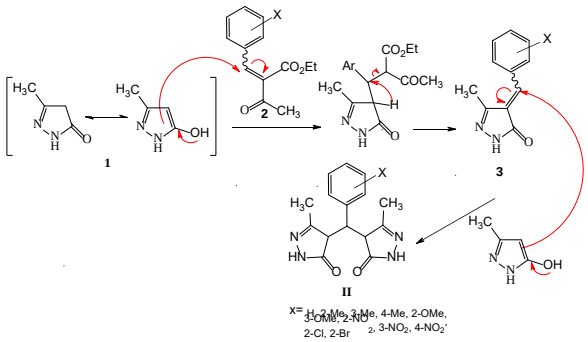

Scheme 2. Proposed reaction pathway for the synthesis of dipyrazolo-1,4-dihydropyridine deriva -tives **II**

3. References

[1] Liu, C.; Li, Z.; Zhao, L.; Shen, L. *ARKIVOC* **2009**, (*ii*), 258.
[2] Chen, J.; Liu, W.; Ma, J.; Xu, H.; Wu, J.; Tang, X.; Fan, Zh.; Wang, P. *J. Org. Chem.* **2012**, *77*, 3475.
[3] Acharya, B.N.; Saraswat, D.; Tiwari, M.; Shrivastava, A.K.; Ghorpade, R.; Apna, S.; Kaushik, M.P. *Eur. J. Med. Chem.*, **2010**, *45*, 430-438.
[4] Moshtaghi Z. A.; Beiranvand M.; Mohammad-Rezaei R.; Naderi S. *Lett. Org. Chem.*, **2020**, *17 (7)*, 548-554.
[5] Soleimani E.; Ghorbani s.; Taran M.; Sarvary A. *C. R. Chimie*, **2012**, *15*, 955–961.
[6] Winters, G. U.S. patent 4954508 , 1990.
[7] Quiroga, J.; Alvarado, M.; Insuasty, B.; Moreno, R. *J. Heterocyclic Chem.* **1999**, *36*, 1311.
[8] Shi, D.-Q.; Shi, J.-W.; Yao, H.; Jiang, H.; Xiang-Shan Wang, X.-Sh. *J. Chin. Chem. Soc.* **2007**, *54*, 1341.
[9] Zare, L.; Mahmoodi, N. O.; Yahyazadeh, A.; Mamaghani, M. *Synth. Commun.* **2011**, *41*, 2323.
[10] Zhao, K.; Lei, M.; Ma, M.; Hu, L. *Monatsh. Chem.* **2011**, *142*, 1169.
[11] Sohal, H. S.; Manvinder Kaur, M.; Khare1, R.; Singh, K. *Am. J. Org. Chem.* **2014**, *4(2)*, 21.
[12] Dabiri, M.; Salehi, P.; Koohsari, M.; Hajizadeh, Z.; MaGee, D. I. *ARKIVOC* **2014**, *iv*, 204.
[13] Quiroga, J.; Portilla, J.; Insuasty, B.; Abonía, R. *J. Heterocyclic Chem.* **2005**, *42*, 61.
[14] Rahat Khan, M. D.; Imam Uddin, M. D. *Bangladesh J. Pharmacol.* **2008**, *3*, 27.
[15] Correa, W. H.; Scott, J. L. *Green Chem.* **2001**, *3*, 296-301.
[16] **General procedure for the synthesis of compounds IIa-j.** A mixture of 3-methyl-1H-pyrazol-5(4H)-one **1** (0.294 g, 3 mmol) and ammonium acetate (0.269g, 3.5 mmol) in EtOH (7 mL) was heated under reflux, and then ethyl 2-benzylidenacetoacetates **2** (3 mmol) was added. The mixture was stirred at reflux temperature till the completion of reaction as indicated by TLC (Table 1). After which it was cooled and the precipitated soild was filtered, washed with cold ethanol and recrystallized from ethanol to afford the pure products **II**. *4,4'-(phenylmethylene)bis(3-methyl-1H-pyrazol-5-ol)* ***(IIa)****:* White solid (78% yield); IR (KBr) (ν_{max}/cm^{-1}): 3400-2000, 1606, 696; ^{1}H NMR (400 MHz, DMSO-d_6): δ (ppm) 2.06 (6H, s, $2CH_3$), 4.82 (1H, s, CH), 7.09-7.22 (5H, m, Ar-H); ^{13}C NMR (100 MHz, DMSO-d_6): δ (ppm) 10.34 (CH_3), 32.76 (CH), 104.21 (C-4), 125.38 (CH, ArH), 127.47 (CH, ArH), 127.69 (CH- ArH), 139.67 (C-ArH), 143.32 (C-3), 161.02 (C-5).

29TH IRANIAN ORGANIC CHEMISTRY CONFERENCE
1_3 NOV, 2023
UNIVERSITY OF QOM, IRAN

SYNTHESIS AND CHARACTERIZATION OF ZnO NANOPARTICLES FOR PHOTOCATALYTIC DEGRADATION OF ACRIDINE ORANGE

Leila Khoshmaram, Fatemeh Zakeran H.*

Department of Chemistry, Faculty of Science, Azarbaijan Shahid Madani University, Tabriz, Iran, l.khoshmaram@gmail.com, fatemezakeran25@gmail.com

Abstract - In the present study, ZnO nanoparticles (NPs) were synthesized from Zinc chloride in two different conditions. The synthesis is based on a simple precipitation method. The nanoparticles' composition, crystallinity and size were investigated and compared by Fourier transformed infrared spectroscopy (FTIR), X-ray powder diffractometry (XRD) and dynamic light scattering (DLS). After complementary characterization, as-prepared ZnO-NPs were further subjected for its photocatalytic behavior. The toxic Acridine Orange dye was degraded by ZnO NPs in indoor light and the disappearance of the dye was monitored by a spectrophotometer.

1. Introduction

Metal oxides and their outstanding properties in various fields have always attracted scientists. Metal oxides have many applications including sensors [1], superconductors [2], catalysts [3], and adsorbents [4]. However, some metal oxides might be a threat to human and animal safety. Zinc Oxide (ZnO) is considered a safe material for human beings and animals; therefore, it can be used as a viable solution for environmental protection [5]. Nanoscience is regarded as an important science since the nanoparticles exhibit distinct features from their bulk materials. There are several chemical methods reported for the preparation of ZnO NPs. For example, sol-gel technique [6], microemulsion synthesis [7], spray pyrolysis and drying [8], RF plasma synthesis [9], and so on.

Dye pollutants are an important source of environmental concern. Most of the organic dyes are not easily degradable by standard biological methods [10].

To briefly explain the mechanism constituting heterogeneous photocatalytic oxidation processes: on absorbing photon having energy greater than its band gap by a semiconductor led to the formation of electron/hole (e^-/h^+) pairs with free electrons produced in the empty conduction band (e_{CB}^-) leaving behind an electron vacancy or "hole" in the valence band (h_{VB}^+). Maintaining charge separation, the electron and hole may migrate to the catalyst surface where they participate in redox reactions with organic substrate. Generation of hydroxyl radical takes place when h^+_{VB} react with surface-bound H_2O or OH^-. Conduction band electron (e_{CB}^-) is picked up by oxygen to generate superoxide radical anion as indicated in the following Eqs. (1)– (3).

$$SC + h\nu \rightarrow e_{CB}^- + h_{VB}^+ \quad (1)$$

$$O_2 + e_{CB}^- \rightarrow O_2^{\bullet -} \quad (2)$$

$$H_2O + h_{VB}^+ \rightarrow OH^\bullet + H^+ \quad (3)$$

It has been suggested that hydroxyl radicals ($OH^\bullet$) and superoxide radical anions ($O_2^{\bullet -}$) are the main oxidizing species in the photocatalytic oxidation processes [11].

ZnO has recently received attention as an active photocatalyst because of its lower cost, simple synthesis process and has similar band gap energy around 3.2ev [12].

In the present paper, a simple precipitation method was used to synthesize ZnO NPs, in which Sodium hydroxide is the precipitation agent. The synthesis was repeated with a slight alteration in the process to examine the outgrowth of the factor. Then, the synthesized ZnO NPs were used in degradation of the acridine orange dye.

2. Experimental

2.1. Reagents

$ZnCl_2$ and NaOH pallets were purchased from Merck and were used as received without any further purification.

2.2. Synthesis of Nanosized ZnO

ZnO NPs were synthesized twice in this work and the process is as follows:

For the first try, 5.5 g of $ZnCl_2$ salt was dissolved in 100 ml of double distilled water with constant stirring. Then, the temperature of the solution was increased to 90°C. By setting the solution at this constant temperature, 16 ml of NaOH 3M solution was slowly added drop by drop touching the wall of the container. The slurry was vigorously stirred for 2 hours at 90°C and then settled down for 2 hours without heating. The solution was filtered and rinsed multiple times until reaching pH=7, then the synthesized ZnO NPs were collected was dried in an oven at 100°C for 3 hours. For the second try, 1.5 ml of HCl 2M was added to the

$ZnCl_2$ solution. After the complete dissolution of salt, the temperature of the solution was increased to 90°C. the proceeding steps were repeated without any changes.
The characterization analysis was done to the resultant ZnO NPs of both syntheses.

3. Results and discussion

3.1. Characterization of the ZnO NPs

FT-IR analysis of the dried ZnO NPs was carried out by the KBr pellet method and the presence of the various vibrational modes in the synthesized NPs was investigated. The phase structure and material identification of ZnO NPs were studied by X-ray diffractometer. The dynamic light scattering technique was employed to visualize the size of the particles.

3.1.1. FTIR analysis

Infrared studies (Fig. 1) were carried out to determine the purity and nature of the nanoparticles. The peaks at 461 and 521 cm^{-1} are signatures of Zn-O vibrational modes, also the peak at 623 cm^{-1} is corresponding to Zn-O deformation mode. These peaks are exactly located in the same wavenumber in both separately synthesized ZnO NPs and the difference is in the sharpness of the peaks. The Zn-O signature peaks of the second synthesis are sharper which might be associated with the complete dissolution of the $ZnCl_2$ salt due to the presence of HCl acid. The bands at 1050–700 cm^{-1} appeared to be due to Zn—O bonds [13]. The additional peaks observed at 3459 and 3566 cm^{-1} are due to O-H stretching vibration and the bands at 1635 or 1630 and 1383 or 1395 cm^{-1} were related to bending mode of H_2O [14]. which declares that despite the drying of samples, moisture could not be completely removed. The FTIR results confirm the NPs synthesized by the proposed method, are ZnO NPs without any significant impurity.

3.1.2. DLS analysis

Size is an important factor in defining NPs. Dynamic light scattering method can be utilized to have an insight into particle size. The particles dispersed into a proper solvent, get exposed to light and the scattered light is analyzed and the result is the hydrodynamic size of the particles. The reflective index used for recording DLS results was 1.33. Fig. 2 indicates that in the first synthesis, almost 50 percent of the dispersed particles have 200nm of diameter size, compared to the second try synthesis with the addition of HCl to $ZnCl_2$ salt that resulted in 40 percent of the dispersed particles' hydrodynamic diameter size is 85.5 nm. This proves that the Zn source must be completely dissolved for smaller-sized particles.

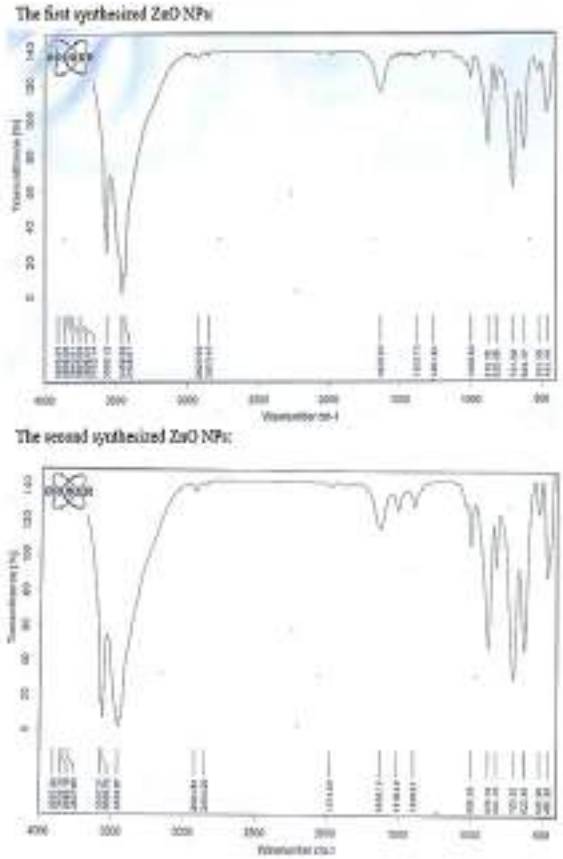

Fig.1. FTIR spectra of the synthesized ZnO NPs.

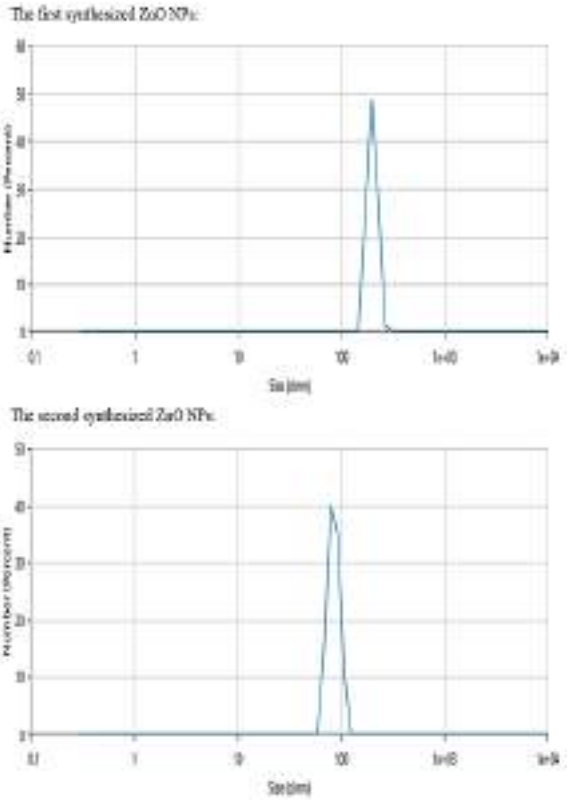

Fig.2. DLS results of the synthesized ZnO NPs.

3.1.3. XRD analysis

The crystalline structure of the samples is determined by X-ray diffraction analysis. XRD patterns for both samples are represented in Fig. 3. The peaks at 2θ of 32.7, 33.6, 37.8, 44.8 and 58.2 responds to (100), (002), (101), (102) and (110) planes [15] confirming the hexagonal unit cells of the synthesized ZnO NPs with lattice constants a = b = 0.324 nm and c = 0.521 nm based on the JCPDS card no. 36-1451 for wurtzite zinc oxide [16].

By examining and comparing the XRD patterns recorded for the first and second synthesized ZnO NPs, the obvious result is that both indicate very similar patterns however the second-time synthesis ZnO NPs have sharper peaks which validate more crystallinity.

3.2. Investigating photocatalytic behavior

To investigate the photocatalytic behavior of ZnO NPs, a specific concentration of acridine orange dye was prepared and a certain weight of NPs was added and continuously stirred. After a very short period of time (about two minutes), bubbles and gas exit were observed on the surface of the stirring liquid. then, the solution was filtered and its absorbance was measured by a spectrophotometer. Also, there was an obvious change in the color of acridine orange solution after adding ZnO NPs (Fig. 4).

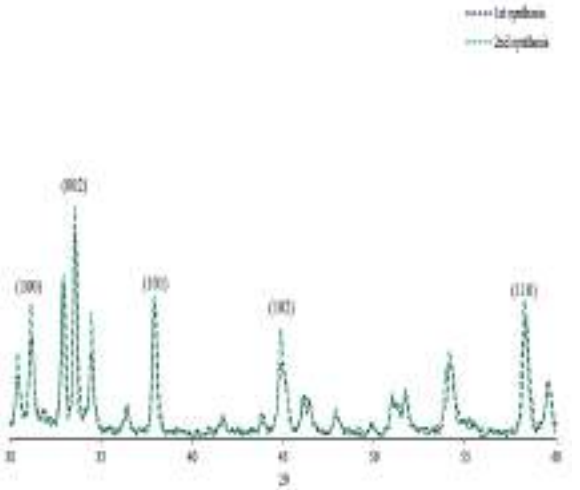

Fig.3. XRD patterns for Synthesized ZnO NPs.

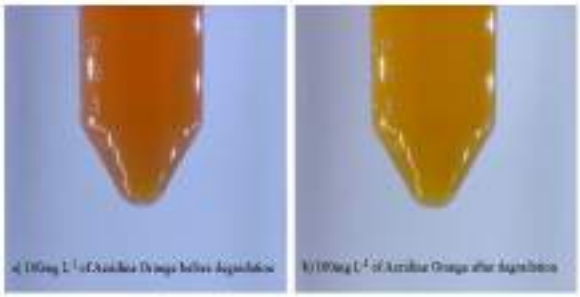

Fig.4. Acridine Orange solution color comparison of a) before, and b) after degradation by ZnO NPs.

Conclusion

In the present paper, we have produced and characterized ZnO NPs in different conditions. The results of the comparison between both ZnO NPs indicate that adding an appropriate amount of HCl assists the complete dissolution of Zn source and the produced NPs are smaller in size and have higher crystallinity. Subsequently, the ZnO NPs were successfully used for degradation of the Acridine Orange dye.

References

[1] M. Yang, J. He, X. Hu, C. Yan, Z. Cheng, Y. Zhao, G. Zuo, Surface and interface physics papers A 155. 2. (2011) 692-698.

[2] V. Pillai, P. Kumar, M. J. Hoa, P. Ayyub, D. O. Shah, J. Advances I Colloid and Interface Science 55 (1995) 241-269.

[3] T. G. Altincekic, I. Boz, S. Aktürk, J Nanosci nanotechnol 8. 2. (2008) 874-877.

[4] R. Han, L. Zoa, X. Zhao, Y. Xu, F. Xu, Y. Li, Y. Wang, Chemical Engineering Journal 149. 1. (2009) 123-131.

[5] A. K. Arora, S. Devi, V. S. Jaswel, J. Singh, M. Kinger, V. D. Gupta, Oriental Journal of Chem, 30. 4. (2014) 1671-1679.

[6] M. S. Tokumoto, S. H. Pulcinelli, C. V. Santilli, V. Briois, J. Phys. Chem. B 107 (2003) 568–574.

[7] M. Singhai, V. Chhabra, P. Kang, D.O. Shah, Mater. Res. Bull. 32 (1997) 239–247.

[8] F. Paraguay D., W. Estrada L., D.R. Acosta N., E. Andrade, M. Miki-Yoshida, J. Thin Solid Films 350. 1. (1999) 192-202.

[9] T. Sato, T. Tanigaki, H. Suzuki, Y. Saito, O. Kido, Y. Kimura, C. Kaito, A. Takeda, S. Kaneko, J. Cryst. Growth 255 (2003) 313–316.

[10] B. Pare, S. B. Jonnalagadda, H. Tomar, P. Singh, V. W. Bhagwat, J. Desalination 232 (2008) 80-90.

[11] M. Faisal, S. B. Khan, M. M. Rahman, A. Jamal, A. M. Asiri, M. M. Abdullah, J. Applied Surface Science 258. 2. (2011) 672-677.

[12] J. H. Sun, S.Y. Dong, Y.K. Wang, S.P. Sun, J. Hazard Mater 172 (2009) 1520.

[13] M.N. Zafar, Q. Dar, F. Nawaz, M. N. Zafar, M. Iqbal, M. F. Nazar, J. Mater Res and Techn 8. 1. (2019) 713-725.

[14] M. Gu, L. Hao, Y. Wang, X. Li, Y. Chen, W. Li, L. Jiang, J. Chemical Physics 534 (2020) 110750.

[15] N. Goswami, D. Kumar Sharma, J. Physica E: Low-dimensional Systems and Nanostructures 42. 5. (2010) 1675-1682.

[16] S. Talam, S. R. Karumuri, N. Gunnam, J. International Scholarly Research Notices (2012).

29TH IRANIAN ORGANIC CHEMISTRY CONFERENCE
1_3 NOV, 2023
UNIVERSITY OF QOM, IRAN

Green synthesis of Se-NPs using *Polylophium involucratum* (Pall.) Boiss. Extract, Characterization and Investigation of its *in vitro* Antioxidant Activity

Shahab Ojani [1], Naser Montazeri [2], Masoud Mohammadi Zeydi[1] and Masoud Ghane[2]*

[1] *Department of Chemistry and Medicinal Chemistry, Tonekabon Branch, Islamic Azad University, Tonekabon, Iran, Shahab_ojani@yahoo.com, Montazer1350@gmail.com.*
[2] *Department of Microbiology, Tonekabon Branch, Islamic Azad University, Tonekabon, Iran*

Abstract - Nowadays, plant-mediated synthesis of metal nanoparticles is a promising alternative to the traditional method of physical and chemical synthesis. In this research, the green synthesis of selenium nanoparticles (Se-NPs) using *Polylophium involucratum* (Pall.) Boiss. seeds extract as a reducing agent by microwave irradiation method and its antioxidant properties have been reported. Green ssynthesis of (Se-NPs) was characterized by UV-Vis, FT-IR, XRD, TEM, and FE-SEM. FT-IR spectroscopy revealed that (Se-NPs) were functionalized with biomolecules that have carbonyl groups, OH groups and other stabilizing functional groups. An absorption band centered on 330 nm was observed, this absorption corresponds to the surface plasmon resonance (SPR) of the (Se-NPs). The structure and composition of (Se-NPs) were analyzed by XRD and showed that the (Se-NPs) are crystalline. The morphological study of (Se-NPs) using TEM suggests that the nanoparticles are spherical with a diameter of 150 nm. The antioxidant activity of the synthesized (Se-NPs) was assayed by the $DPPH^0$ free radical scavenging assay method. The results of radical scavenging activity (%) and IC_{50} of (Se-NPs) were 69.43 % and 0.57 mg/ml respectively. Furthermore, the present study can be continued for their structural elucidation, biomedical application, and pharmacological activity.

1. Introduction

The effect of free radicals, especially Reactive Oxygen Species (ROS), has been well understood in developing several pathological disorders, including diabetes, cardiovascular diseases, cancers, inflammatory, and neurodegenerative diseases (e.g., Parkinson's disease, Alzheimer's disease, etc.) Recently herbs have received remarkable attention as a source of safe and potent substantial free radical sweepers to hinder oxidative stress-related illnesses [1]. Therefore, Nanotechnology is a multidisciplinary research field that covers various technologies such as biology, physics, engineering, chemistry, *etc.* on a scale of 1 to 100 nm. Nano-biotechnology is a branch of nanotechnology that deals with the design, fabrication, and manipulation of Nano-scale materials using a biological approach or in favor of biological systems. Nanomaterial synthesis using biological techniques has attracted considerable attention in the Nano-biotechnology field using various algae, plants, bacteria, fungi, marine organisms, yeasts, and natural biomolecules [2]. The synthesis of metallic nanoparticles (NPs) has attracted considerable attention because of their specific features. Various metals, including gold, silver, copper, zinc, magnesium, selenium, and titanium have been evaluated; the selenium nanoparticles (Se-NPs) have indicated a broad size morphology and distribution with highly reactive aspects. These procedures have made a few groups of inorganic nanoparticles (importantly, metal oxides, metal nanoparticles, and salts). Through the reagents mentioned above, plant-based materials appear to be the best choice, and they are proper for nanoparticle fabrication through 'biosynthesis. Bioactive secondary metabolites flavonoids, phenolic compounds, alkaloids exist in medicinal herbs. They are utilized for curing several illnesses such as infectious diseases and disorders; in addition, they have some benefits in the green synthesis approach. Moreover, capping agents are significant for nanoparticle stabilization. Capped (Se-NPs) indicate better activity than uncapped (Se-NPs). Synthesized green nanoparticles of biological sources such as plants are extensively accomplished since they are less toxic to humans than chemical drugs [3-5]. *Polylophium involucratum* (Pall.) Boiss. ((P. involucratum)), is a wild aromatic plant that belongs to the Umbelliferae (Apiaceae) family. In the north of Iran, it is used as a seasoning and flavoring and this plant has been effective in the treatment of oral and dental infections in the past. Studies on aqueous extracts have revealed that they are rich in coumarins, flavonoids, quinones, phenols, cardiac glycosides, phlobatannins, and terpenoids [6]. Hence, in the present project, we have demonstrated green synthesis of (Se-NPs) using P. involucratum extract, characterization and investigation of its *in vitro* antioxidant activities.

2. Experimental

All used materials/reagents were certified analytical grades; sodium selenite (Na_2SeO_3), ethanol, and etc media were attained from Sigma-Aldrich (St. Louis, MO, USA). Seeds of P. involucratum were collected from the highlands of javaherdeh in Ramsar, identified by the herbarium expert, registered with the code 754. And, in this method, 30 gram of powder of seeds of P. involucratum was mixed with hydroalcoholic exposed to microwave irradiation at 100 W in microwave (model GE 280 S) oven with regular at intervals 10 minute irradiation during 5 minutes. After extracting, the solvent was removed under the vacuum at temperature below 45^{0C} and the extracts were freeze dried. Then, 0.1 g of dried extract of P. involucratum seeds is added into 50 ml deionized water and then stirred for 1 h in a magnetic stirrer at room temperature. Coarse filtering is employed prior to centrifuging the extract at 4000 rpm for 30 min to remove the heavy biomaterials in it. Clear P. involucratum seeds extract is mixed immediately into a 0.1 mM Na_2SeO_3 solution of equal volume. The color change involved in the formation of (Se-NPs). Green synthesis of (Se-NPs) was characterized by UV-Vis, FT-IR, XRD, TEM, and FE-SEM. Then, the phytochemicals which are present in the hydroalcoholic extract of seeds of P. involucratum was determined and quantified by standard procedures and the antioxidant activity of the synthesized (Se-NPs) was assayed by the $DPPH^0$ free radical scavenging assay method [7-10].

3. Results and Discussion

3.1. Quantitative phytochemical analysis

Total phenol contents (TPC) of the extracts were determined according to the Folin-Ciocalteu method and expressed in mg of Gallic acid equivalent per g (mg GAE/g) of extract, by reference to a standard curve (y=47.00 x and R^2=0.979). Total phenol contents in hydroalcoholic extracts of seeds of P. involucratum was 12.93±2 mg GAE/g dry plant material, respectively. Also, the total flavonoid contents (TFC) of the extracts were measured according to the Aluminum Chloride Colorimetric method and expressed in mg of Rutin equivalent per g (mg Ru/g) of extract, by reference to a standard curve (y=8.26 x and R^2=0.995). Total flavonoid contents in hydroalcoholic extracts of seeds of P. involucratum was 7.58±7 Ru/g dry plant materials, respectively. The radical scavenging activity (%) and IC_{50} of hydroalcoholic extracts of seeds of P. involucratum was (57.70 % - 0.66), and radical scavenging activity (%) and IC_{50} (Se-NPs) using hydroalcoholic extracts of seeds of P. involucratum (69.43 % - 0.57) mg/ml respectively. Also, ascorbic acid used as the reference control was (0.0116) μg/ml.

3.2. UV-Vis characterization

Due to the formation of the Se-NPs, Surface Plasmon Resonating (SPR) signal that may have been shown as a wide excitation wavelength (λ max) in the range of a wavelength of 270–400 nm, the creation of (Se-NPs) could be validated using the UV–Vis spectrophotometer. SPR of selenium occurs at 330 nm (Fig. 1.).

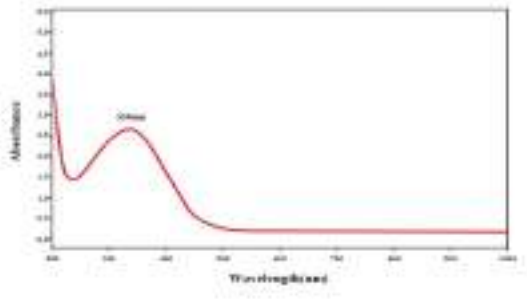

Fig.1. UV–Visible spectrum of synthesized (Se-NPs)

3.3. FT-IR analysis

Biomolecules that are associated with (Se-NPs) are detected via FT-IR. The FT-IR results are given in (Fig 2). The presence of amides, alkenes, alkoxy, alcohols, etc was confirmed via FT-IR, which played vital roles as reducing and capping agents of (Se-NPs) synthesis. These functional groups were also responsible for the stabilization of nanoparticles. Similar results from FT-IR were reported earlier and hence confirmed.

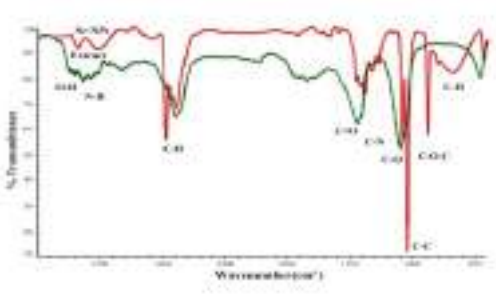

Fig.2. FT-IR spectra of (Se-NPs) obtained using P. involucratum

3.4. XRD results

XRD analysis was used to examine the crystal structure and phase of the produced (Se-NPs) (Fig. 3) shows the XRD pattern of the produced (Se-NPs). The XRD peaks of (Se-NPs) and displays the diffraction characteristics regarding 2θ at 23.78°, 29.6°, 40.5°, 52.2° and 65.46° which represented the Bragg/s reflections at (100), (101), (111), and (210) respectively. The XRD results indicated that the formed (Se-NPs) were highly crystalline for better application.

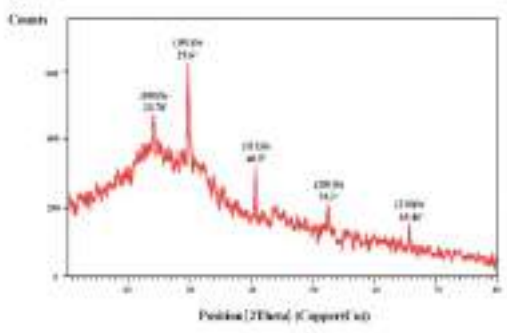

Fig. 3. XRD pattern of (Se-NPs) obtained using P. involucratum

3.5. TEM studies

The formation of (Se-NPs) by hydroalcoholic extract of seeds of P. involucratum was confirmed by the TEM image. The morphological project of (Se-NPs) using TEM suggests that the nanoparticles are spherical with a diameter of 150 nm respectively, (Fig. 4).

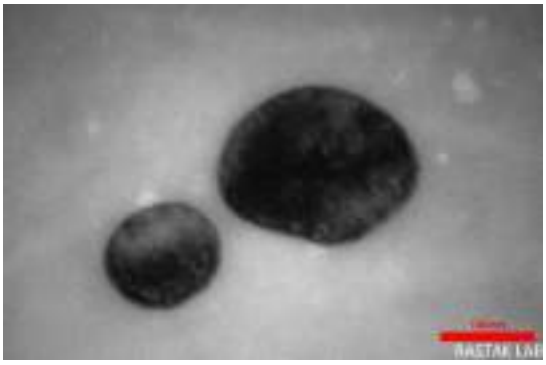

Fig. 4. TEM images indicating the presence of spherical (Se-NPs)

3.6. FE-SEM studies

The morphology and size of (Se-NPs) derived from P. involucratum seeds extract were characterized by field emission scanning electron microscope (Fig. 5). Phytosynthesized (Se-NPs) had been size was 79.15 nm according to FE-SEM images. The nanoparticles were spherical and agglomerated. These synthesized nanoparticles were highly stable.

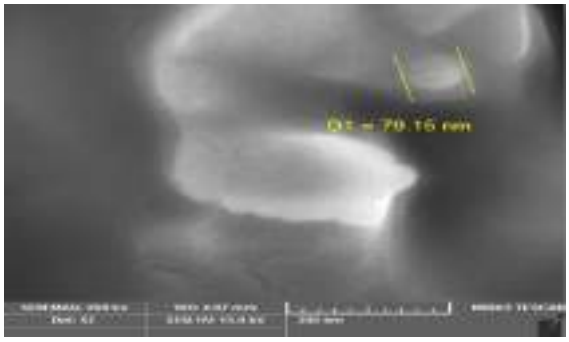

Fig. 5. FE-SEM image of (Se-NPs)

4. Conclusions

In this project, the green synthesis of (Se-NPs) was successfully performed, as indicated by UV-Vis, FT-IR, XRD, TEM, and FE-SEM, demonstrating stable nanoparticles with chemical bonds corresponding to the P. involucratum extract used. The green synthesized (Se-NPs) exhibited good antioxidant potential. Therefore, (Se-NPs) synthesized in this manner exhibit particular potential in biomedical applications such as cancer therapy, targeted chemotherapy, and drug delivery systems. They could also be found in suitable applications as efficient antibacterial and antioxidant agents in the food and pharmaceutical industry.

4. References

[1] M.A. Soobrattee, V.S. Neergheen, A. Luximon-Ramma, OI. Aruoma, T. Bahorun, Mutat. Res. 579 (2005) 13-200.

[2] O. Shoseyov, I. Levy (eds.) Nano-biotechnology: BioInspired Devices and Materials of the Future, 1th edition, Humana Press: Totowa, New Jersey, 2008.

[3] S.A. Dahoumane, M. Mechouet, K. Wijesekera, CDM. Filipe, C. Sicard, D.A. Bazylinski, C, Jeffryes, Green. Chem, 19 (2017) 552-87.

[4] M.B. Marulasiddeshwara, S.S. Dakshayani, M.N. Sharath Kumar, R. Chethana, P. Raghavendra Kumar, S. Devaraja, Mater. Sci. Eng. C Mater. Biol. Appl. 81 (2017) 182-190.

[5] S. Chung, R. Zhou, T.J. Webster, Int. J. Nanomed. 15 (2020) 115-124.

[6] Kh. Pourshamsian, Sh. Ojani, J. Planta Medica. 82 (05) (2016).

[7] H.H. Hussein, O.M. Darwesh, B.B. Mekki, Biocatalys. Agric. Biotechnol. 18 (2019).

[8] M. Bartosiak, J. Giersz, K. Jankowski, Microchem. J. 145 (2019) 1169-1175.

[9] W. Brand-Williams, M.E. Cuvelier, C. Berset, Food Sci Technol. 28 (1995) 25- 30.

[10] P. Banerjee, M. Satapathy, A. Mukhopahayay, P. Das, Bioresour. Bioprocess. 1 (2014) 1-10.

29TH IRANIAN ORGANIC CHEMISTRY CONFERENCE
1_3 NOV, 2023
UNIVERSITY OF QOM, IRAN

Evaluation of Bioactive Metabolites of Hydroalcoholic Extract of *Polylophium involucratum* (Pall.) Boiss. by Phytochemical Analysis

Shahab Ojani [1], *Naser Montazeri* [2*], *Masoud Mohammadi Zeydi*[1] *and Masoud Ghane*[2]

[1] *Department of Chemistry and Medicinal Chemistry, Tonekabon Branch, Islamic Azad University, Tonekabon, Iran, Shahab_ojani@yahoo.com, Montazer1350@gmail.com*
[2] *Department of Microbiology, Tonekabon Branch, Islamic Azad University, Tonekabon, Iran*

Abstract - *Polylophium involucratum* (Pall.) Boiss. is a wild aromatic plant that belongs to the Umbelliferae (Apiaceae) family. The aim of this project, evaluation of bioactive metabolites of hydroalcoholic extract of P. involucratum by phytochemical analysis. The seeds of P. involucratum were collected from Ramsar, Iran and hydroalcoholic extract prepared by microwave assisted extraction method. Qualitative and quantitative phytochemical analysis of hydroalcoholic extract of seeds of P. involucratum was conducted following the standard procedures. The antioxidant potential was evaluated by ($DPPH^0$) assay. Later, the antibacterial activity was screened against on gram positive (*Staphylococcus aureus* and *Bacillus cereus*) as well as gram negative bacteria (*Escherichia coli*) by disk diffusion method. The phytochemical screening of hydroalcoholic extract was terpenoids, flavonoids, phenols, saponins, coumarins, cardiac glycosides, tannins and quinones presented. Our data showed total phenol contents of hydroalcoholic extracts of P. involucratum was 12.93±2 mg GAE/g dry plant material. Total flavonoid contents of hydroalcoholic extracts was 7.58±7 mg RU/g dry plant material. The hydroalcoholic extract of *P. involucratum* exhibited good antibacterial, and antioxidant potential. These findings provide an opportunity to use hydroalcoholic extract in biomedical, cosmetics, and pharmaceutical applications, especially to develop novel antioxidant and antibacterial compounds.

1. Introduction

Medicinal plants are used worldwide by humans as therapeutic resources and as an alternative to conventional medicine in contemporary society. Currently, these natural products play a pivotal role as a source of compounds, and many drugs derived from traditional herbal medicine are used in modern pharmacotherapy. Despite the increasing commercialization of herbal remedy as safe for consumers, these plant materials require monitoring due to their potential adverse and toxic effects. Given this concern, medicinal plants have become the focus of scientific studies due their chemical diversity, which can have unknown biological effects [1-3]. Therefore, quality control is crucial in order to evaluate the safety, efficacy, and validation of medicinal plant use, with regard to the potential risks associated with their chemical composition. Plants produce a wide variety of molecules and highly specific secondary metabolites (e.g., phenolic compounds, and terpenes), which play several roles in plant growth and development processes. Furthermore, these compounds display positive beneficial effects on human health and agricultural production, arousing scientific interest due to their potential application in several industrial areas, and significantly contributing to the economy. Among them, the pharmaceutical industry stands out, as plant secondary metabolites are a promising source of new molecules for drug research and development, with potential for clinical use [4-5]. Nevertheless, many of these chemical compounds can interact with DNA and other biomolecules, promoting alterations at the biochemical, physiological, and molecular levels. *Polylophium involucratum* (Pall.) Boiss. ((P. involucratum)), is a wild aromatic plant that belongs to the Umbelliferae (Apiaceae) family. In the north of Iran, it is used as a seasoning and flavoring and this plant has been effective in the treatment of oral and dental infections in the past. Studies on aqueous extracts have revealed that they are rich in coumarins, flavonoids, quinones, phenols, cardiac glycosides, phlobatannins, and terpenoids [6]. Accordingly, the aim of this project, evaluation of bioactive Metabolites of hydroalcoholic extract of *Polylophium involucratum* (Pall.) Boiss. by phytochemical analysis.

2. Experimental

All used materials/reagents were certified analytical grades; media were attained from Sigma-Aldrich (St. Louis, MO, USA). Seeds of P. involucratum were collected from the highlands of javaherdeh in Ramsar,

identified by the herbarium expert, registered with the code 754. And, in this method, 30 gram of powder of seeds of P. involucratum was mixed with hydroalcoholic exposed to microwave irradiation at 100 W in microwave (model GE 280 S) oven with regular at intervals 10 minute irradiation during 5 minutes. After extracting, the solvent was removed under the vacuum at temperature below 45^{0C} and the extracts were freeze dried. Qualitative phytochemical analysis of hydroalcoholic extracts of seeds of P. involucratum was conducted following the standard procedures [7]. The Folin-Ciocalteu method was used to estimate the total phenols as Gallic acid equivalents. $AlCl_3$ colorimetric assay was used for flavonoid determination [8]. The antioxidant activity was measured in terms of hydrogen donating or radical scavenging ability, using the stable radical, 2,2-Diphenyl-1-picrylhydrazyl [9]. Then, In this research, to assess the antibacterial activity of the hydroalcoholic extract of P. involucratum, the selected bacterial strains are *Staphylococcus aureus* (ATCC: 29213), *Bacillus cereus* (ATCC: 14579) and *Escherichia coli* (ATCC:25922), which will be prepared from American Type Culture Collection and assessed by disc diffusion method based on certain methodology. [10].

3. Results and Discussion

3.1 *in vitro* Qualitative phytochemical analysis

The results of the phytochemical screening of hydroalcoholic extract of seeds of P. involucratum were terpenoids, flavonoids, phenols, saponins, coumarins, cardiac glycosides, tannins and quinones presented. The medicinal actions of plants are unique to a particular plant species or groups, consistent with the concept that the combination of secondary products in a particular plant is taxonomically distinct. Thus the preliminary screening test may be useful in the detection of the bioactive principles and subsequently may lead to the drug discovery and development. The screening of plants for medicinal value has been carried out by numerous researchers with the help of preliminary phytochemical analysis. Phytochemical screening test is of paramount importance in identifying new source of therapeutically and industrially valuable compound having medicinal significance, to make the best and judicious use of available natural wealth. A number of medicinal plants have been chemically investigated by several researchers. These phytochemicals have been shown to possess anti-oxidant, anti-inflammatory, anti-cancer, anti-bacterial, anti-diabetic, anti-pyretic, allergenic, anti-coronary, anti-septic, analgesic, anti-arthritic, sedative, anesthetic, hypo-cholesterolemic, and hepato-protective activities.

3.2. Quantitative phytochemical analysis

Total phenol contents (TPC) of the extracts were determined according to the Folin-Ciocalteu method and expressed in mg of Gallic acid equivalent per g (mg GAE/g) of extract, by reference to a standard curve ($y=47.00$ x and $R^2=0.979$). Total phenol contents in hydroalcoholic extracts of seeds of P. involucratum was 12.93±2 mg GAE/g dry plant material. Also, the total flavonoid contents (TFC) of the extracts were measured according to the Aluminum Chloride Colorimetric method and expressed in mg of Rutin equivalent per g (mg Ru/g) of extract, by reference to a standard curve ($y=8.26$ x and $R^2=0.995$). Total flavonoid contents in hydroalcoholic extracts of seeds of P. involucratum was 7.58±7 Ru/g dry plant materials. The radical scavenging activity (%) and IC_{50} of hydroalcoholic extracts of seeds of P. involucratum was (57.70 % - 0.66) mg/ml respectively. Also, ascorbic acid used as the reference control was (0.0116) μg/ml.

Antioxidant activity was examined because most of the sicknesses in humans are due to free radicals. Free radicals cause many diseases in the human body. Free radicals that are produced in our body are examined by antioxidant monitoring compounds. There are many kinds of antioxidants that are not good for human health, but they are swapped for natural ones. There are many kinds of human diseases, for example, inflammatory diseases, cardiovascular diseases, and cancer, in which antioxidants reduce the oxidative stress in cells and make it useful in many aspects. To avoid artificial antioxidants, more cheap, bioactive, and safe antioxidants have been explored from plants. Many studies have confirmed the antioxidant activity of medicinal plants.

3.2. Antibacterial activity

Antibacterial action in (Fig. 1.) depicts the antibacterial activity of hydroalcohlic extract of seeds of P. involucratum. The results of investigation of the hydroalcohlic extracts of seeds of P. involucratum antibacterial effect on a gram-negative bacterium (*Escherichia coli*) and two gram-positive bacteria (*Staphylococcus aureus* and *Bacillus cereus*) and comparison of this extract antibacterial activity with the antibiotic ampicillin, used as a control, revealed the significant ability of these nanoparticles to inhibit the growth of the investigated bacteria. Based on the results, the zone of inhibition of these hydroalcohlic extracts of seeds of P. involucratum for *Staphylococcus aureus*, *Bacillus cereus*, and *Escherichia coli* was "10, 10, 25" mm, respectively. (The zone of inhibition of antibiotic ampicillin 6 mm).

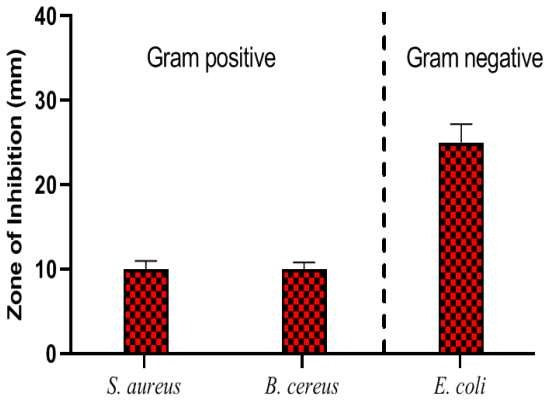

Fig.1. antibacterial activity of hydroalcohlic extract of P. involucratum

The development of new drugs is due to microorganisms having become resistant to many antibiotics due to increased use of drugs, which is decreasing efficiency of conventional medicines. So, it is necessary to find out new antimicrobial agents to fight against diseases.

4. Conclusions

The hydroalcoholic extract of seeds of P. involucratum exhibited good antibacterial and antioxidant potential. Also, the qualitative extract of P. involucratum showed the presence of hydroalcoholic extract of seeds of P. involucratum were terpenoids, flavonoids, phenols, saponins, coumarins, cardiac glycosides, tannins and quinones. Therefore, hydroalcoholic extract P. involucratum exhibit particular potential in biomedical applications such as cancer therapy, targeted chemotherapy and drug delivery system. They could also be found in suitable applications as efficient antibacterial and antioxidants agents in the food and pharmaceutical industry.

4. References

[1] H. Zheng, X. Fu, J. Shao, Y. Tang, M. Yu, L. Li, L. Huang, K. Tang, Trends Plant Sci. in press (2023).
[2] A. Jităreanu, A. Trifan, M. Vieriu, I.-C. Caba, I. Mâr¸tu, L. Agoroaei, Processes. 11 (2023) 83.
[3] M.B.N. Alves, N.B. Barros, C.A.B. Lugtenburg, R.R. Barros, Braz. J. Dev. 8 (2022) 31491.
[4] B.M. Twaij, M.N. Hasan, Int. J. Plant Biol. 13 (2022) 4-14.
[5] A.J. Siddiqui, S. Jahan, R. Singh, J. Saxena, S.A. Ashraf, A. Khan, R.K. Choudhary, S. Balakrishnan, R. Badraoui, F. Bardakci, Biomed. Res. Int. (2022) 5425485.
[6] Kh. Pourshamsian, Sh. Ojani, J. Planta Medica. 82 (05) (2016).
[7] E.C. Trease, W.C. Evans, Pharmacognosy, 16th Edition, W.B. Saunders, Philadelphia, 2009.
[8] L. Lebanov, S. Chung Lam, L. Tedone, T. Sostaric, JA. Smith, A. Ghiasvand, Journal of Chromatography B, 1179, (2021).
[9] W. Brand-Williams, M.E. Cuvelier, C. Berset, Food Sci. Technol. 28 (1995) 25- 30.
[10] M.M. Hassan, Antimicrobial Resistance - A One Health Perspective [Internet]. London, IntechOpen, 2020.

29TH IRANIAN ORGANIC CHEMISTRY CONFERENCE
1_3 NOV, 2023
UNIVERSITY OF QOM, IRAN

Recent advances in the use of nanostructures in biomedicine as smart drug delivery systems

Ali Hossein Rezayan, Hale Alvandi*

Division of Nanobiotechnology, Department of Life Science Engineering, Faculty of New Sciences and Technologies, University of Tehran, P.O. Box 14395-1561, Tehran, Iran, ahrezayan@ut.ac.ir

Abstract: Drug discovery involves highly challenging, laborious, expensive, and time-consuming processes. However, most drugs fail in clinical trials and they are not able to reach the target site. The ineffectiveness of drug delivery to the target tissue and their side effects have led to the attention of new drug delivery methods such as the use of nanostructures. In addition to targeted drug/gene delivery, nanostructures can be used in various biomedical fields such as disease diagnosis and tissue engineering. In recent years, our research team has been focused on the synthesis, and application of nanostructures in diagnosis methods, drug delivery, and wound healing. In this review, we intend to have a brief overview of some reported work in the field of drug delivery systems.

Keywords: Nanostructure, Drug Carriers, Drug Delivery Systems, Biomedicine.

1. Introduction:

Drug discovery and development involve highly challenging, laborious, and expensive processes. The development process of each new drug takes an average of 15 years with an estimated cost of about 802$ million, and this cost is markedly increasing at an annual rate of 7.4%. However, most drugs fail in clinical trials because they are not able to reach the target site. A significant amount of drug is distributed over the normal tissues or organs that are not involved in the pathological process, often leading to severe side effects. An effective approach to overcome this critical issue is the development of drug delivery systems that release the drugs or bioactive agents at the desired site of action. This could increase patient compliance and therapeutic efficacy of pharmaceutical agents through improved pharmacokinetics and biodistribution [1-4]. Drug-delivery systems were developed primarily for traditional routes of administration, such as oral and intravenous, but recently there has been an explosion in research on delivery by so-called nonconventional routes, such as transdermal, nasal, ocular, and pulmonary administration. Drug-delivery applications have expanded from traditional drugs to therapeutic peptides, vaccines, hormones, and viral vectors for gene therapy [1, 3, 4]. Nanocarriers such as dendrimers, liposomes, peptide-based nanoparticles, carbon nanotubes, quantum dots, polymer-based nanoparticles, inorganic vectors, lipid-based nanoparticles, hybrid NPs, and metal nanoparticles are the advanced forms of NPs. The choice of the carrier molecule is of high importance because it significantly affects the pharmacokinetics and pharmacodynamics of the drugs. In recent years, our research team has been focused on the synthesis, surface modification, functionalization, and application of nanostructures in diagnosis methods, drug delivery, and tissue engineering. In this review, we intend to have a brief overview of some reported work in the field of drug delivery systems.

2. Drug/gene delivery:

2.1. Polymer based nanostructure:

During the last two decades, a wide range of natural and synthetic polymers have been used as nanocarriers in drug/gene delivery. Among the most common polymers used for drug/gene delivery are polycaprolactone (PCL), polylactic acid, chitosan, and gelatin. Oroojalian et al. (2017) synthesized aminoglycoside-carboxyalkyl-polyethylenimine-containing nanoplexes for gene delivery. Investigations showed that modifying the surface of nanostructures, in addition to reducing their toxicity, improves the efficiency of gene transfection into megalin receptor-expressing cells [5]. In another study, Oroojalian et al. (2017) used polyamine-polyethylenimine (PEI) nanostructure conjugated polymyxin B for kidney targeting . In vitro, modifying the nanostructure surface increases the delivery efficiency. In vivo, the presence of nanostructure and gene expression in the kidney is significantly higher than in other tissues [6].

Fig. 1. Schematic illustration showing the development of hybrid PLGA/lecithin NPs. The hybrid NPs comprise a hydrophobic

PLGA core and a lipid (lecithin) monolayer shell at the surface of the hydrophobic core [7].

Ahmaditabar et al. (2017) used hybrid nanoparticles consisting of a hydrophobic poly(lactide-co-glycolide) (PLGA) core and a monolayer coating of soy lecithin for the controlled release of N-acetylcysteine (NAC). The size of these nanoparticles (Fig. 1), which were synthesized using a combined nanoprecipitation and self-assembly method, was about 81 nm. Also, the drug entrapment efficiency was 67%. In vitro studies on normal alveolar cells showed that this nanostructure had no cytotoxic effect [7].

2.2. Lipid based nanostructure:

Lipid-based nanostructures with high diversity are one of the most common nanostructures in drug delivery, whose clinical applications have also been confirmed. Among these nanostructures are liposomes, niosomes, and solid lipid nanoparticles. In addition to advantages such as increased permeability and targeted delivery, lipid nanostructures have a simple formulation that enables low-cost industrialization. Hamedinasab et al. (2020) loaded NAC into liposomes (Fig. 2). In this study, liposomes were coated with chitosan to optimize formulation and long-term and controlled drug release. The release of NAC in the simulated lung fluid showed that the drug release from the chitosan-coated liposome reached 38% after 9 hours; While the drug release from the liposome was 51% at the same time. Investigations showed that coating liposomes with chitosan, in addition to improving the cellular uptake, increases nanoparticles remaining time in the rat lung by increasing the stability [8, 9]. Shirvany et al. (2021) used niosome nanoparticles for cefazolin delivery. Investigations showed that loading antibiotics in these nanoparticles causes the stability and maintenance of the drug structure. The slow release of the drug from the niosome along with the fusion of the nanoparticles with the bacterial cell wall, which facilitates the entry of the antibiotic into the bacteria, has caused a disruption in the proteins function and the construction of the bacterial cell wall, which ultimately leads to cell death [10].

Fig. 2 The liposomal formulation was prepared using the thin-film hydration method. NAC: N-acetylcysteine; MLV: multilamellar; SUV: small unilamellar vesicles; DPPC: dipalmitoyl phosphatidylcholine; DPPG: dipalmitoyl phosphatidylglycerol [9].

3. Biomedical applications:

3.1. MRI Contrast Agent:

Magnetic nanoparticles with high stability are suitable for biomedical applications, especially MRI contrast enrichment. Rezayan et al. (2016) modified Fe_3O_4 nanoparticles with carboxyl functionalized polyethylene glycol (PEG) via dopamine (DPA) linker to improve the quality of MRI images and the biocompatibility and stability of nanoparticles (Fig. 3). Compared to unmodified nanoparticles, modified nanoparticles had better cellular uptake in MDA-MB-231 cancer cells. Also, the quality of MRI images improved significantly by using modified nanoparticles [11]. In another study, PEG and D-glucosamine were used to modify the surface of Fe_3O_4. Studies show that normal kidney cells are very sensitive to MRI contrast agents. This is while using modified nanoparticles had very little toxicity for these cells. In vivo, these nanoparticles have a tendency to accumulate in tissues with high metabolism, such as the gastrointestinal tract, and can improve the quality of imaging [12].

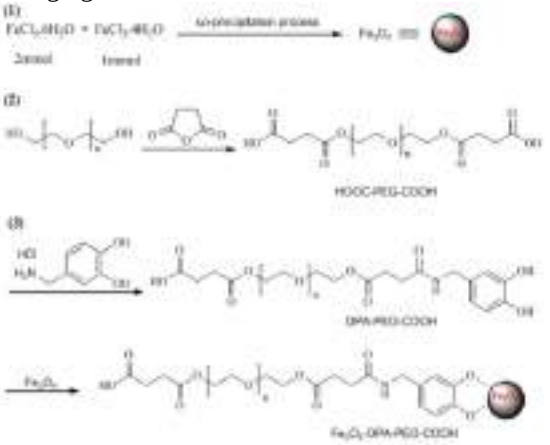

Fig. 3. Fe_3O_4 synthesis via co-precipitation method (1), Synthesis of PEG diacid (2), and immobilization of PEG diacid on Fe_3O_4 nanoparticles via DPA linker (3) [11].

3.2. Wound healing:

The complexity of the wound-healing process has caused the use of modern, bioactive wound dressings based on nanostructures to receive more attention in recent years [13, 14]. Mirmajidi et al. (2021) used a 3-layer wound dressing consisting of chitosan, PCL, and polyvinylalcohol (PVA) containing melatonin for surgical wound repair in rats (Fig. 4). By imitating the structure of the extracellular matrix, the three-layer wound dressing causes proper adhesion of cells and helps to heal the wound faster by stimulating cell proliferation and collagen synthesis [14]. Firoozi et al. (2017) prepared a scaffold containing a polymer network of PCL-polyurethane. This scaffold was synthesized through the reaction of hydroxyl-terminated four-armed star-shaped PCL, 1,4-diisocyanatobutane, and ethylenediamine. Cell studies showed that the presence of PCL in this scaffold stimulates the proliferation and growth of fibroblast cells. The biocompatibility of this scaffold makes it very capable in tissue engineering and skin repair [15].

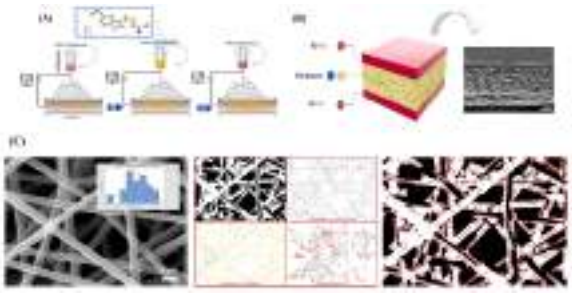

Fig. 4. Fabrication of the three-layer wound dressing (A) Schematic micrograph of three-layer wound dressing (PCL + Cs/ PVA + MEL/ PCL + Cs). (B) SEM images of the three-layer wound dressing of PCL + Cs/ PVA + MEL/ PCL + Cs cross-section. Scale bar = 100 µm. (C) Processing SEM image by imageJ software to optimize PVA nanofibers, scale bar 1 µm [14].

Conclusions:

In this review, the synthesis, surface modification, and application of nanostructures were investigated. Modifying the surface of nanostructures with various biological and chemical molecules, in addition to increasing their stability, also provides the possibility of their targeted delivery. The combination of chemical and biological molecules with the effect on material properties can help to expand the use of nanostructures in the diagnosis and treatment of diseases.

References:

1. O. Afzal, A.S. Altamimi, M.S. Nadeem, S.I. Alzarea, W.H. Almalki, A. Tariq, B. Mubeen, B.N. Murtaza, S. Iftikhar, and N. Riaz. "Nanoparticles in Drug Delivery: From History to Therapeutic Applications", Nanomaterials. 12(24): 4494, 2022.
2. J.H. Park, G. Saravanakumar, K. Kim, and I.C. Kwon. "Targeted delivery of low molecular drugs using chitosan and its derivatives", Advanced drug delivery reviews. 62(1): 28-41, 2010.
3. N. Rohra, M. Gore, S. Dyawanapelly, M. Tambe, A. Gautam, M. Suvarna, R. Jain, and P. Dandekar. "Emerging trends in nanotechnology for diagnosis and therapy of lung cancer", Nanobiotechnology: Human health and environment. Taylor and Francis Group: 105-169, 2018.
4. D. Peer, J.M. Karp, S. Hong, O.C. Farokhzad, R. Margalit, and R. Langer. "Nanocarriers as an emerging platform for cancer therapy", Nano-enabled medical applications: 61-91, 2020.
5. N. Salari, F. Faraji, F.M. Torghabeh, F. Faraji, K. Mansouri, F. Abam, S. Shohaimi, H. Akbari, and M. Mohammadi. "Polymer-based drug delivery systems for anticancer drugs: A systematic review", Cancer Treatment and Research Communications: 100605, 2022.
6. F. Oroojalian, A.H. Rezayan, F. Mehrnejad, A.H. Nia, W.T. Shier, K. Abnous, and M. Ramezani. "Efficient megalin targeted delivery to renal proximal tubular cells mediated by modified-polymyxin B-polyethylenimine based nano-gene-carriers", Materials Science and Engineering: C. 79: 770-782, 2017.
7. P. Ahmaditabar, A.A. Momtazi-Borojeni, A.H. Rezayan, M. Mahmoodi, A. Sahebkar, and M. Mellat. "Enhanced entrapment and improved in vitro controlled release of n-acetyl cysteine in hybrid PLGA/lecithin nanoparticles prepared using a nanoprecipitation/self-assembly method", Journal of cellular biochemistry. 118(12): 4203-4209, 2017.
8. H. Hamedinasab, A.H. Rezayan, M. Mellat, M. Mashreghi, and M.R. Jaafari. "Development of chitosan-coated liposome for pulmonary delivery of N-acetylcysteine", International journal of biological macromolecules. 156: 1455-1463, 2020.
9. H. Hamedinasab, A.H. Rezayan, M.R. Jaafari, M. Mashreghi, and H. Alvandi. "The protective effect of N-acetylcysteine against liposome and chitosan-induced cytotoxicity", Journal of Microencapsulation: 1-9, 2023.
10. A. Shirvany, A.H. Rezayan, H. Alvandi, M. Barshan Tashnizi, and H. Sabahi. "Preparation and evaluation of a niosomal drug delivery system containing cefazolin and study of its antibacterial activity", Iranian Journal of Medical Microbiology. 15(6): 638-657, 2021.
11. A.H. Rezayan, M. Mousavi, S. Kheirjou, G. Amoabediny, M.S. Ardestani, and J. Mohammadnejad. "Monodisperse magnetite (Fe3O4) nanoparticles modified with water soluble polymers for the diagnosis of breast cancer by MRI method", Journal of Magnetism and Magnetic Materials. 420: 210-217, 2016.
12. A.H. Rezayan, S. Kheirjou, M. Edrisi, M. Shafiee Ardestani, and H. Alvandi. "A Modified PEG-Fe3O4 Magnetic Nanoparticles Conjugated with D (+) Glucosamine (DG): MRI Contrast Agent", Journal of Inorganic and Organometallic Polymers and Materials. 32(6): 1988-1998, 2022.
13. F. Chogan, T. Mirmajidi, A.H. Rezayan, A.M. Sharifi, A. Ghahary, J. Nourmohammadi, A. Kamali, and M. Rahaie. "Design, fabrication, and optimization of a dual function three-layer scaffold for controlled release of metformin hydrochloride to alleviate fibrosis and accelerate wound healing", Acta biomaterialia. 113: 144-163, 2020.
14. T. Mirmajidi, F. Chogan, A.H. Rezayan, and A.M. Sharifi. "In vitro and in vivo evaluation of a nanofiber wound dressing loaded with melatonin", International journal of pharmaceutics. 596: 120213, 2021.
15. N. Firoozi, A.H. Rezayan, S.J. Tabatabaei Rezaei, M. Mir-Derikvand, M.R. Nabid, J. Nourmohammadi, and J. Mohammadnejad Arough. "Synthesis of poly (ε-caprolactone)-based polyurethane semi-interpenetrating polymer networks as scaffolds for skin tissue regeneration", International Journal of Polymeric Materials and Polymeric Biomaterials. 66(16): 805-811, 2017.

29TH IRANIAN ORGANIC CHEMISTRY CONFERENCE
1_3 NOV, 2023
UNIVERSITY OF QOM, IRAN

Investigation and comparison of molecularly imprinted polymers based on $CuFe_2O_4$ and Fe_3O_4 nanoparticles.

Sanaz Aftabi[1], Negin Sohrabi[1, 2], and Reza Mohammadi[1]*

[1] *Department of Organic and Biochemistry, Faculty of Chemistry, University of Tabriz, Tabriz, Iran, r.mohammadi@tabrizu.ac.ir*

[2] *Department of Biosystem Engineering, Faculty of Agriculture, University of Tabriz, Tabriz, Iran*

Abstract – In this study molecularly imprinted polymers based on two different nanoparticles ($CuFe_2O_4$ and Fe_3O_4) were investigated and compared. For this purpose, two nanoparticles and then their molecularly imprinted polymers were synthesized using methacrylic acid as monomer, EGDMA as crosslinker and AIBN as initiator in the presence of Tramadol (as template molecule). The SEM and VSM analyzes were used to characterization of these materials. The results showed that the both molecularly imprinted polymers were well synthesized, but their magnetic properties were different and the magnetic saturation value of MIP-Fe_3O_4 was higher than that of MIP-$CuFe_2O_4$. In addition, the magnetic diagram of MIP-Fe_3O_4 has no hysteresis, but the diagram of MIP-$CuFe_2O_4$ has hysteresis. The imprinting factor values of both polymers were calculated using binding tests, and subsequent Scatchard analysis. The results showed that the imprinting factor of MIP-Fe_3O_4 is equal to 1.02 and less than the imprinting factor of MIP-$CuFe_2O_4$ (1.53). Therefore, if the magnetic property is important, MIP-Fe_3O_4 is the best choice, and if the imprinting factor is important, MIP-$CuFe_2O_4$ is more suitable.

1. Introduction

Molecularly imprinted polymers are smart polymers and they have memory that is produced for a specific purpose. Molecularly imprinted polymers are materials in which, during a polymerization process, a polymer is engraved with specific sites specific to the template molecule. The constituent components of molecularly imprinted polymers are monomer, crosslinker, initiator, solvent, and template molecule. molecularly imprinted polymers have very good features such as easy production, high selectivity, and good stability, which has led to their high acceptance in applications such as solid phase extraction and biosensing [1]. The characteristics of molecularly imprinted polymers are influenced by the type of solvent, functional monomer, crosslinker, initiator, and their ratios [2]. The ability to adsorb and entrap Molecularly imprinted polymers is strongly influenced by the number of binding sites, the availability of these sites, washing, and complete removal of the template molecule from the polymer structure, which are issues in traditional Molecularly imprinted polymers that They are synthesized in the form of polymer mass, they are often not observed [3]. To solve these defects and improve the imprinted surface of polymers, in many studies, various nanoparticles and nanocomposites such as TiO_2 [4], Fe_3O_4 [5], rGO/Fe_3O_4 [6], carbon nanotubes [7] etc, have been used in the synthesis and production of molecularly imprinted polymers. Because nanostructures have small dimensions and a large surface-to-volume ratio, they can be used to produce more binding sites and increase the ability of polymer adsorption [8]. Mono and bimetallic magnetic nanoparticles have been synthesized for various applications. Therefore, the aim of the present study is to investigate the effect of the type of nanoparticles on the properties of the molecularly imprinted polymer based on them.

2. Results and Discussion

The SEM analysis results for MIP-Fe_3O_4, MIP-$CuFe_2O_4$ nanoparticles, and polymers are shown in Figure 1. As can be seen, the morphology of both nanoparticles is spherical. After the formation of a molecularly imprinted polymer layer for tramadol drug on the surface of these polymers, their morphology is still spherical, but their particle size has increased, which indicates their successful synthesis. In addition, the results of the VSM analysis are shown in Figure 2. As can be seen, the graph related to the polymer does not have magnetic hysteresis, but MIP-$CuFe_2O_4$ has magnetic hysteresis. Also, the magnetic saturation value of MIP-Fe_3O_4, and MIP-$CuFe_2O_4$ polymers is equal to 23.13 emu/g and 8.39 emu/g, respectively. Therefore, the results of VSM analysis show that the magnetic properties of MIP-Fe_3O_4 are better than MIP-$CuFe_2O_4$ for separation using an external magnetic field.

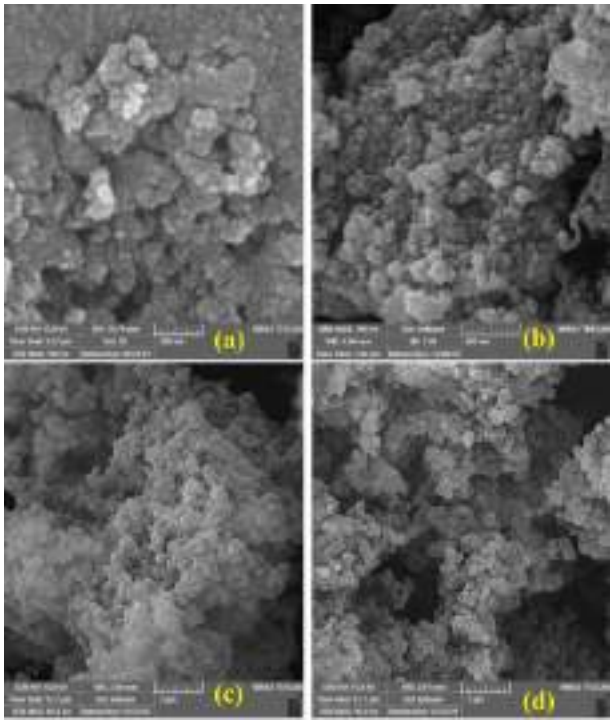

Figure 1. SEM analysis results for a) $CuFe_2O_4$, b) Fe_3O_4, c) MIP-$CuFe_2O_4$, d) MIP-Fe_3O_4

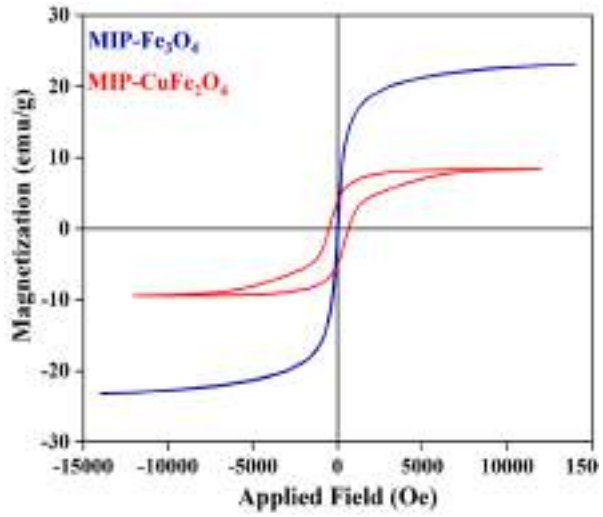

Figure 2. Results of VSM analysis for molecularly imprinted polymers

The results of the binding tests are shown in Table 1. As can be seen, the maximum value of adsorption capacity for MIP-Fe_3O_4 and MIP-$CuFe_2O_4$ molecularly imprinted polymers is higher than the maximum value of adsorption capacity for NIP-Fe_3O_4 and NIP-$CuFe_2O_4$. This indicates the successful imprinting of both desired polymers. In addition, the maximum adsorption capacity of MIP-$CuFe_2O_4$ is higher than MIP-Fe_3O_4. The imprinting factor for MIP-Fe_3O_4 polymer is equal to 1.02 and for MIP-$CuFe_2O_4$ is equal to 1.53. The value of the MIP-$CuFe_2O_4$ imprinting coefficient is higher, so it can be said that MIP-$CuFe_2O_4$ polymer imprinting is more successful than MIP-Fe_3O_4 polymer. Therefore, the selectivity of MIP-$CuFe_2O_4$ is better than the selectivity of MIP-Fe_3O_4. In general, bimetallic nanoparticles have a higher surface-to-volume ratio than monometallic nanoparticles [9, 10]. This has caused more successful and better imprinting of polymers based on $CuFe_2O_4$ bimetallic nanoparticles.

Table 1. Results of Scatchard analysis

Adsorbent	K_D(µmol/L)	Q_{max}(µmol/g)	IF
MIP-Fe_3O_4	22.42	203.23	1.02
NIP-Fe_3O_4	71.43	199.99	
MIP-$CuFe_2O_4$	46.30	434.93	1.53
NIP-$CuFe_2O_4$	113.64	284.57	

3. Conclusions

In this study, two magnetic nanocomposites include Fe_3O_4, and $CuFe_2O_4$ were synthesized by co-precipitation method. Then, the molecularly imprinted polymers based on these nanoparticles were synthesized by methacrylic acid as monomer, EGDMA as crosslinker, AIBN as initiator, and Tramadol as template molecule. The characterization of nanoparticles and polymers were done by used the SEM and VSM analyses. The results showed that these materials were well synthesized, but the magnetic properties of two polymers are different. The magnetic saturation of MIP-Fe_3O_4 was higher than that of MIP-$CuFe_2O_4$. In addition, the magnetic diagram of MIP-Fe_3O_4 has no hysteresis, but the diagram of MIP-$CuFe_2O_4$ has hysteresis. The imprinting factor values and maximum adsorption capacity of both polymers were calculated using binding tests, and then Scatchard analysis. The results showed that the maximum adsorption capacity of MIP-Fe_3O_4 is equal to 203.23µmol/g and maximum adsorption capacity of MIP-$CuFe_2O_4$ is equal to 434.93 µmol/g. In addition, imprinting factor of MIP-Fe_3O_4 is equal to 1.02 and imprinting factor of MIP-$CuFe_2O_4$ is equal to 1.53. Therefore, if the magnetic property is important, MIP-Fe_3O_4 is the best choice, and if the selectivity is important, MIP-$CuFe_2O_4$ is more suitable.

4. References

[1] Niu M, C Pham-Huy, H He. Core-shell nanoparticles coated with molecularly imprinted polymers: a review. Microchimica Acta. 183 (2016) 2677-95.

[2] Khadem M, F Faridbod, P Norouzi, A Rahimi Foroushani, MR Ganjali, SJ Shahtaheri, et al. Modification of carbon paste electrode based on

molecularly imprinted polymer for electrochemical determination of diazinon in biological and environmental samples. Electroanalysis. 29 (2017) 708-15.
[3] Hu M, P Huang, L Suo, F Wu. Polydopamine-based molecularly imprinting polymers on magnetic nanoparticles for recognition and enrichment of ochratoxins prior to their determination by HPLC. Microchimica Acta. 185 (2018) 1-6.
[4] Shen X, L Zhu, J Li, H Tang. Synthesis of molecular imprinted polymer coated photocatalysts with high selectivity. Chemical Communications. (2007) 1163-5.
[5] Zhang Y, R Liu, Y Hu, G Li. Microwave heating in preparation of magnetic molecularly imprinted polymer beads for trace triazines analysis in complicated samples. Analytical Chemistry. 81 (2009) 967-76.
[6] Mehdinia A, S Heydari, A Jabbari. Synthesis and characterization of reduced graphene oxide-Fe3O4@ polydopamine and application for adsorption of lead ions: Isotherm and kinetic studies. Materials Chemistry and Physics. 239 (2020) 121964.
[7] Amatatongchai M, W Sroysee, P Sodkrathok, N Kesangam, S Chairam, P Jarujamrus. Novel three-Dimensional molecularly imprinted polymer-coated carbon nanotubes (3D-CNTs@ MIP) for selective detection of profenofos in food. Analytica chimica acta. 1076 (2019) 64-72.
[8] Yao G-H, R-P Liang, C-F Huang, Y Wang, J-D Qiu. Surface plasmon resonance sensor based on magnetic molecularly imprinted polymers amplification for pesticide recognition. Analytical Chemistry. 85 (2013) 11944-51.
[9] Ma L, N Sun, J Zhang, C Tu, X Cao, D Duan, et al. Polyethylenimine-coated Fe 3 O 4 nanoparticles effectively quench fluorescent DNA, which can be developed as a novel platform for protein detection. Nanoscale. 9 (2017) 17699-703.
[10] Li J, Y Ren, F Ji, B Lai. Heterogeneous catalytic oxidation for the degradation of p-nitrophenol in aqueous solution by persulfate activated with CuFe2O4 magnetic nano-particles. Chemical Engineering Journal. 324 (2017) 63-73.

TITLE: Comparison of activated carbon produced from walnut shell and apple skin: characterization and adsorption ability.

Media Sighar Ghiasi[1,2], Fatemeh Abdi[1], Negin Sohrabi[1,2], and Reza Mohammadi[1]*

[1] *Department of Organic and Biochemistry, Faculty of Chemistry, University of Tabriz, Tabriz, Iran,* Snegin.sohrabi@tabrizu.ac.ir, *r.mohammadi@tabrizu.ac.ir*

[2] *Department of Biosystem Engineering, Faculty of Agriculture, University of Tabriz, Tabriz, Iran.*

Abstract – In this study, apple skin and walnut shell were separated from the desired products and burned in the oven at 200 ˚C, turned into ash and completely powdered. To activate the resulting powders, they were individually placed in sodium hydroxide solution with a concentration of 1 M for 24 hours. Then mentioned powders were separated from the solution and placed in the oven at 700 degrees Celsius for 2 hours, After the mentioned time, activated carbon from apple skin (ASAC) and activated carbon from walnut shell (WSAC) were placed at room temperature to cool completely and were washed several steps with distilled water until their pH reached 6.5-7 and be neutralized. Using SEM, FT-IR and BET analyses, the produced activated carbons were discussed. In addition, their absorption ability for green malachite dye was investigated and their absorption capacity was calculated. The results of this study showed that the activated carbon produced from walnut shell is a more suitable adsorbent than the activated carbon produced from apple skin with its active surface and higher porosity.

1. Introduction

In recent years, there has been an increased emphasis on the preparation of activated carbon from agricultural products and waste Agricultural wastes are among abundant, available and degradable resources for preparing activated carbon. These materials have very little economic value and collecting them is not only costly, but accumulating them in one place may also cause environmental pollution. Activated carbon is prepared from almond shell, hazelnut shell, walnut shell, coconut shell, peach kernel, apricot, cherry, rice bran and wheat bran as a raw material for the production of activated carbon [1]. One of the most effective adsorbents in the surface absorption method to remove pollution is activated carbon, which is used in industrial and urban wastewater treatment to separate dye and organic matter [2]. The advantages of activated carbon include high porosity and active surface, high adsorption capacity and speed, use for a wide range of pollutants, high availability and effectiveness [3, 4]. Activation of carbon materials in order to produce activated carbon, which is the main step of the process, is usually done by two physical and chemical methods. Physical activation is a two-step process including carbonization and high temperature activation. In the physical activation method, the first raw material is carbonized in an environment without the presence of air, to form the initial carbon base. In these conditions, the cellulose and polymer compounds present in the raw material are converted into charcoal and all volatile compounds are lost, then the obtained carbon base is exposed to an active compatibilizing agent at high temperature. The activating agent is generally water vapor, carbon dioxide, oxygen or their mixture, which is able to precipitate with a part of carbon at high temperature and react in the texture of the material, and the porosity of this product depends on several factors such as the type of raw material, Carbonization conditions, type of activating agent, temperature and activation time [5]. In chemical activation, carbonization and activation are done in one step using chemical activating agents such as ZnCl2, KOH, H3PO4, NaOH, etc. Here, the role of the activating agent is to remove water from the structure of the raw material, lower the temperature necessary for carbonization, and prevent the formation of tar during the process, which leads to the creation of a porous structure in the product [5]. Therefore, in this study, activated carbon produced from apple skin and walnut shell was compared.

2. Results and Discussion

The results of FT-IR analysis for both activated carbons are shown in Figure 1. As can be seen in the structure of activated carbon produced from apple skin, absorption peaks in 13678 cm^{-1} are observed, which are caused by free O-H bonds in its structure. Also, other absorption peaks can be observed in 1523 cm^{-1} and 1647 cm^{-1}, which are respectively caused by aromatic C=C and C=O bonds (acidic COOH group) in the structure of ASAC [6]. In addition, there is a strong absorption peak in 1743 cm^{-1}, this peak indicates the bending C=O bond in the ASAC structure [6]. A peak in 3435 cm^{-1} appeared in

spectrum of WSAC that is related to O-H vibration and the band appearing at 1709 cm^{-1} is attributed to carbonyl (C=O) groups. The olefinic (C=C) absorptions cause the band at about 1613 cm^{-1}, while the skeletal C=C vibrations in aromatic rings cause another band at about 1444 cm^{-1}. The appearance of band at 1250 cm^{-1} can be assigned to C-O stretching vibrations. The peak at around 875 and 712 cm^{-1} is ascribed to the aromatic C-H out of-plane vibrations [7]. Therefore, the results of this analysis show that both activated carbons have been properly synthesized and different functional groups have been created on their surface.

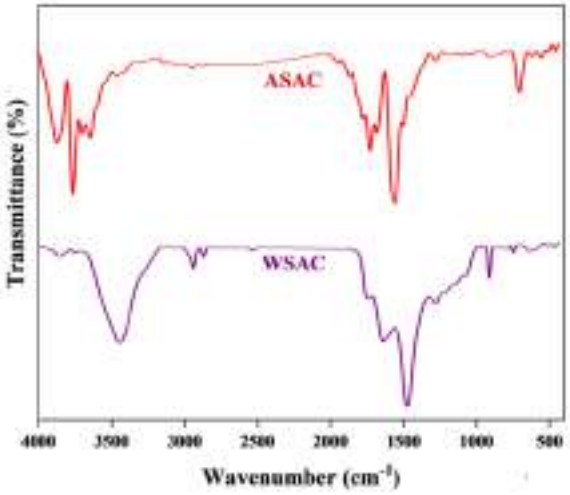

Figure 1- FT-IR analysis results

The results of BET analysis are reported in Table 1. As can be seen, all the parameters related to the value of the active surface for WSAC are higher than ASAC. Also, the values of different parameters related to the amount of porosity also show that the porosity of WSAC is higher than that of ASAC. In addition, the results of SEM analysis also showed that the porosity of activated carbon obtained from walnut shell is higher than that of apple skin (Figure 2).

Table 1- BET analysis results

Parameter	WSAC	ASAC
BET surface area	84.85 m^2/g	15.53 m^2/g
Langmuir surface area	94.38 m^2/g	16.82 m^2/g
t-Plot Micropore Area	85.65 m^2/g	9.58 m^2/g
BJH surface area	106.86 m^2/g	16.69 m^2/g
Total pore volume (by BET)	0.48 cm^3/g	0.06 cm^3/g
BJH Adsorption cumulative volume of pores	0.49 cm^3/g	0.06 cm^3/g
Adsorption average pore diameter (4V/A by BET)	22.77 nm	19.42 nm
BJH Adsorption mean pore diameter	1.85 nm	1.21 nm

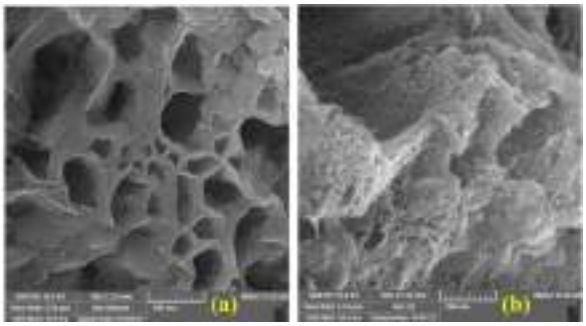

Figure 2- Results of SEM analysis for a) WSAC, b) ASAC

In order to further investigate these two active carbons in the absorption process, experiments were conducted. The tests performed for the absorption of malachite green dye were in the conditions of pH equal to 7, adsorbent dose equal to 1.3 gr, contact time 60 minutes, room temperature and dye concentration equal to 100 ppm. The results showed that the absorbent capacity of WSAC for green malachite dye is equal to 71.85 mg/g and the absorbent capacity of ASAC for green malachite dye is equal to 51.56 mg/g. Therefore, all these results showed that activated carbon produced from walnut shell has higher porosity, active surface and absorption capacity than activated carbon produced from apple skin.

3. Conclusions

The results of this study showed that activated carbon produced from walnut shell has higher porosity, active surface and absorption capacity than activated carbon produced from apple skin.

4. References

[1] Adeleke, A.; Latiff, A.; Radin Mohamed, R. M. S.; Daud, Z.; Ismail, N.; Ahsan, A.; Ab Aziz, N. A.; Ndah, M.; Kumar, V.; Al-Gheethi, E. I. A.; Rosli, M.; Abubakar, M.: Locally Derived Activated Carbon From Domestic, Agricultural and Industrial Wastes for the Treatment of Palm Oil Mill Effluent. Environ. Nanotechnol. Monit. Manag. 2019; pp 35-62.

[2] Cardoso, N.; Lima, E.; Royer, B.; Bach, M.; Dotto, G.; Pinto, L.; Calvete, T. Comparison of Spirulina platensis Microalgae and Commercial Activated Carbon as Adsorbents for the Removal of Reactive Red 120 Dye from Aqueous Effluents. J. Hazard. Mater. 2012, 241.

[3] Foroutan, R.; Mohammadi, R.; Ramavandi, B. Elimination performance of methylene blue, methyl violet, and Nile blue from aqueous media using AC/CoFe2O4 as a recyclable magnetic composite. Environ. Sci. Pollut. Res. 2019, 26.

[4] Afshin, S.; Rashtbari, Y.; Ramavandi, B.; Fazlzadehdavilb, M.; Vosoughi Niri, M.; Mokhtari, s. A.; Shirmardi, M.; Rehman, R. Magnetic

nanocomposite of filamentous algae activated carbon for efficient elimination of cephalexin from aqueous media. Korean J Chem Eng. 2020, 37, 80-92.
[5] Hassan, M. F.; Sabri, M. A.; Fazal, H.; Hafeez, A.; Shahzad, N.; Hussain, M. Recent trends in Activated Carbon Fibers production from various precursors and applications—A comparative review. J. Anal. Appl. Pyrolysis. Ezoic. 2020, 145, 104715.
[6] Pavia, D. L.; Lampman, G. M.; Kriz, G. S.; Vyvyan, J. A.: Introduction to spectroscopy; Cengage learning, 2014.
[7] Okoya, A.; Anjous-Alao, R.; Awokoya, N. Sorption Characteristics of Halogenated Acetonitriles (HANs) in Surface Water onto Activated Carbon Prepared from Walnut Shell. International Research Pure Appl. Chem. 2020, 273-287.

Recent Synthesis Methods Comparison of Lidocaine

*Ali Saberi**

Chemistry Department, Payame Noor University (PNU), P. O. Box 19395-4697 Tehran, I. R. of IRAN, saberi@pnu.ac.ir

Abstract

Lidocaine, also known as Xylocaine, is a commonly used local anesthetic and antiarrhythmic drug. People may encounter lidocaine through dental procedures, routine biopsies, or over-the-counter topical pain-relief products (creams, sprays, and roll-on applicators). Combined with the current background, this work reviewed the general classification methods have shown the potential to be considered as alternative methods for producing lidocaine.

Introduction

Local anaesthetics are widely used in the treatment of both acute and chronic pain, but their usefulness is limited by the short duration of the local anaesthetic effect that generally lasts for only few hours. Lidocaine is a local anaesthetic type amide, that can be considered as a model molecule for hydrophobic drug encapsulation because of its small molecular weight and low water solubility. Lidocaine has a faster onset of action and a higher length of action than amino ester anaesthetics. However, its therapeutic potential is restricted by its short plasma half-life.

Results and Discussions

A two-step synthesis of lidocaine was first developed in 1948 by Lofgren and co-workers is showed in scheme 1 using 2,6-xylidine, diethylamine, 2-chloroacetyl chloride, and acetic acid, having benzene as solvent [1].

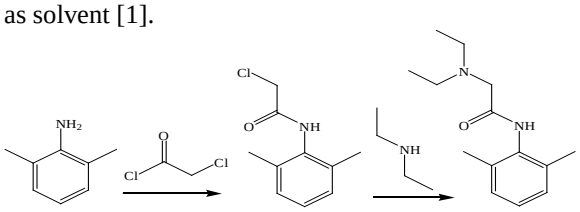

Scheme 1.

Indeed, the two-step synthesis of lidocaine by Reilly has been widely adopted in organic laboratory courses is showed in scheme 2. In this method 2,6-xylidine, diethylamine, 2-chloroacetyl chloride, and acetic acid, toluene as solvent were used [2].

Scheme 2.

Various lidocaine analogues have been synthesized by J. C. S. Costa et al is showed in scheme 3. Changes in the aromatic ring substitution of lidocaine led to enhanced potency and selective antispasmodic activity. Changes in the torsional angles between the aromatic ring and the plane of the aliphatic side chain and increased lipophilicity of the compounds are likely to account for the observed results [3].

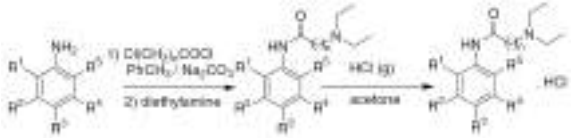

Scheme 3.

Synthesis of lidocaine by Reilly was recently updated by Diner, Blomkvist, and colleagues is showed in scheme 4. Their revised protocol uses the same synthetic strategy as Reilly and as the original patent but features greener choices of solvent, reaction temperature, and base [4].

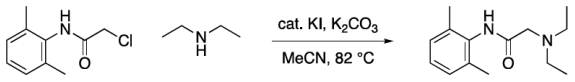

Scheme 4.

Three component synthesis of the topical anesthetic lidocaine with excellent atom economy by David A. V. et al. is showed in scheme 5. Paraformaldehyde, diethylamine, and 2,6-dimethylphenyl isocyanide were combined and conveniently stirred at room temperature for a week in methanol with acetic acid. researchers also evaluated multiple lidocaine synthesis procedures using green chemistry principles and explored the reaction mechanisms of both traditional (N-acylation followed by N-alkylation) and multicomponent lidocaine syntheses. Results from both in-person and remote instruction versions of the experiment are included. [5].

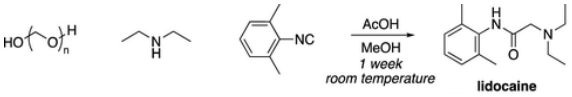

Scheme 5.

Conclusions

All of the mentioned studies show the synthesis of lidocaine by different routes. Among the discussed methods the synthesis of lidocaine Diner, Blomkvist, and colleagues is easier and faster.

Acknowledgments

The author is grateful to Payame Noor University for financial support.

References

[1] Lofgren, N. M.; Lundqvist, B. J. U.S. Patent 2, 441, 498, 1948.

[2] Reilly, T. J., J. Chem. Educ. 76 (1999), 11, 1557 − 1557.

[3] J. C. S. Costa et al., Bioorg. Med. Chem. Lett. 18 (2008), 1162–1166.

[4] Josephson, P.; Nykvist, V.; Qasim, W.; Blomkvist, B.; Dinér, P., J. Chem. Educ., 96 (2019), 7, 1389 − 1394.

[5] Gámez-Montano, and David A. Vosburg, J. Chem. Educ. 99 (2022), 6, 2399–2402.

29TH IRANIAN ORGANIC CHEMISTRY CONFERENCE
1_3 NOV, 2023
UNIVERSITY OF QOM, IRAN

Recent Synthesis Methods Comparison of N-Acetylcysteine

*Ali Saberi**

Chemistry Department, Payame Noor University (PNU), P. O. Box 19395-4697 Tehran, I. R. of IRAN
saberi@pnu.ac.ir

Abstract
N-acetylcysteine (NAC) is mainly administrated as a mucolytic medication, antioxidant supplement, antidote in paracetamol overdose, and a drug for the prevention of diabetic kidney disease. Its effect has been investigated for the treatment of several diseases such as COVID-19. This drug can be synthesized in a single-batch step instead of using a multi-stage process. Combined with the current background, this work reviewed the general classification methods have shown the potential to be considered as alternative methods for producing N-acetylcysteine.

Introduction
Although N-acetylcysteine is an antioxidant and is used as an antidote to paracetamol (acetaminophen) overdose, it also has many other applications supported by clinical evidence. N-acetylcysteine can support the body's antioxidant level during infections, toxic assaults, inflammations, and stresses. It is often prescribed to patients who are at high risk for hepatotoxicity. In addition, N-acetylcysteine is a precursor to make glutathione, which is the major antioxidant in the human body. It was shown that taking N-acetylcysteine as a supplement also increases the levels of glutathione. Glutathione can detoxify a number of toxic compounds, including peroxide, xenobiotics substances, and other radical species. It might also meliorate lung inflammation occurring in influenza. Several studies demonstrate that N-acetylcysteine can be effective in the prevention of diabetic kidney disease (nephropathy). High levels of glucose in the blood due to diabetes can damage kidneys and this may cause a leakage of proteins into the urine. It has been reported that taking N-acetylcysteine through an intravenous route can prevent this kind of kidney damage regarding the scavenging of free radicals with its antioxidant features. It is worth mentioning that most of the research studies in the literature are about the synthesis of N-acetylcysteine derivatives and their clinical examination. However, published articles that indicate an explicit method for the synthesis of N-acetylcysteine are very scarce. This work presents a novel process for chemical synthesis and purification of this drug in a very high yield. The advantage of using the corresponding N-acylbenzotriazole as an effective acylation agent is taken into account to form a peptide bond with L-cysteine amino acid [5].

Results and Discussions
Riera et al. suggested a two-step route to make N-acetylcysteine by acylation of L-cystine and then taking the advantage of reduction methods to reach N-acetylcysteine. In their proposed method, the aim of reducing bis-acetyl-L-cystine is to breakdown the L-cystine's S-S bond and convert it into two S-H bonds resulting two N-acetylcysteine molecules [1].
For the reduction purpose, a reducing agent such as metallic zinc or an electrochemical reduction process were considered. The main problem of this method lies on the separation process where metallic zinc converts into Zn^{2+} ions which contaminate the medium with a high concentration of zinc ions. Therefore, isolating N-acetylcysteine to reach a high grade can be a challenge. On the other hand, managing the residual aqueous solution containing high contents of Zn^{2+} ions is an environmental issue. In this method, the production of hydrogen gas should also be managed due to its potential explosion issue. Moreover, the presence of unconverted zinc in the final product should be addressed by forming the corresponding lead mercaptan, followed by treatment with H_2S gas, removal of formed lead sulphide, and then recrystallization with suitable solvents to obtain purified N-acetylcysteine. N-acetyl-L-cysteine can be made through direct acylation in the presence of sodium acetate is showed in scheme 1 [2,3].

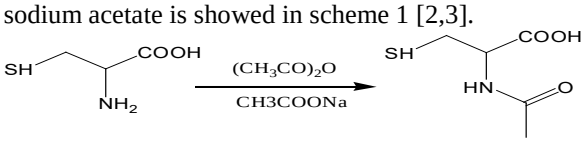

Scheme1.

For this purpose, a suspension of L-cysteine hydrochloride monohydrate is stirred in a reaction vessel containing aqueous tetrahydrofuran under a nitrogen atmosphere, and sodium acetate trihydrate is added. The mixture is stirred at room temperature to ensure the neutralization of the hydrochloride salt,

resulting in the formation of a suspension of equimolar amounts of cysteine and sodium acetate is obtained. The mixture is then chilled by external cooling and acetic anhydride is added dropwise. The resulting suspension is stirred at room temperature and heated at reflux. The resulting suspension of sodium N-acetyl-L-cysteinate is then neutralized by aqueous hydrogen chloride. The resulting sodium chloride is removed by filtration and the product is isolated by distilling the solvent from the filtrate in vacuo. This is followed by crystallization to reach N-acetylcysteine as a white solid.

Besides, following the method proposed by Katritzky et al. is showed in scheme 2 [4] failed to synthesize N-acetylcysteine. Apparently, this is due to the presence of water in their method, as water hydrolyses N-acetylbenzotriazole. Additionally, the presence of acetonitrile in their method is another issue, since acetonitrile may compete with L-cysteine to form a peptide bond.

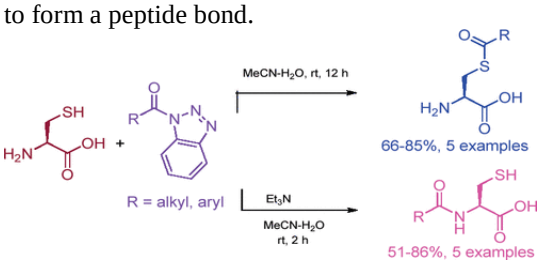

Scheme 2.

Ziaee, F. and Ziaee, M presented an efficient and uncomplicated method for the chemical synthesis of N-acetylcysteine, which is mainly administrated as a mucolytic medication, antioxidant supplement, and an antidote in paracetamol overdose. The work has improved the synthesis process of this drug, using a peptide-making route to achieve a high yield of the product, as the obtained characterization data shows a reaction yield of 94%. The purification process was undertaken in three steps using suitable solvents to reach an excellent purity. Since the proposed method does not use any reduction agents, it can address the concerns that may arise due to the presence of metals such as zinc in the final product is showed in scheme 3 [5].

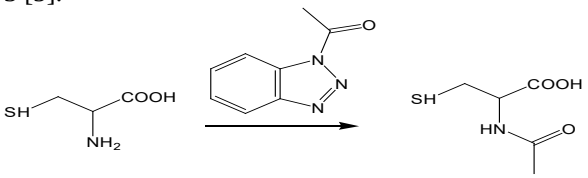

Scheme 3.

Conclusions

All of the mentioned studies show the synthesis of N-acetylcysteine by acetylation of cysteine. Among the discussed methods the synthesis of N-acetylcysteine using sodium acetate and acetic anhydride is the easiest.

Acknowledgments

The author is grateful to Payame Noor University for financial support.

References

[1] Riera, A.A.; Leguey, V.M.; Garcia, V.G.; Garcia, J.G. Universidad de Alicante. Process for the Electrochemical Synthesis of n-acetylcysteine from Cystine. U.S. Patent No. 6,159,352, 12 December 2000.

[2] Vardanyan, R.S.; Hruby, V.J. Synthesis of Essential Drugs, 1st ed.; Elsevier: Amsterdam, The Netherlands, 313–314, 2006.

[3] Martin, T.A.;Waller, C.W. Process for the N-Monoacylation of Cysteine. USA Patent No. 2,029,488, 18 May 1965.

[4] Katritzky, A.R.; Tala, S.R.; Abo-Dya, N.E.; Gyanda, K.; El-Gendy, B.E.D.M.; Abdel-Samii, Z.K.; Steel, P.J., J. Org. Chem., 74 (2009), 7165–7167.

[5] Ziaee, F.; Ziaee, M., Molbank, 2021, 2021, M1288.

29TH IRANIAN ORGANIC CHEMISTRY CONFERENCE
1_3 NOV, 2023
UNIVERSITY OF QOM, IRAN

4,10-Dinitro-2,6,8,12-tetraoxa-4, 10-diazatetracyclo [5.5.0.0^{5,9}.0^{3,11}]-dodecane (TEX) as an insensitive explosive

Hadi Panahi [1]*, *Maryam Hosseinabadi* [2]

[1]*Department of Chemistry, Faculty of Applied Science, Malek-e-Ashtar University of Technology, Isfahan, Iran , Hadi.p814@gmail.com*
[2]*Department of Chemistry, Faculty of Chemistry and Chemical Engineering, Malek-e-Ashtar University of Technology, Tehran, Iran*

Abstract - In this paper, the method of synthesis an insensitive explosive that named 4, 10-Dinitro-2, 6, 8, 12-tetraoxa-4, 10-diazatetracyclo [5.5.0.0^{5,9}.0^{3,11}]-dodecane (TEX) is introduced. Its physical, chemical and functional characteristics have been investigated and some explosive formulations based on it have been reported. TEX can be used as a new molecular explosive material in the insensitive munitions (IM) due to its high density in the ambient temperature and also TEX is fairly insensitive towards mechanical and thermal stimuli.

1. Introduction

The level of safety and sensitivity of ammunition has a direct relationship with the explosives used in their compositions. The use of explosives with a higher level of safety and less sensitivity has attracted the attention of scholars in this field in recent years; Therefore, new molecular explosives have been introduced and offered, but due to their unique characteristics, more costs for their synthesis should be considered [1].

Insensitive high explosives should possess sufficient energy content to be a close match with standard high explosives (HE). In modern insensitive explosives, density plays an important role because the detonation velocity, of an energetic material correlates linearly with density and the detonation pressure, correlates with its square. 2,4,6,8,10,12-hexanitro-2,4,6,8,10,12-hexaazatetracyclo dodecane or CL-20 is the densest stable CHNO-compound with an ambient density of ρ= 2.044 g cm^{-3} [2]. Fig. 1 shows the molecular structures of CL-20. The high density of CL-20 is mainly due to the isowurzitane cage structure of the compound. However CL-20 is very sensitive to both friction (64 N) and impact (4 J) and to thermal stress [2] which is believed to result from steric strain of the nitramine groups. Sensitivity to both friction and impact and the high production cost currently impede large scale use of CL-20 and restrict its use to small items. TEX or 4,10-dinitro-2,6,8,12-tetraoxa-4,10 diazatetracyclo dodecane is a prominent “relative” to CL-20. TEX derives from CL-20 by replacement of four nitramine groups by ether bridges (Fig. 2). As TEX possesses the same isowurzitane cage structure as CL-20 it conserves the very high ambient temperature density of ρ= 1.985 g cm^{-3}, however due to absence of sterically demanding nitramine groups reduces its sensitivity greatly and makes this an interesting insensitive energetic material. Fig. 2 shows the molecular structures of TEX.

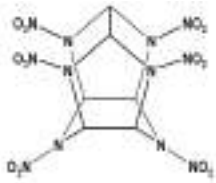

Figure 1- Molecular structures of CL-20

Figure 2- Molecular structures of TEX

TEX also described as dinitro tetra oxa diaza isowurzitane and often abbreviated as, DTIW, TOIW or DNTD is identified via its CAS-No (130919 56-1). It is the second most dense nitramine with an ambient temperature density of ρ= 1.985 g cm^{-3}, an oxygen balance of - 42.7 % [3].

TEX is commercially available from ATK/USA, Explosia/Czech Republic and Rafael/Israel.

Table 1. Shows general properties of TEX. As seen from table 1. TEX is insensitive to friction and impact. Also its density is ρ= 1.985 g cm^{-3} and it is the second densest nitramine.

Table 1. Properties of TEX

Property	Unit	
Formula		C6H6N4O8
Molecular weight	g mol^{-1}	262.13
Oxygen balance	%	-42.7
Density	g cm^{-3}	1.985

No Go Friction Force (BAM)	N	>353
No Go Impact Energy (BAM)	J	23-25
CAS-No	-	130919-56-1

Due to the Availability of the raw materials and the simplicity of the production methods, it is possible to widely use this compound in common high-energy formulation such as composition B.

Overview of synthesis methods

The synthesis of TEX was first reported by Boyer et al [4]. TEX synthesis is mainly a two-step process. In the first step during a condensation reaction in an alkaline medium, the intermediate substance, which is a hexasubstituted piperazyl derivative, is synthesized. In the second step, by increasing the intermediate, to an acidic medium containing at least one nitrate source such as nitric acid and a strong acid such as concentrated sulfuric acid or concentrated hydrochloric acid, TEX compound is synthesized. The raw product is a pale yellow solid (Yellowish white) with a purity of 97% [5]. Due to the abundance of the raw material and the ease of work, the vast majority of articles have chosen the 1, 4-diformyl- 2, 3, 5, 6-tetrahydroxypiperazine (DFTHP) as the raw material. (Scheme 1)

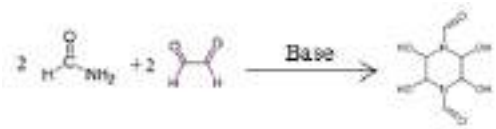

Scheme 1- Synthesis of the precursor DFTHP

The synthesis of DFTHP and its derivatives have been described in the literature [6-9]. Matyáš et al. have revisited the synthesis of DFTHP recently and have achieved yields in the 80 % range using triethylamine as the base in a molar range between 0.1- 0.2 mole per mole formamide [10]. The conventional reaction for the preparation of DFTHP is from the reaction of formamide with glyoxal under alkaline conditions. During the nitration reaction of DFTHP, two processes are carried out, First, the formation of the isowurzitane cage, then the nitrolysis of third-type nitrogens, which occurs along with the removal of formyle groups. The sequence and order of these two processes and the details of the reaction mechanism have not been published so far, but it is known that when the exothermic reaction starts, if the reaction mixture is not cooled properly, the reaction proceeds violently and there is a possibility of explosion [11]. In general, the nitration of DFTHP is done in the following three ways:

1- Nitration of DFTHP with concentrated nitric acid.
2- Nitration of DFTHP with a mixture of nitric acid and concentrated sulfuric acid in the presence of urea.
3- Nitration of DFTHP with nitric acid and oleum in the presence of urea.

Synthesis of TEX with concentrated nitric acid

In this method, intermediate substance (DFTHP) is completely added to concentrated nitric acid at 45°C. In this method, the ratio of intermediate to nitric acid is about 1 to 7. After 5 minutes, the temperature rises to about 65 °C and the reaction mixture is refluxed. After 20 minutes, the reaction temperature rises to 65 °C, which means the beginning of the autocatalytic stage of NO_X production. Then the reaction mixture is quickly cooled to 0 °C until a white precipitate of TEX is formed. The sediment is filtered and washed several times with water until completely neutralized. The efficiency of this process is about 30% and the NMR spectrum shows the purity of TEX more than 95% [12].

Synthesis of TEX with a mixture of nitric acid and concentrated sulfuric acid in the presence of urea

In this method, a mixture of nitric acid and concentrated sulfuric acid is used for synthesis. Urea is also used to remove NO_X gases and prevent product degradation. In this method, the reaction temperature ranges from 50 to 60 degrees Celsius and its efficiency is about 62% [5].

Synthesis of TEX with a mixture of nitric acid and oleum in the presence of urea

In this method, a mixture of nitric acid and concentrated sulfuric acid and oleum 30% is used for synthesis. The reaction temperature keep at 55-60 °C and The reaction is continuously stirred for 2 hours. Product efficiency is reported to be 32% [4, 13].

According to the investigations, the DFTHP synthesis steps are reported in Figure 3.

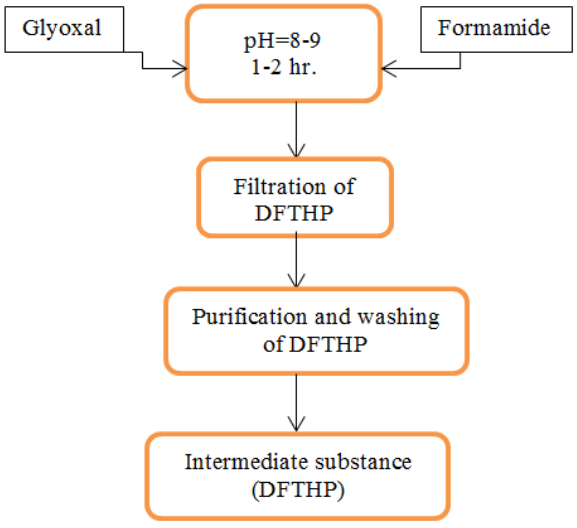

Figure 3- The synthesis of DFTHP

After adding glyoxal and formamide, the pH is maintained in the range of 8 to 9 for 1 to 2 hours. Then filtration of raw material done and by distilled

water washing done. The raw material (DFTHP) should be purified.

After the DFTHP synthesis, by nitration, sedimentation, filtration and purification steps the TEX will be produced. These steps are reported in Figure 4.

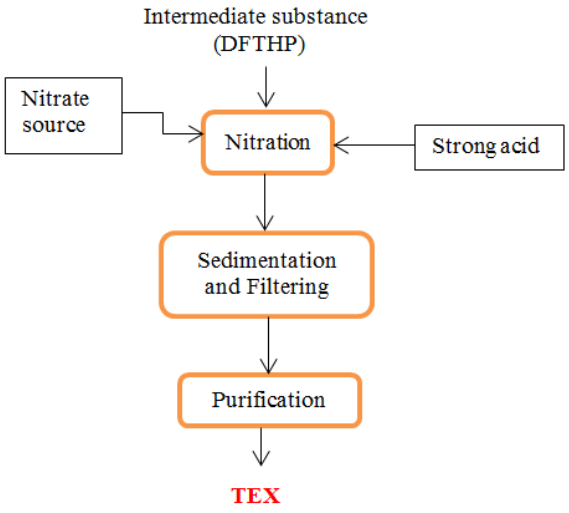

Figure 4 - The synthesis of TEX from DFTHP

TEX based Formulations

TEX due to its suitable explosive properties and low sensitivity can be used in various explosive formulations.

Also in view of its high density TEX is an interesting ingredient in IM-formulations replacing NTO but also RDX. Table 2 displays data on both TEX/TNT and compares with experimental data on NTO/TNT (Ontalite). These data indicate that TEX could be a promising replacement for NTO.

Table 2. Explosive performance of TEX/TNT composites and comparison with NTO/TNT.

Formulation		Exp
Reference	[14]	[15]
Composition	TEX/TNT	NTO/TNT
	75/25	60/40
Density (g cm^{-3})	1.89	1.78
V_d (m s^{-1})	8306	7427

Safety and Sensitivity of TEX and its formulations

Friction & Impact Sensitivity

TEX is not sensitive to friction (> 353 N) [16]. The impact sensitivity for 200 µm grain sample is 33 cm with the ABL machine, > 116.8 cm with the proprietary Thiokol (now ATK) impact hammer [14], 42.5 cm with the NSWC/IH fall hammer [17], 50 cm with the 5 kg fall hammer [18] and 24 J with the BAM fall hammer [19].

Spark Sensitivity

The spark sensitivity of TEX – of unspecified granulometry - has been determined to 13.1 J [20].

Thermal response (Cook Off)

Bulk crystalline TEX (200 µm) yields a mild (burn) response in the Simulated Bulk Auto ignition Temperature Test (SBAT) at 252°C [3]. The 5s deflagration point has been determined to 312 °C in Ref. [2].

Vacuum stability

TEX passes vacuum stability testing at 110°C for 20 h with 0.05 ml g-1 [21] and 0.05 ml g-1 at 100°C after 48 h [14].

2. Results and Discussion

This paper Overview the TEX synthesis methods and its properties. Also this paper displays data on both TEX/TNT and compares with experimental data on NTO/TNT.

As TEX possesses the same isowurzitane cage structure as CL-20 it conserves the very high ambient temperature density of ρ= 1.985 g cm^{-3}, however due to absence of sterically demanding nitramine groups reduces its sensitivity greatly and makes this an interesting insensitive energetic material.

3. Conclusions

TEX is the second most dense nitramine explosive (Density = 1.985 g cm^{-3}) following CL-20. However unlike Cl-20, TEX is friction insensitive, possesses low impact sensitivity (~ 24 J with BAM Impact tester). TEX is synthesized in ~ 40 % overall yield from cheap starting materials in a simple process. Its production does not require any specialized equipment and the associated waste stream (neutralized spent acid) is non-hazardous. Due to the unique features and capabilities of TEX, as well as the low cost of raw materials for its production, TEX can be used for large-scale explosive formulations and IM ammunition.

TEX as an explosive due to its high performance and low sensitivity has been considered as one of the components of explosive compounds. Compared to conventional nitramine solid materials such as RDX and HMX, this material has better thermal stability and less sensitivity to impact and friction.

4. References

[1] STANAG, N. 4439-2010. Policy for introduction and assessment of insensitive munitions (IM). 2010.

[2] Simpson, R.; Urtiew, P.; Ornellas, D.; Moody, G.; Scribner, K.; Hoffman, D. CL-20 Performance Exceeds that of HMX and its Sensitivity is Moderate. *Propellants Explos. Pyrotech* **1997**, *22* (5), 249-255.

[3] Lund, G. K.; Highsmith, T. K.; Braithwaite, P. C.; Wardle, R. B. Insensitive high performance explosive compositions. Google Patents: 1996.

[4] Ramakrishnan, V.; Vedachalam, M.; Boyer, J. 4, 10-dinitro-2, 6, 8, 12-tetraoxa-4, 10-diazatetracyclo [5.5. 0.05, 903, 11] dodecane. *J. Heterocycl. Chem.* **1990**, *31* (3), 479-480.

[5] Highsmith, T. K.; Edwards, W. W.; Wardle, R. B. Synthesis of 4, 10-dinitro-2, 6, 8, 12-tetraoxa-4, 10-diazatetracyclo [5.5. 0.05, 903, 11] dodecane. Google Patents: 1996.

[6] Norman, F. A.; Godfrey, F. 1, 4-diformyl-2, 3, 5, 6-tetrahydroxypiperazine and derivatives and preparation thereof. Google Patents: 1968.

[7] Dinwoodie, A.; Gibson, J.; Parker, J. Base-catalysed reactions of glyoxal. Part II. 2, 3, 5, 6-Tetrahydroxypiperazine-1, 4-disulphonic acid derivatives. *JOC* .**1967**, 496-497.
[8] Currie, A.; Dinwoodie, A.; Fort, G.; Thompson, J. Base-catalysed reactions of glyoxal. Part I. 1, 4-Diformyl-and 1, 4-bis-methylsulphonyl-derivatives of 2, 3, 5, 6-tetrahydroxypiperazines. *JOC* .**1967**, 491-496.
[9] Vail, S. L.; Moran, C. M.; Barker, R. H. The formation of N, N'-dihydroxyethylenebisamides from glyoxal and selected amides. *J. Org. Chem.* **1965**, *30* (4), 1195-1199.
[10] Jalový, Z.; Matyáš, R.; Klasovitý, D.; Zeman, S. Contribution to the Synthesis of 4, 10-Dinitro-2, 6, 8, 12-tetraoxa-4, 10-diazatetracyclo [5.5. 0.05, 903, 11] dodecane (TEX). *J. Energ. Mater.* **2010**, *7* (3), 189-196.
[11] Jalovy, Z.; Maty, R. In The Influence of Reactions Conditions on TEX Synthesis. In *Vth Seminar, New Trends in Research of Energetic Materials, Pardubice, Czech Republic*, 2002; pp 24-25.
[12] Sanderson, A. J.; Hajik, R. M.; Highsmith, T. K.; Johnston, H. E. Synthesis for 4, 10-dinitro-2, 6, 8, 12-tetraoxa-4, 10-diazatetracyclo [5.5. 0.05, 903, 11]-dodecane. Google Patents: 2003.
[13] Wardle, R. B.; Hajik, R. M.; Hinshaw, J. C.; Highsmith, T. K. Process for the large-scale synthesis of 4, 10-dinitro-2, 6, 8-12-tetraoxa-4, 10-diazatetracyclo-[5.5. 0.05, 903, 11]-do decane. Google Patents: 2000.
[14] Braithwaite, P. TEX A promising new insensitive high explosive. In *29^< th> International Annual Conference of ICT (Energetic Materials): Thiokol Propulsion, Brigham City; USA, 1998*, 1998.
[15] Cartridge, H. E. H. M.; Sotsky, L.; Mazzei, R.; Al-Shehab, N. 2006 Insensitive Munitions and Energetic Materials Technology Symposium.
[16] Vágenknecht, J.; Mareček, P.; Trzciński, W. A. Sensitivity and performance properties of TEX explosives. *J. Energ. Mater.* **2002**, *20* (3), 245-253.
[17] Doherty, R. M.; Simpson, R. L. A comparative evaluation of several insensitive high explosives. *Combust Flame* .**1998**, 32-1.
[18] Dudek, K.; Marecek, P.; Vavra, P. Laboratory testing of HNIW mixtures. *J. Energ. Mater.* **2000**, 110-1.
[19] Clement, D.; Koch, E.; Rudolf, K.; Eigenmann, B. 10th Seminar "New Trends in Research of Energetic Materials". *Pardubice, Czech Republic* **2008**, 25-27.
[20] FrIEdl, Z.; Kočí, J. Electric spark sensitivity of nitramines. Part I. Aspects of molecular structure. *Cent. Eur. J. Energ. Mater.* **2006**, *3* (3), 27-44.
[21] Marecek, P.; Pokornà, J.; Vàvra, P. A study of some insensitive explosives. In *Fraunhofer ICT*. 1998; Fraunhofer-Institut Fur Chemische Technologie: pp P52-P52.

29TH IRANIAN ORGANIC CHEMISTRY CONFERENCE
1_3 NOV, 2023
UNIVERSITY OF QOM, IRAN

Copper Cluster as An Anticancer Agent: A DFT Study

*Batoul Alipour and Mohamad Zaman Kassaee**

Department of Chemistry, Tarbiat Modares University, P.O. Box 14115-175, Tehran, Iran,
alipourbatoul@gmail.com, *kassaeem@modares.ac.ir*

Abstract - The Cu cluster is predicted to exhibit carcinogenic or anticancer properties. They can potentially act as carcinogens by promoting the formation of free radicals through the loss of an electron and approaching Cu^+. In contrast, they can also act as anticancer by tending to scavenge free radicals through the attraction of an electron and approaching Cu^-. Herein, we calculate the dual roles of the Cu_3 cluster in scavenging RO•, or generating free radicals from RO–H, at the B_3LYP/ LANL2DZ level in water as solvent. Cu_3 reduces the bond dissociation energy (BDE) of RO–H and decreases the spin density at the oxygen of RO•, suggesting the cleavage of the RO–H bond and the capture of the RO• radical. These are clear evidence for both the RO–H bond breakage and scavenging of RO• radical. Since O–Cu, anchoring bond is responsible for the interaction of Cu_3 and ROH (or RO•), its nature is interpreted utilizing the quantum theory of atoms in molecules (AIM) and the natural bond orbital (NBO). The results indicate that the O–Cu bond is stronger and has more covalent character in RO•–Cu_3 than in ROH–Cu_3. The scavenging properties of copper cluster seems to have a more significant role in their anticancer activity rather than their ability to initiate the formation of free radicals in carcinogenesis.

1. Introduction

Copper clusters have been studied both experimentally [1-4] and theoretically [5-12]. Since they can be described as models of surface they prove helpful for investigating adsorption[13, 14] and heterogeneous catalysis[15] and scavenging free radicals.[16] Free radicals exist within the biological system.[17] They have garnered interest due to their intriguing chemical and pathological properties in living organisms, including their role in energy production and regulation of cell growth [18]. These radicals have a brief lifespan and easily interact with different cellular elements. This phenomenon, known as oxidative stress (OS), results in DNA damage and the development of cancer [19]. Antioxidants (AO) serve as a remedy for OS by intercepting free radicals and preventing cell oxidation. Consequently, the advancement of AO aids in enhancing the overall health of living organisms. Currently, nanoparticles (NPs) have attracted attention as free radical trappers [20-22].

Recently, we used DFT to respond to the question of whether gold clusters promote free radicals or scavenge [23, 24]. Herein, the effects of Cu_3 cluster on radical quenching and promotion using DFT are calculated, and compared.

2. Results and discussion

Here, the effects of Cu_3 cluster on RO–H homolytic bond cleavage and stabilizing RO• radical are assessed at the B_3LYP/LANL2DZ [25-28] level of theory (Fig. 1). The extent of carcinogenicity and anticarcinogenic of copper NPs may be indicated by their ability to generate or quench free radicals. The questions are: (1) How reactive are Cu_3 cluster towards RO• free radicals? (2) Which orbitals of free radicals interact with Cu_3 cluster? (3) What BDE is involved in the reaction with Cu_3 cluster?

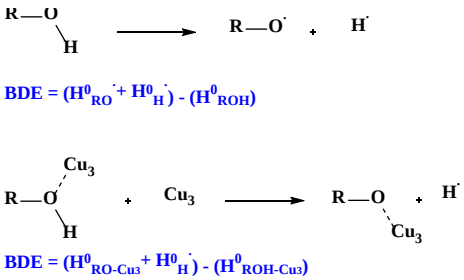

Fig.1. Bond dissociation energy (BDE) of RO–H in the absence (a) and presence of Cu_3 (b) (R = H, methyl, ethyl, *n*-propyl, *i*-propyl, *n*-butyl, *t*-butyl, and phenyl).

2.1. Structure and energy of RO•–Cu_3 and ROH–Cu_3 complexes

To create the initial structures of Cu_3 cluster complexes with RO• and ROH, we positioned the Cu_3 cluster adjacent to the oxygen atoms that possess an abundance of electrons in both RO• and ROH. Fig. 2 shows the optimized structures of the RO•–Cu_3 and ROH–Cu_3 complexes. In these structures, the Cu_3 cluster is positioned adjacent to the oxygen atoms of both RO• and ROH. The electron densities of these oxygen atoms are transferred to the valence orbitals of the copper atoms, resulting in the formation of stable complexes.

Fig.2. Geometric features, including interatomic distances (Å) for ROH–Cu_3 and RO•–Cu_3, at the B_3LYP/LANL2DZ level of theory

triplet	doublet	triplet	doublet
HO•–Cu_3	H_2O–Cu_3	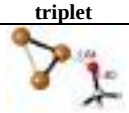 MeO•–Cu_3	MeOH–Cu_3
EtO•–Cu_3	EtOH–Cu_3	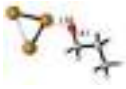 *n*-PrO•–Cu_3	*n*-PrOH–Cu_3
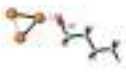 *n*-BuO•–Cu_3	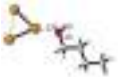 *n*-BuOH–Cu_3	*i*-PrO•–Cu_3	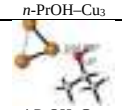 *i*-PrOH–Cu_3
t-BuO•–Cu_3	*t*-BuOH–Cu_3	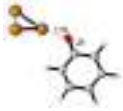 *t*-BuO•–Cu_3	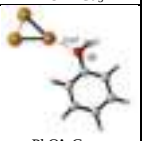 PhO•–Cu_3

The important geometrical and thermodynamic parameters of RO•–Cu_3 and ROH–Cu_3 are compared and contrasted (Table 1). The weak interactions of the Cu_3 cluster with the ROH oxygen atom, O–H and C-O bond distances are not significantly affected, Elongation for C–O occurs more than the O–H bond. Therefore, depending on the R in ROH–Cu_3, the results show that Δr(O–H) and Δr(C–O) with values of 0.001 to 0.002 Å and -0.012 to 0.028 Å, respectively. r(O–Cu) in ROH–Cu_3 appears longer than RO•–Cu_3. Such as O–Cu (2.051 Å) in H_2O–Cu_3 appear longer than those of *r*(O–Cu) of Cu atoms (1.849 Å) in HO•–Cu_3. Also, the results show that *r*(O–Cu) in PhOH–Cu_3 of Cu (2.068 Å) in PhO•–Cu_3 appear longer than those of *r*(O–Cu) of Cu (1.942 Å) in PhO•–Cu_3. For RO•–Cu_3 complexes, the anchoring bond, r(O–Cu), appears shorter than in ROH–Cu_3 complexes (Table 1). Effects of Cu_3 cluster on elongation of C–O bond (Δr(C–O)) in RO•–Cu_3 are generally more than that in ROH–Cu_3 complexes. Comparing E_b values for RO•–Cu_3 and ROH–Cu_3 shows that complexes of radical species (RO•) with Cu_3 cluster enjoy more stability than those with ROH. The highest and lowest absolute values of binding energy (E_b) pertain to HO•–Cu_3 and PhO•–Cu_3, respectively. The effect of the copper cluster on the length of bond between O–Cu_3 shows that when the copper reacts with RO•, the bond length is shorter than when it is complexed with ROH. Thus, the copper cluster has scavenging free radicals properties.

Table 1 Geometric and thermodynamic features, including bond lengths (Å) and binding energies (E_b, kcal/mol) for ROH–Cu_3 and RO•–Cu_3, at the B_3LYP/LANL2DZ level of theory

Compound	r(O–Cu)[a]	Δr(C–O)[b]	Δr(O–H)[b]	E_b
HOH–Cu_3	2.051	0.002	0.002	-12.54
HO•–Cu_3	1.849	-0.012	-	-33.75
MeOH–Cu_3	2.040	0.015	0.001	-13.72
MeO•–Cu_3	1.837	0.035	-	-25.27
EtOH–Cu_3	2.037	0.020	0.001	-14.38
EtO•–Cu_3	1.836	0.040	-	-24.80
n-PrOH–Cu_3	2.033	0.019	0.001	-14.35
n-PrO•–Cu_3	1.836	0.039	-	-24.52
n-BuOH–Cu_3	2.037	0.020	0.002	-15.27
n-BuO•–Cu_3	1.836	0.039	-	-24.52
i-PrOH–Cu_3	2.037	0.024	0.001	-15.96
i-PrO•–Cu_3	1.834	0.034	-	-26.66
t-BuOH–Cu_3	2.034	0.028	0.001	-15.85
t-BuO•–Cu_3	1.834	0.034	-	-27.29
PhOH–Cu_3	2.068	-0.002	0.001	-14.88
PhO•–Cu_3	1.942	0.024	-	-17.88

[a] r(O–Cu) is the anchoring bond length in angstroms.

[b] Δr(C–O) and Δr(O–H) are the differences between the bond lengths of O–C and O–H in the complexed and free forms in angstroms.

[c] The binding energy, E_b, in $kcalmol^{-1}$.

[d] Here, for HOH or HO•, we have Δr(H–O) instead of Δr(C–O).

2.2. Bond dissociation energy (BDE) and spin density (SD)

Bond dissociation energy (BDE) is calculated *via* the effects of Cu_3 cluster on RO•, using O–H BDE in ROH and ROH–Cu_3. The calculations of BDE aim to show the extent to which BDE of RO–H can be affected in the presence of Cu_3 cluster.

Table 2 Calculated O–H BDEs (in $kcalmol^{-1}$) in ROH and ROH–Cu_3 components

ROH	(a) O–H	ROH···•Cu_3	(b) O–H	Δ_1
HOH	116.53	HOH···•Cu_3	39.07	77.46
MeOH	99.61	MeOH···•Cu_3	41.32	58.29
EtOH	99.17	EtOH···•Cu_3	41.15	58.02
n-PrOH	99.09	n-PrOH···•Cu_3	41.56	57.53
n-BuOH	98.46	n-BuOH···•Cu_3	41.84	56.62
i-PrOH	100.44	i-PrOH···•Cu_3	41.92	58.52
t-BuOH	101.17	t-BuOH···•Cu_3	42.08	59.09
PhOH	79.16	PhOH···•Cu_3	28.10	51.06

Δ_1 = (a-b) Δ_2 = (a-c)

We calculated the BDEs for O–H (a, and b) of ROH, and ROH–Cu_3, respectively (Table 2). The BDE of RO–H decreases 51.06 to 59.09 (Δ_1). $kcalmol^{-1}$ in the presence of Cu_3. This decrease is except for HO–H, which decreases significantly in the existence of Cu_3 cluster (Δ_1:77.46 $kcalmol^{-1}$). In other words, Cu_3 cluster facilitate the formation of free radicals by decreasing the BDE of O–H.

The spin density maps for the RO• and their complexes with copper cluster are shown in Fig. 3. Hence, the Cu_3

cluster stabilizes the RO• radical *via* the transfer of spin density.

Fig.3. Spin density maps of RO• and RO•–Cu_3 structures

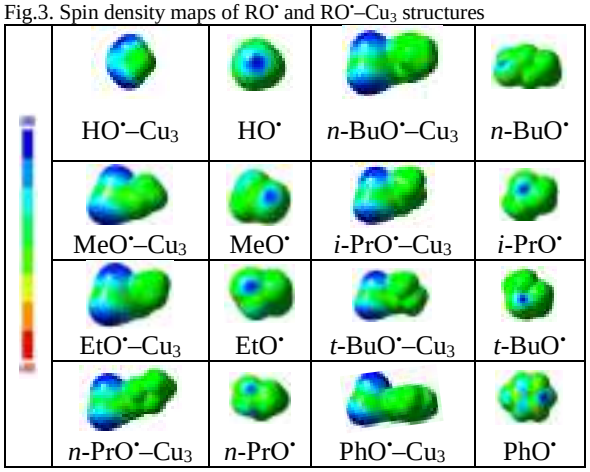

2.3. Atoms in molecules (AIM)

AIM analysis indicates the nature of bonding *via* the properties of electron density by bond critical points (BCPs). At the BCPs, there are topological parameters, including electron density, $\rho(r)$, Laplacian of electron density, $\nabla^2\rho(r)$; electronic kinetic energy density, G(*r*); electronic potential energy density, V(*r*), and electronic energy density, H(*r*) (Table 3).

Table 3 Bond critical point data from AIM analysis for O–Cu in ROH–Cu_3 and RO•–Cu_3 complexes

Compound	$\rho(r)$	$\nabla^2\rho(r)$	G(r)	V(r)	H(r)
HOH–Cu_3	0.053	0.424	0.010	-0.093	0.006
HO•–Cu_3	0.080	0.480	0.123	-0.127	-0.003
HO•–Cu_3	0.061	0.588	0.142	-0.136	-0.005
MeOH–Cu_3	0.054	0.446	0.105	-0.099	0.006
MeO•–Cu_3	0.103	0.791	0.212	-0.227	-0.015
EtOH–Cu_3	0.055	0.454	0.107	-0.101	0.006
EtO•–Cu_3	0.102	0.792	0.212	-0.225	-0.014
n-PrOH–Cu_3	0.057	0.471	0.112	-0.107	0.006
n-PrO•–Cu_3	0.104	0.788	0.212	-0.228	-0.015
n-BuOH–Cu_3	0.057	0.469	0.112	-0.106	0.006
n-BuO•–Cu_3	0.101	0.786	0.210	-0.223	-0.013
i-PrOH–Cu_3	0.056	0.465	0.111	-0.105	0.006
i-PrO•–Cu_3	0.102	0.787	0.210	-0.223	-0.013
t-BuOH–Cu_3	0.057	0.472	0.112	-0.107	0.005
t-BuO•–Cu_3	0.103	0.798	0.213	-0.228	-0.014
PhOH–Cu_3	0.052	0.424	0.099	-0.093	0.006
PhO•–Cu_3	0.079	0.737	0.185	-0.186	-0.0007
PhO•–Cu_3	0.079	0.737	0.185	-0.186	-0.0007
PhO•–Ag_3	0.038	0.245	0.062	-0.062	-0.0003

The sign of $\nabla^2\rho(r)$ at a BCP is distinguished by the G(r)/V(r) ratio. A negative value of $\nabla^2\rho(r)$ indicates a covalent interaction. A positive value of $\nabla^2\rho(r)$, on the other hand, shows a closed-shell electrostatic interaction. At the BCPs, the electronic energy density (H(r)) is defined as H(r) = G(r) + V(r). For O–Cu bonds, the $\rho(r)$ correlates with their values of E_b. For example, the $\rho(r)$ at O– Cu in EtOH–Cu_3 and EtO•–Cu_3 is 0.055 and 0.102, which correlates with their E_b of -14.38 and -24.80, respectively (Table 3). All parameters show that O–Cu bond is more covalent nature in RO•–Cu_3 than in ROH–Cu_3 (Table 3, Fig. 4).

Fig.4. Electron density maps of ROH and RO• complexes with the Cu_3 cluster

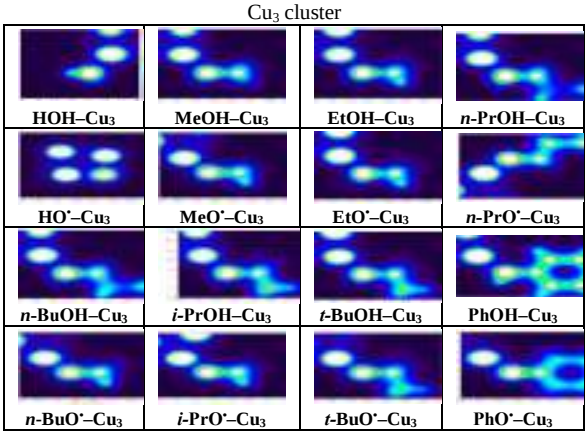

2.4. Natural bond orbital (NBO)

The NBO analysis done to show charge transfer (ΔE_{CT}) O–Cu, in RO•–Cu_3 and corresponding ROH–Cu_3. In anchoring O–Cu bonds, the charge of the lone pair of oxygen atoms is transfered to the antibonding (σ*) and unfilled valence shell nonbonding (n*) orbitals of Cu_3. For RO•–Cu_3 and ROH–Cu_3, the charge transfer energy ΔE_{CT} are calculated (Table 4). The ΔE_{CT} of RO•–Cu_3 is more than that of ROH–Cu_3. For example, the ΔE_{CT} at EtO•–Cu_3 and EtOH–Cu_3 are 33.15 and 14.25, which correlate with their E_b of -24.80 and -14.38, respectively (Table 1, 6).

Table 4 Charge transfer features of ROH and RO•–Cu_3 complexes based on NBO theory

Complex	Interaction	ΔE_{CT}[a]	Complex	Interaction	ΔE_{CT}[a]
HOH–Cu_3	$n_O \rightarrow n^*_{Cu}$	12.45	*n*-BuOH–Cu_3	$n_O \rightarrow n^*_{Cu}$	13.36
HO•—Cu_3	$n_O \rightarrow n^*_{Cu}$	15.60		$n_O \rightarrow \sigma^*_{Cu13\text{-}Cu15}$	3.44
	$n_O \rightarrow \sigma^*_{Cu}$	3.09	*n*-BuO•–Cu_3	$n_O \rightarrow n^*_{Cu}$	30.69
MeOH–Cu_3	$n_O \rightarrow n^*_{Cu}$	12.32		$n_O \rightarrow \sigma^*_{Cu\text{-}Cu}$	4.14
MeO•–Cu_3	$n_O \rightarrow n^*_{Cu}$	31.9	*i*-PrOH–Cu_3	$n_O \rightarrow n^*_{Cu}$	14.27
	$n_O \rightarrow \sigma^*_{Cu\text{-}Cu}$	5.00		$n_O \rightarrow \sigma^*_{Cu\text{-}Cu}$	2.95
EtOH–Cu_3	$n_O \rightarrow n^*_{Cu}$	14.25	*i*-PrO•–Cu_3	$n_O \rightarrow n^*_{Cu}$	32.31
	$n_O \rightarrow \sigma^*_{Cu\text{-}Cu}$	3.02		$n_O \rightarrow \sigma^*_{Cu\text{-}Cu}$	4.14
EtO•–Cu_3	$_O \rightarrow n^*_{Cu}$	33.15	*t*-BuOH–Cu_3	$n_O \rightarrow n^*_{Cu}$	14.64
n-PrOH–Cu_3	$n_O \rightarrow n^*_{Cu}$	13.30		$n_O \rightarrow \sigma^*_{Cu\text{-}Cu}$	2.66
	$n_O \rightarrow \sigma^*_{Cu\text{-}Cu}$	3.56	*t*-BuO•–Cu_3	$n_O \rightarrow n^*_{Cu}$	31.6
n-PrO•–Cu_3	$_O \rightarrow n^*_{Cu}$	31.27		$n_O \rightarrow \sigma^*_{Cu\text{-}Cu}$	1.86
	$n_O \rightarrow \sigma^*_{Cu\text{-}Cu}$	5.47	PhOH–Cu_3	$n_O \rightarrow n^*_{Cu}$	12.36
				$n_O \rightarrow \sigma^*_{Cu\text{-}Cu}$	2.87

[a]The charge transfer energy value, in kcalmol^{-1}, between donor and acceptor orbitals within complexes of ROH and RO•

3. Conclusion

In summary, the E_b in $RO^{\bullet}–Cu_3$ is more than ROH–Cu_3. The ΔE_{CT} confirms these results by showing stronger charge-transfer in $RO^{\bullet}–Cu_3$ than the corresponding ROH–Cu_3. Moreover, AIM analysis illustrates that O–Cu bond is stronger in $RO^{\bullet}–Cu_3$ than in ROH–Cu_3. Copper cluster stabilizes $RO^{\bullet}$ and significantly reduce the BDE of O–H. Also, the spin density map shows that $RO^{\bullet}$ oxygen is dramatically reduced. These data show RO–H bond breakage and its simultaneous trapping of $RO^{\bullet}$ radical by copper cluster. The calculated results show that the copper cluster may function as radical trappers at high concentrations of radicals.

4. References

[1] M. Vogel, A. Herlert, L. Schweikhard, J. Am. Soc. Mass Spectrom. 14 (2003) 614-621.
[2] S. Lecoultre, A. Rydlo, C. Félix, J. Buttet, S. Gilb, W. Harbich, J. Chem. Phys. 134 (2011) 074303.
[3] C. Pettiette, S. Yang, M. Craycraft, J. Conceicao, R. Laaksonen, O. Cheshnovsky, R. Smalley, J. Chem. Phys. 88 (1988) 5377-5382.
[4] L. Ames, R. Barrow, Trans. Faraday Soc. 63 (1967) 39-44.
[5] M. Yang, K.A. Jackson, J. Chem. Phys. 122 (2005) 184317.
[6] C.W. Bauschlicher Jr, S.R. Langhoff, P.R. Taylor, J. Chem. Phys. 88 (1988) 1041-1045.
[7] G. Jeung, M. Pelissier, I. Barthelat, Chem. Phys. Lett. 97 (1983) 369-372.
[8] M. Böyükata, J.C. Belchior, J. Braz. Chem. Soc. 19 (2008) 884-893.
[9] H. Tatewaki, E. Miyoshi, T. Nakamura, J. Chem. Phys. 76 (1982) 5073-5086.
[10] A. Posada-Amarillas, R. Pacheco-Contreras, S. Morales-Meza, M. Sanchez, J.C. Schön, Int. J. Quantum Chem. 116 (2016) 1006-1015.
[11] R. Singh, P. Biswas, P.K. Jha, Int. J. Quantum Chem. 120 (2020) e26239.
[12] V. Gurin, Int. J. Quantum Chem. 104 (2005) 249-255.
[13] A. Clotet, J. Ricart, F. Illas, G. Pacchioni, R. Lambert, J. Am. Chem. Soc. 122 (2000) 7573-7578.
[14] A.A. Ahmed, Chem. Phys. Lett. 753 (2020) 137543.
[15] D. Domınguez-Ariza, C. Sousa, N. Harrison, M. Ganduglia-Pirovano, F. Illas, Surf. Sci. 522 (2003) 185-197.
[16] M. Reina, A. Martínez, Comput. Theor. Chem. 1112 (2017) 1-9.
[17] B. Commoner, J. Townsend, G.E. Pake, Nature 174 (1954) 689-691.
[18] A.A. Alfadda, R.M. Sallam, J. biotechnol. biomed. 2012 (2012).
[19] V. Dhawan, Reactive oxygen and nitrogen species: general considerations, Studies on respiratory disorders, Springer2014, pp. 27-47.
[20] F. Della Pelle, D. Vilela, M.C. González, C.L. Sterzo, D. Compagnone, M. Del Carlo, A. Escarpa, Food Chem. 178 (2015) 70-75.
[21] J. Jeynes, M. Merchant, A. Spindler, A. Wera, K. Kirkby, Physics in Medicine & Biology 59 (2014) 6431.
[22] V. Kumar, P. Guleria, V. Kumar, S.K. Yadav, Science of the total environment 461 (2013) 462-468.
[23] A. Ahmadi, M.Z. Kassaee, A. Fattahi, J. Phys. Org. Chem. 31 (2018) e3776.
[24] A. Ahmadi, M.Z. Kassaee, M. Ayoubi-Chianeh, A. Fattahi, J. Phys. Org. Chem. 34 (2021) e4126.
[25] R.A. Gaussian09, Inc., Wallingford CT 121 (2009) 150-166.
[26] D. Zheng, M. Zhang, G. Zhao, Sci. Rep. 7 (2017) 1-10.
[27] K. Raghavachari, Theor. Chem. Acc. 103 (2000) 361-363.
[28] B. Miehlich, A. Savin, H. Stoll, H. Preuss, Chem. Phys. Lett. 157 (1989) 200-206.

29TH IRANIAN ORGANIC CHEMISTRY CONFERENCE
1_3 NOV, 2023
UNIVERSITY OF QOM, IRAN

Dopamine-conjugated apoferritin for delivery of epirubicin

Ronak Rafipour[1*], *Hasanain Gomhor J. Alqaraghuli*[2], *Soheila Kashanian*[3,4]

[1] *Department of Chemistry, Kermanshah Branch, Islamic Azad University, Kermanshah, Iran, ronak.rafipour@iau.ac.ir*
[2] *Department of Science, College of Basic Education, Al-Muthanna University, Al-Muthanna, Iraq.*
[3] *Department of Applied Chemistry, Faculty of Chemistry, Razi University, Kermanshah, Iran*
[4] *Nano Drug Delivery Research Center, Kermanshah University of Medical Sciences, Kermanshah, Iran*

Abstract – Nanocarriers are drug delivery vehicles, which have attracted the attention of researchers in recent years, particularly in cancer treatment. The encapsulation of anticancer drugs using protein nanocages is considered to be an optimal approach to reducing drug side-effects and increasing the bioavailability of anticancer drugs. Epirubicin (EPR) is an active chemotherapeutic medication used in the treatment of breast cancer. However, the toxicity of this drug against normal cells is a considerable limitation in therapy. EPR toxicity could be reduced using nanocarriers and dual-targeted drug delivery. Dual-targeted drug delivery system was developed by the conjugation of dopamine (DA) with horse spleen apoferritin (HsAFr)-encapsulated EPR to overcome the limitations of chemotherapeutic EPR in breast cancer treatment. HsAFr-EPR-DA complexes could target the scavenger receptors, transferrin receptors 1, and DA receptors, which are overexpressed on breast cancer cells.

1. Introduction

Breast cancer is the most prevalent cancer and the main cause of cancer deaths in women across the world. In 2012, reports estimated the number of cancer cases to be 1.7 million in women, with 522,000 deaths [1]. Anthracyclines are anticancer chemotherapeutic agents, which are broadly utilized in the treatment of breast cancer. The anticancer activity of these drugs is through the inhibition of topoisomerase , which prevents DNA synthesis and leads to cell death. Recent studies have confirmed that anthracyclines increase the risk of clinical cardiotoxicity, thereby leading to heart failure [2]. Protein nanocages have been extensively investigated as drug delivery carriers in bionanotechnology. These agents are considered to be potent nanocarriers owing to their biocompatible, nonimmunogenic, stability, and biodegradable nature [3]. Horse spleen apoferritin (HsAFr) is a spherical protein nanocage, which has been reported to be an effective nanocarrier for the dual-targeted drug delivery of cancer cells since it has more receptors on the membrane of cancer cells compared to normal cells. Furthermore, the surface of HsAFr contains numerous functional groups, which could be modified to prepare targeted ligands. Encapsulation of anticancer drugs in HsAFr nanocages is based on pH-induced HsAFr dissociation and reassembly properties. The subunits of HsAFr could be dissociated in strong acidic or alkaline environments (pH: 2 or 13) and associated by returning the pH to the physiological level (7.4). Dopamine (DA) receptors are found on breast cancer cells; therefore, it is essential to target these receptors as the therapeutic targets in breast cancer. DA is a biochemical substance with the formula of 3,4-dihydroxy-L-phenylalanine (catecholamine), which is secreted from the mussels. DA receptors are a class of G-protein-coupled receptors. DA has five types of receptors, and it has been reported that dopamine type-1 receptor (D1R) is more significantly overexpressed in breast cancer cells than other cancer cell types [4].

2. Materials and methods

2.1 Chemicals

Horse spleen apoferritin (HsAFr) was purchased from Calbiochem (San Diego, CA). Epirubicin hydrochloride was obtained from Kavosh Gostar Darou Company (Tehran, Iran) (manufactured by Ebewe pharma, Unterach am Attersee, Austria). All other materials were purchased from Merck (Kenilworth, NJ).

2.2 Synthesis of HsAFr-EPR-DA complexes

The loading of EPR into HsAFr was achieved as described by H. Gomhor J. Alqaraghuli et al. [5], and the synthesis of HsAFr-EPR-DA complexes was carried out based on the modified methods proposed by Kim et al. and Lee et al. EDC (0.5 mg) and NHS (0.3

mg) were dissolved. in one milliliter of phosphate buffer solution (pH:6.6) for at the temperature of 25°C for 15 minutes in order to prepare the activation buffer. The activation buffer was added to one milligram of EPR-loaded HsAFr drop-wise with slow stirring. After 20 minutes, 0.2 milligram of DA was added, and the pH was adjusted to 6.8 using HCl (0.01 M), and the mixture was incubated for three hours. The solution was dialyzed against 0.01 M phosphate buffer solution (pH: 7.4, 450 ml) in triplicate at two-hour intervals so as to completely drive out the free DA molecules from the HsAFr- EPR-DA complexes.

3. Results and discussion

3.1 Characterization of DA-conjugated EPR-loaded HsAFr

HsAFr showed an absorption peak at 280 nm. Absorption at 280 nanometers reflected the residues of the aromatic amino acid content in the HsAFr protein. On the other hand, the spectrum of red EPR showed the maxima at 481 nanometers. In addition, DA showed an absorption band at 280 nanometers. Absorption at 280 nanometers in DA was due to $\pi \rightarrow \pi^*$ transition in the aromatic rings. The UV-Vis spectra of the HsAFr-EPR-DA complexes were determined as well (Fig 1). The UV-Vis spectra of the HsAFr-EPRDA complexes were also verified in order to investigate the encapsulation of the drug in the apoferritin through the absorption observed at 481 nanometers, and the surface was modified HsAFr with DA through the absorption with high intensity at 280 nanometers.

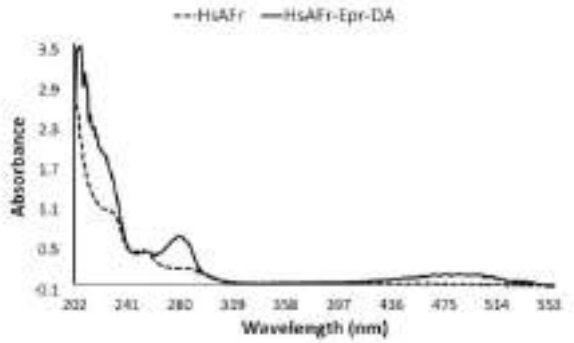

Figure 1. UV–Vis spectra of the HsAFr and HsAFr–Epr-DA.

3.2 Fluorescence spectroscopy

The DA fluorescence spectra in the DA solution and HsAFr-EPR-DA complexes were determined after using the blank HsAFr (Fig 2). The DA fluorescence spectra were recorded at 285-405 nanometers at the excitation wavelength of 279 nanometers . The HsAFr protein in the HsAFr-EPR-DA sample was measured using the Bradford assay to prepare the blank solution of HsAFr. According to the findings, the fluorescence spectra of DA in the DA solution and HsAFr-Epr-DA complex exhibited an emission maximum at the wavelength of 317 nanometers. Moreover, the HsAFr surface was modified with DA in the HsAFr-EPR-DA complex.

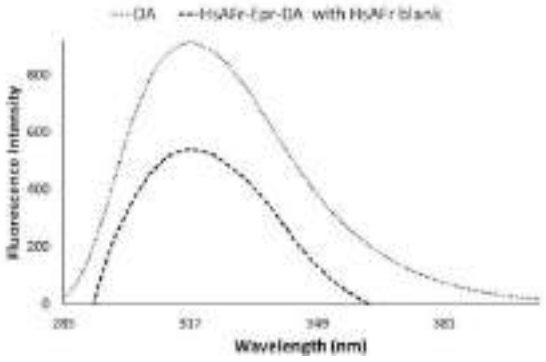

Fig2. Dopamine Fluorescence Spectra in DA Solution and HsAFr-EPR-DA Complexes (Excitation wavelength set at 279 nm; fluorescence spectra exhibited emission maximum at wavelength of 317 nm)

3.3 *In-vitro drug release from HsAFr-DA nanocages*

Fig 3 shows the EPR drug release profile from the HsAFr-DA nanocarriers in phosphate buffer in physiological conditions (pH: 7.4, 37°C) as a function of time. Moreover, the obtained results indicated the acceptable drug release at the pH of 7.4 to be approximately 25.34% of the loaded EPR that was released after eight hours, and 81.39% of the loaded EPR was released after 48 hours. The inner surface of the HsAFr protein nanocage was rich in the acidic residues of glutamate (Glu) and aspartate (Asp) amino acids, resulting in a high negative charge density in the inner cavity of the HsAFr nanocage at physiological pH . At the pH of 7.4, the carboxylic groups of Asp and Glu residues were ionized, and the drug molecules were neutral due to the non-protonation of its amino groups, which in turn led to the reduction of the electrostatic interaction of neutral EPR drug molecules with the negatively charged inner cavity of the apoferritin. This phenomenon led to drug release from EPR-loaded HsAFr-DA over time.

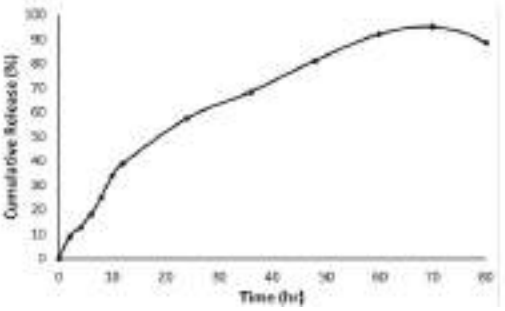

Fig 3. Fig.3. Rate of EPR Drug Release from HsAFr-DA Nanocarriers at pH of 7.4 (Release profiles of EPR in phosphate buffer solution at 37°C as function of time)

4. Conclusions

In the present study, we developed a novel dual-targeted delivery system, and EPR as an anticancer drug was encapsulated in the core of the delivery system, which was composed of the HsAFr protein nanocage with DA utilized as a targeting ligand. Moreover, the ligand-based dual-targeted delivery system could be a new step toward the improvement of anticancer drugs to target cancer cells through a wide range of receptors. The HsAFr- EPR-DA complexes were successfully prepared, and their detailed characterization indicated that the HsAFr protein nanocage was stable after EPR loading and its surface modification with DA.

5. References

[1] L. A. Torre, F, Bray, R. L. Siegel, et al. CA Cancer J Clin. 65(2015) 87-108.
[2] C. Perrino, G. Schiattarella, F. Magliulo, F. Ilardi, G. Carotenuto, et al. CurrVasc Pharmacol. 12 (2014) 106-16.
[3] E. J. Lee, N. K. Lee, I.S. Kim. Adv Drug Deliv Rev. 106 (2016) 157-171.
[4] D. C. Borcherding, W. Tong, E. R. Hugo, D. F. Barnard, S. Fox, K. LaSance. Oncogene. 35 (2016) 3103-3113.
[5] J. A.H. Gomhor, S. Kashanian, R. Rafipour, E. Mahdavian, K. Mansouri. Nanomed Biotechnol. 46 (2018) S847-s854.

29TH IRANIAN ORGANIC CHEMISTRY CONFERENCE
1_3 NOV, 2023
UNIVERSITY OF QOM, IRAN

Adsorptive removal of tetracycline from water using MOF-808 nanoadsorbent

Maryam Noori Keshtkar[1], *Hossein Molavi*[2] *and Seyyed Abbas Musavi*[1] *

[1]*Department of Chemical and Petroleum Engineering, Sharif University of Technology, Tehran, Iran, maryamnoori.ce@gmail.com, musavi@sharif.edu*

[2] *Department of Chemistry, Institute for Advanced Studies in Basic Science (IASBS), Gava Zang, Zanjan 45137-66731, Iran.*

Abstract - Environmental pollution by antibiotics has severely affected human health and development. This paper presents synthesis of MOF-808 and its adsorptive performance for tetracycline (TC) removal. Adsorption kinetics and isotherms were determined from experimental data. The results show that the pseudo-second order kinetic model and the Langmuir isotherm model agree well for the adsorption of TC on MOF-808. The maximum adsorption capacity of TC in MOF-808 is about 254.94 $mg.g^{-1}$, which indicates a great adsorption performance of MOF-808.

Keywords: MOF-808, Tetracycline, Metal-organic framework, Adsorption

1. Introduction

With ongoing economic development and an ever-increasing world population, clean water supply is one of the most important issues worldwide [1]. Tetracycline (TC) is one of the most popular antibiotics and the second largest produced and consumed in the world (approximately over 5,500 tons per year). They are present in varying concentrations in natural water sources, and municipal and industrial wastewater [2]. Highly efficient moisture removal approaches are very important and such approaches should be affordable, robust, and effective. Urgent removal of them from water requires highly efficient methods, and such methods need to be accessible, powerful, and effective. There are various methods for removing antibiotics, among which the adsorption method has the following advantages. It has attracted attention due to its low cost, easy operation, and environmental friendliness. Adsorption removal is a potential method with low cost, a simple system design, and a simple adsorption/regeneration process. Metal-organic frameworks (MOFs) are a new generation of nanoadsorbents that have metal centers and organic ligands that can be used as adsorbents. Since these materials have low density, high accessible surface area, adjustability of pore size, and modification ability, they show very good separation ability and have attracted the attention of many researchers. Because these nanoparticles have the ability to adsorb medicinal compounds, their use will increase the efficiency of the water purification process [3]. In this study we use these materials to increase the efficiency of the process of removing pharmaceutical pollutants from water using the adsorption process. Based on the above perspective, we synthesized MOF-808 as the adsorbent and evaluated its adsorption performance for TC removal from aqueose solution.

2. Experimental

2.1. Materials and method: All used chemical materials such as Zirconium oxychloride octahydrate ($ZrOCl_2 \cdot 8H_2O$, purity≥ 99%), 1,3,5-benzene tricarboxylic acid (BTC, Merck), Dimethylformamide (DMF, Merck), Formic acid (≥ 99%, Merck), methanol (Merck), Tetracycline (TC, Merck) were used without any further purification.

2.2. Synthesis of MOF-808: MOF-808 was synthesized according to the published literatures with a slight modification in activation steps [4]. The centrifugation activation method were employed. In a typical synthesis, 0.257 g of $ZrOCl_2 \cdot 8H_2O$ and 0.056 g of BTC was firstly dissolved in a 1:1 mixture of DMF and formic acid (24 mL) in a screw-cap jar. The solution was ultrasonicated for approximately 15 min to completely dissolve all the MOF precursors. The solution was then put in an oven at 120 ˚C for 48 h and cooled down to room temperature. The resultant white product at the bottom of the jar was collected and activated via centrifugation method. According to this activation method, the synthesized particles were separated by centrifugation, washed several times with DMF and then with methanol under sonication for 15 min to remove the residual reactants. The white particles were solvent-exchanged by immersing in 10 mL of methanol for 5 days, in which every day the particles were washed with fresh methanol under sonication. Finally, the prepared adsorbent materials were dried at 100 ˚C overnight in an oven.

2.3. Adsorption kinetic experiments: The stock solution was prepared by adding a specific amount of TC to deionized water (500 $mg.L^{-1}$). To quantify the adsorption equilibrium time 0.5 $g{\cdot}L^{-1}$ nano-adsorbent (MOF-808) was added to an aqueous solution with a specific concentration of 150 $mg.L^{-1}$, and samples were taken at specific time intervals of 20, 40, 60, 90, 120, 160, 200, 250, 300 min. After adsorption, the nano-adsorbent was separated from the solutions by centrifugation at 3700 rpm for 10 min, and the TC concentrations were calculated using the absorbances obtained from the UV-vis spectrophotometer. Fig.1a illustrates the adsorption capacity versus time intervals.

2.4. Batch experiments and adsorption isotherms: To find the maximum adsorption capacity of TC in MOF-808, adsorption experiments were performed for 4 h (equilibrium time) using 15 mL aqueous solutions at ambient environment (room temperature). The initial concentrations of TC were 50, 80, 100, 120, 150, 200, 250, 300 $mg.L^{-1}$ and 7 mg of MOF-808 nano-adsorbent were added to each solution. Fig.1b shows the adsorption capacity at various equilibrium concentrations.

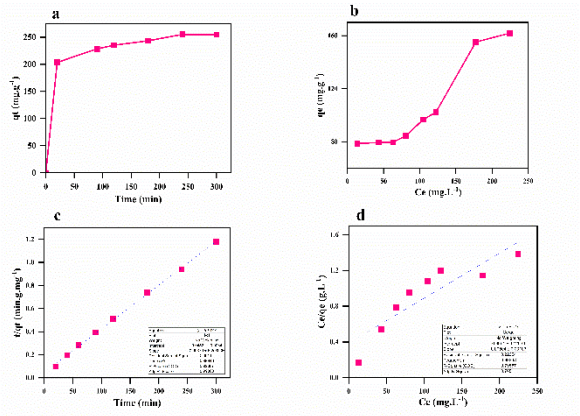

Fig.1. TC adsorption (a) kinetic curve and (b) isotherm over MOF-808, (c) The fitted pseudo-second order kinetic model and (d) the fitted adsorption isotherms by the Langmuir equation.

3. Results and Discussion

The featured powder X-ray diffraction (PXRD) peaks at 2θ values of 4.3, 8.3, and 8.69 can be easily identified in the obtained powders (Fig.2a), indicating (111), (311), and (222) crystal planes, respectively [5]. Fig.2b shows the FTIR spectrum of the synthesized MOF-808 sample. Peaks at 710 and 758 cm^{-1} were assigned to the C–C bond of the benzene ring. Furthermore, the peaks at 1570 and 1400 cm^{-1} are assigned to asymmetric and symmetric stretches of coordinating carboxylates (C=O), respectively, indicating Zr^{4+} and BTC coordination. Specifc surface area of the materials was measured at − 196 ˚C and the calculated BET surface area of the sample is around 589 m^2g^{-1}. A SEM image of MOF-808 was shown in Fig.3. It can be seen that the MOF-808 has a regular ochtahedral structure with particle size of about 500 nm.

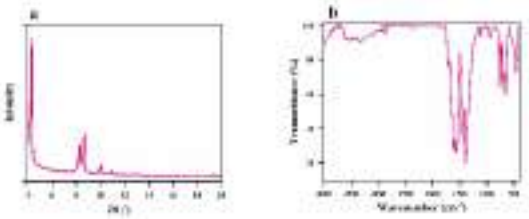

Fig.2. (a) XRD patterns and (b) FTIR spectrum of MOF-808.

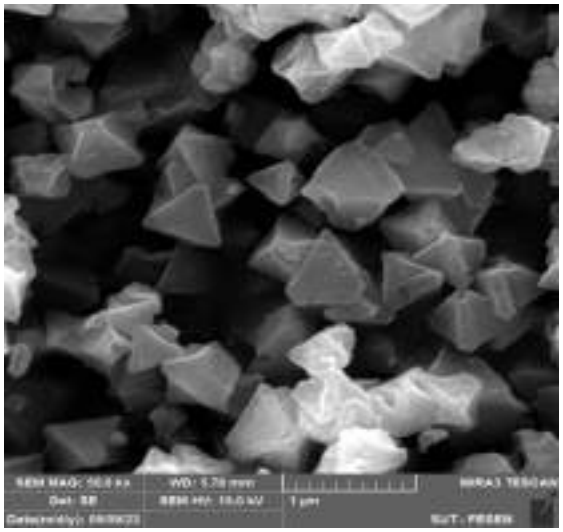

Fig.3. SEM image of MOF-808

4. Conclusions

In this study, we have successfully shown the superiority of MOF-808 as an adsorbent for TC removal. MOF-808 was successfully synthesized using a simple solvothermal method and characterized using BET, XRD and FTIR methods. Adsorption kinetics and isotherms were determined from the experimental data, and the results showed good agreement between the pseudo-second order kinetic model and the Langmuir isotherm model for the adsorption of TC on MOF-808. This nanoadsorbent showed excellent performance of adsorption of TC from water.

5. References

[1] M.B. Ahmed, J.L. Zhou, H.H. Ngo, W. Guo, Adsorptive removal of antibiotics from water and wastewater: Progress and challenges, Science of the Total Environment. 532 (2015) 112–126.

[2] E.Y. Klein, T.P. Van Boeckel, E.M. Martinez, S. Pant, S. Gandra, S.A. Levin, H. Goossens, R. Laxminarayan, Global increase and geographic convergence in antibiotic consumption between 2000 and 2015, Proc Natl Acad Sci U S A. 115 (2018) E3463–E3470.

[3] X. Liu, Y. Shan, S. Zhang, Q. Kong, H. Pang, Application of metal organic framework in wastewater treatment, Green Energy and Environment. 8 (2023) 698–721.

[4] N. Prasetya, K. Li, MOF-808 and its hollow fibre adsorbents for efficient diclofenac removal, Chemical Engineering Journal. 417 (2021).
[5] B. Liu, M. Liu, Z. Xie, Y. Li, A. Zhang, Performance of defective Zr-MOFs for the adsorption of anionic dyes, J Mater Sci. 57 (2022) 5438–5455.

29TH IRANIAN ORGANIC CHEMISTRY CONFERENCE
1_3 NOV, 2023
UNIVERSITY OF QOM, IRAN

Green magnetic nanostructures for solid phase extraction of pesticides

Sharifeh Hormozi Jangi, *Asma Khoobi* *

Department of Chemistry, Faculty of Sciences, University of Sistan and Baluchestan, Zahedan 98135-674, Iran, hormozii77@gmail.com, a.khoobi@science.usb.ac.ir.

Abstract

In order to increase human concerns about the effect of chemicals in agriculture on the ecosystem, accurate, selective and sensitive methods for the analysis of pesticides need to reduce the risk of human health problems caused by pesticides. In the present study, among the synthesized magnetic nanostructures discussed in this research: Cu/$CuFe_2O_4$@MIL-88A(Fe) nanostructures that synthesized by a hydrothermal strategy for solid phase magnetic extraction of chlorpyrifos and phosalone pesticides from water, vegetable and fruit juice samples were selected. The nanocomposites have good absorption capacity, high surface area, and paramagnetic properties. In addition, in this research, polysulfone magnetic nanostructures with high absorption capacity have been reported to extract some pesticide residues from synthesized fruit and vegetable juices.

Keywords: Magnetic nanostructures; Solid phase extraction; Absorbent, Pesticides

1. Introduction

Since in the whole world, 45% of agricultural products are destroyed by various pests, therefore the use of poisons and pesticides is inevitable [1,2]. In the past few decades, the excessive use of various types of pesticides is considered as a direct effect of a significant increase in environmental pollution, which causes various diseases such as congenital disabilities, cancer and etc. that It results from exposure to various pesticides [3,4]. As shown in Fig. 1 [5], the structure of common pesticides, a group of pesticides are organophosphates (OPPs) that are widely used to control pests in fruits and vegetables, including the most common banned pesticides that are widely used to protect a variety of food products in the pesticides used in Iran are chlorpyrifos (CPS) and phosalone (PHO) [6]. It is worth noting that OPPs have been introduced as a priority pollutant by European laws [7]. In the world market, due to the increase in demand to improve the quality of agricultural products, the use of pesticides has been widely used, so when these substances enter the food chain, human health is threatened [8-10], For this reason, we need an efficient method to analyze pesticide residues in products [11]. Despite the development in analysis tools, due to the many complex matrices and low concentration of analyte in pesticides, we need a sample preparation method [12]. Liquid-liquid extraction (LLE) and solid phase extraction (SPE) are two traditional methods for extracting pesticide residues [13,14]. Preparation methods such as SPE and LLE have limited applications due to disadvantages such as the high consumption of dangerous and toxic organic solvents and the high cost of solvents [15], If SPE requires a smaller volume of organic solvents, even though it requires spending a lot of time [16].

In 1990, at first, solid phase microextraction was derived from SPE [17]. Then, single-drop microextraction [18], hollow-Liquid phase microextraction of fiber [19], dispersed liquid-liquid microextraction (DLLME) [20], dispersed solid phase extraction (DSPE) [21], magnetic dispersive solid phase extraction (MDSPE) [22], and several other methods have been introduced. However, in the past years MDSPE and DSPE due to its efficient method, it has attracted everyone's attention [23,24].

There is a possibility of destruction and difficulty of adsorbent accumulation by DSPE, but despite this limitation, this method has been widely used for effective cleaning of pesticides [25].

Recently, magnetic nanoparticles (MNPs) have gained special attention in extraction analysis due to their characteristics such as magnetic properties, morphology uniformity, easy modification of the desired surfaces, and easy modification by magnetic field [26]. Iron oxide ferrites have the formula MFe_2O_4, M here can be a bivalent metal such as nickel, manganese, or copper. Ferrites are widely used for various applications because of their characteristics such as electrical and magnetic properties and they have the ability to be recycled [27].

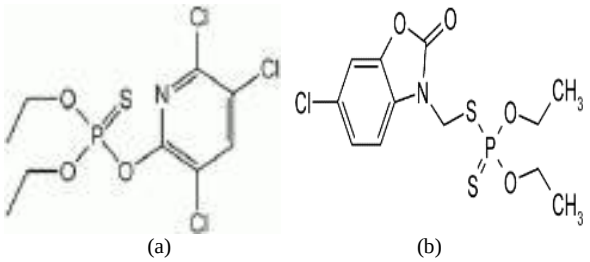

(a) (b)

Fig.1. Structure of (a) Chlorpyrifos and (b) Phosalone.

2. Experimental

2.1. Synthesis of Cu/$CuFe_2O_4$@MIL-88A(Fe)

One of the synthesized magnetic nanostructures are Cu/$CuFe_2O_4$ spherical magnetic nanocrystals that have been synthesized using solvothermal method. Scheme 1. shows a schematic of Cu/$CuFe_2O_4$@MIL-88A(Fe) magnetic nanocomposite [28]**.** In this way, the Cu/$CuFe_2O_4$@MIL-88A(Fe) was synthesized and used as a new magnetic adsorbent to analysis two OPPs using magnetically dispersed solid phase extraction method in different water, vegetable, and fruit juice samples. Cu/$CuFe_2O_4$@MIL-88A(Fe) nanocomposite is a magnetic adsorbent with superior pore accessibility and very large surface area. This material has strong magnetic properties and rapid separation to simplify the extraction process [29].

Scheme 1. Schematic of magnetic Cu/$CuFe_2O_4$@MIL-88A(Fe) nanocomposite.

2.2. Synthesis of PS@MNPs

Polysulfone is used in the automotive industry, medicine, etc. due to its high resistance and unique mechanical properties [30, 31]. The synthesis of PS@MNPs has two steps. In the first step, iron MNPs with zero capacity are formed through the thermal decomposition of [$Fe(CO)_5$]. In the second step, the synthesis includes the phase-inversion precipitation method. This proposed method is briefly presented in Scheme 2 [32].

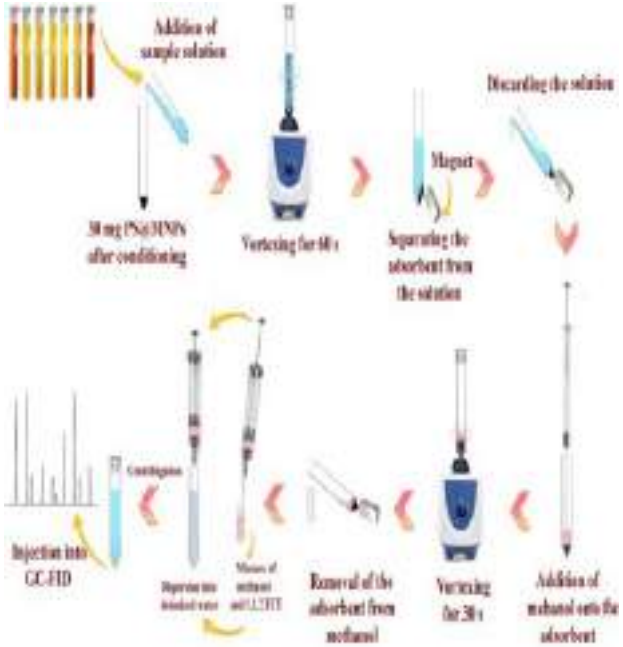

Scheme. 2. A summary of the stages of the extraction process**.**

3. Results and discussion

Fig. 2, shows the morphology and structure of Cu/$CuFe_2O_4$@MIL-88A(Fe) composite and pure Cu/$CuFe_2O_4$ using scanning electron microscopy (SEM) technique. Fig (2a) shows the SEM images of sphere-like Cu/$CuFe_2O_4$ nanocrystals with an average size of 16.64-18.70 nm. Fig. (2b) shows SEM images of Cu/$CuFe_2O_4$@MIL-88A@MIL-88A(Fe) nanocomposite, which clearly shows that we have synthesis with irregular and symmetrical spheres along with roughness of the surface and their great tendency to be magnetized. Fig. (2c) shows the transmission electron microscope (TEM) images, which the internal structure of the spheres is, studied [33].

The TEM images in Fig. 3. shows that the diameter of the spherical particles is in the range of 30-50 nm and it also shows the successful covering of MNPs (with a dark color) with a layer of PSs (with a light color) [34].

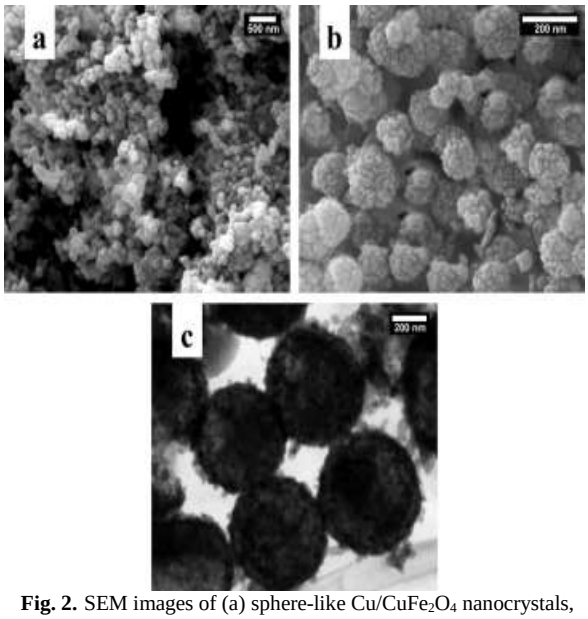

Fig. 2. SEM images of (a) sphere-like Cu/$CuFe_2O_4$ nanocrystals, (b) Cu/$CuFe_2O_4$@MIL-88A@MIL-88A(Fe) nanocomposite, and (c) TEM images of nanocomposite.

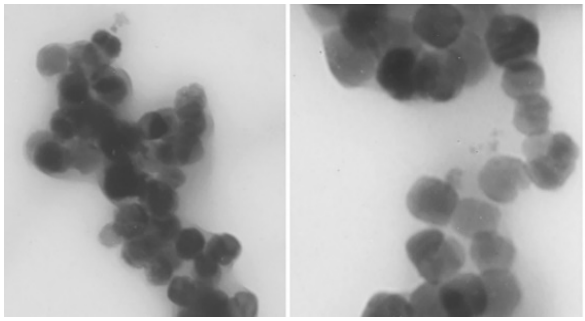

Fig. 3. TEM images PSs.

3. Conclusions

In this research, the synthesis of Cu/$CuFe_2O_4$@MIL-88A(Fe) magnetic nanocomposite was reported for analysis of two OPPs as a magnetic adsorbent in different samples and also to extract pesticide residues from products such as vegetables and water and etc.. In addition, magnetic nanostructures of polysulfone have been synthesized through a simple method with high absorbability and cost-effectiveness.

4. References

[1] Baig, S.A., Akhtera, N.A., Ashfaq, M. and Asi, M.R. (2009). Journal of Agriculture and Environmental Science, 6(5): 513-519.

[2] Bhanti, M. and Taneja, A. (2007). Chemosphere, 69(1): 63-68.

[3] Fernandes, V. C., Freitas, M., Pacheco, J. P. G., Oliveira, J. M., Domingues, V. F., Delerue-Matos, C. 2018. J.Chromatogr. A.

[4] Ramos, J. S. A., Pedroso, T. M. A., Godoy, F. R., Batista, R. E., de Almeida, F. B., Francelin, C., Lee Ribeiro, F., Rocha Parise, M.,de Melo e Silva, D., 2021. Sci. Total Environ.754, 141893.

[5] Barr, D. B., & Angerer, J. (2006). 114(11), 1763-1769.

[6] Salamzadeh, J., Shakoori, A., Moradi, V., 2018. J. Environ. Heal. Sci. Eng. 16, 55–63.

[7] Heidari, H., Ghanbari-Rad, S., & Habibi, E., 2020.J. Food Compos. Anal. 87, 103389.

[8] M.C. Leung, M.H. Silva, A.J. Palumbo, P.N. Lohstroh, S.E. Koshlukova,S.B. DuTeaux, Reprod. Toxicol. 85 (2019) 12 – 18

[9] M. Bjorling-Poulsen, H.R. Andersen, P. Grandjean, Environ. Health 7 (2008) 50 – 72

[10] N. Eevers, J.C. White, J. Vangronsveld, N. Weyens, a review, Adv. Bot. Res. 83 (2017) 277 – 318

[11] M. Nasiri, H. Ahmadzadeh, A. Amiri, A review, Trends Anal. Chem. 123 (2020)115772.

[12] Amini, S., Ebrahimzadeh, H., Seidi, S., Jalilian, N., 2021. Food Chem. 350, 129242.

[13] R.M. Gonzalez-Rodriguez, B. Cancho-Grande, J. Simal-J. Chromatogr. A 1216(2009) 6033 – 6042

[14] G. Font, J. Manes, J. Molto, Y. Pico J. Chromatogr. A 642 (1993) 135 – 161

[15] Fırat Ayyıldız, M., Selin Fındıkoğlu, M., Selali Chormey, D., Bakırdere, S., 2020. J. Food Compos. Anal. 88, 103431.

[16] J. Płotka-Wasylka, N. Szczepańska, M. de la Guardia, J. Trends Anal. Chem. 73 (2015) 19 – 38

[17] C.L. Arthur, J. Pawliszyn, Anal. Chem. 62 (1990) 2145 – 2148

[18] E. Amvrazi, N. Tsiropoulos, J. Chromatogr. A1216 (2009) 2789 – 2797

[19] D.A. Lambropoulou, T.A. Albanis, J. Chromatogr. A 1072(2005) 55 – 61

[20] E. Zhao, W. Zhao, L. Han, S. Jiang, Z. Zhou, J. Chromatogr. A 1175 (2007) 137 – 140

[21] M. Radišić, S. Grujić, T. Vasiljević, M. Laušević, Food Chem. 113 (2009) 712 – 719

[22] W. Liu, Y. Hu, J. Zhao, Y. Xu, Y. Guan, J. Chromatogr. A 1095(2005) 1 – 7

[23] M. Mohammadnejad, Z. Gudarzi, S. Geranmayeh, V. Mahdavi, Microchim. Acta 185 (2018) 495 – 503

[24] S. Akbarzade, M. Chamsaz, G.H. Rounaghi, M. Ghorbani, Anal. Bioanal. Chem. 410 (2018) 429 – 439

[25] Arabi, M., Ostovan A., Bagheri, A., Guo, X., Wang, L., Li, J., Wang, X., Li, B., Chen, L., 2020. Trends Analyt Chem. 128,115623.

[26] Köseoğlu, K., Ulusoy, H. İ., Yilmaz, E., Soylak, M., 2020. J. Food Compos.Anal. 90, 103482.

[27] Kurian, J., Jacob Mathew, M., 2017. J. Magn. Magn. Mater. 428, 204–212.

[28] Li, Z., Guo, C., Lyu, J., Hu, Z., Ge, M., 2019. J. Hazard. Mater.

[29] Sh. Amini, M. Amiri, H. Ebrahimzadeh, Sh. Seidi, S. Hejabri kandeh, J. of Food Composition,.2021.104128.

[30] H.P. Diogo, J.J.M. Ramos J. Therm. Anal. Calorim. 111 (2013)773–779.

[31] M. Zambianchi, A. Aluigi, M.L. Capobianco, F. Corticelli, I. Elmi, S. Zampolli, F. Stante, L. Bocchi, F. Belosi, M.L, Adv. Sustain. Syst. 1 (2017) 1700019.

[32] G. Zhao, L. Zhou, Y. Li, X. Liu, X. Ren, X. Liu, J. Hazard. Mater. 169 (2009) 402 – 410

[33] Satheeshkumar, M.K., Ranjith Kumar, E., Srinivas, C., Prasad, G., Singh Meena, S., Pradeep, I., Suriyanarayanan, N., Sastry, D.L.,2019. J. Magn. Magn. Mater. 484, 120-125

[34] M. Sattari Dabbagh, A. A. Farajzadeh,. Micro chem J,2020, 105238, 158.

29TH IRANIAN ORGANIC CHEMISTRY CONFERENCE
1_3 NOV, 2023
UNIVERSITY OF QOM, IRAN

DFT investigation of a Zn-doped carbon nanocone for the drug delivery of methylated aspirins

*Ali Ghasemi Gol, Jafar Akbari**
Department of Chemistry, Buinzahra Branch, Islamic Azad University, Buinzahra, Iran,
ghasemigolali@gmail.com, jakbari2@gmail.com

Abstract
A zinc-doped (Zn-doped) carbon nanocone (NANO) was investigated in this work for the drug delivery of aspirin (ASP) and eight methylated derivatives (A1-A8). Geometries of the models were optimized and their structural and electronic descriptors were evaluated by performing density functional theory (DFT) calculations. After obtaining the stabilized singular models, interactions of each of A1-A8 and ASP with the NANO substance were examined for the formation of bimolecular complexes. Different levels of strength were achieved for the complexes based on the contributions of two O…Zn interactions. Results of frontier molecular orbitals indicated an advantage of employing such system for detection of the adsorbed ASP substance. Moreover, levels of reactivates and chemical features revealed the significance of methylation on the properties of ASP, which were found clearly through the complex formations. Achievements on molecular orbitals localizations and interactions details proposed the current models for further investigations of aspirin drug delivery processes.

1. Introduction

To this aim, the current work was performed to investigate interactions of aspirin and a representative nanostructure for initiating the first steps of drug delivery assessments. Nanostructures have always been expected to show characteristic features for employing in different fields of applications To approach the goal, quantum chemical density functional theory (DFT) calculations were performed to find the stabilized structures and their desecrators. Indeed, this work was done to learn details of interacting complexes of aspirin and nanocone (ASP@NANO) to propose them for further investigations of drug delivery processes. Hence, computational chemistry tools were employed to recognize the models in accordance with their molecular and atomic contributions to the interaction processes besides knowing the possibility of stabilized complex formations [1].(Tables 1-5 and Figs. 1-4.)

2. Computational details

The models of original aspirin (ASP) and eight methylated derivatives (A1-A8) were obtained (Fig. 1) from the ChemSpider structural bank [2] and they were investigated in this work for participating in interactions with a representative Zn-doped carbon nanocone (NANO) (Fig. 2). The singular models were optimized to obtain the stabilized structures, which were confirmed by the evaluated real vibrational frequencies of infrared (IR) spectra. Next, each of the ASP and A1-A8 models were combined with the NANO substance for examining theformations of ASP@NANO complexes (Fig. 3). As a consequence, nine models of bimolecular complexes were stabilized and their global minimizations were confirmed by the evaluated real vibrational frequencies of IR spectra. Subsequently, structural and electronic descriptors were evaluated for the optimized singular and bimolecular models to assess their physical and chemical features. By the important roles of frontier molecular orbitals for defining molecular electronic features, quantities of energy levels of the highest occupied and the lowest unoccupied molecular orbitals (HOMO and LUMO) were evaluated besides exhibiting their distribution patterns (Tables 1-3). Additionally, representations of electrostatic potential (ESP) surfaces and diagrams of density of states (DOS) were exhibited for the investigating models (Figs. 1-4). The features of quantum theory of atoms in molecules (QTAIM) were evaluated to show the involving atoms and the qualities of interactions for learning details of interactions of ASP@NANO complexes (Table 4). Moreover, the values of quadrupole coupling constants (Cq) were calculated for the oxygen and zinc atoms to show chemical environments of the dominant interacting atoms of ASP and NANO models in the singular and bimolecular states (Table 5). The current calculations were performed using the B3LYP exchange–correlation functional and the 6-31G* basis set as implemented in Gaussian program [3].

3. Results and discussion

The hypothesized idea was supported by the values of energy gap (EG), defined by the calculated energy distances of two characteristic HOMO and LUMO frontier molecular orbitals. The values of EG could somehow mean the level of reactivity for a molecular

model, and such reactivity was changed by the additional of Me groups. The value of chemical hardness (CH); defined by the average value of EG, was obvious for the variations of molecular resistances for participating in further reactions. Next, changes of the level of Fermi energy (EF) showed a diagnostic feature of the molecular models based on their different electronic environments. As a consequence, the original ASP and eight methylated derivatives were found achievable and the impacts of additional of Me groups to the original ASP model were observed by their structural and electronic features. The role of Me group was to change the levels of frontier molecular orbitals besides the observed variations of graphical representations.. Accordingly, the optimization calculations yielded the complex models by participation of these two sites in the interactions. As listed in Table 3, the evaluated values of EB, standing for the values of binding energy, showed slight variations among the models with a maximum of (1 kcal/mol) difference among the models. To ensure that the energies were calculated appropriately by the B3LYP functional, additional single point calculations were performed at the(M062X/6-31G*)level and the results were summarized. the models were found in similar values of EB for formations of ASP@NANO models. To evaluated the values of EB, the formula of EB = EASP@NANO – EASP – ENANO was used, in which the values of basis set superposition error (BSSE) were inserted in the formula to yield the corrected binding energy (EBC) values [4]. Based on such evaluated EB values, the models were ranked in this order: A7N >A3N >A2N >A8N >A5N >ASP@NANO >A1N >A4N >A6N by slight changes of energy strength. It could be also mentioned that all models were in similar levels of strengths and their formations could be found suitable. Based on the performed optimization calculations on formations of interacting ASP@NANO bimolecular models, different features were obtained as shown in Fig. 3 and listed in Table 3 .These features were electron density (Rho), Laplacian of electron density (Del2-Rho), and energy of electron density (H), which were summarized in Table 4. To this aim, the models were analyzed by their features and the results indicated the existence of interactions and their strengths. First, it was known that two O…Zn interactions were available for each of bimolecular complexes. Second, their strength levels were meaningful for the formation of bimolecular complexes. Third, two interactions were not at the same level of strength, in which the keto-like oxygen of carboxylic group (O_2) was at a higher interaction strength in comparison with the keto-like oxygen of acetate group (O_4). In this regard, their features indicated details of such interactions for the formation of ASP@NANO and A1N-A8N models. Distances (D) of these two interactions were also different, in which D1 of the O_2…Zn interaction was at a shorter distance than D_2 of the O_4…Zn interaction. Based on these results, two main points were achieved regarding the existence of O…Zn interactions and their meaningful strengths.. In this regard, the models of this work were analyzed by their atomic descriptors showing some characteristic results. O_2 and O_4 were directly in interactions with the Zn atom of NANO and O1 and O3 were standing behind these two atoms. Interestingly, the values of Cq were decreased for both of O_2 and O_4 from the singular state to the bimolecular state whereas those of O_1 and O_3 were increased at the same direction. This achievement could show the dominant roles of O2 and O4 of ASP and derivatives for contributing to interactions with the Zn atom. Accordingly, the value of Cq of Zn atom was drastically decreased from the singular to the bimolecular state showing its significant contribution to interactions with two oxygen atoms of ASP substances. Based on the evaluated QTAIM descriptors, meaningful strengths were found for two interactions of complexes and the Cq results affirmed the dominant roles of O2 and O_4 for participating in interactions with the Zn atom. Interestingly, the Cq values of O_1 and O3 were increased meaning an electronic environment recovery in the molecular systems by involving O_2 and O_4 in the interactions. As a consequence, details of the models were recognized in both of molecular and atomic scales.

4 . Conclusion:

By the obtained HOMO and LUMO descriptors, additional of methyl groups to the original structure of ASP changed frontier molecular orbitals features and accordingly the levels of reactivity tendencies were changed. The Zn-doped model showed an advantage of employing NANO model in comparison with the original nanocone by providing a specific region of interaction for the substance. Formations of ASP@NANO models were achieved by interactions of oxygen atomic sites and the Zn atom. Accordingly, the bimolecular models were existed by the occurrence of two O…Zn interactions with different strengths for each one but with meaningful strengths for the whole interacting complexes. The evaluated levels of adsorption strengths showed slight changes for the models, in which the original ASP@NANO model was placed in a middle level of adsorption strength order and the methylated models were placed before and after it. Interestingly, the highest stability and the lowest stability were observed for the complex models with two methyl groups, in which the structural positions of the groups determined significant variations of strengths. The obtained atomic results of Cq descriptors also affirmed the dominant roles of O and Zn atoms for participating in interaction.

Table 1
Molecular descriptors of singular aspirin models.*

Model	ChemSpider	Formula	Me	HO
ASP	2157	$C_9H_8O_4$	n/a	−7.
A1	4,421,139	$C_{10}H_{10}O_4$	R1	−6.
A2	10,365,979	$C_{10}H_{10}O_4$	R2	−6.
A3	13,242,596	$C_{10}H_{10}O_4$	R3	−7.
A4	70,472	$C_{10}H_{10}O_4$	R4	−6.
A5	24,706,340	$C_{11}H_{12}O_4$	R2,R4	−6.
A6	24,706,339	$C_{11}H_{12}O_4$	R1,R4	−6.
A7	15,342,070	$C_{11}H_{12}O_4$	R2,R3	−6.
A8	24,706,338	$C_{11}H_{12}O_4$	R1,R3	−6.

*The models were shown in Fig. 1. ChemSpider IDs were

Table 2
Molecular descriptors of singular nanocone m

Model	Formula	HOMO	LUMO
Original	$C_{45}H_{12}$	−4.49	−3.54
NANO	$C_{45}H_{12}Zn$	−4.38	−2.60

*The models were shown in Fig. 2. HOMO, LUMO

Table 3
Molecular descriptors of bimolecular ASP@NANO models.*

Model	ER	BSSE	ER_c	HOMO
ASP@NANO	−23.9	4.0	−19.9	−3.60
A1N	−23.7	4.1	−19.6	−3.37
A2N	−24.4	4.1	−20.3	−3.61
A3N	−24.4	4.0	−20.4	−3.50
A4N	−23.7	4.0	−19.7	−3.62
A5N	−24.1	4.0	−20.1	−3.50
A6N	−23.3	4.0	−19.3	−3.38
A7N	−24.7	4.0	−20.7	−3.54
A8N	−24.3	4.1	−20.2	−3.50

*The models were shown in Fig. 3. ER, BSSE, and ER_c are in kcal/mol. HOMO, LUMO, ED, EP, an

Table 5
O_2 descriptors of O and Zn atoms of singular (S) and bimolecular (B) models.*

Model	O1		O2		O3	
	S	B	S	B	S	B
ASP@NANO	9.18	9.22	9.55	9.59	10.15	10.40
A1N	9.11	9.17	9.54	9.54	10.15	10.45
A2N	9.18	9.40	9.65	9.67	10.54	10.50
A3N	9.18	9.22	9.64	9.58	10.10	10.41
A4N	9.14	9.40	9.66	9.62	10.28	10.31
A5N	9.12	9.12	9.68	9.68	10.28	10.32
A6N	9.12	9.18	9.64	9.61	10.18	10.28
A7N	9.18	9.10	9.64	9.67	10.33	10.42
A8N	9.12	9.18	9.64	9.62	10.28	10.40

*The models were shown in Fig. 1-5. O_2 values are in RMS.

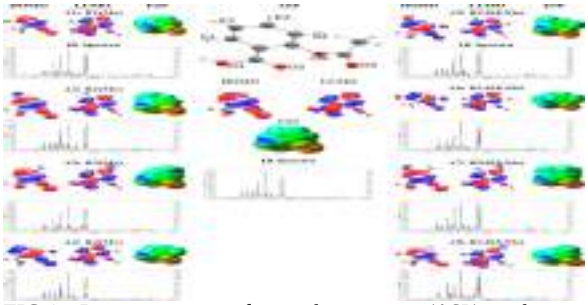

FIG.1. Representations of singular aspirin (ASP) and methylated derivatives (A1-A8).

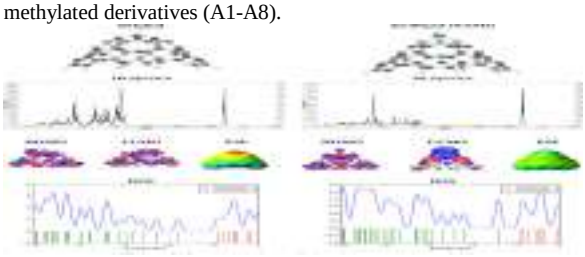

Fig. 2. Representations of singular nanocone models.

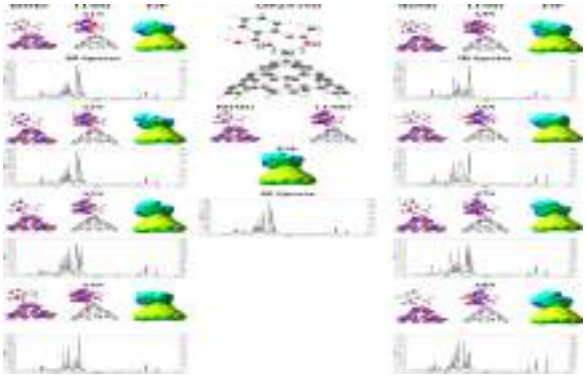

Fig. 3. Representations of bimolecular models; ASP@NANO and A1N-A8N derivatives.

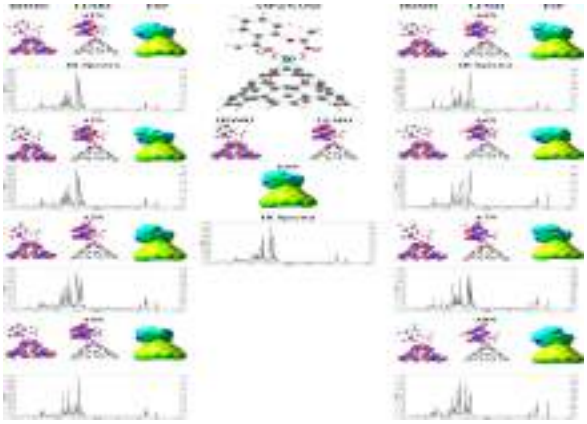

Fig. 4. DOS diagrams of bimolecular models; ASP@NANO and A1N-A8N derivatives.

4. References

[1] A.M. Dhumad, H.J. Majeed, K. Harismah, H. Zandi, In silico approach on ribavirininhibitors for COVID-19 main protease, Biointerface Res. Appl. Chem. 11 (2021)13924.
[2] H.E. Pence, A. Williams, ChemSpider: an online chemical information resource,J. Chem. Educ. 87 (2010) 1123.
3]I.Y. Zhang, J. Wu, X. Xu, Extending the reliability and applicability of B3LYP,Chem. Commun. 46 (2010) 3057.
[4] E.R. Davidson, S.J. Chakravorty, A possible definition of basis set superpositionerror, Chem. Phys. Lett. 217 (1994) 48.

29TH IRANIAN ORGANIC CHEMISTRY CONFERENCE
1_3 NOV, 2023
UNIVERSITY OF QOM, IRAN

Electrosynthesis of Azodicarbonamide (ADCA) from Hydrazodicarbonamide (Biurea)

Mostafa Kiamehr, Elahesadat Miri, Ali Ehsani**

Department of Chemistry, Faculty of Science, University of Qom, Ghadir Blvd, P.O. Box 37146-6611, Qom, Iran, mkiamehr@yahoo.com, m.kiamehr@qom.ac.ir, mirielahe114@gmail.com, ehsani46847@yahoo.com

Abstract - Foaming agents are physical or chemical agents that lighten polymer products and these agents are widely used in polymer industries. In this paper, we introduced new method for preparation of azodicarbonamide (ADCA), which has wide applications as a foaming agent in various chemical industries such as polymer and plastic industries. Initially, hydrazodicarbonamide (biurea) prepared by reaction of urea and hydrazine, then azodicarbonamide prepared via electrochemical (anodic) oxidation of biurea in the presence of potassium bromide as a catalyst. The prepared products have been characterized by FTIR and UV-Vis.

Keywords: Electrosynthesis, Oxidation, Azodicarbonamide, Hydrazodicarbonamide, Biurea

1. Introduction

Azodicarbonamide is a synthetic chemical that exists at ambient temperature as a yellow-orange crystalline solid (Figure 1).

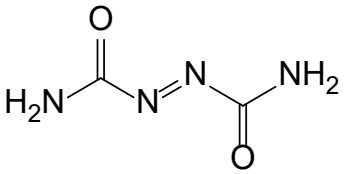

Fig.1. Azodicarbonamide structure.

Azodicarbonamide widely used in industry as a chemical foaming agent [1-3] in the production of numerous products because it is nontoxic, odorless, and non-polluting when decomposed [4].

The gases produced by the decomposition of ADCA are 65% nitrogen gas, 24% carbon monoxide, 5% carbon dioxide, and 5% ammonia [5-7]. It is poorly soluble in water at 20 °C (<50 mg/litre), although it is slightly soluble in hot water. It is insoluble in many organic solvents, but it is soluble in *N*,*N*-dimethyl formamide and dimethyl sulfoxide [8]. The current procedure to synthesis of ADCA is as follow: hydrazodicarbonamide was synthesized from hydrazine hydrate and urea by means of acid condensation reaction [9], then ADCA was synthesized from biurea via oxidation reaction. There are several ways to produce azodicarbonamide by the oxidation of biurea, and these include the chlorate method [10], the chlorine method [11-13], the hydrogen peroxide method [14,15], and the dichromate oxidizing agent framework [16-18]. The oldest and still commonly used process uses dichromate oxidizing agent. The dichromate method employed due to high cost and the pollution generated during chrome is eliminated. Furthermore, chromium compounds are skin irritants and cause health problems if any chromium residues remain in the product. In addition, the deep green color of the chromate ions masks the orange-colored azo compound. Also it is difficult to determine the end point of the reaction and expensive waste disposal problems [19].

Our Anodic oxidation is a new method to produce azodicarbonamide foaming agent. Several characteristics make the electrochemical production of organic compounds superior to classical methods. Since electrons can be considered as redox reactants, it is possible to substitute an electric current instead of dangerous and polluting oxidizing reagents. Furthermore, since the energy of the electrons can be controlled through the applied voltage most of the electrosynthetic reactions take place at room temperature. The electrodes can also be considered as heterogeneous catalysts that can simply be physically removed at the end of the reaction [20], so this method is environmentally friendly.

2. Result and discussion

In this paper, an oxidant-free reagent strategy for the construction of azodicarbonamide using anodic oxidation of biurea was presented. Initially, biurea was produced by adding hydrazine hydrate 85% and urea (3 eq.) in two mouths round-bottom flask, in the presence of H_2SO_4 50% to produce pH value 3-5 with continuous stirring, heating up to 105 ºC, keeping the pH value and temperature, react 9 h to the reaction end point, suction filtration, washing the product by warm

water and air drying at room temperature. The synthesized biurea characterized by IR spectrum and melting point (**Scheme 1**).

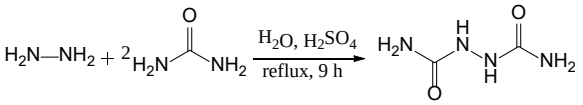

Scheme 1. Synthesis of biurea

In the next step, the synthesized biurea and potassium bromide as a catalyst was suspended in a certain ratio of water and hydrochloric acid. The reaction was performed at 20 ºC with two graphite electrodes as anode and cathode via applying the potential after 45 minutes azodicarbonamide was obtained with 88% yield (**Scheme 2**).

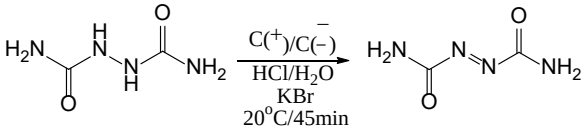

Scheme 2. Electrosynthesis of azodicarbonamide

IR spectra of ADCA and biurea

The IR of ADCA and biurea have been compared in the Figure 2. The IR band assignments of ADCA and biurea are listed in Table 1.

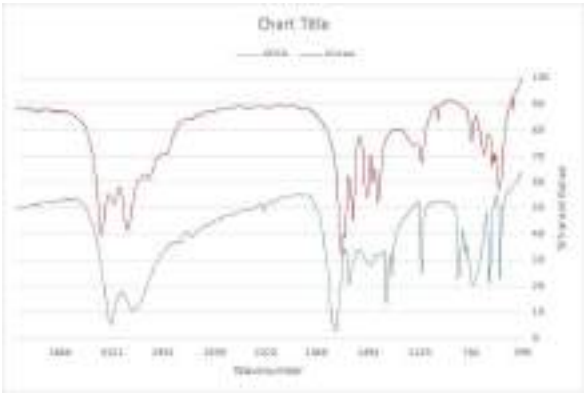

Fig.2. FTIR spectra of ADCA and biurea.

Table 1. Comparison of FTIR (cm^{-1}) spectra of ADCA and biurea.

functional groups	ADCA	biurea
NH_2	3170, 3329	3206, 3394
NH	—	3300
C=O	1731	1686
C−N	1116	1114

FTIR spectras agree with the standard spectra of biurea and azodicarbonamide, indicating that the products are biurea and azodicarbonamide.

UV-Vis spectra of ADCA

The UV-Vis of ADCA shown in the Figure 3. The red spectrum shows commercial or standard ADCA and blue spectrum is for synthesized ADCA.

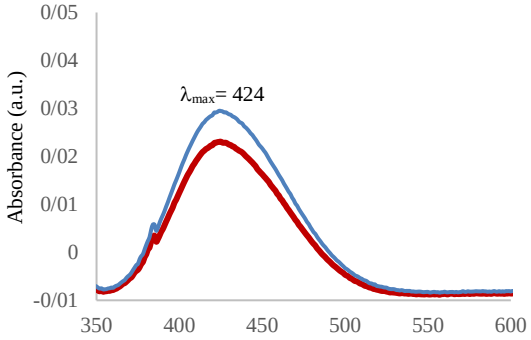

Fig.3. UV-Vis spectra of ADCA

UV-Vis spectra and λ_{max} of product completely agrees with the standard spectra of azodicarbonamide, indicating that the product is azodicarbonamide.

3. Conclusion

It can be concluded that this method is highly efficient for oxidation of biurea to ADCA through anodic oxidation with advantages such as no pollutants, no-chemical reagent, no by-products and high product quality and high yield.

4. References

General procedure for the synthesize of biurea:

In the two mouths round-bottom flask, hydrazine hydrate 85% 3 mL (50 mmol) and distilled water 70 mL were acidified with adding some sulfuric acid 50% (PH= 3-5), then urea 9 g (150 mmol) was added and the reaction mixture was heated to reflux temperature under stirring condition. The reaction mixture was cooled and filtered after 9 h at reflux (pH was kept 3-5 all the times). The filtered precipitate was washed whit warm water (50 mL) and dried at room temperature after 24 hours.

General procedure for the synthesize of ADCA:

1 g (8.5 mmol, 1 eq) biurea and 0.105 g (0.9 mmol, 10 mol%) potassium bromide were suspended in 20 mL water and 30 mL chloride acid with two graphite electrodes as anode and cathode in an undivided cell. The reaction was performed at 20 ºC with vigorous stirring. A constant potential of 0.1 V was applied to reaction media for 5 minutes and then was stopped for 3 minutes, it continued for 6 times (overall 45 min.), then, the resulting yellow precipitate was filtered, washed with water (20 mL) and dried at room temperature.

[1] Xu, C., Sun, C., Wan, H., Tan, H., Zhao, J., & Zhang, Y. Microstructure and physical properties of poly (lactic acid)/polycaprolactone/rice straw lightweight bio-composite foams for wall insulation. Constr. Build Mater, (2022). 354, 129216.
[2] Lei, W., Wang, D., Li, Y., Li, K., Liu, Q., Wang, P., ... & Yang, X. High temperature resistant polymer foam based on bi-functional benzoxazine-phthalonitrile resin. Polym. Degrad. Stab., (2022). 201, 110003.
[3] Liu, B., Essawy, H., Deng, S., Zhao, C., Du, G., Hou, D., ... & Zhang, J. High performance bio-based gelatinized starch-furanic resin derived foam reinforced by microcrystalline cellulose. Ind. Crops. Prod., (2023). 194, 116282.
[4] Younes, A. A., Adam, A. M. A., Refat, M. S., Al-Wasidi, A. S., Almehizia, A. A., Al-Omar, M. A., ... & Asla, K. A. Synthesis of Bivalent Ni (II), Cu (II) and Zn (II) Complexes of Azodicarbonamide in Mixture of Methanol and Aqueous Solvents: Spectral Characterizations and Anti-Microbial Studies. Crystals, (2023). 13(3), 367.
[5] Douibi, L., Gouissem, M., & Guessoum, D. B. Synergic Effect of a combined use of two Chemical Blowing Agents on the Foaming Efficiency of an Extruded Rigid PVC Compound. *Int. J. Eng. Technol. Sci*, (2014). *14*, 60.
[6] Sims, G. L. A., & Jaafar, H. A. S. A chemical blowing agent system (CBAS) based on azodicarbonamide. *J. Cell. Plast*, (1994). *30*(2), 175-188.
[7] Krutko, I., Danylo, I., & Kaulin, V. Kinetics of azodicarbonamide decomposition in the presence of an initiator for obtaining solid foams. *Вопросы химии и химической технологии*, (1), (2019). 26-34.
[8] Cary, R., Dobson, S., Ball, E. & World Health Organization. *Azodicarbonamide*. WHO (1999).
[9] Qi, M., Guo, R., Su, M., Cheng, X., & Zhang, L. Appl. Mech. Mater, (2014). 448, 464
[10] Ignaz, B. Preparation of azodicarbonamide, US patent 3227706A.
[11] Woodrow, W. Oxidation of hydrazoamides to azoamides, US patent 3190873A.
[12] Fuzhen, W., Guodong, H., & Bozhen, W. Clean production method of azodicarbonamide. CN patetnt A, 102408359.
[13] Mei, D., & Haixian, C. Method for producing ADC foaming agent by using chlorine gasoxidized HDCA (biurea) in saturated hydrochloric acid solution. CN patent A, 102675158.
[14] Shihao, C., Xuechen, C., Bing, H., & sheng yang, H. Method for preparing azodicarbonamide by hydrogen peroxide oxidization method, CN patent 103058893A.
[15] Bohm, S., & Wedemeyer, K. Process for the production of azodicarbonamide. US patent A, 4088643.
[16] Kume, H., & Maekawa, T. Preparation of azodicarbonamides.
[17] Hill, H. A. U.S. Patent No. 2,988,545. Washington, DC: U.S. Patent and Trademark Office. (1961).
[18] Williams, M. M., McEwan, W. S., & Henry, R. A. The heats of combustion of substituted triazoles, tetrazoles and related high nitrogen compounds. Chem. Phys, (1957). 61(3), 261-267.
[19] Bohloulbandi, E., & Ahmadi Aval, P. Study on Catalytic Synthesis of Azodicarbonamide with Hydrogen Peroxide as a Green Oxidant. Int J New Chem, (2021). 8(3), 356-364.
[20] Frontana-Uribe, B. A., Little, R. D., Ibanez, J. G., Palma, A., & Vasquez-Medrano, R. Organic electrosynthesis: a promising green methodology in organic chemistry. Green Chem, (2010). 12(12), 2099-2119.

29TH IRANIAN ORGANIC CHEMISTRY CONFERENCE
1_3 NOV, 2023
UNIVERSITY OF QOM, IRAN

Synthesis and characterization of magnetic clay nanocomposite for adsorption methylene blue dye

Fatemeh Jabbarzadeh[1], Negin Sohrabi[1, 2], and Reza Mohammadi[1]*

[1] *Department of Organic and Biochemistry, Faculty of Chemistry, University of Tabriz, Tabriz, Iran, r.mohammadi@tabrizu.ac.ir*

[2] *Department of Biosystem Engineering, Faculty of Agriculture, University of Tabriz, Tabriz, Iran*

Abstract – One of the main pollutants in aqueous sources is industrial dyes. Therefore, in this study, a biocompatible and inexpensive adsorbent has been synthesized and investigated to remove one of the most widely used dyes in Iran. The synthesized adsorbent is natural clay magnetized with iron nanoparticles. FT-IR and SEM analyzes were used to investigate the adsorbent. The results showed that the adsorbent was properly synthesized. Adsorption process conditions were optimized using response surface methodology (RSM) and central composite design (CCD). The results showed that the best conditions for adsorption of methylene blue dye using natural clay/Fe_3O_4 composite are: initial concentration of dye 11 mg/L, contact time equal to 60 minutes, amount of composite 2.2 g/L and pH equal to 8, in which the adsorption efficiency is equal to 98.36%.

1. Introduction

Industrial wastewater is one of the important sources of environmental pollution, so that sometimes the concentration of COD and BOD or the concentration of compounds in them reaches tens of thousands of mg/L [1]. The wastewaters of dyes are one of the important industrial wastewaters that have caused wide-ranging environmental problems [2]. In the textile industry, a wide range of natural and synthetic dyes are used to produce different products. In this industry, various chemical processes and operations are used for materials. Due to the variety of production methods, dyes and chemicals used, textile industries produce wastewaters of different quality and quantity, and for this reason, among the types of industrial wastewaters, they have special complications in the treatment process [3]. In textile processes, about 15% of the used dyes are washed in different stages and entered with their wastewater. [4]. The released of dyes into the environment disturbs its beauty and also causes disruption in the photosynthesis of plants by creating the phenomenon of eutrophication. In addition, these materials can create very dangerous compounds for the environment and humans through chemical reactions such as oxidation, hydrolysis, etc [5].

A group of dyes used in industries, especially textile industries, are anionic and cationic dyes, and cationic dyes are usually more toxic than the anionic type [6]. Among the cationic dyes, methylene blue dye is known as a very widely used and toxic dye (causing cancer) [7]. In recent years, when industrial wastewater treatment has become a global approach, various methods have been used to remove their pollutants in many researches. The basis of these methods depends on the chemical, electrical, thermal and biological properties of the pollutant and the method [8]. The most common methods that have been used over the years to remove these dye molecules are oxidative degradation [9], electrochemical methods [10], membrane separation [11], and adsorption and chemical biodegradation [12]. However, these methods require a lot of energy and cost, and their efficiency is low. But the adsorption method is an effective method for removing dye molecules due to its cheapness and ease of use. The use of adsorbents such as clay is very effective for removing dye molecules, but the problem of its use is its separation from the solution and pollution caused by its sludge. Therefore, in this study, magnetic natural clay (using iron nanoparticles) was used as an adsorbent for methylene blue.

2. Results and Discussion

FT-IR analysis was used to determine the functional groups [13] present in natural clay and clay/Fe_3O_4 composite (Figure 1). The results showed that in natural clay and natural clay/Fe_3O_4 composite a broad absorption peak was observed in the range of 3437-3391 cm^{-1}, which may be due to the tensile vibrations of the OH functional group in the structure of these materials (due to Al-OH, Si-OH and water molecules) [14]. In addition, in the natural clay structure, peaks at wavenumbers of 472, 533, 1016, and 1440 cm^{-1} can be observed, which may be due to the Si-O-Mg, Si-O-Al, Si-O, and carbonate ($CaCO_3$ or Ca,Mg $(CO_3)_2$) vibrations, respectively. After the Fe_3O_4 nanoparticles was deposited in the natural clay structure, the intensity of the absorption peaks in the natural clay

structure changed significantly, which could be due to the interaction between the functional groups on the surface of natural clay with iron nanoparticles. In addition to the magnetic composite structure, absorption vibrations appeared at 570 cm^{-1} due to the Fe-O vibrations, confirming that the Fe_3O_4 nanoparticles are present in the clay/Fe_3O_4[15].

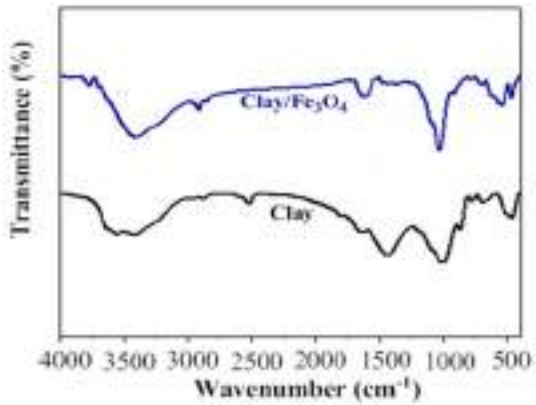

Figure 1. FT-IR analysis results

SEM analysis was used to check the changes made on the surface of the samples and the results are shown in Figure 2. The results showed that natural clay has a porous surface with different pores and roughness, which can be effective in adsorption dyes. After placing Fe_3O_4 nanoparticles on the surface of natural clay, particles with different sizes and almost spherical morphology were observed, which could be caused by the formation of Fe_3O_4 nanoparticles on the surface of natural clay.

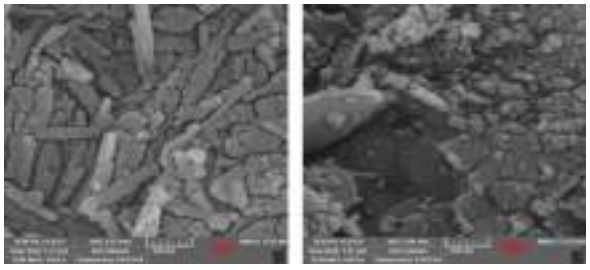

Figure 2. SEM analysis a) Clay, b) Clay/Fe_3O_4

The adsorption process of methylene blue dye using Clay/Fe_3O_4 nanocomposite was optimized using response surface methodology and central composite design. For this purpose, the pH parameters of the solution (3 to 11), dye initial concentration (10 to 50 mg/L), adsorbent dose (0.5 to 2.5 g/L), contact time (20 to 80 min) were investigated. The results of optimal conditions for the adsorption process of methylene blue dye using Clay/Fe_3O_4 nanocomposite are shown in Figure 3. As can be seen, the highest adsorption efficiency of methylene blue dye by natural clay/Fe_3O_4 composite is equal to 98.2% and in the condition of initial dye concentration of 11 mg/L, contact time is equal to 60 minutes, the amount of composite is 2.2 g/L and pH is equal to 8. In order to experimentally investigate these conditions, methylene blue dye adsorption test was performed in the reported optimal conditions and its efficiency was calculated. The efficiency value obtained was 98.36%, which compared with the efficiency value reported by the model for optimal conditions showed that the difference between these is very small. This small difference shows that the central composite design can effectively investigate the conditions of methylene blue dye adsorption process by Fe_3O_4 natural clay composite and determine the optimal conditions.

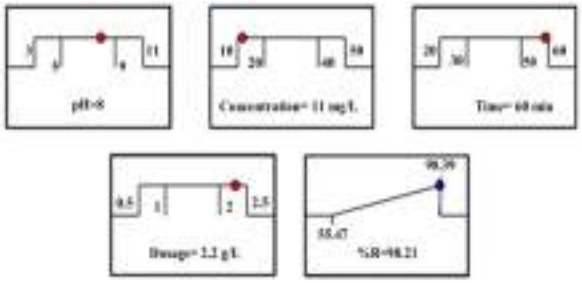

Figure 3. Profile of the optimum conditions for the adsorption of methylene blue dye using clay/Fe_3O_4 nanocomposite

3. Conclusions

The results of the present study showed that magnetic clay nanocomposite can be used as an efficient adsorbent to remove dye pollutants from aqueous solutions. In addition, the response surface methodology and the central composite design are also able to predict the adsorption process of methylene blue dye using natural clay/Fe_3O_4 composite.

4. References

1. Merouani, S., et al., Sonochemical degradation of Rhodamine B in aqueous phase: effects of additives. Chemical Engineering Journal, 2010. 158(3): p. 550-557.

2. Mahmoodi, N.M. and M. Arami, Bulk phase degradation of Acid Red 14 by nanophotocatalysis using immobilized titanium (IV) oxide nanoparticles. Journal of Photochemistry and Photobiology A: Chemistry, 2006. 182(1): p. 60-66.

3. Kos, L. and J. Perkowski, Decolouration of real textile wastewater with advanced oxidation processes. Fibres and textiles in Eastern Europe, 2003. 11(4): p. 81-85.

4. Lourenco, N., J. Novais, and H. Pinheiro, Effect of some operational parameters on textile dye

biodegradation in a sequential batch reactor. Journal of Biotechnology, 2001. 89(2-3): p. 163-174.

5. Saquib, M. and M. Muneer, TiO2-mediated photocatalytic degradation of a triphenylmethane dye (gentian violet), in aqueous suspensions. Dyes and Pigments, 2003. 56(1): p. 37-49.

6. Wang, W.-Y. and Y. Ku, Photocatalytic degradation of Reactive Red 22 in aqueous solution by UV-LED radiation. Water research, 2006. 40(12): p. 2249-2258.

7. Jones, J.J. and J.O. Falkinham, Decolorization of malachite green and crystal violet by waterborne pathogenic mycobacteria. Antimicrobial agents and chemotherapy, 2003. 47(7): p. 2323-2326.

8. Mota, J.P. and S. Lyubchik, Recent advances in adsorption processes for environmental protection and security. 2008: Springer.

9. Gözmen, B., et al., Oxidative degradations of reactive blue 4 dye by different advanced oxidation methods. Journal of Hazardous materials, 2009. 168(1): p. 129-136.

10. Khansorthong, S. and M. Hunsom, Remediation of wastewater from pulp and paper mill industry by the electrochemical technique. Chemical Engineering Journal, 2009. 151(1-3): p. 228-234.

11. Purkait, M., S. DasGupta, and S. De, Micellar enhanced ultrafiltration of eosin dye using hexadecyl pyridinium chloride. Journal of hazardous materials, 2006. 136(3): p. 972-977.

12. Kagalkar, A.N., et al., Biotechnological strategies for phytoremediation of the sulfonated azo dye Direct Red 5B using Blumea malcolmii Hook. Bioresource technology, 2009. 100(18): p. 4104-4110.

13. Taha, A., et al., Multi-component adsorption of Pb (II), Cd (II), and Ni (II) onto Egyptian Na-activated bentonite; equilibrium, kinetics, thermodynamics, and application for seawater desalination. Journal of environmental chemical engineering, 2016. 4(1): p. 1166-1180.

14. Eloussaief, M., et al., Mineralogical identification, spectroscopic characterization, and potential environmental use of natural clay materials on chromate removal from aqueous solutions. Chemical Engineering Journal, 2011. 168(3): p. 1024-1031.

15. Shafiee, M., et al., Application of oak powder/Fe3O4 magnetic composite in toxic metals removal from aqueous solutions. Advanced Powder Technology, 2019. 30(3): p. 544-554.

29TH IRANIAN ORGANIC CHEMISTRY CONFERENCE
1_3 NOV, 2023
UNIVERSITY OF QOM, IRAN

Chrysin: A natural product against depressant

*Faaeze.Younesi, Mansoor.Namazian**

Department of Chemistry, Faculty of Science, University of Yazd, Yazd, Iran, f.younesi7773@gmail.com, namazian@gmail.com

Abstract - This research paper investigates the acidic properties of Chrysin using advanced ab initio calculations. The study examines Chrysin's capability to scavenge reactive oxygen species by delving into the Hydrogen Atom Transfer (HAT) mechanism. Additionally, the research explores the radical scavenging potential of Chrysin by analyzing Radical Stabilization Energies (RSE) and Bond-dissociation energy (BDE). To enhance Chrysin's antioxidant activity and solubility, several similar molecules with different substituents are also analyzed to identify possible design improvements.

1. Introduction

Plants are a rich source of flavonoids and polyphenol derivatives that have various biological and pharmaceutical activities. These plant pigments are found in a variety of fruits and vegetables [1] and are categorized into six subclasses: Flavonols, Flavones, Flavanols, Flavanones, Anthocyanidins, and Isoflavonoids. There are more than 4,000 types of biologically active flavonoids known to us. Chrysin is a bioactive flavonoid with significant health benefits and is used as a pharmaceutical drug to treat various illnesses [2]. It plays a crucial role in preventing conditions such as cancer, oxidative stress, inflammatory disorders, diabetes mellitus, cardiovascular diseases, and obesity [12]. The chemical structure of flavonoids consists of fused A and C rings, and a phenyl B ring attached to position 2 of the C ring, as shown in Figure 1 [3-11].

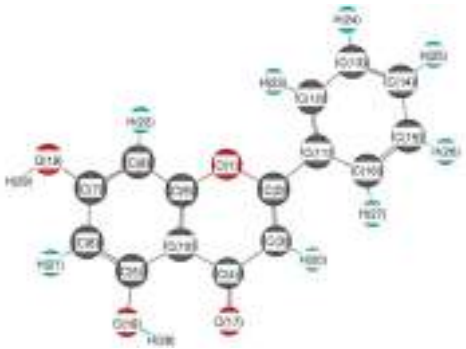

Fig. 1. Structure of Chrysin and practical numbering system adopted for carrying out the calculations.

2. Calculation details

In order to determine the equilibrium molecular geometry, we used the G4 theory method with the 6-31G basis set and the 2df, p method, as recommended by Curtiss et al. To scale vibrational frequencies, we used a factor of 0.9854, which was computed at the same level of theory. Zero-point energies (ZPE) and other thermal corrections were then calculated. To compute the point energy, we used a large basis set of 6-31G(2df,p). Additionally, we calculated solvation energies using a universal solvation model based on solute electron density (SMD) at the M05-2X/6-31G(d) level of theory, as recommended by Truhlar and his co-workers. We conducted all ab initio and DFT calculations using Gaussian 09.

3. Results and discussions

3.1. Reaction Mechanisms

3.1.1. Hydrogen Atom Transfer (HAT)

To investigate the radical scavenging of Chrysin, we also considered the (HAT) mechanism, based on the following reaction:

$$\mathrm{Chry-OH} + \mathrm{R}\cdot \rightarrow \mathrm{Chry-OH}\cdot + \mathrm{R-H} \qquad (1)$$

According to the results of calculations related to the stability of Chrysin radical forms, the most stable radical form of Chrysin compound forms a; Therefore, in this section, the Gibbs free energy changes of the reaction (1) for the conversion of Chrysin into the

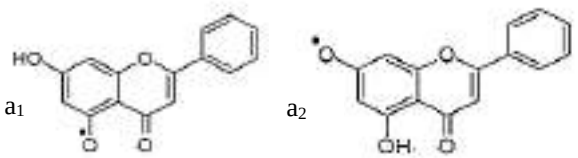

Fig. 2. Radical forms a and b of Chrysin compounds

radical form are reported. The reported negative results related to the reaction of Chrysin with $OH^{\bullet}$ radical show that Chrysin can inhibit this radical based on this mechanism. The comparison of the results also proves that the ability of the anion form a_1 of Chrysin to neutralize the hydroxyl radical is more than the radical form a_2. It was shown based on the calculations made; Energy values for forms a_1 and a_2 are -104.3 KJ and -52.9 kJ, respectively.

3.1.2. Bond-dissociation energy (BDE) and Radical Stabilization Energy (RSE)

Quantitatively describing the antioxidant properties of compounds can be done by determining the stability of radicals. Radical Stability Energy (RSE) and Bond Dissociation Energy (BDE) are two useful parameters for predicting and interpreting chemical reactions related to free radicals. The thermodynamic stability of radicals has been the focus of many theoretical calculations. This method can compare the stability of radicals and the ability of a compound to inhibit free radicals across a wide range of structures. In this study, the Radical Stability Energy for each oxygen-centered radical corresponds to reactions (2):

$$OH^{\bullet} + R - OH \rightarrow H_2O + R - O^{\bullet} \quad (2)$$

$$CH_3^{\bullet} + R - H \rightarrow CH_4 + R^{\bullet}$$

and Bond Dissociation Energy to reactions (4) in the gas phase was obtained:

$$\boldsymbol{R - H \xrightarrow{\Delta E} R^{\bullet} + H^{\bullet}} \quad (3)$$

$$H_2O \rightarrow OH^{\bullet} + H^{\bullet}$$

Radical stability energy and Bond Dissociation Energy were calculated for the compound with different substituents placed in specified positions. The hydrogen atom in the B ring [2] Figure 1 of the compound was used as the reference structure. The calculated values are presented. The amount of radical stability energy decreased from 4.82 kJ/mol for chrysin to 4.74 kJ/mol for the reference structure. The presence of electron-donating substituents, such as NH_2 and CH_3, led to the stability of the resulting radical and a higher RSE related to the substitutions compared to the reference compound. The presence of T-BU and CH_3 substitution did not have much effect on the stability of the composition. Two NH_2 substitutions in R_1 and R_2 positions significantly increased the antioxidant activity of the compound. The effect of substitutions on Chrysin activity was investigated. If hydrogen is separated from the NH_2 substitution, the stability energy of the radical is -131.1 kJ/mol, and if hydrogen is separated from the reference compound, the energy increases to 1.144 kJ/mol, The compound is more stable because of the separation of hydrogen from its reference structure.

3.2. Calculations of pK_a values:

Through the use of density functional theory, we have calculated the pK_a values of Chrysin in an aqueous solution. our model produces pK_a values that are more consistent with experimental data than those obtained through Hartree-Fock calculations using a 6-31G(d,p) basis set. We have examined the impact of relaxation energies on the accuracy of our results. In a recent study, we reported the calculated pKa of Chrysin in an aqueous solution. our calculations were performed using ab initio methods at the Hartree-Fock level and standard 6-31G(d,p) basis sets. We utilized solute-solvent interactions and gas phase energies to obtain

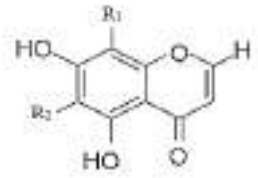

Fig. 3. Structure of the reference compound with R_1 and R_2 substitutions

pK_a values, which were then compared to experimental values. In the current study, we have employed density functional theory, using the B3LYP functional and a larger basis set 6-31G(d,p), to calculate the pK_a values of previously examined Chrysin in the aqueous phase [17].

aqueous solution if it dissociates as follows:

$$Chry \rightarrow H^{+} + Chry^{-} \quad \Delta G^0{}_1 \quad (4)$$

$$Chry + PH - O^{-} \rightarrow Chry^{-} + Ph - OH \quad \Delta G^0{}_3 \quad (5)$$

The equilibrium constant is related to the change in standard Gibbs free energy, therefore, there is a simple relation between and pK_a:

$$\Delta G = -2.303RT \log\left(\frac{Ka}{H2O}\right) \quad (6)$$

The standard change in the Gibbs free energy for the process in water at 298.15 °K.

To calculate, we have used a structure of phenol as a reference molecule.

$$Ph - OH \rightarrow H + + Ph - O^{-} \quad \Delta G^0{}_2 \quad (7)$$

And the Gibbs energy of reaction ΔG_3:

$$\Delta G_3 = \Delta G_1 - \Delta G_2 \quad (8)$$

shows a Thermodynamical cycle proposed to calculate the ΔG_1 From this cycle, ΔG_1 is given by the following expression.

$$\Delta G_3 = \Delta G_{2.gas} - \Delta G_{1.sol} \quad (9)$$

$$pK_a(chry) = \frac{\Delta G3}{2.303RT} + pK_a\,(Ph - OH) \quad (10)$$

first, the Gibbs free energy of the reaction in the gas phase is calculated, and then, using the solvent absorption energies, the Gibbs energy of the reaction in the solution phase is determined. The gas phase contribution to the Gibbs energy can be determined from DFT calculations at the level of B3LYP. Solvation energies have been calculated using a polarizable continuum model (PCM) [13-18]. The zero-point energies, thermal corrections, and entropies have been used to convert the internal energies to Gibbs energies at 298.15 °K. A diffuse basis set, 6-31G(d,p), has been chosen as recommended for anions and molecules with lone pair electrons and from considering the size of studied molecules.Gaussian98 [19] has been employed for all DFT calculations.

3.3. Solvation Energy

It is easier to study the solubility of Chrysin using SMD, a tool introduced by Thruhlar and colleagues. Solvation energies were calculated for all compounds at the M05-2X/6-31G(d) level of theory as recommended [20]. The results indicate that all the solvation energies are considerable in aqueous solutions, meaning that the studied compounds will

have great solubility in water. Among the compounds, Chry-OH has a significantly negative value of solvation energy in water. The results also show solvation energy values and Chrysin compound partition coefficient values for different solvents, including green, yellow, and red solvents. When Chrysin is dissolved in green solvents, the solvation energy increases from -3.13 kJ/mol in a normal octanol solvent to -36 kJ/mol in a water solvent. Therefore, the solvation energy values increase by dissolving Chrysin compounds in polar solvents. Based on the data, the concentration value of the Chrysin compound in all green solvents is negative compared to the concentration of Chrysin in a water solvent. Yellow solvents were also used to calculate the solvation energy of the compound. If Chrysin is dissolved in Methylcyclohexane solvent, the amount of solvation energy is 14 kJ/mol, which reduces to 33 kJ/mol for cyclohexane solvent. The solvation energy values for red solvents have decreased from 4.25 kJ/mol in benzene solvent to 1.31 kJ/mol in Dichloroethane solvent.

Conclusions:

By using the DFT method along with various basis sets, accurate pKa values were obtained that closely matched experimental values. Specifically, using the theoretical level of 6-311G(3df,2p) and method M062X allowed for the successful calculation of pKa with a difference of less than one pKa unit from the experimental value. In order to calculate the solvation energies of the Chrysin molecule, both the SMD continuous solvation model and method the M062X and the level of 6-31G(2df,p) were utilized. The results indicated that the method with a larger basis set was more suitable. It's worth noting that Chrysin is a hydrophilic compound that dissolves easily in the blood and possesses more stable energy values than other solvents.

Reference:

[1] Sulaiman, M.; Ghassan, A.; Al-Amiery, Bagnati Renzo..Food Sci Nutr,101-105, 2014.

[2] Khoo, B. Y.; Chua, S. L.; Balaram, P. Int. J. Mol. Sci, 2188-2199, 2010.

[3] Nijveldt, R.J.; van Nood, E.; van Hoorn, D.E.; Boelens, P.G.; van Norren, K.; van Leeuwen, P.A. Flavonoids: A review of probable mechanisms of action and potential applications. Am. J. Clin. Nutr, 418-425, 2001.

[4] Kale,A.;Gawande,S.;Kotwal,S.Cancerphytotherapeutics: a role for flavonoids at the cellular level. Phytother. Res, 567-577, 2008.

[5] Awad, R.; Arnason, J.T.; Trudeau, V.; Bergeron, C.; Budzinski, J.W.; Foster, B.C.; Merali, Z. Phytochemical and biological analysis of skullcap (Scutellaria lateriflora L.): A medicinal plant with anxiolytic properties. Phytomedicine, 640-649, 2003.

[6] Zheng, X.; Meng, W.D.; Xu, Y.Y.; Cao, J.G.; Qing, F.L. Synthesis and anti-cancer effect of chrysin derivatives. Bioorg. Med. Chem. Lett., 881-884, 2003.

[7] Ernst, E. Herbal remedies for anxiety - a systematic review of controlled clinical trials. Phytomedicine, 205-208, 2006.

[8] Huang, W.H.; Lee, A.R.; Yang, C.H. Anti-oxidative and anti-inflammatory activities of polyhydroxy flavonoids of Scutellaria baicalensis GEORGI. Biosci. Biotechnol. Biochem, 2371-2380, 2006.

[9] Scheck, A.C.; Perry, K.; Hank, N.C.; Clark, W.D. Anti-cancer activity of extracts derived from the mature roots of Scutellaria baicalensis on human malignant brain tumor cells. BMC Complement Altern. Med., 27-35, 2006.

[10] Cole, I.B.; Cao, J.; Alan, A.R.; Saxena, P.K.; Murch, S.J. Comparisons of Scutellaria baicalensis, Scutellaria lateriflora, and Scutellaria racemosa: Genome size, anti-oxidant potential, and phytochemistry. Planta Med, 474-481, 2008.

[11] Parajuli, P.; Joshee, N.; Rimando, A.M.; Mittal, S.; Yadav, A.K. In vitro anti-tumor mechanisms of various Scutellaria extracts and constituent flavonoids. Planta Med, 41-48, 2009.

[12] Saima Naza, Muhammad Imranb, Abdur Raufc, Ilkay Erdogan Orhand, Mohammad Ali Shariatie, Iahtisham-Ul- Haqf, IqraYasming, Muhammad Shahbazh, Tahira Batool Qaisranih, Zafar Ali Shahc, Sergey Plygune,i,j, Mojtaba Heydari, Int. Life Sciences, 116797, 2019.

[13] S. Miertus, E. Scrocco, J. Tomasi, Chem. Phys. 55-117, (1981).

[14] M.T. Cances, V. Mennucci, J. Tomasi, J. Chem. Phys. 107-3032, (1997).

[15] J.B. Foresman, T.A. Keith, K.B. Wiberg, J. Snoonian, M.J. Frisch, J. Phys. Chem. 100-16098, (1996) .

[16] V. Barone, M. Cossi, J. Phys. Chem. A, 102 (1998).

[17] M. Cossi, V. Barone, J. Phys. Chem. A 104-10614, (2000).

[18] M. Cossi, V. Barone, R. Cammi, J. Tomasi, J. Phys. lett. 255-327, (1996).

[19] Peng, A. Nanayakkara, C. Gonzalez, M. Challacombe, P.M.W. Gill, B. Johnson, W. Chen, M.W. Wong, J.L. Andres, C. Gonzalez, M. Head-Gordon, E.S. Replogle, and J.A. Pople, Gaussian, Inc., Pittsburgh PA, 1998.

[20] A.V. Marenich, C.J. Cramer, D.G. Truhlar, Universal solvation model based on solute electron density and on a continuum model of the solvent defined by the bulk dielectric constant and atomic surface tensions, J. Phys. Chem.B,6378–6396,(2009).

29TH IRANIAN ORGANIC CHEMISTRY CONFERENCE
1_3 NOV, 2023
UNIVERSITY OF QOM, IRAN

Efficient synthesis of novel polycyclic quinoline derivatives *via* sequential Ugi 4CR/nucleophilic substitution/Staudinger/aza-Wittig reactions and hydrolysis

Mostafa Kiamehr[*], *Mohadeseh Fathizadeh*

Department of Chemistry, Faculty of Science, University of Qom, Ghadir Blvd, P.O. Box 37146-6611, Qom, Iran, mkiamehr@yahoo.com, mkiamehr@qom.ac.ir, mohafathi1999@gmail.com

Abstract - A sequential transformation of Ugi four-component reaction/ nucleophilic substitution/ Staudinger/ aza-Wittig reactions and hydrolysis was developed for the synthesis of 3-(tetrazolo[1,5-a]quinolin-4-yl)piperazine-2,5-dione derivatives. This method involves the Ugi-4CR of 2-chloro-3-formyl quinolines **1**, amines **2**, 2-chloroacetic acid **3**, and isocyanides **4** for the synthesis of versatile precursors **5**. Then sodium azide (2.5 eq.) was added to the product **5**, followed by Staudinger/aza-Wittig reactions and hydrolysis sequentially. This convergent approach demonstrates high efficiency, involves the use of readily available commercial reagents, and is an example of structural complexity with operational simplicity in a cost-effective manner (**Scheme 1**).

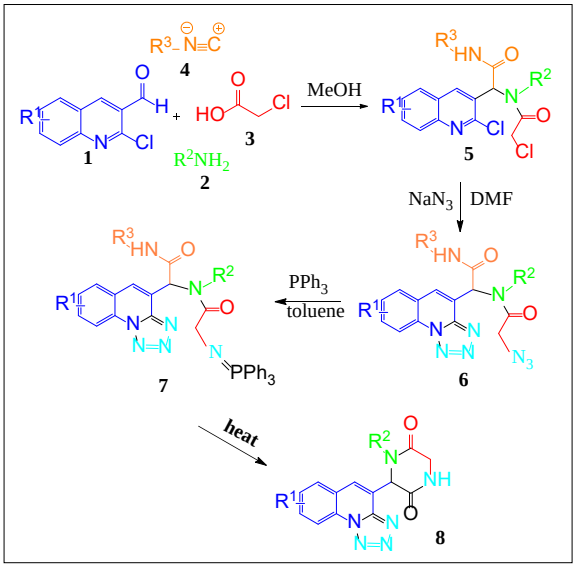

Scheme 1. A sequential transformation of Ugi four-component reaction/ nucleophilic substitution/ Staudinger/ aza-Wittig reactions and hydrolysis

Keywords: Quinoline derivatives, Ugi reaction, Staudinger reaction, Aza-Wittig reaction, Intramolecular cyclization.

1. Introduction

The Ugi reaction is a four-component reaction (4-CR) of carbonyl compounds, carboxylic acids, isocyanides, and amines, during which new compounds are synthesized in one step. Ugi-4CR is suitable for diversity-oriented synthesis and can be used in drug discovery because it facilitates rapid access to diverse compounds [1-2]. Isocyanide-mediated multicomponent reactions (IMCRs), which enable the highly efficient one-pot synthesis of complex molecules from simple materials, are powerful tools in advanced medicinal and combinatorial chemistry [3]. Recently, the combination of IMCRs with subsequent transformations has been shown to be a powerful approach to access numerous highly diverse heterocyclic scaffolds [4-8].

Ugi reaction is a powerful, atom-economical I-MCRs starting from isocyanide, amine, aldehyde (or ketone), and carboxylic acid components that generates a significantly more complex α-acylamino amide adduct [9]. The sequences of classical Ugi isocyanide multicomponent reactions, followed by post-condensation transformations, constitute extremely powerful synthetic tools for the preparation of structurally diverse heterocyclic compounds [10]. On the other hand, aza-Wittig reactions have received increased attention in view of their utility in the synthesis of nitrogen-containing heterocycles [11]. Thus, it is envisioned that combining the efficiency of the Ugi condensation with a post-condensation aza-Wittig reaction would facilitate access to a series of biologically useful heterocycles [12].

Staudinger reaction has been found to be a useful method for the synthesis of amines from azides, and has received increased attention in view of its utility in the synthesis of nitrogen-containing heterocycles [13-15]. Thus, it is envisioned that combination of the IMCRs with a post condensation Staudinger reaction would facilitate access to a series of biologically useful heterocycles [16-17].

2. Result and discussion

Initially, 2-chloro-3-formylquinoline (**1a**), benzyl-amine (**2a**), 2-chloroacetic acid (**3**), and cyclohexyl

isocyanide (**4a**) was stirred at room temperature in methanol for 24 h to afford the corresponding Ugi product **5a** (Scheme 2). After removing the methanol from the reaction media, the obtained white precipitate (**5a**) was dissolved in the DMF as a solvent and then sodium azide (2.5 eq) was added. The reaction temperature increased to 90 ºC, after 6 h the result compound **6a** was obtained with 90% yield (Scheme 3).

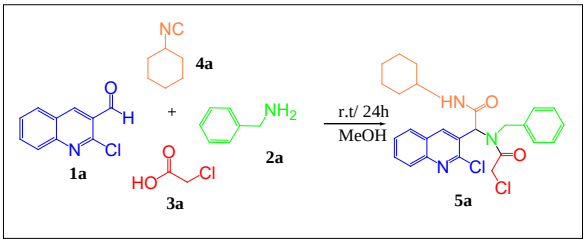

Scheme 2. Overview of Ugi reaction

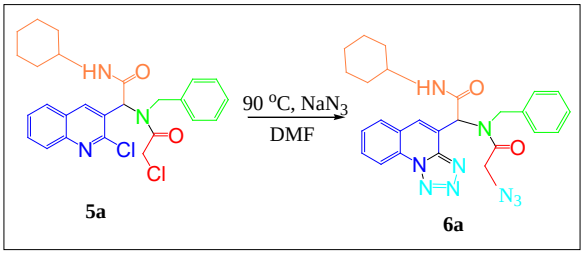

Scheme 3. Nucleophilic substitution reaction of azides to produce substance **6a**

To achieve the desired product **8a**, various conditions were investigated. When the compound **6a** was treated with triphenylphosphine in toluene, the iminophosphorane **7a** was easily formed at 2 h (Scheme 4), then the reaction media was heated at 90 °C for 6 h and compound **8a** was successfully produced in 75% yield (Scheme 5).

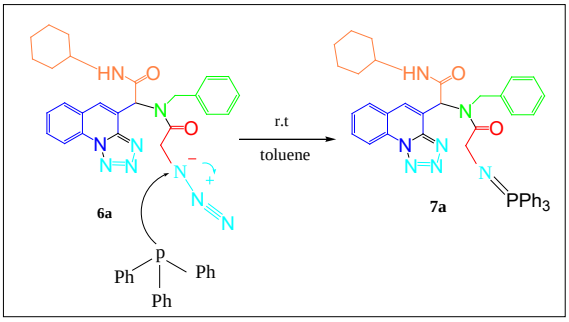

Scheme 4. Staudinger reaction

A plausible mechanism for the formation of product **8a** is shown in Scheme 6. At the beginning, a six-membered ring is formed through attack of the iminophosphoran **7**, then the water which is exist in the toluene solvent enters the reaction. Next the triphenylphosphine oxide and cyclohexylamine are removed (Scheme 6).

Under the mentioned reaction condition, a series of 3-(tetrazolo[1,5-a]quinolin-4-yl)piperazine-2,5-dione derivatives **8** were synthesized using a various 2-chloro-3-formyl quinolines **1**, amines **2** and isocyanides **4** derivatives (Table 1).

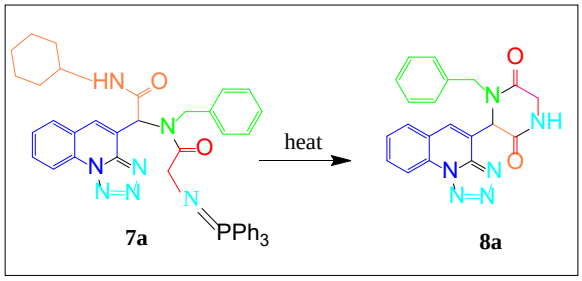

Scheme 5. Aza-Wittig reactions and hydrolysis

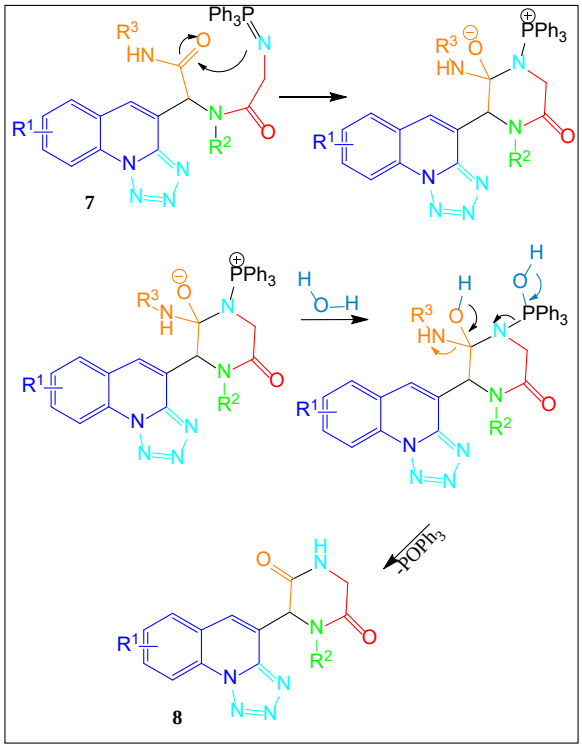

Scheme 6. Mechanism of aza-Wittig reaction in the toluene.

Table 1. Synthesis of 3-(tetrazolo[1,5-a]quinolin-4-yl)piperazine-2,5-dione derivatives **8**

z	R^1	R^2	R^3	Product	Yield (%)
1	H	$C_6H_5CH_2$-	c-C_6H_{11}	**8a**	75
2	H	$C_6H_5CH_2$-	t-Bu	**8a**	68
3	H	$C_4H_3OCH_2$-	c-C_6H_{11}	**8b**	70
4	H	C_6H_5-	c-C_6H_{11}	**8c**	59
5	OMe	$C_6H_5CH_2$-	c-C_6H_{11}	**8d**	65
6	OMe	$C_4H_3OCH_2$-	c-C_6H_{11}	**8e**	60
7	OMe	C_6H_5-	c-C_6H_{11}	**8f**	55
8	Me	$C_6H_5CH_2$-	c-C_6H_{11}	**8g**	72
9	Me	$C_4H_3OCH_2$-	c-C_6H_{11}	**8h**	68
10	Me	C_6H_5-	c-C_6H_{11}	**8i**	60

3. Conclusion

In conclusion, we have successfully developed an efficient route for the synthesis of various derivatives of 3-(tetrazolo[1,5-a]quinolin-4-yl)piperazine-2,5-dione *via* a Ugi reaction/nucleophilic substitution of azides/Staudinger reaction/aza-Wittig reactions and hydrolysis. This method has advantages: no need for catalyst, high bond formation efficiency with good to excellent yield and simple separation. The synthesized substance having important functional groups such as tetrazole ring, quinoline skeleton and piperazine-2,5-dione which have different properties, that can be a potential compound in terms of medicinal properties.

Experimental:

General procedure of the synthesis of Ugi adducts 5:

To a solution of 2-chloro-3-formylquinoline **1** (1 mmol) in MeOH (2 mL), benzylamine **2** (1 mmol), chloroacetic acid **3** (1 mmol), and cyclohexyl isocyanide **4** (1 mmol) were added, respectively. The solution was stirred for 24 h at room temperature. The reaction progress was monitored by TLC. After the completion of reaction, the colorless solid was precipitated and dried for next step.

General procedure of the Synthesis of compounds 6:

The desired Ugi product **5** was dissolved in DMF (5 mL), then sodium azide (162.5 mg, 2.5 mmol) was added to the reaction mixture, then the reaction heated at 90 °C for six hours. The reaction progress was monitored by TLC. After the completion of the reaction, the mixture was cooled to room temperature, and was added H_2O (10 mL) with stirring then the colorless solid was filtered and washed with H_2O to produce product **6**.

General procedure of the Synthesis of compounds 8:

Triphenylphosphine (200 mg, 1 mmol) was added to a solution of compound **6** (1 mmol) in toluene (3 mL) at stirred condition. After stirring for about 2 h, iminophosphorane **7** was formed which was monitored by TLC. Then the solution was heated to 90 °C for 6 h. After the reaction was completed, the solvent was evaporated and the residue was purified by column chromatography to give product.

1-Benzyl-6-(1,2,3,9b-tetraaza-cyclopenta[a]naphthalen-4-yl)-piperazine-2,5-dione (**8a**) as white solid. Mp: 200-203 ºC, ^{1}H NMR (250 MHz, CDCl3): δ 3.98 (1H, d, J = 15 Hz, CH_2), 4.27 (1H, dd, J = 17.4, 2.9 Hz, CH_2), 5.07 (1H, d, J = 17.4 Hz, CH_2), 5.14 (1H, d, J = 15 Hz, CH_2), 5.26 (1H, s, CH), 7.12-7.18 (5H, m, Ar-H), 7.30 (1H, s, NH), 7.75 (1H, t, J = 7.6 Hz, Ar-H), 7.86 (1H, s, Ar-H), 7.92 (1H, t, J = 7.5 Hz, Ar-H), 7.98 (1H, d, J = 7.9 Hz, Ar-H), 8.63 (1H, d, J = 8.3 Hz, Ar-H), ^{13}C NMR (126 MHz, $CDCl_3$): δ 45.9, 47.6, 61.5, 116.7, 121.2, 123.2, 127.9, 128.3, 128.4, 128.6, 129.2, 130.6, 131.9, 134.7, 134.9, 145.4, 164.1 (CON), 164.6 (CON)

4. References

[1] Zhong, Y.; Wang, L.; & Ding, M. W. New efficient synthesis of 2, 3, 4-trisubstituted 3, 4-dihydroquinazolines by a Ugi 4CC/Staudinger/aza-Wittig sequence. *Tetrahedron* 2011, 67(20), 3714-3723.

[2] Golmohammadi, F., Balalaie, S., Fathi Vavsari, V., Anwar, M. U., & Al-Harrasi, A. (2020). Synthesis of Spiro-β-lactam-pyrroloquinolines as Fused Heterocyclic Scaffolds through Post-transformation Reactions. J. Org. Chem., 85(20), 13141-13152.

[3] Zhu, H. Bienaymé, Multicomponent Reactions; Eds.; Wiley-VCH: Weinheim, 2005.

[4] Domling, A., Wang, W., & Wang, K. (2012). Chemistry and biology of multicomponent reactions. Chem. Rev., 2012 112(6), 3083-3135.

[5] Borisov, R. S., Polyakov, A. I., Medvedeva, L. A., Khrustalev, V. N., Guranova, N. I., & Voskressensky, L. G. (2010). Concise approach toward tetrazolo [1, 5-a][1, 4] benzodiazepines via a novel multicomponent isocyanide-based condensation. Org. Lett., 12(17), 3894-3897.

[6] Wang, R., Xu, X. P., Meng, H., Wang, S. Y., & Ji, S. J. (2013). 3-Phenacylideneoxindoles with tosylmethyl isocyanide and MeOH through C–C bond cleavage: facile synthesis of pyrrole and 2H-pyrrolo [3, 4-c] quinoline derivatives. Tetrahedron, 69(6), 1761-1766.

[7] Su, Y., Bouma, M. J., Alcaraz, L., Stocks, M., Furber, M., Masson, G., & Zhu, J. (2012). Organocatalytic enantioselective one-pot four-component Ugi-type multicomponent reaction for the synthesis of epoxy-tetrahydropyrrolo [3, 4-b] pyridin-5-ones. Chem. Eur. J., 18(40), 12624-12627.

[8] Xu, Z., De Moliner, F., Cappelli, A. P., & Hulme, C. (2013). Aldol reactions in multicomponent reaction-based domino pathways: a multipurpose enabling tool in heterocyclic chemistry. Org. Lett., 15(11), 2738-2741.

[9] (a) Domling, A.; Ugi, I. Angew. Chem., Int. Ed. 2000, 39, 3168; (b) Zhu, J.; Bienayme, H. Multicomponent Reactions;Wiley-VCH:Weinheim, Germany, 2005; (c)Domling, A. Chem. Rev. 2006, 106, 17; (d) Kaim, L. E.; Gizzi, M.; Grimaud, L. Org. Lett. 2008, 10, 3417.

[10] (a) Fan, L.; Adams, A. M.; Polisar, J. G.; Ganem, B. J. Org. Chem. 2008, 73, 9720; (b)Velzquez, F.; Venkatraman, S.; Wu, W.; Blackman, M.; Prongay, A.; Girijavallabhan,V.; Shih, N.-Y.; George Njoroge, F. G. Org. Lett. 2007, 9, 3061; (c)Huang, X.; Xu, J.-F. J. Org. Chem. 2009, 74, 8859; (d) Liu, H. X.; Domling, A. J. Org.Chem. 2009, 74, 6895; (e) Krasavin, M.; Shkavrov, S.; Parchinsky, V.; Bukhryakov,K. J. Org. Chem 2009, 74, 2627; (f) Tour, B. B.; Hall, D. G. Chem. Rev. 2009,109, 4439; (g) Kaïm, L. E.; Grimaud, L.;Wagschal, S. J. Org. Chem. 2010, 75, 5343.

[11] (a) Marsden, S. P.; McGonagle, A. E.; McKeever-Abbas, B. Org. Lett. 2008, 10, 2589; (b) Lertpibulpanya, D.; Marsden, S. P.; Rodriguez-Garcia, I.; Kilner, C. A. Angew. Chem., Int. Ed. 2006, 45, 5000; (c) Palacios, F.; Alonso, C.; Aparicio, D.; Rubiales, G.; Santos, J. M. Tetrahedron 2007, 63, 523; (d) Alajarin, M.; Bonillo, B.; Ortin, M.-M.; Sanchez-Andrada, P.; Vidal, A.; Orenes, R.-A. Org. Biomol. Chem. 2010, 8, 4690; (e) Devarie-Baez, N. O.; Xian, M. Org. Lett. 2010, 12, 752.

[12] Sa~nudo, M.; García-Valverde, M.; Marcaccini, S.; Delgado, J. J.; Rojo, J.; Torroba, T. J. Org. Chem. 2009, 74, 2189.

[13] Marsden, S. P., McGonagle, A. E., & McKeever-Abbas, B. (2008). Catalytic aza-Wittig cyclizations for heteroaromatic synthesis. Org. Lett., 10(12), 2589-2591.

[14] Lertpibulpanya, D., Marsden, S. P., Rodriguez-Garcia, I., & Kilner, C. A. (2006). Asymmetric Aza-Wittig Reactions: Enantioselective Synthesis of β-Quaternary Azacycles. Angew. Chem., 118(30), 5122-5124.

[15] Alajarin, M., Bonillo, B., Ortin, M. M., Sanchez-Andrada, P., Vidal, A., & Orenes, R. A. (2010). Domino reactions initiated by intramolecular hydride transfers from tri (di) arylmethane fragments to ketenimine and carbodiimide functions. Org. Biomol. Chem., 8(20), 4690-4700.

[16] Corres, N., Delgado, J. J., García-Valverde, M., Marcaccini, S., Rodríguez, T., Rojo, J., & Torroba, T. (2008). Synthesis of pseudopeptidic [(5H)-6-oxodibenzo [b, f][1, 5] diazocine-5-yl] arylglycinamides by an Ugi 4CC/Staudinger/aza-Wittig sequence. Tetrahedron, 64(9), 2225-2232.

[17] Lecinska, P., Corres, N., Moreno, D., García-Valverde, M., Marcaccini, S., & Torroba, T. (2010). Synthesis of pseudopeptidic (S)-6-amino-5-oxo-1, 4-diazepines and (S)-3-benzyl-2-oxo-1, 4-benzodiazepines by an Ugi 4CC Staudinger/aza-Wittig sequence. Tetrahedron, 66(34), 6783-6788.

29TH IRANIAN ORGANIC CHEMISTRY CONFERENCE
1_3 NOV, 2023
UNIVERSITY OF QOM, IRAN

A novel in-silico study for the guanine-cytosine base pair tautomerization based on double proton transfer

*Zeinab Korkani, Shapour Ramazani**

Department of Chemistry, Faculty of Science, University of Yasouj, Yasouj, Iran, marya.aryaee@yahoo.com, shapour.ramazani@gmail.com,

Abstract - Proton transfer in the Guanine-Cytosine (GC) base pair has been proposed as a possible mechanism for rare tautomer formation and thus a source of spontaneous mutations in DNA. We looked into 23 guanine-cytosine tautomers based on double proton transfer for the first time in this work. 5 transition states, comprising four types of N-H→N, N-H→O, N-H→C, and C-H→N hydrogen transfer, were discovered in these pathways after the various potential energy levels to detect these molecules were explored. The primary base pair GC_1 is the most stable molecule in both the gas phase and solution.

Keywords: DNA, Tautomerism, Base Pair

1. Introduction

Proton transfer is crucial for many different chemical and biological processes [1-4]. Nearly all reactions involving the transfer of multiple protons occur in living things, whether they are enzyme catalysis reactions or DNA mutation processes [5, 6]. The double proton transfer systems play a crucial role in this area because they can act as a template for DNA base pairs [7, 8]. Proton transfer along the DNA's hydrogen bonds can result in the formation of tautomers, causing short-lived point mutations with biological significance. These mutations can further result in gene mutation and, ultimately, cancer. Considered candidates for spontaneous DNA mutation during replication and repair are amino-imino tautomerism and keto-enol [9–11]. Species diversity is provided by spontaneous point mutations, which are of great significance [12–13]. The therapy and treatment of cancer disorders brought on by the higher mutation rates require an understanding of the molecular process behind their occurrence [14]. The methods of generation of rare DNA base tautomers are currently not fully understood, despite the fact that prototropic tautomerism of DNA bases has been thought to be the primary driver of spontaneous point mutations [2–4]. In the next sections, a thorough explanation of the approaches used for achieving reaction pathways, evaluating the energy levels of molecules, and determining the stability of those tautomers will be provided. To better comprehend the inner workings of PT processes, it is crucial to investigate their various physicochemical properties, including energetic (e.g., electronic and Gibbs free energies) and geometric (e.g., lengths and angles). Furthermore, future scientific studies into PT processes in H-bonded complexes of any type and structure may make extensive use of the provided data.

2. Computational Details

Using the GAUSSIAN 09 software package [15], we completed all DFT calculations in the gas phase and aqueous solution in the current work. The calculations were carried out using MPWB1K/6-311++G(d,p) level, and approved to give accurate geometrical structures, normal mode frequencies, barrier heights, and characteristics of inter/intramolecular H-bonds. This level was used to optimize the geometries of the GC base pair and transition states (TS's) of their conversion [16-18]. We have related structures to the transition state or minima by the presence or absence of the imaginary frequency in the vibrational spectra of the complexes, respectively, which were localized on the potential energy landscape using the Synchronous Transit-guided Quasi-Newton (STQN) method [19]. Due to the fact that water molecules typically dominate the environment that affects nucleic acids. Therefore, these molecules might be crucial for DNA's spontaneous mutation [20]. Therefore, the self-consistent reaction field (SCRF) theory via polarizable continuum model (PCM) [21] was utilized at the MPWB1K level to study the effect of solvent on the stability of tautomers.

3. Results and discussions

3.1. Potential energy diagram of proton transfer

There were discovered to be 23 different tautomers for the primary guanine-cytosine base pair, GC_1, which featured four hydrogen transfers (H_8, H_{25}, H_{28}, and H_{29}) between nine transfer sites (C_{15}, C_{18}, N_7, N_{10}, N_{19}, N_{20}, N_{21}, N_{23}, and O_{24}). The compounds under examination are schematically shown in Figure 1, with marks R1 to R25 designating the products of 25 different reactions. The potential energy levels of each pathway were determined using the intrinsic reaction coordinate (IRC).

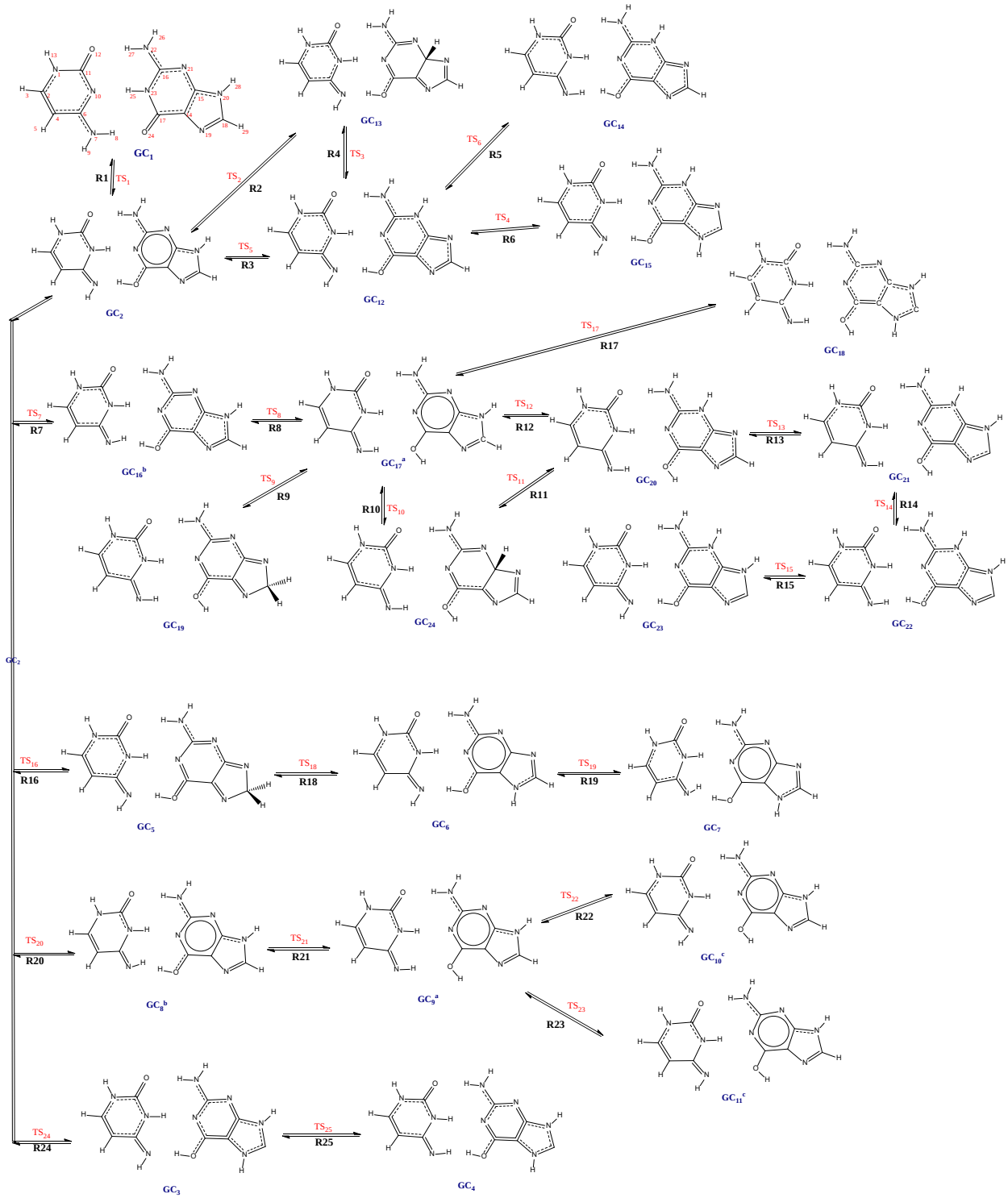

Fig.1. Isomerization diagram of guanine-cytosine tautomers

According to Figure 2, which depicts the isomerization energy diagram of the guanine-cytosine base pair and its tautomers, the potential energy level difference between all tautomers creates 14 tautomers (GC_3, GC_4, GC_5, GC_{12}, GC_{13}, GC_{14}, GC_{15}, GC_{16}, GC_{18}, GC_{19}, GC_{20}, GC_{21}, GC_{22}, and GC_{23}) as well as 9 tautomers (GC_2, GC_6, GC_7, GC_8, GC_9, GC_{10}, GC_{11}, GC_{16}, and GC_{17}) with relative energies greater and less than 100 ($kJ.mol^{-1}$) compared to the main reactant GC_1, respectively. The imaginary frequencies of transition state molecules in Table 1 in these pathways provided valid evidence for these molecules as active complexes with the lowest energy state. Four types of hydrogen transfer reactions were identified in a total of 25 pathways: N–H→N (R1, R3, R12), N–H→O (R1), N–H→C (R2, R9, R10, R16), C–H→N (R4, R6, R11, R13, R17, R18, R24), O-H group orientation change (R8, R14, R21) and N-H group orientation change (R5, R7, R15, R19, R20, R22, R23, R25).

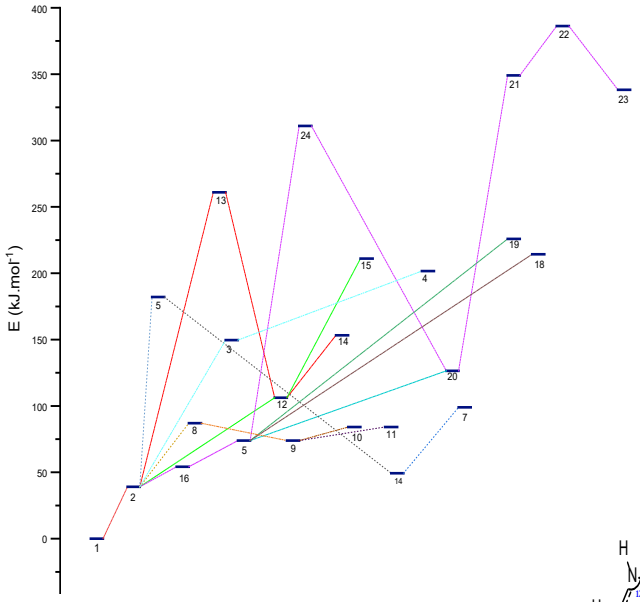

Fig2. The relative energies of different species in the reaction of guanine-cytosine tautomers in kJ.mol^{-1} at the MPWB1K/6-311++ G(d,p) level in gas phase

Table 1 Different structures of transition states (TS), imaginary frequency of TS (cm^{-1}) at MPWB1K/6-311+ G(d,p) level in gas phase (and aqueous solution)

Species	Imaginary frequency
TS1	1353.22i (N23-H25→N10, N7-H8→O24) (DPT) (N23-H25→N10)* (1104.95i)
TS2	1311.03i (N20-H28→C15) (1347.32i)
TS3	1541.21i (C15-H28→N21) (1572.98i)
TS4	1669.16i (C18-H29→N19) (1630.20i)
TS5	2017.96i (N20-H28→N21) (2085.31i)
TS6	1002.66i (C6─N7─H9) (858.82i)
TS7	1002.83i (C6─N7─H9) (873.50i)
TS8	454.52i (C17─O24─H8) (429.16i)
TS9	1514.76i (N20-H28→C18) (1535.61i)
TS10	1295.75i (N20-H28→C15) (1329.60i)
TS11	1514.18i (C15-H28→N21) (1550.02i)
TS12	2027.09i (N21-H28→N20) (2087.53i)
TS13	1721.57i (C18-H29→N20) (1734.35i)
TS14	413.69i (C17─O24─H8) (459.44i)
TS15	1004.41i (C6─N7─H9) (850.68i)
TS16	1520.48i (N20-H28→C18) (1545.68i)
TS17	1612.46i (C18-H29→N19) (1612.09i)
TS18	1449.82i (C18-H28→N19) (1460.15i)
TS19	969.37i (C6─N7─H9) (851.23i)
TS20	1002.92i (C6─N7─H9) (873.76i)
TS21	404.23i (C17─O24─H8) (429.73i)
TS22	1093.57i (C6─N7─H9) (1087.55i)
TS23	1048.29i (C6─N7─H9) (1131.57i)
TS24	1611.93i (N19-H29→C18) (1600.23i)
TS25	983.03i (C6─N7─H9) (852.04i)

As can be observed in Figure 3, among the 25 base pairs of guanine-cytosine, R1 is the most significant conversion. It involves two simultaneous proton transfers, which is known as the double proton transfer phenomena in the gas phase [11, 20, 22–25]. The non-planar ring TS1, which has a barrier of 61.38 kJ.mol^{-1}, transforms GC_1 into GC_2.

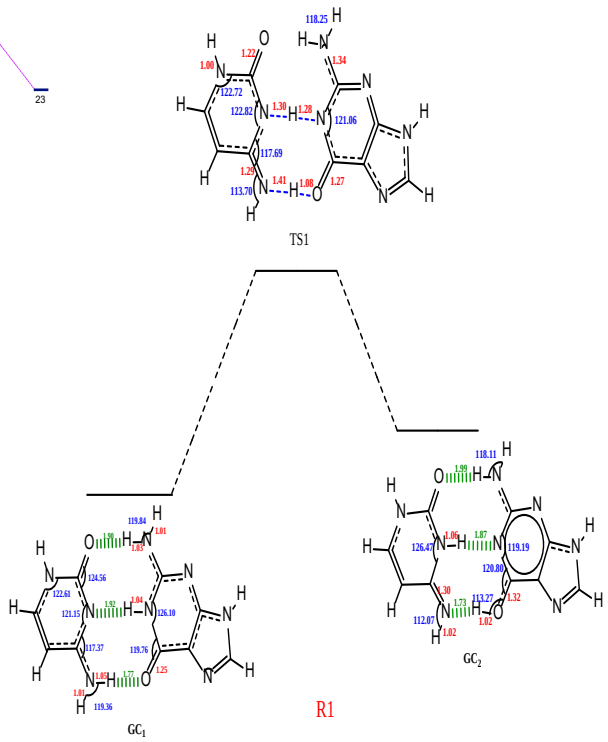

Fig.3. Schematic of the conversion of GC_1 to GC_2 with transition state TS1 in the gas phase

3.2. The comparison of the stability of GC tautomers in the gas phase and aqueous solution

One of the key elements impacting the stability of tautomer structures is electron delocalization. Other significant elements include planar and non-planar ring configurations, as well as functional groups in tautomers. Based on the information in Table 1 and Figure 4, it is possible to order the stability of the guanine-cytosine base pair and its tautomers in declining order as follows:

In the gas phase:

$GC_1 < GC_2 < GC_6 < GC_{16} < GC_9$, $GC_{17} < GC_{11} < GC_{10} < GC_8 < GC_7 < GC_{12} < GC_{20} < GC_3 < GC_{14} < GC_5 < GC_4 < GC_{18} < GC_{19} < GC_{13} < GC_{15} < GC_{24} < GC_{23} < GC_{21} < GC_{22}$.

In the solvent phase:

$GC_1 < GC_2 < GC_6 < GC_{12} < GC_7 < GC_{17} < GC_9 < GC_{10}$, $GC_{11} < GC_8 < GC_{16} < GC_{20} < GC_{14} < GC_5 < GC_3 < GC_{18} < GC_4 < GC_{15} < GC_{13} < GC_{19} < GC_{23} < GC_{21} < GC_{22} < GC_{24}$.

Significant changes in the stability of tautomers in terms of energy have been observed, leading to 11 tautomers becoming more stable in the aqueous phase in accordance with Figure 4 and the arrangements described in the gas and aqueous phases. Examples of tautomers that have improved in stability in the aqueous phase are GC_6, GC_7, GC_{12}, GC_{13}, GC_{14}, GC_{15}, GC_{17}, GC_{18}, GC_{21}, GC_{22}, and GC_{23}.

Additionally, the rotomers GC_8, GC_{10}, GC_7, GC_{11}, GC_{24}, GC_{16}, and GC_{22}, with greater energy in the aqueous phase than in the gas phase, were produced by the rotation of the imine NH in cytosine in GC_6, GC_9, GC_3, GC_{12}, and GC_2. In GC_8 and GC_{16}, respectively, the rotation of the enol OH in guanine had resulted in the formation of the rotomers, which were less stable in the aqueous phase than in the gas phase.

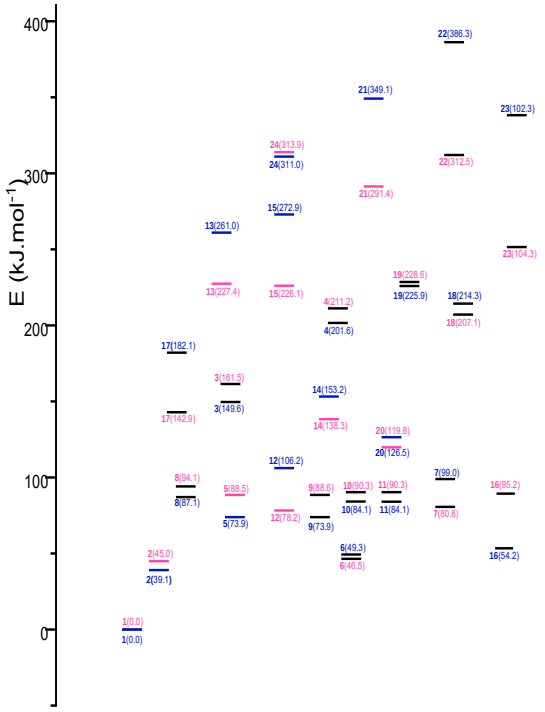

Fig.4. The relative energies of GC tautomers (a) $\Delta E^{Solvent} = \Delta E^{Solvent}_{GC} - \Delta E^{Solvent}_{GC1}$ (in pink) in aqueous solution and (b) $\Delta E^{Gas} = \Delta E^{Gas}_{GC} - \Delta E^{Gas}_{GC1}$(in blue) in gas phase

4. Conclusion

This research successfully examined 23 Guanine-Cytosine tautomers based on double proton transfer and tautomerism's potential energy surfaces. The findings showed that four different forms of hydrogen transfer (N-H→N, N-H→O, N-H→C, and C-H→N) were responsible for the tautomerism reactions. The results demonstrated that GC_1 is the most stable guanine-cytosine base pair in both the gas and solution phases, reiterating the rationale behind the selection of this structure for the double-stranded helical chain of DNA in biological systems. Additionally, structures GC_6, GC_7, GC_{12}, GC_{13}, GC_{14}, GC_{15}, GC_{17}, GC_{18}, GC_{21}, GC_{22}, and GC_{23} are more stable in the solution phase than in the gas phase. This is due to both better delocalization of electrons and functional groups in the cytosine and guanine branches.

5. References

[1] J.M. Mayer, Acc. Chem. Res, 44 (2011) 36-46.

[2] D.R. Weinberg, C.J. Gagliardi, J.F. Hull, C.F. Murphy, C.A. Kent, B.C. Westlake, A. Paul, D.H. Ess, D.G. McCafferty, and T.J. Mayer, Chem. Rev, 112 (2012) 4016-4093.

[3] J.P. Layfield, and S. Hammes-Schiffer, Chem. Rev, 114 (2014) 3466-3494

[4] M. Salamone, and M. Bietti, Acc. Chem. Res, 48 (2015) 2895-2903.

[5] D. Jacquemin, D. Jacquemin, J. Zúñiga, A. Requena, and J.P. Céron-Carrasco, Acc. Chem. Res, 47 (2014) 2467-2474.

[6] J.P. Klinman, and A. Kohen, Annurev-Biochem, 82 (2013) 471-496.

[7] G.L. Barnes, S.M. Squires, and E.L. Sibert, J. Phys. Chem. B, 112 (2008) 595-603.

[8] Z. Smedarchina, W. Siebrand, and A. Fernández-Ramos, J. Chem. Phys, 148 (2018) 102307.

[9] P.O Löwdin, Rev. Mod. Phys, 35 (1963) 724.

[10] P.O Löwdin, Adv. Quantum Chem, Elsevier (1966) 213-360.

[11] L. Slocombe, J. Al-Khalili, and M. Sacchi, Phys. Chem. Chem. Phys, 23(2021) 4141-4150.

[12] E.C. Friedberg, A. Aguilera, M. Gellert, P.C. Hanawalt, J.B. Hays, A.R. Lehmann, T. Lindahl, N. Lowndes,A. Sarasin,and R.D. Wood, DNAREP, 5(2006) 986-996.

[13] H. Lee, E. Popodi, H. Tang, and P.L. Foster, PNAS, 109 (2012) E2774-E2783.

[14] B. Vogelstein,. and K.W. Kinzler, The Genetic Basis of Human Cancer. 1998: McGraw-Hill, Health Professions Division.

[15] J. Frisch, G.W. Trucks, Hs. B. Schlegel, G.E. Scuseria, M.A. Robb, J.R. Cheeseman, G. Scalmani, V. Barone, B. Mennucci, G.A. Petersson, H. Nakatsuji, M. Caricato, X. Li, H.P. Hratchian, A.F. Izmaylov, J. Bloino, G. Zheng, J.L. Sonnenberg, M. Hada, M. Ehara, K. Toyota, R. Fukuda, J. Hasegawa, M. Ishida, T. Nakajima, Y. Honda, O Kitao, H Nakai, T Vreven, JA Montgomery Jr, JE Peralta, F. Ogliaro, M. Bearpark, J.J. Heyd, E. Brothers, K.N. Kudin, V.N. Staroverov, R Kobayashi, J Normand, K Raghavachari, A Rendell, J.C. Burant, S.S. Iyengar, J. Tomasi, M. Cossi, N. Rega, J.M. Millam, M. Klene, J.E. Knox, J.B. Cross, V. Bakken, C. Adamo, J. Jaramillo, R. Gomperts, R.E. Stratmann, O. Yazyev, A.J. Austin, R. Cammi, C Pomelli, J.W. Ochterski, R.L. Martin, K. Morokuma, V.G. Zakrzewski, G.A. Voth, P Salvador, J.J. Dannenberg, S. Dapprich, A.D. Daniels, aÖ. Farkas, J.B. Foresman, J.V. Ortiz, J. Cioslowski, and D.J. Foxet, Gaussian 09 program, revision C. 01. Gaussian Inc, Wallingford, 2010.

[16] Zhao, Y. and D.G. Truhlar, J. Phys. Chem. A, 108 (2004) 6908-6918.

[17] M.J. Frisch, J.A. Pople, and J.S. Binkley, J. Chem. Phys, 80 (1984) 3265-3269.

[18] T. Clark, J. Chandrasekhar, G.W. Günther W. Spitznagel, and P.V.R. Schleyer, J. Comput. Chem, 4 (1983). 294-301.

[19] C. Peng, P.Y. Ayala, H.B. Schlegel, and M.J. Frisch, J. Comput. Chem., 17 (1996) 49-56.

[20] J.P. Cerón-Carrasco, A. Requena, J. Zúñiga, C. Michaux, E. A. Perpète, and D. Jacquemin, J. Phys. Chem. A, 113 (2009) 10549-10556.

[21] J. Tomasi, B. Mennucci, and R. Cammi, Chem. Rev, 105 (2005) 2999-3094.

[22] O.h.O. Brovarets', and D.M. Hovorun, J. Biomol. Struct. Dyn., 37 (2019) 1880-1907.

[23] R. Pohl, O. Socha, P. Slavíček, M. Šála, P. Hodgkinson, and M. Dračínský, Faraday Discuss, 212 (2018) 331-344.

[24] D. Soler-Polo, J.I. Mendieta-Moreno, D.G. Trabada, and J. Ortega, J. Chem. Theory Comput, 15 (2019) 6984-6991.

[25] L. Slocombe, M. Winokan, J. Al-Khalili, and M. Sacchi Commun. Chem., 5 (2022) 144.

29TH IRANIAN ORGANIC CHEMISTRY CONFERENCE
1_3 NOV, 2023
UNIVERSITY OF QOM, IRAN

Simultaneously aromatic ring opening and N-demethylation pathways of photocatalytic degradation of triphenylmethane crystal violet dye

Simin Janitabar Darzi[1], *Hajieh Bastami*[*2]

[1]*Nuclear Science & Technology Research Institute, Nuclear Fuel Cycle Research School, Tehran, Iran, P.O. Box: 14395-836, sjanitabar@aeoi.org.ir*

[2] *Department of Materials and Metallurgical Engineering, Technical and Vocational University (TVU), Tehran, Iran, hbastami@tvu.ac.ir*

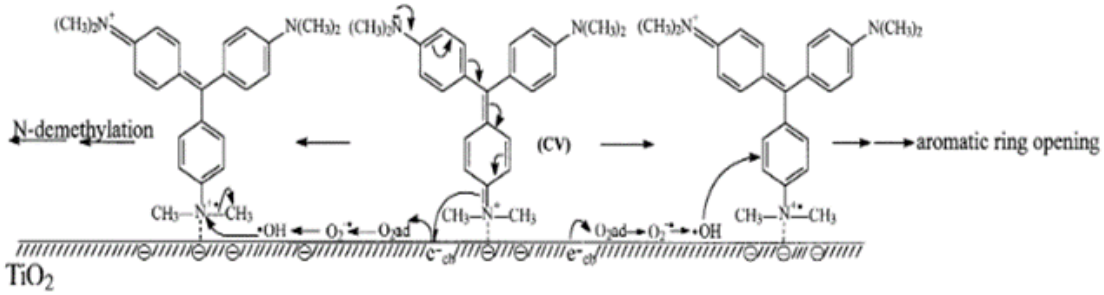

Photocatalytic degradation of Crystal violet dye performs via aromatic ring opening and N-demethylation

Abstract - Crystal violet is a renowned triphenylmethane organic dye which is extensively used in pathobiological applications as well as in different industries such as textile one. The vast use of this dye requires a kind of astonishing effective technique for encountering with the probable environmental pollution raised from this dye. In this research, photocatalytic degradation of Crystal violet using TiO2 was studied. A sol-gel prepared mesoporous TiO2 was applied for this purpose. The prepared TiO2 revealed anatase phase and the band gap related to it was obtained to be 3.2 eV from DRS curve. Photocatalytic degradation of Crystal violet in photocatalytic reaction went through aromatic ring opening and N-demethylation mechanisms.

Keywords: Crystal violet, organic dye, degradation, dye sensitization.

1. Introduction

Nanosized and nanoporous TiO2 photocatalyst can exhibit high specific surface area and a significant activity in degradation of dyes and other effluents. Among the chemical pollutants, organic dyes due to toxic nature, are one of the major contaminants of industrial wastewater. Photocatalytic degradation of organic pollution is an excellent platform as compared to conventional treatment methods of water treatment and remediation from organic dyes [1].

Research on visible light active TiO_2 photocatalysts has grown considerably not only for its merits as an efficient pollution remover, but also for its feasible production, inexpensiveness, biological and photochemical stabilities [2]. The present work investigates crystal Crystalviolet dye degradation as a model of pollutant on the surface of mesoporous TiO2. The study also proposes the mechanism of photodegradation of Crystalviolet at the surface of the photocatalyst.

2. Experimental

2.1. Preparation and characterization of photocatalyst

First, 0.9 g of Pluronic P-123 [HO-[CH_2-CH_2O]a-[CH_2-CH(CH_3)O]b-[CH_2-CH_2O]a-OH] was dissolved in 11 mL of ethanol. To this solution, 1 mL of titanium tetrachloride was added under vigorous stirring. The mixture was maintained in an open beaker at 40°C for 5 days, the evaporated ethanol being filled up every 12 h. Thus, prepared clear yellowish solution could be stored at room temperature for several weeks without apparent changes. Films of different thickness were prepared by spreading various amounts of the stock solution on the glass support. The liquid layer was subsequently gelled in air at 40°C for 7 days and calcined at 400°C for 5 h in air. Finally, the titania

films were peeled off the support. Characterization of the product was carried out by means of Fourier transform infrared spectroscopy (FT-IR), X-ray diffraction (XRD), transmission electron microscopy (TEM), scanning electron microscopy (SEM), Brunauer–Emmett–Teller (BET) specific surface areas, thermogravimetry–differential scanning calorimetry (TG–DSC) and UV–vis absorption spectroscopy.

2.2. Photocatalitic set-up

Photocatalytic performance of TiO_2 photocatalyst towards the Crystal violet dye under visible light was tested by a hand maid set-up. An Osram lamp was used as radiation source and distance between the lamp and reaction container was adjusted at 15 cm. During the reaction, the amount of oxygen existing in the container was held fixed by means of an aquarium pump. The set-up was cooled with a fan and the tests was done at constant temperature around 25◦C. The photocatalyst amount was 1 gL-1 and the concentration of dye was 5 ppm. Prior to starting the photocatalytic reaction, the suspension was stirred in the dark for 30 minutes to guarantee an adsorption-desorption equilibrium among the oxygen, the photocatalyst, and dye molecules. After regular intervals during the photocatalytic reaction, about 5 mL of suspension was picked up and centrifuged. After that, the filtrates were subjected for studding by means of Uv–Vis spectroscopy.

3. Results and discussion

3.1. Characterization TiO2 photocatalyst

FT-IR spectra of the precipitation collected from scraping of the TiO_2 film before and after calcination are shown in Fig. 1. The FT-IR spectrum of the precipitate prior to calcinations (spectrum a) shows a broad peak at 3000–3600 cm-1 , which is assigned to the fundamental stretching vibration of hydroxyl groups (free or bonded) [3]. This is further confirmed by the weak band at about 1615 cm-1 [4], which is as a result of bending vibration of coordinated H2O as well as Ti–OH. The bending vibrational mode of water may appear as shoulders on the spectrum, as in 2800cm-1 [5]. It was reported that the vibration of the Ti–O bonds in the TiO_2 lattice may be located at 500 and 430 cm1 [3]. Other peaks are attributed to the surfactant. After calcinations (spectrum b), the absorption features due to P-123 is almost removed, as evidenced by the significantly reduced characteristic bands at 2850, 2940 and 1080 cm-1.

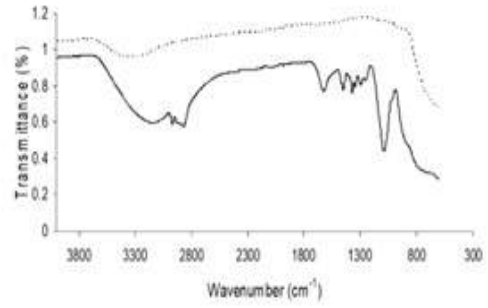

Fig. 1. FTIR analysis of synthesized TiO2 photocatalyst before calcination and after that

Fig.2 presents TEM images of prepared TiO2. According to TEM image the mater composed of granular particles.

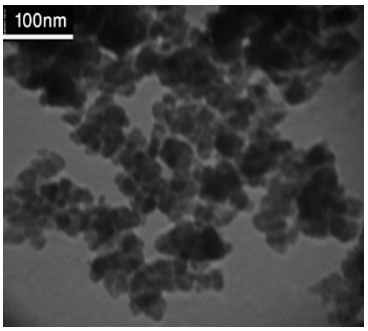

Fig. 2. TEM image of synthesized TiO2 photocatalyst

Fig. 3 reveals the N_2 adsorption-desorption analysis of prepared TiO_2. The hysteresis loop presented in the figure is of kind IV according to IUPAC categorization of mesoporous materials.

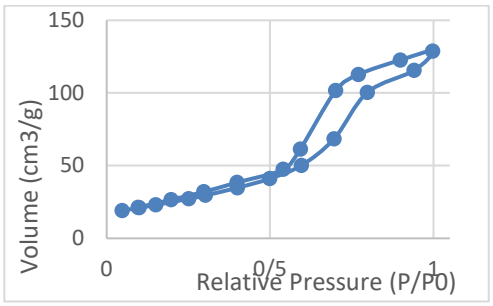

Fig.3 BET surface area of TiO2

3.2. Photodegradation mechanism and reason of hypsochromic shift in Uv-Vis spectra of dye

Figure 4 displays the spectral changes taking place through the degradation of CV at the surface of TiO2 photocatalyst under visible light irradiation. As shown in Figures 2 the maximum absorption (λmax) of the dye is observed at 588.5 nm and the intensity of spectra is decreased with a huge hypsochromic shift in λ max

in photocatalytic degradation pathway. Generally, the wavelengths of light that dye chromophores can absorb depends on the length of conjugated lane of the molecule. If the amount of conjugation in the chromophore system is reduced, a hypsochromic shift in the UV-Vis spectrum will happen. On the other side, according to the literature, when triphenylmethane dyes undergo a photocatalytic degradation, the process of demethylation of amine sites in the chromophore system can occur [6, 7]. It seems that during the decolorization of the CV dye, two reaction pathways including demethylation of amine sites of the chromophore system and breaking of the whole conjugated chromophore skeleton simultaneously takes place. Some reports have acknowledged that a competition between N-demethylation reaction and cleavage of conjugated structure exists [7]. The N-demethylation of CV dye will be performed in a stepwise demeanor to produce mono-, di-, tri-, tetra-, penta-, and hexa-N-demethylated intermediates. The CV dye has six methyl groups at three different amin site. There are two different isomers of di-N-demethylated type intermediates, which differ from each other because of their various kinds of methyl loosing from the amin sites. The di-N-demethylated isomers have four methyl groups due to losing two methyl groups from plain CV. If one methyl group separates from one of amine groups of the CV molecule, the second methyl is removed from another amine site of the dye molecule, and DMMPR is produced. Nevertheless, if removing of both of two methyl groups originate from one amine site, DDPR species is produced. By losing three methyl groups, some different new species are probable for appearing. If each of the three methyl groups can be removed from distinct anime sites, the prepared tri-N-demethylated CV isomer will be MMMPR. DMPR isomer is formed by eliminating of two methyl groups from the one amin sites of the dye, while the latest separated methyl is removed from another amine group. Both of DPR and MMPR isomers have lost four methyl groups from the plain CV structure. The DPR is formed by removing of four methyl groups from two amine sites of the plain CV molecule. However, MMPR is produced by eliminating of two methyl groups from one of amin sites of the CV and simultaneously removing of the other two methyl groups from two distinct amine groups in the dye. Lu et. al. [8] propounded above terms and reported maximum absorption wavelength (λmax) of some N-demethylated species of the CV. According to the literature, λmax of CV (N,N,N',N',N'',N''-Hexamethylpararosaniline or DDDPR), DDMPR, DMMPR, DDPR, MMMPR, DMPR, MMPR, DPR, MPR, and PR (Pararosaniline or hexa-N-demethylated CV) are located at 588.5, 581.0, 579.8, 573.7, 570.0, 566.3, 566.3, 561.5, 554.1, and 543.2 nm, respectively [8]. These reported λmax related to the different intermediates in photodegradation of CV dye were also observed in the absorbance spectra of this dye during our photocatalytic experiment under visible light on the surface of TiO2.

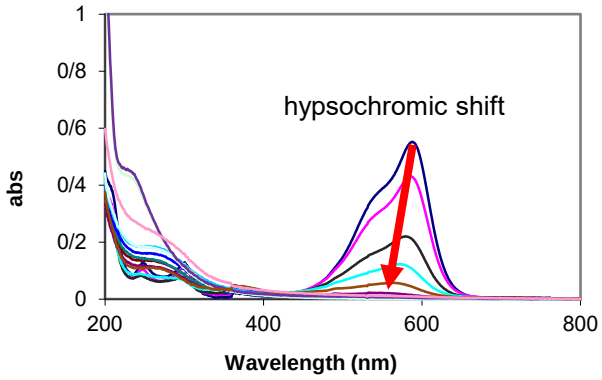

Fig.4. Changes in the absorbance spectra of Crystal violet dye during visible light degradation at the surface of TiO2

4. Conclusion

Visible light photocatalytic degradation of Crystal violet organic dye was performed on the surface of TiO2. As the band gap related to TiO2 was obtained to be 3.2 eV, the photocatalytic performance of this semiconductor cannot simply conduct through electron and hole under incident light whilst, it is proposed its activity be originated from electron and hole transfer between Homo-Lumo levels of absorbed dye and TiO2 valance -conduction bonds.

5. References

[1] M. Ismail, K. khtar, M.I. Khan, T. Kamal, M. A Khan , A. M Asiri , J. Seo , S. B Khan, Pollution, Toxicity and Carcinogenicity of Organic Dyes and their Catalytic Bio-Remediation. 25 (2019) 3645-3663.

[2] S. Janitabar Darzi, Structural and Photocatalytic Activity of Mesoporous N-Doped TiO2 with Band-to-Band Visible Light Absorption Ability. Particulate Science and Technology, 32 2014) 506-511.

[3] R. Zhang, L. Gao, Key. Eng., Mater 573 (2002) 224.

[4] B. Klingenberg, M.A. Vannice, Chem. Mater. 8 (1996) 2755.

[5] K. Schrijnemakers, N.R.E.N. Impens, E.F. Vansant, Langmuir 15 (1999) 5807.

[6] C.C. Chen, H.J. Fan, C.Y. Jang, J.L. Jan, H.D. Lin, C. Lu, J. Photochem. Photobiol. B, 2006, 184, 147–154.

[7] B. Gao, X. Luo, H. Fu, B. Lin, Y. Chen, Z. Gu, Mater. Res. Bull., 2013, 48, 587–594.

[8] C.S. Lu, F.D. Mai, C.W. Wu, R.J. Wu, C.C. Chen, Dyes Pigm., 2008, 76, 706–713

29TH IRANIAN ORGANIC CHEMISTRY CONFERENCE
1_3 NOV, 2023
UNIVERSITY OF QOM, IRAN

Well-Designed Electrospun poly (vinylidene fluoride) /MoO_3 Nanofiber as Triboelectric Nanogenerators

*Rebwar Fatehi, Zahed Shami**

Department of Chemistry, Faculty of Science, University of Kurdistan, Sanandaj, Iran, rebwar1323@gmail.com, z.shami@uok.ac.ir

Abstract: Nanogenerators (TENGs) have emerged as a next-generation sustainable power source for Internet of Things technology. Polyvinylidene fluoride (PVDF) nanofibers have been investigated widely to enhance the TENG performance by controlling their polarity it has great flexibility and can provide power for small independent systems. The triboelectric nanogenerator (TENG) is widely concerned because of their high output energy density. The TENG is used to drive electronics as a power source and to monitor human body motion in real time as a flexible wearable sensor, indicating its feasibility in sustainable and wearable electronics. Leads to enhancing the performance of the TENG. Besides, the nanocomposite maintains high performance of the stability and durability due to the excellent compatibility with PVDF nanofibers containing molybdenum oxide (MoO_3)

Keywords: Nanogenerator, Triboelectric (PVDF) nanofiber, Electrospinning,

1. Introduction:

The Vibration Energy Scavenging Project which is being set up to try to scavenge electrical energy from environmental vibrations and movements a fine technology, converting ambient energy in nature or everyday life into useful electrical energy that offers a sustainable power generation solution for various practical applications. Such ambient energies are being divided into wind, solar, fluid, thermal, and mechanical energy invaluable input sources for power generation when converted. These various energy harvesting technologies are not competing with one another; rather, they can provide complementary power solutions depending on the operating environment and their potential power levels. Triboelectric nanogenerator (TENGs) is one of the great millstones in which harvesting energy technology is being promised. Since Nanogenerators affected by triboelectric properties were first introduced to the world of science and technology in 2012 by Zhang Linwen and his group. They stated that due to mechanical pressure and contact between two layers of materials with high polarity and piezoelectric properties, electron transfer takes place from materials with higher dielectric constant, called cathode, to the material with lower dielectric constant, called anode. The preparation of nanofibers is one of the techniques of making nanogenerators based on triboelectric properties. In this research the efforts was based on using molybdenum oxide(MoO_3) to generate positions in polyvinylidene fluoride(PVDF) nanofibers, synthesized via electrospning system in order to make the electron transfer easier alongside with flexibilities and Elasticity's that PVDF nanofibers can give. The result observed from these nanogenerators led to the lighting of 18 LEDs [1-2].

2. Experimental Section

Polyvinylidene fluoride, dimethylformamide (DMF) and MoO_3 all were being provided from Sigma-Aldrich. The electrospinning solution was being prepared by dissolving 0.2 g MoO_3 in 5 ml of DMF, Then 1.5g the PVDF granules added to the solution. The solution stirred at a temperature of 70 °C for 24 hours to obtain a homogenized solution.

Nanofibers had been prepared via electrospning system. The as-spun nanofibers were being taped to copper plates and were placed facing each other with repeated mechanical taps. The LEDs were attached to the electrical circuit were turned on as a typical application.

3. Results

Formation of PVDF/MoO_3 nanofiber as TENGs hybrid triboelectric nano-generatore confirmed by SEMand XRD analysis. The (021) and (200) diffraction peaks in XRD confirm the presence of MoO_3 particle in PVDF nanofibers. Additionally,

The SEM image as well shows the formation of electrospun nanofibers notably, the fibres have a soft and pure surface, which is the result of MoO_3 presence is in the inner layer of nanofibers. The electrical circuit test applied on the as-spun hybrid nanofibrous structures confirms its triboelectric performance [3].

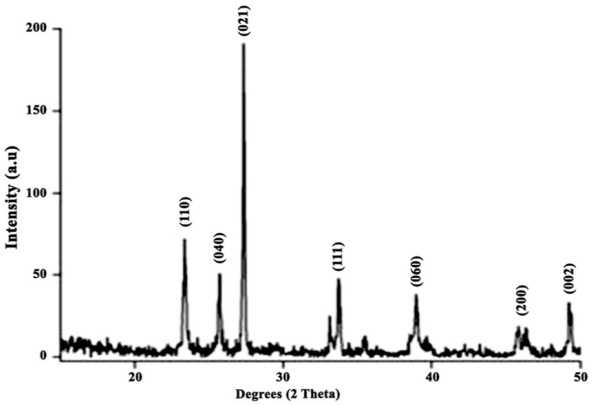

Figure 1. XRD pattern of PVDF/MoO_3 triboelectric nangenerator

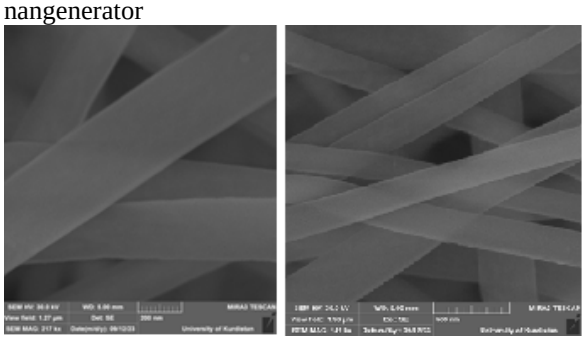

Figure 2. SEM image of PVDF/MoO_3 triboelectric nan generato

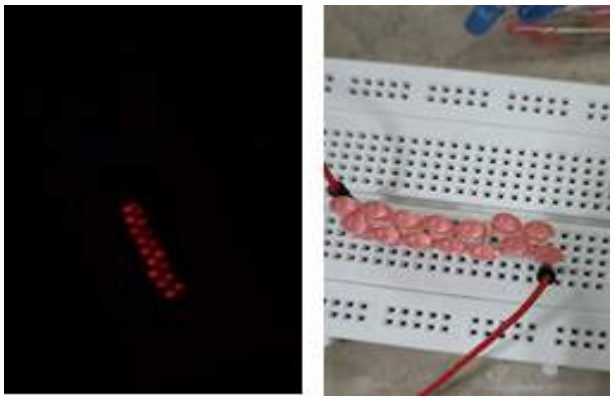

Figure 3. The photo presents the triboelectric nanogenerator performance of the as-spun nanofiber

3. Conclusion

In summary, PVDF electrospun fiber containing MoO_3 nanoparticles was successfully prepared. The SEM and XRD analysis provide the formation the as-spun PVDF/MoO_3 nanofibers. The triboelectric application of these material confirmed by the electrical circuit.

References:

[1] Y Kim, X Wu, Ch Lee, J Hoon oh ACS Appl. Mater. Interfaces 2021, 13, 31, 36967–36975

[2] N. Wang, X.Wang, K. Yan, ACS Applied Materials & Interfaces 2020, 12, 41, 46205-46211.

[3] Z Yang, X Zhang, G Xiang, ACS Appl. Nano Mater. 2022, 5, 11, 16906–16911

29TH IRANIAN ORGANIC CHEMISTRY CONFERENCE
1_3 NOV, 2023
UNIVERSITY OF QOM, IRAN

Aerobic Oxidation of Alcohols Catalyzed by in Situ Generated Gold Nanoparticles inside the Channels of Periodic Mesoporous Organosilica with Ionic Liquid Framework

Babak Karimi,[1,2] Akram Bigdeli[1], Ali Asghar Safari, Mojtaba Khorasani, Hojatollah Vali, and Somaiyeh Khodadadi Karimvand*

[1]*Institute for Advanced Studies in Basic Sciences, Zanjan 45137-66731, Iran, karimi@iasbs.ac.ir, bigdeli.a@iasbs.ac.ir*

[2]*Research Center for Basic Sciences & Modern Technologies (RBST), Institute for Advanced Studies in Basic Sciences (IASBS), Zanjan 45137-66731, Iran.*

Abstract - In situ generated gold nanoparticles inside the nanospaces of periodic mesoporous organosilica with an imidazolium framework (Au@PMO-IL) were found to be highly active, selective, and reusable catalysts for the aerobic oxidation of activated and nonactivated alcohols under mild reaction conditions. The catalyst was characterized by nitrogen adsorption-desorption measurement, thermogravimetric analysis (TGA), transmission electron microscopy (TEM), elemental analysis (EA), diffuse reflectance infrared Fourier transform spectroscopy (DRIFT), X-ray photoelectron spectroscopy (XPS), and inductively coupled plasma atomic emission spectroscopy (ICP-AES). The catalyst was also recovered and reused for at least seven reaction cycles. Data from three independent leaching tests indicated that amounts of leached gold particles were negligible (<0.2 ppm). It is believed that the combination of bridged imidazolium groups and confined nanospaces of PMO-IL might be a major reason explaining the remarkable stabilization and homogeneous distribution of in situ generated gold nanoparticles, thus resulting in the highly active and recyclable catalyst system.

1. Introduction

Selective oxidation of alcohols to the related carbonyl compounds such as aldehydes, ketones, and carboxylic acids is considered as one of the most interesting research topics since the desired products are extensively used in the synthesis of pharmaceutical, agricultural, and fine chemicals [1]. These transformations have been traditionally performed by using stoichiometric amounts of harmful organic as well as inorganic oxidants. Therefore, during the past two decades, from viewpoints of green chemistry and especially atom economy, a plethora of research has been directed toward the development of new and efficient catalytic systems on the basis of molecular oxygen and hydrogen peroxide as green terminal oxidants [2]. In this regard, many sophisticated protocols based on transition-metal catalysts were developed in either homogeneous or heterogeneous form. However, for many practical applications heterogeneous compared to homogeneous catalysis stands with greater promise because of simple recovery of the catalyst as well as minimization of metal contamination in the final products.

Similar to other noble metals, nano and subnano gold particles have shown very interesting activities and selectivities as well as turnover numbers in a variety of catalytic processes.

In this context, it has been well documented that the activity, selectivity, and lifetime of the gold nanoparticles depend not only on size and shape of the particles but can be significantly influenced by the nature of the support, location of gold on the support, and synergistic interactions between gold and supporting materials [3]. In order to prevent the agglomeration of Au nanoparticles and retain high catalytic activity, several stabilizing agents such as polyvinylpyrrolidone (PVP), sugars, surfactants, and various types of solid supports have been used during the synthesis steps and/or when they acted in desired reaction mediums [4]. Although, considerable improvements have been achieved in the catalytic activity, selectivity, and substrate scope, there are still major problems with Au nanoparticles based catalysts. Primarily, the control of the size of Au nanoparticles is highly challenging because of the very low melting point of gold [5]. Recently, we reported the preparation of Au nanoparticles on a bifunctional phenylene/ ethylene periodic mesoporous organosilica (Au@PMO) [6].The catalyst was then successfully employed in the aerobic oxidation of alcohols under ambient temperature. Meanwhile, we discovered that incorporating an appropriate concentration of the bridged imidazolium group inside the framework of mesoporous silica led to innovative functional materials (socalled PMO-IL) which serve as a superior supported ionic liquid and/or effective support for immobilization and stabilization of metal nanoparticles in several synthetically important transformations [7]. It was demonstrated that in these materials the

molecular diversity of IL-like nanostructures that act as effective solid ionic stabilizers for metal nanoparticles is genuinely combined with the advantages of an integrated reaction and purification strategy. In particular, by using XPS studies we showed that Au supported on PMO-IL (Au@PMO-IL) in the form of Au(III) species is an efficient catalyst in the A3-coupling reaction of aldehyde with amine and phenylacetylen to give the corresponding propargylamines [8]. Considering the excellent capability of PMO-IL in the immobilization and stabilization of metal nanoclusters, in our present work, we attempt to explore the use of Au@PMO-IL in the aerobic oxidation of alcohols under mild reaction conditions. With this goal in mind, the aerobic oxidation of several alcohols was investigated for confirming the general applicability of the Au@PMO-IL catalyst in the presence of either Cs2CO3 (close to room temperature) or K2CO3 (at 60- 80 °C). The advantage of our catalyst systems relies on the fact that, contrary to most of the reported gold catalysts, the pregeneration of gold nanoparticles by employing an exogenous reducing agent is not required. More importantly, the open pore structure of Au@PMO-IL not only exposes a highly catalytically active species but also combines the possibility of separating and recycling both ionic liquid and supported Au NPs at the same time, features that are all together of paramount importance for heterogeneous catalysis.

RESULT AND DISCUSSION

The synthesis of bridged ionic liquid 1,3-bis(3-trimethoxysilylpropyl)-imidazolium chloride (BTMSPC) was accomplished according to our reported procedures with a few modifications. The PMO-IL was then prepared using hydrolysis and copolymerization of both BTMSPCl and tetramethoxyorthosilicate (TMOS) in the presence of Pluronic P123 as an effective structure directing agent (SDA) under acidic conditions. The surfactant was then removed with acidic ethanol to provide PMO-IL. The resulting PMO-IL was then used to immobilize anionic gold species (AuCl4-) via a simple ion-exchange-impregnation technique according to our previous reported procedure with slight changes. In this regard, PMO-IL was first sonicated in water to obtain a homogeneous distribution of particles of materials, and then a solution of NaAuCl4 was added to replace some of PMO-IL chloride counterions with AuCl4- until the final catalyst which is denoted as Au@PMO-IL was obtained.

The textural and structural features of the PMO scaffold and Au@PMO-IL were evaluated using nitrogen sorption analysis. Figure 1 displays N2 adsorption-desorption isotherms and BJH pore size distributions (inset) for all materials. N2 adsorption-desorption isotherms exhibit type IV adsorption isotherms with H1 hysteresis loops which are characteristic of mesoporous materials with narrow pore size distributions [9]. As evidenced by these investigations, the shape of the isotherm in Au@PMO-IL is well-retained as compared with that of pristine PMO-IL, suggesting that the structure ordering survived during the mere ion-exchange process [10]. Moreover, narrow pore size distributions for both PMO-IL and Au@PMO-IL indicate high-ordered structure in the mentioned materials (Figure 1, inset). The textural parameters of PMO-IL, fresh Au@PMO-IL, and the recovered catalyst are summarized in Table 1. These results show that after immobilization of the anionic AuCl4- species into the PMO-IL channels, the specific surface area, total pore volume, and average pore diameter decreased from initial amounts of 530 m2 g-1, 0.99 cm3 g-1, and 10.6 nm to 432 m2 g-1, 0.77 cm3 g-1, and 9.2 nm, respectively. On the basis of these measurements, the incorporation of AuCl4- species shows minor effects on the pore size, pore volume, and surface area. While the decrease in nitrogen uptake under a relative pressure of 0.6-0.8 demonstrates successful immobilization of AuCl4- ions inside the mesochannels of PMO-IL, the isotherms clearly reflect the excellent pore opening in the materials after the ion-exchange process.

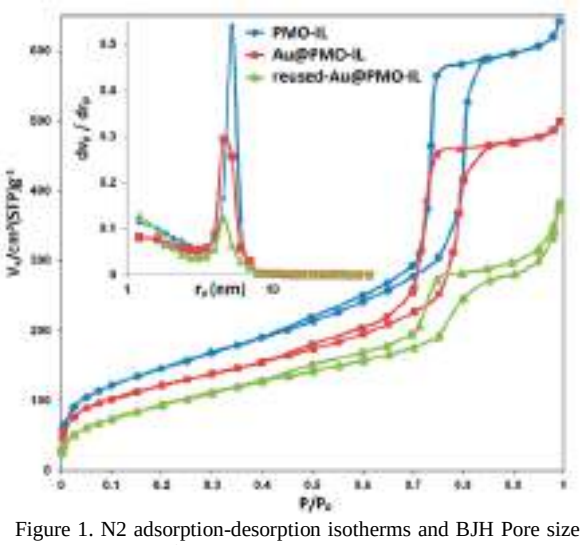

Figure 1. N2 adsorption-desorption isotherms and BJH Pore size distributions (inset) for PMO-IL, Au@PMO-IL and recovered Au@ PMO-IL.

TEM studies were performed on PMO-IL and Au@PMOIL, in order to confirm uniform mesoporous structure in the materials. The TEM image of PMO-IL (Figure 2a) clearly demonstrates formation of a long-range ordered mesoporous structure with an estimated pore size of 10 nm. On the other hand, the TEM image of catalyst Au@PMO-IL also establishes that periodicity in the mesoporous structure is retained during catalyst preparation (Figure 2b). From this image, it is clear that no formation of Au nanoparticles or aggregation occurred either on the external surface or inside the mesochannels of PMO-IL. Overall, these

finding are in good agreement with results obtained by N2 adsorption-desorption analysis (Table1).

Table 1. Textural Properties of the PMO-IL, Au@PMO-IL, and Recovered Au@PMO-IL

material	S_{BET} [a] ($m^2 g^{-1}$)	V_t [b] ($cm^3 g^{-1}$)	D_{BJH} [c] (nm)	F.G. [d] (mmol g^{-1})
PMO-IL	530	0.98	10.6	IL (1.1)
Au@PMO-IL	432	0.77	9.21	Au (0.090)
Recovered Au@ PMO-IL	355	0.58	9.2	Au (0.085)

structure with an estimated pore size of 10 nm. On the other hand, the TEM image of catalyst Au@PMO-IL also establishes that periodicity in the mesoporous structure is retained during catalyst preparation (Figure 2b). From this image, it is clear that no formation of Au nanoparticles or aggregation occurred either on the external surface or inside the mesochannels of PMO-IL. Overall, these finding are in good agreement with results obtained by N2 adsorption-desorption analysis (Table1)

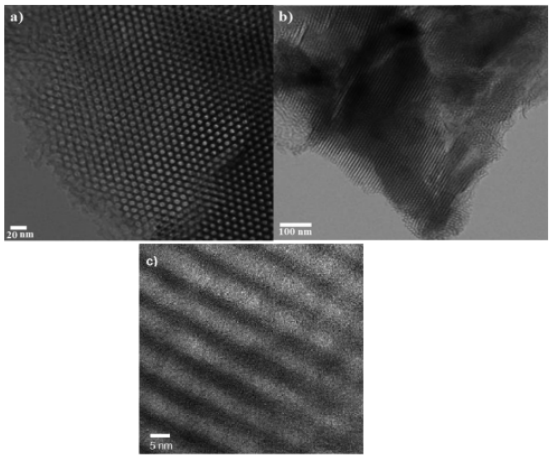

Figure 2. TEM images of PMO-IL (a) and Au@PMO-IL (b and c).

CONCLUSION

In conclusion, among three distinct Au supported catalysts onto periodic mesoporous organosilica with an imidazolium framework (PMO-IL), in situ generated gold nanoparticles inside the nanospaces of PMO-IL (Au@PMO-IL) exhibit superior activity and selectivity and high stability as well as good reusability in the aerobic oxidation of activated and nonactivated alcohols in the presence of either Cs2CO3 (35 °C) or K2CO3 (60 °C) as reaction bases under mild reaction conditions. It was found that the activity is strongly influenced by the method of generating Au nanoparticles inside the wellordered mesopore networks of PMO-IL. Our studies imply that the coexistence of Au (3+) ions and Au (0) on the surface of the catalyst plays a crucial role in enhancement of the catalytic activity. This is most likely explained by the fact that a high local Au (3+) concentration of the surface of the catalyst acts as Lewis acid and coordinates with the substrate, a feature allowing starting alcohols to be present in the nanospaces of the catalyst in high concentrations, where they can more efficiently oxidize at available Au active sites before they can be released back to the solution. The amounts of leached catalyst were very negligible (<0.2 ppm), and the catalyst was recovered in at least seven reaction cycles. The high stability and reusability of the catalyst can be attributed to the presence of ionic liquid in the catalyst, a finding that is in good agreement with a reference catalyst experiment and structural analysis of a sample of the recovered catalyst.

References

[1] M. Hudlicky, Oxidation in Organic Chemistry; ACS Monograph Series, American Chemical Society: Washington, DC, (1990).

[2] S. V. Ley, A. Madfin, B. M. Trost, I. Fleming, Pergamon Press: Oxford, UK, 7 (1991) 251−289. T.V. Krishna, T.M. Mohan, J. Chem. Thermodyn. 47 (2012) 267-275.

[3] Cole-Hamilton, D. J. Science 299 (2003) 1702−1706.

[4] 4) Y. V. Geletii, B. Botar, P. Koegerler, D. A. Hillesheim, D. G. Musaev, C. L. Hill, Angew. Chem., Int. Ed. 47 (2008) 3896−3899.

[5] S. Diez-Gonzalez, N. Marion, S. P. Nolan, Chem. Rev. 109 (2009) 3612−3676.

[6] D. J. Gorin, B. D. Sherry, F. D. Toste, Chem. Rev. 108 (2008) 3351−3378.

[7] R. Li, P. Zhang, Y. Huang, P. Zhang, H. Zhong, Q. Chen, J. Mater. Chem. 22 (2012) 22750−22755.

[8] S. Caron, R. W. Dugger, S. G. Ruggeri, H. A. Ragan, D. H. B. Ripin, Chem. Rev. 106 (2006) 2943−2989.

[9] S. E. Allen, R. R. Walvoord, R. Padilla-Salinas, M. C. Kozlowski, Chem. Rev. 113 (2013) 6234−6458.

[10] Z. Xue, J. Zhang, L. Peng, B. Han, T. Mu, J. Li, G. Yang, Chem. Phys. Chem 15 (2014) 85−89.

[11] J. Chen, Q. Zhang, Y. Wang, H. Wan, Adv. Synth. Catal. 350 (2008) 453−464.

[12] T. K. Slot, D. Eisenberg, D. van Noordenne, P. Jungbacker, G. Rothenberg, Chem. Eur. J. 22 (2016) 12307−12311.

[13] N. Gunasekaran, Adv. Synth. Catal. 357 (2015) 1990−2010.

[14] P. Sangtrirutnugul, T. Chaiprasert, W. Hunsiri, T. Jitjaroendee, P. Songkhum, K. Laohhasurayotin, T. Osotchan, V. Ervithayasuporn, ACS Appl. Mater. Interfaces 9 (2017) 12812−12822.

[15] X. Yao, C. Bai, J. Chen, Y. Li, RSC Adv. 6 (2016) 26921−26928.

29TH IRANIAN ORGANIC CHEMISTRY CONFERENCE
1_3 NOV, 2023
UNIVERSITY OF QOM, IRAN

Green synthesis of MCM-41/Ni nanocomposite and its application for catalytic oxidation of ethanol

Mahdiyeh Ebrahimzadeh[1], *Mohammad Ali Sheikh-Mohseni*[1]* *and Sajad Pirsa*[2]

[1]*Medicinal Plants Group, Shahid Bakeri High Education Center of Miandoab, Urmia University, Urmia, Iran, M.ebrhimzdh@gmail.com, m.a.sh.mohseni@gmail.com.*
2 Department of Food Science and Technology, Faculty of Agriculture, Urmia University, Urmia, Iran.

Abstract - In this research, *equisetum arvense* was used for the green synthesis of MCM-41/Ni nanocomposite. The MCM-41/Ni nanocomposite was used for modification of carbon paste electrode. The electrode was studied for ethanol electrooxidation. The electrochemical and surface characteristics of this electrode were studied by various techniques such as cyclic voltammetry and chronoamperometry, and the catalytic and electrochemical behavior of the modified electrode was studied at different pH, different scanning rates, and different ethanol concentration. The redox couple $Ni(OH)_2$/NiOOH was confirmed in the catalytic oxidation of ethanol. The calibration curve obtained by voltammetric method to investigate the catalytic oxidation of ethanol showed that the electrode can catalyze ethanol in two concentration ranges of 0.01-0.25 M and 0.25-2 M. The oxidation potential of nickel on the modified electrode surface in the presence of ethanol was 0.55 V.

1. Introduction

In the past years, environmental and energy problems have increased in the world. The need for high-efficiency energy conversion systems is now a very good demonstration because fossil fuels are being finished and the need to reduce pollution in the world [1-3]. Therefore, more attention is paid to fuel cells for environmental compatibility, high efficiency, reduced fossil fuel dependency and low temperature. Fuel cells are used as new technologies that can be used for different applications [4, 5].
Most importantly, ethanol is a green fuel that can be made through the fermentation process of sugar-containing sources such as sugar cane, wheat, corn or cellulose containing raw materials such as grass and straw. Therefore, biological ethanol (or bioethanol) is attractive [6, 7]. But the key problem in ethanol fuel cells is the low kinetic of ethanol oxidation at anode electrode. There are many researchers who study the catalytic electro-oxidation of ethanol by different nanocomposites [8, 9]. A novel, green and ecofriendly method for synthesized of nanocomposites is synthesizing with plant materials.
In this study, the MCM-41/Ni nanocomposite was synthesized by plant materials of *equisetum arvense.* This nanocomposite was used as an electrocatalyst for ethanol oxidation.

2. Results and Discussion

2.1. Electrochemical investigation of MCM-41/Ni modified electrode

The effects of potential scan rate in the range of 25 to 3000 mVs^{-1} on the response of the electrode modified with MCM-41/Ni by the CV technique as shown in Fig. 1, The first thing that can be concluded from this figure is the redox behavior of the electrode. This oxidation/reduction behavior is caused by the $Ni(OH)_2$/NiOOH redox couple on the surface of the electrode, which is shown in equation 1. It is obvious that $Ni(OH)_2$ is the oxidation product of nickel during the scanning of anodic potential. This form of nickel on the surface of the electrode is transformed into other forms as shown in equation (1).

$$Ni(OH)_2 + OH^- \longleftrightarrow NiOOH + H_2O + e^- \quad (1)$$

As shown in the inset of figure (1), the current of the anodic and cathodic peaks increases linearly with the increase of potential scan rate. This proportion shows the normal behavior of a redox substance stabilized on the surface.

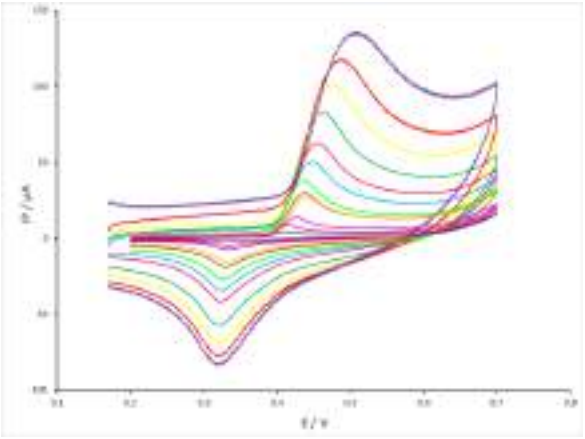

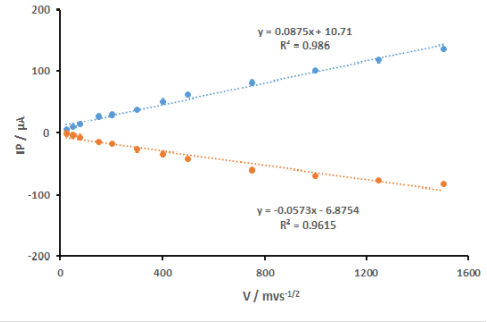

Fig.1. Top) Cyclic voltammograms of MCM-41/Ni modified electrode for different potential scan speeds (from inside to outside: 0.025, 0.05, 0.075, 0.15, 0.2, 0.3, 0.4, 0.5, 0.75, 1.0, 1.250 and 1.5 V/s). Bottom).inset: The plot of anodic and cathodic peak currents versus potential scan speed

The electrochemical behavior of modified electrode at different pH was studied using CV method (Figure 2). The results showed that the electrochemical current of the modified electrode decreases as the pH of the solution decreases. According to equation (2) and related explanations, the presence of hydroxide is necessary for proper redox activity of nickel nanoparticles. Therefore, the electrochemical activity of the Ni modified electrode disappears at pHs lower than 9. As a result, pH = 13 was chosen as the optimal pH.

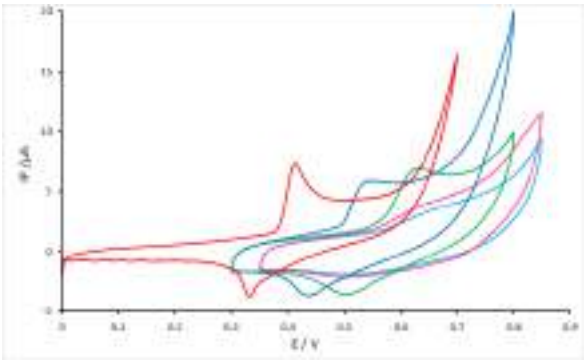

Fig.2. Cyclic voltammograms of electrode modified with MCM-41/Ni at different pH (from left to right 13, 12, 11, 10 and 9)

2.2. Electrocatalytic oxidation of ethanol on the MCM-41/Ni modified electrode

The electrocatalytic activity of the proposed electrode for ethanol oxidation was investigated by (CV) method. The cyclic voltammetric responses of the modified electrode were recorded in the presence and absence of ethanol in a solution with pH = 13.0 (Figure 3).

As this figure shows, the electrochemical behavior of ethanol oxidation during the positive scan is indicated by appearing a new peak in the forward scan at a potential of 0.55 V. In the reverse scan, a new anodic peak also appears which is related to the oxidation of ethanol [10].

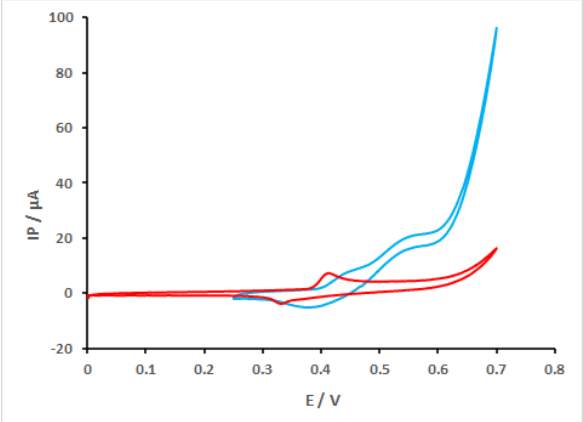

Fig.3. Cyclic voltammetry of MCM-41/Ni modified electrode in presence (blue) and absence (red) of ethanol

Therefore, it can be concluded that the anodic peak current of $Ni(OH)_2$/NiOOH redox couple increases strongly in the presence of ethanol. In fact, ethanol reacts with NiOOH on the electrode surface. These observations suggest a catalytic mechanism for ethanol oxidation at the modified electrode, which is shown in the following equations.

$Ni(OH)_2 + OH \rightarrow NiOOH + H_2O + e$ (2)

$NiOOH + Ethanol \rightarrow Ni(OH)_2 + products$ (3)

In the first step (Eq. (2)), nickel was electrochemically converted to species with a higher oxidation number, NiOOH. In the second step (equation (3)), NiOOH promotes ethanol oxidation. Therefore, there is no mechanism involving direct electron transfer from ethanol to the anode. In this mechanism, it is mentioned that there are two electrochemical processes with overlapping potential values, the oxidation of ethanol and the formation of NiOOH. Ethanol oxidation leads to the corresponding reduction of NiOOH to $Ni(OH)_2$ and NiOOH species are continuously regenerated.

The effect of potential scan rate on the electrocatalytic oxidation of ethanol on the modified electrode surface at pH=13.0 was studied. Figure 4 shows these results**.**

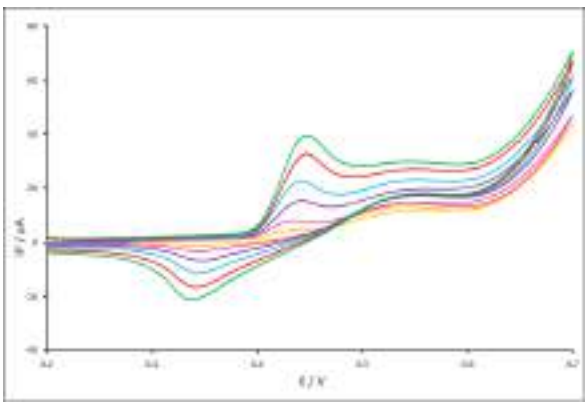

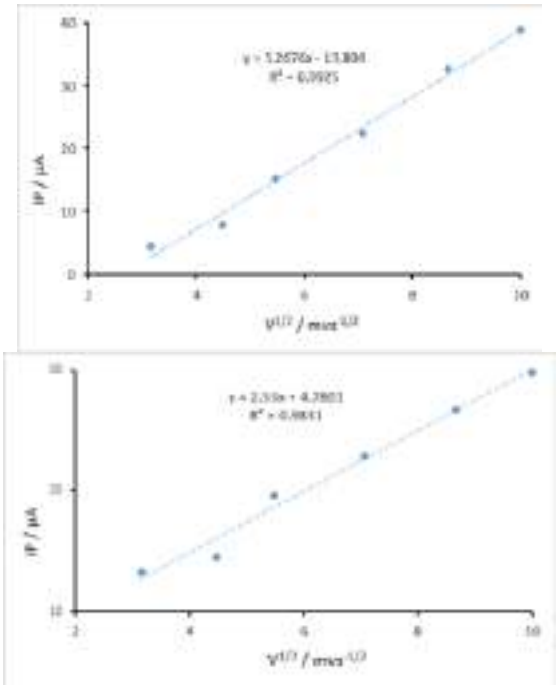

Fig.4. Cyclic voltammogram of the MCM-41/Ni modified electrode in the presence of ethanol at different potential scanning speeds (from inside to outside: 10, 20, 30, 50, 75, 100 mV/s) and pH=13

The results showed that the peak current of ethanol oxidation is proportional to the square of the potential sweep rate in the range of 10-100 mVs^{-1}, which indicates that the electrocatalytic process is controlled by diffusion. Another observation was the increase of the $Ni(OH)_2/NiOOH$ cathodic current peak with increasing scan rate. This observation can be explained by the fact that at high scan rate, there is not enough time for the reaction between NiOOH and ethanol (Equation (3)), and therefore more NiOOH remains for the $Ni(OH)_2/NiOOH$ reduction pathway stays.

2.3. Effect of pH on the catalytic oxidation of ethanol

The electrocatalytic oxidation of ethanol at modified electrode was investigated at different pH from 9 to 13 (Figure 6). The electrocatalytic current of ethanol is the highest at pH=13 and the current of ethanol decreases with the decrease of pH. This behavior is influenced by the behavior of the $Ni(OH)_2/NiOOH$ redox couple at different pHs, which was explained earlier. The electrochemical current of Ni in the electrode decreases with a decrease in the pH of the solution, and as a result, its catalytic activity decreases.

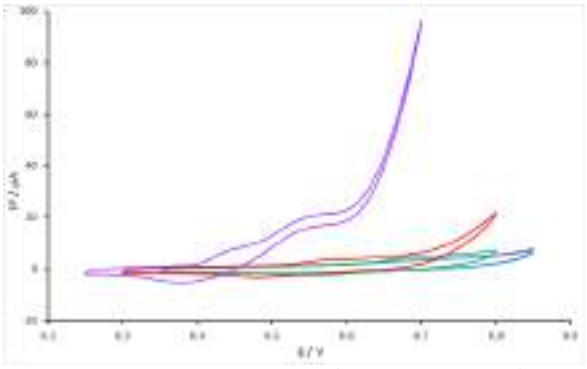

Fig.5. Electrocatalytic oxidation of ethanol on the modified electrode surface at different pH from left to right 13, 12, 11, 10 and 9.

3.4. Effect of ethanol concentration on catalytic oxidation at modified electrode surface

The ability of an electrocatalyst to catalyze oxidation of different fuel concentrations is an important factor. Therefore, the CV method was used to investigate the catalytic oxidation of ethanol at different concentrations. The obtained cyclic voltammograms as shown in Fig. 7, As can be seen, with the increase in ethanol concentration, the catalytic peak current also increases. This behavior is linear from 10 mM to 2 M ethanol concentration and with two different slopes (inset of Figure 6). It can also be concluded that the performance of the proposed electrocatalyst is highest at a concentration of 2 M ethanol.

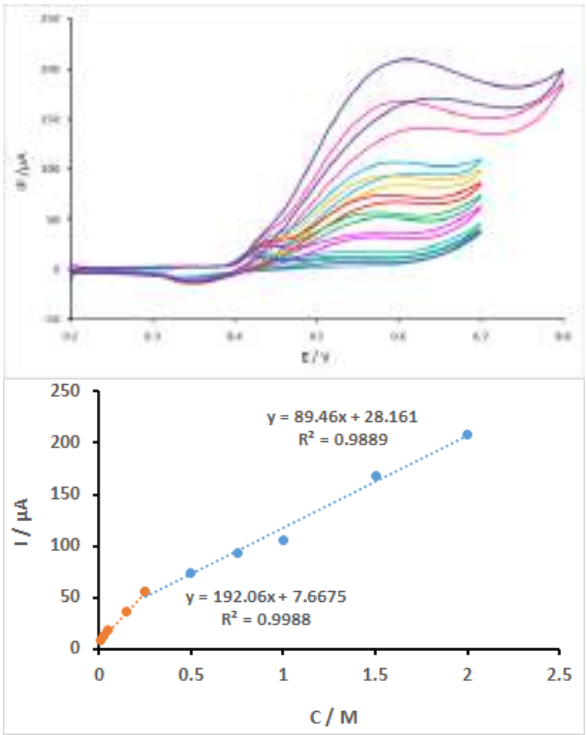

Fig.6. Catalytic oxidation of modified electrode in different concentrations of ethanol (from bottom to top): (0.01, 0.025, 0.05, 0.1, 0.15, 0.25, 0.5, 0.75, 1, 1.5, 2M)

3. Conclusions

In this study, the MCM-41/Ni nanocomposite was synthesized by plant materials of *equisetum arvense*. This nanocomposite was used as an electrocatalyst for ethanol oxidation. The role of $Ni(OH)_2$/NiOOH redox couple in the catalytic oxidation of ethanol was confirmed. The calibration curve obtained by voltammetric method to investigate the catalytic oxidation of ethanol showed that the electrode made in two concentration ranges of 0.01-0.25 M and 2-0.25 M can catalyze ethanol. The oxidation potential of nickel on the modified electrode surface in the presence of ethanol was 0.55 V.

4. References

[1] E. Serrano, G. Rus, J. Garcia-Martinez, Nanotechnology for sustainable energy, Renew. Sust. Energ. Rev. 13 (9) (2009) 2373–2384.

[2] P.D. Lund, Effects of energy policies on industry expansion in renewable energy, Renew. Energy 34 (1) (2009) 53–64.

[3] J. Twidell, T. Weir, Renewable Energy Resources, 3rd edition, Routledge, London, 2015.

[4] Y. Qiao, C.M. Li, Nanostructured catalysts in fuel cells, J. Mater. Chem. 21 (12) (2011) 4027–4036.

[5] M. Liu, R. Zhang, W. Chen, Graphene-supported nanoelectrocatalysts for fuel cells: synthesis, properties, and applications, Chem. Rev. 114 (10) (2014) 5117–5160.

[6] D. Chiaramonti, M. Prussi, M. Buffi, A.M. Rizzo, L. Pari, Review and experimental study on pyrolysis and hydrothermal liquefaction of microalgae for biofuel production, Appl. Energy 185 (2017) 963–972

[7] H. Zabed, J.N. Sahu, A. Suely, A.N. Boyce, G. Faruq, Bioethanol production from renewable sources: current perspectives and technological progress, Renew. Sust. Energ. Rev. 71 (2017) 475–501.

[8] M. Yaldagard, et al. "Ethanol Electro-Oxidation on Catalysts with S-ZrO2-Decorated Graphene as Support in Fuel Cell Applications." Nanomaterials 12.19 (2022): 3327.

[9] V. Hassanzadeh, M.A. Sheikh-Mohseni, and B. Habibi. "Catalytic oxidation of ethanol by a nanostructured Ni-Co/RGO composite: Electrochemical construction and investigation." Journal of Electroanalytical Chemistry 847 (2019): 113200.

[10] M. Fleischmann, K. Korinek, and D. Pletcher. "The oxidation of organic compounds at a nickel anode in alkaline solution." Journal of Electroanalytical Chemistry and Interfacial Electrochemistry 31.1 (1971): 39-49.

Green synthesis of silver nanoparticles using aqueous extract of *Olive Leaf (Olea europaea L. folium)*

Atefeh Golkari [a], *Nasrin Mollania* *[a], *Fariba Mollania* [b], *Toktam Hajjar* [a]

[a] *Department of Biology, Faculty of Basic Sciences, Hakim Sabzevari University, Sabzevar, Iran,*
biochemhsu@gmail.com

[b] *Department of plant production, University of Torbate Heydarieh, Iran.*

Abstract

Today, nanotechnology and the production of nanomaterials have become one of the fields of application in the field of biomedicine.

Silver nanoparticles (AgNPs) have antibacterial, antifungal, and antiviral properties. This study aims to synthesize AgNPs using Olive leaf extract and to optimize the synthesis conditions. The parameters such as pH, reaction temperature, and time were evaluated for this purpose.

Nanoparticles produced using different techniques have been investigated. The UV-Vis peak at 426 nm indicated the presence of the mentioned nanoparticles. The AgNPs formation with an approximate size of 22 nm was confirmed by dynamic light scattering (DLS). This study demonstrates the potential of plant extracts as a safer, cheaper, and more environmentally friendly method for nanoparticles synthesis instead of chemical ways.

Keywords: Silver nanoparticle, Aqueous extract of *Olive leaf*, Dynamic light scattering

1. Introduction

Nanotechnology is a vast interdisciplinary field of research, development, and industrial activity that has been growing rapidly worldwide in the last decade. The increasing use of nanotechnology-based materials offers new solutions to previously unsolved problems [1].

In the last two decades, AgNPs have attracted the attention of researchers due to their wide applications in various fields. AgNPs play a significant role in biology and medicine due to their physical and chemical properties.

The strong toxicity of silver against a wide range of microorganisms is well known, and AgNPs have recently been shown to be a promising antimicrobial agent [2].

AgNPs have anti-inflammatory, antiviral, anti-angiogenic, and anti-platelet activity and cytotoxicity against cancer cells [3, 4].

Many synthesis methods are very expensive and also involve the use of toxic and hazardous chemicals, which may pose potential environmental and biological hazards. Although chemical and physical methods are commonly used for AgNPs synthesis, finding a new effective green synthesis method is crucial to reducing environmental impact. [5].

Biosynthesis is an eco-friendly and reliable method that uses natural agents such as plant extracts, fungi, and microorganisms to produce AgNPs [6].

The use of plant extracts for the biosynthesis of AgNPs has become important in recent years due to the increase in the chemical, physical, biological, and optoelectronic properties of the particles formed by this green process [7].

In many green syntheses, the reduction of silver ions (Ag^+), which was an important step for the production of AgNPs, was performed by secondary metabolites in plant extracts such as proteins, alkaloids, saponins, amino polysaccharide proteins, tannins, and enzymes [8].

Green synthesis of AgNPs using different plant parts extract has been successfully exploited. The olive leaf extract has medicinal properties and therefore it has many metabolites with high antioxidant properties. Therefore, it can be a good candidate for the synthesis of nanoparticles [9].

For example, the natural polyphenols show a wide range of biological activities. Natural polyphenols extracted from Olive leaf has gained popularity in recent days due to several beneficial functions in the

human system. Polyphenols extracted from Olive leaf has anti-inflammatory, anti-tumorogenic, anti-thrombotic, anti-atherogenic, anti-allergic, and anti-inflammatory properties. furthermore, due to high antioxidant potential, the polyphenols can be effective in green synthesis of various nanoparticles [10].

2. Material and methods

2.1 Material

Olive leaf was collected from Sabzevar city of Khorasan Razavi province. AgNO3 salt was purchased from Riedel-deHaën/Sigma-Aldrich (St. Louis, MO, USA). Caustic soda (NaOH) and hydrochloric acid (HCl), obtained from Merck, were used to adjust the extract's pH.

2.2 Preparation of aqueous extract

Olive leaf was collected and washed with deionized water to remove contamination and dried in a dark environment, then the powdered plant samples (10% V/W) were added to an Erlenmeyer. Then, the mixture was heated at 80°C for 30 min with stirring, and the plant's secondary metabolites were separated.

2.3 Synthesis of silver nanoparticles with *Olive leaf* extract

First, the pH of the plant extract was measured. Then, the extract was mixed with AgNO3 at concentrations ranging from 1 to 3 mM to synthesize AgNPs. This mixture was placed at 60°C for 220 minutes at 180 rpm. The reaction mixture turned to a dark brown colour from a brownish-yellow colour within 20 min indicating the synthesis of silver nanoparticles.

Then, the obtained nanoparticles were centrifuged for 20 min at 12,000 rpm for segregation of brown sediment. The UV-Vis method was used to study the synthesis rate of nanoparticles. After optimizing, AgNPs were suspended in deionized ultrapure water and the hydrodynamic particle size was determined by the dynamic light scattering (DLS) technique.

3. Result and Discussion

For nanoparticle biosynthesis analysis, the UV-Vis method was used and the highest absorption peak was observed at 426 nm (Fig. 1). The various factors have an effect on the morphology of AgNPs. In this study, the effect of pH, silver nitrate concentration, temperature, and time were the factors that were investigated in the green synthesis of AgNPs by olive leaf.

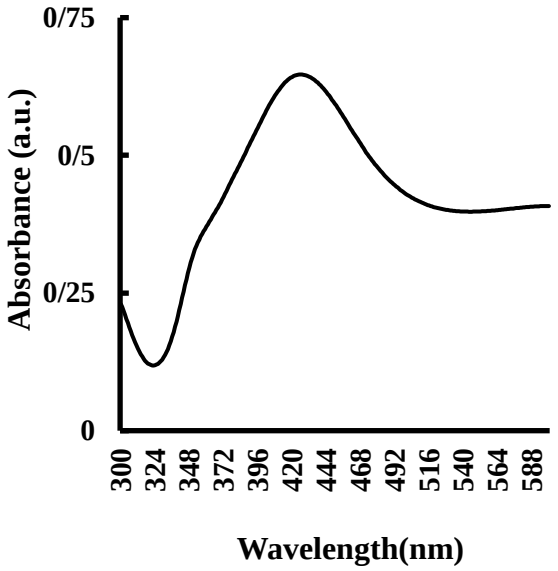

Fig. 1. UV-visible spectra of synthesized AgNPs.

Based on the results, the temperature was found to be an important factor influencing the size, shape, and efficiency of the desired nanoparticle due to the Increased mobility of silver ions at higher temperatures. By examining different pHs, it was realized that the optimal synthesis was done at pH = 8 (Fig. 2). After comparing different times, it was found that the optimum synthesis was obtained at 220 min. The final effective factor was the silver salt concentration. The best UV-Vis peak at 426 nm was obtained with a final concentration of 2 mM.

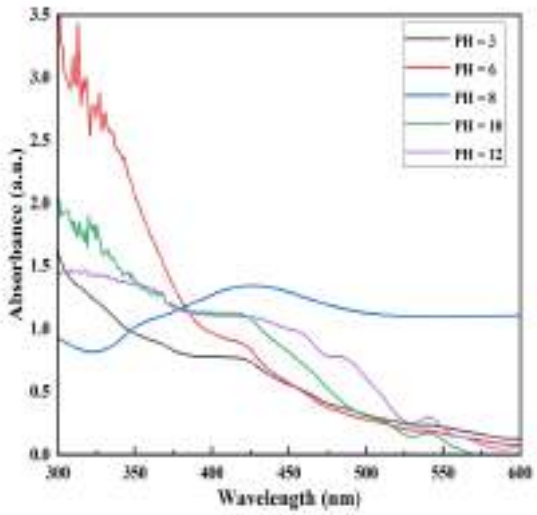

Fig. 2: The effect of pH on nanoparticle biosynthesis.

Fig. 3 shows the DLS pattern of the biosynthesized AgNPs using Olive tree leaf extract. The histogram analysis presented that the average size of synthesized nanoparticles was 22 nm.

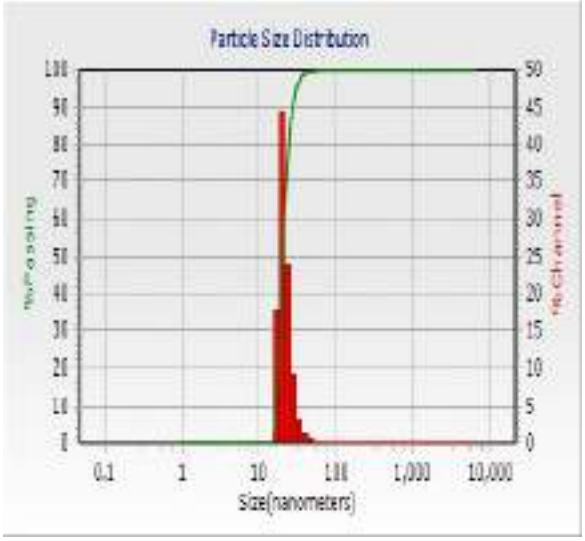

Fig. 3. Particle size distribution analysis of synthesized AgNPs by DLS technique.

4. Conclusion

Based on the above study, it is clear that the olive leaf plant has many medicinal properties and is also a suitable option for the production of AgNPs. One of the advantages of producing nanoparticles by plants is their cost-effectiveness, low risk, and environmental compatibility. On the other hand, these nanoparticles were might functionalized by the functional groups of plant metabolites. Functionalized nanoparticles are useful for drug immobilization and delivery.

5. References

1. Y. Sun, B. Mayers, T. Herricks, and Y. Xia, Nano Lett., 3 (2003), 955-960.
2. H. Li, G. Si-ying, W. Hao, L. Xue-pin, H. Qiang, S. Bi. Mater. Sci. Eng. 32 (2012), 1050-1056.
3. M.N. Nadagouda, G.E. Hoag, R.S. Varma, J. Collins, Crystal Growth & Design, 9 (2009), 4979-4983.
4. M. Safaepour, A. Reza Shahverdi, H. Reza Shahverdi, M. R. Khorramizadeh, and A.R. Gohari. Avicenna J Med Biotechnol, 1 (2009) 111.
5. H. Duan, D. Wang, and Y. Li, Chem. Soc. Rev, 44 (2015), 5778-5792.
6. R. K. Das, V. L. Pachapur, L. Lonappan, M. Naghdi, R. Pulicharla, S. Maiti, M. Cledon, L. M. A. Dalila, S. J. Sarma & S. K. Brar. Nanotechnol. Environ. Eng, 2 (2017) 1-21.
7. M. Valle-Orta, D. Diaz, P. Santiago-Jacinto, A. Vázquez-Olmo, and E. Reguera. J. Phys. Chem. B, 112(2008), 14427-14434.
8. P. Khandel, R. K. Yadaw, D. K. Soni, L. Kanwar & S. K. Shahi. J. Nanostructure Chem. 8 (2018) 217-254.
9. H.M. Alhajri, B.M. Alrfaei, W.S. Alqahtani, S. Alterary, J. Nanophotonics, 15(2021), 036003-036003.
10. A. E. Mahmoud, S. A. Fathy, M. M. Ali, M. K. Ezz, A. T. Mohammed, Grasas Aceites, 69 (2018), 1-12.

29TH IRANIAN ORGANIC CHEMISTRY CONFERENCE
1_3 NOV, 2023
UNIVERSITY OF QOM, IRAN

DFT investigation on $B_{12}N_{12}$ fullerene as SO_2 and COS sensors

*Somayeh Hassani, Afsaneh Maleki**

Department of Chemistry, Omidiyeh Branch, Islamic Azad University, Omidiyeh, Iran,
somaye.*hasani5771*@gmail.com

Abstract

Today, air pollution is one of the most important environmental problems that most developing countries face. The aim of this research work is to investigate the surface adsorption of COS, SO_2 gases on $B_{12}N_{12}$ nanocages and also COS on $AlB_{11}N_{12}$ by computational method. For this purpose, different adsorption arrangements were considered for the absorption of COS gas on the surface of these nanocages, and the desired structures were calculated using the density functional theory (DFT) method using the B3LYP method and using the G+6-31 basis set (d) was optimized.
The negative values of the surface adsorption energy showed that the interaction of gases with nanostructures is experimentally possible. The negative values of enthalpy changes and Gibbs free energy changes showed that the surface adsorption of gases on the adsorbent surface is exothermic and spontaneous. Calculations related to adsorption energy (Eads) and parameters related to chemical activity such as energy gap (Egap), chemical hardness (η), chemical potential (μ), electrophilicity coefficient (ω) and dipole moment of gases were performed on boron nitride nanocages. .
The results show that doping $B_{12}N_{12}$ nano cages with aluminum atoms increases the reactivity of its surface. The values of absorption energy and calculated thermodynamic parameters show that $AlB_{11}N_{12}$ nano cages have better activity than $B_{12}N_{12}$, which is due to the presence of doped aluminum atoms in this nanostructure.
Keywords: $AlB_{11}N_{12}$, $B_{12}N_{12}$, carbonyl sulfide, surface absorption, density dependence theory.

1. Introduction

The current era can be called the carbon era due to the extensive use of carbon in all industrial fields. Since carbon is one of the most amazing elements in nature and has many uses in all areas of human life, the use of this precious element is developing day by day. [1] Carbon in nature has five solid allotropes other than diamond, graphite, nanotube, amorphous carbon and fullerene. that the use of any of the other forms will help people in different fields. One of these elements that researchers use today is fullerene. Since fullerenes are cage-like molecules and have a truncated geometrical shape, one of the researchers' concern is to find a suitable carrier to use this wonderful element. [2]

Borne nitride nanostructures are one of the important nanocarriers whose applications in various aspects have recently received a lot of attention. Boron nitride is a chemical compound with the formula BN, which consists of equal numbers of boron and nitrogen atoms. These nanostructures have attracted the attention of researchers due to a wide range of prominent features such as special mechanical properties, high thermal and chemical resistance, high biocompatibility, the ability to interact with organic molecules, excellent resistance to oxidation at high temperatures, high thermal conductivity, etc. Researchers have been placed. [3]

Since boron nitride is a refractory and chemically resistant chemical compound, the appearance of this compound is colorless crystals. This compound exists in various crystal structures that have the same electrons as a carbon lattice with a similar crystal structure. One of the most important nanostructures that has attracted the attention of many researchers today is the $B_{12}N_{12}$ nanocages. This nanocages is one of the smallest stable boron nitride fullerenes. The $B_{12}N_{12}$ nanocage contains six four-membered rings and eight six-membered rings. In this nanocage, there are two specific N-B bands, one is shared between two six-membered rings and the other is shared between four and six-membered rings. [4]

Today, many hazardous wastes are abundant in nature and these wastes cause gases such as carbonyl sulfide. Carbonyl sulfide is a colorless gas similar to rotten eggs, and it is thought that carbonyl sulfide is the most abundant gas in the troposphere, which is located in the troposphere layer of clouds. Today, due to the importance and wide spread of using different sensors as chemical and physical sorbents and the expansion of the use of different nanocages such as boron nitride nanocages in the industry, many

researchers have been encouraged to use adsorbents. As we know, absorption in nanocages is divided into two physical and chemical levels. Physical absorption is a reversible phenomenon that is the result of attractive forces between solid molecules and the absorbed substance. In this type, there is attraction between molecules and internal forces, one of these forces is van der Waals. Vandals is a very weak force that attracts two molecules to each other, this force does not include electron exchange and chemical bond formation. Chemical adsorption or activated surface adsorption is the result of chemical interactions between the solid and the adsorbed substance. Since the strength of the resulting chemical bond changes significantly in different situations and the identification of chemical compounds is practically difficult, the adhesive forces are usually greater than what is present in physical adsorption. Usually, chemical bonds are strong bonds that have about 100 times the absorption energy of physical absorption. The heat released in chemical absorption is usually high and around the heat of a chemical reaction. The chemical process is generally irreversible, and chemical changes are observed in it with the initial removal and separation of the adsorbed substance. [1]

2. Computational methods

First, the structure of $B_{12}N_{12}$ fullerene was drawn with Nanotube Modeler software. Then the structures of COS and SO_2, fullerene $B_{12}N_{12}$, fullerene doped with aluminum were prepared using Gauss View 3.1 software and geometric optimization was done on them by Gaussin. It should be noted that all calculations were considered at a temperature of 15.298 K and a pressure of 1 atmosphere. All calculations were done using density functional theory and B3LYP/6-31G(d) basis series. This basic series was chosen because in many studies, the results obtained from the basic series were in good agreement with the results.

The studied reaction is generally as follows:

gas+nano cage→gas⁄(nano cage (complex)) (1)

The following formulas are used to calculate the chemical adsorption energy (Ead), enthalpy changes (ΔH), Gypsum free energy changes (ΔG), and entropy (ΔS).

E_ad=(E_complex-(〖 E〗 _(nano cage)+E_gas)) (2)

ΔH=(H_complex-(H_(nano cage)+H_gas)) (3)

ΔG=(G_complex-(G_(nano cage)+G_cos)) (4)

ΔS=(S_complex-(S_(nano cage)+S_cos)) (5)

In relation number 2, E represents the total electron energy of each carbonyl sulfide structure, nanostructure and carbonyl sulfide-fullerene complex after geometric optimization. In relation 3, H is the enthalpy symbol of the studied material. The symbol G in Equation 4 is intended to represent the Gypsum free energy of each structure, which is obtained by adding the total electron energy of each structure with the thermal Gypsum free energy. The symbol S in relation 5 is used to show the entropy of each of the studied structures.

Parameters related to molecular orbitals, including the percentage of gap energy changes (ΔEg), chemical hardness (η), chemical potential (μ) and electrophilicity (ω) were calculated from relations 6 to 9.

ΔE_g=[(E_g2-E_g1)/E_g1]*100% (6)

Eg1 = gap energy of nano cage

Eg2 = energy gap of nano cage complex and gas

η= ((E_LUMO-E_HOMO))/2 (7)

μ= ((E_LUMO+E_HOMO))/2 (8)

ω = μ^2/2η (9)

In the relationships mentioned above, ELUMO and EHOMO are the energy of the lowest unoccupied molecular orbital and the energy of the highest occupied molecular orbital, respectively. [5]

3. Results and discussion

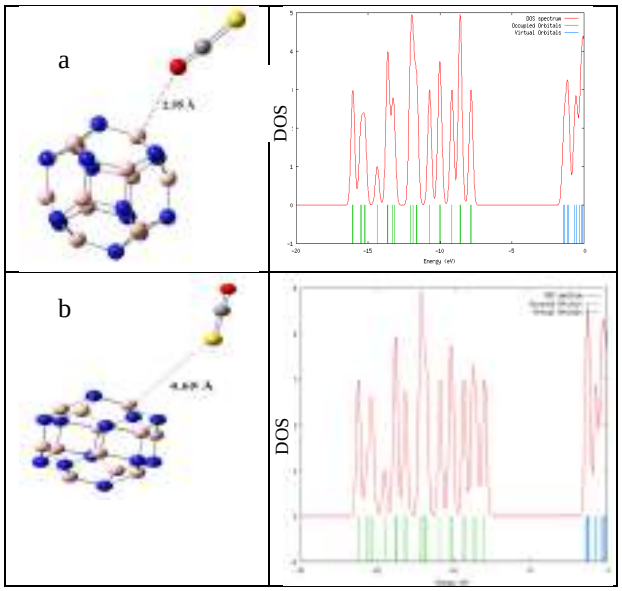

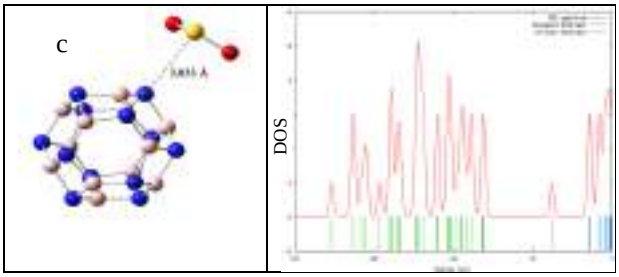

Fig. 1 Models for stable adsorption of COS and SO_2 on the $B_{12}N_{12}$ and their density of state (DOS).

Table 1. HOMO energies (E_{HOMO}), LUMO energies (E_{LUMO}), HOMO–LUMO energy gap (Eg), and Fermi level energy (E_F) of systems.

Structures	Q on gas	d (Å)	HOMO (eV)	LUMO (eV)	ΔE_g (%)	μ_D (Debye)	E_F (eV)	η (eV)
$B_{12}N_{12}$	-	-	-7.71	-0.86	0	0	-4.29	3.43
COS-O/$B_{12}N_{12}$ (a1)	0.08	2.95	-7.85	-1.53	-7.74	1.35	-4.69	3.16
COS-S/$B_{12}N_{12}$ (a2)	0.003	4.65	-7.98	-1.34	-3.07	0.81	-4.66	3.32
SO_2/$B_{12}N_{12}$	0.45	3.03	-8.08	-3.78	-37.2	2.22	-5.93	2.15

Table 2. Adsorption energy (Ead, kcal/mol), HOMO energies (E_{HOMO}), LUMO energies (E_{LUMO}), HOMO–LUMO energy gap (Eg), and Fermi level energy (EF) of systems

Structures	E_{ad} (Kcal/mol)	ΔH_{ad} (Kcal/mol)	ΔS_{ad} (Kcal/mol)	ΔG_{ad} (Kcal/mol)
COS/$B_{12}N_{12}$(a)	-17.69	-16.8۱	-14.0۸	-12.61
COS/$B_{12}N_{12}$(b)	-16.99	-16.68	-14.4۲	-12.38
SO_2/$B_{12}N_{12}$ (c)	-15.51	-14.8۰	-27.15	-6.75

4.conclusion

The purpose of this research is to investigate the absorption of carbonyl sulfide (COS) and sulfur dioxide (SO_2) polluting gases on $B_{12}N_{12}$ and $AlB_{11}N_{12}$ nanocages. Different absorption arrangements have been considered for COS gas absorption on the surface of these nanocages. The desired structures were optimized using the density functional method (DFT) and using the G(d)+6-31 basis set.

Based on the adsorption energy, the formation of COS/$B_{12}N_{12}$ complex is slightly more favorable than SO_2/$B_{12}N_{12}$, which shows that $B_{12}N_{12}$ is a better adsorbent for COS than SO_2. Also, doping the boron nitride nano cage has led to better absorption of COS. Energy gap results show that Al doped nanocage is electronically more sensitive to the presence of COS molecule and is a better sensor compared to pure nanocage. But the pure $B_{12}N_{12}$ nanocage is a better sensor for SO_2 than COS. The absorption of COS gas from the oxygen side was better than from the sulfur side on both nanocages.

5. References

[1] G. Tschumper., Kenny B.; Cundari, Thomas R. (eds.). ReViews in Computational Chemistry. Vol. 26. John Wiley & Sons. (2008). pp. 3990.

[2] M .Tosali , A.Naqipour. http://chemistrytechnology.98.ir.
.

[3] A.Arefe, R, Asmkhani, Department of Chemistry, 2018.

[4] E. Vessally, M.D. Esrafili, R. Nurazar, P. Nematollahi, A. Bekhradnia, , Structural Chemistry.(2017). Vol 28, pp735-748.

[5] M.Sarostani, Scientific Research Journal of Advanced Materials and New Coatings, Volume 1, No.

29TH IRANIAN ORGANIC CHEMISTRY CONFERENCE
1_3 NOV, 2023
UNIVERSITY OF QOM, IRAN

Investigation of stability of guanine and its tautomers in DNA and RNA

*Fatemeh Razavi, Shapour Ramazani**

Department of Chemistry, Faculty of Science, University of Yasouj, Yasouj, Iran, razavineda59@gmail.com
shapour.ramazani@gmail.com

Abstract

In the present research, 16 guanine tautomers were investigated. These tautomers were all the production of N_1 to O_{11} main hydrogen translocation. Some of these tautomers were reported for the first time in the gas and aqueous solution phase. G_1 and G_5 were the most stable tautomers in gas and aqueous solution phase, respectively. The potential energy surface of 16 tautomers and 15 transition states was determined. Since the stability of rare tutomeric forms had a significant effect on stabilization of anomalous DNA (deoxyribonucleic acid) double helix and spontaneous mutation, relative energies of all trajectories were determined.

1. Introduction

Polymeric double strand molecule DNA, which composed of only four types of monomeric organic bases, is the chemical basis of heredity. The organic bases include adenine (A), guanine (G), cytosine (C), thymine (T), and uracil (U). Nucleic acids can adopt complex three-dimensional structures in RNA and DNA, and RNA in turn, can catalyse biochemical reactions in order to regulate a wide variety of biological processes. Such chemical versatility is partly due to the phenomenon of *nucleobase tautomerism*, whereby the bases can adopt both multiple and distinct isomeric forms, known as *tautomers*. For nucleobases, tautomers molecules are known as structural isomers that differ from each other by the position of hydrogen atom and a double bond. Some changes may result in the DNA sequence alteration i.e nucleotides sequence of an organism that called Mutation. While most of these point mutations are benign, they might have various functional consequences, including changes in *gene expression* or *alterations in encoded proteins* so studying the effect of tautomers on biological processes is very important for researchers which helps to develop new therapeutic interventions to reduce harmful mutational events and genetic. *Guanine* with the formula $C_5H_5N_5O$, alternatively as 2-amino-6-hydroxypurine (2-amino-9*H*-purin-6(1*H*)-one) is one of the most important nucleic acid bases existing in both deoxyribose nucleic acid (DNA) and ribonucleic acid (RNA). Here we are challenging to identify *guanine* tautomers by ab initio calculations. In fact, theory and experiments are complementary to each other so no wonder to say that application of theoretical calculations were urgent to devote relatively higher energy tautomers of guanine in the gas phase [1].

3. Results and Discussion

All *ab initio* calculations were carried out using Gaussian09 at 298.15 K optimizing the gas and solvent phase geometries including reactants, products and transition states at the MP2/6-311++g(d,p). In order to attain more accurate energies for the stationary points along the PES, single-point calculations were carried out on the optimized MP2 geometries at the CCSD(T) level with the 6-311+g(d) basis set [2,3]. Harmonic vibrational frequencies were obtained at MPWB95 level with the 6-31+g(d,p) basis set [4]. The harmonic frequencies were scaled by a factor of 0. 9501 to increase their alignment with the vibrational frequencies beheld in the experimental setting [5]. In order to identify all stationary points, the connection between desired reactants and products was confirmed by conducting minimum energy path (MEP) calculations in in such a way that all calculated transition states became the subject in order to calculate the intrinsic reaction coordinate (IRC) [6].

4. Conclusions

In this article those tautomers of guanine which can be created from hydrogen abstraction from N_1 to O_{11} i.e. N_1-H→ O_{11} were investigated. Fig. 1 provides a depiction of the under consideration molecules, which are the result of 15 distinct reactions and labelled as R1 to R15. Table 1 presents the Relative energies of all guanine tautomers at different levels of theory (in kJ/mol^{-1}) in gas and aqueous phases Fig. 2 represents the energy diagram of guanine and its tautomers at the CCSD (T) level in gas and aqueous solution phase. Reaction coordinate calculation (IRC) was utilized to acquire the potential energy surface of the pathway.

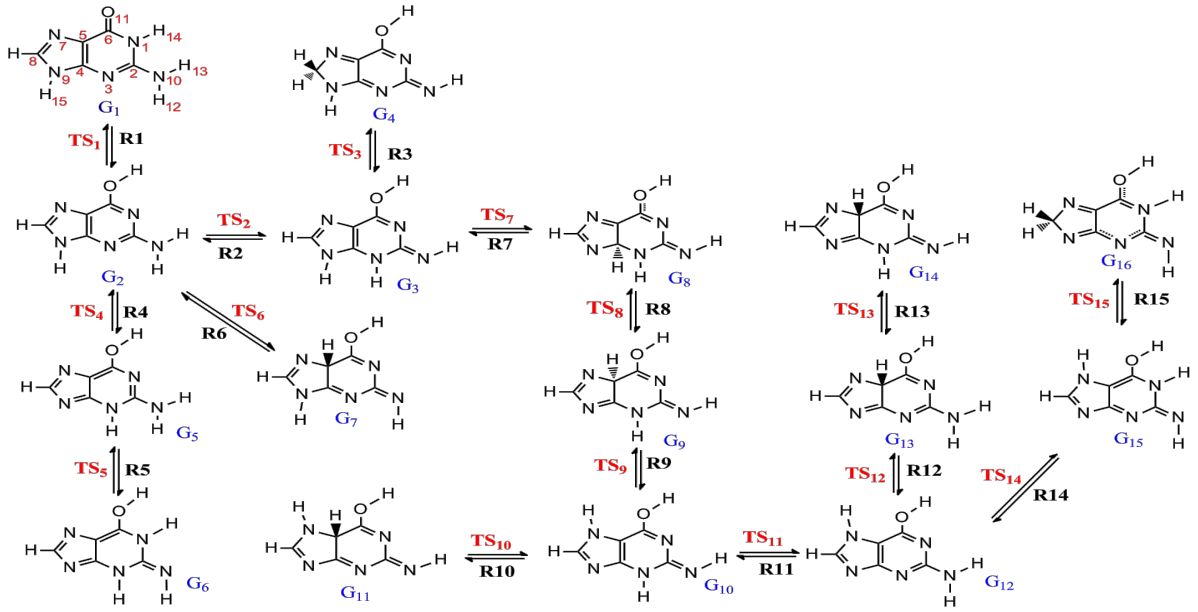

Fig 1. Isomerisation diagram for tautomers of guanine

Table 1. Relative energies of all guanine tautomers at different levels of theory (in kJ mol^{-1}) in gas (and aqueous) phases.

R	Mp2	mpwb95	CCSD	CCSD(T)	ZPE
G1	0.00 (0.00)	0.00 (0.00)	0.00 (0.00)	0.00 (0.00)	315.29 (314.84)
G2	0.75 (19.92)	-1.68 (24.31)	1.60 (23.75)	0.31 (21.6)	315.55 (314.55)
G3	98.36 (100.79)	93.97 (99.92)	94.36 (99.4)	93.9 (98.67)	314.13 (313.24)
G4	188.05 (188.31)	195.48 (197.63)	168.23 (169.67)	163.53 (165.61)	311.10 (302.42)
G5	59.48 (-3.72)	60.81 (59.92)	65.64 (66.81)	61.64 (62.95)	314.80 (314.01)
G6	141.44 (58.87)	138.96 (136.69)	139.37 (141.87)	137.07 (138.83)	312.84 (313.46)
G7	174.80 (182.84)	189.61 (197.6)	151.43 (160.59)	149.55 (159.06)	312.06 (311.84)
G8	213.11 (239.24)	236.97 (267.25)	189 (-34.92)	186.05 (215.04)	312.12 (312.13)
G9	159.12 (182.57)	166.07 (193.44)	134.97 (160.67)	133.52 (159.11)	312.77 (312.84)
G10	81.29 (97.08)	74.66 (93.56)	76.71 (94.83)	75.52 (93.43)	314.28 (313.62)
G11	188.79 (186.82)	202.72 (197.9)	162.04 (165.14)	158.60 (162.42)	311.85 (312.00)
G12	12.86 (27.63)	11.85 (32.18)	14.86 (31.7)	12.00 (28.52)	314.78 (314.23)
G13	145.95 (158.41)	147.73 (161.83)	123.94 (138.18)	120.86 (135.25)	312.06 (311.16)
G14	159.12 (181.62)	166.07 (192.48)	134.98 (159.32)	133.53 (157.81)	312.77 (311.88)
G15	165.16 (147.69)	154.16 (140.42)	158.76 (144.31)	154.62 (140.67)	311.04 (311.85)
G16	289.09 (265.17)	298.31 (278.13)	281.35 (352.61)	271.04 (340.85)	307.10 (307.37)
TS1	142.19 (2282.10)	142.13 (156.01)	158.13 (169.35)	148.68 (159.72)	301.57 (293.74)
TS2	218.83 (2372.87)	218.42 (239.81)	237.85 (255.76)	227.2 (244.60)	299.58 (291.88)
TS3	2683.43 (2695.87)	590.41 (619.68)	589.80 (616.19)	551.87 (577.76)	287.33 (285.85)
TS4	270.38 (2434.37)	284.05 (308.07)	302.46 (324.15)	286.19 (307.69)	299.15 (292.43)
TS5	258.86 (2398.35)	260.12 (262.91)	281.21 (282.30)	270.18 (271.18)	287.79 (287.31)
TS6	394.73 (2565.40)	418.80 (431.66)	421.05 (431.85)	402.77 (413.40)	298.69 (290.17)
TS7	2467.50 (2479.86)	325.42 (352.76)	344.45 (370.13)	324.01 (349.40)	291.70 (290.84)
TS8	2449.8 (2461.43)	296.32 (322.39)	310.88 (334.48)	294.17 (317.92)	293.91 (293.28)
TS9	2435.97 (2454.49)	284.48 (314.19)	306.56 (334.78)	287.78 (315.97)	292.58 (291.45)
TS10	2686.61 (2533.40)	471.76 (449.76)	559.61 (562.72)	528.00 (535.34)	286.80 (290.27)
TS11	219.52 (2376.95)	218.71 (241.90)	239.72 (259.78)	227.2 (247.08)	299.67 (292.21)
TS12	2397.46 (2408.73)	238.07 (262.80)	265.39 (287.01)	244.64 (266.29)	292.51 (291.36)
TS13	325.3 (2488.72)	331.12 (351.81)	324.65 (343.13)	312.95 (331.43)	297.23 (288.97)
TS14	247.57 (2385.73)	243.72 (248.11)	265.09 (265.55)	253.07 (254.00)	297.94 (291.54)
TS15	2538.95 (2515.37)	370.84 (359.88)	404.77 (396.14)	378.5 (371.86)	290.20 (291.12)

Fig.2 The energy diagram of guanine and its tautomers at the CCSD (T) level in gas (black) and aqueous solution (red) phase

The PES of the path is presented in Fig. 3. whole transition state molecules were observed and determination of their imaginary frequency provided an evidence for these molecules to be as the activated complex of the pathway with the lowest energy state. Table 2 demonstrates the Imaginary frequency and structures of transition states at the MPWB95 level. The relative free energy, enthalpy and entropy of different structures are shown in table 3.

Four types of hydrogen transfer reactions were detected: N-H→C (R1, R3, R6, R7, R10, R12, R15), C-H→N (R9), C-H→C (R8), N-H→N (R2, R4, R5, R11, R13, R14). The aforementioned reactions are classified into two distinct categories depending on the produced production: enol and amine functional groups (R1, R4, R11, R12), enol and imine functional groups (R2, R3, R5, R6, R7, R8, R9, R10, R13, R14, R15). The stability of given sequence G_1 to G_{16} can be presented in ascending order as follows: In gas phase:

G_1>G_2>G_{12}>G_5>G_{10}>G_3>G_6>G_{13}>G_9>G_{14}>G_{15}>G_7>

G_4>G_{11} >G_8>G_{16}

In solvent phase:

G_5>G_1>G_2>G_{12}>G_6>G_{10}>G_3>G_{15}>G_{13}>G_{14}>G_9>G_7>

G_{11}>G_4> G_8>G_{16}

As shown in figure 1, First reaction started with the relocation of hydrogen from N_1 to O_{11} in G_1 [2-amino-1H-purin-6(9H)-one] and creation of G_2 [2-amino-9H-purin-6-ol] (R1). G_1 and G_2 were connected through TS_1 transition state (planar transition state with 1958.70i (1981.22i) cm^{-1} imagine frequency) with 148.68 (159.72) kJ/mol barrier energy in which G_1 was 0.31 (21.6) kJ/mol more stable than G_2. G_3 was created from G_2 (2-imino-3,9-dihydro-2H-purin-6-ol) via TS_2 (planner ring structure-1955.83i (2020.39i) cm^{-1}) (R2) in which H_{12} migrated to N_3 from N_{10}. The barrier energy of TS_2 was found to be 226.90 (223) kJ/mol. By hydrogen migration from N_3 atom to C_8, G_4 (2-imino-8,9-dihydro-2H-purin-6-ol) formed from G_3 via TS_3 that has both enol and imino functional groups. The barrier energy of R3 is 457.97 (473.14) kJ/mol. TS_3 is a non planar ring structure (1788.31i (1736.50i) cm^{-1} imaginary frequency). G_4 is 69.62 (66.94) kJ/mol more unstable than G_4. If H_{15} in G_3 translocated to N_3, G_5 (2-amino-3H-purin-6-ol) formed from G_2 via TS_4 (non planar ring- 2021.51i (2037.98i) cm^{-1} imagine frequency) (R4). TS_4 is a Non Planar ring with 2021.51i (2037.98i) cm^{-1} imagine frequency. The barrier energy of G_2 → G_5 was 285.88 (286.09) kJ/mol. The relative energy of G_2 is 61.33 (41.35) kJ/mol lower than the relative energy of G_5. Translocation of H_{13} to N_1 (R5) frequency with planar ring structure) resulted in G_6 (2-imino-2,3-dihydro-1H-purin-6-ol) creation. The energy barrier of G_5→G_6 were 29.6 (21.57) and 208.54 (208.23) kJ/mol. G_6 is ((75.43 (75.88) kJ/mol) more unstable than G_5 in both gas and solution phase. By translocation of H_{13} from N_{10} to the C_5 (R6) G_7 [(S)-2-imino-5,9-dihydro-2H-purin-6-ol] produced via planer ring transition state (TS_6) with imaginary frequency 283.38i (185.70i) cm^{-1} from G_2. The barrier energy of TS_6 was 402.46 (391.80) kJ/mol in which G_2 was 149.24 (137.46) kJ/mol more stable than G_7.

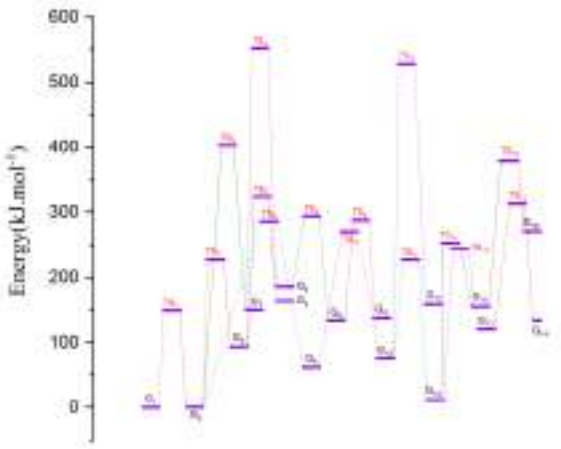

Fig.3 Potential energy serface of guanine tautomerism pathway

Table 2: Imaginary frequency and structures of transition state at the MPWB95 level.

Species	Structure	Imaginary freq. (cm^{-1})
TS_1	Planar ring	1958.70i (1981.22i)
TS_2	Planar ring	1955.83i (2020.39i)
TS_3	Non planar ring	1788.31i (1736.50i)
TS_4	Non Planar ring	2021.51i (2037.98i)
TS_5	Planar ring	1945.29i (2009.35i)
TS_6	Non planar ring	1791.15i (1800.96i)
TS_7	Planar ring	-1587.13i (-1597.73i)
TS_8	Planar ring	1306.19i (1291.12i)
TS_9	Non planar ring	1661.35i (1685.22i)
TS_{10}	Non Planar ring	1942.76i (459.06i)
TS_{11}	Planar ring	1985.34i (2025.35i)
TS_{12}	Planar ring	1606.54i (1640.92i)
TS_{13}	Non Planar ring	1996.88i (2031.18i)
TS_{14}	Planar ring	1833.33i (1969.44i)
TS_{15}	Planar ring	1489.76i (1537.15i)

Table 3. The relative free energy, enthalpy and entropy of different structures.in the gas phase.

Isomer	ΔH (Kj/mol)	ΔG (Kj/mol)	ΔS (Kj/mol.K)
G_1	0.00	0.00	0.00
G_2	-2.17	-1.67	-1.673E-03
G_3	96.21	96.06	5.019E-04
G_4	193.22	192.25	3.232E-03
G_5	61.14	61.20	-2.113E-04
G_6	141.52	140.86	2.201E-03
G_7	189.62	189.77	-5.019E-04
G_8	237.99	237.89	3.258E-04
G_9	164.91	165.11	-6.957E-04
G_{10}	73.22	72.72	1.664E-03
G_{11}	202.65	202.78	-4.227E-04
G_{12}	11.51	11.69	-6.076E-04
G_{13}	147.63	147.56	2.466E-04
G_{14}	164.90	165.11	-6.957E-04
G_{15}	155.16	153.69	4.905E-03
G_{16}	298.96	298.17	2.668E-03
TS_1	141.64	142.67	-3.461E-03
TS_2	222.97	223.44	-1.585E-03
TS_3	548.10	550.69	-8.700E-03
TS_4	287.38	287.51	-4.403E-04
TS_5	200.85	201.36	-1.708E-03
TS_6	418.31	420.87	-8.586E-03
TS_7	279.48	139.65	4.690E-01
TS_8	105.44	107.81	-7.943E-03
TS_9	166.83	168.40	-5.275E-03
TS_{10}	519.04	520.63	-5.319E-03
TS_{11}	147.94	149.24	-4.385E-03
TS_{12}	272.32	273.57	-4.192E-03
TS_{13}	182.80	183.75	-3.214E-03
TS_{14}	232.14	231.89	8.190E-04
TS_{15}	267.85	271.04	-1.067E-02

TS_7 connected G_3 and G_8 via a planar structure with 1587.13i (1597.72i) cm^{-1} imaginary frequency. In this reaction (R7), Hydrogen from N_9 in G_3 translocated to C_4 in G_8. The barrier energy of TS_7 is 230.11 (250.73) kJ/mol. The production G_8 is 92.15 (116.37) kJ/mol more stable than G_3. Next reaction happened between G_8 and G_9 ((R)-2-imino-3,5-dihydro-2H-purin-6-ol) via TS_8 (R8) that is a planar ring (1306.19i (1291.12i) cm^{-1} imaginary frequency) in which H_{15} migrated from C_4 to C_5. In this reaction (R8), The donor (C_4) and acceptor (C_5) atoms are Adjacent. TS_8 has 108.12 (102.88) kJ/mol barrier energy. G_8 is 52.53 (55.93) kJ/mol more unstable than G_9. TS_9 is the transition state between G_9 and G_{10} (2-imino-3,7-dihydro-2H-purin-6-ol). This molecule is a Non planar ring with 1661.35i (1685.22i) cm^{-1} imaginary frequency. In TS_9, H_{15} from C_5 translocated to N_7 in G_{10} (R9). G_{10} is 58 (65.68) kJ/mol more stable than G_9. The barrier energy of TS_9 is 154.26 (156.86) kJ/mol.

G_{11} (2-imino-3,9-dihydro-2H-purin-6-ol) formed from G_{10} via TS_{10} (a non planner ring (1942.76i (459.06i) cm^{-1} imaginary frequency) by changing the position of hydrogen from N_3 to C_5 (R10). TS_{10} has 452.48 (441.91) kJ/mol barrier energy. G_{10} is 83.08 (-69.00) kJ/mol more stable than G_{11}. In R11, H_{12} from N_3 in G_{10} translocated to N_{10} and formed G_{12} (2-amino-7H-purin-6-ol) via TS_{11}. This transition state is a planar ring with 1985.34i (2025.35i) cm^{-1} imaginary frequency. The barrier energy of TS_{11} is 151.68 (153.65) kJ/mol. G_{12} can be converted to G_{13} ((S)-2-amino-5H-purin-6-ol)) (R12) via a planar ring (1606.54i (1640.92i) cm^{-1} imaginary frequency) transition state (TS_{12}). In this reaction the barrier energy is 232.64 (237.77) kJ/mol. The stability of G_{12} is supposed to be 108.86 (106.73) kJ/mol less than the stability of G_{13}. In the next reaction (R13), G_{13} converted to G_{14} ((S)-2-imino-3,5-dihydro-2H-purin-6-ol) in which these two molecules linked to each other via TS_{13}. TS_{13} is a Non Planar ring with 1996.88i (2031.18i) imaginary frequency. In this reaction H_{12} from N_{10} migrated to N_3. The barrier energy of this reaction is 192.09 (196.18) kJ/mol. G_{13} is 12.67 (22.56) less stable than G_{14}. G_{12} converts to G_{15} (2-imino-2,7-dihydro-1H-purin-6-ol) (R14). TS_{14} linked these two tautomers. TS_{14} is a planar ring structure (1833.33i (1969.44i) cm^{-1} imaginary frequency). The barrier energy of TS_{14} is 241.08 (225.49) kJ/mol and G_{15} is 142.62 (112.15) kJ/mol less stable than G_{12}. In R15, G_{16} created from G_{15} via TS_{15} (planar ring-1489.76i (1537.15i) cm^{-1} imaginary frequency). G_{15} needs 223.88 (231.19) kJ/mol energy to pass the barrier energy. G_{16} is 116.42 (200.18) kJ/mol less stable than G_{15}.

References

[1] Shukla, M. K., & Leszczynski, J. (2013). Tautomerism in nucleic acid bases and base pairs: a brief overview. *Wiley Interdisciplinary Reviews: Computational Molecular Science*, *3*(6), 637-649.

[2] L.A. Curtiss, P.C. Redfern, K. Raghavachari, V. Rassolov, and J.A. Pople, J. Chem. Phys. 110, 4703 (1999).

[3] J.A. Pople, M. Head-Gordon, and K. Raghavachari, J. Chem. Phys. 87, 5968 (1987).

[4] James W McIver Jr, *Accounts of Chemical Research* 7 (3), 72 (1974); O Ermer, *Tetrahedron* 31 (16), 1849 (1975).

[5] I.M. Alecu, J. Zheng, Y. Zhao, and D.G. Truhlar, J. Chem. Theory Comput. 6, 2872 (2010)

[6] C. Gonzales and H.B. Schlegel, J. Phys. Chem. 94, 5523 (1990).

29TH IRANIAN ORGANIC CHEMISTRY CONFERENCE
1_3 NOV, 2023
UNIVERSITY OF QOM, IRAN

Chemoselective Reduction of *α,β*-Unsaturated Carbonyl Compounds *via* CS_2/*t*-BuOK System: Dimethyl sulfoxide as a Hydrogen Source

*Saideh Rajai-Daryasarei, Mir Sadra Hosseini, Saeed Balalaie**

Peptide Chemistry Research Institute, K. N. Toosi University of Technology, P.O. Box 15875-4416, Tehran 19697-64499, Iran, saideh.rajai@yahoo.com, balalaie@kntu.ac.ir

Abstract -We herein report a novel and practical approach to access saturated ketones from unsaturated ketone derivatives via CS_2/*t*-BuOK system in DMSO. The *in-situ* generation of xanthate salt through reaction of carbon disulfide and potassium *tert*-butoxide is essential to this transformation. Deuterium-labelling experiments demonstrated that DMSO can act as hydrogen donor.

1. Introduction

Selective reduction reactions are one of the most fundamental transformations in organic chemistry, which have been extensively used for the synthesis of various natural products, agrochemicals, pharmaceuticals, and functional materials. Among these reduction methodologies, chemoselective reduction of α,β-unsaturated carbonyls into saturated carbonyls has attracted considerable attention due to them wide applications in the construction of industrial chemicals and pharmaceuticals (Fig 1).[1]

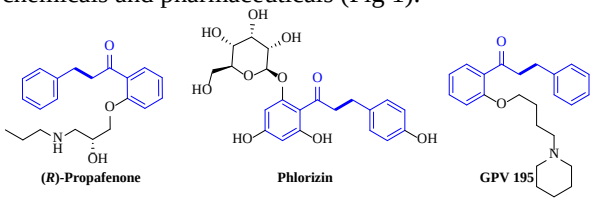

Fig1. Examples of bioactive molecules containing dihydrochalcones.

Over the past decades, great efforts have been devoted to develop the selective reduction of C=C bond of α,β-unsaturated carbonyls. Some of the reported methods are using various transition-metal catalyst systems, such as Rh, Ru, Pd, Ir, and other metal complexes with various hydrogen donors such as H_2, water, alcohols, formic acid, hydrosilanes, borohydrides, (para)formaldehyde, *etc* (Scheme 1a).[2] However, these strategies usually suffered from certain limitations such as application of expensive catalysts, long reaction times, generation of toxic waste, difficult separation of the products, and poor functional group tolerance which restrict their industrial and pharmaceutical application to some extent. Hence, developing an efficient and novel transition-metal-free system for the selective reduction of a C=C bond of α,β-unsaturated carbonyls using cheap hydrogen donor under sustainable conditions is still highly desirable. In 2018, Zhou, Liu and co-workers reported selective reduction of a C=C bond in an α,β-unsaturated carbonyls under transition-metal-free conditions using Se/DMF/H_2O system (Scheme 1b, (i)).[3] Xia and co-workers disclosed an electrochemical strategy for the reduction of a C=C bond in an α,β-unsaturated carbonyls using methanol and ammonium chloride as hydrogen sources (Scheme 1b, (ii)).[4]

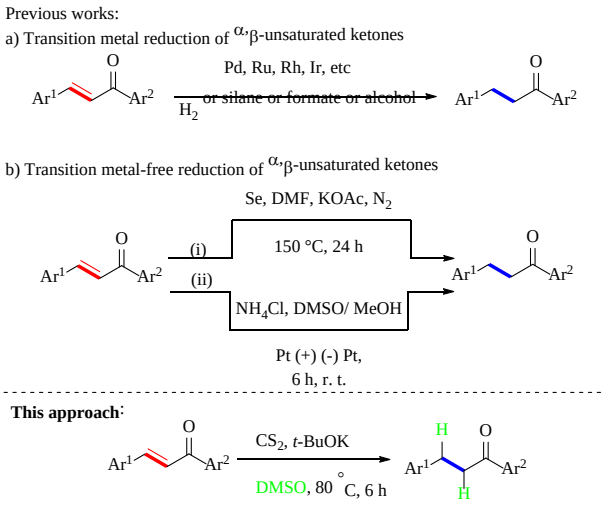

Scheme 1. Strategies to selective reduction of C=C bond in α,β-unsaturated carbonyls.

On the other hand, the development of simple, novel and environmentally friendly strategies for the synthesis of organic compounds is an important task in synthetic chemistry. In recent years, xanthates have found widespread use in organic transformations due to their high reactivity and availability, and are readily prepared from reaction of inexpensive alcohols and carbon disulfide on a large scale. Xanthates and their derivatives are applied as a sulfur reagent in construction of sulfur-containing heterocycles, preparation of some ligands and have important applications in radical transformations.[5] In 2019, Melchiorre and co-workers reported photochemical generation of radicals from alkyl electrophiles using xanthate salts as a catalyst to form carbon–carbon bond.[5a] Recently preparation of various 4-substituted

isothiazoles,[5b] and oxime ethers using xanthate salts.[5h] Inspired by these metal-free reduction systems and recent advances in the field of using xanthate in radical processes, we herein report a method to access saturated ketones from unsaturated ketone derivatives *via* CS_2/*t*-BuOK system. In this approach, the desired xanthate salt acts as a mediator as well as DMSO serves as the hydrogen source and reaction solvent. The xanthate is generated *in-situ* through carbon disulfide and potassium tert-butoxide reaction.

2. Results and discussion

On the onset of our investigation, reaction of chalcone **1a** with carbon disulfide/ potassium *tert*-butoxide system was chosen as the model substrate to optimize the reaction conditions (Table 1). When substrate **1a** reacts with carbon disulfide (4.0 eq.) in the presence of potassium *tert*-butoxide (4.0 eq.) as a base in toluene for 6 hours at 80 °C, no desired product **2a** was delivered (entry 1). Various other solvents including, PhCl, DMF, DMSO, NMP, CH_3CN, and DCE were examined (entries 2-7). Solvent screening indicated that DMSO is the best solvent for this transformation and the desired product **2a**, was obtained with 85% yield (entry 4). Carrying out the reaction at 50 °C and the room temperature led to afford the desired product **2a**, with a 43% and trace yields, respectively (entries 8 and 9). Notably, decreasing the amount of potassium *tert*-butoxide to 3 and 2 equivalents decreased the yield to 65% and 15%, respectively (entries 10 and 11). Decreasing the amount of carbon disulfide failed to improve the yield of the desired product (entries 12 and 13). As a note, when the model reaction was conducted under N_2 atmosphere, the yield of the desired product was not changed (entry 14). Finally, the best results with 85% yield and remarkably high selective reduction of double bond to afford ketone **2a** were obtained when the reaction of substrate **1a** was carried out with carbon disulfide (4.0 eq.) in the presence of potassium tert-butoxide (4.0 eq.) in DMSO at 80 °C for 6 hours. It should be mentioned, the combination of CS_2/*t*-BuO^-K^+ with DMSO acts as the actual reducing agents in this transformation.

Table 1: Optimization of reaction conditions[a]

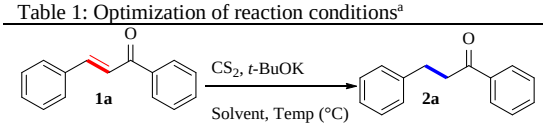

Entry	Equiv. of CS_2/ *t*-BuOK	Solvent	Temp (°C)	Yield of **2a** (%)[b]
1	4: 4	$PhCH_3$	80	nr
2	4: 4	PhCl	80	nr
3	4: 4	DMF	80	nr
4	**4: 4**	**DMSO**	80	85
5	4: 4	NMP	80	80
6	4: 4	CH_3CN	80	nr
7	4: 4	DCE	80	nr
8	4: 4	DMSO	50	43
9	4: 4	DMSO	rt	trace
10	4: 3	DMSO	80	65
11	4: 2	DMSO	80	15
12	3: 4	DMSO	80	60
13	2: 4	DMSO	80	trace
14	4: 4	DMSO	80	83

[a]Reaction conditions: chalcone 1a (0.25 mmol), carbon disulfide (4.0 eq.), base (4.0 eq.), DMSO (1 mL) for 6 h at 80 °C. [b]Isolated yields. [C]N_2 atmosphere.

With the optimized conditions identified, we explored the substrate scope for the chemoselective partial reduction of chalcones double bond. The results are summarized in Scheme 2. A variety of substituents chalcones were found to be compatible under the standard conditions, resulting in the desired products **2**, with a range of good to excellent yield values. Chalcones with electron- neutral (H), electron-donating (methyl, methoxy, and dimethylamino), halides, or electron-withdrawing (trifluoromethyl and nitro) groups on the aromatic ring (Ar^1) and phenyl ring (Ar^2) were tolerated well, providing the desired reduced products **2a-2m** with 81-91% yields. Further investigation showed that chalcones bear electron-withdrawing and electron-donating groups on both aromatic rings, are well responsive to the reaction conditions and provide desired products **2n-2u** with 76-92% yields. It is noteworthy that 2-furyl-, 2-thienyl, 1-naphthyl- and 2-naphthyl- substituted chalcones were identified suitable for this selective reduction where the corresponding products **2v-y** were obtained with 82-87% yields. Unfortunately, coumarin, styrene and diphenylacetylene were not compatible with this transformation, and the corresponding products **2z-2ab** were not detected after 8 hours.

Several control experiments were conducted to better understand the reaction mechanism (Scheme 3). When TEMPO as the radical scavenger was added to the reaction under the standard conditions, the formation of desired product **2i** was tremendously repressed (Scheme 3a). These results indicates that this transformation presumably proceeds *via* a radical pathway. Xanthate **A** was successfully synthesized through reaction carbon disulfide (CS_2) and potassium tert-butoxide (*t*-BuOK) according to the previous literature,[6] and the carrying out reaction in the presence of intermediate **A** led to corresponding product **2a**, with 86% yield (Scheme 3 b).

This observation demonstrates that the *in-situ* generation of xanthate **A** acts as a key step in this selective reduction reaction. When the model reaction was conducted under N_2 atmosphere, no change in the yield of the reduced product was observed (Scheme 3c). To further understand the reaction mechanism and the hydrogen source in the reduction reaction, deuterium-labeling experiment was performed using DMSO-d_6, and deuterium containing product was obtained with 84% yield (Scheme 3d). This indicates that the DMSO acts as the hydrogen donor in this

Scheme 2: Substrate Scope for the Construction of Dihydrochalcones.[a]

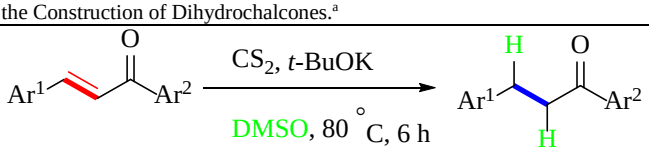

1a-y **2a-y**

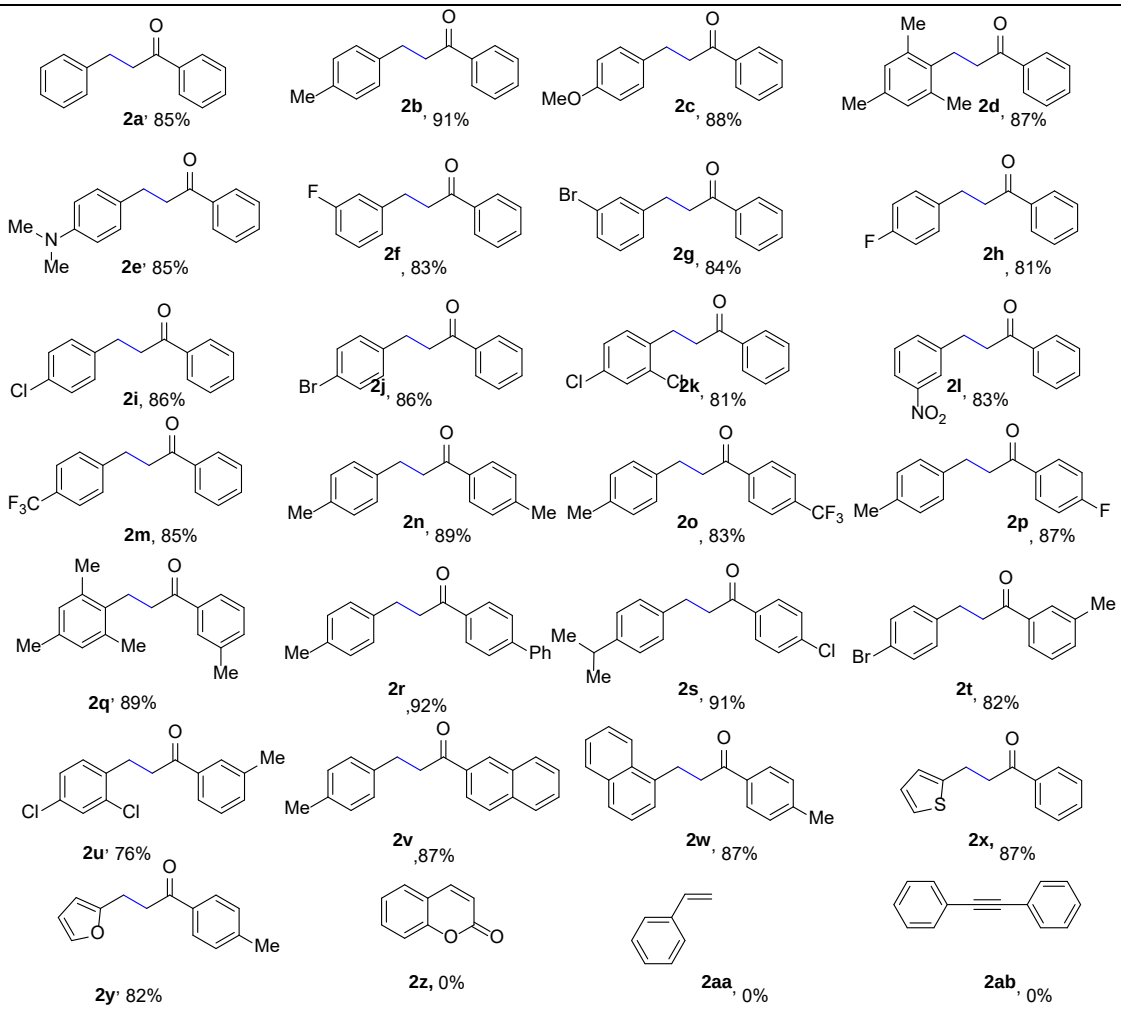

[a]Reaction conditions: Chalcone **1** (0.25 mmol), CS_2 (4.0 eq.), *t*-BuOK (4.0 eq.), DMSO (1.0 mL), 80 °C, 6 h.

reaction. In addition, to show the practicability of the selectivity of the reaction, the gram-scale synthesis of **2a** was performed (Scheme 3e).

Based on our presented experimental data and the previous reports on xanthates,[1a, 5, 7] a plausible mechanism for this selective reduction reaction is proposed in Scheme 4. Initially, carbon disulfide (CS_2) reacted with potassium tert-butoxide (*t*-BuOK) to deliver xanthate **A**. Subsequently, nucleophilic attack by xanthate **A** to the chalcone 1, followed by protonation process by DMSO result in xanthate ester **B**. Then, xanthate ester **B** undergoes the homolytic cleavage of the C−S bond, affording the benzyl radical intermediate **C**, which can be stabilized through conjugation with the aryl group, and releasing dithiocarbonyl radical **D**, which converts to byproduct dixanthogen **E**. The detection of a TEMPO-adduct X by HRMS analysis (please see the page S81 in the Supporting Information). Finally, radical intermediate **C** undergoes abstract a hydrogen atom from DMSO to deliver the desired product **2**. According to bond-dissociation energy (BDE) of both alpha-C-H bond of phenyl alkyl ketone and DMSO, abstraction of H atom of DMSO by the alkyl radical species **C** is likely feasible.

In summary, we have successfully developed a novel and efficient chemoselective reduction protocol to convert unsaturated carbonyl compounds to saturated ketones using CS_2/*t*-BuOK system to form in-situ xanthate under reaction conditions. Mechanistic studies indicated that reaction proceeded *via* radical pathway and DMSO served as

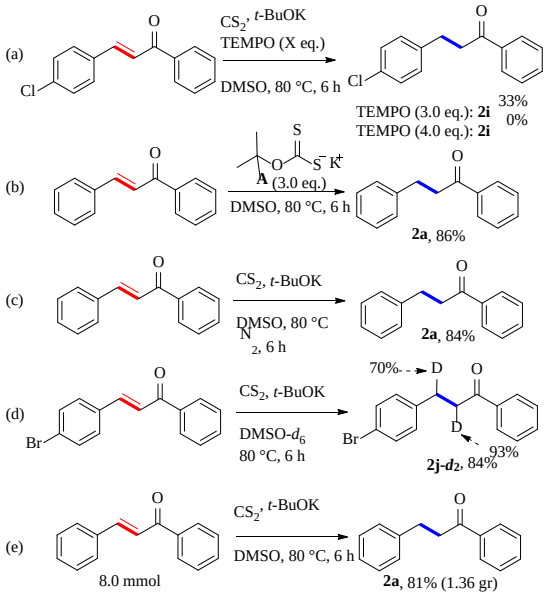

Scheme 3. Mechanistic Experiments.

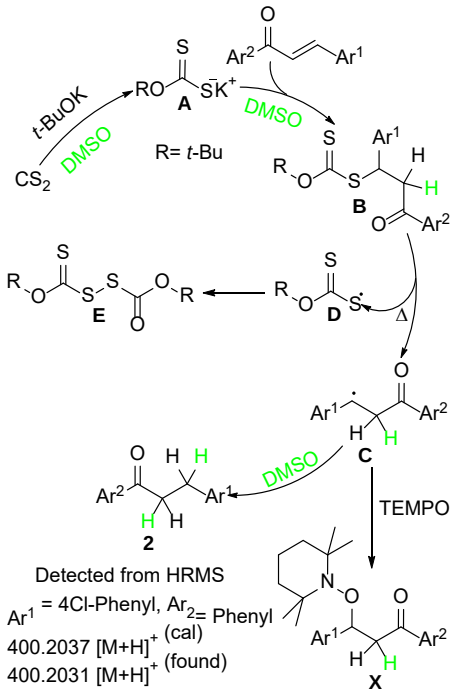

Scheme 4. Proposed reaction mechanisms.

the hydrogen source and reaction solvent. Additionally, the use readily available reagents (CS_2 and *t*-BuOK), operational simplicity, wide functional group tolerance, and ability to gram-scale synthesis are the advantages of the reported method.

3. References

[1] (a) W. Ding, Q. Song, *Org. Chem. Front.* **2016**, *3*, 14-18; (b) W. Li, X. F. Wu, *Eur. J. Org. Chem.* **2015**, *2015*, 331-335; (c) D. Wang, D. Astruc, *Chem. Rev.* **2015**, *115*, 6621-6686; (d) J. Mendes-Burak, B. Ghaffari, C. Copéret, **2019**, *55*, 179-181; (e) X. Hu, G. Wang, C. Qin, X. Xie, C. Zhang, W. Xu, Y. Liu, *Org. Chem. Front.* **2019**, *6*, 2619-2623; (f) J. Kozłowska, B. Potaniec, B. Żarowska, M. Anioł, *RSC Adv*. **2018**, *8*, 30379-30386; (g) T. Song, Y. Duan, Y. Yang, *Catal. Commun.* **2019**, *120*, 80-85; (h) Z. Wei, Y. Gong, T. Xiong, P. Zhang, H. Li, Y. Wang, *Catal. Sci. Technol*. **2015**, *5*, 397-404; (i) S. Lau, D. Gasperini, R. L. Webster, *Angew. Chem. Int. Ed.* **2021**, *60*, 14272-14294; (j) R. Nie, Y. Tao, Y. Nie, T. Lu, J. Wang, Y. Zhang, X. Lu, C. C. Xu, *ACS Catal.* **2021**, *11*, 1071-1095; (k) R. Prasanna, S. Guha, G. Sekar, *Org. Lett.* **2019**, *21*, 2650-2653; (l) N. Garg, H. P. Somasundharam, P. Dahiya, B. Sundararaju, *Chem. Commun*. **2022**, *58*, 9930-9933; (m) D. J. Lowes, W. A. Guiguemde, M. C. Connelly, F. Zhu, M. S. Sigal, J. A. Clark, A. S. Lemoff, J. L. Derisi, E. B. Wilson, R. K. Guy, R. K. *J. Med. Chem.* **2011**, *54*, 7477-7485; (n) J. R. Ehrenkranz, N. G. Lewis, C. Ronald Kahn, J. Roth, *Diabetes Metab. Res. Rev.* **2005**, *21*, 31-38; (o) T. Langer, M. Eder, R. D. Hoffmann, P. Chiba, G. F. Ecker, *Arch. Pharm.* **2004**, *337*, 317-327.

[2] (a) S. -J. Chen, G.-P. Lu, C. Cai, *RSC Adv.* **2015**, *5*, 13208-13211; (b) B. Ding, Z. Zhang, Y. Liu, M. Sugiya, T. Imamoto, W. Zhang, *Org. Lett.* **2013**, *15*, 3690-3693; (c) D. B. Bagal, Z. S. Qureshi, K. P. Dhake, S. R. Khan, B. M. Bhanage, *Green Chem.* **2011**, *13*, 1490-1494; (d) S. Ganji, S. Mutyala, C. K. P. Neeli, K. S. R. Rao, D. R. Burri, *RSC Adv.* **2013**, *3*, 11533-11538; (e) Z. Baán, Z. Finta, G. Keglevich, I. Hermecz, *Green Chem.* **2009**, *11*, 1937-1940; (f) C. A. Mebi, R. P. Nair, B. J. Frost, *Organometallics* **2007**, 26, 429-438; (g) T. Song, Z. Ma, Y. Yang, *ChemCatChem* **2019**, *11*, 1313-1319.

[3] H.-C. Li, C. An, G. Wu, G.-X. Li, X.-B. Huang, W.-X. Gao, J.-C. Ding, Y. -B. Zhou, M.-C. Liu, H.-Y. Wu, *Org. Lett*. **2018**, 20, 5573-5577.

[4] B. Huang, Y. Li, C. Yang, W. Xia, *Chem. Commun.* **2019**, *55*, 6731-6734.

[5] (a) B. Schweitzer-Chaput, M. A. Horwitz, E. De Pedro Beato, P. Melchiorre, *Nat. Chem*. **2019**, *11*, 129-135; (b) G. Huang, J. Li, X. Ji, L. Chen, Q. Liu, X. Chen, Y. Huang, Y. Li, *Chem. Commun*. **2020**, *56*, 5763-5766; (c) J. Li, J. Li, X. Ji, Q. Liu, L. Chen, Y. Huang, Y. Li, *Adv. Synth. Catal.* **2021**, *363*, 1059-1068; (d) S. Z. Zard, Acc. *Chem. Res*. **2018**, *51*, 1722-1733; (e) S. K. Rout, G. Marghem, J. Lan, T. Leyssens, O. Riant, *Chem. Commun*. **2019**, *55*, 14976-14979; (f) L. Anthore-Dalion, Q. Liu, S. Z. Zard, *J. Am. Chem. Soc.* **2016**, *138*, 8404-8407; (g) X. Luo, Y. Li, X. Chen, Z. Song, J. Liang, C. Liao, Z. Zhu, L. Chen, *Org. Biomol. Chem.* **2019**, *17*, 7315-7319; (h) Z. Zhu, X. Tang, J. Cen, J. Li, W. Wu, H. Jiang, *Chem. Commun*. **2018**, *54*, 3767-3770; (i) X. Luo, X. Chen, L. Chen, K. Zhang, Y. Li, *Chem. Commun.* **2019**, *55*, 2170-2173; (j) W.-H. Bao, X. Wu, *J. Org. Chem.* **2023**, 88, 3975-3980; (k) M. Z. Aldin, A. Maho, G. Zaragoza, A. Demonceau, L. Delaude, *Dalton Trans.* **2018**, *47*, 13926-13938; (l) E. Katlenok, S. Smirnov, A. Y. Ivanov, S. Makarenko, K. Balashev, *Opt. Spectrosc.* **2017**, *122*, 426-434.

[6] A. W. Mott, G. Barany, *J. Chem. Soc. Perkin Trans 1.* **1984**, 2615-2621.

[7] (a) Y. Qin, J. Lu, Z. Zou, H. Hong, Y. Li, Y. Li, L. Chen, J. Hu, Y. Huang, *Org. Chem. Front.* **2020**, *7*, 1817-1822; (b) C.-H. Ma, L. Zhao, X. He, Y.-Q. Jiang, B. Yu, *Org. Chem. Front.* **2022**, *9*, 1445-1450; (c) G. Huang, J. Li, J. Li, J. Li, M. Sun, P. Zhou, L. Chen, Y. Huang, S. Jiang, Y. Li, *J. Org. Chem.* **2020**, *85*, 13037-13049; (d) E. de Pedro Beato, D. Mazzarella, M. Balletti, P. Melchiorre, *Chem. Sci.* **2020**, *11*, 6312-6324.

29TH IRANIAN ORGANIC CHEMISTRY CONFERENCE
1_3 NOV, 2023
UNIVERSITY OF QOM, IRAN

Synthesis and spectroscopic study of two new phosphorus compounds: (2-Cl-C_6H_4O)(2-Cl-$C_6H_4CH_2NH)_2P(O)$ and (C_6H_5)(4-CH_3-$C_6H_4NH)_2P(O)$

*Azadeh Naraghi and Mehrdad Pourayoubi**

Department of Chemistry, Faculty of Science, Ferdowsi University of Mashhad, Mashhad, Iran, azadehnaraghi@yahoo.com, pourayoubi@um.ac.ir.

Abstract – The phosphorus signals of (2-Cl-C_6H_4O)(2-Cl-$C_6H_4CH_2NH)_2P(O)$ diamidophosphoester (**I**), and (C_6H_5)(4-CH_3-$C_6H_4NH)_2P(O)$ phosphonicamide (**II**) appear at 13.30 and 8.62 ppm, respectively. The NH protons of (**I**) reveal a doublet of triplets with apparent coupling constants of 7.3 and 14.6 Hz (due to vicinal hydrogen-hydrogen and geminal phosphorus-hydrogen couplings). The phosphorus-carbon coupling constants $^nJ_{PC}$ (n = 2 and 3) in (**I**) and $^mJ_{PC}$ (m = 1, 2, 3 and 4) in (**II**) were evaluated.

Keywords: Diamidophosphoester, Phosphonicamide, Phosphorus-carbon coupling constant, Phosphorus-hydrogen coupling constant

1. Introduction

The phosphorus-nitrogen compounds, typically amidophosphoesters/phosphonicamides, are well-known for different applications in flame retardants, and manufacturing of drugs [1–3]. Nuclear magnetic resonance (NMR) is a beneficial technique to study of these compounds, due to the existence of NMR-active nuclei (^{31}P, ^1H, ^{13}C). Moreover, NMR spin-spin coupling constants are used to prove the assignment of signals, and analysis related to conformation/configuration [4].

In this work, the synthesis and spectroscopic characterization of two new phosphorus compounds, belonging to diamidophosphoester and phosphonicamide families are investigated. These compounds are (2-Cl-C_6H_4O)(2-Cl-$C_6H_4CH_2NH)_2P(O)$ (Scheme 1), and (C_6H_5)(4-CH_3-$C_6H_4NH)_2P(O)$ (Scheme 2). Some topics related to the phosphorus-hydrogen and phosphorus-carbon coupling constants were issued.

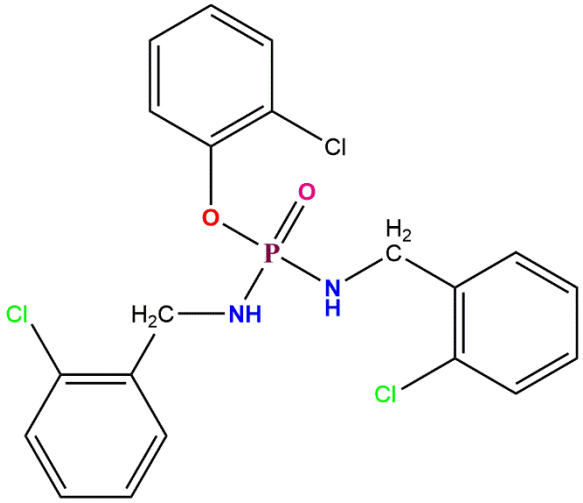

Scheme 1. Chemical structure of (2-Cl-C_6H_4O)(2-Cl-$C_6H_4CH_2NH)_2P(O)$.

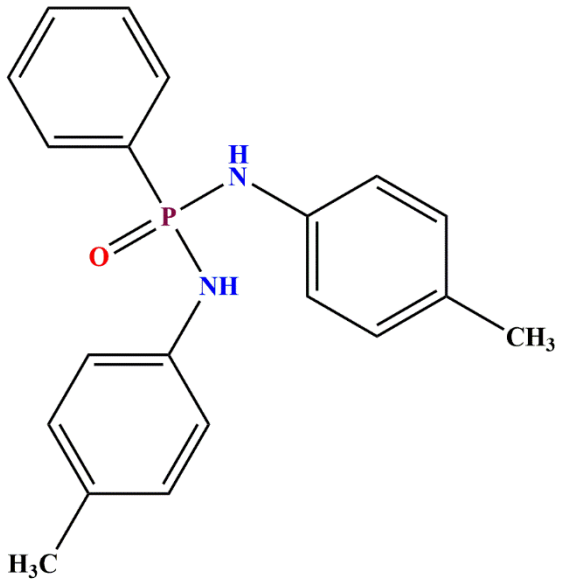

Scheme 2. Chemical structure of (C_6H_5)(4-CH_3-$C_6H_4NH)_2P(O)$.

2. Experimental

2.1. Synthesis and Identification:

Synthesis of (2-Cl-C_6H_4O)(2-Cl-$C_6H_4CH_2NH)_2P(O)$ (I): To a solution of (2-Cl-C_6H_4O)$Cl_2P(O)$ in dry $CHCl_3$, a solution of 2-chlorobenzylamine and triethylamine in the same solvent (1:2:2 mole ratio) was added dropwise and stirred for 4 hours. Initial temperature is 0 °C (ice-bath) to start the reaction, which warms to room temperature during the reaction time. After removing the solvent (under a vacuum), the resulting solid was washed with distilled water to separate the $[(C_2H_5)_3NH]Cl$ salt. The product was dried in air, and the solid substance was re-crystallized in a mixture of chloroform and normal hexane.

$^{31}P\{^1H\}$-NMR (121.78 MHz, DMSO-d_6, 295.6 K): δ = 13.30 (*s*) (Fig. 1). $^{13}C\{^1H\}$-NMR (75.65 MHz, DMSO-d_6, 296.2 K, TMS): δ = 42.42 (*s*), 122.32 (*d*, *J* = 3.0 Hz), 125.07 (*d*, *J* = 6.8 Hz), 125.43 (*s*), 127.38 (*s*), 128.43 (*s*), 128.70 (*s*), 129.19 (*s*), 129.22 (*s*), 130.58 (*s*), 132.01 (*s*), 138.17 (*d*, *J* = 6.0 Hz), 148.01 (*d*, *J* = 5.9 Hz) (Fig. 2). ^{1}H-NMR (300.81 MHz, DMSO-d_6, 295.5 K, TMS): δ = 4.26 (*dd*, *J* = 11.7 Hz, 7.2 Hz, 4H, CH_2), 5.80 (*dt*, *J* = 14.6 Hz, 7.3 Hz, 2H, NH), 7.40 (*m*, 12H) (Fig. 3). IR (KBr, cm^{-1}): 3273, 3161, 3068, 3005, 2919, 1586, 1481, 1437, 1246, 1200, 1122, 1043, 1011, 932, 817, 748, 687 (Fig. 4).

Synthesis of (C_6H_5)(4-CH_3-$C_6H_4NH)_2P(O)$ (II): To a solution of (C_6H_5)$Cl_2P(O)$ in dry $CHCl_3$, a solution of *p*-toluidine in the same solvent (1:4 mole ratio) was added dropwise and stirred for 4 hours. Initial temperature to start the reaction is 0 °C (ice-bath), which warms to room temperature during the reaction time. After removing the solvent (under a vacuum), the resulting solid was washed with distilled water to separate the [4-CH_3-$C_6H_4NH_3$]Cl salt. The product was dried in air, and the solid substance was re-crystallized in a mixture of chloroform and normal hexane.

$^{31}P\{^1H\}$-NMR (121.78 MHz, DMSO-d_6, 295.5 K): δ = 8.62 (*s*) (Fig. 5). $^{13}C\{^1H\}$-NMR (75.65 MHz, DMSO-d_6, 296.1 K, TMS): δ = 20.67 (*s*), 118.28 (*d*, *J* = 6.7 Hz), 128.81 (*d*, *J* = 13.5 Hz), 129.33 (*s*), 129.61 (*s*), 132.07 (*d*, *J* = 10.2 Hz), 132.10 (*d*, *J* ≈ 1.9 Hz, overlapped), 133.56 (*d*, *J* = 152.7 Hz), 140.05 (*s*) (Fig. 6). ^{1}H-NMR (300.81 MHz, DMSO-d_6, 295.3 K, TMS): δ = 2.18 (*s*, 3H, CH_3), 6.95 (*d*, *J* = 8.4 Hz, 4H), 7.08 (*d*, *J* = 8.4 Hz, 4H), 7.47–7.59 (*m*, 3H), 7.80–7.87 (*m*, 4H, CH & NH) (Fig. 7). IR (KBr, cm^{-1}): 3241, 3179, 3001, 2615, 1616, 1579, 1515, 1443, 1385, 1282, 1235, 1174, 1125, 1029, 932, 811, 747, 697 (Fig. 8).

3. Results and discussion

3.1. NMR spectroscopy:

The phosphorus signals ($^{31}P\{^1H\}$-NMR) appear at 13.30 and 8.62 ppm for **I** and **II**, respectively.

In the ^{1}H-NMR spectrum of **I**, the NH proton appears at 5.80 ppm with a *dt* (doublet of triplets) fine structure, due to geminal (^2J) phosphorus-hydrogen and vicinal hydrogen-hydrogen (^3J) couplings (14.6 and 7.3 Hz). The signal at 4.26 ppm (doublet of doublets) associates to the CH_2 protons with apparent *J* values of 11.7 and 7.2 Hz. These values associate to the couplings with phosphorus nucleus and the NH proton, respectively. For **II**, the peak of NH proton is mixed with the peak of two aromatic protons (belonging to the phenyl group directly attached to phosphorus).

The *ipso*- carbon atom of 2-Cl-$C_6H_4CH_2$ moiety and the *ipso*-/*ortho*- carbon atoms of 2-Cl-C_6H_4O group show couplings with phosphorus. These carbon atoms, respectively with a three and two/three bonds separation from phosphorus reveal doublets in the $^{13}C\{^1H\}$-NMR spectrum. Typically, the doublet at 148.01 ppm ($^2J_{PC}$ = 5.9 Hz) associates to the *ipso*-carbon atom of the 2-Cl-C_6H_4O moiety. This coupling constant is comparable with the one observed for an analogous compound ($C_6H_5O)_2$(4-CH_3-C_6H_4-*R*-(+)CH(CH_3)NH)P(O) with the calculated values of 6.5 Hz for both signals at 151.10 and 151.23 ppm. The reason for the observation of two signals in literature compound is the presence of chiral fragment and observation of two sets of carbon signals related to two diastereotopic C_6H_5O groups [5].

All carbon atoms of phenyl group directly attached to phosphorus in compound **II** show couplings with phosphorus (^1J, ^2J, ^3J and ^4J). The doublet centred at 133.56 (^1J = 152.7 Hz) is related to the *ipso*-carbon atom. The signal of *para*-carbon atom (about 132.10 ppm) is mixed with the neighboring signal, and from the shapes of these two overlapped signals the ^4J value is estimated to be about 1.9 Hz. The doublets at 132.07 and 128.81 ppm (*J* = 10.2 and 13.5 Hz) are assigned to the *ortho*- and *meta*-carbon atoms.

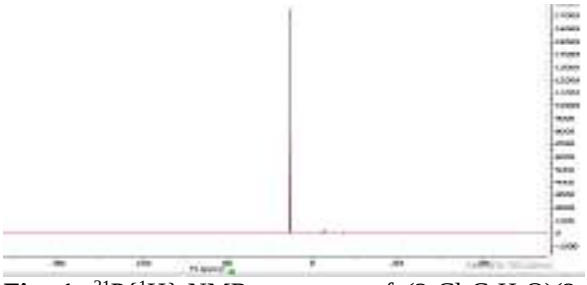

Fig. 1. $^{31}P\{^1H\}$-NMR spectrum of (2-Cl-C_6H_4O)(2-Cl-$C_6H_4CH_2NH)_2P(O)$.

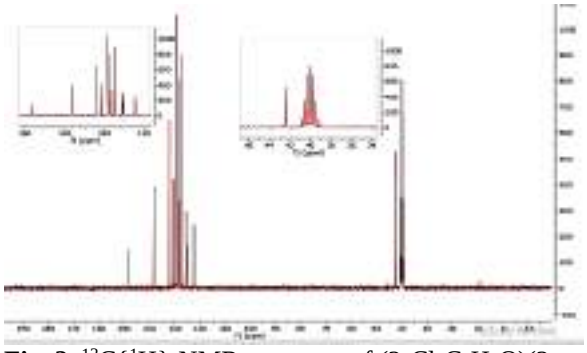

Fig. 2. $^{13}C\{^{1}H\}$-NMR spectrum of (2-Cl-C_6H_4O)(2-Cl-$C_6H_4CH_2NH)_2P(O)$.

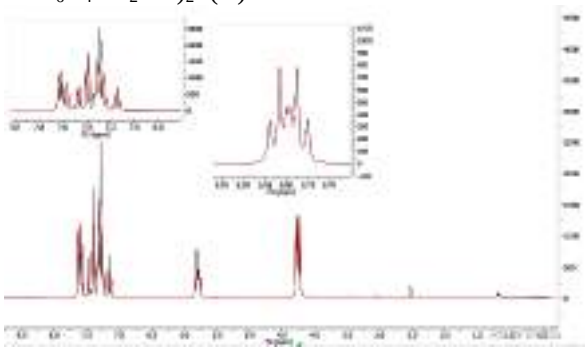

Fig. 3. ^{1}H-NMR spectrum of (2-Cl-C_6H_4O)(2-Cl-$C_6H_4CH_2NH)_2P(O)$.

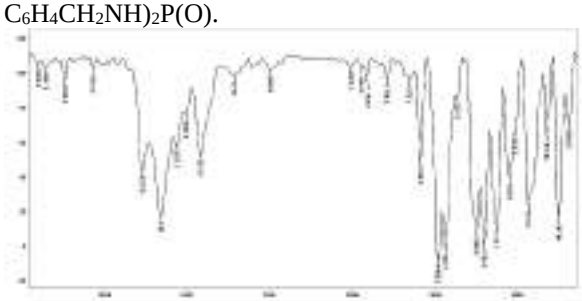

Fig. 4. IR spectrum of (2-Cl-C_6H_4O)(2-Cl-$C_6H_4CH_2NH)_2P(O)$.

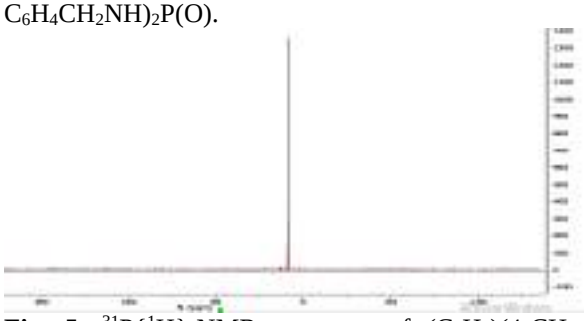

Fig. 5. $^{31}P\{^{1}H\}$-NMR spectrum of (C_6H_5)(4-CH_3-$C_6H_4NH)_2P(O)$.

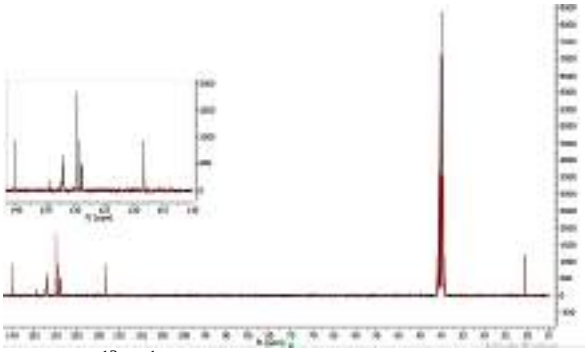

Fig. 6. $^{13}C\{^{1}H\}$-NMR spectrum of (C_6H_5)(4-CH_3-$C_6H_4NH)_2P(O)$.

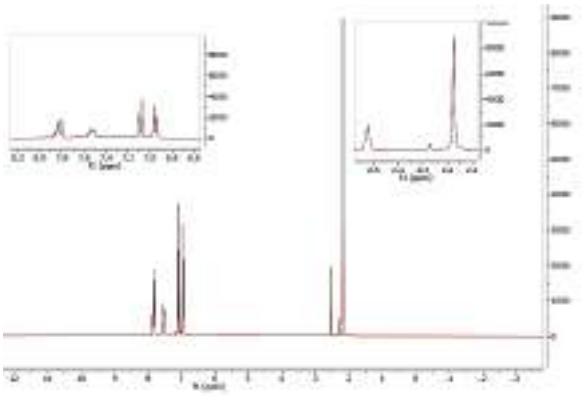

Fig. 7. ^{1}H-NMR spectrum of (C_6H_5)(4-CH_3-$C_6H_4NH)_2P(O)$.

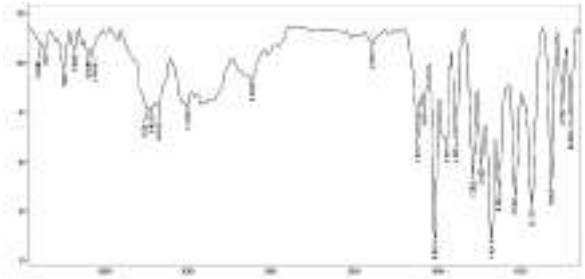

Fig. 8. IR spectrum of (C_6H_5)(4-CH_3-$C_6H_4NH)_2P(O)$.

4. References

[1] C. Nguyen, J. Kim, Macromol. Res. 16 (2008) 620–625.

[2] A. Binici, G. Elmas, A. Okumuş, R. Güzel, H. Şimşek, Z. Kılıç, Phosphorus Sulfur Silicon Relat. Elem. 198 (2023) 21–33.

[3] A. Binici, G. Elmas, V. Okumuş, S. Erden Tayhan, T. Hökelek, B. N. Şeker, Z. Kılıç, J. Biomol. Struct. Dyn. 41 (2023) 298–318.

[4] F. Sabbaghi, M. Pourayoubi, J. Chem. React. Synthesis 13 (2023) 222–231.

[5] N. Lal Zakaria, M. Pourayoubi, M. Eghbali Toularoud, M. Dušek, E. Skorepova, Acta Cryst. C 77 (2021) 186–196.

29TH IRANIAN ORGANIC CHEMISTRY CONFERENCE
1_3 NOV, 2023
UNIVERSITY OF QOM, IRAN

Assessing the drug delivery of ibuprofen by the assistance of metal-doped graphenes: Insights from density functional theory

Sahar Esfehani, Jafar Akbari Somayeh Soleimani-Amiri*

Department of Chemistry, Buinzahra Branch, Islamic Azad University, Buinzahra, Iran, jakbari2@gmail.com

Abstract- Quantum chemical density functional theory (DFT) calculations were performed to examine features of metaldoped graphene (MG) models for adsorbing the popular ibuprofen (IBU) drug substance towards approaching the drug delivery features. The M-doped atoms were titanium (Ti), chromium (Cr), iron (Fe), nickel (Ni), and zinc (Zn) with even number of electrons not to make a perturbation to the paired electronic systems of MG models.
The models were optimized in singular and bimolecular states yielding the highest adsorption strength (-77.768 kal/mol) for TiG-IBU model and the lowest adsorption strength (-7.990 kal/mol) for ZnG-IBU model. Further analyses of molecular orbital features indicated a very high reactivity for the singular ZnG model preventing it from participating in a strong adsorption process. On the other hand, a medium reactivity was found for TiG model. Benefits of MG-based diagnosis process were also observed to make useful the models for employing in the smart drug delivery process of IBU drug substance.

1. Introduction

the topic of drug development has been currently found very important for keeping the levels of human health systems in this process, a carrier could be used to adsorb the drug substance. Regard, the advantages of nano-based drug delivery processes for approaching a targeted platform were reported by the results of earlier works Ibuprofen among highly Nonsteroidal anti-inflammatory drugs (NSAIDs) are used to treat pain, fever, and inflammation. But due to non-selective inhibition, some side effects may occur for patients. In this regard, the representative models of metal-doped graphenes were investigated in the current work for adsorbing the ibuprofen drug substance towards approaching the carrier role of drug delivery purposes. Consequently, the models were optimized and their descriptors were evaluated to approach an insightful point regarding the investigations of metal-doped graphenes towards the drug delivery of ibuprofen [1-4].

2. Computational details

The principal models of this work were shown in Fig. 1 including ibuprofen (IBU) with the formula of C13H18O2 and metal-doped graphenes (MG) with the formula of C42H16M by a variating M atom among titanium (Ti), chromium (Cr), iron (Fe), nickel (Ni), and zinc (Zn). It is worth to mention that the criterion for using these types of transition metal atoms for doping the graphene was to keeping the even total number of electrons avoiding the existence of systems electron splitting. Accordingly, the charge and multiplicity were assigned by 0 and 1. Such singular models were assigned by A0, A1, A2, A3, A4, and A5 as shown in Fig. 2. Optimization calculations were performed to stabilize geometries of the models to provide minimized energy structures for involving in further electronic investigations. The bimolecular models were created using the already optimized structures of singular models to approach B1, B2, B3, B4, and B5 models as shown in Fig. 3. ing the investigations of metal-doped graphenes towards the drug delivery of ibuprofen. To this aim, density functional theory (DFT) quantum chemical calculations were performed using the wB97XD/6-31G* method/basis set as implemented in the Gaussian program [2]. Additionally, energies of molecular models were calculated by including the water solvent using the (PCM) method (Table 4) for showing the impacts of humidity or water solvating on the obtained energy features of the models and their stabilities [1-4]. An identical initial configuration of bimolecular models was inserted in the new optimization calculations to obtain the minimized structures of interacting systems. The models were subsequently analyzed by evaluating the related structural and electronic features. Infrared (IR) spectra of all singular and bimolecular models (Fig. 4) were evaluated to obtain the minimized structures of interacting systems. The models were subsequently analyzed by evaluating the related structural and electronic features. Infrared (IR) spectra of all singular and bimolecular models (Fig. 4) were evaluated to show variations of vibrational strengths of the optimized models before and after involving in the interactions. Table 1 exhibits the adsorption descriptors of bimolecular models

including adsorption energy, interaction type and distance, density of all electrons, Laplacian of electron density, and energy density, in which the last three descriptors belong to the analysis of quantum theory of atoms in molecules (QTAIM) [3]. To evaluate the values of adsorption energy, an equation of (EAds = EMG-IBU – EMG – EIBU) was used. Table 2 exhibits atomic charges for the interacting M and O atoms, in which they belong to the natural bond orbital (NBO) analysis [3]. Table 3 exhibits evaluated values of frontier molecular orbitals (FMOs) related descriptors including energy levels of the highest occupied and the lowest unoccupied molecular orbitals (HOMO and LUMO). Additionally, the related features including energy gap (EG = LUMO – HOMO), chemical hardness (η = (LUMO – HOMO)/2)chemical potential (μ = (HOMO + LUMO)/2), and electrophilicity index ($\omega = \mu^2/2\eta$) were evaluated for the models. The graphical HOMO and LUMO distribution patterns of the optimized models were also exhibited in Figs. 2 and 3 and variations of their lower and upper levels were illustrated in Fig. 5 through density of states (DOS) diagrams [4]. Consequently, the models were optimized and their descriptors were evaluated to approach an insightful point regarding the investigations of metal-doped graphenes towards the drug delivery of ibuprofen. To this aim, density functional theory (DFT) quantum chemical calculations were performed using the wB97XD/6-31G* method/basis set as implemented in the Gaussian program [3]. Additionally, energies of molecular models were calculated by including the water solvent using the (PCM) method (Table 4). for showing the impacts of humidity or water solvating on the obtained energy features of the models and their stabilitiesfor showing the impacts of humidity or water solvating on the obtained energy features of the models and their stabilitiesumidity or water solvating on the obtained energy featuresof the models and their stabilities [4].

3. Results and discussion

First, the molecules were investigated individually and then as two molecules.The exhibited results of A1- A5 could reveal a featured role for each Mdoped atom in the surface model with specific HOMO and LUMO properties for involving in further interactions and reactions. Significant variations of the IR peaks were observed in two regions of 1700–1000 cm−1 and 1000–500 cm−1 confirming the combinations of MG and IBU models for the formation of bimolecular MG-IBU models.The results of adsorption energy revealed different levels of interaction strength for the bimolecular models, in which this order was found: B1 > B2 > B4 > B3 > B5. The models with two M…O interactions (B1, B2, and B4) were in a higher strength than those models with one M…O interaction (B3 and B5). In this regard, B1 model was placed at the highest level

4. Conclusion

The results indicated that each MG model had its own tendency for adsorbing the IBU drug substance, in which TiG model was at the highest tendency and ZnG model was at the lowest tendency. The molecular orbital features indicated a very high reactivity for ZnG making it unstable for participating in a strong adsorption whereas the reactivity of TiG was indeed at a medium level. NBO atomic charges yielded different chemical features for the M-doped atoms for interacting with the oxygen atoms of IBU. There were two oxygen atoms close to each other in IBU, but not both of them were involved in all interactions with the M-doped atom of MG models. FeG-IBU and ZnG-IBU models were in one M…O interactions and their strengths were lower than two interacting TiG-IBU, CrG-IBU, and NiG-IBU models. The NBO atomic charges and FMO features helped to reach a point that the models should be carefully selected for managing the adsorption of IBU dug substance. If a strong adsorption or a weak adsorption is required, the models will be in different states of structural and electronic features. , Weaker models showed a possibility of releasing the adsorbed drug from the carrier under the existence of humidity. For providing information for managing the initial step of selecting a carrier for the drug delivery of IBU, all investigated MG models of this work could be proposed in general. Each MG-IBU bimolecular model shoed a featured specification for approaching the purpose. A full protection of IBU or a medium protection could be provided by the MG surfaces, in which measuring DOS diagrams could provide even a diagnosis tool of smart drug delivery process.

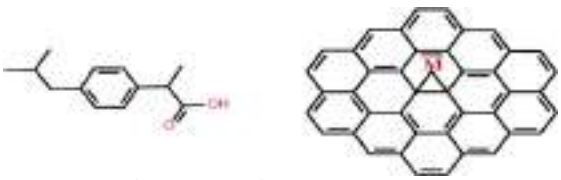

Fig. 1. Ibuprofen (IBU) at left and metal-doped graphene (MG) at ri

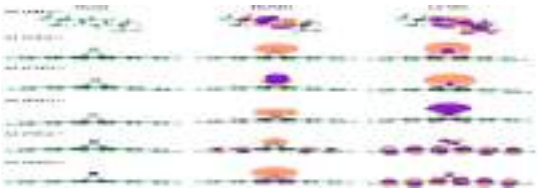

Fig. 2. Optimized configurations and HOMO-LUMO distribution patterns of singular models.

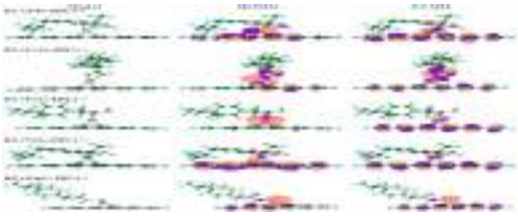

Fig. 3. Optimized configurations and HOMO-LUMO distribution patterns of bimolecular models.

Fig. 4. IR spectra of singular and bimolecular models.

Fig. 5. DOS diagrams of singular and bimolecular models.

Table 1
Adsorption descriptors for bimolecular (B) models evaluated by the wB97XD/ 6-31G* calculations.
a For ibuprofen; the keto oxygen was assigned by O1 and the enol oxygen was assigned by O2.

Model	Adsorption energy (kcal/mol)	Interactiona	Distance (Å)	Density of all electrons (au)	Laplacian of electron density (au)	Energy density (au)
B1 (TiG-IBU)	−77.768	Ti…O1	1.856	0.137	0.572	−0.037
		Ti…O2	2.185	0.102	0.316	−0.011
B2 (CrG-IBU)	−45.567	Cr…O1	1.889	0.113	0.649	−0.028
		Cr…O2	2.953	0.095	0.204	−0.009
B3 (FeG-IBU)	−37.184	Fe…O1	1.788	0.131	0.873	−0.017
B4 (NiG-IBU)	−43.750	Ni…O1	2.023	0.121	0.215	−0.011
		Ni…O2	1.992	0.146	0.423	−0.026
B5 (ZnG-IBU)	−7.990	Zn…O2	1.899	0.106	0.429	−0.013

Table 2
NBO atomic charges (e) for singular (A) and bimolecular (B) models evaluated by the wB97XD/6-31G* calculations.
a For ibuprofen; the keto oxygen was assigned by O1 and the enol oxygen was assigned by O2. For Δ, the charge quantities of singular and bimolecular states were compared; e.g. ΔM = MBimolecular – MSingular and so on.

Modela	M	ΔM	O1	ΔO1	O2	ΔO2
A0 (IBU)	–	–	−0.572	–	−0.711	–
A1 (TiG)	0.725	–	–	–	–	–
A2 (CrG)	0.616	–	–	–	–	–
A3 (FeG)	0.443	–	–	–	–	–
A4 (NiG)	0.498	–	–	–	–	–
A5 (ZnG)	0.146	–	–	–	–	–
B1 (TiG-IBU)	1.186	0.461	−0.634	−0.062	−0.751	−0.04
B2 (CrG-IBU)	0.821	0.205	−0.671	−0.099	−0.691	0.020
B3 (FeG-IBU)	0.662	0.219	−0.661	−0.089	−0.679	0.032
B4 (NiG-IBU)	0.812	0.314	−0.624	−0.052	−0.776	−0.065
B5 (ZnG-IBU)	0.859	0.713	−0.515	0.057	−0.851	−0.140

Table 4
The calculated adsorption energy (kcal/mol) in gas and PCM-water included phases evaluated by the wB97XD/6-31G* calculations.

Phase	B1	B2	B3	B4	B5
Gas	−77.768	−45.567	−37.184	−43.750	−7.990
Water	−65.252	−26.936	−20.671	−28.313	6.261

References

[1] Z. Zhang, P. Ma, R. Ahmed, J. Wang, D. Akin, F. Soto, B.F. Liu, P. Li, U. Demirci, Advanced point-of-care testing technologies for human acute respiratory virus detection, Adv. Mater. 34 (2022) 2103646.

[2] X. Zhang, Y.Y. Qu, L. Liu, Y.N. Qiao, H.R. Geng, Y. Lin, W. Xu, J. Cao, J.Y. Zhao, Homocysteine inhibits pro-insulin receptor cleavage and causes insulin resistance via protein cysteine-homocysteinylation, Cell Rep. 37 (2021) 109821.

[3] A.M. Tamaddon, F. Saadati, H. Khosropanah, A. Dehghani Nazhvani, G.H. Yousefi, Histologic evaluation of new doxycycline gel formulation for subgingival application in experimental periodontitis in rats, Int.J.Sci.Res.Dent.Med.Sci. 2 (2020) 107.

[4] S. Chakravarthi, B. Karikalan, Molecular biomarkers for lung adenocarcinoma: a short review, Curr.Cancer Ther.Rev. 17 (2021) 97.

Pd nanoparticles decorated of g-C_3N_4 for Suzuki cross-coupling reaction of aryl halides with phenylboronic acid

Neda Seyedi ***

Department of Chemistry, Faculty of Science, University of Jiroft, Jiroft, Iran, nedaseyedi@ujiroft.ac.ir

Abstract

In this study, Pd nanoparticles synthesized on the surface of g-C3N4. The structure of the prepared catalyst was confirmed using XRD, and SEM. It was applied as an efficient catalyst for the Suzuki cross-coupling reaction. The synthesized catalyst could be recovered and reused five times without any loss of activity.

1. Introduction

The Pd-catalyzed reaction of the C–C bond is one of the most effective and multifaceted tools in advanced organic chemistry [1]. Typically, Suzuki cross-coupling reactions are performed under homogeneous and heterogeneous conditions using a variety of palladium catalytic reaction [2]. Despite the relatively high efficiency of homogeneous systems, the recovery of the costly and potentially toxic palladium catalysts remains as a pressing problem in the development toward a greener, more sustainable chemical industry [3]. Heterogeneous catalysts are preferred to homogeneous catalysts because of their facile recyclability and easy compatibility with continuous flow systems [4]. Recently, for the synthesis of heterogenous catalyst, solid materials, including silica, carbon nanotubes, polymers, metal oxides, dendrimers and graphene layers, activated carbon, zeolites and nanoparticles [5] have been used as solid supports for the homogeneous catalysts. Nowadays, graphite carbon nitrite (g-C_3N_4) has been applied in the preparation of organic compounds as a solid support. A few papers are found which used g-C_3N_4 as a solid support for palladium ions and/or palladium nanoparticles catalyst in the C–C cross-coupling reactions. In this research, we synthesized Pd NPs on the g-C_3N_4 as a support. The catalytic activity of this catalyst was studied on the ross-coupling reaction of aril halides with phenylboronic acid. The results showed that this catalyst had excellent activity and easily separated from reaction mixture without significant decrease in catalytic activity.

2. Results and Discussion

2.1. Characterization:

To obtain information on the morphology and structure of Pd NPs, the catalyst was characterized.

The XRD pattern of catalyst exhibited in Fig.1. The diffraction peak of these two materials was found at 27.6°, which was related to (002) crystallographic face of the graphite support. Also, diffraction peaks at 2θ = 40.02, 46.91 and 69.05 can be attributed to the reflections of the 111, 200 and 311 crystalline planes of Pd, respectively [6].

The FE-SEM image of catalyst (Fig. 2) showed the small spherical particles accumulated on the of g-C_3N that represent the synthesized Pd NPs.

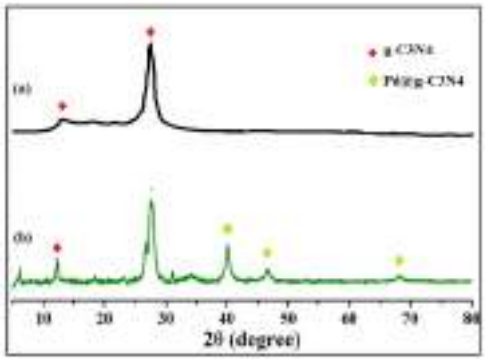

Fig.1. The XRD pattern of a) g-C3N4, b) Pd@g-C3N4

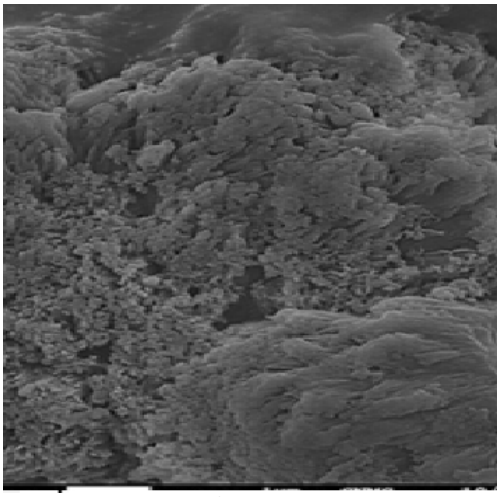

Fig. 2. FE-SEM image of Pd NPs@g-C_3N_4

2.2. Suzuki cross-coupling reaction of different aryl halides with phenyl boronic acids using PdNPs@g-C_3N_4

To study catalytic activity of the prepared PdNPs@g-C_3N_4 catalyst, The Suzuki cross-coupling reaction of aryl halides with phenylboronic acid was investigated. The coupling of iodobenzene with phenylboronic acid was chosen as a model reaction. The reaction gave the desired product in an almost quantitative yield at 50 °C in 1 h by using Na_2CO_3 and (water/ethanol) as a base and solvent, respectively.

Results of the coupling reaction between different aryl halides and phenylboronic acids (with or without electron donating/with-drawing chemical groups attached to their benzene ring) over the PdNPs@g-C_3N_4 catalyst under optimized condition are presented in Table 1.

Table 1. Synthesis of biphenyl derivatives in the presence of PdNPs@g-C_3N_4

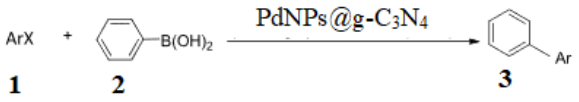

Entry	Compound	ArX	X	Yield
1	3a	C_6H_5	I	95
2	3b	4-OCH_3	I	93
3	3c	4-NO2	I	82
4	3d	4-CH3	I	92
5	3e	4-OCH3	Br	90
6	3f	C_6H_5	Cl	60

Reaction condition: phenylboronic acid (1.5 mmol), aryl halide (1 mmol), Na_2CO_3 (2 mmol), catalyst (15 mg)

As seen, aryl halides with electron-withdrawing or releasing groups reacted with phenylboronic acid to afford the corresponding products in high yields.

Reusability of the catalyst was tested by carrying out repeated runs of the reaction on the same batch of the catalyst in the case of the model reaction. The results show that this catalyst can be reused five times without any significant loss in activity performance (Fig. 3)

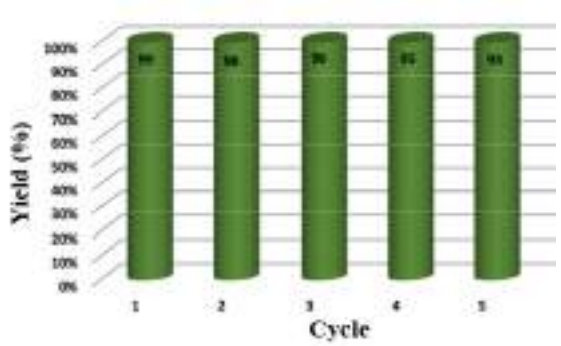

Fig. 3. Recyclability of PdNPs@g-C_3N_4 for the Suzuki–Miyaura coupling reaction of phenylboronic acid (1.1 mmol), iodobenzene (1 mmol), Na_2CO_3 (2 mmol) and PdNPs@g-C_3N_4, (15 mg), EtOH/H_2O (4 mL), 50 °C

.3. Conclusion

In conclusion, Pd nanoparticles were decorated on the surface of g-C_3N_4. The immobilized palladium was found to be effective in the Suzuki coupling of various aryl halides and especially less reactive aryl chlorides with phenyl boronic acid. This new heterogeneous catalyst showed the following compensations: (a) simple preparation; (b) easy separation (c) reusability for several times without any significant loss in its catalytic activity.

4. References

Experimental:

Synthesis of Pd@ g-C_3N_4:

the g-C_3N_4 was prepared by heating melamine in a muffle furnace according to the previously reported method [7].5.0 g melamine was placed into an alumina crucible, heated up to 500 °C with a heating rate of 10 °C min^{-1} After cooling to room temperature, the pale-yellow block was ground to obtain g-C_3N_4 powder.

For the preparation of Pd NPs@g-C_3N_4, 0.5 g g-C_3N_4 support was dispersed in 50 mL deionized water with sonication for 1 h. then, aqueous solution of $PdCl_2$ (0.01 M) and NaCl (0.04 M) was added into the mixture and then sonicated in the ultrasonic bath for 1 h. Then, 0.7 mL freshly-prepared $NaBH_4$ (0.5 M) solution was added to this suspension and the mixture was stirred overnight. Finally, the obtained catalysts were isolated by filtration, washed with sufficient deionized water and dried under vacuum at 50 °C overnight [4].

[1] F. F. Xu, J. Q. Chen, D. Y. Shao, P. Q. Huang, Nat. Commun. 14 (2023) 6251.
[2] A. K. King, A. Brar, G. Li., M. Findlater, Organometallics, 42 (2023), 2353-2358.
[3] A. Corma, H. Garcia, Top. Catal. 48 (2008) 8-31.
[4] N. Seyedi, K. Saidi, H. Sheibani, catal. Lett. 148 (2018) 277-288.
[5] R. G. Franzén, J. Comb. Chem.2 (2000) 195-214.
[6] N. Wang, L. Ma, J. Wang, Y. Zhang, R. Jiang, ChemPlusChem 84 (2019) 1164-1168.
[7] A. Nasri A, B. Jaleh B, Z. Nezafat Z, M. Nasrollahzadeh, S. Azizian, H. W. Jang, M. Shokouhimehr, Ceram. Int. 47 (2021) 3565-72.

29TH IRANIAN ORGANIC CHEMISTRY CONFERENCE
1_3 NOV, 2023
UNIVERSITY OF QOM, IRAN

Multicomponent Reactions towards Nitrogen Heterocycles

Ali Ramazani[1,2]*, and Seyedmohammad Hosseininezhad*[1,3]

[1]*Department of Chemistry, Faculty of Science, University of Zanjan, Zanjan 45371-38791, Iran, aliramazani@znu.ac.ir*
[2]*Research Institute of Modern Biological Techniques (RIMBT), University of Zanjan, Zanjan 4537138791, Iran*
[3]*Department of Chemistry, Faculty of Science, Babol Noshirvani University of Technology, Babol, Iran*

Abstract Nitrogen heterocycles are important structural units that are widely found in drugs, chemicals, bioactive natural products, etc. Due to the wide range and wide application of these compounds, the synthesis of nitrogen-containing heterocycles using multi-component reactions has been one of the hot topics. The purpose of this review is to summarize the reactions of triphenylphosphine in two, three, and four multicomponent reactions, the use of green nano catalyst, and also the effect of the solvent in multicomponent reactions for the synthesis of nitrogen heterocyclic compounds. For simplicity, we organized this review based on the following:

1. Introduction
2. Use of (*N-i*socyanimino)triphenylphosphorane
2.1. Two-Component Reactions of (*N-i*socyanimino)triphenylphosphorane
2.2. Three-Component Reactions of (*N-i*socyanimino)triphenylphosphorane
2.3. Four-Component Reactions of (*N-i*socyanimino)triphenylphosphorane
3. Use of green nanocatalyst
4. The effect of solvent on the selective synthesis of nitrogen-containing heterocyclic compounds
5. Conclusion

1. Introduction

Among the large and diverse families of organic compounds, heterocycles can be mentioned, in the meantime, nitrogen heterocycles have attracted a lot of attention because they are important structural subunits. These heterocycles have many applications in medicines, cosmetics, dyes, bioactive natural products, agricultural chemicals, etc [1]. According to the studies conducted among the top-selling small molecule drugs, more than 80% of these drugs contained at least one nitrogen heterocycle. Meanwhile, common nitrogen heterocycle skeletons such as triazines, triazoles, tetrazoles, indoles, and indazoles have shown that they have various biological activities [2]. Among other important applications of nitrogen heterocycles is the use of these compounds as mediators in the field of pharmaceutical industry, material chemistry and organic synthesis [3]. Considering the importance and practicality of nitrogen heterocyclic compounds in science and industry, these compounds have always been a hot topic in organic synthesis [4]. Regarding organic synthesis, multi-component reactions (MCRs) have gained a special place among chemists for many years, because by connecting three or more raw materials, high-complexity products with high atom economy and wide biological properties are produced. In the meantime, the use of MCRs for the synthesis of nitrogen heterocyclic compounds has become a powerful tool over the years [5]. In this review, we have briefly discussed the use of multicomponent reactions for the synthesis of nitrogen-containing heterocyclic compounds. Meanwhile, reactions involving the use of (*N* Isocyanimino)triphenylphosphorane in two-, three-, and four-component reactions, the use of green nanocatalyst, and the effect of the solvent on the selectivity of nitrogen heterocycles have been discussed.

2. Use of (*N-i*socyanimino)triphenylphosphorane

2.1. Two-component reactions of (*N-i*socyanimino)triphenylphosphorane

In 2007, (N-isocyanimino)triphenylphosphorane (2) and benzoic acids (1) reacted together (ratio 1:1) in CH_2Cl_2 at room temperature to produce the 2-aryl-1,3,4-oxadiazoles (3) (83-93% yields) and triphenylphosphine oxide (4) (Fig. 1). The important points of the method are high yields, ease of work-up, mild reaction conditions, and no side reactions which makes it a useful addition to modern synthetic methodologies[6].

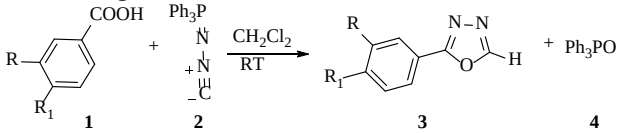

Fig. 1. Synthesis of 2-aryl-1,3,4-oxadiazoles[6].

2.2. Three-component reactions of (*N-i*socyanimino)triphenylphosphorane

Ramazani et al. [7] synthesized 1,3,4-oxadiazole derivatives (8) via the reaction between (N-isocyanimino)triphenylphosphorane (6), aromatic (or heteroaromatic) carboxylic acids (5), and aromatic bis-aldehydes (7) (ratio= 1:1:1) in CH_3CN at room temperature for 20 h (Fig. 2). the desired products were obtained in 70-85% yields. The advantages of the reaction are mild and clean conditions, easy work-up, and no side reactions.

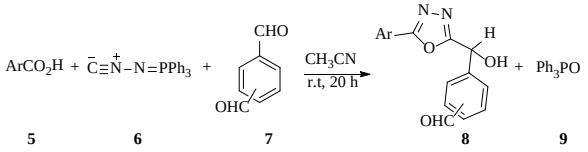

Fig. 2. Synthesis of Fully Substituted 1,3,4-Oxadiazole Derivatives from (N-isocyanimino)triphenylphosphorane[7].

In the other research, electron-poor α-haloketone derivatives (12) were reacted with aromatic carboxylic acid derivatives (10) and (N-isocyanimino) triphenylphosphorane (11) in CH_2Cl_2 at room temperature in a 1:1:1 ratio and produced the disubstituted 1,3,4-oxadiazoles (83-88% yields) (Fig. 3). This synthetic method due to the simple and mild conditions, high yields, and ease of work-up makes it a good addition to modern synthetic methodologies [8].

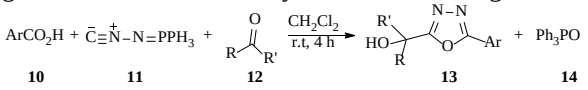

Fig. 3. Synthesis of disubstituted 1,3,4-oxadiazoles [8].

In 2012, fully substituted 1,3,4-oxadiazoles (18) were synthesized via the reaction between cyclobutanone (17), aromatic (or heteroaromatic) carboxylic acids (15), and N –isocyaniminotriphenylphosphorane (16) (ratio= 1:1:1) in CH_3CN at room temperature for 20 h (Fig. 4). The products were produced up to 87% yields. It should be noted that in this method the products were synthesized by intramolecular aza-Wittig closure. The important points of the method are mild and neutral conditions, an easy and simple route, ease of work-up, and no side reactions. All of these advantages make this method useful for modern synthetic methodologies[9].

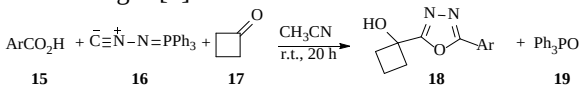

Fig. 4. Synthesis of fully substituted 1,3,4-oxadiazoles[9].

2.3. Four-component reactions of (*N-isocyanimino*)triphenylphosphorane

In 2010, 2,5-disubstituted 1,3,4-oxadiazoles (24) were synthesized via the reaction between an aromatic aldehyde (21), a carboxylic acid (22), a secondary amine (20), and (N-isocyanimino)triphenylphosphorane (23) in CH_2Cl_2 at room temperature for 2 h by an aza-Wittig closure of intramolecular (Fig. 5). The desired products were obtained in 78-94% yields. The important and advantageous point of the reaction is no use of an activation and catalyst. Also, these heterocyclic compounds could be biologically active scaffolds. It should be noted that a secondary amine is essential because the Mumm rearrangement is no longer possible [10].

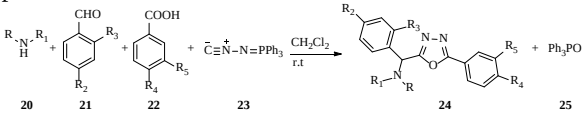

Fig. 5. Synthesis of 2,5-disubstituted 1,3,4-oxadiazoles[10].

In the next research, Ramazani et al. [11] synthesized disubstituted 1,3,4-oxadiazoles (30) via the reaction between a primary amine (26), a carboxylic acid (29), biacetyl (27), and (N-isocyanimino)triphenylphosphorane (28) in CH_2Cl_2 at room temperature (Fig. 6). The reaction was done by the Ugi-4CR/aza-Wittig sequence and the products were obtained in 72-87% yields. It should be noted that this method has good potential for the synthesis of types of disubstituted 1,3,4-oxadiazoles because of the neutral ring closure conditions, the ease of the synthetic method, and also no side reactions.

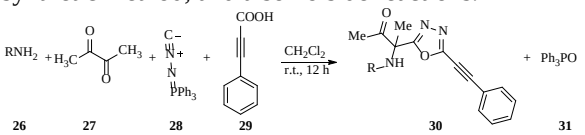

Fig. 6. Synthesis of disubstituted 1,3,4-oxadiazoles [11].

3. Use of green nanocatalyst

Ramazani et al.[12] synthesized 3-pyrrolin-2-one derivatives (35) via the reaction between diethyl acetylenedicarboxylate (33), aldehyde (34), and aniline derivatives (32) in the presence of magnetic cobalt ferrite nanoparticles functionalized with citric acid in EtOH under ultrasound irradiation (Fig. 7). The acidic nanocatalyst used in the reaction was reusable, green, and efficient. The desired products were produced up to 92%. This method was a green route for the synthesis of substituted 3-pyrrolin-2-one derivatives which has environmental, economic, simple separation, and easy work-up advantages.

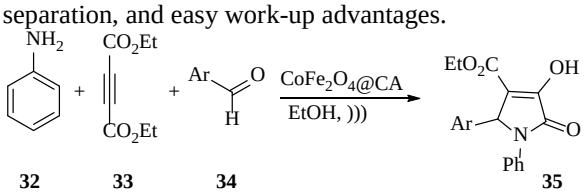

Fig. 7. Synthesis of 3-pyrrolin-2-one derivatives under ultrasound irradiation[12].

In 2018, Ramazani et al.[13] synthesized 2-amino-4,6-diarylnicotinonitrile derivatives (40) via the reaction between acetophenone (38), malononitrile (37), ammonium acetate (39), and aromatic aldehydes (36) in solvent-free conditions under microwave irradiation

(Fig. 8). It should be noted that this method used $CoFe_2O_4@SiO_2$-SO_3H as an organic-inorganic hybrid heterogeneous catalyst and the recovery of the catalyst was simple. The important advantages that could mentioned are high yields of products (85-92% yields), catalyst recovery at least five times, shorter reaction times, and easy work-up which achieves the high purity of products.

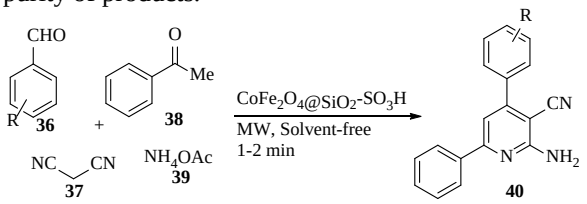

Fig. 8. Synthesis of 2-amino-4,6-diarylnicotinonitrile derivatives under solvent-free condition[13].

4. The effect of solvent on the selective synthesis of nitrogen-containing heterocyclic compounds

Ramazani et al.[14] via the reaction between acetylene diesters (41), benzhydroxamic acids (43), and trialkyl(aryl) phosphines (42) synthesized two important classes of heterocyclic compounds namely 1,4,2-dioxazoles (44) and N-benzoylaziridines (45) (Fig. 9). In this method, intermediate solvation plays a key step role in product selectivity. It should be noted that this method conformed to the highly cis-selective formation of the N-benzoylaziridines. In addition, the mentioned method via the green method prepared 1,4,2-dioxazoles by a β-cyclodextrin nanoreactor in aqueous media.

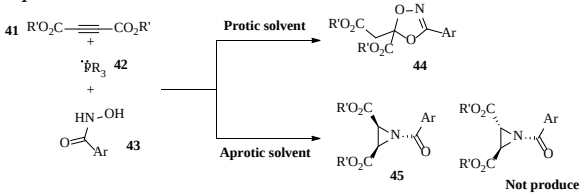

Fig. 9. Synthesis of 1,4,2-dioxazoles and N-benzoylaziridines[14].

5. Conclusion

In this review, recent advances in the synthesis of nitrogen heterocycle compounds using isocyanide, green nanocatalysts and the effect of solvent on the selectivity for the formation of nitrogen heterocycles were discussed. According to the results, the nitrogen heterocycles synthesized by isocyanides have no side reactions and have an easy purification process, and the products have high efficiency. Regarding the green nano catalysts, it should be said that the reactions were carried out under ultrasonication, which improved the reaction time, and also these catalysts were effective on the reaction efficiency. In addition, purification was easy in these reactions. We propose to expand the one-pot reactions for the synthesis of heterocyclic compounds to the gram scale in different reactions

6. References

[1] a) T. Eicher, S. Hauptmann, A. Speicher, The Chemistry of Heterocycles: Structures, Reactions, Synthesis, and Applications 3rd, Completely Revised and Enlarged Edition, Wiley-VCH, Weinheim, 2012; b) J. J. Li, Heterocyclic Chemistry in Drug Discovery, Wiley-VCH, Weinheim, 2013; c) A. P. Taylor, R. P. Robinson, Y. M. Fobian, D. C. Blakemore, L. H. Jones, O. Fadeyi, Org. Biomol. Chem. 2016, 14, 6611-6637.

[2] a) E. Vitaku, D. T. Smith, J. T. Njardarson, J. Med. Chem. 2014, 57, 10257-10274; b) R. D. Taylor, M. MacCoss, A. D. G. Lawson, J. Med. Chem. 2014, 57, 5845-5859; c) M. Baumann, I. R. Baxendale, Beilstein J. Org. Chem. 2013, 9, 2265-2319; d) M. Baumann, I. R. Baxendale, S. V. Ley, N. Nikbin, Beilstein J. Org. Chem. 2011, 7, 442-495; e) S. W. Youn, H. J. Yoo, E. M. Lee, S. Y. Lee, Adv. Synth. Catal. 2018, 360, 278-283.

[3] For selected reviews, see: a) P. Yin, Q. Zhang, J. M. Shreeve, Acc. Chem. Res. 2016, 49, 4-16; b) M. M. D. Roy, E. Rivard, Acc. Chem. Res. 2017, 50, 2017-2025; c) L. Li, T.-D. Tan, Y.-Q. Zhang, X. Liu, L.-W. Ye, Org. Biomol. Chem. 2017, 15, 8483-8492; d) E. Peris, Chem. Rev. 2018, 118, 9988-10031; e) H. Gao, Q. Zhang, J. M. Shreeve, J. Mater. Chem. A. 2020, 8, 4193-4216;

[4] Liu, J., Jiang, J., Zheng, L., & Liu, Z. Q. (2020). Recent advances in the synthesis of nitrogen heterocycles using arenediazonium salts as nitrogen sources. Advanced Synthesis & Catalysis, 362(22), 4876-4895.

[5] Isambert, N., & Lavilla, R. (2008). Heterocycles as key substrates in multicomponent reactions: the fast lane towards molecular complexity. Chemistry–A European Journal, 14(28), 8444-8454.

[6] Souldozi, A., & Ramazani, A. (2007). The reaction of (N-isocyanimino) triphenylphosphorane with benzoic acid derivatives: a novel synthesis of 2-aryl-1, 3, 4-oxadiazole derivatives. Tetrahedron Letters, 48(9), 1549-1551.

[7] Ramazani, A., Ahmadi, Y., & Mahyari, A. (2011). One-pot efficient synthesis of fully substituted 1, 3, 4-oxadiazole derivatives from (N-isocyanimino) triphenylphosphorane, carboxylic acids, and aromatic bis-aldehydes. *Synthetic Communications*, *41*(15), 2273-2282.

[8] Ramazani, A., Ahmadi, Y., Rouhani, M., Shajari, N., & Souldozi, A. (2010). The reaction of (N-isocyanimino) triphenylphosphorane with an electron-poor α-haloketone in the presence of aromatic carboxylic acids: A novel three-component reaction for the synthesis of disubstituted 1, 3, 4-oxadiazole derivatives. *Heteroatom Chemistry*, *21*(6), 368-372.

[9] Holagh, M. V., MAHARRAMV, A. M. O., Allahverdiyev, M. A. O., Ramazani, A., Ahmadi, Y., & Souldozi, A. (2012). One-pot synthesis of fully substituted 1, 3, 4-oxadiazole derivatives from aromatic carboxylic acids, cyclobutanone and N-isocyaniminotriphenylphosphorane. Turkish Journal of Chemistry, 36(1), 179-188.

[10] Ramazani, A., & Rezaei, A. (2010). Novel one-pot, four-component condensation reaction: An efficient approach for the synthesis of 2, 5-disubstituted 1, 3, 4-oxadiazole derivatives by a Ugi-4CR/aza-wittig sequence. Organic letters, 12(12), 2852-2855.

[11] Ramazani, A., Abdian, B., Nasrabadi, F. Z., Shajari, N., & Ranjdoost, Z. (2012). Four-component preparation of disubstituted 1, 3, 4-oxadiazoles from (N-isocyanimino) triphenylphosphorane, phenylacetylenecarboxylic acid, biacetyl and primary amines. Bull. Korean Chem. Soc, 33(11), 3701.

[12] Ahankar, H., Ramazani, A., Ślepokura, K., Lis, T., & Kinzhybalo, V. (2019). Magnetic cobalt ferrite nanoparticles functionalized with citric acid as a green nanocatalyst for one-pot three-component sonochemical synthesis of substituted 3-pyrrolin-2-ones. Research on Chemical Intermediates, 45, 5007-5025.

[13] Hosseinzadeh, Z., Ramazani, A., Ahankar, H., Ślepokura, K., & Lis, T. (2019). Synthesis of 2-amino-4, 6-diarylnicotinonitrile in the presence of CoFe 2 O 4@ SiO 2-SO 3 H as a reusable solid acid nanocatalyst under microwave irradiation in solvent-freeconditions. Silicon, 11, 2169-2176.

[14] Aghahosseini, H., Ramazani, A., Jalayer, N. S., Ranjdoost, Z., Souldozi, A., Ślepokura, K., & Lis, T. (2018). Vinylphosphonium salt-mediated reactions: A one-pot condensation approach for the highly cis-selective synthesis of N-benzoylaziridines and the green synthesis of 1, 4, 2-dioxazoles as two important classes of heterocyclic compounds. Organic letters, 21(1), 22-26.

Stereoelectronic effects: A new approach in organic chemistry

Mohammad Ali Zolfigol*

Department of Organic Chemistry, Faculty of Chemistry and Petroleum Sciences, Bu-Ali Sina University, Hamedan 6517838683, Iran. zolfi@basu.ac.ir & mzolfigol@yahoo.com

Keywords: Electrostatic, Stereoelectronic, Anomeric effect

Chemical reactivity is complex. Chemical reactivity is determined via various factors such as steric, electrostatic, stereoelectronic, overall energy, structure etc. In this lecture, the role of stereoelectronic concepts as a conceptual bridge between structure and reactivity will be discussed. Stereoelectronic effects, i.e., the stabilizing interactions of orbitals in space are based on the quantum nature of molecular bonding. Stereoelectronic stabilization can be "switched on" when the geometry is favorable for orbital overlap. Orbital size matching is very important for suitable overlapping. Generally, Stereoelectronic effects (intramolecular delocalizing interactions) are classified as conjugation, hyperconjugation (positive, negative and neutral), and σ-conjugation. To the best of our knowledge, the interactions that involve π-bonds and p-orbitals are referred to as conjugation. Interactions between σ- and π-orbitals are classified as hyperconjugation, whereas the interactions between two σ-orbitals are called σ-conjugation. In practice, σ-conjugation is often treated as another pattern of hyperconjugation. Negative hyperconjugation (or anomeric effect) involves the transfer of electron density from a good donor (usually, a lone pair) into an acceptor σ*-orbital. The anomeric effect (AE) is one of the famous concepts in organic chemistry. Recently, we and our coworkers have reviewed the role of AE in organic synthesis comprehensively [1-2]. Stereoelectronic effects and AE act as a major role in the biological molecules such as oxidation/reduction reactions of NADH/ NAD^+ and NADPH/$NADP^+$ systems. Various kinds of stereoelectronic effects and AE have been reported (**Scheme 1**).

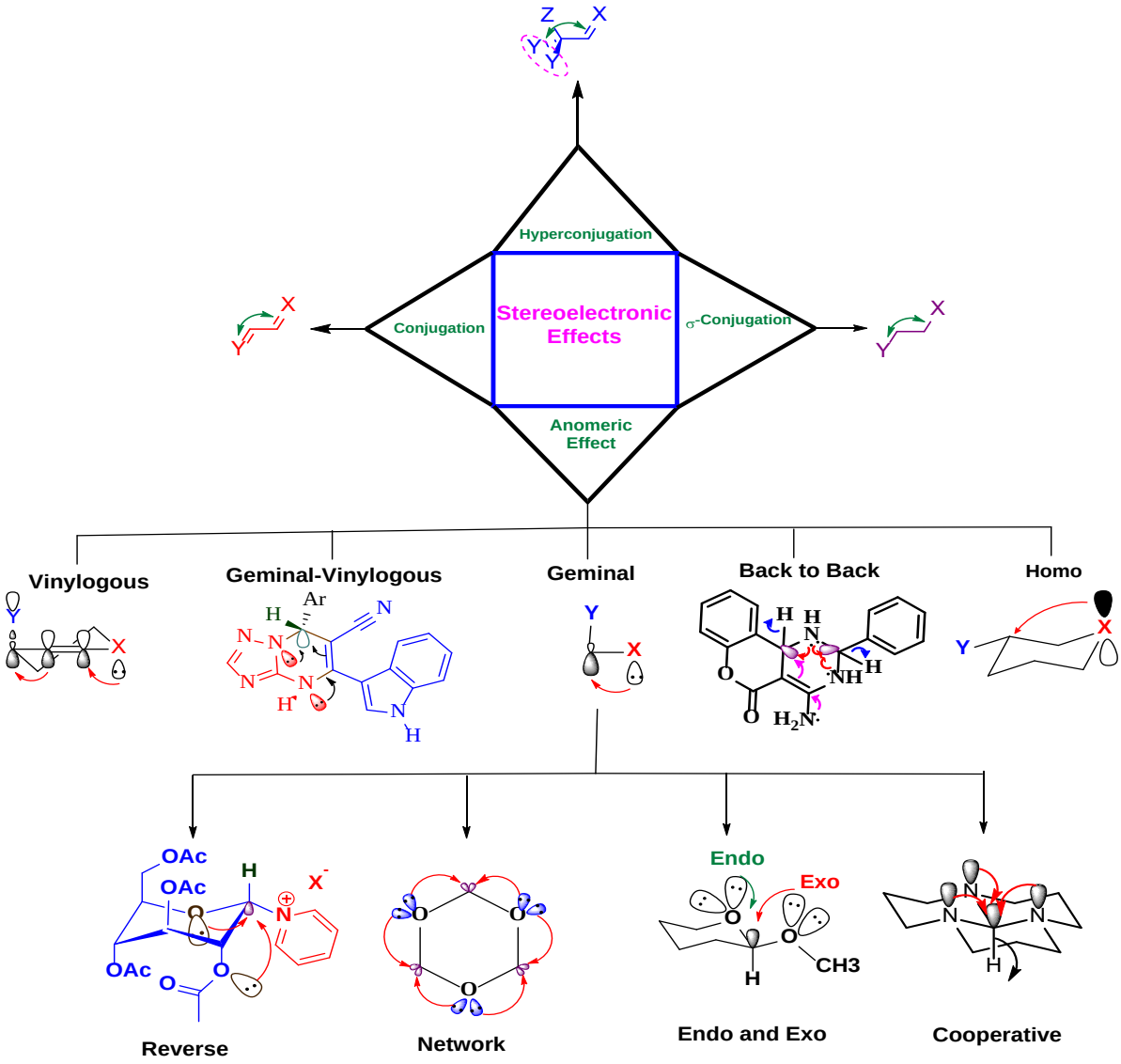

Scheme1: Various kinds of stereoelectronic and anomeric effects.

References

[1] Alabugin, I. V.; Kuhn, L.; Medvedev, M. G.; Krivoshchapov, N. V.; Vil, V. A.; Yaremenko, I. A.; Mehaffy, P.; Yarie, Terent'ev, M. A. O.; Zolfigol, M. A., Stereoelectronic power of oxygen in control of chemical reactivity: the anomeric effect is not alone, *Chem. Soc. Rev.* **2021**, *50*, 10253-10345.

[2] Alabugin, I. V.; Kuhn, L.; Krivoshchapov, N. V.; Mehaffy, P.; Medvedev, M. G. Anomeric effect, hyperconjugation and electrostatics: lessons from complexity in a classic stereoelectronic phenomenon, *Chem. Soc. Rev.* **2021**, *50*, 10212-10252.

29TH IRANIAN ORGANIC CHEMISTRY CONFERENCE
1_3 NOV, 2023
UNIVERSITY OF QOM, IRAN

Effect of CuO nanoparticles on thermal kinetics of nitrocellulose-based propellants

Vahid Mirzajani,[1] Hamed Nazarpour-Fard,[2] Khalil Farhadi,[1] Ali Ghobadian[3]*

[1] Department of Analytical Chemistry, Faculty of Chemistry, Urmia University, Urmia, Iran
[2] Department of Polymer Engineering, Faculty of Engineering, Lorestan University, Khoram-Abad, Iran
[3] Department of Chemistry, Faculty of Science, Lorestan University, Khoram-Abad, Iran

Abstract: The copper oxide nanoparticles (nano-CuO)/nitrocellulose (NC)/triethyleneglycol dinitrate (TEGDN)/diaminoglyoxime (DAG) nanocomposites were successfully prepared. The CuO nanoparticles significantly altered the thermal pattern of the studied energetic materials (confirmed by TGA and DSC methods), e.g., the temperatures corresponded to the DSC peaks were changed by increasing the nano-CuO amount. Moreover, the catalyst resulted in the decrement in the activation energy of the decomposition stage by ~30-50 kJ mol^{-1} and also improved the thermal stability of TEGDN/NC/DAG composite.
Keywords: Propellants, Combustion, CuO nano-catalyst, Kinetic, Thermodynamic

1. Introduction

Nano-sized metal oxides have been attracting much attention due to their unique physical and chemical characteristics [1, 2, 3, 4, 5, 6, 7-9]. CuO nanostructures are of particular interest because of their appealing traits and promising usages in energetic materials [10, 11-12]. Also, they have been employed as a heterogeneous catalyst in the combustion of hydrocarbons and also the improvement of thermal conductivity of materials [10]. Energetic materials are extensively applied in the numerous defense-related areas, de-construction, joining, airbag igniters, soldering etc [7-10]. Enhancing the combustion performance of the solid propellants or energetic samples has always been an important issue for various researchers [1, 7-9]. The particles with the size in the nano-scale have been exhibited the elevated catalytic characteristics [1, 7-9]. Thus, substituting the traditional catalysts in the solid propellants by nano-catalysts could be the important and attractive studying field for improving the combustion performance of the energetic materials [1, 7-9, 13].
The oxidized transition metal oxides (TMOs) have been found as important chemicals with the wide-variety of usages in the various fields [2]. Among them, nano-sized transition metal oxides have been revealed a remarkable effect on decomposition improvement of energetic samples [3, 14-15] that can show fantastic physico-chemical behaviors [2]. It is clear that obtaining information about the thermal stability of nanoparticles in the different formulations is essential [8, 18-19].
Thus, we aimed at the studying the catalytic performance of the nano-sized CuO on the thermal behavior of the TEGDN/NC/DAG composite. It can be hoped that this study can open the new insight toward further studies on the characteristics of TEGDN/NC/DAG nanocomposite type propellants.

2. Materials and methods

All the materials used here were as the onse used in the previous reported our study [20-21]. Also, all the synthesis protocols of the propellant samples was as same as the method used in the previous studies [22-23]. SEM microscopy (KYKY-EM3200, CHINA) was utilized to investigate the morphology of the prepared nanocomposites. The thermal analysis of the energetic mateials were performed by a thermal analyzer (Mettler TA4000) and a DSC 1 (Mettler Toledo Co., Switzerland).

3. Results and discussion

3.1. Characterization of the prepared composite and nanocomposites

On the basis of the SEM micrograph in Figure 4(a), it is clear that ES-1 has the homogeneous morphology and no agglomeration of the components was exhibited in its SEM image. While, Figures 4 (b-d) and Figures S1-S3 are the SEM results for ES-2, ES-3 and ES-4, respectively. As could be seen, the nanoparticles were uniformly distributed through the structure of the samples and no meaningful agglomeration was appeared in the SEM images.

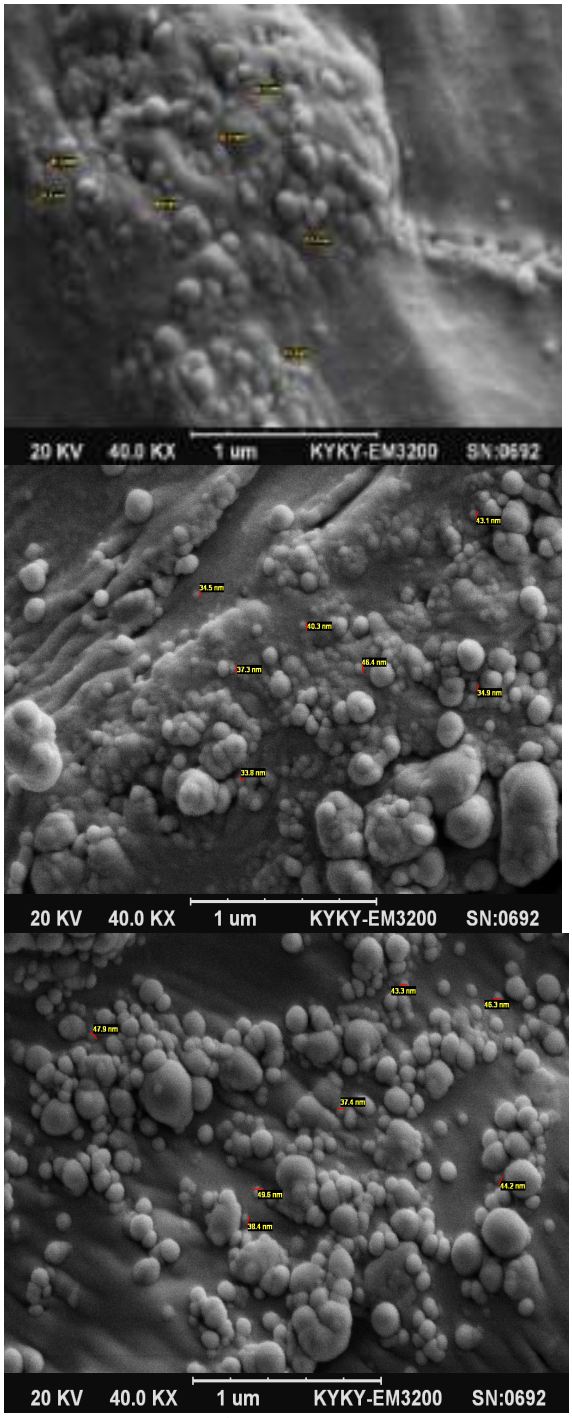

Figure1. SEM images of the 1%, (b) 2% and (c) 3% nano-CuO incorporated nanocomposites.

3.2. Thermal behavior of the samples

3.2.1. The nano-CuO incorporated nanocomposites

The catalytic activity of the nanoparticles on the thermal decomposition of the TEGDN/NC/DAG energetic compositions were studied *via* the two techniques of TG-DTG at the heating rate of 10 °C min^{-1} and DSC thermal analysis at the heating rates of 2, 5, 7 and 10 °C min^{-1} for all the samples (Figures 5 and 6).

Al the samples showed the exothermic peak at the DSC traces and the corresponding single mass loss stage in TG analysis. The parent TEGDN/NC/DAG sample exhibited the single mass loss stage starting at 195 ˚C with the mass loss about 80.3%, while the DSC peak temperature of this sample occurred at 197 ˚C. DSC curve of the 1% nano-CuO contained sample (ES-2) revealed the sharp exothermic event with the onset temperature of 197 ˚C and the peak temperature of 200 ˚C. The TG analysis of ES-2 exhibited the mass loss of ~70.5%. DSC curve of the sample containing 2% nano-CuO (ES-3) similarly showed a sharp exothermic behavior which starts from 195 ˚C and is maximized at the temperature of 200 ˚C. Whereas the mass loss of ES-3 in thermogravimetry analysis was around 71.2%. But, ES-4 (the sample containing 3% nano-CuO) exhibited the similar peak starting from 188 ˚C and maximizing at the temperature of 200 ˚C. While the corresponding mass loss of this sample was about 70.5%.

A summary of the DSC results for TEGDN/NC/DAG energetic compositions containing the different amounts of the CuO nanoparticles are presented in Table 3. According to the DSC data, it could be concluded that nano-CuO enhances the decomposition temperature of TEGDN/NC/DAG energetic composite. Additionally, the heat of decomposition for the energetic compositions were enhanced upon adding 2 and 3 wt% of nano-CuO to the samples. The described changing trend in the heat of decomposition for the studied samples can be found in Figure 7. As seen in this figure, the sample containing 3 wt% of the nano-catalyst has the highest heat of decomposition.

Additionally, it is worth mentioning that on the basis of Figure 6, the DSC peaks of the samples were shifted to the higher temperatures upon increasing the heating rate. Table 3 reveals these shifts in the peak temperatures quantitatively.

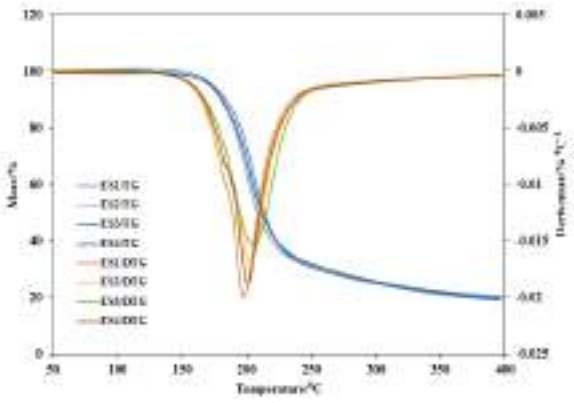

Figure 5. TG-DTG curves for the energetic composites and nanocomposites at the heating rate of 10 °C min^{-1}.

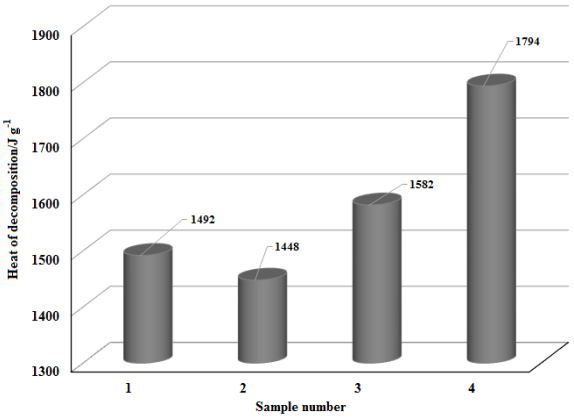

Figure 7. The heats of decomposition for the energetic composite and nano-composites at the different heating rates.

Table 3. Maximum peak temperature of the energetic composite and nanocomposites at the different heating rates.

Heating Rate (°C min^{-1})	Decomposition Temperature (°C)			
	ES-1	ES-2	ES-3	ES-4
2	183	184	184	184
5	187	190	192	192
7	192	192	199	195
10	197	200	200	200

3.3 Theoretical section

The first utilized protocol for measuring the Arrhenius parameters was Kissinger [24], in which E_a is obtained by using Eq.1 (Table 4). φ is the DSC heating rate, T_m is the temperature corresponding to the highest heat flow or to the peak temperature at the maxima, and R is the universal gas constant. The activation energy data for the prepared propellants were measured by the DSC data at the several heating rates (Table 3). Plotting $Ln\,(\frac{\varphi}{T_m^2})$ against $1/T_m$ led to the linear curves for all the samples which confirmed that the thermal decomposition of the samples undergoes no distinction at the different heating rates [25]. It is worth to mention that, the slope of the linear curves is equal to $-E_a/R$. In the next stage, Arrhenius factor or log (A/S^{-1}) was evaluated *via* the following equation recommended by ASTM E698 (Eq.2) [26].

$$Ln\,\frac{\varphi}{T_m^2} = Ln\,\frac{AR}{E_a} - \frac{E_a}{R\,T_m} \qquad (1)$$

$$A = \frac{[\varphi E_a \exp(\frac{E_a}{RT_m})]}{RT_m^2} \qquad (2)$$

The resulted data of Arrhenius factor (A) and activation energy for the propellants have been shown in Table 5.

Table 5. The computed kinetic parameters of the major exothermic decomposition step for the high energy nanocomposites and pure sample

Method	ES-1			
	E_a kJ mol^{-1}	log$A$ s^{-1}	r	Q
Kissinger	185	19	0.9495	0.2556
	ES-2			
Kissinger	158	16	0.9307	0.2967
	ES-3			
Kissinger	151	15	0.9831	0.1472
	ES-4			
Kissinger	176	18	0.9947	0.0829

3.4. The Thermal stability of TEGDN/NC/DAG and TEGDN/NC/DAG/CuO

The TG/DSC thermograms for the TEGDN/NC/DAG and TEGDN/NC/DAG/CuO samples can be seen in Figures 5 and 6. ES-1 and the nanocomposites revealed the similar thermal patterns and exhibited a single exothermic occurrence during their decomposition reaction. However, the decomposition of the nanocomposites was occurred at the higher temperatures and their activation energy values were lower as compared to ES-1. This means that nano-CuO leads to the more easily decomposition reaction and the decrement of the activation energy by around 30–50 kJ mol^{-1}. Also, as can be seen in Table 7, the positive values of $\Delta H^{\#}$ and $\Delta G^{\#}$ for the samples reveals that they need the heat introduction for starting the decomposition, i.e., their decomposition reaction is not spontaneous. The catalytic performance of the metal oxides (e.g., Fe_2O_3, Mn_2O_3 and CuO) is assigned to their electron configuration (the partially filled d-orbitals) and the relatively small sizes causing a less electrical shielding that it results in the high tendency to extra electrons or negative charges [4-5, 15-17].

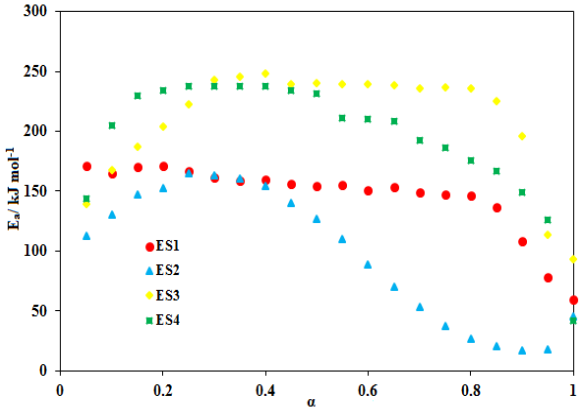

Figure 8. The activation energy values for the energetic composite and nano-composites at the several heating rates.

4 Conclusion

The results of the study exhibited that the decomposition temperature of the nanocomposites is higher than that of the parent TEGDN/NC/DAG. However, the nanocomposites revealed the lower values for the activation energy and frequency factor. The CuO nanoparticles indicated the elevating influence on the thermal decomposition while they reduced the activation energies by more than 30-50 kJ mol^{-1}. The catalytic performance of the nanoparticles was defined on the basis of its electronic configuration.

References

[1] W. Pang, L. T. De Luca, X. Fan, F. Maggi, H. Xu, W. Xie, X. Shi, *J. Combust. Sci. Technol*. **2016**, *188*, 315.
[2] H. Nayak, A. K. Jena, *Int. J. Sci. Res*, **2014**, *3*, 381.
[3] I. P. S. Kapoor, P. Srivastava, G. Singh, *Propellants. Explos. Pyrotech.* **2009**, *34*, 351.
[4] M. Shimokawabe, R. Furuichi, T. Ishii. *Thermochimica. Acta*. **1977**, *20*, 347.
[5] A. A. Said, E. A. Hassan, K. M. Abd El-Salam, *J. Surf. Technol*. **1983**, *20*, 123.
[6] P. Chen, F. Q. Zhao, Y. Luo, R. Z. Hu, S. L. Gao, Y. M. Zheng, M. Z. Deng, Y. Gao, *Chin. J. Chem.* **2004**, *22*, 1056.
[7] A. A. Gromov, A. V. Sergienko, E. M. Popenko, K. V. Slyusarsky, K. B. Larionov, E. L Dzidziguri, A. Y Nalivaiko, *Propellants. Explos. Pyrotech*. **2020**, *45*, 730
[8] V. Bagalkote, D. Grinstein, B. Natan, *Propellants. Explos. Pyrotech.* **2018**, *43*, 136.
[9] A. A. Vargeese, K. Muralidharan, V. N. Krishnamurthy, *Propellants. Explos. Pyrotech.* **2015**, *40*, 260.
[10] Q. Zhang, K. Zhang, D. Xu, G. Yang, H. Huang, F. Nie, C. Liu, S. Yang, *Prog. Mater. Sci.* **2014**, *60*, 208.
[11] M. Mahinroosta, *J. Nanostructure. Chem*. **2013**, 3 (47), 1.
[12] J. Wang, S. He, Z. Li, X. Jing, M. Zhang, Z. Jiang, *J. Chem. Sci.* **2009**, *121*, 1077.
[13] J. Rocco, J. Lima, A. Frutuoso, K. Iha, M. Ionashiro, J. Matos, M. Suárez-Iha, *J. Therm. Anal. Calorim*. **2004**, *75*, 551.
[14] S. Martins, J. B. Fernandes, S. C. Mojumdar, *J. Therm. Anal. Cal*, **2015**, *119*, 831.
[15] M. Ravanbod, H. R. Pouretedal, *J. Therm. Anal. Cal*. **2016**, *124*, 1091
[16] H. Iwakura, N. Kakuta, A. Ueno, K. Kishi, J. Kato, *Ind. Eng. Chem. Res*. **1991**, *30*, 778.
[17] Z. Feng, Y. Pan, Y. Wu, J. Zhao. *Hua-xue Tongbao*, 1988, 9, 43.
[18] P. J. Wilkinson, M. C. Weaver, G. Kister, P. P Gill, *Propellants. Explos. Pyrotech*. **2021**, 47, e202100142,
[19] S. Touidjine, K. M. Boulkadid, D. Trache, S Belkhiri, A. Mezroua, *Propellants. Explos. Pyrotech*. **2022**, 47, p.e202000340.
[20] N. A. Straessler, A. J. Paraskos, M. P. Kramer, *Methods of producing nitrate esters*, US Patent 20120130115A1, Northrop Grumman Corporation, USA, **2012**.
[21] S. M. Pourmortazavi, K. h. Farhadi, V. Mirzajani, S. Mirzajani, I. Kohsari, *J. Therm. Anal. Calorim*. **2016**, *125*, 121.
[22] M. B. Talawar, P. S. Makashir, J. K. Nair, S. M. Pundalik, T. Mukundan, S. N. Asthana, S. N. Singh, *J. Hazard. Mater*. **2005**, *125*, 17.
[23] J. H. Yi, F. Q. Zhao, W. L. Hong, S. Y. Xu, R. Z. Hu, Z. Q. Chen, L. Y. Zhang, *J. Hazard. Mater*. **2010**, 176, 257.
[24] H. E. Kissinger, *J. Anal. Chem.* **1957**, *29*, 1702.
[25] A. S. Tompa, R. F. Boswell, *J. Thermochim. Acta*. **2000**, *357*, 169.
[26] ASTM E698-11. *Standard test method for Arrhenius kinetic constants for thermally unstable materials using differential scanning calorimetry and the Flynn/Wall/Ozawa method*. ASTM International, West Conshohocken, 2011. doi: 10. 1520/E0698-11. Accessed 2017.

29TH IRANIAN ORGANIC CHEMISTRY CONFERENCE
1_3 NOV, 2023
UNIVERSITY OF QOM, IRAN

A NEW APPROACH FOR IMPROVING WATER SOLUBILITY OF PROGESTERONE BY ENCAPSULATION WITH CARBOXYMETHYL-β-CD

*Mehrdad Hadadian, Reza Allahyari, B. Mahdavi**

Department of Chemistry, Faculty of Science, Hakim Sabzevari University, Sabzevar, Iran,
haddadian24@gmail.com, b.mahdavi@hsu.ac.ir

Abstract

Progesterone is a steroid hormone mainly associated with female reproductive functions and formulated to treat sexually transmitted diseases and nervous disorders. However, its low water solubility limits its absorption and bioavailability. So, the formation of inclusion complexes with cyclodextrins is an excellent way to improve its solubility. For this purpose, progesterone was encapsulated in carboxymethyl-β-cyclodextrin (CM-β-CD). UV-Vis, FT-IR, and XRD analyses were performed to characterize the formed inclusion complex.

1. Introduction

Progesterone (Pro) is a sexual steroid hormone associated with female reproductive functions like preparing the uterus for embryo implantation and sexual behavior [1]. this hormone is mainly produced by the ovaries, adrenal cortex, and central nervous system (CNS) of both male and female mammals [2]. Progesterone is used as a medication mainly in hormone therapy for menopausal symptoms and low sex hormone levels in women [3]. It also treats gynecological disorders and supports pregnancy [4].

Cyclodextrins (CDs) are chemical compounds of natural origin, which are derived from bacterial degradation of starch through the metabolic action of cyclodextrin glycosyl transferase enzyme (GCTase) [5]. Cyclodextrins are natural cyclic carbohydrates that consist of 6, 7, and 8 glucose units (αCD, βCD, γCD, respectively). CDs have a hollow hydrophobic interior and a hydrophilic outer surface [6]. That makes these compounds have one of the simplest systems for capsule formation and a high ability to encapsulate various organic and inorganic molecules [7]. With this feature, cyclodextrins can improve the stability and dissolution of the guest in water by forming complexes [8]. β-CD is the most widely used cyclodextrins type because of pore size, availability, and low price. But its poor solubility in water led us to use β-CD derivatives. For this purpose, we modified the cyclodextrin to obtain carboxymethyl-β-cyclodextrin (CM-β-CD) to exhibit satisfying aqueous solubility [9].

This study aimed to form a PRO/CM-β-CD inclusion complex to increase the water solubility and bioavailability of Progesterone. Characterization of PRO/CM-β-CD inclusion complex was prepared by Fourier-transform infrared (FT-IR) spectroscopy and X-ray diffractometry (XRD)

2. Materials and methods

2.1 Materials

In this study, the following chemicals were used: β-cyclodextrin (β-CD, from Merck), Progesterone (from Sigma-Aldrich, >98%.), Sodium hydroxide (NaOH, from Merck), monochloroacetic acid (from Sigma-Aldrich), Hydrochloric acid (HCL, from Merck), methanol (from Merck) and Milli-Q water was used throughout this study.

2.2 Methods

2.2.1 Preparation of carboxymethyl-β-CD (CM-β-CD)

CM-β-CD was prepared following the procedure of literature [10]. Briefly, β-CD (1 g) and NaOH (0.93 g) were dissolved in water (3.7 mL), and 16.3% monochloroacetic acid (2.7 mL) was added. The reaction mixture was stirred at 50 °C for 5 h. After that, the solution was cooled to room temperature, and pH was adjusted (6–7) by adding HCl solution. The obtained neutral solution was poured into non-solvent methanol, and the resulting white precipitate product was filtered and dried at room temperature for 24 h.

2.2.2 Preparation of Pro/CM-β-CD inclusion complex

For this section, 0.98gr of CM-β-CD was dissolved in deionized water (1mL). Also, 0.16 gr of Progesterone was solubilized in methanol (4 mL). then, the progesterone solution was added to CM-β-

CD solution slowly and stirred at room temperature for 24 h. Next, the reaction mixture was ultrasonicated at 30 °C for 30 min and rested at 4 °C for 12 h. Finally, the precipitated complex was filtered and washed with methanol to purify the product, Finally, freeze-drying was applied for further studies [11].

2.2.3 Characterization of inclusion complex

2.2.3.1 Fourier-transform infrared (FT-IR) spectroscopy

FT-IR spectra of Pro, CM-β-CD, and Pro/CM-β-CD inclusion complex were obtained using PerkinElmer Spectrum IR Version 10.6.2 at the range of 400 - 4000 cm^{-1} at room temperature.

2.2.3.2 X-ray diffractometry (XRD)

The XRD patterns of Pro, CM-β-CD, and Pro/CM-β-CD inclusion complex were obtained by a Multipurpose X-ray Diffraction Multipurpose Diffractometer (X'Pert Pro MPD, Malvern PANalytical, UK) with Cu Ka radiation powered at voltage 45kV and current 40mA. The diffraction angle (2θ) was between 6°- 90° and the scanning rate was 2°/min.

2.2.4 solubility studies

solubility studies were performed according to the reported procedure [12]. Summarily, 0.004, 0.005, 0.007, 0.01, 0.02, and 0.025gr of Pro/CM-β-CD were added to 10 mL deionized water and stirred for 10 min. at room temperature. After attaining the equilibrium, the samples were filtered. Then, the maximum absorbance of Pro/CM-β-CD was measured by a UV–Vis spectrophotometer (Jena Speko l2000 spectrophotometer) at the range of 200 – 500 nm.

3. Results and discussion

3.1. Characterization of Pro/CM-β-CD complex

FT-IR analysis. FT-IR is an adequate technique to identify the formation of CD-Drug complexes. As the inclusion complexes between host and guest molecules are formed, their peaks' intensity might change or some peaks undergo disappearance, broadening, or shifting to lower or upper wavenumbers[13]. Fig1. represents the FT-IR spectra of progesterone, CM-β-CD, and inclusion complex. The spectrum of progesterone shows strong peaks at 1658 and 1696 cm^{-1}, contributing to C=O stretching bands. Small speaks at 2851 and 2900 are ascribed to C-H stretching bands. CM-β-CD spectra show strong peaks at 1020 and 1151 which are attributed to the stretching vibration of C-O bands. Moreover, the bending vibration of CH_2 bands is recorded at around 1373 cm^{-1}, and the stretching vibration of C-H bands is observed at

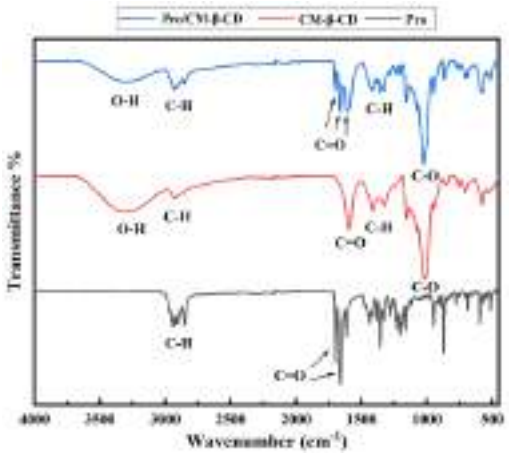

Figure 1. FT-IR spectra of Pro, CM-β-CD, and Pro/CM-β-CD inclusion complex.

2916 cm^{-1}. Besides, the strong peak at 1592 cm^{-1} is attributed to the carbonyl-stretching band, and the prominent peak at 3297 cm^{-1} results from the O-H bands. The spectra of Pro/CM-β-CD indicate the formation of the inclusion complex. The peaks at 1600, 1662, and 1700 cm^{-1} are implied the presence of both host and guest molecules. In addition, some changes are observed for the both stretching and bending vibration of C-H bands. Also, the intensity of the broad O-H band is decreased which could confirm the encapsulated product.

XRD analysis. As the formation of an inclusion complex has detected by FT-IR analysis, we are used XRD analysis to endorse our findings. In microcrystalline or powder states, X-ray diffraction is a useful method for the detection of CDs and their complexes. Every similarity between the XRD patterns of single components and the final product is a confirmation of the synthesis of the inclusion complex. In addition, the appearance, disappearance, shift, and diffraction of peaks are evidence for the interactions of components[14]. As indicated in Fig. 2. CM-β-CD is amorphous with two distinct peaks at angles of 2θ ~31.35° and 45.13°. The XRD pattern of progesterone shows many sharp peaks due to its crystalline nature. The peaks are found at 10.47, 12.58, and 16.78 2θ values. the XRD of Pro/CM-β-CD shows a crystalline quite different pattern from the superimposition of amorphous CM-β-CD and crystalline Pro with strong peaks at 2θ values of 10.47, 12.58, 16.58, 31.35, and 45.13 which indicate the presence of both host and guest molecules and the successful formation of the inclusion complex.

3.2 Aqueous solubility of Pro/CM-β-CD

According to the literature[15]. The solubility of Pro was only 16 μg.mL^{-1} and the water solubility of Pro/CM-β-CD inclusion complex was calculated by Zhang method. Fig. 3. depicts the UV-Vis spectra of aqueous solution of Pro/CM-β-CD with different concentrations. As shown in Fig. 3 the absorption of Pro/CM-β-CD is increased until reaching the saturated solution at 2 g.L^{-1}. Adding an excess amount of inclusion complex leads to mis assessing the absorption peaks because of the formation of a cloudy solution. Moreover, peak intensity is dependent on the concentration of Pro/CM-β-CD. according to our findings, it is obvious that the CM-β-CD capsule increases the solubility of progesterone in water to 2 g.L^{-1} by forming the inclusion complex.

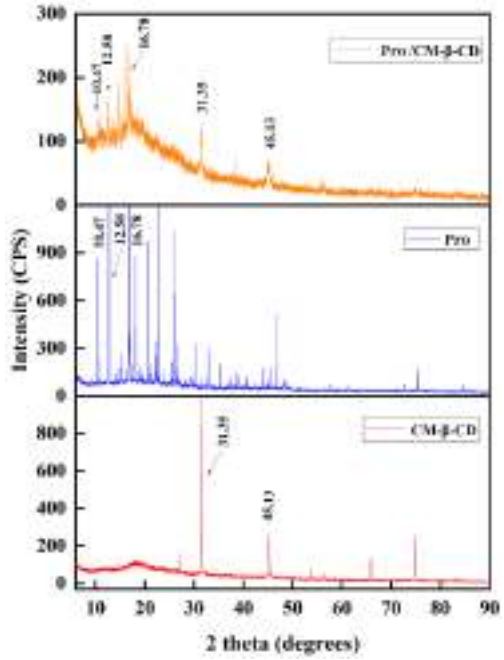

Figure 1. XRD patterns of Pro, CM-β-CD, and PRO/CM-β-CD inclusion complex.

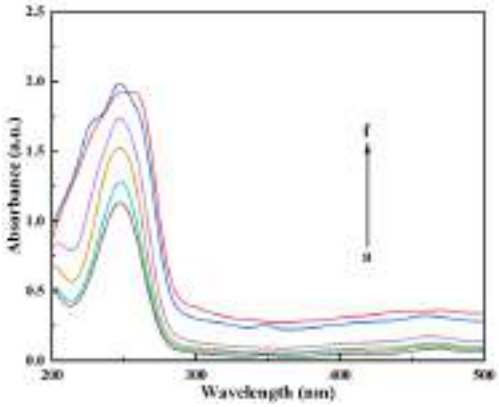

Figure 2. (A) UV-Vis spectra of Pro/CM-β-CD with different concentrations in deionized water: (a)0.004, (b)0.005, (c)0.007, (d)0.01, (e)0.02, (f)0.025.

4. Conclusion

The inclusion complex of progesterone with CM-β-CD is characterized by different analysis. The results show that the water solubility of progesterone tremendously increases after the encapsulation process. Due to the importance of progesterone in sexual and nervous diseases, and the environmentally friendly synthesis of the Pro/CM-β-CD complex, this product should be considered as a wise step in the formulation of progesterone for healthcare products or medicines.

5. References:

[1] Wu, S.-P., R. Li, and F.J. DeMayo, *Progesterone receptor regulation of uterine adaptation for pregnancy.* Trends in endocrinology & metabolism, 2018. **29**(7): p. 481-491.

[2] Mensah-Nyagan, A.G., et al., *Neurosteroids: expression of steroidogenic enzymes and regulation of steroid biosynthesis in the central nervous system.* Pharmacological reviews, 1999. **51**(1): p. 63-82.

[3] Kuhl, H., *Pharmacology of estrogens and progestogens: influence of different routes of administration.* Climacteric, 2005. **8**: p. 3 - 63.

[4] Choi, S.-J., *Use of progesterone supplement therapy for prevention of preterm birth: review of literatures.* Obstetrics & gynecology science, 2017. **60**(5)

[5] Di Cagno, M.P., *The potential of cyclodextrins as novel active pharmaceutical ingredients: a short overview.* Molecules, 2016. **22**(1): p. 1.

[6] Ciobanu, A., D. Landy, and S. Fourmentin, *Complexation efficiency of cyclodextrins for volatile flavor compounds.* Food research international, 2013. **53**(1): p. 110-114.

[7] Astray, G., J. Mejuto, and J. Simal-Gandara, *Latest developments in the application of cyclodextrin host-guest complexes in beverage technology processes.* Food Hydrocolloids, 2020. **106**: p. 105882.

[8] Jin, Z.-Y., *Cyclodextrin chemistry: preparation and application.* 2013: World Scientific.

[9] Zou, C., et al., *Study on the inclusion and solubilization processes of inclusion complex of carboxymethyl-β-cyclodextrin with CDOTP.* Journal of Molecular Liquids, 2014. **191**: p. 48-52.

[10] Badruddoza, A., et al., *Synthesis of carboxymethyl-β-cyclodextrin conjugated magnetic nano-adsorbent for removal of methylene blue.* Colloids and Surfaces A: Physicochemical and Engineering Aspects, 2010. **367**(1-3): p. 85-95.

[11] Kaur, K., R. Jindal, and D. Jindal, *Synthesis, characterization and studies on host-guest interactions of inclusion complexes of metformin hydrochloride with β–cyclodextrin.* Journal of Molecular Liquids, 2019. **282**: p. 162-168.

[12] Zhang, W., et al., *Investigation of water-soluble inclusion complex of hypericin with β-cyclodextrin polymer.* Carbohydrate polymers, 2013. **95**(1): p. 366-370.

[13] Mura, P., *Analytical techniques for characterization of cyclodextrin complexes in the solid state: A review.* Journal of pharmaceutical and biomedical analysis, 2015. **113**: p. 226-238.

[14] Abarca, R.L., et al., *Characterization of beta-cyclodextrin inclusion complexes containing an essential oil component.* Food chemistry, 2016. **196**: p. 968-975.

[15] Vinarov, Z., P. Dobreva, and S. Tcholakova, *Effect of surfactant molecular structure on Progesterone solubilization.* Journal of drug delivery science and technology, 2018. **43**: p. 44-49.

List of Authors

first name	last name/n.o.page
Ali	A.Mohammadi 197,198,357
Mahtab	Abareshi 76
Niloofar	Abbasi 85
Mahsa	Abbasiazad 281
Alireza	Abbassi 496,615
Zahra	Abdi 21,348
Fatemeh	Abdi 730
Fatemeh	AbdiyanMobarakeh 348
Tooba	Abdizadeh 247,250
Fatemeh	AbdolahAbyaneh 469
Erfan	Abdoli 196
Mohammad	Abdollahi 454
Mahdiye	Abdollahi 557
A.	Abdolmaleki 555
Amir	Abdolmaleki 710,546
Shahrzad	Abdolmohammadi 599
M.	AbedinMoghanaki 357
Mina	AbkarAras 571
Nastaran	Abudnejad 408
Mohsen	Adeli 303,312,322
Hadi	Adibi 360
Abbas	Afkhami 68
Jalil	Afshar 315,316
Sanaz	Aftabi 727
Kimia	Aghaie 313
Ghasem	Aghapour 22
Ghasem	Aghapour 22,40,43
Hamid	Aghavandi 230,231,280
Hosein	Ahangar 549
Atieh	Ahmadi 17
Atieh	Ahmadi 17
Hossein	Ahmadi 204,287,549
Masoomeh	Ahmadi 206
Fatemeh	Ahmadi 22
Maryam	Ahmadi 580
Majid	Ahmadlouydarab 623
Fatemeh	Ajormal 112,113
Ali	Akbari 170,171
Jafar	Akbari 754,802
AliReza	Akbarzadeh 586
Nabaa	Al_timimi 496
Hassan	Alamgholiloo 175
Sedigheh	Alavinia 213
MirMohammad	AlaviNikje 416
Jalal	Albadi 609

Hassan Alehdaghi 704
Mohammad Ali Ghasemzadeh 93,246,472,528
Hamid Alimohammadi 498,504
Mahboobeh Alimoradi 331,332
Heshmatollah Alinezhad 116
Sakineh Alipour 16
Batoul Alipour 321
Batoul Alipour 321,741
Zahra Alishahi 180
Reza Alizadeh 285,288
Nina Alizadeh 319
Mahsasadat Alizadeh 340
Vali Alizadeh 463,466
Reza Allahyari 816
Zahraa Alsudani 634
Hale Alvandi 261,724
Roya Alzoha 615
Ameneh Amani 132,133,305,493
Fatemeh Amarloo 376,381
Ali Hossein Amini 423
Rana Amini 423
Hanieh Amini Moghaddam 95
Hanieh Amini Tazehkand 248
Kamran Amiri 313,328,347
Mostafa Amiri 568,658
Maryam Anafcheh 689
Hossein Anaraki-Ardakani 249,683
Mohammad Anary-Abbasinejad 110
Nafiseh Annabestani 662
Ghazale Anvarian-Asl 88
Avat Arman Taherpour 28,29
Ala Arvish 173
Fahimeh Asadi 102
Azar Asadi 400
Sajad Asadi 498,504
Saeedeh Asadian 111
Shadi Asgari
Shadi Asgari 393,395
Sakineh Asghari 120
Zahra Ashoori 214,215
Fatemeh Ashouri Mirsadeghi 70
Elham Ashuri Moghaddam 125
Masoome Atef 86
Ali Ayati 308
Parisa Azarang 513
Seyedeh Bahareh Azimi 165,306
Shahla Azimi 270

Saeid Azimi 654
Jahangir Azizi 146
Amir Azizi 255,257
Saeid Azizian 181
Nasrin Azizi Balabeigloo 87
Pooria Babaei 144,138,242
Parisa Babaei 27,30
Hadi Babaei 351,352
M.R. Babaei 356
Kosar Babanezhad Harikandei 367
Mohammad Babazadeh 328
R. Babereh 239
Alireza Badiei 393,395
Somaye Badri 175
Siamak Baghari 351
Massoumeh Bagheri 10,174,263,293
Sara Bagheri 312
A. Bagheri 605,607
Fatemeh Zahra Bagherinezhad 286
Ghodsieh Bagherzade 522
Mojtaba Bagherzadeh 202
Nastran Baghfar 596,626
Shima Bahrami 460
Niloufar Bahramipanah 224
Mahsa Bakhshian 50
Mina Bakhtiari 311
Mohsen Bakhtiarian 320,326
Saeed Balalaie 328,347,348,362,795
Masomeh Balali 188,202
Abdolhamid Bamoniri 32,34,35,36,46,94,97,179
Alireza Banan 48,49,244,414,415
Maedeh Barabadi 704
Morteza Bararjanian 367
Mohammad Bashiri 145
Behnaz Bastami 322
Hajieh Bastami 733
Elham Bastani 696
Yadollah Bayat 182,358
Mohammad Bayat 214,215,289
Mohamad Bayat 358
Samira Bayazidi 278
A. Behboudi Amlashi 353,354,356,357
Javad Beheshtian 469
Aliasghar Behzadi 189
Haniyeh Behzadi 384
Fatemeh Behzadpour 534
Masoumeh Beiranvand 121,128

Amin	Benrashid 121
Siamak	Beyranvand 312
Nadia	Beyzae 686
Akram	Bigdeli 778
Rahman	Bikas 112,113
Asghar	Bodaghi 678
Mohammad Ali	Bodaghi Fard 204,402
Zahra	Borghebani 52
Maryam	Borzooei 302
Ali	Chanaani 431
Zeinab	Chehrazi 101
Zahra	Chenani 201
Seyed Mohammad Amin	Daei Naseri 540
Sajjad	Damiri 44,45
Mansoureh	Daraie 14,308
Ziba	Daroughezadeh 143,234
Fatemeh	Darvish 21
Mohammad	Dashteh 182
Azimeh	Davarpanah 546,710
Reyhaneh Sadat	DavarpanahShahri 342
Zahra	Davarzani 367
Negin	Dehghan 632
Shiva	Dehghan Abkenar 166
Nasrin	Dehghani 219
Zahra	Dehghani 69
Fatemeh	Dehghani Tafti 513
Yasser	Delavar 185
Mina	Delkhani 387
Somayeh	Dolatabadi 686
Khalilollah	Dolatmand 698
Esmail	Doustkhah 364
Atefe	Dovlatabadi 323
M.	Ebrahimi 354
Sattar	Ebrahimi 701,707
Ali	Ebrahimi Turkamani 137
Mahdiyeh	Ebrahimzadeh 781
Ali	Ehsani 337,757
Hamidreza	Ejraee 537
Hamid	Emadi 71,79,80
A.S.	Emami Meibodi 338
Mina	Erfani Ghazian 185,191
Sahar	Esfehani 802
Hossein	Eshghi 176
Mahboobe	Eskandari 19
Rasoul	Esmaeely Neisiany 686
Ali	Esmaeili 609
Karim	Esmaeilpour 44

Hamid Reza Ezatpour 53
Bahare Fadaei Tehrani 44
Zahra Fahimi 223
Mohammadreza Fakhimi Abarghouei 209
Nasrin Fallah 331,332
Abdollah FallahShojaei 249,272,275
Fatemeh Famarini 367
Mahnaz Farahi 158
B. Farajmand 239
Ayda Farajollahi 265,266
Hajar Farhadi 612
Khalil Farhadi 812
Amir Farkhondeh 18
Homayoun Faroughi Niya 190
Mahrokh Farrokh 38,39
Haniyeh Farrokhi 263
Fahimeh Farshi Azhar 174,580,602,675
Muhammad Saleh Faryabi 170,171
Faezeh Farzandi 33
Maryam Fatahpour 190
Rebwar Fatehi 776
Mahdi Fatehi Marj 543,668
Roghayeh Fathi 126,127
Mohadeseh Fathizadeh 766
Alireza Fattahi 189
Seyedeh Samaneh Feizabadi 292
Fariba Fotouki 540
Sara Fotovati 152,163
Rahim Ghadari 139,140,167
Ali Ghaffarinejad 154
Morteza Ghafoori 498,504
Hossein Ghafuri 154,156
Pouya Ghamari Kargar 522
Mohammad Mehdi Ghanbari 636
Masoud Ghane 718,721
Hale Ghanei 543
Milad Ghani 237
Alireza Gharehkhani 83
Maryam Ghasemi 206
Zarrin Ghasemi 220,222
Shahram Ghasemi 565
Ali Ghasemi Gol 754
Shahram Ghasemimir 79,80
Abdollah Ghasemi Pirbalouti 591
Hassan Ghasemnejad Bosra 54
Mohammad Ali Ghasemzadeh 93,246,472,528
Mojtaba Ghashghaee 20

Mehdi Ghavidel 443
Sobhan Ghazimoradi 15
HamidReza Ghenaatian 463,466
Ali Ghobadian 812
Hamed Gholami 162,241
Parisa Gholami Hasan Abadi 98
Mohammad Gholinejad 19,122
Mostafa Gholizadeh 18,229
Ali Gholmi 591
Fatemeh Ghomi 246
Fatemeh Ghorbani 161,235
Arash Ghorbani-Choghamarani 230,231,280
Ramin Ghorbani-Vaghei 213,245
Atefeh Golkari 785
Fatemeh Golmiri 71,484
Fatemeh Golmiri 71,484
Mahsa Golmohamadi 59
Hadis Goudarzi 60,63
Fatemeh Gourkani 31
Abdolrasoul H.Ebrahimabadi 199
Davood Habibi 13,60,63,121,128,193
Elham Habibzadeh 282
Setareh Habibzadeh 531
Mehrdad Hadadian 816
Samane Haddadi 78
Hamid Hadi 343,344
Mahsa Hadian 220
Vahideh Hadigheh Rezvan 27,87
Mina Haghdadi 50,54
Behzad Haghighi 323
Ali Haghighi Asl 387,389
Maryam Haghpanah 659
Fateme Hajati 54
Leila Hajiaghababaei 166,169
Motahare Hajihasani Bafghi 35
Mobina Hajihosini 133
Maryam Hajjami 38,39,82,83,106,129,162,241,264,287
Toktam Hajjar 785
Fatemeh Hamdi 665
Farahnaz Hamdi Holasoo 42
Hanieh Hamedi 108
Hanieh Hamedi Haghi 228
Farahnaz Hamzehee Harzanji 345
Maryam Hariri 46
Katayoun Hasanpour 275
Elaheh Hashemi 267
Payman Hashemi 303

Amin Hashemi Aghdam 227,228
Somayeh Hassani 788
Zahra Hassanpour 367
A.R. Hassanpour Golshani 354
Halimeh Hassanzadeh 291
Masoumeh Hatami 74
Saba Hatamipour 257
Behnaz Havakhah Hallaj 53
Reza Hazbavi 82
Nourallah Hazeri 190,617,671
Aida Heidari 318
Mohammad Amin Heidari 400
Akbar Heydari 177
Masumeh Heydari 197,198
SeyedehFatemeh Hojati 52
Sharifeh Hormozi Jangi 325,751
FahimehSadat Hoseini 355
Maryam Hosseinabadi 737
Amir Hosseini
Atenasadat Hosseini 327,329
Masoumehossadat Hosseini 423
MirSadra Hosseini 795
Akram Hosseinian 159,160
Mojtaba Hosseinifard 204,287
Seyed Mohammad Hosseininezhad 807
Mona Hosseini-Sarvari 145
Mahdieh Hosseinpoor Fini 94
Malihesadat Hosseiny 376,381,487
L. Hosseiny Nejad 605
Hossein Hosseinzadeh 243
Rahman Hosseinzadeh 37
Zhila Hosseinzadeh 419
Soghra Hossinimotlagh 562
Seyedeh Soghra Hossini Motlagh 574
Zahra Imani 36
Gholamhasan Imanzadeh 66, 152, 163
Zahra Inanloo 224
Hasanain Gomhor J.Alqaraghuli 648, 745
Thomas J.J.Müller 347
Noorhan J.M.Al-Juaifari 55
Fatemeh Jabbarzadeh 760
Khosrow Jadidi 423
Masoumeh JadidiNejad 177
Nadia Jafaei 184, 269
Masoumeh Jafari 169
Behzad Jafari 268
Fariba Jafari 273, 274

Ahmad Jafari 280
Leila Jafari 293
Fariba Jafari-Soghieh 53
Azar Jahanbakhshi 158
Shabnam Jahanbani Korabbaslo 139, 140
Mohammadali Jalali 397, 525
Soheila Jamali 450
Seifollah Jamalpour 101
Majid JamshidiLotf 359
Fatemeh Janati 516, 519
Fatemeh Janghorban 164, 283
Simin Janitabar Darzi 583, 599, 773
Hafez Janizadeh 304
Samira Javadi 13
Ali Javadi 246, 528
Siamak Javanbakht 108, 146, 227, 228, 243, 254, 309
Mohammad Javanmardi 48, 49, 415
Shahrzad Javanshir 134
Payam Joharchi 165
Sadegh Joudian 252
Somaye Kaboli 307
Babak Kaboudin 20, 25
Mina Kadkhodazadeh 285,288
S. Kafash 555
Sima Kalhor 109
Hamid R. Kalhor 124
Mehdi Kalhor 164, 283, 349
Hamid Reza Kalhor 61,65,107
Mohammad Kamangar 328
Zahra Karbalaie 194, 195, 225, 226
Shirin Karimi 122
Sepahbod Karimi 131
Farzaneh Karimi 367
Babak Karimi 41, 74, 75, 778
Nasser Karimi 537
Rahman Karimi-Nami 183, 187
Soheila Kashanian 648, 745
Bahareh Kavasi 671
Yasin Kaykha 431
Foad Kazemi 18
Abbas Kebritchi 478, 537
Narjes Keramati 428, 612
Elahe Keshavarz 361
Mohammad Hossein Keshavarz 45
Seyed Mojtaba Keshavarz 49
Seyed Mojtaba Keshavarz 49, 414, 415
Moghadaseh KeshvariKenari 120

Hassan Keypour 188, 202
Maryam Khademian 270
Soheila Khaghaninejad 96, 258
Ghazaleh khajeh Saeidi 51
Maryam Khajenoori 387, 389
Samad Khaksar 363
Behzad Khalili 454
Ebrahim Khalilzadeh 560
Omid Khanbeiki 79, 80
Ardeshir Khazaei 99, 100, 204
Sadegh Khazalpour 133, 305
Neda Khedri 115
Rahimeh Khezri 122
Azita Khodabandeh 114
Somaiyeh Khodadadi Karimvand 778
Mohammad Mehdi Khodaei 320, 326
Hosein Khodakarami 193
Asma Khoobi 325, 751
Fereshteh Khorasani 178
Mojtaba Khorasani 84, 85, 88, 89, 103, 252, 778
Alireza Khorshidi 251, 260
Yalda Khoshakhlagh Ostad 350
Maryam Khoshdoun 105
Abbas Khoshhal 374
Leila Khoshmaram 580, 602, 675, 715
Farideh Khoshsokhan 452
Kaveh Khosravi 217
Fahimeh Khouini 450
Mostafa Kiamehr 78, 223, 337, 384, 757, 766
AliReza Kiasat 276,91,101
AliReza Kiasat 91, 101, 276
Hamzeh Kiyani 143, 234, 609
Eisa Kohan Baghkheirati 704
Tayyebeh Koneshlou 212,216
Samaneh Koosha 213
Zeinab Korkani 769
Ehsan Koushki 292, 330
Masoumeh Kramati 260
Peter Langer 268
Mojtaba Lashkari 190
Majid M.Heravi 130, 136, 161, 235, 317, 340, 689
José M.Sansano 122
Abbas Madhi 447, 460
Amir Hossein Madhi 447, 460
Mohamad Mahani 92
Mohammad Mahdavi 334
Behnam Mahdavi 47, 62, 114, 330,816

Maryam Mahdavi 528
Seyed Mohammad Mahdi Nouri 327, 329
Shirin Mahjabin 210
Marzieh Mahmoodi Keshtiban 73, 90
Tannaz Mahmoudi 194, 195, 225, 226
Shaya Mahmoudian 411, 437
Maryam MahmoudianiGilan 60, 63, 128, 193
Aliasghar Mahmoudi Kharazm 242
Leila Makvandi 45
Abbas Maleki 224
Sara Maleki 303
Behrooz Maleki 37, 53, 116, 120
M. Maleki 607
Afsaneh Maleki 788
Dina Mallah 97
Masoume Malmir 130, 136, 161, 235, 340
Maryam Manafi Moghadam 639
Elahe Mashhadi 98, 310
Bakhshali Massoumi 73, 90
E. Masudi 356
Leila Matin 58
Firouz Matloubi Moghaddam 372
Masoumeh Mazloumi 296, 297
Hassan Mehrad-Majd 315, 316
Ali Mehrafarine 560
Maryam Mehrdadian 133, 305
Jamshid Mehrzad 315, 316, 487, 490
Amin Mehrzad 560
Sayedeh Mansoureh Memarzadeh 591
Azadeh Meshkini 452
Janan Metghalchi Langroudi 296, 297
Tara Miladi 271
Elham Mir 617, 671
Shefa Miraninezhad 278
Narjes Sadat Mireei 138
Boshra Mirhosseini-Eshkevari 93, 472
Marzie Sadat Mirhosseyni 26, 33
Elahesadat Miri 337, 757
Zohreh Mirjafary 55
Bibi Fatemeh Mirjalili 35, 97
Babak Mirtamizdoust 341, 384
Fatemeh Mirzaei Eslamlou 256
Vahid Mirzajani 812,
Azam Moazeni Bistgani 192, 434
Akbar Mobaraki 419
Sara Mobashsher Aghdam 167
Abolfazl Moein 478

M.H. Moeini 239
Sh. Moeini-Far 238, 239
Mahtab Moeinimehr 28, 29
Alieh Moeinipour 68
Roya Moeinzadeh 273, 274
Parisa Mofatehnia 317
Nazanin Moghadam 513
Nahid Moghaddam 75
Leyla Moghaddam Banaem 583
Alireza Mohaghegh Hazrati 469
Masoud MohamadiVala 358
Mohammad Reza Mohammad Azimi 335, 336
Mohammad Mahdi Mohammad-Hasani 333
Reza Mohammadi 108, 126, 127, 146, 227, 228, 243, 254, 309, 727, 730, 760
Leila Mohammadi 141, 142
Mina Mohammadi 174, 475, 501
A.A. Mohammadi 356
Zahra Mohammadi 40
Samira Mohammadi 510
Masoud Mohammadi 57, 58
Ghodsi Mohammadi Ziarani 26, 33, 77, 86, 117, 173, 200, 219, 393, 395
Somayyeh Mohammadian-Gezaz 374, 379
Kazem Mohammadiannejad 102
Milad Mohammadi Rasooll 39, 118, 119
Mohammad Reza Mohammadizadeh 31, 35
Masoud Mohammadi Zeydi 718, 721
Leyla Mohammadkhani 317, 689
Rahim MohammadRezaei 293
Kolsum Mohammadsharifi 265, 266
Ali Mohammadzadeh 309
Parisa Moharrami Korblagh 34, 36, 46
Maryam Mohebbi 367
Nasrin Mohseni 565
Sara MohseniTavana 117
Hojjat Mohsenpour 351, 352
Mohammad Majid Mojtahedi 125
Javad Mokhtari Aliabad 212, 216
Fatemeh Molaei Yielzoleh 11, 123
Hossein Molavi 211, 748
Hoda Mollabagher 125, 507
Ali Reza Molla Ebrahimlo 652
Saeed Mollaei 475, 501
Nasrin Mollania 248, 286, 291, 342, 662, 686, 704, 785
Fariba Mollania 248, 291, 785
Hamid Mollania 286, 342, 704
Madjid Momeni Moghaddam 292
Niaz Monadi 565

Arezo Monem 60, 63
Naser Montazeri 718, 721
Leila Moradi 17, 95, 192, 434, 557
Hesamodin Moradi 41
Ramtin Moradi Chafjiri 34
Mohsen Moradian 111, 186
Enayatollah Moradi Rufchahi 70, 152, 163
Ali Morsali 253, 281, 282, 298, 369
M.R. Morshedi 356
Zohreh Mortezaei 172
Adeleh Moshtaghi Zonouz 304, 571, 652, 713
Mostafa Moslempoor 549
Zeinab Motamedi 81
Alireza Motavalizadehkakhky 307, 327, 329, 376, 381, 487, 490
Maryam Moudi 286
Maryam Mousapour 256
Seyed Mahdi Mousavi 397, 525
Farimah Mousavi 565
Seyedeh Maryam Mousavi 93
Mehdi Mousavi Kamazani 428
Elahe Sadat Mousavi-Kherad 166
S.Morteza Mousavi-Khoshdel 510
Seyyed Abbas Musavi 748
A. MusaviAzar 353,356
Zahra Naderi 74
Mehri NadiriNiri 620
Mahtab Naeim 232,233,259
Hossein Naeimi 513
Farzaneh Naghdi 249
Ali Naghipour 232,259
Moein Najafabadi 629
Jamshid Najafpour 166,169
Kolsoom Najafzadeh 355
Carmen Nájera 122
Reza Najjar 623
Faeze Namayandeh-Niasar 186
Hassan Namazi 147,148,207,208
Mansoor Namazian 763
Shadi Namdar 104
Fatemeh Namjoyan 251
Azadeh Naraghi 799
Sina Nasiri 623
Farough Nasiri 69
Shima Nasri 214,215
Somayeh Nasrian 10
Mahmoud Nasrollahzadeh 134, 154, 156,
Fatemeh Nasseri 153,155

Mohammad Ali Nasseri 153,155
Forough Nasuhipur 222
Elahe Navaee Lavasani 61
Amene Navaser 124
Mahdiyeh Navazeni 204
Monireh Navazeni 217
Behrouz Nayebzadeh
Behrouz Nayebzadeh 313,328
Mahboobeh Nazari 255
Hamed Nazarpour-Fard 812
Ehsan Nazarzadeh Zare 278
Mohammad Taghi Nazeri 206
Maryam Nazifi 240
Razieh Nejat 642,645
Faezeh Nemati 367
Davood Nematollahi 370
Zahra Nezafat 134
Fatemeh Nezafatpour 129
Alireza Nezamzadeh-Ejhieh 339
Neda Niknam 135
E. NiknamAsl 353
Abbas Nikoo 73,90
Kobra Nikoofar 11,123
Nedasadat Nikoo kalam Azim 334
Ahmad Nikseresht 57,58
Maryam Noori 106,748
Yasmin Noori 276
Maryam Noori Keshtkar 748
Mohammad Nori Ali Beg Candy 304
Nader Noroozi Pesyan 59, 64, 81, 104, 135, 168, 175, 210
Masoomeh Norouzi 271,279,302
Fatemeh Norozi 531
Nader Noshiranzadeh 112,113
Keyvan Nosrat Zadegan 560
Behrouz Notas 206
Sayed Ahmad Nourbakhsh 591
Tohid Nouri 89
Farita Nourizadeh 591
Shahab Ojani 718,721
Maryam Oudi 110
Nahid Pahlavani 267
Hadi Panahi 737
Amin Parvizi Moghadam 632
Zahra Pasandeh 602
Arsalan Pashapour 115
Narjess Peyman 346
Zeinab Piraman 107

Fatemeh Pirani 176
Sajad Pirsa 781
Malihe Pooresmaeil 147,148,207,208
Poya Portaher 31
Mehdi Pourahmad 305
Behjat Pouramiri 391
Mehrdad Pourayoubi 203,205,345,346,350,799
Maryam Pourjamal 272
Ali Pourjavadi 16
Mozhdeh Pourmansouri 84
SeiedAli Pourmousavi 278
Sepideh Pourrohani 588
Ahmad Poursattar Marjani 265,266
Mohammad R.Mosleh 197,198
Mohammad Rad 298
Abdolhamid Raeisi 636
Amirali Rafati 23,24
Ronak Rafipour 648, 745
Fatemeh Rahgozar 65
Yadegar Rahimi 183
Samira Rahimi 692
Somayeh Rahmati 552
Setareh Rahmatzadeh 650
Hossein Asghar Rahnama 248
Saideh Rajai-Daryasarei 795
Ali Ramazani 639, 807
Shapour Ramazani 769, 791
Sara Ramezani 291
Navid Ramezanian 185,191
Sorour Ramezanpour15
Reza Ranjbar-Karimi 102,178
Sara Rashidi 308
Marzieh Rashidipour 322
Somayeh Rashtabadi 220
Asra Rashtiani 245
Mohadeseh Rashvand 103
S.Ghasem Rasooll
Negin Rasoulian 136
Zeinab Rastegaran 33
Zahra Rastipour 115
Sayed Ali Akbar Razavi 282
Fatemeh Razavi 791
Mostafa Razban 713
Fatemeh Rezaei 116
Monireh Rezaei 289
Reza Rezaei 583
Mohammad Rezaei-Gohar 313

M. Rezaei Sameti 605,607
Esmail Rezaei Seresht 47,62,114
AliHossein Rezayan 261,724
Sobhan Rezayati 253
Mohammad Reza Rokhian 698
Frank Rominger 347
Pardis Roozbahani 586
Romina Roozbeh 428
Elham Rostami 596,626,285,288,
Mohsen Rostamian 32
Akbar Rostami-Vartooni 333, 334
Mohammad Rostamizadeh 692,694,
Sadegh Rostamnia 149,150,194,195,225,226,290,335,336,365
Morteza Rouhani 212,216
Zohreh Saadati 408
Mohammad Sabaeiand 101
Fahimeh Sabbaghi 203,205
Ali Saberi 733,735
Nasrin Saberi Harooni 513
Seyyed Javad Sabounchei 359
Hosin Sabri 352
Ali Sabzalipour 25
Marzie Sadat Mirhosseyni 26,33
Malihe Sadat Hosseiny 376,381,487,490
Mohammad Sadegh Aghili 440
Seyyed Hojjat Sadeghi 149,150,194,195,225,226
Azam Sadeghi 172
Bahareh Sadeghi 300,301
alireza Sadeghi-avalshahr 342
Fatemeh Sadeghi Erami 457
Akbar Saednya 137
Jafar Saeidi 315,316
Hamid Saeidian 55, 212, 216, 224
Leyla Saeifard 347
Javad Safaei-Ghomi 138, 179, 242, 310
Maliheh Safaiee 28, 29
Hadis Safarbeigi 279
Reza Safari 343, 344,
Somayeh Safari 402
AliAsghar Safari 778
Rahim Safarpour 207,208
Maryam Saffari 11,123
Maryam Saffaridarbarzi 123
Reza Sahraei 259
Mohammad Ali Saidiansar 19
Mohaddeseh Sajjadi 154,156
Sabah Salahvarzi 534

Haniyeh Salari Jaieni 345
Peyman Salehi 367
Mahboobeh Salehpour 408
Jaber Salehzadeh 69
Mohammad Sepehr Salimi 211
Fatemeh Salimi 331,332
Faezeh Salmanpour 64
Fatemeh Sardarabadi 47
Alireza Sardarian 650
Mohsen Sargordanfard Arani 443
Yaghoub Sarrafi 588,37,270,423
Afshin Sarvary 531,632,262
Mohsen Sayadi 232,233,236
Hassan Sepehrmansourie 38, 39, 72, 99, 100, 109, 118, 119, 204, 299, 311, 314, 333
Moslem Setoodehkhah 397,525
Neda Seyedi 805
Fatemeh Seyedi-Ardabil 339
Seyed Amir Hossein Seyed Mousavi
Zahra Seyedzade 349
Samereh Seyfia 12
Seyyed Abolfazl Seyyedi 66
Amir Seyyedi Saghezchi 187
Soulmaz Seyyed Shahabi 131
Ahmad Shaabani 206,366
Sina Shaabanzadeh 371
Shima Shabani 179
Darya Shabani Domoula 318,324
Yadollah Shad 698
Saied Shafiei Navid 237,588
Seyyed Mohammad Shahcheragh 105
Ali Shahdadi 692,694
Elaheh Shahmoradi 112, 113
AshrafSadat Shahvelayati 166,169
Mehdi Shakourian-Fard 463,466
Mohammad Nasir Shambayati 162,241
Zahed Shami 776
Nikoo Shamkhali 77
Farzaneh Shamsa 487,490
Mohammad Mehdi Shams Nateri 498,504
Somayeh Shariatzadeh-Kyasari 168
H. Shayani-Jam 238,239
Esmaeil Sheibani 549, 696
Nafisehsadat Sheikhan 51,56
Mohammad Ali Sheikh-Mohseni 781
Mahla Sheikhveisi 190
Hamideh Shirazi 405
Sahar Shiri 675

Farhad Shirini 256, 296, 297
Maryam Shojaeifard 55
Reihaneh Siahkar 192
Zahra Siahpour 129, 264
Media Sighar Ghiasi 730
Alireza Simiari 389
Stavroula Skoulika 12
Ehsan Soheyli 259
Negin Sohrabi 727, 730, 760
Vahid Sokhanvaran 323
Somayeh Soleimani-Amiri 802
Reza Taghavi 290
Saeed Taghizadeh Khorasanian 62
Samaane Taghvaeinia 416
Salman Taheri 240, 507
Valid Taheri 423
Pouya Taheri 71, 484
Aazar Tahghighi 513
Mahmood Tajbakhsh 14, 71, 308, 484, 588
Hassan Tajik 296, 297
Aref Tanavardi-Nasab 92
Elham Tavakoli 38, 99, 100
Amir Mahdi Tavassoli 277, 284
Reza Teymouri Mofrad 318, 324
Morteza Torabi 67, 151, 180, 181, 196, 217, 277, 284
Zahra Torkashvand 72
Mat UzirWahit 411
Mohammad Reza Vaezi 141, 142
Arash Vahdatkhah 254
Morteza Vahedpour 450
Hojatollah Vali 778
Zohreh Valipour 37
M.R. Yaftian 238, 239
Yasaman Yaghini 319, 338
Fereshteh Yaghoobi 295, 577
Hooriye Yahyaei 273, 274
Asieh Yahyazadeh 152, 163
Alireza Yaqubzadeh 698
Hossein Yarahmadi 157
Meysam Yarie 67, 151, 180, 181, 196, 277, 284
Issa Yavari 12,371,405
Kimia Yavari 56
Kimia Yavari 56
Zahra Younesi 14
Faaeze Younesi 763
Ali Yousefi 199
Afsaneh Yousefi Monfared 522

Afsaneh	Yousefi Monfared 522
Miguel	Yuse 122
Mohamad	Z.Kassaee 552
Abedin	Zabardasti 312
Ehsan	Zahedi 327,329
Forough	Zahedpour 115
Elham	ZahiriRad 43
Fatemeh	Zakeran 715
Hassan	Zaliboieni 440
Reza	Zamani Chehrania 244
Mohammad	Zaman Kassaee 153,155,321,741
Mohammad Reza	Zamanloo 66
Fatemeh	Zamiran 200
Mahmoud	Zarei 100, 109, 287, 299, 311, 314, 333
Narges	Zarei 151, 181
Mohadese	Zarei 218, 221
Armin	Zarei 639
Fatemeh	Zarezadeh 314
Ali	Zarnegaryan 218, 221, 562, 574
Fatemeh	Zeidabadi 330
Mojgan	Zendehdel 96
Rahele	Zhiani 327,329,376,381,487,490
Mohammad	Zirak 286
Maryam	Zirak 481
Azim	ZiyaeiHalimehjani 368
Gholamhossein	Zohuri 185,191
Farzad	Zolfaghari
Farzad	Zolfaghari 91,276
Maedeh	Zolfalizadeh 222
Mohammad Ali	Zolfigol 38, 39, 72, 99, 100, 109, 118, 119, 151, 180, 181, 182, 196, 204, 217, 277, 284, 287, 299, 810
Ali	Zraatkarmoghaddam 665

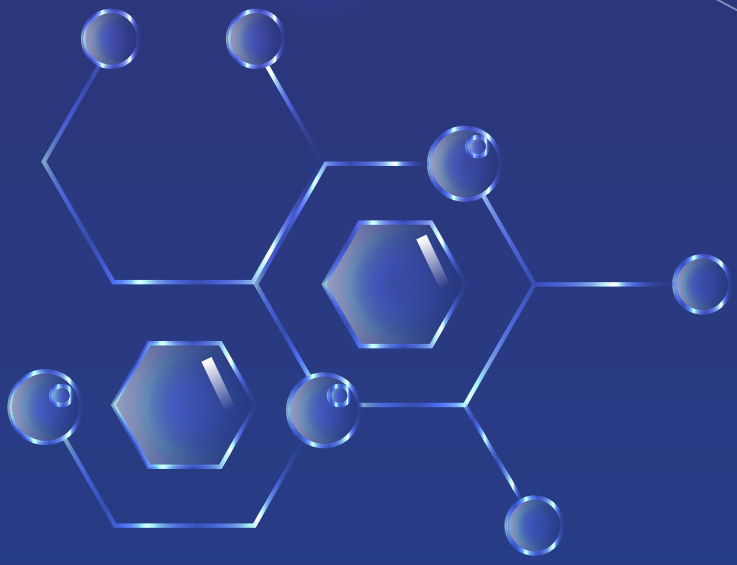

29th Iranian Organic Chemistry Conference

UNIVERSITY OF QOM, IRAN